

Vol. 20, No. 4, December, 2021

ISSN (Print): 0972-6268; ISSN (Online) : 2395-3454

NATURE ENVIRONMENT & POLLUTION TECHNOLOGY

*A Multidisciplinary, International Journal
on Diverse Aspects of Environment*



Technoscience Publications

website: www.neptjournal.com



Technoscience Publications

A-504, Bliss Avenue, Balewadi,
Opp. SKP Campus, Pune-411 045
Maharashtra, India

www.neptjournal.com

Nature Environment and Pollution Technology

(An International Quarterly Scientific Research Journal)

EDITORS

Dr. P. K. Goel (Chief Editor)

Former Head, Deptt. of Pollution Studies
Y. C. College of Science, Vidyanagar
Karad-415 124, Maharashtra, India

Dr. K. P. Sharma

Former Professor, Deptt. of Botany
University of Rajasthan
Jaipur-302 004, India

Published by : Mrs. T. P. Goel, Technoscience Publications, A-504, Bliss Avenue, Balewadi, Pune-411 045, Maharashtra, India

Managing Office : Technoscience Publications, A-504, Bliss Avenue, Balewadi, Pune-411 045, Maharashtra, India

E-mail : contact@neptjournal.com; journalnept@gmail.com

INSTRUCTIONS TO AUTHORS

Scope of the Journal

The Journal publishes original research/review papers covering almost all aspects of environment like monitoring, control and management of air, water, soil and noise pollution; solid waste management; industrial hygiene and occupational health hazards; biomedical aspects of pollution; conservation and management of resources; environmental laws and legal aspects of pollution; toxicology; radiation and recycling etc. Reports of important events, environmental news, environmental highlights and book reviews are also published in the journal.

Format of Manuscript

- The manuscript (*mss*) should be typed in double space leaving wide margins on both the sides.
- First page of *mss* should contain only the title of the paper, name(s) of author(s) and name and address of Organization(s) where the work has been carried out along with the affiliation of the authors.

Continued on back inner cover...

Nature Environment and Pollution Technology

Vol. 20, No. (4), December 2021

CONTENTS

1. **B.Q. Zhao, R.Z. Gao, D. Xia, L. Xia, W.Q. Zhu and W.N. Xu**, Vegetation Community Characteristics Under Different Vegetation Eco-restoration Techniques at Xiangjiaba Hydropower Station 1381-1392
2. **Xiaole Huang, Wennian Xu, Yu Ding, Dong Xia, Shiyuan Xiong, Daxiang Liu and Bo Pan**, Impact of Wetting and Drying Cycles on the Mechanical Properties and Microstructure of Vegetation-growing Concrete 1393-1402
3. **Zakiya Tabassum† and Rajalakshmi Mudbidre**, Treatment and Disposal Methods of Concentrate Stream of Seawater Reverse Osmosis- A Review 1403-1414
4. **J. R. Reyes-Santiago, L. A. García-Villanueva, G. Fernández-Villagómez and P. Guzmán-Guadarrama**, Geochemical Characterization and Saturation Index (Si) in the Montebello Lagunar System Liquidamber Lagoon, Chiapas Mexico 1415-1425
5. **Jie Ma, Jianghong Wang, Song Chen, Hongbao Dai, Jingyu Zhao, Haitao Zhang and Zhichun Li**, Hydrochemical Characteristics, Quality Assessment and Solute Source Identification of Coal Bearing Fractured Aquifer in Dingji Coal Mine, Huainan Coalfield, China 1427-1436
6. **K. J. Naveen Kumar and J. Prakash**, Bioremoval of Different Heavy Metals in Industrial Effluent by the Resistant Fungal Strain *Aspergillus niger* 1437-1448
7. **Nguyen Ngan Ha, Tran Thi Thu Huong, Pham The Vinh and Tran Thi Van**, Surface Water Pollution Risk From Vietnam Water Quality Index (VN-WQI) in the Ca Mau City, Mekong Delta 1449-1464
8. **Shuai Wang*, Huifang Wang*, Luzeng Hu*, Zhipeng Lu*, Muqing Qiu* and Xin Zhong**, The Construction of Magnetic MnFe₂O₄@TpPa-1 Composite Materials and the Adsorption Removal Performance of Organic Pollutants in Solution 1465-1474
9. **R. He, H.P. Jiao, N. He, Y.Y. Chang, H.Y. Jiang, Y. Zhang, Y.Q. Li and R. Jiang**, Seasonal Variation of Zooplankton Communities and the Effects of Environmental Factors in the Seawater Near Taishan Nuclear Power Station 1475-1484
10. **Lakhvir Singh and Balraj Singh Brar**, A Review on Rice Straw Management Strategies 1485-1493
11. **M.I. Antoshchenko, V.Y. Tarasov, Ye.S. Rudniev and O.I. Zakharova**, On the Issue of Establishing the Stages of Coal Metamorphism for Predicting the Hazardous Properties of Coal Seams 1495-1503
12. **C. Prabhu, V. Rajasekar and T. Prakash**, Characterisation and Assessment of Physicochemical Properties of Grapeseed Methyl Ester Using Predictive Correlations and ASTM Standards For CI Engine Application 1505-1513
13. **Sonam Chaturvedi, Bikarama Prasad Yadav and Nihal Anwar Siddiqui**, An Assessment of Machine Learning Integrated Autonomous Waste Detection and Sorting of Municipal Solid Waste 1515-1525
14. **Ruqin Gao, Lu Pan, Yingrui Huang, Zhaoyang Wu and Bingtao Liu**, Adsorption Behavior of Hydroquinone by Diatomite-based Porous Ceramsite 1527-1534
15. **Xinjie Deng**, Spatiotemporal Evolution and Pattern Differences of Environmental Sanitation Facilities in Rural China: Taking the Improvement of Water and Latrines as an Example 1535-1543
16. **J. S. Berame, M. B. Hojilla, E. Trinidad, N. L. Lawsin, J. A. Orozco, I. J. Arevalo and Zeba F. Alam**, Strategies and Approaches Towards Environmental Biomonitoring of Freshwater Ecosystems in Philippines 1545-1553
17. **Somil Thakur and Bhaskar Das**, Investigation on Microbial Fuel Cells Fabricated from Recyclable Materials for Energy Generation and Wastewater Treatment 1555-1563
18. **R. Rajasekaran and P. K. Suresh**, Cell Death Induction Potential in Seed Extracts- Hidden and Bioactive Phytochemical Treasures 1565-1575
19. **W.N. Galang, I.D.F. Tabañag and M.E. Loretero**, Estimation of Biomass Availability in Panglao Island Using SENTINEL-2 MSI 1577-1584
20. **Ren Shuangqing, Men Baohui and Shen Yaoduo**, Water Quality Evaluation of Wenyu River in Beijing by Matter Element Model 1585-1591
21. **Xudong Hu, Jiazhen Gao, Mingtao Zhou, Songtao Peng, Wennian Xu and Chenyuan Wang**, Impact of Drying and Wetting Cycles on Vegetation Cement-soil Physical and Mechanical Properties 1593-1600
22. **Joaquin Ortiz**, Advances in Microfiltration and Ultrafiltration Technology for Greywater Treatment: A Review 1601-1609
23. **Barsha Roy and P. K. Suresh**, Toxic Effect of Antibiotics on Freshwater Algal Systems and the Mechanisms of Toxicity: A Review 1611-1619
24. **Hizbullah Rahmani, Wafaurahman Wafa and Fayaz Gul Mazloun Yar**, The Importance of Public Awareness in Environmental Protection: A Case Study in Paktika, Afghanistan 1621-1626
25. **Xin Youyang, Li Xiuzhong and Shang li**, Environmental Efficiency of Construction Industry with onsiderations to Carbon Emission: A Case Study in Henan, China 1627-1634
26. **Xiongfei Cai, Die Xu, Shijie Zhao, Li Lei, Ji Wang and Bin Xuan**, Analysis and Evaluation on Characteristics of Heavy Metal Pollution in the Coastal Farmland Soil along the Wuma River 1635-1642

27. **Y. Jin, L.Y. Mo, L.T. Qin and J.F. Dai**, Study on the Joint Toxicity of Multi-component Mixtures of Quaternary Ammonium Compounds 1643-1651
28. **Cailing Xue, Ailinaizaier Ainiwaer, Jiazhen Gao and Zhaohui Qin**, Erosion Resistance and Fertility of Frost-Resistant Ecological Substrate in Alpine Region 1653-1660
29. **U.S.P.R. Arachchige**, Briquettes Production as an Alternative Fuel 1661-1668
30. **Wang Lijuan**, Influencing Factors of Carbon Emissions in the Construction Industry Based on Logarithmic Mean Divisia Index: A Case Study of China 1669-1675
31. **M. K. Yadav and A. K. Srivastava**, Solid Selective Catalytic Reduction: A Promising Approach towards Reduction of NO_x Emission from Exhaust of CI Engines 1677-1684
32. **Nithya Gopinath, Madhu G. and Joseph Francis**, Upflow Anaerobic Filter for the Treatment of Wastewater from a Natural Rubber Latex Concentration Unit 1685-1693
33. **A.T. AbdAllah, A.M. Alhababy, M.G. Shamsy, M.S. AbdelDayem and Sahar H. Haroun**, Temporal and Spatial Distribution of Zooplankton Inhabiting Sandy and Muddy Shore Habitats at Jazan Coastal Area 1695-1701
34. **Megat Ahmad Kamal Megat Hanafiah, Shariff Ibrahim, Nur Izah Fasihah Mohamad Subberi, Nesamalar Kantasamy** and Is Fatimah**, Application of Cationic Surfactant Modified Mengkuang Leaves (*Pandanus atropicus*) for the Removal of Reactive Orange 16 from Batik Wastewater: A Column Study 1703-1708
35. **Tianxin Li, Fang Zhang and Minjie Zhang**, Study on the Prevention and Control of Fe and Mn Pollution by Resistant Mixed Bacteria in Simulated Mining Area 1709-1716
36. **Chunwei Han**, Environmental Regulations, Environmental Subsidies and Enterprise Investment for Environmental Protection: Evidence from Pollution Enterprises of China 1717-1724
37. **C. Mani Kumar, Shahid Ali, P. Sri Lakshmi, G. Raja Kullayappa and K. Tanveer Alam**, Low-Cost IoT Enabled Embedded System for Measurement of Environmental Pollutants 1725-1732
38. **S. M. D'Sa, D. Patnaik, V. Acham and S. Jadhao**, Correspondence Between Technology Options Available for Chemical Industries and the Levels of the Waste Management Hierarchy: A Case Study Approach 1733-1740
39. **Latifa Mirzatika Al-Rosyid, Harmin Sulistiyaning Titah, Irwan Bagyo Santoso and Sarwoko Mangkoedihardjo**, Review on BOD/COD Ratio Toxicity to *Daphnia magna*, *Artemia salina* and *Brachydanio rerio* 1741-1748
40. **Bharath A., Manjunatha M., Ranjitha B. Tangadagi, Preethi S. and Mukund Dangeti**, Assessment of LULC Changes for Hesaraghatta Watershed Using GIS Tools and Remote Sensed Data 1749-1756
41. **V. Hariram, J. Godwin John, Subramanyeswara Rao, S. K. Baji Babavali, S. Muni Lokesh, D. Tejeswar Reddy and S. Seralathan**, Biodiesel Extraction from Chicken Fat and Its Effect on the Performance and Emission Characteristics of the Diesel Engine 1757-1763
42. **C. Borpujari and A. K. Bora**, GIS-Based Digital Terrain Analysis of Assam-Meghalaya Foothills in Kamrup District, Assam 1765-1771
43. **Quansheng Li, Kai Zhang, Yingming Yang, Shan Chong, Wenfeng Du and Yunlan He**, Spatiotemporal Variation Characteristics of Groundwater Quality in A Semi-Arid Steppe Area in Northwest China 1773-1779
44. **Xiaoxue Zhang, Faming Sun, Jie Yang, Jian Li, Jing Liang, Mei Yang and Wen Liu**, Situation and Treatment Methods of Ecological and Environmental Problems during the Process of Urbanization in Rural Areas of China 1781-1787
45. **A. D. Vyas, K. Mahale and R. Goyal**, A GIS-Based Methodology to Determine Effect of Vehicular Pollution at Ward Level: Case Study of Jaipur City 1789-1801
46. **Xiaowen Qiu**, Dynamic Relationship Between China's Environmental Protection Investment and Regional Environmental Pollution 1803-1809
47. **Xin Huang and Lin Qiu**, Assessment of Soil Environment Pollution Based on Fuzzy Pattern Recognition Model 1811-1816
48. **P. V. Hirapure, S. A. Paranjape, V. S. Sarodaya, B. A. Mehere and V. J. Upadhye**, Evaluation of Cytotoxicity and Genotoxicity of Water from Nag River, Nagpur, India 1817-1823
49. **A. Thakur, S. Sharma and K. Qanungo**, A Study on the Effect of Soil and Sediment Types on the Fugacity Based Multimedia Partitioning of a Contact Fungicide Fluopyram: An Equilibrium Quality Criterion (EQC) Level 1 Approach 1825-1830
50. **Q. Zhong and X.M. Liu**, Monitoring Methods of Marine Pollution Range Based on Big Data Technology 1831-1836
51. **V. Sai Kumar, P. Hari Prasad Reddy and Ch. Rama Vara Prasad**, Micro-Fabric Transformations of Ball Clay in Alkaline Environment 1837-1842
52. **M. Praveen Kumar**, Seasonal Variation of Dissolved Lead Speciation in Tagus Estuary, Portugal 1843-1847
53. **R. Sivarethinamohan and S. Sujatha**, Environmental Management: Pragmatic Suitability of Low Cost Activated Carbon in Lead (II)Ion Removal by Continuous Mode of Adsorption 1849-1853
54. **Kai Wang and Xin Yang**, Impact of Government Regulation on Emission Reduction of Environmental Pollutants in China 1855-1861

**The Journal
is
Currently
Abstracted
and
Indexed
in:**



Scopus CiteScore (2020) = 0.6

Ulrich's (Refereed) database

Zetoc

J-Gate

Centre for Research Libraries

Connect Journals (India)

Research Bible (Japan)

Elektronische
Zeitschriftenbibliothek (EZB)

CNKI Scholar (China National
Knowledge Infrastructure)

AGRIS (UN-FAO)

CNKI Scholar (China National Knowledge Infrastructure)

NAAS Rating of the Journal (2019) = 3.85

Scopus®, SJR (0.154) 2020

EI Compendex of Elsevier

Chemical Abstracts, U.S.A.

Pollution Abstracts, U.S.A.

Paryavaran Abstract,
New Delhi, India

Electronic Social and Science
Citation Index (ESSCI)

CrossRef (DOI)

Google Scholar

Environment Abstract, U.S.A.

WorldCat (OCLC)

CSA: Environmental Sciences and Pollution Management

Indian Science

SHERPA/RoMEO

Access to Global Online Research in Agriculture (AGORA)

Present in UGC-CARE List (Group II)

Index Copernicus (2019) = 111.88

Indian Science Abstracts,
New Delhi, India

Elsevier Bibliographic
Databases

Zoological Records

Indian Citation Index (ICI)

EBSCO: Environment Index™

DOAJ

ProQuest, U.K.

British Library

JournalSeek

Geobase

Directory of Science

UDL-EDGE (Malaysia) Products like *i*-Journals, *i*-Focus and *i*-Future

www.neptjournal.com

Nature Environment and Pollution Technology

EDITORS

Dr. P. K. Goel (Chief Editor)

Former Head, Deptt. of Pollution Studies
Yashwantrao Chavan College of Science
Vidyanagar, Karad-415 124
Maharashtra, India

Dr. K. P. Sharma

Former Professor, Ecology Lab, Deptt. of Botany
University of Rajasthan
Jaipur-302 004, India
Rajasthan, India

Manager Operations: Mrs. Apurva Goel Garg, C-102, Building No. 12, Swarna CGHS, Beverly Park, Kanakia, Mira Road (E) (Thane) Mumbai-401107, Maharashtra, India (**E-mail: operations@neptjournal.com**)

Business Manager: Mrs. Tara P. Goel, Technoscience Publications, A-504, Bliss Avenue, Balewadi, Pune-411 045, Maharashtra, India (**E-mail: contact@neptjournal.com**)

EDITORIAL ADVISORY BOARD

1. **Dr. Prof. Malay Chaudhury**, Department of Civil Engineering, Universiti Teknologi PETRONAS, Malaysia
2. **Dr. Saikat Kumar Basu**, University of Lethbridge, Lethbridge AB, Canada
3. **Dr. Sudip Datta Banik**, Department of Human Ecology Cinvestav-IPN Merida, Yucatan, Mexico
4. **Dr. Elsayed Elsayed Hafez**, Deptt. of of Molecular Plant Pathology, Arid Land Institute, Egypt
5. **Dr. Dilip Nandwani**, College of Agriculture, Human & Natural Sciences, Tennessee State Univ., Nashville, TN, USA
6. **Dr. Ibrahim Umaru**, Department of Economics, Nasarawa State University, Keffi, Nigeria
7. **Dr. Tri Nguyen-Quang**, Department of Engineering Agricultural Campus, Dalhousie University, Canada
8. **Dr. Hoang Anh Tuan**, Deptt. of Science and Technology Ho Chi Minh City University of Transport, Vietnam
9. **Mr. Shun-Chung Lee**, Deptt. of Resources Engineering, National Cheng Kung University, Tainan City, Taiwan
10. **Samir Kumar Khanal**, Deptt. of Molecular Biosciences & Bioengineering, University of Hawaii, Honolulu, Hawaii
11. **Dr. Sang-Bing Tsai**, Zhongshan Institute, University of Electronic Science and Technology, China
12. **Dr. Zawawi Bin Daud**, Faculty of Civil and Environmental Engg., Universiti Tun Hussein Onn Malaysia, Johor, Malaysia
13. **Dr. Srijan Aggarwal**, Civil and Environmental Engg. University of Alaska, Fairbanks, USA
14. **Dr. M. I. Zuberi**, Department of Environmental Science, Ambo University, Ambo, Ethiopia
15. **Dr. Prof. A.B. Gupta**, Dept. of Civil Engineering, MREC, Jaipur, India
16. **Dr. B. Akbar John**, Kulliyah of Science, International Islamic University, Kuantan, Pahang, Malaysia
17. **Dr. Bing Jie Ni**, Advanced Water Management Centre, The University of Queensland, Australia
18. **Dr. Prof. S. Krishnamoorthy**, National Institute of Technology, Tiruchirapally, India
19. **Dr. Prof. (Mrs.) Madhoolika Agarwal**, Dept. of Botany, B.H.U., Varanasi, India
20. **Dr. Anthony Horton**, Envirocarb Pty Ltd., Australia
21. **Dr. C. Stella**, School of Marine Sciences, Alagappa University, Thondi -623409, Tamil Nadu, India
22. **Dr. Ahmed Jalal Khan Chowdhury**, International Islamic University, Kuantan, Pahang Darul Makmur, Malaysia
23. **Dr. Prof. M.P. Sinha**, Dumka University, Dumka, India
24. **Dr. G.R. Pathade**, H.V. Desai College, Pune, India
25. **Dr. Hossam Adel Zaqoot**, Ministry of Environmental Affairs, Ramallah, Palestine
26. **Prof. Riccardo Buccolieri**, Deptt. of Atmospheric Physics, University of Salento-Dipartimento di Scienze e Tecnologie Biologiche ed Ambientali Complesso Ecotekne-Palazzina M S.P. 6 Lecce-Monteroni, Lecce, Italy
27. **Dr. James J. Newton**, Environmental Program Manager 701 S. Walnut St. Milford, DE 19963, USA
28. **Prof. Subhashini Sharma**, Dept. of Zoology, University of Rajasthan, Jaipur, India
29. **Dr. Murat Eyvaz**, Department of Environmental Engg. Gebze Inst. of Technology, Gebze-Kocaeli, Turkey
30. **Dr. Zhihui Liu**, School of Resources and Environment Science, Xinjiang University, Urumqi, China
31. **Claudio M. Amescua García**, Department of Publications Centro de Ciencias de la Atmósfera, Universidad Nacional Autónoma de México
32. **Dr. D. R. Khanna**, Gurukul Kangri Vishwavidyalaya, Haridwar, India
33. **Dr. S. Dawood Sharief**, Dept. of Zoology, The New College, Chennai, T. N., India
34. **Dr. Amit Arora**, Department of Chemical Engineering Shaheed Bhagat Singh State Technical Campus Ferozepur -152004, Punjab, India
35. **Dr. Xianyong Meng**, Xinjiang Inst. of Ecology and Geography, Chinese Academy of Sciences, Urumqi, China
36. **Dr. Sandra Gómez-Arroyo**, Centre of Atmospheric Sciences National Autonomous University, Mexico
37. **Dr. Manish Sharma**, Research and Development Cell, Bahra University, Shimla Hills, Shimla, India
38. **Dr. Wen Zhang**, Deptt. of Civil and Environmental Engineering, New Jersey Institute of Technology, USA



Vegetation Community Characteristics Under Different Vegetation Eco-restoration Techniques at Xiangjiaba Hydropower Station

B.Q. Zhao^(**), R.Z. Gao^(**), D. Xia^{**}, L. Xia^(**), W.Q. Zhu^(**) and W.N. Xu ^(**)†

*Key Laboratory of Disaster Prevention and Mitigation, China Three Gorges University, Yichang, Hubei 443002, China

**Engineering Research Center of Eco-environment in Three Gorges Reservoir Region, Ministry of Education, China Three Gorges University, Yichang, Hubei 443002, China

†Corresponding author: Wennian Xu; xwn@ctgu.edu.cn

Nat. Env. & Poll. Tech.
Website: www.neptjournal.com

Received: 27-10-2020

Revised: 08-01-2021

Accepted: 22-01-2021

Key Words:

Vegetation eco-restoration techniques

Vegetation community

Species diversity

Disturbed area

ABSTRACT

The objective of this study is to understand the characteristics of vegetation communities under different vegetation eco-restoration models (vegetation concrete eco-restoration technique, frame beam filling soil technique, thick layer base material spraying technique, and external soil spray seeding technique). Vegetation coverage, dominant species, species composition, and species diversity of vegetation community under different vegetation eco-restoration modes were analyzed by field survey. The vegetation community of the abandoned slag slope was unstable due to the simple vegetation community structure. The species and number of the thick layer base material spraying slope were low and fail to form a healthy multilayer community structure due to the invasion of *Leucaena leucocephala* (Lam.) de Wit. Studying the allelopathy of *Leucaena leucocephala* (Lam.) de Wit and seeking the best species composition that can coexist with it is significant to promote the positive succession of the vegetation community. The frame beam filling soil technique, external-soil spray seeding technique, and vegetation concrete eco-restoration technique can effectively promote the succession process of the vegetation community and have well water and soil conservation capacity. These findings suggest that artificial vegetation eco-restoration measures can effectively promote vegetation eco-restoration and the positive succession of vegetation community of disturbed slopes. The research results can provide scientific advice for vegetation eco-restoration and subsequent control and management of disturbed slopes in the Xiangjiaba project, and also can be helpful to other similar projects.

INTRODUCTION

Engineering disturbance can bring serious environmental problems (Ghanbarpour & Hipel 2009, Cao et al. 2018). However, a large number of hydropower stations have been built because of the demand for clean energy (Zhou & Chen 2012, Wang et al. 2019, Gyanwali et al. 2020). The construction of a hydropower station changes the surface structure on a large scale and results in vegetation destruction and strong ecosystem disturbance (Sati 2015). Take Xiangjiaba hydropower station as an example, the disturbed area accounts for more than 50% of the total construction area (Zhou et al. 2016, Xue et al. 2016a). The excavation disturbance results in the original overburden stripping and backfilling disturbance of the slope to form a loose exposed slope body, and the degradation of the slope ecosystem is extremely prominent, which affects the ecological environment and landscape of hydropower development projects (Li et al. 2018a). Therefore, it has become a key topic to reconstruct the vegetation of the disturbed slope of hydropower projects on the premise of ensuring the safety of the project (Cao et al. 2010, Xu et

al. 2017). Though the instability of slope can be solved by traditional slope treatment methods, it is difficult to restore the natural vegetation and ecosystem functions. Vegetation eco-restoration technology can meet the demands of slope stability and vegetation reconstruction (Xu et al. 2006, Zhao et al. 2017). The vegetation restoration of disturbed slope should be carried out on the premise of fully considering the site conditions and restoration objectives. Healthy vegetation ecosystems are reconstructed by adopting artificial vegetation eco-restoration measures (Alday et al. 2010). A large number of scholars have studied the vegetation restoration of different engineering disturbed slopes from aspects of vegetation restoration technology selection, species allocation model, and vegetation succession law (Chiu 2004, Zhang et al. 2013, Xue et al. 2016b, Chen et al. 2018). The suitability of species for colonization should be taken into account when a plant is selected to use in vegetation restoration. Abiotic conditions, such as soil salinity, soil moisture, hydric stress, and limiting nutrients, could hinder plant establishment of the selected species (Tormo et al. 2006). Both vegetation type and its effect on controlling soil

erosion should be considered when implementing vegetation restoration (Duan et al. 2016). Matesanz & Valladares (2007) carried out a multispecies controlled experiment simulating eight different communities with species typically used in the revegetation of gypsum motorways slopes and found that the selection of the species to use in gypsum motorway slopes is crucial for the outcome of the vegetation restoration. Inadequate species selection can render poor results in the long term, and appropriate native species could allow more gradual and stable colonization of the slopes (Matesanz & Valladares 2007). Bochet & García-Fayos (2015) built a large database of 296 species 10 traits based on the leaf, seed, and root measurements for selecting suitable species based on morphological and functional plant traits. Vegetation growth can effectively reduce soil erodibility of steep gully slope lands in semi-arid regions, and grassland is more effective than shrub on vegetation-restored gully slope lands on the Loess Plateau (Zhang et al. 2019). Grasses should be prioritized for the improvement of soil conditions during the implementation of vegetation restoration projects in highly fissured areas (Peng et al. 2020). Herbaceous-only vegetation restoration is not suitable for long-term restoration on disturbed slopes, whereas the composition of herbs, shrubs, and trees is a better vegetation construction model for the ecological restoration of disturbed slopes (Li et al. 2018b). To study the vegetation community structure characteristics of the engineering disturbed slope, this study takes the vegetation communities under different vegetation eco-restoration modes in the Xiangjiaba engineering disturbed area as the research object. By analyzing the vegetation community classification, species composition, and species diversity under different vegetation restoration modes, we can understand the structural characteristics of vegetation communities under different vegetation eco-restoration models, reveal the adaptive mechanism of vegetation communities constructed by artificial vegetation eco-restoration techniques to the habitat conditions in the disturbed area of Xiangjiaba project. The research results can provide a theoretical basis for the ecological restoration of the disturbed slope.

MATERIALS AND METHODS

Description of Experimental Sites

The study was conducted at Xiangjiaba hydropower station, which is located at the convergence of Sichuan and Yunnan provinces, southeast of China. The experimental sites are in the upper Yangtze River's primary preventative region for soil and water conservation. The area is characterized by a subtropical monsoon climate with an annual average precipitation of 1078 mm, and approximately 90% of the total precipitation occurs between May and October. We considered typicality in vegetation eco-restoration technique and similarity in evolutionary time when selecting the sites. The selected experimental sites were vegetation concrete eco-restoration slope (VC), frame beam filling soil slope (FB), thick layer base material spraying slope (TB), external-soil spray seeding slope (SS), abandon slag slope (AS), and natural forest (NF). A brief description of the study sites is presented in Table 1. The unrestored disturbance site (AS) and the undisturbed site (NF) were served as control and used for comparison with those from the disturbed site to determine whether the vegetation eco-restoration technique had an effect on vegetation community characteristics.

Methods of Vegetation Investigation

The combination of field survey and quadrat sampling method was used to investigate vegetation community in all plots. 5 m × 5 m quadrats of tree and shrub layer or 1 m × 1 m quadrats of herb layer were set in every plot according to the types of vegetation, and quadrat was set 5 times repeatedly. The total coverage, name of each plant, fractional coverage, growth forms, average height, and plants numbers were recorded in every quadrat. The important values of different species are calculated according to the results of the quadrat investigation and the related data recorded in every quadrat (Xia 2010, Niu 2013, Liu et al. 2016).

$$IV = \frac{RH + RF + RC}{3} \quad \dots(1)$$

Table 1: A brief description of the study sites.

Site	Technique	Latitude	Longitude	Altitude (m)	Slope gradient (°)	Eco-restoration time
VC	Vegetation concrete eco-restoration technique	28°38'N	104°24'E	328.50	63	2004.12
FB	Frame beam filling soil technique	28°38'N	104°24'E	288.9	40	2004.11
TB	Thick layer base material spraying technique	28°38'N	104°26'E	388.9	51	2004.12
SS	External-soil spray seeding technique	28°39'N	104°23'E	473.9	30	2005.06
AS	Abandon slag slope	28°38'N	104°24'E	520.5	42	
NF	Natural forest	28°39'N	104°23'E	502.4		

Where IV is an important value, RH is the ratio of the height of a plant species to the height of all plant species in the quadrat, RF is the ratio of the frequency of a plant species to the frequency of all plant species in the quadrat, RC is the ratio of the coverage of a plant species to the fractional coverage of all plant species in the quadrat. The diversity of the vegetation community is calculated by the following equation in Table 2 (Xia 2010, Niu 2013, Liu et al. 2016).

RESULTS AND DISCUSSION

Coverage and Species Composition of Vegetation Community

Vegetation coverage is the most visual influence of engineering disturbance on the environment. As shown in Fig. 1, vegetation coverage on the disturbed slope of Xiangjiaba hydropower station changed from 45.0% to 97.0%. The veg-

Table 2: Formula used to calculate vegetation community diversity index.

Vegetation community diversity index		Formula
The species diversity index of vegetation community	<i>Shannon-Wiener</i> diversity index (SW)	$SW = -\sum_{i=1}^S P_i \ln P_i$
	<i>Simpson</i> diversity index (SP)	$SP = 1 - \sum_{i=1}^S (P_i)^2$
	<i>McIntosh</i> diversity index (MI)	$MI = \frac{N - \sqrt{\sum_{i=1}^S (N_i)^2}}{N - \sqrt{N}}$
The species richness index of vegetation community	<i>Margalef</i> richness index (MA)	$MA = (S - 1) / \ln N$
	<i>Menhinick</i> richness index (ME)	$ME = S / \sqrt{N}$
	<i>Monk</i> richness index (MO)	$MO = S / N$
The species evenness index of vegetation community	<i>Pielou</i> evenness index (J_{SW})	$J_{SW} = SW / \ln S$
	<i>Alatato</i> evenness index (J_A)	$J_A = \frac{\left(\sum_{i=1}^S (P_i)^2\right)^{-1} - 1}{\exp(SW) - 1}$
	<i>Simpson</i> evenness index (J_S)	$J_S = \frac{SP}{1 - 1/S}$
The similarity diversity index of vegetation community	<i>Jaccard</i> similarity diversity (JC)	$JC = \frac{a}{(b+c) - a}$
	<i>Sorensen</i> similarity diversity (SR)	$SR = \frac{2a}{b+c}$
	<i>Mountford</i> similarity diversity (MT)	$MT = \frac{2a}{2bc - ab - ac}$

Note: S is the numbers of plant species in the quadrat, $P_i = N_i/N$ is the ratio of the individual numbers of species i to the individual numbers of all species, N_i is the individual numbers of species i , N is the individual numbers of all species in the quadrat, a is the numbers of the same plant species in two quadrants, and b and c is the numbers of all plant species in two quadrants.

etation coverage of FB was 96.1%, which is slightly higher than the vegetation coverage of other artificial sample sites. Based on the statistical analysis of families, genera, and species, the vegetation community in different vegetation

eco-restoration modes has been preliminarily analyzed (Table 2). The vegetation community of NF was belonging to 18 families, 22 genera, and 23 species. The vegetation community of AS was a total of 8 families, 14 genera, and

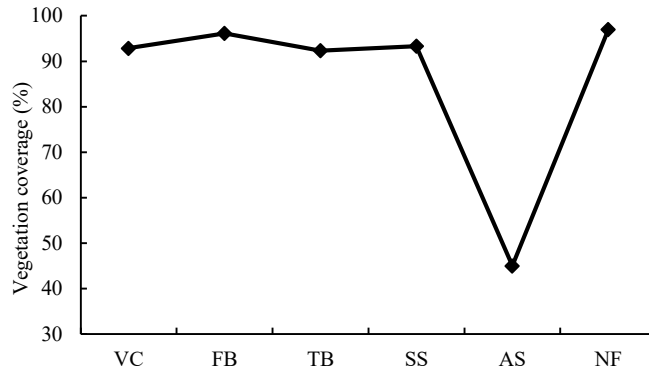


Fig.1: Vegetation coverage in different vegetation eco-restoration modes.

Table 3: Family, genus, and species in different vegetation eco-restoration modes.

Number	Latin name	Site					
		VC	FB	TB	SS	AS	NF
1	<i>Liliaceae</i>						1/1
2	<i>Plantaginaceae</i>				1/1		
3	<i>Labiatae</i>	1/1			1/1		
4	<i>Euphorbiaceae</i>		2/2				
5	<i>Aquifoliaceae</i>						1/1
6	<i>Leguminosae</i>	4/4	4/4	3/3	2/2		2/2
7	<i>Pteridaceae</i>			1/1			
8	<i>Lygodium</i>		1/1	1/1	1/1		1/1
9	<i>Gramineae</i>	4/4	10/11	3/3	5/5	4/4	2/2
10	<i>Betulaceae</i>						1/1
11	<i>Malvaceae</i>		1/1				
12	<i>Compositae</i>	1/1	6/6		3/3	3/3	
13	<i>Fagaceae</i>						1/1
14	<i>Gesneriaceae</i>		1/1		1/1	1/1	
15	<i>Gleicheniaceae</i>				1/1		1/1
16	<i>Malvaceae</i>		1/1				
17	<i>Polygonaceae</i>				1/1		
18	<i>Lindsaeaceae</i>						1/1
19	<i>Asclepiadaceae</i>		1/1				
20	<i>Verbenaceae</i>	2/2	2/2				
21	<i>Loganiaceae</i>		1/1				
22	<i>Ranunculaceae</i>						1/1
23	<i>Equisetaceae</i>				1/1		

Table cont....

Number	Latin name	Site					
		VC	FB	TB	SS	AS	NF
24	<i>Lythraceae</i>				1/1		
25	<i>Rosaceae</i>		1/1		1/1		2/2
26	<i>Solanaceae</i>		1/1				
27	<i>Caprifoliaceae</i>						1/1
28	<i>Umbelliferae</i>		1/1		1/1		
29	<i>Moraceae</i>	1/1	3/3	1/1		1/1	
30	<i>Cyperaceae</i>						1/1
31	<i>Theaceae</i>						2/3
32	<i>Phytolaccaceae</i>	1/1					
33	<i>Pinaceae</i>						1/1
34	<i>Oleandraceae</i>		1/1	1/1	1/1	1/1	
35	<i>Amaranthaceae</i>	1/2	1/1			2/2	
36	<i>Scrophulariaceae</i>					1/1	1/1
37	<i>Urticaceae</i>		1/1				
38	<i>Commelinaceae</i>		1/1				
39	<i>Rutaceae</i>					1/1	1/1
40	<i>Lauraceae</i>						1/1
41	<i>Oxalidaceae</i>		1/1		1/1		
Total (family)		8	20	6	15	8	18
Total (genus)		15	41	10	22	14	22
Total (species)		16	42	10	22	14	23

15 species, and much simpler than NF. The FB had the most plant species in artificial vegetation eco-restoration sites and totaled 20 families, 41 genera, and 42 species, and 40% of the total number of species were *Gramineae* and *Compositae*. The TB had the simplest species, and belonging to 6 families, 10 genera, and 10 species. And the dominant species were *Gramineae* and *Leguminosae*, making up for 60% of the total species.

Growth Forms of Vegetation Community

The growth forms of vegetation community under different vegetation eco-restoration modes were shown in Fig. 2 and classified by trees, shrubs, lianas, perennial herbs, and annual herbs or biennial herbs. Growth forms of different vegetation eco-restoration modes were different significantly. Perennial herbs and shrubs accounted for 43.75% and 31.25% of the vegetation community in VC, respectively. Perennial herbs accounted for 42.86% of the vegetation community in FB. The growth forms of the vegetation community in VC and FB were diverse and included all five growth forms. There were only trees, perennial herbs, and annual herbs or biennial herbs, and herbs were dominant and accounted for 78.57%

of total species in AS. There were trees, shrubs, perennial herbs, and annual herbs or biennial herbs in TB, and the quantities of trees, shrubs, and annual herbs or biennial herbs were almost equal. There were only trees, shrubs, perennial herbs, and annual herbs or biennial herbs in SS. Perennial herbs were dominant and accounted for 59.09% of the total species, and trees and lianas only accounted for 9.09% in total. Trees and shrubs were dominant in NF, and shrubs, trees, and perennial herbs accounted for 34.78%, 30.43%, and 26.09%, respectively.

Important Value of Plant Species

As shown in Table 4, the species composition of vegetation communities in different vegetation eco-restoration modes was surveyed, and vegetation species of all plots were 87 in total. Plant species composition and dominant species were obviously different. Some initial herb species disappeared gradually in VC, FB, and SS, and the importance value of some alien invasive species was increasing, especially some trees, shrubs, and lianas, and the vegetation community began to change from herb layer to herbs-shrubs-lianas layer. The dominant species of TB was *Leucaena leucocephala* (Lam.)

de Wit with an importance value of 57.14%. Some initial species in TB disappeared gradually, such as *Festuca elata* Keng ex E. Alexeev, *Medicago sativa* L., and *Cynodondactylon* (Linn.) Pers. The importance values of invasive species *Broussonetia papyrifera* (L.) L'Hér. ex Vent. and *Sophora xanthantha* C. Y. Ma was 9.46% and 5.61%, respectively. The importance value of dominant species *Alnus cremastogyne* Burk. was 12.21% in NF.

The Diversity Indexes of Vegetation Community

As shown in Fig. 3, the species diversity index of vegetation communities in different vegetation eco-restoration modes was different, but the highest value of species diversity indexes appeared in NF. The lowest *Shannon-Wiener* diversity index appeared in VC. The changing trend of the *McIntosh* diversity index and *Simpson* diversity index were similar in all plots. The lowest species diversity index occurred in AS.

The change trends of species richness indexes of all plots were basically identical (Fig. 4). The highest value of the *Margalef* diversity index and *Menhinick* diversity index appeared in FB, and the lowest value of the *Margalef* diversity index and *Menhinick* diversity index appeared in TB. The *Monk* diversity index of NF (0.223) was the highest, and the *Monk* diversity index of TB (0.075) was the lowest. *Simpson* evenness index and *Alatato* evenness index in NF were both the highest, but *Simpson* evenness index and *Alatato* evenness index of the abandon slag slope (AS) were both the lowest (Fig. 5). The *Pielou* evenness index of NF was the highest (0.923), and the *Pielou* evenness index of VC was the lowest (0.498). As shown in Table 5, the range of *Jaccard* similarity index, *Sorensen* similarity index, and *Moutford* similarity index was 0.000~0.244, 0.000~0.393, and 0.000~0.043 respectively. The lowest size of the three similarity indexes all appeared between VC and NF.

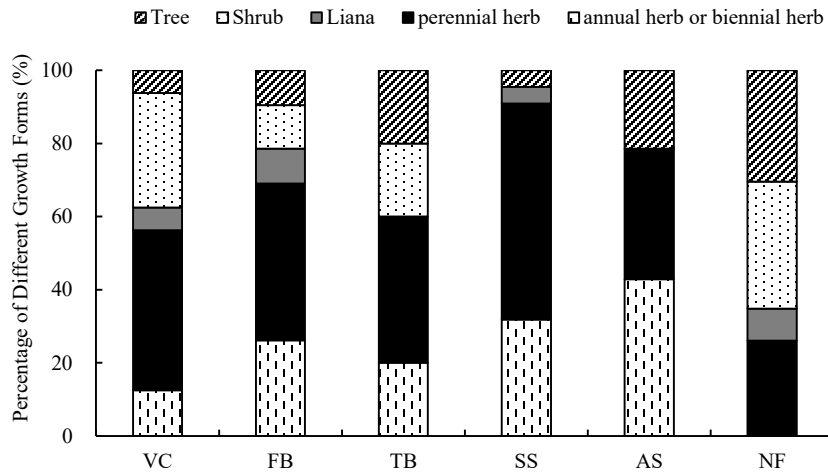


Fig. 2: Growth forms of vegetation community in different vegetation eco-restoration modes.

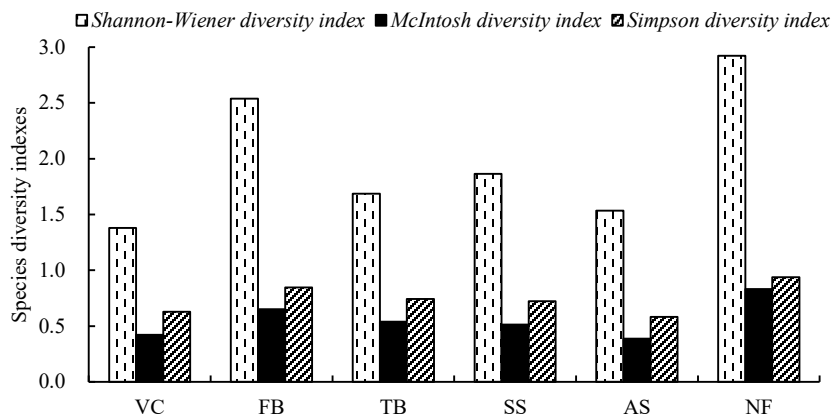


Fig. 3: Species diversity indexes of vegetation community in different vegetation eco-restoration modes.

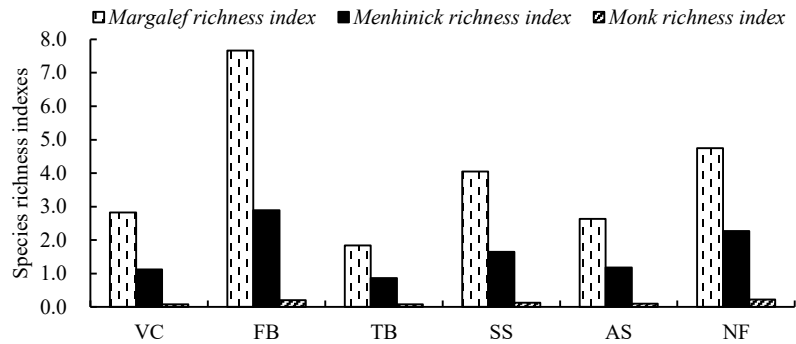


Fig. 4: Species richness indexes of vegetation community in different vegetation eco-restoration modes.

DISCUSSION

Vegetation community characteristics can be used as a measuring index to describe the process of vegetation restoration (Wang et al. 2012). And according to a large number of studies, vegetation community characteristics include vegetation coverage, species composition, dominant species, and species diversity (Ding & Zang 2005, Ruiz-Jaen & Aide 2010, Wortley et al. 2013). Vegetation coverage is an important index to evaluate the growth status of vegetation communities and the ability of conservation of soil and water, and low vegetation coverage is easier to lead to soil erosion than high vegetation coverage (Yuan et al. 2016, Chen et al. 2019). There was a litter difference between artificial vegetation eco-restoration plots in vegetation coverage, which basically reached the level of vegetation coverage of NF. However, there were differences in community species composition among various plots. Species composition is an important index to describe community characteristics (Ding & Zang 2005). The number of species in FB (20 families, 41 genera, and 42 species) increased greatly compared to AS, but the plants were primarily herb and accounted for 69.05% of the total species. The species composition among artificial

vegetation eco-restoration plots was different but was dominant by perennial plants all, and vegetation community structure began to change from herb layer to herbs-shrubs-lianas layer mixed. Perennial plants being dominant, especially the trees and shrubs showed that the vegetation community is stable (Fike & Niering 1999). The important value of the dominant species reflects the complexity of vegetation community structure, and dominant species influence both species and functional composition of the vegetation community (Kompala-Baba et al. 2020). The important value of a dominant species called *Leucaena leucocephala* (Lam.) de Wit was far higher than other accompanying species in TB, which showed that the complexity of vegetation community structure was low. The invasive plants can affect native plants by producing allelochemicals (Mignoni et al. 2017).

The α diversity is an important index to describe community characteristics, which include species diversity indexes, species richness index, and species evenness index (Zhang et al. 2005, Wang et al. 2006). The α diversity level of vegetation community was discussed from three aspects: the number of species, the individual difference of species, and the evenness of species distribution (Zhang et al. 2005,

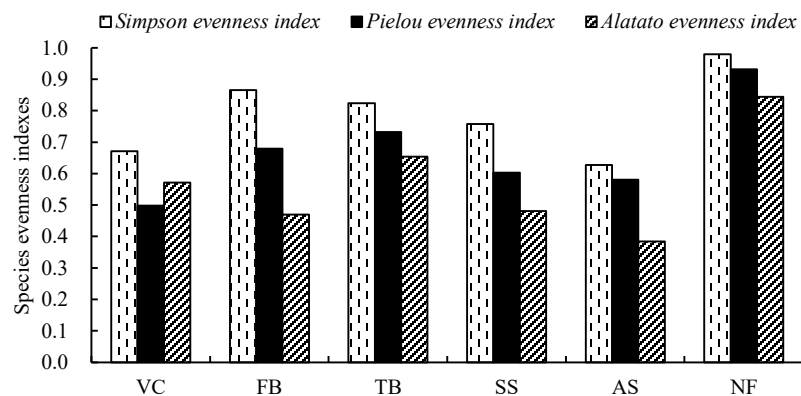


Fig. 5: Species evenness indexes of vegetation community in different vegetation eco-restoration modes.

Table 4: Species composition and important value of vegetation community in different vegetation eco-restoration modes.

Number	Latin name	IV (%)					
		VC	FB	TB	SS	AS	NF
1	<i>Artemisia argyi</i> Levl. et Van.		4.42			4.72	
2	<i>Smilax china</i>						1.33
3	<i>Imperata cylindrica</i> (L.) Beauv.		11.47		15.49	3.98	
4	<i>Saccharum arundinaceum</i> Retz.	4.30					
5	<i>Plantago depressa</i> Willd.				1.96		
6	<i>Clerodendrum bungei</i> Sterd.	2.88	1.23				
7	<i>Solanum torvum</i> Swartz		1.00				
8	<i>Euphorbia humifusa</i> Willd. ex Schlecht.		0.59				
9	<i>Ilex chinensis</i> Sims						4.25
10	<i>Indigofera amblyatha</i>	6.49					
11	<i>Commelina bengalensis</i>		0.93				
12	<i>Urena procumbens</i> Linn.		1.50				
13	<i>Pteris cretica</i> Linn. var. <i>nervosa</i> (Thunb.) Ching et S.H. Wu			5.57			
14	<i>Festuca elata</i> Keng ex E. Alexeev				6.89		
15	<i>Pueraria lobata</i> (Willdenow) Ohwi	8.74	3.26		5.23		
16	<i>Setaria viridis</i> (L.) Beauv.		1.11			15.66	
17	<i>Broussonetia papyrifera</i> (L.) L'Hér. ex Vent.	7.68	4.58	9.46		6.50	
18	<i>Lygodium japonicum</i> (Thunb.) Sw.		3.81	3.42	1.82		1.19
19	<i>Albizia julibrissin</i> Durazz.						6.55
20	<i>Polygonum orientale</i> L.				2.93		
21	<i>Lespedeza bicolor</i> Turcz.	2.94		4.73			
22	<i>Zanthoxylum bungeanum</i> Maxim.					10.75	
23	<i>Artemisia annua</i>				3.72		
24	<i>Sophora xanthantha</i> C. Y. Ma	2.46		5.61			
25	<i>Themeda villosa</i> (Poir.) A. Camus		1.13				
26	<i>Pogonatherum crinitum</i> (Thunb.) Kunth				2.28		
27	<i>Lonicera japonica</i> Thunb.						1.59
28	<i>Arthraxon hispidus</i> (Thunb.) Makio	11.81	7.83	4.95	3.39	3.86	
29	<i>Citrus reticulata</i>						1.87
30	<i>Alternanthera philoxeroides</i>	1.69					
31	<i>Conandron ramondioides</i> S. et Z.		0.86		2.90	2.49	
32	<i>Melia azedarach</i> Linn.		3.41				
33	<i>Pennisetum alopecuroides</i> (L.) Spreng.	25.61	1.42				
34	<i>Diplopterygium glaucum</i> (Thunb. ex Hoult.) Nakai				7.08		2.49
35	<i>Quercus mongolica</i> Fisch. ex Ledeb.						4.92
36	<i>Arundo donax</i>	4.19					
37	<i>Metaplexis japonica</i> (Thunb.) Makino		1.45				
38	<i>Humulus japonicus</i>		0.64				
39	<i>Digitaria sanguinalis</i> (L.) Scop.		1.68	4.31	1.91	2.74	
40	<i>Pinus massoniana</i> Lamb.						6.96
41	<i>Alternanthera sessilis</i> (L.) DC.	3.64	1.98			5.58	
42	<i>Miscanthus sinensis</i> Anderss.		1.52				1.59
43	<i>Paulownia tomentosa</i> (Thunb.) Steud.					7.55	7.09
44	<i>Vitex negundo</i> L.	9.39	0.91				
45	<i>Eleusine indica</i> (L.) Gaertn.		0.63				
46	<i>Rubus hirsutus</i> Thunb.						3.35

Table cont....

Number	Latin name	IV (%)					
		VC	FB	TB	SS	AS	NF
47	<i>Ficus tikoua</i> Bur.		0.93				
48	<i>Alnus cremastogyne</i> Burk.						12.21
49	<i>Leptochloa chinensis</i> (L.) Nees		1.17				
50	<i>Senecio scandens</i> Buch.-Ham. ex D. Don				2.65		
51	<i>Carex breviculmis</i> R. Br.						2.52
52	<i>Celosia argentea</i> L.					3.57	
53	<i>Oplismenus undulatifolius</i> (Arduino) Beauv.			9.54			
54	<i>Bidens pilosa</i> Linn.		2.89			5.28	
55	<i>Camellia japonica</i> L.						5.18
56	<i>Lindera glauca</i> (Sieb. et Zucc.) Bl						5.76
57	<i>Phytolacca acinosa</i> Roxb.	2.76					
58	<i>Cnidium monnieri</i> (L.) Cuss.		0.90				
59	<i>Nephrolepis cordifolia</i> (L.) Presl		2.03	3.84	1.91	3.54	
60	<i>Mosla scabra</i> (Thunb.) C. Y. Wu et H. W. Li	2.32					
61	<i>Hydrocotyle sibthorpioides</i> Lam.				2.31		
62	<i>Sesbania cannabina</i> (Retz.) Poir.		1.53		2.37		
63	<i>Potentilla chinensis</i> Ser.				2.00		
64	<i>Equisetum arvense</i> L.				2.23		
65	<i>Sapium sebiferum</i> (L.) Roxb.		2.71				
66	<i>Sphenomeris chinensis</i> (L.) Maxon						2.72
67	<i>Miscanthus floridulus</i> (Lab.) Warb. ex Schum. et Laut.		1.80				
68	<i>Capillipedium parviflorum</i> (R. Br.) Stapf.		9.73				
69	<i>Eurya nitida</i> Korthals						2.65
70	<i>Prunella vulgaris</i> L.				1.82		
71	<i>Conyza canadensis</i> (L.) Cronq.		4.01		2.77	5.45	
72	<i>Boehmeria spicata</i> (Thunb.) Thunb.		2.55				
73	<i>Cirsium setosum</i> (Willd.) MB.		1.21				
74	<i>Leucaena leucocephala</i> (Lam.) de Wit			57.14			
75	<i>Rosa rubus</i> Lévl. et Vant.		2.16				
76	<i>Paeonia delavayi</i> Franch.						3.65
77	<i>Rosa multiflora</i> Thunb.						2.76
78	<i>Erigeron annuus</i> (L.) Pers.		0.69				
79	<i>Camellia oleifera</i> Abel.						3.73
80	<i>Caesalpinia decapetala</i> (Roth) Alston		1.30				
81	<i>Crotalaria pallida</i> Ait.		0.77				
82	<i>Oplismenus compositus</i> (L.) Beauv.						2.83
83	<i>Eupatorium coelestinum</i> L.	3.09	1.30				
84	<i>Wisteria sinensis</i>						4.46
85	<i>Lagerstroemia indica</i> L.				22.90		
86	<i>Buddleja lindleyana</i>		3.15				
87	<i>Oxalis corniculata</i> Linn.		0.78		1.21		

Liu 2015). As a result of the positive succession of the vegetation community, the α diversity increased. (Wang et al. 2006). The results of the α diversity indexes embody the structure and complex degree of vegetation community, and artificial vegetation eco-restoration patterns can promote the recovery of vegetation community effectively (Pueyo et al.

2006). The β diversity indexes of vegetation communities focus on reflecting the different degrees of species structure and composition among different vegetation communities and expressing heterogeneity among communities (Han et al. 2009). Results of this study showed that species composition among all plots was different, especially between

Table 5: Species similarity indexes among vegetation communities in different vegetation eco-restoration modes.

Site	Species similarity indexes		
	Jaccard similarity index	Sorensen similarity index	Mountford similarity index
VC-FB	0.160	0.276	0.018
VC-TB	0.182	0.308	0.037
VC-SS	0.056	0.105	0.006
VC-AS	0.111	0.200	0.017
VC-NF	0.000	0.000	0.000
FB-TB	0.106	0.192	0.017
FB-SS	0.185	0.313	0.017
FB-AS	0.244	0.393	0.039
FB-NF	0.032	0.062	0.002
TB-SS	0.143	0.250	0.026
TB-AS	0.200	0.333	0.043
TB-NF	0.031	0.061	0.005
SS-AS	0.200	0.333	0.030
SS-NF	0.047	0.089	0.004
AS-NF	0.028	0.054	0.003

NF and artificial vegetation eco-restoration plots, and the disturbed vegetation community needs a long time to return to the natural level.

Decrease or even loss of soil and water conservation function is a prominent problem of engineering disturbed slope while increasing the surface vegetation coverage is the most direct and effective method to control soil erosion (El Kateb et al. 2013, Wang et al. 2016). Numerous studies have shown that community structure with primary near-surface herbs can effectively intercept rainfall and weaken the role of rainwater erosion through the interception precipitation and extend infiltration time to reduce slope runoff (Zhou & Shangguan 2008, Du et al. 2017, Zhang et al. 2017, Gao et al. 2020). Vegetation coverage of the four artificial vegetation eco-restoration sample sites increased obviously than AS, especially in VC and FB which herbaceous were main dominant species. Therefore, it can be considered that the vegetation concrete eco-restoration technology, the frame beam filling soil technology, and the external-soil spray seeding technology can improve soil and water conservation function of engineering disturbed slope effectively. In TB, *Leucaena leucocephala* (Lam.) de Wit resulted in the species and quantity of vegetation community is low, and fail to form the healthy multilayer community structure. Therefore, the surface vegetation coverage of TB was much lower than the other three artificial vegetation eco-restoration sample sites. Studying the allelopathy of *Leucaena leucocephala* (Lam.) de Wit and seeking the best species composition that can coexist with it is significant to

promote the positive succession of the vegetation community in TB. It is also of great significance to improve the soil and water conservation function of the disturbed slope.

CONCLUSIONS

The results of field investigation and analysis undertaken in disturbed slopes at Xiangjiaba hydropower station have revealed that there was a big difference in vegetation community characteristics between different vegetation eco-restoration modes. The vegetation coverage, species numbers, growth type composition, and family, genus, and species of vegetation community of AS were significantly lower than that of artificial vegetation eco-restoration slopes and NF. The simple vegetation community structure indicates that the vegetation community of AS was unstable. The absolute advantage of the two perennial plants indicates that the vegetation community of VC is in a stable state. The species and number of TB were low and fail to form a healthy multilayer community structure due to the invasion of *Leucaena leucocephala* (Lam.) de Wit. It is significant to study the allelopathy of *Leucaena leucocephala* (Lam.) de Wit and seek the best species composition that can coexist with it. The frame beam filling soil technique, external-soil spray seeding technique, and vegetation concrete eco-restoration technique can effectively promote the succession process of the vegetation community. And the absolute advantage of herbs in FB, SS, and VC can also prove that these three techniques have good water and soil conservation capacity.

ACKNOWLEDGMENTS

This research was supported by the CRSRI Open Research Program (CKWV2019763/KY), the National Focal Research Program of China (2017YFC0504902), and the National Natural Science Foundation of China (51979147).

REFERENCES

- Alday, J.G., Marrs, R.H. and Martínez-Ruiz, C. 2010. The importance of topography and climate on short-term revegetation of coal wastes in Spain. *Ecol. Eng.*, 36(4): 579-585.
- Bochet, E. and García-Fayos, P. 2015. Identifying plant traits: A key aspect for species selection in the restoration of eroded roadsides in semiarid environments. *Ecol. Eng.*, 83: 444-451.
- Cao, S.X., Xu, C.L., Ye, H.H., Zhan, Y. and Gong, C. 2010. The use of air bricks for planting roadside vegetation: A new technique to improve the landscaping of steep roadsides in China's Hubei Province. *Ecol. Eng.*, 36(5): 697-702.
- Cao, W., Omran, B.A., Lei, Y.K., Zhao, X., Yang, X.M., Chen, Q. and Tian, G.H. 2018. Studying early-stage slope protection effects of vegetation communities for Xinnan Highway in China. *Ecol. Eng.*, 110: 87-98.
- Chen, J., Xiao, H.B., Li, Z.W., Liu, C., Wang, D.Y., Wang, L.X. and Tang, C.J. 2019. Threshold effects of vegetation coverage on soil erosion control in small watersheds of the red soil hilly region in China. *Ecol. Eng.*, 132: 109-114.
- Chen, W., Chen, Y. and Yang, S. 2018. Optimization of Slope Vegetation System Based on Entropy Method and Relative Entropy Evaluation Method. *Bull. Soil Water Conser.*, 38(2): 313-317 (In Chinese).
- Chiu, P.K.B. 2004. Slope bioengineering in Hong Kong: A study of substrate properties and vegetation development. The Chinese University of Hong Kong (In Chinese).
- Ding, Y. and Zang, R.G. 2005. Community characteristics of early recovery vegetation on abandoned lands of shifting cultivation in Bawangling of Hainan Island, South China. *Journal of Integrative Plant Biology*, 47(5): 530-538.
- Du, X.Y., Liang, Y.Z., Xia, Z.Y., Xia, D., X, W.N. and Wang, Y.K. 2017. Soil nutrient loss characteristic of gravel soil slope on different vegetation patterns. *J. Soil Water Cons.*, 31(1): 61-67 (In Chinese).
- Duan, L.X., Huang, M.B. and Zhang, L.D. 2016. Differences in hydrological responses for different vegetation types on a steep slope on the Loess Plateau, China. *J. Hydrol.*, 537: 356-366.
- El Kateb, H., Zhang, H.F., Zhang, P.C. and Mosandl, R. 2013. Soil erosion and surface runoff on different vegetation covers and slope gradients: A field experiment in Southern Shaanxi Province, China. *Catena*, 105: 1-10.
- Fike, J. and Niering, W. A. 1999. Four decades of old-field vegetation development and the role of *Celastrus orbiculatus* in the northeastern United States. *J. Veg. Sci.*, 10(4): 483-492.
- Gao, J.B., Jiang, Y., Wang, H. and Zuo, L.Y. 2020. Identification of dominant factors affecting soil erosion and water yield within ecological red line areas. *Rem. Sens.*, 12(3): 399.
- Ghanbarpour, M.R. and Hipel, K.W. 2009. Sustainable development conflict over freeway construction. *Environ. Dev. Sustain.*, 11(2): 241-253.
- Gyanwali, K., Komiyama, R. and Fujii, Y. 2020. Representing hydropower in the dynamic power sector model and assessing clean energy deployment in the power generation mix of Nepal. *Energy*, 11: 77-95.
- Han, D.Y., Li, H.Y. and Yang, Y.F. 2009. -diversity patterns of plant community in fragmented habitat in a degenerated meadow in Songnen Plain, China. *Chinese Geographical Science*, 19(4): 375-381.
- Kompala-Baba, A., Sierka, E., Dyderski, M.K., Bierza, W. and Woniak, G. 2020. Do the dominant plant species impact the substrate and vegetation composition of post-coal mining spoil heaps? *Ecol. Eng.*, 143, 105685.
- Li, B., Li, T., Xu, N.W., Dai, F., Chen, W.F. and Tan, Y.S. 2018a. Stability assessment of the left bank slope of the Baihetan Hydropower Station, Southwest China. *Int. J. Rock Mech. Min. Sci.*, 104: 34-44.
- Li, R.R., Kan, S.S., Zhu, M.K., Chen, J., Ai, X.Y., Chen, Z.Q., Z, J.J. and Ai, Y.W. 2018b. Effect of different vegetation restoration types on fundamental parameters, structural characteristics, and the soil quality index of artificial soil. *Soil Till. Res.*, 184: 11-23.
- Liu, X.Q., Zhang, X., Zhang, L.F., Li, Y.N., Zhao, L., Xu, S.X., Li, H.Q., Ma, R.R., Niu, B., Gao, Y.B. and Gu, S. 2016. Effects of enclosure duration on the community structure and species diversity of an alpine meadow in the Qinghai-Tibet Plateau. *Acta Ecologica Sinica*, 36(16): 5150-5162 (In Chinese).
- Liu, Y. 2015. Plant Diversity and Ecosystem Multifunctionality in Constructed Wetlands. Zhejiang University (In Chinese).
- Matesanz, S. and Valladares, F. 2007. Improving revegetation of gypsum slopes is not a simple matter of adding native species: Insights from a multispecies experiment. *Ecol. Eng.*, 30(1): 67-77.
- Mignoni, D.S.B., Simões, K. and Braga, M.R. 2017. Potential allelopathic effects of the tropical legume *Sesbania virgata* on the alien *Leucaena leucocephala* related to seed carbohydrate metabolism. *Biol. Invas.*, 20(1): 165-180.
- Niu, X. 2013. Studies on Revegetation and Restoration Effects of Yimin Opencast Mining Wasteland. Inner Mongolia Agricultural University (In Chinese).
- Peng, X.D., Dai, Q.H., Ding, G.J., Shi, D.M. and Li, C.L. 2020. Impact of vegetation restoration on soil properties in near-surface fissures located in karst rocky desertification regions. *Soil and Till. Res.*, 200: 104620.
- Pueyo, Y., Alados, C.L. and Ferrer-Benimeli, C. 2006. Is the analysis of plant community structure better than common species-diversity indices for assessing the effects of livestock grazing on a Mediterranean arid ecosystem? *J. Arid Environ.*, 64(4): 698-712.
- Ruiz-Jaen, M.C. and Aide, T.M. 2010. Restoration success: How is it being measured? *Restor. Ecol.*, 13(3): 569-577.
- Sati, V.P. 2015. Landscape vulnerability and rehabilitation issues: a study of hydropower projects in Garhwal region, Himalaya. *Nat. Hazards*, 75(3): 2265-2278.
- Tormo, J., Bochet, E. and García-Fayos, P. 2006. Is seed availability enough to ensure colonization success? An experimental study in road embankments. *Ecol. Eng.*, 26(3): 224-230.
- Wang, L., Wang, Y., Du, H.B., Zuo, J., Li, R.Y.M., Zhou, Z.H., Bi, H.H. and Garvlehn, M.P. 2019. A comparative life-cycle assessment of hydro-, nuclear and wind power: A China study. *Appl. Energy*, 249: 37-45.
- Wang, W.Y., Wang, Q.J. and Wang, H.C. 2006. The effect of land management on plant community composition, species diversity, and productivity of alpine Kobersia steppe meadow. *Ecol. Res.*, 21(2): 181-187.
- Wang, X.D., Yu, J.B., Zhou, D., Dong, H.F., Li, Y.Z., Lin, Q.X., Guan, B. and Wang, Y.L. 2012. Vegetative ecological characteristics of restored reed (*Phragmites australis*) wetlands in the Yellow River Delta, China. *Environ. Manag.*, 49(2): 325-333.
- Wang, Z.J., Jiao, J.Y., Rayburg, S., Wang, Q.L. and Su, Y. 2016. Soil erosion resistance of "Grain for Green" vegetation types under extreme rainfall conditions on the Loess Plateau, China. *Catena*, 141: 109-116.
- Wortley, L., Hero, J.M. and Howes, M. 2013. Evaluating ecological restoration success: A review of the literature. *Restor. Ecol.*, 21(5): 537-543.
- Xia, Z.Y. 2010. Earlier Succession and Stability of Artificial Vegetation Community on Disturbed Slope in Xiangjiaba Hydropower Station. Wuhan University (In Chinese).
- Xu, W.N., Xia, D., Zhao, B.Q., Xia, Z.Y., Liu, D.X. and Zhou, M. T. 2017. Research on Slope Eco-Restoration Technique for Hydroelectric Projects Disturbed Area. Science Press, Beijing (In Chinese).
- Xu, X.L., Zhang, K.L., Kong, Y.P., Chen, J.D. and Yu, B.F. 2006. Effectiveness of erosion control measures along the Qinghai-Tibet highway, Tibetan plateau, China. *Transp. Res. D Trans. Environ.*, 11(4): 302-309.
- Xue, H.L., Xu, W.N. and Liu, D.X. 2016a. Changes of soil fertility and

- enzyme activity on different standing conditions under two slope ecological restoration patterns. *Bull. Soil Water Conserv.*, 36(4): 182-187 (In Chinese).
- Xue, O., Wei, T.X., Liu, F. and Li, Y.Y. 2016b. Modeling the degree of coupling and interaction between plant community diversity and soil properties on highway slopes. *J. Beijing Forestry Univ.*, 38(1): 91-100 (In Chinese).
- Yuan, Z.Q., Yu, K.L., Epstein, H., Fang, C., Li, J.T., Liu, Q.Q., Liu, X.W., Gao, W.J. and Li, F.M. 2016. Effects of legume species introduction on vegetation and soil nutrient development on abandoned croplands in a semi-arid environment on the Loess Plateau, China. *Sci. Total Environ.*, 541: 692-700
- Zhang, B.J., Zhang, G.H., Yang, H.Y. and Wang, H.Y. 2019. Soil resistance to flowing water erosion of seven typical plant communities on steep gully slopes on the Loess Plateau of China. *Catena*, 173: 375-383.
- Zhang, J., Zhao, H., Zhang, T., Zhao, X. and Drake, S. 2005. Community succession along a chronosequence of vegetation restoration on sand dunes in Horqin Sandy Land. *J. Arid Environ.*, 62(4): 555-566.
- Zhang, Q.L., Wang, Z.L., Wang, D.D. and Liu, J.E. 2017. Advances in researches on the effects of grassland vegetation on soil erosion in Loess Plateau. *Adv. Earth Sci.*, 32(10): 1093-1101 (In Chinese).
- Zhang, Y., Zhao, T.N., Shi, C.Q., Wu, H.L., Li, D.X. and Sun, Y.K. 2013. Evaluation of vegetation and soil characteristics during slope vegetation recovery procedure. *Trans. Chinese Soc. Agri. Eng.*, 29(3): 124-131 (In Chinese).
- Zhao, B.Q., Xia, Z.Y., Xun, W.N., Yang, S., Xia, D. and Wang, Z.G. 2017. Review on the research of slope eco-restoration technique for engineering disturbed area. *Water Resources and Hydropower Engineering*, 48(2): 130-137 (In Chinese).
- Zhou, J. and Chen, G. 2012. Effect analysis of load characteristics on operation stability of hydropower stations. *Energy Procedia*, 17: 946-953.
- Zhou, M.T., Hu, X.D. and Xu, W.N. 2016. Trend prediction of soil fertility of various substrate slopes. *Bull. Soil Water Conserv.*, 36(4): 107-111 (In Chinese).
- Zhou, Z.C. and Shangguan, Z.P. 2008. Effect of ryegrasses on soil runoff and sediment control. *Pedosphere*, 18(1): 131-136.



Impact of Wetting and Drying Cycles on the Mechanical Properties and Microstructure of Vegetation-growing Concrete

Xiaole Huang*, Wennian Xu*†, Yu Ding*, Dong Xia**, Shiyuan Xiong*, Daxiang Liu* and Bo Pan*

*College of Civil Engineering and Architecture, China Three Gorges University, Yichang Hubei Province, 443002, China

**College of Hydraulic & Environmental Engineering, China Three Gorges University, Yichang Hubei Province, 443002, China

†Corresponding author: Wennian Xu; xwn@ctgu.edu.cn

Nat. Env. & Poll. Tech.
Website: www.neptjournal.com

Received: 22-10-2020

Revised: 17-12-2020

Accepted: 22-01-2021

Key Words:

Vegetation-growing concrete
Wetting and drying cycles
Structural damage

ABSTRACT

Vegetation-growing Concrete (VC), as a new type of cemented soil, is usually used for plants growing on the surface of high and steep rocky slopes. With the widespread application of VC substrate, a pressing problem arises to ensure its durability under wetting and drying conditions. To explore the greatest possible impact on the mechanical properties and microstructure features of VC substrate, an experimental program including triaxial test, SEM analysis, and ultrasonic testing was implemented. The results showed that wetting and drying cycles can significantly decrease more than 40-percent of peak strength, 60-percent of residual strength, and 50-percent of cohesion for VC substrate under ultimate conditions. The fundamental cause of reduction in mechanical performance was found to be the weakening of the bond between soil particles. And it was discovered that structural damage increased as the number of wetting and drying cycles increased but at a slower rate. Based on the tested results, linear functions between the loss extent parameters of mechanical performance and the structural damage variable were established for the VC substrate. Finally, the action mechanisms of wetting and drying cycles for VC substrate were discussed, and the main influential factors were proposed.

INTRODUCTION

Traditional cemented soils are artificially improved soil made by natural soils and cement. The cement added can improve the mechanical properties of natural soils and make the newly cemented soil meet higher load requirements (Hayano et al. 2013). VC substrate, developed by China Three Gorges University (Xu & Wang 2001), is made of natural soil, cement, organic materials, and Amendment of Habitat Material (AHM), and can be regarded as an ecological cemented soil. This ecological cemented soil provides a number of advantages, including good caking properties for maintaining the integrity of the VC substrate and rock mass, as well as optimal conditions for plant growth. In recent years, VC substrate has been widely used for ecological restoration of high steep rock slopes in China and has achieved satisfying ecological and social benefits (Liu et al. 2018).

The essential criterion for VC substrate to attach to a sloped surface and be used as a plant growth substrate is durability. As a new material in environmental engineering, VC substrate is constantly exposed on the ground, and its endurance is affected by climate conditions. Among them, the wetting and drying cycle is one of the most common

climate actions during periods of frequent rainfall and high temperatures. Numerous studies have investigated the influences of wetting and drying cycles on the mechanical properties of various types of soils. In general, natural soil is not durable under wetting and drying cycles. The strength can be reduced gradually with the increasing times of the cycles and reach the lowest level within 3~5 cycles (Pineda et al. 2014, Sayem et al. 2016).

Engineers and researchers are devoted to the development of all types of soil improvement technology to improve the engineering properties of natural soil. Among them, cement stabilization technology is one of the alternative solutions and has been extensively used in traditional engineering, for instance, subgrade engineering. The cement content is crucial in determining the improvement of mechanical properties under wetting and drying cycles. Zhang (2018) and Wang et al. (2018) showed that the strength of cemented soil with less than 10% cement decreased with wetting and drying cycles, while for cemented soils with more than 10% cement, it was found that the strength increased first and then decreased. However, no matter whatever the amount of cement is, the strength of cemented soils will eventually be

reduced, reaching a minimum value, as long as the times of wetting and drying cycles are large enough. In other words, there is a minimum value for wetting and drying cycle times, wherein the mechanical properties of soil are most affected by wetting and drying cycles (Zhang et al. 2014). The number of the minimum cycles was found to be about 5 times for cemented fine-grained soil (Yu 2012, Tan & Chen 2014), and the number for cemented sand seems much bigger, for instance, 12 times, as reported by Wang et al. (2017).

From the above studies, the reduction in mechanical properties of cemented soil during wetting and drying cycles is found to be highly dependent on the quantity of cement used and the type of soil. VC substrate is a new type of ecological cemented soil with specific components, but there is limited information available about the influences of wetting and drying cycles. The objective of this research is to evaluate the mechanical properties under the most serious situations of wetting and drying cycles, meanwhile, analyzing the change features of their microstructures, and pointing out the inner relationship between macro-mechanical performance and the microstructure.

MATERIALS AND METHODS

Materials: Planting soil, cement, organic materials (air-dried sawdust in this study) and the AHM are four basic materials of VC substrate in the tests. The planting soil used

was yellow-brown soil collected from the shallow surface of the earth in Yichang of Hubei, China. The soil was then air-dried and broken into pieces to pass through 2.0 mm. The air-dried moisture content of the soil was 1.93% and the specific gravity was 2.65. The cement used was composite Portland cement (P.C. 32.5) with a specific gravity of 3.1. The air-dried sawdust used had a moisture content of 5.80%, and the density of its solid particles was $0.54 \text{ g}\cdot\text{cm}^{-3}$, which was equal to the average density of commonly used woods in China. The AHM is made of mineral powders containing iron, phosphorus, calcium, and silicon as main materials, and water-retaining agents, and compound fertilizer as auxiliary materials.

By weight of air-dried planting soil, the amount of cement, sawdust, and AHM in VC substrate were 8%, 6%, and 4%, respectively; their volumetric ratios were 6.97%, 28.35%, and 3.74 percent, respectively. From the mixture proportion, we know that planting soil and sawdust are the two main compositions of VC substrate. Based on the data of particle size distributions of planting soil and sawdust, the exact particle size distribution of VC substrate was calculated, as shown in Table 1 and Fig. 1. It is necessary to explain that during the calculation, cement and AHM particles were included in the “0.074” particles category. According to the China Standard for Engineering Classification of Soil, GB/T 50145-2007, the VC substrate was classified as cemented sand with a low proportion of fine-grained soil.

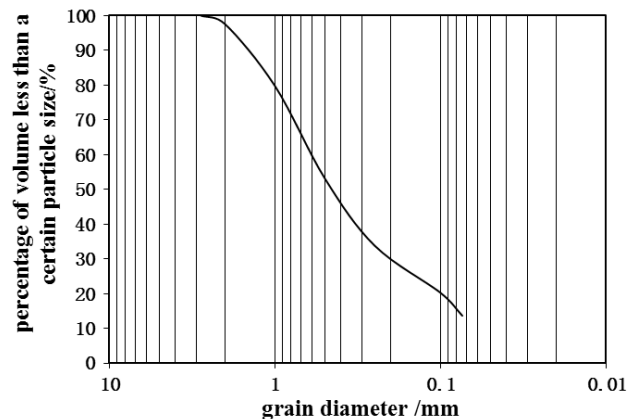


Fig. 1: Grain distribution curve of VC substrate.

Table 1: Particle size distributions.

Particle size(mm)	2.8-2	2-1	1-0.5	0.5-0.25	0.25-0.1	0.1-0.074	<0.074
Planting soil	-	21.34	25.46	19.88	16.88	8.17	8.27
Sawdust	12.08	12.03	40.74	24.76	7.04	3.34	-
VC	2.46	17.80	26.61	19.34	13.57	6.56	13.64

The XRD spectrum of VC substrate was studied by using DY2198 XDR equipment. The tested XRD spectrum and the mineral compositions are shown in Fig. 2 and Table 2, respectively.

Preparation of Samples: Batches of VC samples were prepared with an initial water content of 20% and a dry density of 1.35 g.cm⁻³. First, the four basic materials of one single sample were mixed in a container for more than 3 min. Water was then added into it, after standing for another 3 min, this mixture was stirred again to obtain a uniform distribution of moisture. The final mixture was then compacted into standard samples which were 80 mm in height and 39.1 mm in diameter according to the China Standard for Geotechnical Testing Method, GB/T 50123-2019. Finally, the standard samples were kept in an air-conditioned room at 25±2°C and relative humidity of >90% for 7 days.

Wetting and Drying Cycles: The vacuum saturation method and drying method were applied for wetting and drying, respectively. The samples were first flooded with water for 48 hours and then were placed into a drier for drying for 12 hours. The temperature for drying was set at 45-55 °C to simulate ambient temperature that VC substrate may encounter under strong sun in summer. The combination of one wetting

and the subsequent drying process was referred to as one wetting and drying cycle. At the end of one cycle, samples were allowed to cool slowly at laboratory temperature and then flooded with water for the next cycle.

Samples were divided into four groups and marked as WDC0, WDC5, WDC10, and WDC0-10. Among them, WDC0 corresponded to the control substrate without wetting and drying cycles; From the viewpoint of practice, VC substrate would turn into a root-soil composite gradually with plants growing after the project finished. To evaluate the worst effects on VC substrate by wetting and drying cycles, the root effect in the early growth stage was ignored. And the WDC10 substrate, which was considered as the most serious state by wetting and drying cycles was treated by 10 times of the cycle. WDC5, with 5 times wetting and drying cycles, could be considered as an intermediate sample between WDC0 and WDC10. WDC0-10 was prepared to measure the acoustic velocity of VC substrate with 0~10 times treatment of wetting and drying cycles.

Testing Program: Three kinds of testing methods were used: triaxial test, SEM test, and ultrasound velocity test.

The instrument used for the triaxial test was a TSZ30-2.0 automatic strain-controlled tri-axial shear apparatus

Table 2: Mineral composition.

Composition	Quartz	Albite	Illite	Calcite	Montmorillonite	Dolomite
Mass fraction (%)	56	14	10	9	8	3

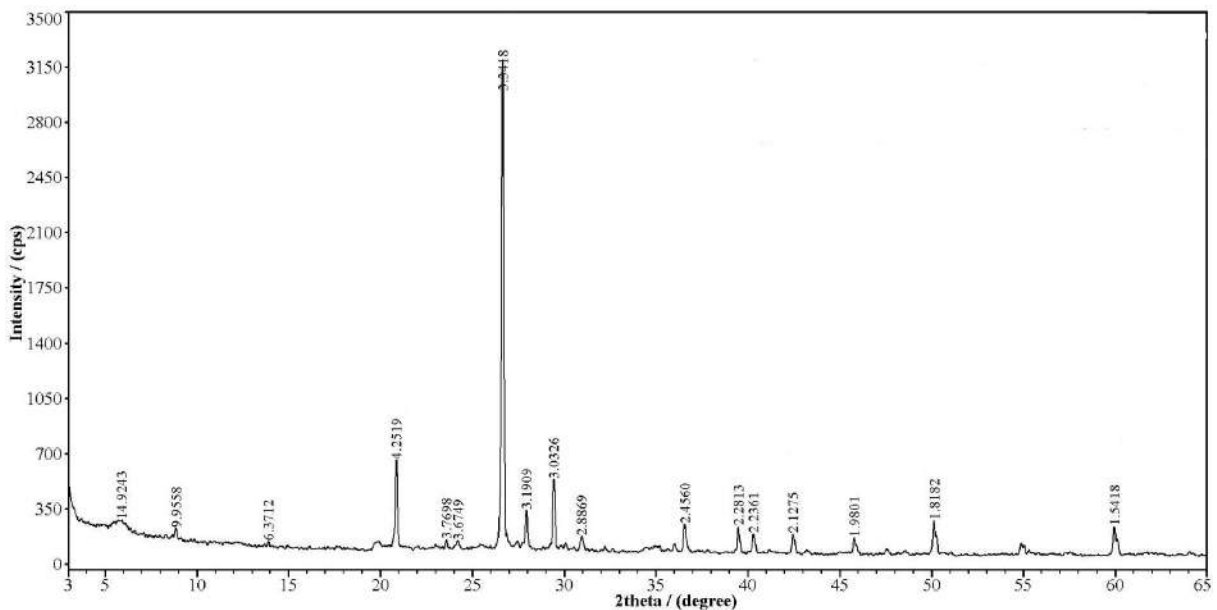


Fig. 2: X-ray powder diffraction spectrum of VC substrate.

developed by Nanjing Soil Instrument Co., Ltd. (China). An unconsolidated, undrained triaxial method was taken and the confining pressures were 10, 30, and 50 KPa. During the test, the strain rate was fixed at a big rate of $4.5 \text{ mm}\cdot\text{min}^{-1}$ as some researchers have reported that shear rates influence on soil structure can be neglected when normal stress in the test is low (Yang et al. 2014). The maximum deviator stress corresponding to the stress-strain curve was taken for the peak strength and deviator stress at the axial strain of 15% was taken for the residual strength. A JSM-7500F Cold Field Emission Scanning Electron Microscope (produced by JEOL) was used for the SEM test to analyze the micro-structure of the substrate. The soil specimen, with dimensions of $5 \text{ mm} \times 5 \text{ mm} \times 2 \text{ mm}$, was cut off in the middle section of the standard cylinder sample and was scanned under the amplification of 500 times and 1000 times. The instrument used for the acoustic velocity test was Nonmetal Ultrasonic Detector, model ZBL-U510. The test voltage was set at 500V; the sampling time interval was $0.4 \mu\text{s}$. To improve

the sample-transducer contact and enhance the measurement accuracy or stability, the transducer surface of the detectors was evenly coated with Vaseline before testing.

RESULTS AND DISCUSSION

Characteristics of Strain-Stress Curves: The stress-strain curve of the WDC0, WDC5, and WDC10 substrate under confining pressures of 10, 30, and 50 KPa are shown in Fig. 3.

These curves have a similar variation trend which could be divided into four stages: compaction stage, elasticity stage, yielding stage, and softening stage. Taking curves at 10 KPa for example, it can be seen that there are some differences in the curves of the substrate with different wetting and drying cycles. For the substrate WDC10, which had experienced 10 wetting and drying cycles, the axial strain in the compaction stage was higher than that of the control substrate WDC0 at the same deviator stress; the axial strain of the intermediary substrate WDC5 was between the substrate WDC0 and

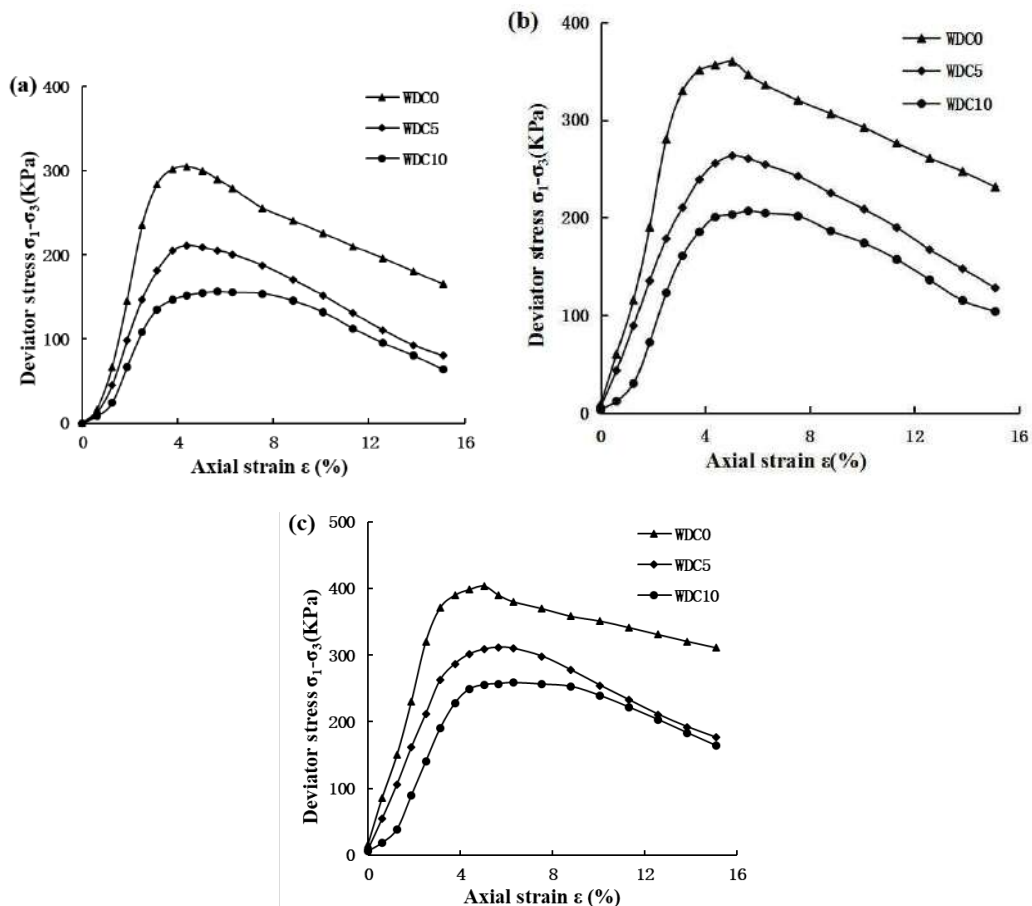


Fig. 3: Stress-strain curves of VC substrate. (a) 10KPa; (b) 30KPa; (c) 50KPa.

WDC10. The initial slope in the elasticity stage, the deviator stress in the yielding stage, and softening stage of the WDC10 were lower than that of the WDC0, and those of the WDC5 substrate was still somewhere in between. Similar results can be observed at confining pressure of 30 and 50KPa. These results indicate that wetting and drying cycles lead to negative effects on the mechanical properties of VC substrate. And these effects indicate the link between times of wetting and drying cycles and mechanical properties.

For the same times of the cycles, the compacted behaviors of VC substrate were weakened to some extent when confining pressure increased up to 50 KPa; but the deviator stress showed an increasing trend with confining pressure. These beneficial effects of the enhancement in deformation property and increase in strength are mainly due to the lateral restraining of confining pressure, as being described in various studies. Despite the effects of confining pressure, we won't further discuss the confining pressure impact on VC substrate for two reasons. First, this research mainly focused on the effects of wetting and drying cycles, not confining pressure. Second, VC substrate is a kind of topsoil with only 10 cm in thickness, the confining pressure difference is low and far less than that used in current tests.

Strength Behaviors: Fig. 4 shows the peak strength and residual strength of the substrate WDC0, WDC5, and WDC10 under 10, 30, and 50KPa confining pressure. It is shown that for a given confining pressure, there are great differences among the three substrate samples in peak strength and residual strength, though their sequences of peak strength

and residual strength were the same as the deviator stress mentioned above.

Compared with the control WDC0, the peak strength of the substrate WDC5 decreased by 30.8%, 26.8%, and 22.8% at confining pressure of 10, 30, and 50 KPa, while for the substrate WDC10, it decreased by 48.7%, 42.5%, and 40.0%. As for residual strength, the declines of the substrate WDC5 and WDC10 were much higher than that in peak strength. Take the case of 10 KPa confining pressure as an example, the residual strength of the substrate WDC5 and WDC10 decreased by 51.4% and 61.4%, about 20.6% and 12.7% higher than that of peak strength, respectively. These results show that wetting and drying cycles can decrease the strength of VC substrate by up to 50% of peak strength and 60% of residual strength. The results also indicate that the reduction of peak strength in the first five cycles was higher than that in the second five cycles, implying that effects by wetting and drying cycles gradually weakened as the cycles continued.

The cohesion and friction angle of the three substrate samples were calculated according to the data of peak strength at 10, 30, and 50KPa confining pressure. The results are listed in Table 3. It can be seen from the figure that the decline of cohesion for the substrate WDC5 and WDC10 were 34.0% and 54.0%, respectively, which is similar to the results of the data of peak strength. However, there was no effect on friction angle. Obviously, the impact of wetting and drying cycles on the macro-strength of VC substrate was mainly the weakening of bonding properties.

Table 3: Cohesion and friction angle.

Sample code	WDC0	WDC5	WDC10
Cohesion $C(KPa)$	75.39	49.72	34.69
Friction angle $\psi(^{\circ})$	33.63	33.86	34.00

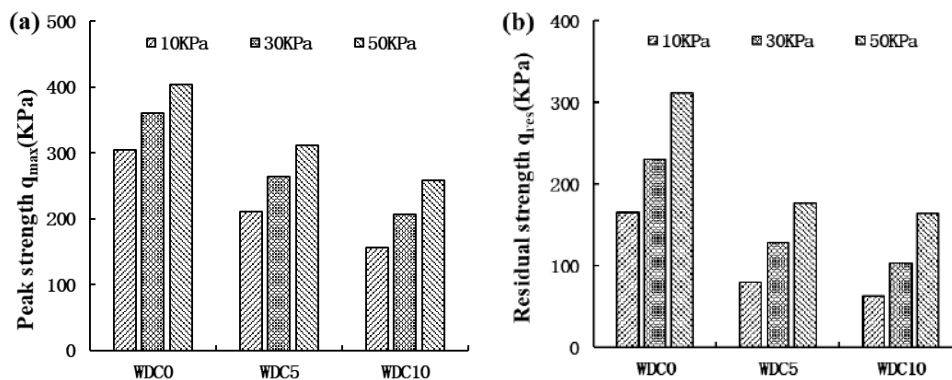


Fig. 4: Peak strength and residual strength of VC substrate. (a) peak strength; (b) residual strength.

Structural Damage: Fig. 5 shows the SEM micrographs of the substrate WDC0, WDC5, and WDC10. As shown in Fig. 5(a), the substrate WDC0 represents a relatively dense matrix with good integrity. This matrix has few pore spaces, which are scattered randomly, and almost has no visible cracks.

Compared with the WDC0, the substrate WDC5 had more pore spaces and poor integrity. The pore spaces were bigger in size and mainly distributed in the interface between skeleton solid particles and debris particles as well as in the debris particle collection region. The biggest pore space of the WDC5 was almost double in size of that in the WDC0 substrate. Additionally, cracks can be observed in the edge of some skeleton particles within the scope of this micrograph. Overall, the substrate WDC5 (Fig. 5(b)) can be considered as a matrix with a partial cementation structure. Unlike the substrate WDC0 and WDC5, the WDC10 resembles a loosen matrix with poor integrity. As can be seen in Fig. 5(c), many pore spaces had been produced and uniformly distributed in the substrate. There were some skeleton particles observed in WDC10 substrate, but they were few, indecipherable clear, and their combination with debris particles was poor. It seemed that the debris particles area and part of the surface of skeleton particles were covered by a layer of floccule, presenting a

flocculate-like structure in VC substrate. The former may be due to the failure of bonding between debris particles; the latter is for the peeling and covering of the debris particles cemented on the surface of skeleton particles, which is also due to the bonding loss between solid particles.

Based on the analysis, wetting and drying cycles can do damage to the structure of VC substrate and change its structure from cemented dense state to loosen state. Hence, the weakening of the bond between solid particles was the predominant aspect of the damage to the VC substrate caused by wetting and drying cycles. This bond loss is what leads to the weakening deviator stress-strain behavior and reduction in the strength parameters of VC substrate as manifested in Fig. 3 and Fig. 4. This can also adequately explain the reduction in cohesion. It is worth noting that the pore size in WDC10 substrate does not change much compared with that in WDC5, which may be due to the filling or covering of the tiny floccule as mentioned above.

The ultrasonic wave method is a non-destructive way to measure structural damage and is widely used to analyze the damage evolution of soils. In this study, ultrasonic waves of the substrate labeled WDC0-10 were measured and a damage variable D which was described by Gong et al. (2018) was defined using the following formula.

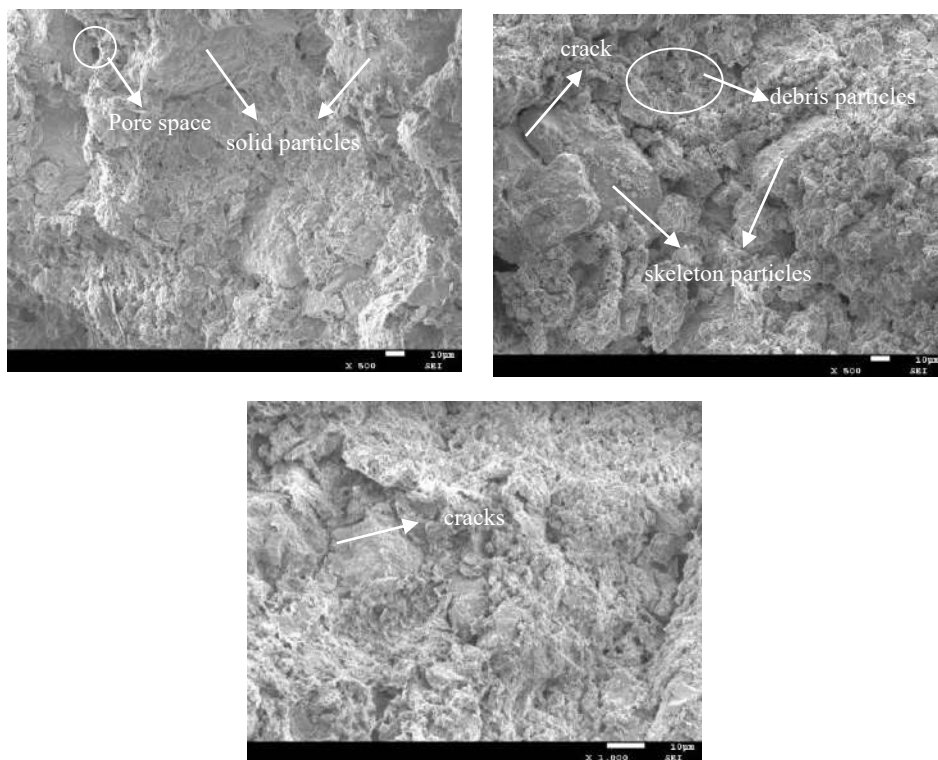


Fig. 5: SEM micrographs of (a) WDC0 substrate; (b) WDC5 substrate; and (c) WDC10 substrate.

$$D=1-(V_T/V_0)^2 \quad \dots (1)$$

Where, D is the structural damage variable; V_T is the ultrasonic wave velocity of the WDC0-10 substrate with n times of wetting and drying cycles ($0 < n < 10$, and n is an integer); the value of V_0 is equal to $0.662 \text{ km} \cdot \text{s}^{-1}$.

Fig. 6 shows the relationship between the structural damage variables and times of wetting and drying cycles. It can be seen that the structural damage variable (D) increases nonlinearly as the number of wetting and drying cycles (n) increases, with a slowing rate of increase. This shows that structural damage accumulates as the number of wetting and drying cycles increases and that this cumulative behavior becomes less obvious as the cycles continue (Pineda et al. 2014).

The dynamics change of D during wetting and drying cycles was well described by a semi-logarithmic relationship with a coefficient correlation of 0.90, as shown in formula (2).

$$D = 0.1686 \ln(n) + 0.1976 \quad \dots (2)$$

The semi-logarithmic fitting is compatible with the results of a similar experiment conducted by Wei et al. (2015) on expansive soil, proving that this method is feasible for VC substrate. In practice, of course, this function combined with the SEM micrographs, as shown in Fig. 5, gives a reference for relevant researchers and engineers to evaluate the damage degree of VC substrate: the VC substrate possesses the partial cementing state when the structural damage variable ranges from 0 to 0.4; however, when the structural damage variable is beyond 0.6, it will be in a loose state. In Fig. 6, though the structural damage variable D at 10 times of wetting and drying cycles was highest, it does not represent the most severe damage state for VC substrate, because within the times of the wetting and drying cycles in this study, the structural damage variable D was still in a slightly upward trend and had not reached steady state. This indicates that the VC substrate at 10 cycles was not completely destroyed,

this notion is confirmed by the existing skeleton particles in Fig. 5 (c).

Relationships between Strength Loss and Structural Damage: Studies have shown that strength change of soil is a macro-reflection of the microstructural damage. In this research, the internal relations of strength loss and structural damage can provide a theoretical basis for mechanical properties of VC substrate under wetting and drying cycles, and it is also popularized in other damage factors. For this purpose, the strength loss rate was defined to evaluate the degree of strength reduction (Gong et al. 2018), as shown in the following formula (3) ~ (5):

$$\Delta q_{\max} = 1 - q_{\max T} / q_{\max 0} \quad \dots (3)$$

$$\Delta q_{\text{res}} = 1 - q_{\text{res} T} / q_{\text{res} 0} \quad \dots (4)$$

$$\Delta C = 1 - C_T / C_0 \quad \dots (5)$$

Where, Δq_{\max} , Δq_{res} , and ΔC are the peak strength loss rate, residual strength loss rate, and cohesion loss rate; $q_{\max 0}$, $q_{\text{res} 0}$, and C_0 are the values of the peak strength, residual strength, and cohesion of the substrate WDC0; $q_{\max T}$, $q_{\text{res} T}$, and C_T are the values of the peak strength, residual strength, and cohesion of the substrate WDC5 or WDC10, respectively. It is noted that the friction angle of the VC substrate was analyzed here because the impact of wetting and drying cycles on it had not been found in this study.

Fig. 7 shows the relationships between the strength loss rate and structural damage variables of VC substrate. It was found that the strength loss rates of peak strength, residual strength, and cohesion were linearly correlated with the structural damage variables, and the fitted effect was preferable. The fitting results obtained were consistent with the findings concluded by Wang et al. (2016).

Damage Mechanism of Wetting and Drying Cycles

The microstructural damage or macro-strength reduction of soil matrixes during wetting and drying cycles are usually

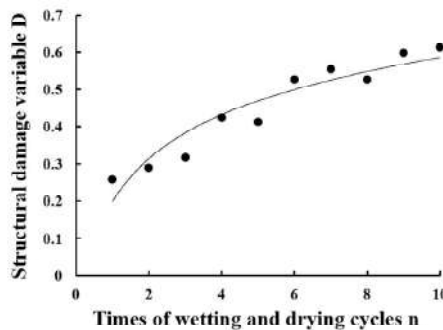


Fig. 6: Damage variables of VC substrate.

associated with the water-physical properties of their components. In this section, we will discuss the relevant properties in the aspects as follows.

Minerals: Hydrophilic minerals are usually considered to be a disadvantage factor as they extensively exist in natural soils and can expand or contract when the moisture content of soil changes (Deng et al. 2017). The expansion and contraction deformation of hydrophilic minerals may result in compression and tension between the contact surfaces of solid particles and thereby weaken the bond between soil particles. As the wetting and drying cycles continue, the compression and tension take place alternately in time and continue to repeat one another. These cyclic stresses in the soil will eventually lead to damage to soil structure or weakening of mechanical properties at a macro level (Muntaha 2017).

As listed in Table 2, the VC substrate contained two kinds of hydrophilic minerals: montmorillonite and illite with a total content of 18% by weight, which were also the only two clay minerals in VC mixtures. Because montmorillonite and illite have high hydrophilicity, they can expand and contract

significantly in volume during wetting and drying cycles, and because they were the primary clay cementing materials for solid particles in the VC substrate, their effects on structural damage would manifest as a weakening of the soil-particle bond, as shown in Fig. 5. In addition, it is worth noting that the content of montmorillonite and illite measured by the XRD method was much higher than that of the clay particles but less than 0.074 mm in the particle analysis test, as shown in Table 1. This indicates that part of montmorillonite and illite minerals existed in bigger solid particles and their expansion and contraction deformation during wetting and drying cycles may be the reason for the cracks in skeleton particles. Furthermore, the VC substrate is an alkaline cemented soil and its pH value can reach 12. We cannot rule out the possibility that quartz and albite might dissolve in alkali solution and accelerate soil structural damage as Qiu et al. (2007) reported.

Sawdust: Sawdust is the second-largest component of VC substrate, and its content was high up to 28.35% by volume. As a kind of woody material, sawdust has the properties of

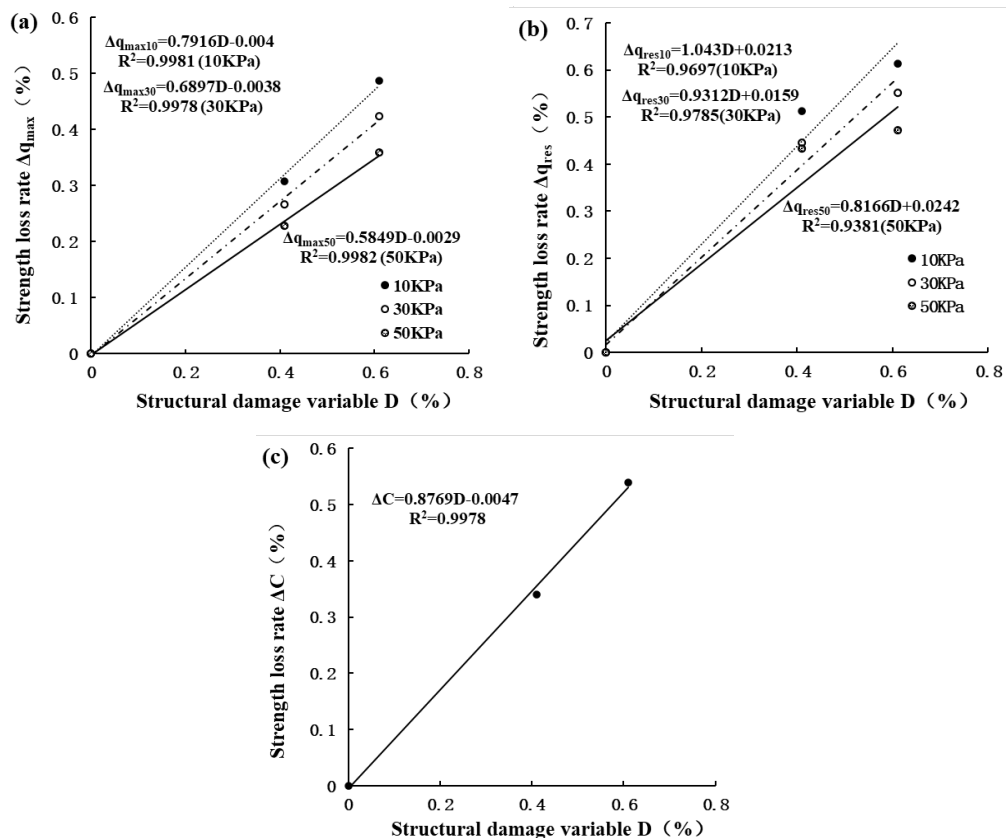


Fig. 7: Relationship between strength loss rate and damage degree of VC specimens. (a) peak strength loss rate; (b) residual strength loss rate; (c) cohesion loss rate.

wet-swelling and dry-shrinkage. When the moisture content is below the fiber saturation point, woody materials may expand in volume after absorbing water and shrink after losing water. This swelling and shrinkage deformation have more or less the same impact on soil structure as hydrophilic minerals do. To further diagnose the possibility of this volumetric deformation of sawdust during wetting and drying cycles, the water content of sawdust was measured before wetting. The test result showed that its water content before wetting (or at the end of drying) was 8.53%, which was significantly lower than the average fiber saturation point of woods in China, as 28% reported by Ai and Zhang (2016). This indirectly confirmed that sawdust could cause damage to the soil structure.

In general, the structural damage of VC substrate during wetting and drying cycles was a comprehensive effect by the expansion and contraction of hydrophilic minerals, as well as the swelling and shrinkage of the sawdust. It should note that the structural damage of VC substrate can also be accelerated by matric suction during wetting and drying cycles.

CONCLUSION

This research was conducted to further our understanding of the durability of the VC substrate under wetting and drying cycles. Based on the findings and results, the following main conclusions can be drawn:

- (1) Wetting and drying cycles affected the features of the strain-stress curves of the VC substrate. Compared with the control substrate WDC0, the initial compaction property of the WDC10 substrate was more pronounced and the initial slope and deviatoric stresses were low. It was also found that the relevant properties of the WDC5 substrate were at an intermediate level between WDC0 and WDC10 substrate.
- (2) The peak strength, residual strength, and cohesion of the WDC10 substrate were decreased by more than 40-percent, 60-percent, and 50-percent, respectively. The corresponding decrease for the substrate WDC5 was about 20-percent in peak strength, 50-percent in residual strength, and 30-percent in cohesion. However, no influence was found on friction angle.
- (3) The weakening of the bond between solid particles was the predominant aspect of the damage to the VC substrate caused by wetting and drying cycles. The actions of wetting and drying cycles ultimately made the VC substrate change from a dense matrix to a loose matrix with plenty of pore space.
- (4) The structural damage of VC substrate accumulated with the increase of the times of wetting and drying cycles,

but at a slower rate, and it followed a semi-logarithmic function. And it was found that the strength loss rates of VC substrate increased linearly with the structural damage variable.

- (5) The mechanisms actions of wetting and drying cycles on structural damage or mechanical properties of VC substrate include the expansion and contraction of hydrophilic minerals, the swelling and shrinkage of the sawdust, and the driving effects of the matric suction.

ACKNOWLEDGEMENTS

This research was supported by the National Key Research and Development Program of China (Grant No. 2017YFC0504902-05), the National Natural Science Foundation of the People's Republic of China (Grant Nos. 51979147 and 51678348), the Natural Science Foundation of Hubei Province (Grant Nos. 2016CFA085 and 2017ACA189), and the Research Fund for Excellent Dissertation of China Three Gorges University (2019BSPY006).

REFERENCES

- Ai, M.Y. and Zhang, X.F. 2016. Practice and application for wood drying. Chemical Industry Press, pp. 6-9.
- Deng, H.F., Fang, J.C., Li, J.L., Xiao, Y. and Zhou, M.L. 2017. Mechanical properties of red-bed soft rock on the saturated state. *J. China Coal Soc.*, 42(8): 1994-2002. (in Chinese)
- Gong, J.Q., Deng, G.Q. and Shan, B. 2018. Ultrasonic test and microscopic analysis of reactive powder concrete exposed to high temperature. *J. Hunan Univ. (Nat. Sci.)*, 45(1): 68-76. (in Chinese)
- Hayano, K., Dong, P.H. and Morikawa, Y. 2013. Physical and mechanical properties of cement-treated granular soils with respect to the geotechnical application. *AIP Conf. Proceed.*, 1542: 301-304.
- Liu, D.X., Zhang, B.H., Yang, Y.S., Xu, W.N., Ding, Y. and Xia, Z.Y. 2018. Effect of organic material type and proportion on the physical and mechanical properties of vegetation-concrete. *Adv. Mater. Sci. Eng.*, 7(3): 1-8.
- Muntaha, M. 2017. The effect of drying-wetting cycle's repetition to the characteristic of natural and stabilization residual soils Jawa Timur-Indonesia. *IOP Conf. Series-Mater. Sci. Eng.*, 267: 012030.
- Pineda, J.A., Romero, E., Gracia, M.D. and Sheng, D. 2014. Shear strength degradation in claystone due to environmental effects. *Geotechnique*, 64(6): 493-501.
- Qiu, L.W., Zhao, W. and Liu, K.Y. 2007. Alkali diagenesis and its application in Jiyang Depression. *Petrol. Geol. Recov. Efficiency*, 14(2): 10-15. (in Chinese)
- Sayem, H.M., Kong, L.W. and Yin, S. 2016. Effect of drying-wetting cycles on saturated shear strength of undisturbed residual soils. *Amer. J. Civil Eng.*, 4(4): 143-150.
- Tan, W.C. and Chen, P.H. 2014. Study on characteristics of cement-modified expansive soil under drying-wetting cycles. *Hunan Comm. Sci. Technol.*, (3): 34-35. (in Chinese)
- Wei, B.X., Huang, Z. and Yang, J. 2015. Research on the relationship between shear strength and damage variable of expansive soil based on wave velocity. *J. Highway Transp. Res. Dev.*, 32(6): 39-45. (in Chinese)
- Wang, H.X., Ke, R., Tan, Y.Z., Wu, J. and Huang, L.B. 2018. Deterioration characters of solidified/stabilized sediments by dry-wet circulations. *Bull. Chinese Ceramic Soc.*, 37(9): 2704-2709. (in Chinese)

- Wang, Y., Li, X. and Zheng, B. 2016. Experimental study on mechanical properties of clay soil under compression by ultrasonic test. *Eur. J. Environ. Civ. Eng.*, 5: 1-20.
- Wang, T., Weng, X.Z., Zhang, J., Jiang, L., Liu, P.C. and Zhang, S. 2017. Strength characteristics of fiber-reinforced solidified sand under dry-wet cycles. *J. Railw. Sci. Eng.*, 14(4): 721-729. (in Chinese)
- Xu, W.N. and Wang, T.Q. 2001. A Kind Of Greening Agent Used for Vegetation-Growing Concrete. P. China. Beijing, China
- Yu, X.J. 2012. Test study on engineering properties of low liquid limit silt and improved soil under wetting-drying cycle. *J. Shijiazhuang Tiedao Univ. (Nat. Sci.)*, 25(1): 86-94. (in Chinese)
- Yang, J., Yang, Z., Zhang, G.D. and Tang, Y.W. 2014. Influence of shear rate and lime-ash content on shear strength index of weathered sand. *J. Lanzhou Univ. Technol.*, 40(5): 126-130. (in Chinese)
- Zhang, J. 2018. Experimental study on compressive strength and durability of polypropylene fiber reinforced cemented soil under drying and wetting cycles. *J. China Foreign Highway*, 38(6): 235-238. (in Chinese)
- Zhang, Z.H., Jiang, Q.H., Zhou, C.B. and Liu, X.T. 2014. Strength and failure characteristics of jurassic red-bed sandstone under cyclic wetting-drying conditions. *Geophys. J. Int.*, (2): 1034-1044.



Treatment and Disposal Methods of Concentrate Stream of Seawater Reverse Osmosis- A Review

Zakiya Tabassum† and Rajalakshmi Mudbidre

Department of Chemical and Biological Engineering, R. V. College of Engineering, Bengaluru, Karnataka, India

†Corresponding author: Zakiya Tabassum; nazeerzakiya@gmail.com

Nat. Env. & Poll. Tech.
Website: www.neptjournal.com

Received: 27-07-2020

Revised: 28-09-2020

Accepted: 15-10-2020

Key Words:

Treatment & Disposal methods
Seawater reverse osmosis
SWRO
Concentrate stream

ABSTRACT

The exponentially multiplying population of the world demands increasing freshwater resources. The limited resources comprising less than 3% of the earth's water resources are getting polluted at an alarming rate. To deal with this situation, seawater reverse osmosis is being carried out at large scales across the globe. The concentrate generated in return is two times more concentrated in terms of total dissolved solids when compared to the feed. The adverse effects of the concentrate stream on the marine ecosystem and further pollution of water cause an immediate need to treat the concentrate. In this review, the harm caused by the direct discharge of concentrate stream has been discussed and therefore volume minimization using treatment methods has been addressed. The treatment methods are mainly classified into four types; membrane-based, thermal-based, electricity-based, and chemical-based methods. Integrated methods, which have been mainly tested on a pilot scale for zero liquid discharge, have also been discussed. The treatment methods that are probable for seawater concentrate treatment falling under the above categories for other concentrate sources have also been attended to. Finally, the disposal methods employed for the discharge of the leftover concentrate have been addressed. Thermal methods are well established but require a lot of energy compared to other methods whereas chemical methods can be economic due to the profit obtained from recovered chemicals, but they are mostly employed for pretreatment. Electricity-based and membrane-based methods are emerging technologies. It was also found that seawater reverse osmosis concentrate is usually discharged directly and therefore integrated methods based on zero liquid discharge are to be implemented. To compensate for the intensive research required for zero liquid discharge to become a reality, innovative and environmentally-friendly disposal methods are available to cut the resultant footprint.

INTRODUCTION

Reverse osmosis is a procedure that uses membrane technology to purify wastewater or water streams that are unfit for drinking or domestic use. It produces potable water that can be used as a substitute for natural freshwater resources. Reverse osmosis is the process in which water flows from a highly concentrated stream through a semi-permeable membrane to the fresh waterside giving out permeate stream and concentrate stream. The permeate stream is the water with the least quantities of total dissolved solids (Greenlee et al. 2009). Meanwhile, the concentrate stream has 1.5-2 times the dissolved solids as compared to the feed water (Younos 2005, Qasim et al. 2019). It has a smaller footprint, allowing the system to efficiently combine with other methods to enhance the overall recovery. Even then, researchers have looked into its high energy consumptions and carbon dioxide emissions (Heihsel et al. 2019). Countries in the Middle East did not rely on Reverse Osmosis (RO) earlier but with the rising prices of oil and fuel, they are increasingly switching to RO treatment (Tularam & Ilahee 2007).

NEED FOR REVERSE OSMOSIS

Nearly 3% of the Earth's water sources are fresh, divided unevenly across the countries. According to an estimate, over one billion people do not have fresh water sources in the world (Subramani & Jacangelo 2014). Freshwater resources available to us in nature are depleting day by day due to a drastic increase in population across the globe. The ever-increasing population demands higher quantities of freshwater resources to satisfy the daily needs of people. Countries such as the United States, Vietnam, Bangladesh, and India are encountering the problem of increasingly saline groundwater causing an increased demand for seawater treatment (Tularam & Ilahee 2007). The water stress index is the ratio of withdrawal of freshwater to the available freshwater resources. A value of 40% indicates water shortage, and water shortages may lead to increased prices, unavailability of freshwater to all spheres of the population (Fritzmann et al. 2007). As the water resources are getting depleted drastically due to this, various treatment methods have been employed for treating saline sources of water.

Amongst these, RO is found to be the most efficient method due to its lower energy requirements, higher recovery, and good quality of permeate obtained. The 330,000 m³.day⁻¹ Sea Water Reverse Osmosis (SWRO) plant in Ashkelon, Israel, and the 136,000 m³.day⁻¹ Tuas SWRO plant in Singapore are some of the high capacity RO plants (Pérez-González et al. 2012). Fujairah SWRO plant was also built in 2005 with a capacity of 170,500 m³.day⁻¹ in the Middle Eastern region (Sanza et al. 2007). Apart from seawater, other sources of water are also treated by RO technology. International Desalination Association has classified brackish water as water containing TDS levels from 1000 mg.L⁻¹ to 10,000 mg.L⁻¹. Brackish water reverse osmosis can be carried out at a much lower energy consumption of 0.5-2.5 kWh.m⁻³ compared to seawater reverse osmosis which has an energy consumption of 3-4 kWh.m⁻³ (Xianhui et al. 2019). Thermal-based technologies are most commonly used in Middle Eastern countries because they have a surplus of fuel resources and its cheap price in comparison to other countries (Xu et al. 2013). But due to the large volumes of seawater available, the SWRO process should be made as efficient as probable to bring down the cost of energy consumption.

NEED TO TREAT THE CONCENTRATE

As mentioned before, RO gives out a concentrated stream that has 1.5-2 times more dissolved solids. Numerous problems are caused to the environment by this concentrated stream. The concentrate stream endangers the marine ecosystem in the area where it has been discharged. The areas receiving the concentrate undergo various degradations such as pH variations, eutrophication, and accumulation of heavy metals such as zinc, copper, iron, chromium, and nickel (Greenlee et al. 2009, Subramani & Jacangelo 2014, Rautenbach & Linn 1996, Chelme Ayala et al. 2009, Ng et al. 2008). Along with this, the concentrate stream upon disposal directly goes to the bottom of the sea due to the high concentration of total dissolved solids causing an increase in its density. The heavy metals present in these dissolved solids upon going to the bottom harm the aquatic animals and ecosystem including the coral reefs. Plenty of species such as the benthic community that inhabit the bottom of the sea disappear from the discharge zone (Li et al. 2019, Medeazza 2005, Mickley 2006, Missimer & Maliva 2018, Mondal et al. 2020, Panagopoulos et al. 2019). Due to all these adverse impacts, direct disposal of concentrate is restricted or banned by various organizations of different countries. To manage this problem, treatment of the concentrate must be done prior to discharge not just to prevent the adverse effects but also to minimize the volume of the concentrate. Treating the concentrate helps to provide an additional

freshwater resource, minimizes the concentrate volume, and precipitates/extracts valuable chemicals (Li et al. 2012, Xu et al. 2009). The selection of the best treatment method for the reverse osmosis concentrate is mainly dependent on the characteristics of the concentrate, its density, and volume (Mickley 2006).

METHODS OF TREATMENT AND DISPOSAL

Certain methods like zero liquid discharge methods end up with complete elimination of concentrate stream. Zero liquid discharge is based on the principle of maximizing the recovery in the first RO process, thereby highly reducing concentrate volume (Ning & Troyer 2009). Methods such as thermal-based or membrane-based methods help reduce the volume but do not completely terminate the concentrate stream. The disposal of this concentrated stream can be done using various disposal techniques. Some of the disposal methods are surface discharge, deep well injection, evaporation ponds, etc. In some cases, dispersion models have been used to determine the point of discharge that causes the least impact on the environment but even this shows limited change or benefit. The cost of discharge is usually around 5-33% of the total cost of the process depending on concentrate characteristics, concentration, and volume. Direct disposal may lead to certain environmental issues such as an increase in salinity beyond threshold limits, the concentration of metals, the concentration of nutrients that harm the environment, elevated temperatures, etc. Therefore, thorough research must be carried out before the disposal of concentrate (Voutchkov 2011). In this review, the different treatment technologies of the concentrate for concentrate volume minimization along with integrated techniques, which try to achieve zero liquid discharge, have been discussed. Disposal methods employable after concentrate treatment also have been addressed. The various benefits of treatment methods such as the recovery of valuable salts decreased costs due to the profit gained, and benefits to the environment have been reviewed.

TREATMENT METHODS OF CONCENTRATE STREAM

The direct disposal of the concentrate generated by the seawater reverse osmosis process is not possible due to the high volume of concentrate generated in most cases. To deal with this problem, various treatment technologies have been developed and amended for the volume minimization of the concentrate stream. Intermediate treatment of the concentrate between RO stages spikes the efficiency of the system. These treatment methods can be broadly divided into thermal-based, membrane-based, electricity-based, and

chemical-based methods. Integrated methods of treatment have also come into place.

THERMAL BASED METHODS

Thermal-based methods have been intensely researched and are well established industrially. The efficiency is high for thermal-based methods with the disadvantage being the high-energy requirement. Middle Eastern countries and countries with cheap fuel sources utilize thermal-based methods majorly in comparison with other treatment methods. The given Table 1 explains their properties.

MEMBRANE-BASED METHODS

Due to the depleting fuel resources around the world and the need to replace fuel-based technology with renewable technologies, thermal-based methods are not being used in most countries. Membrane-based methods have become quite popular due to the relatively less energy required and the high efficiency attained as discussed in Table 2.

A study of MD simulated an increase in the water recovery of a 40,000 m³.day⁻¹ plant from 40-89%. The total brine volume after treatment with MD decreased by a factor of 5.5. When highly ideal conditions were used, the minimum spe-

Table 1: Thermal based methods.

Sl. No.	Method	Properties	Advantages	Disadvantages	References
1.	Multiple Effect Evaporation (MEE)/ Vapor Compression (MVC)	In solution's vapor pressure is reduced within the system to make the solution boil at a lower temperature. The evaporator admits the concentrate feed into the tube side in series where it undergoes boiling. In MVC, the principle difference is that the vapor produced on evaporation is compressed using a compressor, for reuse as steam.	<ul style="list-style-type: none"> • They are the most cost-effective amongst the evaporation methods. • Steam used for boiling condenses over the tube walls and is reused for heating. • They have a simple geometry and are easy to operate, resulting in high efficiency. • They do not depend on weather conditions. 	Fossil fuel requirements and the high cost of energy sources are the main drawbacks.	(Morillo et al. 2014)
2.	Dewvaporation	The concentrate upon heating by hot air evaporates and condenses in the form of dew on one face of the heat transfer surface.	<ul style="list-style-type: none"> • Scaling can be avoided as evaporation occurs at the air-liquid interface. • Dewvaporation using solar energy combined with a chimney attains not just freshwater but also generates power. • At high heating power of 4.9 kW, 48 g.min⁻¹ of freshwater was seen to be the highest. 	There is a higher footprint as the tower operates at atmospheric pressure. The energy requirements are considerably high making it suitable only for high scale plants. To produce 1000 gallons of pure water, 2.6 X 10 ⁶ BTU of heat will be required. 32.14% was the highest thermal efficiency obtained for seawater desalination.	(Hamieh & Beckman 2006, Cao et al. 2020)
3.	Wind Aided Intensive Vaporization (WAIV)	Based on the principle of simultaneous humidification-dehumidification. In this method, intensely packed towers wetted with concentrate streams are evaporated using high-speed wind. These towers are vertical hydrophilic trays with the wind passing in a parallel direction. The heat flux at the wetted surface caused by the temperature difference between the warmer wind and cooler water surface causes evaporation.	<ul style="list-style-type: none"> • A demonstration in Australia showed that WAIV's efficiency was found to be 10 times higher than evaporation ponds. • It doesn't cause salt drift. • It has the lowest specific energy consumption of 1 kWh.m⁻³. • Wind energy is the main source of energy. • It has reduced land requirements. 	This method may have a drop-off in efficiency. Industrial research is needed to keep a tab on the detection of groundwater pollution.	(Gilron et al. 2003, Panagopoulos et al. 2019)

Table 2: Membrane-based methods.

Sl. No.	Method	Properties	Advantages	Disadvantages	References
1.	Membrane Distillation (MD)	It operates on the same principle as distillation except that it uses a membrane to form support between the vapor-liquid interface. Only the volatile component of the solution passes through the hydrophobic membrane. The driving force is the vapor pressure gradient between heated feed and cooled water. The most suitable MD for desalination purposes is direct contact membrane distillation. Here, a hydrophobic membrane is placed between hot brackish water concentrate and cold pure water	<ul style="list-style-type: none"> • MD isn't energy-intensive, as it requires a temperature between 60-80°C. • The volume of the membrane with respect to the equipment provides a large contact area. • It can be coupled with cheaper heat sources such as geothermal, solar, and waste energy. • The water produced was purer when compared to that of the other membrane processes. • MD membranes are resistant to oxidation in comparison with nanofiltration and RO membranes. 	<ul style="list-style-type: none"> • The hindrance to this method is the conductive heat loss that occurs at the MD membrane, thereby increasing the energy costs. • The research on this method should focus on the development of new membranes such that heat loss is less and scaling is eluded. • The CaCO₃ and CaSO₄ cause scaling, which can be reversible by washing and chemical cleaning. 	(Lawson 1997, Xianhui et al. 2019, Office 2003), Mericq et al. 2010)
2.	Forward Osmosis (FO)	A concentrated solution called draw solution, in this case, concentrate stream causes osmotic pressure differential and carries out dilution of the stream.	<ul style="list-style-type: none"> • FO has a lower energy requirement compared to RO • It has a reduced specific energy consumption of 4.49 kWh.m⁻¹ in comparison with a double RO system of 6.43 kWh.m⁻¹. • No external pressure is required. • Membrane fouling is also relatively low and easily reversible. 	<ul style="list-style-type: none"> • Concentration polarization is high. • Suitable draw solutions that provide a strong driving force are hard to find. • To reduce the concentration polarization, hydraulic configurations need to be optimized. • Scaling takes place in real systems due to the presence of organics. 	(Zhang et al. 2011, McCutcheon & Elimelech 2006, Shaffer et al. 2012, Subramani & Jacangelo 2014, Kazner et al. 2014, Martinetti et al. 2009, Liyanaarachchi et al. 2020).
3.	Bipolar Membrane Electrodialysis (BMED)	Bipolar membrane electro-dialysis is an electro-dialysis process carried out with the help of bipolar membranes. This gives mixed acids and bases as the product. Mono polar cation and anion exchange membranes with alternating bipolar membranes are installed as a whole. The membranes split water into protons and hydroxides, Protons combine with anions to form acids meanwhile hydroxides combine with cations to form bases.	<ul style="list-style-type: none"> • It is a source of valuable metals. • One of the recent studies shows BMED powered by photovoltaic energy overcame the energy consumption issue. • Byproducts reduce the environmental impact of the process of treating seawater concentrate. 	<ul style="list-style-type: none"> • There is limited stability of the ion exchange membranes. • When the salt concentrations are very high, the separation of acids and bases is hindered as salts also permeate through the bipolar membrane and precipitate. 	(Badruzzaman et al. 2009, Morillo et al. 2014, Jones et al. 2019, Strathmann 2010).

cific energy consumption of 7.7 kWh.m⁻³ was obtained with feed and distillate temperatures of 60°C and 20°C (Deshmukh et al. 2018). Similarly, to understand the efficiency of FO, it was used to concentrate brine from TDS 70,000 mg.L⁻¹ to 225,000 mg.L⁻¹. 60% of water recovery was obtained using FO (Subramani & Jacangelo 2014). In the case of BMED, upon carrying out Life Cycle Impact Assessment with climate change as the factor, it was seen that the resultant

water had TDS similar to seawater and hence direct discharge is quite possible (Herrero-Gonzalez et al. 2020).

ELECTRICITY BASED METHODS

Electricity-based methods are quite efficient for desalination. They also achieve recovery of valuable products from the seawater concentrates such as precious metals and other

Table 3: Electricity based methods.

Sl. No.	Method	Properties	Advantages	Disadvantages	References
1.	Electrodialysis (ED)	There is a cathode and an anode between which a series of alternating cation and anion-selective semi-permeable membranes are present. The cations pass through the cation-selective membrane and get attracted to the anode, which is negatively charged. Similarly, the anions pass through the anion-selective membrane and get attracted to the cathode, which is positively charged.	<ul style="list-style-type: none"> • It is well established. • Hollow membrane fibers between the ion exchange membranes decrease the concentration polarization. • It can operate with residual chlorine up to 1 mg.L⁻¹, controlling fouling. • The salt concentration is increased from 0.2-2% to 12-20% with 1-7 kWh.m⁻³ energy requirement. 	<ul style="list-style-type: none"> • It has a high cost of generation. • It is only used for low concentrations of salts. • Fouling occurs by the presence of colloidal materials and organics. • It may have a high energy consumption if low selective membranes are employed. • Industrially, batch ED processes are carried out but continuous supply is mostly required and needs to be further explored. 	(Korngold et al. 2005, Xu et al. 2013)
2.	Electrodialysis Metathesis (EDM)	This method is also based on electrodialysis in which repeating units of the following are present; NaCl solution compartment, dilute compartment, cation exchange membrane, anion exchange membrane, two concentrate compartments, monovalent selective anion, and cation exchange membrane. This configuration separates the feed into two streams of highly soluble salts; sodium with anions and chloride with cations.	<ul style="list-style-type: none"> • This method is excellent at concentrating ions and recombining them simultaneously. • In a recent project, EDM was used to concentrate the seawater brine and further sodium and chlorine were produced making it economically efficient. 	<ul style="list-style-type: none"> • This method doesn't help remove organics from the water. • High voltages give high specific energy consumption, which in the above-mentioned study reached up to 1.77 kWh.kg⁻¹ TDS for a voltage of 8V. 	(Bond & Veerapaneni 2011, Chen et al. 2019)

economic salts. The disadvantage of this method is quite obvious, namely, its high-energy requirements to fulfill the electricity demand. The following Table 3 below describes the different aspects of the methods.

In a recent study where seawater desalination was carried out in a two-stage ED plant, energy consumption was found to be around 3.6kWh.m⁻³ where the concentration decreased to 11.4mM, which is according to the standards prescribed (Doornbusch et al. 2019). Whereas, Electro Dialysis Metathesis (EDM) is not commonly used and so far, has only been used at lab scale and not industrially. Electrodialysis metathesis helped increase water recovery to 99% with BWRO feed and can be used as a secondary treatment.

CHEMICAL-BASED PROCESSES

Chemical-based processes mentioned in Table 4 mainly focus on the recovery of chemical products from the concentrate stream of SWRO. This is because it increases the environmental benefits by reducing the volume of the discharge while increasing the economic benefits by producing valuable chemicals simultaneously. Various chemical-based methods have been employed for treatment. Although, some may increase costs due to the added cost of

chemicals whereas others generate profit when byproduct chemicals are of value to other industries.

As mentioned, the by-products formed to make this category economic most of the time. SAL-PROC processes have been tested for installations with a capacity of up to 822-7991 m³.day⁻¹. The recovery rates in the four plants in Oman were found to be 70% on average (Schantz et al. 2018). A recent study used to treat 17.5 t.h⁻¹ seawater concentrate; the Chlor-alkali process was the last treatment step to produce chlorine and alkali. 208.4 kg.h⁻¹ of NaOH was obtained including the caustic soda required in the process (Du et al. 2018). When chemical softening was accompanied by a secondary step of RO, 95% overall water recovery was obtained. In another study, flocculants were also used to enhance precipitation and remove hardness by floc formation (Ordóñez et al. 2012).

INTEGRATED PROCESSES

Integrated processes are the combination of different processes into a flow where the final product is seen to have enhanced recovery as compared to single methods. Certain integrated processes such as a combination of RO with a membrane reactor have achieved up to 88.94% recovery but

Table 4: Chemical-based methods.

Sl. No.	Method	Properties	Advantages	Disadvantages	References
1.	SAL-PROC	This is a patented process used for the extraction of dissolved elements from seawater in a sequential process and gives out valuable chemicals in the slurry, crystalline, and liquid forms. In one of the studies at the laboratory scale, sodium bicarbonate, sodium carbonate, ammonium chloride was obtained from concentrated brine by ammoniating the solution and bubbling carbon dioxide through the brine solution. It is a simple process of evaporation and cooling that is accompanied by chemical and mineral processing.	<ul style="list-style-type: none"> • The recovery of valuable salts from these waste concentrate streams improves the cost-effectiveness of the desalination process. • In an estimation that took place regarding desalination of the Petroleum Development Oman's (PDO) four desalination plants, commercial salts worth USD 895,000 could be recovered at the most using this process. • Chemical recovery can make an expensive process economic due to the profit gained. 	<ul style="list-style-type: none"> • The storage of chemicals required, chemicals produced will generate a significant footprint. • It will also have high investment costs due to the continuous need for reactant chemicals. 	(Jibril & Ibrahim 2001, Morillo et al. 2014, Ahmed et al. 2003)
2.	Chlor-alkali	This potential process of profitable concentrate treatment is similar to BMED where an electrochemical cell is used to oxidize chloride ions to chlorine gas and sodium ions and water to sodium hydroxide.	<ul style="list-style-type: none"> • Hydrogen gas obtained at the cathode can be used on-site, as a commodity, or released into the atmosphere. • If a membrane electrolytic cell is used, pure NaOH will be produced that deals with environmental concerns. • The chlorine produced by SWRO concentrate treatment can be utilized for the disinfection of drinking water. • When a cost analysis was carried out on this method, it was concluded that after ten years, the profit obtained could pay off the capital costs. 	<ul style="list-style-type: none"> • The brine has to be free of Ca, Mg, Ba, Sr, and organic matter. • The profitability was sensitive to changes in the prices of the product. • The energy demand for generating chlorine from the concentrate stream is approximately 2100 kWh.t⁻¹chlorine. Therefore, unless the product generates enough profit, the energy consumption will be quite disadvantageous. 	(Schantz et al. 2018, Shahmansouri et al. 2015, Morillo et al. 2014)
3.	Chemical Softening	Chemical softening is done by the addition of chemicals to the concentrate, giving out the precipitate. This process commonly precipitates Ca ²⁺ , Mg ²⁺ , and Sr ²⁺ . Dosing alkaline chemicals such as Ca(OH) ₂ , NaOH, and Na ₂ CO ₃ precipitates scaling chemicals such as CaCO ₃ . A Solid Contact Reactor was used to carry out softening and the precipitate was separated from water efficiently.	<ul style="list-style-type: none"> • In 2014, this method was used to treat seawater brines from Mediterranean and Red Sea RO plants and synthetic seawater. • The efficiencies obtained for calcium were 89%, 95%, and 95.5% respectively. 	<ul style="list-style-type: none"> • There is a high chemical demand for precipitation of the scalants. • Large quantities of waste sludge are produced. • There is a requirement for a filtration step before sending the feed for secondary RO. • Retardation of the rate of desupersaturation due to the presence of antiscalants is another drawback. 	(Qu et al. 2009, Gabelich et al. 2007), Schantz et al. 2018, Sorour et al. 2015)
4.	Degasification	Degasification/CO ₂ stripping can be used for obtaining carbon dioxide from seawater RO concentrate. In one of the studies when carbonate-rich RO concentrate was treated, air stripping the CO ₂ precipitated the solids with increasing pH.	<ul style="list-style-type: none"> • An environmental and economically favorable way of removing CO₂ is by stripping CO₂ using aeration, without the use of any chemicals. • The recovery increases due to an increase in pH 	<ul style="list-style-type: none"> • Blockage of air aperture nozzles can take place, leading to diminished air flow rate, and a decrease in CaCO₃ precipitation rate. • There is a requirement for additional chemicals. • The production of large quantities of sludge can be a hindrance. • Availability of area for storage of chemicals, and space requirements of the respective reactors are also possible concerns. 	(Hasson et al. 2011, Segev et al. 2011, Cohen & Kirchmann 2004)

haven't been researched further (Lew et al. 2005). In a study, the concentrate was treated using the ED-Pellet Reactors combination (Tran et al. 2012). Whereas in another study RO concentrate with EDR was tested and gave a high recovery (Turek et al. 2009). Studies that combined ultrafiltration, activated carbon filtration, and nanofiltration giving high recoveries, have also been studied (Heijman et al. 2009). Some of the methods have been discussed in Table 5.

8400m³/day of concentrated brine from Pozo Izquierdo desalination plant with a capacity of 33000m³/day was used to test Chlor-alkali/chemical precipitation combination. Once the brine was treated, it was fed to an electrolyzer to separate chlorine gas and NaOH. The results showcased a production of 253.71kt/y NaOH, 2.82kt/y hydrogen, and 101.16 kt.y⁻¹

chlorine. In HERO, the combined overall recovery was seen to be 90% (Subramani & Jacangelo 2014). Another alternative to SPARRO is a two-pass process. Firstly, a tubular nanofiltration (NF) system with seeded slurry recycle was employed and in the second step, a spiral wound RO system was used. It's called a double pass preferential precipitation RO system. It achieved a recovery of up to 92-96% (Peters et al. 2007).

DISPOSAL METHODS

If treatment methods are ZLD type then there won't be any residue left over. But when treatment methods cannot suffice to eliminate residue, disposal methods should be opted to take care of the concentrate leftover. Carrying out treatment

Table 5: Integrated methods.

Sl. No.	Method	Properties	Advantages	Disadvantages	References
1.	WAIV/MCr	In this method, the BW was first pre-treated and then passed through RO. Upon recovery, the concentrate was further treated using WAIV. WAIV super concentrates were fed to the MCr semi-pilot plant.	<ul style="list-style-type: none"> NaCl can be crystallized in different shapes and sizes. The cost of treatment can be reduced to 64% by using WAIV instead of evaporation ponds. In the presence of antiscalants, 88% recovery was possible. The combined system was able to obtain up to 88.9% recovery. The savings for this system was over one magnitude greater than the reduction in the footprint for concentrate disposal. 	<ul style="list-style-type: none"> A fouling layer may be found in the MCr unit. The external substances existing in the brine may deter the kinetics of crystallization, causing a reduced growth or inferior product quality. 	(Subramani & Jacangelo 2011, Tullaram et al. 2007)
2.	Chlor-alkali/Chemical Precipitation	Chlor alkali feed must be free of Ca, Mg, Ba, Sr, to obtain chlorine gas. Thus, an integrated method combining Chlor-alkali with chemical precipitation was tested. A multiple-effect evaporator was used to carry out chemical precipitation. Calcium, sulfates, and magnesium were removed with chemical precipitation.	<ul style="list-style-type: none"> Using the concentrate stream reduced the energy required to start with fresh seawater directly. The hydrogen gas generated can be used to generate electricity in the plant. This method is economic as it involves the production of economic products 	This method needs further research and may have high-energy consumption depending on the electrolytic cell used.	(Morillo et al. 2014)
3.	High-Efficiency RO (HERO)	RO concentrate is treated with ion exchange to remove hardness and degasification methods, and a secondary RO treatment is carried out in the end. Carbon dioxide removal is obtained using the degasification step. The RO concentrate was treated with weakly acidic cationic exchange resins that caused the removal of divalent ions	<ul style="list-style-type: none"> Due to the degasification, an increase in pH increased the recovery of the secondary RO. Weakly ionized species such as SiO₂ and boron were reduced by a factor of 10 or more. 	<ul style="list-style-type: none"> Its estimated energy requirements were from 11-19 kWh.m⁻³. Complete coverage of the membrane with aluminosilicate was obtained. This is a patented process, hence leads to high capital costs. 	(Xinyang et al. 2012)
4.	Slurry Precipitation and Recycling RO (SPARRO)	Crystals such as gypsum are added to the concentrate solution, upon which scaling compounds precipitate on the seed compounds rather than on the membrane surface. A hydro-cyclone removes the crystals formed in the concentrate.	Overall recovery was estimated to be greater than 90%.	<ul style="list-style-type: none"> When the seed slurry is recirculated within the membrane system, plugging might occur. To avoid this, tubular membrane systems are desirable. 	(Peters et al. 2007)

methods is important because it reduces the volume by a large factor but disposal methods should also be discussed (Table 6) to identify the ideal disposal method for each process. When installing a desalination plant, the site location should be chosen such that no other sources of discharge are present or where a stream is available for its dilution to carry out the disposal effectively and in an environmentally acceptable manner (Mauguin & Corsin 2005).

CONCLUSION

The disposal of SWRO concentrate directly into the sea would cause adverse effects to the marine ecosystem of the sea, especially at the point of discharge. To avert this adverse damage to the aquatic life, treatment methods are to be developed to minimize the volume of concentrate or better yet, eliminate it. Zero liquid discharge is based on improving or maximizing the efficiency of the primary RO treatment. Treatment methods were divided based on the main princi-

Table 6: Disposal methods.

Sl. No.	Method	Properties	Advantages	Disadvantages	References
1.	Direct discharge	The discharge entering receiving water such as the sea forms a highly saline plume that may sink, float or stay in the water depending on the density of the water.	It is the most cost-effective and simple method.	<ul style="list-style-type: none"> • The concentrate goes directly to the bottom of the sea due to its high density, causing harm to the marine ecosystem as they consume heavy metals in the dissolved solids. • Plenty of degradation and depletion of marine life has been witnessed. 	(Younos et al. 2005, Chelme-Ayala et al. 2009, Li et al. 2012, Abdul-Wahab 2007, Leong et al. 2014).
2.	Dis-charge to trenches	Some small desalination plants use this method where they make use of perforated pipes buried at shallow depths parallel to the sea.	<ul style="list-style-type: none"> • Concentrate seeps slowly away from the shore, diffusing and dispersing with no impact on the benthic community, • It does not affect animal life such as nesting sea turtles. 	The apt way of construction of this method is to be tested further and a successful design should be accomplished.	(Missimer & Maliva 2018)
3.	Single pipe discharge	A single pipe with an inclined open end is available. When the concentrate is sent through the pipe to deep waters, it ascends at the end and descends back to the bottom of the seawater due to gravity.	It can be used at a large depth to avoid harm to marine life and coastal environments near the surface. <ul style="list-style-type: none"> • If the seabed is inclined, upon passing down, the concentrate gets diluted due to the level difference. 	The natural dilution of this concentrate depends on waves, currents, bathymetry, and tides present at the point of discharge.	(Missimer & Maliva 2018, Bleninger & Morelissen 2015, Younos et al. 2005)
4.	Discharge mixed with cooling water	The cooling water used in power plants can be mixed with the concentrate water before its discharge into the sea. The factors to consider for this are the difference in the densities of the cooling water and the concentrates, momentum, and velocity of the water getting discharged.	<ul style="list-style-type: none"> • The power plant will acquire a stable customer for electricity, as desalination plants require electricity for operation. • The heavy saline discharge draws the lighter cooling water into the entire depth of ocean water, accelerating its mixing and blending with ambient water in the sea. 	<ul style="list-style-type: none"> • This can only be done if the power plant is present at the site of the RO plant. • It only works if the power plant cooling water discharge flow is greater than the proposed RO intake flow. 	(Younos et al. 2005, Missimer & Maliva 2018, Voutchkov 2011)
5.	Deep well injection	The discharge zone is usually a dolomite transmissivity fractured zone called the boulder zone. The well depth can be from 0.2-1.6 miles below the Earth's surface. Florida is considered a safe location geologically for deep well injection.	<ul style="list-style-type: none"> • The concentrate stays underground permanently. • It doesn't harm aquatic life. 	<ul style="list-style-type: none"> • If the geography of the area does not permit the injection, this method cannot be used. • In the United States, earthquakes have been linked to this. Increased pressure causes the weakening of a pre-existing fault leading to earthquakes. • When the pore pressure increases more than the effective normal stress across the fault, the movement of concentrate takes place. This may result in the start of an earthquake. • The overall cost of this system is high because of the monitoring wells, tests for leakage, tests for strength during pressure, etc. 	(Chelme-Ayala et al. 2009, Li et al. 2012, Younos et al. 2005, Missimer & Maliva 2018, Leong et al. 2014)

Table cont....

Sl. No.	Method	Properties	Advantages	Disadvantages	References
6.	Diffusers	It involves the use of a diffuser attached at the end of the discharge pipe. Diffusers essentially comprise a series of nozzles that spread the concentrate amongst the seawater to prevent its accumulation at the bottom of the sea. The diffuser and the ambient seawater zone sandwich the mixing zone.	<ul style="list-style-type: none"> • In a study in Spain, a substantial decrease in the population of polychaetes families was found due to a salinity of 49ppt. • When a diffuser was employed, later on, the polychaete families returned to the area due to salinity reduction. • In Perth Seawater Desalination Plant in Australia, the University of Western Australia analyzed that negligible impacts were present in the surrounding environment due to the discharge. 	The dilution zone depends on diffuser design, size and shape of mixing zone, prevailing marine currents, and concentrate salinity.	(Voutchkov 2011, Missimer & Maliva 2018, Christie & Bonnélye 2009)
7.	Reflux	The concentrate is sent back to the feed to increase the water recovery as well as decrease the concentrate volume.	<ul style="list-style-type: none"> • The normal RO systems operated with a reflux rate of 60%. • Increasing the reflux rates up to 75% was also probably for BWRO systems. 	Careful measures must be taken to not give high reflux rates as it increases the salinity beyond tolerable levels deteriorating the membrane life.	(Younos et al. 2005)
8.	Evaporation ponds	This method will be useful for areas with high evaporation rates, low annual rainfall, and cheap land costs. These ponds may be shallow with 25-45cm depths.	It is easy to operate and construct.	Seepage prevention should be managed to prevent underground aquifer contamination, land-intensive.	(Xinyang et al. 2012, Schantz et al. 2018, Chelme Ayala et al. 2009, Leong et al. 2014)
9.	Agriculture	In some areas of Palestine, the olive and jujube tree is irrigated by concentrate from the desalination plant. This is carried out without an assessment of the impact caused on the soil, trees, and land around it.	Minimizes the price of concentrate treatment as it irrigates salt-resistant crops.	Saline aquaculture development limits due to the usage of concentrate therefore reuse for agriculture is highly site-specific.	(Li et al. 2012, Al-Agha & Mortaja 2005, Younos et al. 2005)

ple involved, namely; membrane-based, electricity-based, thermal-based, and chemical-based methods.

Thermals methods are conventional and well-established methods, which are popularly used in countries with high fuel resources and cheaper sources. These methods are however losing popularity due to the harm caused to the environment by the gas emissions along with the large expense of fuel for their functioning. The membrane-based methods are attaining popularity due to their lower energy requirements and better quality of the water recovered. The problem with these may be the life cycle due to scaling and fouling of membranes and therefore would require care to prevent added expenses. Chemical-based methods, although requiring expensive chemicals are also economic, considering the profit gained from the recovered chemicals. However, these have only

been utilized as a pretreatment step in reverse osmosis of water. Electricity-based methods are very expensive due to the additional requirement of electricity which again adds to the environmental concerns, even though they are found to be quite efficient.

Apart from these, integrated methods employ two or more methods based solely on the characteristics, volume, and concentrations of the concentrate stream generated. These methods aim for zero liquid discharge to eliminate the aspect of disposal. These newly developed methods have mostly been tested at pilot scales and require further examination of economic aspects before being employed industrially. Although membrane and chemical methods are developing, an optimum solution would be to develop an integrated system involving one or more types of treatment methods suitable

for the characteristic feed water and test it at a pilot scale before industrial usage. This would most likely give the best results for a system and can be tuned such that low energy is required but high efficiency is obtained. At the pilot scale, brackish water has been tested but seawater treatment must also be carried out to attain sufficient data.

The common disposal methods used to dispose of the minimized concentrate are discussed where evaporation ponds are found to be effective in only certain areas. They can be used if appropriate geography is found. Methods such as discharge into the sea have been made more efficient using single pipe discharge, trenches, and diffusers. Innovative discharge methods such as agriculture, recycle, reflux, and incineration have also been discussed which could help in the reuse and utilization of the waste stream in a more advantageous way. Despite the efforts in developing integrated methods, increasingly environment-friendly disposal methods need to be developed to ensure that current waste streams are disposed of securely. The establishment of integrated methods at an industrial scale is currently far off as prior pilot testing is compulsory. Until then, a safe disposal method should be established for existing waste streams such as discussed in the paper.

AUTHOR'S PERSPECTIVE

In the authors' perspective, as emphasized by the conclusion, the integrated system can theoretically provide zero liquid discharge. Even in situations where it doesn't attain zero discharge, a simple environment-friendly disposal method such as direct discharge with the help of a diffuser will have a lesser amount of environmental impact. As seen in the integrated methods section, the recovery rates are higher than 90% and this can be improved further with increased efficiency and better research. The minimal amount of concentrate left can be disposed of with the help of environmental measures to direct discharge. The authors highly encourage this system but plenty of further research is needed in this arrangement.

ACKNOWLEDGMENT

The research and publication support provided by the Department of Chemical Engineering of R.V. College of Engineering along with the support from project coordinator Dr. M.A. Lourdu Antony Raj and Head of the Department Dr. Vinod Kallur is gratefully acknowledged.

REFERENCES

Abdul-Wahab and S. A. 2007. Characterization of water discharges from two thermal power/desalination plants in Oman. *Environmental Engineering Science*, 24(3): 321-337.

- Ahmed, M., Arakel, A., Hoey, D., Thumarukudy, M.R., Goosen, M.F.A., Al-Haddabi, M. and Al-Belushi, A. 2003. Feasibility of salt production from inland RO desalination plant rejects brine: A case study. *Desalination*, 158(1-3): 109-117.
- Al-Agha, M.R. and Mortaja, R.S. 2005. Desalination in the Gaza strip: Drinking water supply and environmental impact. *Desalination*, 173(2): 157-171.
- Badruzzaman, M., Oppenheimer, J., Adham, S. and Kumar, M. 2009. Innovative beneficial reuse of reverse osmosis concentrate using bipolar membrane electro dialysis and electrochlorination processes. *Journal of Membrane Science*, 326(2): 392-399.
- Bleninger, T. and Morelissen, R. 2015. Intakes and Outfalls for Seawater Reverse-Osmosis Desalination Facilities. In: *Environmental Science and Engineering book series (ESE)*. Proceedings of Innovation and Environmental Impacts. 397-449.
- Bond, R. and Veerapaneni, V. 2011. Zero liquid discharge desalination of brackish water with an innovative form of electro dialysis: Electro dialysis metathesis. In: *American Water Works Association Annual Conference and Exposition 2011, Proceedings of ACE 2011*, July, 4289-4317.
- Cao, F., Liu, Q. and Xiao, H. 2020. Experimental study of a humidification-dehumidification seawater desalination system combined with the chimney. *Int. J. Photoenergy*, 19: 704.
- Chelme-Ayala, P., Smith, D.W. and El-Din, M.G. 2009. Membrane concentrate management options: A comprehensive critical review. *Can. J. Civ. Eng.*, 36(6): 1107-1119.
- Chen, Q.B., Ren, H., Tian, Z., Sun, L. and Wang, J. 2019. Conversion and pre-concentration of SWRO reject brine into high solubility liquid salts (HSLs) by using electro dialysis metathesis. *Sep. Purif. Technol.*, 213(38): 587-598.
- Christie, S. and Bonn elye, V. 2009. Perth, Australia: Two-Year Feedback on the Operation and Environmental Impact. In: *IDA World Congress Dubai, UAE*. ftp://ftp.sccwrp.org/pub/download/DOCUMENTS/BrinePanel/Resources/Perth_2YrReport.pdf. Accessed 03/07/2020.
- Cohen, Y. and Kirchmann, H. 2004. Increasing the pH of wastewater to high levels with different gases - CO₂ stripping. *Water Air Soil Pollut.*, 159(1): 265-275.
- Deshmukh, A., Boo, C., Karanikola, V., Lin, S., Straub, A. P., Tong, T., Warsinger, D. M. and Elimelech, M. 2018. Membrane distillation at the water-energy nexus: Limits, opportunities, and challenges. *Energy and Environmental Science*, 11(5): 1177-1196.
- Doornbusch, G.J., Tedesco, M., Post, J.W., Borneman, Z. and Nijmeijer, K. 2019. Experimental investigation of multistage electro dialysis for seawater desalination. *Desalination*, 464: 105-114.
- Du, F., Warsinger, D.M., Urmi, T.I., Thiel, G.P., Kumar, A. and Lienhard, J.H. 2018. Sodium hydroxide production from seawater desalination brine: Process design and energy efficiency. *Environ. Sci. Technol.*, 52(10): 5949-5958.
- Fritzmann, C., L wenberg, J., Wintgens, T. and Melin, T. 2007. State-of-the-art of reverse osmosis desalination. *Desalination*, 216(1-3): 1-76.
- Gabelich, C.J., Williams, M.D., Rahardianto, A., Franklin, J.C. and Cohen, Y. 2007. High-recovery reverse osmosis desalination using intermediate chemical demineralization. *J. Membrane Sci.*, 301(1-2): 131-141.
- Gilron, J., Folkman, Y., Savliev, R., Waisman, M. and Kedem, O. 2003. WAIV - Wind aided intensified evaporation for reduction of desalination brine volume. *Desalination*, 158(1-3): 205-214.
- Greenlee, L.F., Lawler, D.F., Freeman, B.D., Marrot, B. and Moulin, P. 2009. Reverse osmosis desalination: Water sources, technology, and today's challenges. *Water Res.*, 43(9): 2317-2348.
- Hamieh, B.M. and Beckman, J. R. 2006. Seawater desalination using Dewvaporation technique: theoretical development and design evolution. *Desalination*, 195(1-3): 1-13.
- Hasson, D., Segev, R., Lisitsin, D., Liberman, B. and Semiat, R. 2011. High recovery brackish water desalination process devoid of precipitation chemicals. *Desalination*, 283: 80-88.

- Heihsel, M., Lenzen, M., Malik, A. and Geschke, A. 2019. The carbon footprint of desalination: An input-output analysis of seawater reverse osmosis desalination in Australia for 2005–2015. *Desalination*, 454: 71-81.
- Heijman, S.G.J., Guo, H., Li, S., van Dijk, J.C. and Wessels, L.P. 2009. Zero liquid discharge: Heading for 99% recovery in nanofiltration and reverse osmosis. *Desalination*, 236(1-3): 357-362.
- Herrero-Gonzalez, M., Admon, N., Dominguez-Ramos, A., Ibañez, R., Wolfson, A. and Irabien, A. 2020. Environmental sustainability assessment of seawater reverse osmosis brine valorization by means of electro dialysis with bipolar membranes. *Environ. Sci. Pollut. Res.*, 27(2): 1256-1266.
- Jibril, B.E.Y. and Ibrahim, A.A. 2001. Chemical conversions of salt concentrate from desalination plants. *Desalination*, 139(1-3): 287–295.
- Jones, E., Qadir, M., Van Vliet, M.T.H., Smakhtin, V. and Kang, S.M. 2019. The state of desalination and brine production: A global outlook. *Sci. Total Environ.*, 657: 1343-1356.
- Kazner, C., Jamil, S., Phuntsho, S.K., Shon, H., Wintgens, T. and Vigneswaran, S. 2014. Forward osmosis for the treatment of reverse osmosis concentrate from water reclamation: Process performance and fouling control. *Water Sci. Technol.*, 69(12): 2431-2437.
- Korngold, E., Aronov, L., Belayev, N. and Kock, K. 2005. Electro dialysis with brine solutions oversaturated with calcium sulfate. *Desalination*, 172(1): 63-75.
- Lawson, M. 1997. Membrane distillation. nanostructured polymer. *Membranes*, 1: 419-455.
- Leong, J., Tan, J., Charrois, J. and Ladewig, B.P. 2014. Review of high recovery concentrate management options. *Desal. Water Treat.*, 52(40-42): 7609-7627.
- Lew, C.H., Hu, J.Y., Song, L.F., Lee, L.Y., Ong, S.L., Ng, W.J. and Seah, H. 2005. Development of an integrated membrane process for water reclamation. *Water Sci. Technol.*, 51(6-7): 455-463.
- Liyanaarachchi, S., Jegatheesan, V., Shu, L., Shon, H.K., Muthukumar, S. and Li, C.Q. 2020. Evaluating the feasibility of forwarding osmosis in diluting ro concentrate using pretreatment backwash water. *Membranes*, 10(3): 65-89.
- Martinetti, C.R., Childress, A.E. and Cath, T.Y. 2009. High recovery of concentrated RO brines using forward osmosis and membrane distillation. *J. Membrane Sci.*, 331(1-2): 31-39.
- Mauguin, G. and Corsin, P. 2005. Concentrate and other waste disposals from SWRO plants: Characterization and reduction of their environmental impact. *Desalination*, 182(1-3): 355-364.
- McCutcheon, J.R. and Elimelech, M. 2006. Influence of concentrative and dilutive internal concentration polarization on flux behavior in forwarding osmosis. *Journal of Membrane Science*, 284(1-2): 237-247.
- Medeazza, M.G.L. 2005. Direct and socially-induced environmental impacts of desalination. *Desalination*, 185(1-3): 57-70.
- Mericq, J.P., Laborie, S. and Cabassud, C. 2010. Vacuum membrane distillation of seawater reverse osmosis brines. *Water Res.*, 44(18): 5260-5273.
- Micklely, M.C. 2006. Membrane concentrate disposal: practices and regulation. *Desal. Water Purif. Res. Develop. Program*, 123(69): 298.
- Missimer, T.M. and Maliva, R.G. 2018. Environmental issues in seawater reverse osmosis desalination: Intakes and outfalls. *Desalination*, 434: 198-215.
- Mondal, P., Yadav, B.P. and Siddiqui, N.A. 2020. Removal of lead from drinking water by bioadsorption technique: an eco-friendly approach. *Nat. Environ. Poll. Techn.*, 19(4): 1675-1682.
- Morillo, J., Usero, J., Rosado, D., El Bakouri, H., Riaza, A. and Bernaola, F.J. 2014. Comparative study of brine management technologies for desalination plants. *Desalination*, 336(1): 32-49.
- Ng, H.Y., Lee, L.Y., Ong, S.L., Tao, G., Viawanath, B., Kekre, K., Lay, W. and Seah, H. 2008. Treatment of RO brine-towards sustainable water reclamation practice. *Water Sci. Technol.*, 58(4): 931-936.
- Ning, R.Y. and Troyer, T. L. 2009. Random reverse osmosis process for zero-liquid discharge. *Desalination*, 237(1-3): 238-242.
- Office, D. 2003. Novel Membrane And Device For Direct Contact Membrane Distillation-Based Desalination Process : Phase Ii New Jersey Institute of Technology. New Jersey Institute of Technology, Newmark. <https://www.usbr.gov/research/dwpr/reportpdfs/report096.pdf>. Accessed 06/06/2020
- Ordóñez, R., Moral, A., Hermsilla, D. and Blanco, A. 2012. Combining coagulation, softening, and flocculation to dispose of reverse osmosis retentates. *J. Ind. Eng. Chem.*, 18(3): 926-933.
- Panagopoulos, A., Haralambous, K.J. and Loizidou, M. 2019. Desalination brine disposal methods and treatment technologies: A review. *Sci. Total Environ.*, 693: 133545.
- Pérez-González, A., Urriaga, A. M., Ibañez, R. and Ortiz, I. 2012. State of the art and review on the treatment technologies of water reverse osmosis concentrates. *Water Res.*, 46(2): 267-283.
- Peters, T., Pintó, D. and Pintó, E. 2007. Improved seawater intake and pre-treatment system based on Neodren technology. *Desalination*, 203(1-3): 134-140.
- Qasim, M., Badrelzaman, M., Darwish, N.N., Darwish, N.A. and Hilal, N. 2019. Reverse osmosis desalination: A state-of-the-art review. *Desalination*, 459: 59-104.
- Qu, D., Wang, J., Wang, L., Hou, D., Luan, Z. and Wang, B. 2009. Integration of accelerated precipitation softening with membrane distillation for high-recovery desalination of primary reverse osmosis concentrate. *Sep. Purif. Technol.*, 67(1): 21-25.
- Rautenbach, R. and Linn, T. 1996. High-pressure reverse osmosis and nanofiltration, a “zero discharge” process combination for the treatment of wastewater with severe fouling/scaling potential. *Desalination*, 105(1-2): 63-70.
- Sanza, M.A., Bonnelyea, V. and Cremerb, G. 2007. Fujairah reverse osmosis plant: 2 years of operation. *Desalination*, 203(1-3): 91-99.
- Schantz, A.B., Xiong, B., Dees, E., Moore, D.R., Yang, X. and Kumar, M. 2018. Emerging investigators series: Prospects and challenges for high-pressure reverse osmosis in minimizing concentrated waste streams. *Environ. Sci.: Water Res. Technol.*, 4(7): 894-908.
- Segev, R., Hasson, D. and Semiat, R. 2011. Improved high recovery brackish water desalination process based on fluidized bed air stripping. *Desalination*, 281(1): 75-79.
- Shaffer, D.L., Yip, N.Y., Gilron, J. and Elimelech, M. 2012. Seawater desalination for agriculture by integrated forward and reverse osmosis: Improved product water quality for potentially less energy. *J. Membr. Sci.*, 415-416: 1-8.
- Shahmansouri, A., Min, J., Jin, L. and Bellona, C. 2015. Feasibility of extracting valuable minerals from desalination concentrate: A comprehensive literature review. *J. Clean. Prod.*, 100: 4-16.
- Sorour, M.H., Hani, H.A., Shaalan, H.F. and Al-Bazedi, G.A. 2015. Schemes for salt recovery from seawater and RO brines using chemical precipitation. *Desal. Water Treat.*, 55(9): 2398-2407.
- Strathmann, H. 2010. Electro dialysis, a mature technology with a multitude of new applications. *Desalination*, 264(3): 268-288.
- Subramani, A. and Jacangelo, J.G. 2014. Treatment technologies for reverse osmosis concentrate volume minimization: A review. *Sep. Purif. Technol.*, 122: 472-489.
- Tran, A.T.K., Zhang, Y., Jullok, N., Meesschaert, B., Pinoy, L. and Van der Bruggen, B. 2012. RO concentrate treatment by a hybrid system consisting of a pellet reactor and electro dialysis. *Chem. Eng. Sci.*, 79: 228-238.
- Tularam, G.A. and Ilahee, M. 2007. Environmental concerns of desalinating seawater using reverse osmosis. *J. Environ. Monit.*, 9(8): 805-813.
- Turek, M., Was, J. and Dydo, P. 2009. Brackish water desalination in RO-single pass EDR system. *Desal. Water Treat.*, 7(1-3): 263-266.
- Voutchkov, N. 2011. Overview of seawater concentrate disposal alternatives. *Desalination*, 273(1): 205-219.

- Xianhui, L., Hasson, D., Semiat, R. and Shemer, H. 2019. Intermediate concentrate demineralization techniques for enhanced brackish water reverse osmosis water recovery: A review. *Desalination*, 466: 24-35.
- Xinyang, L., Zhang, L. and Wang, C. 2012. Review of disposal of concentrate streams from nanofiltration (NF) or reverse osmosis (RO) membrane process. *Adv. Mater. Res.*, 518-523: 3470-3475.
- Xu, P., Cath, T.Y., Robertson, A.P., Reinhard, M., Leckie, J.O. and Drewes, J. E. 2013. A critical review of desalination concentrates on management, treatment, and beneficial use. *Environ. Eng. Sci.*, 30(8): 502-514.
- Xu, P., Cath, T., Wang, G. and Dolnicar, S. 2009. Critical Assessment of Implementing Desalination Technology. The Drinking Water Inspectorate. <http://dwi.defra.gov.uk/research/completed-research/reports/dwi70-2-208exsum.pdf>. Accessed 12/07/20
- Younos, T. 2005. Environmental issues of desalination. universities council on water resources. *J. Contemp. Water Res. Educ.*, 132: 11-18.
- Zhang, S., Wang, K.Y., Chung, T.S., Jean, Y.C. and Chen, H. 2011. Molecular design of the cellulose ester-based forward osmosis membranes for desalination. *Chem. Eng. Sci.*, 66(9): 2008-2018.



Geochemical Characterization and Saturation Index (SI) in the Montebello Lagunar System Liquidambar Lagoon, Chiapas Mexico

J. R. Reyes-Santiago, L. A. García-Villanueva†, G. Fernández-Villagómez and P. Guzmán-Guadarrama

Department of Sanitary and Environmental Engineering, Engineering School, National Autonomous University of Mexico, Mexico

Corresponding author: L.A.García-Villanueva; lagvillanueva@ingenieria.unam.edu

Nat. Env. & Poll. Tech.
Website: www.neptjournal.com

Received: 20-06-2020

Revised: 30-09-2020

Accepted: 18-10-2020

Key Words:

Agricultural waste
Erosion risk
Loss of fertile soil
Water quality

ABSTRACT

The “Lagunas de Montebello” National Park located in Chiapas, Mexico, is well known for its crystal blue water bodies, some of which, in 2003, started to change color from crystalline to cloudy brown, and occasionally emit a foul smell, contains white-yellowish supernatant debris and dead fish. To determine the causes of the changes in the water characteristics of the “Liquidambar” lagoon of the Montebello lagoon system, a physicochemical characterization was carried out over the first six meters of the water column, together with geochemical speciation analysis and the saturation index calculation for different minerals. Water was classified as calcium-sulfated and the main mechanism that controlled its chemistry was rocks dissolution. Sulfide was found at all sampled depths in the range of 0.11 to 1.13 mg.L⁻¹. The concentration of sulfate in the water column ranged from 249.21 to 298.7 mg.L⁻¹, carbonate ranged from 140.5 to 261.4 mg.L⁻¹, calcium and magnesium ranged from 94.5 to 146.9 mg.L⁻¹ and 34.2 to 38.3 mg.L⁻¹, respectively. Likewise, oxygen was also found to be oversaturated on the surface with a value of 9.32 mg.L⁻¹. The speciation results and SI indicated that the mineral phases calcite, aragonite, and dolomite were oversaturated, being greater on the surface. The results suggested the possibility that the turbidity, the coloration change, and the whitish supernatant were due to the precipitation of carbonate minerals, microbiologically influenced by the photosynthetic activity in the upper layer of the lagoon water.

INTRODUCTION

Geochemistry studies the redistribution of the elements and compounds through natural and anthropogenic environments, and in the case of water, it studies the processes that control its chemical composition. These processes are identified through the analysis of the water physicochemical parameters, which allows identifying characteristics acquired by its interaction with geological mediums such as quality, origin, the type of rocks through which it flows, its flow patterns, and even the residence time in the watershed and aquifers (Appelo & Postma 2005, García et al. 2014, Nordstrom & Campbell 2014)

The main processes that control water chemistry are atmospheric precipitation, dissolution of the crust minerals, and evaporation (Appelo & Postma 2005, Marandi & Shand 2018, Zhu & Schwartz 2010).

Some other mechanisms that modify the water chemistry are processes that involve chemical reactions, such as silicates dissolution, which requires acid-base reactions, redox reactions, most of them biologically assisted, that exert a significant influence over some elements such as O, C, S,

N, and Fe. Ion exchange and absorption can also be mentioned as processes that influence water chemistry (Appelo & Postma 2005, Singhal & Gupta 2010, Stumm 2007, Zhu & Schwartz 2010).

The dissolution and precipitation of minerals, as well as ion exchange, are rapid processes that are controlled by chemical equilibrium. On the contrary, redox transformations and silicates dissolution, are slow processes and controlled by kinetics. The majority of water solutes produced by the above-described processes are Ca²⁺, Na⁺, Mg²⁺, K⁺, HCO₃⁻, Cl⁻, SO₄²⁻ and H₄SiO₄ and the source of these is described in Table 1 (Zhu & Schwartz 2010).

Mineral saturation calculations using the saturation index (SI) can assist in predicting the existence of reactive minerals. This is defined as (Appelo & Postma 2005):

$$SI = \log (IAP/K_{sp})$$

Where IAP is the ion activity product, which is obtained from the water chemical analysis, and K_{sp} is the solubility product constant. When SI=0, the balance between dissolved ions and a solid mineral has been reached, that is, saturation has been reached. On the other hand, SI>0 indicates over-

Table 1: Origin of the main chemical water components.

Component	Source
Na ⁺	Feldspar, rock salt, zeolite, atmosphere, cation exchange
K ⁺	Feldspar, mica
Mg ²⁺	Dolomite, serpentite, pyroxene, amphibole, olivine, mica
Ca ²⁺	Carbonate, gypsum, feldspar, pyroxene, amphibole
Cl ⁻	Rock salt, atmosphere
HCO ₃ ⁻	Carbonates, organic matter
SO ₄ ²⁻	Atmosphere, gypsum, sulfides
NO ₃ ⁻	Atmosphere, organic matter
Si	Silicate
Fe ²⁺	Silicates, Siderite, Hydroxides, Sulfides
PO ₄ ³⁺	Organic matter, phosphates

Source: Appelo & Postma (2005)

saturation, so the mineral will tend to precipitate to achieve balance. When $SI < 0$, water is under saturated with respect to the mineral phase, so it will tend to dissolve until the balance is reached (Appelo & Postma 2005).

Mineral precipitation occurs when the *IAP* that compose it, exceeds the *Kps*. For precipitation to occur, an oversaturation condition must exist. In natural water bodies, it has been observed that an $SI > 1$ is required, i.e., the *IAP* is 10 times the value of *Kps* (Appelo & Postma 2005, Dupraz et al. 2009, Homa & Chapra 2011).

The minerals precipitation mediated by microorganisms can be classified according to their degree of intervention in the process. The secretion of one or more metabolic by-products that react with ions or chemicals in the environment, resulting in mineral particle deposition, is known as biologically induced precipitation. It is especially significant in anaerobic environments or oxic-anoxic interfaces because the source of electron acceptors are sulfates and/or various metals including iron and manganese. On the other hand, biologically controlled precipitation is that in which biological activity controls nucleation, growth, morphology, and the final location of minerals; some examples of it are the formation of shells and exoskeletons. Finally, biologically influenced precipitation is that in which environmental parameters, rather than microbial activity, are responsible for precipitation. In this case, microorganisms exercise some influence over the environment, leading to precipitation, for example, the carbon minerals precipitation derived from the increase of pH generated by photosynthesis (Dupraz et al. 2009, Homa & Chapra 2011).

Photosynthesis is one of the most effective biological processes in biologically influenced precipitation in aquatic

environments with hard water. Photosynthetic carbon fixation removes CO₂ from the environment, sometimes at a faster rate than the diffusion replacement to the higher activity layer, resulting in HCO₃⁻ dissociating to CO₂ and OH⁻ raising the pH and favoring the precipitation of CaCO₃. At the same time, CO₂ removal displaces the balance towards calcium carbonate formation. The net reaction of CaCO₃ photosynthesis and precipitation process is (Dupraz et al. 2009, Homa & Chapra 2011, Karami et al. 2019).



The CaCO₃ formation has more than one environmental impact, since calcite precipitation, when oversaturated, causes reduction of water clarity (Karami et al. 2019, Walsh et al. 2019)

Abiotically, the physicochemical processes that lead to precipitation are: water evaporation (which concentrates the ions until reaching saturation), and degassing (which modifies the carbonates balance favoring precipitation) (Dupraz et al. 2009).

The “Lagunas de Montebello” National Park, located in the state of Chiapas, Mexico, is a protected natural area that houses a karstic origin lagoon system formed by approximately sixty lagoons that vary in size and shape. The park houses some of the most beautiful scenery in the Mexican territory, largely for the water color and clarity of its lagoons (Durán et al. 2014, IMPLAN Comitán 2015).

For decades, the region’s socio-economic pressure to land-use change, deforestation, the increase in agricultural and livestock activities, as well as the increase of population, have altered water quality in the basin (IMPLAN Comitán 2015, Mora et al. 2017).

In 2003, residents of the Liquidambar Lagoon area began to report water changes in the coloration and transparency of the water, as well as whitish-yellow supernatant debris, bubbling, foul odor, and fish death. This phenomenon, with the passage of time, has been identified in other lagoons too, and it commonly occurs between December to February (Alcocer et al. 2016, 2018, García et al. 2014, IMPLAN Comitán 2015, Mora et al. 2017, Oseguera & Alcocer 2016).

Studies have been carried out for the physical, chemical, biological and toxicological characterization of the Lagunar System of Montebello, Chiapas. However, the causes of spatial and temporal change in the water quality of the lagoons have not been identified (CONAGUA – CONACYT 2013).

STUDY AREA

The Lagunas de Montebello National Park is in the state of Chiapas in Mexico and borders Guatemala. It is delimited by the coordinates 16°5' and 16°10' latitude and 91°38' and 91°97' longitude (Fig. 1). It covers an area of approximately 61 km², and it is located at the southeastern end of the Río Grande basin in Comitán (CONAGUA - CONACYT 2013, Durán et al. 2014, Mora et al. 2017).

This region's climate is semi-humid temperate with rainfall all year long, the total average precipitation is 1800 mm, and the annual average temperature is 17°C. The Montebello Lagunar System is composed of about sixty lagoons, some of which are superficially connected. However, the waters that feed the system are mainly underground and are part of the

Río Grande basin in Comitán (Durán et al. 2014, IMPLAN Comitán 2015, Mora et al. 2017).

The soil of the system is predominantly composed of sedimentary cretaceous rocks, chemically limestone, and dolomites. At greater depth, paleocene turbidite can be found. Finally, there are Eocene and Miocene units composed of continental clastic deposits (Durán et al. 2014, Mora et al. 2016).

The Lagunar system of Montebello Park is composed of 50-60 water bodies. Some of the main bodies are Balametik, Liquidambar, San Lorenzo, Yalmuz, Bosque Azul, Monte Bello, Cinco Lagos, Pojoj, Tzisco, and Dos Lagunas, which stand out for their size, morphology, and economic importance, as well as for being subjects of study (Alcocer et al. 2016, Mora et al. 2017).

According to their water chemistry, the lagoons can be classified into two large groups: lagoons with carbonate calcium water and lagoons with sulfate calcium water. The lagoons in the first group receive the discharge from the Río Grande, and have been classified as eutrophic, and mesotrophic (Durán et al. 2014, Mora et al. 2017, Vera et al. 2015).

MATERIALS AND METHODS

Sampling

The sampling was performed in the Liquidambar Lagoon in July of 2018. The change of color was observed for the

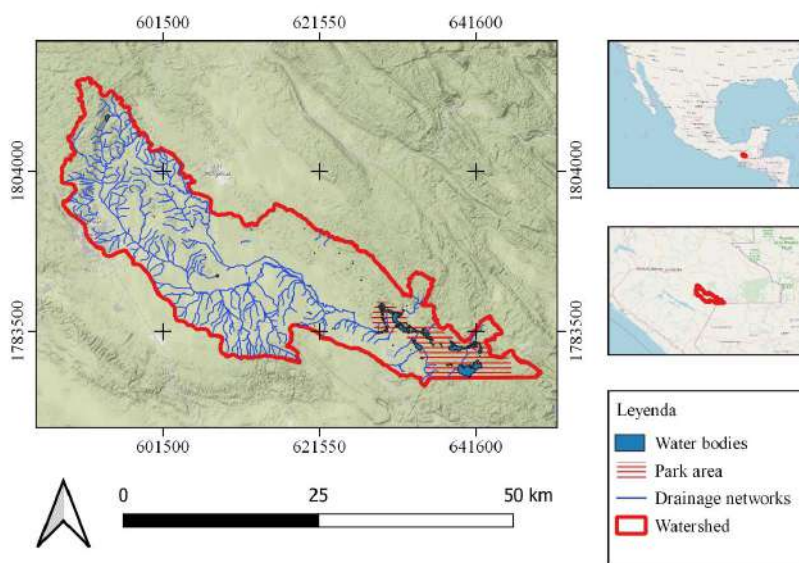


Fig. 1: Geographical location of the Lagunas de Montebello National Park

Source: Modified from SIATL-INEGI

first time in this lagoon (Vera et al. 2015). The sampling point coordinates are latitude 1786736, length 629915, UTM projection; Datum WGS 84 (Fig. 2), with an elevation of 1457 masl.

The samples were taken with a Van Dorn bottle, at 7 different depths, the first at 0.5 m under the water mirror and later at 1, 2, 3, 4, 5, and 6 m. They were filtered through a 0.45-micron nitrocellulose membrane of 25 mm diameter. To provide pressure, swinnex filter holders and a 5 mL syringe were used. Samples taken for ion analysis were stored in 50 mL corning polypropylene centrifuge tubes.

For the sulfide samples, 8 drops of 2N zinc acetate were added as a preservative and 4 drops of NaOH 6N to bring the sample to a pH above 8, and ensure that the sulfides remain dissolved when the zinc sulfide precipitate is formed.

For the biochemical oxygen demand (BOD_5), chemical oxygen demand (COD), and alkalinity tests, one-liter polypropylene bottles were filled completely, without leaving air space. The samples were kept on ice until analysis.

Sample Characterization.

For the field parameters (temperature, pH, dissolved oxygen (DO), redox potential (EH)) a multiparametric Hanna Instruments model HI 9829 probe was used.

Alkalinity was determined by volumetric titration using HCl 0.02N to the turn of bromocresol green; the determina-

tion was made within 7 h after the first sampling.

The dissolved anions and cations, except for sulfide, were analyzed using the chromatography technique of ions with conductometric detection.

The ion sulfide concentration determination was done by reverse titration. An excess iodine solution of 0.0025N was added to the sample to react with the sulfide, then the remaining iodine was titrated with sodium thiosulphate 0.0025N ($Na_2S_2O_3$) using starch as an indicator, method 4500-S2- F (Clescerl et al. 1999). The COD was analyzed using the Hach reagent kit "COD ultra-low range" which has a measurement range of 1 to 40 $mg.L^{-1}$ and consists of a closed reflux test.

The ultimate carbonaceous biochemical oxygen demand (U-CBOD) was performed using Winkler bottles following the technique for BOD_5 (5210 B) using 2-chloro-6-(trichloromethyl) pyridine (TCMP 2-Chloro-6-(trichloromethyl) pyridine) as nitrification inhibitor, and resaturating oxygen when it reached 2 $mg.L^{-1}$ values, (Clescerl et al. 1999). The values were taken for 60 days until there was no more oxygen consumption. An equipment YSI model 58 YSI was used for measuring DO.

Modeling Focus

Before starting the analysis and interpretation of the data, the review of the chemical data quality collected during

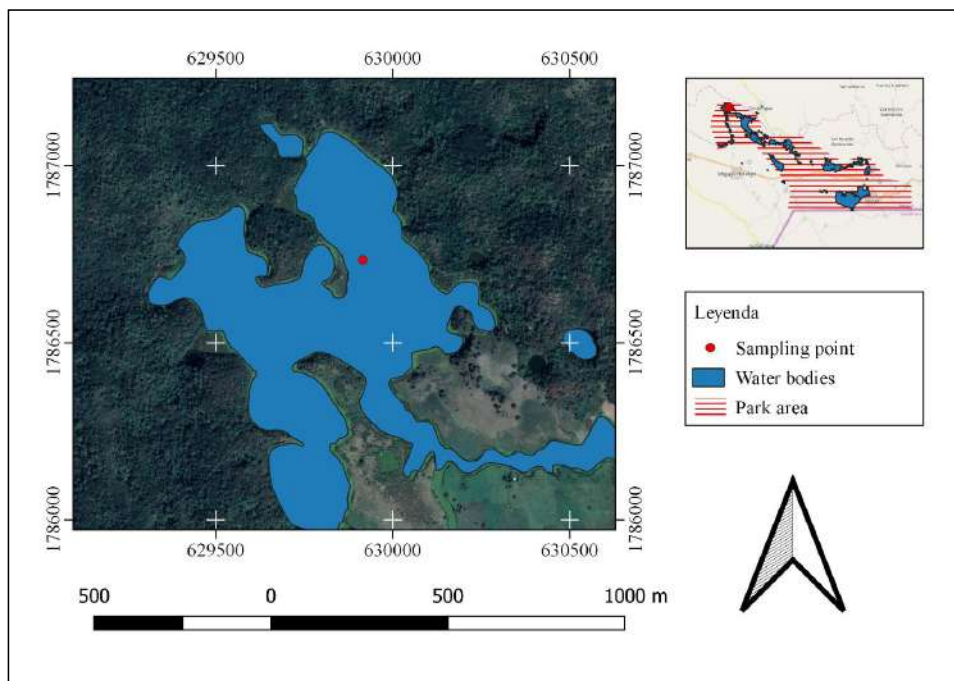


Fig. 2: Sample site.

sampling and samples characterization is necessary. The ionic balance of the collected samples had an error of less than 5% in all cases (Zhu & Anderson 2010). To identify the family to which water belongs, and the geochemical processes that control the water chemistry in the Liquidambar lagoon, chemical data was used to generate diagrams of Piper, Gibbs, and Stiff.

To determine whether the minerals in the water precipitate, dissolve, or are in balance, a geochemical speciation analysis was performed, and saturation rates of minerals of interest and those that might be present were obtained, using the numerical model PHREEQC version 3.0 and the minteqv4 database (Parkhurst & Appelo 2013).

RESULTS AND DISCUSSION

Physicochemical Characterization of Water

Table 2 shows the Liquidambar lagoon water physico-chemical characteristics sampled in July 2018. The lagoon was found stratified with clinogram profiles for temperature, pH, EH, DO, Cl⁻, Na⁺, and K⁺. The properties that showed ortho profiles were TDS, EC, U-CBOD, COD, alkalinity, S²⁻, HCO₃⁻, SO₄²⁻, Ca²⁺ and Mg²⁺.

The clines, or change areas, were observed at different depths, being able to categorize the properties in two groups

according to the observed profile, from 2 to 5 m, for temperature, pH, alkalinity, TDS, EC, and EH, and from 4 to 5 m, for Cl⁻, Mg²⁺, Ca²⁺, HCO₃⁻, Na⁺, SO₄²⁻ and K⁺.

The concentration variations between the surface and the 6 m were 120.9 mg.L⁻¹ for bicarbonates, 52.4 mg.L⁻¹ for calcium, 49 mg.L⁻¹ for sulfates, 4.06 mg.L⁻¹ for magnesium, -2.86 mg.L⁻¹ for sodium, -0.28 mg.L⁻¹ for potassium, and at last, -0. mg.L⁻¹ for chlorides and 1.01 for S(II-).

The NO₃⁻, NO₂⁻, PO₄³⁻, Br⁻, F⁻ concentrations were found below the technique detection limit and could not be determined. The NH₄⁺ could be found at 5 and 6-m depth with values of 2.05 and 2.25 mg.L⁻¹ respectively- at the upper points the concentration was below the detection limit.

For physicochemical properties, these variations were -1.06 for pH, -3.3°C for temperature, 222.8 mg.L⁻¹ for TDS, 86 mg.L⁻¹ for alkalinity, and -406 for EH. The variation reported by DO was 6.01 mg.L⁻¹, while for dissolved U-CBOD it was 7.5 mg.L⁻¹.

The different profiles developed from the variables of the Laguna Liquidambar water are shown in Fig. 3.

Hydrogeochemical Classification

The Piper graph (Fig. 4) shows that water from the Liquidambar Lagoon can be classified as sulfated calcium-type

Table 2: Summary of the main physiochemical characteristics of the water in Laguna Liquidambar.

Sample	Depth [m]	T [°C]	pH	TDS [ppm]	EC [µS.cm ⁻¹]	EH [mV]	U-CBOD [mg.L ⁻¹]	Alkalinity [mg.L ⁻¹]	DO [mg.L ⁻¹]
L0	0.5	25.5	8.3	543.7	414.0	400.9	305.5	90.0	9.3
L1	1.0	25.3	8.2	541.8	408.0	394.6	260.7	92.0	6.9
L2	2.0	25.4	8.2	538.9	409.0	406.7	239.4	92.0	6.0
L3	3.0	24.3	7.7	579.9	429.0	76.5	249.2	118.0	5.5
L4	4.0	23.6	7.7	614.9	448.0	33.7	198.5	124.0	5.0
L5	5.0	22.9	7.2	734.8	506.0	-4.2	351.6	168.0	3.8
L6	6.0	22.2	7.3	766.5	526.0	-5.1	508.2	176.0	3.3

Table 2 Cont....

Sample	Depth [m]	S ²⁻ [mg.L ⁻¹]	HCO ₃ ⁻ [mg.L ⁻¹]	Cl ⁻ [mg.L ⁻¹]	SO ₄ ²⁻ [mg.L ⁻¹]	Na ⁺ [mg.L ⁻¹]	K ⁺ [mg.L ⁻¹]	Ca ²⁺ [mg.L ⁻¹]	Mg ²⁺ [mg.L ⁻¹]
L0	0.5	0.11	140.5	9.9	249.6	11.9	3.1	94.5	34.2
L1	1.0	0.11	136.3	10.2	251.8	11.4	3.1	94.6	34.3
L2	2.0	0.15	132.7	11.1	249.2	11.8	4.3	95.3	34.4
L3	3.0	0.16	160.3	12.2	252.6	11.5	3.5	105.5	34.4
L4	4.0	0.18	181.4	10.6	260.5	11.7	3.0	112.2	35.5
L5	5.0	0.84	229.2	9.2	302.1	8.7	3.0	144.4	38.2
L6	6.0	1.13	261.4	9.3	298.7	9.0	2.8	146.9	38.3

water (Singhal & Gupta 2010). Likewise, it is observed that all samples are located in areas 1, 4, and 6 of the diagram, so it can be noticed that the alkaline earth elements exceed the alkaline, the strong acids exceed the weak acids, and the carbonated hardness exceeds 50%.

The Liquidambar Lagoon water is located in the “Rock Dominance” area, according to the Gibbs graph (Fig. 5), as the process that controls the water chemistry is the dissolution of the medium, which indicates that the water in the lagoon is partially in equilibrium with the basin material (Appelo & Postma 2005, Marandi & Shand 2018).

In the Stiff graph (Fig. 6) it can be observed that at greater depth the calcium, magnesium, bicarbonate, and sulfate ions have a higher concentration. For sodium, potassium, and chlorides there is a slight decrease as depth increases.

Similarly, the graphs for Piper, Stiff (Fig. 5 and Fig. 6) show that surface water, compared to bottom water, has a lower concentration of total dissolved solids. This variation can be attributed to rainwater since, in the Gibbs graph (Fig. 4). Surface samples move away to the area where the main mechanism controlling the water chemistry is atmospheric

precipitation. The Stiff graph also shows that sodium and chlorides increase their concentration as they approach the surface, indicating atmospheric input (Appelo & Postma 2005, Singhal & Gupta 2010).

Saturation State

The results show that all the depths studied are oversaturated with respect to the calcite mineral phase, having on the surface the maximum value, which is 0.86. On the other hand, the samples showed oversaturation with respect to the mineral phase's aragonite and dolomite (ordered and disorderly) in the first 4 m of the water column, having a maximum of 0.68 for aragonite and 1.66 for ordered dolomite. The SI of the three calcium minerals decreases with respect to depth.

On the other hand, the SI for gypsum is between -1.19 and -0.98, indicating that the gypsum dissolution process can continue (Appelo & Postma 2005).

The saturation index calculation results suggest that a carbonate precipitation bleaching event may happen (whiting event), which is a phenomenon that occurs in the water column of hard water lakes during the productive warm pe-

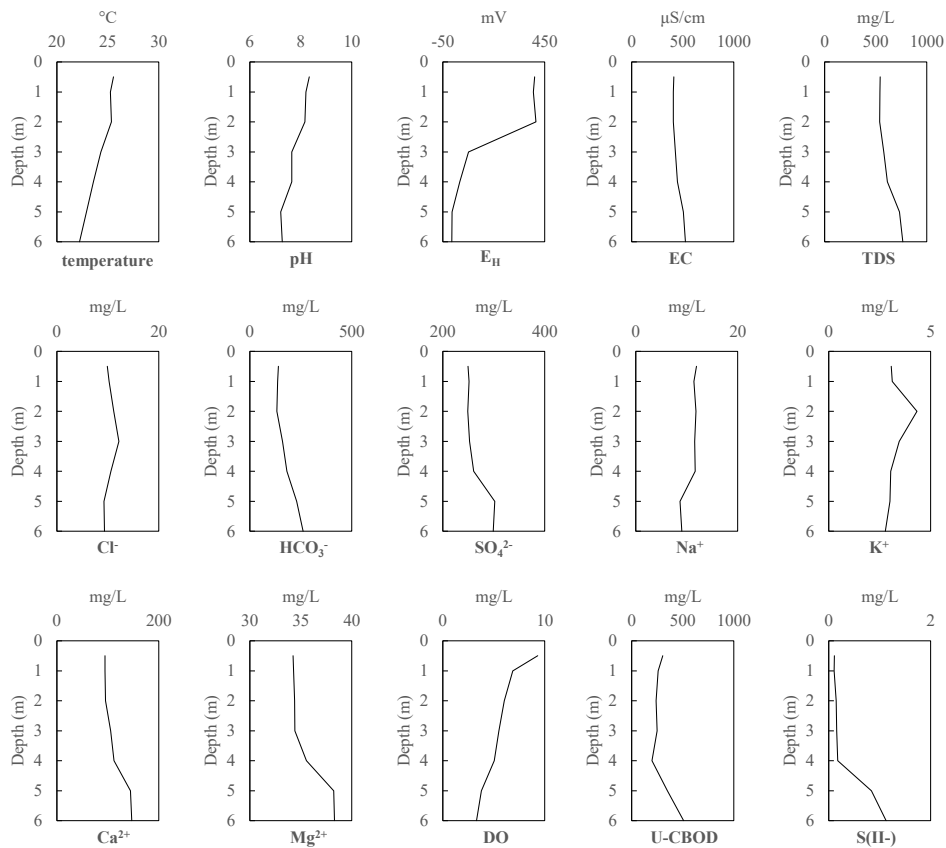


Fig. 3: Physicochemical properties profiles for water in the Liquidambar Lagoon.

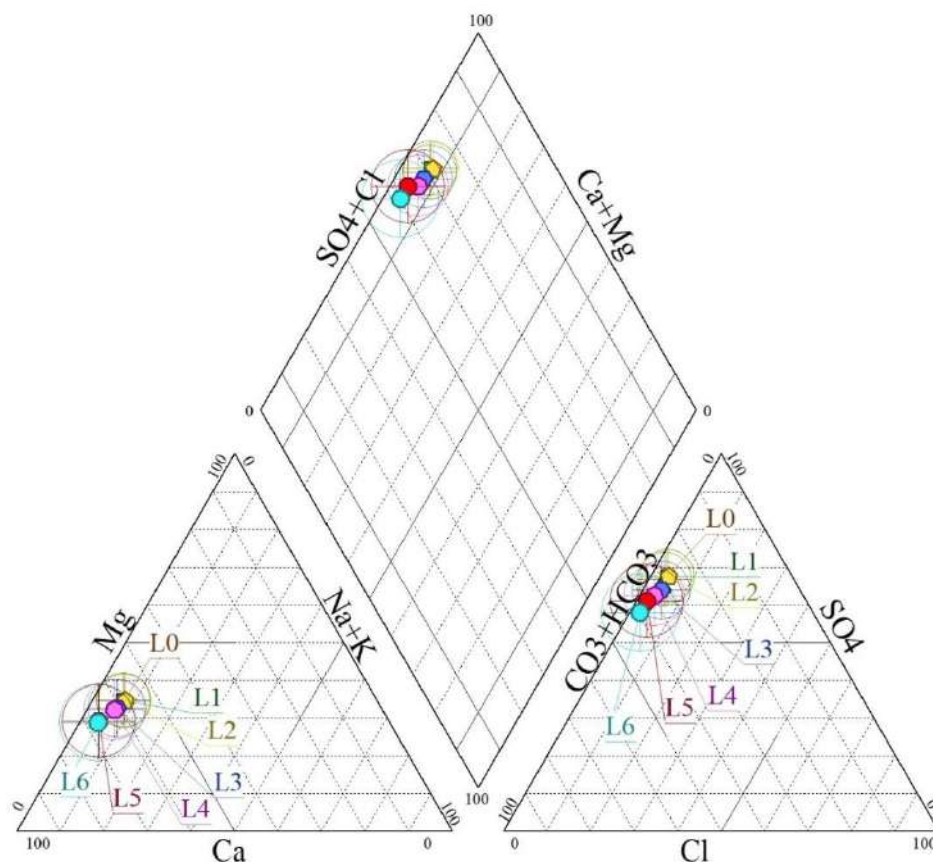


Fig. 4: Piper diagram of the water in Liquidambar Lagoon.

riod. This is one of the forms of internal inorganic particles production that provides turbidity and is a light attenuation component (Dupraz et al. 2009, Karami et al. 2019, Walsh et al. 2019).

Some studies indicate that carbonate precipitation occurs both biotically and abiotically induced, being photosynthesis, the process that most influences carbonate mineral precipitation, by increasing pH dissociating bicarbonate (HCO_3^-) into carbon dioxide (CO_2) and hydroxide ions (OH^-), which in turn reduces the solubility of carbonate minerals. Likewise, degassing CO_2 is another process that impacts the solubility of carbonates by altering the equilibrium of the dissolution reaction of CaCO_3 (Dupraz et al. 2009).

As shown in Table 2, the pH is higher on the surface and descends with depth, which explains a higher SI of carbonate minerals on the surface (Appelo & Postma 2005). Likewise, the oxygen oversaturation on the surface with a value of 9.32 mg.L^{-1} (Table 2) suggests photosynthetic activity, so this could be the cause of the increase in pH. Finally, speciation results show that the concentration of CO_2 in lagoon water

exceeds saturation. According to Henry's law, the partial atmospheric CO_2 pressure that would correspond to the CO_2 concentration of water is $6.02 \times 10^{-4} \text{ atm}$, considering the partial atmospheric CO_2 pressure of $4.08 \times 10^{-4} \text{ atm}$. This suggests that the degassing process is occurring, which would be an additional factor contributing to the increase in SI on the surface (Dupraz et al. 2009, Karami et al. 2019, Stumm 2007).

A graphical comparison of the SI profiles in the water column (Table 3, Fig. 7) shows the effect of depth on the SI of the main mineral phases in the water of the Liquidambar lagoon.

Redox Conditions (State)

According to the results, the EH in the water column is in the reduction range for O_2 , Mn^{4+} , Fe^{2+} and NO_3^- , as well as organic matter oxidation and in S^{2-} . Two changes can be observed in the EH profile trend corresponding to the $\text{Fe}^{3+}/\text{Fe}^{2+}$ and $\text{NO}_3^-/\text{NH}_4^+$ transformations, which occur in the 100mV and 400mV areas (Fig. 8) (Appelo & Postma 2005, Stumm 2007).

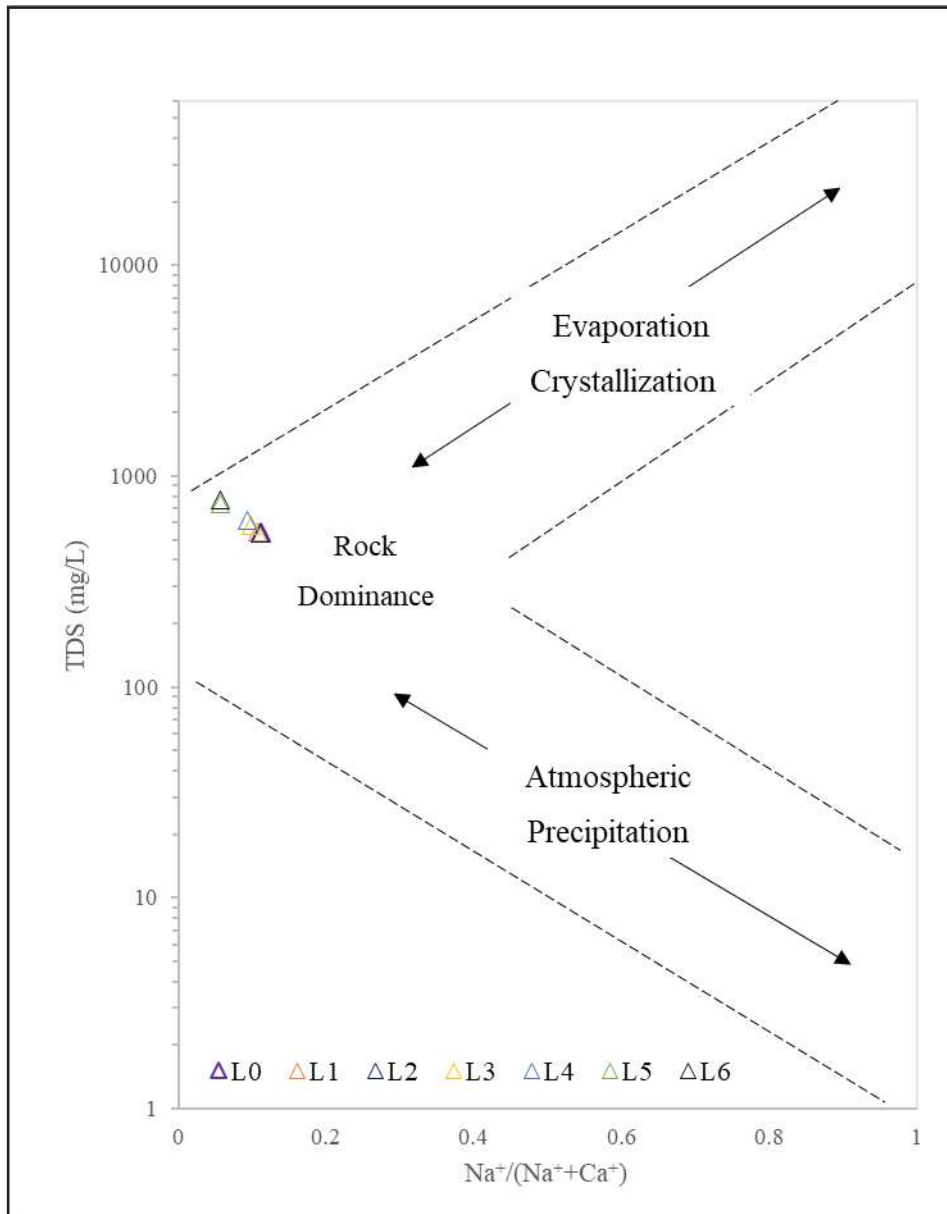


Fig. 5: Gibbs' diagram of water in the Liquidambar Lagoon.

Furthermore, S^{2-} was also observed in all the depths sampled, in coexistence with O_2 , so the suboxic zone was not defined (Murray et al. 1989). ($[\text{O}_2] < 3\mu\text{M}$; $[\text{S}^{2-}] < 0.2\mu\text{M}$). Minimal concentrations were found at $103\mu\text{M}$ for O_2 and $3.5\mu\text{M}$ for S^{2-} . Due to the presence of oxygen, it is unlikely that the sulfate reduction reaction is occurring at the sampled depth, on the contrary, the coexistence of these turns out to be uncommon due to the oxygen presence, S^{2-} is rapidly oxidized (Hargrave et al. 2008). This coexistence occurs

in oxy-anoxic transition zones mainly in sediments though, it has been observed also in the water column. Sulfide is rarely observed within anoxic environments (Findlay et al. 2014, Knossow et al. 2015), so it can be assumed that S^{2-} is the result of diffusion transport or a recent mixing event in the water column.

Carbonaceous dissolved oxygen demand was found to be almost constant up to 4 m deep, where it increased substantially, possibly due to oxygen depletion.

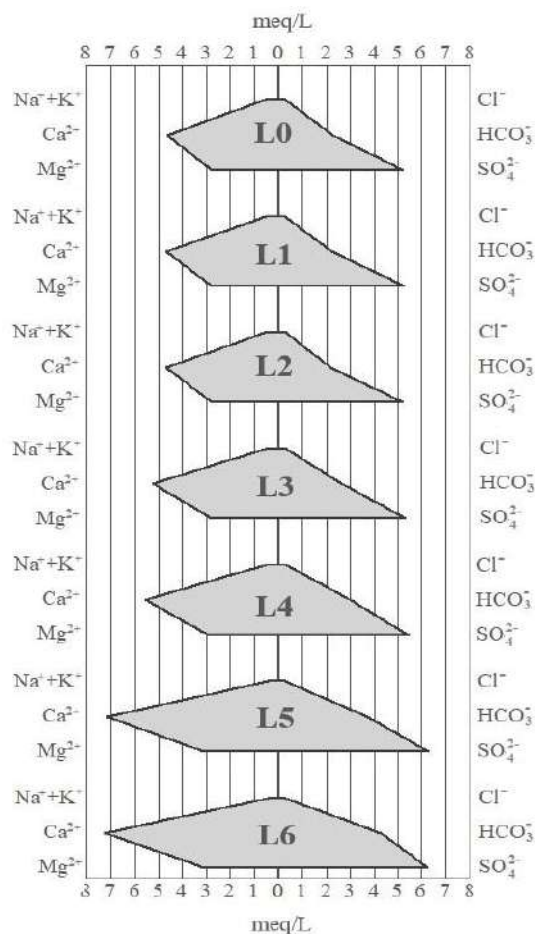


Fig. 6: Stiff diagram of the water in the Liquidambar lagoon

Table 3: SI of the main mineral phases in the water at the Liquidambar lagoon

Sample	Depth [m]	Anhydrite	Aragonite	Calcite	Dolomite [disordered]	Dolomite [ordered]	Gypsum	Huntite	Magnesite
L0	0.5	-1.44	0.68	0.86	1.11	1.66	-1.19	-1.08	-0.37
L1	1	-1.43	0.54	0.72	0.83	1.38	-1.18	-1.66	-0.5
L2	2	-1.43	0.5	0.68	0.74	1.29	-1.18	-1.84	-0.55
L3	3	-1.39	0.09	0.27	-0.14	0.41	-1.14	-3.65	-0.99
L4	4	-1.37	0.15	0.34	-0.04	0.52	-1.11	-3.46	-0.92
L5	5	-1.24	-0.14	0.05	-0.7	-0.15	-0.98	-4.88	-1.28
L6	6	-1.24	-0.02	0.17	-0.49	0.08	-0.98	-4.45	-1.15

CONCLUSION

Based on the results it is concluded that the mineral phases of aragonite, calcite and dolomite are oversaturated so turbidity, color change, and whitish supernatant could be due to the precipitation of carbonate minerals, microbiologically

influenced by photosynthesis activity in the upper layer of lagoon water.

Likewise, foul odor and death of fishes may happen due to the presence of sulfides in the surface layer of the lagoon, as well as their release during the mixing periods in the win-

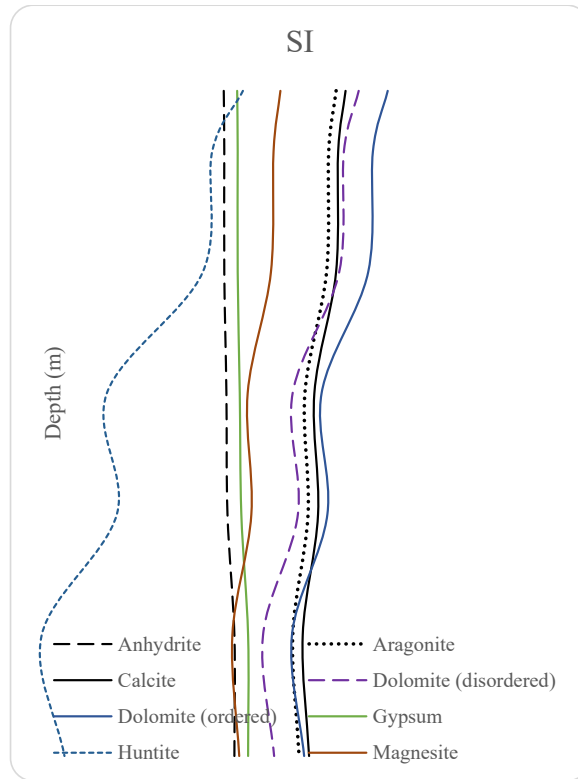


Fig. 7: The SI profiles of the main mineral phases in the Liquidambar lagoon water

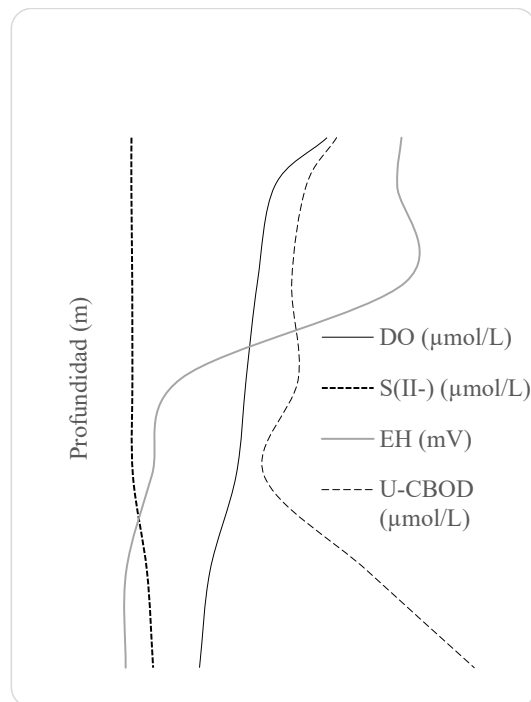


Fig. 8: Profiles of main redox species in the water of the Liquidambar lagoon

ter season, combined with low oxygen concentrations and concentrations of organic matter measured as BOD.

ACKNOWLEDGEMENT

To the General Directorate of Academic Personnel Affairs (DGAPA), through the Program of Support for Research Projects and Technological Innovation (PAPIIT), for financial support to the project with code IA108117.

REFERENCES

- Alcocer, J., Merino-Ibarra, M., Oseguera, L.A. and Escolero, O. 2018. Anthropogenic impacts on tropical karst lakes: "Lagunas de Montebello," Chiapas. *Ecohydrology*, 11(8), e2029.
- Alcocer, J., Oseguera, L.A., Sánchez, G., González, C., Martínez, J. and González, R. 2016. Bathymetric and morphometric surveys of the Montebello Lakes, Chiapas. *J. Limnol.*, 75: 11-19
- Appelo, C.A.J. and Postma, D. 2005. *Geochemistry, Groundwater, and Pollution*. 2nd edition. CRC Press, Taylor & Francis Group, London, UK.
- Clescerl, L.S., Greenberg, A.E. and Eaton, A.D. (Eds.). 1999. *Standard Methods for the Examination of Water and Wastewater: User Guide*. 20th edition. The American Public Health Association, Washington DC, USA.
- Comisión Nacional del Agua y Consejo Nacional de Ciencia y Tecnología (CONAGUA - CONACYT). 2013. *Hydrological and Water Quality Study Of The Montebello Lagoon System*, Chis. (No. 1). Mexico
- Dupraz, C., Reid, R.P., Braissant, O., Decho, A.W., Norman, R.S. and Visscher, P.T. 2009. Processes of carbonate precipitation in modern microbial mats. *Earth-Sci. Rev.*, 96(3): 141-162.
- Durán, I., Escolero, O., Muñoz-Salinas, E., Rodríguez, M. and Silva-Romo, G. 2014. Geomorphological mapping at 1: 50000 scale of Lagunas de Montebello National Park, Chiapas (Mexico). *Bullet. Mexican Geol. Soc.*, 66: 263-277.
- Findlay, A. J., Gartman, A., MacDonald, D. J., Hanson, T. E., Shaw, T. J. and Luther, G. W. 2014. Distribution and size fractionation of elemental sulfur in aqueous environments: The Chesapeake Bay and the Mid-Atlantic Ridge. *Geochim. Cosmochim. Acta*, 142: 334-348.
- García, L.A., Escolero, O. and Fernández, G. 2014. Hydrogeochemistry Lake San Lorenzo in Montebello, Chiapas (Mexico). *Colombian Association of Sanitary and Environmental Engineering*, Bogota, Columbia.
- Hargrave, B.T., Holmer, M. and Newcombe, C.P. 2008. Towards a classification of organic enrichment in marine sediments based on biogeochemical indicators. *Marine Pollut. Bull.*, 56(5): 810-824.
- Homa, E.S. and Chapra, S.C. 2011. Modeling the impacts of calcite precipitation on the epilimnion of an ultraoligotrophic, hard-water lake. *Ecol. Model.*, 222(1): 76-90.
- Instituto Municipal de Planeación de Comitán de Domínguez (IMPLAN Comitán). 2015. *Management Plan for the Rio Grande basin, Lagunas de Montebello, Chiapas, Mexico*. http://transparencia.comitan.gob.mx/ART74/I/DESARROLLO_RURAL/plan_de_gestion_cuencas.pdf
- Karami, F., Balci, N. and Guven, B. 2019. A modeling approach for calcium carbonate precipitation in a hypersaline environment: A case study from a shallow, alkaline lake. *Ecol. Complex.*, 39: 100774.
- Knossow, N., Blonder, B., Eckert, W., Turchyn, A.V., Antler, G. and Kamysny, A. 2015. Annual sulfur cycle in a warm monomictic lake with sub-millimolar sulfate concentrations. *Geochem. Trans.*, 16: 7.
- Marandi, A. and Shand, P. 2018. Groundwater chemistry and the Gibbs Diagram. *Appl. Geochem.*, 97: 209-212.
- Mora, L., Bonifaz, R. and López-Martínez, R. 2016. Geomorphological units of the Río Grande de Comitán basin, Lagos de Montebello, Chiapas-México. *Bullet. Mexican Geol. Soc.*, 68(3): 377-394.
- Mora, L., García, L.A., Ramos, Y.R., Bonifaz, R. and Escolero, O. 2017. Description of chemical changes in a large karstic system: Montebello, Mexico. *Proced. Earth Planet. Sci.*, 17: 829-832.
- Murray, J.W., Jannasch, H.W., Honjo, S., Anderson, R.F., Reebergh, W.S., Top, Z., Friederich, G.E., Codispoti, L. A. and Izdar, E. 1989. Unexpected changes in the oxic/anoxic interface in the Black Sea. *Nature*, 338(6214): 411-413.
- Nordstrom, D.K. and Campbell, K.M. 2014. Modeling Low-Temperature Geochemical Processes. In Drever, J.I. (ed.), *Surface and Ground Water, Weathering, and Soils*, In *Treatise on Geochemistry*. 2nd edition, Vol. 7. Elsevier, The Netherlands, pp. 27-68.
- Oseguera, L.A. and Alcocer, J. 2016. Concentration and Vertical Distribution of Particulate Carbon (Total And Organic) In Paz, F.J. and Torres, R. (eds.), *Current State of Knowledge of the Carbon Cycle and its Interactions in Mexico: Synthesis to 2015*. Mexican Carbon Program in collaboration with the Center for Global Change and Sustainability in the Southeast, A.C and the International Center for Linking and Teaching of the Universidad Juárez Autónoma de Tabasco, Mexico, pp. 457-463.
- Parkhurst, D.L. and Appelo, C.A.J. 2013. *Description of Input and Examples for PHREEQC Version 3: A Computer Program for Speciation, Batch-Reaction, One-Dimensional Transport, and Inverse Geochemical Calculations*. U.S. Geological Survey, USA, p. 159.
- Singhal, B.B.S. and Gupta, R.P. 2010. *Applied Hydrogeology of Fractured Rocks*. 2nd edition. Springer, New York.
- Stumm, W. 2007. Chemical Processes Regulating the Composition of Lake Waters. In O Sullivan, P.E. and Reynolds, C.S. (eds.), *The Lakes Handbook*. John Wiley & Sons, Hoboken, NJ, USA, pp. 79-106
- Vera, M.N., Hernández, P., Alcocer, J., Ardiles, V. and Oseguera, L.A. 2015. Concentration and Vertical Distribution of Chlorophyll-A Phytoplankton in the Lakes of Montebello, Chiapas. In Alcocer, J., Merion-Ibarra, E. and Escobar-Briones, E. (eds.), *Research Trends in Tropical Limnology: University Perspectives in Latin America*. Asociación Mexicana de Limnología, AC, Instituto de Ciencias del Mar y Limnología, UNAM, and Consejo Nacional de Ciencias y Tecnología, pp. 107-114.
- Walsh, J.R., Corman, J.R. and Munoz, S.E. 2019. Coupled long-term limnological data and sedimentary records reveal new control on water quality in a eutrophic lake. *Limnol. Oceanogr.*, 64(S1): S34-S48. <https://doi.org/10.1002/lno.11083>.
- Zhu, C. and Anderson, G. 2010. *Environmental Applications of Geochemical Modeling*. Cambridge University Press, Cambridge.
- Zhu, C. and Schwartz, F. 2010. Hydrogeochemical processes and controls on water quality and water management. *Elements*, 7: 169-174.



Hydrochemical Characteristics, Quality Assessment and Solute Source Identification of Coal Bearing Fractured Aquifer in Dingji Coal Mine, Huainan Coalfield, China

Jie Ma^{*(**)}†, Jianghong Wang^{***}, Song Chen^{*(**)}, Hongbao Dai^{****}, Jingyu Zhao^{*(**)}, Haitao Zhang^{*(**)} and Zhichun Li^{****}

*School of Resources and Civil Engineering, Suzhou University, Suzhou, Anhui, China

**Key Laboratory of Mine Water Resource Utilization of Anhui Higher Education Institute, Suzhou, Anhui, China

***Dingji Coal Mine of Huaihu Coal Power Co., Ltd, Huainan, Anhui, China

****School of Environment and Surveying Engineering, Suzhou University, Suzhou, Anhui, China

†Corresponding author: Jie Ma; ahszumajie@163.com

Nat. Env. & Poll. Tech.
Website: www.neptjournal.com

Received: 11-10-2020

Revised: 15-12-2020

Accepted: 13-01-2021

Key Words:

Solute source

Hydrochemical facies

WQI

Irrigation assessment

Multivariate analysis

ABSTRACT

Coal-bearing fractured aquifer is regarded as one of the most dynamic mine water inrush sources, and after pumping and treating, it can be used as a water supply for coal mine production, coal preparation plant, rural irrigation, and even reserved drinking water source. Hence, this study focuses on the hydrochemical characteristics, ion source, and water quality evaluation with respect to drinking and irrigation of the coal-bearing fractured aquifer in Dingji coal mine, Huainan coalfield, China. Descriptive statistics and hydrochemical classification diagrams including the Piper diagram and Chadha rectangular diagram were carried out to depict the hydrochemical characteristics and facies. The water quality of the aquifer was assessed for irrigation and drinking purposes using the WHO threshold value, water quality index (WQI), SAR, % Na and RSC. Hydrochemical formation mechanism and solute origin of major ions were explained by Gibbs diagram, bivariate diagrams, and multivariate statistical analysis. The results show that the dominant hydrochemical facies are the Cl-Na type and the HCO₃-Na type. The sequence of ions is Na⁺ > Ca²⁺ > Mg²⁺ for cations, and HCO₃⁻ > Cl⁻ > SO₄²⁻ > CO₃²⁻ for anions. The main solute sources are controlled by various factors including the dissolution of halite, sulfate, and carbonate rocks, the weathering of silicate, and cation exchange. Water quality assessment based on WQI suggests that none of the samples fall under the excellent category, even 32.5% is not suitable for direct drinking. Meanwhile, the samples of the aquifer are generally unsuitable for irrigation. Before utilization for irrigation and even drinking, appropriate water treatment should be applied to guarantee its security during usage.

INTRODUCTION

Since the 21st century, with the rapid development of economics and changes in the global environment, mankind is being confronted with even more environmental pollution, climate warming, ecological degradation, and water resources shortage, etc.

Coal resource exploitation accounts for more than 75% of China's energy production (Liu et al. 2007). With the increasing mining depth and usage demand, mine hazards such as water, fire, dust, gas, and roof have become more dynamic and disastrous, inducing huge economic losses and massive casualties. Among these, water inrushes always occur owing to complicated geologic and hydrogeological conditions. For a long time, scholars and specialists in the prevention and control of mine water disasters have focused on how to

ensure production safety and avoid stoppages, casualties, and repeated economic losses. In recent decades, many researchers have offered efficient and effective ways to reduce the mine geological hazards (Gui & Lin 2016, Mahato et al. 2018). Meanwhile, relevant scholars have taken an interest in mine water treatment and resource utilization research, providing technical and theoretical support for safe, green, and efficient mining (Zhang et al. 2020, Sun et al.2020, Gu 2015, Jiang et al. 2018).

The research scopes of mine water prevention and controlling have been conducted from the initial hydro-geological and hydro-chemical conditions appraisal, and gradually involved the coupling analysis of the hydro-chemical field, hydro-dynamic field, water temperature field, and others. In addition, assessment of drinking water, irrigation evaluation, and water inrush identification are also hot topics in

mine water research. In view of the sustainable utilization of water resources, and prevention and controlling of water inrush, the objectives of this study were to: (1) analyze the hydrochemical characteristics and types of the coal-bearing aquifer, (2) appraise and understand the water quality for irrigation and drinking, (3) explain the mechanism of water-rock interactions and identify the solute sources of major ions.

BACKGROUND OF STUDY AREA

Location and climate

The Dingji mine is a new type of coal mine with the integration of coal and electricity, which is affiliated to Huaihu Coal Power Co., Ltd. The study area is situated in Huainan coalfield with coal production of 6 million tons per year, and lies between latitudes $32^{\circ}47' 26''$ - $32^{\circ}54' 31''$ and longitudes $116^{\circ}32' 53''$ - $116^{\circ}42' 37''$ (Fig. 1). It approximately extends 12-15 km long from east to west and 4-11 km wide from north to south, covering a total area of around 95.7 km^2 . The coal mine is located in the midstream of the Huaihe River, and the altitudes range between 21 m and 23 m above mean sea level, with a terrain tendency of high in the northwest and low in the southeast.

The study area belongs to a semi-humid climate and has four distinct seasons, warm in spring, hot in summer, cool in autumn, and cold in winter. According to Fengtai

County Meteorological Bureau's data, the average annual temperature is 15.1°C , with a maximum value of 41.4°C and a minimum value of -22.8°C . Annual precipitation and evaporation are 320.44 mm and 1610.14 mm, respectively. The rainfall season is concentrated from June to August.

Geology and hydrogeology

Huainan coalfield is located in the southeast of the North China Plate. The regional notable structure form is a synclorium, and the Dingji coal mine lies in the middle-north part. The overall structural form of the mine is a monocline structure inclined to the east, and the formation dip is gentle. Basic fine-grained rock and syenite porphyry among Yanshanian intrusion are well developed, with a maximum thickness of 87.87m.

From the bottom to top, the strata of the coal mine, as evidenced by huge drillings, mainly consists of Ordovician (O_{1+2}), Carboniferous (C_2 and C_3), Permian (P_{1s} , P_{1x} , P_{2s} , and P_{2sj}), Triassic (T), Paleogene (E), Neogene (N) and Quaternary (Q). The mid-lower Ordovician Majiagou formation (O_{1+2}) consisted of limestone and dolomitic limestone with breccias limestone and shale, and the maximum exposure thickness by drilling is 93.42 m. The middle Carboniferous Benxi formation (C_2) is composed mainly of mudstone and aluminous mudstone, the upper Carboniferous Taiyuan formation (C_3) comprises 12 to 13 layers of thin limestone and

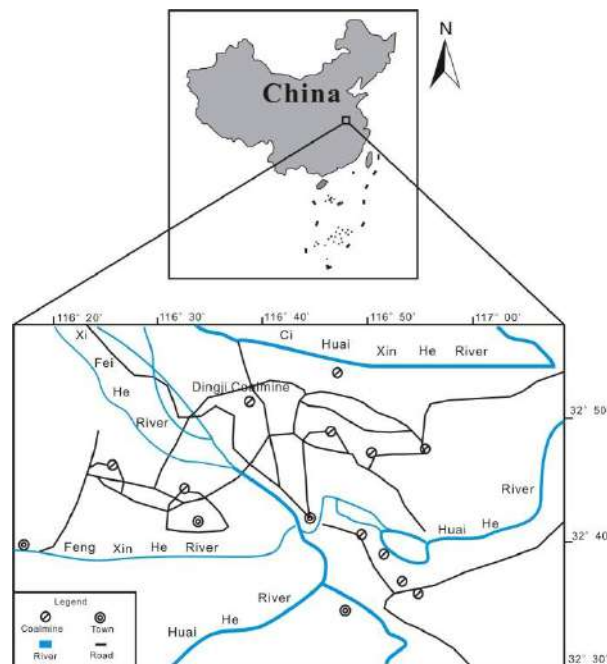


Fig. 1: Location of the study area (Dingji Coal mine).

some intercalations, such as mudstone and sandstone. The average thickness of the two formations is 7.18 m and 110.27 m, respectively. The lower Permian Shanxi formation (P_{1s}), the lower Xiashihezi formation (P_{1x}), the Upper Shangshihezi formation (P_{2s}), and the Upper Sunjiagou formation (P_{2sj}) is about 81 m, 135 m, 510 m, and 260 m thick, respectively. The Permian formation lithology is mainly composed of sandstone with different particle sizes and mudstone. The Triassic Series is made up of purplish-red sandstone, siltstone, and mudstone, and its thickness is unknown. The Paleogene Series consisted of motley glutenite, the Neogene Series comprised argillaceous conglomerate, clay, and medium sand, and the Quaternary sediment composed of silty sand, fine sand, and sandy clay.

According to lithologic characteristics, hydraulic connection, and pump testing, from shallow to deep, the main groundwater system can be divided into three types: loose porous aquifer, coal-bearing fractured aquifer, and karst fractured aquifer. The shallow part of the loose porous aquifer is recharged by precipitation and lateral inflow of surface rivers. The deep part of the loose porous aquifer confined by water-resisting lays has a limited recharge and water content is mainly static reserves. Similarly, due to the effective water-resisting lays, the water abundance of the coal-bearing fractured aquifer is primarily static reserves, and the unit water flow is 6.76×10^{-4} - 3.48×10^{-2} L·(s·m) $^{-1}$. With a large thickness of hidden strata, the karst fractured aquifer belongs to a relatively enclosed confined aquifer. By now, ten water bursting accidents have occurred in the coal mine. The sources of water inrush are mainly coal-bearing fractured aquifer and loose porous aquifer, and the water bursting volume is about 10-130 m 3 ·h $^{-1}$.

MATERIALS AND METHODS

Sampling and Measurements

In this study, 40 coal-bearing fractured aquifer samples were collected from the water inrush points of the roadway. To guarantee the accuracy and reliability of the hydrochemical analysis, before sampling, each in-situ sample was rinsed

3-5 times with the groundwater to be collected and the sampling container was white pollution-free plastic bottles. All collection, treatment, preservation, and analytic standard methods referred to technical requirements for hydrochemistry approach in coal mine water control of Ministry of Coal Industry Standard of the People's Republic of China (MT/T 672-1997), and the hydrochemical indicator test was conducted by the Gas and Water Quality of Rescue Team of Huai-he River Energy Group Coal Company, which has participated in national mine rescue works. The selected parameters for the analysis included the total dissolved solids (TDS), pH, and major ions (SO_4^{2-} , Cl^- , CO_3^{2-} , HCO_3^- , Ca^{2+} , Mg^{2+} and Na^+).

Methods

For this study, MyStat 12.0 was applied for the descriptive statistics. Correlation analysis, Piper diagram, and Chadha rectangular diagram were used to determine the hydrochemical type of the samples. Gibbs diagram and bivariate diagrams were employed to explain the mechanism of solute formation and ion source. WHO standard, water quality index (WQI), %Na, and RSC were carried out for both drinking and irrigation evaluation. In addition, with the help of SPSS 16.0, multivariate statistical methods including cluster analysis and principal component analysis/factor analysis, known as effective tools for minimizing the effects of measurement unit difference and interpreting the hidden factors accounting for the various parameters, were conducted to further delineate the solute composition of the coal-bearing fractured aquifer.

RESULTS AND DISCUSSION

Major Ion Concentration

The physicochemical parameters and major ion compositions were summarized in Table 1, including the minimum, maximum, mean, coefficient of variation and standard deviation. Among the cations, the concentration of Ca^{2+} , Mg^{2+} and Na^+ were in the range of 1.6-32.1, 0.0-15.6, 304.9-2680.6 mg·L $^{-1}$, respectively. The concentration range of CO_3^{2-} , HCO_3^- , Cl^- and SO_4^{2-} were 0.0-264.0, 353.9-3295.1, 45.0-2442.5 and

Table 1: Physicochemical parameters and major ion composition (expressed in mg/L, except pH).

Statistics	Ca $^{2+}$	Mg $^{2+}$	Na $^+$	CO $_3^{2-}$	HCO $_3^-$	Cl $^-$	SO $_4^{2-}$	TDS	pH
Min	1.6	0.0	304.9	0.0	353.9	45.0	1.4	873.6	8.0
Max	32.1	15.6	2680.6	264.0	3295.1	2442.5	234.4	6320.5	9.3
Mean	8.9	4.1	1382.4	54.0	1660.9	965.7	55.8	3301.5	8.7
SD	6.9	3.9	568.1	63.7	978.4	405.4	68.3	1306.0	0.3
CV	0.78	0.96	0.41	1.18	0.59	0.42	1.22	0.40	0.03

1.4-234.4 mg.L⁻¹, respectively. According to the average value, the relative order was Na⁺ > Ca²⁺ > Mg²⁺ for cations, and HCO₃⁻ > Cl⁻ > SO₄²⁻ > CO₃²⁻ for anions.

The coal-bearing fractured aquifer showed a slightly alkaline nature with an average of 8.7. The TDS values of the samples varied from 873.6 to 6320.5 mg.L⁻¹, with a mean content of 3301.5 mg.L⁻¹. 50% and 47.5% of the samples were categorized into brackish water (1000-3000 mg.L⁻¹) and saline water (3000-10000 mg.L⁻¹), respectively. This relatively high salt content is concerned with Na⁺ and Cl⁻, which indicated that the salinity of the aquifer was closely related to the prolonged water-interaction interaction.

The CVs values of most parameters (except for pH), which were higher than 0.3, showed an apparent spatial and temporal variation. Therefore, long-term exploitation and mine water pumping also have a predominant and universal effect on the solute concentrations and hydrochemical types.

Correlation analysis was conducted to evaluate the relationship between parameters of the aquifer (Table 2) using SPSS 16.0. According to the results, a strong correlation between Na⁺-HCO₃⁻ (r=0.851) and Na⁺-Cl⁻ (r=0.810) were observed. This showed that the halite dissolution and the silicate weathering provided solute components, such as feldspar. Additionally, a positive correlation can be obtained between Mg²⁺-Ca²⁺ (r=0.765), Ca²⁺-SO₄²⁻ (r=0.569), and Mg²⁺-SO₄²⁻ (r=0.562), implying that sulfate dissolution, such as gypsum and magnesium sulfate, occurs. Besides this, a negative correlation can be observed between different parameters, such as Ca²⁺-Na⁺ (r=-0.381), Ca²⁺-HCO₃⁻ (r=-0.467), Mg²⁺-Na⁺ (r=-0.482), and Mg²⁺-HCO₃⁻ (r=-0.610), indicating that ion-exchange reactions also occurred during the interaction between water and aquifer.

Hydrochemical facies

Hydrochemical facies can be probed using the Piper diagram. As shown in Fig. 2, all samples are classified into sodium

type with respect to cations, and bicarbonate and chloride type with respect to anions. 50.5% of samples can be categorized as HCO₃-Na water type, remaining 49.5% samples are classified into Cl-Na water type (EI Alfay et al. 2019, Zaki et al. 2019).

Interpretation and classification of the hydrochemical type of the coal-bearing aquifer can also be conducted using the Chadha rectangular diagram (Fig. 3) (Liu et al. 2020, Wu et al. 2019). According to the difference in milliequivalent percentage between (Ca²⁺+Mg²⁺) and (Na⁺+K⁺), and (CO₃²⁻+HCO₃⁻) and (SO₄²⁻+Cl⁻), this diagram can be divided into eight sub-fields. Results of hydrochemical data are plotted on the Chadha's diagram (Fig. 3), which is in confirmation with the output of Piper trilinear diagram, showing that the plots mainly fall under the field 7 and 8 with typical water of Cl-Na and HCO₃-Na, respectively.

Overall, scatter plots of the two diagrams depicting hydrochemical facies demonstrated that the weathering of silicate and the dissolution of evaporite play a vital role in the solute composition of the aquifer.

Source Identification

The hydrochemical formation mechanism of major ions has been widely discussed by Gibbs diagrams (Shirke et al. 2020, Ahmad et al. 2019). In this study, the plots of the Gibbs diagram fall within the evaporation dominance area with respect to cations (Fig. 4a), implying that the dissolution of halite is the dominant mechanism controlling solute composition. For anions (Fig. 4b), the scatters of the Gibbs diagram disperse in both the evaporation dominance and rock dominance, suggesting water-rock interaction also plays an important role in influencing the anion content.

This interaction can be confirmed by the bivariate diagrams between ions. The 1:1 ratio of Na/Cl indicates the pure dissolution of halite during water-rock interaction, and the plots display a linear relationship in the bivariate

Table 2: Correlation analysis between parameters of the aquifer (n=40).

	Ca ²⁺	Mg ²⁺	Na ⁺	CO ₃ ²⁻	HCO ₃ ⁻	Cl ⁻	SO ₄ ²⁻
Ca ²⁺	1.000						
Mg ²⁺	0.765**	1.000					
Na ⁺	-0.381*	-0.482**	1.000				
CO ₃ ²⁻	-0.232	-0.259	0.301	1.000			
HCO ₃ ⁻	-0.467**	-0.610**	0.851**	0.055	1.000		
Cl ⁻	-0.105	-0.110	0.810**	0.261	.412**	1.000	
SO ₄ ²⁻	0.569**	0.562**	-0.347*	-0.153	-.385*	-0.233	1.000

**Correlation is significant at the 0.01 level (2-tailed).

*Correlation is significant at the 0.05 level (2-tailed).

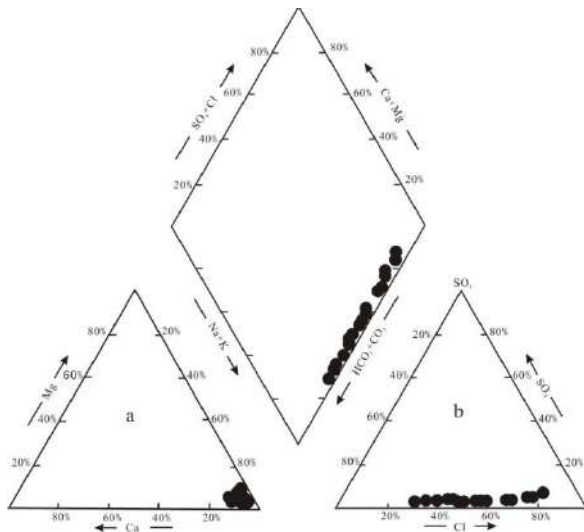


Fig. 2: Piper diagram of the aquifer's samples.

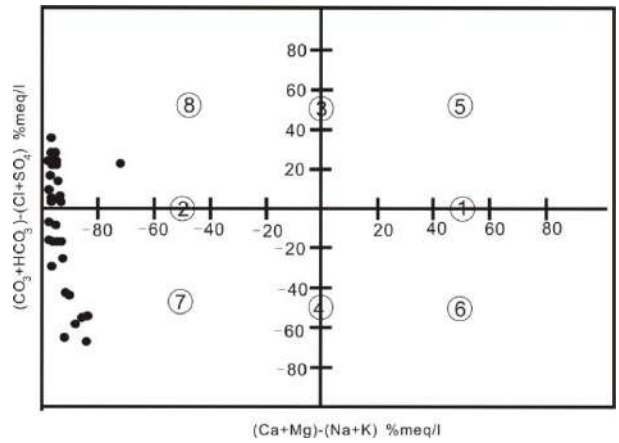


Fig. 3: Chadha rectangular diagram of the aquifer's samples.

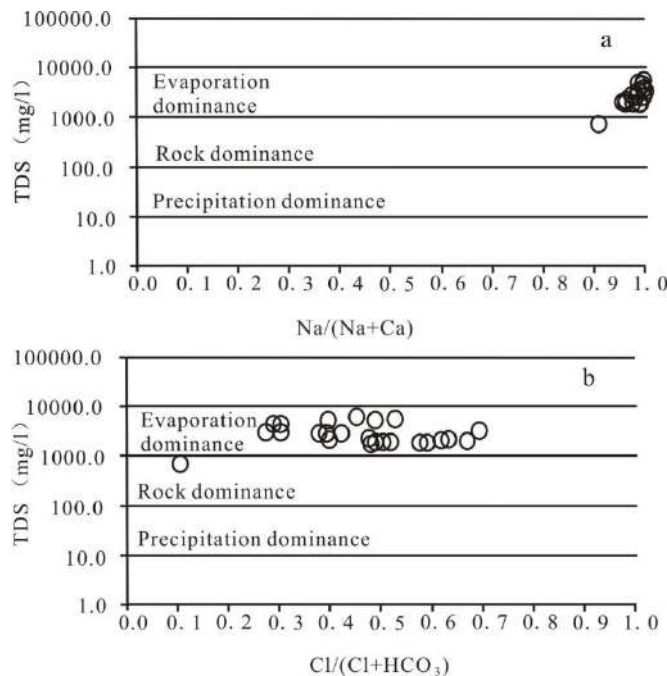


Fig. 4: Gibbs diagrams: a TDS versus Na/(Na+Ca), b TDS versus Cl/(Cl+HCO₃).

diagram. However, all points are under the 1:1 line (Fig. 5a), showing that Na⁺ content exceeds Cl in the samples. Excessive Na⁺ can be acquired from cation exchange and/or the weathering of silicate minerals (Li et al. 2018, Jalali 2007). The scatter plots of (Ca²⁺+Mg²⁺) versus (SO₄²⁻+HCO₃⁻) and (Ca²⁺+Mg²⁺-SO₄²⁻-HCO₃⁻) versus (Na⁺-Cl) further verify the above-mentioned two functions. Samples plotted on

the (Ca²⁺+Mg²⁺) versus (SO₄²⁻+HCO₃⁻) diagram fall under in the (SO₄²⁻+HCO₃⁻) area (Fig. 5b), suggesting that the dissolution of sulfate and the weathering of silicate are the main interaction in this process and redundant Na⁺ can be obtained from the weathering of silicate minerals, such as albite. Meanwhile, excessive Na⁺ can also be acquired from the cation exchange, the ratio of (Ca²⁺+Mg²⁺-SO₄²⁻-HCO₃⁻)

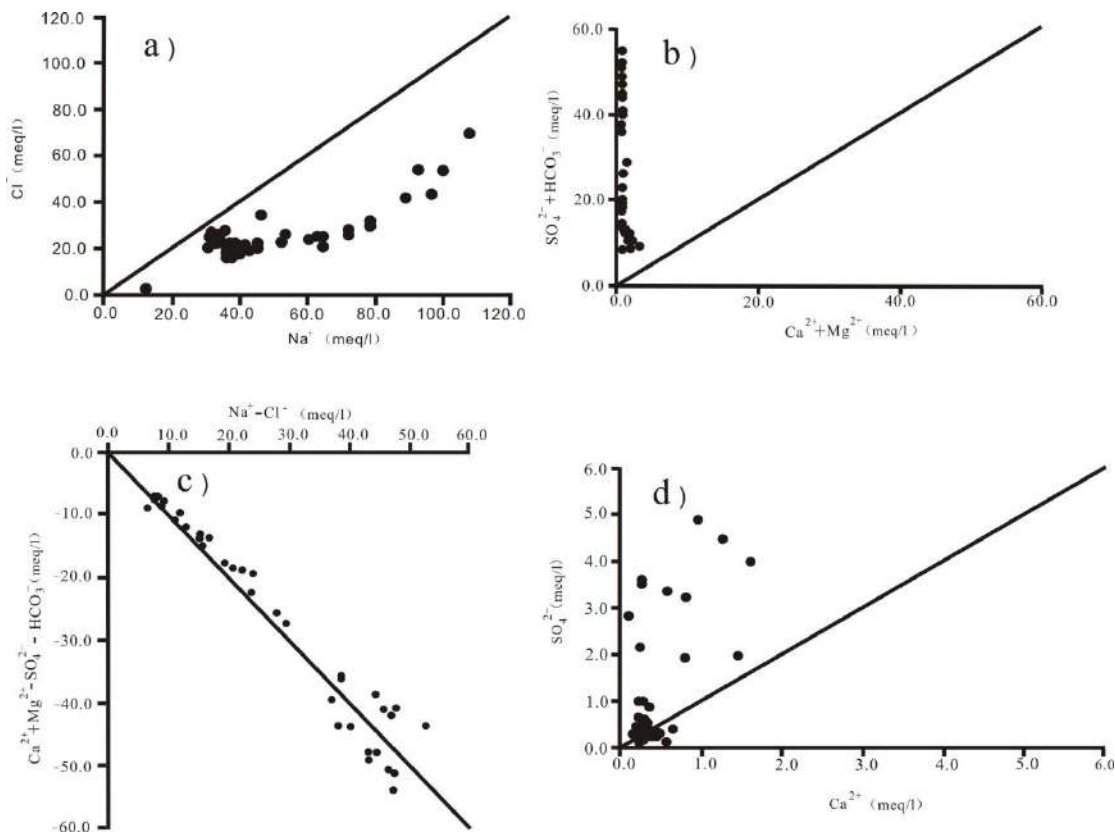


Fig. 5: Plots of (a) Na^+ versus Cl^- ; (b) $(\text{Ca}^{2+} + \text{Mg}^{2+})$ versus $(\text{SO}_4^{2-} + \text{HCO}_3^-)$; (c) $(\text{Ca}^{2+} + \text{Mg}^{2+} - \text{SO}_4^{2-} - \text{HCO}_3^-)$ versus $(\text{Na}^+ - \text{Cl}^-)$; (d) Ca^{2+} versus SO_4^{2-} .

$(\text{Na}^+ - \text{Cl}^-)$ is plotted along and around the line of -1 (Fig. 5c), which indicate that cation exchange also plays a vital role in the major hydrochemical process. The 1:1 ratio between Ca^{2+} and SO_4^{2-} proved the sole dissolution of sulfate, which is widespread in coal-bearing fractured aquifers. However, most scatters were above the 1:1 line (Fig. 5d), suggesting other water-rock interactions offered excessive sulfate anion, for instance, the oxidation of hydrogen sulfide during the mining period. The ratio of $\text{Ca}^{2+}/\text{Mg}^{2+}$ can be used to infer their origins, for example, dolomite dissolution with the ratio is 1, calcite dissolution with the ratio is between 1 and 2, while the silicate mineral dissolution and/or weathering with a ratio more than 2 (Varol & Davraz 2014). The ratio of $\text{Ca}^{2+}/\text{Mg}^{2+}$ of the studied aquifer varied from 0.3 to 3.6. Three samples have a ratio of 1 indicating the dissolution of dolomite, and 11 samples with the ratio ranging from 1 to 2 characterize the dissolution of calcite, 13 samples have a ratio > 2 which indicates the effect of silicate minerals. Nevertheless, due to the low concentration of Ca^{2+} and Mg^{2+} , the dissolution of carbonate rocks plays a finite contribution to the solute composition.

Principal Component Analysis/Factor Analysis

The principal component /factor analysis (PCA/FA) with Varimax rotation was applied. Eigenvalues of 1.00 or greater were selected as the new variables. Factor loading with >0.75 , $0.75-0.5$, and $0.5-0.3$ were classified as strong, moderate, and weak, respectively (Palma et al. 2010, Pejman et al. 2009). Two factors explained 70.25% of the variance were extracted, and the results of PCA/FA were summarized in Table 3. The first varifactor (VF1) accounted for 36.11% of the variance. Strong positive loading for Ca^{2+} and Mg^{2+} , and moderate positive loading for SO_4^{2-} represented the dissolution of sulfate. The second varifactor (VF2) explained 34.14% of the variance. VF2 exhibited strong positive loading for Na^+ and Cl^- , and moderate positive loading for HCO_3^- . VF2 was attributed to the dissolution of halite and the weathering of silicate.

Cluster Analysis

Cluster analysis is the method of grouping the variables into different clusters based on their similarities. In this study, a hierarchical cluster was performed by means of Ward's

Table 3: Principal component analysis of the aquifer’s hydrochemical variables.

component	Before Rotation		After Rotation	
	FC1	FC 2	VF1	VF2
Ca ²⁺	-0.74	0.52	0.89	-0.12
Mg ²⁺	-0.80	0.45	0.89	-0.22
Na ⁺	0.86	0.48	-0.30	0.94
CO ₃ ²⁻	0.37	0.12	-0.19	0.34
HCO ₃ ⁻	0.83	0.13	-0.51	0.66
Cl ⁻	0.58	0.72	0.07	0.92
SO ₄ ²⁻	-0.67	0.37	0.74	-0.19
Eigen Values	3.52	1.40	2.53	2.39
Var/%	50.30	19.95	36.11	34.14
Cum/%	50.30	70.25	36.11	70.25

method using the squared Euclidean distances for similarity measure (Kamble & Vijay 2011). A total of 40 samples are used for cluster analysis, and a dendrogram with two significant clusters is composed as shown in Fig. 6. Cluster 1 includes Na⁺, HCO₃⁻, Cl⁻ and CO₃²⁻, these components are related to the dissolution of halite and the weathering of silicate minerals. Cluster 2 comprised Ca²⁺, Mg²⁺ and SO₄²⁻, which implies the dissolution of sulfate minerals, such as gypsum and magnesium sulfate.

Drinking assessment

The pumped coal-bearing fractured water can be converted into groundwater by infiltration, and the quality of the sub-surface water will affect human health. In comparison to the standard limit proposed by WHO (2011) which is listed in Table 4 (Talib et al. 2019), all of Ca²⁺, Mg²⁺ and SO₄²⁻ contents are below the limit, showing the suitability for drinking. Whereas the concentration of Na⁺ and HCO₃⁻ are all above the limit, and some samples show more than ten times than the WHO standard. The majority of Cl⁻, TDS and pH values

WATER QUALITY ASSESSMENT

Table 4: Weight and relative weight of each chemical parameter.

Chemical parameters	WHO Standard (2011)	Weight (w _i)	Relative weight (W _i)
Ca ²⁺	200	3	0.103
Mg ²⁺	150	3	0.103
Na ⁺	200	4	0.138
HCO ₃ ⁻	250	1	0.034
Cl ⁻	250	5	0.173
SO ₄ ²⁻	250	5	0.173
TDS	1000	5	0.173
pH	8.5	3	0.103
/	/	Σ=29	Σ=1

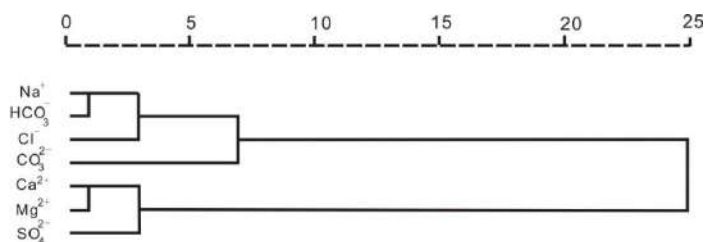


Fig. 6: Cluster analysis of the aquifer’s hydrochemical variables.

exceed the WHO standard, which indicates that these indices are inadequate for drinking purposes and even lead to a series of diseases such as hypertension, renal failure, etc.

The water quality index (WQI) is well-suited for classification and appraisal for drinking purposes, with the advantages of converting a large number of water quality data into a single value (Talib et al. 2019, Kumar & James 2013). Three calculation steps are as follows: (1) The first step involves the relative weight calculation. Based on the importance to the water quality, eight parameters (TDS, SO_4^{2-} , Cl^- , Na^+ , Ca^{2+} , Mg^{2+} , pH, and HCO_3^-) have been given the assigned weight between 1 and 5 according to its importance. (2) The second step is the calculation of quality rating for each parameter, and the WHO standard is listed in Table 4. (3) The third step is the calculation of the water quality index.

The calculated WQI values can be classified as excellent (<50), good (50-100), poor (100-200), very poor (200-300), and unsuitable (>300) for human consumption. The computed WQI values are summarized in Table 5, and the values vary from 73.9 to 504.8. None of the samples fall under the excellent, 2.5% of the samples represent "good water", 37.5% show "poor water", 27.5% indicate "very poor", and 32.5% exhibit "unsuitable water", which suggest that these samples are not suitable for direct drinking. Hence, prior to drinking, thorough water quality treatment measures and the environmental monitoring system need to be conducted to ensure the discharged water reaching the emission standard.

Irrigation assessment

High salinity and strong alkalinity will lead to a harmful effect on crop growth and yields. The indices used for

irrigation appraisal mainly contain sodium adsorption ratio (SAR), %Na, and residual sodium carbonate (RSC) (Berhe 2020, Adimalla et al.2018, Kaur et al. 2017). The classification criteria of irrigation water quality were summarized in Table 6. SAR, which indicates the content of sodium in irrigation water or soil solution, is the most general parameter for appraising the degree of soil alkalization. %Na is used for representing the risk of alkali hazard caused by irrigation water, and high content can reduce the permeability and poor drainage of the soil. RSC is employed to assess alkali damage degree, and the negative RSC indicates that there is no excess carbonate to react with Na^+ , so it will not increase alkali damage. On the contrary, positive RSC can bring out alkali damage to the water.

As given in Table 7, the SAR value ranges within 12.6-214.1 with a mean of 106.9, indicating that all of the samples are unacceptable for irrigation. Only one sample with a SAR of 12.6 is good for irrigation. The computed %Na of the present study's samples ranges from 86.7-99.7 with an average of 98.0, suggesting that the aquifer is unsuitable for irrigation. The calculated RSC values are in the range of 3.7-53.4 with a mean of 28.2, and 100% of the samples are classified into unsuitable categories for irrigation purposes.

Overall, the samples of the aquifer are generally unsuitable for irrigation. Long-term utilization of this aquifer water may give a rise to sodium hazards and affect crop growth and yields. Therefore, centralized treatment and discharge should be implemented before irrigation to ensure regional sustainable development.

CONCLUSIONS

Coal-bearing fractured aquifer is regarded as one of the most

Table 5: Classification of the aquifer's samples according to WQI.

Calculated value	Threshold	No. of samples	Percentage (%)
Min	73.9	<50	0
		50-100	1
Max	504.8	100-200	15
		200-300	11
Mean	257.0	>300	13
			32.5

Table 6: Classification criteria of irrigation water quality based on SAR, %Na, and RSC.

SAR	Irrigation water quality	%Na	RSC	Irrigation water quality
<10	Excellent quality	<30	< 1.25	Suitable
10-18	Good quality	30-60	1.25-2.5	Marginally suitable
18-26	Acceptable quality	>60	>2.5	Unsuitable
>26	Unacceptable quality	-	-	-

Table 7: Results of irrigation water quality assessment.

	SAR	%Na	RSC
Min	12.60	86.70	3.70
Max	214.10	99.70	53.40
Mean	106.90	98.00	28.20

dynamic mine water inrush sources, and it can be used for irrigation and even reserved drinking water sources after effective and safe treatment. In the present study, hydrochemical characteristics, ion source, and water quality evaluation with respect to drinking and irrigation of the coal-bearing fractured aquifer in Dingji coal mine, Huainan coalfield, China were discussed in detail. The results showed that the relative order of major ion composition was $\text{Na}^+ > \text{Ca}^{2+} > \text{Mg}^{2+}$ for cations, and $\text{HCO}_3^- > \text{Cl}^- > \text{SO}_4^{2-} > \text{CO}_3^{2-}$ for anions, respectively. Piper diagram and Chadha rectangular diagram demonstrated the main hydrochemical facies are Cl-Na type and HCO_3^- -Na type. Gibbs diagram, bivariate diagrams, and multivariate statistical analysis suggest that water-rock interactions of the aquifer include the dissolution of halite, sulfate, and carbonate, the weathering of silicate and cation exchange, etc. The computed WQI values vary from 73.9 to 504.8, and none of the samples fall under the excellent, 2.5% of the samples represent “good water”, 37.5% show “poor water”, 27.5% indicate “very poor”, and 32.5% exhibit “unsuitable water”. According to SAR, %Na and RSC, the samples of the aquifer are generally unsuitable for irrigation. Long-term water quality monitoring should be carried out to dynamically grasp the variation and deal with it in time.

ACKNOWLEDGMENTS

This research was supported by the Excellent Top-Notch Talents Cultivation Foundation of Colleges and Universities, Anhui Province, China (gxbjZD2020091, gxyqZD2020047, gxgnfx2020106, and gxgnfx2020107), the Natural Science Research Foundation of Colleges and Universities, Anhui Province, China (KJ2019A0677 and KJ2019A0667), the Science Project of Suzhou University, Anhui Province, China (2019yzd01 and 2016ykyf02), and the Doctoral Research Foundation of Suzhou University, Anhui Province, China (2017jb01).

REFERENCES

Ahmad, S., Umar, R. and Arshad, I. 2019. Groundwater quality appraisal and its hydrogeochemical characterization – Mathura City, Western Uttar Pradesh. *J. Geol. Soc. India*, 94: 611-623.

Adimalla, N., Li, P. and Venkatayogi, S. 2018. Hydrogeochemical evaluation of groundwater quality for drinking and irrigation purposes and integrated interpretation with water quality index studies. *Environ. Process*, 5: 363-383.

Berhe, B.A. 2020. Evaluation of groundwater and surface water quality suitability for drinking and agricultural purposes in Kombolcha town area, eastern Amhara region, Ethiopia. *Appl. Water Sci.*, 10: 127-143.

El Alfy, M., Abdalla F., Moubark, K. and Alharbi, T. 2019. Hydrochemical equilibrium and statistical approaches as effective tools for identifying groundwater evolution and pollution sources in arid areas. *Geosci. J.*, 23: 299-314.

Gui, H. and Lin, M. 2016. Types of water hazards in China coalmines and regional characteristics. *Nat. Hazards*, 84: 1501-1512.

Gu, D. 2015. Theory framework and technological system of coal mine underground reservoir. *J. China Coal Society*, 40(2): 239-246. (in Chinese).

Jiang, S., Huang, J., Xu, Z., Sun, Y., Liu, Q., Zhang, L. and Cui, L. 2018. Feasibility study of the construction of groundwater reservoir in the goaf of the Xuzhou Coal Mines. *J. Eng. Geol. Hydrogeol.*, 45(5): 17-23. (in Chinese)

Jalali, M. 2007. Hydrochemical Identification of Groundwater Resources and Their Changes under the Impacts of Human Activity in the Chah Basin in Western Iran. *Environ. Monit. Assess.*, 130: 347-364.

Kaur, T., Bhardwaj, R. and Arora, S. 2017. Assessment of groundwater quality for drinking and irrigation purposes using hydrochemical studies in Malwa region, southwestern part of Punjab, India. *Appl. Water Sci.*, 7: 3301-3316.

Kumar, P.J.S. and James, E.J. 2013. Development of water quality index (WQI) model for the groundwater in Tirupur district, South India. *Chin. J. Geochem.*, 32: 261-268.

Kamble, S.R. and Vijay, R. 2011. Assessment of water quality using cluster analysis in the coastal region of Mumbai, India. *Environ. Monit. Assess.*, 178: 321-332.

Liu, J., Wang, H., Jin, D., Xu, F. and Zhao, C. 2020. Hydrochemical characteristics and evolution processes of karst groundwater in Carboniferous Taiyuan formation in the Pingdingshan coalfield. *Environ. Earth Sci.*, 79: 151-164.

Li, P., Wu, J., Tian, R., He, S., He, X., Xue, C. and Zhang, K. 2018. Geochemistry, Hydraulic Connectivity and Quality Appraisal of Multilayered Groundwater in the Hongdunzi Coal Mine, Northwest China. *Mine Water Environ.*, 37: 222-237.

Liu, G., Zheng, L., Qi, C. and Zhang, Y. 2007. Environmental geochemistry and health of fluorine in Chinese coals. *Environ. Geol.*, 52: 1307-1313.

Mahato, M.K., Singh, P.K., Singh, A.K. and Tiwari, A.K. 2018. Assessment of hydrogeochemical processes and mine water suitability for domestic, irrigation, and industrial purposes in East Bokaro Coalfield, India. *Mine Water Environ.*, 37: 493-504.

MT/T 672-1997. 1997. Ministry of Coal Industry of the People's Republic of China. Technical requirement for hydrochemistry approach in coal mine water control.

Palma, P., Alvarenga, P., Palma, V.L., Fernandes, R.M., Soares, A.M.V.M. and Barbosa, I.R. 2010. Assessment of anthropogenic sources of water pollution using multivariate statistical techniques: A case study of the Alqueva's reservoir, Portugal. *Environ. Monit. Assess.*, 165: 539-552.

Pejman, A.H., Nabi Bidhendi, G.R., Karbassi, A.R., Mehrdadi, N. and Bidhendi, M.E. 2009. Evaluation of spatial and seasonal variations in surface water quality using multivariate statistical techniques. *Int. J. Environ. Sci. Technol.*, 6(3) : 467-476.

- Shirke, K.D., Kadam, A. K. and Pawar, N.J. 2020. Temporal variations in hydro-geochemistry and potential health risk assessment of groundwater from lithological diversity of the semi-arid region, Western Gujarat, India. *Appl. Water Sci.*, 10: 156-175.
- Sun, Y., Chen, G., Xu, Z., Yuan, H., Zhang, Y., Zhou, L., Wang, X., Zhang, C. and Zheng, J. 2020. Research progress of water environment, treatment, and utilization in coal mining areas of China. *Journal of China Coal Soc.*, 45(1): 304-316. (in Chinese)
- Talib, M.A., Tang, Z., Shahab, A., Siddique, J., Faheem, M. and Fatima, M. 2019. Hydrogeochemical Characterization and Suitability Assessment of Groundwater: A Case Study in Central Sindh, Pakistan. *Int. J. Environ. Res. Public Health*, 16: 886-906.
- Varol, S. and Davraz, A. 2014. Assessment of geochemistry and hydrogeochemical processes in groundwater of the Tefenni plain (Burdur/Turkey). *Environ. Earth Sci.*, 71: 4657-4673.
- Wu, J., Zhou, H., He, S. and Zhang, Y. 2019. Comprehensive understanding of groundwater quality for domestic and agricultural purposes in terms of health risks in a coal mine area of the Ordos basin, north of the Chinese Loess plateau. *Environ Earth Sci.*, 78: 446-462.
- Zhang, S., Wang, H., He, X., Guo, S., Xia, Y., Zhou, Y., Liu, K. and Yang, S. 2020. Research progress, problems, and prospects of mine water treatment technology and resource utilization in China. *Crit. Rev. Environ. Sci. Technol.*, 50(4): 331-383.
- Zaki, S.R., Redwan, M., Masoud, A. and Abdel Monein, A.A. 2019. Chemical characteristics and assessment of groundwater quality in Halayieb area, the southeastern part of the Eastern Desert, Egypt. *Geosci. J.*, 23, 149-164.



Bioremoval of Different Heavy Metals in Industrial Effluent by the Resistant Fungal Strain *Aspergillus niger*

K. J. Naveen Kumar*[†] and J. Prakash*

*Department of P.G. Studies and Research in Microbiology, Kuvempu University, Jnana Sahyadri, Shankaraghatta-577 451, Shivamogga District, Karnataka, India

[†]Corresponding author: K. J. Naveen Kumar; naviekj@gmail.com

Nat. Env. & Poll. Tech.

Website: www.neptjournal.com

Received: 22-10-2020

Revised: 02-01-2021

Accepted: 13-01-2021

Key Words:

Aspergillus niger

Bioleaching

Heavy metals

Oxalic acid

Submerged fermentation

ABSTRACT

Developing countries are increasingly concerned with pollution due to toxic heavy metals in the environment. Unlike most organic pollutants which can be destroyed, toxic metal ions released into the environment often persist indefinitely circulating and eventually accumulating throughout the food chain thus posing a serious threat to mankind. The use of biological materials for heavy metal removal or recovery has gained importance in recent years due to their good performance and low cost. Among the various sources, both live and inactivated biomass of organisms exhibits interesting metal binding capacities. Their complex cell walls contain high content of functional groups like amino, amide, hydroxyl, carboxyl, and phosphate which have been implicated in metals binding. In the present study, *Aspergillus niger* was used to analyze the metal uptake from an aqueous solution. The determination of Cu^{+2} , Pb^{+2} , Cd^{+2} , Zn^{+2} , Co^{-2} and Ni^{+2} in samples was carried out by differential Pulse Anodic Voltammetry (DPASV) and the Voltammograms. Production of oxalic acid was carried out by submerged fermentation. The organism used in the present study has the ideal properties to sequester toxic metals and grow faster.

INTRODUCTION

Fungi are ubiquitous in nature and can be found in soil, sediments, and aquatic environments such as lakes, ponds, rivers, marine water, wastewater, industrial effluents, etc. They are heterotrophic organisms, mostly aerobic or microaerophilic in nature. Fungi exist in a variety of morphological and physical states, which makes it difficult to quantify and identify them by cultural techniques. Cultural methods for fungi are similar to those of bacteria but must be modified to inhibit bacterial growth. They can also be used for the recovery of the metals from ores or even other forms (Elizabeth & Priyadarshini 2004, Abdul & Sirajuddeen 2006, Acosta-Rodriguez et al. 2018).

Metals in general are a class of chemical elements that form lustrous solids, which are good conductors of heat and electricity. However not all metals fit this definition, for example, mercury is a liquid. Metals such as arsenic, boron germanium, and tellurium are generally considered metalloids or semimetals in that their properties are intermediate between metals and those of non-metals. The metals associated with metal pollution are arsenic (As), cadmium (Cd), copper (Cu), chromium (Cr), mercury (Hg), lead (Pb), and zinc (Zn). Toxic metals include those with no known biological function. These include argentinum

(Ag), cadmium (Cd), tin (Sn), mercury (Hg), tellurium (Tl), lead (Pb), aluminum (Al), and metalloids like germanium (Ge), antimony (Sb), and silicon (Si). The metalloids exert different toxic effects than metals because they have different chemistries (Akthar & Mohan 1995, Aneja 2001, Barros et al. 2003).

Metal pollution results when human activity disrupts normal biogeochemical activities or by the disposal of concentrated metal wastes. Sometimes a simple metal is involved, but more often a mixture of metals is present (Bishnoi et al. 2004, Chatterjee et al. 2006). Mining ore refinement, nuclear processing, and the industrial manufacture of batteries, metal alloys, electrical components, paints, preservatives, and insecticides are some of the examples of processes that produce metal by-products. Examples of specific metal contaminants include copper and zinc salts that are extensively used as pesticides in agricultural settings, silver salts that are used to treat skin burns, lead which is utilized in the production of batteries, cable sheathing pigments, and alloys (Khasim Beebi et al. 1999, Hussain et al. 2004, Kumar & Selvisabhanayakam 2006). Other examples include mercury compounds that are used in electrical equipment, paints, thermometers, fungicides, as preservatives in pharmaceuticals and cosmetics, and triorganotin compounds such as tributyltin chloride and triphenyltin chloride, which can be

used as antifouling agents in marine paints because of their toxicity to plankton of bacteria (Mani & Mohini 2005).

Thus, while metals are ubiquitous in nature, human activities have caused metals to accumulate in the soil. Such contaminated soils provide a metal sink from which surface waters, groundwaters, and redox zone can become contaminated. Metal contamination has occurred for centuries since metals have been mined and used extensively throughout human history. Atmospheric metal concentration has also increased. Contaminated soil contributes to high metal concentrations in the air through metal volatilization. Several methods have been employed for the detection of metals (Naseem Akthar & Mohan 1995, Essoka & Umaru 2006). One among them is stripping voltammetry, among the electroanalytic techniques, differential pulse anodic stripping voltammetry is the most sensitive and suitable for detection of the heavy metal ions like cadmium, copper, zinc, lead, etc., because of low cost and easy operation (Asha & Juwarkar 1988, Acharya et al. 2004).

Bioleaching is a simple and effective technology for metal extraction from low-grade ores and mineral concentrates. The process involves the transformation of solid compounds into soluble and extractable elements which can be recovered. It represents a 'clean technology' with low cost and low energy consumption as compared to conventional methods. Metal recovery from sulfide minerals is based on the activity of chemolithotrophic bacteria, mainly *Thiobacillus ferrooxidans* and *Thiobacillus thiooxidans* which convert insoluble metal sulfides into soluble metal sulfates (Esposito et al. 2001, Fawzy et al. 2017). Non-sulfide ores and minerals can be treated by heterotrophic bacteria and by fungi. In these cases, metal extraction is due to the production of organic acids and chelating and complexing compounds excreted into the environment. At present bioleaching is used essentially for the recovery of copper, uranium, and gold and the main techniques employed are heap, dump, and in situ leaching. Tank leaching is practiced for the treatment of refractory gold ores (Ghaed et al. 2001, Hossain 2006). Bioleaching has also some potential for metal recovery and detoxification of industrial waste products, sewage sludge, and soil contaminated with heavy metals. The present work is undertaken with the following to study the bioleaching property of *Aspergillus niger*.

MATERIALS AND METHODS

Sample Collection

The industrial effluent samples were collected from the outlet five different times, near the bus stop Bhadravathi, Shimoga, and Karnataka using screw-capped plastic bottles

of 1.5 L capacity. The collected samples were preserved in the laboratory at room temperature.

Isolation of *Aspergillus niger* from Industrial Effluent by Serial Dilution Method

One mL of industrial effluent sample was taken in a test tube containing nine mL of sterile distilled water and shaken well in a vortex mixer. From this stock, various dilutions were prepared from 10^{-1} to 10^{-7} , using sterile distilled water. One mL of the diluted sample was poured into Petri plates containing the Potato Dextrose agar medium. Streptomycin was added to the molten medium after autoclave and the plates were incubated at $28 \pm 2^\circ\text{C}$ for 4 to 5 days to identify the fungi. Distinct fungal colonies grown on Potato Dextrose agar medium were isolated from repeated plating (Aneja 2001).

Identification of Fungi

Fungal morphology was studied macroscopically by observing colony features (color and surfaces) under a Stereo binocular microscope and microscopically by staining with Lacto phenol cotton blue and observed under binocular compound microscope for the conidia, conidiophores, and arrangement of spores (Funder 1961, Domsch 1980, Subramanian 1983).

Metal Detection

The sample was allowed to settle for a week. The liquid was decanted. The slurry was centrifuged for 15 min at 7000 rpm. The supernatant was decanted and the solid residue was collected and dried at $40\text{-}50^\circ\text{C}$ using the hot air oven. After drying, the residue was ground well using a pestle and mortar. The resultant mixture was weighed and preserved and a part of which was sent for metal analysis using stripping voltammetry (Schinner & Bungstaller 1989, Vijendra & Chandel 2001).

Processing for Bioleaching

The fermentation broth was prepared using glucose, peptone, malt extract, and double-distilled water. 200 mL of fermentation broth was poured into four different 250 mL conical flasks. The flasks containing media were sterilized at 121°C for 20 min. After cooling, the media was inoculated with *A. niger* at aseptic conditions. The flasks were then kept on the rotary shaker for 10 days at 120 rpm at 29°C . Titrations were carried out on the 10th day to estimate the oxalic acid production. 1.5 mg of the mixture was taken in the tea bag and suspended in the medium and left for bioleaching for 10 days (Satchanska et al. 2005).

Bioaccumulation Process

Metal used for analysis: Heavy metals such as zinc oxide and nanoparticles like nickel hydroxide, zinc hydroxide.

Preparation of stock solution: A stock solution of 500 ppm is prepared by dissolving 250 mg of the metal in 500 mL of double-distilled water. From this stock solution 20 ppm, 40 ppm, 60 ppm, 80 ppm, and 100 ppm concentrations were prepared.

Protocol for bioaccumulation process: Clean conical flasks were labeled with the metal concentration, organism to be inoculated, and the name of metal. 50 mL of sabouraud's dextrose broth was added. The respective metal concentration of 20 mL volume was added. Two loopful of the organism (*A. niger*) was inoculated. The flasks were incubated at room temperature for 7 days.

Metal detection: The residual metal in the aqueous solution was detected by using Atomic Absorption Spectroscopy (AAS). AAS is an instrument where the metal concentration in a solution is determined by aspirating a metal solution into an air acetylene flame to atomize the metal. A metal-specific lamp is placed into the AAS and is used to determine the differences in the light absorbance between a sequence source and the metal solution. The difference affects the amount of metal present.

Analysis of Complex Formation using UV Spectroscopy

After 10 days, the leachate and the control broth were made to undergo UV spectroscopy for the detection of complex formation. UV visible spectra of the controlled broth were recorded in water as a solvent. Then, 2 mL of the solution was taken and diluted with 2 mL of water (Jamil & Kumar

1997, Jyotsna 2003).

Processing: The incubated samples were filtered through Whatman No 1 filter paper to separate fungal mat and supernatant. The supernatant was decanted to another flask and the fungal biomass obtained was dried in a hot air oven at 250°C for 30 min. The supernatant obtained was subjected to a digestion process.

Digestion: To analyze the residual metal present in the supernatant, the supernatant was digested using concentrated nitric acid. The sample was digested in the following way. 100 mL of sample was taken in a beaker and 5 mL of concentrated nitric acid was added. The beaker was placed on a hot plate at 100°C. When the volume of the sample was reduced to 20 mL, then 5 mL of concentrated nitric acid was added. A Petri dish lid was placed on the beaker and evaporated to dryness. Then, 20-30 mL of distilled water was added, stirred well, and filter through Whatman No. 1 filter paper. Then the solution was made up to 100 mL by adding distilled water. The filtered solution obtained was subjected to atomic absorption spectroscopy (AAS) for the detection of residual metal.

Statistical analysis: All the results were statistically analyzed using SPSS software to determine the mean of three replicates and its standard error value from independent experiments.

RESULTS AND DISCUSSION

Isolation of *Aspergillus niger* from Industrial Effluent

Fungal morphology was studied macroscopically by observing colony features (color and surfaces) under a Stereo binocular microscope and microscopically by staining with

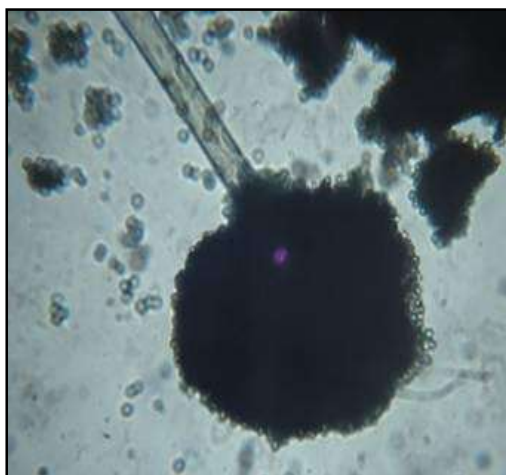


Fig. 1: Macroscopic and Microscopic view of *Aspergillus niger*.

Lacto phenol cotton blue and observed under a binocular compound microscope (Fig. 1).

Production of Oxalic acid by Submerged Fermentation Process

Production of oxalic acid was done by submerged fermentation process (Fig. 2).

Metal Detection

The processed sample was found to contain heavy metals like zinc, copper, cadmium, lead, cobalt, and nickel. The determination of Cu^{+2} , Pb^{+2} , Cd^{+2} , Zn^{+2} , CO^{-2} , and Ni^{+2} in the sample was carried out by Differential Pulse Anodic Voltammetry (DPASV) and the Voltammograms as shown in Fig. 3 and 4.

The results of the samples analyzed by DPASV were as follows, $\text{Cu} = 0.95 \text{ mg.kg}^{-1}$, $\text{Co} = 0.036 \text{ mg.kg}^{-1}$, $\text{Pb} = 0.50 \text{ mg.kg}^{-1}$, $\text{Ni} = 0.195 \text{ mg.kg}^{-1}$ and $\text{Zn} = 3.10 \text{ mg.kg}^{-1}$

Preliminary Work

Initially, we wanted to know the effect or binding capacity of the oxalic acid with the metals present in the industrial effluent sample. So, we started a preliminary test in which 10% oxalic acid (10 gm of oxalic acid in 100 mL distilled water) solution was prepared. To this, the processed sample was suspended using the teabag.

After two days the strength of the oxalic acid was estimated. Interestingly, it was found that the strength of the oxalic acid had decreased. Therefore, we allowed the experimental setup to stand for another five days. Finally,

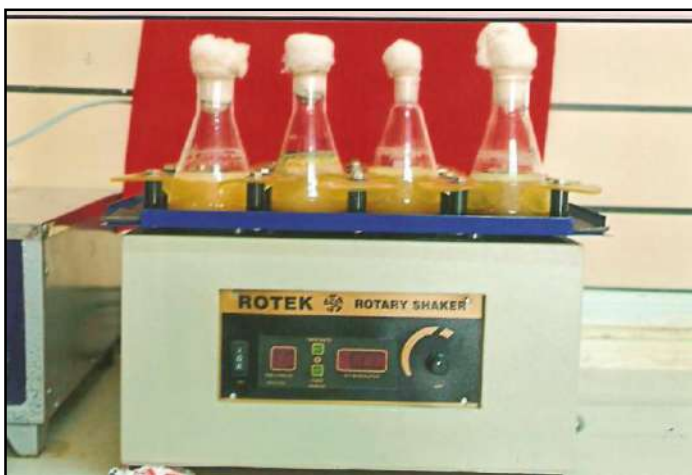


Fig. 2: Production of oxalic acid using malt extract broth by submerged fermentation process on a rotary shaker at 120 rpm.

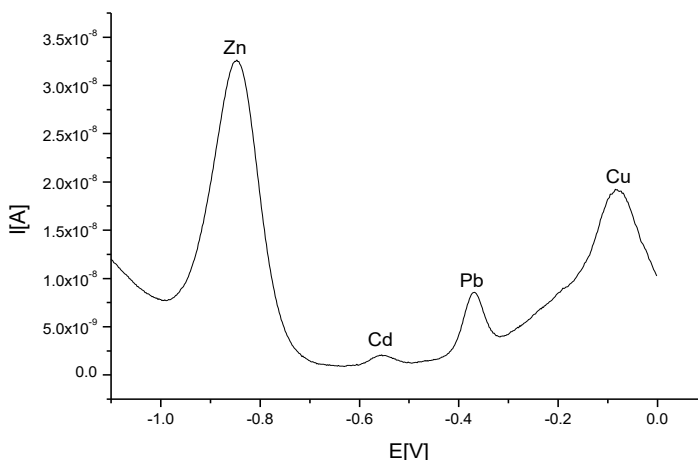


Fig. 3. Stripping voltammogram of the sample extracted from industrial effluent

Note: pH 2.25, Deposition potential -1.25 V, Deposition time 120 sec, modulation amplitude 20 mV, modulation time 0.5 sec, interval time 0.2 sec

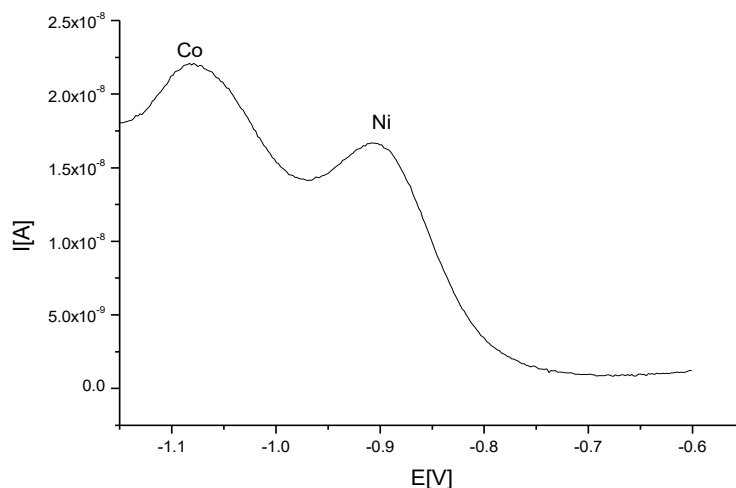


Fig. 4: Stripping voltammogram of the sample extracted from industrial effluent

Note: pH 9.2, Deposition potential -1.25 V, Deposition time 120 sec, modulation amplitude 20 mV, modulation time 0.5 sec, interval time 0.2 sec

after five days, final titration was carried out and it was observed that the strength of the oxalic acid had further decreased.

By observing the above results, fermentation broth containing glucose, peptone, and malt extract was used for the cultivation of *A. niger* and thereby oxalic acid production (Table 1).

Bioleaching

As expected, it was found that the strength of the fermented broth was decreasing. This was confirmed by the titrations performed (Table 2).

The decrease in the strength of the oxalic acid in the broth

confirmed the process of bioleaching. This was possible because more and more carboxylic (COO^-) groups formed complexes with the metal ions through coordination bonds. This gradually brought down the acidity of the broth, thereby indicating the progress of the bioleaching process.

After comparison, there was a decrease in controlled broth and leachate. In the control, it was due to fungal activity, whereas in leachate it was due to both fungal activity as well as bioleaching.

Detection of Complex Formation

The complex formation was further confirmed by UV spectrophotometry. UV visible spectra were recorded in Shimad-

Table 1: Oxalic acid production was estimated through titration assay.

Date	Sample taken	Trial No.	Initial reading	Final reading	Vol. of NaOH consumed	Strength of NaOH	Strength of oxalic acid
14-02-2019	Control	1	0	7.9	7.9	1	1.58
		2	7.9	15.8	7.9	1	1.58
	Leachate	1	0	7.9	7.9	1	1.58
		2	7.9	15.8	7.9	1	1.58
16-02-2019	Control	1	0	7.9	7.9	1	1.58
		2	7.9	15.8	7.9	1	1.58
	Leachate	1	0	7.3	7.3	1	1.46
		2	7.3	14.6	7.3	1	1.46
24-02-2019	Control	1	0	7.9	7.9	1	158
		2	15.3	23.2	7.9	1	158
	Leachate	1	0	7.1	7.1	1	1.42
		2	7.1	14.2	7.1	1	1.42

Table 2: Oxalic acid production was estimated from fermented broth through titration assay.

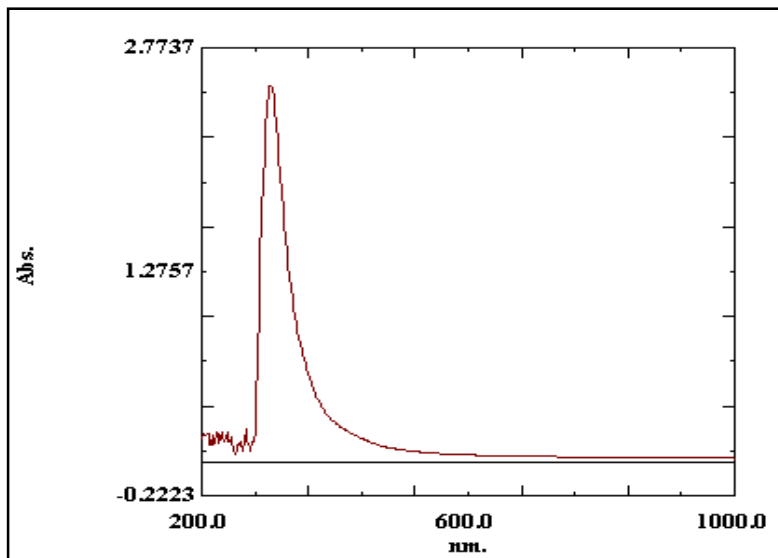
Days	Sample taken	Trial No.	Initial reading	Final reading	Vol. of NaOH consumed	Strength of NaOH	Strength of oxalic acid
10 days	Control	1	0.00	10.00	10.00	0.10	0.200
		2	10.00	20.00	10.00	0.10	0.200
	Broth-1	1	0.00	10.40	10.40	0.10	0.208
		2	11.00	21.40	10.40	0.10	0.208
	Broth-2	1	0.00	10.80	10.80	0.10	0.216
		2	11.00	21.80	10.80	0.10	0.216
20 days	Control	1	13.10	18.50	5.40	0.10	0.109
		2	24.50	30.00	5.50	0.10	0.109
	Broth-1	1	0.00	3.90	3.90	0.10	0.078
		2	3.90	7.80	3.90	0.10	0.078
	Broth-2	1	7.80	10.50	2.70	0.10	0.053
		2	10.50	13.10	2.60	0.10	0.053

zu UV visible-1650 PC spectrophotometer. The spectra of both control and treated broth are displayed below.

The absorption (λ_{max}) of the control was observed in the range of 304 nm (Fig. 5). But in the case of broth two, an additional peak was observed in the range of 524 nm, which confirms the formation of a complex metal with oxalic acid (Fig. 6).

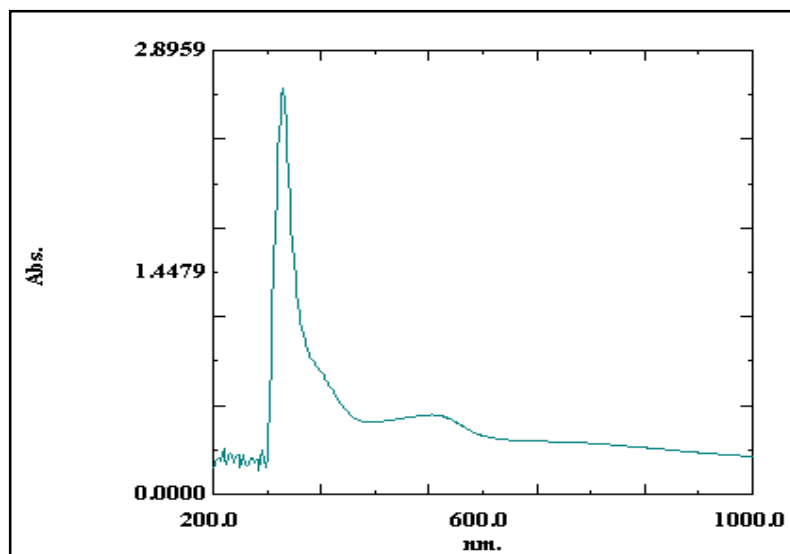
The effect of zinc oxide, zinc hydroxide, and nickel hydroxide on the cell growth in terms of the dry weight of biomass at different concentrations was reported (Table

3, 4 and 5) (Fig. 7, 8 and 9). It can be seen that a high concentration of zinc inhibited growth up to control values. A higher concentration of zinc accumulates in a concentration-dependent manner up to 60 ppm in the medium. *A. niger* was fairly effective in removing zinc oxide, zinc hydroxide, and nickel hydroxide from metal solution at a concentration ranging from 20-100 ppm. The results showed the concentration of heavy metals and nanoparticles remaining in the solution and accumulated by the organism.



Sl. No.	Wave length (nm)	Absorption
1	956.0	0.030
2	304.0	2.524
3	274.0	0.074

Fig. 5: Spectra analysis of control broth.



Sl. No.	Wave length (nm)	Absorption
1	524.0	0.518
2	304.0	2.646
3	434.0	0.467

Fig. 6: Spectra analysis of treated broth.

 Table 3: Bioaccumulation of zinc oxide (Heavy metals) by *Aspergillus niger*.

Initial conc. (mg/L)	Graph value	Conc. of metal remaining (mg/L)	conc. of metal accumulation (mg/L)	% of removal	Dry wt. of Biomass (mg)
Control	0	0	0	0	343
20	3.1830	4.085	15.915	75%	315
40	6.5598	7.201	32.799	80%	280
60	6.120	29.35	30.65	50%	259
80	5.9909	50.0455	29.9545	36%	180
100	5.1204	74.398	25.602	25%	180

 Table 4: Bioaccumulation of zinc hydroxide (nanoparticle) by *Aspergillus niger*.

Initial conc. (mg/L)	Graph value	Conc. of zinc hydroxide in metal solution (mg/L)	conc. of zinc hydroxide accumulation (mg/L)	% of removal of zinc	Dry wt. of Biomass (mg)
Control	00	0	00	0	260
20	1.7320	11.34	8.66	40%	175
40	1.5540	32.23	7.70	19.4%	143
60	1.5192	52.404	7.596	12.5%	90
80	1.19161	74.042	5.958	7.3%	75
100	0.5862	97.069	2.931	2.9%	60

DISCUSSION

Water plays an important role in the world economy. The majority (71%) of the Earth's surface is covered by water, but freshwater constitutes a minuscule fraction (3%) of the total. Water fit for human consumption is obtained from freshwater bodies. Approximately, 70% of the freshwater goes to agriculture. This natural resource is becoming scarce

at many places and its unavailability is a major social and economic concern (Khatik et al. 2006, Lohani et al. 2007, Ahmady-Asbchin & Bahrami 2011). Though access to safe drinking water has improved over the last few decades, it is estimated that five million deaths per year are caused due to consumption of polluted drinking water or drought. In many developing countries, 90% of all wastewater still

Table 5: Bioaccumulation of nickel hydroxide (nanoparticles) by *Aspergillus niger*.

Initial conc. (mg/L)	Graph value	Conc. of nickel hydroxide in metal solution (mg/L)	conc. of nickel accumulation (mg/L)	% of removal of nickel	Dry wt. of biomass (mg)
Control	0	0	0	0	290
20	2.2640	8.68	11.32	55%	147
40	1.8903	30.5485	9.4515	22%	90
60	1.5540	52.23	7.77	11.6%	75
80	1.0822	74.589	5.411	6.7%	60
100	0.6264	96.868	3.132	3.1%	60

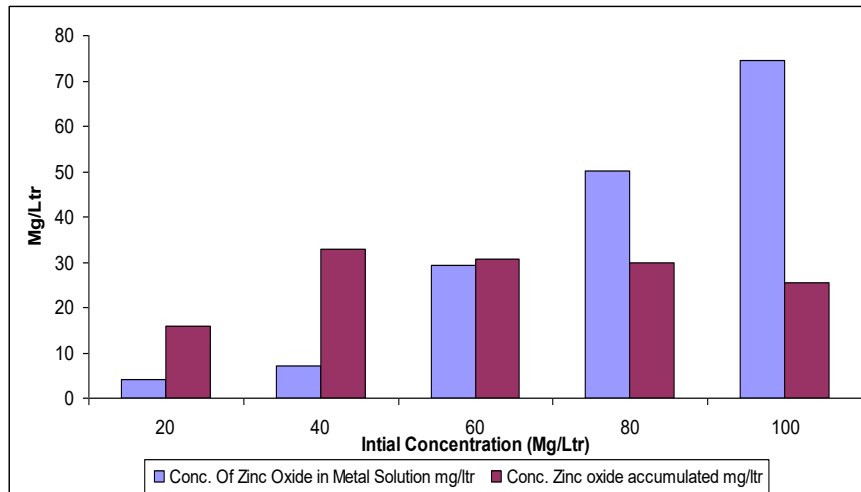


Fig. 7: Graph indicating the residual and accumulated concentration of zinc oxide.

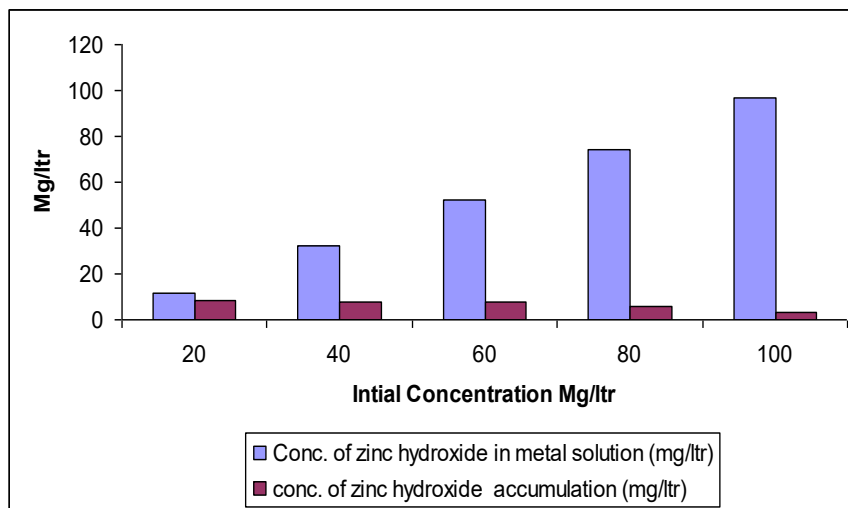


Fig. 8: Graph indicating the residual and accumulated concentration of zinc hydroxide.

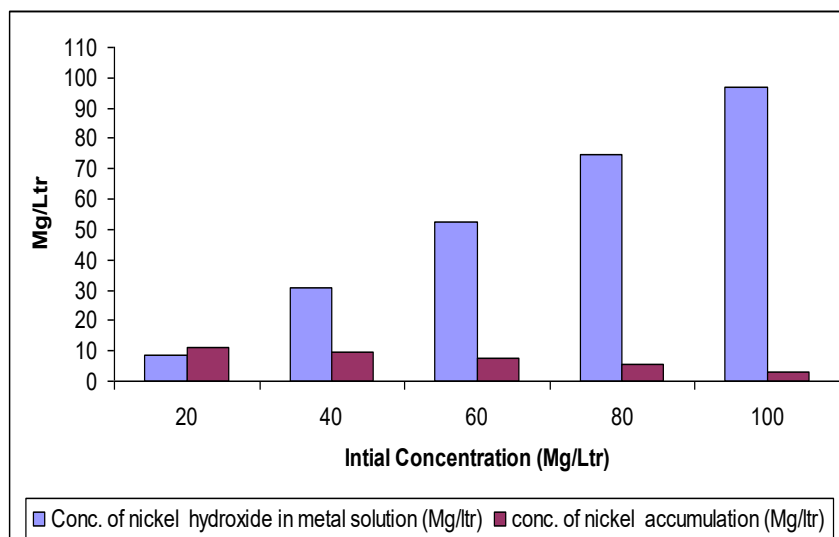


Fig. 9: Graph indicating the residual and accumulated concentration of nickel hydroxide.

goes untreated into the freshwater bodies making it unfit for human consumption, which either leads to scarcity or affects the human population. The concern to protect freshwater bodies for a healthy population is a challenge in recent times. Industrialization to a larger degree is responsible for the contamination of the environment especially water where lakes and rivers are overwhelmed with a large number of toxic substances (Muraleedharan et al. 1991, Murali et al. 2003, Korrapati & Pydi Setty 2012).

Heavy metals are reaching hazardous levels when compared with other toxic substances. Heavy metals are a unique group of naturally occurring compounds. Their continuous release leads to overconsumption and accumulation (Rai et al. 1998, Dhar et al. 2005, Essoka & Umaru 2006, Fawzy et al. 2017). As a result, people around the globe are exposed to adverse consequences of these heavy metals. Many industries (fertilizers, metallurgy, leather, aerospace, photography, mining, electroplating, pesticide, surface finishing, iron and steel, energy and fuel production, electrolysis, metal surface treating, electro-osmosis, and appliance manufacturing) discharge waste containing heavy metals either directly or indirectly into the water resources. Toxic heavy metals, which are of concern are chromium (Cr), lead (Pb), zinc (Zn), arsenic (As), copper (Cu), nickel (Ni), cobalt (Co), cadmium (Cd), and mercury (Hg) (Seide et al. 2000, Vlatka et al. 2001, Siddiquee et al. 2015). As these metals are not biodegradable, they tend to accumulate in living organisms and lead to various diseases and disorders which ultimately threaten human life. They can cause ill health, even when present in the range of parts per billion (ppb). Biosorption has emerged as an attractive option over conventional methods

for the removal of heavy metal ions from effluents discharged from various industries which ultimately reach and pollute freshwater bodies (Samal et al. 2004, Parihar et al. 2007, Ruta et al. 2010).

The bioaccumulation capacity of *A. niger* over a concentration ranging from 20 ppm to 100 ppm was estimated for zinc oxide heavy metal, zinc hydroxide nanoparticle, and nickel hydroxide. *A. niger* was fairly effective in removing zinc oxide, nanoparticles like zinc hydroxide, and nickel hydroxide from the media supplemented with metal solution observed in Figs. 7, 8 and 9.

At low concentrations, such as 20 ppm, there was a nearly complete accumulation of heavy metal (zinc oxide) in the medium. As the concentration of heavy metal increased in the medium, accumulation by the organisms varied. There was a decrease in the percentage of uptake of metal by fungal biomass. There was 80% removal of zinc oxide heavy metal at an initial concentration of 20 ppm to 25% at a final concentration of 100 ppm.

The results were compared with the work done by Asha & Juwarkar (1988). In her work on bioaccumulation of zinc by *Penicillium* sp., the percentage removal of zinc was 70% at a concentration of 100 ppm to 25% at a final concentration of 600 ppm.

Elizabeth & Priyadarshini (2004) had reported that metal up to a concentration of 50 ppm inhibits the growth of organisms. It can be seen that a high concentration of zinc inhibited the growth of the organism than control. Growth of organism was observed on the third day of incubation in control but in test samples, growth of organism was observed

on the seventh day. This reflects that metals had an effect on the growth of the organism.

The effect of nanoparticles on the accumulation and growth of organisms was comparatively low when compared to that of heavy metals. The accumulation of zinc hydroxide drastically reduced from 40% to 2.9% from an initial concentration of 20 ppm to a final concentration of 100 ppm respectively. Likewise, nickel had an effect on growth and accumulation. The percentage removal of nickel hydroxide reduced from 55% at 20 ppm to 3.1% at 100 ppm. This present work was compared with the work conducted by Hussain et al. (2004), who investigated the effect of carbon-60 on two common soil bacteria *E. coli* and *B. subtilis*. At a concentration of 2.5 mg.L⁻¹ of carbon-60, inhibition of the bacterial growth was observed. Reduction in the dry weight of biomass was observed as the concentration of metal i.e. nanoparticles increased in the medium.

Microorganisms capable of tolerating unfavorable conditions evolved their use as biosorbents in the removal of metal ions from wastewaters. They include bacteria, yeast, algae, and fungi. Experiments focused on the use of dead and or living microorganisms offer options for the type of remediation to perform. However, the use of dead microbial biomass for the binding of metal ions has been preferred over living biomass because of the absence of the requirement of nutrients and monitoring BOD and COD in effluents. Hence, the use of dead biomass is economical. These biosorbents can effectively sequester metal ions in the solution and decrease the concentration from the ppm to ppb level efficiently; therefore, they are considered ideal candidates for the treatment of complex wastewaters with high volume and low concentration of metal ions. A large quantity of materials of microbial origin has been investigated as biosorbents for the removal of metal ions extensively. Reports do not include the use biomass of any pathogens for water treatment (Rezza et al. 1997, Barros et al. 2003, Dhar et al. 2005, Chatterjee et al. 2006).

Fungi are also considered economic and eco-friendly biosorbents because of their characteristic features, that is, easy to grow, high yield of biomass, and ease of modification (chemically and genetically). The cell wall of fungi shows excellent binding properties because of distinguishing features like chitin, lipids, polyphosphates, and proteins among different species of fungi. The cell wall of fungi is rich in polysaccharides and glycoprotein which contain various metal-binding groups like amines, phosphates, carboxyls, and hydroxyls. Fungal organisms are used in a wide variety of fermentation processes. Hence, they can be easily produced at the industrial level for the biosorption of metal ions from a large volume of contaminated water resources. Besides, the

biomass can be easily and cheaply obtained from inexpensive growth media or even as by-products from many fermentation industries. Further, fungi are less sensitive to variations in nutrients and other process parameters like pH, temperature, and aeration. Because of their filamentous nature, they are easy to separate by means of simple techniques like filtration (Khasim Beebi et al. 1999, Ghaed et al. 2001, Rajendran et al. 2003, Segaran et al. 2020).

In the present study, we have isolated the *A. niger* from industrial effluent. This strain is more efficient for metal absorption from industrial water. This strain is widely used for the bioleaching process. Production of oxalic acid was using malt extract broth by submerged fermentation. The processed sample was found to be containing heavy metals like zinc, copper, cadmium, lead, cobalt, and nickel.

The mechanism of biosorption is a complex process that involves the binding of sorbate onto the biosorbent. Many natural materials can be used as biosorbents which involve the seventy-four biosorption binding of metal ions by physical (electrostatic interaction or van der Waals forces) or chemical (displacement of either bound metal cations (ion exchange) or protons) binding, chelation, reduction, precipitation, and complexation. Biosorbents contain chemical/functional groups like amine, amide, imidazole, thioether, sulfonate, carbonyl, sulfhydryl, carboxyl, phosphodiester, phenolic, imine, and phosphate groups that can attract and sequester metal ions (Ramteka 2000, Sarkar & Gupta 2003, Srinath et al. 2003).

A. niger is a heterotrophic microorganism that is widely applied in current bioleaching technology and has been extensively researched by local and foreign scholars. To date, bioleaching technology research is mainly related to metal removal in urban fly ash, waste catalyze, and minerals, and is mainly engaged in the screening and optimization of bioleaching process conditions. However, research on the leaching of heavy metals in urban sludge by *A. niger*, as well as on agricultural adaptability and environmental risks after sludge leaching, are lacking. The toxicity of heavy metals not only depends on concentration but also revolves around bioavailability.

CONCLUSION

It can be concluded that both titrimetric data and UV spectral data confirm the decrease in the acidity and complex formation respectively, which in turn confirms the bioleaching process of the metals extracted from the industrial effluent. Decrease in the individual metal concentrations will be carried out and the use of the bioleaching process in the removal of metal from the effluents has to be evaluated. The effect of

nanoparticles on the accumulation and growth of organisms was comparatively low when compared to that of heavy metals. The accumulation of zinc hydroxide drastically reduced from 40% to 2.9% from an initial concentration of 20 ppm to a final concentration of 100 ppm respectively. Likewise, nickel had an effect on growth and accumulation. The percentage removal of nickel hydroxide reduced from 55% at 20 ppm to 3.1% at 100 ppm. Finally, these results suggest the potential applicability of *A. niger* for the remediation of heavy metals from polluted industrial effluent.

ACKNOWLEDGEMENTS

The authors gratefully acknowledge the Department of Microbiology, Kuvempu University, Shivamogga, Karnataka, India, for providing necessary facilities and support for the completion of this work. They are indebted to their family and friends for their good wishes for the success of this work.

REFERENCES

- Abdul, J.A. and Sirajuddeen J. 2006. Heavy metal concentration of ground-water in Reltavaithatai area, Thiruchirappalli, Tamil Nadu. *J. Ecotoxicol. Environ. Monit.*, 16: 443-446.
- Acharya, C., Kar, R.N., Shukla, L.B. and Misra, V.N. 2004. Fungal leaching of manganese oil. *Transactions of the Indian Institute of Metals*, 57(5): 501-508.
- Acosta-Rodriguez, I., Cardenas-Gonzalez, J.F., Perez, A.S.R., Oviedo, J.T. and Juarez, V.M.M. 2018. Bioremoval of different heavy metals by the resistant fungal strain *Aspergillus niger*. *Bioinorg. Chem. Appl.*, 2018: 1-7.
- Ahmady-Asbchin, S. and Bahrami, A.M. 2011. Nickel biosorption by immobilized biomass of *Bacillus* sp. from aqueous solution. *Adv. Environ. Biol.*, 5: 1656-1663.
- Akthar, M.D. and Mohan P.M. 1995. Bio-mediated removal of toxic metal ions from polluted lake waters and industrial effluents by fungal biosorbent. *Curr. Sci.*, 59: 1028-1030.
- Aneja, K.R. 2001. Experiments in microbiology, plant pathology, and biotechnology. *New Age Int. Publ.*, 4: 157-162.
- Asha, J. 1988. Bioaccumulation of zinc by *Penicillium* sp. *Curr. Sci.*, 57: 251-252.
- Barros, L.M., Macedo, G.R., Duarte, M.M.L., Silva, E.P. and Lobato, A.K. 2003. Biosorption of cadmium using the fungus *Aspergillus niger*. *Braz. J. Chem. Eng.*, 20(3): 1-6.
- Bishnoi, N.R., Bajaj, M. and Sanatomba, S. 2004. Biosorption of zinc (II) using *Spirogyra* species from electroplating effluent. *J. Environ. Biol.*, 26: 661-664.
- Chatterjee, R., Das, M. and Maiti, S.K. 2006. Evaluation of phytoremediation of copper mine waste from Mosaboni, East Singhbhum. *Indian J. Environ. Protect.*, 26(3): 233-239.
- Dhar, N.R., Khoda, A.K., Khan, A.H., Bala, P. and Karim, M.F. 2005. A study of effects of acid activated saw dust on the removal of different dissolved tannery dyes (acid dyes) from aqueous solutions. *J. Environ. Sci. Eng.*, 47: 103-108.
- Domsch, K.H., Games, W. and Anderson, T.H. 1980. *Compendium of Soil Fungi*. Academic Press, London, pp. 1-858.
- Elizabeth, K.M. and Priyadarshini, B.H. 2004. Bioremediation of toxic pollutants by marine algae from Vishakhapatnam city. *Indian J. Environ. Protect.*, 24: 134-137.
- Esposito, A., Pagnanelli, F., Lodi, A., Solisio, C. and Veglio, F. 2001. Biosorption of heavy metals by *Sphaerotilus natans*: An equilibrium study at different pH and biomass concentrations. *Hydrometallurgy*, 60: 129-141.
- Essoka, P.A. and Umaru, J.M. 2006. Industrial effluent and water pollution in Kakuri area, Kaduna south, Nigeria. *J. Ind. Pollut. Control*, 22(1): 53-58.
- Fawzy, E.M., Abdel-Motaal, F.F. and El-Zayat, S.A. 2017. Biosorption of heavy metals onto different eco-friendly substrates. *J. Bioremediat. Biodegrad.*, 8(3): 1-7.
- Funder, S. 1961. *Practical Mycology Manual for Identification of Fungi*. 2nd edition. BrÃ,gger, Norway, pp. 1-120.
- Ghaed, S., Shirazi, E.K. and Marandi, R. 2001. Biosorption of Copper Ions by *Bacillus* and *Aspergillus* Species. *Adsorp. Sci. & Technol.*, 31(10): 869-890.
- Gupta, R., Ahuja, P., Khan, S., Saxena, R.K. and Mohapatra, H. 2000. Microbial biosorbents: Meeting challenges of heavy metal pollution in aqueous solutions. *Curr. Sci.*, 78: 967-973.
- Hossain, S.M. 2006. Studies on bacterial growth and copper (II) biosorption using *Bacillus subtilis*. *Indian J. Environ. Protect.*, 26: 1101-1107.
- Hussain, H., Ibrahim, S.F., Kandeel, K. and Moawad, H. 2004. Biosorption of heavy metals from wastewater using *Pseudomonas* sp. *Electron. J. Biotechnol.*, 7: 1-7.
- Jamil, K. and Kumar, B.M. 1997. Studies on the utilization of waste biomass *Alternaria eichhorniae* in the biosorption of lead, cadmium, and nickel. *Indian J. Environ. Protect.*, 17: 745-748.
- Jyotsna, L. 2003. Bioaccumulation: A method of metal removal and recovery from wastewater. *Indian J. Environ. Protect.*, 23: 1401-1407.
- Khasim Beebi, S.K., Chandana Lakshmi, M.V.V., Sridevi, V., Elizabeth K.M. and Chaitanya, K.V.K. 1999. Bioconcentration of nickel ions from single metal aqueous solutions by bacteria. *Indian J. Environ. Protect.*, 27(1): 75-80.
- Khatik, S.K., Thakur, R. and Sharma, G.D. 2006. Lead: the heavy metal in soil water and plant environment. *J. Ind. Pollut. Control*, 21(2): 233-244.
- Korrapati, N. and Pydi Setty Y. 2012. Studies on biosorption of chromium ions from wastewater using biomass of *Aspergillus niger* species. *J. Bioremediat. Biodegrad.*, 3(7): 1-4.
- Kumar, T.R. and Selvisabhanayakam, S. 2006. Impact of heavy metal zinc on protein metabolism in the fat body, testes seminal vesicles and margs of *Laccotrephes rubber* (Linn.) (Heteroptera: Nepidae) in relation to reproduction. *Environ. Ecol.*, 24(2): 529-531.
- Lohani, M.B., Rupinwar, D.C., Dhar, D.N. and Amarika, S. 2007. Spectroscopic analysis of Heavy metal concentration in the river Gomti at Lucknow. *Indian J. Environ. Protect.*, 27(2): 162-164.
- Mani, V.H. and Mohini, M. 2005. Toxic metals and environmental pollution. *J. Ind. Pollut. Control*, 21(1): 101-107.
- Muraleedharan, T.R., Iyengar, L. and Venkobachar, C. 1991. Biosorption: An attractive alternative for metal removal and recovery. *Curr. Sci.*, 61: 380-384.
- Murali, S., Absar Ahmad, M.I. and Ravi, K. 2003. Biosynthesis of metal nanoparticles using fungi and actinomycetes. *Curr. Sci.*, 85: 163-169.
- Naseem Akthar, M.D. and Mohan, P.M. 1995. Bio-mediated removal of toxic metal ions from polluted lake waters and industrial effluents by fungal biosorbent. *Curr. Sci.*, 59: 1028-1030.
- Parihar, D.K., Lawrence, K., Sharma, V., Lawrence, R. and Ramteke, P.W. 2007. Activity of catalase and peroxidase for assessment of river water quality. *Indian J. Environ. Protect.*, (2): 142-144.
- Rai, L.C., Sarita, S. and Pradhan, S. 1998. Biotechnological potential of naturally occurring and laboratory grown *Microcystis* in biosorption of nickel and cadmium. *Curr. Sci.*, 74: 461-464.
- Rajendran, P., Muthukrishnan, J. and Gunasekaran P. 2003. Microbes in heavy metal remediation. *Indian J. Exp. Biol.*, 41: 935-944.

- Ramteka, P.W. 2000. Biosorption of nickel (II) by *Pseudomonas stutzeri*. J. Environ. Biol., 21: 219-221.
- Rezza, I., Salinas, E., Calvente, V., Benuzzi, B., Snaz, M.I. and Tosethi, D. 1997. Extraction of lithium from spodumene by bioleaching. Lett. Appl. Microbiol., 25: 172-176.
- Ruta, L., Paraschivescu, C., Matache, M., Avramescu, S. and Farcasanu, I.C. 2010. Removing heavy metals from synthetic effluents using "kamikaze" *Saccharomyces cerevisiae* cells. Appl. Microbiol. Biotechnol., 85(3): 763-771.
- Samal, A.C., Bhar, G. and Santra, S.C. 2004. Biological process of arsenic removal using selected microalgae. Indian J. Exp. Biol., 42: 522-528.
- Sarkar, S. and Gupta, A. 2003. Treatment of chrome plating wastewater (Cr6+) using activated alumina. Indian J. Environ. Health, 45: 73-82.
- Satchanska, G., Rencheva, E.N., Atanasova, R., Groudeva, V., Trifonova, R. and Golovinoky, E. 2005. Microbial diversity in heavy metal polluted waters. Biotechnol. Equip., 19(3): 61-67.
- Schinner, F. and Bungstaller, W. 1989. Extraction of zinc from industrial waste by a *Penicillium* sp. Appl. Environ. Microbiol., 55(5): 1153-1156.
- Segaran, G., Uma Anitha, K.P.G. and Sathivelu, M. 2020. Evaluation of antioxidant, total phenol and phytoconstituents of *Curvularia* sp., a fungal endophyte of *Boerhaavia diffusa* L. Res. J. Biotechnol., 15: 117-122.
- Seide, H., Ondruschka, J., Morgenstern, P., Wennrich, R. and Hoffmann P. 2000. Bioleaching of heavy metal contaminated sediments by indigenous *Thiobacillus* spp. metal solubilization and sulphur oxidation in the presence of surfactants. Appl. Microbiol. Biotechnol. 6(15): 854-857.
- Siddiquee, S., Rovina, K., Sujjat, A., Laila, N., Suryani, S and Chaikaew, P. 2015. Heavy metal contaminants removal from wastewater using the potential filamentous fungi biomass: A review. J. Microb. Biochem. Technol., 7(6): 384-393.
- Srinath, T., Garg, S.K. and Ramteke, P.W. 2003. Biosorption and elution of chromium from immobilized *Bacillus Coagulans* biomass. Indian J. Exp. Biol., 41: 986-990.
- Subramanian, C.V. 1983. Hyphomycetes taxonomy and biology. Academic Press, London, 1 & 2: 1-930.
- Vijendra, S. and Chandel, C.P. 2006. Analytical study of heavy metals of industrial effluents at Jaipur, Rajasthan (India). J. Environ. Sci. Eng., 48(2): 103-108.
- Vlatka, Z.G., Tomas, C.S., Grba, S., Lutlisky, L. and Kozlek, D. 2001. Chromium uptake by *Saccharomyces cerevisiae* and isolation of glucose tolerance factor for yeast biomass. J. Biosci., 26: 217-223.



Surface Water Pollution Risk From Vietnam Water Quality Index (VN-WQI) in the Ca Mau City, Mekong Delta

Nguyen Ngan Ha*, Tran Thi Thu Huong*, Pham The Vinh*† and Tran Thi Van**(***)

*Southern Institute of Water Resources Research (SIWRR), Ho Chi Minh City, 70000, Vietnam

**Faculty of Environment and Natural Resources, Ho Chi Minh City University of Technology (HCMUT),
268 Ly Thuong Kiet Street, District 10, Ho Chi Minh City, Vietnam

***Vietnam National University Ho Chi Minh City, Linh Trung Ward, Thu Duc District, Ho Chi Minh City, Vietnam

†Corresponding author: Pham The Vinh; vinhsiwrr@gmail.com

Nat. Env. & Poll. Tech.
Website: www.neptjournal.com

Received: 10-11-2020

Revised: 15-01-2021

Accepted: 22-01-2021

Key Words:

Multiple linear regression
Satellite image
VN-WQI
Water quality
Ca Mau city

ABSTRACT

This paper presents the study of integrating the remote sensing technology with in-situ ground observation for assessing the status of water quality in Ca Mau city through the Vietnam Water Quality Index (VN-WQI). The Sentinel-2 image and in-situ surface water samples were collected on 20 February 2020 for this study. The sample results were then specified by samples' coordination. Besides, Sentinel-2 imaging was processed by radiometric and atmospheric correction, geometric registration, and extracted pixel spectral values from the sample locations. The multiple linear regressions of seven water quality parameters including BOD₅, COD, NH₄, PO₄, TSS, pH, Coliform with surface water's pixel spectral values from the satellite images were calculated and used to simulate water quality parameters on the satellite image. They were integrated into the VN-WQI to estimate, classify, and evaluate the general surface water quality of the Ca Mau city. The results show that there is a regressive correlation between measured data and image spectral values, and the simulation also well fits with the data with an acceptable error. The surface water quality of Ca Mau city is heavily polluted with almost all water quality parameters recognized at B1 to above B2 level according to the QCVN08-MT:2015/BTNMT. In terms of VN-WQI, the results also illustrate the low quality of surface water and heavy pollution only used for water transportation, not for domestic use. This approach can be a powerful method in spatially monitoring water quality and supporting environment management.

INTRODUCTION

Water is a critical factor that determines the success of strategies, planning, socio-economic development, ensures national security, water security, etc. but not like petroleum that can be replaced by other fuels such as electricity, biofuel, gas, etc. Water, although renewable, is a finite and irreplaceable resource. Many studies, actions, solutions, strategies, and more activities have been put in place and implemented to protect the Earth's water resources. In the field of water quality assessment, the remote sensing method is considered one of the optimal technology solutions for estimating water quality (Gholizadeh et al. 2016).

Citizens of Ca Mau city have been suffering from extremely polluted surface water as a result of river water containing high levels of organic compounds, nutrients, suspended particles, and microorganisms. In the face of this alarming situation, it is necessary to put in efforts and a lot of actions to overcome these environmental disasters and improve water quality. Assessing the water quality is one of

the first actions taken into consideration. At present, the city still uses the traditional method of in-situ measurement with laboratory analysis. However, the number of water samples is not enough and cannot fully cover the surface water network of the city due to lack of human resources, budget, and the time required to conduct a field study. Moreover, this method is accurate at the point scale but does not give either the spatial or temporal view of water quality needed for accurate assessment or management of water bodies (Ritchie et al. 2003). Therefore, remote sensing technology is one of the best solutions to improve the cons of the in-situ measurement method by extracting spatial-temporal information on water quality with a high spatial resolution (Lim & Choi 2015).

The assessment of water quality by applying remote sensing technology has been recognized in numerous studies and research projects. Many of those consider the correlation between water quality parameters and pixel values of satellite images. Alparslan et al. (2007) assessed the water quality at Ömerli Dam, Turkey by using the Landsat 7-ETM satellite data and measured water quality parameters (chlorophyll-a,

suspended solid matter, Secchi disk, and total phosphate). The study showed that Landsat TM satellite data and water quality parameters at various locations of Ömerli Dam can be related through a regression analysis to constitute a model, which can be used to measure water quality parameters over the entire lake surface (Alparslan et al. 2007). Abdullah (2010) estimated multiple water indices by developing water quality models based on Landsat 8 image and four mathematical methods (NSFWQI, CCMEWQI, OWQI, and AWWQI) for twenty stations in Dokan Lake, Iraq. The thesis concluded that the AWWQI model gives the best results with the coefficient R^2 . Therefore, the relationship between the image bands of the Landsat OLI image and the water indicators is consistent (Abdullah 2010). In 2014, Waxter's study conducted a linear regression between Landsat 5 and in situ measurement of Hazardous Algae Blooms in North and South Tenmile Lakes in coastal Oregon, United States. Results show a good linear correlation between turbidity and radiance, which are inversely related in algal-dominated lakes (Waxter 2014). Another similar study is from Kapalanga (2015). The study had used Landsat 8 images to estimate multiple water parameters for the Olushandja dam in North-central Namibia. The author then concluded that the developed regression algorithms are best fit to predict water quality parameters from satellite data. Remote sensing is therefore recommended for frequent and continuous monitoring of Olushandja Dam as it has the ability to provide information about surface water quality (Kapalanga 2015). El-Zeny and El-Kafrawy (2016) also applied the regression model between calibrated Landsat 8 image and water parameters on Burullus Lake (El-zeny & El-Kafrawy 2016). In 2017, Gholizadeh & Melesse (2017) developed a multiple linear regression model for Florida Bay between the optical bands in the region from blue to near-infrared and all the possible band ratios to explore the relationship between the reflectance of the waterbody and observed data. They used Landsat 5 for data in the wet season and Landsat 8 for data in the dry season. The model gave high coefficients and is good to monitor and predict the spatiotemporal variations of the studied water quality parameters in Florida Bay (Gholizadeh & Melesse 2017). With the small scale of the study area as the Bin El reservoir, Karaoui et al. (2019) applied Sentinel-2 images to simulate the surface water indices (chlorophyll-a, dissolved oxygen, nitrates). The in-situ sampling was carried out in the Bin El Ouidane Reservoir (Azilal Province), followed by the analysis of physicochemical parameters in the laboratory. These measurement results were compared with the reflectance in each sampling location to investigate the correlations between bands and laboratory chemical analysis results. The correlation results showed that they can be transformed to predictive models by stepwise regression (Karaoui et al. 2019). In Vietnam, Dinh (2018) applied VNREDSAR-1A

data (Vietnam's satellite images) to monitor the surface water of the Hanoi region. The study has built up the optimal model for calculating the four water indicators for two areas of the lagoon and the Red River. The research results had demonstrated the effectiveness and reliability of remote sensing technology in assessing and monitoring surface quality compared with traditional research methods (Dinh 2018). In 2019, Vo et al. (2019) Published a study on the applicability of Landsat imagery to estimate suspended sediment concentrations (SSC) on Tien and Hau rivers, Mekong Delta. The research results had identified a linear regression model with variables such as reflectance coefficients from the green and red channels capable of applying SSC estimation for the study area. The results showed that there is a strong correlation between the actual measured SSC data series and the estimated SSC according to the equation. Therefore, it is possible to study the changes of SSC on the river in the direction of the satellite image approach (Vo et al. 2019).

Based on the correlation between the water parameters and satellite image's pixel values, this paper applies the remote sensing technology for estimating seven water parameters include biochemical oxygen demand (BOD_5), chemical oxygen demand (COD), ammonium (NH_4), phosphate (PO_4), total suspended solids (TSS), pH and coliforms. The regression model was constructed between the in-situ measurements sampling points and four bands (blue, green, red, near-infrared) of the Sentinel-2 image. Both in-situ data and Sentinel-2 were collected on 20 February 2020. Furthermore, the VN-WQI was used in combination with Decision 1460/QD-TCMT to present and map the overall state of surface water quality in Ca Mau.

MATERIALS AND METHODS

Study Area

Ca Mau city, located in the east of Ca Mau province, is one of the driving forces of the Mekong Delta's core economic zone (Fig. 1).

There are four types of land use in Ca Mau city which include residential areas, shrimp ponds, aquaculture areas, and perennial crop farms. Aquaculture land accounts for 57.1 % of the city's total area. Residential areas and shrimp ponds are in second and third place, with 25.2 % and 11.9 %, respectively. Perennial cropland makes up only 0.4 % of the total land area. The rest of the city has a water layer of 5.3 %.

Datasets

Satellite Image

The satellite image used in this study is the Sentinel-2 MSI

level 2A (S2A) acquired on 20 February 2020 collected from the European Space Agency (ESA). The Level-2A product provides Bottom of Atmosphere (BOA) reflectance images derived from the associated Level-1C products. Each Level-2A product is composed of $100 \times 100 \text{ km}^2$ tiles in cartographic geometry (UTM/WGS84 projection) (ESA, 2020). There are 13 bands in the Sentinel 2 image. According to the principle of spectral reflection on the electromagnetic spectrum, water objects have strong reflectivity in short wavelengths. Besides that, from many previous studies about the relationship between surface water quality and satellite pixel values, this study utilized $10 \text{ m} \times 10 \text{ m}$ of resolution image with its four bands blue (band 2), green (band 3), red (band 4), and near-infrared (band 8) to determine the multiple linear regression between the field data and the satellite reflectance values (Engman & Gurney 1991, Seyhan & Dekker 1986, Zhu et al. 2011, Fiorani et al. 2006, Imen et al. 2014, Chang et al. 2014).

Field Data

We conduct field sampling in the dry season to reduce the cloud or rain effects from the weather conditions, and to consist of the Sentinel 2A image captured time samples collected from 10:00 to 10:45 am on 20 February 2020. We divided into three teams to collect 51 samples from major

rivers, canals, and lakes in the study area. Fig. 2 shows the sampling routes and 51 sample locations.

Spatial Data

Instead of satellite images and field samples, spatial data such as administrative boundaries, existing land use, canals, and street networks can be used for satellite geo-processing, extracting the study area, developing the water quality zoning maps, and analyzing the results.

Mathematical Approach

There are five main stages in this study which include (1) Collecting and assessing in-situ data following the National technical regulation of surface water quality QCVN08-MT:2015/BTNMT; (2) Pre-processing the Sentinel 2A image; (3) Specifying pixel spectral values with the measured data; (4) Calculating and applying the multiple linear regression on the satellite image; (5) Applying VN-WQI from Decision 1460/QĐ-TCMT and establishing the classification map of surface water quality (VN-WQI map) (Fig. 3).

Preprocessing of Satellite Image

The image preprocessing stage was implemented in three

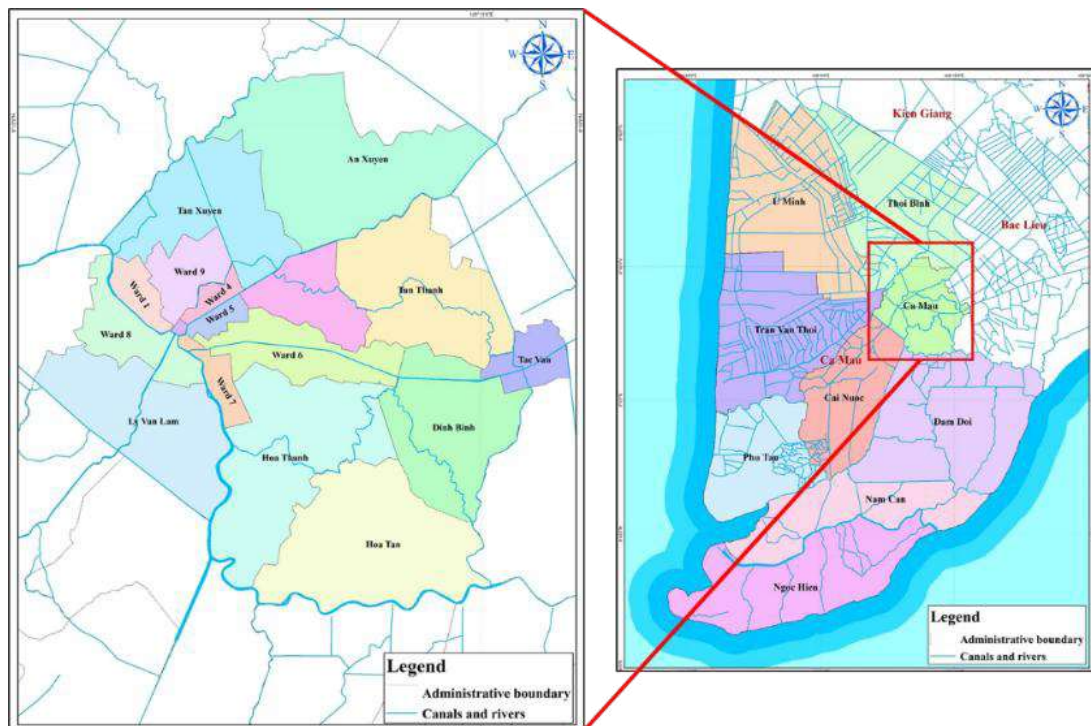


Fig. 1: Ca Mau city location.

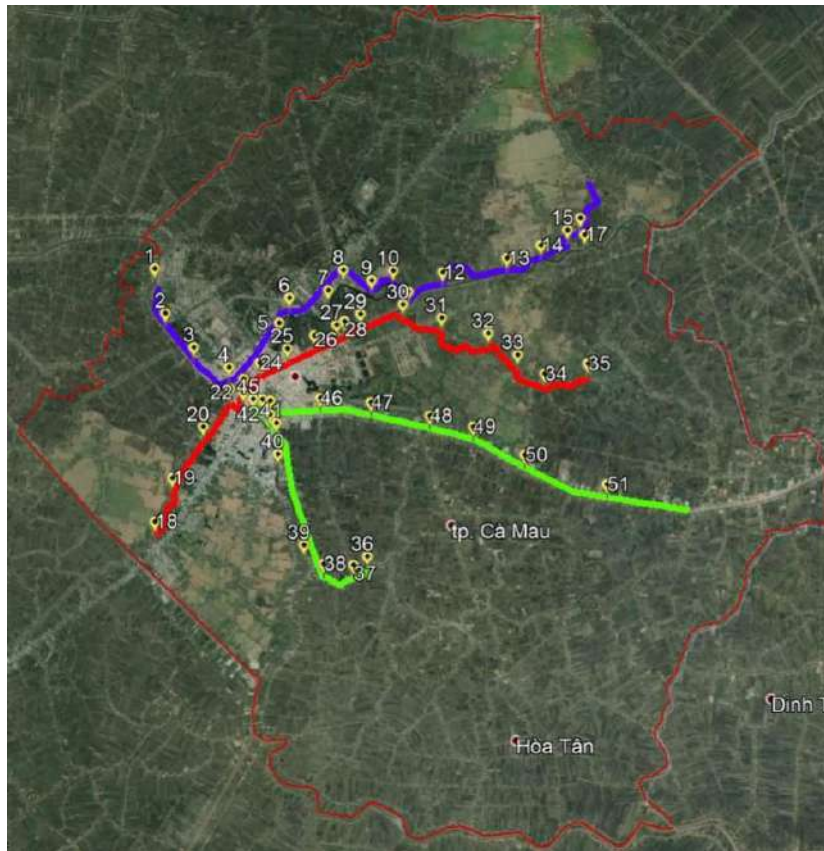


Fig. 2: The study sites with sampling routes and sample locations.

steps include (1) spatial resampling, (2) radiometric calibration, and (3) geoprocessing.

The S2A product requires spatial resampling since the bands are measured at different spatial resolutions. Due to the size of the study area, a resolution of 10 m is required to retrieve the best pixel values. The resampling used band 2 with 10 m to up-sampling with a larger spatial resolution (20m and 60m) onto a grid with a higher spatial resolution. This step is done by the Nearest neighbor sampling method whereas every pixel value in the output product is set to the nearest input pixel value. Each output cell value in the nearest neighbor method is the unmodified value from the closest input cell (ESA 2019).

The next step is the radiometric calibration to convert the surface reflectance into the radiance values as the S2A has already been calibrated from the raw DN (Digital Numbers) into the surface reflectance by using solar irradiance in each wavelength at the time of acquisition. In this study, the FLASH method was applied to four bands of resampled S2A products mentioned above. This computation has the general form:

$$L_{\lambda} = \text{gain} * \text{cell value} + \text{offset} \quad \dots(1)$$

Where L_{λ} is the radiance [Watts/(m²*steradian* μ m)]

The last step is geoprocessing the calibrated S2A to reduce the error that comes from satellite shooting angles. This study used the Ground Control Point (GCP) method for the image geo-reference. Five control points were selected for the geo-reference. The Root Mean Square Error (RMSE) showed 0.26 which is below 0.5 as the required rule.

Surface Water Layer Extraction

The iso cluster unsupervised classification method was utilized for the surface water extraction. The iso cluster algorithm is an iterative process for computing the minimum Euclidean distance when assigning each candidate cell to a cluster (ESRI 2020a). Generally, the more cells contained in the extent of the intersection of the input bands, the larger the values for minimum class size and sample interval should be specified (ESRI 2020b).

$$Z = \frac{(X - \text{oldmin}) \times (\text{newmax} - \text{newmin})}{(\text{oldmax} - \text{oldmin})} + \text{newmin} \quad \dots(2)$$

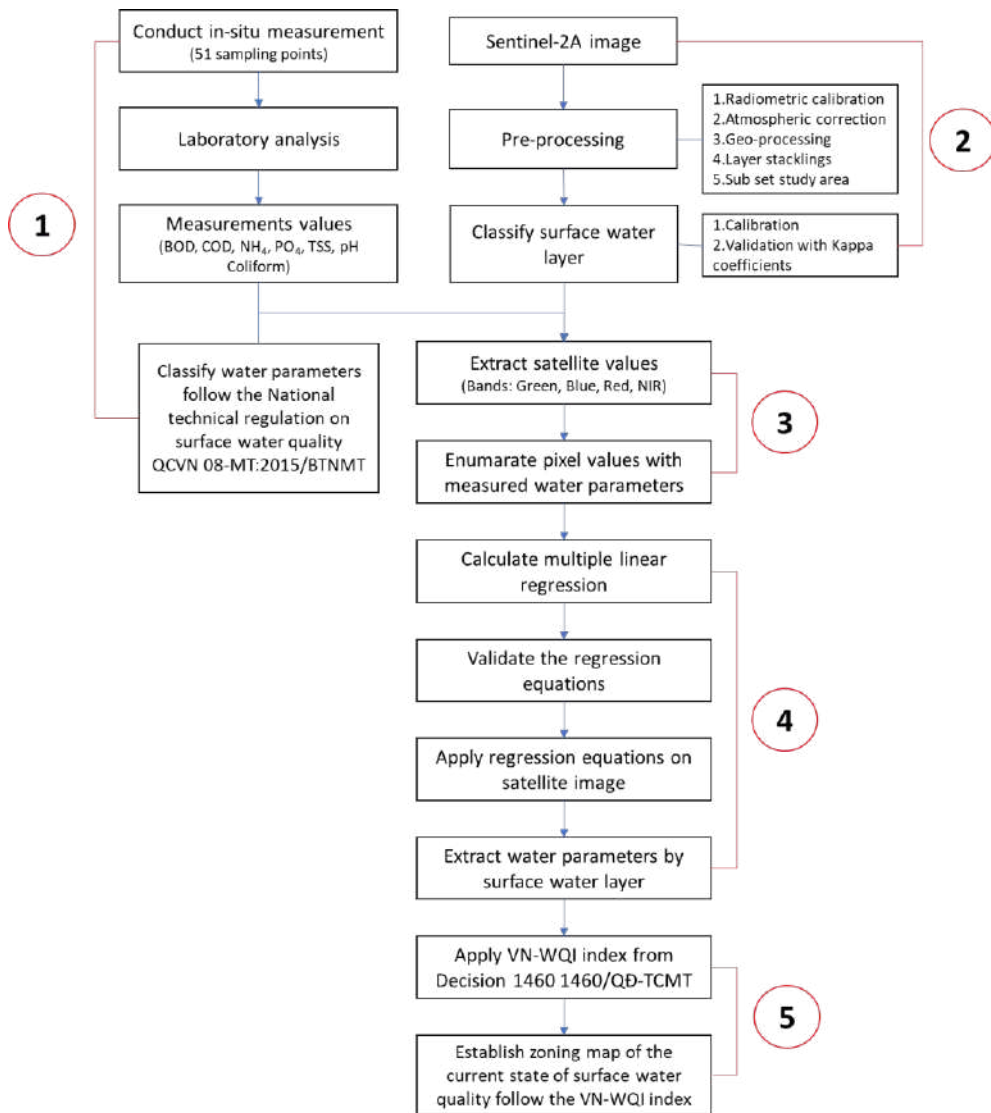


Fig. 3: Different steps for the WQI mapping process.

Where Z is the output raster with new data ranges; X is the input raster; oldmin is the minimum value of the input raster; oldmax is the maximum value of the input raster; newmin is the desired minimum value for the output raster; newmax is the desired maximum value for the output raster.

Multiple Linear Regression Calculation

The multiple linear regression between measured parameters (BOD₅, COD, NH₄, PO₄, TSS, pH, and Coliform) and the satellite pixel values (bands 2, 3, 4, 8) of 38 out of 51 sample locations was conducted. The regression function is expressed in detail in equation 3.

$$y_i = a + bx_{i,B2} + cx_{i,B3} + dx_{i,B4} + ex_{i,B8} \dots(3)$$

Where i is a study site; y_i is the measured parameter of the study site i; (dependent variable); x_i is the pixel values of the study site i in bands blue, green, red, or NIR (independent variable). B2, B3, B4, B8 are bands blue, green, red, and NIR respectively.

These regression equations then are validated by five statistical indices in Excel software: R square (R²), adjusted R square (Adj. R²), t-Stat, p-value, and Significance-F (Sig. F).

After applying the validated regression equation on the S2A, three parameters include Bias, RMSE, and Percentage

of Error (PE) were calculated to validate the simulated results with the measured values. These parameters are defined as equations 4, 5, 6.

$$\text{Bias} = \text{Bias} = \frac{1}{n} \sum_{i=1}^n (X_i - Y_i) \quad \dots(4)$$

$$\text{RMSE} = \sqrt{\frac{1}{n} \sum_{i=1}^n (X_i - Y_i)^2} \quad \dots(5)$$

$$\text{PE} = \frac{1}{n} \sum_{i=1}^n \left| \frac{X_i - Y_i}{X_i} \right| \times 100 \quad \dots(6)$$

Where X_i, Y_i are estimated values and ground data values, respectively, n is the number of samples.

The regressions equations accepted as the above parameters meet the following criteria: $R^2 \geq 0.8$, $\text{adj. } R^2 \geq 0.8$, $t\text{-Stat} \geq |2|$, $p\text{-value} \leq 0.05$, and $\text{Sig. } F \leq 0.05$

VN-WQI Calculation

From the multiple water quality parameters, the integrated index to provide the general assessment of water quality is required. The VN-WQI is utilized to classify the water quality of the study area. This index was calculated based on the Decision 1460/QD-TCMT regarding the promulgation of Technical Guidelines for calculation and publication of the Vietnam Water Quality Index (VN-WQI). VN-WQI was calculated from five groups of parameters including (Group I) pH index; (Group II) Crop protection agent; (Group III)

Heavy metal parameters; (Group IV) Organic and Nutrient parameters; and (Group V) microorganism parameters.

To calculate the WQI, it is necessary to select at least three out of five specified groups (from Group I to Group V), of which three parameters from Group IV are required. Therefore, this paper chooses to calculate seven criteria: BOD₅, COD, NH₄⁺, P-PO₄³⁻, TSS (Group IV), Coliform (group V), and pH (Group I). The summary formula of VN-WQI is shown as equation 7.

$$WQI = \frac{WQI_I}{100} \times \frac{\left(\prod_{i=1}^n WQI_{II}\right)^{1/n}}{100} \times \frac{\left(\prod_{i=1}^m WQI_{III}\right)^{1/m}}{100} \times \left[\frac{1}{k} \sum_{i=1}^k WQI_{IV} \times \frac{1}{l} \sum_{i=1}^l WQI_V \right]^{1/2} \quad \dots(7)$$

Where $WQI_I/WQI_{II}/WQI_{III}/WQI_{IV}/WQI_V$ are the results of WQI by groups I to V, respectively. These WQIs are calculated and classified following the Decision 1460/QD-TCMT (Table 1).

RESULTS AND DISCUSSIONS

Ground Measured Water Quality Parameter Assessment by Sampling Locations

The National technical regulation on surface water quality, QCVN 08-MT:2015/BTNMT, governs four groups for the classification of surface water sources for the purposes of assessing and controlling water quality for various purposes. These four values are described in Table 2. The limit values for each water parameter are shown in Table 3.

Table 1: Surface water quality classified by VN-WQI.







		VN-WQI index	
WQI value range	Water quality	Color	Utilization purpose
90-100	Very good		Good for domestic water supply purposes
75-90	Good		For domestic water supply purposes but need appropriate treatment measures
50-75	Average		For irrigation and other similar purposes
25-50	Poor		For water transportation and other similar purposes
10-25	Very poor		Heavily polluted water, needing treatment measures in the future
<10	Heavily polluted		Toxic water, need to take measures to overcome and treat

Table 2: Classification of surface water quality by QCVN 08-MT:2015/BTNMT.

Group	Description
A1	Good use for domestic water supply and other purposes, such as A2, B1, and B2
A2	For domestic water supply, but must apply the appropriate treatment technology, conservation of aquatic animals and plants, or other purposes, such as B1 and B2
B1	For irrigation purposes or other purposes requiring similar quality standards or for the purposes as B2
B2	Water transport and other purposes with low-quality water requirements

From the classification standard (Table 2), Fig. 4 illustrates the surface water quality of 51 samples taken in the study area on 20 February 2020. Water characteristics obtained from Ca Mau’s principal rivers, canals, and lakes, as shown in Table 3, generally indicate poor surface water quality, with the majority of the results falling between B1 and B2. In detail, except for the pH value is in group A1 all the other parameters have values from B1 to B2 level and even exceed the B2 level. Especially TSS and PO₄, most of the values are above B2. This data indicates that the state of surface water quality is severely polluted, indicating that the local government must take suitable actions and implement solutions to enhance water quality.

Multiple Linear Regression Results

The regression was conducted from the statistic of in-situ

surface water quality parameters with pixel spectral values of four bands (blue, green, red, and NIR) at 38 sample locations as mentioned before. However, in our first calculation, we observed that each parameter correlated with different bands combinations according to the *t*-Stat and the *p*-value. In general, the *t*-stat $\geq |2|$ and *p*-value ≤ 0.05 show that the parameter and satellite band have a good relationship. Otherwise, they have a weak correlation.

The first calculation result is presented in Table 4. From this table, NH₄ and pH have a good relationship with all four bands. The BOD₅ and COD do not correlate with the NIR band with *t*-stat below $|2|$. The same situation with PO₄ and Coliform parameters. Last, the TSS parameter only correlates with bands green and red. Therefore, we removed bands that do not have a good relationship with water parameters, and then recalculated and derived new regression equations (Table 5).

Table 3: Limit values of surface water quality QCVN 08-MT:2015/BTNMT.

No.	Parameter	Unit	Limit values			
			A1	A2	B1	B2
1	BOD ₅ (20°C)	mg/L	4	6	15	25
2	COD	mg/L	10	15	30	50
3	NH ₄ ⁺	mg/L	0.3	0.3	0.9	0.9
4	PO ₄ ³⁻	mg/L	0.1	0.2	0.3	0.5
5	TSS	mg/L	20	30	50	100
6	pH	-	6-8.5	6-8.5	5.5-9	5.5-9
7	Coliform	MPN/100 ml	2,500	5,000	7,500	10,000

Table 4: Statistic of *t*-Stat and *p*-value from regression analysis.

Water quality parameter	Parameter/Band	BLUE	GREEN	RED	NIR
BOD ₅	<i>t</i> Stat	39.245	-44.410	17.608	0.865
	<i>P</i> -value	0.000	0.000	0.000	0.000
COD	<i>t</i> Stat	14.811	-16.889	7.072	0.701
	<i>P</i> -value	0.000	0.000	0.000	0.000
NH ₄	<i>t</i> Stat	9.152	6.598	-20.754	51.535
	<i>P</i> -value	0.000	0.000	0.000	0.000
PO ₄	<i>t</i> Stat	36.151	-40.856	13.297	0.674
	<i>P</i> -value	0.000	0.000	0.000	0.000
TSS	<i>t</i> Stat	-1.089	-38.498	61.365	1.215
	<i>P</i> -value	0.000	0.000	0.000	0.000
pH	<i>t</i> Stat	2.237	-17.509	15.312	22.692
	<i>P</i> -value	0.000	0.000	0.000	0.000
Coliform	<i>t</i> Stat	-178.232	157.395	82.680	-0.036
	<i>P</i> -value	0.000	0.000	0.000	0.000

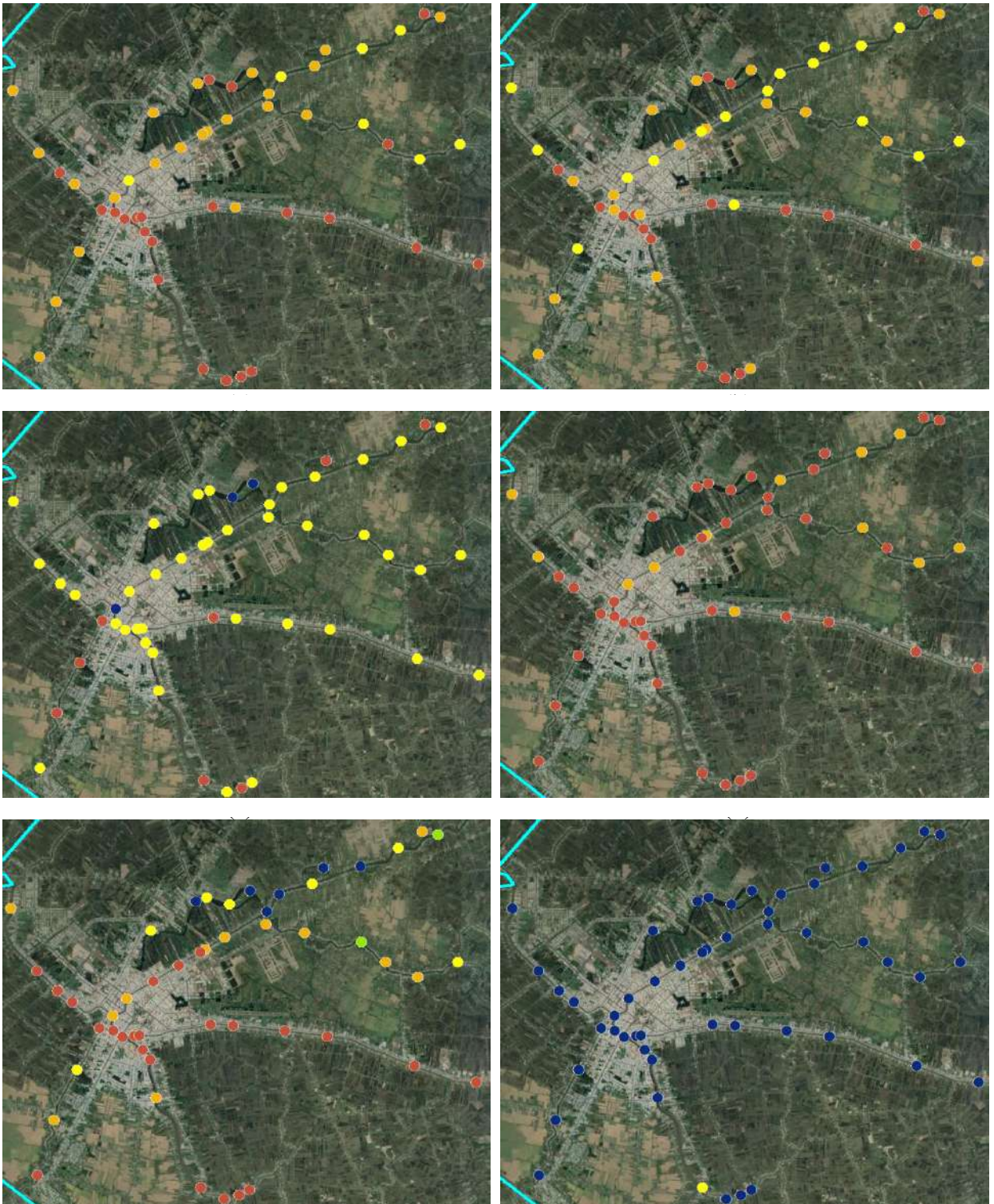


Fig. 4 Cont....

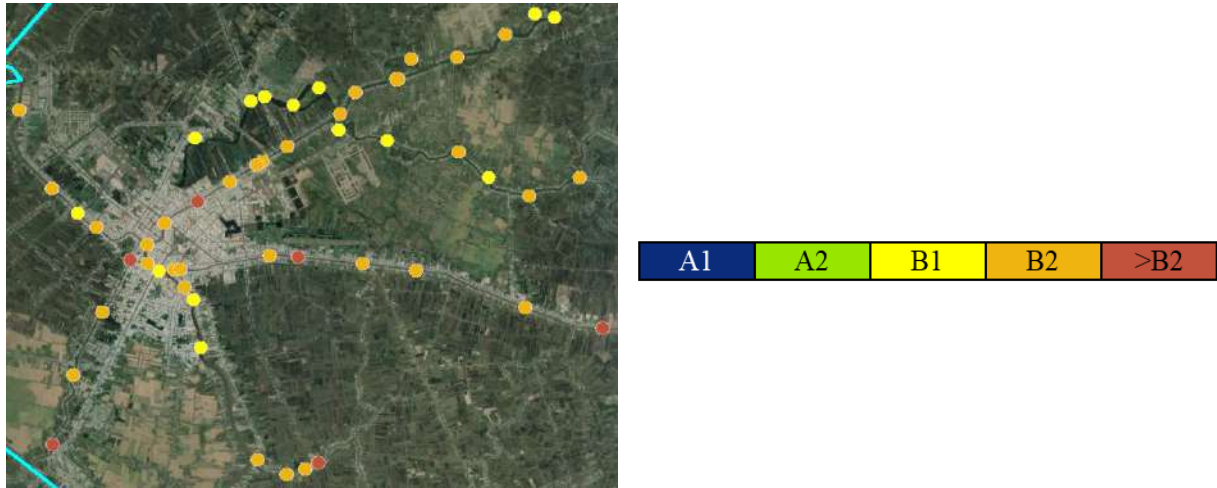


Fig. 4: Classification of measured surface water quality by QCVN 08-MT:2015/BTNMT: (a) BOD₅, (b) COD, (c) NH₄, (d) PO₄, (e) TSS, (f) pH, and (g) Coliform

From Table 5, the regressions equations of all water quality parameters show its R² and adjusted R² above 0.9, and significance F below 0.05. Therefore, the measured parameters and satellite bands have a significant regressive correlation. Thus, water quality parameters can be achieved by applying these regression equations on the

S2A. 13 remaining measured data was used to evaluate the simulation results by applying the derived regression equations and the statistical parameters include bias, percentage error (PE), and RMSE. Table 6 presents the simulation results of 13 remaining measured data and its validation.

Table 5: Recalculated multiple linear regression equations.

Water quality parameter	Regression equation derived	R ²	Adj. R ²	Sig. F
BOD ₅	25.57 + 14167.79 x B - 16071.25 x G + 5222.30 x R	0.988	0.987	0.000
COD	40.70 + 22453.20 x B - 25817.64 x G + 9021.55 x R	0.930	0.923	0.000
NH ₄	-0.009 + 108.99 x B + 78.35 x G - 198.09 x R + 189.53 x N	0.992	0.991	0.000
PO ₄	1.094 + 590.20 x B - 665.99 x G + 178.03 x R	0.986	0.984	0.000
TSS	44.20 - 55467.75 x G + 69783.92 x R	0.998	0.998	0.000
pH	7.20 + 56.033 x B - 437.31 x G + 307.42 x R + 175.540 x N	0.985	0.983	0.000
Coliform	6076.83 - 2025482.56 x B + 1783177.80 x G + 290083.64 x N	0.970	0.970	0.000

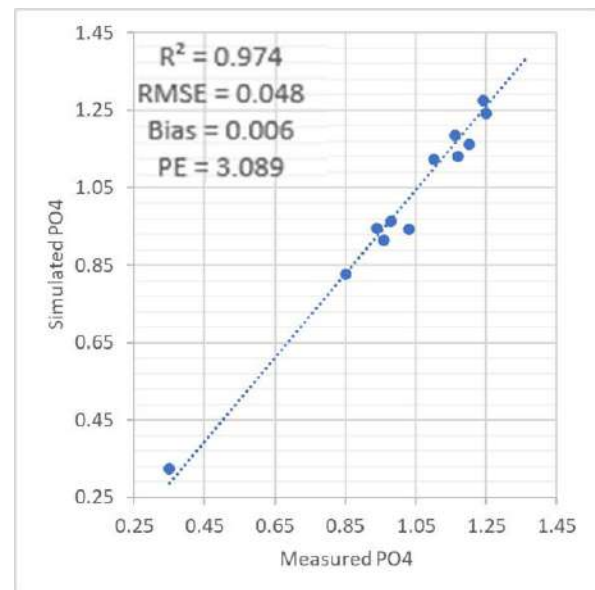
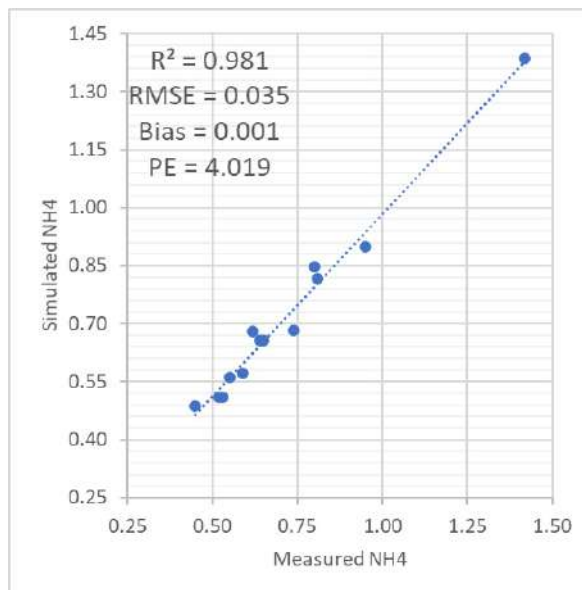
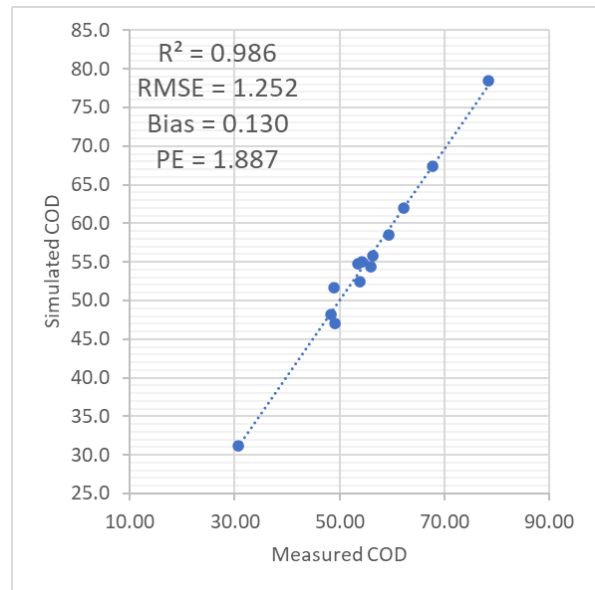
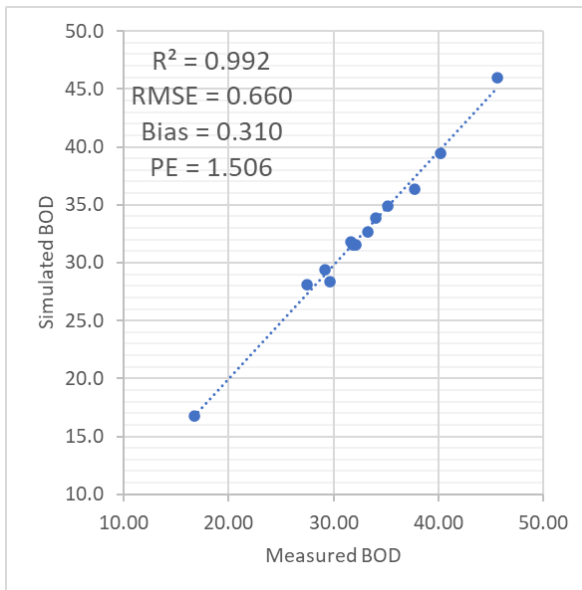
(B is band blue, G is band Green, R is band red and N is band near-infrared)

Table 6: The area percentage of the simulation results classified by QCVN 08-MT:2015/BTNMT.

Parameter/Level	A1	A2	B1	B2	>B2
BOD	4.82	3.31	22.80	43.78	25.29
COD	7.03	5.16	28.23	49.95	9.63
NH ₄	2.87		46.59		50.54
PO ₄	4.82	7.07	7.69	17.59	62.83
TSS	2.18	1.83	6.36	37.43	52.21
pH	0.003	0.03	5.13	45.05	49.79
Coliform	99.30		0.69		-

The simulation results from the 13 remaining samples are very close to the in-situ measurements (Fig. 5). The bias of seven parameters are all less than 3 with 0.31 (BOD_5), 0.13 (COD), 0.001 (NH_4), 0.006 (PO_4), -1.66 (TSS), 0.009 (pH), and -2.82 (Coliform). However, the estimated Coliform is still accepted and can illustrate a good simulation. The percentage error also witnessed good values with all values is under 5% with 1.51% (BOD_5), 1.89% (COD),

4.02% (NH_4), 0.006 (PO_4), 3.09% (TSS), 0.95% (pH), and 0.60% (Coliform). The RMSE also presents the strong relationship between estimated and measured data with 0.66 (BOD_5), 1.25 (COD), 0.03 (NH_4), 0.05 (PO_4), (2.14) TSS, 0.06 (pH), and 24.7 (Coliform). Therefore, the simulation results achieved from the estimated regression equations and the S2A can indicate the real water quality data with reliable accuracy.



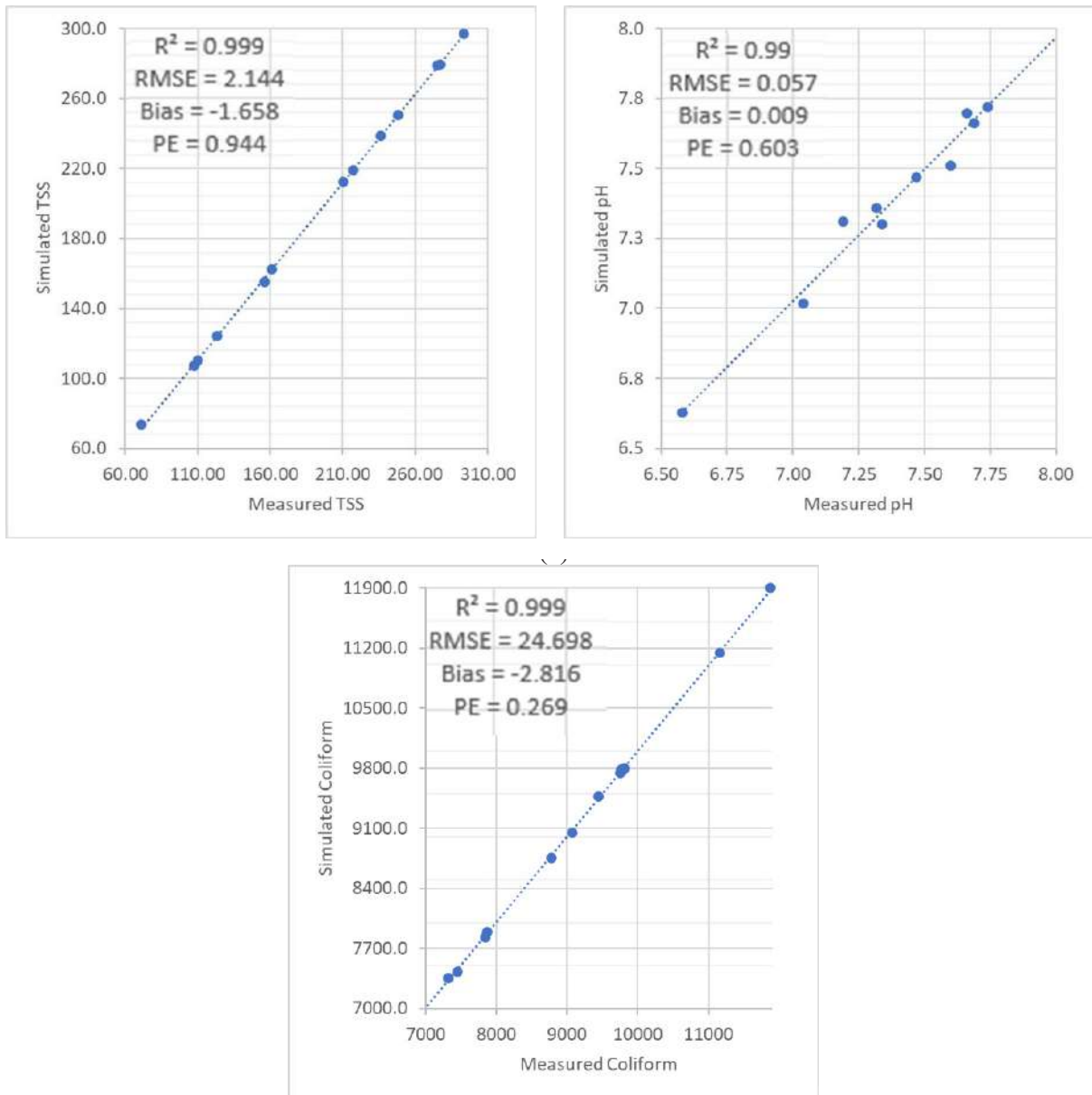


Fig. 5: Comparison of water quality parameters derived from Sentinel-2A and measured data on 20 February 2020: (a) BOD₅, (b) COD, (c) NH₄, (d) PO₄, (e) TSS, (f) pH, and (g) Coliform

Water Quality Parameters Derived from Sentinel-2A

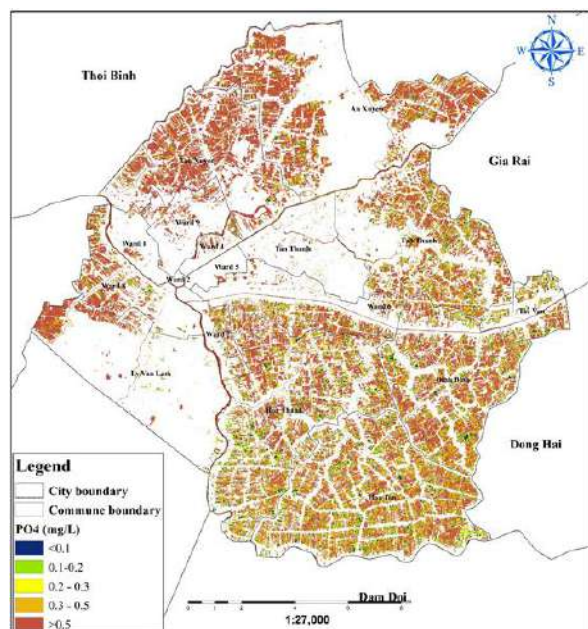
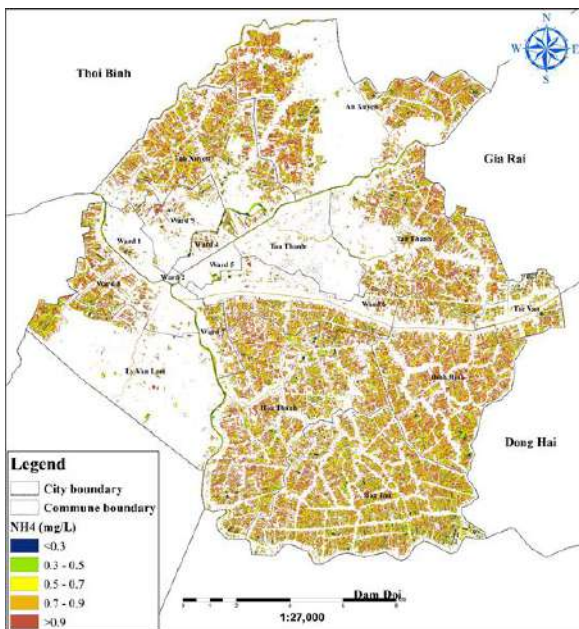
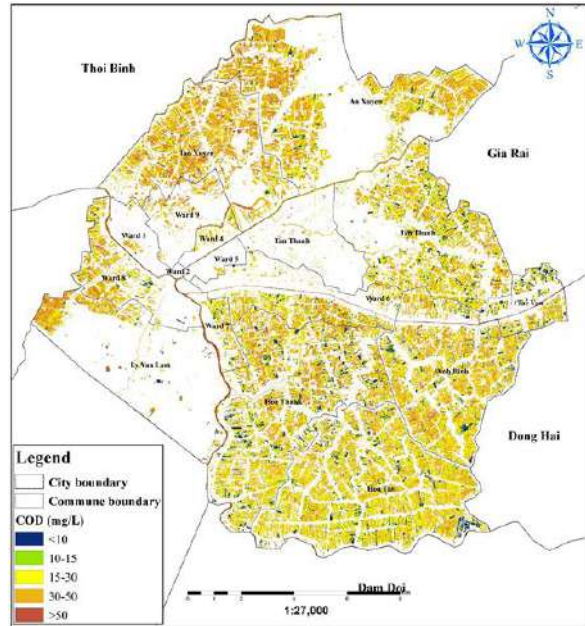
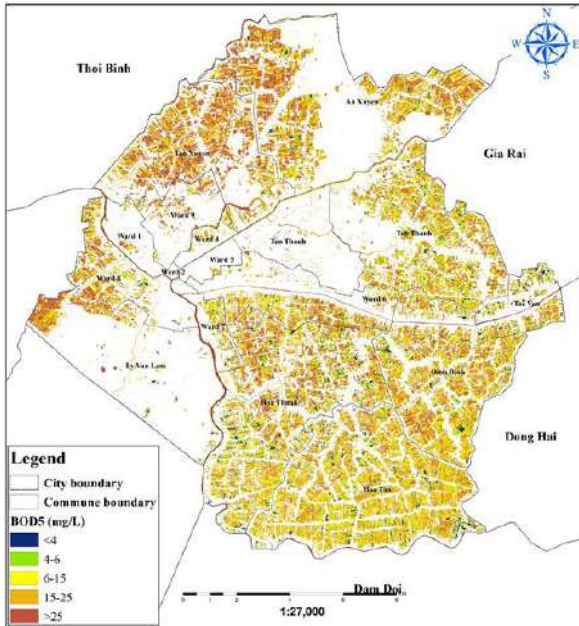
Table 6 is the area percentage of the simulated water quality parameters by concentration level classified by QCVN 08-MT:2015/BTNMT.

With BOD₅, level B2 (15-25 mg.L⁻¹) covered the most of surface water area with 43.78% of the area. On the other hand, levels A1 (<4 mg.L⁻¹) and A2 (4-6 mg/L) levels covered

a small area with only 4.82% and 3.31%. The same trend appears in COD when 49.95% of the study area was level B2 (30-50 mg.L⁻¹). Levels A1 and A2 still came last with 7.03% and 5.16% of the distribution area. In terms of NH₄, 50.54% of the Ca Mau city’s surface water is distributed above the B2 level (>0.93 mg.L⁻¹). In contrast, the A-level (A1 and A2) assigned only 2.87%. In PO₄ parameters, the concentration above 0.5 mg.L⁻¹ (above B2 level) accounted for the highest

proportion, at 62.83% of the total area. Meanwhile, the lowest figures can be seen in the percentage of A1 level ($<0.1 \text{ mg.L}^{-1}$), at nearly 4.8%. TSS parameter has a similar trend with the PO_4 when more than 100 mg.L^{-1} of TSS (above B2 level) covered most of the city's surface water area with 52.21% of the total area. Meanwhile, A1 and A2 levels have the lowest figures, at 2.18% and 1.83%. In the Coliform parameter, the proportions of above B2 ($>10,000$

MPN/100mL) and B2 (7,500-10,000 MPN100mL) levels were high, at 49.79% and 45.05% while the level A1 allocated only about 0.003% respectively. In contrast to the above parameters, the A-level (A1 and A2) of pH, which ranges from 6 to 8.5, is predominantly found in surface water, accounting for 99.30% of the total. Meanwhile, the B-level (B1 and B2) covered a very small area, about 0.69% of the area.



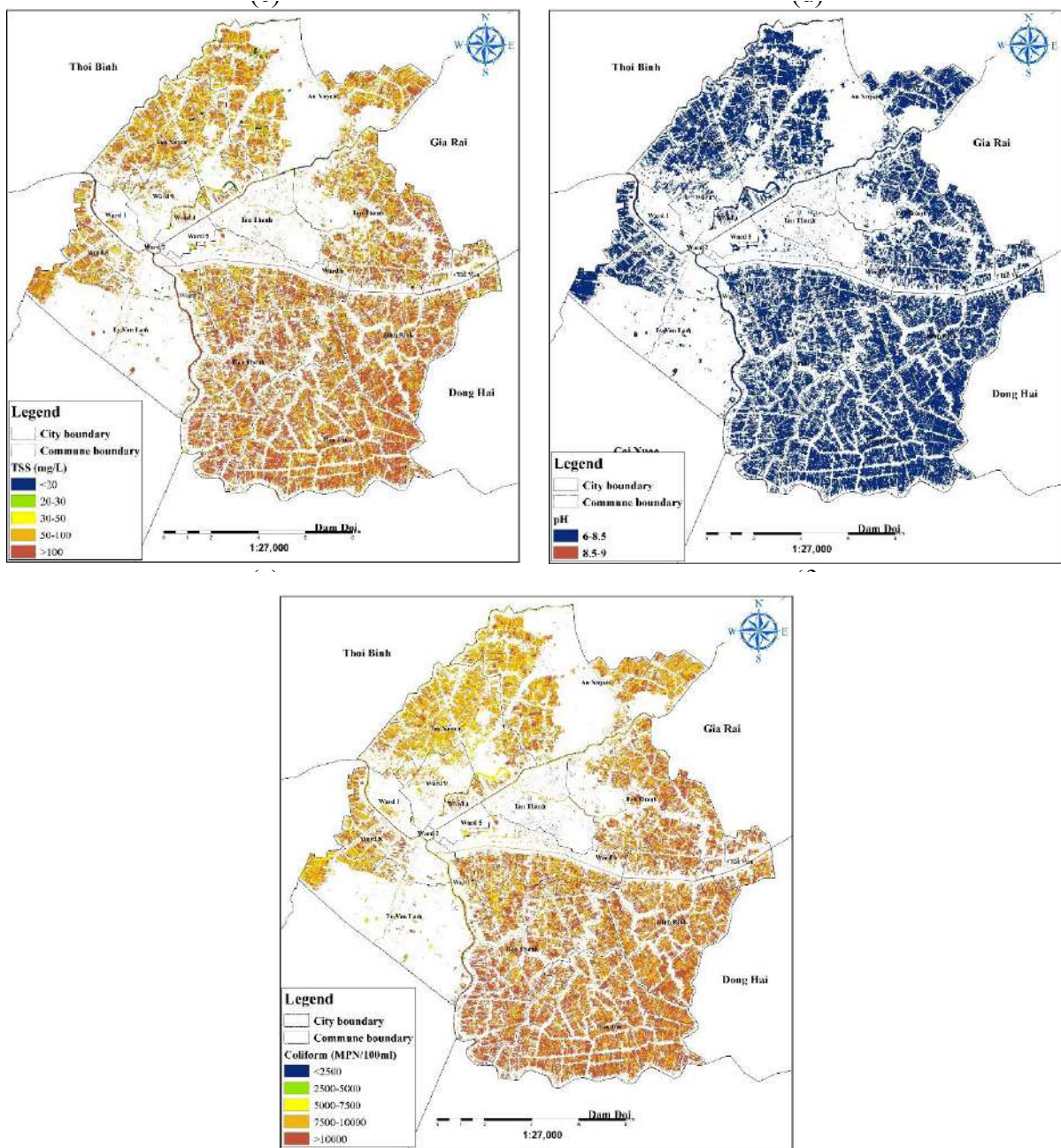


Fig. 6: Seven parameters with limit value ranges for water quality analysis by QCVN 08-MT:2015/BTNMT achieved from the S2A: (a) BOD₅, (b) COD, (c) NH₄, (d) PO₄, (e) TSS, (f) pH, and (g) Coliform.

In general, except for pH, all other parameters have a very high concentration (equivalent B1, B2, and above B2 levels) that appeared in most surface water in Ca Mau city. Meanwhile, the A-level (A1 and A2) comprises a small area in which water is used for drinking. With the current status of the seven water quality parameters at the image acquisition

time, the surface water of Ca Mau city seems heavily polluted. However, the concentration levels of each parameter have a fragmented distribution and cannot provide the overall assessment of the surface water quality. Therefore, the VN-WQI index was used to derive the general surface water quality from the above seven parameters.

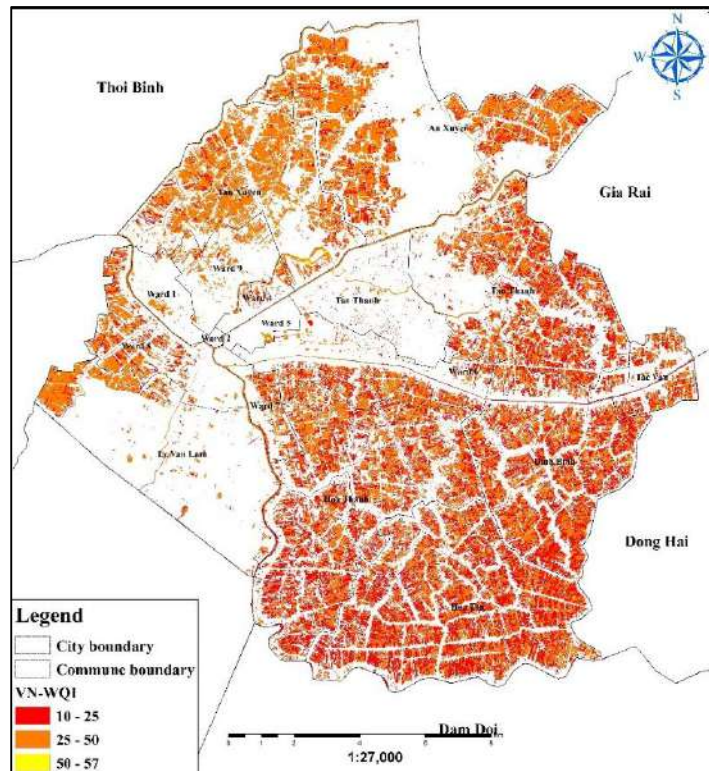


Fig. 7: General surface water quality classified by VN-WQI.

General Surface Water Quality Classification by VN-WQI

To have a general assessment for the surface water quality, the VN-WQI was conducted and its result was classified according to the Decision 1460/QD-TCMT approved by Vietnam Environment Administration (2019) mentioned in the above VN-WQI in the above section. The results are illustrated in Table 7 and Fig. 7. In general, statistical results showed that there are three WQI levels detected in the study area, 10-25, 25-50, and 50-75, and have an uneven distribution. WQI levels 10-25 and 25-50 are most detected in surface waters of Ca Mau city, with levels 10-25 occurring most in the south and the east while 25-50 mainly distributed in the northwest and the northeast of this city. As a result, the surface water quality in Ca Mau city is low, with a level of 10-25 indicating that the water is extremely polluted and will require treatment in the future, and a level of 25-50 indicating that the water is only

utilized for water transportation and other similar reasons. On the other side, the surface water used for irrigation and other similar purposes contained a small proportion (level 50-75), and there was no surface water area that suitable for domestic water supply.

More specifically, level 50-75 has a low figure of 0.11 % and is dispersed around the city. It's particularly common in the Tan Xuyen district. The WQI 10-25 level, on the other hand, accounts for around 41% of the entire surface water area in Ca Mau city, with most of it concentrated in the city's south and east. The area distribution on the side of levels 25-50 accounted for the highest percentage of the total area distribution at 58.7%. Levels 25-50, like levels 10-25, are dispersed around the city. However, it concentrated in the northwest and northeastern areas. Both of these WQI levels mainly occur in aquaculture and industrial areas, residential area, and shrimp ponds in An Xuyen, Hoa Tan, Hoa Thanh, Ly Van Lam districts, and Tan Thanh commune.

Table 7: Distribution of VN-WQI result by classification level.

VN-WQI classification level	10-25	25-50	50-75
Area (ha)	3874.14	5529.06	10.56
Percentage of area (%)	41.15	58.73	0.11

One of the reasons to explain this situation is that the wastewater comes from industrial parks, specifically Hoa Trung Industrial park located in the south of the city. There are currently nine industrial production establishments (five seafood processing facilities and four processing facilities for chitin and fish sauce) that generate a lot of odors, exhaust gas, polluted wastewater. There is no centralized industrial wastewater treatment system. The majority of the manufacturing facilities are near the Luong The Tran canal, and many of the dumping locations are beneath riverbank dwellings, making it difficult to regulate the discharge. Also, due to the production characteristics of chitin and fish sauce, there is a lot of odor widely dispersed. Many facilities have not installed the odor collection and treatment system. Song Doc industrial cluster and the contiguous area have 12 industrial production establishments (three seafood processing facilities and nine fishmeal facilities) that generate a lot of smoke, odor, and wastewater from industrial production activities. Over more, the type of fishmeal production with the separated rice husk boiler technology generates a lot of dust and gas emissions into the surrounding environment. Many small businesses that produce chitin and perform basic processing on aquatic items do not have wastewater treatment facilities, therefore pollution levels are rising near the industrial park. The PC also determines that the residential areas concentrated in the inner Ca Mau and Song Doc town (Tran Van Thoi district) are regularly polluted due to indiscriminate waste in the vacant land, ponds. Up to now, this area has formed spontaneous landfills with large volumes (Huynh 2018). Moreover, in residential areas, domestic wastewater and leachate from spontaneous landfills are discharged directly into rivers and canals of this city, also causing serious surface water pollution.

CONCLUSIONS

The results showed that the measured data and the satellite image values have a significant linear relationship. The obtained linear regression formula has high reliability and accuracy. Therefore, the determination of surface water quality parameters by the remote sensing method is feasible. From the obtained linear regression equation, a comparison between the results of real measurements and simulations for the remaining 13 samples was performed. The results obtained are real measurements and simulations for high similarity with the RMSE index, bias index, and percentage error. Thus, the simulation results are similar to actual measured data, and this result can be used in assessing the existing surface water quality of Ca Mau city.

Surface water quality parameters were calculated and classified according to QCVN08-MT:2015/BTNMT. The results show that except for pH values obtained at level A

(A1 and A2), in which water is used for domestic purposes, the remaining parameters are distributed in the levels from B1 to above B2 level as water used for irrigation and water transportation. When considering the VN-WQI index, the two levels 10-25 and 25-50 accounted for a large percentage of the distribution in the surface water area of the whole region and concentrated in the aquaculture, industrial, and residential areas. Meanwhile, the level 50-75 (water used for irrigation purposes) only accounts for a low rate, and the other two are 75-90 and 90-100 (water used for domestic purposes) did not present in surface water areas of the city. Thus, this result indicates that the city's surface water is heavily polluted and can be only used for water transportation.

In conclusion, the method of evaluating surface water quality by satellite image is feasible, and the obtained results are highly accurate and are a reliable reference for other methods such as water quality assessment by a mathematical model. However, this method still has some limitations, such as depending on the quantity and accuracy of the actual measured data, the reflected spectral values are susceptible to atmospheric and cloud errors, limited by image resolution.

ACKNOWLEDGEMENTS

This research is funded by the Vietnam Ministry of Science and Technology under grant number KC.08.30. We address our sincere gratitude to the SIWRR for supporting the research and the ESA for providing the Sentinel-2 image data source.

REFERENCES

- Abdullah, H.S.E. 2010. Water Quality Assessment for Donkan Lake Using LST8 OLI Satellite Images (Thesis). BSc. Irrigation Engineering, University of Sulaimani, Faculty of Engineering, Irrigation Engineering Department.
- Alparslan, E., Aydoğan, C., Tufekci, V. and Tufekci, H. 2007. Water quality assessment at Ömerli Dam using remote sensing techniques. *Environ. Monit. Assess.*, 135(1-3): 391-398.
- Chang, N.B., Vannah, B.W., Yang, Y.J. and Elovitz, M. 2014. Integrated data fusion and mining techniques for monitoring total organic carbon concentrations in a lake. *International Journal of Remote Sensing* 2014, 35: 1064-1093.
- Dinh T.T.H. 2018. Study on building a technological process to monitor surface water in the Hanoi area from VNREDSAT-1 data (Vietnamese). Thesis (Master), Hanoi University of Mining and Geology, Faculty of Geosynthetic-Map Engineering, Hanoi.
- El-Zeny, A. and El-Kafrawy, S.B. 2016. Assessment of water pollution induced by human activities in Burullus Lake using Landsat 8 operational land imager and GIS. *Egypt. J. Remote. Sens. Space Sci.*, 20: 49-56.
- Engman, E.T. and Gurney, R.J. 1991. *Remote Sensing in Hydrology*, Chapman and Hall Ltd, London.
- ESA. 2019. Algorithm Theoretical Basis Document Sentinel 2Global Mosaics. S2GM-SC2-ATBD-BC-V1.3.1.2019. [online]: https://usermanual.readthedocs.io/en/stable/_downloads/fe714f-8693d5a208b3684847d762192f/S2GM-SC2-ATBD-BC-v1.3.2.pdf [Accessed 3 October 2020].

- ESA. 2020. User Guides - Sentinel-2 MSI - Level-2A Product - Sentinel Online. [online] Earth.esa.int. Available at: <<https://earth.esa.int/web/sentinel/user-guides/sentinel-2-msi/product-types/level-2a>> [Accessed 3 October 2020].
- ESRI. 2020a. How ISO Cluster Works. [online]: <https://desktop.arcgis.com/en/arcmap/10.3/tools/spatial-analyst-toolbox/how-iso-cluster-works.htm#GUID-7B5D7C52-3F6C-4744-BA77-8C4D1C0A27F0> [Accessed 3 October 2020]
- ESRI. 2020b. Iso Cluster Unsupervised Classification. [online]: <https://desktop.arcgis.com/en/arcmap/10.3/tools/spatial-analyst-toolbox/iso-cluster-unsupervised-classification.htm> [Accessed 3 October 2020]
- Fiorani, L., Fantoni, R., Lazzara, L., Nardello, I., Okladnikov, I. and Palucci, A. 2006. Lidar calibration of satellite sensed cdom in the Southern Ocean. *EARSeL eProc.*, 5: 89-99.
- Gholizadeh, M. H. and Melesse, A. M. 2017. Study on spatiotemporal variability of water quality parameters in Florida bay using remote sensing. *J. Rem. Sens. GIS*, 06(03): 14-39
- Gholizadeh, M., Melesse, A. and Reddi, L. 2016. A comprehensive review on water quality parameters estimation using remote sensing techniques. *Sensors*, 16(8): 1298.
- Huynh, H. 2018. Four “Black Spots” Of Environmental Pollution In Ca Mau. Vietnamese. [online] Dan Tri International News. Available at: <https://dantri.com.vn/moi-truong/bon-diem-den-o-nhiem-moi-truong-o-ca-mau-20180415144101599.htm> [Accessed 23 September 2020].
- Imen, S., Chang, N.B. and Yang, Y.J. 2014. Monitoring spatiotemporal total organic carbon concentrations in Lake Mead with integrated data fusion and mining (IDFM) technique. 2014 IEEE International Conference on Systems, Man, and Cybernetics (SMC), San Diego, CA, USA, 5-8 October 2014, pp. 1-9.
- Kapalanga, M. 2015. Assessment and Development of Remote Sensing-Based Algorithms for Water Quality Monitoring in Olushandja Dam, North-Central Namibia (Thesis). Master of Science, University of Zimbabwe, Department of Civil Engineering.
- Karaoui, I., Abdelkrim, A., Abdelghani, B., Mohammed, H., Sabri El, M., Kamal Ait, O. and Driss, E. 2019. Evaluating the potential of Sentinel-2 satellite images for water quality characterization of artificial reservoirs: The Bin El Ouidane Reservoir case study (Morocco). *Meteorol. Hydrol. Water Manag.*, 7(1): 31-39.
- Lim, J. and Choi, M. 2015. Assessment of water quality based on Landsat 8 operational land imager associated with human activities in Korea. *Environ. Monit. Assess.*, 187(6): 313-339.
- Ritchie, J. C., Zimba, P. V. and Everitt, J. H. 2003. Remote sensing techniques to assess water quality. *Photogramm. Eng. Remote Sens.*, 69(6): 695-704.
- Seyhan, E. and Dekker, A. 1986. Application of remote sensing techniques for water quality monitoring. *Hydrobiol. Bull.*, 20: 41-50.
- Vietnam Environment Administration. 2019. Decision 1460/QĐ-TCMT: On the Issuing of Technical Guide to Calculation and Disclosure Viet Nam Water Quality Indicator (VN_WQI). Ha Noi: Vietnam Environment Administration, pp.1-6.
- Vo, T. P. L., Vo, Q. T. and Le, V.H. 2019. Application of Landsat images to estimate suspended sediment concentration in the Hau and Tien rivers (Vietnamese), Can Tho University. *J. Sci.*, 55(2): 134-144.
- Waxter, M.T. 2014. Analysis of Landsat Satellite Data to Monitor Water Quality Parameters in Tenmile Lake, Oregon (Thesis). Master of Science, Portland State University, Civil and Environmental Engineering.
- Zhu, W., Yu, Q., Tian, Y.Q., Chen, R.F. and Gardner, G.B. Estimation of chromophore dissolved organic matter in the Mississippi and Atchafalaya river plume regions using above surface hyperspectral remote sensing. *J. Geophys. Res. – Oceans*, 2011: 116.



The Construction of Magnetic $\text{MnFe}_2\text{O}_4@\text{TpPa-1}$ Composite Materials and the Adsorption Removal Performance of Organic Pollutants in Solution

Shuai Wang*, Huifang Wang*, Luzeng Hu*, Zhipeng Lu*, Muqing Qiu* and Xin Zhong*†

*College of Life Science, Shaoxing University, Huancheng West Road 508, Shaoxing, 312000, P.R. China

†Corresponding author: Xin Zhong; zhongxinmagic@163.com

Nat. Env. & Poll. Tech.
Website: www.neptjournal.com

Received: 19-11-2020

Revised: 29-01-2021

Accepted: 22-02-2021

Key Words:

MnFe_2O_4

COFs

TpPa-1

Adsorption

Bisphenol A

ABSTRACT

$\text{MnFe}_2\text{O}_4@\text{TpPa-1}$ adsorbent was developed by co-precipitation and solvothermal method, using β -ketoenamine linked covalent organic frameworks (COFs, TpPa-1) as supporting material to alleviate the aggregation of MnFe_2O_4 . The properties were characterized by XRD, FT-IR, SEM, TEM, VSM, pH_{pzc} , and N_2 adsorption-desorption. The experimental results showed that the pseudo-second-order and Langmuir model best described the adsorption process, suggesting that the adsorption process was chemisorption and spontaneous endothermic reaction, and the maximum adsorption capacity of Bisphenol A (BPA) was $926.65 \text{ mg}\cdot\text{g}^{-1}$. The main adsorption mechanism of BPA was hydrogen bonding and π - π conjugation between active functional groups in the TpPa-1 skeleton and BPA. Furthermore, the magnetic $\text{MnFe}_2\text{O}_4@\text{TpPa-1}$ showed good regeneration ability, indicating that $\text{MnFe}_2\text{O}_4@\text{TpPa-1}$ could be used in water treatment.

INTRODUCTION

In the past few decades, large numbers of toxic chemicals have been released into the environment due to the rapid industrialization and growth of the world population (Ji et al. 2015, Gómez-Pastora et al. 2017, Waclawek et al. 2017). These pollutants include azo dyes, antibiotics, endocrine disruptors, pesticides, and so on, most of which were persistent and not easily removed from natural ecosystems (Guan et al. 2013, Liu et al. 2014, Mohan et al. 2014, Liang et al. 2017, Guan et al. 2018). Furthermore, organic pollutants, particularly persistent ones with toxic, carcinogenic, and biorefractory functional groups, may pose a major threat to human health and ecological balance (Duan et al. 2015, Tian et al. 2018, Fu et al. 2019). Therefore, it is important to treat those pollutants effectively (Paethanom & Yoshikawa 2012; Tan et al. 2015, Abdel-Shafy & Mansour 2016, Li et al. 2018). At present, some treatment methods, such as adsorption, chemical reaction, bioremediation, etc. are applied to the organic pollutants in solution (Poletto 2016, Qiu et al. 2018, Rivas & Solís 2018, Jayawardhana et al. 2019, Wang et al. 2018, 2020).

Covalent organic frameworks (COFs) were first reported to be successfully produced in 2005 (Wang & Zhuang 2019). Since then, their properties have been investigated extensively. The main characteristics of COFs are (1) Low density, which is constructed by some light chemical elements such

as C, H, O, N; (2) Regular pore structures that self-assemble into periodic and highly ordered pore formations. Thereby, their specific surface area, pore size, and pore shape could be easily adjusted; (3) Excellent chemical stability connected by covalent bond, resulting in considerably improved thermodynamic and chemical stability; (4) Diverse structure, synthesized by designing a variety of construction units and connection methods; (5) Functionalized, specific functional groups could be introduced to construction units in the initial stage (Wang & Zhuang 2019). Besides, COFs are the long-range orderly pore structure and crystalline organic porous materials, named as "Organic Zeolites". COFs materials application research in the environmental field is still in its early stages. COFs were mainly used for atmospheric governance research in the early research period. In recent years, it has been gradually applied to wastewater treatment (Liu et al. 2018).

COF-TpPa-1 was selected, which was connected by imine bonds ($-\text{C}=\text{N}-$) and arranged periodically in a two-dimensional plane layer. Through π -conjugation, interlayer covalent bond interlocking, and interlayer non-covalent interaction, COF-TpPa-1 was formed as a layer-by-layer structure in the plane and vertical direction (Kandambeth et al. 2012, He et al. 2017). TpPa-1 materials had excellent chemical stability. This advantage was particularly important for its application in the wastewater treatment industry.

However, the TpPa-1 material existed in powder form. The preparation procedure was complicated and the reaction conditions were harsh. As a result of these difficulties, its applicability in the field of water environment has been greatly limited. If MnFe_2O_4 was combined with TpPa-1, it could be compensated for each other in terms of application limitations. MnFe_2O_4 had a small specific surface area, while TpPa-1 had a high specific surface area, regular pores, and rich foreign elements. MnFe_2O_4 could also impart magnetic properties to powdered TpPa-1, allowing it to be easily recycled, reused, and at a lower cost. Furthermore, TpPa-1 could provide a carrier platform for MnFe_2O_4 particles to prevent their agglomeration. Therefore, combining TpPa-1 with MnFe_2O_4 not only enriched the types and properties of COFs but also made up for the application limitations of the TpPa-1 with MnFe_2O_4 . This research could provide a new solution for wastewater treatment.

In this experiment, MnFe_2O_4 @TpPa-1 adsorbent was developed by co-precipitation and solvothermal method, using β -ketoenamine linked covalent organic frameworks (COFs, TpPa-1) as supporting material to alleviate the aggregation of MnFe_2O_4 . The properties were characterized by XRD, FT-IR, SEM, TEM, VSM, pHpzc, and N_2 adsorption-desorption. The adsorption experiments of Bisphenol A (BPA) by MnFe_2O_4 @TpPa-1 were carried out. The adsorption mechanism and regeneration ability of BPA by MnFe_2O_4 @TpPa-1 were discussed in detail.

MATERIALS AND METHODS

Materials

$\text{MnCl}_2 \cdot 4\text{H}_2\text{O}$, $\text{FeCl}_3 \cdot 6\text{H}_2\text{O}$, Arsenazo III, BPA, trialdehyde phloroglucinol (Tp), P-phenylenediamine (Pa), dioxane, acetic acid, methanol, and N,N-dimethyl formamide (DMF) were obtained from Shanghai Maclin Biochemical Technology Co., Ltd. HNO_3 and NaOH were purchased from Shanghai Chemical Reagent Co., Ltd. All the above reagents were of analytical grade or advanced purity and used directly without further purification. The ultrapure water was used in the experimental process.

Preparation of MnFe_2O_4

0.1 $\text{mol} \cdot \text{L}^{-1}$ Mn^{2+} ions and 0.2 $\text{mol} \cdot \text{L}^{-1}$ Fe^{3+} ions were prepared by $\text{MnCl}_2 \cdot 4\text{H}_2\text{O}$ and $\text{FeCl}_3 \cdot 6\text{H}_2\text{O}$, respectively. The mixture solution of 0.1 $\text{mol} \cdot \text{L}^{-1}$ Mn^{2+} ions and 0.2 $\text{mol} \cdot \text{L}^{-1}$ Fe^{3+} ions were added into the 250 mL of Erlenmeyer flask. Then, 100 mL 3 $\text{mol} \cdot \text{L}^{-1}$ NaOH solution slowly was added into the Erlenmeyer flask at a preheating temperature of 95°C. After continuous stirring and aging for 2 h, the solution was filtered, washed, and dried at 60°C for 12 h.

Preparation of MnFe_2O_4 @TpPa-1

63 mg of Tp was dissolved into a mixture of (1+1) mesitylene and dioxane under ultrasonic conditions. Then, 100 mg of MnFe_2O_4 was added into the solution for 30 min under ultrasonic conditions. Then, 48 mg of Pa-1 was added into the solution for 30 min under ultrasonic conditions. Finally, 0.5 mL of 3 $\text{mol} \cdot \text{L}^{-1}$ acetic acid was added into the solution for 3 days at a temperature of 120°C. The supernatant was washed with DMF until it was clear. After that, they were washed twice more with acetone. Then, they were dried under vacuum at 80°C for 12 h. MnFe_2O_4 @TpPa-1 was obtained for adsorption experiments.

Adsorption Experiments

Effect of pH: 2 mg of MnFe_2O_4 and 2 mg of MnFe_2O_4 @TpPa-1 were added to 25 mL and 50 $\text{mg} \cdot \text{L}^{-1}$ of BPA solutions, respectively. The value of pH in the solution was adjusted from 1 to 10 with the 0.01 $\text{mol} \cdot \text{L}^{-1}$ HNO_3 or NaOH solution. Then, the mixture solution was put in a shaker at 25°C and 150 rpm for 24 h. The concentration of BPA was determined at equilibrium contact time.

Adsorption kinetics: 2 mg of MnFe_2O_4 and 2 mg MnFe_2O_4 @TpPa-1 materials were added to 100 mL and 50 $\text{mg} \cdot \text{L}^{-1}$ of BPA solution, respectively. The value of pH in the solution was adjusted to 2.0 with 0.01 $\text{mol} \cdot \text{L}^{-1}$ HNO_3 solution. Then, the mixture solution was put in a shaker at 25°C and 150 rpm for 24 h. The concentration of BPA was determined at different contact time.

Adsorption thermodynamics: 2 mg of MnFe_2O_4 and 2 mg MnFe_2O_4 @TpPa-1 materials were added to 100 mL and 15 $\text{mg} \cdot \text{L}^{-1}$, 25 $\text{mg} \cdot \text{L}^{-1}$, 50 $\text{mg} \cdot \text{L}^{-1}$, 75 $\text{mg} \cdot \text{L}^{-1}$, and 100 $\text{mg} \cdot \text{L}^{-1}$ of BPA solution, respectively. The value of pH in the solution was adjusted to 2.0 with 0.01 $\text{mol} \cdot \text{L}^{-1}$ HNO_3 solution. Then, the mixture solution was put in a shaker at a different temperature (25°C, 35°C, and 45°C) and 150 rpm for 24 h. The concentration of BPA was determined at equilibrium contact time.

Adsorption-desorption of the experiment: 2 mg of MnFe_2O_4 and 2 mg of MnFe_2O_4 @TpPa-1 were added to 25 mL and 50 $\text{mg} \cdot \text{L}^{-1}$ of BPA solutions, respectively. The value of pH in the solution was adjusted to 2.0 with 0.01 $\text{mol} \cdot \text{L}^{-1}$ HNO_3 solution. Then, the mixture solution was put in a shaker at 25°C and 150 rpm for 24 h. The concentration of BPA was determined at equilibrium contact time. After the adsorption experiment was over, a magnet was used for solid-liquid separation. The obtained material was dried at 60°C for 12 h. Then, the obtained material was washed three times with methanol solution (Luo et al. 2019). After that, the above tests were repeated.

Analytical Method

The crystal structure of the sample was determined by X-Ray Diffraction (XRD) (Emoyrean diffractometer, Panalytical, Holland). The surface functional groups were detected by Fourier Transform Infrared Spectroscopy (FT-IR) (NEXUS). The morphology and particle size of the material were characterized by FE-SEM (Hitachi S4800) and TEM (FEI Tecnai F20 S-TWIN), respectively. The surface area and pore size distribution were measured by the N₂ adsorption-desorption method (ASAP 3020). Magnetic properties of materials were determined by Model 6000 (Quantum Design, USA). The surface charge properties of materials (Zeta potential) were determined by Malvern ZEN3690.

The concentration of BPA was measured by UV-spectrophotometer at 276 nm. The adsorption capacity of BPA by MnFe₂O₄/MnFe₂O₄@TpPa-1 was calculated using the following formula.

$$q_e = \frac{(C_0 - C_e)V}{m} \quad \dots(1)$$

Where, C_0 was initial concentration (mg.L⁻¹), C_e is the concentration at adsorption equilibrium (mg.L⁻¹), q_e is adsorption amount at adsorption equilibrium (mg.g⁻¹), V is the volume of solution (L), m is the mass of the adsorbent (g).

RESULTS AND DISCUSSION

The Characteristic of MnFe₂O₄@TpPa-1

The microstructure of the MnFe₂O₄@TpPa-1 was observed by SEM and TEM. The results are shown in Fig. 1. As shown from Fig.1(a), TpPa-1 was in the shape of a sea urchin. MnFe₂O₄ with a particle size of about 50 nm was distributed on the surface of TpPa-1. It could effectively prevent the accumulation of MnFe₂O₄. Additionally, the sea urchin-like morphology could give the MnFe₂O₄@TpPa-1 composite a high specific surface area and more adsorption sites. This structure facilitated its adsorption capacity.

Fig. 2(a) shows the FT-IR spectra of TpPa-1, MnFe₂O₄, and MnFe₂O₄@TpPa-1. The adsorption peaks at 3450 cm⁻¹ and 1630 cm⁻¹ were the O-H stretching vibration and bending vibration adsorption peaks, respectively.

This result indicated that the preparation of MnFe₂O₄ contained a large amount of -OH functional groups. The adsorption peaks at 430 cm⁻¹ and 578 cm⁻¹ corresponded to the characteristic peaks of Mn-O and Fe-O, respectively (Ghobadi et al. 2018). Compared with MnFe₂O₄, MnFe₂O₄@TpPa-1 not only had the above-mentioned characteristic adsorption peak but also had the characteristic peak of C=N

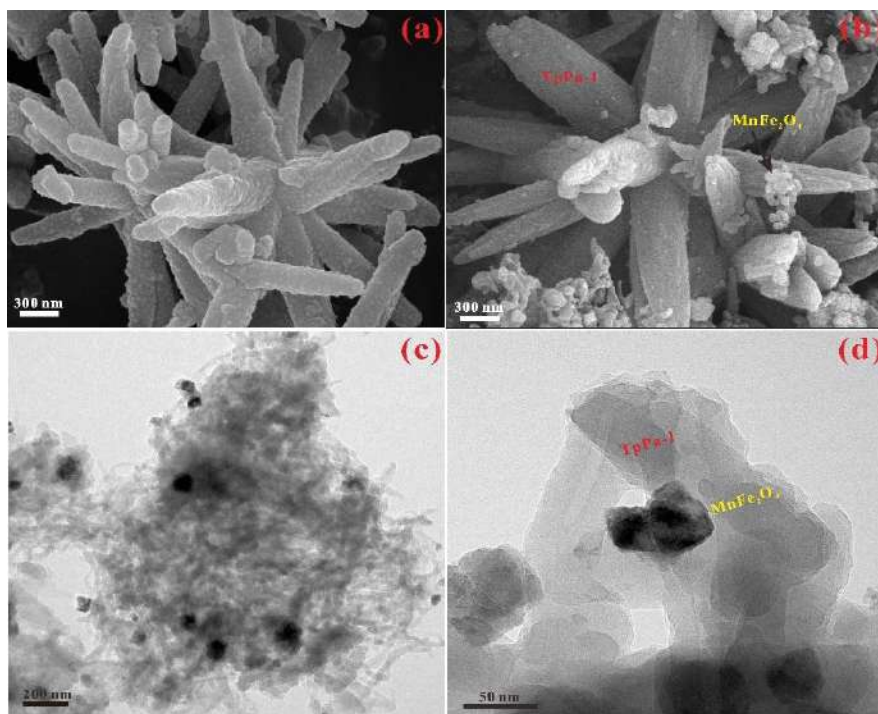


Fig. 1: SEM and TEM images of TpPa-1 and MnFe₂O₄@TpPa-1, SEM: (a) TpPa-1; (b) MnFe₂O₄TpPa-1; TEM: (c-d) MnFe₂O₄@TpPa-1

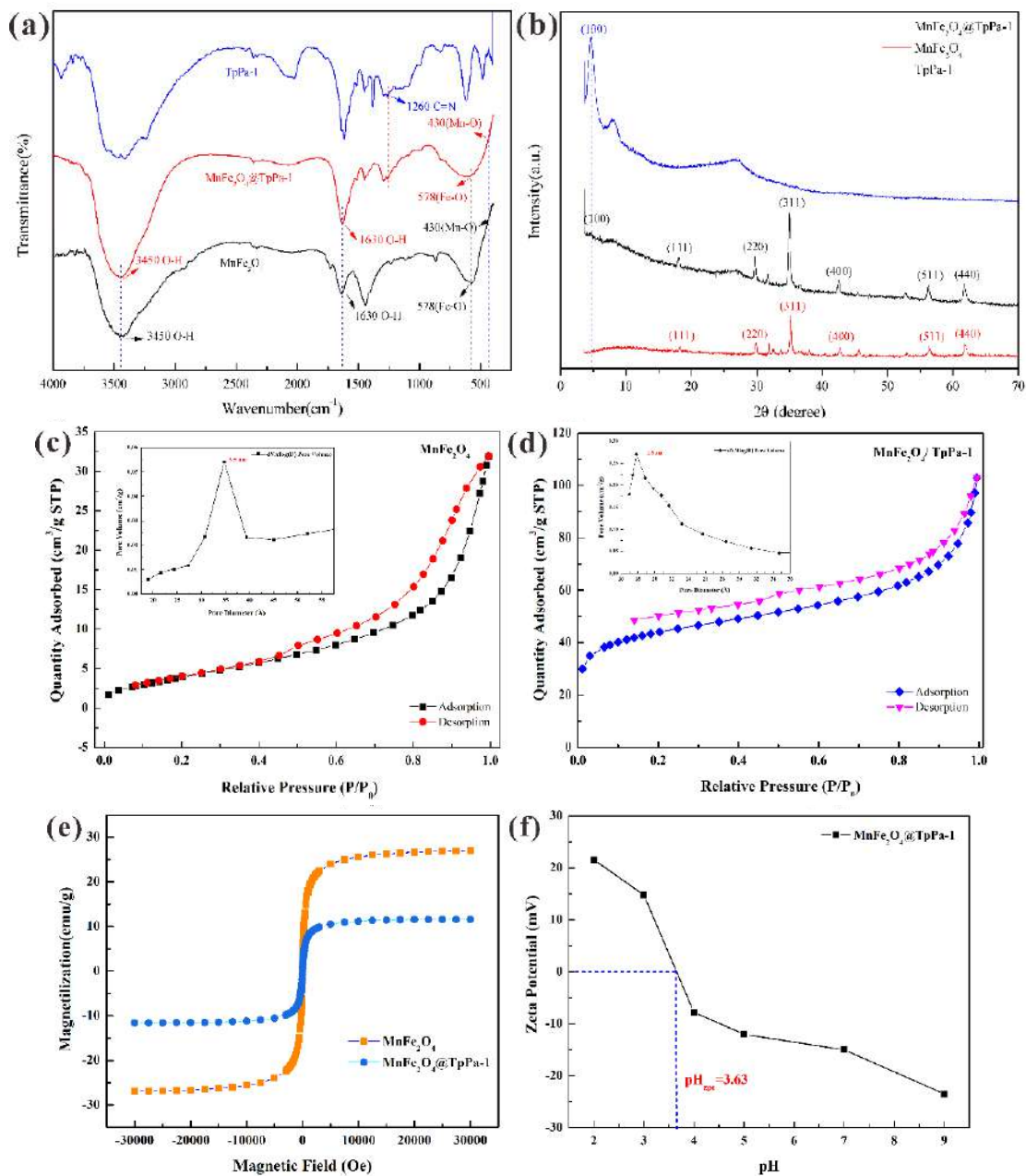


Fig. 2: (a) the FT-IR spectra of TpPa-1, MnFe_2O_4 and $\text{MnFe}_2\text{O}_4@\text{TpPa-1}$; (b) the XRD spectra of TpPa-1, MnFe_2O_4 and $\text{MnFe}_2\text{O}_4@\text{TpPa-1}$; N_2 adsorption-desorption isotherm of MnFe_2O_4 (c) and $\text{MnFe}_2\text{O}_4@\text{TpPa-1}$ (d); (e) the magnetic hysteresis curves of MnFe_2O_4 and $\text{MnFe}_2\text{O}_4@\text{TpPa-1}$ at room temperature and (f) Zeta potential of $\text{MnFe}_2\text{O}_4@\text{TpPa-1}$.

at 1260 cm^{-1} which belongs to the framework of TpPa-1 (Kandambeth et al. 2012).

It indicated that $\text{MnFe}_2\text{O}_4@\text{TpPa-1}$ composite materials were successfully synthesized. The XRD spectra of TpPa-1, MnFe_2O_4 , and $\text{MnFe}_2\text{O}_4@\text{TpPa-1}$ are shown in Fig.2(b). From the XRD pattern of MnFe_2O_4 , some obvious diffraction peaks at $2\theta = 18.03^\circ$, 29.65° , 34.92° , 42.43° ,

56.08° , and 61.56° could be observed. They corresponded to crystal planes (111), (220), (311), (400), (511), and (440), respectively, which were consistent with the standard card of MnFe_2O_4 (JCPDS Card NO. 10-0319) (Li et al. 2019). The XRD pattern of $\text{MnFe}_2\text{O}_4@\text{TpPa-1}$ was consistent with MnFe_2O_4 . It indicated that MnFe_2O_4 maintained good crystallinity in the composite materials. Furthermore, the

diffraction peak of MnFe₂O₄@TpPa-1 at 2θ=4.7° was attributed to the (100) crystal plane of TpPa-1 (Kandambeth et al. 2012). This result further proved that the MnFe₂O₄@TpPa-1 composite materials were successfully prepared.

Fig. 2(c-d) was the N₂ adsorption-desorption isotherm of MnFe₂O₄ and MnFe₂O₄@TpPa-1, respectively, and the internal inset figures were the pore size distribution diagram of MnFe₂O₄ and MnFe₂O₄@TpPa-1. The specific surface area, pore-volume, and pore size of MnFe₂O₄ were 15.4 m².g⁻¹, 0.04 cm³.g⁻¹, and 3.5 nm, respectively. MnFe₂O₄@TpPa-1 composite materials had type IV isotherm. It suggested that it was a mesoporous material. Its specific surface area, pore, volume, and pore size were 235.5 m².g⁻¹, 0.17 cm³.g⁻¹, and 1.8 nm, respectively. The magnetic hysteresis curves of MnFe₂O₄ and MnFe₂O₄@TpPa-1 at room temperature are shown in Fig. 2(e). The saturation magnetization of the material was 26.94 and 11.52 emu.g⁻¹, respectively, which was sufficient to ensure the solid-liquid separation of the adsorbent and the aqueous solution under the condition of an external magnetic field (Hyun et al. 2012).

Effect of pH

To investigate the influence of pH on adsorption capacity, the adsorption experiments were carried out at a different pH in solution. Fig. 3 showed the effect of pH on the removal of BPA by MnFe₂O₄ and MnFe₂O₄@TpPa-1.

When pH was 2.0, the adsorption capacity of MnFe₂O₄ and MnFe₂O₄@TpPa-1 for BPA reached the maximum. When pH < 9.0, most BPA mainly existed in molecular form. However, when pH ≥ 9.0, BPA existed in the form of anionic BPA (HBPA⁻ and BPA²⁻). As shown from Fig. 2(f), the Zeta potential of MnFe₂O₄@TpPa-1 was 3.63. When the pH in the solution was lower than 3.63, the surface of MnFe₂O₄@TpPa-1 was positively charged. It indicated that

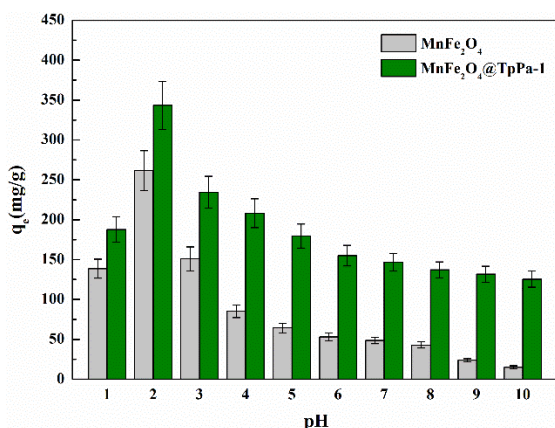


Fig. 3: Effect of pH on BPA adsorption onto MnFe₂O₄ and MnFe₂O₄@TpPa-1

the removal of BPA mainly relied on π-π conjugation and hydrogen bonding (Zhong et al. 2020a, 2020b). When the pH of the solution was higher than 3.63, the surface of MnFe₂O₄@TpPa-1 was a negative charge. The electrostatic repulsion between MnFe₂O₄@TpPa-1 and BPA was enhanced, thereby reducing the amount of adsorption of BPA.

Adsorption Kinetics

The effect of contact time on the adsorption of BPA by MnFe₂O₄ and MnFe₂O₄@TpPa-1 are shown in Fig. 4. It could be seen from Fig. 4(a) that the adsorption capacity of MnFe₂O₄ and MnFe₂O₄@TpPa-1 on BPA gradually increased with the increase of the reaction time. The adsorption capacity increased rapidly at the first stage of 30 minutes, and the adsorption sites on MnFe₂O₄ and MnFe₂O₄@TpPa-1 were continuously occupied. After 5 h, the adsorption sites on the surface tended to be saturated, causing the adsorption to gradually reach equilibrium. Compared with MnFe₂O₄, MnFe₂O₄@TpPa-1 had a higher adsorption capacity and faster adsorption rate for BPA. This was mainly the reason that MnFe₂O₄@TpPa-1 contained a higher specific surface area, larger pore volume, and various active surface functional groups (C=N, -OH, -NH₂) (Ding et al. 2015).

The pseudo-first-order, pseudo-second-order dynamic model, and intra-particle diffusion model were used to further explore the removal process of BPA by MnFe₂O₄ and MnFe₂O₄@TpPa-1. The pseudo-first-order model, the pseudo-second-order model, and the intra-particle diffusion model were as follows:

$$\ln(q_e - q_t) = \ln q_e - k_1 t \quad \dots(2)$$

$$\frac{t}{q_t} = \frac{1}{k_2 q_e^2} + \frac{t}{q_e} \quad \dots(3)$$

$$q_t = k_p t^{1/2} + C \quad \dots(4)$$

Where, q_e and q_t (mg.g⁻¹) are the adsorption capacity of BPA at equilibrium and t , respectively. k_1 (min⁻¹), k_2 (g min⁻¹mg⁻¹), and k_p (g/mg min^{0.5}) are the rate constants of the pseudo-first-order, pseudo-second-order dynamics model, and the intra-particle diffusion model, respectively. The results are shown in Fig. 4b-d and Table 1.

By comparing the correlation coefficient (R²) value, it could be found that the pseudo-second-order kinetic model was more suitable for describing the adsorption process of BPA by MnFe₂O₄ and MnFe₂O₄@TpPa-1. It was suggested that the adsorption process was controlled by chemical adsorption or strong surface complexation. Furthermore, the internal particle diffusion model was used to study the adsorption and diffusion mechanism. The result is

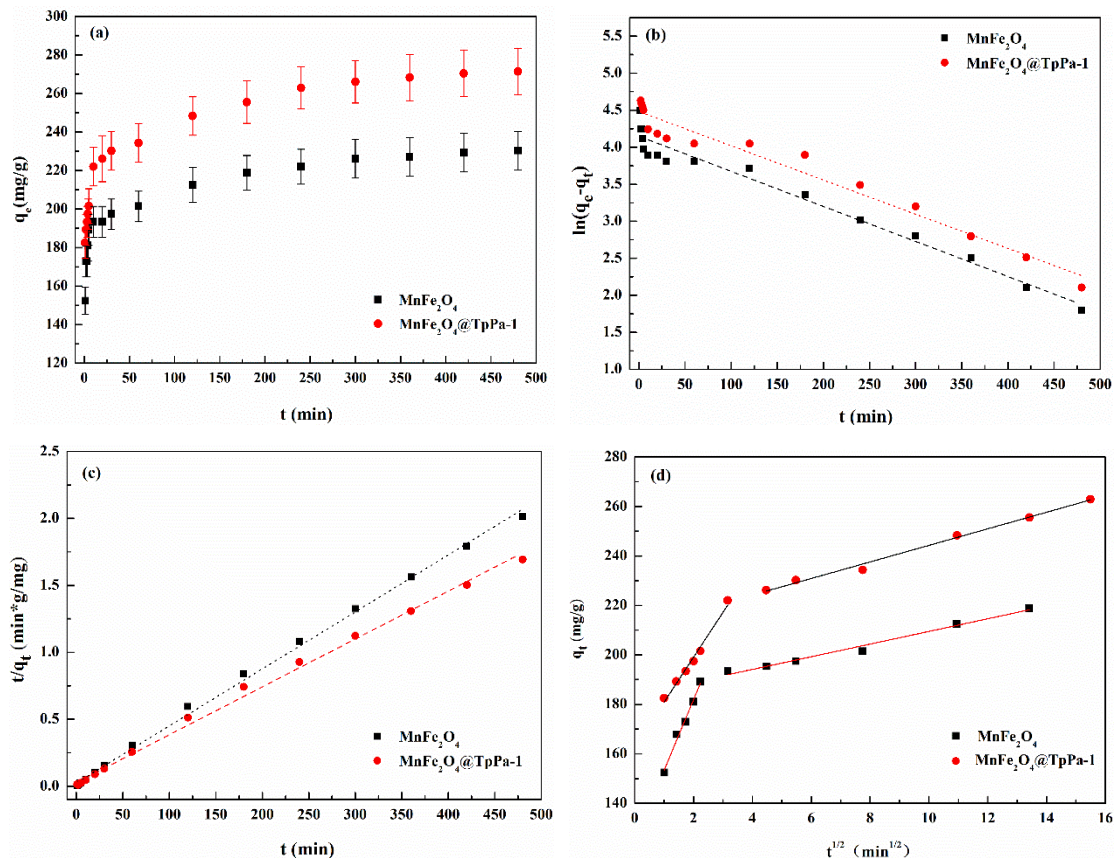


Fig. 4: (a) Effect of contact time on the adsorption of BPA by MnFe_2O_4 and $\text{MnFe}_2\text{O}_4@\text{TpPa-1}$; (b) the pseudo-first-order model; (c) the pseudo-second-order model, and (d) the intra-particle diffusion model.

Table 1: The parameters of the kinetic models of BPA adsorption onto MnFe_2O_4 and $\text{MnFe}_2\text{O}_4@\text{TpPa-1}$.

Adsorbents	Pseudo-first-order			Pseudo-second-order			Intra-particle-diffusion		
	k_1 (min^{-1})	q_e ($\text{mg}\cdot\text{g}^{-1}$)	R^2	k_2 ($\text{g}\cdot\text{mg}^{-1}\cdot\text{min}$)	q_e ($\text{mg}\cdot\text{g}^{-1}$)	R^2	k_p ($\text{g}\cdot\text{mg}^{-1}\cdot\text{min}^{0.5}$)	C	R^2
MnFe_2O_4	0.005	63.43	0.9649	7.2×10^{-4}	238.09	0.9979	28.49	124.93	0.9809
							2.56	183.86	0.9810
$\text{MnFe}_2\text{O}_4@\text{TpPa-1}$	0.005	88.23	0.9604	4.7×10^{-4}	285.71	0.9967	18.14	162.80	0.9823
							3.35	210.80	0.9910

shown in Fig. 4(d). The fitting curve showed two-stage adsorption. Additionally, the fitting curve did not pass through the origin of the coordinate. It indicated that the adsorption process was affected by many factors. The first stage was the adsorption of BPA by MnFe_2O_4 and $\text{MnFe}_2\text{O}_4@\text{TpPa-1}$, which involved the instantaneous adsorption of BPA and film diffusion. In the second stage, internal diffusion occurs as BPA diffuses in the pores of MnFe_2O_4 and $\text{MnFe}_2\text{O}_4@\text{TpPa-1}$. Therefore, the adsorption process for BPA by MnFe_2O_4 and $\text{MnFe}_2\text{O}_4@\text{TpPa-1}$ was affected by chemical

adsorption, strong surface complexation, and internal particle diffusion.

Adsorption Thermodynamics

The adsorption capacity of BPA by MnFe_2O_4 and $\text{MnFe}_2\text{O}_4@\text{TpPa-1}$ was investigated under the conditions of different initial concentrations of BPA and different temperatures (25°C, 35°C, and 45°C). The experimental results were fitted with Langmuir and Freundlich models, respectively (Equation 5 and Equation 6). The fitting results were shown

in Fig.5, and the relevant parameters were listed in Table 2.

$$Q_e = \frac{K_L Q_{max} C_e}{K_L C_e + 1} \quad \dots(5)$$

$$Q_e = K_F C_e^{1/n} \quad \dots(6)$$

Where, C_e (mg.L⁻¹) is the concentration at adsorption equilibrium. Q_e (mg.g⁻¹) is the amount of adsorption at adsorption equilibrium. Q_{max} (mg.g⁻¹) is the maximum adsorption capacity and K_L (L.mg⁻¹) is the constant of the Langmuir model. K_F and n are Freundlich constant.

The experimental results showed that the adsorption capacity of BPA by MnFe₂O₄ and MnFe₂O₄@TpPa-1 increased continuously with the increase of the initial concentration. By comparing the value of R², the Langmuir model was more fitted with the adsorption process of BPA by MnFe₂O₄ and MnFe₂O₄@TpPa-1. It indicated that the adsorption process of BPA was single-layer adsorption. Calculated by the Langmuir model, the maximum adsorption capacity of BPA by MnFe₂O₄ and MnFe₂O₄@TpPa-1 was 515.03 mg.g⁻¹ and 926.65 mg.g⁻¹, respectively.

Thermodynamic parameters of DG⁰, DH⁰ and DS⁰ were calculated by the formula (7-9). Fig. 6 shows the linear plots

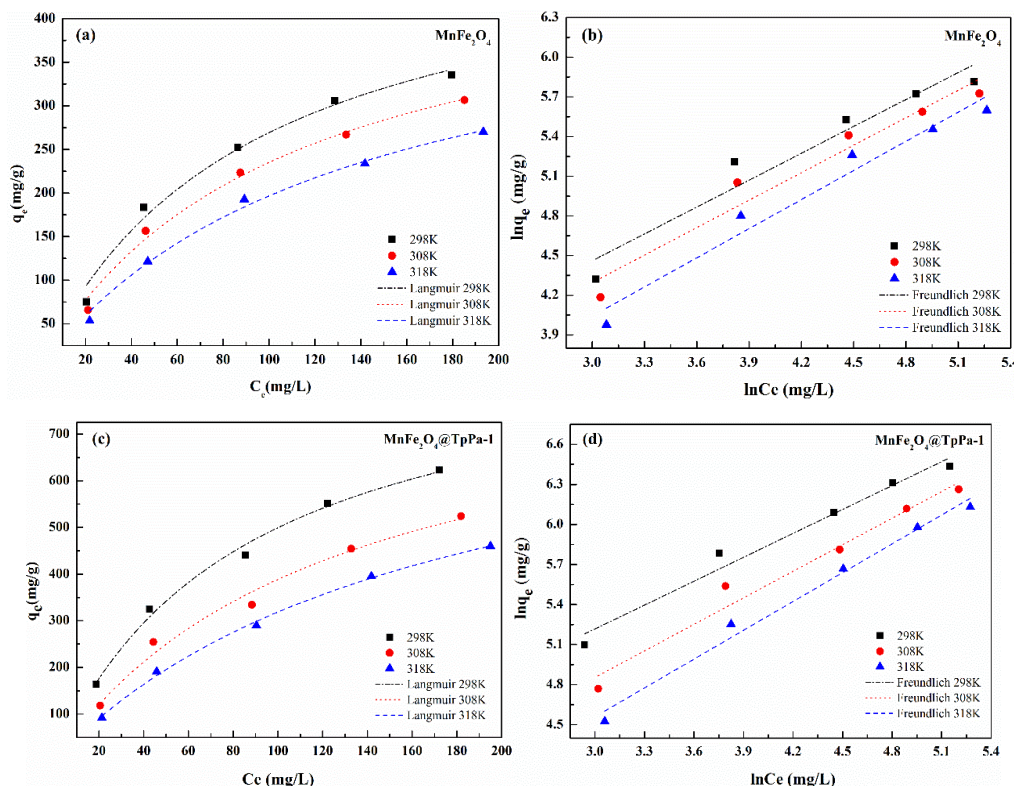


Fig. 5: The Langmuir model and Freundlich model of BPA adsorption onto MnFe₂O₄ (a-b) and MnFe₂O₄@TpPa-1(c-d).

Table 2: The parameters of Langmuir and Freundlich model for MnFe₂O₄ and MnFe₂O₄@TpPa-1 adsorption of BPA.

Adsorbents	T(K)	Langmuir model			Freundlich model		
		q _{max} (mg.g ⁻¹)	K _L (L.mg ⁻¹)	R ²	K _F (mg ^{1-1/n} .g ⁻¹ .L ^{-1/n})	1/n	R ²
MnFe ₂ O ₄	298	515.03	0.010	0.9823	11.32	0.677	0.9214
	308	482.47	0.009	0.9878	9.18	0.692	0.9351
	318	459.35	0.007	0.9906	6.29	0.734	0.9534
MnFe ₂ O ₄ @TpPa-1	298	926.65	0.011	0.9913	30.75	0.596	0.9705
	308	877.12	0.007	0.9805	17.53	0.662	0.9632
	318	866.28	0.005	0.9973	11.02	0.719	0.9835

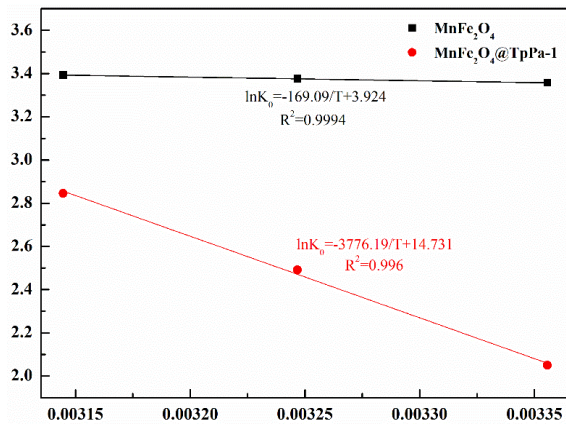


Fig. 6: The linear plots of $\ln K_0$ versus $1/T$ at three different temperatures ($T = 298\text{--}318\text{K}$).

of $\ln K_0$ versus $1/T$ at three different temperatures. Thermodynamic parameters of BPA adsorption onto MnFe_2O_4 and $\text{MnFe}_2\text{O}_4@\text{TpPa-1}$ are listed in Table 3.

$$\Delta G^0 = -RT \ln K_0 \quad \dots(7)$$

$$\Delta G^0 = \Delta H^0 - T\Delta S^0 \quad \dots(8)$$

$$\ln K_0 = \frac{\Delta S^0}{R} - \frac{\Delta H^0}{RT} \quad \dots(9)$$

At different temperatures, the calculated ΔG^0 values were all less than zero and decreased as the temperature increased. It was suggested that the adsorption process is a spontaneous reaction. However, the values of ΔH^0 were all positive, indicating that the adsorption process was an endothermic reaction. The main reaction mechanism was the chemical adsorption process. In addition, the values of ΔS^0 were all greater than zero, indicating that the degree of the disorder increased at the solid-liquid interface.

Adsorption-Desorption of Experiment

The biggest disadvantage of COFs as adsorbents is the relatively high price of synthetic raw materials. In actual application, the cost of adsorbent is a very important

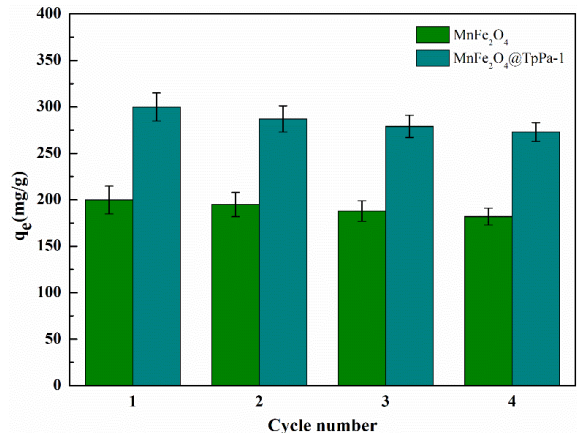


Fig. 7: The adsorption-desorption cycles of MnFe_2O_4 and $\text{MnFe}_2\text{O}_4@\text{TpPa-1}$.

economic factor. Therefore, it is very important to investigate the recycling performance of composite materials, to reduce the cost of adsorbent used. The adsorption-desorption cycles of MnFe_2O_4 and $\text{MnFe}_2\text{O}_4@\text{TpPa-1}$ are shown in Fig. 7.

In this study, MnFe_2O_4 and $\text{MnFe}_2\text{O}_4@\text{TpPa-1}$ are used for four cycles. After four cycles of recycling, the adsorption of MnFe_2O_4 and $\text{MnFe}_2\text{O}_4@\text{TpPa-1}$ on BPA gradually decreased. It might be due to the depletion of active functional groups and non-renewable active sites during the adsorption process. However, $\text{MnFe}_2\text{O}_4@\text{TpPa-1}$ had a relatively high level of adsorption. It indicated that $\text{MnFe}_2\text{O}_4@\text{TpPa-1}$ had good regeneration ability. Therefore, it had good application prospects.

CONCLUSIONS

In this experiment, $\text{MnFe}_2\text{O}_4@\text{TpPa-1}$ composite material with high specific surface area, pore volume, and abundant active functional groups was prepared. $\text{MnFe}_2\text{O}_4@\text{TpPa-1}$ showed excellent adsorption capacity of BPA and good application prospects. In the research of adsorption kinetic, the pseudo-second-order kinetic model was more suitable to

Table 3: Thermodynamic parameters of BPA adsorption onto MnFe_2O_4 and $\text{MnFe}_2\text{O}_4@\text{TpPa-1}$.

Adsorbents	T(K)	$-\Delta G^0$ (kJ.mol ⁻¹)	ΔS^0 (J.(mol.K) ⁻¹)	ΔH^0 (kJ.mol ⁻¹)
MnFe_2O_4	298	4.84	24.32	2.41
	308	5.08		
	318	5.32		
$\text{MnFe}_2\text{O}_4@\text{TpPa-1}$	298	5.10	122.47	31.40
	308	6.33		
	318	7.56		

describe the adsorption process of BPA by MnFe₂O₄@TpPa-1. It indicated that the adsorption process was controlled by chemical adsorption or strong surface complexation. In the research of adsorption thermodynamics, the Langmuir model was more fitted to the adsorption process of BPA by MnFe₂O₄@TpPa-1. It was suggested that the adsorption process was chemical adsorption, and the adsorption process was a spontaneous and endothermic reaction. The maximum adsorption capacity of Bisphenol A (BPA) was 926.65 mg.g⁻¹. The main adsorption mechanism of BPA was hydrogen bonding and π - π conjugation between active functional groups in the TpPa-1 skeleton and BPA. In addition, magnetism MnFe₂O₄@TpPa-1 exhibited good regeneration ability, indicating MnFe₂O₄@TpPa-1 had good regeneration ability, indicating that MnFe₂O₄@TpPa-1 could be used in water treatment.

ACKNOWLEDGEMENTS

This work is supported by the National Natural Science Foundation of China (No. 21876115) and the Natural Science Foundation of Zhejiang Province, China (LGF19C030001, LGF20C030001, and LGF21C030001). The authors are very grateful for their supports. Additionally, Shuai Wang and Huifang Wang contributed equally to this work.

REFERENCES

- Abdel-Shafy, H.I. and Mansour, M.S.M. 2016. A review on polycyclic aromatic hydrocarbons: source, environmental impact, effect on human health and remediation. *Egypt. J. Pet.*, 25: 107-123.
- Ding, C.C., Cheng, W.C., Sun, Y.B. and Wang, X.K. 2015. Novel fungus-Fe₃O₄ bio-nano composites as high-performance adsorbents for the removal of radionuclides. *J. Hazard. Mater.*, 295: 127-137.
- Duan, X., Sun, H., Kang, J., Wang, Y., Indrawirawan, S. and Wang, S. 2015. Insights into heterogeneous catalysis of persulfate activation on dimensional-structured nanocarbons. *ACS Catal.*, 5: 4629-4636.
- Fu, H.C., Ma, S.L., Zhao, P., Xu, S.J. and Zhan, S.H. 2019. Activation of peroxymonosulfate by graphitized hierarchical porous biochar and MnFe₂O₄ magnetic nanoarchitecture for organic pollutants degradation: Structure dependence and mechanism. *Chem. Eng. J.*, 360: 157-170.
- Ghobadi, M., Gharabaghi, M., Abdollahi, H., Boroumand, Z. and Moradian, M. 2018. MnFe₂O₄-Graphene oxide magnetic nanoparticles as a high-performance adsorbent for rare earth elements: Synthesis, isotherms, kinetics, thermodynamics, and desorption. *J. Hazard. Mater.*, 351: 308-316.
- Gómez-Pastora, J., Dominguez, S., Bringas, E., Rivero, M.J, Ortiz, I. and Dionysiou, D.D. 2017. Review and perspectives on the use of magnetic nano photocatalysts (MNPCs) in water treatment. *Chem. Eng. J.*, 310: 407-427.
- Guan, R., Yuan, X., Wu, Z., Jiang, L., Li, Y. and Zeng, G. 2018. Principle and application of hydrogen peroxide-based advanced oxidation processes in activated sludge treatment: a review. *Chem. Eng. J.*, 339: 519-530.
- Guan, Y., Ma, J., Ren, Y., Liu, Y., Xiao, J., Lin, L. and Zhang, C. 2013. Efficient degradation of atrazine by magnetic porous copper ferrite catalyzed peroxymonosulfate oxidation via the formation of hydroxyl and sulfate radicals. *Water Res.*, 47: 5431-5438.
- He, S., Zeng, T., Wang, S., Niu, H. and Cai, Y. 2017. Facile synthesis of the magnetic covalent organic framework with a three-dimensional bouquet-like structure for enhanced extraction of organic targets. *ACS Appl. Mater. Interf.*, 9: 2959-2965.
- Hyun, S.P., Davis, J.A., Sun, K. and Hayes, K.F. 2012. Uranium(VI) reduction by iron(II) monosulfide mackinawite. *Environ. Sci. Technol.*, 46: 3369-3376.
- Jayawardhana, Y., Gunatilake, S.R., Mahatantila, K., Ginige, M.P. and Vithanage, M. 2019. Sorptive removal of toluene and m-xylene by municipal solid waste biochar: simultaneous municipal solid waste management and remediation of volatile organic compounds. *J. Environ. Manag.*, 238: 323-330.
- Ji, Y., Dong, C., Kong, D., Lu, J. and Zhou, Q. 2015. Heat-activated persulfate oxidation of atrazine: implications for remediation of groundwater contaminated by herbicides. *Chem. Eng. J.*, 263: 45-54.
- Kandambeth, S., Mallick, A., Lukose, B., Mane, M.V., Heine, T. and Banerjee, R. 2012. Construction of crystalline 2D covalent organic frameworks with remarkable chemical (acid/base) stability via a combined reversible and irreversible route. *J. Am. Chem. Soc.*, 134: 19524-19527.
- Li, C., Chen, C., Lu, J., Cui, S., Li, J., Liu, H., Li, W. and Zhang, F. 2018. Metal-organic framework derived CoMn₂O₄ catalyst for heterogeneous activation of peroxymonosulfate and sulfanilamide degradation. *Chem. Eng. J.*, 337: 101-109.
- Li, N., Li, W. and Fu, F. 2019. Removal of chromium (VI) by MnFe₂O₄ and ferrous ion: synergetic effects and reaction mechanism. *Environ. Sci. Pollut. Res.*, 26: 30498-30507.
- Liang, P., Zhang, C., Duan, X., Sun, H., Liu, S., Tade, M.O. and Wang, S. 2017. An insight into metal-organic framework derived N-doped graphene for the oxidative degradation of persistent contaminants: formation mechanism and generation of singlet oxygen from peroxymonosulfate. *Environ. Sci.: Nano*, 4: 315-324.
- Liu, S., Xie, J., Su, Q., Du, G., Zhang, S., Cao, G., Zhu, T. and Zhao, X. 2014. Understanding Listeria mechanism and performance of MnFe₂O₄ by in situ TEM observation on its electrochemical process in nano lithium battery. *Nano Energy*, 8: 84-94.
- Liu, Z., Wang, H., Ou, J., Chen, L. and Ye, M. 2018. Construction of hierarchically porous monoliths from covalent organic frameworks (COFs) and their application for bisphenol A removal. *J. Hazard. Mater.*, 355: 145-153.
- Luo, S., Chen, H., Wu, S., Yang, C. and Cheng, J. 2019. Enhanced removal of bisphenol A from aqueous solution by aluminum-based MOF/sodium alginate-chitosan composite beads. *Chemosphere*, 237: 124493-124511.
- Mohan, D., Sarswat, A., Ok, Y.S. and Pittman, C.U. 2014. Organic and inorganic contaminants removal from water with biochar, a renewable, low cost and sustainable adsorbent: A critical review. *Bioresour. Technol.*, 160: 191-202.
- Paethanom, A. and Yoshikawa, K. 2012. Influence of pyrolysis temperature on rice husk char characteristics and its tar adsorption capability. *Energies*, 5: 4941-4951.
- Poletto, M. 2016. Thermogravimetric analysis and kinetic study of pinewood pyrolysis. *Brazilian J. Wood Sci.*, 7: 111-118.
- Qiu, M.Q., Wang, M., Zhao, Q.Z., Hu, B.W. and Zhu, Y.L. 2018. XANES and EXAFS investigation of uranium incorporation on nZVI in the presence of phosphate. *Chemosphere*, 201: 764-771.
- Rivas, F.J. and Solís, R.R. 2018. Chloride promoted oxidation of tritosulfuron by peroxymonosulfate. *Chem. Eng. J.*, 349: 728-736.
- Tan, X., Liu, Y., Zeng, G., Wang, X., Hu, X., Gu, Y. and Yang, Z. 2015. Application of biochar for the removal of pollutants from aqueous solutions. *Chemosphere*, 125: 70-85.
- Tian, W., Zhang, H., Sun, H., Tade, M.O. and Wang, S. 2018. One-step synthesis of flour-derived functional nanocarbons with hierarchical pores for versatile environmental applications. *Chem. Eng. J.*, 347: 432-439.

- Wacławek, S., Lutze, H.V., Grübel, K., Padil, V.V.T., Černík, M. and Dionysiou, D.D. 2017. Chemistry of persulfates in water and wastewater treatment: A review. *Chem. Eng. J.*, 330: 44-62.
- Wang, H., Yang, N.C. and Qiu, M.Q. 2020. Adsorption of Cr(VI) from aqueous solution by biochar-clay derived from clay and peanut shell. *J. Inorg. Mater.*, 35: 301-308.
- Wang, J. and Zhuang, S. 2019. Covalent organic frameworks (COFs) for environmental applications. *Coordin. Chem. Rev.*, 400: 213046.
- Wang, W., Deng, S., Ren, L., Li, D., Wang, W., Vakili, M., Wang, B., Huang, J., Wang, Y. and Yu, G. 2018. Stable covalent organic frameworks as efficient adsorbents for high and selective removal of an aryl-organophosphorus flame retardant from water. *ACS Appl. Mater. Interf.*, 10: 30265-30272.
- Zhong, X., Liang, W., Lu, Z. and Hu, B.W. 2020a. Highly efficient enrichment mechanism of U(VI) and Eu (III) by covalent organic frameworks with intramolecular hydrogen bonding from solutions. *Appl. Surf. Sci.*, 504: 144403.
- Zhong, X., Lu, Z., Liang, W. and Hu, B.W. 2020b. The magnetic covalent organic framework as a platform for high-performance extraction of Cr (VI) and bisphenol A from aqueous solution. *J. Hazard. Mater.*, 393: 122353.



Seasonal Variation of Zooplankton Communities and the Effects of Environmental Factors in the Seawater Near Taishan Nuclear Power Station

R. He*§, H.P. Jiao***§, N. He**†, Y.Y. Chang**, H.Y. Jiang***, Y. Zhang****, Y.Q. Li**** and R. Jiang*†

*The Pearl River Hydraulic Research Institute, Guangzhou 510611, China

**Yichun University, Yichun 336000, China

***Guangdong Province Research Center for Geoanalysis, Guangzhou 510070, China

****Taishan Nuclear Power Joint Venture Co., Ltd., Jiangmen 518034, China

§These two authors contributed equally to this work

†Corresponding author: N. He; hen201236@163.com

Nat. Env. & Poll. Tech.
Website: www.neptjournal.com

Received: 07-01-2021

Revised: 03-03-2021

Accepted: 11-04-2021

Key Words:

Zooplankton
Community structure
Seasonal variations
Environment factors
Taishan nuclear power station

ABSTRACT

In the seawater near Taishan Nuclear Power Station, Zooplankton community composition and abundance, the biomass of major taxa, vertical distribution pattern, together with several environmental factors were investigated to evaluate the variation tendency as the seasons change. The structure characteristics of the zooplankton community were analyzed by Margalef species richness (d), Shannon-wiener species diversity index (H'), Pielou evenness index(J'), zooplankton dominant (Y), and dominant species replacement rate (R). There are 48 species within 11 classes of zooplankton identified, including 32 species of copepods. Zooplankton species richness changed obviously in the four seasons, Spring saw the highest (8010.00 ind.m⁻³), followed by winter (5100.00 ind.m⁻³), autumn (1713.75 ind.m⁻³), and summer (1196.25 ind.m⁻³). Similar trends were observed for the wet biomass, which was highest in spring (215.90 mg.m⁻³), followed by winter (181.70 mg.m⁻³), summer (78.56 mg.m⁻³), and autumn (24.69 mg.m⁻³), which gave an annual average of 125.21 mg.m⁻³. The results indicate that the abundance and biomass in spring were significantly higher than those in other seasons. Altogether 8 dominant species were identified along the whole year: *Acrocalanmus gibber*, *Bestiolina amoyensis*, *Paracalanus parvus*, *Acartia danae*, *Mesocyclops leuckarti*, *Noctiluca scientillans*, *Penilla avirostris*, and *Lucifer penicilliger*. The annual average Shannon-Wiener diversity index, Margalef diversity index, Pielou evenness index were 1.75, 1.83, and 0.74, respectively. The effects of environmental factors on the zooplankton community were studied by R and canonical correspondence analysis (CCA). According to Pearson correlation analysis and canonical correspondence analysis, the most important environmental factors influencing the changes of zooplankton species composition, abundance and distribution were water temperature, salinity, and pH in the whole year.

INTRODUCTION

Nuclear power has played an important role in energy development. However, due to warmer waters brought by heatwaves, many nuclear facilities have already reduced their output in the recent decade. More and more people begin to pay close attention to the threat of nuclear power stations on marine life and the coastal environment, particularly after the Fukushima incident. Nuclear reactors are located near a river or the ocean since they are the most water-intensive energy-producing technology. That may bring temperature drainage, residual chlorine, radioactive materials, and other problem (Chen et al. 2017, Jiang & Hou, 2015, Jiang & Wang 2020, Muthulakshmi et al. 2019).

Zooplankton communities are the vital secondary producers and main drivers of the biological pump in the Marine food web (Muthulakshmi et al. 2019, Goncalves

et al. 2012, Wu et al. 2011, Steinberg & Landry 2017). Since they are highly sensitive to environmental conditions, zooplankton communities are good indicators of the coastal environment change impacts and have been widely used to study such changes and their impacts (Batchelder et al. 2013). Buesseler et al. (2016) had found that when the temperature reached 37.0°C ~ 37.6°C, large zooplankton disappeared and Copepods dropped dramatically in the eastern Indian Ocean due to thermal drainage. Taishan Nuclear Power Station is located about 1.2 km to the northeast of Chixi town, Taishan city in Guangdong province.

There have been relevant studies on the zooplankton community in the coastal waters (Alagan et al. 2020, Asgari & Steiner, 2017, Lin, et al. 2021, Maja et al. 2018, Richardson et al. 2019, Sonia et al. 2019, Thirunavukkarasu et al. 2020), however, few studies on zooplankton community

characteristics in the waters near the nuclear power plant have been reported (Ding et al. 2019).

In this paper, four quarterly background surveys of the zooplankton community in this area from 2015 to 2016 were investigated, focusing on its community structure, abundance distribution, and seasonal changes. The relationship between the zooplankton community and several environmental factors including temperature, salinity, pH, and nutrient salts was also discussed. Our result intended to provide fundamental information for the sustainable utilization of resources in the seawater near Taishan Nuclear Power Station.

MATERIALS AND METHODS

Study Site

The zooplankton samples were collected in the seawater near Taishan Nuclear Power Station from Dec. 2015 to Sept. 2016, including 10 points along the coast station (S1-S10) and another 10 offshore (S11-S20) (Fig. 1).

Sampling

The 20 stations were sampled quarterly from December 2015 to September 2016 for reflecting their variation in four seasons: winter (20-21, December 2015), spring (28-30, March 2016), summer (25-26, June 2016), and autumn (21-23, September 2016).

At each station, water temperature, salinity, and pH were

measured in situ with a multi-parameter water quality meter along with sample collection. For quantitative investigation, 5 L water samples were collected from different sampling sites by an organic glass water extractor and then filtered by a 25# plankton net (with 200 64- μm apertures); And then 50 mL was collected in plastic bottles and immediately fixed with 5% formalin solution. The identifications were analyzed by Olympus SZ61 stereomicroscope after being settled and concentrated to 5 mL. The phyletic analysis was conducted referring to the Chinese Marine plankton map, and Chinese phytoplankton map, and Chinese zoological freshwater copepods.

Data Analysis

The structure characteristics of the zooplankton community were analyzed by Margalef species richness (d), Shannon-wiener species diversity index (H') (Shannon & Weaver 1949), Pielou evenness index (J') (Pielou 1969), zooplankton dominant (Y) and dominant species replacement rate (R) (Walkusz et al. 2009, Zervoudaki et al. 2009), calculated as below:

$$\text{Species richness index: } d = (S - 1) / \log_2(N) \quad \dots(1)$$

(S - the number of phytoplankton species, N - the number of individuals of all species)

$$\text{Species diversity index: } H' = \sum (n_i/N) \log_2(n_i/N) \dots(2)$$

(n_i - the total number of individuals of the i^{th} species, N - the total number of individuals of all species)

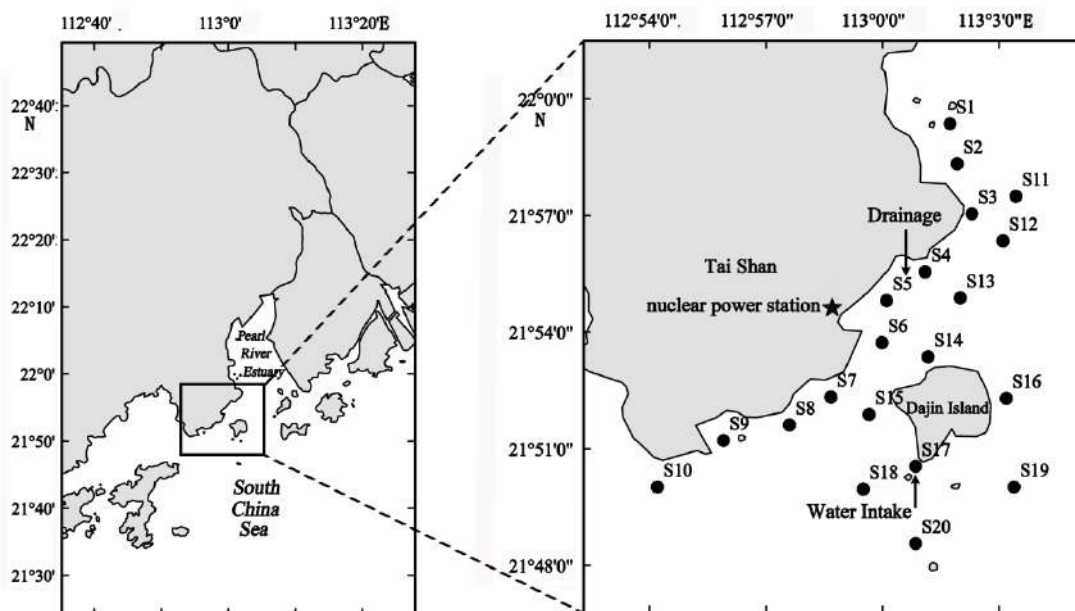


Fig. 1: Map of the different sampling stations. Intake point: Coastwise (S1-S10) and Offshore (S11-S20).

Species evenness index: $J' = H'/\log 2S$... (3)

(H' - the diversity index, S - the number of species in the sample)

Dominant index: $Y = \frac{n_i}{N} f_i$, ≥ 0.02 indicates dominant species ... (4)

(n_i - the total number of the i^{th} species, f_i - the frequency of this species in each sample, N - the total number of all samples)

Replacement rate of dominant species: $R = \frac{a+b-2c}{a+b-c} \times 100\%$... (5)

(a , b - dominant species of the two adjacent periods; c - the number of common dominant species.)

The R Programming Language *cor* and *cor.test* functions were used for correlation analysis. The biodiversity of the zooplankton community was analyzed by large multivariate statistical software PRIMER6.0. Redundancy analysis (RDA) was performed on zooplankton species and environmental data using Canoco5.0. Canonical-correlation analysis (CCA) was conducted between six water environmental factors (water temperature, salinity, pH, COD, nitrate-nitrogen, and labile phosphate) measured at 20 stations and the abundance of 25 optimal zooplankton species.

RESULTS

Species Composition

A total of 48 species of zooplankton taxa (excluding 13 planktonic larvae) belonging to 11 taxonomic groups were identified in seawater around Taishan as shown during the seasonal surveys in Table 1. At the taxonomic level, copepods were numerically the most abundant with 32 species recorded (RA 66.67%), followed by Sergestidae (RA 6.25%, 3 species). The taxonomic groups with 2 species were Cladocera, Rotifera, and Hydromedusae, respectively. The rest classes that had only 1 species recorded were Planktonic mollusks, Cumacea, Isopoda, and Amphipoda, respectively.

The community was predominant by low salt neritic ecological groups, such as *Acartia clausi*, *Acartia pacifica*, *Acartia spinicauda*, *Euterpina acutifrons*, *Labidocera sinilobata*. There were also a few estuarine groups recorded (such as *Sinocalanus tenellus*, *Schmackeria poplesia*, *Centropages tenuiremis*), as well as salty groups (such as *Paracalanus parvus*, *Acartiella sinensis* Shen, *Centropages furcatus*) and tropical groups (such as *Acartia danae*, *Acrocalanmus gibber*, *Acartia erythraea*, *Lucifer intermedius*) (Table 1). In terms of seasonal variation, autumn and winter saw the most complex zooplankton community with 28 species, followed by summer (19 species) and spring (15 species) successively.

Zooplankton Abundance and Biomass

In the present study, the zooplankton abundance showed a noticeable change among the study stations and between different seasons (Fig. 2). Zooplankton abundance ranged from 75.00 to 9600.00 ind.m⁻³ in all the samples investigated with an annual average of 4005.00 ind.m⁻³. The highest average abundance was observed in spring (8010.00 ind./m³) and followed by winter (5100.00 ind.m⁻³), autumn (1713.75 ind.m⁻³), and summer (1196.25 ind.m⁻³). It presented seasonal changes as: spring > winter > autumn > summer.

The biomass of zooplankton samples ranged from 2.63 to 815.10 mg.m⁻³ with an annual average of 125.21 mg.m⁻³. The total biomass of zooplankton showed similar trends with the zooplankton abundance. In general, maximum biomass occurred in spring (215.90 mg.m⁻³), and then followed a declining trend in the order of winter (181.70 mg.m⁻³), summer (78.56 mg.m⁻³), and autumn (24.69 mg.m⁻³), showing obvious seasonal changes (Fig. 3).

From the perspective of the horizontal distribution shown in Figs. 2-3, the abundance and biomass of zooplankton in near-shore samples collected in spring were significantly different from those in open-sea samples but similar in the other three seasons. In spring, zooplankton abundance and biomass were dramatically higher in near-shore than in open-sea samples with 3.50 times and 3.22 times, respectively. The zooplankton was mainly distributed in the neritic area, while its abundance and biomass were low. This distribution pattern of zooplankton was contributed by the high abundance of *Noctiluca scintillans* as shown in Table 2. The zooplankton showed different distribution patterns in summer, which was mainly distributed in the estuary region to the north of the sampling station and higher compared to other stations (Fig. 2). This is because the *N. scintillans* is still dominant in the summer (Table 2). In addition, the zooplankton was mainly distributed in the southern part of the sampling area in autumn, because *Penilla acirostris* and *Tortanus forcipatus* largely appeared (Table 2) and planktonic larvae were detected at the same time. However, the abundance distribution of zooplankton was relatively uniform in winter (Fig. 2), mainly dominated by copepods (Table 2).

Dominant Zooplankton Species and Their Seasonal Variations

In the present study, 8 dominant species were found in surface seawater near Taishan during the investigation (not including 2 phytoplankton). Apparently, there were substantial seasonal changes in the zooplankton dominant species, from *A. gibber*, *Bestiolina amoyensis*, *P. parvus*, *Acartia danae*, and *Mesocyclops leuckarti* in winter, *N. scintillans* in spring and summer to *P. acirostris* and *Lucifer penicilliger* in autumn.

Table 1: Species composition of surface zooplankton.

S.No	Family/Species	Ecotype	S.No.	Family/Species	Ecotype
Copepod			Cladocera		
1	<i>Cyclops vicinuss</i>	Freshwater	36	<i>Ecadne tergestina</i>	
2	<i>Pseudodiaptomus inopinus</i>	Freshwater	37	<i>Penilla acirostris</i>	
3	<i>Acartia clausi</i>	Nearshore low Salinity	Rotifers		
4	<i>Acartia pacifica</i>	Nearshore low Salinity	38	<i>Brachionus plicatilis</i>	Wide-temperature- salinity group
5	<i>Acartia spinicauda</i>	Nearshore low Salinity	39	<i>Asplanchna priodonta</i>	Freshwater group
6	<i>Paracalanus crassirostris</i>	Nearshore low Salinity	Hydra jellyfish		
7	<i>Euterpina acutifrons</i>	Nearshore low Salinity	40	<i>Moerisia</i> sp.	
8	<i>Microsetella norvegica</i>	Nearshore low Salinity	41	<i>Aequorea conica</i>	
9	<i>Oithona brevicornis</i>	Nearshore low Salinity	Protozoan		
10	<i>Oithona simplex</i>		42	<i>Noctiluca scintillans</i>	
11	<i>Oithona nana</i> Giesbrecht		Amphipoda		
12	<i>Bestiolina amoyensis</i>	Nearshore low Salinity	43	<i>Gammaridea</i> sp.	
13	<i>Labidocera euchaeta</i>	Nearshore low Salinity	Phytoplankton mollusks		
14	<i>Labidocera sinilobata</i>	Nearshore low Salinity	44	<i>Creseis acicula</i>	
15	<i>Tortanus forcipatus</i>	Nearshore low Salinity	Cumacea		
16	<i>Tortanus dextrilobatus</i>	Nearshore low Salinity	45	<i>Cumacea</i> sp.	
17	<i>Temora turbinata</i>	Nearshore low Salinity	Isopods		
18	<i>Acartia danae</i>	Tropical taxa	46	<i>Microniscus</i> sp.	
19	<i>Acartia erythraea</i>	Tropical taxa	Other		
20	<i>Acartia negligens</i>		47	<i>Cypridina bairdii</i>	
21	<i>Candacia</i> sp.	Tropical taxa	Planktonic larvae		
22	<i>Acrocalanus gibber</i>	Tropical taxa	49	Zoea larvae (Brachyura)	
23	<i>Mesocyclops leuckarti</i>	Tropical taxa	50	Nauplius larvae (Cirripedia)	
24	<i>Sinocalanus tenellus</i>	Tropical taxa	51	Nauplius larvae (Copepoda)	
25	<i>Schmackeria poplesia</i>	Tropical taxa	52	Copepoda larvae	
26	<i>Sinocalanus laevidactylus</i>	Tropical taxa	53	Ophiuroidea	
27	<i>Centropages tenuiremis</i>	Tropical taxa	54	<i>Cylla serrata</i>	
28	<i>Paracalanus parvus</i>	Wide salinity group	55	Gastropoda larvae	
29	<i>Acartiella sinensis</i> Shen	Wide salinity group	56	Mysidacea larvae	
30	<i>Centropages furcatus</i>	Wide salinity group	57	Polychaeta larvae	
31	<i>Pseudodiaptomus penicillus</i>		58	Macrura larvae	
32	<i>Canthocalanus pauper</i>		59	Penaenus orientalis	
Sergestidae			60	Eriocheir sinensis	
33	<i>Lucifer hansenii</i>		61	Eriocheir sinensis	
34	<i>Lucifer penicilliger</i>	Warm water species	Total = 61		
35	<i>Lucifer intermedius</i>	Tropical taxa			

To understand how the dominant species changed in different seasons, the replacement rate of the dominant species and the population turnover rate were calculated. The replacement rate of dominant species in spring-summer, summer-autumn, autumn-winter, and winter-spring was

calculated as 0%, 100%, 100%, and 100%, respectively. Successively, the population turnover rate was 53.57%, 77.27%, 76.79%, and 67.44%, respectively. Except for the same dominant species were found in spring and summer, the corresponding replacement rate was above 50%. As a result,

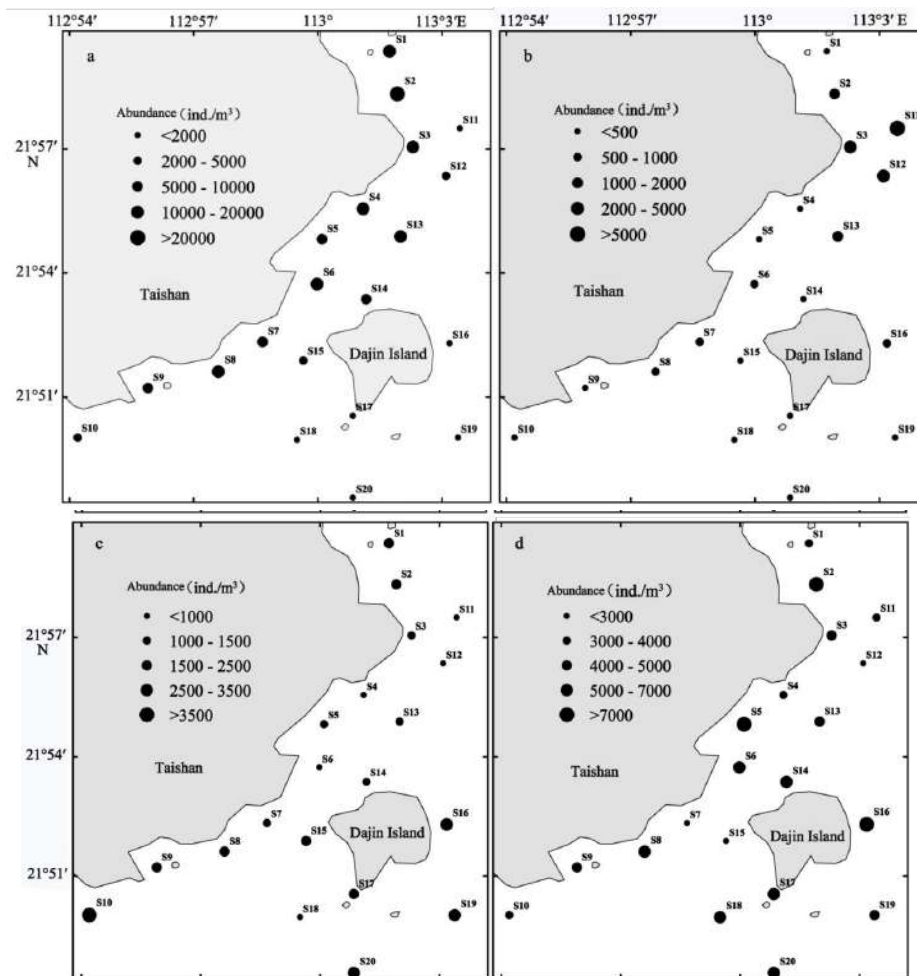


Fig. 2: Average abundance of zooplankton in different seasons (a: Spring, b: Summer, c: Autumn, d: Winter) from Dec. 2015 to Sep. 2016.

the seasonal replacement rate of zooplankton was relatively high in the whole year.

Species Diversity and Seasonal Variation

As shown in Table 3, the abundance index such as Pielou's index (d), the diversity index (H'), and the Evenness index (J') during investigation time across seasons exhibited a common trend. Pielou's index (d) was in the range of 0.2–3.1, with an annual average of 1.75. The diversity index (H') was in the range of 0.00–3.28, with an annual average of 1.83. The Evenness index (J') was in the range of 0.09–1.00, with an annual average of 0.74. The zooplankton diversity index over the 4 seasons in 2015–2016 was the lowest in spring and followed an increasing trend till winter. While at other times, these values were lower due to the explosive growth of some dominant species.

Effects of Environmental Factors

Environmental factors play important roles in the seasonal succession of the zooplankton community. As showed in Table 4, the results of correlation analysis were performed to evaluate the influence of environmental factors (water temperature, salinity, pH, COD, nitrate-nitrogen, and labile phosphate) on the zooplankton community (species, abundance, biomass, and diversity index). The population and abundance of zooplankton were found to be positively correlated with salinity and pH, while negatively correlated with COD. Zooplankton biomass was positively correlated with nitrate-nitrogen and labile phosphate, while negatively correlated with water temperature. The diversity index of zooplankton was positively correlated with water temperature, salinity, and pH, while negatively correlated with COD and nitrate-nitrogen.

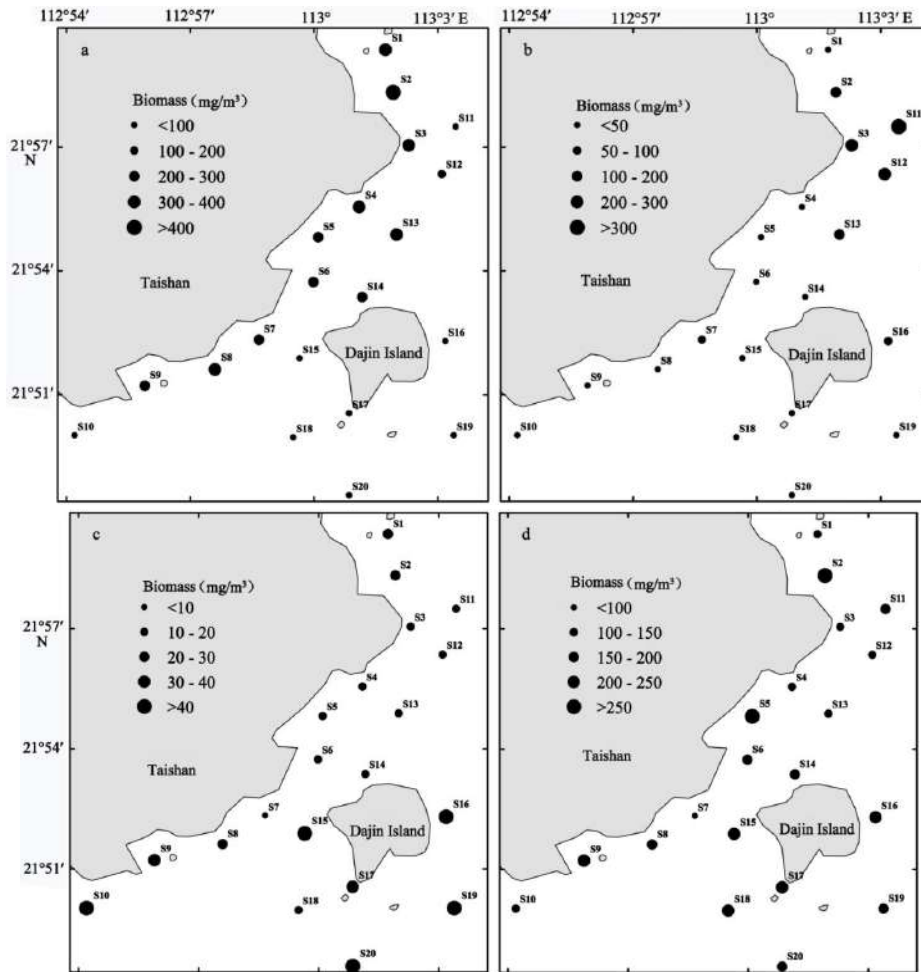


Fig. 3: Horizontal distribution of average biomass of zooplankton in different seasons (a: Spring, b: Summer, c: Autumn, d: Winter) from Dec. 2015 to Sep. 2016.

Table 2: Dominant species of zooplankton.

No.	Dominants	Spring				Summer				Autumn				Winter			
		f%	A	A%	Y	f%	A	A%	Y	f%	A	A%	Y	f%	A	A%	Y
1	<i>Acrocalanus gibber</i>	*	*	*	*	*	*	*	*	5.0	18.75	1.22	-	13.00	780	15.29	0.13
2	<i>Bestiolina amoyensis</i>	*	*	*	*	*	*	*	*	*	*	*	*	5.29	450	5.56	0.05
3	<i>Paracalanus parvus</i>	*	*	*	*	5.0	7.5	0.63	-	15	18.75	1.22	-	16.41	930	11.48	0.16
4	<i>Acartia danae</i>	5.0	3.75	0.05	-	10	18.8	1.57	-	40	56.25	3.67	0.01	2.65	300	3.70	0.03
5	<i>Mesocyclops leuckarti</i>	*	*	*	*	*	*	*	*	*	*	*	*	2.12	270	3.33	0.02
6	<i>Noctiluca scintillans</i>	90	7642.5	95.41	0.86	100	915	76.49	0.76	10	11.25	0.73	-	*	*	*	*
7	<i>Penilla acirostris</i>	*	*	*	*	*	*	*	*	55	247.5	16.14	0.09	*	*	*	*
8	<i>Lucifer penicilliger</i>	*	*	*	*	*	*	*	*	75	165	10.76	0.08	*	*	*	*

f% - frequency of occurrence; A - abundance (ind.m³); A% - abundance percentage; Y - dominance

Note: Means the dominance Y < 0.01, *means not shown

Table 3: Seasonal variation of diversity and evenness of zooplankton.

Season	Pielou's index (<i>d</i>)		Diversity index (<i>H'</i>)		Evenness index (<i>J'</i>)	
	Mean	Range	Mean	Range	Mean	Range
Spring	0.93	0.33-2.49	0.62	0.00-2.35	0.29	0.09-0.96
Summer	1.28	0.62-2.23	1.55	0.64-2.45	0.80	0.28-0.97
Autumn	2.03	0.69-3.05	2.47	1.38-3.22	0.90	0.79-0.99
Winter	2.75	1.95-3.75	2.66	2.00-3.28	0.98	0.91-1.00
Annual Mean	1.75	0.33-3.75	1.83	0.00-3.28	0.74	0.09-1.00

Table 4: Pearson correlation analysis between parameters of zooplankton and environmental factors.

Environment factors	Number of species		Abundance		Biomass		Diversity index	
	<i>R</i>	<i>P</i>	<i>R</i>	<i>P</i>	<i>R</i>	<i>P</i>	<i>R</i>	<i>P</i>
Temperature T	-0.040	0.724	-0.144	0.203	-0.577	0.000**	0.257	0.021*
Salinity S	0.468	0.000**	0.363	0.000**	-0.074	0.515	0.503	0.000**
pH	0.456	0.000**	0.625	0.000**	-0.210	0.062	0.728	0.000**
Chemical Oxygen Demand COD	-0.272	0.015*	-0.683	0.000**	0.167	0.139	-0.622	0.000**
nitrate-nitrogen (NO ₃)	-0.187	0.100	-0.005	0.967	0.395	0.000**	-0.268	0.016*
labile phosphate (PO ₄)	0.035	0.756	0.205	0.068	0.435	0.000**	-0.094	0.409

Note: *indicated *P* level was 0.05. **indicated *P* level was 0.01

To further explore the correlations between zooplankton community structure and environmental factors, the canonical correlation analysis (CCA) between the abundance of 25 optimal zooplankton species and six water environmental factors was conducted, as showed in Table 5.

All the characteristic values of CCA sequencing explain 18.7% of the variation degree of zooplankton. The characteristic values of the first two sequencing axes were 0.662 and 0.529, which together explain 15% of the change degree of the zooplankton community. The correlation coefficients between 25 species and 6 water environmental factor sequencing axes (the first axis and the second axis) were 0.956 and 0.886, indicating a close correlation between the zooplankton and the water environmental factors. Thus, the results of CCA were credible. Furthermore, the Monte Carlo test showing that the first axis was significantly different from other axes ($P < 0.01$) made the ranking results of CCA analysis more convincing.

The distinct clusters in species biplot of CCA analysis clearly revealed that the zooplankton spatio-temporal variation may be caused by different environmental variables. Furthermore, among all the environmental variables, the most important factors affecting the structure of the plankton community were COD, pH, and salinity, which is consistent with Pearson correlation analysis results shown in Table 4. In addition, CCA results divided 25 species of major zooplankton into three groups. The species of group I, including *A. gibber*, *B. amoyensis*, etc., were positively correlated with salinity, pH, and labile phosphate, while

negatively correlated with COD. On the contrary, group III (*P. acirostris*, *C. larva*, etc.) was positively correlated with COD but negatively correlated with salinity, pH, and labile phosphate. Group II (*L. penicilliger*, *C. furcatus*, etc.) presented a positive correlation with temperature and a negative correlation with nutrient salts.

Zooplankton species number 1-8 is shown in Table 2. 9. *Centropages furcatus* 10. *Acartia spinicauda* 11. *Oithona brevicornis* 12. *Schmackeria poplesia* 13. *Cycylla serrata* 14. *Paracalanus crassirostris* 15. Nauplius larvae 16. Copepoda larva 17. *Acartia pacifica* 18. *Canthocalanus pauper* 19. *Sinocalanus tenellus* 20. *Lucifer intermedius* 21. *Penaenus orientalis* 22. *Eriocheir sinensis* 23. *Eriocheir sinensis* 24. *Temora turbinata* 25. *Labidocera sinilobata*

Table 5: Summary statistics for the axes of CCA performed on zooplankton.

items	Sequencing axis			
	1	2	3	4
Characteristic value	0.662	0.529	0.172	0.123
Correlation of species and environmental factors	0.956	0.886	0.710	0.713
Cumulative percentage of species	8.30	15.0	17.1	18.7
Cumulative percentage of the relationship between species and environment	41.1	74.0	84.7	92.3
Four sort the total eigenvalues	7.96			
Sum of all canonical eigenvalues	1.61			

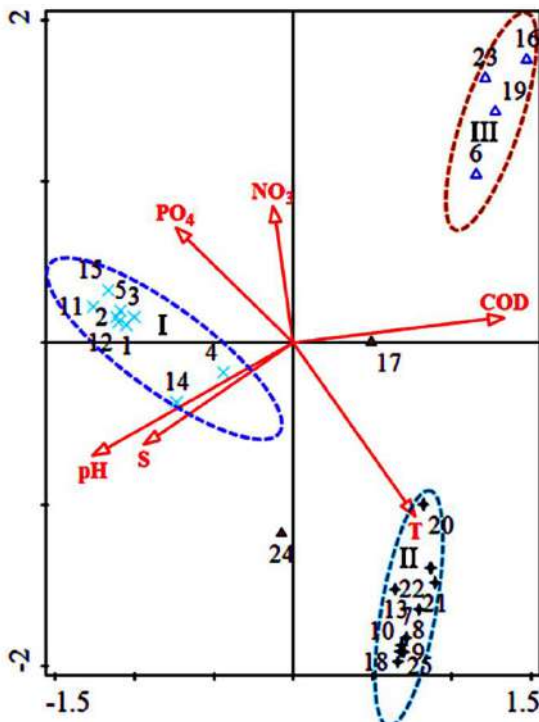


Fig. 4: Canonical correlation analysis between zooplankton species and environmental factors.

DISCUSSION

Effects of Environmental Factors and Phytoplankton

In the water, environmental conditions are complex and changing, affecting zooplankton species and communities. Temperature, salinity, and phytoplankton were the important factors influencing the distribution of zooplankton. During this study, a significant variation of water temperature exhibited a seasonal pattern: which increased after spring and reached a maximum in summer, decreased in autumn, and dropped to a minimum in winter. While the salinity showed higher values in winter and autumn than in spring and summer.

The concentration and rich nutrient content of phytoplankton were significantly correlated with the water quality characteristics in different seasons (Alagan et al. 2020, He et al. 2018, Lin et al. 2021, Shi et al. 2018, 2020, Wang et al. 2020). These environmental conditions affected the distribution of zooplankton and thus caused seasonal changes of the zooplankton community (Muthulakshmi et al. 2019, Thirunavukkarasu et al. 2020). Pearson correlation showed that all six environmental factors had affected zooplankton in different aspects, while pH, salinity, and temperature were the most significant factors that influenced the 25 major zooplankton species.

The number of phytoplankton peaked in spring because of adequate nutrient salt, which had reached the level of red tide. With abundant food, low temperature, and low salinity, *N. scintillans* thrived and become the most dominant species ($Y = 0.86$). S2 stood up with 31125 ind.m^{-3} among all the sample stations as shown in Fig. 3. Additionally, as a group III species (as discussed in 3.5), *N. scintillans* displayed a significant negative correlation with water temperature and salinity. A red tide of *N. scintillans* had occurred several times in the neritic areas of China, resulting in the death of mollusks such as scallops and oysters, and bringing huge economic losses to the fishery (Baliarsingh et al. 2016). In this survey, the massive propagation of *N. scintillans* was mainly distributed in near-shore and the Pearl River estuary area (with similar environmental conditions of previous *N. scintillans*-related red tides) (Mikaelyan et al. 2014). It indicates risks of occurrence of red tides caused by *N. scintillans*. In addition, low salinity zooplankton groups near the shore and estuaries such as *Acartia pacifica* and *Sinocalanus laevidactylus* were detected. In summer, the abundance of phytoplankton decreased significantly when water temperature increased and salinity decreased. Although the abundance of *N. scintillans* decreased, they remained the dominant species ($Y=0.76$). *N. scintillans* is mainly distributed in the pearl river estuary sea areas such as Station S3, S11, and S12, among which S11 presented the maximum abundance of 4650 ind.m^{-3} . As salinity increased while the autumn temperature was still high, the density of phytoplankton as a food source decreased, and thus, replacement of dominant zooplankton species had taken place: *P. acirostris* and *L. penicilliger* became the dominant species, while the planktonic larvae began to multiply and became the absolute group. It can be seen from Fig. 4 that *Nauplius larvae*, belonging to group I, showed a positive correlation with salinity, while *Penaenus orientalis* and *Eriocheir sinensis* (in group II) were mainly positively correlated with temperature. The relationship between different species of planktonic larvae and environmental factors is quite different, which is consistent with previous research results (Fanjul et al. 2018). In winter, dominant species became *P. parvus*, *A. gibber*, *B. amoyensis*, and *A. danae daphnia* with both temperature and phytoplankton abundance decreasing, which were all negatively correlated with temperature.

Other Effects

It is important to note in particular that the direct effect of the nuclear power plants on the environmental changes was due to the increase in the temperature for the temperature drainage, which became a major factor affecting the marine ecological environment (Alibek 2016, Jiang & Wang et al. 2020, Muthulakshmi et al. 2019). In this study, the differ-

ences in the abundance distribution of zooplankton between the four voyage outlets and the neighboring stations were compared. As a result, zooplankton abundance near the outlet was not much different from that at the adjacent stations in spring; What mattered was the distance from shore: zooplankton abundance was higher at near shore stations than that at the stations in the open sea, indicating significant influence from tides. In summer, zooplankton abundance around the outlet and the south sea area is lower than that in the North Sea area, which indicates that the estuary runoff may have a great influence on the distribution of zooplankton. However, zooplankton abundance around the outlet is lower than those found at non-outlet stations in autumn, which is more likely related to temperature drainage from the nuclear power plant. The situation in winter is more complex with zooplankton distributed quite randomly. In conclusion, temperature drainage seems did affect zooplankton distribution in autumn.

CONCLUSION

In the seawater near Taishan Nuclear Power Station, a total of 48 species of zooplankton taxa belonging to 11 taxonomic groups were identified. At the taxonomic level, copepods covered the vast majority of zooplankton and they were mainly composed of low salinity groups near the shore, which is typical of subtropical flora. The differences in zooplankton density, biomass, and diversity indices were significant in different seasons. The results indicate that the abundance and biomass in spring were significantly higher than those in other seasons. However, the zooplankton diversity index was the lowest in spring and showed an upward trend till winter. According to Pearson correlation analysis and canonical correspondence analysis, pH, salinity, and temperature were the principal factors affecting the distribution of zooplankton. By comparing the results among the study stations and between different seasons, it seems that the zooplankton community in the survey area was mainly determined by different seasons, estuary runoff, and tide. This study will be helpful in the further understanding of the threat of the Taishan Nuclear Power Station on the marine life and the coastal environment, and in providing scientific guidance for the protection of the ecological environment of surrounding seas.

ACKNOWLEDGEMENT

This paper was granted by State Key Laboratory of Organic Geochemistry, GIGCAS (No. SKLOG202011 and No. SKLOG202007), the Jiangxi Province Natural Science Foundation of China (No.20202BAB213021), the Guangdong Province Natural Science Foundation of China (No.

2017A030313329), and the National Natural Science Foundation of China (No. 51409287).

REFERENCES

- Alibek, I. 2016. Mathematical modeling of the discharged heat water effect on the aquatic environment from thermal power plant under various operational capacities. *Appl. Math. Model.*, 40(2): 1082-1096.
- Alagan, M., Natesan, U., Ferrer, V.A. and Venugopalan, V.P. 2020. Effects of environmental variables on phytoplankton in the coastal waters of Kalpakkam with special emphasis on thermal discharge from a power plant, southeast coast of India. 6th International Scientific Conference Geobalcanica, 12-13May 2020, Ohrid, North Macedonia, Geobalcanica, Macedonia, pp. 31-45
- Asgari, M. and Steiner, C.F. 2017. Interactive effects of productivity and predation on zooplankton diversity. *Oikos*, 130(8): 45-57.
- Baliarsingh, S.K., Lotliker, A.A., Trainer, V.L., Wells, M.L., Parida, C., Sahu, B.K., Srichandan, S., Sahoo, S., Sahu, K.C. and Kumar, T.S. 2016. Environmental dynamics of red *Noctiluca scintillans* bloom in tropical coastal waters. *Marine Pollution Bulletin*, 111(1-2): 277-286.
- Batchelder, H.P., Daly, K.L. and Davis, C.S. 2013. Climate impacts on zooplankton population dynamics in coastal marine ecosystems. *Oceanography*, 26: 34-51.
- Buesseler, K., Dai, M.H., Aoyama, M., Benitez-Nelson, C. and Morris, P.J. 2016. Fukushima Daiichi-derived radionuclides in the ocean: Transport, fate, and impacts. *Annu. Rev. Mar. Sci.*, 9(1): 1.1-1.31.
- Chen, X., Ji P., Wu Y.H., Zhao, Y.J. and Zeng, L. 2017. Coupling simulation of overland flooding and underground network drainage in a coastal nuclear power plant. *Nucl. Eng. Des.*, 325: 129-134.
- Ding, X.W., Tian, W., Zhai, A.F., Kang, B. and Zhu, Q. 2019. Research on water intake, usage, and drainage impact demonstration for coastal nuclear power plants. *IOP Conf. Ser - Earth Environ. Sci.*, 36: 515-539.
- Fanjul A., Iriarte A., Villate F., Uriarte, I., Atkinson, A. and Cook, K. 2018. Zooplankton seasonality across a latitudinal gradient in the Northeast Atlantic Shelves Province. *Continental Shelf Research: A Companion Journal to Deep-Sea Research and Progress in Oceanography*.
- Goncalves, A.M.M., Azeiteiro U.M., Pardal M.A. and Troch, M.D. 2012. Fatty acid profiling reveals seasonal and spatial shifts in the zooplankton diet in a temperate estuary. *Estuar. Coast. Shelf Sci.*, 109: 70-80.
- He, R., Jiang, R., Zhu, X.P., Guo, W., Li, Z.X. and Xu, N. 2018. Seasonal variation of phytoplankton and its relationship with environmental factors in sea waters near Taishan. *Chinese Journal of Ecology*.
- Jiang, S. and Hou, J. 2015. The impact analysis for the marine environment which caused by the thermal discharge of the power plant. *International Forum on Energy, Environ. Sci. Mater.*, 6: 35-51
- Jiang, R. and Wang, Y.S. 2020. Modeling the ecosystem response of the semi-closed Daya bay to the thermal discharge from two nearby nuclear power plants. *Ecotoxicology*, 29(2):11-23.
- Lin, J., Zou, X. and Huang, F. 2021. Quantitative analysis of the factors influencing the dispersion of thermal pollution caused by coastal power plants. *Water Res.*, 188: 116558.
- Maja, M.K., Lidia, D.G. and Agata, W. 2018. Influence of environmental factors on the population dynamics of key zooplankton species in the Gulf of Gdańsk (Southern Baltic Sea). *Oceanologia*, S0078323418300691.
- Mikaelyan, A.S., Malej, A., Shiganova, T.A., Turk, V., Sivkovitch, A.E., Musaeva, E.I., Kogovsek, T. and Lukashova, T.A. 2014. Populations of the red tide forming dinoflagellate *Noctiluca scintillans* (Macartney): A comparison between the Black Sea and the northern Adriatic Sea. *Harmful Algae*, 33: 29-40.
- Muthulakshmi, A.L., Natesan, U., Ferrer, V.A., Deepthi, K. and Narasimhan, S.V. 2019. Impact assessment of nuclear power plant discharge on zooplankton abundance and distribution in coastal waters of Kalpakkam, India. *Ecol. Proces.*, 8(1): 22.

- Pielou, E.C. 1969. *An Introduction to Mathematical Ecology*, Wiley-Interscience, New York, pp. 1-28.
- Richardson, J., Feuchtmayr, H., Miller, C., Hunter, P.D., Maberly, S.C. and Carvalho, L. 2019. The response of cyanobacteria and phytoplankton abundance to warming, extreme rainfall events, and nutrient enrichment. *Glob. Change Biol.*, 25(1).
- Shannon, C.E. and Weaver, W. 1949. *The Mathematical Theory of Communication*, University of Illinois Press, Urbana IL, pp. 1-125.
- Shi, Y.Q., Niu, M.X., Zuo, T., Wang, J. and Pakhomov, E.A. 2020. Inter-annual and seasonal variations in zooplankton community structure in the Yellow Sea with the possible influence of climatic variability. *Prog. Oceanogr.*, 185: 102349.
- Shi, Y.Q., Zuo, T., Yuan, W., Sun, J.Q. and Wang, J. 2018. Spatial variation in zooplankton communities in relation to key environmental factors in the Yellow Sea and the East China Sea during winter. *Cont. Shelf Res.*, 170: 33-41.
- Sonia, R.R., Ricardo, G.G., Carlos, C. and Acua, J.L. 2019. Seasonal and vertical dynamics in the trophic structure of a temperate zooplankton assemblage. *Limnol. Oceanogr.*, 64: 434-451.
- Steinberg, D.K. and Landry, M.R. 2017. Zooplankton and the ocean carbon cycle. *Annu. Rev. Mar. Sci.*, 9: 413-444.
- Thirunavukkarasu, S., Vasanthi, R., Karunasagar, G. and Munuswamy, N. 2020. Coastal water quality impact on community structure and genotoxicity of marine zooplankton. *Reg. Stud. Marine Sci.*, 39: 18-31
- Walkusz, W., Kwasniewski, S., Falk-Petersen, S., Hop, H. and Weslawski, J.M. 2009. Seasonal and spatial changes in the zooplankton community of Kongsfjorden, Svalbard. *Polar Res.*, 28(2): 1-17.
- Wang, M.L., Wang, Y.T., Chen, H., Sun, F.L. and Wang, Y.S. 2020. Phytoplankton community, structure, and succession delineated by partial least square regression in Daya Bay. *The South China Sea*, 29: 751-761.
- Wu, J.X., Yan, B.L., Feng, Z.H., Li, Y. and Shen, X. 2011. Zooplankton ecology near the Tianwan Nuclear Power Station. *Acta Ecol. Sin.*, 31(22): 6902-6911.
- Zervoudaki, S., Nielsen, T.G. and Carstensen, J. 2009. Seasonal succession and composition of the zooplankton community along a eutrophication and salinity gradient exemplified, by Danish waters. *J. Plankton Res.*, 31(12): 1475-1492.



A Review on Rice Straw Management Strategies

Lakhvir Singh† and Balraj Singh Brar

Yadavindra College of Engineering, Punjabi University Guru Kashi Campus, Talwandi Sabo, Punjab, India

†Corresponding author: Lakhvir Singh; er.lakhvir723@gmail.com

Nat. Env. & Poll. Tech.
Website: www.neptjournal.com

Received: 02-11-2020

Revised: 15-02-2021

Accepted: 22-02-2021

Key Words:

Rice Straw

Burning

Pollutions

Treatments

Environment friendly

ABSTRACT

Rice straw is one of the organic materials and natural residue of rice crop or paddy material and is the third-largest residue from agriculture after sugarcane bagasse and maize straw. Southeast Asian countries produce approximately 80% of rice production in the world. It leads to a large quantity of rice straw as a by-product every year. Surplus rice straw is a focal issue associated with storage of rice straw, removal of entire straw from the field, and very little time between the cultivation of the crop. Stubble burning is a quick, cheap, and efficient way to prepare the soil bed for wheat, the next crop. Rice straw has both nutrient and calorific values. Straw is the only organic material available in significant quantities to most rice farmers. About 40 percent of the nitrogen (N), 30 to 35 percent of the phosphorus (P), 80 to 85 percent of the potassium (K), and 40 to 50 percent of the sulfur (S) taken up by rice remains in vegetative plant parts at crop maturity. Straw is either removed from the field, burned in situ, piled or spread in the field, or incorporated in the soil. Open burning of the crop residue kills useful microflora of soil, leads to soil degradation, and contributes to harmful greenhouse gases such as SO₂, NO₂, CH₄, N₂O, carbon monoxide in the atmosphere including the hydrocarbon and particulate matter. Therefore, rice straw burning is a serious creator of environmental pollution. The study investigated environment-friendly options of rice straw such as bedding material for cattle, mushroom cultivation, nutrition in the soil, power generation, combustion material, pellet making, bio-gas, bio-ethanol, bio-char, acoustic material, 3D objects, cardboard and composite board, packaging materials, production of bio-composite, cement bricks, and handmade paper. The key purpose of this paper is to provide environmentally friendly alternatives to rice straw instead of open field burning.

INTRODUCTION

Rice crop or paddy is a type of grass (Gramineae) and belongs to the genus *Oryza*. The rice *Oryza glaberrima* and rice *Oryza sativa* were domesticated in Africa and Asia respectively. Many other places have been proposed for the origin of *O. sativa* such as northern Thailand and India. In southern China, Yangzi valley is one of the domesticated rice places (Dobermann & Fairhurst 2002, Singh et al. 1995). The *O. sativa* is cultivated in a wide range of environments. It is cultivated from lowland paddy fields to high altitude terraces, equatorial tropics to sub-tropical mid-latitude, and from swamps to upland rice. The maximum yield of paddy is obtained in the dry season, because of less cloud cover. With lesser cloud cover, the photosynthetic active radiations (PAR) are more as compared to the wet season (Dobermann & Fairhurst 2002).

The primary harvesting season for rice is from June to October for different regions and climates (Zhiqiang et al. 2011). For most of the traditional varieties, the growing season is of about 260 days. But in the case of modern varieties, the growing season reduces to 90-110 days. For increasing crop production, the shortening of the growing season plays a very important role. The time for crop maturity is usually

extended because of a deficiency in phosphorus and other nutrients. Modern varieties of rice were introduced in the year 1960. Most of the paddy rice farmers cultivate is nitrogen (N) responsive and short straw varieties (Dobermann & Fairhurst 2002).

Rice straw is one of the organic materials and natural residue of rice crop or paddy material, which is easily available to most farmers worldwide (Dobermann & Fairhurst 2002). Globally, it is the third-largest residue from agriculture after sugarcane bagasse and maize straw (McLaughlin et al. 2016).

Problems in Paddy Straw Management: Worldwide and in India

Southern and Southern Eastern Asia is the main producer of rice. From this region, China, India, Indonesia, Bangladesh, and Vietnam are the main rice-producing countries. That is why this region is the main focus of the study problem related to rice straw and its management (Bakker et al. 2013). As rice is the 2nd largest cereal crop after wheat, more than 580 million tonnes of rice straw, a biomass, is produced every year (Nasr et al. 2015, Reddy & Yang 2006). In India, 43.95 million hectares of land are under paddy cultivation, which produced nearly 106.54 million tonnes of rice and

160 million tonnes of straw in the last few years. Usually, the ratio of rice grain to straw produced is 1:1.5. In the year 2013–14, Punjab, a small northern state of India, alone produced approximately 11.27 million tonnes of rice (about 10.6 % of India's total production) and 16.90 million tonnes of rice straw (Chandra et al. 2017, Yadav et al. 2015).

It is noted that, traditionally, a major part of wheat straw is used as animal feed, but rice straw is of very low-quality roughage and hence not preferred as feed for the animals (Bakker et al. 2013). Compared to wheat straw, a very little part of rice straw is used in brick kilns, animal production/grooming, mushroom cultivation, making of cardboards, as a fuel for biomass power plants, and many applications in industrial processes (Chandra et al. 2017, Yadav et al. 2015).

Losses to the Environment and Soil Fertility Due to Traditional Handling of Rice Straw

Open-field burning of rice straw leads to air, water, and land pollution, which is an enormous problem for the environment. Moreover, it contributes to climate change and increased ozone levels. In India, farmers of Punjab and Haryana states follow mechanized agriculture because of a shortage of labor and they need to prepare their field quickly for the cultivation of the next crop (Verma 2014). Open-field burning of crop residue produces very harmful gases like SO_2 , NO_2 , CH_4 , N_2O , and carbon monoxide in the atmosphere including hydrocarbon and particulate matter (Pushpa & Sinha 2011). Punjab Agriculture University, Ludhiana (PAU) estimated that crop residue contains carbon of about 6 million tonnes which upon open field burning, produces 22 million tonnes of carbon dioxide within a time period of 15-20 days (Kumar et al. 2015). The Supreme Court of India took a serious note of pollution due to stubble burning in Northern Indian states such as Punjab, Haryana, Delhi, and Uttar Pradesh (Kaur 2017).

The several nutrients detached from rice straw, rice grain, and combined (straw and grain) are as given in Table 1: To manage the current situation of stubble burning, alternative (Scientific methods) uses of rice straw need to be found, which are economical to farmers rather than a burden. Presently, many farmers have been using the traditional method of burning crop stubble which is easy, inexpensive, and efficient. The study recommends some approaches that (if used appropriately) will profoundly assist in arresting the issues of burning agricultural stubble in the country and beyond (Vagg 2015). The two main processing technologies for the conversion of rice straw to energy are: biochemical/biological and thermochemical. Thermochemical processing comprises liquefaction, pyrolysis/gasification, and combustion. Biochemical processing comprises fermentation and

digestion (Dobermann & Fairhurst 2002, Bakker et al. 2013).

The main objective of this paper is to review the various rice straw management strategies and respective hurdles.

Flow Diagram of Rice Straw Management Alternatives

The state of the art of rice straw management techniques has been broadly classified as per the flow chart given below:

The flow chart shows two main classifications of rice straw management: in-field options and off-field options which are described as follows. The in-field options for rice straw management are further classified as direct open-field burning of rice straw and incorporation of rice straw into paddy soil is another strategy to manage rice straw. The off-field options are further classified into three main categories: agriculture/ dairy, energy production, and manufacturing. In the agriculture/ dairy category, rice straw is used for bedding material, mushroom cultivation, and compost purpose. The energy production category is divided into power generation (thermal) and bio-chemical. The power generation (thermal) category is further classified as generation of power from rice straw, rice straw as combustion material, and pallet making from rice straw. Another category of energy production is the biochemical process. With the help of biochemical processes bioethanol, biogas and biochar can be prepared from rice straw. Other miscellaneous uses of rice straw for manufacturing are as follows: acoustic material, 3D objects, cardboard composite, cement bricks, and handmade paper.

Recent Review of Paddy Straw Management Endeavors

To recent reviews of different rice straw management techniques are further discussed, as shown in the flow chart:

Recent Review of in-Field Options for Rice Straw Management

There are two key in-field options for rice straw management: open burning of rice straw and preparation of compost from the rice straw. These are further discussed below in detail:

- **Open burning of rice stubble in the field:** The burning of rice straw has a very harmful effect on the environment because of the generation of a large quantity of

Table 1: Values of Nutrients Removed (Dobermann & Fairhurst 2002).

	Removal of Nutrients in kg/tonne				
	P_2O_5	N	K_2O	Mg	Ca
By rice straw	2.3	7.0	17.5	2.0	3.5
By rice grain	4.6	10.5	3.0	1.5	0.5
Straw and grain	6.9	17.5	20.5	3.5	4.0

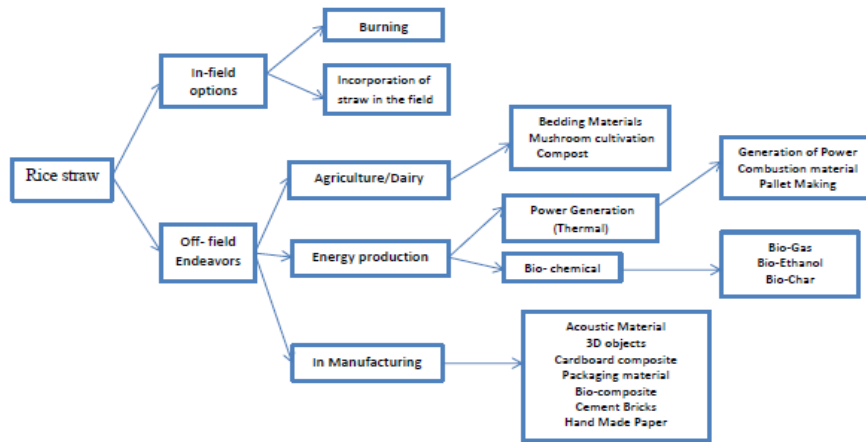


Diagram 1: Rice straw management alternatives.

CO₂ gas that contributes to the greenhouse effect. It also affects the respiratory system of the local population of that area (Zayed & Abdel-Motaal 2005). Paddy residue left by harvesters takes one-and-half months to decompose while farmers do not have sufficient time to sow their next crop, wheat. Stubble burning is a quick, cheap, and efficient way to prepare soil bed for wheat, the next crop (Chandra et al. 2017, Yadav et al. 2015). During the rice straw burning, lots of nutrients are lost as discussed in section 3 of this paper. So the farmers have to add various fertilizers and nutrients to compensate for the loss, which is an additional economic burden (Zhiqiang et al. 2011) (McLaughlin et al. 2016).

- **Incorporation of rice straw in the field:** The burning of crop residue leads to soil degradation (Yadav et al. 2015). Researchers are continuously working to develop rapid and simple composting methods for the conversion of waste rice straw into organically rich nutrients for the soil. In agriculture, the use of compost improves crop yield problems by 4-9 % (Verma 2014).

To accelerate the breakdown process, some special fungus is added and it gives successful results just in 3 months. The addition of cow dung also provides the required environment for enzymes and microbes (Vagg 2015). A study showed that before incorporation, rice straw treated with *Trichoderma harzianum*, *Pleurotus sajorcaju*, and cow dung slurry enhanced the nutrients content and organic carbon of soil. It further increases straw yield and grains (Fig. 1) (Sanathimmappa et al. 2015).

Recent Review of Off-Field Options for Rice Straw Management

In off-field options, first, the rice straw is moved from the

field and then converted into bundle form. The various off-field options are discussed as below:

Rice Straw Uses in Agriculture and Dairy Purpose

Use of rice residue as bedding material for cattle: The Punjab Agricultural University, Ludhiana advised the farmers to use rice straw as bedding material in winters for cattle (Fig. 2). Rice straw provides a dry, clean, comfortable, non-slippery, and hygienic environment which prevents the chances of lameness and injury. Healthy legs ensure better milk production and reproductive efficiency of animals (Kumar et al. 2015, Kargbo et al. 2010, Singh et al. 1995).

Paddy straw for mushroom cultivation: In 2017-18, India cultivated rice in an approximate area of 45.10 Mha and produced 111.01 MMT with a productivity rate of 3.52 MT.ha⁻¹. Mushrooms were first cultivated in India in Coimbatore by Thomas et al. (1943). As per the FAO (Food and Agriculture Organization) statistics, in 2016, India produced 29992 tonnes of mushrooms and ranked 5th in the world in mushroom production. Cultivation of mushrooms requires rice straw with some special moisture, length, and temperature (Yoshiro & Duoug 2015, Kaushik et al. 2018).



Fig. 1: Incorporation of rice straw in the field.

The factors required for the proper growth of mushrooms are relative humidity of about 75-85% and 35°C temperature (Thiribhuvanamala et al. 2012). The production cycle of paddy straw mushrooms is 15 days only (Fig.3) (Kaushik et al. 2018) (Tripathy 2010).

Rice straw as nutrients for the soil: Rice straw has both nutrient and calorific values (Yoshiro & Duoug 2015). In composting process, the degradation of organic wastes by communities of microbial takes place (Tang et al. 2007). The composting process has many advantages like bulk and mass reduction, high C/N ratio (carbon to nitrogen), and sanitation. The produced compost is stable and used in agricultural applications and also helps in the growth of plants (Abdelhamid et al. 2004). Because of the high C/N ratio, rice straw resists microbial activity. So for better results, composting of rice straw is done with some other organic wastes. Composting process converts the unstable ammonia to stable organic material, can destroy the pathogens, and reduce waste, thus, meeting the requirements to be used as fertilizers. In the composting process, factors that affect the quality of compost are the C/N ratio, moisture content, temperature, ph. value, degree of aeration, and structure (Physical) of the waste material (Rashad et al. 2010, Li et al. 2007).

Rice Straw for Energy Production

Power generation (thermal) from rice straw: Power can be generated by using rice straw as a fuel or raw material deliberated below one by one:

Rice straw for generation of power: Currently, bioenergy is the largest renewable energy source globally and accounts for more than 2/3rd of the renewable energy mix. In the overall energy scenario, bioenergy accounts for 13% –14% of the total energy consumption (Fig. 4). Crop residues, in particular, are one of the largest biomass resources globally and the best options for use to produce bioenergy (Yadav et al. 2015, Kargbo et al. 2010). In India, Punjab Biomass

Power Limited in village Ghanaur of Patiala Distt. (Punjab) was the first power plant working on rice straw for the production of power with a capacity of 12 MW Power (Vagg 2015). In Zimbabwe, 47 % of the energy consumed is taken from biomass and a major part of this biomass is the residue of crops (Yadav et al. 2015). The thermal efficiency of rice straw is approximately 60-75 % which may further depend on the technology used in its combustion. The two main obstacles for rice straw to be considered as a biomass fuel are logistics and consistency of product (Vagg 2015). Uniform combustion of straw takes place when baled form of straw is converted into shredded form (Verma 2014).

Rice straw as combustion material: Rice straw can also be used as a feedstuff, fuel, industrial raw material, and fertilizer. For the combustion of agriculture wastage, combustors are used as grate-fired and fluidized bed or suspension burners systems. Grate-firing systems have many benefits like low investment cost, handle rice straw contains 65% water by weight, and little dust particles in flue gases. For the combustion of both biomass and coal, fluidized beds combustors are used. Fluidized beds combustors have higher combustion intensity when compared to the grate-firing system, and NO₂ emission is highly controlled in fluidized beds system (Zhiqiang et al. 2011). It was investigated that if the moisture content in a baled straw is more than 25 %, then fermentation of straw starts. Moreover, it is expensive to transfer straw with moisture from one place to another (Zhiqiang et al. 2011).

Lots of parameters should be considered while designing a large-scale rice straw combustion system. These parameters are volatile matter content, the mean value, the possibility of moisture, agglomeration characteristics, ash composition, ash content, and energy content of the fuel. Various by-products like bottom ash, fly ash, etc. produced have economic value, and these may be further used in the manufacturing of bricks, cement, embankments, and construction of roads (Verma 2014) (Fig. 5).



Fig. 2: Rice straw as bedding material for cattle.



Fig. 3: Rice straw for mushroom cultivation.

Rice stubble for pellets making: In pallet manufacturing, initially, the raw material (biomass) is crushed and then pressed for increasing density and forming. Then, solid pellets of biomass fuel are formed which are small in size. The pellet fuel has more efficiency, easy to store, and can solve the problem of coal and pollution. Pellet biomass fuel (Fig.6) has many advantages: high combustion efficiency, small volume, easy transportation, and storage. These advantages of pellet biomass fuel replace coal, wood, gas, oil, etc. as fuel. It is usually used in hot water boilers, life stoves, biomass power plants, and industrial furnaces (Verma 2014).

Energy Production from rice straw by biochemical methods: By applying different treatments to rice straw, different types of energy can be created. These are discussed as follows:

Biogas from rice straw: For the production of biogas from rice straw, underground containers usually have 2.5 m width, 4 m height, with a dome shape on top, and constructed with cement and bricks (Fig. 7). At the top of the container, a way for the gas outlet is provided and at the bottom, there is a way for the water inlet. A half-meter thick layer of rice straw and a layer of cow dung are placed alternately on the straw layer. These steps are repeated continuously till the complete filling of the plant. Later the plant is filled with water, and the fermentation process begins and production of biogas starts

after one week. From one tonne of straw, 5-6 cubic meters of biogas is produced for 4 months continuously. By-products from the plant are utilized as fertilizers (Vagg 2015).

Rice straw for Bioenergy (Biogas) with a New Approach

Dr. B.S. Chadha investigated that before using rice straw for the production of biogas, several extraordinary value products are extracted from it. Generally, these products are hemicellulose, cellulose, and lignin (Dhap & Singh 2017, Nasr et al. 2015). Rice straw has hemicellulose 19-27 %, cellulose 32-47 %, ashes 18.8 % and lignin 5-25 % (Yoswathana & Phuriphapat 2010). Cellulose is extracted in solid form, some of it as a sugar-rich hydrolysate, and most of the hemicellulose is extracted as hydrolysates. With help of hydrolysis, hemicellulose and cellulose release xylooligosaccharides which are sugar polymer and ethanol is its last product. Highly valuable lignin is extracted during thermochemical pretreatment of rice straw by nano-filtration technique (membrane). Extracted lignin is non-toxic in nature that makes it a raw material for tire, cement application, computer's silica chip, antioxidants, manufacturing of carbon fiber, grease, and foams of polymers (Vagg 2015).

Rice straw for bioethanol production: As population increases, the demand for petroleum, diesel, coal, etc.



Fig. 4: Power generation from rice stubble.



Fig. 5: Rice straw as combustion material.



Fig. 6: Rice straw for pellets production.



Fig. 7: Bio-gas from rice straw.

increases, and the supply of these non-renewable sources also increases but its availability decreases gradually. The creation of ethanol from the cellulosic material of rice straw solves various problems (environment, energy, and economic) faced globally. Nowadays for transportation purposes, bioethanol fuel is recommended. Combustion of bioethanol produces volatile organic compounds, CO, NO in very low concentrations and does not release CO₂ in the atmosphere (Dhap & Singh 2017). In recent years, from a list of renewable resources, ethanol is an alternate fuel to different fossil fuels. 205 billion liters of bioethanol is produced from rice straw each year, i.e. 5% of its total consumption of fuel (Yoswathana & Phuriphat 2010) (Fig 8.).

For the extraction of bioethanol from the rice straw as raw material, there are three main steps are: In the first step, during the pretreatment, lignin is removed and then converted into monomeric sugar (hexose and pentose).

In the second step, hydrolysis takes place for proper cleaning of the polymer of hemicellulose and cellulose by using enzymes for the production of glucose monomers. In the third step, the fermentation process takes place for the production of bioethanol from glucose. There are different pretreatment processes for the production of bioethanol such as chemical (sodium chloride and sodium hydroxide, Alkaline hydrogen peroxide), physical (Milling, Milling and autoclaving, Milling and gamma irradiation, subcritical water, Ultrasonic), or biological. May be a combination of chemical and physical (Phosphoric acid, Aqueous-ammonia soaking, Sulfuric acid, Sodium hydroxide, wet air oxidation lime) treatments can be applied for the production of bioethanol (Dhap & Singh 2017).

Rice straw for biochar: Biochar is a type of charcoal that is derived biologically with thermochemical pyrolysis of rice straw (biomass). Pyrolysis is a thermochemical decom-

position of organic materials at an elevated temperature in absence of oxygen. In the pyrolysis process, larger molecules break down into small molecules. Although biochar can never add nutrients itself in soil, it increases the pH value in an area that is acidic in nature. So, with the help of biochar (Fig. 9), there may be a reduction in greenhouse gases, increase in crop yield, and the soil is provided with more fertility (Yoshiro & Duoug 2015).

Manufacturing From Rice Straw

In different types of manufacturing, trend changes to using biodegradable raw materials in various kinds of production. Some of these are discussed below:

Rice straw for manufacturing of acoustic material: The construction of acoustic material is divided into 2 different stages. In the first stage, the rice straw must be dried for a week to remove the moisture present in the straw. After that, it is heated usually at 80°C for 5 min in the oven for complete evaporation of moisture. The raw material was then cut into 5 to 10 mm. To have a compact structure, the fibers were then mixed with a binding agent, namely, polyurethane. The composition of the fibers and the binder was roughly 90% and 10% by weight, respectively. In the second stage of fabrication, the mixture is hot-pressed into a mold of a round shape 33 mm in diameter so that it must fit into an impedance tube during the sound absorber test (Fig. 10).

Putra et al. (2013) fabricated different absorber samples with different thicknesses of 10 mm and 20 mm. For each thickness, the weight of the fiber is given for 2 grams and 4 grams which yields different fiber densities. The bulk density for each sample can be simply calculated by the ratio of the total mass of the sample and its volume. The sample with more density showed more fibers in the same thickness i.e. pores size reduced that leads to more sound energy loss. The experimental results show that this natural fiber can be utilized as a potential alternative acoustic material.

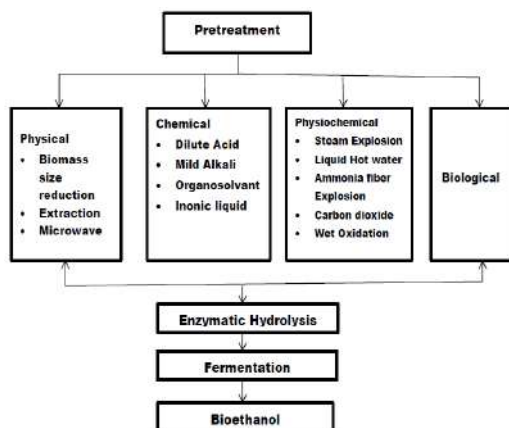


Fig. 8: Production of bio-ethanol from rice straw (Tayab et al. 2018).



Fig. 9: Bio-Char from the rice straw.

With a thickness of 20 mm and 3 grams of fiber weight, the absorption coefficient is more than 0.5 above 1 kHz and can reach 0.8 on average above 1.5 kHz, comparable with the performance of synthetic glass wool with the same thickness. By introducing a single layer of polyester fabric to the sample's facing, further improvement of sound absorption can be obtained (Putra et al. 2013).

It is studied that from a mixture of rice straw and wood particles, sound-absorbing composites can be manufactured. Wood particles used up to 20 % by wt. as a raw material for sound absorbing composites without a decrease in bonding strength (Yang et al. 2003).

Mixing with plastics for 3D objects: Recently a company in China invented an eco-friendly material- straw-based plastic - made from rice and wheat stalks and can be used in 3D printing. It is prepared from the dried straw of crops like rice straw, wheat straw, corn stalk, etc., mixed with plastic and plastic additives. The process starts with shredding the straw to 1.5~2mm pieces. Then they mix the straw dust with polypropylene, adding a silane coupling agent and ethylene bis(stearamide) as additives. The mixture is then extruded into granules using a twin-screw extruder. After the transformation, the granules have even particle size and are more stable for further processing. The plastic granules can be heated up to 160~180 °C for injection molding. Using special filament extruders, the company has turned these plastic granules into filament for 3D printers. The 3D printed object created using the straw-based filament has the color of natural wood and the texture of plant fiber on the surface. It has also a nice surface finish and high strength (Verma 2014).

Rice straw for cardboard and composite board: Composite boards manufactured (Fig. 11) from rice straw and waste tire particles have better flexural properties than insulation boards, plywood, wood particle boards, and fibreboards (Yang et al. 2004). So, rice straw is an alternate source of fiber in the manufacturing of cardboard, and hence, it reduces the cutting down of trees for the purpose of making cardboard.

In the production of paper and cardboard, more than 65% of rice straw is transformed into useful pulp (Verma 2014).

Manufacturing of packaging materials: The good resilience and compact resistance property of rice straw make it useful for the manufacturing of virtuous packaging material replacing costly petroleum-based products (Verma 2014, Singh et al. 1995).

For the production of biocomposite: Agro-based biocomposite (Fig. 12) is prepared by using the eco-polyalcohol polymer-based adhesive system from rice straw. In the manufacturing of lignocellulosic composite, formaldehyde-based adhesives are used worldwide because of their noble adhesive properties. Epidemiology studies have inferred a possible association between formaldehyde exposure and increase risk of cancer. In the manufacturing of composite rice straw, three types of sizes are used. Their particle sizes are $<4.75\text{mm}<2.63\text{mm}<\text{RS}<4.75\text{mm}$, $1\text{mm}<\text{RS}<2.63\text{mm}$, and $500\ \mu\text{m}<\text{RS}<1\text{mm}$. For blending of these particles, polyalcohol polymer-based adhesives are used. The mass percentage of adhesive to dry rice straw of 12-16 % was used. Hot pressing of material at 130°C temperature and pressure at 140 bars for 7 min takes place in the manufacturing of board. The final dimension of rice straw composite was approximately 8 mm thickness and density ranged from 905-1001 $\text{kg}\cdot\text{m}^{-3}$. The performance of the prepared board with environmental impact, commercial UF, and binding treated RS was compared. The TS and water absorption capability of the composite were measured after 24 h immersion in distilled water at 20 °C. Thermogravimetric analysis of rice straw composite takes place with the help of Perkin Elmer, performed at 50 $\text{cc}\cdot\text{min}^{-1}$ nitrogen flow rate and $10^\circ\text{C}\cdot\text{min}^{-1}$ heating rate under non-isothermal conditions. The results showed that incorporating PVA up to 17 % to starch increased the bonding strength. Moreover, this trend can reverse with more PVA quantity (20-67 %). Also, a pressing temperature of 130°C, pressing time of 7 min, and adhesive synthesized from 17 % PVA and 83 % corn starch contribute to higher bond strength. Due to



Fig. 10: Acoustic material from rice straw.



Fig. 11: Cardboard of rice straw.

the applied pressure, compression of fibers takes place which leads to reduction of voids and porosity in the manufactured board that gives higher water-resistant property and density (Basta et al. 2013).

Rice straw-cement bricks: Rice straw is also being used for the production of lightweight cement bricks (Fig. 13) that are used as fillers in the construction of buildings (skeleton types). The burned product of biomass power plant left behind contains high silica contents and is used in the manufacturing of bricks (Vagg 2015). Allam & Garas (2010) investigated that a sun-baked mud brick without straw had strength less than 6 kp.cm^{-2} , however, with the addition of straw, these bricks become three times stronger, about 20 kp.cm^{-2} . Moreover, the straw used in the production of bricks also provides thermal insulation to it. Coarse and fine aggregates were batched by volume using wooden boxes with the desired volume. Cement was added by weight using only whole bags of 50 kg to ensure uniform proportions of mix. The chopped rice straw was added to the mixture according to the previously mentioned quantities. The dry mixes were batched outdoors in a rotating power-driven revolving mixer of 100 liters capacity before adding water. Then the bricks were molded and vibrated and then de-molded immediately



Fig. 12: Bio-composite of rice straw.



Fig. 13: Rice straw cement bricks.

after compaction. These samples were placed for curing purposes and water sprayed twice a day up to 7 days for the proper gaining of strength in bricks. It was investigated that bricks prepared by this method maintain compression stress up to 115 kg.cm^{-2} moreover; the production cost reduced by 25% as compared to pure cement bricks (Allam & Garas 2010).

Rice straw for handmade paper: Agriculture residue has high fibrous lignocellulose and a large quantity of hollocellulose content which makes it a raw material for the paper industry (Kadam et al. 2000). In this technology, acetic acid pulping in presence of H_2SO_4 as a catalyst is used under different conditions. The main reaction variables are the concentration of Acetic acid (%), catalyst (HCl or H_2SO_4 %) concentration, the ratio of liquid to straw, reaction time, and temperature. Good quality of pulp is produced, when acetic acid concentration is 85%, liquid to straw ratio is taken as 10, the reaction temperature is 90°C , H_2SO_4 concentration is 1%, and reaction time taken in pulp production is 180 min. The produced pulp is used to manufacture handmade paper (Fig. 14) and carry bags because of better mechanical properties (Pushpa & Sinha 2011).

CONCLUSION

Proper utilization of rice straw is not only the responsibility of farmers; government should have to make proper laws and regulations to check stubble burning. There must be public awareness regarding rice straw management and compulsory training must be given to farmers related to rice straw management. To curb the menace of stubble burning during the post-harvesting season in the state, the Punjab Pollution Control Board (PPCB) has urged all owners to ensure the attachment of Super Straw Management System (SMS) with their self-propelled combine harvesters. The Super Straw Management System (SMS) cuts the residue rice straw into small pieces and spread it in the fields. Uses of rice straw also provide some financial support to farmers. Rice straw can be used for different purposes as a fuel that may reduce greenhouse and other harmful gases. In this way, the environment can be protected from the future critical situation of pollution. The technology should be such that rice straw can be transported from the field to industry with minimum effort otherwise all efforts are a failure. Private players have to use their new and old technologies for better practice of stubble by setting up units locally. It has been already discussed that rice straw can replace non-renewable energy fuel. These steps save the environment for our future generation. Small power thermal plants may also replace their fuel and operate on stubble in the future. The government should implement subsidies plans to promote the consumption of these



Fig. 14: Rice straw hand made paper.

biofuels. In India and other countries, local authorities can be more responsible in setting specific prohibitions. Some NGOs (Non-Government Organization) have also started microfinance in Bangladesh and Indonesia for small-scale renewable energy projects.

REFERENCES

- Abdelhamid, M. T., Horiuchi, T. and Oba, S. 2004. Composting of rice straw with oilseed rape cake and poultry manure and its effects on faba bean growth and soil properties. *Elsevier*, 93: 183-189.
- Allam, M. and Garas, G. 2010. Recycled chopped rice straw-cement bricks: An analytical and economical study. *Trans. Ecol. Environ.*, 140: 79-86.
- Bakker, R., Elbersen, W., Poppens, R. and Lesschen, J. P. 2013. Rice Straw and Wheat Straw Potential Feedstocks for the Biobased Economy. Wageningen UR, Food & Biobased Research, NL Agency Ministry of Economic Affairs, The Netherlands.
- Basta, A., El-Saied, H. and Lotfy, V. 2013. Performance of rice straw-based composites using environmentally friendly polyalcoholic polymer-based adhesive system. *Pigment. Resin Technol.*, 42(1): 24-31.
- Chandra, R., Trivedi, A., Jha, B., Verma, A. R. and Vijay, V. K. 2017. Energy Generation from Paddy Straw. *Akshay Urja, Delhi*.
- Dhap, N. and Singh, H. 2017. Pretreatment of rice straw for bio-ethanol production: A review. *J. Chem. Pharm. Res.*, 9(4): 216-220.
- Dobermann, A. and Fairhurst, T. 2002. Rice straw management. *Better Crops Int.*, 16: 1-11.
- Sanathimmappa, H.G., Gurumurthy, B.R., Jayadeva, H.M., Rajanna, D. and Shivanna, M.B. 2015. Effective Recycling of Paddy Straw through Microbial Degradation for Enhancing Grain and straw Yield in Rice. *IOSR Journal of Agriculture and Veterinary Science*, 8(1), 70-73.
- Kadam, K.L., Forrest, L.H. and Jacobson, W.A. 2000. Rice straw as a lignocellulosic resource: Collection, processing, transportation, and environmental aspects. *Elsevier Sci.*, 18: 369-389.
- Kargbo, F.R., Xing, J. and Zhang, Y. 2010. Property analysis and pretreatment of rice straw for energy use in grain drying: A review. *Agric. Biol. J. North Amer.*, 1(3): 195-200.
- Kaur, A. 2017. Crop residue in Punjab agriculture: Status and constraints. *J. Krishi Vigyan*, 5(2): 22-26.
- Kaushik, S., Ipsita, D. and Kumar, S. 2018. Paddy straw mushroom: A natural scavenger who helps in malnutrition and environmental protection. *Int. J. Microbiol. Res.*, 10(5): 1183-1185.
- Kumar, P., Kumar, S. and Joshi, L. 2015. Socioeconomic and Environmental Implications of Agricultural Residue Burning. Springer, London.
- Li, X., Zhang, R. and Pang, Y. 2007. Characteristics of dairy manure composting with rice straw. *Bioresour. Tech.*, 99: 359-367.
- McLaughlin, O., Mawhood, B., Jamieson, C. and Slade, R. 2016. Rice Straw for Bioenergy: The Effectiveness of Policymaking and Implementation in Asia. 24th European Biomass Conference and Exhibition at Amsterdam, The Netherlands, 6-9 June 2019, pp. 1-16
- Nasr, A.M., Badawi, M.H., Demerdash, M.A. and Barakat, O.S. 2015. Bioconversion of Rice straw into Ethanol: Fungi and yeasts are the Backbone Microbiota of the process. *Int. J. Curr. Microbiol. Appl. Sci.*, 4(12): 382-401.
- Pushpa, J. and Sinha, A. 2011. Application of rice straw as raw material for the production of handmade paper. *IPPTA*, 23(2): 145-148.
- Putra, A., Abdullah, Y., Efendy, H., Mohamad, W. and Salleh, N. 2013. Biomass from paddy waste fibers as sustainable acoustic material. *Adv. Acoust. Vib.*, 2013: 1-7.
- Rashad, F.M., Saleh, W.D. and Moselhy, M.A. 2010. Bioconversion of rice straw and certain agro-industrial wastes to amendments for organic farming systems: 1. Composting, quality, stability, and maturity indices. *Elsevier*, 101: 5952-5960.
- Reddy, N. and Yang, Y. 2006. Properties of high-quality long natural cellulose fibers from rice straw. *J. Agric. Food Chem.*, 54(21): 8077-8081.
- Singh, R.B., Saha, R.C., Singh, M., Chandra, D., Shukla, S.G., Walli, M. and T.K. 1995. Rice Straw- its Production and Utilization in India. ICAR, New Delhi.
- Tang, J.C., Shibata, A., Zhou, Q. and Katayama, A. 2007. Effect of temperature on reaction rate and microbial community in composting of cattle manure with rice straw. *J. Biosci. Bioeng.*, 104(4): 321-328.
- Tayyab, M., Noman, A., Islam, W., Waheed, S., Arafat, Y. and Ali, F. 2018. Bioethanol production from lignocellulosic biomass by environment-friendly pretreatment methods: A review. *Appl. Ecol. Environ. Res.*, 6(5): 225-249.
- Thiribhuvanamala, G., Krishnamoorthy, S., Monoranjitham, K., Praksasm, V. and Krishnan, S. 2012. Improved techniques to enhance the yield of paddy straw mushroom (*Volvariella volvacea*) for commercial cultivation. *Afr. J. Biotechnol.*, 11(64): 12740.
- Tripathy, A. 2010. Yield evaluation of paddy straw mushrooms (*Volvariella Spp.*) on various lignocellulosic wastes. *Int. J. Appl. Agric. Sci.*, 5(3): 317-326.
- Vagg, A. 2015. Rice Straw Utilisation. Nuffield Australia Farming Scholars, Australia.
- Verma, D. 2014. Technologies for stubble use. *J. Agric. Life Sci.*, 1(2): 106-110.
- Yadav, M., Prawasi, R., Satyawar, R.P., Kumari, K. and Karamdeep, R. 2015. Assessment of Rice Straw Burning and its power generation potential in major rice-growing districts of Haryana, India. *Int. J. Sci. Eng. Technol. Res.*, 4(5): 1287-1293.
- Yang, H., Kim, D. and Kim, H. 2003. Rice straw-wood particle composites for sound absorbing wooden construction materials. *Biosour. Technol.*, 86(2): 17-121.
- Yang, H., Kim, D., Lee, Y., Kim, H., Jeon, J. and Kang, C. 2004. Possibility of using waste tire composite reinforced with rice straw as construction material. *Biosour. Technol.*, 95(1): 61-65.
- Yoshiro, H. and Duoug, P.T. 2015. Current Situation and possibilities of Rice Straw Management in Vietnam. University of Tsukuba.
- Yoswathana, N. and Phuriphipat, P. 2010. Bioethanol Production from Rice Straw. *Energy Res. J.*, 1(1): 26-31.
- Zayed, G. and Abdel-Motaal, H. 2005. Bio-active composts from rice straw enriched with rock phosphate and their effect on the phosphorous nutrition and microbial community in the rhizosphere of cowpea. *Elsevier*, 96, 929-935.
- Zhiqiang, L., Xu, A. and Zhao, T. 2011. Energy from the combustion of rice straw: Status and challenges to China. *Energy Power Eng.*, 3: 325-331.



On the Issue of Establishing the Stages of Coal Metamorphism for Predicting the Hazardous Properties of Coal Seams

M.I. Antoshchenko*, V.Y. Tarasov*†, Ye.S. Rudniev** and O.I. Zakharova***

* Department of Mining, Volodymyr Dahl East Ukrainian National University, 93400, Severodonetsk, Ukraine

**Department of Electrical Engineering, Volodymyr Dahl East Ukrainian National University, 93400, Severodonetsk, Ukraine

***Department of Chemistry and Industrial Safety Measures, Volodymyr Dahl East Ukrainian National University, 93400, Severodonetsk, Ukraine

†Corresponding author: V.Y. Tarasov; tarasov@snu.edu.ua; vatarasov81@gmail.com

Nat. Env. & Poll. Tech.
Website: www.neptjournal.com

Received: 05-12-2020

Revised: 15-02-2021

Accepted: 24-02-2021

Key Words:

Coal
Metamorphism
Elemental composition
Coal seams
Hazardous properties

ABSTRACT

The characteristic stages of metamorphic transformations of mines are established according to the increase in the elemental content of carbon and changes in other components of organic matter. Stages of metamorphism transformations with an average carbon content of more than 93.6% can significantly differ in properties due to the unpredictability of the ratio between the components of organic matter. At these stages, even a minimal difference between the components can be the reason for the emergence of new properties of the coal seams. As the influence of the processes of metamorphism increases, the boundaries of the stages, determined by the percentage of carbon, narrow. The established stages of the transformation of reservoirs in terms of the individual proportion of the components in carbonization practically do not differ from the boundaries of the stages determined by the elemental composition of organic matter. It is noted that the average carbon content at the stages of seam metamorphism, determined by the yield of coke, in most cases does not coincide with the ranges of changes in the average carbon content, established by the individual content of the components or their share in carbonization. The inconsistency of the boundaries in the stages of seam metamorphism makes it unacceptable to use the coke yield as the main criterion for assessing the conversion of coal and even more so the manifestation of hazardous properties of coal seams.

INTRODUCTION

At present, it is generally accepted that some mining accidents are associated with the properties of fossil coals, which appeared as a result of geological processes and metamorphic transformations of the original organic matter. This is confirmed by the fact that the indicators of the degree of coal metamorphism are used in the modern regulatory framework of Ukraine (Antoshchenko et al. 2020) to predict gas release, gas-dynamic phenomena, endogenous fires, and the dust-generating capacity of coal seams. One of the main signs of increased metamorphic transformation of coals is an increase in the elemental content of carbon (C_0) and a decrease in other components in the original organic matter (Thomas 2020). This, being one of the basic principles of metamorphic transformations, is not observed when predicting the hazardous properties of coal seams. Changes in the elemental composition of the initial organic matter, as the main indicator of the degree of coal metamorphism, are not considered at all in the regulatory framework (Antoshchenko et al. 2020). The methods for determining the degree of coal

metamorphism in the documents under consideration were developed based on the experience of applying industrial classifications. They envisaged, first, the determination of the technological properties of coals associated with their tendency to cokeability and calorific value.

The degree of metamorphism was initially characterized by the amount of coke yield to organic matter (K) and moisture content (W) (Ahamed et al. 2019). These indicators, for the most part, directly characterize the consumer properties of coal. In the course of upgrading industrial classifications, approximately 30 indicators were also investigated, which, in aggregate, more clearly define the technological properties of coals than carbon (C_0) and W . The modern industrial classification provides for the use of 10 indicators. The content of carbon (C_0), as one of the main indicators of metamorphic transformations, is not considered. The maximum moisture capacity for an ashless state (W_{max}^{af}) is limitedly used only for dividing brown coals into types. The volumetric yield of volatile substances during the thermal decomposition of coals into a dry ash-free state (V_v^{def}) for anthracites became

one of the main indicators of the stages of metamorphism in industrial classifications (GOST 25543-2013 2014, GOST 6382-2007 2008) and regulatory framework (Antoshchenko et al. 2020). Essentially, thermal decomposition (GOST 6382-2007 2008) is an artificial continuation of the stages of coal transformation at temperatures (900°C), significantly higher than the transformation temperature of coal (300-500°C) and anthracite (500-650°C) (Klymenko et al. 2019). The composition and characteristics of coals have changed over geological time, although thermal degradation products do not directly characterize this transformation. The expediency of using indicators and establishing the consumption properties of coals is confirmed by successful experience in the application of industrial classification (GOST 25543-2013 2014). Such a possibility of experimental verification is absent when predicting the hazardous properties of coal seams.

Recurring accidents in coal mines indicate the importance of enhancing the regulatory framework in terms of predicting the hazardous properties of coal seams. Its main disadvantage is the use of indicators that do not directly characterize the change in the elemental composition and properties of coals in the process of their metamorphic transformations. Application of indicators V^{daf} and V^c , without due scientific justification, is copied from industrial classifications. The latter provides for the systematization of coals according to indicators characterizing their suitability for industrial use (ASTM D388-15, 2012). The coal grades are established according to these indicators. They are commonly used to describe coal variations that are similar in genetic, basic energy, and technological properties. Industrial classifications do not provide for forecasting the manifestation of hazardous properties of coal seams during mining operations.

When determining the propensity of coal seams to manifest their dangerous properties based on genetic factors, the definition of metamorphism according to ASTM D388-15 (2012) should be taken into account. It consists of the transformation of brown coal sequentially into coal and anthracite as a result of changes in the chemical composition, structure, and physical properties of coal in the depths, mainly under the influence of elevated temperature and pressure. None of the indicators used in the regulatory framework fully comply with this definition. A direct change in the composition of the initial organic matter is not considered with an increase in metamorphism as an increase in the carbon content and a decrease in the content of other components.

MATERIALS AND METHODS

The research methodology was developed based on modern knowledge in the field of geological science, chemical

analysis of coals, mining experience, and the results of statistical processing of extensive material obtained in different coal basins by many researchers. During the research, the basic principles were observed, according to which the metamorphism of fossil coals manifests itself in a change in the elemental composition of the original matter and its properties. The change in carbon content in an individual ratio with each component of organic matter should be directly characterized by classification indicators. These basic principles of metamorphism manifestation are not considered by the modern regulatory framework (Antoshchenko et al. 2020) and the current industrial classification (GOST 25543-2013. 2014).

According to the known industrial classifications, the stages of metamorphic transformations of coal seams cannot be determined for several reasons:

- The main indicators of the degree of coal metamorphism are based on the determination of the products of thermal coal decomposition. This process is an artificial continuation of the stages of the transformation of organic matter that took place in natural conditions in the past geological time periods;
- Most of the classification indicators are determined for dry ashless mass, which does not correspond to the conditions for finding coal in coal seams. In all cases, there is the presence of moisture and mineral impurities;
- Conditional coal grades are determined for their industrial use. They are artificially established according to a set of several indicators that are not directly related to the change in the elemental composition of organic matter and the manifestation of hazardous properties during mining;
- Seam moisture is not considered in the composition of organic matter, which excludes its influence on the physical state of the coal seams.

The method assumed that the main components of organic matter are carbon (C_o), hydrogen (H_o), nitrogen (N_o), sulfur (S_o), oxygen (O_o), and moisture (W). Their total content at all stages of reservoir metamorphism is 97.5% and more. The average compositions of the Donetsk basin coals at different stages of seam metamorphism were taken for analysis based on the results of processing more than a thousand samples. Their results completely coincide with the average values of the elemental composition of organic matter obtained in other coal basins when processing about three thousand more data pairs (Thomas 2020, Klymenko et al. 2019, Qi 2020). The obtained results of statistical processing of such a quantity of experimental data do not raise doubts about their reliability.

The change in the content of the components of organic matter (C_o , O_o , H_o , S_o , N_o) and moisture (W) at different

Table 1: Information on the average composition of the Donetsk basin coals at different stages of seam metamorphism.

Indicators, %	Stages of metamorphic transformations of formations and the composition of the original organic matter									
	I	II	III	IV	V	VI	VII	VIII	IX	X
K	52÷55	55÷60	60÷65	65÷70	70÷75	75÷80	80÷85	85÷90	90÷95	95÷100
\bar{K}	53,5	57,5	62,5	67,5	72,5	77,5	82,5	87,5	92,5	97,5
V_k	48÷45	45÷40	40÷35	35÷30	30÷25	25÷20	20÷15	15÷10	10÷5	5÷0
\bar{V}_κ	46,5	42,5	37,5	32,5	27,5	22,5	17,5	12,5	7,5	2,5
\bar{W}	7,34	6,44	2,59	1,59	1,15	0,99	0,88	0,78	1,29	3,32
\bar{C}_0	80,19	81,57	84,29	86,43	88,33	89,53	90,43	91,46	92,67	93,65
\bar{H}_0	5,34	5,31	5,31	5,21	5,10	4,81	4,60	4,30	3,75	1,93
\bar{N}_0	1,43	1,44	1,44	1,46	1,52	1,51	1,51	1,38	1,32	1,05
\bar{S}_0	2,28	1,83	1,42	1,24	1,10	1,04	1,06	1,03	1,00	0,74
\bar{O}_0	10,76	9,85	7,54	5,66	3,95	3,11	2,40	1,83	1,26	0,63

stages of metamorphism are given in Table. 1. The initial criterion for determining the stages of metamorphism was the yield of coke to organic matter (K). According to the K values from 52 to 100%, the conversion of seams from young coal to anthracite was evenly divided into 10 stages. The average values of the yield of coke (\bar{K}) at each stage were determined by the average values of the components of organic matter ($\bar{C}_0, \bar{H}_0, \bar{N}_0, \bar{S}_0, \bar{O}_0$) and moisture content (\bar{W}) in the initial samples (Ahamed et al. 2019). Graphite ($C_0 \approx 100\%$) is accepted as the final member of the coal metamorphism series. The main component of organic matter at all stages of transformation is carbon. Its minimum value for bituminous coals is about 70%. Average values of carbon content at the considered 10 stages of metamorphism of formations varied in the range of 80,19÷93,65% (Table 1).

The average amount of removed fluids (\bar{V}_κ), formed at different stages of formation transformation, is determined from the ratio:

$$\bar{V}_\kappa = 100 - \bar{K}, \% \quad \dots(1)$$

RESULTS AND DISCUSSION

With this definition \bar{V}_κ , its values will slightly exceed the average yield of volatile substances during the thermal decomposition of coal (\bar{V}^{daf}). The \bar{V}^{daf} composition considers only gaseous decomposition products, and the presence of pyrogenetic moisture and coal tar is not excluded in the

removed fluids. This once again confirms the inconsistency of the indicator \bar{V}^{daf} with the metamorphic transformations of seams.

As the metamorphic processes intensified (growth of \bar{K}), a one-sided increase in the carbon content occurred (Fig. 1a). Simultaneously with these processes, a decrease in the sum of the remaining components ($\Sigma \bar{H}_0, \bar{N}_0, \bar{S}_0, \bar{O}_0$) of organic matter was observed (Fig. 1b, curve 7). The individual change in the content of organic matter components was not so unambiguous. The most intense decrease in oxygen content was observed in stages I-IV, then a more gradual decrease in stages V-X was observed almost to zero (Fig. 1b, curve 2). The hydrogen content remained practically unchanged at stages I-VI and then decreased according to a nonlinear dependence (Fig. 1b, curve 3). The content of nitrogen and sulfur underwent minor changes (Fig. 1b, curves 5 and 4). In addition to the considered components of organic matter ($\bar{C}_0, \bar{H}_0, \bar{N}_0, \bar{S}_0, \bar{O}_0$), it includes seam moisture (\bar{W}). \bar{W}^a determination methods do not allow it to be considered together with other components ($\bar{C}_0, \bar{H}_0, \bar{N}_0, \bar{S}_0, \bar{O}_0$) in a 100% composition of organic matter.

The \bar{W} percentage is related to the original coal sample. The reduction in moisture content took place intensively at the initial stages (I-III) of the transformation of mine layers (Fig. 1 b, curve 6). Then its reduction was insignificant (stages IV-VII, Table 1), and an increase was observed at stages VIII-X. Such an ambiguous change in the \bar{W} indica-

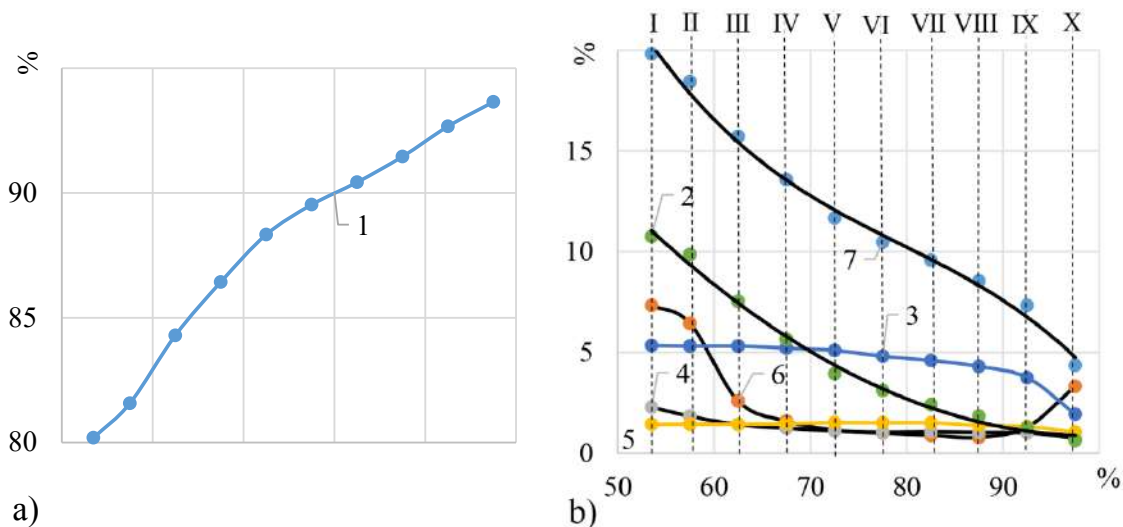


Fig. 1: Change in the average content of organic matter components from the yield of coke at different stages of metamorphic transformations of coal seams.

1, 2, 3, 4, 5, 6 – curves of average carbon (\bar{C}_0), oxygen (\bar{O}_0), hydrogen (\bar{H}_0), sulfur (\bar{S}_0), nitrogen (\bar{N}_0), and moisture (\bar{W}) content in organic matter respectively; 7 – a curve of change in the sum of components of organic matter ($\bar{H}_0, \bar{N}_0, \bar{S}_0, \bar{H}, \bar{O}_0$); I-X – stages of metamorphic transformations of seams by coke yield.

tor certainly affects the processes of metamorphism and the manifestation of the hazardous properties of coal seams. This is evidenced by the change in the position of \bar{W} the series of ranking indicators for the coke yield (Table 2). As the processes of metamorphism intensify at stages I-VI, the role of \bar{W} , in comparison with other components, decreases. In the ranking, \bar{W} moves from the third position to the sixth. Then, at the final stages IX-X, the importance in the ranking series rises again.

Carbon content holds the indisputable top position in the evaluation ranks at all stages of reservoir transformation. The presence of other components ($\bar{H}_0, \bar{N}_0, \bar{S}_0, \bar{O}_0$) and moisture (\bar{W}) in the organic matter directly depends on the \bar{C}_0 content. This gives grounds to use the change in the ratio between carbon content and other components, instead of the coke yield, for characterizing the stages of metamorphism of coal seams.

The \bar{C}_0 ratio to the sum of the hydrogen (\bar{H}_0) and oxygen (\bar{O}_0) content was defined as an indicator of carbonation (Sen & Banerjee 2015). The use of only two components to determine the carbonation index (C_n) does not give a complete picture of the effect of the nitrogen (\bar{N}_0), sulfur (\bar{S}_0), and moisture (\bar{W}) content on the increase in carbon (\bar{C}_0) with the intensification of metamorphic processes. It is more expedient to consider all the main components of organic matter ($\bar{H}_0, \bar{N}_0, \bar{S}_0, \bar{O}_0$) and moisture (\bar{W}) when determining the C_n indicator. The carbonation index C_n^Σ corresponding to the sum of the components of organic

matter, according to Table 1, was calculated using the equation:

$$C_n^\Sigma = \frac{\bar{C}_0}{\bar{H}_0 + \bar{N}_0 + \bar{S}_0 + \bar{O}_0} \quad \dots(2)$$

Similarly, roughly, since \bar{W} is not part of the 100% content of organic matter components, the carbonation index for the moisture content was calculated:

$$C_n^W = \frac{\bar{C}_0}{\bar{W}} \quad \dots(3)$$

The results of determining the indicators C_n^Σ and C_n^W for different stages of seam metamorphism are shown in Table 3.

The general carbonation index (C_n) is associated with C_n^Σ and C_n^W through the expression:

$$\frac{1}{C_n} = \frac{1}{C_n^\Sigma} + \frac{1}{C_n^W} \quad \dots(4)$$

Taking the C_n^{-1} value per unit for each stage of seam metamorphism, we determined the shares of participation, respectively, and the sum of the organic matter components (ΔC_n^Σ) and moisture (ΔC_n^W):

$$\Delta C_n^\Sigma = \frac{1}{C_n^\Sigma} \cdot \frac{1}{C_n}, \quad \dots(5)$$

$$\Delta C_n^W = \frac{1}{C_n^W} \cdot \frac{1}{C_n}, \quad \dots(6)$$

Table 2: Ranking the content of organic matter and moisture components in coal samples.

Rank	Metamorphism stages									
	I	II	III	IV	V	VI	VII	VII	IX	X
Ranking of components by coke yield										
1	\bar{C}_0	\bar{C}_0	\bar{C}_0	\bar{C}_0	\bar{C}_0	\bar{C}_0	\bar{C}_0	\bar{C}_0	\bar{C}_0	\bar{C}_0
2	\bar{O}_0	\bar{O}_0	\bar{O}_0	\bar{O}_0	\bar{H}_0	\bar{H}_0	\bar{H}_0	\bar{H}_0	\bar{H}_0	\bar{H}_0
3	\bar{W}	\bar{W}	\bar{H}_0	\bar{H}_0	\bar{O}_0	\bar{O}_0	\bar{O}_0	\bar{O}_0	\bar{N}_0	\bar{H}_0
4	\bar{H}_0	\bar{H}_0	\bar{W}	\bar{W}	\bar{N}_0	\bar{N}_0	\bar{N}_0	\bar{N}_0	\bar{W}	\bar{N}_0
5	\bar{S}_0	\bar{S}_0	\bar{N}_0	\bar{N}_0	\bar{W}	\bar{S}_0	\bar{S}_0	\bar{S}_0	\bar{O}_0	\bar{S}_0
6	\bar{N}_0	\bar{N}_0	\bar{S}_0	\bar{S}_0	\bar{S}_0	\bar{W}	\bar{W}	\bar{W}	\bar{S}_0	\bar{N}_0
Ranking of components in relation to carbon \bar{C}_0 content										
1	\bar{O}_0	\bar{O}_0	\bar{O}_0	\bar{O}_0	\bar{H}_0	\bar{H}_0	\bar{H}_0	\bar{H}_0	\bar{H}_0	\bar{W}
2	\bar{W}	\bar{W}	\bar{H}_0	\bar{H}_0	\bar{O}_0	\bar{O}_0	\bar{O}_0	\bar{O}_0	\bar{W}	\bar{H}_0
3	\bar{H}_0	\bar{H}_0	\bar{W}	\bar{W}	\bar{N}_0	\bar{N}_0	\bar{N}_0	\bar{N}_0	\bar{N}_0	\bar{N}_0
4	\bar{S}_0	\bar{S}_0	\bar{N}_0	\bar{N}_0	\bar{W}	\bar{W}	\bar{S}_0	\bar{S}_0	\bar{O}_0	\bar{S}_0
5	\bar{N}_0	\bar{N}_0	\bar{S}_0	\bar{S}_0	\bar{S}_0	\bar{S}_0	\bar{W}	\bar{W}	\bar{S}_0	\bar{O}_0
Ranking of components by the percentage of participation in carbonation										
1	\bar{O}_0	\bar{O}_0	\bar{O}_0	\bar{O}_0	\bar{H}_0	\bar{H}_0	\bar{H}_0	\bar{H}_0	\bar{H}_0	\bar{H}_0
2	\bar{H}_0	\bar{H}_0	\bar{H}_0	\bar{H}_0	\bar{O}_0	\bar{O}_0	\bar{O}_0	\bar{O}_0	\bar{O}_0	\bar{W}
3	\bar{W}	\bar{W}	\bar{N}_0	\bar{N}_0	\bar{N}_0	\bar{N}_0	\bar{N}_0	\bar{N}_0	\bar{N}_0	\bar{N}_0
4	\bar{S}_0	\bar{S}_0	\bar{S}_0	\bar{S}_0	\bar{S}_0	\bar{S}_0	\bar{S}_0	\bar{S}_0	\bar{S}_0	\bar{S}_0
5	\bar{N}_0	\bar{N}_0	\bar{W}	\bar{W}	\bar{W}	\bar{W}	\bar{W}	\bar{W}	\bar{W}	\bar{O}_0

The calculated values for each stage of metamorphism are shown in Table 3. The proportions of participation of the sum of the organic matter components (ΔC_n^Σ) and moisture (ΔC_n^W) in carbonization change significantly with an increase in the carbon content (Fig. 2a).

For this reason, we corrected the initial values $\bar{H}_0, \bar{N}_0, \bar{S}_0, \bar{O}_0$ and \bar{W} for each stage, multiplying them, respectively, by ΔC_n^Σ and ΔC_n^W (Table 3). Correction of the $\bar{H}_0, \bar{N}_0, \bar{S}_0, \bar{O}_0$ and \bar{W} values on the proportion of their participation in carbonization (ΔC_n^Σ and ΔC_n^W) practically did not affect the changes in the series of ranking of components

in comparison with the series of ranking in terms of coke yield (Table 2). In the early stages of metamorphism (I, II), the main components affecting carbonization were oxygen content (\bar{O}_0) and moisture (\bar{W}). At the next stages, oxygen and hydrogen (III, IV), hydrogen and oxygen (V ÷ VIII), hydrogen and moisture (IX), moisture and hydrogen (X) sequentially occupied the leading positions. The compared ranks of ranking the organic matter components in terms of the yield of coke and the index of carbonation practically do not differ among themselves and in the arrangement of the remaining members of these rows. For example, at the final stage (X), they are located in the same order - \bar{W} ,

$\overline{H}_0, \overline{N}_0, \overline{S}_0, \overline{O}_0$.

This indicates that when establishing the stages of seam metamorphism, taking into account their classical definition (ASTM D388-15, 2012), it is possible to use the value of

carbon content (\overline{K}) in organic matter instead of the coking index (\overline{C}_0).

An additional argument for the acceptance of the carbon content as the main fission criterion at the stage of

Table 3: Results of determination of carbonization indices for organic matter components at different stages of metamorphic transformations of seams.

Indicators	Carbon content in organic matter, \overline{C}_0 , %									
	80,19	81,57	84,29	86,43	88,33	89,53	90,43	91,46	92,67	93,65
C_n^Σ	4,05	4,43	5,37	6,37	7,57	8,55	9,45	10,71	12,64	21,53
C_n^W	10,93	12,67	32,5	54,36	76,81	90,43	102,76	117,26	71,84	28,21
$(C_n^\Sigma)^{-1}$	0,25	0,23	0,19	0,16	0,13	0,12	0,11	0,09	0,08	0,05
$(C_n^W)^{-1}$	0,09	0,08	0,03	0,02	0,013	0,011	0,01	0,009	0,014	0,035
$(C_n^\Sigma)^{-1+}$	0,339	0,31	0,22	0,18	0,143	0,131	0,120	0,099	0,094	0,085
ΔC_n^Σ	0,730	0,74	0,86	0,89	0,910	0,92	0,92	0,91	0,85	0,59
ΔC_n^W	0,270	0,26	0,14	0,11	0,090	0,08	0,08	0,09	0,15	0,41
\overline{H}_0	5,34	5,31	5,31	5,21	5,10	4,81	4,60	4,30	3,75	1,93
$\overline{H}_0 \cdot \Delta C_n^\Sigma$	3,90	3,93	4,56	4,64	4,64	4,81	4,23	3,91	3,19	1,14
\overline{N}_0	1,43	1,44	1,44	1,46	1,52	1,51	1,51	1,38	1,32	1,05
$\overline{N}_0 \cdot \Delta C_n^\Sigma$	1,04	1,07	1,24	1,30	1,38	1,39	1,39	1,26	1,12	0,62
\overline{S}_0	2,28	1,83	1,42	1,24	1,10	1,04	1,06	1,03	1,00	0,74
$\overline{S}_0 \cdot \Delta C_n^\Sigma$	1,66	1,35	1,22	1,10	1,00	0,96	0,98	0,94	0,85	0,44
\overline{O}_0	10,76	9,85	7,54	5,66	3,95	3,11	2,40	1,83	1,26	0,63
$\overline{O}_0 \cdot \Delta C_n^\Sigma$	7,96	7,30	6,47	5,04	3,60	2,86	2,21	1,67	1,07	0,38
\overline{W}	7,34	6,44	2,59	1,59	1,15	0,99	0,88	0,78	1,29	3,32
$\overline{W} \cdot \Delta C_n^W$	1,98	1,67	0,67	0,41	0,30	0,26	0,23	0,20	0,34	0,86
C_n^H	20,30	20,77	18,44	18,63	19,04	20,21	21,38	23,39	29,05	82,15
C_n^N	75,65	76,23	67,98	66,48	64,01	64,41	65,06	72,59	82,74	151,05
C_n^S	47,45	60,42	69,1	78,57	88,33	93,26	92,28	97,30	109,02	212,84
C_n^O	10,07	11,2	13,01	17,15	24,6	31,30	40,92	54,77	86,61	246,44
C_n^W	41,98	48,84	125,81	210,8	294,43	344,35	393,17	457,3	272,56	108,9
$(C_n^H)^{-1}$	0,049	0,048	0,054	0,054	0,053	0,049	0,047	0,043	0,034	0,012
$(C_n^N)^{-1}$	0,013	0,013	0,015	0,015	0,016	0,016	0,015	0,014	0,012	0,007
$(C_n^S)^{-1}$	0,021	0,017	0,014	0,013	0,011	0,011	0,011	0,010	0,009	0,005
$(C_n^O)^{-1}$	0,098	0,089	0,077	0,058	0,041	0,032	0,024	0,018	0,012	0,004
$(C_n^W)^{-1}$	0,024	0,020	0,008	0,005	0,003	0,003	0,003	0,002	0,004	0,009
$\Sigma(C_n^i)^{-1}$	0,206	0,187	0,168	0,145	0,124	0,111	0,10	0,087	0,071	0,037
ΔC_n^H	0,237	0,257	0,32	0,37	0,43	0,44	0,47	0,49	0,48	0,32
ΔC_n^N	0,063	0,070	0,09	0,10	0,13	0,14	0,15	0,160	0,17	0,19
ΔC_n^S	0,101	0,09	0,08	0,09	0,09	0,10	0,110	0,11	0,13	0,14
ΔC_n^O	0,478	0,47	0,46	0,40	0,33	0,29	0,24	0,21	0,17	0,11
ΔC_n^W	0,121	0,11	0,05	0,03	0,02	0,03	0,03	0,02	0,05	0,24

seam metamorphism is the individual graphs of the mutual changes in the components of organic matter (Fig. 3). The intersection points of the curves characterizing the individual change in the organic matter components indicate not only a change in the chemical composition but also a change in the physical and mechanical properties. With this assumption, the initial stage of seams metamorphism (I) corresponds to a carbon content of less than 83%. The upper limit of 83% is determined by points 6 and 7 of curve intersection 4, 5, and 2, 3. Curves 4 and 5, respectively, characterize the change in the content of nitrogen (\bar{N}_0) and sulfur (\bar{S}_0), and curves 2 and 3 the content of hydrogen (\bar{H}_0) and oxygen (\bar{O}_0) and moisture (\bar{W}). Similarly, the upper limit ($\bar{N}_0 = 87\%$) of stage II was determined by points 8 and 9. They correspond to the intersection of curves 3, 4 and 1, 2, which determine, respectively, the moisture content (\bar{W}) and nitrogen (\bar{N}_0) and sulfur (\bar{S}_0), and curves 2 and 3 - oxygen (\bar{O}_0) and hydrogen (\bar{H}_0) content.

The upper limit of stage III ($\bar{C}_0 = 89\%$) is determined by point 10 of curve intersection 3 and 5. The points of

intersection 11 and 12 correspond to the end of stage IV (curves 3, 5, and 1, 4). Point 13 corresponds to the intersection of curves 3, 4 (stage V). The intersection of curves 1 and 5 at point 14 defines stage VI. Stages VII and VIII differ by tenths of a percentage of carbon, and the limits of stages IX - X cannot be determined from the available data (Table 4), since in this case, the carbon content is less than 93.6%. Stages of seam metamorphism at $\bar{C}_0 > 93.6\%$ can differ significantly in properties due to the unpredictability of the ratio between the organic matter components. At these stages, even a slight difference between the components can be the reason for the emergence of new properties of the coal seams. As the influence of the processes of metamorphism increases, the boundaries of the stages, determined by the percentage of carbon, narrow.

According to the method described above (equations 2-6,.) the corrected shares of individual participation in the carbonization of hydrogen (ΔC_n^H), oxygen (ΔC_n^O), nitrogen (ΔC_n^N), sulfur (ΔC_n^S), and moisture (ΔC_n^W) were calculated.

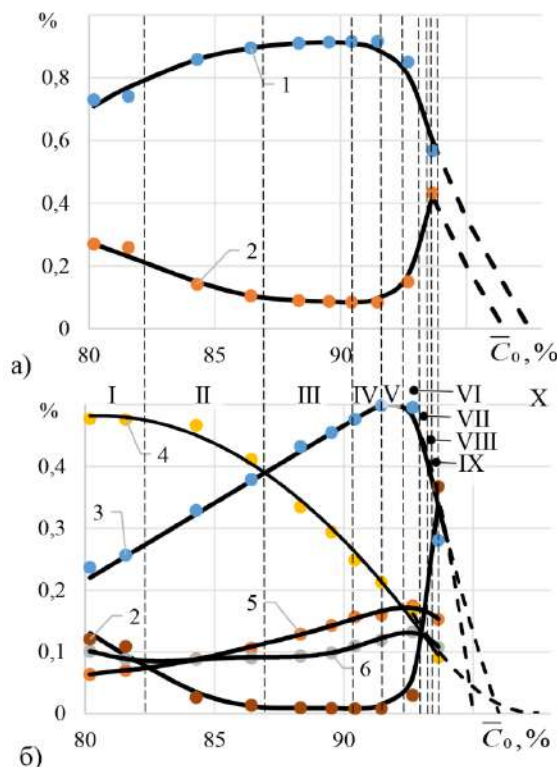


Fig. 2: The dependence of the change in the share of participation in the carbonization of layers of organic matter components on the average carbon content (\bar{C}_0).

1, 2 – curves of changes in the share of participation in carbonization, respectively, the sum of components (C_n^Σ) of organic matter ($\bar{H}_0, \bar{N}_0, \bar{S}_0, \bar{O}_0$) and moisture ΔC_n^W ; 3, 4, 5, 6 – curves of changes in the proportion of participation in carbonization of hydrogen (ΔC_n^H), oxygen (ΔC_n^O), nitrogen (ΔC_n^N) and sulfur (ΔC_n^S), respectively; I, II, III, IV, V, VI, VII, VIII, IX, X – stages of seam metamorphism.

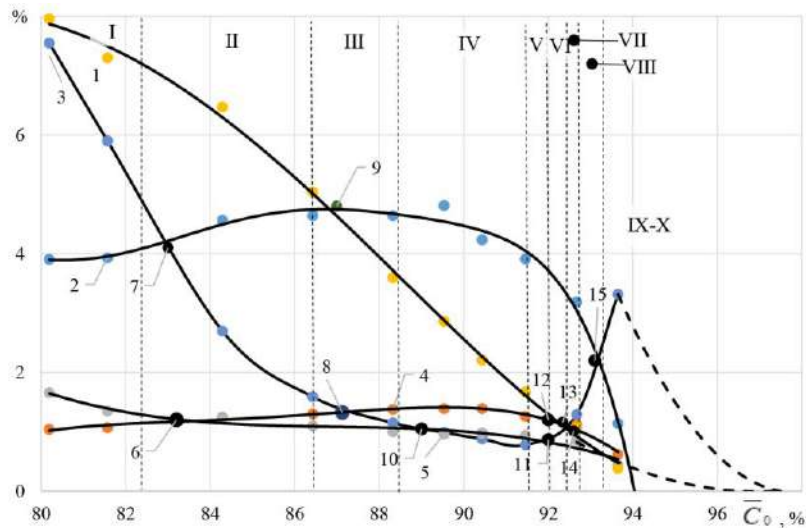


Fig. 3: Dependence of the average values of the content of components in organic matter on carbon.

1, 2, 3, 4, 5, – curves of the average content in organic matter, respectively, of oxygen (\bar{O}_0), hydrogen (\bar{H}_0), moisture (\bar{W}), nitrogen (\bar{N}_0) and sulfur (\bar{S}_0); 6, 7, 8, 9, 10, 11, 12, 13, 14 – characteristic points of curve intersections defining the boundaries of the stages of layer metamorphism; I, II, III, IV, V, VI, VII, VIII, IX, X – stages of seam metamorphism, determined by the characteristic points of curve intersection.

Table 4: Change of elemental content of carbon in organic matter at different stages of reservoir transformation.

Stage determination criterion	Stages of seam metamorphism and carbon content, %									
	I	II	III	IV	V	VI	VII	VII	IX	X
Coke yield, \bar{K} , %	80,19	81,57	84,29	86,43	88,33	89,53	90,43	91,46	92,67	93,5
Carbonation according to the individual content of moisture and organic matter components	80,0- 83,0	83,0- 87,0	87,0- 89,0	89,0- 92,0	92,0- 92,7	92,7- 93,0	93,0- 93,2	93,2- 93,6	over 93,6	
Individual share of participation of organic matter components in carbonization	80,0- 83,4	83,4- 86,0	86,0- 90,4	90,4- 91,8	91,8- 92,5	92,5- 93,2	93,2- 93,4	93,4- 93,6	over 93,6	

Their values (Table 3) changed significantly in the process of metamorphic transformations of seams. There are also differences in the ranks of ranking according to the proportion of the participation of components in carbonization in comparison with the ranks ranked according to the elemental organic matter composition (Table 2). The presence of moisture plays a significant role in the early stages (I, II) of reservoir transformation. At the next stages (III-IX), the proportion of its influence on carbonation is minimal in comparison with other components. At the last stage (X), the role of moisture increases again, and it returns to one of the leading places in the ranking. After reaching a carbon content of more than 93.6%, a sharp decrease in the share of participation in carbonization (Fig. 2b) of all other components (\bar{H}_0 , \bar{N}_0 , \bar{S}_0 , \bar{O}_0 and \bar{W}) is predicted. In this case, their total share in organic matter will not exceed 6.4%, which undoubtedly affects the properties of coal seams during mining.

The established stages of seam transformation in terms of the individual share of the components in carbonization practically do not differ from the limits of the stages established by the elemental composition of organic matter (Fig. 2b, Table 4). It should also be noted that the average carbon content at the stages of seam metamorphism, determined by the coke yield, in most cases does not coincide with the ranges of variation established by the individual content of the components or their share in carbonization (Table 4). The inconsistency of the limits of the stages of seam metamorphism makes it unacceptable to use the coke yield as the main criterion for assessing the conversion of coal and even more so the manifestation of hazardous properties of seams.

CONCLUSION

The conducted research and the results obtained allowed us to draw conclusions that are important for improving the regulatory framework for safe mining of coal seams:

- The indicators of the yield of volatile substances during the thermal decomposition of coals currently used in the regulatory framework are not directly related to the stages of seam transformation in natural conditions. Thermal decomposition under artificial conditions is the next stage in the transformation of coals at a higher temperature;
- The main indicators of the regulatory framework are determined for the dry ash-free state of organic matter (*daf*), which does not correspond to its state in coal seams during mining;
- The use of indicators of the volatile substances released during the thermal decomposition of coals to characterize the hazardous properties of coal seams is borrowed from industrial classifications without proper justification. They only conditionally characterize the brands of coal for their industrial use by genetic and basic energy and technological characteristics;
- The stages of metamorphism, according to the GOST definition, characterize the degree of change in the chemical composition, structure, and properties of coal, achieved during coal formation and determining its position in the genetic series: brown coal - hard coal - anthracite. None of the indicators of the regulatory framework correspond to this definition of the degree of metamorphism;
- One of the main signs of an increase in the degree of metamorphism is an increase in the carbon content in organic matter and a decrease in the sum of the remaining components;
- According to technical and elemental analysis, the presence of seam moisture is not considered in the composition of organic matter, which unreasonably excludes its influence on the physicochemical state of the mines;
- The main components of organic matter are carbon,

hydrogen, nitrogen, sulfur, oxygen, and moisture. Their total content at all stages of formation transformation is close to 100%;

- In the process of metamorphic transformations of coal seams, there is an ambiguous change in the ratio between the main components of the elemental composition of organic matter;
- The hazardous properties of coal seams are determined not only by the elemental composition of organic matter but also by the share of each component in carbonization.

REFERENCES

- Ahamed, M. A. A., Perera, M. S. A., Matthai, S. K., Ranjith, P. G. and Dong-yin, L. 2019. Coal composition and structural variation with rank and its influence on the coal-moisture interactions under coal seam temperature conditions: A review article. *J. Pet. Sci. Eng.*, 180: 901-917.
- Antoshchenko, M., Filatieva, E., Yefimtsev, V. and Tarasov, V. 2020. Peculiarities of using classification indicators of the coal metamorphism degree for predicting the hazardous coal seams properties. *E3S Web of Conf.*, 01014: 1-10.
- ASTM D388-15. 2012. Standard Classification of Coals by Rank, ASTM International, West Conshohocken, PA
- GOST 25543-2013. 2014. Brown Coals, Hards Coals, and Anthracites. Classification According to Genetic and Technological Parameters: State Standard of the USSR. *Izd-vo Standartov, Moscow.*
- GOST 6382-2007. 2008. Solid Mineral fuel: Methods for Determination of Volatile Matter Yield. *Izd-vo Standartov, Moscow.*
- Klymenko, V., Gutsul, V., Bondarenko, V., Martynenko, V. and Stets, P. 2019. Modeling of the kinetics of the gas hydrates formation on the basis of a stochastic approach. *Solid State Phen. Trans. Tech. Publ. Ltd.*, 109-98 :291
- Qi, Y. (ed.) 2020. *Geology of Fossil Fuels-Coal*. Proceedings of the 30th International Geological Congress, 4-14 August 2020, Beijing, China. CRC Press, London, p. 168.
- Sen, S. and Banerjee, S. 2015. Identifying Relationship Amongst Vitrinite/Inertinite Ratio (V/I), Cleat Parameters, Vitrinite Reflectance, O/C Ratio and Permeability of Coal Seams and V/I Ratio as Exploration Tool: Study from Raniganj Coal Bed Methane Block, Essar Oil Limited, India. In Mukherjee, S. (ed.), *Petroleum Geosciences: Indian Contexts*. Springer, Cham, pp. 205-217.
- Thomas, L. 2020. *Coal Geology*. John Wiley & Sons, New York.



Characterisation and Assessment of Physicochemical Properties of Grapeseed Methyl Ester Using Predictive Correlations and ASTM Standards For CI Engine Application

C. Prabhu†, V. Rajasekar and T. Prakash

Department of Automobile Engineering, College of Engineering and Technology, SRM Institute of Science and Technology, Kattankulathur-603203, Tamilnadu, India

†Corresponding author: C. Prabhu; prabhuc@srmist.edu.in

Nat. Env. & Poll. Tech.
Website: www.neptjournal.com

Received: 29-12-2020
Revised: 20-02-2021
Accepted: 22-02-2021

Key Words:

Grapeseed methyl ester
Winery waste
Property prediction
CI engine

ABSTRACT

In the present work, a detailed investigation of the physio-chemical characteristics of grapeseed methyl ester (GSME) obtained from winery biomass waste has been carried out to evaluate its suitability as an energy alternate, for CI engines. GSME was subjected to Gas chromatography and mass spectrometry analysis from which fatty acids compositions were determined followed by other interpretations such as carbon number, number of double bonds, etc. Two different predictive correlations were identified from the literature for predicting the properties that are considered important, for using GSME as a fuel. The predicted properties of GSME are compared with the experimental results obtained through standard ASTM procedures, for diesel, neat grapeseed oil (GSO) and GSME, respectively. Further, the influence of the structural and compositional characteristics of GSME on the physicochemical properties like density, kinematic viscosity, lower calorific value, etc. has been evaluated and found to be closer to diesel.

INTRODUCTION

Diesel engines are the most sought-after systems deployed in the transportation sector, in power generation gensets for their utmost efficacy and low-cost factor. Conversely, as non-renewable fuel energy, diesel is also a major source of particulate matter (PM) causing adversities in health (Raheman & Phadatare 2004). Albeit consistent efforts are being put up to mitigate these effects by investigating various possible energy resources, hardly there has been any significant development. However, with respect to compression ignition (CI) engine application, the options are limited to mainly biodiesel (BD), as these come with the advantage of requiring fewer engine modifications. These BDs can be extracted from edible or non-edible sources. However, it is preferred to extract it from a non-edible resource (Singh et al. 2010) although it contains a high free fatty acid (FA) content, viscosity, and density, (Atabani et al. 2013, Gui et al. 2008). Thus far, many second-generation fuels such as sunflower, rapeseed, palm oil, etc. (Shahid & Jamaal 2008), and third-generation fuels like waste cooking oil, waste tire oil, algae oil, bryophyte, etc. (Atabani et al. 2013, Sirohi et al. 2019) have been tested in CI engine application. Since the sources from which these oils are obtained are different, there exists a difference in FA contents and its percentage

composition as well. Several research works have been carried to establish a correlation between the composition of the BD's and its properties.

Ramírez-Verduzco et al. (2012) had analyzed and presented in their work the characterization of the methyl ester of beef tallow and soybean oil. The impact of the molecular weight (MW) and unsaturation of the oils on the physicochemical properties were discussed in their work. Lapuerta et al. (2010) in their study had made attempts to compile the densities of ethyl esters and methyl esters available in the literature, at 15°C, based on the chain length and unsaturation degree. Mehta and Anand (2009) had formulated an approach in determining the heating values of processed and straight vegetable oils based on the bond energies of their corresponding fatty esters. The closeness of predictions for the processed and straight vegetable oils with the existing experimental data was said to be within 3%. Tong (2010) developed a model involving the fatty acid methyl ester (FAME) components for the determination of cetane number (CN) of various BDs. MW and carbon number of the FA chain were correlated by developing two different regression equations. Islam et al. (2013) had examined the BD of different microalgal species by characterization through Preference Ranking Organisation Method for Enrichment Evaluation (PROMETHEE) to calculate the salient properties

like iodine value, kinematic viscosity, etc. Efforts were made by Chuck et al. (2009) to generate a model for FAME composition using Matlab environment, fitting a quadratic response for saturation and average chain length.

Rao & Rao (2008) had investigated the influence of (BD) properties on the engine characteristics. Two BD fuels namely, coconut oil and sesame seed oil methyl ester respectively, were selected. The authors had indicated that as the ratio of carbon to hydrogen (C/H) increases, the fuel had a tendency to produce more smoke emissions. The work carried out by Salamanca et al. (2012) showed the impact of the molecular structure of the moderately unsaturated palm oil and highly unsaturated linseed oil biodiesel and their blend (50% by volume) on PM emission. The sample oils were characterized using gas chromatography analysis and tested in an engine and compared with diesel soot emission.

Motivation for the Present Study

One of the progressive areas of business is the winery industry, which is a major source of voluminous liquid and solid waste, which mainly comprise grape pomace and seeds and serves as a source of oil (Fernández et al. 2010, Muhlack et al. 2018). Often, the handling, treatment, and discarding procedures of these solid wastes are complex and costlier (Ohnishi 1990, Bustamante et al. 2008). This opens up a broad avenue for extracting oil from winery waste, particularly, the grape seeds, and evaluate the suitability of GSO as fuel for CI engine applications. Moreover, not much work has been reported on the assessment of physiochemical characteristics and property prediction of the biofuel produced from grapeseed of winery industry waste which is the prime novelty of this work.

Hence, in the present work, the physiochemical characteristics of neat GSO and GSME were tested through ASTM standards and further subjected to Gas Chromatography-Mass Spectrometry analysis (GC-MS). The presence of different

FAs in the oils with its percentage composition can be found through this analysis (Hariram et al. 2020). Several other interpretations such as the presence of double bonds in each FA (indicating unsaturation level), carbon number, and the MW of the individual FA present in the oil were made. A comparative analysis was carried out between the physiochemical properties obtained through standard ASTM procedures and that of predicted values. These predicted values are obtained from the already established predictive correlations from literature, that is based on the inherent characteristics of the fuel such as carbon number, number of double bonds, etc., as these provide a close approximation of the physiochemical properties (Da Silva et al. 2017, Chai et al. 2014).

MATERIALS AND METHODS

Transesterification

In view of the fact that the viscosity of neat GSO chosen for this work was higher, the same has been converted into BD. Although several methods are available for reducing the viscosity of neat vegetable oil into BD. Trans-esterification is one of the methods which is most common and efficient (Martín 2010). As the free fatty acid (FFA) content of NGSO was lower (0.25%), it was subjected to a single stage of esterification. The separated BD was then water washed twice and heated up to obtain the final yield of nearly 80 %.

Characterisation of Grapeseed Methyl Ester

To determine the nature of oil obtained and the extent to which a given sample of oil can be used as fuel, and FA profile analysis of GSME was carried out using Agilent GCMS. The specification of the GCMS setup is provided in Table 1.

Physiochemical Properties Measurement

One of the important aspects on which the performance of an

Table 1: Specifications of the GCMS setup.

GCMS for FA profile	ASTM D6584
Instrument Model	AGILENT GCMS : MSD 5977A AND GC7890B
Column	Agilent 19091S-433:93.92873 HP-5MS 5% phenyl methyl silox -60°C to 325°C (325°C) 30mX250µmX0.25µm
Software	MASS HUNTER Data compared with NIST library
Condition	Scan range: 30-300amu Injection volume: 1µL through auto sampler Split ratio: 100:1 Helium gas 18.129psi : (1.489mL/min) MSD Transfer line temp : 250°C Injector temp :250°C
Temperature program	80°C for 2min then ramped 130°C at 10°C/min then 210°C at 30°C/min hold for 30min with a total run time 44mins and Solvent delay of 2min

engine depends is the physicochemical properties of the fuel. As far as BDs are concerned, the physiochemical properties, which in turn are governed by the individual fatty esters present, could greatly influence the engine performance and combustion-related parameters, like, the mass of fuel injected fuel penetration. and atomization, etc. (Lapuerta et al. 2010). Hence, properties like the acid value, viscosity, density, cetane index, iodine value, and heating value of the FAME have been determined. The instruments and methods used for the measurements of properties are indicated in Table .2. For cetane index calculation, the procedure prescribed in ASTM D4737 was followed (Aleme & Barbeira 2012).

Calculated Cetane Index = 45.2+(0.0892)

$$\frac{(T_{10N})+[0.131+(0.901)(B)][T_{50N}]+[0.0523-(0.420)(B)]}{[T_{90N}]+[0.00049] [(T_{10N})^2-(T_{90N})^2]+107(B)+(60)(B)^2}$$

Calculated Cetane Index by Four Variable Equation

$$D = \text{Density at } 15^{\circ}\text{C, g/mL, } B = [\exp^{(-3.5)(D-0.85)}] - 1$$

$$T_{10} = 10 \% \text{ recovery temperature, } ^{\circ}\text{C, } T_{10N} = T_{10} - 215$$

$$T_{50} = 50 \% \text{ recovery temperature, } ^{\circ}\text{C, } T_{50N} = T_{50} - 260$$

$$T_{90} = 90 \% \text{ recovery temperature, } ^{\circ}\text{C, } T_{90N} = T_{90} - 310$$

Predictive Correlations

The overall properties of the BD will be based on each fatty

ester that constitutes the BD. In turn, the characteristics of the individual fatty esters are governed by the structural features of the FA and its percentage composition. Researchers have formulated several correlations based on the fatty ester’s inherent chemical characteristics such as the chemical structure, MW, double bonds, etc., Islam et al. (2013). The correlations that have been used in this work are shown in Table 3.

RESULTS AND DISCUSSION

Gas Chromatography-Mass Spectrometry Results

Fig.1 shows the various peaks obtained at different intervals for GSME using GCMS and provides absolute quantification of the FAME’s present in GSME. The values thus obtained from the spectral peaks of the GCMS is analyzed and the outcome indicates the presence of different fatty esters in GSME like methyl linoleate (C18:2-39.83%), methyl stearate (C18:0 - 25.13%), methyl palmitate (C16:0 - 17.37%), methyl myristate (C14:0 - 3.048%) and methyl laurate (C12:0 - 2.378%) in major proportion by weight along with other compounds. Furthermore, double bonds in methyl linoleate and methyl eicosenoate and its percentage content, evidently indicate, that the oil is moderately unsaturated. The compounds which are present in very minor proportions have not been considered for analysis in this work. In addition, as the physicochemical

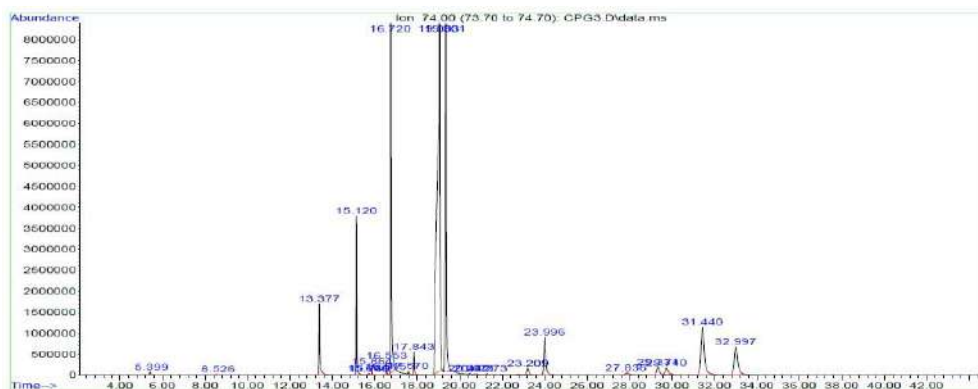


Fig. 1: Chromatogram generated by GCMS for GSME.

Table 2: Instruments and Standards for property measurement.

S.No.	Properties	Instruments used	Measurement Standards	Accuracy
1.	Specific gravity @15°C	Weighted bulb hydrometer	ASTM D1298	±0.001
2.	Viscosity @40°C	Glass Viscometer Brook Field Viscometer	ASTM D445	± 0.003 cSt or mm ² /s
3.	Heating value, MJ/kg	CC01/M3 Bomb calorimeter	ASTM D240	±0.001°C
4.	Iodine value	Wij’s method	IS 548 Part 1, 1964	-
5.	Cetane Index	Distillation temperature (90 % recovered) – Thermo-couple, Flask, with distillation arrangement	ASTM D4737	±0.1°C

Table 3: Predictive correlations based on carbon, hydrogen, oxygen, MW, and number of double bonds.

Properties	Correlations based on MW, Carbon number, Hydrogen, and Oxygen content, and Number of double bonds of the FAME (FAME)	References
Density	$D = 0.8463 + 4.9/M_i + 0.018N_{db}$ where M_i is the MW of the i^{th} FAME and N is the number of double bonds in the FAME	... (I) Ramirez et al. (2012)
	$D = 851.471 + [250.718db + 280.899]/1.214 + n$ Where db is the number of double bonds in the FAME, n is the carbon number of the FAME.	... (II) Lapuerta et al. (2010)
Viscosity	$\ln(V_i) = -12.503 + 2.496\ln(M_i) - 0.178N_{db}$ where M_i is the molecular weight of the i^{th} FAME and N is the number of double bonds in the FAME	... (I) Ramirez et al. (2012)
	$\eta = 0.235N_c - 0.699N_{DB}$ where η is the kinematic viscosity of the FAME, Where N_c = No. of carbon atoms, N_{DB} = No. of double bonds	... (II) Chang & Liu (2009)
Lower heating value	$LHV = 0.0109(C/O)\exp^3 - 0.3516(C/O)\exp(2) + 4.2000(C/O) + 21.066 - 0.11N_{db}$ where C and O are the percentage weights of Carbon and Oxygen respectively and N_{db} is the number of double bonds in the FAME	... (I) Mehta & Anand (2009)
	$LHV = 0.0011(H/O)\exp^3 - 0.0785(H/O)\exp(2) + 2.0409(H/O) + 20.992 - 0.100N_{db}$ where C , H , and O are the percentage weight of carbon, hydrogen, and oxygen, respectively	... (II) Mehta & Anand (2009)
Cetane Number	$CN = -52.974 + (13.767 - 1.202db + 0.152db^2)X - 0.351X^2$ Where db is the number of double bonds in the FAME, and 'X' is the Carbon number of the FA	... (I) Tong et al. (2011)
	$CN = -23.523 + (2.366 + 6.299e^{-0.411db})n X \exp^{-0.018n}$ Where db is the number of double bonds in the FAME, and n is the Carbon number of the FA	... (II) Lapuerta et al. (2010)
Iodine Value	$IV = (\% C_{16:1} X 0.95) + (\% C_{18:1} X 0.86) + (\% C_{18:2} X 1.723) + (\% C_{18:3} X 2.616) + (\% C_{20:1} X 0.785) + (\% C_{22:1} X 0.723)$ $C x:y$ – where x is the carbon number and y is the number of double bonds	... (I) Da Silva et al. (2017)
	$IV = \Sigma(254 X D X A_f)/MW$ where D is the density, A_f is the percentage content and MW_i is the MW of the FAME's	... (II) Islam et al. (2013)

properties of the FAME has larger dependability on the inherent chemical characteristics such as carbon number, the number of double bonds, MW, etc., a close prediction of the physicochemical properties of the methyl ester can be arrived at (Tong 2010, Knothe 2005, Maroto et al. 2010).

Several interpretations that have been made from the different compounds identified from the sample of GSME have also been listed in Table.4. Further, it is seen that with the increasing carbon number, the MW of the fatty esters increases while the percentage content of oxygen decreases. The data thus interpreted, was substituted in two different correlations that have been chosen from different literature for each property such as density, viscosity, heating value, etc. which are considered to be important from the point of view of the performance of GSME in a CI engine. The predicted property values thus derived from the correlations are indicated in the parenthesis and further been quantified based on the percentage composition of the individual fatty esters, as indicated in Table.5.

Physical Properties Variation

Although the dependence of properties on structural characteristics of the ester may not be clearly evident from the

values based on the FA percentage composition, the actual predicted values (in parenthesis) in Table 5 do exhibit a correlation as explained below. For instance, methyl caprylate which has an oxygen weight percentage of 22.19 has a heating value of 33.75 MJ.kg^{-1} while methyl 18-methyl nonadecanoate with an oxygen percentage of 9.79 has a heating value of 40.69 MJ.kg^{-1} , clearly indicating that with the increasing oxygen percentage, the fatty esters tend to have a proportionally lower energy density, while carbon number has a positive correlation with heating value. In a similar context, a correlation can be arrived, between the MWs of the individual ester composition with density, cetane index, and kinematic viscosity respectively, while a close correlation can also be arrived at, between lower heating value (LHV) of the esters and C:H and C:O, respectively.

Fig. 2 shows the variation of density with MW of individual fatty ester composition. Although there is a decreasing trend for density with an increase in MW from $158.13 \text{ g.mol}^{-1}$ for methyl caprylate to $284.27 \text{ g.mol}^{-1}$ for methyl margarate, a sharp deviation from this trend is noticed for methyl linoleate and methyl eicosenoate. On the other hand, viscosity and cetane index has a positive correlation with MW. It is

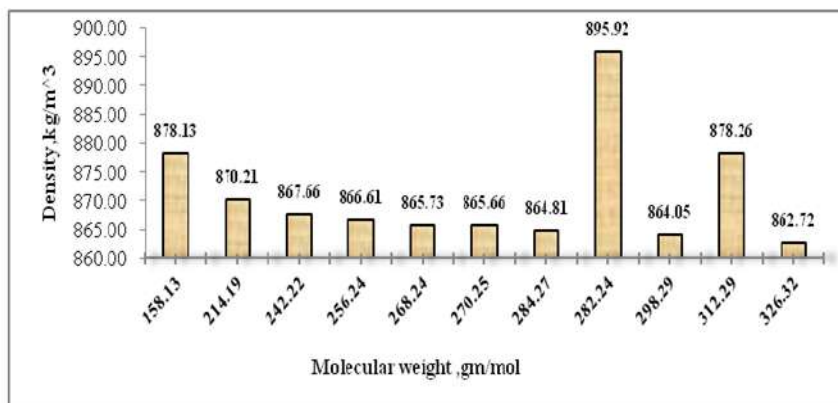


Fig. 2: Variation of density (avg) with a molecular weight.

Table 4: Percentage content of the fatty esters, number of double bonds, and weight percentage of C, H, and O.

S. No.	Compound Name	Per-centage content	Molecular formula	Carbon Number	No. of double bond	Molecular Weight (g/mol)	C (%)	H (%)	O (%)	C:H	C:O
1	Methyl Caprylate	0.141	C ₉ H ₁₈ O ₂	9	0	158.13	68.4	11.2	20.1	6.12	3.40
2	Methyl Laurate	2.378	C ₁₃ H ₂₆ O ₂	13	0	214.19	72.9	12.2	14.8	5.96	4.91
3	Methyl Myristate	3.048	C ₁₅ H ₃₀ O ₂	15	0	242.22	74.4	12.5	13.1	5.96	5.67
4	Methyl Pentadecanoate	0.17	C ₁₆ H ₃₂ O ₂	16	0	256.24	74.9	12.6	12.4	5.96	6.04
5	Methyl Palmitoleate	0.285	C ₁₇ H ₃₂ O ₂	17	0	268.24	76.1	12.0	11.9	6.34	6.42
6	Methyl Palmitate	17.37	C ₁₇ H ₃₄ O ₂	17	0	270.25	75.5	12.7	11.8	5.97	6.42
7	Methyl Margarate	0.647	C ₁₈ H ₃₆ O ₂	18	0	284.27	76.0	12.8	11.2	5.96	6.80
8	Methyl Linoleate	39.829	C ₁₈ H ₃₄ O ₂	18	2	282.24	76.6	12.1	11.3	6.31	6.80
9	Methyl Stearate	25.13	C ₁₉ H ₃₈ O ₂	19	0	298.29	76.5	12.8	10.7	5.97	7.18
10	Methyl Eicosenoate	0.343	C ₂₀ H ₄₀ O ₂	20	1	312.29	76.9	12.9	10.2	5.97	7.56
11	Methyl 18-methyl Nonadecanoate	2.657	C ₂₁ H ₄₂ O ₂	21	0	326.32	77.3	13.0	9.7	5.96	7.93
12	Weight of C, H and O in the mixture (g/mol).	-	-	-	-	2816.62	2113.7	350.4	351.78	-	-
13	Composition in the mixture by weight percent	-	-	-	-	-	75.06	12.44	12.48	-	-

understood that the viscosity increases from 1.63 cSt to 5.96 cSt, and the cetane index increases from 42.65 to 91.26, for the ester composition having MW's from 158.13 g.mol⁻¹ to 326.32 g.mol⁻¹ respectively, for GSME. However, a similar deviation in the trend is observed for methyl linoleate and methyl eicosenoate as shown in Fig.3.

The reason that can be cited for such a deviation in trend for density, viscosity, and cetane index for both the fatty esters mentioned above could be due to the presence of double bonds in it, at a fairly considerable proportion making the oil moderately unsaturated. It can be seen that the iodine values computed through both the predictive correlation have values

Table 5: Predicted properties using correlations based on number of double bonds, carbon number, and weight percentage of C, H and O.

S.No.	Compound Name	Iodine value I	Iodine value II	Viscosity based on % FFA, (cSt)	Viscosity based on % FFA, (cSt) (I)	Viscosity based on % FFA, (cSt) (II)	LHV based on % FFA (MJ/kg), (I)	LHV based on % FFA (MJ/kg), (II)	Density based on % FFA, (kg/m ³) (I)	Density based on % FFA, (kg/m ³) (II)	Cetane Index based on % FFA (I)	Cetane Index based on % FFA (II)
1	Methyl Caprylate	0	0	0.01 (2.12)	0.01 (31.71)	0.01 (1.14)	0.04 (31.71)	0.05 (33.2)	1.24 (877.29)	1.24 (878.97)	0.06 (42.49)	0.06 (42.8)
2	Methyl Laurate	0	0	0.07 (3.06)	0.82 (34.50)	0.06 (2.44)	0.82 (34.50)	0.85 (35.57)	20.67 (869.18)	20.72 (871.23)	1.59 (66.67)	1.56 (65.62)
3	Methyl Myristate	0	0	0.11 (3.53)	1.08 (35.56)	0.10 (3.32)	1.08 (35.56)	1.11 (36.5)	26.41 (866.53)	26.48 (868.80)	2.27 (74.55)	2.31 (75.70)
4	Methyl Pentadecanoate	0	0	0.01 (3.76)	0.06 (36.00)	0.01 (3.82)	0.06 (36.00)	0.06 (36.9)	1.47 (865.42)	1.48 (867.79)	0.13 (77.44)	0.14 (80.43)
5	Methyl Palmitoleate	0	0	0.01 (4.01)	0.10 (36.43)	0.01 (4.28)	0.10 (36.43)	0.10 (36.8)	2.46 (864.57)	2.47 (866.89)	0.03 (79.62)	0.24 (84.95)
6	Methyl Palmitate	0	0	0.69 (4.02)	6.33 (36.43)	0.76 (4.36)	6.33 (36.43)	6.48 (37.3)	150.15 (864.43)	150.58 (866.89)	13.83 (79.62)	14.76 (84.95)
7	Methyl Margarate	0	0	0.03 (4.23)	0.24 (37.6)	0.03 (4.95)	0.24 (37.6)	0.24 (37.6)	5.59 (863.54)	5.60 (866.09)	0.52 (81.1)	0.58 (89.29)
8	Methyl Linoleate	68.58	71.12	1.22 (3.07)	14.57 (36.58)	1.50 (3.78)	14.57 (36.58)	14.81 (37.17)	358.33 (899.66)	355.35 (892.19)	19.43 (48.78)	17.26 (43.33)
9	Methyl Stearate	0	0	1.12 (4.47)	9.33 (37.13)	1.40 (5.58)	9.33 (37.13)	9.53 (37.9)	226.80 (862.73)	227.45 (865.37)	20.58 (81.88)	23.48 (93.43)
10	Methyl Eicosenoate	0.27	0.28	0.01 (4.24)	0.13 (37.32)	0.02 (5.57)	0.13 (37.32)	0.13 (38.2)	3.02 (879.99)	3.01 (876.53)	0.21 (60.96)	0.23 (67.77)
11	Methyl Nona-decanoate	0	0	0.13 (4.94)	1.00 (37.70)	0.19 (6.98)	1.00 (37.70)	1 (38.4)	22.89 (861.32)	22.96 (864.12)	2.16 (81.34)	2.69 (101.17)
Total (based on %FFA)		68.85	71.4	3.41	33.71	4.08	33.71	34.39	819.02	817.35	61.01	63.30
Average (E+I)/2		70.12		3.74 cSt	34.05 MJ/kg				818.18 kg/m ³		62.16	

Values inside the parenthesis () indicate predicted property values.

of 68.85 and 71.4 respectively, thereby reinforcing the above statement. Giakoumis (2013) had reported in their work for different BDs, a drop in viscosity level and cetane index for unsaturated esters, while it increased for saturated esters. Similar correlations used by Chang and Liu (2010) based on the number of carbon atoms and double bonds resulted in an average relative deviation of 6.78 % for 30 experimental data points for MW and 13.97 % deviation for kinematic viscosity prediction for 60 experimental data points. Compared to the average percentage deviation between the experimental and predicted value of the various BDs used by them, the observed deviation in this work for MW and kinematic viscosity is comparatively lesser as can be inferred from Table 6.

Generally, the lower heating value for BD ranges from an average of 33 MJ.kg^{-1} to 38 MJ.kg^{-1} which is nearly 10 to 12% lower than diesel fuel. For GSME, the variation of LHV with carbon to oxygen ratio and carbon to hydrogen ratio for its fatty ester composition is shown in Fig.4 and 5 respectively. The lower heating value was found to be 31.28 MJ.kg^{-1} for the low MW, methyl caprylate, while it is 36.81 MJ.kg^{-1} for the higher MW, methyl 18-methyl nonadecanoate. However, a very close correlation can be observed between LHV and C:O and C:H, respectively. It is therefore evident, that as the oxygen content in the fatty esters decreases or the carbon content increases, the lower heating value of the esters increases. Further, FAMES with similar C:O but lower C:H ratios (i.e. more hydrogen) exhibit greater LHV which was the case for methyl palmitoleate and methyl palmitate. However, with progressively greater levels of unsaturation, the energy content reduces. Similar results have been reported by Ramírez-Verduzco et al. (2012).

Comparison of Experimental and Predicted Property Results

Since the present investigation deals with the characterization and evaluation of properties of GSO for use in CI engine application, a comparison of the properties of neat GSO and GSME (predicted and test results) is made with diesel. It can be inferred from Table. 6, that NGSO has a specific gravity, kinematic viscosity, cetane index, and heating value of 0.91, 26.42 cSt, 48, and 36.54 MJ.kg^{-1} respectively, while for diesel it is 0.83, 3.8 cSt, 46, and 42.8 MJ.kg^{-1} , respectively. Although the cetane value of neat GSO is closer to diesel, the kinematic viscosity and density are much higher than diesel which could lead to increased fuel consumption, poor atomization, and combustion.

Further, the density, kinematic viscosity, lower heating value, and cetane index of GSME determined through ASTM standards and the average of I and II predicted from correlations are shown in Table.6 with their percentage variation, respectively. Since the percentage variation between the experimental results and the predicted results are not high, it can be concluded that the determination of the properties using predictive correlations are in close agreement with the experimental values and also falls within the acceptable range specified in the international standards as can be seen in Table .6.

Moreover, as the properties of GSME is closer to diesel, lower fuel consumption and better atomization compared to NGSO can be expected, eventually leading to better performance, combustion, and emission characteristics when used as a fuel for CI engine application.

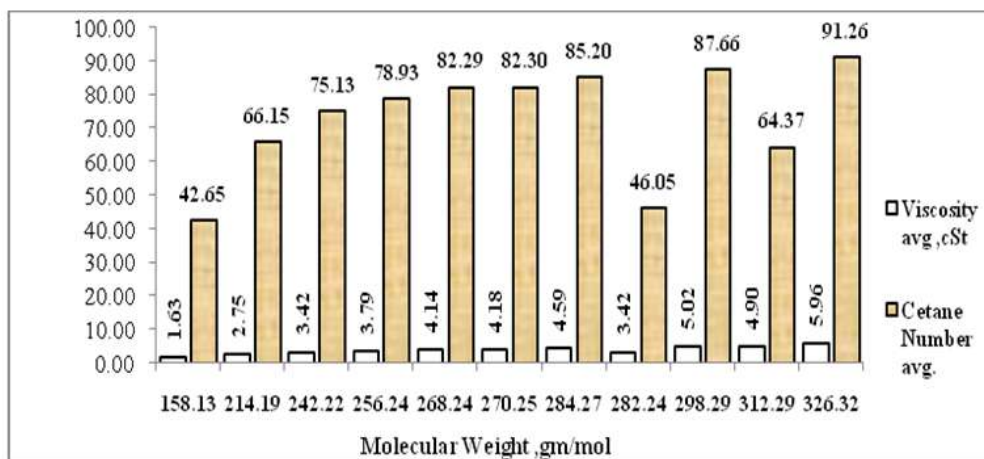


Fig. 3: Variation of kinematic viscosity_(avg) and cetane index_(avg) with MW.

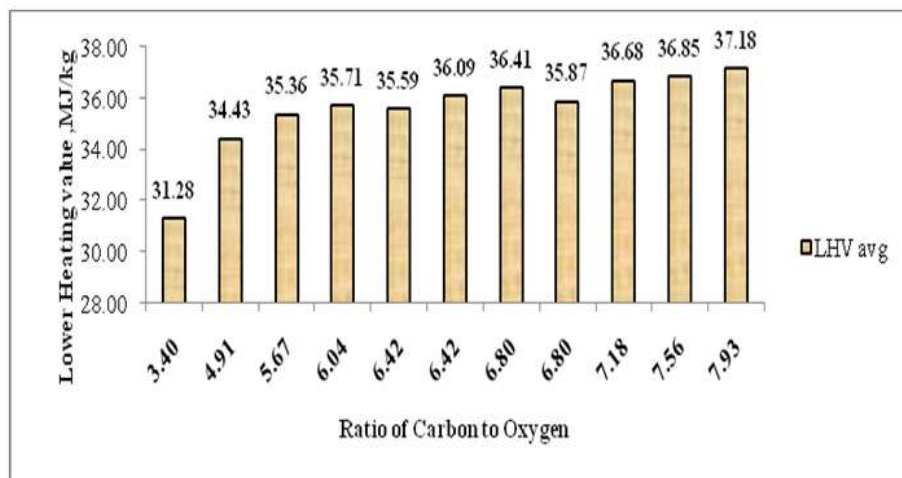


Fig. 4: Variation of lower heating value $_{(avg)}$ with carbon to oxygen ratio for GSME.

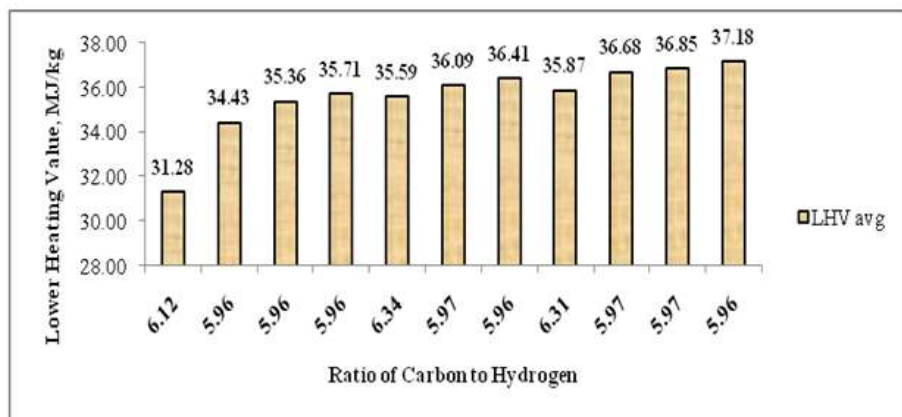


Fig. 5: Variation of lower heating value $_{(avg)}$ with carbon to hydrogen ratio for GSME.

CONCLUSIONS

1. The inputs to predictive correlations such as MW, number of double bonds, carbon number, etc. were interpreted from GCMS analysis for individual fatty ester composition.
2. A close correlation is observed between individual fatty ester MW and density, kinematic viscosity, and cetane index, respectively. For saturated esters of GSME, with an increase in MW, density decreases from 878.13 kg.m^{-3} to 862.72 kg.m^{-3} for methyl caprylate to methyl margarate having MW of 158.13 g.mol^{-1} and 284.27 g.mol^{-1} respectively. However, this effect is contradicting for methyl linoleate and methyl eicosenoate which are unsaturated.
3. Similarly, viscosity and cetane index have a positive correlation with MW. It is understood that the viscosity increases from 1.63 cSt to 5.96 cSt and the cetane index increases from 42.65 to 91.26 for the ester composition having MWs from 158.13 g.mol^{-1} to 326.32 g.mol^{-1} respectively for GSME.
4. In addition, C:O and C: H are found to have a close correlation with the lower heating value of the fuel with lower carbon to oxygen ratio exhibiting lower LHV, and lower carbon to hydrogen ratio exhibiting higher LHV.
5. Experimental evaluation of properties of GSME through ASTM standards is in close agreement with predicted values.

On the whole, as the properties of GSME are closer to

Table 6: Property comparison of NGSO and GSME with diesel.

Properties	Experimental			Average values predicted (based on % FFA) for GSME	(Experimental & Predicted) % variation
	Diesel	NGSO	GSME		
Density @ 15°C	830	910	841	818.18	2.75
Kinematic viscosity (cSt), (40°C)	3.80	26.42	4.04	3.74	7.71
Low Heating Value (MJ/kg)	42.8	36.54	36.82	34.05	7.82
Cetane Index	47	46.3	59.99	62.16	3.55
Iodine Number	-	72	66	70.12	6.05

diesel, lower fuel consumption and better atomization compared to NGSO can be achieved, eventually leading to better performance, combustion, and emission characteristics when used as fuel for CI engine application.

REFERENCES

- Almeida, H.G. and Barbeira, P.J., 2012. Determination of flash point and cetane index in diesel using distillation curves and multivariate calibration. *Fuel*, 102: 129-134.
- Atabani, A.E., Silitonga, A.S., Ong, H.C., Mahlia, T.M.I., Masjuki, H.H., Badruddin, I.A. and Fayaz, H. 2013. Non-edible vegetable oils: A critical evaluation of oil extraction, FA compositions, BD production, characteristics, engine performance, and emissions production. *Renew. Sust. Energy Rev.*, 18: 211-245.
- Bustamante, M.A., Moral, R., Paredes, C., Pérez-Espinosa, A., Moreno-Caselles, J. and Pérez-Murcia, M.D., 2008. Agrochemical characterization of the solid by-products and residues from the winery and distillery industry. *Waste Manag.*, 28(2): 372-380.
- Chai, M., Tu, Q., Lu, M. and Yang, Y.J. 2014. Esterification pretreatment of free fatty acid in BD production, from laboratory to industry. *Fuel Process. Technol.*, 125: 106-113.
- Chang, A.F. and Liu, Y.A. 2010. Integrated process modeling and product design of BD manufacturing. *Ind. Eng. Chem. Res.*, 49(3): 1197-1213.
- Chuck, C.J., Bannister, C.D., Hawley, J.G., Davidson, M. G., La Bruna, I. and Paine, A. (2009). A predictive model to assess the molecular structure of BD fuel. *Energy Fuels*, 23(4): 2290-2294.
- Da Silva, F.L., do Nascimento, J.R., de Melo, L.N., de Freitas, J.A.S., Bortoluzzi, J.H. and Meneghetti, S.M.P., 2017. Study of correlations between composition and physicochemical properties during methyl and ethyl BD synthesis. *Ind. Crops Prod.*, 95: 18-26.
- Fernández, C.M., Ramos, M.J., Pérez, Á. and Rodríguez, J.F. 2010. Production of BD from winery waste: Extraction, refining and transesterification of GSO. *Bioresour. Technol.*, 101(18): 7019-7024.
- Giakoumis, E.G. 2013. A statistical investigation of BD physical and chemical properties, and their correlation with the degree of unsaturation. *Renewable Energy*, 50: 858-878.
- Gui, M.M., Lee, K.T. and Bhatia, S. 2008. Feasibility of edible oil vs. non-edible oil vs. waste edible oil as BD feedstock. *Energy*, 33(11): 1646-1653.
- Hariram, V., Karthikeyan, N.B., Seralathan, S., Premkumar, T.M. and John, J.G. 2020. Spectroscopic characterization of palm stearin BD derived through base catalyzed transesterification process. *Nature Environ. Pollut. Technol.*, 19(3): 981-990.
- Islam, M.A., Magnusson, M., Brown, R.J., Ayoko, G.A., Nabi, M.N. and Heimann, K. 2013. Microalgal species selection for BD production based on fuel properties derived from fatty acid profiles. *Energies*, 6(11): 5676-5702.
- Knothe, G. 2005. Dependence of BD fuel properties on the structure of fatty acid alkyl esters. *Fuel Process. Technol.*, 86 (10): 1059-1070.
- Lapuerta, M., Rodríguez-Fernández, J. and Armas, O. 2010. Correlation for the estimation of the density of fatty acid esters fuels and its implications. A proposed BD cetane index. *Chem. Phys. Lipids*, 163(7): 720-727.
- Maroto, J.A., Quesada-Pérez, M. and Ortiz-Hernández, A.J. 2010. Use of kinematic viscosity data for the evaluation of the molecular weight of petroleum oils. *J. Chem. Educ.*, 87(3): 323-325.
- Martín, C. 2010. Fractional characterization of jatropa, neem, moringa, trisperma, castor, and candlenut seeds as potential feedstocks for BD production in Cuba. *Biomass Bioenerg.*, 34(4): 533-538.
- Mehta, P.S. and Anand, K. 2009. Estimation of a lower heating value of vegetable oil and BD Fuel. *Energy Fuels*, 23(8): 3893-3898.
- Muhlack, R.A., Potumarthi, R. and Jeffery, D.W. 2018. Sustainable wineries through waste valorization: A review of grape marc utilization for value-added products. *Waste Management*, 72, 99-118.
- Ohnishi, M. 1990. Chemical composition of lipids, especially triacylglycerol, in grape seeds. *Agric. Biol. Chem.*, 54(4):1035-1042.
- Raheman, H. and Phadatar, A.G. 2004. Diesel engine emissions and performance from blends of karanja methyl ester and diesel. *Biomass and Bioenerg.*, 27(4): 393-397.
- Ramírez-Verduzco, L.F., Rodríguez-Rodríguez, J.E. and Jaramillo-Jacob, A. R. 2012. Predicting cetane number, kinematic viscosity, density and higher heating value of BD from its FAME composition. *Fuel*, 91(1): 102-111.
- Rao, V.P. and Rao, B.V.A. 2008. Influence of Physical and Chemical Properties of Two BD Fuels on Performance, Combustion and Exhaust Emission Characteristics in a DI-CI Engine. ASME 2008 Internal Combustion Engine Division Spring Technical Conference.
- Salamanca, M., Mondragón, F., Agudelo, J.R., Benjumea, P. and Santamaría, A. 2012. Variations in the chemical composition and morphology of soot induced by the unsaturation degree of BD and a BD blend. *Combust. Flame*, 159(3): 1100-1108.
- Shahid, E.M. and Jamal, Y. 2008. A review of BD as a vehicular fuel. *Renew. Sust. Energy Rev.*, 12(9): 2484-2494.
- Singh, P.J., Khurma, J. and Singh, A. 2010. Preparation, characterization, engine performance, and emission characteristics of coconut oil-based hybrid fuels. *Renew. Energy*, 35(9): 2065-2070.
- Sirohi, S., Yadav, C. and Banerjee, D. 2019. Biofuel from Bryophyta as an alternative fuel for the future. *Nature Environ. Pollut. Technol.*, 18(3): 889-895.
- Tong, D. 2010. Cetane number prediction of BD from the composition of the fatty acid methyl esters. *J. Amer. Oil Chem. Society*, 88(3): 415-423.



An Assessment of Machine Learning Integrated Autonomous Waste Detection and Sorting of Municipal Solid Waste

Sonam Chaturvedi†, Bikarama Prasad Yadav and Nihal Anwar Siddiqui

Sustainability Cluster, University of Petroleum and Energy Studies (UPES), Bidholi Energy Acres, Dehradun-248007, India

†Corresponding author: Sonam Chaturvedi; sonam.dobriyal@gmail.com

Nat. Env. & Poll. Tech.
Website: www.neptjournal.com

Received: 19-03-2021

Revised: 15-04-2021

Accepted: 18-04-2021

Key Words:

Municipal waste management

Machine learning

CNN

Image processing

ABSTRACT

Municipal solid waste deposition in metropolitan areas has become a major concern that, if not addressed, can lead to environmental degradation and possibly endanger human health. It is important to adopt a smart waste management system in place to cope with a range of waste materials. This research aims to develop a smart modelling method that could accurately predict and forecast the production of municipal solid waste. An integrated convolution neural network and air-jet system-based framework developed for pre-processing and data integration were developed. The results showed that machine learning algorithms could be used to detect different types of waste with high accuracy. The best performers were obtained from neural network models, which captured 72% of the information variation. The method proposed in this study demonstrates the feasibility of developing tools to assist urban waste through the supply, pre-processing, integration, and modelling of data accessible to the public from a variety of sources.

INTRODUCTION

The World Bank study found that nearly 4 billion tonnes of solid waste are generated in the world every year, and only cities are the biggest contributors to this number, with waste expected to rise by 70 % by 2025 (Gupta et al. 1998). Researchers estimate that the accumulation of waste from the least developed countries will rise significantly over the next 25 years (Sharholi et al. 2008). With the growing number of businesses in the urban areas, solid waste disposal is becoming a big concern for the municipality. The principal method of waste disposal is landfill, which is inefficient and costly, and which pollutes the natural environment. For example, the landfill may cause health problems to the people living near the landfill site. Another traditional means of handling waste is burning waste, which contributes substantially to air pollution. Moreover, some compounds are combined to blend the air and cause cancer. Hence waste must be recycled to improve the air quality and protect the health of humans, and waste needs to be separated into various categories which can be recycled in different ways. This work addresses the present details on waste disposal selections at Dehra Dun Uttarakhand, and also the possible indirect and direct effect of waste control tasks on individual wellness, even though principal concentration is primarily on MSW. In India, the primary concern with garbage management is the filling of lands and

properties, with draining of wastes also being considered in some cases. The fact that there is evidence of negative health consequences to those living near landfill sites is one of the most significant effects of this entire review of the research. There are strong indications that germs originating in sewer treatment plants are more likely to cause gastrointestinal problems. For decades, the majority of waste produced on the earth has been steadily increasing, particularly in rich nations. Though information on waste sources can be dismal and unreliable, current estimates suggest that more than two billion tonnes of municipal solid waste (MSW) is generated globally each year. The amount of MSW produced in the OECD countries in 2006 was more than 620 million tonnes, or 580 pounds per person (Gupta et al. 2006). Huge quantities of wastes are generated in more complex nations like India, from industries and households, even though generation per capita is far less than $0.5 \text{ kg.day.capita}^{-1}$ in India, and remains comparatively small when compared to waste generation in OECD countries. (up to $2.1 \text{ kg.day.capita}^{-1}$ in the USA) (Rathi 2006). However, this overlooks the fact that cities generate a significant portion of MSW. The forecasts for China's municipal garbage generation were based on three distinct waste development scenarios (i.e., waste generation increasing slowly from $0.9 \text{ kg.day.capita}^{-1}$ to $1.2 \text{ kg.day.capita}^{-1}$ to $1.5 \text{ kg.day.capita}^{-1}$) (Kumar et al. 2017). Even if waste generation is very low, the total amount of MSW

generated in 2030 would be double that of the United States. Despite the fact that China's GDP growth rate is no longer double-digit, the international financial crisis is unlikely to have an impact on the countries' estimated waste generation. A number of high-profile and widely condemned pollution incidents involving improper waste management have caused people to be concerned about lack of controls, weak policies, environmental harm, and overall health impact. As a result of this positive effect, several federal governments have been forced to start a new regulatory strategy to manage hazardous, dangerous, and unsustainable waste management strategies. In Western nations, landfilling is still the most important disposal system. In 2000, in western Europe, around 18 percent of MSW was incinerated and 25% was recycled, while incineration and recycling accounted for around 6% and 9% in eastern and central Europe, respectively (Talyani et al. 2008). Hence, waste recycling in Western Europe is increasing (Talyan et al. 2008). As regulations are highly

effective and also landfilling is often an expensive choice, alternative ways are considered. The quantity of waste landfilled in the United Kingdom and Italy, for example, has decreased substantially.

In 1995, Italy and the United Kingdom both landfilled 93 % and 83% of MSW, respectively, but by 2005, the figures had dropped to 58 percent for Italy and 42 percent for the United Kingdom. The disposal of sewage sludge affects the environment as the sludge may contain harmful components such as pathogenic organisms, organic compounds, heavy metals, and excess phosphorus and nitrogen. Water that is discharged from factories, for example, can pollute rivers and lakes with substances like chemicals, waste, and dyes. This water pollution can kill wildlife and harm the overall ecosystem, and the effects of polluted water have left several plants and animal species endangered.

Table 1: State-wise waste generation in India.

State	Total waste generation TDP	Percentage of waste processing	Estimated per capita waste
Andaman & Nicobar	70	30%	0.45
Andhra Pradesh	5,980	8%	0.33
Arunachal Pradesh	110	15%	0.30
Assam	650	0%	0.13
Bihar	3,703	0%	0.28
Chandigarh	340	100%	0.30
Chhattisgarh	1,896	0%	0.27
Dadra & Nagar Haveli	35	0%	0.12
Daman & Diu	85	0%	0.25
Delhi	8,390	52%	0.46
Goa	183	25%	0.18
Gujarat	9,227	28%	0.31
Haryana	3,490	25%	0.33
Himachal Pradesh	300	20%	0.41
Jammu & Kashmir	1,792	2%	0.46
Jharkhand	3,750	0%	0.42
Karnataka	8,784	34%	0.33
Kerala	1,576	50%	0.07
Madhya Pradesh	5,079	12%	0.23
Maharashtra	26,820	10%	0.48
Manipur	176	50%	0.18
Meghalaya	268	58%	0.40
Mizoram	253	4%	0.40
Nagaland	270	0%	0.37
Odisha	2,460	2%	0.32
Puducherry	495	20%	0.52
Punjab	3,900	10%	0.34
Rajasthan	5,037	15%	0.26
Sikkim	49	0%	0.20
Tamil Nadu	14,532	15%	0.38
Telangana	5,520	18%	0.39
Tripura	407	0%	0.32
Uttar Pradesh	19,180	7%	0.39
Uttarakhand	1,013	0.5%	0.29
West Bengal	8,674	0%	0.27

Table 1 shows the statewide distribution of the waste generation in India. In India, around 8.8 million tonnes of sewer waste are implemented or removed each year, with approximately 60% of it being suitable for agricultural use (Patil & Shekdar 2001). Sewage sludge has potential fertilizer properties and can be used to enrich agricultural soils due to its high nitrogen, phosphorus, and organic matter content. Dried sludge is often used as manure. Sludge is nothing but accumulated solid content from the wastewater. It is often used as manure because those are biodegradable materials that are made mostly of food and human waste which acts as good manure for the plants. Therefore, sludge is often used as manures.

The types of waste control systems used in each country are usually based on financial considerations, but they also include different factors based on the type of waste to be disposed of. For example, if coal burning has been used to heat buildings and homes, large amounts of coal ash may be disposed of alongside additional municipal waste. Because coal ash contains high levels of metals and other toxins, ash when combined with urban waste in landfills may be difficult to eliminate. In addition, coal ash tends to make incineration more expensive. Thus it is very harmful to coal ash to be released into the environment. Spills of coal ash can pollute waterways, groundwater, drinking water, and the air. The number and types of categories into which wastes are divided usually depends on the collection system used and the final destination of the wastes. Waste separation at the source enables the removal of substances that are hazardous (inflammable, poisonous), that can which can be recycled, or composted. Effective segregation of wastes means that less waste goes to landfills which makes it cheaper and better for people and the environment. ... Segregated waste is also often cheaper to dispose of because it does not require as much manual or mechanical sorting as mixed waste. Hence, for the effective disposal and treatment methods of waste, knowing the composition of wastes is important.

PLASTIC WASTE SEPARATION METHODS

Direct Methods

The hydro-cyclone separates materials of various densities using centrifugal power. This method is often used to separate materials, such as acrylonitrile butadiene styrene, polyethylene high impact polystyrene, and polyvinyl chloride (Kannangara et al. 2018). Different types of variables affect the buoyancy of a particular material, such as thickness, shape, and separation level from other materials, and are used to separate other parts from MSW. In the process called jiggling, a water stream is pulsed, or moved by pistons upward and downward, through the material bed. Under the influence

of this oscillating motion, the bed is separated into layers of different densities, the heaviest concentrate forming the lowest layer and the lightest product the highest. Important to this process is a thorough classification of the feed since particles less than one millimeter in size cannot be separated by jiggling (Kontokosta et al. 2018). The waste is decomposed into small fragments and mixed with water. Air is dispersed into the mixture of water and waste mesh under high tension. The dispersed air is then moved into the lightness field under pneumatic tension. This permits the water-waste mixture's foam to expand outwards. The hydrophobicity of the attached plastic fragments binds them together.

Indirect Sorting

X-ray transmission (XRT) is a fast circuit arranging method that requires just a few milliseconds to capture X-ray images. A high-intensity beam of radiation is used by the imaging module. Once the material is assimilated, part of this beam is transferred to the identifier under the test material. To extract details about the atomic density of the material, the radiation detected by the indicator is dissected. Two types of X-ray sorting systems exist: Double x-ray energy (DE-XRT) and X-ray fluorescence (XRF) (Guo et al. 2020). The experience of XRF can be used to retrieve plastic waste fragments. Unfortunately, this process is only for recovering PVC from different types of plastic. The XRF approach is focused on the acceptance of individual molecules from an external laser source, which allows the release of X-ray photons (Abbasi & Hanandeh 2016). The emitted photons form a mark for atomic weight, which helps determine the type of material. The spectral signature of plastic is a superposition of the spectral signatures of parts that can be classified using ML. Another approach for sorting waste is Energy Dispersive X-ray fluorescence, which uses markers applied to the polymer structure to sort plastic particles. These marks are framed by a number of materials dispersed within the material, maximizing the polypropylene arrangement's selectivity (Adedeji & Wang 2019). The X-ray is focused on a small area of material and guided to the detector. The signal is then transferred from the identifier to the handling unit. The radiation source is monitored by this unit, whose spectral signature is dissected and used to distinguish materials with unique marker concentrations. Detecting dim polymers and grim waste with XRF is a non-destructive process.

Optical Based Sorting

For the most part, techniques use real characteristics while ignoring visual properties such as colour, patterns, surface, and scale while organizing waste. Optical sorting (sometimes called digital sorting) is the automated process of sorting solid products using cameras and/or lasers. Organizing methods

that rely on highlights such as form and concealment. This approach incorporates a 3D shading camera and a laser beam on the transportation axis. This method is known as triangulation checking because it creates triangles on the camera image of the fundamental laser beam. For the plastic segmentation, the technique achieves an accuracy of 99 percent. Ghostly imaging is a strategy based on phantom reflectance estimations and image handling procedures. There are a few unusual imaging techniques that use NIR (near-infrared), VIS (visual image spectroscopy), and HSI (hyperspectral imaging) (Srinilta & Kanharattanachai 2019). A hyperspectral sensor generates images on an infinite range of small spectral types, and the following framework investigates spectroscopic data (Gyawali et al. 2004). The transport system transfers tiny volumes of waste under the phantom camera, securing photos. The knowledge is pre-prepared and reduced in the accompanying point. An exceptional equation is then used to play out the material grouping. A swarm of packed air spouts is placed at the end of the transport line, and depending on the classifier's selection, one of the spouts is set off by loss-specific canisters (Ding et al. 2018). Waste control can also be achieved by the use of computerized logic. The recycling in the work is carefully designed by a major improvement in the neural network algorithm for the grouping of unique types of recyclable articles. In a layered organization, this new model has reduced the number of boundaries from 121 to about 3 million (Dixit & Vaze 2013). In previous studies, they proposed the concept of programmed recycling of plastic and metal waste in conjunction with another method

for monetary motivation of end-user works. The utilization of AI to characterize waste turned into the principal help for specialists. The prospects got by neural organizations in the field of picture arrangement and acknowledgment show that it is possible to assemble viable frameworks additionally in the field of waste determination, however, the intricacy of the entire framework should be rearranged.

WASTE SORTING METHODOLOGY

Plastic wastes can be segregated into different types once it has been separated from MSW using a computerized image processing method. The device we utilize has an RGB sophisticated camera and a computer with programming for the classification of heavy waste. Airflow, on the other hand, is used to transfer waste to a specified container, with the assumption that the waste can be sent separately through the conveyor belt. In the neural network image pre-processing, the object used in this framework uses image processing methods. To identify objects, deep learning methods are used.

The local arrangement of pixels is crucial for perceiving the shape of an object. CNN usually contains a convolving layer, a grouping layer, and a fully connected layer. The convolutional layer and grouping layer are stacked one on top of the other (Thanawala et al. 2020, Ma et al. 2020). Fig. 2 presents the CCN methodology used in MSW sorting.

Due to the small size of images, an approach for data enhancement was used for the pre-processing of images. This approach was chosen because of the different orientations of

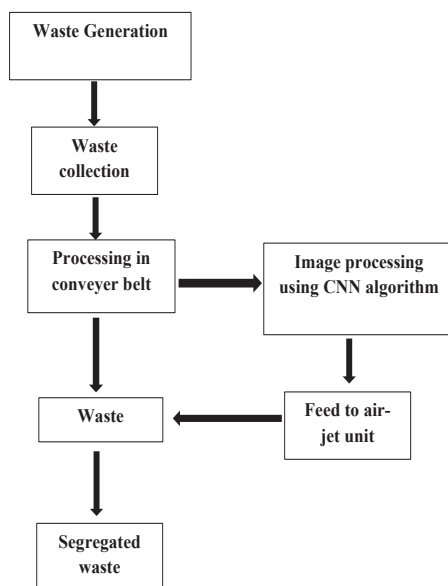


Fig. 1: Block diagram of the proposed technique for waste sorting.

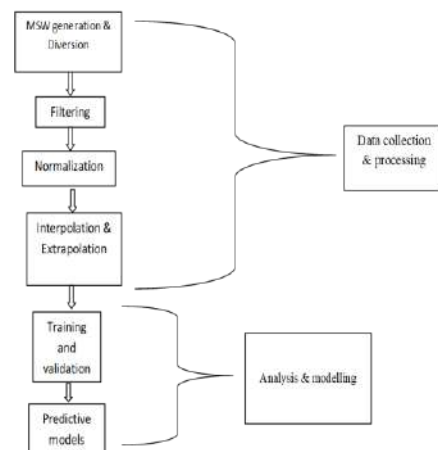


Fig. 2: The CNN methodology used in MSW sorting (Ma et al. 2020).

waste matters. Some of the approaches include a random selection from the image, translation of the image, random scaling of the image, and image sharing. This approach makes the dataset as large as possible. The described approach was updated based on the preformed model ResNet-50, and it is depicted in Fig. 1. Certain steps are involved with CNN layers, allowing it to classify the input images. The conversion layer convolves the input image using a set of 3x3 filter window sizes, which was chosen to differentiate artifacts in small and local features (Ikhlal 2018). The basic features and primitive characteristics are extracted from the input images and first layers respectively. Moreover, the complex layers and detailed features are extracted from the probability of loss function (Softmax function). The proposed model was built on the pre-formed ResNet-50 model, which was trained on ImageNet images with a resolution of 256x256 and classified into 1000 categories. As shown in Fig. 2, a preformed ResNet-50 model has been formed on the image data set, and a weight set has been acquired, but we removed the top classification layer by setting the include_top = False, only the feature is extracted from the network (Chu et al. 2018). The extracted features are fed to the multi-class SVM model, which performs classification based on the extracted features.

SVM can be utilized to resolve classification and regression problems. It is a machine learning technique and is considered one of the best classification algorithms. With this algorithm, the data article is plotted as a specific point in the n-dimensional space versus the characteristic standards of a particular coordinate. The objects in SVM can be classified depending on the hyperplane separation for each multidimensional data. We find the hyperplane where the minimum distance is greater for training data (Talyan et al. 2008).

$$\min_{\gamma, w, b} 1/2 \|w\|^2$$

$$\text{s.t } y^i(w^T x^{(i)} + b) \geq 1, i=1 \dots m \quad \dots(1)$$

Equation (1) shows the optimization of SVM. Here, w and b represent the parameters of the constraint function y^i . For example, $x^{(i)}$ is the i^{th} example of m . The nominal geometric margin of the training samples is also represented by m (Ibrahim et al. 2019). Following the identification of waste, the system's air jets start and separate the various types of waste using air blow. As a result, the entire system may be used to detect, identify, and segregate various types of wastes, and channel them into their respective slots.

RESULTS AND DISCUSSION

The research phase consists of few steps where the first

step is to identify the waste after collecting it. As the identification phase started a lot of complex algorithms come into operation. First, the image of the waste is captured, after that, the image is passed through algorithms to extract the information such as color gradient, edge detection output, RGB output, and OpenCV histogram. All the necessary outputs for this project are given below. As waste passes through the conveyor belt, the feed from the waste detecting unit is provided to the air-jet system, which can determine which type of waste is entering the system and how much air thrust is required to channelize the specific waste to its designated slot.

The CNN algorithm, which was used to detect and identify different types of wastes, was successful in identifying the different types of wastes, as shown in Fig. 3. The waste images are captured for edge detection in the detection process, which is a sophisticated method. The Canny edge filter or canny algorithm is used in the edge detection process. A wide range of information may be extracted from image data using edge detection, making it easier for the system to grasp what kind of material it is recognizing.

The Canny algorithm uses a Gaussian filter to smooth the image and to remove noises. It helps the viewers to understand the intensity gradient of the image. The gradient algorithm step identifies the edge intensity and direction by measuring the image using the edge detection operator. Edges correspond to a change of pixels' intensity. To identify this, a better procedure is to utilize filters that focus on the change in intensity for both the directions such as horizontal (x) and vertical (y). When the image is smoothed, the derivatives I_x and I_y w.r.t. x and y are calculated. It can be implemented by convolving I with Sobel kernels K_x and K_y , respectively:

$$K_x = \begin{pmatrix} -1 & 0 & 1 \\ -2 & 0 & 2 \\ -1 & 0 & 1 \end{pmatrix} \quad \dots (2)$$

$$K_y = \begin{pmatrix} 1 & 2 & 1 \\ 0 & 0 & 0 \\ -1 & -2 & 1 \end{pmatrix} \quad \dots (3)$$

Then the magnitude G and the slope θ of the gradient are calculated as follows.

$$|G| = \sqrt{(I_x^2 + I_y^2)} \quad \dots (4)$$

$$\theta(x,y) = \arctan(I_y/I_x) \quad \dots(5)$$

Overall, the canny algorithm helps to lower the error rate in the field of edge detection of image data. The edge detection of various types of waste is shown below where the canny algorithm successfully works. Fig. 4 shows the detected edge of the cardboard, glass, metal, paper, and plastic wastes.

The convolution neural network (CNN) has been applied to the sample data of the waste of different types to train the data set and provide a convenient conclusion for the system to recognize the type of waste that has been collected, the convolution neural network (CNN). CNNs are employed in image processing because of their high accuracy for classification and recognition since they create a hierarchical model of networks through which image data is processed

and exact outputs are produced. With an open CV histogram and RGB analysis, the processed output of municipal solid wastes such as cardboard, glass, metal, paper, and plastic are shown in Fig. 5

It should be understood from these outputs that it is possible to classify and identify different types of municipal solid wastes by using the CNN algorithm using this waste detection system. In an image processing context, the his-



Fig. 3: Sample waste data successfully detected by CNN algorithm.

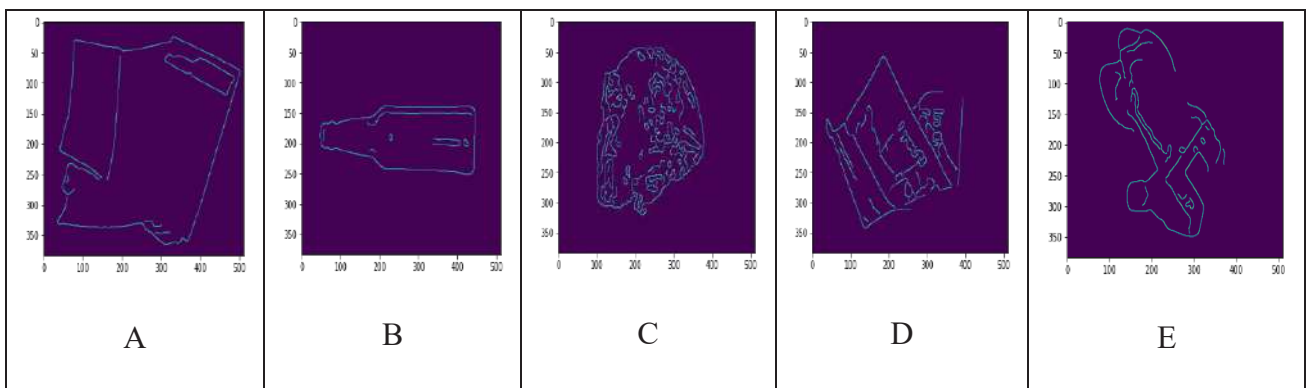
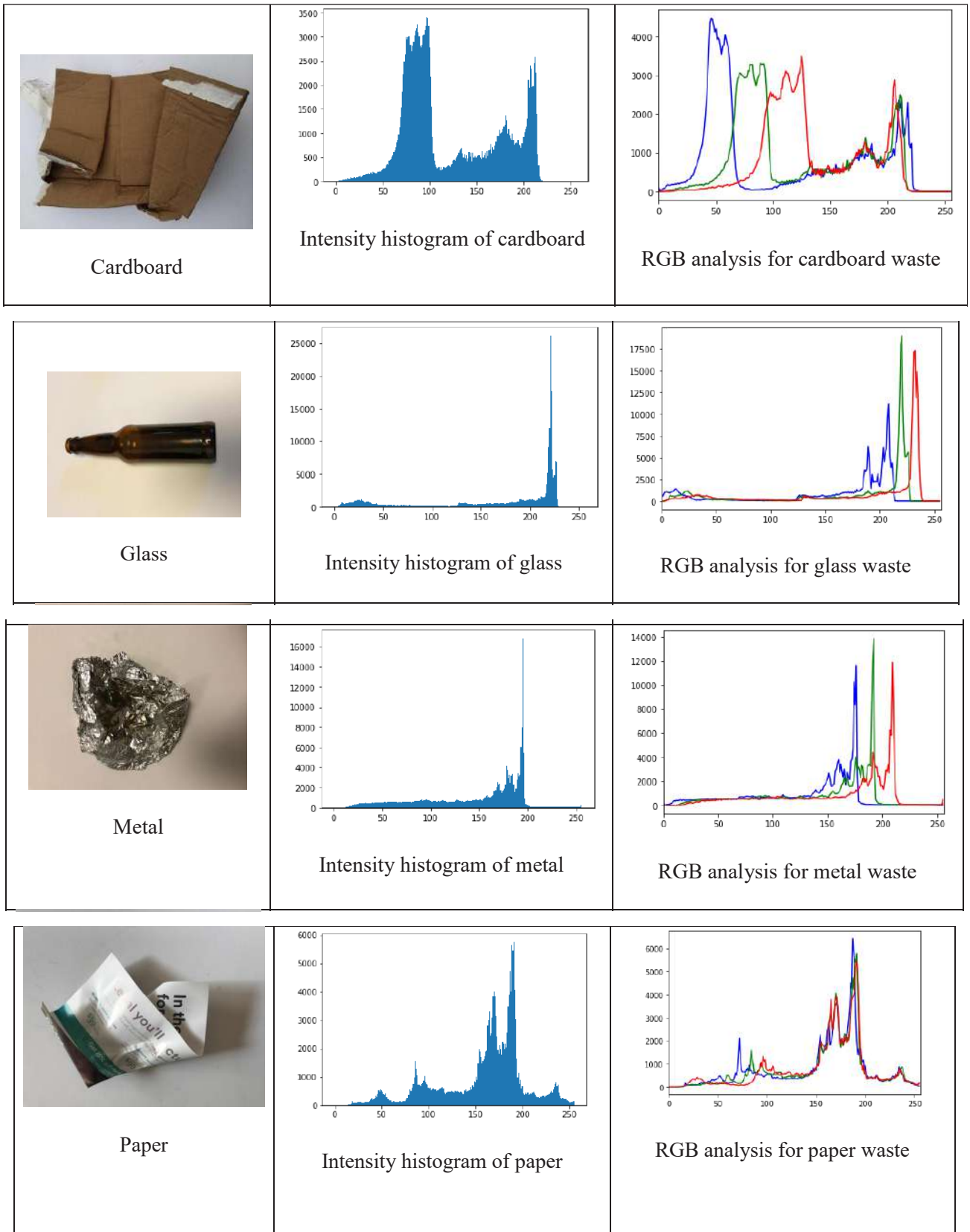


Fig. 4: Edge detection of (A) Cardboard, (B) Glass, (C) Metal, (D) Paper and (E) Plastic.



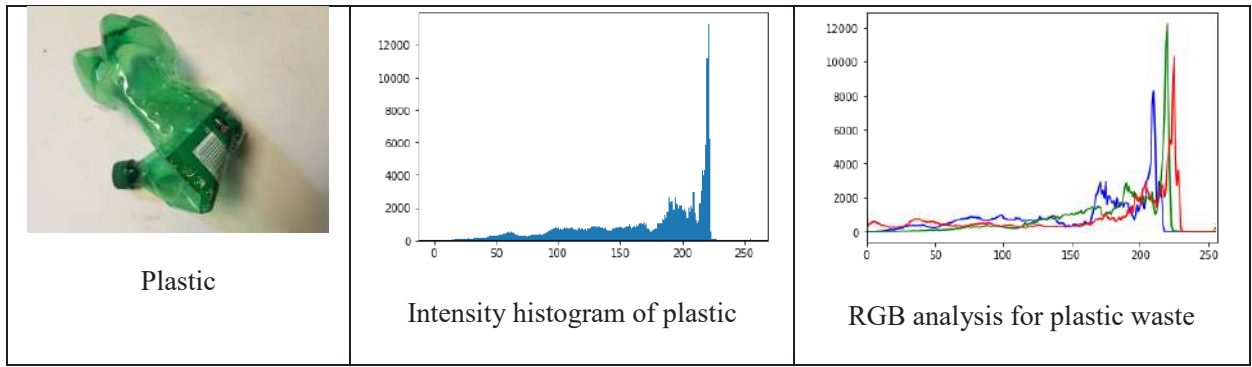
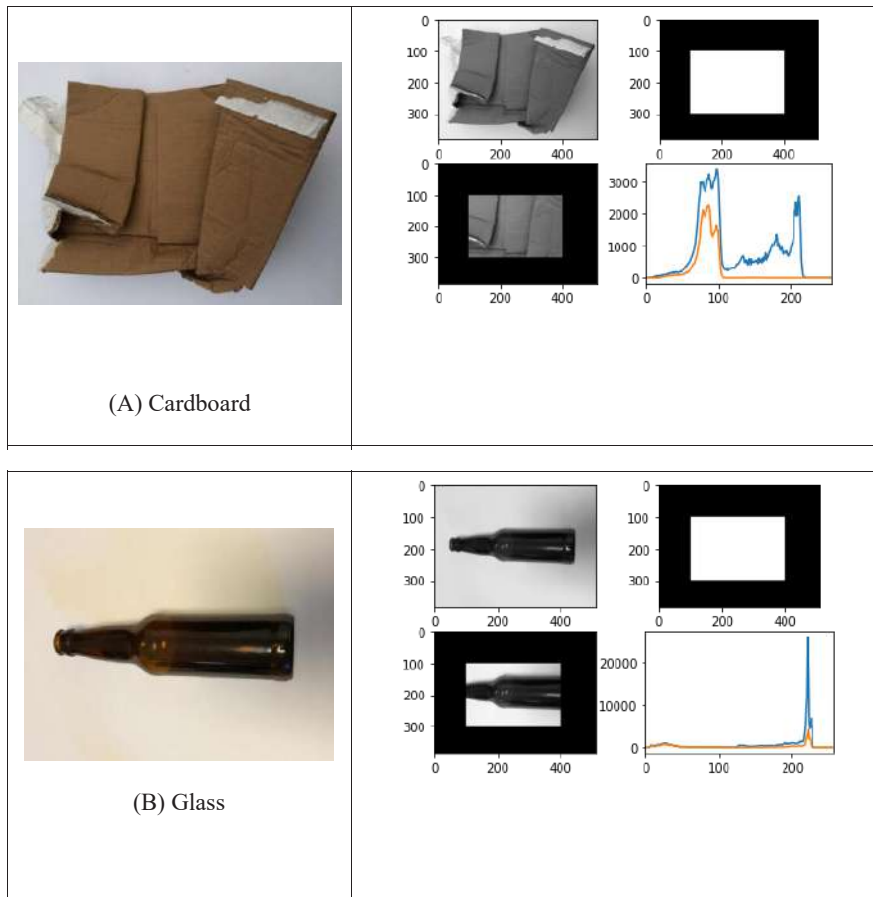


Fig. 5: List of different types of waste elements that have been analyzed for this paper with open CV histogram and RGB analysis.

ogram of an image normally refers to a histogram of the pixel intensity values. This histogram is a graph showing the number of pixels in an image at each different intensity value found in that image. The intensity histogram is a graphical representation of any object that allows us to understand how many different color values appear in an image or, in other words, it helps to know the intensity distribution of an image.

These histograms (Fig. 6) provide masked data of various kinds of wastes, which helps us and the proposed system to understand and identify the type of wastes and separating the wastes in a particular manner. Fig. 7 shows the detection accuracy plot of the applied technique.

This study has proved to be an effective solution for the detection and segregation of different types of wastes.



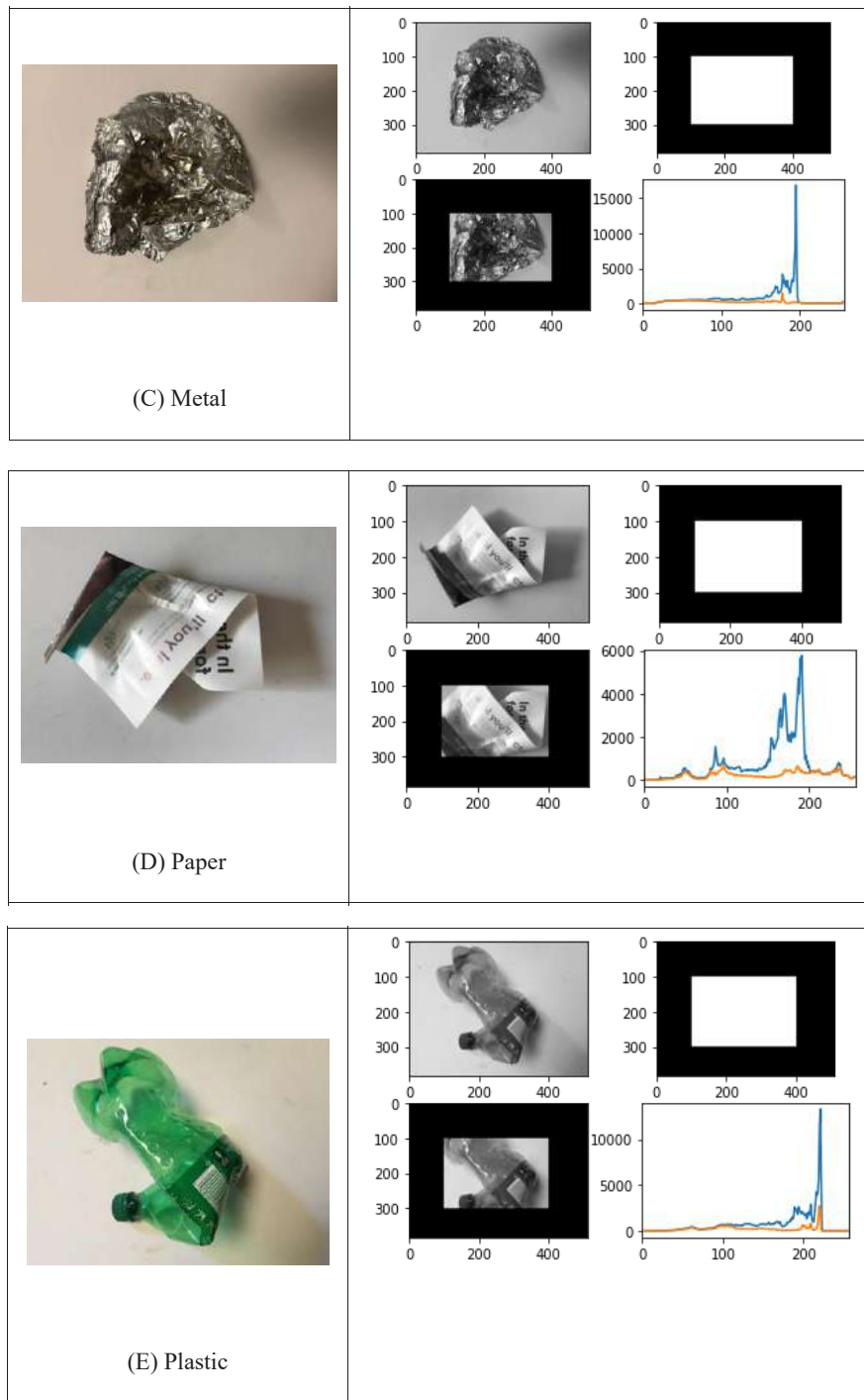


Fig. 6: Histogram with mask and without mask of different types of wastes (A) cardboard (B) glass (C) metal (D) paper (E) plastic.

Municipalities facing big challenges with solid waste management will quickly fix their issues by implementing this type of system where they only need to gather the waste from workers, while the majority of the waste segregating jobs would be handled automatically by this system. It will

allow municipalities to maintain clean and healthy cities.

CONCLUSIONS

In this study, we developed MSW generation and manage-

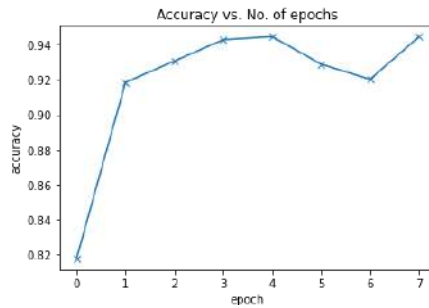


Fig. 7: Detection accuracy plot of the applied technique.

ment models to solve waste-related problems for Dehradun. The developed model is capable of detecting the MSW and can sort it by its form. CNN and decision tree AI algorithms were used to build the models. The neural network approach was based on unparalleled models than the choice tree approach. It rendered MSW detection models with a test data accuracy rate of 72%. Results demonstrate that given sufficient financial logical factors, AI techniques can deliver high precision for waste detection applications. The existing model for the identification of waste can be extended across India in light of the fact that the financial limits of the information can be defined using assessment information that is available to all regions in India.

The ability to predict waste generation allows municipalities to plan and maximize their waste management operations. The current research model could be used to identify waste automatically, reducing human work, and preventing diseases and pollution. With an accuracy of 87 percent, our model was validated against the waste data set. As a result, it delivers a more efficient and effective waste segregation approach that may be used with or without manual effort. If images are added to the informational index, the accuracy of the framework can be considerably improved. In general, we will improve our framework to include an option to classify and detect more waste items, by transforming a portion of the edges/boundaries used. Our future work will be focused to train the model using large sample data so that it can identify different types of waste materials with high precision.

ACKNOWLEDGEMENT

The authors would like to thank UPES Dehradun for facilitating the space to carry out the research work. Corresponding author thanks to Mr. Saikat Banerjee and Sourav Basu of CubicX India for the great support in terms of the data processing and analysis. Thanks to Dr. Sudhir Kumar Chaturvedi, Associate Professor, UPES Dehradun for the great support in drafting the manuscript. Also, thankful to Dr. Surya Prakash Tiwari, Assistant Professor, King Fahad

University of Petroleum & Minerals for the continuous help in the improvement of this paper.

REFERENCES

- Abbasi, M. and Hanandeh, A. 2016. Forecasting municipal solid waste generation using artificial intelligence modeling approaches. *Waste Manag.*, 56: 13-22.
- Adedeji, O. and Wang, Z. 2019. Intelligent waste classification system using deep learning convolutional neural network. *Procedia Manuf.*, 35: 607-612.
- Chu, Y. Huang, C. Xie, X., Tan, B., Kamal, S. and Xiong, X. 2018. Multilayer hybrid deep-learning method for waste classification and recycling. *Comput. Intell. Neurosci.*, 35: 194-198.
- Dixit, N. and Vaze, V. M. 2020. Waste separation of degradable solids using convolutional neural network (CNN). *Mukt Shabd J.*, 9(8): 1374-1376
- Ding, Z., Zhu, M., Tam, V.W., Yi, G. and Tran, C.N. 2018. A system dynamics-based environmental benefit assessment model of construction waste reduction management at the design and construction stages. *J. Cleaner Prod.*, 176: 676-692.
- Guo, H.N., Wu, S.B., Tian, Y.J., Zhang, J. and Liu, H.T. 2020. Application of machine learning methods for the prediction of organic solid waste treatment and recycling processes: A review. *Bioresour. Technol.*, 11: 124-134.
- Gupta, S., Mohan, K., Prasad, R., Gupta, S. and Kansal, A. 1998. Solid waste management in India: Options and opportunities. *Resour. Conserv. Recycl.*, 24(2): 137-54.
- Gyawali, D., Regmi, A., Shakya, A., Gautam, A. and Shrestha, S. 2004. Comparative analysis of multiple deep CNN models for waste classification. *arXiv*, 2004: 21
- Ikhlayel, M. 2018. Development of management systems for sustainable municipal solid waste in developing countries: A systematic life cycle thinking approach. *J. Cleaner Prod.*, 180: 571-86.
- Ibrahim, K., Savage, D.A., Schirel, A., Intrevado, P., and Interian, Y. 2019. ContamiNet: Detecting contamination in municipal solid waste. *Comput. Vis. Pattern Recognit.*, 28: 1-8.
- Kumar, S., Smith, S.R., Fowler, G., Velis, C., Kumar, S.J., Arya, S., Rena, K. R. and Cheeseman, C. 2017. Challenges and opportunities associated with waste management in India. *Royal Soc. Open Sci.*, 4(3): 160-174.
- Kannagara, M., Dua, R., Ahmadi, L. and Bensebaa, F. 2018. Modeling and prediction of regional municipal solid waste generation and diversion in Canada using machine learning approaches. *Waste Manag.*, 74:3-15.
- Kontokosta, C.E., Hong, B., Johnson, N.E. and Starobin, D. 2018. Using machine learning and small area estimation to predict building-level municipal solid waste generation in cities. *Comput. Environ. Urban Syst.*, 70:151-62.

- Ma, S., Zhou, C., Chi, C., Liu, Y. and Yang, G. 2020. Estimating physical composition of municipal solid waste in China by applying artificial neural network method. *Environ. Sci. Technol.*, 54(15): 9609-9617.
- Patil, A.D. and Shekdar, A.V. 2001. Health-care waste management in India. *J. Environ. Manag.*, 63(2): 211-20.
- Rathi, S. 2006. Alternative approaches for better municipal solid waste management in Mumbai, India. *Waste Manag.*, 26(10): 1192-200.
- Sharholly, M., Ahmad, K., Mahmood, G. and Trivedi, R.C. 2008. Municipal solid waste management in Indian cities—A review. *Waste Manag.*, 28(2): 459-67.
- Srinilta, C. and Kanharattanachai, S. 2019. Municipal Solid Waste Segregation with CNN. In 2019 5th IEEE International Conference on Engineering, Applied Sciences and Technology (ICEAST) China, 2-5 July 2019, Luang Prabang, Laos, pp. 465-491.
- Talyan, V., Dahiya R.P. and Sreekrishnan, T.R. 2008. State of municipal solid waste management in Delhi, the capital of India. *Waste Manag.*, 28(7): 1276-1287.
- Thanawala, D., Sarin, A. and Verma, P. 2020. An Approach to Waste Segregation and Management Using Convolutional Neural Networks. International Conference on Advances in Computing and Data Sciences, Singapore.



Adsorption Behavior of Hydroquinone by Diatomite-based Porous Ceramsite

Ruqin Gao*, Lu Pan*, Yingrui Huang*, Zhaoyang Wu**† and Bingtao Liu*

*School of Environmental and Municipal Engineering, North China University of Water Resources and Electric Power, Zhengzhou 450046, China

** Zhengzhou Institute of Multipurpose Utilization of Mineral Resources, CAGS, Zhengzhou 450006, China

†Corresponding author: Zhaoyang Wu; wzy500@sina.com

Nat. Env. & Poll. Tech.
Website: www.neptjournal.com

Received: 16-07-2020

Revised: 13-12-2020

Accepted: 26-05-2021

Key Words:

Diatomite-based porous ceramsite
Hydroquinone
Adsorption kinetics
Moving-boundary model
Liquid film diffusion

ABSTRACT

Diatomite-based porous ceramsite is a new kind of environmental material. In this study, ceramsite was prepared by wet grinding, a rolling-ball method, and high temperature-calcination using diatomite as the main raw material with the addition of a pore-forming agent and sintering assistant. X-ray diffraction, scanning electron microscopy, and mercury injection, were used to analyze the structure and characteristics of the prepared materials. Using hydroquinone as the target pollutant, the adsorption behavior of diatomite-based porous ceramsite was investigated. Results indicated that the diatomite-based porous ceramsite had a pore size ranging from 500 to 3000 nm, a specific surface area of $6.14 \text{ m}^2 \cdot \text{g}^{-1}$, and a porosity of 47.8%. When pH was 7, the removal rate and adsorption capacity of the hydroquinone by the diatomite-based porous ceramsite was 91.2% and $4.56 \text{ m}^2 \cdot \text{g}^{-1}$, respectively. In the adsorption process of hydroquinone by diatomite-based porous ceramsite, the diffusion of a liquid membrane was dominant, which could be better described by the quasi-first-order kinetic equation. The Langmuir and Koble-Corrigan equations had a higher fitting degree of data for the adsorption isotherms. The adsorption characteristics of the diatomite-based porous ceramsite are in accordance with the fixed-point adsorption of a single molecular layer and belong to a heterogeneous composite adsorption system. The correlation coefficient R^2 and k value of hydroquinone adsorption by the diatomite-based porous ceramsite determined by the liquid film diffusion model were 0.848 and 0.0417, respectively.

INTRODUCTION

Diatomite is unicellular algal debris that is deposited in the ocean or lakes and can form diatomite. Diatomite is a non-metallic porous mineral that has a small density, a large specific surface area, good adsorption properties, is chemically stable, and has pores with the size of 50 - 800 nm (Iuchaurroudo et al. 2016, Zahra et al. 2018, Tan et al. 2018, Font et al. 2018). Hydroquinone is an important chemical raw material and chemically synthesized intermediate that is widely used in photographic developer, antioxidants, and synthetic ammonia co-solvents in rubber. Hydroquinone is an important organic pollutant that is highly toxic and difficult to degrade. It can be easily oxidized into benzoquinone which is more toxic to the central nervous system and liver in humans. It is also one of the main pollutants in industrial wastewater which can cause great harm to organisms and the environment (Ergürhan et al. 2018, Yıldız et al. 2005, Xu et al. 2019, Li et al. 2013).

Ceramsite is a new type of porous material that has a small bulk density, high porosity, good chemical and thermal stability, can be easily regenerated at low cost with good mechanical strength. Ceramsite can be made of clay, sludge,

or fly ash that is mixed with sintering aids and pore-forming agents. These are ground, balled, and calcined at high temperature, and are widely used in construction materials, sewage treatments, the petrochemical industry, and gardening (Chen et al. 2010, Qin et al. 2015, Che et al. 2018, Li et al. 2019, Wang et al. 2019a, Wu et al. 2016, Podder & Majumder 2016). In this study, diatomite-based porous ceramsite was prepared and its adsorption effect on hydroquinone was elucidated. The results provide a theoretical basis for exploring the efficient utilization of diatomite, the optimal allocation of resources, and the sustainable development of the environment.

MATERIALS AND METHODS

Material and Reagent

Diatomite was produced by Linjiang Beifeng Diatomite Company, Jilin Province, (The mass fractions of main compositions included: 70.38% SiO_2 , 2.37% Al_2O_3 , 1.42% K_2O , and 10.58% CaO). The pore-forming agent was carbon powder, provided by Nanjing Greifa Carbon Material Company; Bauxite powders (325 mesh), $\text{Al}_2\text{O}_3 \geq 65\%$, was produced by Yangquan Haotianwei Refractory Company;

Quartz was purchased from the Xinhui Mining Processing Plant in Lingshou County, China, and feldspar was obtained from Yantai Yitao Mining Company. The aforementioned raw materials were industrially pure. The analytically pure sodium silicate was used as a dispersant obtained from Beijing Tongguang Fine Chemical Company, and the analytically pure hydroquinone was purchased from Qingdao Yousuo Chemical Technology Company.

Sample Preparation and Characterization

Diatomite, the pore-forming agent, sintering aid, water, and dispersant (a mass ratio of 82: 6: 18: 120: 2), were added to the ball mill with a grinding medium (ZrO₂ ceramic ball with $\phi \approx 8$ mm) and ground for 20 min. The materials were then put into an oven and dried at 105°C. The diatomite-based porous ceramsite was obtained by dispersing, rolling, and calcining in a box resistance furnace at 1020°C for 2 h.

A Japan JSM-6490LV SEM was employed to observe the micromorphology of the ceramsite. The pore size distribution of samples was detected using an American Auto Pore IV 9500 mercuryporosimeter. An ultraviolet-visible spectrophotometer produced by LAMBDA of PerkinElmer Company in the United States was used to detect the absorbance of hydroquinone wastewater at 288 nm. The pH value of hydroquinone wastewater was measured with JY-pH 2.0 pH agent (Shimazu, Japan). The porosity of diatomite-based porous ceramsite was determined using the Archimedes method.

Adsorption Experiment

In this experiment, 1g of the diatomite-based porous ceramsite was placed into a 150 mL conical flask, and 50 mL of hydroquinone solution at a concentration of 50 mg.L⁻¹ was added. The conical flask was sealed and placed into a constant temperature shaking table for shaking. The pH was adjusted to 2-9 with 0.1 mol.L⁻¹ HCl or NaOH solution (25°C, 120 r.min⁻¹, 24 h). After the supernatant was filtered by a 0.45

µm membrane filter, its absorbance was measured to be 288 nm using an ultraviolet spectrophotometer. According to the Lambert-Beer law, if the absorbance of the maximum wavelength of a solution has a good linear relationship with the concentration of the solution, so the adsorption q_e and the removal rate r of hydroquinone can be calculated from the absorbance.

$$r = \frac{(C_0 - C_e)}{C_0} \times 100\% \quad \dots(1)$$

$$q_e = \frac{V \times (C_0 - C_e)}{m} \quad \dots(2)$$

Where: C_0 is the concentration of hydroquinone before adsorption (mg.L⁻¹); C_e represents the concentration of hydroquinone at adsorption equilibrium (mg.L⁻¹); m is the mass of adsorbent (g); V is the volume of solution (L).

Establishment of Adsorption Kinetic, Adsorption Thermodynamic and Dynamic Boundary Models

Adsorption kinetics, adsorption thermodynamic, and dynamic boundary models (Li et al. 2015, Jing et al. 2018, Zhu et al. 2016, Duan et al. 2011, Qu et al. 2018, Cheng et al. 2017, Chiara et al. 2019) of diatomite-based porous ceramsite to hydroquinone are listed in Tables 1-3 respectively.

RESULTS AND DISCUSSION

Micromorphology of the Diatomite-based Porous Ceramsite

Fig. 1 shows the SEM image of the diatomite-based porous ceramsite. The diatomite particles basically maintain the original pore structure (The small holes are distributed in the plate-shaped particles). Due to high-temperature calcination, the smaller holes on the diatomite particles disappear. The plate-shaped particles and tiny particles (sintering aids and pore-forming agents) are stacked to form a large gap. A large

Tables 1: Adsorption kinetics of diatomite-based porous ceramsite to hydroquinone.

Models	Equations
Quasi-first-order kinetic model	$q_t = q_e (1 - e^{-k_1 t})$
Quasi-second-order kinetic model	$q_t = \frac{k_2 q_e^2 t}{(1 + k_2 q_e t)}$
Elovich model	$q_t = a + k \ln t$
Double-constant model	$q_t = e^{(a+k \ln t)}$

Where q_t (mg.g⁻¹) is the adsorption capacity at the time of t , q_e (mg.g⁻¹) is the adsorption capacity at equilibrium; C_e and C_t (µmol.L⁻¹) represent the adsorption concentrations at equilibrium and t , respectively; K and k_0 denote the adsorption rate constant and a is the remaining constant.

Tables 2: Adsorption thermodynamics of diatomite-based porous ceramics to hydroquinone.

Models	Equations
Langmuir adsorption isotherm	$q_e = \frac{q_m k_L C_e}{1 + k_L C_e}$
Toth adsorption isotherm	$q_e = \frac{q_m C_e}{(k_{Th} + C_e)^i}$
Redlich-Peterson adsorption isotherm	$q_e = \frac{AC_e}{1 + BC_e^g}$
Koble-Corrigan adsorption isotherm	$q_e = \frac{AC_e^n}{1 + BC_e^n}$

Where q_e ($\text{mg}\cdot\text{g}^{-1}$) is the adsorption capacity at equilibrium, q_m ($\text{mg}\cdot\text{g}^{-1}$) is the maximum adsorption capacity; C_e represents the concentration of adsorbate in the solution at equilibrium; k_L is the Langmuir isotherm constant (related to the energy of adsorption); k_F stands for the Freundlich isotherm constant (related to adsorption capacity and strength of adsorbents); k_{Th} is the Toth isotherm constant.

Tables 3: Dynamic boundary model of diatomite-based porous ceramics to hydroquinone.

Models	Equations
Liquid film diffusion	$\ln(1-F) = -k_t$
Intragranular diffusion	$1 - 3(1-F)^{2/3} + 2(1-F) = k_t$
Chemical reaction	$1 - (1-F)^{1/3} = k_t$

Where, F is the adsorption fraction at time t , $F = qt/q_e$; k (min^{-1}) is the rate constant.

number of three-dimensional pores form an organic hole between the aggregated particles and the particles.

Pore Structure Characteristics of the Diatomite-based Porous Ceramsite

The pore diameter distribution curves of the diatomite-based porous ceramics (Fig. 2) are mainly concentrated at 500 to 3,000 nm. The results of the pore size distribution, porosity, and specific surface area of the diatomite-based porous ceramics (before and after toner addition) by the mercury injection are displayed in Table 4. It can be seen, after adding

the toner, the pore size is widely distributed, the specific surface area is larger, and the porosity is higher. Thus the adsorption capacity of the material is greatly improved.

Effect of pH on the Adsorption of Hydroquinone by the Diatomite-based Porous Ceramsite

Fig. 3 illustrates the effect of pH on the adsorption of hydroquinone by the diatomite-based porous ceramics. When the pH is in the range of 2-7, the adsorption capacity and removal rate of the hydroquinone by the diatomite-based porous

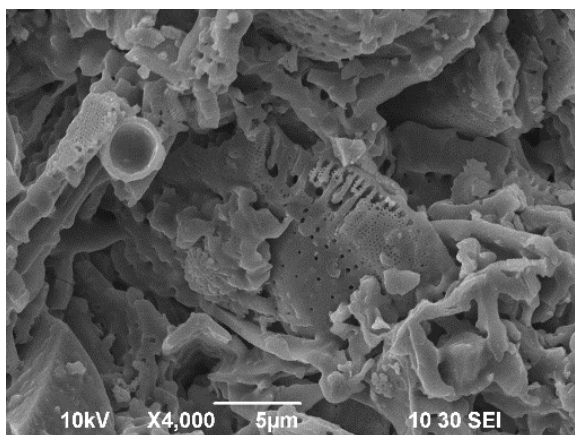


Fig. 1: SEM micrographs of the diatomite-based porous ceramics.

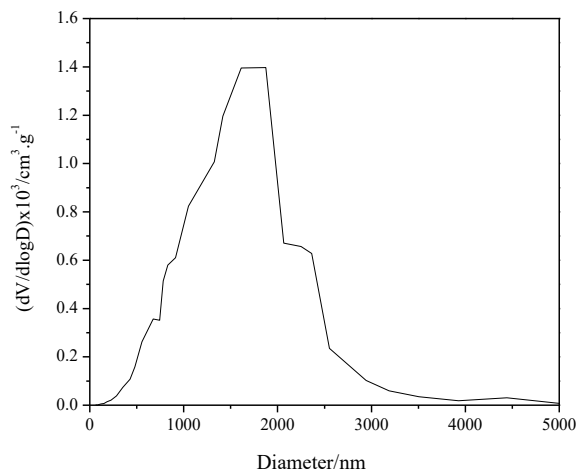


Fig. 2: Pore size distribution of the diatomite-based porous ceramics.

Table 4: Pore size distribution, porosity, and specific surface area of the diatomite-based porous ceramsite.

Pore structure index	Specific surface area ($\text{m}^2 \cdot \text{g}^{-1}$)	Mean pore diameter (nm)	Pore size distribution (nm)	Porosity (%)
No carbon powder	3.21	723.4	460~1800	23.7
With carbon powder	6.14	1493.8	500~3000	47.8

ceramsite increase with increasing pH. When the pH is 7, the removal effect is most efficient. The adsorption capacity and removal rates are $4.56 \text{ mg} \cdot \text{g}^{-1}$ and 91.2%, respectively. When the pH is greater than 7, the adsorption capacity of the diatomite-based porous ceramsite to hydroquinone decreases significantly. This may be due to the degree of dissociation of hydroquinone being lower under acidic conditions. With an increase in pH, the degree of dissociation of hydroquinone increases, which is conducive to adsorption. In the alkaline environment, the hydroxyl group of hydroquinone is further dissociated. The hydrogen bond between the hydroquinone and the solvent water takes up too many adsorption sites, which leads to a decrease in the removal rate of hydroquinone by the diatomite-based porous ceramsite. Therefore, the pH value of the solution was adjusted to 7 in subsequent experiments.

Adsorption Kinetic Analysis

According to the equations in Table 1, the non-linear kinetic adsorption models such as the quasi-first-order dynamic model, the quasi-second-order kinetic model, the Elovich model, and the double-constant model were respectively fitted. The non-linear kinetic adsorption of hydroquinone by the diatomite-based porous ceramsite is illustrated in Fig. 4, and the relevant parameters are shown in Table 5.

Fig. 4 shows that the adsorption process of hydroquinone

by the diatomite-based porous ceramsite occurs in two stages. The adsorption capacity increases rapidly in the range from 0 to 120 min. When t is 120 min, the adsorption capacity reaches $4.35 \text{ mg} \cdot \text{g}^{-1}$. After 120 min, the adsorption capacity increases slowly and gradually become stable. Finally, at 1,440 min, the adsorption capacity reaches $4.4 \text{ mg} \cdot \text{g}^{-1}$. This is because in the first stage, there is a large number of adsorption sites on the surface of ceramsite, and the adsorption amount increases rapidly. In the second stage, hydroquinone in the solution occupies a large number of adsorption sites on the surface of ceramsite, resulting in slow adsorption. According to Table 1, the correlation coefficient ($R^2 = 0.979$) of the quasi-first-order kinetic equation is greater than that of the quasi-second-order kinetic equation ($R^2 = 0.953$), the Elovich model, and the double constant.

The adsorption process of hydroquinone by the diatomite-based porous ceramsite can be accurately demonstrated by quasi-first-order and quasi-second-order kinetic equations. The quasi-first-order kinetic model is based on the assumption that the adsorption process is controlled by diffusion steps. The quasi-second-order kinetic model is based on the assumption that the adsorption rate is controlled by the chemical adsorption mechanism. The quasi-second-order kinetic model includes all adsorptions, such as liquid film diffusion, intraparticle diffusion, and chemical adsorption (Zhang et al. 2018, Pholosi et al. 2020). The adsorption of

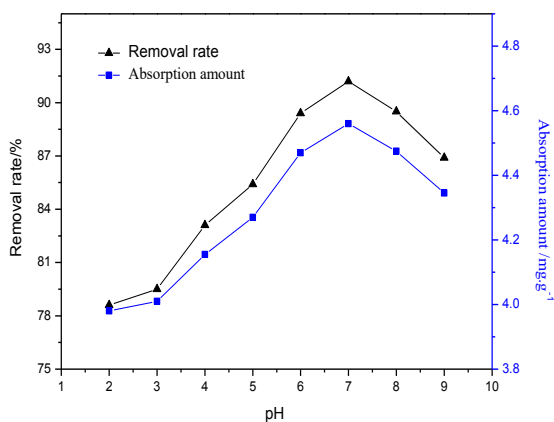


Fig. 3: Effect of pH on adsorption of the diatomite-based porous ceramsite.

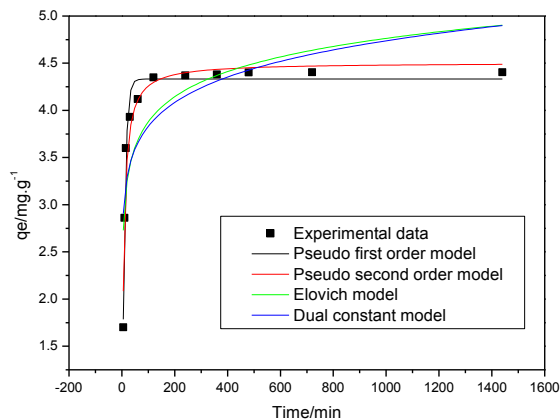


Fig. 4: Nonlinear dynamic fitting curve.

hydroquinone by the diatomite-based porous ceramicsite is dominated by liquid film diffusion. The quasi-first-order kinetic model can describe the whole adsorption process and is, therefore, more accurate in describing the adsorption process of hydroquinone by the diatomite-based porous ceramicsite.

Adsorption Thermodynamic Analysis

The adsorption isotherm equations (Langmuir, Koble-Corrigan, Toth, and Redlich-Peterson) were used to fit the experimental data of the adsorption of hydroquinone by the diatomite-based porous ceramicsite (Cui et al. 2019, Mudzielwana et al. 2019, Raganati et al. 2018, Lonappana et al. 2018, Wang et al. 2019b). The fitting results are shown in Fig. 5, and the fitting parameters are summarized in Table 6.

From Fig. 5 and Table 6, the Langmuir and Koble-Corrigan equations can well fit the data of the adsorption isotherm. The Langmuir equation is an adsorption isothermal model based on single molecular layers, that is, adsorption only occurs on the outer surface of the adsorbent. The Koble-Corrigan equation can be used to present the composite adsorption system of uniform adsorption and uneven adsorption, which shows that the adsorption process is more complex and related to the porous composite characteristics of ceramicsite. The adsorption characteristics of diatomite-based porous ceramicsite conform to the fixed-point adsorption of a single molecular layer. Each active adsorption site on the ceramicsite only adsorbs one molecule, and there is no transfer or interaction between single molecules adsorbed on the site. The

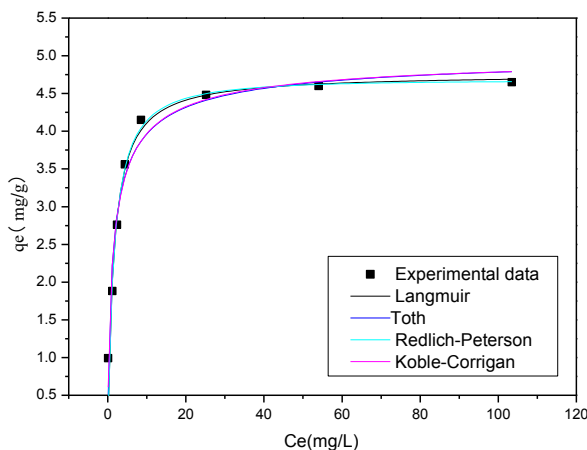


Fig. 5: Thermodynamic nonlinear fitting diagram.

Table 5: The fitting parameters of the kinetic adsorption model.

Kinetic model	Pseudo-first-order model			Pseudo-second-order model		
HQ	R^2 0.979	q 4.33256	k 0.10615	R^2 0.953	Q 4.50573	K 0.03816
Kinetic model	Elovich model			Double-constant model		
HQ	R^2 0.669	a 2.10892	k 0.38423	R^2 0.603	a 0.91768	k 0.09233

Table 6: Fitting parameters of the thermodynamic model of adsorption.

Model	Langmuir model			Toth model				
HQ	R^2 0.9503	q 4.7608	k 0.63128	R^2 0.944	q 5.0735	k 0.775	t 0.6494	
Model	Koble-Corrigan model			Redlich-Peterson model				
HQ	R^2 0.9535	a 3.5976	b 0.7152	n 0.7181	R^2 0.9406	A 2.8528	B 0.5756	g 1.0100

maximum adsorption capacity is a fixed value. Meanwhile, the adsorption on the surface of ceramsite is heterogeneous and belongs to a heterogeneous composite adsorption system.

Dynamic Boundary Analysis

A Dynamic boundary model can be used to describe the adsorption behavior of porous adsorbents. The adsorption process on the surface of the diatomite-based porous ceramsite is divided into three steps: 1) liquid film diffusion, 2) intragranular diffusion, 3) adsorption chemical reaction on the active groups inside the particles. According to Table 1, the linear fitting of the dynamic boundary model is shown in Fig. 6, and the fitting parameters are summarized in Table 7.

From the fitting parameters in Table 7, the liquid film diffusion model exhibits a higher fitting degree for

the adsorption of hydroquinone by the diatomite-based porous ceramsite with a correlation coefficient $R^2 = 0.848$, followed by the fitting degrees of the internal diffusion model of particles, and the chemical reaction model, which indicated that the adsorption rate of hydroquinone on the surface of ceramsite is mainly controlled by the liquid film diffusion (Hosokawa et al. 2018, Sun et al. 2017). This data demonstrated that the adsorption mechanism of hydroquinone by diatomite-based porous ceramsite is mainly through micropores on the ceramsite surface and the charge adsorption on the material surface (Jegasothy et al. 2004, Sun et al. 2018, Li et al. 2018). The K value can be used to measure the speed of adsorption. The K value of the liquid film diffusion model is 0.04173, which is much larger than that fitted by the intragranular diffusion and chemical

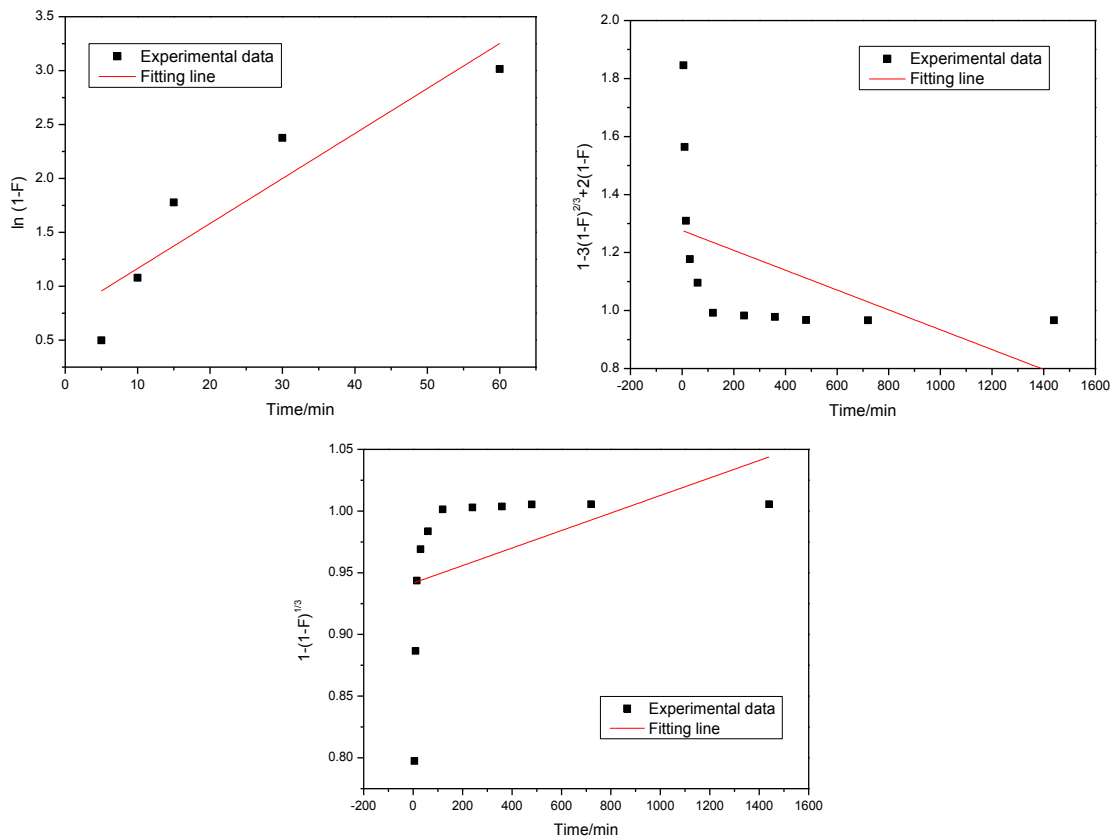


Fig. 6: The fitting lines of dynamic boundary models on the diatomite-based porous ceramsite.

Table 7: The fitting result of the dynamic boundary model.

Fitting parameters	Liquid film diffusion	Intragranular diffusion	Chemical reaction
k	0.04173	0.00193	0.00164
R^2	0.84775	0.17884	0.13333

reaction models. These results indicated that the liquid film diffusion is relatively rapid in the adsorption process, while the intragranular diffusion and chemical reactions are relatively slow in the adsorption process.

CONCLUSION

Diatomite-based porous ceramsite has a high porosity, a specific surface area, and a better adsorption performance for hydroquinone. When the pH is 7, the removal rate and adsorption capacity of hydroquinone in the sample can reach 91.2% and 4.56 mg.g⁻¹, respectively. The quasi-first-order kinetic, and the quasi-second-order kinetic equations have a high fitting degree for the adsorption data of the diatomite-based porous ceramsite. The diffusion of the liquid films dominates the adsorption process of hydroquinone by ceramsite and the quasi-first-order kinetic equation is more accurate. The Langmuir and Koble-Corrigan equations can well fit the adsorption isotherm data. The adsorption characteristics of the diatomite-based porous ceramsite conform to the fixed-point adsorption of a single molecular layer. The adsorption on the surface of ceramsite is heterogeneous and seen as a heterogeneous composite adsorption system. The fitting results of the dynamic boundary model and the experimental data indicated that the liquid film diffusion model has a high fitting degree for the adsorption process of hydroquinone by the diatomite-based porous ceramsite, with a correlation coefficient of $R^2 = 0.848$ and adsorption rate of $k = 0.04173$. The adsorption mechanism of hydroquinone by the diatomite-based porous ceramsite mainly occurs in the micropores on the ceramsite surface, and the charge adsorption on the material surface.

ACKNOWLEDGEMENTS

This work was financially supported by the National Natural Science Foundation of China (Grant no. 51378205), the Science and Technology Department, Henan Province (Grant no. 182102311080), and a Special project of geological and mineral evaluation of China Geological Survey (Grant no. YMZB-2017014F).

REFERENCES

- Che, T.K., Pan, B.F. and Jian, O.Y. 2018. The laboratory evaluation of incorporating ceramsite into HMA as fine aggregates. *Constr. Build Mater.*, 186: 1239-1246.
- Chen, Y.C., Shi, J.W., Rong, H., Zhou, X., Chen, F.Y., Li, X.L., Wang, T. and Hou, H.B. 2010. Adsorption mechanism of lead ions on porous ceramsite prepared by co-combustion ash of sewage sludge and biomass. *Sci. Total Environ.*, 702: 135017.
- Cheng, S., Zhang, L.B., Xia, H.Y., Peng, J.H., Shu, J.H., Li, C.Y., Jiang, X. and Zhang, Q. 2017. Adsorption behavior of methylene blue onto wasted rived adsorbent and exhaust gases recycling. *RSC Adv.*, 7: 27331-27341.
- Chiara, G., Panayiotis, T., Chanan, E., Rachel, P., David, A.D., Tod, P., David, P., Georg, H. and Angelos, M. 2019. Adsorption behavior of organic molecules: a study of benzotriazole on Cu (111) with spectroscopic and theoretical methods. *Langmuir*, 35(4): 882-893.
- Cui, Z.X., Gan, J.Z., Xue, Y.Q., Zhang, J., Zhang, R., Liu, J.Y. and Hao, J. 2019. Adsorption selectivity of cubic nano-CeO₂ and effect of particle size on adsorption thermodynamics. *Fluid Phase Equilib.*, 502: 112277.
- Duan, L.H., Guo, Y.S. and Yang, J.Q. 2011. Study on the effect of a magnetic field on Pb(II) removal using modified chitosan. *Adv. Chem. Eng. Sci.*, 2: 101-107.
- Ergürhan, O., Parlak, C., Alver, O. and Senyel, M. 2018. Conformational and electronic properties of hydroquinone adsorption on C₆₀ fullerenes: Doping atom, solvent, and basis set effects. *J. Mol. Struct.*, 1167: 227-231.
- Font, A., Soriano, L., Reig, L., Tashima, M., Borrachero, M.V., Monzó, J. and Payá, J. 2018. Use of residual diatomaceous earth as a silica source in geopolymer production. *Mater. Lett.*, 223: 10-13.
- Hosokawa, S., Hayashi, K. and Tomiyama, A. 2018. Evaluation of adsorption of surfactant at a moving interface of a single spherical drop. *Exp. Therm. Fluid Sci.*, 96: 397-405.
- Iuchaurroudo, N., Font, J., Ramos, C. P. and Haure, P. 2016. Natural diatomites: Efficient green catalyst for Fenton-like oxidation of orange. *Appl. Catal. B: Environ.*, 181: 481-494.
- Jegasothy, S., Slatara, N.K.H., Denecker, C., Sherrington, D.C., Leic, Z. and Sutherland, A.J. 2004. Kinetics of oxidation of hydroquinone by polymer-supported hypervalent iodine oxidant, iodoxybenzoic acid. *Chem. Eng. J.*, 105: 1-10.
- Jing, Q.X., Wang, Y.Y., Chai, L.Y., Tang, C.J., Huang, X.D., Guo, H., Wang, W. and You, W. 2018. Adsorption of copper ions on porous ceramsite prepared by diatomite and tungsten residue. *Trans. Non-ferrous Met. Soc. China*, 28: 1053-1060.
- Li, G. T., Feng, Y. M. and Chai, X. Q. 2015. Equilibrium and thermodynamic studies for adsorption of 1, 4- Benzoquinone by fly ash. *Nat. Environ. Pollut. Technol.*, 14: 865-869.
- Li, L. L., Fan, L. L., Sun, M., Qiu, H. M., Li, X. G., Duan, H. M. and Luo, C. N. 2013. Adsorbent for hydroquinone removal based on graphene oxide functionalized with magnetic cyclodextrin-chitosan. *Int. J. Biological Macromolecules*, 58: 169-175.
- Li, T. T., Liu, Y. M., Wang, T., Wu, Y. L. and He, Y. L. Yang, R. and Zheng, S. R. 2018. Regulation of the surface area and surface charge property of MOFs by multivariate strategy: Synthesis, characterization, selective dye adsorption, and separation. *Micropor. Mesopor. Mat.*, 272: 101-108.
- Li, X., Shi, X.S., Yang, Z.M., Xu, X.H. and Guo, R.B. 2019. Effects of recyclable ceramsite as the porous bulking agent during the continuous thermophilic composting of dairy manure. *J. Cleaner Prod.*, 217: 344-351.
- Lonappana, L., Rouissia, T., Brara, S.K., Vermab, M. and Surampallic, R.Y. 2018. An insight into the adsorption of diclofenac on different biochars: Mechanisms, surface chemistry, and thermodynamics. *Bioresour. Technol.*, 249: 386-394.
- Mudzielwana, R., Gitari, M.W. and Ndungu, P. 2019. Performance evaluation of surfactant modified kaolin clay in As(III) and As(V) adsorption from groundwater: adsorption kinetics, isotherms, and thermodynamics. *Heliyon*, 5: e02756.
- Pholosi, A., Naidoo, E.B. and Ofomaja, A.E. 2020. Intraparticle diffusion of Cr(VI) through biomass and magnetite coated biomass: A comparative kinetic and diffusion study. *S. Afr. J. Chem. Eng.*, 32: 39-55.
- Podder, M.S. and Majumder, C.B. 2016. Sequestering of As(III) and As(V) from wastewater using a novel Neem leaves/MnFe₂O₄ composite biosorbent. *Int. J. Phytoremediat.*, 18: 1237-1257.
- Qin, J., Cui, C., Cui, X. Y., Hussain, A. and Yang, C. M. 2015. Preparation and characterization of ceramsite from lime mud and coal fly ash. *Constr. Build Mater.*, 95: 10-17.

- Qu, J.L., Li, Q., Luo, C., Cheng, J. and Hou, X.M. 2018. Characterization of flake boron nitride prepared from the low-temperature combustion synthesized precursor and its application for dye adsorption. *Coatings*, 8(6): 214.
- Raganati, F., Alfe, M., Gargiulo, V., Chirone, R. and Ammendola, P. 2018. Isotherms and thermodynamics of CO₂ adsorption on a novel carbon-magnetite composite sorbent. *Chem. Eng. Research. Des.*, 134: 540-552.
- Sun, S., Chen, L.Y., Sun, H.L. and Zha, T.Y. 2018. Adsorption and charge transfer of lithium at electrified graphene/electrolyte interface. *Electrochim. Acta.*, 259: 1089-1094.
- Sun, X.L., Wang, Z.G. and Fu, Y.Q. 2017. Adsorption and diffusion of sodium on graphene with grain boundaries. *Carbon*, 116: 415-421.
- Tan, G.Q., Wu, Y., Liu, Y. and Xi, D. 2018. Removal of Pb(II) ions from aqueous solution by manganese oxide coated rice straw biochar – A low-cost and highly effective sorbent. *J. Taiwan Inst. Chem. Eng.*, 84: 85-92.
- Wang, H.Y., Wang, B.D., Li, J.H. and Zhu, T.L. 2019. Adsorption equilibrium and thermodynamics of acetaldehyde/acetone on activated carbon. *Sep. Purif. Technol.*, 209, 535-541.
- Wang, X.K., Zheng, G.D., Chen, T.B., Nie, E. Q., Wang, Y.W., Shi, X.X. and Liu, J.W. 2019. Application of ceramsite and activated alumina balls as recyclable bulking agents for sludge composting. *Chemosphere*, 218: 42-51.
- Wu, H. M., Fan, J.L., Zhang, J., Ngo, H.H., Guo, W. S., Liang, S., Lv, J.L., Lu, S.Y., Wu, W.Z. and Wu, S.Q. 2016. Intensified organics and nitrogen removal in the intermittent-aerated constructed wetland using a novel sludge-ceramsite as substrate. *Bioresour. Technol.*, 210: 101-107.
- Xu, C., Jiang, L., Qin, X.L., Jin, C., Liu, L.J., Yu, S. and Xian, M. 2019. Enhancement mechanism behind the different adsorptive behaviors of nitro/amine modified hyper crosslinked resins towards phenols. *J. Taiwan Inst. Chem. Eng.*, 102: 340-348.
- Yıldız, N., Gönülşen, R., Koyuncu, H. and Çalimli, A. 2005. Adsorption of benzoic acid and hydroquinone by organically modified bentonites. *Colloids Surf. A: Physicochem. Eng. Aspects*, 260: 87-94.
- Zahra, A., Jamshid, E.L., Jamil, K. and Robab, H.L. 2018. Properties of sustainable cement mortars containing a high volume of raw diatomite. *Sust. Mater. Technol.*, 16: 47-53.
- Zhang, L.K., Liu, X.Y., Wang, W.D., Li, Y.M., Sun, P., Shang, S.P. and Jiang, Q.H. 2018. Characteristics and mechanism of lead adsorption from aqueous solutions by oil crops straw-derived biochar. *Trans. Chin. Soc. Agric. Eng.*, 34: 218-226.
- Zhu, J., Wang, P., Lei, M.J., Zhang, W.L. and Chen, Y. 2016. Composite modification of diatomite and its adsorption characteristic of Cd²⁺ in aqueous solutions. *Acta Sci. Circum.*, 36: 2059-2066.



Spatiotemporal Evolution and Pattern Differences of Environmental Sanitation Facilities in Rural China: Taking the Improvement of Water and Latrines as an Example

Xinjie Deng†

Yiwu Industrial and Commercial College, Yiwu Zhejiang 322000, China

†Corresponding author: 24250987@qq.com

Nat. Env. & Poll. Tech.
Website: www.neptjournal.com

Received: 01-02-2021

Revised: 25-04-2021

Accepted: 28-04-2021

Key Words:

Rural sanitation facilities
Spatiotemporal evolution
Improvement of latrines
GWR model

ABSTRACT

Based on the panel data of water and latrine improvement in rural China from 2003 to 2016, this paper explores the spatiotemporal evolution pattern of rural sanitation facilities and analyzes the spatial heterogeneity of influencing factors of rural sanitation facilities by using the Geographically Weighted Regression (GWR) model. The conclusions are as follows: the gap between the western and the eastern regions of China is gradually narrowing; the spatial differences of rural environmental sanitation facilities in provinces were obvious, showing high-high and low-low agglomeration types. Additionally, years of education per capita, population density, and government investment all have a significant positive impact on the improvement of water and latrines. And the proportion of the minority population has a significant negative impact on the improvement of water. The net income per capita, traffic density, and residential investment per capita are significantly positively correlated with the improvement of water and latrines. But the difference is that the impact on the improvement of water is an obviously east-west band and decreases successively, and the impact on the improvement of latrines shows a dual pattern of polarization between north and south.

INTRODUCTION

The lack of environmental health services in rural areas is an important cause of the health inequality between urban and rural residents, which will have an important impact on the development of rural human capital, and may lead to the further expansion of the income gap between urban and rural areas. Rural environmental sanitation differs due to differences in geographic environment, natural endowments, and socio-economic conditions. Therefore, clarifying the conditions of rural environmental sanitation facilities and the influencing factors of their spatial differentiation has important theoretical and practical value for formulating differentiated policies to promote the equalization of environmental sanitation public services.

The research on rural environmental sanitation facilities has always been a hot topic of continuous research in various countries. The initial research contents included the investigation on the status quo of rural environmental sanitation facilities (Tao 2009), health impact (Miao 2008, Andres et al. 2017, Jalan & Ravallion 2003, Zhang 2012), willingness to pay for improvement (Abramson et al. 2011, Miao et al. 2012) and equity research (Yang et al. 2013, Phansalkar 2007). Later, studies involving regional differences or spatial distribution of rural environmental

sanitation facilities gradually emerged. Some scholars used the method of statistical description to reveal the provincial differences between rural drinking water and sanitary latrines and the correlation between them and socioeconomic development (Wenjie 2019). Subsequently, the geographic information system (GIS) and spatial analysis methods were gradually applied to the study. Scholars either included environmental sanitation facilities in public services (Ma et al. 2011), physical capital (Liu et al. 2017), or human settlement environment indicators (Zhu et al. 2015) to analyze their spatial differentiation pattern and agglomeration trend or analyze the spatially related characteristics and causes of a certain type of environmental sanitation facilities (Wan et al. 2010).

The existing results provide an important theoretical basis and methodological reference for further research. However, the rural environmental sanitation facilities as a whole are rarely studied. Moreover, GIS and spatial analysis methods overemphasize the content of geographic maps, exaggerate the existing problems, and do not fully reflect the real situation such as influencing factors (Lejano 2008). However, the geographically weighted regression (GWR) model can reflect the spatial differences of the influencing factors of the research objects, which takes both influencing

factors and spatial characteristics into account. In addition, in terms of model construction and data, scholars either used time series or panel data for global regression, often ignoring the existence of spatial nonstationarity, or the GWR model was used to process the spatial cross-section data, ignoring the time dimension. Based on the “individual effect” analysis of the spatial panel data of water and latrine improvement in 30 provinces in China from 2003 to 2016, this paper uses the GWR model to analyze the economic, geographical and social factors affecting the environmental sanitation facilities, and explores the spatiotemporal differentiation characteristics and influencing factors of the environmental sanitation facilities in rural China. This enriches the spatial analysis methods of related research, and in practice provides a basis for policymaking to improve the level of environmental sanitation public services in rural areas.

MATERIALS AND METHODS

This paper conducts an empirical study on the panel data of 420 observational values from 2003 to 2016 in 30 provinces of China (except Tibet, and not including Hong Kong, Macao, and Taiwan). Data was obtained from China Statistical Yearbook, China Rural Statistical Yearbook, China Health Statistical Yearbook, China Environmental Statistical Yearbook, China Population, and Employment Statistical Yearbook, and China Transport Statistical Yearbook. Missing data was supplemented by the trend extrapolation method. The name, unit, and statistical description of each variable are shown in Table 1. The abbreviation for the variable is in parentheses.

Spatial autocorrelation analysis: When there is a potential interdependence between the observed data of some variables in the same distribution region, the spatial autocorrelation method can be used for spatial analysis. Based on the spatial

autocorrelation model, this paper analyzes the spatial agglomeration characteristics of water and latrine improvement in 30 provinces of China. Spatial autocorrelation analysis includes two aspects, one is global spatial autocorrelation analysis. It is used to test whether there is a correlation among neighboring provinces. Moran's I index can be used to analyze the study area, and its formula is,

$$I = \frac{n}{\sum_i \sum_j W_{ij}} \cdot \frac{\sum_i \sum_j W_{ij} (x_i - \bar{x})(x_j - \bar{x})}{\sum_i (x_i - \bar{x})^2} \quad \dots(1)$$

Here, n is the number of provinces, and W_{ij} is the spatial adjacent weight matrix of i and j of each province in China. When the two are adjacent, W_{ij} is 1; otherwise, it is 0. And x_i is the mean of the observed value of i province. At a given significance level, Moran's I is greater than 0, indicating a positive correlation. Otherwise, it indicates a negative correlation. The higher the value is, the higher the correlation degree is, and vice versa. Moran's I equal zero means the distribution is random.

The second is the local spatial autocorrelation analysis. This analysis method can be used to test the degree of spatial correlation and spatial difference of the study area. In this paper, the Moran scatter plot is used to measure the spatial local correlation. Its formula (Anselin 1995) is as follows,

$$I_i = \frac{(x_i - \bar{x}) \sum_j W_{ij} (x_j - \bar{x})}{\sum_i (x_i - \bar{x})^2 / n} \quad \dots(2)$$

Geographically Weighted Regression (GWR) model:

GWR model is an extension of the ordinary linear regression model and a new method used to study the complexity, autocorrelation, and variability of spatial data. Its purpose is to explore the influence of independent variables on dependent variables with spatial changes. Fotheringham et al. (1998) embedded the spatial position of the data into the regression parameters and performed point-by-point parameter estima-

Table 1: Variable statistics and variable description.

Variables	Unit	Mean	Std. dev.	Min	Max
Cumulative benefit rate of water improvement (Benefit_water)	%	93.92	7.605	55.41	100
Cumulative benefit rate of latrine improvement (Benefit_latrine)	%	64.30,	18.30	21.50	99.80
Net income per capita (NIPC)	Yuan per person	6949	4339	1565	26000
Years of education per capita (YEPC)	Year	7.380	0.688	5.139	9.304
Population density (PD)	People.km ⁻²	207.8	149.6	3.973	734.6
Traffic density (TD)	km.km ⁻²	0.682	0.474	0.0310	2.184
Cumulative investment in water improvement per capita (Invest_water)	Yuan per person	785.0	1123	0	8755
Cumulative investment in latrine improvement per capita (Invest_latrine)	Yuan per person	84.47	115.9	0	590.6
Cumulative residential investment per capita (CRIPC)	Yuan per person	3471	3382	73.38	21000
Annual average temperature (AAT)	Centigrade	14.52	5.072	4.300	25.40
Annual precipitation in major cities (APMC)	Mm	909.2	528.1	0	2940
The proportion of minority population (PMP)	%	12.36	15.85	0.260	59.52

tion using the locally weighted least square method. It should be pointed out that the weight here is the distance function between the geospatial position of the regression point and the geospatial position of other observation points. The regression coefficient changes with the change of the spatial position, and the formula are as follows (Cui et al. 2012):

$$y_{it} = \alpha_i + \beta_0(u_i, v_i) + \sum_{k=1}^n \beta_k(u_i, v_i) X_{ikt} + \varepsilon_{it} \quad \dots(3)$$

In the formula, y_{it} is the cumulative benefit rate of water or latrine improvement in each province every year; α_i represents the individual fixed effect vector. The subscript i of all variables represents the individual and t represents the time. Symbol (u_i, v_i) is the coordinate of i province, and $\beta_k(u_i, v_i)$ is the regression coefficient of the k variable of i province. X_{ikt} is the explanatory variable matrix, and ε_{it} is the error term, obeying the normal distribution with constant variance. Since spatial panel data is used in this paper, each variable has two attributes of both time dimension and space dimension.

With regard to the selection of explanatory variable X_{ikt} in the GWR model, existing literature has emphasized the socio-economic and cultural factors at the family level (Cheng & Wang 2006), while this paper mainly discusses the geographical environment and socio-economic factors at the regional level. Some scholars have proposed that income, the proportion of ethnic minorities, education level, and average temperature in winter will affect the local environmental sanitation level (Miao & Chen 2016), and government investment in environmental sanitation facilities also plays a decisive role (Peng & Lu 2010). In addition, since this paper focuses on the spatial heterogeneity of rural environmental sanitation facilities, the spatial network characteristics of

population distribution and roads are the most obvious. Therefore, they are included in the explanatory variable of the GWR model in this paper. Taking into account China's special national conditions, the distribution characteristics of rural sanitation facilities, and the availability of data, this article finally selects 9 indicators including net income per capita, years of education per capita, population density, traffic density, government investment in water improvement (or latrine improvement) per capita, cumulative investment per capita in residential buildings, annual average temperature, annual precipitation in major cities, and proportion of ethnic minority populations as explanatory variables.

RESULTS AND DISCUSSION

Spatiotemporal changes of rural water and latrines in

China: According to the natural discontinuity method, the coverage rate of water improvement and latrine improvement is divided into four levels: low, lower, higher, and high. For comparison of water improvement, two time sections in 2005 and 2014 were taken. While for comparison of latrine improvement, two time sections in 2005 and 2016 were taken, as shown in Fig. 1 and Fig. 2. In terms of water improvement, Beijing, Tianjin, and Shanghai are at a high level all the time. Hebei, Shandong, Jiangsu, and Guangxi were upgraded from a higher level to a high level. Heilongjiang, Jilin, Hubei, and Jiangxi rose from a higher level to a high level. The western provinces of Xinjiang, Gansu, and Inner Mongolia saw a rapid increase in the benefit rate of water improvement. From the perspective of latrine improvement, the provinces with a high level of benefit of latrine improvement have moved from the central and eastern regions to the eastern coastal areas.

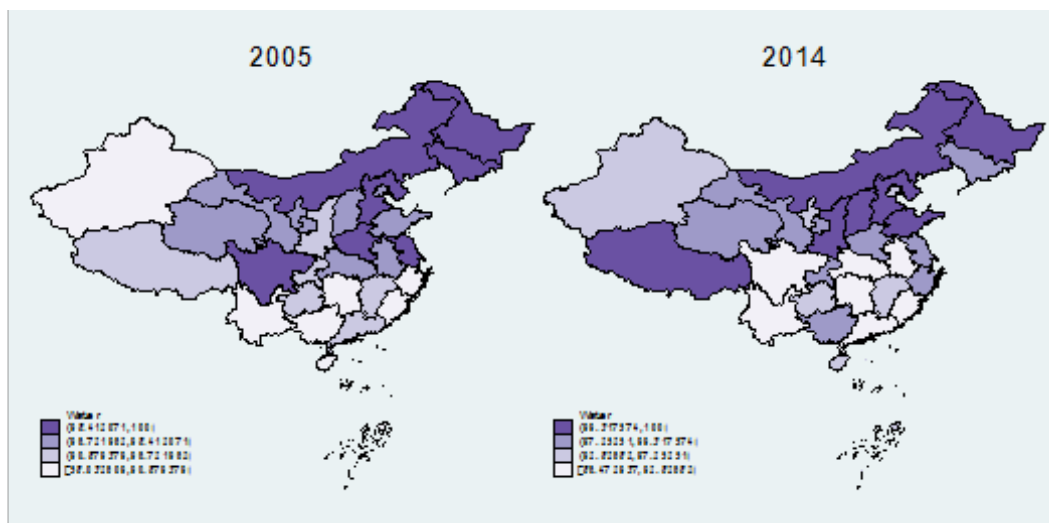


Fig. 1: Spatial evolution of water improvement in rural China in 2005 and 2014.

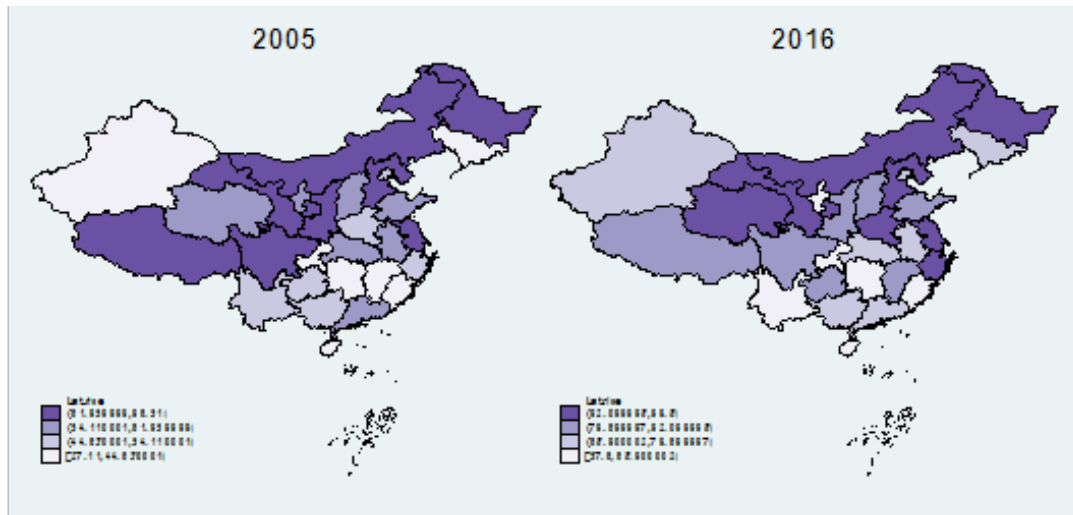


Fig. 2: Spatial evolution of latrine improvement in rural China in 2005 and 2016.

The specific performance is: Hubei, Jiangxi, and Guangxi have been reduced from high-level to higher-level areas; Three provinces of Guangdong, Fujian, and Jiangsu have been upgraded from high-level to higher-level areas; The three municipalities, Shandong and Zhejiang have always been at a high level. Generally speaking, the provinces with higher coverage of rural sanitation facilities in China are located in the northeast and eastern coastal areas, and the rural sanitation facilities in the central provinces are divided. The provinces in the western region are currently at the same level as the central provinces with rapid progress, and the gap with the eastern provinces is gradually narrowing.

Spatial autocorrelation analysis: The global autocorrelation index Moran's I of water improvement in 2014 and latrine improvement in 2016 was calculated using Stata13 software, global autocorrelation model, and formula (1).

The values are 0.25 and 0.35, and the significance levels are 0.01 and 0.001, respectively. $Z(I)$ is also greater than the critical value of 2.58. This indicates that there is a spatial correlation between rural environmental sanitation facilities in China. Global Moran's I can examine the overall relevance of space, but it will cover up its local spatial heterogeneity (Whittington et al. 1993). While local Moran's I scatter plot can reveal the differences in regional economic development. Therefore, local Moran's I scatter plots of water improvement in 2005 and 2014 and latrines improvement in 2005 and 2016 (Fig. 3 and Fig. 4) were extracted in this paper to explore the spatial relevance and development imbalance of local environmental sanitation in rural China.

According to Moran's I scatter plot, the spatial correlation degree of environmental sanitation facilities between a province and its neighboring provinces can be divided

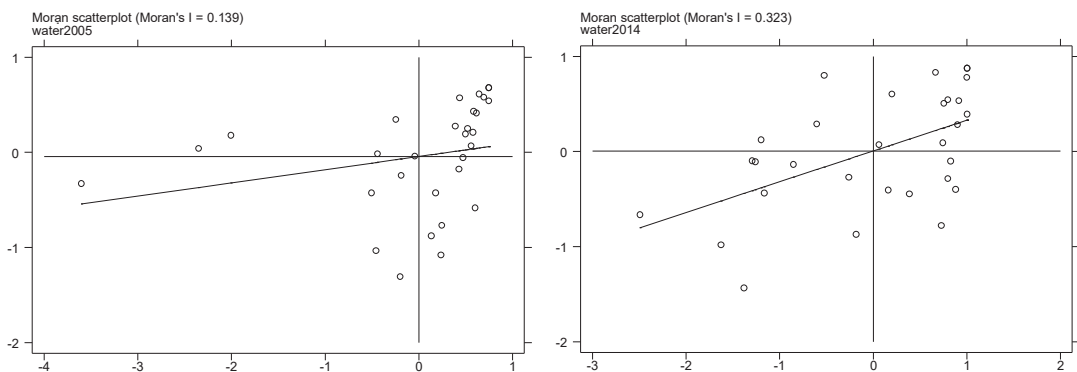


Fig. 3: Local Moran's I scatter plot of rural water improvement in China in 2005 and 2014.

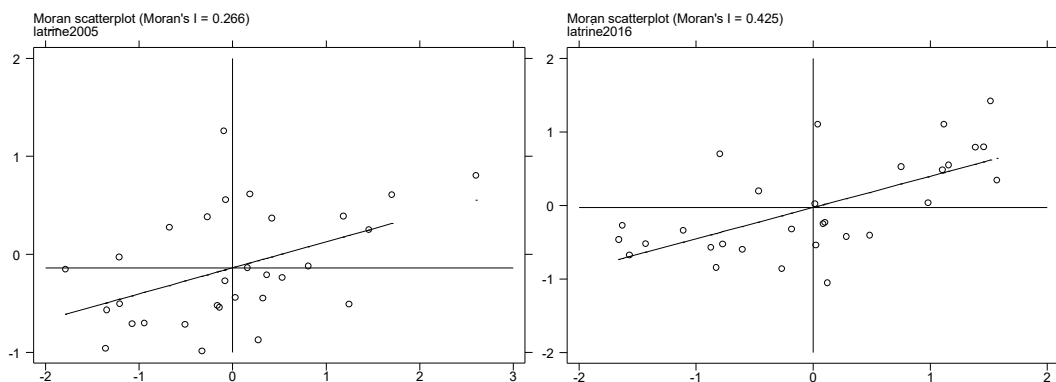


Fig. 4: Local Moran's I scatter plot of latrine improvement in rural China in 2005 and 2016.

into four types. In the first quadrant, the spatial difference is small, and the coverage rate of environmental sanitation facilities is high, which belongs to the “high-high (H-H)” type. In the third quadrant, the spatial difference is small, and the coverage rate of environmental sanitation facilities is low, which belongs to the “low-low (L-L)” type. In the second quadrant, there is a large spatial difference between a province and its neighboring provinces. The province itself has a high coverage rate of environmental sanitation facilities, while the neighboring provinces have a low coverage rate, which belongs to the “high-low (H-L)” type. In the fourth quadrant, there is also a large spatial difference between a province and its neighboring provinces, and the province itself has a low coverage rate, while the neighboring provinces have a high coverage rate, which belongs to the “low-high (L-H)” type. As can be seen from Fig. 3, the number of regions distributed in the first quadrant is highly dense in both time sections. That is, the H-H type occupies the superiority in quantity, but the intensity is reduced to a certain extent. And the distribution location is no longer so concentrated. The number of regions in the third quadrant begins to increase. This indicates that the gap between the eastern and western regions of rural water reform has been alleviated, but it still cannot change the dual pattern. As can be seen from Fig. 4, the number of areas distributed in the first and third quadrants shows an increasing trend. In conclusion, rural environmental sanitation facilities in China show agglomeration characteristics, which is consistent with the analysis results of the spatiotemporal evolution.

Analysis of influencing factors of the spatial distribution of rural environmental sanitation facilities: Through the above autocorrelation analysis, rural environmental sanitation facilities in China have spatial autocorrelation and significant regional differences. To further explore its formation mechanism, this paper uses the GWR model to analyze its influencing factors by using provincial spatial

panel data of rural environmental sanitation facilities in China from 2003 to 2016.

Considering the reference frame, mixed regression was first carried out, and the regression results are shown in the OLS model in Table 2. Due to the different conditions of each province, there may be missing variables that do not change over time, so the fixed-effect (FE) model is considered. The output also contains an F -test with the null assumption that the individual effect u_i for all provinces is 0. Since the p -value of the regression results of fixed effect of water and latrine improvement is 0.000 in F -test, the null hypothesis is strongly rejected. That is, the individual effect of provinces exists, and mixed regression should not be used. Although the above results have basically confirmed the existence of individual effects in provinces, individual effects may still exist in the form of random effects (RE). After the regression results of the random effects of water and latrine improvement and the LM test to test the individual effects, the LM test strongly rejects the null hypothesis that “there is no individual random effect”. So there are also individual random effects of provinces. Hausmann's test is used to determine whether to use fixed-effects or random-effects models. But Hausmann's test results cannot strongly reject the null hypothesis “ $H_0: u_i$ is not related to x_{it} or z_i ”. Therefore, the random effects of provinces should be considered. Because the “GWR” command in Stata13 software does not have “re” or “fe” options, spatial panel data cannot be processed. In this paper, each variable was transformed by “random effect”, and then the GWR model was carried out. See Table 2 for the regression results of water and latrine improvement.

The geographically weighted regression analysis of water improvement: See Fig. 5 and Fig. 6 for the output of the GWR model. Among the regression coefficients of various factors affecting water improvement, the absolute value of the coefficient of years of education per capita is the largest, which is significant at the level of 5%. Years of education

Table 2: Regression results of influencing factors of water and latrine improvement in rural China.

	Water				Latrine			
	OLS	FE	RE	GWR	OLS	FE	RE	GWR
NIPC	0.000** (0.000)	-0.000 (0.000)	-0.000 (0.000)	-0.000 (0.000)	0.002*** (0.000)	0.001*** (0.000)	0.001*** (0.000)	0.001*** (0.001)
YEPC	0.615 (0.576)	2.442** (0.982)	2.009** (0.818)	2.192** (0.859)	0.436 (0.959)	2.740** (1.369)	2.456** (1.240)	2.499** (1.249)
PD	0.010*** (0.004)	0.012 (0.007)	0.011** (0.005)	0.011** (0.005)	0.030*** (0.006)	0.027** (0.010)	0.027*** (0.008)	0.026*** (0.008)
TD	-1.948 (1.456)	-1.023 (1.864)	-1.369 (1.620)	-1.257 (1.667)	-0.378 (2.482)	6.178** (2.442)	5.282** (2.272)	5.405** (2.277)
Invest_water	0.000 (0.000)	0.002*** (0.000)	0.001*** (0.000)	0.001*** (0.001)	0.025*** (0.006)	0.023*** (0.009)	0.022*** (0.008)	0.022*** (0.008)
Invest_latrine	0.000 (0.000)	0.000 (0.000)	0.000 (0.000)	0.001 (0.000)	0.001** (0.000)	0.001*** (0.000)	0.001*** (0.000)	0.001*** (0.001)
AAT	-0.257*** (0.097)	0.014 (0.190)	-0.139 (0.137)	-0.100 (0.149)	-0.574*** (0.166)	0.025 (0.259)	-0.035 (0.214)	-0.026 (0.218)
APMC	0.002* (0.001)	0.001 (0.001)	0.001 (0.001)	0.001 (0.001)	0.009*** (0.002)	0.001 (0.001)	0.002 (0.001)	0.002 (0.001)
PMP	-0.226*** (0.025)	0.000 (0.000)	-0.223*** (0.056)	-0.220*** (0.071)	-0.093** (0.040)	0.000 (0.000)	-0.053 (0.108)	-0.051 (0.116)
_cons	90.151*** (4.186)	72.205*** (7.223)	80.299*** (6.226)	17.758*** (5.034)	38.280*** (7.080)	19.827** (10.065)	22.777** (9.586)	4.293*** (1.855)
N	420	420	420	420	420	420	420	420
F	35.139	9.810	9.69	10.387	117.999	114.687	7.201	7.834
Quasi-R ²	0.423	0.170	0.168	0.180	0.715	0.678	0.705	0.767

Note: The parentheses are the standard deviations of the coefficient. ***, ** and * indicate that the variable is significant at the level of 1%, 5% and 10%, respectively.

per capita has the greatest impact on water improvement in Xinjiang, Inner Mongolia, Shaanxi, Sichuan, Chongqing, and Guizhou, followed by Shanxi, Anhui, Jiangxi, Henan, Hubei, and Hunan in the central region, and less in Shandong, Jiangsu, Shanghai, Zhejiang, and Fujian in the eastern region. Generally speaking, the impact of education level on rural water improvement in China shows an obvious trend of decreasing in turn. It can be seen that improving the education level of rural residents in underdeveloped areas, especially in the western region, has a significant role in promoting the improvement of safe drinking water facilities. The proportion of the ethnic minority population is the second most important factor affecting rural water improvement. The larger the value, the lower the coverage rate of rural water improvement. The provinces with the larger absolute value of the impact coefficient mainly include provinces where ethnic minorities live in concentrated communities such as Xinjiang, Guizhou, Hunan, Sichuan, Inner Mongolia, and Qinghai. There is no obvious correlation between rural water

improvement and the size of the minority population in the provinces of Northeast and South China.

Population density is the third most important factor affecting rural water improvement. The provinces with a large impact coefficient mainly include the densely populated five provinces of Shanxi, Henan, Hubei, Chongqing, and Sichuan, as well as the sparsely populated western province Xinjiang. The possible reason is that the water improvement project is difficult to construct in places with low population density, and it is easy to develop in places with high population density because of the economies of scale. The benefit rate of rural water improvement is significantly positively correlated with the government investment per capita in water improvement at 1%. Fig. 5 shows the regression coefficient of the government's cumulative water improvement investment per capita, which is the largest in Xinjiang, Sichuan, Chongqing, Guizhou, Guangxi, and Hubei in the west. In other central provinces, eastern and northeastern provinces,

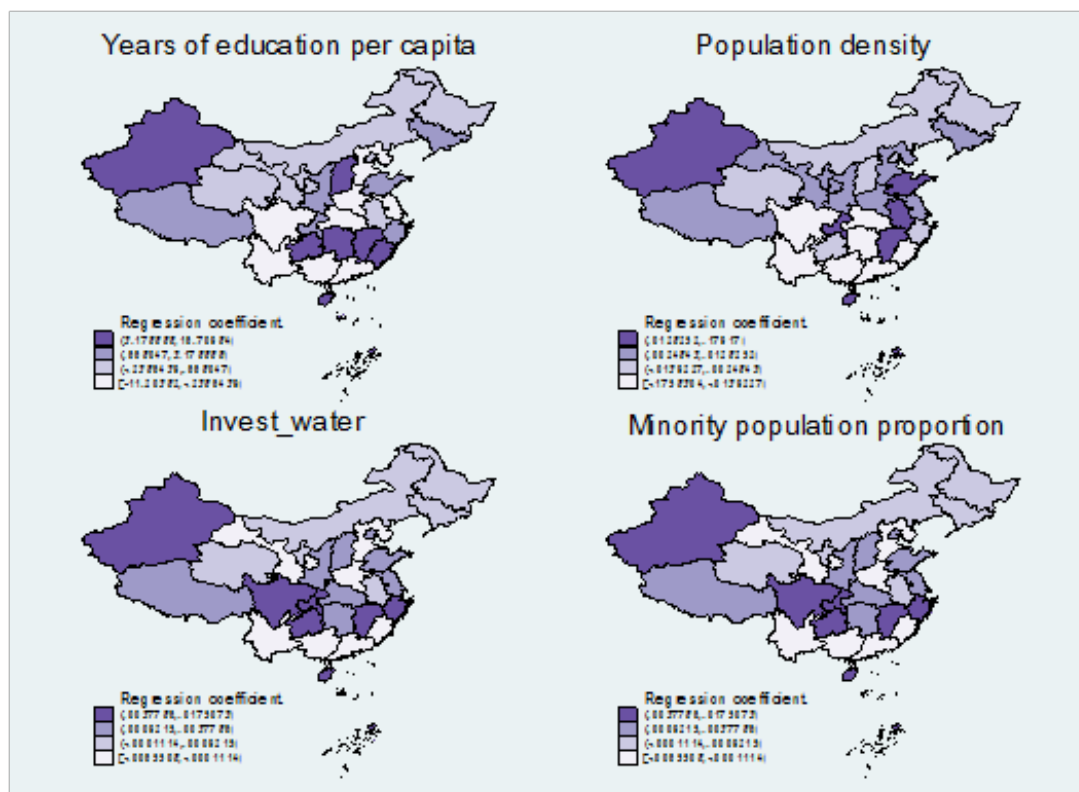


Fig. 5: Distribution of regression coefficients of GWR model for rural water improvement in China.

the regression coefficient is small. It shows that the water improvement cannot be separated from the promotion of the government and the support of government investment funds. In the western provinces, which are relatively undeveloped areas, the improvement of water in rural areas is more dependent on government financial support.

The geographically weighted regression analysis of latrine improvement: The impact of net income per capita on rural latrine improvement is significant at 1%, and an increase in net income per capita of 1,000 Yuan can increase the coverage of rural latrine improvement by 1%, showing a large impact. The provinces with larger regression coefficients of net income per capita include Inner Mongolia, Jilin, Shanxi, Anhui, Fujian, Guangxi, and Hainan, involving the four major regions of China. It shows that the impact of net income per capita on latrine improvement is not differentiated by region. Although the years of education per capita has a significant impact on rural latrine improvement at the level of 5%, its impact coefficient is relatively large. High-value areas are mainly distributed in the six provinces of Hubei, Anhui, Jiangsu, Jiangxi, Fujian, and Zhejiang in the middle and lower reaches of the Yangtze River, and Xinjiang in the western region. The low-value areas are distributed in Qinghai, Inner Mongolia, Shanxi, Hebei, and Shandong in

the north. It shows that years of education per capita has a polarized dual pattern of impact on rural latrine improvement in the northern and southern provinces. Population density also has a positive impact on the latrine improvement in rural areas, and the highest value areas are mainly found in the northern provinces of Xinjiang, Inner Mongolia, Shaanxi, Heilongjiang, and Liaoning. The difference in latrine habits between northern and southern areas, coupled with the lack of people, makes the incentive to improve latrines even less strong.

The influence of traffic density on rural latrine improvement is significant at the level of 5%, and its regression coefficient is the largest among the six influencing factors. However, there are no obvious regional distribution characteristics between high- and low-value areas of the influence coefficient. It shows that the influence of traffic density is regional, and the improvement of traffic conditions also contributes to the improvement of latrines in rural areas. The average coefficient of the impact of cumulative government investment per capita on latrine improvement in rural areas is 0.022, indicating that every 100 Yuan increase in cumulative government investment per capita can increase the coverage rate of latrine improvement by 2.2%, which is far greater than the impact of net income per capita. The high-value areas

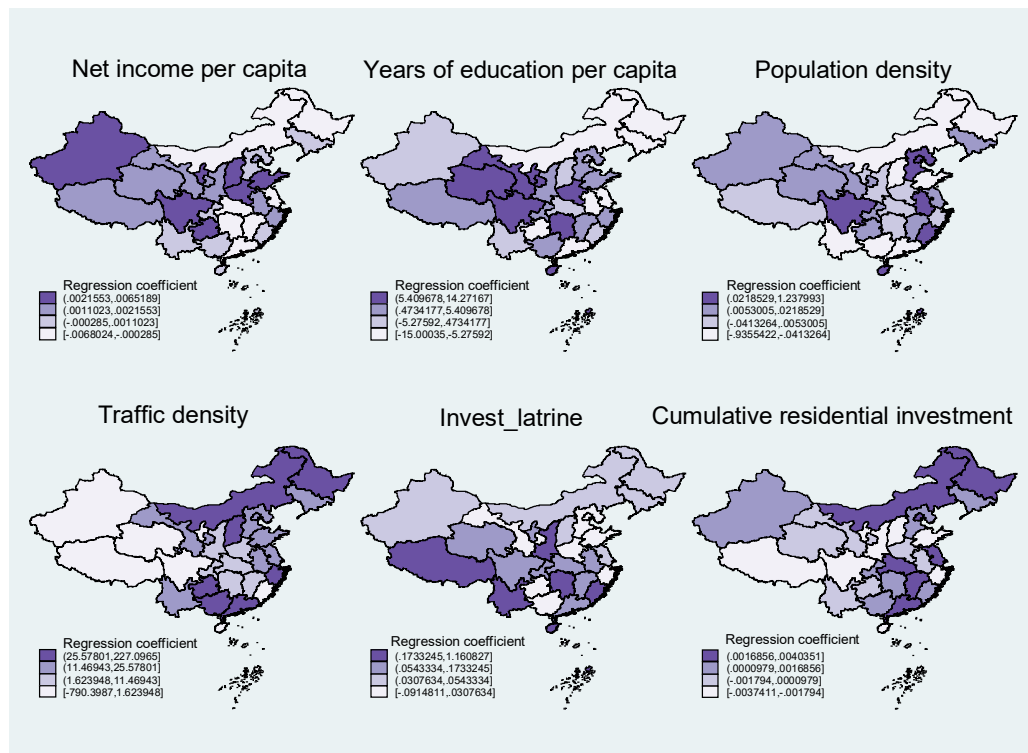


Fig. 6: Regression coefficient distribution of GWR model for latrine improvement in rural China.

are mainly concentrated in the southwest of China, including Yunnan, Guizhou, Hunan, Sichuan, Chongqing, Ningxia, and Shaanxi. The low-value areas are mainly concentrated in the northeast and eastern coastal provinces. The impact of cumulative government investment per capita on rural latrine improvement decreases from west to east in a banding manner. The distribution of the regression coefficient on the map of the impact of the cumulative residential investment per capita is similar to that of the cumulative government investment. The difference is that the overall regression coefficient is far less than that of cumulative government investment per capita in latrine improvement.

CONCLUSIONS

This article takes China's rural water and latrine improvements as an example, uses spatial autocorrelation and local Moran's I scatter plots to analyze the spatiotemporal evolution characteristics of rural sanitation facilities in China from 2003 to 2016, and uses the GWR model further to analyze the driving factors of the difference in coverage of environmental sanitation facilities from a spatial perspective. The spatial autocorrelation analysis of rural environmental sanitation facilities in China shows that there is a certain spatial correlation and dependence among rural environ-

mental sanitation facilities in different provinces, which has obvious spatial agglomeration characteristics, namely high-high agglomeration, and low-low agglomeration. There is a decreasing trend in the low-low type and high-high type of water improvement, while there is an increasing trend in the low-low type and high-high type of latrine improvement.

The analysis results of the GWR model show that among the explanatory variables, there is a significant positive correlation between the number of years of education per capita and the improvement of water and latrines. The difference is that the impact of education level on rural water improvement decreases in an obvious band from west to east, while the impact on rural latrine improvement shows a dual pattern of polarization between the northern and southern provinces. The population density is significantly positively correlated with the improvement of water or latrines. The difference is that it mainly has a significant impact on the improvement of water in northern provinces such as the Northwest and Northeast, and has no obvious impact on the six central provinces. The cumulative government investment in improving water and latrines is the third major factor affecting rural water and latrine improvements in China. The western provinces are more dependent on government investment, while the eastern provinces are less dependent.

In addition, the proportion of the ethnic minority population is significantly negatively correlated with the improvement of water. The provinces with greater influence are also mainly located in areas where ethnic minorities live. Traffic density and net income per capita have a significant impact on the improvement of latrines.

ACKNOWLEDGMENTS

We acknowledge the financial support of the Education Department of Zhejiang Province of China (No. FG2020203).

REFERENCES

- Abramson, A., Becker, N., Garb, Y., and Lazarovitch, N. 2011. Willingness to pay, borrow and work for rural water service improvements in developing countries. *Water Resour. Res.*, 47(11): 553-561.
- Andres, L., Briceño, B., Chase, C. and Echenique, J.A. 2017. Sanitation and externalities: evidence from early childhood health in rural India. *J. Water Sanit. Hyg. Dev.*, 7(2): 272-289.
- Anselin, L. 1995. Local indicators of spatial association: LISA. *Geogr. Anal.*, 27(2): 93-115.
- Cheng, P. and Wang, P. 2006. Influences of modes of production and life upon environment and sanitation in ethnic rural areas: taking Chengbu County in Hunan Province, Longsheng County in Guangxi Autonomous Region, Liping in Guizhou Province as the example. *J. Cent. South Univ. for National. – Human. Social Sci. Edn.*, 26(5): 56-59.
- Cui, C., Jiang, S. and Zhang, Z. 2012. The analysis of spatial variability of influencing factors to county economy in Hebei based on BGWR. *Econ. Geogr.*, 32(2): 39-45.
- Fotheringham, A.S., Charlton, M.E. and Brunson, C. 1998. Geographically weighted regression: a natural evolution of the expansion method for spatial data analysis. *Environ. Plan A - Econ. Space*, 30(11): 1905-1927.
- Jalan, J. and Ravallion, M. 2003. Does piped water reduce diarrhea for children in rural India? *J. Econom.*, 112(1): 153-173.
- Lejano, R.P. 2008. Technology and institutions: a critical appraisal of GIS in the planning domain. *Science Technology & Human Values*, 33(5): 653-678.
- Liu, C., Liu, Y. and Wang, C. 2017. Spatial characteristics of livelihood assets of poor farmers and its influential factors in loess hilly region: a case study of Yuzhong County, Gansu Province. *Econ. Geogr.*, 37(12): 153-162.
- Ma, H., Han, Z. and Jiang, H. 2011. The characteristics and spatial differences of basic public services of cities at the prefecture-level and above in China. *Econ. Geogr.*, 31(2): 212-217.
- Miao, Y. 2008. Access to health resources and the health problems of farmers: An empirical analysis from rural China. *Chin. Popul. Sci.*, 3: 47-55.
- Miao, Y. and Chen, W. 2016. Rural water and environmental sanitation: achievements and challenges. Social Science Literature Press, Beijing, China, pp. 44.
- Miao, Y., Yang, Z. and Zhou, H. 2012. Study on willingness to pay for environmental hygiene improvement of rural residents and its influencing factors: taking latrine improvement as an example. *Manage. World*, 9: 89-99.
- Peng, Y. and Lu, Y. 2010. Analysis of the spatio-temporal evolution of the economic development difference in the Chengyu Economic Zone. *Econ. Geogr.*, 30(06): 912-917.
- Phansalkar, S. J. 2007. Water, equity and development. *Iwmi Res. Rep.*, 3(3): 1-25.
- Tao, Y. 2009. Investigation of drinking water and environmental sanitation in rural China. *J. Environ. Health*, 26(1): 1-2.
- Wan, K., Yu, S. and Hu, Q. 2010. A spatial econometric analysis of rural drinking water safety in Zhejiang. *Rural Water Conserv. Hydro. China*, 4: 136-139.
- Wenjie, Y. 2019. Macroscopic factor decomposition of non-point source pollution of chemical fertilizer: scale, structure, and constraint. *Nature Environ. Pollut. Technol.*, 18(1): 323-327.
- Whittington, D. 1993. Household demand for improved sanitation services in Kumasi, Ghana: a contingent valuation study. *Water Resour. Res.*, 29(6): 1539-1560.
- Yang, H., Bain, R., Bartram, J., Gundry, S., Pedley, S. and Wright, J. 2013. Water safety and inequality in access to drinking water between rich and poor households. *Environ. Sci. Technol.*, 47(3): 1222.
- Zhang, J. 2012. The impact of water quality on health: evidence from the drinking water infrastructure program in rural China. *J. Health Econ.*, 31(1): 122-134.
- Zhu, B., Zhang, X. and Yin, X. 2015. Evaluation of rural human settlements quality and its spatial pattern in Jiangsu Province. *Econ. Geogr.*, 35(3): 138-144.



Strategies and Approaches Towards Environmental Biomonitoring of Freshwater Ecosystems in Philippines

J. S. Berame^{*(**)}†, M. B. Hojilla^{*(***)}, E. Trinidad^{*(****)}, N. L. Lawsin^{*(*****)}, J. A. Orozco^{*(*****)},
I. J. Arevalo^{*(*****)} and Zeba F. Alam^{*}

*De La Salle University, Manila, Philippines

**Caraga State University, Butuan City, Philippines

***West Visayas State University, Iloilo City, Philippines

****Our Lady of Fatima University, Valenzuela City, Philippines

***** Pamantasan ng Lungsod ng Muntinlupa, Muntinlupa City, Philippines

*****Philippine Normal University, Taft Avenue, Manila, Philippines

*****Colegio San Agustin, Laguna, Philippines

†Corresponding author: Julie S. Berame; Janveel@yahoo.com

Nat. Env. & Poll. Tech.

Website: www.neptjournal.com

Received: 11-02-2021

Revised: 20-03-2021

Accepted: 14-04-2021

Key Words:

Biomonitoring

Aquatic ecosystems

Heavy metals

Organic pollutants

Bioremediation

ABSTRACT

The Philippines, like many other Asian countries, is struggling to combat the current widespread aquatic pollution levels caused by anthropogenic activities. Environmental biomonitoring is an efficient tool to detect and monitor the fluctuating toxicity levels in a dynamic ecosystem using bioindicators like algae, macrophytes, zooplankton, insect, bivalve mollusks, gastropod, fish, amphibians, and others to assess the extent and levels of pollution in aquatic ecosystems. The present review deliberates on the biomonitoring techniques such as bioaccumulation, biochemical alterations, population, and community-level approaches to evaluate the current status with respect to the extent and levels of pollution in the aquatic ecosystems in the Philippines which also is one of the biodiversity hotspots. Therefore, the potential applications for biomonitoring are proposed to mainly include evaluation of actual aquatic pollutions, bioremediation, toxicology prediction, and research on toxicological mechanisms. The purpose of such evaluations is to critically analyze and help stakeholders to come up with a strategic action plan with recommendations on a low-cost, sensitive, and effective bioindicator for rapid and efficient environmental biomonitoring.

INTRODUCTION

The Philippines with 7,641 islands is endowed with 421 principal rivers with 18 major river basins, and 79 natural lakes, which constitutes the freshwater ecosystem (EMB 2013). The Philippine archipelago has a coastline of 36,289 km which is the sixth longest coastline in the world, with the West Philippine Sea on the western side, the Philippine Sea on the east, and the Celebes Sea on the south (World Atlas 2020). There are 18 major river basins with the Cagayan River being the largest with a catchment area of 25,649 km² (DPWH, 2004). Both the freshwater as well as marine water ecosystems are at threat due to numerous anthropogenic activities such as urbanization, overexploitation of the natural resources, and more leading to the loss of aquatic biodiversity (PEMSEA 2016). These human activities can lead to physicochemical and biological changes in an ecosystem which should be identified accurately, rapidly, and before major destruction can occur to the ecosystem (Hughes et al. 2004).

In the Philippines, more attention has been drawn to the wide occurrence of heavy metal pollution in the aquatic environment due to mining activities, cyanide, and many illegal uses of harmful chemicals in the country. These heavy metals may transform into permanent metallic compounds with high toxicity levels of metals like mercury and cyanide levels in the water, which can bioaccumulate in the aquatic plants, organisms' vital organs, and get magnified in the food chain, thus threatening human health as well (Jin et al. 2004). The observed effects such as abnormal development of fetus, procreation failure, and immunodeficiency have been exhibited due to aquatic heavy metal exposure and are a serious threat in the country particularly in Luzon and Mindanao where big mining sites are found (Chang et al. 2009). Hence, monitoring and prevention of heavy metal pollution are one of the hot topics in environmental research, not only in the Philippines but in other progressive countries globally.

Therefore, it is of utmost importance to continuously monitor the ecosystems to identify the source of contam-

ination, reduce their impact and restore their health status since a healthy ecosystem has the resilience to quickly and completely recover from the risks or threats that generally have detrimental effects on the composition, structure and/or function of an ecosystem (Fu-Liu & Shu 2000). The effects of a chemical toxin in a living organism at the level of molecules, organelles, cells, tissues, organs, organisms, populations, communities, ecosystems, and biomes can be assessed through biomonitoring. Over the years, the use of biological monitoring has become more reliable as it provides a complete spectrum of information for proper management of water bodies by integrating, detecting, and using highly diverse flora and fauna to evaluate the health of the aquatic bodies (Li et al. 2010).

In the country, many macro-organisms like fish, macroinvertebrates, macrophytes, protozoa, and others are used for environmental biomonitoring (Marzin et al. 2012). Due to the consistency between the selected organisms and the corresponding living space, biomonitoring can directly provide information on the potential effects and actual cumulative toxicities of pollutants, reflecting the harmful and consistent effect in the environment. The alterations in the physiology, molecules, functions, or number of organisms are the effect indicators whereas the accumulation of materials or toxins from the surroundings can be studied as accumulation bioindicators (Tellez & Merchant 2015). The stomach contents of fishes like *Oncorhynchus mykiss* and *Salmo trutta* and prey diversity can be used to evaluate the pollution levels in the water bodies (Fierro et al. 2015). The bioindicators used in the environmental biomonitoring also give the accumulative changes in an aquatic body over a period of time (Herman & Nejadshemi 2015). Hence, the biomonitoring of aquatic bodies can be done by focusing on the bioconcentration or bioaccumulation of toxins/pollutants in aquatic organisms (Deben et al. 2015, García-Seoane et al. 2018), or at the molecular level using biochemical biomarkers such as proteins to understand the molecular responses to contaminants in the living organisms which has led to the new development of a new field of environmental proteomics (Li et al. 2018). Thus, this review aims to come up with suggestions on low cost, sensitive, and effective bioindicators that can be used for rapid and efficient biomonitoring of the contaminated freshwater aquatic ecosystems in the country that can help the stakeholders to come up with an effective strategy to monitor the pollution levels in the aquatic bodies.

MATERIALS AND METHODS

Search strategy: The literature search was conducted based on a thematic technique for systematic reviews and Boolean search methodology for the years 2014–2020 from Google

Scholar, Sci-Hub, and Web of Science. Search terms such as bioassessment, biomonitoring, aquatic ecosystems, and freshwater pollutions, Philippines, etc. were used and from the search results, a total of around 30 publications were selected for the review. The low numbers of relevant publications are indicative of the limited research on environmental biomonitoring conducted in the country.

Inclusion criteria: The data from publications was extracted and information was collected on the study type, pollutants investigated, type of biomarker and matrix, measurement techniques, and quality assurance of the methodology used to carry out the research. Biomonitoring research articles were extensively analyzed and upon further examination, 6 studies were excluded from the present study due to the criteria such as results being reported in earlier studies. The published articles were reviewed, assessed, and ranked independently based on their quality of the study using the criteria such as the specificity of the biomarkers used, the analytical techniques, the quality of the study design, sample handling, and quality assurance.

Data Analysis

The information and data presented in the research papers included were analyzed, reviewed, and further evaluated by a third abstractor if required.

Techniques and Approaches for Biomonitoring of Aquatic Bodies

Bioaccumulation: This is an important process where over a period of time an increase in the concentration of a pollutant/chemical in a biological organism may occur compared to the chemical's concentration in the environment. Bioaccumulation occurs when an organism absorbs a toxic substance at a rate greater than that at which the substance is lost. This results from a disturbance to the dynamic equilibrium between exposure from the outside environment and uptake, excretion, storage, and degradation within an organism. Hence often, the bioaccumulation approach is used to monitor heavy metal contamination in the aquatic environment. For organic pollutants, a bivalve, *Mya arenaria* has been identified as a bioindicator to monitor the tributyltin chloride (TBT) pollution in the marine environment with the Bioconcentration factor (BCF) of *M. arenaria* ranging from 15 538 to 91 800 after 28 days of exposure (Zhou & Guibin 2006). The rapid uptake and low rate of elimination of TBT reactions displayed first-order kinetics.

Biochemical alterations: With the development of biological techniques, research on the interaction between the pollutants and biological macromolecular such as protein, enzyme, and nucleic acid may indicate the action mechanism

of the pollutants. The alteration in the biological process can be used as a bioindicator to assess the environmental quality hence many biomarkers have currently been developed such as metallothionein, oxidative stress, cyto-toxicological responses such as genotoxicity, lysosomal alterations, immunocompetence, and gencholinerase activities (Siddig et al. 2016). Some special proteins can be purified to serve as a biomarker for metal exposure as well. Chlorophyll fluorescence, as a potential valuable ecotoxicological endpoint, could be used with a range of aquatic phototrophs for the assessment of aquatic pollution including heavy metals (Ralph et al. 2007). The main advantages are that it is rapid, non-invasive, and non-destructive, while the major weakness is the lack of clear ecological relevance.

Use of Proteomic Analysis: The biomonitoring of the aquatic environment has also been carried out using the proteomic analysis using Annelids (Roohi-Shalmaaee et al. 2019); crustaceans (Vellinger 2016), and fishes (Catteau et al. 2021). The impact of oxidative stress on tissues such as muscles, liver, gills, kidneys, brain, or skin, etc has been studied to understand the mechanism (Zhang et al. 2019). The changes in the proteome of goldfish (*Carassius auratus*) subjected to heat shock and toxins like herbicides and fungicides as a response to cellular stress further confirm that proteomic analysis can be used as a tool for environmental biomonitoring in the aquatic environment (Beese et al. 2012). The Chinese rare minnow (*Gobiocypris rarus*) exposed to benzotriazole were reported to exhibit alteration in the heat shock proteins and catalase enzyme levels (Liang et al. 2021). The mollusks were also reported to be suitable environmental sentinels with their protein expression strongly affected by the pollutants (Campos et al. 2012).

Population and Community-Level Approaches: Population-level (density, size distribution) and community-level (species richness metrics, multivariate analysis of community composition) responses of the aquatic organisms to pollution in the aquatic ecosystem, are of much significance for the evaluation of the ecological balance induced by water qualities in the studied area. Single or various populations may be involved for different aims. The protozoan communities get affected by heavy metal pollution and can be used for biomonitoring by using the species richness, individual abundance, and biodiversity index as endpoints (Cairns et al. 2009). The response of testate amoebae communities was used as a bioindicator to monitor the heavy metal pollution in the groundwater, stream water, and aquatic bryophytes in the Lanmuchang stream, Guizhou Province, China (Zhang & He 2010).

Freshwater Ecosystem

In the Philippines, the Department of Environment and

Natural Resources (DENR) is the government agency responsible for the conservation, management, development, and proper utilization of natural resources. DENR has classified the bodies of freshwater into different categories based on their intended beneficial use (DAO No. 2016-08) (DENR Administrative Order No. 2016-26 2016). This criterion was formulated in 1978 and was revised in 1990 in DAO No. 34. The criterion was further modified in 2016 to support the changing needs of our environment; thus DAO 2016-08 was crafted. Hence, DENR also added the use of the effluent standards to analyze the conditions of the different bodies of water and classify them accordingly (Table 1).

Freshwater Environment

The National Water Resources Board (NWRB) has identified 18 major river basins, 421 principal rivers and the Bureau of Fisheries and Aquatic Resources (BFAR) of the Department of Agriculture has listed 79 lakes in the Philippines (BFAR 2015). Besides this, an estimated 3.7 million cubic meters of groundwater is extensively used of which 54% is used for domestic purposes and 25 % for irrigation (DENR 2013). The Department of Environment and Natural Resources (DENR) is the government agency that is responsible for the conservation, management, development, and proper utilization of natural resources including water. To assess the water quality, DENR has taken into account 33 parameters to generally classify the water bodies into different categories based on their intended beneficial use as defined in DAO No, 2016-08 in Table 1. The first criteria were formulated in 1978 and then were revised in 1990 in DAO No. 34 and further modified in 2016 to support the changing needs of the environment. Using these parameters, the water quality of various inland surface water bodies including the 55 principal rivers, 76 minor rivers, and 4 big lakes was monitored (Table 2).

According to the criteria of Dissolved oxygen (DO) used for water quality testing, 59% of the tested water bodies qualified with “Good” water quality and 29% with “Fair” water quality in terms of Dissolved oxygen (DO) compliance. However, the main four rivers of the NCR namely-Parañaque River (1.6%), the Pasig River (4.4%), Navotas-Malabon-Tullahan-Tinejeros River (7.2%), and San Juan River (11.5%) had the lowest DO compliance (Gorme et al. 2010). The discharge of wastewater and other untreated waste causes low DO levels in the aquatic bodies making it difficult for the aquatic organisms to survive as they require at least 5 milligrams per liter ($\text{mg}\cdot\text{L}^{-1}$) of dissolved oxygen. In terms of BOD, the higher the BOD value, the greater is the degree of pollution where most aquatic organisms perish if the BOD level is above $7 \text{ mg}\cdot\text{L}^{-1}$. 57% of the water bodies

Table 1: Effluent standards for the classification of water bodies (DENR 2013).

Parameter	Unit	Water Body Classification								
		AA	A	B	C	D	SA	SB	SC	SD
Ammonia as NH ₃ -N	mg/L	NDA	0.5	0.5	0.5	7.5	NDA	0.5	0.5	7.5
BOD	mg/L	NDA	20	30	50	120	NDA	30	100	150
Boron	mg/L	NDA	2	3	3	12	NDA	2	20	80
Chloride	mg/L	NDA	350	350	450	500	NDA	n/a	n/a	n/a
COD	mg/L	NDA	60	60	100	200	NDA	60	200	300
Color	TCU	NDA	100	100	150	300	NDA	100	150	300
Cyanide as Free Cyanide	mg/L	NDA	0.14	0.14	0.2	0.4	NDA	0.04	0.2	0.4
Fluoride	mg/L	NDA	2	2	2	4	NDA	3	3	6
Nitrate as NO ₃ -N	mg/L	NDA	14	14	14	30	NDA	20	20	30
pH (Range)		NDA	6.0-9.0	6.0-9.0	6.0-9.5	5.5-9.5	NDA	6.5-9.0	6.0-9.0	5.5-9.5
Phosphate	mg/L	NDA	1	1	1	10	NDA	1	1	10
Selenium	mg/L	NDA	0.02	0.02	0.04	0.08	NDA	0.02	0.2	0.4
Sulfate	mg/L	NDA	500	500	550	1,000	NDA	500	550	1,000
Surfactants (MBAS)	mg/L	NDA	2	3	15	30	NDA	3	15	30
Temperature (h)	°C change	NDA	3	3	3	3	NDA	3	3	3
Total Suspended Solids	mg/L	NDA	70	85	100	150	NDA	70	100	150
Arsenic	mg/L	NDA	0.02	0.02	0.04	0.08	NDA	0.02	0.04	0.08
Barium	mg/L	NDA	1.5	1.5	6	8	NDA	1.5	2	8
Cadmium	mg/L	NDA	0.006	0.006	0.01	0.02	NDA	0.006	0.01	0.02
Chromium as Hexavalent Chromium (Cr ₆₊)	mg/L	NDA	0.02	0.02	0.02	0.04	NDA	0.1	0.1	0.2

met the BOD compliance though most of these water bodies are classified as Class A or Class C. Paranaque River, San Juan, Pasig, and Meycauyan Rivers failed to meet the BOD compliance in most of their sampling events (Gorme et al. 2010) (Table 3).

Table 2: Monitored water quality parameters per type of water body (DENR 2013).

Water Body	Water Quality Parameter
Inland surface waters	Dissolved oxygen (DO) Biochemical oxygen demand (BOD) Total suspended solids (TSS) Phosphates Nitrates Heavy metals Cyanide as free cyanide
Ground Water	Fecal coliform Nitrates Salinity (chloride content)
Coastal and marine waters	Fecal coliform Total coliform DO

Table 4 shows the status of the top 11 largest rivers in the Philippines and its classification based on the Environmental Management Bureau (EMB). Laguna de Bay is the largest freshwater lake in the Philippines and was categorized as class C with fishery water for the propagation of growth of fish and other aquatic resources, recreational water class II - for boating, fishing, or similar activities, and agriculture, irrigation, and livestock watering.

Sources of Pollution

The water bodies inside the country as well as that surround the landmass are contaminated and polluted. The prevailing water pollution has greatly affected the lives of the Filipinos. The identified sources of water pollution are- (1) Industrial wastes with heavy metals like lead, mercury, chromium, cadmium, cyanide, and more (Olivares et al. 2019); (2) Agricultural wastes including organic wastes such as decayed plants, dead animals, livestock manure, soil runoff; and non-organic wastes, like pesticides and fertilizers; (3) Domestic sewage that may contain pathogens capable of causing diseases to humans and animals (Olivares et al.

Table 3: Priority principal rivers subject to regular monitoring in the Philippines (Tuddao & Gonzales 2016).

Rivers	Location (Luzon and Mindanao Regions)	Class	DO (mg.L ⁻¹)	BOD (mg.L ⁻¹)
Meycauayan River	Region III	C	0.88	88.67
Marilao River	Region III	C	2.06	43.48
Bocau River	Region III	C	2.52	27.03
Imus River	Region IVA	C	5.09**	10.63
Ylang-ylang River	Region IVA	C	4.6	4.9
Tagbruos River	Region IVB	C	4.81	9.65
Calapan River	Region IVB	C	1.3	6.39
Salog River	Region V	C	5.81	3.55
Balos River	Region V	C	7	2
Sagumayon River	Region V	C	4.11	22.16
Balili River	CAR	A	5.9	59.5

Table 4: Top ten largest lakes and their classification in the Philippines (BFAR 2015).

Lake	Location (Luzon & Mindanao Lakes)	Area (ha)	Region	Water Body Classification and Usage of Freshwater
Laguna de Bay	Laguna and Rizal	89,076	4-A	C
Lake Lanao	Lanao del Sur	34,000	10	A
Taal Lake	Batangas	24,356	4-A	B
Lake Mainit	Surigao del Norte-Agusan del Norte	17,430	CARAGA	A
Agusan Marsh Lake	Agusan del Sur	14,000	CARAGA	No Classification
Naujan Lake	Oriental Mindoro	7,899	4-B	B
Lake Buluan	South Cotabato	6,134	2	No classification
Lake Bato	Camarines Sur	3,792	5	B
Lake Pagusi	Agusan	2,534	8	No classification
Lake Labas	South Cotabato	2,141	7	No classification
Lake Lumao	Agusan	168	8	No classification

2019) and (4) Other sources such as oil, mine or chemical spills and illegal dumping in or near water sources (Andrews 2018).

Kind of Pollutants

Heavy Metals are inorganic pollutants that pose a negative impact on the environment especially on aquatic organisms, plants, and even humans (Marrone 2016). Heavy metals are indirectly and directly discharged into the environment through mining, agriculture, factories, and commercial wastes. Since heavy metals in their ionic form are soluble in water, they tend to settle down at the sediments and bottom of the rivers where they can accumulate to toxic levels which can harm the aquatic life and humans who consume the fish and other seafood (Vestil & Lim 2016). Heavy metals such as lead, cadmium, arsenic, and mercury are toxic and may cause harm to organisms (Walag and Canencia, 2018). In terms of total mercury, all monitored rivers were declared

safe with mercury levels within the maximum limit of 2 micrograms per liter (ug.L⁻¹) with the exception of four rivers, of Agno, Malguit, Panique, and Tubay (Walag et al. 2018). For Cadmium, 8 out of the 18 water bodies tested, were found to be compliant to the maximum limit of 0.01 mg.L⁻¹ and for Lead, 7 out of 18 water bodies met the maximum limit of 0.05 mg.L⁻¹ though it is important to point out that there were concerns that the data has been derived from a very small number of sampling events (Canencia et al. 2016).

Organic Pollutants are organic compounds that can cause toxicity to aquatic plants and animals. One of the most toxic organic pollutants are the endocrine disruptive chemicals (EDCs) which are the external agents that can disrupt the hormonal activities of an organism, thus affecting the homeostatic mechanisms, reproduction, development, or behavior of an organism (Pielou 1998). Furthermore, EDCs can increase the chances of having cancer in humans (Rachon 2016).

Impact of Freshwater Pollution on Public Health

Water pollution is considered one of the major environmental problems that the Philippines should prioritize because it can greatly affect the lives of the Filipino people, especially the ones living near the bodies of water. According to the Environmental Management Bureau (EMB), only 47% out of the Philippines' 127 freshwater bodies retain good water quality which is intended for human usage. The impact of water pollution on the Filipino people living beside the riverbanks was determined based on the following: (a) waterborne viruses and bacteria that contaminate drinking water that can lead to gastrointestinal diseases such as diarrhea, cholera, and various skin diseases; (b) bioaccumulation of toxins that are being built-up over a period of time in the adipose tissues of an organism (Paulaa & Andow 2016). Water-borne diseases like diarrhea and cholera also account for some diseases associated with polluted water (Andrews & Gabriella 2018).

Deteriorating water quality also negatively impacts the growth of crops and livestock and overall soil quality, leading to reduced agricultural yields. A decrease in productivity, including smaller crop yield, results in a lower household income and similarly, it can also reduce food supply to man. Furthermore, access to clean water is an important component of preventing malnutrition and decreasing infant mortality. Heavy metals are known to enter the body and can cause nausea/vomiting, diarrhea, kidney and liver failure, cognitive and neuromuscular dysfunction besides genetic alterations resulting in structural defects (Jan et al. 2015).

Impact of Freshwater Pollution in the Environment

As water pollution puts the health of people at risk, there were direct and indirect effects on the environment such as the eutrophication of lakes. This results in algal blooms, which may lead to the depletion of oxygen available for other freshwater organisms. The depletion of oxygen can cause morphological stress to the other organisms living in these bodies of water, decreasing their overall ability to survive. The draining of fertilizers and pesticides leading to algal bloom and eutrophication, disposal of untreated sewage both from domestic and industrial sources and the deposition of sediment in the riverbeds due to deforestation is the major causes of deterioration in the health of the aquatic ecosystems in the Philippines (Andrews 2018).

Biomarkers Used for Freshwater Environment

Biomarkers refer to any physiological, biochemical, and histological changes in a living organism that can be used as indicators of exposure to chemical contaminants such as heavy metals and organic compounds (Reboa et al. 2019). Hence, biomarkers are being employed in ecotoxicology

to analyze the trends and effects of toxins in an aquatic environment and serve as indicators of exposure to toxicants (Ippolito et al. 2016). Biomarkers in aquatic ecosystems are used to detect environmental stressors and pollutants that may affect environmental conditions such as temperature, pH, oxygen content, and more (Berra et al. 2016). Hence, the development of sensitive biochemical markers is very much needed to detect the conditions of aquatic ecosystems and monitor the status of the environment. The erythrocytes of Nile Tilapia (*Oreochromis niloticus*) have been used as biomarkers to detect the presence of genotoxic pollutants in Taal Lake, Batangas, where micronucleus test, chromosomal aberration analysis, and comet assay was used to assess the DNA damage in the fish exposed to the genotoxic pollutants in the waters of the Taal Lake (Hallare et al. 2016). The low levels of enzyme- acetylcholinesterase (AChE) in the brain and muscles of white goby using the rapid colorimetric method indicated the exposure to the organophosphates and carbamate pesticides in the Laguna Lake (Fajardo & Ocampo 2018). The benthic macroinvertebrate assemblages were used for biomonitoring of water quality of the Iligan river (Maagad 2012) and of three Estuary sites in Iligan city (Superada & Tampus 2015). The water quality of Gibong River in Agusan del Sur was monitored by assessing the diversity of macroinvertebrates (Peligro & Jumawan 2015).

The biological assemblage such as macroinvertebrates, diatoms, and coliform was used as bioindicators of the status of water quality and habitat degradation of the Cagayan de Oro River (Sinco et al. 2014). Bioaccumulation of heavy metals like Cu and Zn was reported in various species of gastropods and bivalves in the estuaries near the mining town in the Camarines Norte region where biomonitoring was conducted over a period of two years (Carino et al. 1993). Riparian Channel and Environmental (RCE) Inventory was done to evaluate the integrity of the riparian vegetation. The presence of lead in the hepatopancreas of the melon conch was used to determine the concentration of lead in Bacoor Bay, Cavite (Sia Su et al. 2015). Hence, the environmental biomonitoring of a freshwater ecosystem can be done using biomarkers though for each area or region a suitable biomarker needs to be identified.

Factors and Sources of Freshwater Pollution

There is a wide array of factors of marine water pollution in the Philippines. One such factor is the location of the water bodies. Indirectly connected to Manila Bay via the Pasig River is Laguna de Bay, the largest lake in the Philippines. As a semi-enclosed estuary, Manila Bay is surrounded by the highly urbanized National Capital Region (NCR) provinces of Bataan, Pampanga, Bulacan Cavite. Both the Pampanga and Pasig River basins (two main contributory areas) drain their

waters to Manila Bay. Domestic and agro-industrial wastes, including discharge of municipal wastes, find their way to Manila Bay via these two (Pasig and Pampanga) River Basins.

Metro Manila, considered a megacity, having a population of 10 million or more (UNDESAPD 2018) is one big source of pollution in the water bodies. Metro Manila and some of the other major cities in the Philippines have seen rapid economic growth and development, leading to haphazard urbanization with many environment-related challenges such as an increase in greenhouse gas emissions, rise in solid waste generation, and overall decline in air and water quality (DENR 2013). The agricultural farms in the neighboring provinces surrounding Metro Manila are the source of pesticides that settle down in the sediments of the rivers adversely affecting the benthic dwellers, filter feeders, and the flora/fauna present in the water bodies (Bajet et al. 2010). An increasing number of informal settlers along the Pasig riverbanks contributed to an increase in solid waste generation, clogging the waterways and deterioration in water quality. So much so that Pasig River, once known to have pristine waters is now labeled as the "Toilet Bowl" of Metro Manila (Gorme et al. 2010).

Government Policies on Aquatic Environment

A number of policies have been put together by the government to prevent the damage and protect the aquatic ecosystems. One of the earliest laws that have been formulated was the Commonwealth Act 383 (1938), which prohibited the dumping of different types of wastes that can cause an elevation or block the course of streams in rivers. Subsequently, Presidential Decrees (PD) such as National Pollution Control Decree (PD 984) was devised to ban the throwing or disposal of any gaseous or liquid pollutants in water, air, and land resources. PD 1067 of 1976 or the Water Code of the Philippines was developed to conserve and regulate the use of water and management of water resources. Furthermore, RA No. 9275 (Clean Water Act) was developed to control wastewater discharges.

CONCLUSION

In conclusion, biomonitoring provides direct evidence of alterations that occur in the major freshwater ecosystems in the Philippines due to environmental pollution. Integrated information on the water quality can be reflected based on the biomonitoring of aquatic metal pollution, which offers the potential effects and actual toxicities. Notable progress has been achieved due to the biomonitoring efforts with respect to industrial, agricultural, and domestic pollution in aquatic ecosystems in the country. Several biomarkers at the cellular levels have been developed due to the sensitive responses of the organisms that can alert us about the toxic

effects induced by current water pollution levels as well as help us to understand the potential toxicological mechanism which can help to undertake precautions and preventions to combat pollution levels. Hence, developing comprehensive monitoring approaches in freshwater ecosystems is very important through constant sampling and testing to monitor the level of toxicity in the aquatic environment, perform a toxicological study on aquatic organisms to determine the extent of the impact on freshwater organisms, determine health risks at individual and group levels through biomonitoring, and conduct an information campaign activities on biomonitoring to educate the members of the local community on the possible occurrence of toxicity induced by pollutants in the aquatic ecosystems.

RECOMMENDATIONS

The use of mollusks as a bioindicator in biomonitoring is the best way to monitor the aquatic environment. The following actions are recommended for the freshwater environmental biomonitoring: (1) strict implementation of Environmental Laws on biomonitoring in a freshwater environment in the Philippines; (2) develop comprehensive monitoring approaches in the freshwater environment through constant sampling and testing to monitor the level of toxicity in the aquatic environment; (3) perform a toxicological study on aquatic organisms to determine the extent of the impact on freshwater organisms; (4) determine health risks at individual and group levels through biomonitoring, and (5) conduct an information campaign activity on biomonitoring to educate the members of the community on the possible occurrence of poisoning and the importance of biomonitoring in a freshwater environment.

ACKNOWLEDGMENT

The study was supported by the University Research Coordination Office, De La Salle University, Manila, Philippines, (URCO) grant 77 F U 3TAY18-2TAY20.

REFERENCES

- Alimi, B. 2016. Risk factors in street food practices in developing countries: A review. *Fd. Sci. Hum. Wellness*, 5(3): 141-148.
- Andrews, G. and Gabriella, F. 2018. Resolving the water pollution crisis in the Philippines: The implications of water pollution on public health and the economy. *Pepperdine Pol. Rev.*, 10: 1-15
- Bajet, C., Carvalho, F.P., Villeneuve, J., Cattini, C. and Navarro-Calingacion, M. 2010. Chlorinated hydrocarbons in sediments from Manila Bay, the Philippines. *Inter. J. Environ. Stud.*, 67(4): 493-504.
- Besse, J.P., Geffard, O. and Coquer, M. 2012. Relevance and applicability of active biomonitoring in continental waters under the water framework directive. *TrAC Tren. in Analyt. Chem.*, 36, 113-127
- Berra, F., Felletti, F. and Tessarollo, A. 2016. Stratigraphic architecture of a transensional continental basin in low-latitude semiarid conditions:

- the permian succession of the central Orobic basin. *J. of Sedimen. Res.*, 86 (4): 408-429.
- Bureau of Fisheries and Aquatic Resources (BFAR). 2015. In *Turbulent Seas: The Status of Philippine Marine Fisheries*. Coastal Resource Management Project, The Philippines. p. 378.
- Cairns, J., Dahlberg, M., Kenneth L. Dickson, K., Smith, N. and Waller, W. 2009. The relationship of fresh-water protozoan communities to the MacArthur-Wilson equilibrium model. *Am. Nat.*, 103: 933.
- Campos, I., Aguado, D., Ferrer, J., Gil, L., Soto, J. and Vivancos, J. 2012. A voltammetric electronic tongue as tool for water quality monitoring in wastewater treatment plants. *W. Res.*, 46(8): 2605-2614.
- Canencia, M. and Walag, A. 2016. Physico-chemical parameters and macrobenthic invertebrates of the intertidal zone of Gusa, Cagayan de Oro City, Philippines. *Inter. J. of the Bioflux Soc.*, 8(1): 71- 82.
- Carino, V.C., Casway, A.A. and Rivero, H.I. 1993. Use of Mollusks (*Gastropoda* and *Bivalves*) as a Biological Indicator of Cu and Zn Pollution in the Estuaries of a Mining Town in Camarines Norte(Philippines). *Proceeding of the Second National Malacological Convention, Laguna, the Philippines*, pp. 93-100.
- Catteau, A. Bado-Nilles, A., Beaudouin, R., Tebby, C., Joachim, S., Palluel, O., Turiès, C., Chrétien, N. and Nott, K. 2021. Water quality of the Meuse watershed: assessment using a multi-biomarker approach with caged three-spined stickleback (*Gasterosteus aculeatus* L.). *Ecotoxicol. Environ. Saf.*, 208: 111-207.
- Chang, K.H., Amano, A., Miller, T. W., Isobe, T., Maneja, R., Siringan, F.P., Imai, H. and Nakano, S. 2009. Pollution study in Manila Bay: Eutrophication and its impact on plankton community. *Inter. Stud. Environ. Chem. Res.*, 51: 261-267.
- Deben, S., Aboal, J.R., Carballeira, A., Cesa, M., Real, C. and Fernandez, J.A. 2015. Inland water quality monitoring with native bryophytes: A methodological review. *Ecol. Indic.*, 53: 115e124.
- DENR Administrative Order No. 2016-26. 2016. Guidelines for the implementation of the coastal and marine ecosystem management program (CMEMP). Retrieved January 12, 2020 from <https://server2.denr.gov.ph/uploads/rmd/d/d/ao-2016-26.pdf>
- DENR 2013. DENR administrative order no. 2013-22. Supreme court e-library, 24 -No. 4. Retrieved August 16, 2021 from <https://elibrary.judiciary.gov.ph/thebookshelf/showdocs/10/67621>
- DPWH 2004. Flood control project implementation system for principal rivers in the Philippines. Retrieved August 15, 2021 from <https://www.scribd.com/document/470675949/Study-on-Flood-Control-Project-for-Rivers-in-the-Philippines>.
- Environmental Management Bureau (EMB). 2013. List of classified water bodies as of 2013. Retrieved October 23, 2019 from <http://www.emb.gov.ph/portal/Portals/24/Classified%20Waterbodies/2013/Classified%20WB%202019Region%204a.pdf>.
- Fajardo, L. and Ocampo, P. 2018. Inhibition of acetylcholinesterase activities in whitegoby, *Glossogobius giurinus* from the East Bay of Laguna Lake, Philippines. *Inter. J. Agric. Tech.*, 14(7): 1181-1192.
- Fierro, P., Bertrán, C., Mercado, M., Peña-Cortés, F., Tapia, J., Hauenstein, E., Caputo, L. and Vargas-Chacoff, L. 2015. Landscape composition as a determinant of diversity and functional feeding groups of aquatic macroinvertebrates in southern rivers of the Araucanía, Chile. *Lat. Amer. J. Aqua. Res.*, 43: 186-200.
- Fu-Liu, X. and Shu, T. 2000. On the study of ecosystem health: State of the art. *J. Envi. Sci.*, 12: 33-38.
- García-Seoane, R., Fernandez, J.A., Villares, R. and Aboal, J.R. 2018. Use of macroalgae to biomonitor pollutants in coastal waters: Optimization of the methodology. *Ecol. Indic.*, 84, 710e726.
- Gorme, J.B., Maniquiz, M.C., Song, P. and Kim, L.H. 2010. The water quality of the Pasig River in the City of Manila, Philippines: Current status, management, and future recovery. *Environ. Engr. Res.*, 15(3): 173-179.
- Hallare, A.V., Ocampo, K.A., Tayo, P. K. and Balolong, M. 2016. Genotoxic stress-induced by intensive aquaculture activities in Taal Lake, the Philippines on circulating fish erythrocytes using the comet assay and micronucleus test. *Adv. Environ. Bio.*, 10(1): 273-283.
- Herman, M. and Nejadhashemi, A. 2015. A review of macroinvertebrate- and fish-based stream health indices. *Ecohydrol. Hydrobiol.*, 15: 53-67.
- Hughes, T., Baird, H., Bellwood, D., Card, M. and Connolly, S. 2004. Climate change, human impacts, and the resilience of coral reefs. *Science*, 301(5635): 929-933.
- Ippolito, G., Petersena, E., Wilsonb, M., McCloskeyd, B., Mwabae, P. and Batease, M. 2016. Rapid spread of zika virus in the Americas - implications for public health preparedness for mass gatherings at the 2016 Brazil Olympic games. *Inter. J. of Infec. Dis.*, 44, 11-15.
- Jan, A.T., Azam, M., Siddiqui, K., Ali, A., Choi, I. and Haq, Q.M. 2015. Heavy metals and human health: Mechanistic insight into toxicity and counter defense system of antioxidants. *Int. J. Mol. Sci.*, 16(12): 29592-29630.
- Jin, L. 2017. Cadmium Biomonitoring Summary. Centers for Disease Control Prevention. CAS No, 7440-43-9
- Liang, C., Willey, J., Pollock, T., Thomson, E. and Walker, M. 2021. Exposure load: Using biomonitoring data to quantify multi-chemical exposure burden in a population. *Inter. J. of Hyg. and Environ. Hlth.*, 34: 113-204.
- Li L., Zheng B. and Liu L. 2010. Biomonitoring and bioindicators used for river ecosystems: Definitions, approaches, and trends. *Procedia Environ. Sci.*, 2: 1510-1524.
- Li, C., Pulin, Z., Wei, L., Wei, D., Jia, O. and Chang, C.C. 2018. Molecular biological methods in environmental engineering. *Water Environ. Res.*, 90: 1371-1391.
- Maagad, L. 2012. Benthic Macroinvertebrates and Water Quality of Iligan River. (Unpublished master's thesis). Mindanao State University-Iligan Institute of Technology, Iligan City, Philippines
- Marrone, R. 2016. Water Pollution in the Philippines: Causes and Solutions. BORGEM. Retrieved November 6, 2020 from <http://www.borgenmagazine.com/water-pollution-in-the-philippines>.
- Marzin, A., Archambault, V., Belliard, J., Chauvin, C., Delmas, F. and Pont, D. 2012. Ecological assessment of running waters: Do macrophytes, macroinvertebrates, diatoms, and fish show similar responses to human pressures? *Ecol. Indic.*, 23: 56-65.
- Mehana, E.E., Khafaga, A.F., Elblehi, S.S., Abd El-Hack, M.E., Naiel, M.A. and Bin-Jumah, M. 2020. Biomonitoring of heavy metal pollution using acanthocephalans parasite in the ecosystem: An updated overview. *Animals*, 10: 811.
- Olivares, R., Sta Maria, E. and Sombrito, E. 2019. Environmental assessment of metal pollution in Manila Bay surface sediments. *Phil. J. Sci.*, 149(S1): 183-195.
- Pielou, E.C. 1998. *Fresh Water*. The University of Chicago Press, Chicago & London.
- Paulaa, D. and Andow, D. 2016. Uptake and bioaccumulation of Cry toxins by an aphidophagous predator. *Environ. Poll.*, 209: 164-168.
- Peligro, V. and Jumawan, J. 2015. Aquatic macroinvertebrates diversity and riparian channel and environmental inventory in Gibong River, Philippines. *J. Ento. Zool. Stud.*, 3(5): 398-405.
- PEMSEA. 2006. *Sustainable Development and Management of Manila Bay: A Focus on Water Quality*. PEMSEA, Quezon City, pp. 1-5
- Presidential Decree No. 600. 1974. Prevention and control of marine pollution. Retrieved November 15, 2019 from <http://www.coastguard.ov.ph/images/philcoastguard/PresidentialDecree/PD600.pdf>
- Presidential Decree No. 984. 1976. Providing for the revision of Republic Act No. 3931, commonly known as the pollution control law, and for other purposes. Retrieved January 28, 2020 from <http://r12.emb.gov.ph/wp-content/uploads/2016/04/presidential-decree-no984.pdf>
- Presidential Decree No. 1067. 1976. A decree instituting a water code, thereby revising and consolidating the laws governing the ownership,

- appropriation, utilization, exploitation, development, conservation, and protection of water resources. Retrieved December 16, 2020 from https://www.lawphil.net/statutes/presdecs/p_d1976/pd_1067_1976.html
- Rachon, D. 2016. Endocrine-disrupting chemicals (EDCs) and female cancer: Informing the patients. *Rev. Endoc. Meta. Dis.*, 16: 359-364.
- Ralph, P., Smith, R., Macinnis-Ng, C. and Seery, C. 2007. Use of fluorescence-based ecotoxicological bioassays in monitoring toxicants and pollution in aquatic systems: Review. *Toxicol. Environ. Chem.*, 89(4): 589-607.
- Reboa, A., Mandich, A., Cutroneo, L., Carbone, C., Malatesta, A. and Capello, M. 2019. Baseline evaluation of metal contamination in teleost fishes of the Gulf of Tigullio (north-western Italy): Histopathology and chemical analysis. *Mar. Pol. Bul.*, 141: 16-23.
- Republic Act 9275. 2004. An act providing for comprehensive water quality management and other purposes. <https://emb.gov.ph/wp-content/uploads/2015/09/RA-9275.pdf>
- Roohi-Shalmaa, N., Mousavi-Nadushan, R., Mostafavi, P., Shahbazzadeh, D. and Bagheri, K. 2019. Ecological adaptation of the Persian Gulf polychaete in a polluted area: proteomics concerning dominant defensive biomarkers. *Inter. J. of Environ. Sci. and Tech.*, 17: 1937-1946.
- Sia Su, G., Ramos, G. and Barcelon, E. 2015. Lead bioaccumulation and the imposex effect of *Volema (Pugilina) cochlidium* in Bacoor Bay, Philippines. *J. of Fish. Sci.*, 9(3):001-004.
- Siddig, A.A., Ellison, A.M., Ochs, A., Villar-Leeman, C. and Lau, M.K. 2016. How do ecologists select and use indicator species to monitor ecological change? Insights from 14 years of publication in ecological indicators. *Ecol. Indic.*, 60: 223-230.
- Sinco, A., Sendaydiego, J., Saab, L., Mojica, G., Tampus, G. and Rondez, A. 2014. Riverine biota as indicators of water quality in tropical Cagayan de Oro River, Philippines. *Int. J. of the Bioflux Society*, 6(2): 23-35
- Superada, J. and Tampus, A. 2015. Macroinvertebrates as Indicators of Water Quality in Three Estuary Sites in Iligan City, Philippines. *J. Multidiscip. Stud.*, 4: 85.
- Tellez, M. and Merchant, M. 2015. Biomonitoring heavy metal pollution using an aquatic apex predator, the American alligator, and its parasites. *PLoS One*, 10: e0142522.
- Tuddao, V. and Gonzales, E. 2016. Updates on Water Environment Management in the Philippines. Retrieved August 15, 2021 from http://wepa-db.net/activities/2016/20161130/PDF/11%20Philippines_Country%20updates_FINAL%20PHILIPPINE%20REPORT%20Updates%20on%20Water%20Environment%20Management%20FINAL%20REVISED.pdf
- UNDESAPD (United Nations, Department of Economic and Social Affairs, Population Division). 2018. World urbanization prospects: The 2018 revision, 2020-9-21. Retrieved August 15, 2021 from <http://creativecommons.org/licenses/by/3.0/igo/> (2018)
- Vellinger, D. 2016. Lead contamination in flint-An abject failure to protect public health. *N. Engl. J. Med.*, 374:1101-1103.
- Vestil, J. and Lim, C. 2016. Special Report: Heavy Metals and More. SunStar Philippines, Cebu City, The Philippines, pp. 1-4.
- Walag, A., Canencia, O. and Fiedler, B. 2018. Water quality: Mindanao Island of the Philippines. Translating National Policy to Improve Environmental Conditions Impacting Public Health Through Community Planning, pp. 219-253.
- White, P. 2012. Oil Spill Preparedness and Response for Mariculture Parks in the Philippines - AquaPark Working Report, Akvaplan-Niva, BFAR, pp. 1-28
- World Atlas. 2020. Maps of the Philippines. Retrieved August 15, 2021 from <https://www.worldatlas.com/maps/philippines>
- Zhang, Z. and He, L. 2010. Two new species of Pyemotes closely related to *P. tritici* (Acari: Pyemotidae). *Zootaxa*, 2723: 1-40.
- Zhou, Q. and Jiang, G. 2006. Butyltin accumulation in freshwater clam *Mya arenaria*: An evaluation of its suitability for monitoring butyltin pollution. *Chemosphere*, 63: 1-8.



Investigation on Microbial Fuel Cells Fabricated from Recyclable Materials for Energy Generation and Wastewater Treatment

Somil Thakur and Bhaskar Das†

Department of Environmental and Water Resources Engineering, School of Civil Engineering, VIT, Vellore, Tamil Nadu 632014, India

†Corresponding author: Bhaskar Das; bhaskar.ju@gmail.com

Nat. Env. & Poll. Tech.
Website: www.neptjournal.com

Received: 12-01-2021

Revised: 26-02-2021

Accepted: 16-03-2021

Key Words:

Bio-electricity
Renewable energy
Sustainability
Wastewater treatment

ABSTRACT

Microbial fuel cells (MFC) have gained focus due to their diversity in operating conditions & substrates for the generation of sustainable green energy. In the present study, novel MFC has been fabricated using the recyclable aluminum can as air-cathode and graphite rod as anode for the treatment of domestic wastewater and simultaneous power generation. Three different substrate (COD) concentrations, high ($>800 \text{ mg.L}^{-1}$), medium ($250 \text{ mg.L}^{-1} - 800 \text{ mg.L}^{-1}$) and low ($<250 \text{ mg.L}^{-1}$) were used. The maximum COD removal efficiencies, voltage generation, power densities were found to be 80%, 0.71 V, and 304.46 mW.m^{-2} respectively in high strength wastewater setup. In both medium and low strength wastewater setups, after 288 hours, the COD was reduced below 50 mg.L^{-1} thus limiting the electricity generation substantially. Setup with low-strength wastewater produced a maximum CE (%) of 13.80. Overall results showed that although high-strength wastewater produced better and maximum power densities, medium and low-strength wastewater setups were more consistent in energy generation throughout the experiment.

INTRODUCTION

Rapid urbanization and intense industrialization have increased the consumption of energy sources substantially in recent decades (Zou et al. 2016). The present energy requirement is majorly dependent upon the non-renewable sources mostly fossil fuels, which sums of around 80% of the global energy supply (Gielen et al. 2019). Although these sources are considered to be available in abundance, they are depleting quickly like never before due to excessive resource utilization. Moreover, the conversion of fossil fuels into energy poses numerous adverse effects on the environment, leading to the emission of carbon dioxide, SO_x and NO_x gases which are harmful to the environment (César et al. 2015). Taking this into account, researchers have been working on alternative energy sources in the form of renewable energy, e.g., solar energy, wind energy, geothermal, energy from biomass, etc. Among these, Microbial Fuel Cell (MFC) technology has also emerged as an environment-friendly solution that takes on the concept of energy from biomass, thus providing wastewater treatment and energy generation from it simultaneously without requiring any external power source with additional benefits of minimal to no emission of greenhouse gases (Chen & Smith 2018). MFC's use anaerobic microorganisms to decompose the organic matter in the anodic compartment and breaking it down into CO₂,

hydrogen ions, and electrons. The electrons are transported on anode through soluble shuttle or direct transfer with the help of exo-electrogenic bacteria and are transferred through the external circuit to the cathode (Choudhury et al. 2017, He et al. 2017). The hydrogen ions (protons) are transferred from anode to cathode chamber through fluidized media and meet with the electrons in the cathode compartment thus completing the circuit. Depending upon the reactor design and electrode configurations MFC's can be of various types, e.g., Single chamber MFC, Double chamber MFC, air cathode MFC, benthic MFCs, stacked MFC and MFC integrated with various treatment methodologies (He et al. 2017, Ezziat et al. 2019). Double chamber MFC's have two compartments, one typically referred to as an anode chamber and one as a cathode chamber which are joined by some cation mediator (e.g., Nafion membrane, salt bridge, etc.). However, the required redox potential for MFC can also be maintained in single-chambered systems (Logan et al. 2006). Anoxic anode zone and aerobic cathode zone maintained in a single compartment can create a redox gradient facilitate the transfer of electrons from anode to cathode (Seeber et al. 2015).

The substrate is considered the most important biological factor in MFC which can be pure or complex in nature (Wu et al. 2020). Among the different substrates, municipal wastewater is the most studied due to its

diverse microbial community, significance, and inherent energy potential. It has been found that municipal wastewater contains approximately ten times the energy in the form of biomass that will be required to treat it (Maktabifard et al. 2018).

The available studies on MFC systems indicate limiting factors such as internal resistance and the capital cost for the installation especially for the electrode materials (Feng et al. 2014, Ge & He 2016). Anode material directly influences microbial growth, electron transfer, should have biocompatibility, low resistance, and a large surface area for the microorganism to sustain. For fulfilling that, carbonaceous materials like carbon cloth, graphite plate/rod, and carbon brush are commonly used as anode material (Luo & He 2016). The cathode influences the power generation due to lower Oxygen Reduction Potential (ORR) than the organic anaerobic oxidation in the anode (Kannan & Kumar 2016). To overcome this ORR barrier, the design of the cathode mainly focuses on catalysts or artificial electron mediators to promote higher ORR in the cathode. Some of the abiotic cathodes commonly used are platinum (Pt), transition metal oxides activated carbonaceous material electroconductive polymers, and metal macrocyclic compounds (Zuo et al. 2007, Narayanan & Thakur 2010). The electrodes are one of the major components of MFC based on performance and economic consideration (Choudhury et al. 2017). Though there are possibilities to reduce the cost of electrode material without compromising the performance, there is inadequate information regarding low cost, indigenous, reusable/recyclable electrode material as most of the studies on MFC focus on optimization of design parameters and operating conditions. Wang et al. (2011) used recycled coated tire crumbs in the anode and air cathode and found PD and CE of 421 mWm^{-2} and 25.1% respectively for a single chamber MFC of 140 mL volume. The 2-4 layers of graphite coating in the tire crumbs achieved the specific surface area 10 times more than same-size graphite granules whereas the cost of the electrode is almost 1000 times less. Lefebvre et al. (2012) fabricated a two-chamber MFC with Inconel 718, a recycled scrap material, as cathode with carbon cloth for synthetic wastewater as substrate and achieved maximum acetate removal of 99.7%, PD of 36 Wm^{-3} . Using the recycled material, they reduced the cost of the electrode from 50% to 26% without reduction of performance and leaching of metal even after one year of operation. Low cost commercially available carbon fiber (CF) coated with nickel (Ni), used as cathode material (Luo & He 2016) showed Ni-CF have better performance in respect to electricity generation and cost-effectiveness when compared with carbon cloth CC, which is a conventional electrode material for the cathode. Another recent work (Thakur & Das 2020) used fabricated

composite anode made of *Luffa aegyptiaca* (natural scrubber) and graphite plate for the treatment of municipal wastewater and RO concentrate mix and achieved maximum removal of 95.83%, 87.61%, and 94.06% of COD, TDS, and TSS respectively with a maximum voltage of 0.530 mV and NER of $19.51 \text{ Whkg}^{-1}\text{COD}^{-1}$. The integration of low cost highly porous and locally available material increased the COD, TSS, and TDS removal efficiency and achieved more NER when compared with the MFC system without a natural scrubber.

The aluminum beverage can represent about 80% of total aluminum waste globally which contains 97% metal aluminum. Around 475 billion cans are produced each year, with differing percentages of them being recycled in different nations (Yoo et al. 2007). According to a report by the United States Environmental Protection Agency (US EPA 2015), the recycling rate of aluminum used in packaging and beverage industries is just 32.8 % while in India it stands at 25%. It is clear that this metal has some return value but is not being recycled up to the extent. Apart from the recycling, the waste aluminum cans have served as a useful metal in several studies which investigated other value-added applications like the synthesis of zeolite nanostructure (Abdelrahman 2018), hydroxysodalite nanoparticles (Abdelrahman & Hegazey 2019), hydrogen generation through PEM (Martínez et al. 2007), synthesis of $\gamma\text{-Al}_2\text{O}_3$ (Abdelkader et al. 2018), etc. In a previous study, aluminum was used as an electrode material, and the more conductive nature of aluminum alloy mesh was found to lower internal resistance (Chen et al. 2013). The electrical performance of aluminum alloy mesh carbon cloth electrodes is enhanced in comparison with conventional carbon cloth electrodes. In the present study, recyclable aluminum cans have been used as air cathode in MFCs with graphite rod as anode and different strengths (high, medium, and low) of domestic wastewater as substrate. An unconventional approach was adopted in this study to fabricate the setup by not providing any PEM and letting the ions flow with the help of surface transfer. In most high-voltage domestic electrical applications, short circuits would cause circuit damage, but because energy generation in normal MFCs is substantially lower, this preliminary investigation was designed to see how much energy might be generated without utilising PEM while using recyclable materials. All the available studies with high strength wastewater correspond either to industrial (tannery (Palanisamy et al. 2020), dairy (Mansoorian et al. 2016), pharmaceutical (Velvizhi & Venkata Mohan 2011)) or synthetic wastewater. Hence, high strength domestic sewage wastewater has been considered as substrate in MFCs. Further the results were compared with other studies on MFC using domestic wastewater as substrate.

MATERIAL AND METHODS

Fabrication

Cylindrical aluminum cans made up of 3004-H19 alloy with characteristics (Matweb 2020) as mentioned in Table 1 (diameter - 66 mm & height - 115 mm), generally used as beverage cans, were used as the containment as well as cathode while graphite rods of 10 mm diameter, 50 mm height (48 mm effective) were used as an anode. Each of them was cleansed with 0.5M aqueous HCL solution and rinsed ultrasonically with double distilled water. Anode chambers were sealed and made airtight with the help of thermocol and edges were sealed with epoxy to maintain an anaerobic environment, while cathode chambers were kept open to the atmosphere for an anaerobic environment. Copper wires were used to connect anode and cathode via an external open circuit connected with a multimeter (Fig. 1).

Wastewater Collection

Wastewater was collected from two different treatment plants of VIT Vellore. Raw wastewater (R1, R2) was collected from the inlet chamber of the wastewater treatment plants; primary treated wastewater (S1, S2) was collected from the outlet of the settling chambers; secondary treated wastewater (T1, T2) was collected from the secondary clarifier outlets of the activated sludge system. As per the COD concentration, they were classified as high strength, medium strength & low strength wastewater respectively. The influent COD concentrations are mentioned in Table 2.

Operation

A total of six systems were fabricated with an anode volume of 165 mL each and operated at room temperature (25-30 °C). Influent wastewater was classified with different COD range [39] (i.e.- High wastewater strength (R1, R2 > 800 mg.L⁻¹), Medium strength (250 < S1, S2 < 800) & Low strength (0 < T1, T2 < 250). COD was analyzed using COD digester [Spectroquant TR320] (APHA 2017), voltage (open circuit) with multimeter [MAS830L], pH with digital pH meter [Hanna HI98107]. COD represents the degree of organic pollution in water bodies (Li et al. 2018) which is being consumed by microbes for the generation of energy in MFCs. pH also plays a vital role in wastewater treatment (Yaseen & Scholz 2019) as variation in pH can affect the functioning of microbial activity. Electrogenic microbial culture (geobacter, shewanella, etc.) is neutrophilic and can only sustain in a pH range of 6-8. Normalized energy recovery (NERs) is considered as an important parameter for comparison between different MFCs because of its non-dependence on the size of the reactor while considering wastewater flow rate and organic removal efficiency for its calculation (Das et al. 2019). COD removal, NERs, Power, PD & CE were calculated by using Equation (1), (2), (3), (4) & (5) respectively:

$$\text{COD Removal Efficiency} = \frac{C_i - C_e}{C_i} \times 100 \quad \dots(1)$$

$$\text{Power(P)} = \text{Current(I)} \times \text{Voltage(V)} \quad \dots(2)$$

$$\text{Power Density (PD)} = \frac{\text{Power}}{\text{Area of anode}} \quad \dots(3)$$

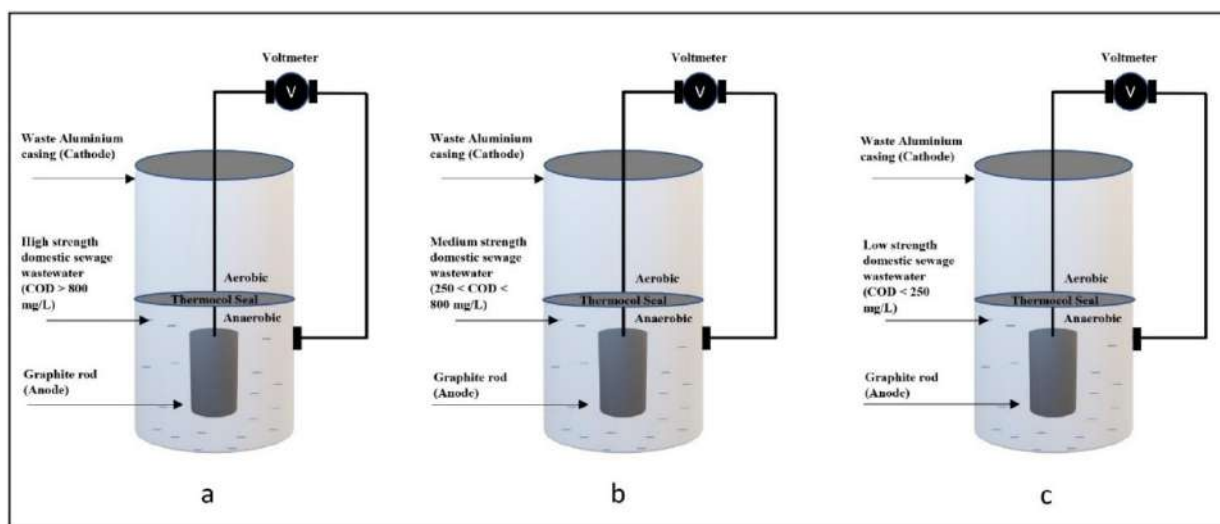


Fig. 1: Schematic diagram of experimental systems representing; (a) – System with high strength wastewater (R1, R2), (b) – System with medium strength wastewater (S1, S2), (c) – System with low strength wastewater (T1, T2).

$$\text{Normalized Energy Recovery (NERs)} = \frac{P * t}{\Delta\text{COD}} \dots(4)$$

$$\text{Coulombic Efficiency (CE)} = \frac{M \int_0^t I dt}{F b v_a \Delta\text{COD}} \dots(5)$$

where, C_i = Initial COD (mg.L^{-1}), C_e = Final COD (mg.L^{-1}), $\text{DCOD} = C_i - C_e$. P = Power, t = time(hours), DCOD = Removed COD, M = Molecular weight of oxygen (32), V = Voltage, I = Current, F = Faraday's constant (96485), $b = 4$ (number of electrons exchanged per mole of oxygen), v_a = Volume of Anode.

RESULTS AND DISCUSSION

COD Removal and pH

COD removal has been calculated with the help of Equation (1). All systems showed gradual COD removal during the experiment in similar trends (Fig. 2). R1 and R2, which had the highest COD loading showed cumulative removal of 83.33% & 91.66%. A gradual reduction in COD was

because of slowly increasing microbial activity in the anode zone of systems which led to anaerobic degradation of organic matter. COD removal efficiencies were calculated after every 72 hours and its variation has been mentioned in Fig. 2(d), while cumulative values have been mentioned in Table 2. Anaerobic microbial culture degraded the organic matter and converted it into electrons and hydrogen ions. The trends of COD reduction in all systems were almost similar. However, more COD removals were achieved by R1, R2 because of the presence of more available biomass but it did not work synergistically with energy generation which has been discussed later. It was also found that the stability of systems with low organic loading was better. The COD removal efficiencies of the present study, when compared with available literature considering domestic wastewater as substrate, were similar at different substrate concentrations (Tatinclaux et al. 2018, Zhang et al. 2015, Ahn et al. 2014) as presented in Table 2.

The pH of influent wastewater was in the range of 7.0-9.0. pH decreased gradually with time in all systems. However, the pH of systems with high-strength wastewater

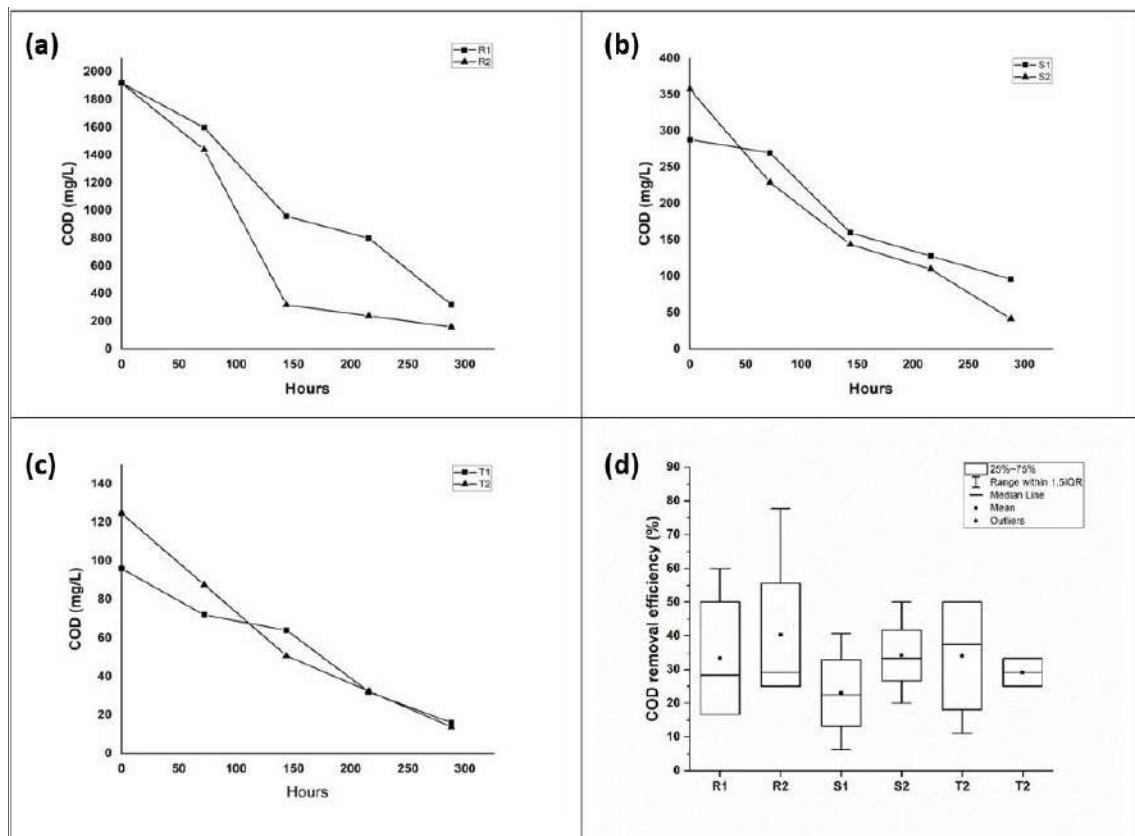


Fig. 2: The reduction in COD (mg.L^{-1}) with respect to time. (a) – High strength wastewater (R1, R2), (b) – Medium strength wastewater (S1, S2), (c) – Low strength wastewater (T1, T2), (d) – Box plot showing the variability of COD removal efficiencies in all systems.

Table 1: Characterization of the Aluminum casing (Matweb 2020).

Alloy 3004- H19			
Mechanical properties		Element properties	
Hardness, Brinell	79	Aluminum, Al	95.5 - 98.2 %
Tensile Strength, Ultimate	295 MPa	Copper, Cu	<= 0.25 %
Tensile Strength, Yield	285 MPa	Iron, Fe	<= 0.70 %
Elongation at Break	2% @Thickness 1.60 mm	Magnesium, Mg	0.80 - 1.3 %
		Manganese, Mn	1.0 - 1.5 %
Modulus of Elasticity	69.0 GPa	Other, each	<= 0.05 %
Poissons Ratio	0.35	Other, total	<= 0.15 %
Shear Modulus	25.0 GPa	Silicon, Si	<= 0.30 %
Shear Strength	180 MPa	Zinc, Zn	<= 0.25 %

was lowest. It can be linked to COD removal and voltage generation, since abundant biomass undergoing anaerobic reactions in R1 and R2 may have resulted in the formation of higher amounts of acids and acetate, lowering the pH to 6.9 in R1 by the end of the experiment. However, due to the higher initial pH of R1, R2, very little energy generation was detected. Throughout the trial, the pH of the medium and low strength wastewater systems was in the range of 7 to 9.

Voltage Generation

R1 and R2 produced maximum voltages of 0.67 and 0.71 V respectively. This can be related directly to the COD removal by the systems (Fig. 2), as maximum COD removals by R1 and R2 were between 72-144 hours when the voltage generations were also maximized. However, R1 and R2 showed slower electrochemical activity initially because of high organic loading and lower pH, but once the electrochemical culture was achieved, this high organic loading helped them to reach the highest voltage peaks in the end. Also, variation of voltage in R1 and R2 is significant as compared to other systems which shows the inconsistency of performance in the case of high strength substrates. In the case of S1, S2, T1 and T2, voltage generations were quite efficient from the initiation of the experiment and they produced peak voltages of 0.61, 0.66, 0.36, and 0.41 V respectively. Electrochemical activities started earlier in these systems due to lower organic loading, thus leading to higher voltage generations, but due to less substrate available, after reaching the peak, it started to decline by the end of the experiment (Fig. 3). The voltage generation of similar studies considering domestic wastewater as a substrate has been included in Table 2. The maximum voltage generated from the present study is comparable with previous results (Ahn & Logan 2013) in all substrate concentrations.

Power Density and Normalized Energy Recovery

Power Density (PD) signifies power generated by a system with respect to the surface area of the electrode (mW.m^{-2}). Maximum PDs obtained by different systems have been mentioned in Table 2. Although maximum PDs were obtained by R1 and R2, the lower average values show that their power generation consistencies were low. Medium strength wastewater managed to produce approximately similar maximum PDs with much better average values and consistency. These consistencies were also verified by Normalized Energy Recovery (NERs) [Fig. 4]. Systems with high-strength wastewater produced maximum NERs of 0.22 kWh/kgCOD during 216 -288 hours, medium-strength wastewater produced 0.79 kWh/kgCOD during 144-216 hours, and low strength wastewater produced NERs of 0.65 kWh/kgCOD during 72-144 hours. In the case of low strength wastewater systems, there is an increasing trend of NERs till 144 hours, after which it started decreasing from 0.65 kWh/kgCOD to 0.15 kWh/kgCOD by end of the experiment. It was observed that decrease of COD value below 50 mg.L^{-1} limits the generation of energy which reduces the NERs for low strength wastewater substantially. The less NERs during the initial phase for high-strength wastewater systems were due to more activation time required to produce electrons because of high pH and organic loading. Though during 144-288 hours, NERs values for these systems showed increasing trends and superseded the decreasing trend of systems with low strength, medium-strength wastewater systems achieved maximum NERs values during 144-216 hours and then declined.

Coulombic Efficiency

The T1 achieved the highest CE of 22.11 %, showing that exoelectrogens were able to use that percentage of electrons

Table 2: Performance of single chamber MFCs considering domestic wastewater as substrate.

S.No.	Type	Substrate concentration	Type of MFC	Working volume	Anode	Cathode	Voltage	COD removal (%)	Max Power Density	Coulombic Efficiency (%)	Reference	
1	Batch	155 ± 36 to 232 ± 84	SC-MFC; No membrane	130 mL	Graphite brush anodes	Carbon cloth	0.41 ± 0.05 V	>90	120 mW/m ²	-	(Ahn et al. 2014)	
2	Continuous	410	SC-MFC; with 2 cathodes	Variable flow rate (30-140 mL/h)	Graphite fiber brushes	Activated carbon with polyvinylidene fluoride (PVDF) binder	-	64.8 ± 1.7	Power - 1.30 to 1.36 mW	18 ± 5 to 29 ± 3	(Kim et al. 2015)	
		410	SC-MFC; Single anode single cathode	Variable flow rate (20-100 mL/h)			-	69.0 ± 0.4	Power - 1.00 to 1.22 mW	18 ± 2 to 36 ± 2		
3	Batch	303.69	SC-MFC with separator	130 mL	Graphite fiber brush	Carbon cloth	0.58 V	62.4 to 94.1	328.11 mW/m ²	9.2 to 31.4	(Ahn & Logan 2013)	
		303.69	SC-MFC without separator				0.54 V	81.5 to 93.3	282.29 mW/m ²	1.5 to 23.3		
4	Batch	545 ± 5	SC-MFC without cloth separator	140 mL	Carbon fiber brush	Carbon cloth cathode with a Pt catalyst without a separator (Pt-NS)	-	82 ± 0	315 ± 16 mW/m ²	26 ± 1	(Stager et al. 2017)	
	Batch	330 ± 5	SC-MFC with cloth separator				Activated carbon cathode (AC-CS)	-	59 ± 3	161 ± 14 mW/m ²		19 ± 1
	Continuous	1050 ± 2	SC-MFC without cloth separator				Activated carbon cathode with a cloth separator (AC-CS)	-	28 ± 5	257 mW/m ²		7 ± 2
5	Batch	223 ± 6	SC-MFC; No membrane	26 mL	Graphite fiber brush	Carbon cloth with Pt. catalyst layer	-	55 (Approx.)	-	21	(Zhang et al. 2015)	
6	Batch	237.3 ± 8.0	SC-MFC; Mn coating	2000 mL	Circular graphite plate	Carbon Cloth	0.5 V	45.55	48.4 ± 10.16 mW/m ²	-	(Tatinclaux et al. 2018)	
		293.3 ± 81.5	SC-MFC; Pt coating				0.45 V	27.98	65.4 ± 4.6 mW/m ²	-		
7	Batch	1920	SC-MFC; No membrane	165 mL	Graphite rod	Aluminium sheet	0.67 V	83.33	267.19 mW/m ²	0.01 to 0.25	This study	
		1920	SC-MFC; No membrane				0.71 V	91.66	304.46 mW/m ²	0.04 to 4.55		
		288	SC-MFC; No membrane				0.61 V	66.66	224.21 mW/m ²	2.58 to 9.33		
		360	SC-MFC; No membrane				0.66 V	82.22	259.24 mW/m ²	1.27 to 9.86		
		96	SC-MFC; No membrane				0.36 V	83.33	78.27 mW/m ²	4.80 to 22.11		
		128	SC-MFC; No membrane				0.41 V	75	98.27 mW/m ²	4.05 to 9.97		

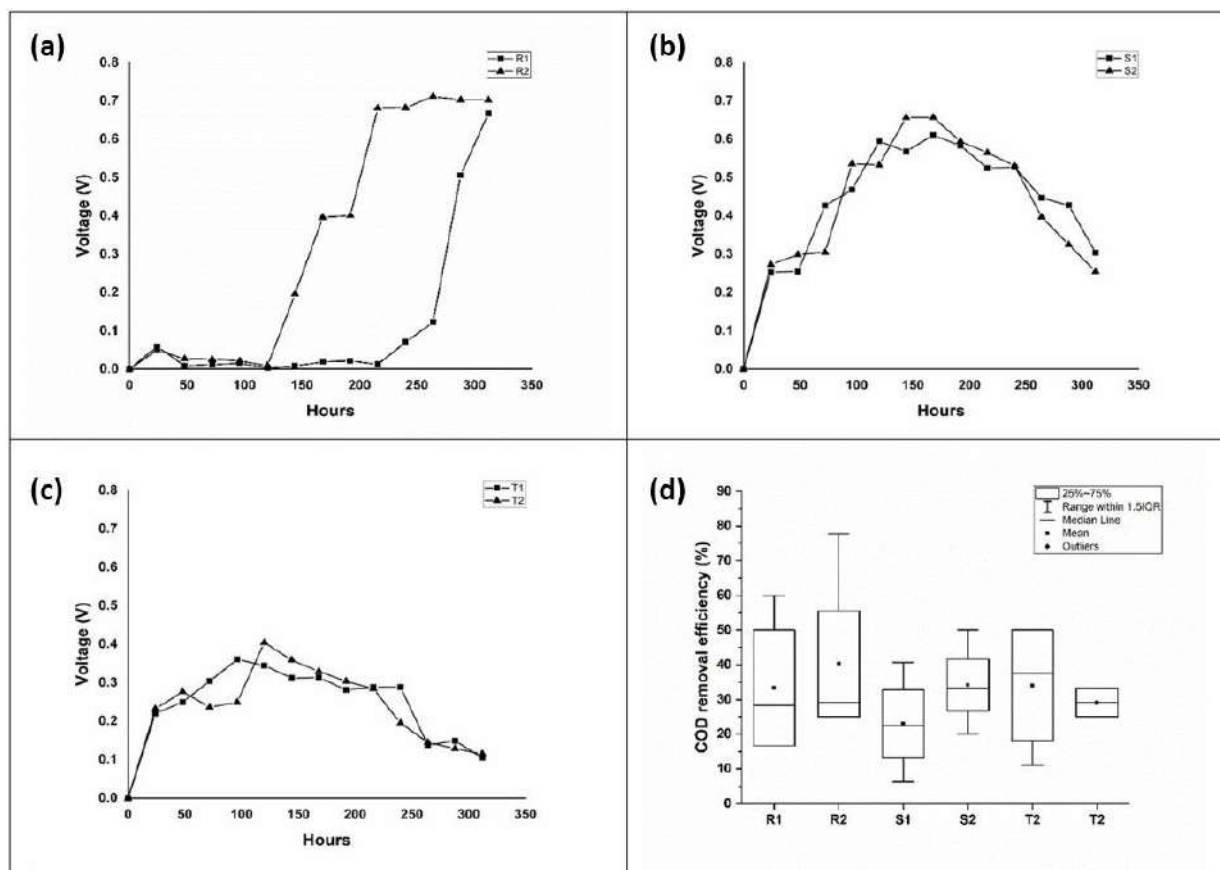


Fig. 3: Voltage generation with respect to time; (a) – High strength wastewater (R1, R2), (b) – Medium strength wastewater (S1, S2), (c) – Low strength wastewater (T1, T2), (d) – Box plot showing the variability of voltage generation in all systems.

generated from the substrate for energy generation. R1 and R2 utilized only a small fraction of electrons generated in form of current (Max CE in R1, R2 = 0.25%, 4.55%), which indicates less electron settlement on the anode. This might be due to higher internal resistance due to the settleable non-conductive particles which are available in raw wastewater. As wastewater was collected from different treatment plants, the difference in CE of R1 and R2 might be due to the varying concentrations of other constituents like nitrates, phosphates, and chlorides. The possibilities of electron loss due to alternate electron acceptors like dissolved oxygen or short-circuiting also cannot be ruled out (Kim et al. 2015). Short-circuiting in systems can be avoided by coating the internal surface of the cathode zone with proton exchange membranes but the cost of fabrication will increase substantially. For further comparison of performance, the average CE of similar substrate concentrations was considered. Systems with high-strength wastewater produced an average CE of 2.40%, medium-strength wastewater produced 9.59%, and

low-strength wastewater produced 13.80% which has been shown in Fig. 4. In the case of low strength wastewater systems, there is an increasing trend of CE till 144 and 216 hours respectively, after which it decreased from 13.80 to 5.66%. This implies a depleted substrate in these systems, as they gradually decreased after reaching a maximum value. Initial CE was low in systems with high wastewater strength, but it steadily grew over time, indicating the development of electrogenic microbial growth over the course of 216-288 hours.

CONCLUSION

The overall performances were satisfactory, as COD reduction and energy generation were comparable with similar MFC designs. Systems with high organic loading removed more COD than other systems and produced more maximum voltages. However, in terms of electrochemical activities, they struggled to deliver initially and systems with lower organic loading performed better, thus providing more energy recovery and coulombic efficiency. Higher COD loading

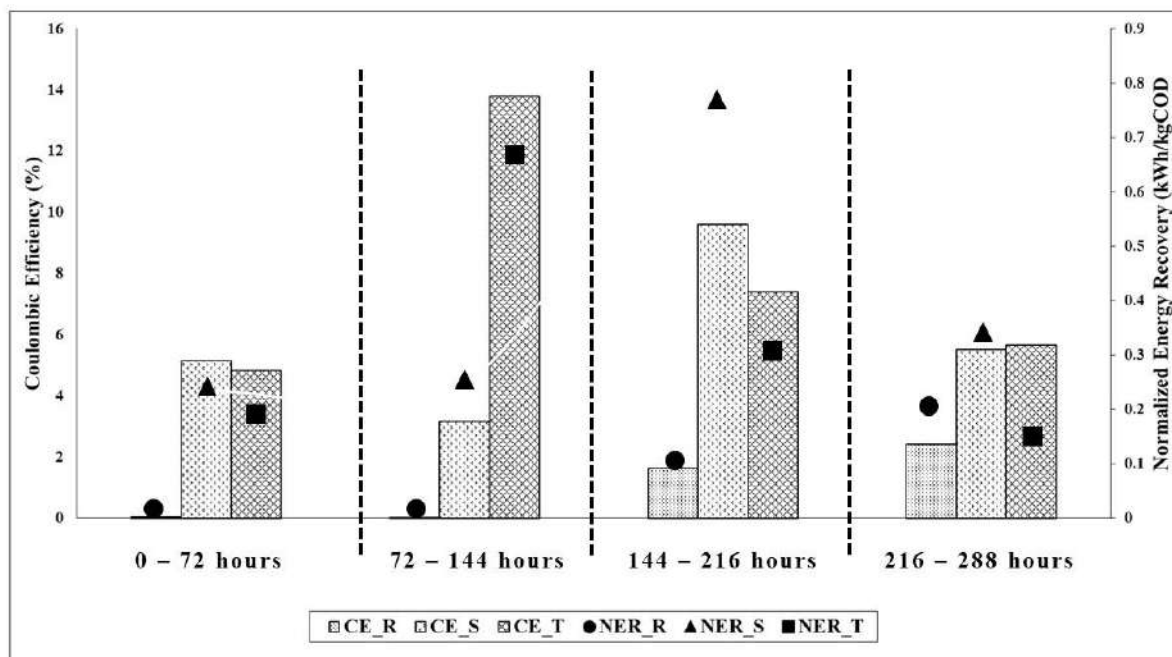


Fig. 4: The variation of Coulombic efficiency (CE) & Normalized Energy recovery with time [represented as {CE_R, NER_R (Average of R1, R2)}, {CE_S, NER_S (Average of S1, S2)} and CE_T, NER_T (average of T1, T2)}].

required more time in starting electrochemical activities of MFCs and have more energy losses. On the other hand, lower organic loading can utilize produced electrons efficiently but might need new substrate feed after some operation time. They even have more stability and give equivalent performance as systems with high organic loading. The short circuit did not seem to affect the performance but still, a detailed study for obtaining the mechanism of electron transfer and relation of performance with other constituents like nitrates, sulfates, and chlorides are required. Also, after observing the overall performance of fabricated MFC's in comparison to other studies, the use of recyclable/reusable materials is recommended after proper pretreatment.

ACKNOWLEDGEMENT

The authors acknowledge the help of VIT, Vellore, India for the financial & technical support provided under Seed Fund for Research (RGEMS) to carry out this research work.

ABBREVIATIONS

MFC	Microbial Fuel Cell
R1, R2	Experimental systems with high strength wastewater
S1, S2	Experimental systems with medium strength wastewater
T1, T2	Experimental systems with low strength wastewater
COD	Chemical Oxygen Demand

NER	Normalized Energy Recovery
PD	Power density
CE	Coulombic Efficiency

REFERENCES

- Abdelkader, A., Osman, A.I., Halawy, S.A. and Mohamed, M.A. 2018. Preparation and characterization of mesoporous γ -Al₂O₃ recovered from aluminum cans waste and its use in the dehydration of methanol to dimethyl ether. *J. Mater. Cycles Waste Manag.*, 20: 1428-1436. <https://doi.org/10.1007/s10163-018-0702-0>
- Abdelrahman, E.A. 2018. Synthesis of zeolite nanostructures from waste aluminum cans for efficient removal of malachite green dye from aqueous media. *J. Mol. Liq.*, 253: 72-82. <https://doi.org/10.1016/j.molliq.2018.01.038>
- Abdelrahman, E.A. and Hegazy, R.M. 2019. Utilization of waste aluminum cans in the fabrication of hydroxysodalite nanoparticles and their chitosan biopolymer composites for the removal of Ni(II) and Pb(II) ions from aqueous solutions: Kinetic, equilibrium, and reusability studies. *Microchem. J.*, 145: 18-25. <https://doi.org/10.1016/j.microc.2018.10.016>
- Ahn, Y., Hatzell, M.C., Zhang, F. and Logan, B.E. 2014. Different electrode configurations to optimize the performance of multi-electrode microbial fuel cells for generating power or treating domestic wastewater. *J. Power Sources*, 249: 440-445. <https://doi.org/10.1016/j.jpowsour.2013.10.081>
- Ahn, Y. and Logan, B.E. 2013. Domestic wastewater treatment using multi-electrode continuous flow MFCs with a separator electrode assembly design. *Appl. Microbiol. Biotechnol.*, 97: 409-416. <https://doi.org/10.1007/s00253-012-4455-8>
- APHA. 2017. Standard methods for the examination of water and wastewater. 23rd edition. American Public Health Association, Washington DC, USA.

- César, A.C.G., Carvalho, J.A. and Nascimento L.F.C. 2015. Association between NO_x exposure and deaths caused by respiratory diseases in a medium-sized Brazilian city. *Brazilian J. Med. Biol. Res.*, 48: 1130-1135. <https://doi.org/10.1590/1414-431X20154396>
- Chen, S. and Smith, A.L. 2018. Methane-driven microbial fuel cells recover energy and mitigate dissolved methane emissions from anaerobic effluents. *Environ. Sci. Water Res. Technol.*, 4: 67-79. <https://doi.org/10.1039/c7ew00293a>
- Chen, Y.M., Wang, C.T., Yang, Y.C. and Chen, W.J. 2013. Application of aluminum-alloy mesh composite carbon cloth for the design of anode/cathode electrodes in *Escherichia coli* microbial fuel cell. *Int. J. Hydrogen Energy*, 38: 11131-11137. <https://doi.org/10.1016/j.ijhydene.2013.01.010>
- Choudhury, P., Uday, U.S.P., Mahata, N., Nath Tiwari, O., Narayan Ray, R., Kanti Bandyopadhyay, T. and Bhunia, B. 2017. Performance improvement of microbial fuel cells for wastewater treatment along with value addition: A review on past achievements and recent perspectives. *Renew. Sustain. Energy Rev.*, 79: 372-389. <https://doi.org/10.1016/j.rser.2017.05.098>
- Das, B., Thakur, S., Chaitanya, M.S. and Biswas, P. 2019. Batch investigation of constructed wetland microbial fuel cell with reverse osmosis (RO) concentrates and wastewater mix as substrate. *Biomass and Bioenergy*, 122: 231-237. <https://doi.org/10.1016/j.biombioe.2019.01.017>
- Ezziat, L., Elabed, A., Ibsouda, S. and El Abed, S. 2019. Challenges of microbial fuel cell architecture on heavy metal recovery and removal from wastewater. *Front. Energy Res.*, 7: 1-13. <https://doi.org/10.3389/fenrg.2019.00001>
- Feng, Y., He, W., Liu, J., Wang, X., Qu, Y. and Ren, N. 2014. A horizontal plug flow and stackable pilot microbial fuel cell for municipal wastewater treatment. *Bioresour. Technol.*, 156: 132-138. <https://doi.org/10.1016/j.biortech.2013.12.104>
- Ge, Z. and He, Z. 2016. Long-term performance of a 200 liter modularized microbial fuel cell system treating municipal wastewater: Treatment, energy, and cost. *Environ. Sci. Water Res. Technol.*, 2: 274-281. <https://doi.org/10.1039/c6ew00020g>
- Gielen, D., Boshell, F., Saygin, D., Bazilian, M.D., Wagner, N. and Gorini, R. 2019. The role of renewable energy in the global energy transformation. *Energy Strateg. Rev.*, 24: 38-50. <https://doi.org/10.1016/j.esr.2019.01.006>
- He, L., Du, P., Chen, Y., Lu, H., Cheng, X., Chang, B. and Wang, Z. 2017. Advances in microbial fuel cells for wastewater treatment. *Renew. Sustain. Energy Rev.*, 71: 388-403. <https://doi.org/10.1016/j.rser.2016.12.069>
- Kannan, M.V. and Kumar, G.G. 2016. Current status, key challenges, and its solutions in the design and development of graphene-based ORR catalysts for microbial fuel cell applications. *Biosens. Bioelectron.*, 77: 1208-1220. <https://doi.org/10.1016/j.bios.2015.10.018>
- Kim, K.Y., Yang, W. and Logan, B.E. 2015. Impact of electrode configurations on retention time and domestic wastewater treatment efficiency using microbial fuel cells. *Water Res.*, 80: 41-46.
- Lefebvre, O., Shen, Y. and Ng, H.Y. 2012. Optimization of a microbial fuel cell for wastewater treatment using recycled scrap metals as a cost-effective cathode material. *Bioresour. Technol.*, 127C: 158-164. <https://doi.org/10.1016/j.watres.2015.05.021>
- Li, J., Luo, G., He, L.J., Xu, J. and Lyu, J. 2018. Analytical approaches for determining chemical oxygen demand in water bodies: A review. *Crit. Rev. Anal. Chem.*, 48: 47-65. <https://doi.org/10.1080/10408347.2017.1370670>
- Logan, B.E., Hamelers, B., Rozendal, R., Schröder, U., Keller, J., Freguia, S., Aeltermann, P., Verstraete, W. and Rabaey, K. 2006. Microbial fuel cells: Methodology and technology. *Environ. Sci. Technol.*, 40: 5181-5192. <https://doi.org/10.1021/es0605016>
- Luo, S. and He, Z. 2016. Ni-coated carbon fiber as an alternative cathode electrode material to improve the cost efficiency of microbial fuel cells. *Electrochim. Acta.*, 222: 338-346. <https://doi.org/10.1016/j.electacta.2016.10.178>
- Maktabifard, M., Zaborowska, E. and Makinia, J. 2018. Achieving energy neutrality in wastewater treatment plants through energy savings and enhancing renewable energy production. *Rev. Environ. Sci. Biotechnol.*, 17: 655-689. <https://doi.org/10.1007/s11157-018-9478-x>
- Mansoorian, H.J., Mahvi, A.H., Jafari, A.J. and Khanjani, N. 2016. Evaluation of dairy industry wastewater treatment and simultaneous bioelectricity generation in a catalyst-less and mediator-less membrane microbial fuel cell. *J. Saudi Chem. Soc.*, 20: 88-100. <https://doi.org/10.1016/j.jscs.2014.08.002>
- Martínez, S.S., Albañil Sánchez, L., Álvarez Gallegos, A.A. and Sebastian, P.J. 2007. Coupling a PEM fuel cell and the hydrogen generation from aluminum waste cans. *Int. J. Hydrogen Energy*, 32: 3159-3162. <https://doi.org/10.1016/j.ijhydene.2006.03.015>
- Matweb. 2020. Characteristics of Aluminum 3004-H19. http://www.matweb.com/search/datasheet_print.aspx?matguid=ec6a8753c110472ebcead3a2f95457ba&n=1
- Narayanan, A. and Thakur, M. 2010. Quadratic electro-optic effect in the non-conjugated conductive polymer iodine-doped poly(β -pinene) measured at longer wavelengths including 1.55 μ m. *Solid State Commun.*, 150: 375-378. <https://doi.org/10.1016/j.ssc.2009.11.036>
- Palanisamy, D., Chockalingam, L.R. and Murugan, D. 2020. Microbial fuel cell for effluent treatment and sustainable power generation. *Energy Sources, Part A Recover. Util. Environ. Eff.*, 1: 1-13. <https://doi.org/10.1080/15567036.2020.1796844>
- Seeber, R., Zanardi, C. and Inzelt, G. 2015. Links between electrochemical thermodynamics and kinetics. *ChemTexts.*, 1: 18. <https://doi.org/10.1007/s40828-015-0018-9>
- Stager, J.L., Zhang, X. and Logan, B.E. 2017. The addition of acetate improves the stability of power generation using microbial fuel cells treating domestic wastewater. *Bioelectrochemistry*, 118: 154-160. <https://doi.org/10.1016/j.bioelechem.2017.08.002>
- Tatinclaux, M., Gregoire, K., Leininger, A., Biffinger, J.C., Tender, L., Ramirez, M., Torrents, A. and Kjellerup, B. V. 2018. Electricity generation from wastewater using a floating air cathode microbial fuel cell. *Water-Energy Nexus*, 1: 97-103. <https://doi.org/10.1016/j.wen.2018.09.001>
- Thakur, S. and Das, B. 2020. Performance evaluation of microbial fuel cell with sewage wastewater and RO concentrate using composite anode made of Luffa aegyptiaca. *Environ. Prog. Sustain. Energy*, 76: e13504. <https://doi.org/10.1002/ep.13504>
- US EPA. 2015. Advancing Sustainable Materials Management: Facts and Figures 2013, United States Environmental Protection Agency.
- Velvizhi, G. and Venkata Mohan, S. 2011. Biocatalyst behavior under self-induced electrogenic microenvironment in comparison with anaerobic treatment: Evaluation with pharmaceutical wastewater for multi-pollutant removal. *Bioresour. Technol.*, 102: 10784-10793. <https://doi.org/10.1016/j.biortech.2011.08.061>
- Wu, Q., Jiao, S., Ma, M. and Peng, S. 2020. Microbial fuel cell system: A promising technology for pollutant removal and environmental remediation. *Environ. Sci. Pollut. Res.*, 27: 6749-6764. <https://doi.org/10.1007/s11356-020-07745-0>
- Yaseen, D.A. and Scholz, M. 2019. Impact of pH on the treatment of artificial textile wastewater containing azo dyes using pond systems. *Int. J. Environ. Res.*, 13: 367-385. <https://doi.org/10.1007/s41742-019-00180-1>
- Yoo, S.J., Yoon, H.S., Jang, H.D., Hong, S.T., Park, H.S., Park, S.U., Kwak, D.H. and Lee, S.I. 2007. Synthesis of aluminum ethoxide from used aluminum cans. *Korean J. Chem. Eng.*, 24: 872-876. <https://doi.org/10.1007/s11814-007-0057-z>
- Zhang, X., He, W., Ren, L., Stager, J., Evans, P.J. and Logan, B.E. 2015. COD removal characteristics in air-cathode microbial fuel cells. *Bioresour. Technol.*, 176: 23-31. <https://doi.org/10.1016/j.biortech.2014.11.001>
- Zou, C., Zhao, Q., Zhang, G. and Xiong, B. 2016. Energy revolution: From a fossil energy era to a new energy era. *Nat. Gas Ind. B.* 3: 1-11. <https://doi.org/10.1016/j.ngib.2016.02.001>
- Zuo, Y., Cheng, S., Call, D.F. and Logan, B. 2007. Scalable tubular membrane cathodes for microbial fuel cell applications. *ACS Natl. Meet. B. Abstr.*, 41: 3347-3353.



Cell Death Induction Potential in Seed Extracts- Hidden and Bioactive Phytochemical Treasures

R. Rajasekaran and P. K. Suresh†

Department of Biomedical Sciences, SBST, VIT, Vellore-632014, India

†Corresponding author: P. K. Suresh; p.k.suresh@vit.ac.in

Nat. Env. & Poll. Tech.
Website: www.neptjournal.com

Received: 17-04-2021

Revised: 20-05-2021

Accepted: 25-05-2021

Key Words:

Seed extracts
Cell death
GSPs
Drug-delivery potential

ABSTRACT

Seeds have been known to possess bioactive components with anti-cancer properties. This study aims to demonstrate the processes by which seed extracts from various sources induce cell death. Several assays have been employed to demonstrate the induction of cell death by the respective seed extracts. This review also underscores the importance of Grape Seed Proanthocyanidins (GSPs) in terms of inducing the aforesaid physiological form of seed extract-induced cell death. Furthermore, this review highlights the critical and pressing need to conduct comparative HTS-based strategies (with a battery of cell lines representing different cancers) to identify the major seed extracts that can reproducibly serve to augment the cell death induction capabilities of the existing battery of chemotherapeutic drugs/ natural alternatives.

INTRODUCTION

Seed extracts are known to be rich in phenolic and flavonoid compounds, minerals, vitamins, fatty acids. Such extracts and bioactive compounds extracted from various seed sources have exhibited therapeutic potential in drug development for various human diseases and disorders. They have exhibited high antioxidant and anticancer properties (Liu et al. 2016), anti-inflammatory (Chene et al. 2016), antibacterial (Al-Mamun et al. 2016), and hepatoprotective effects (Mahli et al. 2015, Ogaly et al. 2015). In terms of its anti-cancer properties, demonstration of the improved induction of cell death would be the proof-of-concept strategy for screening and selecting the best seed/solvent(s) combination for anticancer drug development. This review will address a gap in the literature by critically analyzing existing research, discussing future challenges, and bringing readers up to date on seed extract-mediated cell death (*in vitro* and *in vivo*). The rationale behind this approach is that cell death resistance, exhibited by tumorigenic and their relatively recalcitrant subsets (stem cells) is one of the hallmarks of cancer. Hence, the administration of extracts from seed sources may be a feasible and viable strategy for cell death induction. Our approach of selecting and discussing research papers based on work carried out on extracts of seeds from diverse sources would provide an impetus to perform High-Throughput Screening (HTS) of the various extracts and/or the bioactive components contained therein. This strategy would enable

us to rank order them in terms of their efficacy in inducing cell death. Also, the experimental design should ensure that the various seasonal and dormancy-related variations in the levels of the bioactive components are taken into account. Last but not least, this experimental design can be extended to evaluate crude extract-synthesized natural molecule derivative combinations for possible synergy in cell death induction potential.

Selected Seed Extracts and Apoptosis -*In vitro* Approaches

A plant extract-based chemotherapeutic strategy can complement surgery and radiotherapy and possibly reduce, if not eliminate, the undesirable, inevitable side-effects associated with the current arsenal of anti-cancer drugs. A vast majority of FDA-approved new plant compounds are used for cancer therapy and have shown good results in clinical trials and therapeutic applications (Seca & Pinto 2018). The papers cited and discussed concern mechanistic information about the involvement of either or both extrinsic and intrinsic mechanisms of cell death, as well as empirical measurements of seed extract-induced cell death. In certain cases, *in vitro*, antioxidant assays have been employed to correlate ROS levels with cell death induction. This paper gives an overview of the cell death-inducing potential of extracts from a variety of plant flora that is indigenous to different parts of the world. This approach highlights the ubiquitous presence of

significant bioactive molecules in seeds, despite qualitative and quantitative differences in their content, warranting a systematic screening of seed extracts for the selection of the best seed/extract-cancer pair for cell death induction.

Acacia belongs to the Fabaceae family and Mimosoideae subfamily, seen predominantly in the African and Australian continents. Cytotoxic effect of ACS extract was determined by 3-(4,5-dimethylthiazol-2-yl)-2,5-diphenyltetrazolium bromide assay, using concentrations of 0.1–1000 $\mu\text{g.mL}^{-1}$ for 24 h. *A. catechu* ethanol seed extract was treated SCC-25 cells with 25 and 50 $\mu\text{g.mL}^{-1}$. At the end of treatment period, apoptotic marker gene expressions such as caspase 8, 9, Bcl-2, Bax, and cytochrome c were evaluated by semiquantitative reverse transcription-polymerase chain reaction. Morphological changes of ACS treated SCC-25 cells was evaluated by acridine orange/ethidium bromide (AO/EB) dual staining. Nuclear morphology and DNA fragmentation was evaluated by propidium iodide (PI) staining. *Areca catechu* ethanol seed extract treatment caused cytotoxicity in SCC-25 cells with an IC₅₀ value of 100 $\mu\text{g.mL}^{-1}$. Apoptotic markers caspases 8 and 9, cytochrome c, Bax gene expressions were significantly increased upon ACS extract treatment indicate the apoptosis induction in SCC-25 cells. This treatment also caused significant downregulation of Bcl-2 gene expression. Staining with AO/EB and PI shows membrane blebbing, and nuclear membrane distortion further confirms the apoptosis induction by ACS treatment in SCC-25 cells (Lakshmi et al. 2017).

Adenium obesum is a flowering plant, which is part to the Apocynaceae family and is indigenous to certain parts of Africa. The cytogenotoxic potential of *Adenium obesum* seed extracts was evaluated in MCF-7 cells. A growth inhibition assay was performed and it was shown that the IC₅₀ of a crude Methanol-based extract was 337 $\mu\text{g.mL}^{-1}$. After a 12hour exposure to 200 $\mu\text{g.mL}^{-1}$ and 300 $\mu\text{g.mL}^{-1}$ of a methanolic extract of this seed, flow cytometric evaluation showed that 37% and 35% of cells were in the early and late apoptosis stages. At the same time point and identical concentrations, the results of the comet assay provided adequate evidence in terms of the total DNA damage score being 614 and 617 respectively. Due to the aforesaid demonstrated properties, this extract may be exploited and further evaluated for its anticancer potential (Ali et al. 2019).

The avocado, a flowering plant, has been reported to originate from certain parts of Mexico and is a member of the Lauraceae family. Free radical scavenging capabilities of the Colored Avocado Seed Extract (CASE) was determined using the Oxygen Radical Acceptance Capacity (ORAC) and the lipid hydroperoxides reduction assays. At a concentration of 500 $\mu\text{g.mL}^{-1}$, the ORAC value was 2012 \pm 300

Trolox equivalents/mg. Further, there was a 33% reduction in the lipid hydroperoxide formation (emulsion was oil-in-water), at the same concentration of CASE. In terms of the half-maximal effects (19 to 132 $\mu\text{g.mL}^{-1}$), a wide range of inhibitory concentrations was measured, following a 48hour *in vitro* exposure of a battery of cell lines (MCF7; H1299; HT29; LNCaP) to the CASE. In LNCaP cells, the IC₅₀ value for CASE was 42 $\mu\text{g.mL}^{-1}$ at the 12hour time point. A G₀/G₁ cell cycle arrest was observed and the expression of cyclin D1 and E2 (Western blot (WB) assay) were decreased, despite differences in the exposure period. The extent of the cell cycle arrest was 70 and 84% respectively at the IC₅₀ and IC₆₀ concentrations. Concentration-dependent elevations in cell death were determined based on Annexin V-FITC/PI measurements of phosphatidylserine externalization. In the same cell line, WB assay showed that cell death was correlated with elevations in caspase-3 expression as well as cleaved PARP levels relative to control values. Similarly, WB results showed a correlated decrease in the translocation of NF- κ B to the nucleus (Davatgaran et al. 2017).

The Apricot belongs to the *Prunus* genus and its species is *Armeniaca*, even though related species are also considered to form part of this family. Variations in cellular behavior were demonstrated depending on the source of the kernel extracts at the 100, 500, and 1000 $\mu\text{g.mL}^{-1}$ concentrations respectively. The main bioactive principle in the kernels associated with cyanide production is amygdalin. This bioactive component inhibits cytochrome c oxidase –an important enzyme in the Electron Transport Chain (ETC). This, in turn, affects ATP production, and hence, this results in the shift from apoptosis to necrosis. The extracts from the Chinese apricots (CAK) produced a time and concentration-dependent decrease in cell numbers following incubation for 24 as well as for 48 hours. However, after exposure for 3 days, solvent effects were seen in the case of the 100 $\mu\text{g.mL}^{-1}$ (CAK-hydrophilic) as well as in 1000 $\mu\text{g.mL}^{-1}$ (CAK-hydrophilic and CAK-lipophilic). However, biphasic temporal and concentration-dependent variations were demonstrated in HT-29 cells by all the apricot kernels of the South African variety. At the 24-hour time point, the South African apricot (SAK) kernels increased cell proliferation at the 100 and 1000 $\mu\text{g.mL}^{-1}$ concentrations, while the cell numbers decreased at the intermediate 500 $\mu\text{g.mL}^{-1}$ concentration. Similar, albeit statistically insignificant, effects were observed following a 48hour incubation period. Marked variation in this cellular behavior was exhibited at 72 h. As in the case of the 24hour time point, the lowest, as well as the highest concentration of all the SAK extracts, tested inhibited cell proliferation. However, there was a substantial increase in cell numbers, following exposure to 500 $\mu\text{g.mL}^{-1}$ of the extract. A similar trend was seen in the case of the extracts from the South Af-

rican Peach kernels (SPK). The lack of a correlation between the morphological changes and possible apoptotic-related phenomenon (Hoechst33342-based staining) indicated that their observed irregularities in shape as well as in cell volume were plausibly not linked to apoptosis in the case of the SAK and SPK extracts. In the case of the 100 $\mu\text{g}\cdot\text{mL}^{-1}$ Chinese peach Hydrophilic (CPK-H) extract (24 h exposure), membranous protrusions (blebbing) was seen, while at 48 hours, the Chinese Apricot Total (CAK-T) extract at a concentration of 100 $\mu\text{g}\cdot\text{mL}^{-1}$, exhibited irregularities in the cellular morphology. In general, the cell cycle analysis data (of all the extracts) was that there was a significant increase in the S phase cells, despite the lack of a definite dose-dependent trend. The temporary nature of the block may be attributable to the cell being able to withstand the damage during the process of replication. This may explain the observed decrease in cell numbers following a 24-hour exposure to the Chinese kernel extracts (Cassiem et al. 2019).

Alcea rosea is an ornamental plant in the Malvaceae family. The ethyl acetate extract of *Alcea rosea* (AR; Hollyhock) was tested (hexosaminidase assay) at a concentration range of 0–100 $\mu\text{g}\cdot\text{mL}^{-1}$ for its anti-proliferative effects in two colon cancer cell lines (HCT116 and SW480) at three different time point (24, 48 and 72 hours). Results clearly indicated the dose and time-dependent nature of the growth inhibition in both the cell lines with a correlated decrease in Ki-67 (a marker indicative of the proliferation status). In both the cell lines, these extracts inhibited the cells in the transition between the G_0 and G_1 phase at 24 and 48 hours. In addition, this block could be correlated with a decrease in the levels of Cyclin B and D1 based on WB data. The apoptosis data, as well as the molecular correlates (cleaved PARP; decreases in Bcl-xL; an elevation in the Bax levels and an increase in fully cleaved caspase-3), provided fairly definitive evidence of this AR seed extract's capabilities to induce cell death by apoptosis. Next, the colony-forming potential was assessed following treatment of both cell lines with AR for a week. Serial passaging and replating were done to demonstrate the dose-dependent decrease in the number and size of colon spheres (thereby providing inferential evidence of a decrease in the number of stem cells). WB analysis of cell lysates obtained from 2D cultures of both cell lines was done, after their treatment with the AR extract. In this 2D model system, a decrease in the stem cell markers was observed (ALDH1A1, Dcl1, and CD44e), and this may be correlated with the decrease in the number and size of colon spheres. This data was correlated with a concomitant decrease in β -catenin, plausibly linked to increases in WIF1 (a Wnt antagonist). The increased expression of the antagonist could be correlated with decreases in EZH2 signaling (an epigenetic regulator involved in the expression

of the antagonist). Also, components of the Notch pathway (Notch-ICD and Hes1) were decreased following treatment with AR extract. Due to its apoptotic potential, analytical characterization would aid in the identification of the probable bioactive component, that may have most plausibly contributed to this controlled form of cell demise. In this regard, HPLC-based preliminary analysis has provided them with some pointers for the delineation of the principal active components that can be developed to target colon cancer (Ahmed et al. 2016).

Cell line studies have shown that *Aesculus hippocastanum* (the horse chestnut –flowering plant belonging to the soapberry and lychee family Sapindaceae) seed extracts have several pharmacological properties, including anti-inflammatory and cell death induction potential. The major bioactive principle is considered to be β -escin or escin (Penta tricyclic terpene). However, this report is the first of its kind, wherein the cytotoxicity and cell death potential of escin was evaluated using C6 glioma and A549 cells. The combination of cytotoxicity and cell death assays employed include MTT, Annexin V–FITC. This design was extended to measure Caspase-3 and Bax protein expression, apart from TEM-based detection and correlation of the escin-induced apoptosis with the other cell death assays. Based on the MTT assay, the IC50 values for the C6 glioma and A549 cells respectively were 23 and 16.3 $\mu\text{g}\cdot\text{mL}^{-1}$ (24 and 48-hour exposure) and 14 and 11.3 $\mu\text{g}\cdot\text{mL}^{-1}$ (24 and 48-hour exposure). In the flow cytometry assay to detect apoptotic cells, at the concentration range tested (3.5, 7, 14, 21 $\mu\text{g}\cdot\text{mL}^{-1}$), the early and late apoptotic events were 1.6, 6.0, 26.2, 31.6% and 2.4, 4.6, 7.1, 32.2% respectively. Also, it was reported that the relative sensitivity of A549 cells was greater than the C6 glioma cells in terms of escin-induced apoptosis. This finding was corroborated by TEM-based imaging (14 and 21 $\mu\text{g}\cdot\text{mL}^{-1}$) wherein cell rounding; alterations in the cellular organization; cell shrinkage, DNA condensation, and disruption of the organelle membranes were observed. At the 7 $\mu\text{g}\cdot\text{mL}^{-1}$ concentration, the vacuoles containing cellular material were evident along with slight damage to the membranes. Caspase-3 activity was measured using flow cytometry following a 24 exposure of A549 cells to escin—the major bioactive principle. Results clearly indicated at doses (3.5, 7, 14, and 21 $\mu\text{g}\cdot\text{mL}^{-1}$), there was a dose-dependent increase in the caspase-3 positive cells (2.6, 8.4, 10.3, and 13 % respectively). Immunohistochemical findings documenting the induction of Bax at the 14 and 21 $\mu\text{g}\cdot\text{mL}^{-1}$ concentrations provided indirect evidence of the involvement of the mitochondrial pathway in escin-mediated cell death in A549 cells. In terms of the cell cycle analysis, a general trend was observed in terms of an increase in the concentration resulting in a greater number of cells arrested at the G_0/G_1 phase (even though there is some discrepancy

between the information in the body of the text and the tabular column) (Ciftci et al. 2015).

The citrus fruits, belonging to the citrus family, are very popular throughout the world and are horticulture crops. Bioactive molecules were extracted from the various parts of the citrus fruit. Specifically, this study involved the identification of hesperidin, neohesperidin, and naringin. Subsequently, MTT-based cytotoxicity measurements were made following the treatment of HepG2 cells to either the crude ethanolic extract or bioflavonoids ($0\text{--}200\ \mu\text{g}\cdot\text{mL}^{-1}$) for 24 hours. The IC₅₀ value is approximately $200\ \mu\text{g}\cdot\text{mL}^{-1}$ with the bioflavonoids causing a greater decrease in the cell viability. In terms of toxicity of hesperidin, naringin, and neohesperidin, the IC₅₀ values showed that Hesperidin was the most toxic to HepG2 cells with an IC₅₀ value of $150.43 \pm 12.32\ \mu\text{M}$. At all the concentrations tested, the IC₁₀ (15%), IC₂₀ (19.7%) and IC₅₀ (22.3%) values for Hesperidin provided evidence of a dose-dependent increase in early apoptotic cells. This result was based on flow cytometric findings, following staining with Annexin V-FITC/PI. The role of certain initiator caspases (Caspase-9 and Caspase-8), as well as the principal executioner caspase (caspase-3), was evaluated based on their ability to cleave p-NA (a substrate which can be detected based on its λ_{max} at 410 nm) from substrates that are selective for each of the three caspases. The leakage of a dye into the cytoplasm indicative of the loss of the mitochondrial transmembrane potential was observed in Hesperidin-treated HepG2 cells. Dose-dependent increases in the leakage of this dye (ionic fluorochrome, 3,3'-dihexyloxycarbocyanine iodide (DiOC₆)) and the consequent decrease in fluorescence intensity was observed in these cells. An interesting finding was the absence of induction of ROS levels, based on the fluorescence intensity changes in Hesperidin-treated HepG2 cells at the 4-hour time point (DCFH-DA assay). Further, the earlier demonstration of dose-dependent increases in apoptosis was further corroborated based on the down-regulation of the anti-apoptotic Bcl-xL protein, whereas there was an increment in the Bax, Bak, and tBid protein levels the involvement of t-bid provides evidence of cross-talk between the intrinsic and the extrinsic pathways in hesperidin-mediated cell death in HepG2 cells (Banjerdpongchai et al. 2016).

Dorema glabrum is a member of the Apiaceae family and is widely prevalent in North-Western; South Western and Central Asia. Limited data on the root-based bioactive principles of this plant is available. However, this study reports on the anti-cancer potential of seed extracts of this plant. Extraction; fractionation followed by preparative HPLC resulted in the isolation of three phenolic compounds, including diglucosyl caffeoyl ester; 4-O- β -D-glucopyranosylcaffeic acid, and Umbelliferone 7-O- β -D-glucoside (skimming). These compounds

were obtained from the methanolic extract of the seeds since this extract gave the best result in the MTT assay. All the three (3) isolated compounds were tested in the CAOV-4 human ovarian cancer cells and the MTT assay was performed at the 24, 48, and 72-hour time points. Following exposure of these cells for 2 days, the IC₅₀ values for the $197\ \mu\text{M}$, $254\ \mu\text{M}$, and $216\ \mu\text{M}$ concentrations respectively were 99.7, 87.3, and $70.03\ \mu\text{g}\cdot\text{mL}^{-1}$. Based on the comet assay, exposure of CAOV-4 cells for 48 hours all the three (3) compounds exhibited double-strand breaks (indicative of possible interaction of these compounds with DNA). The toxicity and DNA damaging potential were correlated with the percentage of FITC-labeled annexin V cells. Diglucosyl caffeoyl ester caused cell death by apoptosis. The mode of cell demise was attributed to being due to necrosis in the case of 4-O- β -D-glucopyranosylcaffeic acid as well as Umbelliferone 7-O- β -D-glucoside (skimming) (Eskandani et al. 2014).

The seeds of *Descurainia sophia* (Brassicaceae (Cruciferae) family) have been reported to be part of the Korean medicine system. The ethanolic extract of *Descurainia sophia* seeds (EEDS) has ingredients that have cytotoxic (helveticoside) and anti-inflammatory potential (quercetin and syringaresinol) and this finding provided the researchers a basis for further evaluating its anticancer/cell death potential in suitable cell culture-based model systems. The involvement of the extrinsic pathway in augmenting cell death was demonstrated by this seed extract sensitizing A549 cells to TRAIL-mediated cell death. This augmentation of cell death was mediated, in major part, by the upregulation of the death receptors DR4 and DR5, at both the mRNA and protein levels in the TRAIL refractory A549 cells. This increased cell death in A549 cells was demonstrated based on combination treatment involving exposure to a certain concentration of EEDS and exogenously administered TRAIL. The involvement of DR5 was further verified by inhibiting this increase in cell death following a decrease in the CCAAT/enhancer-binding protein homologous protein (CHOP). This provided evidence for the involvement of its transcription in EEDS-mediated upregulation of DR5 (Park et al. 2016).

The plethora of published data on Grape Seed Extracts (GSE) and the bioactive components contained therein has necessitated the inclusion of the salient findings with respect to their cell death induction potential as well as details with respect to the model system and the methodologies adopted (Table 1).

CHALLENGES AND FUTURE DIRECTIONS

Extraction and Solvent System

The techniques selected to extract bioactive principles from

Table 1: Grape seed extracts and key findings *in vitro* and *in vivo*.

S.No.	Extract/ Compound Name	Cell Line/Animal Model	Concentration range- IC 50/ Treatment time	Major Findings	Reference
1	GSPs	HeLa, SiHa	0-100 $\mu\text{g.mL}^{-1}$ 40 and 80 $\mu\text{g.mL}^{-1}$	Dose-dependent decrements and in the mitochondrial membrane potential increase in Bak-1 and decrease the level of Bcl-2 protein was seen in both cell lines and other apoptotic	Chen et al. (2014)
2	GSPs	Ca9-22 and HGF-1	50-200 $\mu\text{g.mL}^{-1}$ IC50-150 $\mu\text{g.mL}^{-1}$	5-27% in sub G1;14-73% Annexin V positive; 2-63% DCFH-DA ROS level and decrease of 100-15% decrease of Rh123; 3-36% Increase of phosphorylated γH2AX protein (marker for double strand breaks)	Yen et al. (2015)
3	RSV-GSE	8 months old AOM-induced rodent Model	0.12% W/W of drug fed after 16 Weeks after 6week subcutaneous injection of AOM	50% decline in tumor with no GI toxicity compared with Sulindac \downarrow in Nuclear β -catenin correlated with c-myc and cyclin D1, $\Delta\Psi\eta$ (18%), P53, Bax cleaved PARP and Cyt C & ther was concomitant \downarrow in 50% CSCs, Bcl-2. Experimental manipulation of the p53 levels -a shRNA system -involvement of this protein in regulating Cox2 levels and not on RSV-GSE-mediated decrements - β -catenin; c-myc and cyclin-D1 levels.	Reddivari et al. (2016)
4	GSE/ GSPs/ (+)-catechin and (-)-epi- catechin with oligomers being pre- dominant	BIU87	0-200 $\mu\text{g.mL}^{-1}$	Dose-dependent toxicity; 48%-79% PI-based G1 block, Increase in Cyclin D1 & CDK4; 9-41% apoptotic cells and hyper condensed cells and fragmented nuclei was seen in 24h treatment. Survivin levels decreased and caspase-3 expression was elevated in a dose-dependent manner.	Liu et al. (2015)
5	GSPs	Tca8113	0-200 $\mu\text{g.mL}^{-1}$ IC 50 of 24, 48 & 72 hours was 86.36, 43.65 and 31.17 $\mu\text{g.mL}^{-1}$ respectively	Dose-dependent toxicity, 3-47% increased apoptosis, 28-76% migratory capabilities, and MMP-2 and MMP-9; also increase in Bax and decrease in Bcl-2. Phosphorylation of Akt as well as NF- κB activation and translocation to the nucleus was inhibited.	Yang et al. (2017)
6	Aqueous GSE	A431	50-200 $\mu\text{g.mL}^{-1}$ IC50-111.11 $\mu\text{g.mL}^{-1}$	Dose-dependent toxicity, roundedness, irregular and cytoplasmic vacuolation of cells; Increase in ROS, 16 % apoptotic cell death, while 80.6% of them were eliminated by secondary necrosis. IC 50 of seed extract 60% loss in $\Delta\Psi\eta$, 49% apoptotic, and 48% necrotic cells at the 24-hour time point.	Nirmala et al. (2018)
7	GSPs/RSV	MCF-7& MDA MDB-231	GSP-20, 40 $\mu\text{g.mL}^{-1}$, RES-10, 20 $\mu\text{M.ml}^{-1}$	The combination of RSV and GSP shows a significant difference when compared with a parental group, and an increase in Bax and decreased Bcl-2 was seen in both cell lines. At 20 $\mu\text{g.mL}^{-1}$ GSP + 10mM RSV decrease the DNMT and HDAC activity	Gao & Tollefsbol (2018)
8	GSPs/GSE	ECA109	0-400 $\mu\text{g.mL}^{-1}$. IC50 12h- 66.442 \pm 13.54, 24h-51.713 \pm 12.69, 48h-37.158 \pm 13.07	Higher the dose and time of GSPE 80 $\mu\text{g.mL}^{-1}$ for 48h - higher the inhibition of IL-6, and COX-2 and with BAY11-7082 is stronger inhibition when compared when treated alone; and also \downarrow of IKK, I κ B, p-I κ B in dose-dee pendent and \uparrow of mRNA and protein expression of p50, and p65 and BAY-11 alone there is no decrease in IKK and mRNA levels.	Guo et al. (2018)

Table cont...

S.No.	Extract/ Compound Name	Cell Line/Animal Model	Concentration range- IC 50/ Treatment time	Major Findings	Reference
9	GSP B2	HT29 and LoVo cells	0-200 $\mu\text{g.mL}^{-1}$ HT29 IC50=15 μM and LoVo IC50=12 μM at 48 hrs.	Procyanidin (6, 12, 24 μM) shows a dose-dependent increase in the number of the autophagosome, high expression GPF-LC3, Beclin1, LCII, and Agt5 - and expression of LC3I was inhibited. 1-12% - \uparrow apoptosis and upregulation of Bax, Caspase-3, and \downarrow Bcl-2. 3MA reversed the inhibition of apoptosis and concluded the inhibition of autophagy reduction leads to anti-apoptosis	Zhang et al. (2019)
10	GSP	NSCLC-A549& H23; SCLC- DMS114 & pre- malignant 1198	0-30 $\mu\text{g.mL}^{-1}$	GSE shows a dose-dependent increase in 6-keto PGF1 α and 15HETE inhibition of (COX-2)/prostaglandin E2 (PGE2) eicosanoid pathways.	Mao et al. (2016)
11	GS Catechin and Epicatechin	<i>In vivo</i> -HCC animal model	25,50,100 mg.kg^{-1}	GS shows \downarrow pre-neoplastic foci formation; 4&10fold decrease respectively in the number and the area of GST-P in the livers of treated rats. GSEs effects-liver: \uparrow apoptosis induction; \downarrow cell proliferation, oxidative stress, and HDAC activity and inflammation markers (COX-2, iNOS, NF- κ B -p65 and p- TNF receptor expression).	Hamza et al. (2018)
12	GSP	H441	0-10 $\mu\text{g.mL}^{-1}$	Plain SLN is non-toxic. They show dose-dependent, high bioavailability, and GSE-loaded SLN - antioxidant effect for a longer duration than free GSE indicative of controlled release of their payload.	Castellani et al. (2018)
13	GS-GA, CAT, epi- CAT	MCF-7	0.05–100 $\mu\text{g.mL}^{-1}$	Higher GJIC –alteration in the functionality of the Connexin proteins already present in the cells and/or the opening of the gap shut abnormally. Immunolocalization of the Cx43 protein in MCF-7 cells -treated with different GSE concentrations (2 h or 24 h)	Leone et al. (2019)
14	GSP B2	<i>In vivo</i> - CCl4- induced mouse Liver model	150 mg.kg^{-1}	HSCs <i>in vivo</i> and <i>in vitro</i> - \downarrow VEGF-A, HIF-1 α , α -SMA, Col-1, and TGF- β 1; SAG and cyclopamine –proved PB2 targets in the Hh pathway	Feng et al. (2019)
15	GSPs	A375 & Hs294t	0-60 $\mu\text{g.mL}^{-1}$	\uparrow -Dose-dependent toxicity, 12-30% apoptosis, downregulation of Bcl-2, Bc-x1 and β -Catenin. GSPs (0.2 and 0.5%, w/w) supplemented with AIN76A (control diet) –xenograft Model -greatly inhibited the growth of melanoma cells and decreased the growth of Mel928 (β -catenin-activated), did not inhibit the xenograft growth of Mel1011 (β -catenin-inactivated) cells.	Vaid et al. (2016)
16	GSE	HNSCC- Detroit 562 and FaDu cells		GSE activated AMP-activated protein kinase (AMPK) and decreased Akt/mTOR/4E-BP1/S6K signaling in both Detroit 562 and FaDu cells. FaDu xenograft tumor model -GSE feeding of nude mice –activation of AMPK and autophagy induction	Shrotriya et al. (2015a)
17	GSE& RSV	4NQO-induced tongue cancer in C57BL/6	100 $\mu\text{g.mL}^{-1}$	GSE and Res –multiple possible mechanisms –prophylactic efficacy -pleiotropic effects on cell proliferation, apoptosis, cellular metabolism, and autophagy	Shrotriya et al. (2015b)

GSPs- Grape seed Procyanidins, GSE- Grape seed extract, RSV- Resveratrol, IC50- 50% of cell growth inhibitory concentration, AOM- Azoxymethane, GI- Gastrointestinal, $\Delta\Psi\text{m}$ -Mitochondrial membrane potential, DNMT- DNA methyltransferase, HDAC- Histone deacetylases, 3-MA- 3-Methyladenine, COX-2- cyclooxygenase-2, (PGE2)- Prostaglandin E2, iNOS- inducible Nitric oxide synthase, NF- κ B- nuclear factor-kappa B, p-TNF- phosphorylated tumor necrosis factor receptor, GST-P- placental Glutathione-S-transferase, GJIC- gap-junction-mediated cell-cell communications, Hh-Hedgehog pathway, SAG- Smoothed agonist, HSC-Hepatic stellate cell lines, α SM- Smooth muscle actin, Col-1-Collagen type 1, VEGF-A –Vascular endothelial growth factor A, 4NQO- 4-nitroquinoline-1- oxide.

seeds as well as their optimization is a pivotal first step for succeeding in developing a drug with chemotherapeutic potential. Different techniques were employed to extract and remove the compounds from seed extracts. The chemical (solvent-based) extraction and classical Soxhlet, maceration, distillation, and physical-based methods like cold press extraction technique is widely used to extract the compounds. The major drawbacks of this technique were its time-consuming nature as well as the volume of organic solvents used (De Castro & Garcia 1998). The green extraction method has been used extensively in the past 2 decades. These methods include advanced techniques like ultrasound, microwave, and supercritical CO₂ extraction, used singly or in combination, which can be optimized for the maximal extraction of bioactive active compounds from seeds (Casazza et al. 2010, Chemat et al. 2012, Singh et al. 2014, Zhang et al. 2018). Sometimes seeds may be requiring additional steps (pulverization, pre-leaching methods), which facilitate the subsequent extraction of compounds from the seed matrix (Bimakr et al. 2013, Dhobi et al. 2009, Dabas et al. 2019).

Synergistic effect of seed extracts when combined with two or more compounds basis for crude seed extract-based research for drug development potential

Despite some factors, such as seasonal variations that may impact the levels of bioactive components in the seeds as well as seed-to-seed variability, crude extracts have potential in terms of their anti-cancer efficacy. Once the extraction process is optimized (Please see Fig. 1 for the experimental flow that can be adopted as a teaching and research tool for the systematic extraction of bioactive principles from seed and other plant sources), these extracts should be tested in suitable *in vitro* and *in vivo* cancer models. Reproducibility in the therapeutic effect warrants optimization of the efficacy of the formulation involving these extracts. Also, toxicity evaluation needs to be done in drug development involving crude extracts from seed sources. Also, in certain cases, the crude extracts may synergize with currently available chemotherapeutic drugs and are elaborated upon below with suitable examples.

A study showed that Taxol (paclitaxel) is a powerful anti-cancer drug widely used against several types of malignant tumors. The effects of Taxol-encapsulated liposomes (T) alone and in combination between *Eruca sativa* seed extract on nuclear factor kappa B (NF- κ B), cyclooxygenase-2 (COX-2), and B-cell lymphoma-2 (Bcl-2) gene expression levels were investigated in rat mammary gland carcinogenesis induced by 7,12 dimethylbenz(α) anthracene (DMBA)

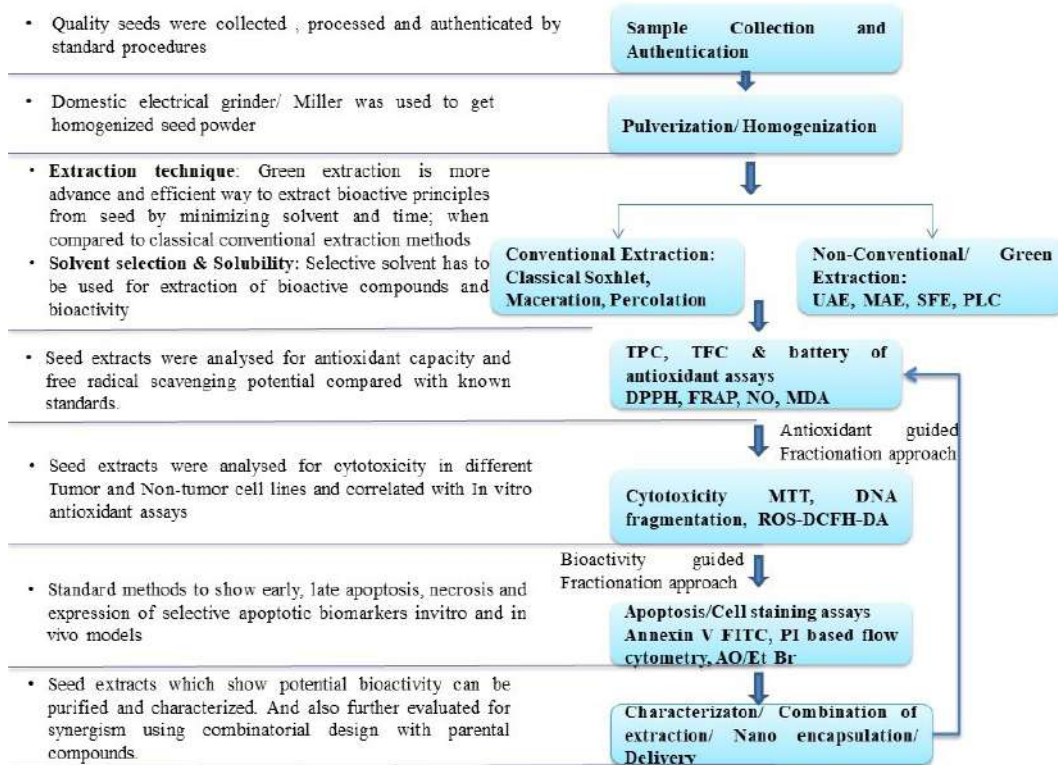


Fig. 1: Schematic representation of steps involved in the identification of apoptotic potential of seed extracts.

using qRT-PCR. Results showed that DMBA increased NF- κ B, COX-2, and Bcl-2 gene expression levels and lipid peroxidation (LP) while decreasing glutathione-S-transferase (GST) and superoxide dismutase (SOD) activities and total antioxidant concentration (TAC) compared to the control group. T and T-SE treatment reduced NF- κ B, COX-2, and Bcl-2 gene expression levels and LP. Hence, T and T-SE treatment appeared to reduce inflammation and cell proliferation, while increasing apoptosis, GST and SOD activities, and TAC (Shaban et al. 2016). A study showed the synergistic effects of GSPs and Res on inhibiting MDA-MB-231 and MCF-7 human breast cancer cells. Our results of 3-(4,5-dimethylthiazol-2-yl)-2,5-diphenyltetrazolium bromide (MTT) assays and clonogenic assays indicate that treatments with the combinations of GSPs and Res synergistically decreased

cell viability and posttreatment cell proliferation in both cell lines (Gao et al. 2018). Chavoshi et al. (2017) showed that a combination of silibinin (a molecule extractable from a seed source), paclitaxel, and cisplatin show a synergistic effect, in MCF-7 breast cancer cells than when treated alone (Chavoshi et al. 2017). A 70% ethanolic extract of *Blepharis persica* seed combined with Doxorubicin induces toxicity, apoptosis, necrosis, downregulation of Bcl2, and upregulation of Bax protein in the HT29 cell line (Aghaabbasi et al. 2020). Czajkowska et al. (2017) reported that the novel octahydropyrazino[2,1-a:5,4-a']di-isoquinoline derivative combined with *Nigella sativa* showed a synergistic effect in terms of cell toxicity, apoptosis, and mitochondrial membrane potential (Czajkowska et al. 2017). A study evaluated the anticancer potential of methanolic extracts of Berberis

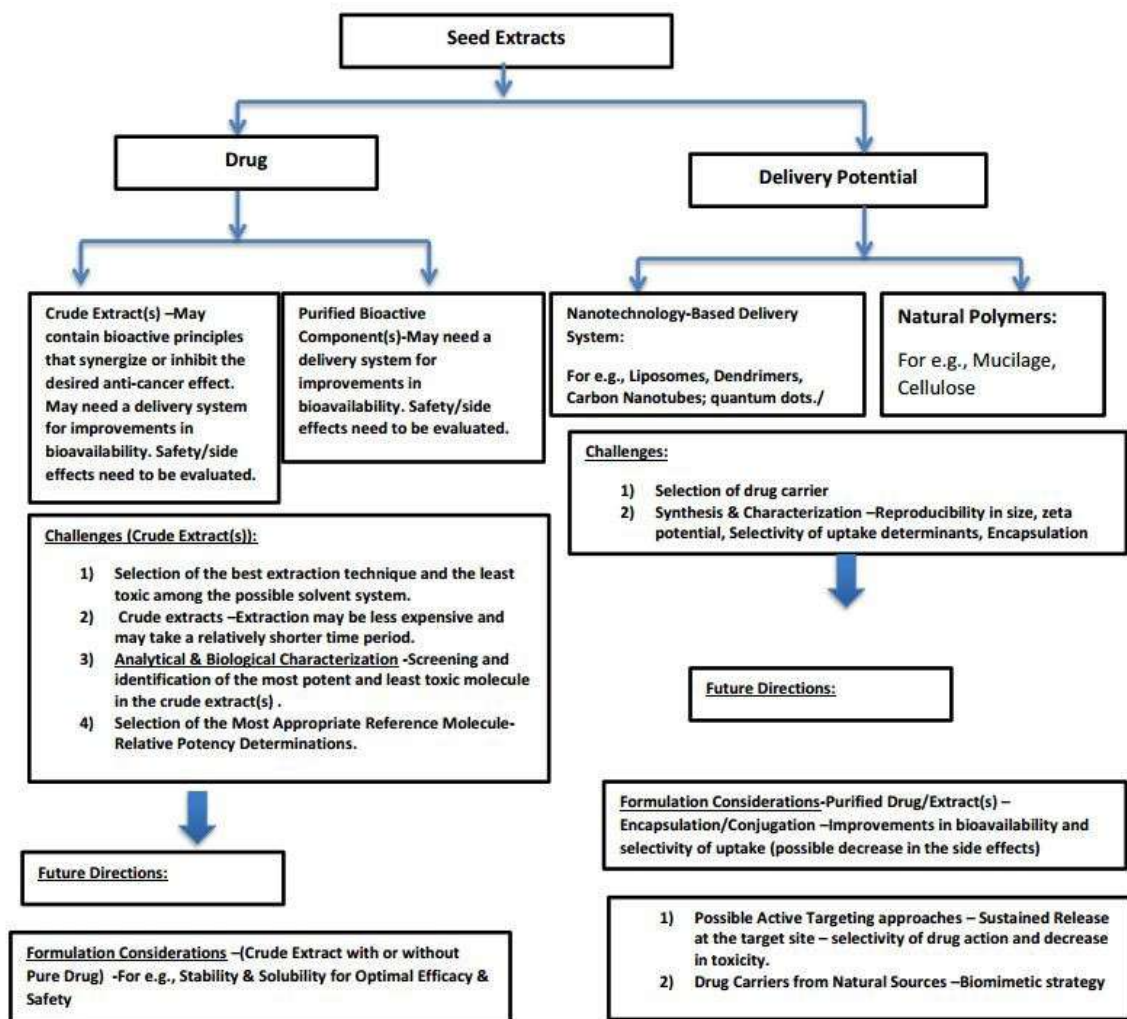


Fig. 2: Experimental flow for seed extracts/ or compounds as drug/delivery developmental system.

aristata root and *Azadirachta indica* seeds prepared by various extraction techniques in human osteosarcoma (HOS) cells. Soxhlation extract of *B. aristata* (BAM-SX) and sonication extract of *Azadirachta indica* (AIM-SO) were most effective in inducing apoptosis in parental drug-sensitive, as well as resistant cell type developed by repeated drug exposure. (27.82 $\mu\text{g}\cdot\text{ml}^{-1}$ and 28.65 $\mu\text{g}\cdot\text{ml}^{-1}$) toxicity (Sengupta et al. 2017).

These aforesaid promising findings provide a sound rationale for the need to delineate the best bioactive principles or a combination thereof, that can possibly enhance the anti-cancer potential of currently available synthetic drugs as well as those of natural origin. Also, Fig. 2 provides a strategy for the encapsulation and subsequent increments in uptake and the subsequent cell death potential of seed extracts singly and/or in combination with other molecules (natural or synthetic in origin).

CONCLUSIONS

Our discussion clearly provides evidence of the beneficial apoptotic effects of seed extracts from diverse sources in different *in vitro* and *in vivo* model systems. Also, this review highlights the need to perform an HTS-based screening strategy to short-list the major seed sources, thereby hastening the drug development process. Moreover, this review underscores the need for the inter-laboratory validation of protocols as well as for defining certain variables, like the dormancy status of the seeds. Furthermore, this design can be extended to identifying specific seed extract-drug combinations that can reliably synergize and augment cell death.

ACKNOWLEDGEMENT

The authors acknowledge the infrastructural support and constant encouragement provided by the management of the Vellore Institute of Technology (VIT). We also thank DST (SERB) for funding the project on drug delivery systems [(SB/SO/HS-157 (2013))] and for creating the scientific ambiance, that served to encourage all the research scholars and the project students in the laboratory. This work was funded, in part, by the Vellore Institute of Technology. Also, the Council of Scientific & Industrial Research (CSIR), New Delhi, has provided additional financial support in the form of a Senior Research Fellowship (09/844(0075)/2019-EMR 1) to the lead author.

ABBREVIATIONS

GSP: grape seed proanthocyanidins, HTS: High throughput screening, Annexin V-FITC/PI: Annexin A5-Fluorescein isothiocyanate/ propidium iodide, FDA: US Food and Drug

administration, PARP: Poly (ADP-ribose) polymerase, WIF1: WNT Inhibitory Factor 1, ALDH1A1: Aldehyde Dehydrogenase 1 Family Member A1, Dcl1: Doublecortin Like Kinase1, EZH2: Enhancer of zeste homolog 2, MTT: 3-(4,5-Dimethylthiazol-2-yl)-2,5-diphenyltetrazolium bromide, TEM: Transmission electron microscope, DiOC₆: Ionic fluorochrome, 3,3'-dihexyloxycarbocyanine iodide, DCFH-DA: 2',7'-Dichlorofluorescein Diacetate, TRAIL: Tumor necrosis factor-related apoptosis-inducing ligand, CCAAT: enhancer-binding protein delta (CEBPD), DLBCL: Diffuse large B-cell lymphoma, AR: Androgen Receptor, PSA: Prostate Specific Antigen, TUNEL: Terminal deoxynucleotidyl transferase dUTP nick end labeling, AKT: Protein kinase B, GSK3 β : Glycogen synthase kinase 3 beta, SLN: solid lipid nanoparticles, RES: Resveratrol, GST: Glutathione S-transferases, SOD: Superoxide dismutase, DMBA: 7,12 dimethylbenz(α) anthracene, OX26 mAb: anti-transferrin receptor monoclonal antibody.

REFERENCES

- Aghaabbasi, K., Askari, N., Kumleh, H.H., Torkzadeh-Mahani, M. and Ramzani-Ghara A. 2020. The *Blepharis persica* seed hydroalcoholic extract synergistically enhances the apoptotic effect of doxorubicin in human colon cancer and gastric cancer cells. *Mol. Biol. Rep.*, 47(2): 843-853.
- Ahmed, I., Roy, B.C., Subramaniam, D., Ganie, S.A., Kwatra, D., Dixon, D., Anant, S., Zargar, M.A. and Umar, S. 2016. An ornamental plant targets epigenetic signaling to block cancer stem cell-driven colon carcinogenesis. *Carcinogenesis*, 37(4): 385-396.
- Ali, A.Q., Farah, M.A., Abou-Tarboush, F.M., Al-Anazi, K.M., Ali, M.A., Lee, J., Hailan, W.A. and Mahmoud, A.H. 2019. Cytogenotoxic effects of *Adenium obesum* seeds extract on breast cancer cells. *Saudi J. Biol. Sci.*, 26(3): 547-553.
- Al-Mamun, M.A., Husna, J., Khatun, M., Hasan, R., Kamruzzaman, M., Hoque, K.M.F., Reza, M.A. and Ferdousi, Z. 2016. Assessment of anti-oxidant, anticancer and antimicrobial activity of two vegetable species of *Amaranthus* in Bangladesh. *BMC Compl. Altern. Med.*, 16(1): 1-11.
- Banjerpongchai, R., Wudtiwai, B., Khaw-On, P., Rachakhom, W., Duangnil, N. and Kongtawelert, P. 2016. Hesperidin from Citrus seed induces human hepatocellular carcinoma HepG2 cell apoptosis via both mitochondrial and death receptor pathways. *Tumor Biol.*, 37(1): 227-237.
- Bimakr, M., Rahman, R.A., Saleena Taip, F., Adzahan, N.M. and Islam Sarker, Z. 2013. Ultrasound-assisted extraction of valuable compounds from winter melon (*Benincasa hispida*) seeds. *Int. Food Res. J.*, 20(1).
- Casazza, A.A., Aliakbarian, B., Mantegna, S., Cravotto, G. and Perego, P. 2010. Extraction of phenolics from *Vitis vinifera* wastes using non-conventional techniques. *Journal of Food Engineering*, 100(1): 50-55.
- Cassiem, W. and de Kock, M. 2019. The anti-proliferative effect of apricot and peach kernel extracts on human colon cancer cells *in vitro*. *BMC Compl. Altern. Med.*, 19(1):1-12.
- Castellani, S., Trapani, A., Spagnoletta, A., Di Toma, L., Magrone, T., Di Gioia, S., Mandracchia, D., Trapani, G., Jirillo, E. and Conese, M. 2018. Nanoparticle delivery of grape seed-derived proanthocyanidins to airway epithelial cells dampens oxidative stress and inflammation. *J. Transl. Med.*, 16(1): 1-15.
- Chavoshi, H., Vahedian, V., Saghaei, S., Pirouzpanah, M.B., Raeisi, M. and Samadi, N. 2017. Adjuvant therapy with silibinin improves the efficacy of paclitaxel and cisplatin in MCF-7 breast cancer cells. *Asian Pac. J.*

- Cancer Prev., 18(8): 2243.
- Chemat, F., Vian, M.A. and Cravotto, G. 2012. Green extraction of natural products: concept and principles. *Int. J. Mol. Sci.*, 13(7): 8615-8627.
- Chen, Q., Liu, X.F. and Zheng, P.S. 2014. Grape seed proanthocyanidins (GSPs) inhibit the growth of cervical cancer by inducing apoptosis mediated by the mitochondrial pathway. *PLoS One*, 9(9): 107045.
- Chene, G., Baillif, V., Van Goethem, E., Branka, J.E., Ionescu, T., Robert, G. and Lefeuvre, L. 2015. *In vitro* and *in vivo* anti-inflammatory effect of a biotechnologically modified borage seed extract: Evidence for lipid pro-resolving mediators' implication in the enhancement of psoriatic and atopic dermatitis lesions. *J. Cosmet. Dermatol. Sci. Appl.*, 5(02): 151.
- Ciftci, G.A., Işcan, A. and Kutlu, M. 2015. Escin reduces cell proliferation and induces apoptosis on glioma and lung adenocarcinoma cell lines. *Cytotechnology*, 67(5): 893-904.
- Czajkowska, A., Gornowicz, A., Pawlowska, N., Czarnomysy, R., Nazaruk, J., Szymanowski, W., Bielawska, A. and Bielawski, K. 2017. Anticancer Effect of a Novel Octahydropyrazino [2, 1-a: 5, 4-a'] diisoquinoline Derivative and Its Synergistic Action with *Nigella sativa* in Human Gastric Cancer Cells. *BioMed Res. Int.*, 2017.
- Dabas, D., Elias, R.J., Ziegler, G.R. and Lambert, J.D. 2019. *In vitro* antioxidant and cancer inhibitory activity of a colored avocado seed extract. *Int. J. Food Sci.*, 2019: 63-84.
- Davatgaran-Taghipour, Y., Masoomzadeh, S., Farzaei, M.H., Bahram-soltani, R., Karimi-Soureh, Z., Rahimi, R. and Abdollahi, M. 2017. Polyphenol nanoformulations for cancer therapy: Experimental evidence and clinical perspective. *Int. J. Nanomed.*, 12: 2689.
- De Castro, M.L. and Garcia-Ayuso, L.E. 1998. Soxhlet extraction of solid materials: an outdated technique with a promising innovative future. *Anal. Chim. Acta*, 369(1-2): 1-10.
- Dhobi, M., Mandal, V. and Hemalatha, S. 2009. Optimization of microwave-assisted extraction of bioactive flavonolignan-silybinin. *J. Chem. Metrol.* 3(1).
- Eskandani, M., Dadizadeh, E., Hamishehkar, H., Nazemiyeh, H. and Barar, J. 2014. Geno/cytotoxicity and apoptotic properties of phenolic compounds from the seeds of *Dorema glabrum* Fisch. *CA. BioImpacts-BI*, 4(4): 191.
- Feng, J., Wang, C., Liu, T., Li, J., Wu, L., Yu, Q., Li, S., Zhou, Y., Zhang, J., Chen, J. and Ji, J. 2019. Procyanidin B2 inhibits the activation of hepatic stellate cells and angiogenesis via the Hedgehog pathway during liver fibrosis. *J. Cell. Mol. Med.*, 23(9): 6479-6493.
- Gao, Y. and Tollefsbol, T.O. 2018. Combinational proanthocyanidins and resveratrol synergistically inhibit human breast cancer cells and impact epigenetic-mediating machinery. *Int. J. Mol. Sci.*, 19(8): 2204.
- Guo, F., Hu, Y., Niu, Q., Li, Y., Ding, Y., Ma, R., Wang, X., Li, S. and Xie, J. 2018. Grape seed proanthocyanidin extract inhibits human esophageal squamous cancerous cell line eca109 via the nf-kb signaling pathway. *Medicinski Arhiv.*, 2018: 56-71
- Hamza, A.A., Heeba, G.H., Elwy, H.M., Murali, C., El-Awady, R. and Amin, A. 2018. Molecular characterization of the grape seeds extract's effect against chemically-induced liver cancer: *In vivo* and *in vitro* analyses. *Sci. Rep.*, 8(1): 1-16.
- Lakshmi, T., Ezhilarasan, D., Nagaich, U. and Vijayaragavan, R. 2017. *Acacia catechu* ethanolic seed extract triggers apoptosis of SCC-25 cells. *Pharmacogn. Mag.*, 13: S405.
- Leone, A., Longo, C., Gerardi, C. and Trosko, J.E. 2019. Pro-apoptotic effect of grape seed extract on MCF-7 involves the transient increase of gap junction intercellular communication and Cx43 up-regulation: A mechanism of chemoprevention. *Int. J. Mol. Sci.*, 20(13): 3244.
- Liu, J., Zhang, W.Y., Kong, Z.H. and Ding, D.G. 2016. Induction of cell cycle arrest and apoptosis by grape seed procyanidin extract in human bladder cancer BIU87 cells. *Eur. Rev. Med. Pharmacol. Sci.*, 20(15): 3282-3291.
- Liu, Y., Ma, S.S., Ibrahim, S.A., Li, E.H., Yang, H. and Huang, W. 2015. Identification and antioxidant properties of polyphenols in lotus seed epicarp at different ripening stages. *Food Chem.*, 185: 159-164.
- Mahli, A., Koch, A., Czech, B., Peterburs, P., Lechner, A., Haunschild, J., Müller, M. and Hellerbrand, C. 2015. Hepatoprotective effect of oral application of a silymarin extract in carbon tetrachloride-induced hepatotoxicity in rats. *Clin. Phytoscience*, 1(1): 1-8.
- Mao, J.T., Smoake, J., Park, H.K., Lu, Q.Y. and Xue, B. 2016. Grape seed procyanidin extract mediates antineoplastic effects against lung cancer via modulations of prostacyclin and 15-HETE eicosanoid pathways. *Cancer Prev. Res.*, 9(12): 925-932.
- Nirmala, J.G., Celsia, S.E., Swaminathan, A., Narendhirakannan, R.T. and Chatterjee, S. 2018. Cytotoxicity and apoptotic cell death induced by *Vitis vinifera* peel and seed extracts in A431 skin cancer cells. *Cytotechnology*, 70(2): 537-554.
- Ogaly, H.A., Eltablawy, N.A., El-Beahry, A.M., El-Hindi, H. and Abd-El-salam, R.M. 2015. Hepatocyte growth factor mediates the antifibrogenic action of *Ocimum bacilicum* essential oil against CCl4-induced liver fibrosis in rats. *Molecules*, 20(8): 13518-13535.
- Park, J.S., Lim, C.J., Bang, O.S. and Kim, N.S. 2016. Ethanolic extract of *Descurainia sophia* seeds sensitizes A549 human lung cancer cells to TRAIL cytotoxicity by upregulating death receptors. *BMC Compl. Altern. Med.*, 16(1): 1-8.
- Reddivari, L., Charepalli, V., Radhakrishnan, S., Vadde, R., Elias, R.J., Lambert, J.D. and Vanamala, J.K. 2016. Grape compounds suppress colon cancer stem cells *in vitro* and a rodent model of colon carcinogenesis. *BMC Compl. Altern. Med.*, 16(1): 1-12.
- Seca, A.M. and Pinto, D.C. 2018. Plant secondary metabolites as anticancer agents: successes in clinical trials and therapeutic application. *Int. J. Mol. Sci.*, 19(1): 263.
- Sengupta, P., Raman, S., Chowdhury, R., Lohitesh, K., Saini, H., Mukherjee, S. and Paul, A. 2017. Evaluation of apoptosis and autophagy inducing potential of *Berberis aristata*, *Azadirachta indica*, and their synergistic combinations in parental and resistant human osteosarcoma cells. *Front. Oncol.*, 7: 296.
- Shaban, N., Abdel-Rahman, S., Haggag, A., Awad, D., Bassiouny, A. and Talaat, I. 2016. The combination between taxol-encapsulated liposomes and *Eruca sativa* seed extract suppresses mammary tumors in female rats induced by 7, 12 Dimethylbenz (a) anthracene. *Asian Pac. J. Cancer Prev.*, 17(1): 117-123.
- Shrotriya, S., Deep, G., Lopert, P., Patel, M., Agarwal, R. and Agarwal, C. 2015a. Grape seed extract targets mitochondrial electron transport chain complex III and induces oxidative and metabolic stress leading to cytoprotective autophagy and apoptotic death in human head and neck cancer cells. *Mol. Carcinog.*, 54(12): 1734-1747.
- Shrotriya, S., Tyagi, A., Deep, G., Orlicky, D.J., Wisell, J., Wang, X.J., Sclafani, R.A., Agarwal, R. and Agarwal, C. 2015b. Grape seed extract and resveratrol prevent 4-nitroquinoline 1-oxide induced oral tumorigenesis in mice by modulating AMPK activation and associated biological responses. *Mol. Carcinog.*, 54(4): 291-300.
- Singh, M., Jha, A., Kumar, A., Hettiarachchy, N., Rai, A.K. and Sharma, D. 2014. Influence of the solvents on the extraction of major phenolic compounds (punicalagin, ellagic acid and gallic acid) and their antioxidant activities in pomegranate aril. *J. Food Sci. Technol.*, 51(9): 2070-2077.
- Vaid, M., Singh, T., Prasad, R. and Katiyar, S.K. 2016. Bioactive proanthocyanidins inhibit growth and induce apoptosis in human melanoma cells by decreasing the accumulation of β -catenin. *Int. J. Oncol.*, 48(2): 624-634.
- Yang, N., Gao, J., Cheng, X., Hou, C., Yang, Y., Qiu, Y., Xu, M., Zhang, Y. and Huang, S. 2017. Grape seed proanthocyanidins inhibit the proliferation, migration and invasion of tongue squamous cell carcinoma cells through suppressing the protein kinase B/nuclear factor- κ B signaling

- pathway. *Int. J. Mol. Med.*, 40(6): 1881-1888.
- Yen, C.Y., Hou, M.F., Yang, Z.W., Tang, J.Y., Li, K.T., Huang, H.W., Huang, Y.H., Lee, S.Y., Fu, T.F., Hsieh, C.Y. and Chen, B.H. 2015. Concentration effects of grape seed extract in anti-oral cancer cells involving differential apoptosis, oxidative stress, and DNA damage. *BMC Complem. Altern. Med.*, 15(1): 1-9.
- Zhang, Q.W., Lin, L.G. and Ye, W.C. 2018. Techniques for extraction and isolation of natural products: A comprehensive review. *Chinese Med.*, 13(1): 1-26.
- Zhang, R., Yu, Q., Lu, W., Shen, J., Zhou, D., Wang, Y., Gao, S. and Wang, Z. 2019. Grape seed procyanidin B2 promotes autophagy and apoptosis in colorectal cancer cells via regulating PI3K/Akt signaling pathway. *OncoTargets Ther.*, 12: 4109.



Estimation of Biomass Availability in Panglao Island Using SENTINEL-2 MSI

W.N. Galang ^(**)†, I.D.F. Tabañag ^{***} and M.E. Loretero ^{****}

*School of Engineering, University of San Carlos, Cebu City, Cebu, Philippines

**College of Engineering and Computer Studies, Holy Name University, Tagbilaran City, Bohol, Philippines

***Department of Chemical Engineering, University of San Carlos, Cebu City, Cebu, Philippines

****Department of Mechanical and Manufacturing Engineering, University of San Carlos, Cebu City, Cebu, Philippines

†Correspondence: W.N. Galang; naborgalang@gmail.com

Nat. Env. & Poll. Tech.

Website: www.neptjournal.com

Received: 18-10-2020

Revised: 17-01-2021

Accepted: 22-01-2021

Key Words:

Biomass assessment
Geographical information system (GIS)
Normalized difference vegetation index (NDVI)
Remote sensing (RS)
Theoretical energy potential

ABSTRACT

Remote Sensing (RS) technology using SENTINEL-2 Multispectral Instrument (MSI) imagery was used in the estimation of residual biomass' available energy potential. The estimation was done in Panglao Island, within the province of Bohol, Philippines. Estimation of biomass availability was processed using Geographical Information System (GIS) software incorporating the calculation of Normalized Difference Vegetation Index (NDVI) to extract information on land resources and its spatial distribution. It was found that the majority of vegetation cover on the island is in the form of perennial woody plants and coconut trees. Coconut production on the island of Panglao contributed 1.26% of the total cultivation area for the province based on processed captures of Sentinel-2 imagery. The residue concentration amounted to 2,865 tons of coconut residues based on the RPR method. This amount of residues can be translated to 52.92 TJ of theoretical energy potential. The result of this study may serve as a baseline for the locality to consider the utilization of agricultural residues such as coming from coconut trees to support the use of indigenous resources for energy generation.

INTRODUCTION

In the Philippines, the problem of electricity demand is expected to continually increase by end of 2040. Biomass residues from agricultural crops, plantations, or residual forest products can be used as an alternate source. As of 2016, biomass accounted for 25.5 percent of the country's indigenous energy source. The household sector accounted for the majority of biomass consumption. It is the most preferred fuel among households because of its abundance, accessibility, and affordability, particularly in rural areas. Similarly, biomass gradually increased its contribution to the power industry, with its fuel input to electricity generation more than doubling from 2015 to 2016. Despite the Department of Energy's (DOE) order dated May 2018 to ensure access to electricity for areas that remain unserved and underserved by distribution companies and electric cooperatives, there are still rural areas without electricity.

The term biomass refers to any organic material derived from plants. Biomass comes from green plants through photosynthesis that converts sunlight into plant material. Biomass resource can be considered as an organic material, in which solar energy is stored in chemical bonds. When the bonds between adjacent carbon, hydrogen, and oxygen

molecules are broken by digestion, combustion, or decomposition, these substances release the stored, chemical energy (McKendry, 2002). Biomass basically can be divided into three major groups, wood biomass, non-wood biomass, and secondary fuels (Calle et al. 2007).

Panglao is an island located in the Central Visayas region of the Visayas island group and bounded by the Bohol Sea in the north of south-central Philippines. The power plants located in Leyte and Cebu through Leyte-Bohol Transmission Interconnection is the prime power supplier of Bohol including that of the island of Panglao. In 2015, power plants outside of Bohol supplied 68.86 MW, or 89 percent, of the province's peak demand through the Leyte-Bohol Interconnection, while the remaining 8.4 MW or 11 percent is collectively supplied by the three mini-hydro plants inside Bohol. According to Bohol's projected energy demand, total energy consumption was 344.66 GWh in 2015 and is expected to increase to 440.10 GWh by 2020 (Provincial Planning and Development Office, 2018).

The island of Panglao has sources of potential energy from agricultural products waste. The potential agricultural product wastes that can be utilized as an alternative energy source are coconut husks and shells. The underlying issue,

however, is a lack of certainty about the entire availability and potential of coconut residues on the island. An assessment of biomass availability for bioenergy as an initial step is necessary. Several factors should be identified and addressed, including land resources, the spatial distribution of resources, and geographic factors of the resources, to assess the spatial distribution and quantity of residual biomass accurately.

Different types of satellite imageries can be used in identifying agricultural crop areas, one of the initial processes involved in the assessment. Aside from locating residue sources, these images are also used in generating agricultural maps. These maps are used as the primary input data in the estimation of biomass availability in a given area.

The rapid development of remote sensing (RS) has led to increasing usage of high-resolution data regarding space, time, and spectrum to extract vegetation information and improve parameters, which enables biomass estimation with increased accuracy. The instruments used for RS have a wide range of coverage, from airborne cameras to sensors onboard satellites. The development of RS methods provides a better understanding of the relationship between leaf reflectance changes and physio-ecological factors of vegetation. Available satellite, aerial, and ground remote sensing platforms offer different spatial- and temporal-resolution information for energy crop management.

The main reason for using RS data, apart from the ability to cover large areas, is its ability to offer useful information on crop activity and health in a practical, non-destructive way (Ahamed et al. 2013, Moulin et al. 1998, Onojeghuo et al. 2018). The ground-based RS data excel in establishing the calibration model for biomass yield prediction and providing references for aerial and satellite RS which can cover a wide

range of biomass production systems (Ahamed et al. 2011, Ali et al. 2016).

This study considers the advantage of RS wide range coverage. The remote sensing spatio-temporal data provided by SENTINEL-2 Multispectral Instrument (MSI) samples 13 spectral bands. There are four bands at 10 meters, six bands at 20 meters, and three bands at 60 meters spatial resolution images. These bands are being used in the analysis of land cover and crop activity.

This study aims to come up with an assessment approach considering the unavailability of data to establish information on biomass resource estimation by the usage of remote sensing imagery. The results provide a baseline of information on biomass resources available in Panglao Island using the remote sensing images from SENTINEL-2 Multispectral Instrument (MSI). It could be an initial step for promoting the use of indigenous resources for energy generation.

MATERIALS AND METHODS

The study was conducted within the scope of Panglao Island. It has an area of 91.12 km² (35.18 sq mi) see Fig. 1. The island is within the province of Bohol and comprises two municipalities, Dauis and Panglao, respectively. Panglao Island is located southwest of Bohol and southeast of Cebu. It belongs to the fourth climatic type, which is characterized by rainfall more or less evenly distributed throughout the year. The dry season starts from January to May while the rest of the year is generally wet. Rainfall distribution is influenced by the prevailing air streams, the intertropical convergence zone (ITCZ), and the island's topography. The study sites were more of a 90% level to nearly level topography, 10% rolling to the undulating slope, and about 5% rolling to moderately



Fig. 1: Area of study, the island of Panglao.

steep. In general, the location of Panglao has a terrain that ranges from plain, hilly to mountainous. The island itself is made of Maribojoc limestone, the youngest of the limestone units found in the western area of the province.

The acquired data taken from SENTINEL-2, with its mission coverage and high revisit frequency provides generation of geoinformation from local to international scales. This data may be modified and adapted by users for application in spatial planning and monitoring of the environment, water, forest, land carbon, resources, and global crop. The fundamental level of Sentinel-2 MSI products is provided in granules of a fixed size. For ortho rectified products, Level-1C and Level-2A are the images divided into 100 km tiles in UTM/WGS84 projection. The availability of data for general users is given in the Level-1C and Level-2A products.

Band Combinations Using the Spatio-Temporal Images

Initially, the study involved the use- of Sentinel-2 images using the QuantumGIS, a free and open-source cross-platform desktop application that supports viewing, editing, and analysis of geospatial data based from the QGIS Official Website. The selection of specific bands from the Sentinel-2

image via disabling the other bands enables to identify the requirement of the study area, indicating the specific location in the search parameters including the search date and filters to be applied to obtain the adjusted symbology for the study area. The adjusted symbology was from Sentinel-2 bands: Band 2- Blue, Band 3- Green, and Band 4-Red with 10m resolution with tile number T51PWL taken as of May 10, 2019, see Fig. 2 and Fig. 3.

The basis to determine the density of greenness of the Earth's surface, satellites measure the distinct colors or wavelengths of visible and near-infrared sunlight reflected by the plants. Green plants look green because chlorophyll preferentially absorbs light, certain wavelengths of this spectrum are absorbed and other wavelengths are reflected.

The NDVI is one of the most common indices widely applied for monitoring vegetation dynamics at regional and global scales (Vrieling et al. 2013, Zhu et al. 2013). NDVI was preferred as it is a numerical indicator that can be used as a proxy for plant biomass (Dube et al. 2014). This index varies between -1 and 1 in which the values less than zero during the growing season indicate no vegetation cover while values more than zero in the growing season describe

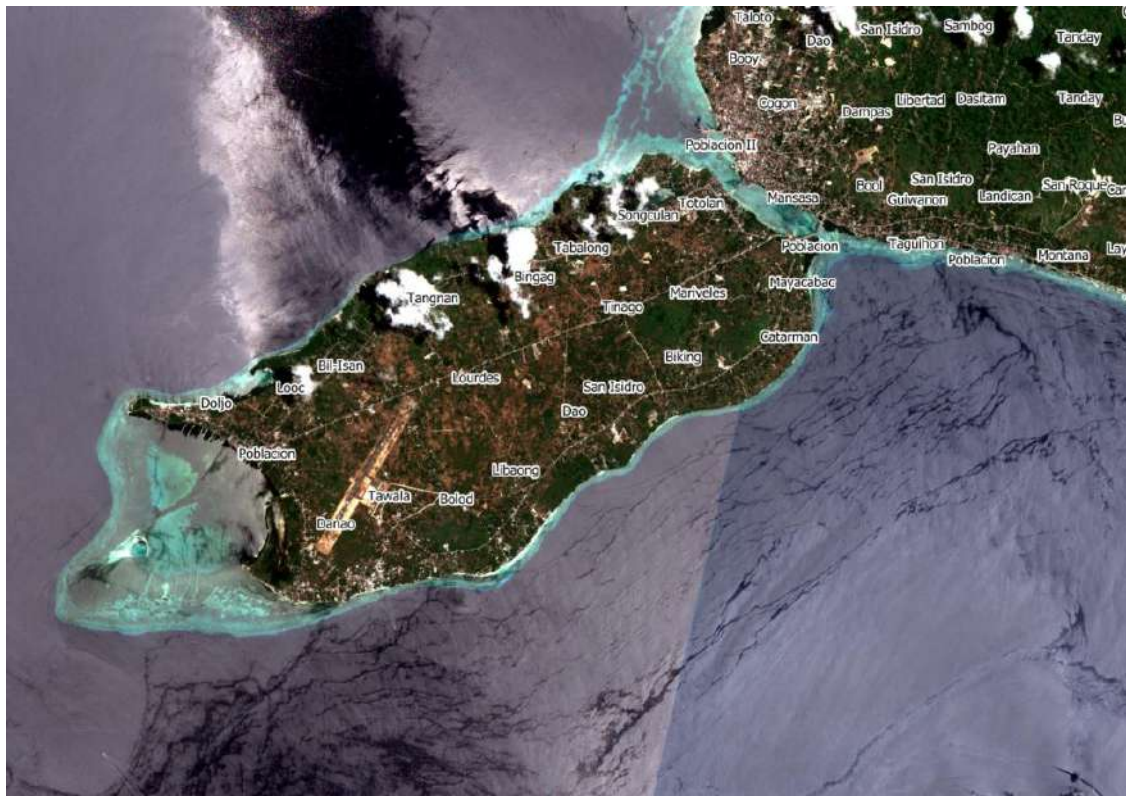


Fig. 2: Sentinel-2 image of Panglao Island with adjusted symbology.



Fig. 3: Panglao Island with band 4 and band 8.

available vegetation cover. The NDVI was calculated using the following formula (Choubin & Malekian 2017):

$$NDVI = (NIR - Red) / (NIR + Red) \quad \dots (1)$$

where *NDVI* is the Normalized Difference Vegetation Index, *NIR* is a reflection in the Near Infrared band and *Red* is a reflection in the red band.

The generated vegetation cover from NDVI calculation is the basis to define the cultivation area related to the plantation density of the crop under study. The measurement forms part of the biomass residue calculation.

Biomass Residue Calculation

The basic data necessary to perform any assessment about available agricultural residues include the type of crop and crop surface, crop yield, plantation density, and residue to product ratio. A sufficient number of average values referred to the last harvests performed in the area were used to ensure data representation.

One of the most common methodologies to assess residual biomass is to consider the crop yield and a residue to product ratio, previously estimated at a regional or local

level, using the following equation:

$$Pr = Y * RPR \quad \dots (2)$$

where, *Pr* corresponds to the potential crop residue produces (t.year⁻¹); *Y* corresponds to the crop yield by the locality (t.year⁻¹); *RPR* corresponds to the residue-to-product ratio, which relates the generated crop residue to the total crop produced.

The estimation is considered a Residue-to-Product Ratio (RPR). This method uses an average value of residue generation (Koopmans & Koopenjan 1997). The significant differences between RPR's used in different studies depend on several factors, mostly caused by variations in weather, crop type grown, water availability, soil fertility, farming practice, among others. The RPR used in this study considered the average ratios from related literature.

The RPR method of residue estimation considered the possibility of varying productiveness depending on the geographic distribution of plantations. This method is the most commonly used to estimate the biomass residue production of agricultural crops because the RPR method considers the crop species, harvest season, cultivation methods, among

other factors, representing the reality of the production area (Rahman et al. 2012, Voivontas et al. 2001).

Theoretical Energy Potential Calculation

$$TEP = Pr * LHV \quad ..(3)$$

where, *TEP* corresponds to the Theoretical Energy Potential; *Pr* relates to the potential crop residue produces (t year⁻¹); *LHV* shows the lower heating value of the plant as MJ.kg⁻¹.

Theoretical biomass energy potential was calculated in previous literature in similar ways (Milhau & Fallot 2013, Ozturk & Bascetincelik 2006, Riva et al. 2014, Okello et al. 2013, Iye & Bilsborrow 2013, Singh 2015).

The methodology was applied to the island of Panglao. The biomass distribution was computed using Eq(2) with parameters from Table 1. It utilizes the satellite image captures from Sentinel-2 to determine the coconut crop area and be able to determine the yield in relation to the statistical data through the Census of Agriculture and Fisheries 2017 record from the Philippine Statistics Authority August 2019 report.

The computation of residues on the island allows for the calculation of theoretical energy potential using Eq(3). The values for the lower heating value of coconut husk and shell were based on related literature indicated in Table 1.

The Sentinel-2 Multispectral Instrument (MSI) image provides a high spatial resolution that aids the band classification process to define the parameters for calculating the vegetation cover of the island. Since crop statistical data with respect to each barangay or village on the island is unavailable, the images captured by Sentinel-2 gathered since 2015 recorded the latest possible land cover changes.

The distinct colors or wavelengths of visible and near-infrared sunlight reflected by the plants must be observed to determine the density of green on a certain land area. The pigment in plant leaves, chlorophyll, strongly absorbs visible light from 0.4 to 0.7 μm for use in photosynthesis. On the

other hand, the cell structure of the leaves strongly reflects near-infrared light from 0.7 to 1.1 μm. Hence, the more leaves a plant has, the more these wavelengths of light are affected, respectively. Fig. 4 indicates the NDVI calculated for Panglao Island that ranges from -0.77 to 0.86.

Biomass Residue Availability from Agricultural Abundance

Calculations of NDVI from Eq(1) for a given pixel always result in a number that ranges from minus one (-1) to plus one (+1). However, no green leaves give a value close to zero. A zero means no vegetation and close to +1 (0.8 - 0.9) indicates the highest possible density of green leaves. Fig. 5 provides an overview of vegetation cover in Panglao Island.

RESULTS AND DISCUSSION

The existing energy infrastructures in Bohol do not use biomass even though securing energy and power from different sources is a priority set by recent policies. Given the availability and potential of biomass, especially the crops residues, residual biomass can be a significant source of energy and power in the province. The result of the vegetation cover map as processed in GIS software leads to identifying areas with residual biomass in the form of coconut husk and shells.

The summary of vegetation cover for respective barangays or villages is listed in Table 2. The vegetation cover for a potential biomass source accounts for 12.62 percent of Panglao Island's total land area. The majority of vegetation cover on the island is in the form of perennial woody plants and coconut trees. Due to municipal policy on tourism and the identification of built-up areas, there are areas on the island with a plus one value for vegetation cover that was not included in the calculation for potential crop residue. The island of Panglao is well-known for its white-sand beaches, and while there are tourist zones with coconut trees, they are not meant for coconut production but rather for tourism. Nevertheless, there are several areas with an abundance of forest trees, shrubs, and agricultural crops. Identified areas with vegetation cover were field validated for the agricultural crop in the form of coconut presence and abundance for potential residue collection.

The coconut trees on the island of Panglao covered 1.26% of the total cultivation area of the province based on the vegetation cover of Sentinel-2 imagery. In 2017, coconut yield potentially reached 2,054 metric tons with a residue concentration amounting to 2,865 tons based on the RPR method. This amount of residues can be translated to 52.92 TJ of theoretical energy potential. (see Table 3).

Table 1: Overview of the RPR and LHV used in this study.

Parameters	Coconut Residues	
	Husk	Shell
RPR (t _{residue} /t _{product})	1.60	0.65
	0.419	0.12
LHV (MJ/kg)	18.62	18.09

Residue-to-product ratio based on (Massaquoi 1990, Bhattacharya 1993, Ryan 1991, Singh 2008)



Fig. 4: Panglao island NDVI, ranges from -0.77 to 0.86.

Estimation of Biomass Residues and Energy Potential in Panglao Island

The island has the potential to produce 2073.74 tons of coconut husk and 790.88 tons of coconut shell in a cultivation area of 444 hectares. Considering the average energy content

for coconut, the theoretical energy generation potential from coconut residues turned out to be 52.92 terajoules. The contributions of different barangays or villages for the coconut residues to theoretical energy generation are summarized in Table 3, considering the fact that all of the residual biomass is recoverable. According to the analysis, using unused residues



Fig. 5: Panglao island vegetation cover.

from agriculture crop sources can generate potential energy with 100 percent waste recovery. However, if the recovery rate is lower, the amount of energy that may be produced is proportionately lower. It must be noted that the amount of energy is mostly based on available biomass resources which are currently unutilized.

The amount of theoretical energy potential recovered is still low compared to the demand of 33,553 total population of Panglao in the 2015 Bohol Census. However, the island of Panglao has several areas with an abundance of coconut trees being a landmass separated from the mainland of the province. The surrounding coconut trees on the island provide the potential for renewable energy when its residues are fully collected and utilized for bioenergy.

CONCLUSION

The resource assessment approach evaluated the energy potential of agricultural residues using Sentinel-2 MSI images. It has a resolution of 10 to 60 m in the visible, near-infrared, and short-wave infrared spectral zones. The captured images include 13 spectral channels, ensuring that differences in vegetation status and temporal changes. The unavailability of data to establish information on biomass resource estimation was bridged by the usage of remote sensing imagery, including the advantage of wide range coverage.

Biomass availability assessment accounts for an overview of the distribution and abundance of biomass resources that can be explored for electricity generation. An agricultural residue is an indigenous form of biomass residue that is widely available for waste to energy utilization. The increasing energy demand shall be sustained when alternative options for renewable and sustainable energy sources are assessed for its availability. This study may serve as a baseline for creating policies and strategies of the local government to fully utilize the potential of the agricultural sector.

Table 2: Estimation of coconut distribution areas in Panglao.

Name of Barangay	Area (sqm)
Bil-Isan	1121426.75
Danao	1313519.74
Doljo	464776.26
Looc	500944.16
Songculan	98922.84
Tabalong	21345.7
Totolan	919853.53

Estimation based on attribute data generated from vegetation cover

Table 3: Panglao coconut bioenergy potential.

Name of Barangay	Potential Crop Residue (t year ⁻¹)		Theoretical Energy Potential (TJ)
	Husk	Shell	Coconut Residues
Bil-Isan	523.68	199.72	13.36
Danao	613.38	233.93	15.65
Doljo	217.04	82.77	5.54
Looc	233.93	89.22	5.97
Songculan	46.19	17.62	1.18
Tabalong	9.97	3.80	0.25
Totolan	429.55	163.82	10.96

Estimation based on *Pr* and *TEP* calculations

ACKNOWLEDGMENT

This study was supported by the Department of Science and Technology, Science Education Institute under the Engineering Research and Development for Technology program. We are grateful to DOST for the financial support given and the University of San Carlos, School of Engineering for the accessibility and use of available facilities.

REFERENCES

- Ahamed, T., Tian, L., Ryoza, N. and Takigawa, T. 2013. Remote sensing applications of estimating biomass for energy crops: Development of ground-based sensing systems. *Remote Sens- Tech. Appl. Technol.*, 6(1): 31-53.
- Ahamed, T., Tian, L., Zhang, Y. and Ting, K.C. 2011. A review of remote sensing methods for biomass feedstock production. *Biomass Bioenerg.*, 35(7): 2455-2469. <https://doi.org/10.1016/j.biombioe.2011.02.028>.
- Ali, I., Cawkwell, F., Dwyer, E., Barrett, B. and Green, S. 2016. Satellite remote sensing of grasslands: From observation to management. *J. Plant Ecol.*, 9(6): 649-671. <https://doi.org/10.1093/jpe/rtw005>.
- Calle, F., Rosillo, P., Groot, S.L.H. and Woods, J. 2007. *The Biomass Assessment Handbook: Bioenergy For A Sustainable Environment*. Earthscan Publications Ltd, London, UK.
- Choubin, B. and Malekian, A. 2017. Combined gamma and M-test-based ANN and ARIMA models for groundwater fluctuation forecasting in semiarid regions. *Environ. Earth Sci.*, 76(15): 1-10. <https://doi.org/10.1007/s12665-017-6870-8>.
- Dube, T., Gumindoga, W. and Chawira, M. 2014. Detection of land cover changes around Lake Mutirikwi, Zimbabwe, based on traditional remote sensing image classification techniques. *Afr. J. Aquat. Sci.*, 39(1): 89-95. <https://doi.org/10.2989/16085914.2013.870068>.
- Iye, E. L. and Bilsborrow, P. E. 2013. Assessment of the availability of agricultural residues on a zonal basis for medium- to large-scale bioenergy production in Nigeria. *Biomass Bioenerg.*, 48: 66-74. <https://doi.org/10.1016/j.biombioe.2012.11.015>.
- Koopmans, A. and Koopenjan, J. 1997. *Agricultural and Forest Residues-Generation, Utilization, and Availability*. Reg. Consul. Modern Appli. Biomass Energ., 9: 23.
- McKendry, P. 2002. Energy production from biomass (Part 1): Overview of biomass. *Bioresour Technol.*, 83(1): 37-46. [https://doi.org/10.1016/S0960-8524\(01\)00118-3](https://doi.org/10.1016/S0960-8524(01)00118-3).

- Milhau, A. and Fallot, A. 2013. Assessing the potentials of agricultural residues for energy: What the CDM experience of India tells us about their availability. *Energy Policy*, 58: 391-402. <https://doi.org/10.1016/j.enpol.2013.03.041>.
- Moulin, S., Bondeau, A. and Delecolle, R. 1998. Combining agricultural crop models and satellite observations: from field to regional scales. *Int. J. Remote Sens.*, 19: 1021-1036.
- Okello, C., Pindozi, S., Faugno, S. and Boccia, L. 2013. Bioenergy potential of agricultural and forest residues in Uganda. *Biomass Bioenerg.*, 56: 515-525. <https://doi.org/10.1016/j.biombioe.2013.06.003>.
- Onojeghuo, A.O., Blackburn, G.A., Huang, J., Kindred, D. and Huang, W. 2018. Applications of satellite 'hyper-sensing' in Chinese agriculture: Challenges and opportunities. *Int. J. Appl. Earth Observ. Geoinform.*, 64: 62-86. <https://doi.org/10.1016/j.jag.2017.09.005>
- Ozturk, H.H. and Bascetincelik, A. 2006. Energy exploitation of agricultural biomass potential in Turkey. *Energy Explor. Exploit.*, 24(4-5): 313-330. <https://doi.org/10.1260/014459806779398802>
- Provincial Planning and Development Office 2018. Bohol Island Power Development Plan (BIPDP). <http://www.ppdobohol.lgu.ph/plan-reports/development-plans/bohol-island-power-development-plan-bipdp/> (accessed September 2020).
- Rahman, M.M. and Paatero, J.V. 2012. A methodological approach for assessing the potential of sustainable agricultural residues for electricity generation: South Asian perspective. *Biomass Bioenerg.*, 47(0): 153-163. <https://doi.org/10.1016/j.biombioe.2012.09.046>.
- Riva, G., Foppapedretti, E. and Caralis, C. 2014. Handbook on Renewable Energy Sources- Biomass Energy Supply.
- Singh, J. 2015. Overview of the electric power potential of surplus agricultural biomass from an economic, social, environmental and technical perspective: A case study of Punjab. *Renew. and Sust. Energ Rev.*, 42: 286-297. <https://doi.org/10.1016/j.rser.2014.10.015>.
- Voivontas, D., Assimacopoulos, D. and Koukios, E. G. 2001. Assessment of biomass potential for power production: A GIS-based method. *Biomass and Bioenerg.*, 20(2): 101-112. [https://doi.org/10.1016/S0961-9534\(00\)00070-2](https://doi.org/10.1016/S0961-9534(00)00070-2).
- Vrieling, A., De Leeuw, J. and Said, M. Y. 2013. Length of the growing period over Africa: Variability and trends from 30 years of NDVI time series. *Remote Sens.*, 5(2): 982-1000. <https://doi.org/10.3390/rs5020982>.
- Zhu, Z., Bi, J., Pan, Y., Ganguly, S., Anav, A., Xu, L., Samanta, A., Piao, S., Nemani, R. R. and Myneni, R. B. 2013. Global data sets of vegetation leaf area index (LAI)3g and fraction of photosynthetically active radiation (FPAR)3g derived from global inventory modeling and mapping studies (GIMMS) normalized difference vegetation index (NDVI3G) for the period 1981 to 2. *Remote Sens.*, 5(2): 927-948. <https://doi.org/10.3390/rs5020927>.



Water Quality Evaluation of Wenyu River in Beijing by Matter Element Model

Ren Shuangqing, Men Baohui† and Shen Yaoduo

School of Water Resources and Hydropower Engineering, North China Electric Power University, Beijing 102206, China

†Corresponding author: Men Baohui; menbh@ncepu.edu.cn

Nat. Env. & Poll. Tech.
Website: www.neptjournal.com

Received: 20-10-2020

Revised: 11-01-2021

Accepted: 22-01-2021

Key Words:

Water resources

Matter element analysis

Multiple super-scale weighting method

Correlation degree

Wenyu river

ABSTRACT

River water quality is an important indicator for identifying river changes and analyzing river health, and has an important impact on the ecological environment of the river basin. In this paper, the matter-element analysis method based on the coupling weight method is used to evaluate the water environment of the water quality measured data of Wenyu River in 2019, which provides a reference for water quality management and protection. Through the establishment of the object element to be evaluated, the classical domain, the section domain, the normalization of the evaluation standard, and the measured data, three representative indicators such as DO, NH₃-N, and COD_{cr} are selected as the object element to be evaluated. The standard value corresponding to the water quality standards of Grade I to V is the classic domain. The weight of river indicators is determined by the coupling of the ordinary objective weighting method and the multiple super-scale weighting method. After the weight is determined, the correlation degree is calculated and the matter-element analysis model for water quality evaluation is established. The results showed that the water quality of the Wenyu River in May 2019 was still mainly Grade V water, which was in line with the actual water quality situation. It shows that the method meets the feasibility and practicability in water quality evaluation and is relatively reliable.

INTRODUCTION

Wenyu River, located in the northeast of Beijing, was once known as the Mother River of Beijing. It is the only river that originated locally in Beijing. It originated from the foothills of Jundu Mountain. Three tributaries, Nansha River, Dongsha River, and Beisha River, meet at the upper reaches of the Wenyu River. In recent years, the population on both sides of the Wenyu River has increased sharply and businesses have been densely populated. Large amounts of domestic sewage and industrial wastewater have been injected into the Nansha River and Beisha River. The Wenyu River, which used to have a clear stream, is no longer clear. At present, there are many methods to evaluate the water environment. The commonly used methods include fuzzy comprehensive evaluation, set pair analysis, attribute recognition, and analytic hierarchy process (Wen 1984). Among them, the fuzzy comprehensive evaluation method uses the membership function to fuzzify the boundary of the evaluation object, although it can objectively reflect the actual situation. This method overemphasizes the extreme value and consumes far too much useful data, and each method for calculating the weight coefficient has its own set of limitations (Ming & Jianqiang 2013). With the improvement of the theory, the matter-element analysis theory established by Chinese mathematician Cai Wen in the 1980s has progressed from the initial matter-element analysis to the current extenics,

forming a rigorous theoretical system (Xueqiang et al. 2001, Zhemin 2005). The matter-element analysis method is a multivariate data quantitative evaluation approach that is based on the matter-element model, extension set, and correlation function theory, and can solve the incompatibility problem (Huber 1985). When determining the weights of evaluation indicators, commonly used methods such as expert evaluation method and analytic hierarchy process are highly subjective, and it is easy to cause deviations in results due to differences in the subjective value judgment standards of each person. Whereas in the ordinary objective weighting method, the weights are obtained directly based on the original data of the evaluation indicators and processed by statistical methods. Therefore, the distribution of the weights in this method will be affected by the randomness of the sample data, and cannot reflect the independence of the indicators, nor can it highlight the main influencing factors in the weights. Wang Mingtao mentioned the combination weighting method in his article -A comprehensive analysis method on determining the coefficients in multi-index evaluation (Mingtao 1999). As each weighting method has its own advantages and disadvantages, it is more reasonable to combine the weights obtained by various methods to determine the final weight. Compared with the basic matter-element analysis, this paper improves the calculation method of its weight coefficient. Based on the ordinary objective weighting method, it is supplemented by

the multiple super-scale weighting method. These two methods are weighted linearly and corresponding coefficients are given according to the actual conditions, and finally, the weight coefficient of the selected index is obtained. In this paper, the matter-element model based on coupling weight is applied to evaluate the water quality of The matter-element analysis method is a multivariate data quantitative evaluation approach that is based on the matter-element model of the Wenyu River.

MATERIALS AND METHODS

Build a Matter-Element Model

Determination of elements to be evaluated: The ordered triple “R = (P, C, X)” is used as the basic unit to describe things, which is called the matter element. Among them, P represents things, C represents the characteristics of P, and X represents the value of P with respect to C.

If a thing P is described by n features C1, C2,..., Cn and the corresponding values X1, X2,..., Xn, it is called an n-dimensional matter element and expressed as:

$$R = \begin{bmatrix} P & C_1 & X_1 \\ & C_2 & X_2 \\ & \vdots & \vdots \\ & C_n & X_n \end{bmatrix} \dots(1)$$

For the unit to be evaluated, the data obtained from the actual measurement is expressed in matter elements, which are called matter elements to be evaluated.

Determination of the Level of the Matter Element Set

Determination of the Classic Domain

$$R_j = (N_j, C_i, X_{ji}) = \begin{bmatrix} N_j & C_1 & X_{j1} \\ & C_2 & X_{j2} \\ & \vdots & \vdots \\ & C_n & X_{jn} \end{bmatrix} = \begin{bmatrix} N_j & C_1 & (a_{j1}, b_{j1}) \\ & C_2 & (a_{j2}, b_{j2}) \\ & \vdots & \vdots \\ & C_n & (a_{jn}, b_{jn}) \end{bmatrix} \dots(2)$$

In the formula, N_j is the j-th level divided; C_i represents the characteristics of level N_j; X_{ji} is the range of values specified by N_j with respect to C_i, that is, the numerical range of each level with respect to the corresponding characteristics.

Determination of Section Domain

$$R_0 = (N_0, C_i, X_{pi}) = \begin{bmatrix} P_0 & C_1 & X_{p1} \\ & C_2 & X_{p2} \\ & \vdots & \vdots \\ & C_n & X_{pn} \end{bmatrix} = \begin{bmatrix} N_j & C_1 & (a_{j1}, b_{j1}) \\ & C_2 & (a_{j2}, b_{j2}) \\ & \vdots & \vdots \\ & C_n & (a_{jn}, b_{jn}) \end{bmatrix} \dots(3)$$

In the formula, P₀ represents the whole level; X_{pi} is the range of values taken by P₀ with respect to C_i.

Determination of the Degree of Relevance of each Level of the Object to be Evaluated

Establish correlation function based on extension set theory and specific conditions:

$$K_j(x_i) = \begin{cases} \frac{-\rho(x_i, X_{ji})}{|X_{ji}|} & x_i \in X_{ji} \\ \frac{\rho(x_i, X_{ji})}{\rho(x_i, X_{pi}) - \rho(x_i, X_{ji})} & x_i \notin X_{ji} \end{cases} \dots(4)$$

Among them,

$$\rho(x_i, X_{ji}) = |x_i - 0.5(a_{ji} + b_{ji})| - 0.5(a_{ji} - b_{ji})$$

$$\rho(x_i, X_{pi}) = |x_i - 0.5(a_{pi} + b_{pi})| - 0.5(a_{pi} - b_{pi})$$

$$|X_{ji}| = |a_{ji} - b_{ji}|$$

For each feature C_i, w_{ij} is the weight coefficient. Let K_i(P) = ∑_{i=1}ⁿ w_{ij} * k_j(X_i), and K_j(P) is called the degree of relevance of the unit P to be evaluated at the quality level j.

Calculation of Weight Coefficient

The multiple super-scale weighting method

In the water quality evaluation process, the greater the weight of the evaluation index, the higher the impact of the index on the water quality. The multiple super-scale weighting method can highlight the main influencing factors and assign weights according to the degree of impact of the indicators on the water quality (Lunyan et al. 2018). It can not only avoid subjectivity in the evaluation but also make the evaluation more objective and reasonable. The calculation formula is as follows:

$$w_{1i} = \frac{x_i/s_i}{\sum_{i=1}^n (x_i/s_i)} \dots(5)$$

In the formula: w_{1i} is the weight of the indicator; x_i is the monitored value (or evaluation value) of the indicator; S_i is the average value of the indicator in the 5 standard levels.

Ordinary Objective Empowerment Method

For the threshold value x_{jj} (j = 1,2, ..., n) of the evaluation level N_i(i = 1,2, ..., m), the weight coefficient is

$$w_{2ij} = x_{ij} / \sum_{i=1}^n x_{ij} \dots(6)$$

i = 1,2, ..., n, j = 1,2, ..., m

The calculation is given in Table 1.

Table 1: Weight coefficient calculation table.

x_{ij}	N_1	N_2	...	N_m
c_1	x_{11}	x_{12}	...	x_{1m}
c_2	x_{21}	x_{22}	...	x_{2m}
...
c_n	x_{n1}	x_{n2}	...	x_{nm}

Coupling weight method (Fan et al. 2020)

The multiple super-scale weighting method can highlight the role of the most important pollutant factor in water quality assessment while taking into account the difference in standard values of different pollutants (Mingmei et al. 2015). Taking into account the actual water quality of the Wenyu River, this article uses the common objective weighting method, supplemented by the coupling weight method of the multiple super-scale weighting method to assign the weight of the river water quality index. Calculated as follows:

$$w_i = \alpha w_{1i} + \beta w_{2i} \quad \dots(7)$$

In the formula: w_{1i} and w_{2i} represent the weights of the multiple super-scale weighting method and the common weighting method respectively; α and β represent the corresponding weighting coefficients of the two methods respectively. According to the actual situation of the river, combining the advantages of each method, take $\alpha=0.4$, $\beta= 0.6$; w_i is the coupling weight corresponding to the i -th index.

Conclusion of matter-element analysis

If $k_a = \max(j)[k_j(P)]$ ($j=1, 2, \dots, m$), then $R \in Ra$, that is, the unit P to be evaluated belongs to the a level.

RESULTS AND DISCUSSION

Application of matter element analysis in water quality evaluation of Wenyu River

According to the actual conditions around the Shahe Reservoir and Wenyu River, combined with the water quality

Table 2: Water quality monitoring values and standard values.

Monitoring indicators	Evaluation standard						mg/L
	I	II	III	IV	V	average	Monitoring value
COD _{cr}	15	15	20	30	40	24	67
NH ₃ -N	0.15	0.5	1	1.5	2	1.03	1.89
DO	8	6	5	3	2	4.8	5.02

of the study area over the years and existing literature data, five water quality measurement sections and several monitoring indicators are selected: Shahe reservoir (116.335°E, 40.130°N), Mafang (116.397°E, 40.142°N), Lutuan gate (116.470°E, 40.120°N), Xinbao Gate (116.120°E, 40.062°N) and Xinbao Gate sewage outlet (116°, 40°) were selected on the mainstream of Wenyu River, as shown in Fig. 1.

Select three water quality monitoring indicators such as DO, NH₃-N, and COD_{cr}, and plot the data obtained from the monthly measurement from March to December 2019, as shown in Fig. 2, 3, and 4.

It can be seen from the measured water quality data that DO is significantly higher in spring and autumn than in summer, and there is no significant difference between different sampling points. The COD index of the water samples from the five sampling sites exceeded the standard more times and showed a rising trend at the sewage outlet of Xinbao Gate. The ammonia nitrogen of the water sample at Xinbao gate is higher than that of the other four water samples during the same period.

Determine the element to be evaluated

There are many surface water environmental quality indicators given in the “Surface Water Environmental Quality Standard” (GB3838-2002). Taking into account the actual measurement results and calculation results and other factors, the following three representative indicators are selected here: COD_{cr}, NH₃-N, DO. The monitored values of Shahe Reservoir on May 19 and the standards at all levels are shown in Table 2.

The object element to be evaluated is:

$$R = \begin{bmatrix} \text{COD}_{cr} & 67 \\ \text{NH}_3 - \text{N} & 1.89 \\ \text{DO} & 5.02 \end{bmatrix}$$

Determining the Classical Domain

Take the value range corresponding to the water quality standards of Class I to V to construct the matter element matrix of the classical domain as follows:



Fig. 1: Location of sampling points.

$$R(1) = \begin{bmatrix} \text{COD}_{cr} & (0,15) \\ \text{NH}_3 - \text{N} & (0,0.15) \\ \text{DO} & (6,8) \end{bmatrix}$$

$$R(2) = \begin{bmatrix} \text{COD}_{cr} & (0,15) \\ \text{NH}_3 - \text{N} & (0.15,0.5) \\ \text{DO} & (5,6) \end{bmatrix}$$

$$R_p = \begin{bmatrix} \text{COD}_{cr} & (0,40) \\ \text{NH}_3 - \text{N} & (0,2) \\ \text{DO} & (0,8) \end{bmatrix}$$

$$R(3) = \begin{bmatrix} \text{COD}_{cr} & (15,20) \\ \text{NH}_3 - \text{N} & (0.5,1) \\ \text{DO} & (3,5) \end{bmatrix}$$

$$R(4) = \begin{bmatrix} \text{COD}_{cr} & (20,30) \\ \text{NH}_3 - \text{N} & (1,1.5) \\ \text{DO} & (2,3) \end{bmatrix}$$

$$R(5) = \begin{bmatrix} \text{COD}_{cr} & (30,40) \\ \text{NH}_3 - \text{N} & (1.5,2) \\ \text{DO} & (0,2) \end{bmatrix}$$

Data Normalization Processing

Because the interval of the quantitative value of each evaluation index is not exactly the same, some evaluation indexes (such as COD_{cr}, NH₃-N) have a smaller value and a higher grade, while others (such as DO) have the opposite, so normalize each evaluation index and evaluation standard (Yinqin et a. 2013). For COD_{cr}, etc.: $d_i = x_i/x_5$; for DO, etc.: $d_i = 1.0 - (x_i - x_5)/x_1$.

Determine Section Domain

Generally, the lower limit of the section domain is 0, and the upper limit is the highest standard. So

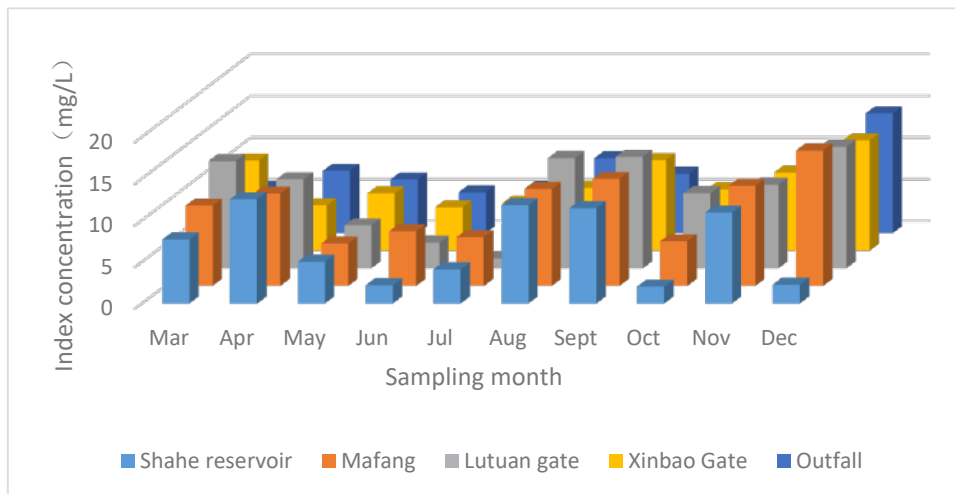


Fig. 2: Statistics of DO monitoring data.

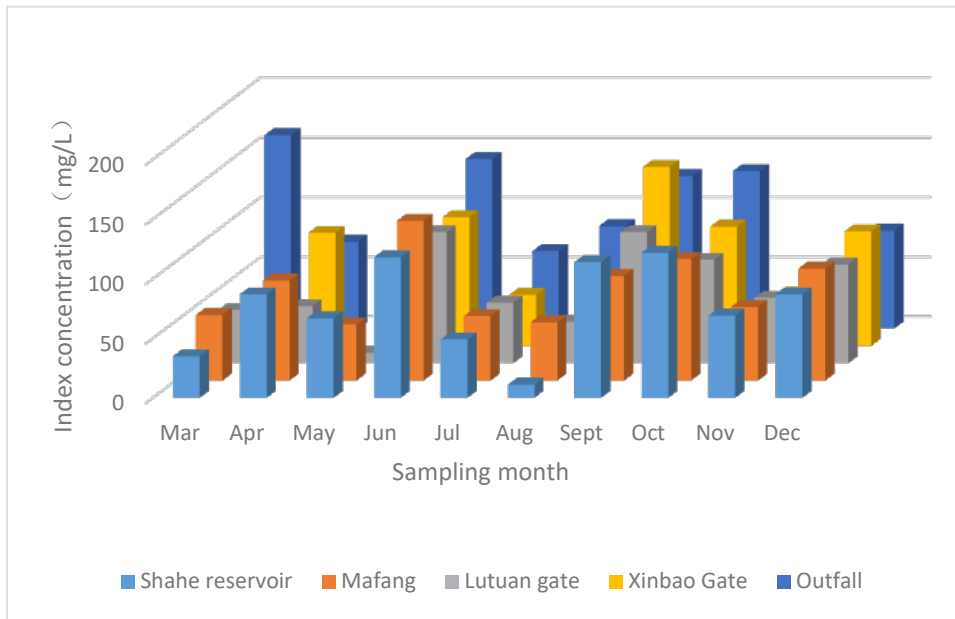


Fig. 3: Statistics of COD_{cr} monitoring data.

In the formula: d_i , x_i , x_1 , x_5 are the normalized standard value, unnormalized standard value, and the grade I and V standard value respectively.

$$R_{01} = \begin{bmatrix} \text{COD}_{cr} & (0,0.375) \\ \text{NH}_3 - \text{N} & (0,0.075) \\ \text{DO} & (0,0.25) \end{bmatrix}$$

The normalization of the grading standards is shown in Table 3.

The normalized classical domain and node domain are as follows:

$$R_{02} = \begin{bmatrix} \text{COD}_{cr} & (0,0.375) \\ \text{NH}_3 - \text{N} & (0.075,0.25) \\ \text{DO} & (0.25,0.5) \end{bmatrix}$$

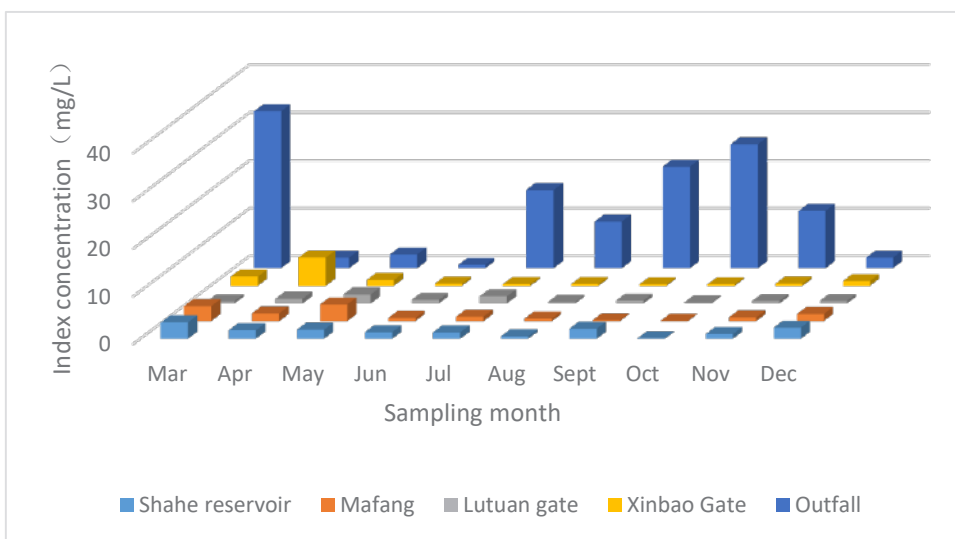


Fig. 4: Statistics of NH₃-N monitoring data.

Table 3: Classification standards after normalization

indicators	COD _{cr}	NH ₃ -N	DO
Grade I	0.375	0.075	0.25
Grade II	0.375	0.25	0.5
Grade III	0.5	0.5	0.625
Grade IV	0.75	0.75	0.875
Grade V	1	1	1

$$R_{03} = \begin{bmatrix} \text{COD}_{\text{cr}} & (0.375, 0.5) \\ \text{NH}_3 - \text{N} & (0.25, 0.5) \\ \text{DO} & (0.5, 0.625) \end{bmatrix}$$

$$R_{04} = \begin{bmatrix} \text{COD}_{\text{cr}} & (0.5, 0.75) \\ \text{NH}_3 - \text{N} & (0.5, 0.75) \\ \text{DO} & (0.625, 0.875) \end{bmatrix}$$

$$R_{05} = \begin{bmatrix} \text{COD}_{\text{cr}} & (0.75, 1) \\ \text{NH}_3 - \text{N} & (0.75, 1) \\ \text{DO} & (0.875, 1) \end{bmatrix}$$

The node domain RP of the model is determined according to the value range of normalized standard value and the measured data. R_x is determined according to the measured data after normalization as follows.

$$R_X = \begin{bmatrix} \text{COD}_{\text{cr}} & 1.675 \\ \text{NH}_3 - \text{N} & 0.945 \\ \text{DO} & 0.6225 \end{bmatrix} \quad R_P = \begin{bmatrix} \text{COD}_{\text{cr}} & (0,1) \\ \text{NH}_3 - \text{N} & (0,1) \\ \text{DO} & (0,1) \end{bmatrix}$$

Calculation of Weight Coefficient and Correlation

The weight coefficient w_{1i} can be determined according to the multiple super-scale weighting method.

$$W_{1\text{COD}_{\text{cr}}} = 0.467; w_{1\text{NH}_3-\text{N}} = 0.260; w_{1\text{DO}} = 0.273$$

Determine the weight coefficient w_2 according to the ordinary objective empowerment method, and the results are shown in Table 4.

Table 4: Weight coefficient w_2 .

a_{ij}	a_{i1}	a_{i2}	a_{i3}	a_{i4}	a_{i5}
a_{1j}	0.5357	0.3333	0.3077	0.3158	0.3333
a_{2j}	0.1072	0.2222	0.3077	0.3158	0.3333
a_{3j}	0.3571	0.4445	0.3846	0.3684	0.3334

Table 5: Weight coefficient w_i .

a_{ij}	a_{i1}	a_{i2}	a_{i3}	a_{i4}	a_{i5}
a_{1j}	0.5082	0.3868	0.3714	0.3763	0.3868
a_{2j}	0.1683	0.2373	0.2886	0.2935	0.304
a_{3j}	0.3235	0.3759	0.34	0.3302	0.3092

The coupling weight coefficient w_i can be obtained from formula (7), as shown in Table 5.

Using the weight coefficient to calculate the comprehensive correlation degree, $K_1(P) = -1.2946$, $K_2(P) = -1.1165$, $K_3(P) = -1.1274$, $K_4(P) = -1.6234$, $K_5(P) = -0.0571$, the evaluation result of this water sample is Grade V water.

CONCLUSIONS

The matter-element analysis method takes the evaluation index and its characteristic value as matter-element, obtains the classic domain, node domain, and weight coefficient of the model to calculate the correlation degree, and establishes a quality evaluation model with multiple index parameters of water quality. The evaluation results can be expressed by quantitative values. Reflect the difference of monitoring values, thereby reflecting the comprehensive level of direct water quality, and classify water quality accordingly. This evaluation method reflects the comprehensive impact of different evaluation factors on water quality.

The coupling weight method effectively highlights the most important pollution factors through two-value coupling and avoids the contingency of data evaluation. The evaluation process is concise and clear. It uses specific numerical calculations and quantitative instead of qualitative, which is closer to the actual situation. Not only can accurately reflect the overall situation of water quality, but also can intuitively show the weight of each measurement index in the water quality pollution factors.

The above-mentioned method was used to evaluate the actual water quality data of the five monitoring sections of the Wenyu River in May. The results showed that the water sample from the Shahe Reservoir at the sampling point on May 19, 2019, was Grade V water. Compared with the actual situation, the evaluation result is close to reality and the evaluation result is credible. In summary, in water quality evaluation, the matter-element analysis method based on coupling weights is an effective method, which can provide a lot of help for the scientific research work of water quality evaluation projects.

ACKNOWLEDGMENTS

This work was supported by the funds for the undergraduate innovative experiment plan of North China Electric Power University, and the Famous Teachers Cultivation planning for Teaching of North China Electric Power University (the Fourth Period).

REFERENCES

- Fan, G., Lan, Z. and Xiaoyi, S. 2020 Analysis of the spatial characteristics of Ulungur Lake water quality based on improved comprehensive water quality index. *South-to-North Water Trans. Water Sci. Technol.*, 18(1): 127-137.
- Huber, P. J. 1985. Projection pursuit (with discussion). *J. Ann. Statist.*, 13(2): 435-475.
- Lunyan, W., Yongchao, C., Huimin, L. and Yanchao, Z. 2018. Water environment quality evaluation based on cloud model: A case study of Jialu River in Zhengzhou *Water-Saving Irrig.*, 7: 61-70.
- Ming, He. and Jianqiang, Z. 2013. River water quality assessment based on matter-element analysis method *J. Environ. Sci. Manag.*, 38(3): 172-175.
- Mingmei, G., Tao, S. and Kun, Z. 2014. Dynamic fuzzy comprehensive evaluation on the atmosphere environmental quality of Jinan city based on the multiple super-scale weighting method. *J. Arid Land Resour. Environ.*, 28(09): 150-154.
- Mingtao, W. A. 1999. Comprehensive analysis method on determining the coefficients in multi-index evaluation. *J. Sys. Eng.*, 17(2): 56-61.
- Wen, C. 1984. Method of matter elements analysis. *J. Busefal*, 20: 51-56.
- Xueqiang, X. and Junjun, Z. 2001. A comprehensive evaluation of Guangzhou urban sustainable development. *Acta Geog. Sin.*, 56(1): 54-63.
- Yinqin, F., Tingting, L. and JIAO, H. W. 2013. Application of matter element analysis method to water quality evaluation in Yellow River. *J. Water Resour. Water Eng.*, 24(2): 166-169.
- Zhemin, L. 2005 Heavy metals pollution in vegetable fields and its prevention. *J. Arid Land Resour. Environ.*, 19(2): 101-104.



Impact of Drying and Wetting Cycles on Vegetation Cement-soil Physical and Mechanical Properties

Xudong Hu*(**), Jiazhen Gao*(**), Mingtao Zhou*(**)†, Songtao Peng***, Wennian Xu*(**) and Chenyuan Wang**

*Hubei Key Laboratory of Disaster Prevention and Mitigation, College of Civil Engineering and Architecture, China Three Gorges University, Yichang, 443002, China

**College of Civil Engineering & Architecture, China Three Gorges University, Hubei Yichang, 443002, China

***Dagu Hydropower Branch, Huadian Tibetan Energy Co., Ltd., Tibet Shannan 856200, China

†Corresponding author: Mingtao Zhou; zmt@ctgu.edu.cn

Nat. Env. & Poll. Tech.
Website: www.neptjournal.com

Received: 05-11-2020

Revised: 15-12-2020

Accepted: 22-01-2021

Key Words:

Vegetation cement-soil
Drying-wetting cycles
Crack
Initial water content

ABSTRACT

The physical and mechanical properties of the ecological slope protection substrate will be affected by long-term variation of the meteorological condition, resulting in the stability of the substrate being reduced. So an artificial substrate of vegetation cement-soil was selected as the research object to prepare specimens with the different initial moisture content of 13%, 19%, 25%, 31%, 37%, and 43%. And a series of tests are conducted to investigate the evolution of the physical and mechanical properties under drying-wetting cycling conditions. Typical results of the vegetation cement-soil evolution can be divided into three stages: cement hydration stage, shrinkage stage, and stabilization stage. In terms of different initial moisture content, the shrinkage cracks number, cracks length, crack width, and cracks surface area are increased first and then stabilize with the increase of the number of drying-wetting cycles. In contrast, the cohesion and internal friction angle of the vegetation cement-soil is reduced with the increase of the number of cycles. Comprehensive analysis shows that the initial moisture content of vegetation cement soil ranges from 25% to 31% is the optimal choice to ensure substrate stability in production practice.

INTRODUCTION

Vegetation cement-soil is an artificial substrate prepared from soil, cement, organic material, a special additive named Runzhi (a patent invented by China Three Gorges University), water, in a certain proportion for cut slope revegetation. The patent and related research clearly indicate the optimal mass proportioning of vegetation cement-soil is 100 (soil): 6 (cement): 6 (organic material): 3 (Runzhi additive) (Xu et al. 2012). As a result, the artificial substrate has both physical and mechanical properties of soil and cement, such as scour resistance, stability, expansion, and contraction (Xu et al. 2012). The vegetation cement-soil has been widely applied on various cut slopes revegetation in southern China (Liu et al. 2012, Zhao 2018) which are often subjected to alternating mega temperature and rainstorm weather changes. In such a case, the physical and mechanical properties of the vegetation cement soil are inevitably influenced by the drying-wetting process.

Alternate drying-wetting cycle (DWC) are recognized as important factors that can affect the soil's physical and mechanical properties (Kuwano et al. 2011, Rao &

Revanasiddappa 2006), and reshape the cement stability as well (Suddepong et al. 2018). For example, the expansive soil shows significant swelling or shrinkage characteristics when the soil gains or loses water, respectively, and cracks gradually develop as the number of DWC increases (Ye et al. 2018). Due to the difference in the content of organic matter, and mineralogy, the cracks of clay soil show a denser crack pattern with a smaller aperture under the repeated drying-wetting cycles (Diel et al. 2019, Wang et al. 2016). In addition to the abovementioned characteristics, the soil strength reduces significantly during the drying-wetting process. However, the strength of cement-soil shows an increase first, then a decreasing trend when the number of DWC increases, and it changes with different water content (Zhang et al. 2014, Zhang 2018). As an artificial composite ecological restoration substrate, the physical and mechanical properties of vegetation cement soil are different from the soil and cement. Moreover, limited works of literature consider the influence of initial moisture content on the soil and cement physical and mechanical properties during the drying-wetting process.

The effect of initial moisture content on the strength of cement is obvious (Zhang et al. 2014), especially in cement soil. Hence, the initial moisture content is selected as a variable in this paper, and the distribution of cracks is considered. Laboratory simulation tests of drying-wetting cycles are conducted to measure the swelling, shrinkage, and crack development. The binary image processing technology is used to quantitatively analyze the development of cracks. Moreover, the direct shear test is carried out to determine its shear strength after several times of drying-wetting cycles. Finally, the optimal initial moisture content could be obtained by the method of comparative analysis.

MATERIALS AND METHODS

Materials Source: The materials include soil, cement, organic matter, Runzhi additive, and water. The yellow-brown soil was selected according to its physical properties (Table 1). The yellow-brown soil was collected from the botanical garden of China Three Gorges University and passed through sieves of 2 mm mesh size. P.O 32.5 ordinary Portland cement, with a dry density of $3.10 \times 10^{-3} \text{ g} \cdot \text{mm}^{-3}$, was purchased from Yichang Huaxin Cement Factory. Sawdust of *Metasequoia glyptostroboides* was adopted as organic matter produced from Yichang Yemingzhu Saw Mill. The Runzhi additive, including mineral powder, water-retaining agent, and complex fertilizer, shows weak acidity that can neutralize the basicity of the cement in the vegetation cement-soil.

Referring to the weak expansive soil sharply influenced depth by climate is mainly 1.6 ~ 2.3 cm in southern China (Xiang & Dong 2012), and the size of repeated ring specimens was intended to be $\Phi 61.8 \text{ mm} \times 20 \text{ mm}$. The preparation of the specimen complied with the National Standard for Soil Test Method (GB/T 50123-2019), and the proportion was 100 (soil): 6 (cement): 6 (organic material): 3 (Runzhi additive). The minimum and saturated moisture contents of vegetation cement soil were 13%, 43%, respectively (Xu et al. 2012). Therefore, we made three groups (Group A, Group B, Group C) of specimens with 6 different initial moisture content at 5% intervals, which were 13%, 19%, 25%, 31%, 37%, and 43%, respectively. The prepared specimens of Group A were

taken for the free swelling test directly without curing, but the Groups B and C were maintained under standard curing conditions (temperature 20°C and relative humidity 95%) for 7 days. One group (Group A) was a control specimen, Groups B and C were used to conduct the drying-wetting cycles test, and Group C would take a direct shear test after each drying-wetting cycle test. Moreover, the mineral composition of the vegetation cement-soil specimen can be seen in Table 2 according to the X-ray analysis.

Test Method and Equipment: When the curing was finished, the specimens of Groups B and C were taken out to perform the drying-wetting cycling tests. In the drying process, the specimens were placed in an oven (DHG-9035A) with a temperature of $40 \pm 1^\circ\text{C}$ for 24 h. In order to obtain the evolution of cracks after the drying process, an HD digital camera was used to take a photograph of the top surface of the specimen, and the distance between camera and specimen was always equivalent. In the subsequent wetting process, a GDB-1 type stacked saturator was used to wetting the specimens. Referring to the drying-wetting cycles of residual soils conducted by Kong et al. (2009), the number of our drying-wetting cycles was set to 8 times, and each specimen should be taken out to measure the expansion and contraction after the drying-wetting cycles. Group A was placed at laboratory conditions (temperature 20°C and relative humidity 95%) during the free swelling test. Each specimen in Group A was wrapped with plastic film to let them expand and contract freely. The WZ-2 dilatometer was used to measure the expansion and contraction every 2h same as the Group B.

Each initial moisture content specimen in Group C has been made to six parallel samples divided into Group C-1, Group C-2, Group C-3, Group C-4, Group C-5, Group C-6. The number of C-1 to C-6 represents the times of drying and wetting cycles test. For example, Group C-1 only conducted one cycle test of drying and wetting. Moreover, the drying-wetting cycling tests of Group C and Group B were conducted at the same time. When the drying-wetting cycling tests were finished, the ZJ Quadruplex Strain Controlled Direct Shear Apparatus was used to conduct the direct shear tests.

Table 1: Physical properties of yellow-brown soil.

Specific gravity	Density $\text{g} \cdot \text{cm}^{-3}$	Natural moisture content $\omega/\%$	Porosity $I/\%$	Liquid limit $\omega_L/\%$	Plastic limit $\omega_P/\%$	Plasticity index IP (%)	Liquidity index IL (%)
2.58	1.79	16.3	40.18	31.7	16.9	14.8	1.1

Table 2: Mineral composition of the specimens.

Composition	Quartz/SiO ₂	Albite/Na ₂ O·Al ₂ O ₃ ·6SiO ₂	Illite	Calcite/CaCO ₃	Montmorillonite	Dolomite
Mass fraction/%	56	14	10	9	8	3

Data Processing Method: First, Photoshop software was used to correct the images and convert them into grayscale images. Then, Matlab software was used to binarize the images and remove the miscellaneous points. A threshold was set to turn the crack areas into black and the other areas into white. Finally, the contour and centerline vectors were also carried out by Matlab software to estimate the cracks area, width, and length. According to the geometric characteristics of cracks on the surface of the specimens, four indicators were used for quantitatively analyzing the generation of the cracks (Chu 2015, Li et al. 2014). The calculation formulas are as follows:

$$\delta_a = \frac{\sum_{i=1}^{n_i} A_i}{A} \quad \dots(1)$$

$$\delta_b = \frac{\sum_{i=1}^{n_i} l_i}{A} \quad \dots(2)$$

$$\delta_c = \frac{\bar{l}}{\bar{d}} \quad \dots(3)$$

$$\delta_d = \frac{A_0 - A}{A} \times 100\% \quad \dots(4)$$

Where, *i* is the number of cracks in the survey; *A_i* represents the crack area, mm²; *A* is the surface area of the specimen, mm²; *l_i* represents the crack length, mm; \bar{l} represents the average length of the crack, mm; \bar{d} represents the average interval of crack, mm²; *d_a*, *d_b*, *d_c*, and *d_d* represents the crack area ratio, length ratio, width ratio, and surface

shrinkage ratio, respectively; *A₀* represents the initial surface area of the specimen, which is equal to 3000 mm².

RESULTS AND DISCUSSION

Free and Cyclic Swelling-Shrinkage: The evolutions of control Group A under laboratory conditions is shown in Fig. 1. As shown in Fig. 1, for the specimens with a curing time of nearly 180 h, the shrinkage of the vegetation cement soil can be divided into three stages. Initially, the specimens, with different initial moisture content, were sharply shrunk due to the hydration reaction between cement and water within 2 hours, and the maximum shrinkage reached 0.4 mm. After the cement hydration stage, the shrinkage of the specimens showed a linear increase and entered the stage of shrinkage. The increasing rates of 13%, 19%, 25%, 31%, 37%, and 43% initial moisture content specimens were 0.017, 0.014, 0.013, 0.012, 0.013, and 0.019, respectively. The initial moisture content of 43% specimen in the period of shrinkage was the longest (nearly 110 h) among them, and the shortest (80 h) was the specimen with 13% initial moisture content. Finally, the shrinkage of vegetation cement-soil gradually stopped under laboratory conditions, showing a stabilization stage.

After each time of the drying-wetting cycle, the shrinkage would be measured to calculate the swelling-shrinkage rate (Fig. 2). The shrinkage rate was increased as a power func-

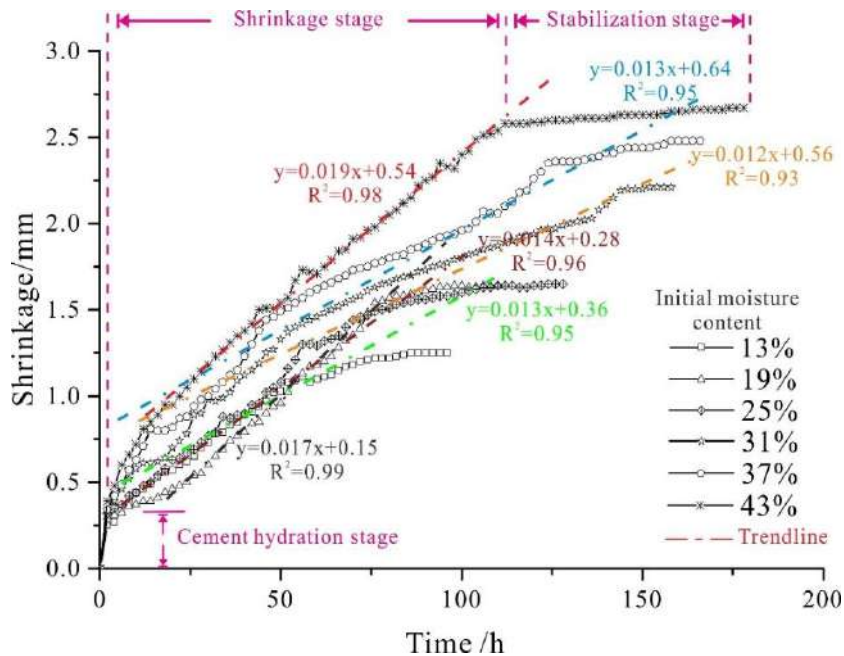


Fig. 1: Free shrinkage time course curve of the control specimens (Group A) under laboratory conditions.

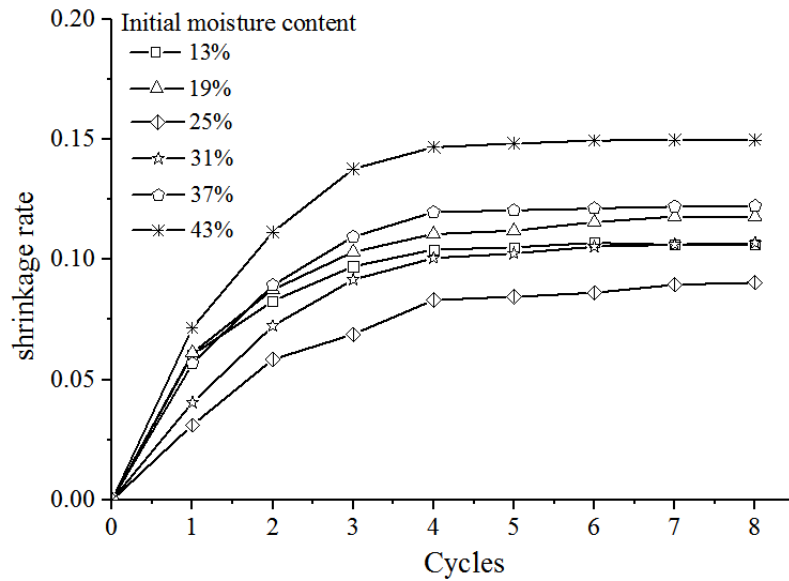


Fig. 2: Cyclic shrinkage rate of Group B during the drying-wetting cycles.

tion with the increase of the cycles. Moreover, the shrinkage rates of each initial moisture content were tiny, indicating the vegetation cement-soil has the effect of restoring itself to its original state after shrinking or expanding. In terms of different initial moisture content, the shrinkage of the specimen with an initial moisture content of 25% was the smallest with 0.08, and the specimen with an initial moisture content of 43% is the largest with 0.15. Moreover, it can be found

that the shrinkage rates of each specimen were becoming steady after the 4th cycle. Compared to the control Group A under laboratory conditions, the shrinkage of different initial moisture content in Group B was larger than that in Group A.

Distribution of Surface Cracks: The binary image of specimen cracks evolution after drying and wetting cycles is shown in Table 3. Group A, which was placed in the laboratory condition without experiencing the drying and

Table 3: Binary image of cracks after drying and wetting cycles.

Initial moisture content	13%	19%	25%	31%	37%	43%
Group A N=0						
Group B N=3						
Group B N=4, 5,...8						

Note: N represents the number of drying and wetting cycles

wetting cycles, has no obvious cracks. After 3 times of drying and wetting cycles, the cracks gradually emerged except for 13% initial moisture content. The length, width, and area of the cracks started to appear and the cracks increasing rate rose with the increase of the drying-wetting cycles. 13% and 43% initial moisture content specimens were on the edge of disintegration after 5 to 8 cycles of drying-wetting, especially the 13% initial moisture content specimen because of the lowest initial moisture content leading to the specimen become loose. 19% and 37% initial moisture content specimens were only divided into several small pieces by cracks, and a large number of cracks were also produced, but the integrity was not destroyed. 25% and 31% initial moisture content specimens saved a complete structure with only a few cracks and performed best among them. Therefore, when the slope ecological restoration project is implemented, the initial moisture content of the vegetation cement soil should be controlled between 25% and 31% to enhance the stability of the project.

The characteristic parameters of average crack width, area ratio, length ratio, and surface area shrinkage were increased with the increase of the number of drying and wetting cycles in Fig. 3a, b, c, d, and stabilized after the 4th cycle. The highest average crack width after 5 to 8 drying and wetting cycles was the specimen with 13% initial moisture content, and the value reached 0.26 cm. In the contrast, the smallest was the 25% initial moisture content with the peak width of 0.15 cm, followed by the 31% initial moisture content with a peak width of 0.16 cm (Fig. 3a). And the stable area ratio of each specimen was 8.3%, 5.6%, 2.9%, 4.5%, 5.1%, and 7.2%, respectively (Fig. 3b). The evolution of crack width was consistent with crack area, and the adhesive force of 25% and 31% initial moisture content specimens were performed best.

The peak value of length ratio was 0.31, 0.26, 0.19, 0.20, 0.23, and 0.29, respectively (Fig. 3c). The largest one is a 13% initial moisture content specimen, and the smallest one is a 25% initial moisture content specimen. The length ratio results implied that the vegetation cement-soil with 19% initial moisture content performed worst, but the one with 25% initial moisture content was the best. Moreover, it can be seen from Fig. 3d that the surface shrinkage of the specimens with an initial moisture content of 13% and 43% was significantly higher than that of other specimens. Comprehensively, the crack evolution of vegetation cement-soil with an initial moisture content of 25% or 31% was the lowest compared to others, which proved once again that the vegetation cement-soil with the initial moisture content between 25% and 31% had high stability.

Post-Cyclic Shear Strength: Results of the direct shear tests

conducted on Group C-1, C-2, C-3, C-4, C-5, and C-6 are given in Fig. 4a, b. The cohesive force and internal friction angle were reduced with the increase of the drying-wetting cycle. After 4 cycles, the reduction trend of the cohesive force and internal friction gradually slows down. Without the drying-wetting cycle, the cohesive force of each initial moisture content specimen ranges from 42 kPa to 53 kPa (Fig. 4a). The internal friction angle of each specimen was distributed from 27° to 31° (Fig. 4b). After 8 cycles, the cohesive force of each initial moisture content specimen reduced to 32.5 kPa, 33 kPa, 36 kPa, 34.8 kPa, 32.8 kPa, and 30.7 kPa, respectively. The maximum reduction value of 16.6 kPa was at 13% initial moisture content specimen, and the minimum reduction value of 11.6 kPa was at 43% initial moisture content specimen. As well as the internal friction angle, the maximum reduction value of 5.2° was at 19% initial moisture content specimen, and the minimum reduction value of 3.3° was at 25% initial moisture content specimen. Fig. 4a, b indicated that the vegetation cement-soil with 19% and 25% initial moisture content performed well.

Vegetation Cement-Soil Physical Properties: Due to the proportion of soil in vegetation cement-soil reaches 80%, the evolution of vegetation cement-soil physical properties is closely related to the physical property of the yellow-brown earth we selected. It is known from Table 2 that the illite and montmorillonite in the yellow-brown earth account for 18%, and the illite and montmorillonite will produce 30% to 40% and 50% to 60% unequal swelling during the wetting process, respectively (Ambroise et al. 1985, Jiang et al. 2013, Yang et al. 2010). As a result, the shrinkages of specimens were larger than the swelling no matter under laboratory conditions or during drying-wetting cycles (Figs. 1, 2). Unlike the expansive soil, which is dominated by the characteristic of swelling ranging from 13% to 6% after 4 drying-wetting cycles (Wang et al. 2015), the vegetation cement-soil is dominated by the physical properties of shrinkage ranging from 8% to 15% under different initial moisture content condition (Fig. 2). An appropriate proportion of cement in the vegetation cement-soil, which was obtained after many trials (Xu et al. 2012), plays a vital role to enhance its strength to avoid swelling.

Although the main characteristic of vegetation cement soil is shrinkage, the swelling could not be ignored during the wetting process. The hydrophilic substances of illite and montmorillonite would make the micro-cracks and pores emerged in the weak parts of cement soil (Walker et al. 1995), causing the weakening of the connectivity between particles. With the recurrence of the drying-wetting cycle, the micro cracks and pores acted as a path for water migration, and the particles and clay minerals were repeatedly eroded

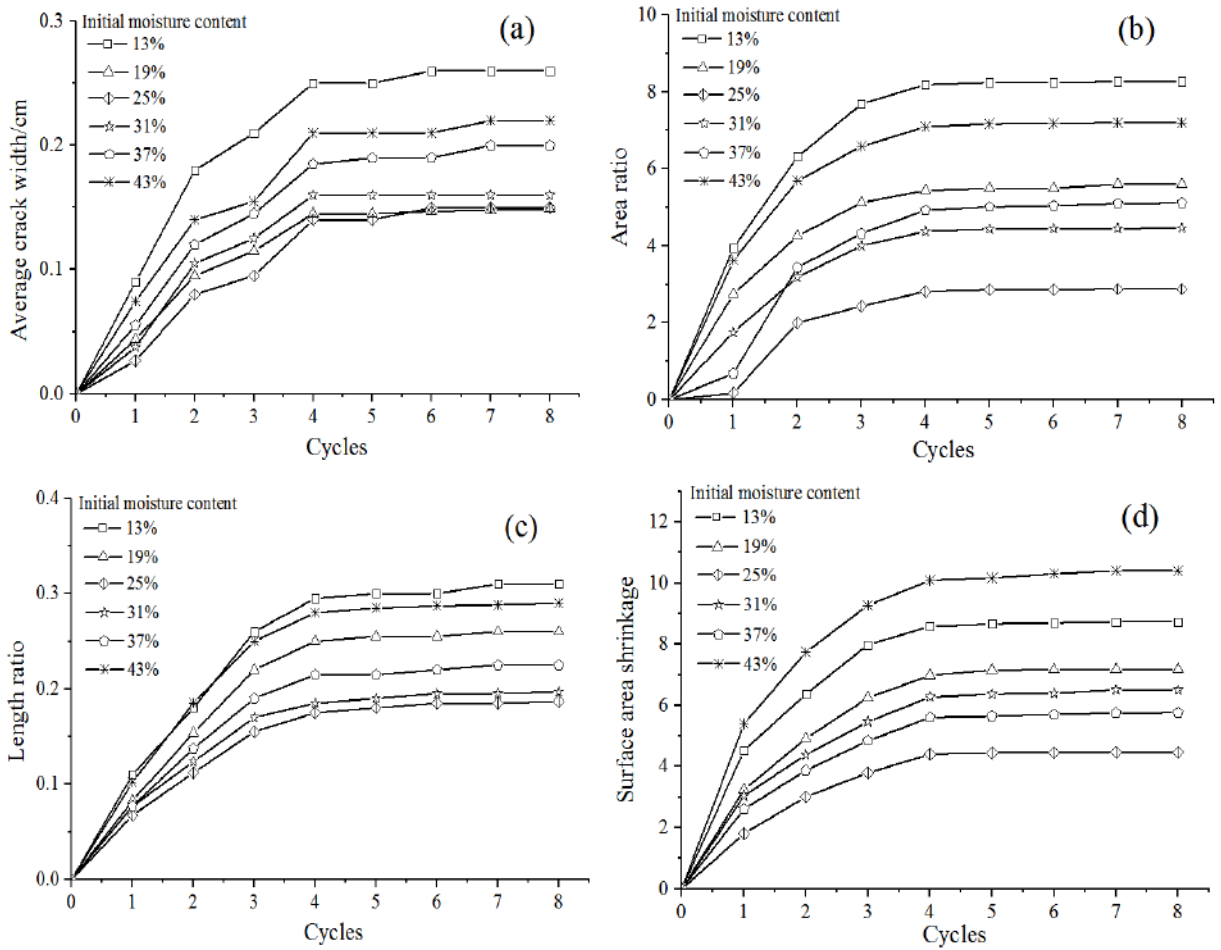


Fig. 3: Evolution of vegetation cement-soil under the drying and wetting cycles (a) Average crack width curve; (b) Area ratio curve; (c) Length ratio curve; (d) Surface area shrinkage curve.

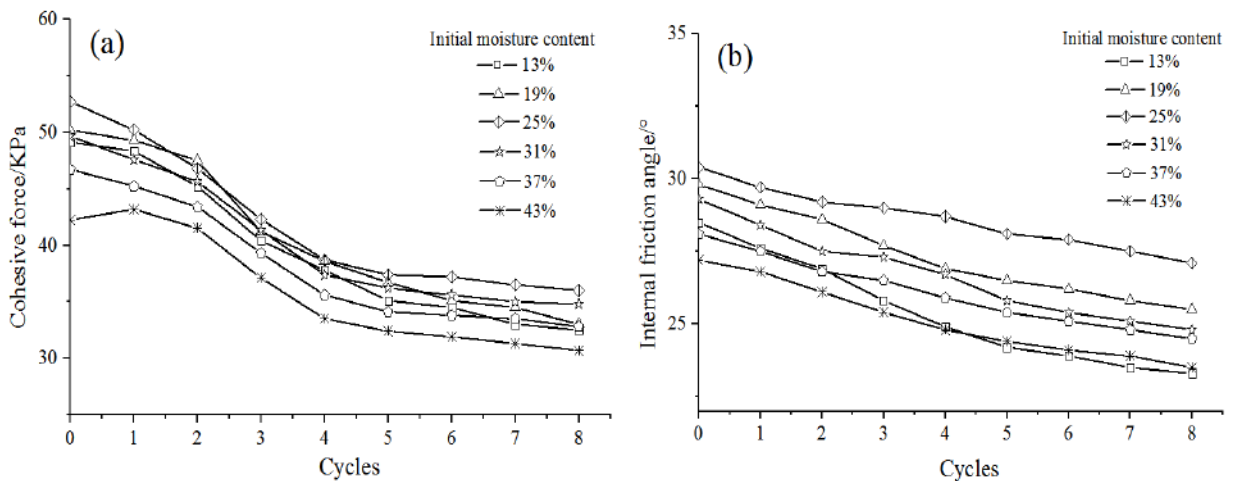


Fig. 4: Vegetation cement-soil mechanical-cycle curves (a) Cohesive force curve; (b) Internal friction angle curve.

and dissolved by water (Kamei et al. 2013), resulting in the pores of vegetation cement-soil increased to destroy its structural and produce cracks eventually. Moreover, the main provider of strength, ettringite crystals, would pulverize and disintegrate after the carbonation reaction between cement and soil during the drying process, generating substances such as calcium carbonate, calcium sulfate, and large pores (et al. 2013), leading to the strength reduced. Pedreño-Rojas et al. (2019) found that the wood chips can cause micro-structure damage and strength loss of composite materials after drying-wetting cycles. Liu et al. (2018) further proved that the organic material, such as sawdust, has a remarkable effect on the physical and mechanical properties of cement soil during drying-wetting cycles, and it could cause damage to cement-soil structures.

Vegetation Cement-Soil Mechanical Properties: For the yellow-brown earth, the influence of soil moisture content and dry bulk density on the shear strength has been explored by Wang et al. (2018). Results showed that the cohesion of yellow-brown earth, with different moisture content (25%, 27%, 29%, 31%, 33%), ranges from 10 kPa to 40 kPa under the dry bulk of 1.1 g.cm^{-3} , and the internal friction angle distributes from 25° to 30° . Compared to the yellow-brown earth and concrete, the vegetation cement-soil has a medium shear strength. For the cohesion, the shear strength of vegetation cement-soil reduces with the increase of the cycles and the smallest cohesion is larger than 30 kPa, which has improved compared to the yellow-brown earth. Due to the small amount of cement mixed in the vegetation cement-soil, the internal friction angle is similar to yellow-brown earth. Despite the fact that vegetation has a lower shear strength than concrete, the purpose of developing vegetation cement-soil is to function as a specific substrate for restoring the cutting slope (Liu et al. 2018). As an artificial substrate, the vegetation cement-soil is not only widely applied in China (Liu et al. 2013), but also spread to Sudan (Mohammed et al. 2018). Hence, the shear strength improved significantly can ensure the stability of slope revegetation as well as the function of revegetation.

Effect of Initial Moisture Content: Unlike yellow-brown earth (Wang et al. 2016) or expansive soil, the vegetation cement-soil contains 6% organic matter. Liu et al. (2018) chose rice husks, sawdust, and corn distillers' and unhulled rice distillers' grain to research the effect of different organic matters on the vegetation cement-soil, and found that they have a remarkable effect on the substrates' porosity and mechanical properties due to the response of organic matter to water. Studies indicate that a higher porosity will reduce the strength of artificial materials like cement (Chen et al. 2013). However, organic matter can retain water to change the pore structure. Zheng et al. (2001) also pointed out that

the weights of the organic matter which reached 5% among the solid material are suitable for plant growth, but Xu et al. (2012) insisted that plants can still grow effectively at the organic matter proportioning of 6% as well. Hence, we can alter the initial moisture content instead of organic matter and cement to control the function of vegetation cement-soil. It was found that the surface image of the specimen with 25% initial moisture content was the most complete by the comparison of different initial moisture content (Table 3). Based on the crack evolution (Table 3) and shear strength (Fig. 4), plant cement soil with a higher or lower initial moisture content would be more easily damaged by wetting swelling and drying shrinkage. In addition, the length and width of cracks were also affected by the initial moisture content, and the results were consistent with others studies (Tang et al. 2011). Compared to the cement and organic matter, the phenomenon in the paper of vegetation cement soil can be blamed on the initial moisture content during the drying and wetting cycles. Therefore, this paper focused on analyzing the impact of initial moisture content and providing an optimal initial moisture content of vegetation cement soil for enhancing the stability of the artificial substrate.

CONCLUSION

The following conclusions are drawn: (1) At laboratory temperature, the shrinkage of vegetation cement-soil presents three stages of cement hydration, shrinkage, and stabilization, and the shrinkage stage is the main characteristic of vegetation cement-soil during the drying-wetting cycles. (2) The specimens with different initial moisture content will produce cracks under the drying and wetting cycles, and the shrinkage cracks number, cracks length, cracks width, and cracks surface area are increased with the increase in the number of cycles and then tend to steady. But the cohesion and internal friction angle of the vegetation cement-soil are reduced. (3) The initial moisture content is the key factor affecting the vegetation cement-soil fissures. The specimen with initial moisture content from 25% to 31%, which has optimal stability and is suitable for application in production practice.

ACKNOWLEDGEMENTS

This work has been supported by the Foundation for creating high-end talent-leading characteristic carriers of China (Grant No. B19-004-01), Key Laboratory of Mountain Hazards and Earth Surface Processes, Chinese Academy of Sciences (Grant No. KLMHESP-20-02), National Key R&D Program of China (Grant No. 2017YFC0504902-02) and China Huadian Corporation Research Foundation (Grant No. 12IJD201800018).

REFERENCES

- Ambrose, J., Murat, M. and Péra, J. 1985. Hydration reaction and hardening of calcined clays and related minerals V. Extension of the research and general conclusions. *Cem. Concr. Res.*, 15(2): 261-268.
- Chu, W.J. 2015. The Characteristics and Rule of Deformation Crack Propagation Under the Wet and Dry Cycles Shrink: The Role of Red Clay Swelling. Master thesis, Guizhou University, Guizhou.
- Chen, X.D., Wu, S.X. and Zhou, J.K. 2013. Influence of porosity on compressive and tensile strength of cement mortar. *Constr. Build. Mater.*, 40: 869-874.
- Diel, J., Vogel, H.J. and Schlüter, S. 2019. Impact of wetting and drying cycles on soil structure dynamics. *Geoderma*, 345: 63-71.
- Jiang, Z.M., Ma, H.J., Tian, B.T. and Jiang S.P. 2013. Study on swelling property of tuff in Lancang Lead Ore by micro-analysis. *Subgrade Eng.*, (2): 83-85, 88. (in Chinese)
- Kamei, K., Ahmed, A. and Ugai, K. 2013. The durability of soft clay soil stabilized with recycled Bassanite and furnace cement mixtures. *Soils Found.*, 53(1): 155-165.
- Kong, L.W., Sayem, H.M. and Tian, H.H. 2018. Influence of drying-wetting cycles on soil-water characteristic curve of undisturbed granite residual soils and microstructure mechanism by nuclear magnetic resonance (NMR) spin-spin relaxation time (T₂) relaxometry. *Can. Geotech. J.*, 55(2): 208-216.
- Kuwano, R., Suwal, L.P. and Beltran-Galvis, A.L. 2011. Change of physical and mechanical properties of sandy soil due to repeated water infiltration. *Deform. Charac. Geomater.*, 46(11): 829-833.
- Li, W., Liu, G.S. and Yao, T. 2014. Improvement of methods for crack image processing and crack feature extraction of expansive soil. *Rock Soil Mech.*, 35(12): 3619-3626. (in Chinese)
- Liu, D.X., Xu, W.N., Cheng, Z.L., Zhou, Z.J., Cai, X.Y. and Zhao, B.Q. 2013. Improvement test on frost resistance of vegetation-concrete and engineering application of test fruitage. *Environ. Earth Sci.*, 69: 161-170.
- Liu, D.X., Zhao, B.H., Yang, Y.S., Xu, W.N., Ding, Y. and Xia, Z.Y. 2018. Effect of organic material type and proportion on the physical and mechanical properties of vegetation-concrete. *Adv. Mater. Sci. Eng.*, (6): 1-8.
- Mohammed, A., Xu, W.N. and Xia, Z.Y. 2018. Ecological and bioengineering studies for stabilizing the Wad Medani-Sennar roadside slope linking the Gezira and Sennar States. *Adv. Civil Eng.*, (1): 1-11.
- Pedreño-Rojas M.A., Morales-Conde M.J., Rubio-de-Hita P. and Pérez-Gálvez F. 2019. Impact of wetting-drying cycles on the mechanical properties and microstructure of wood waste-gypsum composites. *Materials*, 12(11): 1829.
- Rao, S.M. and Revanasiddappa, K. 2006. Influence of cyclic wetting drying on collapse behavior of compacted residual soil. *Geotech. Geol. Eng.*, 24: 725-734.
- Suddepong, A., Intra, A., Horpibulsuk, S., Suksiripattanapong, C., Arulrajah, A. and Shen, J.S. 2018. Durability against wetting-drying cycles for cement-stabilized reclaimed asphalt pavement blended with crushed rock. *Soils Found.*, 58(2): 333-343.
- Tang, C.S., Cui, Y.J., Shi, B., Tang, A.M. and Liu, C. 2011. Desiccation and cracking behavior of clay layer from the slurry state under wetting-drying cycles. *Geoderma*, 166: 111-118.
- Walker, P.J. 1995. Strength, durability, and shrinkage characteristics of cement stabilized soil blocks. *Cem. Concr. Compos.*, 17(4): 301-310.
- Wang, B.T., Zhang, C.H., Qiu, X.L., Ji, E.Y. and Zhang, W.H. 2015. Research on wetting-drying cycles' effect on the physical and mechanical properties of expansive soil improved by OTAC-KCl. *Adv. Mater. Sci. Eng.*, 3(2): 1-7.
- Wang, D.Y., Tang, C.S., Cui, Y.J., Shi, B. and Li, J. 2016. Effects of wetting-drying cycles on soil strength profile of silty clay in micro-penetrometer tests. *Eng. Geol.*, 206: 60-70.
- Wang, N., Zhao, Y.P., Guo, X.P., Zhang, J.C. and Liu, S.L. 2018. Effects of soil moisture content and dry bulk density of different vegetation types on slope soil shear strength. *J. Soil Water. Conserv.*, 38(6): 88-102. (in Chinese)
- Xiang, W. and Dong, X.J. 2012. Study of swelling characteristic of the weak expansive soil in Luwangfen for South-to-North water diversion project. *Rock Soil Mech.*, 33(4): 986-992. (in Chinese)
- Xu, W.N., Xia, Z.Y., Zhou, M.T., Liu, D.X. and Xia, D. 2012. The Vegetation Concrete Eco-Restoration Technology Theory and Practice. China Water & Power Press, Beijing. (In Chinese)
- Yang, K., Li, Z. 2010. Research on montmorillonite hydration expansion mechanisms. *J. Chin. Ceram. Soc.*, 29(5): 1154-1158. (in Chinese)
- Ye, H., Chu, C.F., Xu, L., Guo, K.L. and Li, D. 2018. Experimental studies on drying-wetting cycle characteristics of expansive soils improved by industrial wastes. *Hindawi*, 2018: 1-9.
- Zhang, J. 2018. Experimental study on compressive strength and wet-dry cycle durability of polypropylene fiber cement soil, *J. China Foreign Highway*, 38(6): 235-238. (in Chinese)
- Zhang, J., Gao, Y. and Luosun, Y.M. 2014. Shrinkage stress in concrete under dry-wet cycles: An example with a concrete column. *Mech. Time-Depend. Mater.*, 18(1): 229-252.
- Zhao, B.Q., Xia, L., Xia, D., Liu, D.X., Xia, Z.Y., Xu, W.N. and Zhao, J. 2018. Effect of cement content in vegetation concrete on soil physico-chemical properties, enzyme activities, and microbial biomass. *Nat. Environ. Pollut. Technol.*, 17(4): 1065-1075.
- Zheng, B.F., Zhang, J.Y. and Li, S.C. 2001. Study on basic features of thick layer base material. *Subgrade Eng.*, 3: 1-4. (in Chinese)
- Zhou, X.L., Liu, C.W., Feng, B., Guo, B.B., Lu, Y.H. and Zhang, L.W. 2019. Effects of dry-wet circulation on cement-based composite filling materials. *Chinese J. of Eng.*, 41(12): 1609-1617. (in Chinese)
- Zhou, J., Xu, H.Z. and Hu, W.J. 2013. Impact of wetting-drying cycle effects on the stability of expansive soil slopes, *Chinese J. Geotech. Eng.*, 35(zk2): 152-156. (in Chinese)



Advances in Microfiltration and Ultrafiltration Technology for Greywater Treatment: A Review

Joaquin Ortiz

ORJOLabs SpA, Morandé 835 Street, office N°518, Santiago, Chile

†Corresponding author: Joaquin Ortiz; joaquin.ortiz.t@orjolabs.cl

Nat. Env. & Poll. Tech.
Website: www.neptjournal.com

Received: 31-10-2020

Revised: 29-12-2020

Accepted: 22-01-2021

Key Words:

Greywater
Microfiltration
Ultrafiltration
Bioreactors
Filtering membranes

ABSTRACT

Advances in microfiltration and ultrafiltration technology for the treatment of greywater are important today because everything surrounding the use and preservation of water is an issue that increases in importance over the decades, and our planet will be seriously affected by the consequences of climate change, making water availability uncertain. Hence, wastewater recycling and its cyclical use have become a major topic in the scientific and engineering communities. The objective of this research is focused on compiling and updating all the advances in wastewater treatment, with emphasis on Greywater, in which components have a lower pollutant load than the rest of wastewater. In addition, microfiltration and ultrafiltration technologies were the technology selected to investigate in this investigation because they have the local potential for a second use of the wastewater before the discharge of contaminated water to the sanitation network. This research was carried out using words related to the exposed topic, such as “microfiltration”, “ultrafiltration”, “cleaning wastewater” and “greywater” in the search for documents in scientific search engines, selecting those that covered the topic and could be used to create this document. The results that were developed in this investigation, indicate that there is no generalized consensus on how to treat this greywater, nor how to qualify it. Additionally, it is important to note that despite the fact that urban greywater treatments have given good results, with the widespread use of bioreactors for this task, and the existence of various treatment alternatives for liquid waste that have shown good price-value ratio, studies related to greywater treatments using porosities are still in the incipient stages.

INTRODUCTION

Today our water resources are more threatened around the world than ever before, due to rapid population growth, as well as industrial use of water, thus large bodies of water are required to create a good or perform a service.

On the other hand, as a consequence of man’s various activities, wastewater is generated, which varies from one location to the other, but urban areas are characterized as areas where wastewater is being the most generated, and the fluid that does not come from the restroom is referred to as Greywater. Given the abundance of such wastewater, recycling is one of the main options when seeking new water sources in water-scarce regions, and wastewater treatment provide an effluent of sufficient quality that can be beneficially used instead of discharged.

There is greater interest in the reuse of grey water, given that its pollutant load is lower than that of other wastewater, and it can be attributed to some second use before its subsequent discharge into the waste network. Pore filters are good for use in cleaning these fluids since their equipment is not too complex, and the technology would

help to recirculate a significant amount of water and reduce demand for water within the same community (Li et al. 2009, Yokomizu 1994).

The focus of this research synthesis is on the updating of data related to this topic, as well as its future forecast. Despite the possible limitations to be solved in the process of cleaning Greywater by UF/MF, it continues to be a tentative and sustainable operation that allows people to reduce water consumption and decrease the impact of the human footprint on the deterioration of the ecosystem.

WORKING METHODOLOGY

The work methodology in this review is the search, compilation, study, segregation, synthesis, and formulation of conclusions from scientific publications related to the issue of wastewater recycling using the technology of filtration

Initially, an exhaustive investigation was carried out in scientific search engines as “Scopus”, “Web of science”, “Scencedirect”, “Researchgate”, “SciELO” and “Google Scholar” with the keywords “microfiltration”, “ultrafiltration”, “water treatment” and “greywater”, having a preference to publications of the last decade although ad-

mitting more old material. As a result of this procedure, all publications whose abstract coincided with the focus of this synthesis were analyzed, obtaining a list of publications that were compiled for the study of the advance of Greywater recycling in microfiltration and ultrafiltration technologies in the last decade.

After a detailed review of all the articles set, we proceeded to classify them according to the objective of this study, and from those we proceeded to extract the information linked to the topic of this study. Finally, some conclusions were established from the material found in the scientific library.

GREY WATER

Greywater is all wastewater generated in urban buildings without the presence of fecal contamination. Greywater constitutes 50-80% of total domestic wastewater, and the flow in developed countries is estimated between 90 and 120 L, produced by one person per day (Li et al. 2009). The chemical composition of Greywater is variable, however, its physicochemical characteristics vary in a certain range that is presented in Table 1. Likewise, there are also certain common contaminants that can occur in Greywater, such as Parabens, preservatives (Metilparabens (MP), ethylparaben (P), propylparaben (PP), butylparaben (BP), isobutyl parabens (isoBP)), Fragrances: (Tonalide, galaxolide HCA), surfactants (Triclosan, BaCl₂, nonylphenol), UV Filters, plasticizers, anionic Surfactants, among others) (De Gisi et al. 2015)

Numerous studies have been conducted on greywater treatment with different technologies that vary in both complexity and performance. However, specific guidelines for Greywater reuse are not available or sufficient and studies on the assessment of appropriate technologies for Greywater

reuse/recycling are scarce. Nevertheless, despite the few existing data in the bibliography, there are some environmental standards in some countries that regulate the quality of recycled water from Greywater should have. In the rest of the world, countries where there is no standard definition of Greywater, this one is treated as wastewater without any distinction from other liquid contaminants, and it is treated in common areas of cleaning and disinfection

GREY WATER TREATMENT TECHNOLOGIES

There are different Greywater treatment technologies, categorizing in physical, chemical, and biological treatments. Most of these technologies are preceded by a solid-liquid separation pretreatment and followed by disinfection as a post-treatment (Li et al. 2009).

Physical treatments include coarse sand, soil, and filtration by membranes, followed mainly by a disinfection step since coarse filtration has only a limited effect on the removal of contaminants present in Greywater (March et al. 2004).

Regarding the chemical cleaning processes of Greywater, there are not many technologies about them, which include coagulation, photocatalytic oxidation, ion exchange, and granular activated carbon (Li et al. 2009).

In terms of biological treatments, there are several processes, such as rotating biological contactor, sequencing batch reactor, anaerobic sludge blanket, and constructed wetland and membrane bioreactor (MBR), that have been applied for Greywater treatment, often preceded by a physical pretreatment step, such as sedimentation, use of septic tanks or detection. In addition, most biological processes are followed by a filtration step (e.g. sand filtration) and/or a disinfection step to meet non-potable reuse standards (Li et al. 2009, Jefferson et al. 2004)

Table 1: Characteristics of the different categories of Greywater.

Characteristics	Bathroom	Laundry	Kitchen	Mixed
pH (-)	6,4-8,1	7,1-10	5,9-7,4	6,3-8,1
SST (mg.L ⁻¹)	7-505	68-465	134-1.300	25-183
Turbidity (NTU)	44-375	50-44	298,0	29-375
COD (mg.L ⁻¹)	100-633	231-2.950	26-2.050	100-700
DBO (mg.L ⁻¹)	50-300	48-472	536-1.460	47-466
TN (mg.L ⁻¹)	3,6-19,4	1,1-40,3	11,4-74	1,7-34,3
TP (mg.L ⁻¹)	0,11->48,8	ND- >171	2,9- >74	0,11-22,8
Total Coliforms (CFU.100 mL ⁻¹)	10-2,4x10 ⁷	200,5-7x10 ⁵	>2,4x10 ⁸	56-8,03x10 ⁷
Faecal Coliforms (CFU.100 mL ⁻¹)	0-3,4x10 ⁵	50-1,4x10 ³	-	0,1-1,5x10 ⁸

After Li et al. (2009)

GREYWATER TREATMENT THROUGH ULTRAFILTRATION AND MICROFILTRATION

Filtration is one of the key processes in water treatment, and with the advance of technology, this mechanism has improved over the years. Microfiltration (MF) is defined as a surface of variable shape, with pore sizes ranging from 10 nanometers to 1,000 Armstrong. Ultrafiltration (UF) is also defined as a porous surface, with the difference that pore sizes can vary from 1000 to 50 Armstrong (Koyuncu et al. 2015).

Worldwide, global investment in MF was \$1.6 billion in 2013 and projected to be \$2.6 billion by 2018. Global investment in UF was \$882 million in 2013 and was projected at \$1.2 billion in 2015 (Koyuncu et al. 2015).

These surfaces are made of membranes, whose characteristics vary according to the material they are made of, as well as the physical characteristics they have depending on the purpose they are intended to achieve. The most commonly used membranes are polymeric, due to their low cost, are easy to shape, and have some chemical and thermal resistance. The most used polymers are cellulose acetate, PVDF, PA, PP, and PES (Koyuncu et al. 2015).

However, ceramic membranes are better than polymers because they have better pore distribution, higher porosity, better separation characteristics, greater chemical, and mechanical stability, and are optimal for Greywater treatment because unlike polymers they resist bacterial activity better, which gives them a longer life. Some characteristics of UF and MF membranes are presented in Table 2.

It is important to adjust a hypothetical model that collects representative average data from different samples in other

studies to evaluate the performance of these membranes in the treatment of Greywater, with their varying properties due to the difference that happens from their origin (Eriksson et al. 2002). A model of water was hypothetically created by Friedler (2004). From this model, different efficiencies can be evaluated, and it is possible to see the potential of the cleaning process for these waters. Table 3 shows the physical characteristics of this hypothetical fluid.

PHYSICAL TREATMENT OF GREYWATER

Physical processes alone are not sufficient to ensure adequate reduction of organic and inorganic contaminants. However, the process to be used depends on the purpose for which it is intended (Li et al. 2009)

For example, Kyu-Hong et al. (1998) demonstrated that the application of a tubular membrane of both UF and MF meets the quality standards for secondary uses such as bathing water in hotels according to the Israeli legislation (Israel Ministry of the Environment, 2001).

Regarding the physical cleaning of grey water, Bhattacharya et al. (2013) discussed the potential of ultrafiltration and microfiltration ceramic membranes in tubular membranes. The experiment carried out in this study is the treatment of Greywater driven by a difference in pressure of nitrogen gas in the liquid. The fluid is driven into treatment in three different spatial arrangements, one where the water is treated by microfiltration, another by ultrafiltration, and in the third configuration, the Greywater passes through a microfiltration filter and then by an ultrafiltration filter. In addition, they compared the effects of treated versus untreated Greywater in the *Chrysalidocarpus Lutescens* plant, because it represents

Table 2: Characteristics of MF and UF membranes.

	Micro filtration (MF)	Ultra filtration (UF)
Mode of operation	Crossflow and dead point of operation	Crossflow and dead point of operation
Accuracy of operation	0,1-3 bar (transmembrane)	0,5-10 bar (transmembrane)
Mechanism of separation	Separation based on the size of the particle	Separation based on the size of the particle
Molecular size of the separation	Solids: >0,1µm Separation of particles	Colloids: 20.000 - 200.000 Da Solids: >0,5 µm Macromolecule separation
Type of membrane	Predominantly symmetrical polymer ceramic membranes	Composed of asymmetric polymer or ceramic membrane
Type of module	Spiral winding, hollow fiber, tube modules, plate or cushion modules	Spiral winding, hollow fiber, tube modules, plate or cushion modules
Negligible osmotic pressure	Negligible osmotic pressure	Negligible osmotic pressure
Thickness of the separation layer	symmetrical = 10-150 µm asymmetrical = 1 µm	0,1-1,0 µm

After Koyuncu et al. (2015)

Table 3: Synthetic greywater (SGW, nine samples).

Parameters	Units	<i>m</i>	σ	min	max
pH		6.76	0.30	6.29	7.29
Conductivity	$\mu\text{S}/\text{cm}$	188	18	159	212
Turbidity	NTU	24	16	4	42
Suspended Solids	$\text{mg}\cdot\text{L}^{-1}$	72	14	41	87
COD	$\text{mg O}_2\cdot\text{L}^{-1}$	454	33	391	505
DBO ₅	$\text{mg O}_2\cdot\text{L}^{-1}$	65	6	58	75
DOC	$\text{mg}\cdot\text{L}^{-1}$	132	14	106	149
A-surfactants	$\text{mg}\cdot\text{MBAS}\cdot\text{L}^{-1}$	49.1	11.5	33.5	69.8
Total coliforms	$\text{CFU}\cdot 100\text{ mL}^{-1}$	3.8×10^3	2.5×10^5	9.6×10^4	8.4×10^5
Fecal coliforms	$\text{CFU}\cdot 100\text{ mL}^{-1}$	9.6×10^3	1.4×10^4	1.6×10^2	4.1×10^4
<i>Enterococcus</i>	$\text{CFU}\cdot 100\text{ mL}^{-1}$	2.7×10^3	2.6×10^3	5.3×10^1	8.2×10^3

m: average; σ : standard deviation; min: minimum; max: maximum; After Friedler (2004)

well the soil quality during its development (Bhattacharya et al. 2013).

As a result of this experiment, MF retained turbid materials and suspended solids (almost 99% removal), with 75% COD removal. However, there were several harmful particles that passed the filter. UF had good retention of turbidity and suspended solids (over 99%), oils, and microorganisms, in addition to a COD reduction of 86%. As for the mixed process, where MF and then UF were used, a large amount of contaminants were eliminated, in addition to having a 92% decrease in COD (Bhattacharya et al. 2013).

In the experiment of the *Chrysalidocarpus Lutescens* plant, the quality of the treated water and its interaction with the soil was tested by irrigating this plant with untreated water and water treated with the three techniques outlined. Normal growth was observed in all cases. Bhattacharya concluded that the water treated by physical filters could have a second use that does not involve human consumption (Bhattacharya et al. 2013)

On the other hand, according to Blumental (2000), the physical treatment of Greywater without the addition of any biological additives does not have enough study evidence to conclude its safety with the environment. However, the treated waters meet the physical-chemical criteria of standards for agricultural use in the United Kingdom, because filter-treated Greywater is considered to meet standards for a second use

Majouli et al. (2012) described the preparation of a tubular membrane made of Moroccan ceramics, driven by a pressure difference between the fluid in the system. The contaminants are retained in the tube while the treated water exits through the pores.

The results obtained by measuring the effectiveness of the process in the study, which does not focus on Greywater but explicitly states that the results can be extrapolated for this type of pollutant, are promising; they observed the removal of 97 percent of turbidity, making the water usable for secondary purposes such as agriculture. The most outstanding aspect of this study was the use of Moroccan ceramics, which is easily available in Morocco, and after applying a physical treatment, the shape and porosity of the filter are applied, being ready for use at a laboratory level (Majouli et al. 2012).

Chihi et al. (2019) introduced another microfiltration membrane, replacing the cylindrical shape (which is the most common) with a flat ceramic filter, which has not been evaluated for the use of Greywater but has been tested for the use of industrial water. The operation of this flat plate filtration is from stimulating the flow of water through pressure differences, retaining pollutant particles on the filter.

The main advantage of this flat plate membrane is that its main raw material is Tunisian clays, which are cheap and abundant, and it has to be put in treatment to give the shape, quantity, and quality of pores desired. The plates have good physical, chemical, and biological stability, good pore distribution, and may be more economical to operate (Chihi et al. 2019).

Saja et al. (2017) described the preparation of a flat plate membrane made of Moroccan ceramics, for the treatment of industrial waters on a laboratory scale, also scalable to Greywater.

The membrane model is a microfiltration plate with an average pore size of 1.7 μm and 52% physical space porosity on its surface. It is installed in a system that pumps water

to this filter. The treatment removes 97 percent of turbidity, allowing the water to be used for secondary purposes such as agriculture while also meeting water quality criteria. It also has the potential to improve the quality, quantity, and affordability of Moroccan ceramics (Saja et al. 2017).

PHYSICAL-BIOLOGICAL TREATMENTS OF GREYWATER

Greywater treatment through UF/MF can be optimized by adding biological material which turns the technology into a physical-biological treatment. Over the surface of the filters, which contain the particles that pollute the liquid, bacterial activity is introduced, which destroys the contaminants in the water, boosting the effectiveness of the membranes and, as a result, the cleanliness of the treated liquid. (Ramona et al. 2004).

The process over the membrane is a bio-action carried out on the membranes with porosities of sizes corresponding to microfiltration and ultrafiltration. This is achieved by adding biological material on the surface to remove complex chemical contaminants and then filtering them from the membrane. This type of mechanism is called “membrane bioreactors” (MBR) and has been widely tested, with acceptable results for secondary use water without further treatment (Jefferson et al. 2000, Jefferson et al. 2004, Ramona et al. 2004). According to the regulations for reusing Greywater, it must comply with hygienic aesthetic aspects, environmental tolerance, and economic stability (Kyu-Hong et al. 1998, Nolde 2005, Jong et al. 2010).

The so-called “membrane bioreactors” deliver a cleaner water quality than the physical membranes, however, they are more expensive, and the effluent that these processes deliver is always non-potable secondary use water, although they do not need to be further treated and can be discharged to the environment (Li et al. 2009, Jefferson et al. 2004).

However, Jong et al. (2010) found with a study of Greywater after a traditional MF membrane bio-reactor treatment, that although the physicochemical parameters satisfy those required by Jung’s Korean standard (Jung’s Korean Standard 2004), it is definitely not safe to use this water for secondary use without subsequent treatment. There is still a significant presence of bacterial load harmful to health, and the ecosystem after this process.

Samples of *Escherichia coli* *Staphylococcus aureus*, and *Salmonella tyohimmurion* were measured in the Greywater effluent once it was treated under the conditions of those studies. The measurement showed that it was lower than that of the entrance, but with sufficient presence to be able to generate environmental or health problems, which prevents a safe secondary use.

Continuing with the main topic, Drews (2010) exposed the advantages and disadvantages of this type of reactor with ultrafiltration pore size. The positive characteristics are the benefits in the form of reduction of the CO₂ footprint, the reduction of excess sludge, and the high liquid flow, while as disadvantages are the decrease in production and performance over time, frequent cleaning, damage, and maintenance, difficult aeration and loss of permeability, among others. Another major impediment to bio-reactors is the costs associated with implementation and operation, which are proven by the existence of cost estimates for the submerged membrane bio-reactor (traditional bio-reactor, more studied in the literature), for the treatment of Greywater (Humeau et al. 2011).

This is demonstrated by a market study, such as the one conducted by Hourlier et al. (2010), where it presents market data for an ultrafiltration submerged membrane reactor, for a community of 50 inhabitants and a community of 500 people, of 60-second operation, with 5 seconds of pause, 20 seconds of counter-current water and 5 seconds of rest, in

Table 4: Fixed costs related to equipment (MBR).

Parameter	50 inhabitants (3m ³ .day ⁻¹)	500 inhabitants (30m ³ .day ⁻¹)
Total investment cost	38.100 €	183.800 €
Cost of the process	36.000 €	180.000 €
Membrane área	59 m ²	589 m ²
Area per module	60 m ²	100 m ²
Module unit	1	6
Raw Greywater storage tank	750 €	1.200 €
Permeate storage tank	750 €	1.200 €
Heat Exchanger/ Air Compressor	600 €	1.400 €

After Hourlier et al. (2010)

a cyclical process, with a membrane pressure of 0.5 bar to treat Greywater.

All of the above is carried out according to the model of Hourlier et al. (2010). This study takes into account direct costs (fixed costs, equipment, depreciation, and maintenance), variable costs (electricity consumption, chemicals), indirect costs (administrative charges, contingency costs, insurance), and possible benefits. The results are presented in the following Tables 4 to 6.

Hence, given the data observed in the tables, it is concluded that the average operating costs are 7.4 euros.m⁻³, with a plant capacity of 3 m³.day⁻¹ for 50 people, and 30 m³.day⁻¹ for 500 people, with average direct costs of 4.4 euros.m⁻³. Therefore, although the submerged membrane bioreactor is the most studied and widely used bio-reactor, it has the disadvantage of being very expensive and difficult to operate, which makes it only profitable in small communities like a building (Li et al. 2009, Jefferson et al. 2004, Ramona et al. 2004).

In addition to the previously mentioned limitations, including their cost, bio-reactors present another main dis-

advantage, corresponding to their fouling. To solve this, various techniques are usually used, among which are physical techniques such as: backwashing, optimization of process parameters, different membrane configurations, application of ultrasonic technology (Jie et al. 2012, Hwang et al. 2009, Schoeberl et al. 2005, Xu et al. 2011).

And additionally, they also use chemical techniques such as: adding chemical coagulants (ferric sulfate, alumina, aluminum salts, among others) or add adsorbent materials like carbon or zeolites (Lee et al. 2001, Hu & Stuckey 2007, Tian et al. 2010, Wu & Huang 2008)

As a result of all these limitations of traditional membrane bioreactors, several alternatives have emerged with some improvement or update in their process. Some examples are:

- a) Bani-Melhem et al. (2014) discussed a type of traditional membrane reactor, submerged, varying from the common bioreactor in its configuration uses of tubular hollow fiber with porosities of submerged ultrafiltration, which treats water for 42 days and at 13 kpa. The water is driven by a vacuum pump that forces it to pass filtered through ultrafiltration bio-membranes. This

Table 5: Variable costs related to equipment (MBR).

	50 inhabitants (3m ³ .day ⁻¹)	500 inhabitants (30m ³ .day ⁻¹)
Cost of working	2.650 €.year ⁻¹	8.875 €.year ⁻¹
Total time of working	106 h.year ⁻¹	355 h.year ⁻¹
Inspection, maintenance and revision	20 h.year ⁻¹	48 h.year ⁻¹
Consumable Supplies	72 h.year ⁻¹	288 h.year ⁻¹
Frequency	1,5/month	6/month
Duration of intervention	4 h	4 h
Sowing of the Bio-reactor	8 h.year ⁻¹	8 h.year ⁻¹
Frequency	1/year	1/year
Duration of intervention	8 h	8 h
Membrane replacement	6 h.year ⁻¹	11 h.year ⁻¹
Duration of the replaced module	4 h.year ⁻¹ r	8 h.year ⁻¹
Duration of intervention	2 h.year ⁻¹	3 h.year ⁻¹

After Hourlier et al. (2010)

Table 6: Indirect costs related to equipment (MBR)

	50 inhabitants (3m ³ .day ⁻¹)	500 inhabitants (30m ³ .day ⁻¹)
Membrane replacement cost	1.500 €	13.500 €
Membrane unit cost	3.000 €	4.500 €
Number of units of the module	1	6
Membrane lifetime	2 years	2 years

After Hourlier et al. (2010)

MBR technology is a good option to treat Greywater with good removal of organic substances, surfactants, and microbes without further steps. After 40 days, at 13 kpa and 25°C, a DQO removal of 89%, 95.2% color, complete removal of suspended particles, ammonia removal of 89.4%, phosphorus removal of 56%, and COD removal of 89.3% were noticed

- b) Ding et al. (2017) discussed gravity membrane reactors with microfiltration flat plate membrane size as an alternative to MBRs. They are thought to be equally as capable as other forms of bioreactors, and they are less expensive because they do not require energy to propel the effluent. In the experiment, the study compares two gravitational membrane reactors, one which is aerated and the other is not aerated.

The conclusion reached in this study is that MBR has higher efficiency than the reactors proposed in this research. The experiments carried out in the reactors, provide good effluent effectiveness for both reactors, being aerated with better results. However, these do not reach the quality of MBRs, although it is more profitable to build them, and they need more physical space (4-5 times the non-aerated, meanwhile 2 times the other one) to treat the same amount of water with the same quality as bio-classic membrane reactors.

- c) Jaborni & Podmirseg (2014) discussed a semi-tubular fixed with porous in the surface of the membrane bio-reactor with submerged ultrafiltration porosity size, except for having a sand pre-filter and using a smaller volume in each unit. As a result of the use of the pre-filter, the membranes do not get dirty, the flows are stabilized beforehand, the membranes do not use catalysts, the flow is clean of physical impurities, and fixed membranes are used because in that configuration the recycling of the microorganisms on the membrane increases.

They concluded that the effectiveness of this type of reactor complies with the international standards of the International Standard/American National Standard (2011) on treatment systems for residential and commercial in-situ water reuse. However, the amount of flow is lower and the energy expenditure is higher compared to the conventional submerged membrane bio-reactor.

- d) Huelgas & Funamizu (2010) described a submerged ultrafiltration flat plate bio-reactor with a constant TMP since the water flow is from a difference in level between the inlet and the reactor. Finally, the effluent is clean, with a COD reduction of 96% and suspended particles eliminated greater than 99% after 86 days, indicating that the efficiency and output flow are lower than a typical membrane bio-reactor.

- e) Bani-Melhem & Smith (2012) exposed two reactors that treat Greywater in the same conditions at the same time; a traditional membrane bioreactor, and a submerged UF membrane bio-reactor, with the exception of an electrocoagulation pre-treatment for the elimination of microorganisms. As a result, the permeate flow is faster than one without pre-treatment, the turbidity decreased by 97%, compared to 95% for a traditional one, and in both the color disappeared almost 100%, (the color by 94% in the modified one and by 91% in the traditional one). Suspended solids were also almost completely eliminated in both processes, and coliforms dropped by approximately 40% in both cases. The COD dropped by 89% in the modified process and by 86% in the unmodified one.

In conclusion, the improvements to the reactor provide a better quality effluent, but not in a significantly considerable quantity, therefore it does not have an economic projection because its implementation entails higher economic costs without being profitable.

- f) Finally, Jabornig & Favero (2013) discussed the treatment of Greywater with non-fixed bed bio-layer, with a tubular membrane of ultrafiltration porosity, called "BF-MBR; biofilm membrane bioreactor. The study exposed in this study is divided into two compartments; the first one with non-fixed bio-layers and the other one with membrane modules that act as filtration, and the sludge is recirculated, producing a higher flow than the conventional one, and more economical to maintain.

The effluents from this equipment meet the NSF/ansi350 (NFS 2017) criteria, with a DOC reduction of 64%, a BOD turbidity of 83%, and almost 100% suspended solids.

CONCLUSIONS

Research and implementation of Greywater reuse through treatments that include microfiltration and ultrafiltration are still in an early stage, with a lack of significant studies seeking improvements to the traditional model. There is also no shortage of industrial-scale implementations and scaling up to treat effluents collected from a community.

According to what has been studied, analyzed, and sought in this research, there is not a large amount of literature that addresses the deficiencies of this technology for the treatment of Greywater, the possible improvements, the associated costs, among others. The amount of information available concerning assembly in the implementation of this technology at a city or industrial level is limited, as investments in this sector of the industry are sparse. Despite the above, there are compelling historical studies that guarantee that water

treatment by submerged membrane bio-reactors, (which are the most commonly used types of filters in this topic), is successful for secondary use water discharge without any post-treatment.

There is also a lack of studies on the treatment of Greywater by physical treatments, the vast majority of the literature focuses on the treatment of industrial water. In spite of that, it can be determined that water treated in this way can be reused in a closed circuit from a separate collection for uses that do not demand such high water quality, such as the use of this water for toilets, recirculating water within a community before being discharged to the sanitation network

It should also be noted that the pattern for defining Greywater and its characteristics is variable, depending on local regulations defined in some countries, while in the rest of the world, discharge water is considered discharge water without any special name, and there is no global regulation for its treatment, so its regularization is dependent on the geographical. It is to be hoped that in the future those places that do not have special legislation for this type of fluid discharge, will carry out an environmental agenda that can take advantage of the benefits of treating Greywater differentiated from the rest of the fluids that are loaded into the network sanitation.

It is expected that, in the future, the amount of research into Greywater treatment by MF/UF will increase, and that, as a result, scientific progress will improve the technical and economic flaws in this industry, motivating various governments and institutions to implement this technology in situ to alleviate global water demand.

REFERENCES

- Bani-Melhem, K. and Smith, E. 2012. Greywater treatment by a continuous process of an electrocoagulation unit and a submerged membrane bioreactor system. *Chem. Eng. J.*, 198-199: 201-210.
- Bani-Melhem, K., Al-Qodah, Z., Al-Shannag, M., Qasameh, A., Rasool M. and Alkasrawi, M. 2014. On the performance of real greywater treatment using a submerged membrane bioreactor system. *J. Membr. Sci.*, 476: 40-49
- Bhattacharya, P., Sarkar, S., Ghosh, S., Majumdar, S., Mukhopadhyay, A. and Bandyopadhyay, S. 2013. Potential of ceramic microfiltration and ultrafiltration membranes for treatment of greywater for effective reuse. *Desal. Water Treat.*, 5(22-24): 4323-4332
- Blumental, U., Peasey, A., Palacios, G. and Mara, D. 2000. Guidelines for wastewater reuse in agriculture and aquaculture: Recommended revisions based on new research evidence. *Well Study*
- Chihi, R., Bliidi, I., Trabelsi-ayadi, M. and Ayari, F. 2019. Elaboration and characterization of a low-cost porous ceramic support from natural Tunisian bentonite clay. *Comptes Rendus Chimie.*, 22(2-3): 188-197.
- De Gisi, S., Casella, P., Notarnicola, M. and Farina, R. 2015. Greywater in buildings: A mini-review of guidelines, technologies and case studies. *Civil Eng. Environ. Sys.*, 33 (1): 35-54.
- Ding, A., Liang, H., Li, G., Szivak, I., Traber, J. and Pronk, W. 2017. A low energy gravity-driven membrane bioreactor system for greywater treatment: Permeability and removal performance of organics. *J. Membr. Sci.*, 542: 408-417.
- Drews, A. 2010. Membrane fouling in membrane bioreactors: Characterisation, contradictions, cause, and cures. *J. Membr. Sci.*, 363 (1-2): 1-28. <https://doi.org/10.1016/j.memsci.2010.06.046>
- Eriksson, E., Auffarth, K., Henze, M. and Ledin, A. 2002. Characteristics of grey wastewater. *Urban Water*, 4(1): 85-104. [https://doi.org/10.1016/S1462-0758\(01\)00064-4](https://doi.org/10.1016/S1462-0758(01)00064-4)
- Friedler, E. 2004. Quality of individual domestic Greywater streams and their implication for on-site treatment and reuse possibilities. *Environ. Technol.*, 25 (9): 997-1008. <https://doi.org/10.1080/09593330.2004.9619393>
- Hourlier, F., Masse, A. and Jaouen, P. 2010. Formulation of synthetic Greywater as an evaluation tool for wastewater recycling technologies. *Environ. Technol.*, 31(2): 215-223.
- Hu, A. and Stuckey, D. 2007. Activated carbon addition to a submerged anaerobic membrane bioreactor: effect on performance, transmembrane pressure, and flux. *J. Environ. Eng.*, 133(1): 73-80.
- Huelgas, A. and Funamizu, N. 2010. Flat-plate submerged membrane bioreactor for the treatment of higher-load Greywater. *Desalination*, 250(1): 162-166.
- Humeau, P., Hourlier, F., Bulteau, G., Massé, A., Jaouen, P., Gerente, C., Faur, C. and Le Cloirec, P. 2011. Estimated costs of implementation of membrane processes for on-site Greywater recycling. *Water Sci. Technol.*, 63(12): 2949-56.
- Hwang, K., Chan, C. and Tung, T. 2009. Effect of backwash on the performance of submerged membrane filtration. *J. Membr. Sci.*, 330(1-2): 349-356.
- International Standard/American National Standard (ANSI). 2011. Onsite residential and commercial water reuse treatment systems. NSF, Ann Arbor, USA.
- Israel Ministry of the Environment 2001. Joint Committee for Effluent Reuse, Appendix, Quality Criteria Recommendations for Unrestricted Irrigation and Discharge into Streams.
- Jabornig, S. and Favero, E. 2013. Single household Greywater treatment with a moving bed biofilm membrane reactor (MBBMR). *J. Membr. Sci.*, 446: 277-285.
- Jabornig, S. and Podmirseg, S. 2014. A novel fixed fiber biofilm membrane process for on-site Greywater reclamation requiring no fouling control. *Biotechnol. Bioeng.*, 112(3): 484-493.
- Jefferson, B., Laine, A., Judd S. and Stephenson, T. 2000. Membrane bioreactors and their role in wastewater reuse. *Water Sci. Technol.*, 41(1):197-204.
- Jefferson, B., Palmer, A., Jeffrey, P., Stuetz, R. and Judd, S. 2004. Greywater characterization and its impact on the selection and operation of technologies for urban reuse. *Water Sci. Technol.*, 50 (2): 157-164.
- Jie, L., Liu, L., Yang, F., Liu, F. and Liu, Z. 2012. The configuration and application of helical membrane modules in MBR. *J. Membr. Sci.*, 392-393: 112-121.
- Jong, J., Lee, J., Kim, J., Hyun, K., Hwang, T., Park, J. and Choung, Y. 2010. The study of pathogenic microbial communities in Greywater using membrane bioreactor. *Desalination*, 250(2): 568-572.
- Koyuncu, R., Sengur, T., Turken, S., Guclu, M. and Pasaoglu, E. 2015. Advances in Water Treatment by Microfiltration, Ultrafiltration, and Nanofiltration. Woodhead Publishing, Sawston, UK, pp. 83-128,
- Kyu-Hong, A., Ji-Hyeon S. and Ho-Young C. 1998. Application of tubular ceramic membranes for reuse of wastewater from buildings. *Water Sci. Technol.*, 38(4-5); 373-382.
- Lee, J., Kim, J. Kang, I., Cho, M., Park, P. and Lee, C. 2001. Potential and limitations of alum or zeolite addition to improving the performance of a submerged membrane bioreactor. *Water Sci. Technol.*, 43(11): 59-66.
- Li, F., Wichmann, K. and Otterpohl, R. 2009. Review of the technological approaches for greywater treatment and reuses. *Sci. Total. Environ.*, 407(11): 3439-49.

- Majouli, A., Tahiri, S., Younssi, S., Loukili, H. and Albizane, A. 2012. Elaboration of new tubular ceramic membrane from local Moroccan perlite for microfiltration process: Application to treatment of industrial wastewaters. *Ceramics Int.*, 38(5): 4295-4303
- March, J., Gual, M. and Orozco, F. 2004. Experiences on Greywater re-use for toilet flushing in a hotel (Mallorca Island, Spain). *Desalination*, 164(3): 241-247.
- NSF. 2017. NSF/ANSI 350 Onsite residential and commercial water reuse treatment.
- Nolde, E. 2005. Greywater recycling systems in Germany results, experiences, and guidelines. *Water Sci. Technol.*, 51(10): 203-10
- Ramona, G., Green, M., Semiat, R., and Dosoretz, C. 2004. Low strength Greywater characterization and treatment by direct membrane filtration. *Desalination*, 170(3): 241-250.
- Saja, S., Bouazizi, A., Achiou, B., Ouammou, M., Albizane, A., Bennazha, J. and Alami Younssi, S. 2017. Elaboration and characterization of a low-cost ceramic membrane made from natural Moroccan perlite for treatment of industrial wastewater. *J. Environ. Chem. Eng.*, 6(1): 451-458
- Schoeberl, P., Brik, M., Bertoni, M., Braun, R. and Fuchs, W. 2005. Optimization of operational parameters for a submerged membrane bioreactor treating dyehouse wastewater. *Sep. Purif. Technol.*, 44(1): 61-68.
- Tian, J., Chen, Z., Nan, J., Liang, H. and Li, G. 2010. Integrative membrane coagulation adsorption bioreactor (MCABR) for enhanced organic matter removal in drinking water treatment. *J. Membr. Sci.*, 352(1-2): 205-212. <https://doi.org/10.1016/j.memsci.2010.02.018>
- Wu, J. and Huang, X. 2008. Effect of dosing polymeric ferric sulfate on fouling characteristics, mixed liquor properties, and performance in a long-term running membrane bioreactor. *Sep. Purif. Technol.*, 63(1): 45-52.
- Xu, M., Wen, X., Yu, Z., Li, Y. and Huang, X. 2011. A hybrid anaerobic membrane bioreactor coupled with online ultrasonic equipment for digestion of waste-activated sludge. *Bioresour. Technol.*, 102(10): 5617-5625.
- Yokomizu, T. 1994. Ultrafiltration membrane technology for regeneration of building wastewater for reuse. *Desalination*, 98(1-3): 319-326.



Toxic Effect of Antibiotics on Freshwater Algal Systems and the Mechanisms of Toxicity: A Review

Barsha Roy and P. K. Suresh†

School of Biosciences and Technology, VIT, Vellore-632 014, India

†Corresponding author: P. K. Suresh; p.k.suresh@vit.ac.in

Nat. Env. & Poll. Tech.
Website: www.neptjournal.com

Received: 20-01-2021
Revised: 18-02-2021
Accepted: 24-02-2021

Key Words:

Antibiotics
Non-target organisms
Green algae
Toxicity
Mode-of-action

ABSTRACT

Antibiotics are used to treat bacterial infections in humans and animals and also act as a growth promoter for poultry. Due to incomplete metabolism, these antibiotics are excreted in the environment in their parental forms and accumulates in the aquatic ecosystem. Besides the evolution of antibiotic-resistant bacteria, these drugs can damage non-target organisms. Green algae are highly sensitive to different antibiotics. Damage in the algal population will cause imbalances in the ecosystems. Till now, the mechanisms of antibiotic toxicity towards algae have not been completely elucidated. It was observed that antibiotics mainly affected the photosynthetic machinery and decreased the carbon fixation process, finally resulting in algal growth inhibition. This present review deals with antibiotics classification, various routes of antibiotics exposure to the freshwater environment, sensitivity towards the different classes of antibiotics, possible Mode-of-Action (MOA) on algal systems, and gaps that need to be filled. Significant gaps include the unavailability of proper eco-toxicological data for antibiotics. Moreover, they exist in nature as complex mixtures, and their behavior in the ecosystem may vastly differ from the parent molecules. To improve our understanding of antibiotic responses mechanism in real-life scenarios, mixture toxicity studies may be the first step.

INTRODUCTION

After the discovery of penicillin in 1929, antibiotics are widely used to treat different bacterial infections in humans and animals. They are also used for aquaculture and live-stock development (Liang et al. 2013). From the years 2000 to 2010, the use of antibiotics has increased significantly throughout the world where India became a major contributor. Seasonal variations in terms of the usage of antibiotics were observed (Van Boeckel et al. 2014). By the year 2030 antibiotic consumption will increase by approximately 67% (Van Boeckel et al. 2015).

India has produced a considerable amount of antibiotics in the past. Ninety percent (90%) of the antibiotics, used in humans and other farm animals, are excreted in their unaltered forms through urine and feces. In India, the purchase rate of antibiotics, without an authorized prescription, is high. Hence, the residues are also proportionally higher than those areas where usage is based on doctor's prescription (Mutyar & Mittal 2014). From 2000 to 2010, it has been reported that the use of antibiotics has increased by 36% with 75% of the increases attributable to be due to indiscriminate use and release of antibiotics by the citizens of Brazil, Russia, India, China, and South Africa (BRICS) (Laxminarayan et al. 2016). For this reason, countries like India facing an increasing threat of

infectious diseases spiraling out of control (Laxminarayan et al. 2013, 2016).

In 2017, antibiotics were mostly used in India to treat pneumonia or lower respiratory tract infection; followed by the treatment of skin and soft tissues; central nervous system infection; bronchitis, and infection of the cardiovascular system. Besides these, antibiotics have also been used to treat intra-abdominal sepsis, upper respiratory tract, bone/joint, and gynecological infections. For medical prophylaxis, mostly the antibiotics ceftriaxone, piperacillin-tazobactam, and meropenem are prescribed. In contrast, for surgical prophylaxis, antibiotics prescribed frequently are cefuroxime, amikacin, and ceftriaxone (Singh et al. 2019). Prolonged use of antibiotics after the operation could increase the formation of antibiotic resistance genes (Hagel & Scheuerlein 2014).

This widespread use of antibiotics contributed to the genesis of antibiotic-resistant bacteria, with significant detrimental impacts on human health (Smith et al. 2013). Due to the increased and indiscriminate usage of antibiotics, significant amounts of them are discharged into the aquatic environments from diverse sources, such as during the process of manufacturing, human or animal excreta, and emission from the Wastewater Treatment Plants (WWTPs) (Deng et al. 2016, Wu et al. 2016b, Yan et al. 2013). Some of the primary sources, including hospitals, poultry farms,

farmlands, and aquacultures (Fairbairn et al. 2016, Noguera-Oviedo & Aga 2016, Pal et al. 2014), and some of the uncontrolled sources like septic tanks, leaking sewage lines, landfills, and inaccurately disposed-off waste (González-Pleiter et al. 2019) are responsible for antibiotic disposal into the freshwater system. Antibiotics from these sources are major determinants for the acquisition of antibiotic resistance genes that may cause permanent damage to the genetic pool of the exposed ecosystem (Yang et al. 2014). The harmful impact on the micro-organisms can occur even at low concentrations (ng or $\mu\text{g L}^{-1}$) (Liu et al. 2017).

Antibiotics can be classified into 11 major classes based on their MOA towards the bacteria (González-Pleiter et al. 2019). Commonly found antibiotics in an aquatic ecosystem are tetracyclines (TCs), sulphonamides (SAs), macrolides (MLs), and quinolones (QNs). In an aqueous environment, antibiotics caused toxicity and the formation of antibiotic resistance genes in aquatic micro-organisms (Dong et al. 2016). The other primary concern is the toxicity of antibiotics on other aquatic organisms, which are not their direct targets. Previous studies have shown that antibiotics caused acute and chronic toxicity to the different aquatic species, including algae, crustaceans, and fishes (Huang et al. 2014, Seoane et al. 2014, Wang et al. 2016). In aquatic environments, climatic condition can alter their chemical structures. They can also be degraded by photochemical reactions, which play a major role in determining the fate of the antibiotics (Liu et al. 2017).

As organic manure, livestock waste-containing antibiotic residues have been used in farms which increased the quantity of antibiotics into the soil than pesticides. Some of these antibiotic residues can be present in their biologically active form and can cause significant harm to the environment (Xiang et al. 2016). Generally, freshwater algae showed higher sensitivity towards antibiotics than marine algae. At very low concentrations, both Ciprofloxacin (CIP) and Erythromycin (ERY) inhibited cellular growth in freshwater algae (González-Pleiter et al. 2019). Almost all the antibiotic classes (very low EC_{50} values) showed higher toxicity towards different algae. Some of the antibiotics can even induce intracellular Reactive Oxygen Species (ROS) inside blue-green algae (González-Pleiter et al. 2019), which are highly sensitive to antibiotics.

Unicellular green algae are the major producers of the ecosystem and form the base in the food chain. Any changes in the algal population can disrupt the ecological balance in the food chain (Mutiyar & Mittal 2014). Algae are highly sensitive to many toxicants, including antibiotics. Laboratory-based toxicity studies can be performed easily on algae, which makes them a biomonitoring tool to evaluate the toxic potential of contaminants (Mutiyar & Mittal 2014). Due to

the bioaccumulation of different pollutants, they can also act as a biomarker (Barhoumi & Dewez 2013).

Previous studies found the effects of antibiotics by mainly focussing on the mechanisms of evolution of antibiotic-resistant bacteria. But it was observed that antibiotics can also pose a significant threat to the non-target organisms in the ecosystem. Green algae were found to be affected dramatically by antibiotics. The present review focused on the different antibiotics and detailed the severe damages caused to the algal populations. This study also tried to find out possible mechanisms behind the toxicity of the algae caused by the antibiotics.

Antibiotics of Serious Eco-Toxicological Concern Available in Freshwater Ecosystems

Antibiotics exist as persistent pollutants both in terrestrial and aquatic ecosystems. Its bioaccumulation, in the environment, may plausibly explain its concentrations exceeding the therapeutic concentration (Brandt et al. 2015). It has become mandatory to identify the sources of the antibiotics from where they are released into the environment to control antibiotic usage and to regulate their release.

ROUTES OF EXPOSURE OF ANTIBIOTICS TO THE AQUATIC ENVIRONMENT

Initially, antibiotics were isolated from natural sources like fungus. Hence, antibiotics were present in the environment long before humans identified them to treat bacterial infections. During the twentieth century, mass production of antibiotics began, which resulted in antibiotic-mediated selection pressures in the entire bacterial population (Larsson 2014). The identification of chemical structures of antibiotics isolated from natural sources led to their mass production in the laboratory (Mazel & Davies 1999). Their increased production leads to their higher release in the environment. The concentrations of various antibiotics in several Asian countries were found to be in the range of mg.L^{-1} (Gothwal & Shashidhar 2015). One primary source is sewage through which antibiotics can enter the environment. Antibiotics can be released into the soil through animal manure, or they can be applied directly to the plants to fight against plant pathogens (Shade et al. 2013). Antibiotics can be present in the aquatic environment in both their parental and metabolites forms.

Incomplete metabolism by humans or animals resulted in the release of almost 50–80% of antibiotics in their parental form. The remaining are released into the environment as metabolites through the urine and feces of the treated organisms (Manzetti & Ghisi 2014). Because of incomplete elimination by sewage treatment plants these antibiotics

can be discharged into the different freshwater systems (Wu et al. 2016a). Improper disposal of expired or unused antibiotics resulted in their presence in WWTPs and landfills, which further can contaminate the freshwaters (et al. 2018). Drug wastage can be reduced by prescribing a lower dose. This will eventually prevent their excessive release into the environment. Based on the present release data, public health-associated individuals can issue guidelines about the “environmentally safe dose” that can be released into the environment (Daughton & Ruhoy 2013). Before awarding a marketing license to the antibiotics, a proper environmental risk assessment should have to perform (EMA 2006).

ANTIBIOTICS OF MAJOR THREAT TOWARDS THE ENVIRONMENT

It is important to identify the key marker antibiotics that can cause adverse effects in the environment. The identification of certain antibiotics may be due to their higher usage in humans than others, e.g., penicillin, SAs, macrolide, and quinolone. The current challenges are to estimate their nature and duration of persistence, apart from their release characteristics into the environment (Välitalo et al. 2017). Table 1 represents the different antibiotic classes with their MOA towards bacteria and the resistance mechanism in bacteria. It was observed that antibiotics CIP, norfloxacin (NOR), enrofloxacin (ENR), trimethoprim (TMP), sulfamethoxazole

(SMX), oxytetracycline (OTC), chlorotetracycline (CTC), azithromycin (AZM), and ERY were found in very high quantities in the freshwater samples taken from the environment ($> 1 \mu\text{g. L}^{-1}$) (Ngumba et al. 2016, Wei et al. 2011, 2012). The persistence property and half-life of antibiotics vary significantly with temperature, pH, and geographical locations (Andreozzi et al. 2004, Braschi et al. 2013, Mitchell et al. 2014).

RATIONALE FOR MODELLING THE ECOSYSTEM RELATED TO ANTIBIOTIC DISCHARGE

For the modeling, the crucial determinants among all the variables are biosorption potential, dilution effects, the biodegradability of the antibiotics, and photolysis. Besides these, seasonal variation also plays a role in the modeling. Chronic exposure to varying amounts of antibiotics plays a significant role in these effects. Hence, the characterization of samples from water bodies as well as the algal species present, which may be sentinels of environmental damage is necessary. In a paper, it had been demonstrated that ofloxacin, sulfamethoxazole, and sulfadiazine were the important antibiotics to be considered for risk assessment and that algae were a good model for testing toxicity (Zhang et al. 2020). In this context, complementary modeling approaches involving the Concentration Addition (CA)

Table 1: Classes of antibiotics, their examples, MOA and resistance mechanism in bacteria.

Antibiotic Class	Example	MOA	Mechanism of Resistance
β -Lactam	Penicillin G, ampicillin, amoxicillin	Inhibits synthesis of cell wall and assembly of murein	Cell wall protein modification
Aminoglycosides	Streptomycin, gentamicin	Protein synthesis inhibition (30S inhibitor)	Modification of the ribosomal binding site and/ or producing aminoglycoside modifying enzymes
Macrolides	Erythromycin, roxithromycin, clarithromycin, tylosin, spiramycin	Protein synthesis inhibition (50S inhibitor)	Methylation of the rRNA in gram-positive bacteria
Quinolones	Oxolinic acid, nalidixic acid, flumequine	Inhibits DNA replication (DNA gyrase)	Alteration of DNA gyrase and mutation of the porins of the outer membrane
Fluoroquinolones	Ciprofloxacin, enrofloxacin, norfloxacin, ofloxacin	Inhibits DNA replication (DNA gyrase)	Same as quinolones
Tetracyclines	Tetracycline, oxytetracycline, minocycline, chlorotetracycline	Protein synthesis inhibition (30S inhibitor)	Alteration in the binding site and inducing efflux in <i>E. coli</i>
Sulfonamides	Sulfadiazine, sulfadimethoxine, sulfamethoxazole	Inhibits folic acid synthesis	Resistance mediated by plasmid and integron, and mutation in chromosomes
Lincosamides	Clindamycin, lincomycin	Protein synthesis inhibition (50S inhibitor)	23S subunit of rRNA gets methylate
Rifamycins	Rifamycin	RNA synthesis inhibition (RNA polymerase)	Mutation in the β -chain of the RNA polymerase enzyme
Chloramphenicol	Chloramphenicol	Protein synthesis inhibition (50S inhibitor)	Antibiotic inactivation by the enzyme chloramphenicol acetyltransferase
Diaminopyrimidine	Trimethoprim, iclaprim	Inhibits folic acid synthesis	Replacement of antibiotic target by dihydrofolate reductase

and Independent Action (IA) models may help in the better extrapolation of laboratory-based data. Hormesis, as well as the adsorption process of cefradine and its rate, were studied in *Chlamydomonas reinhardtii*. Optimization of the reaction conditions (temperature, pH, and algal cell density) was done using the Box-Benken design. The dissolved organic matter, specifically the excited triplet state, contributed by the natural biofilms (BDOM), played a significant role in the photodegradation of oxytetracycline. Since the results were at variance with that seen in the case of fulvic acid (inhibition of photodegradation), characterization of these variables in their natural habitat would improve our ability to predict the relative contributions made by individual antibiotics to overall toxicity towards the algal system (Hua et al. 2018). The triplet state, reactive extracellular organic matter (EOMs) in *Chlorella vulgaris* was found to account for the majority of the degradation of chlorotetracycline, by the mechanism of the electron transfer process (Tian et al. 2019).

DIFFERENT ANTIBIOTICS TOXICITY ON GREEN ALGAE

The original rationale behind the development of antibiotics was to eliminate the pathogenic forms without harming the host organism selectively. But as these environmental pollutants (both the parent and/or the altered forms) can persist longer in their active form even in very low concentrations

(ng.L^{-1} – $\mu\text{g.L}^{-1}$), they may pose a significant risk of bioaccumulation in the food chain (Huang et al. 2014). Therefore, toxicity testing of these antibiotics became important. For this, different methods are available for performing acute and chronic toxicity experiments in the various test organisms (Brausch et al. 2012). The most commonly used micro-organisms are cyanobacteria (Ebert et al. 2011), proteobacteria (Backhaus et al. 2000), and multiple species of green algae and microalgae (González-Pleiter et al. 2013, Magdaleno et al. 2015). Algae are one of the best organisms to test the ecotoxicity of any chemical as they are cost-effective, very much sensitive towards pollutants, easy to maintain in the laboratory, and the results obtained are reliable.

Among the algal species, *Pseudokirchneriella subcapitata* is used more commonly for toxicity testing (Baumann et al. 2015, Kolar et al. 2014). Except this, other different species have been also used for antibiotic toxicity testing (De Vasconcelos et al. 2017, Ebert et al. 2011, Seoane et al. 2014, Wang et al. 2019). Previously, the median effective concentration (EC_{50}) or median lethal concentration (LC_{50}) was used to determine the toxicity of an antibiotic on unicellular green algal species and were ranked accordingly (Sebaugh 2011). From Table 2, we can see that macrolides and OTC were most toxic with an EC_{50} value below 1 mg.L^{-1} . The sensitivity of *C. vulgaris* was found to be less when compared with other algal species tested. Previous

Table 2: EC_{50} values of different antibiotics on different green algal species.

Antibiotic Class	Antibiotic Name	Algal species	EC_{50} value (mg/L)	References	
β -Lactum	Amoxicillin	<i>P. subcapitata</i>	>2000	(Magdaleno et al. 2015)	
			>1500	(González-Pleiter et al. 2013)	
Macrolides	Clarithromycin	<i>D. subspicatus</i>	0.0371	(Baumann et al. 2015)	
			<i>P. subcapitata</i>	0.23	(Villain et al. 2016)
				0.35	(González-Pleiter et al. 2013)
Quinolones	Enrofloxacin	<i>D. subspicatus</i>	0.038	(Machado and Soares 2018)	
			<i>P. subcapitata</i>	5.57	(Ebert et al. 2011)
				18.7	(Robinson et al. 2005)
	Ciprofloxacin	<i>D. subspicatus</i>	>8	(Ebert et al. 2011)	
			<i>P. subcapitata</i>	113	(Magdaleno et al. 2015)
				39	(Martins et al. 2012)
	Ofloxacin	<i>P. subcapitata</i>	187	(Robinson et al. 2005)	
			12.1	(Robinson et al. 2005)	
			1.44	(Isidori et al. 2005)	
Norfloxacin	<i>C. vulgaris</i>	10.4	(Eguchi et al. 2004)		
		<i>P. subcapitata</i>	>80	(González-Pleiter et al. 2013)	
			16.6	(Eguchi et al. 2004)	
Tetracyclines	Tetracycline	<i>P. subcapitata</i>	3.31	(González-Pleiter et al. 2013)	
			<i>C. vulgaris</i>	3.58	(Siedlewicz et al. 2020)
				1.04	(Kolar et al. 2014)
Sulfonamides	Sulfamethoxazole	<i>Green algae</i>	1.53	(Johnson et al. 2015)	
Diaminopyrimidine	Trimethoprim	<i>P. subcapitata</i>	129	(Kolar et al. 2014)	
			83.8	(De Liguoro et al. 2012)	

studies have shown that EC_{50} values will be in the range of $\mu\text{g.L}^{-1}$ to mg.L^{-1} (Yang et al. 2008). Earlier experiments proved that sulphonamides (Białk-Bielińska et al. 2011), tetracyclines (Yang et al. 2013), and macrolides (Baumann et al. 2015) had severe effects on algal growth and development in terms of growth inhibition. Sometimes, antibiotics showed hormesis, i.e., the same antibiotics when used in lower doses can stimulate algal growth, but if applied in higher concentrations, showed growth inhibition effects (Baumann et al. 2015, González-Pleiter et al. 2013). Algae can induce defense mechanisms against oxidative stress caused by antibiotics. Increasing concentrations of Norfloxacin affect the activity of two antioxidative enzymes viz. catalase (CAT) and glutathione S-transferase (GST). Similarly, OTC can change the activity of CAT and peroxidase enzymes (Vilvert et al. 2017).

In reality, antibiotics are found as a mixture with other antibiotics or some other contaminants such as heavy metals, nanoparticles, or the metabolites of antibiotics themselves. So it is necessary to identify the relative contributions made by the antibiotic to the toxicity towards algae in complex mixtures. A variety of antibiotics like tylosin and macrolides or other antibiotics with sulfonamides showed simple additive effects. Synergistic effects could be seen in the binary mixture of the same classes of antibiotics like sulfonamides and trimethoprim. A combination of tetracycline with the 7-aminocephalosporanic acid showed antagonistic effects (Gao et al. 2013, Liu et al. 2018). Previous studies also showed that working on the antibiotic mixture was more important than the individual molecules. One of the early studies evaluated the toxicity of antibiotic combinations of ERY and ENR to *C. vulgaris* where the mixture showed synergism. This result could be correlated with an increase in antioxidant enzymes as well as in MDA and glutathione content (Wang et al. 2019). In another study, 16 chemicals with different MOA were tested in algal systems. These concentration-response analyses were performed for 16 different biocides and mixtures with all 16 substances. It was found that the IA model was better than the CA in predicting the toxicity of algal systems. The alternative hypothesis of CA resulted in an overestimation of mixture toxicity, but differences between observed and predicted effect concentrations did not exceed a factor of 3.2 (Faust et al. 2003).

MODELLING APPROACHES TO DETERMINE THE TOXICITY OF MIXTURES

Generally, concentration addition (CA) and independent action (IA) are the two models used to determine the combined effects of the mixture of different chemicals. CA model is used when the components in the mixture display a similar

kind of MOA; whereas, the IA model is applicable where the MOA is different for the components present in the mixture (Nweke et al. 2015). CA model can be depicted as follows:

$$IC_{x(mix)} = \left(\sum_{i=1}^n \frac{\pi_i}{IC_{xi}} \right)^{-1} \quad \dots(1)$$

Where n denotes the total number of components, π_i represents the proportion of i^{th} component in the mixture so that summation of π_i should be equals to 1, IC_{xi} is the concentration of the i^{th} component which give the effect x when acted individually.

IA model can be mathematically expressed as:

$$E(C_{mix}) = 1 - \prod_{i=1}^n [1 - E(C_i)] \quad \dots(2)$$

Where $E(C_{mix})$ is the total effect caused by the mixture containing n number of components, C_i denotes the concentration of the i^{th} compound, and $E(C_i)$ is the effect caused by the component individually.

After determining the effects of individual components, the effect of the mixture can be predicted by applying these CA and IA models. Then the predicted value is compared with the obtained value. The ratio between the observed and predicted value denotes the interaction present between the components of the mixture. A value less than 1 denotes antagonism between the components; whereas a value greater than 1 shows synergism. If the value equals 1 then it is said that components in the mixture present additive effects (Li et al. 2014).

PROBABLE DIFFERENTIAL ALGAL TOXICITY MECHANISM(S) OF ANTIBIOTIC TOXICITY

As mentioned in the earlier sections, it was observed that some antibiotics also affected many non-target organisms like eukaryotic green algae (De Liguoro et al. 2012, de Vasconcelos et al. 2017) besides being toxic to the target organism, i.e., bacteria. However, there were no specific trends observed for algal sensitivity towards antibiotics. This observation suggests that there can be variation in species sensitivity depending on the use of antibiotics. Until now, researchers have focused on morphological changes like inhibition of cellular growth and cytotoxicity (González-Pleiter et al. 2013, Magdaleno et al. 2015). Photosynthesis mechanism damage by oxidative stress and the antioxidant defense mechanisms are used to determine the molecular mechanism(s) of antibiotic toxicity. An antibiotic like amoxicillin did not show any kind of toxicity towards the algal system. The cause may be due to its toxic effects on the formation of the bacterial cell wall. Hence, they do not cause any harm to algae (González-Pleiter et al. 2013). It was also found out that the eukaryotic algal photosynthetic

mechanism was explicitly inhibited by antibiotics (Liu et al. 2011). From Table 2, it is evident that macrolide antibiotics like clarithromycin and erythromycin are highly toxic towards freshwater algal species with very low EC_{50} values (Baumann et al. 2015, González-Pleiter et al. 2013, Machado and Soares 2018, Minguez et al. 2016, Villain et al. 2016). In bacteria, this group of antibiotics inhibits protein synthesis by binding with the 50S ribosomal subunit. The algal chloroplast contains homologs of bacterial 70S ribosomes. Maybe this is why antibiotics affect the photosynthetic machinery of eukaryotic algal species (Villain et al. 2016). It was also observed that erythromycin inhibited several photosynthetic mechanisms like carbon assimilation, electron transport, and photophosphorylation (Liu et al. 2011). It can be said that antibiotics cause toxicity to the algal species by interfering or inhibiting the pathways responsible for chloroplast metabolism, which results in the dysfunction of the photosynthetic apparatus and eventually reduces cell growth (Matsumoto et al. 2012, Wang et al. 2015). Another study found out that tetracyclines affected the mitochondrial translation process (Moullan et al. 2015). Previous studies also showed that antibiotics like roxithromycin, when exposed to the algae *C. pyrenoidasa* for 21 days (long-term exposure), increased the SOD, CAT, and MDA, which suggested that the antibiotic caused oxidative stress in the algae (Li et al. 2020). It was also found out that eukaryotic algae are less sensitive towards levofloxacin (LEV) and oxytetracycline when compared with the blue-green algae (Zhou et al. 2020). Again, the effects of the same antibiotic may vary when exposed to different organisms (Han et al. 2020).

C. vulgaris exposed to environmentally relevant concentrations of sulfamethoxazole, and norfloxacin (less than ten days) showed significant cell-density inhibition ($p < 0.05$) when compared with the control group. Antioxidant enzymes, like, SOD, CAT, and peroxidase (POD) activities also varied with respect to control, which proved that these antibiotics caused oxidative stress (Niu et al. 2019). Triclosan, one of the broad-spectrum antibiotics and can be detected in the aquatic system, was found to be highly toxic to the algae. It was also observed that the by-products of triclosan were more toxic than their parent compound (Dann & Hontela 2011). It was noted that at high concentrations, LEV significantly inhibited the algal growth and increased oxidative stress to the system. LEV also inhibited the photosynthesis mechanism (Wan et al. 2014).

REMOVAL AND/OR DEGRADATION OF ANTIBIOTICS BY ALGAL POPULATION

It was also noted that algae played a significant role in the removal and or degradation of antibiotics. This removal

mechanism might be because of the self-defense mechanism. It was found out that the half-lives of the antibiotic florfenicol were between 3.53 to 7.63 days. It was also observed that at the concentration of 46 mg.L^{-1} , the removal efficiency by *Chlorella sp.* was almost 97%. Further, this algal species showed nearly 74% removal despite the presence of a high concentration (159 mg.L^{-1}) of the antibiotic. These results suggested that this *Chlorella sp.* (an alga known to have considerable bioremediation potential) has shown promise in the removal of florfenicol antibiotics as well (Song et al. 2019). In another study, scientists evaluated the bioremediation properties of four algal species. The removal of ten antibiotics (belong to three classes: sulphonamides, macrolides, and fluoroquinolones) was evaluated. This study demonstrated that variation was based on the antibiotics' dissipation potential and also on algal species variation. The study showed the degradation products of the antibiotics had lower toxicity than their parental products (Kiki et al. 2020). It is also essential to design the experiment properly to understand the contribution of different abiotic factors (Li et al. 2020).

FUTURE CHALLENGES

Most of the studies, to date, have focussed on the effects of a single antibiotic on the freshwater algal system. As mentioned earlier, antibiotics can be mostly found as a mixture of toxicants. In the mixture, they may show additive, synergistic, or antagonistic effects on the algae when compared with the individual toxicant. It is necessary to investigate the toxic effects of the mixture to get more realistic data (Roose-Amsaleg & Laverman 2016). Though there are some studies performed to evaluate toxicities of mixtures on algal species (González-Pleiter et al. 2013, Magdaleno et al. 2015, Wang et al. 2019), mechanistic details are inadequate in the laboratory setting.

Moreover, there is a lack of adequate eco-toxicological data available for all the antibiotics, despite their presence in the environment in large amounts (e.g., azithromycin). In contrast, some antibiotics (like tetracycline and oxytetracycline) got more recognition than others. The reason behind this is not known.

CONCLUSION

From this review, it can be concluded that the ever-increasing production and excessive usage of persistent antibiotics can be classified as an emerging pollutant. Though antibiotics are specific to treat several bacterial infections, they can exhibit toxic effects on non-target organisms. Eukaryotic green algae are one of the most critical non-target organisms studied for determining antibiotic toxicity. Species sensitivity may vary

depending on the antibiotic exposed. Until now, the mechanistic approach of evaluating the toxicity of antibiotics in algae has not been explored systematically. There are still huge gaps found in the eco-toxicological data of antibiotics, as their toxicity can be altered due to their interactions with other toxicants in the environment. Moreover, environmental factors such as humidity, temperature, pH, as well as other variables like BDOM, can also modify the toxicity of antibiotics. Toxicity evaluation of antibiotics is expected to aid the regulators to modify existing guidelines for proper antibiotic disposal.

ACKNOWLEDGEMENT

The authors thank the management of VIT for their unstinted and constant support and for creating the scientific ambiance that made possible the compilation of this review possible.

REFERENCES

- Andreozzi, R., Caprio, V., Ciniglia, C., De Champdoré, M., Lo Giudice R. and Marotta, R. 2004. Antibiotics in the environment: occurrence in Italian STPs, fate, and preliminary assessment on algal toxicity of amoxicillin. *Environ. Sci. Technol.*, 38: 6832-6838.
- Backhaus, T., Scholze, M. and Grimme, L. 2000. The single substance and mixture toxicity of quinolones to the bioluminescent bacterium *Vibrio fischeri*. *Aquat. Toxicol.*, 49: 49-61.
- Barhoumi, L. and Dewez, D. 2013. Toxicity of superparamagnetic iron oxide nanoparticles on green alga *C. vulgaris*. *BioMed Res. Int.*, 13: 36-49.
- Baumann, M., Weiss, K., Maletzki, D., Schüssler, W., Schudoma, D. and Kopf, W. 2015. Aquatic toxicity of the macrolide antibiotic clarithromycin and its metabolites. *Chemosphere*, 120: 192-198.
- Bialk-Bielińska, A., Stolte, S., Arning, J., Uebers, U., Bösch, A. and Stepnowski, P. 2011. Ecotoxicity evaluation of selected sulfonamides. *Chemosphere*, 85: 928-933.
- Brandt, K.K., Amézquita, A., Backhaus, T., Boxall, A., Coors, A. and Heberer, T. 2015. Ecotoxicological assessment of antibiotics: a call for improved consideration of microorganisms. *Environ. Int.*, 85: 189-205.
- Braschi, I., Blasioli, S., Fellet, C., Lorenzini, R., Garelli, A. and Pori, M. 2013. Persistence and degradation of new β -lactam antibiotics in the soil and water environment. *Chemosphere*, 93: 152-159.
- Brausch, J.M., Connors, K.A., Brooks, B.W. and Rand, G.M. 2012. Human pharmaceuticals in the aquatic environment: a review of recent toxicological studies and considerations for toxicity testing. *Rev. Environ. Contam. Toxicol.*, 218: 1-99.
- Dann, A.B. and Hontela, A. 2011. Triclosan: environmental exposure, toxicity, and mechanisms of action. *J. Appl. Toxicol.*, 31: 285-311.
- Daughton, C.G. and Ruhoy, I.S. 2013. Lower-dose prescribing: minimizing "side effects" of pharmaceuticals on society and the environment. *Sci. Total Environ.*, 443: 324-337.
- De Liguoro, M., Di Leva, V., Dalla Bona, M., Merlanti, R., Caporale, G. and Radaelli, G. 2012. Sublethal effects of trimethoprim on four freshwater organisms. *Ecotoxicol. Environ. Saf.*, 82: 114-121.
- De Vasconcelos, E., Dalke, C. and De Oliveira, C. 2017. Influence of select antibiotics on *Vibrio fischeri* and *Desmodesmus subspicatus* at $\mu\text{g L}^{-1}$ concentration. *Environ. Manag.*, 60: 157-164.
- Deng, W., Li, N., Zheng, H. and Lin, H. 2016. Occurrence and risk assessment of antibiotics in river water in Hong Kong. *Ecotoxicol. Environ. Saf.*, 125: 121-127.
- Dong, D., Zhang, L., Liu, S., Guo, Z. and Hua, X. 2016. Antibiotics in water and sediments from Liao River in Jilin Province, China: occurrence, distribution, and risk assessment. *Environ. Earth Sci.*, 75: 1202.
- Ebert, I., Bachmann, J., Kühnen, U., Küster, A., Kussatz, C. and Maletzki, D. 2011. Toxicity of the fluoroquinolone antibiotics enrofloxacin and ciprofloxacin to photoautotrophic aquatic organisms. *Environ. Toxicol. Chem.*, 30: 2786-2792.
- Eguchi, K., Nagase, H., Ozawa, M., Endoh, Y.S., Goto, K. and Hirata, K. 2004. Evaluation of antimicrobial agents for veterinary use in the ecotoxicity test using microalgae. *Chemosphere*, 57: 1733-1738.
- EMA E 2006. Guideline on the environmental risk assessment of medicinal products for human use. *EMEA/CHMP/SWP/4447/00 Committee for Medicinal Products for Human Use (CHMP), London, UK.*
- Fairbairn, D.J., Karpuzcu, M.E., Arnold, W.A., Barber, B.L., Kaufenberg, E.F. and Koskinen, W.C. 2016. Sources and transport of contaminants of emerging concern: A two-year study of the occurrence and spatiotemporal variation in a mixed land-use watershed. *Sci. Tot. Environ.*, 551: 605-613.
- Faust, M., Altenburger, R., Backhaus, T., Blanck, H., Boedeker, W. and Gramatica, P. 2003. Joint algal toxicity of 16 dissimilarly acting chemicals is predictable by the concept of independent action. *Aquat. Toxicol.*, 63: 43-63.
- Gao, L., Shi, L. and Yuan, T. 2013. Growth inhibitive effect of typical antibiotics and their mixtures on *Selenastrum capricornutum*. *J. Environ. Public Health*, 30: 475-478.
- González-Pleiter, M., Gonzalo, S., Rodea-Palomares, I., Leganés, F., Rosal, R. and Boltes, K. 2013. Toxicity of five antibiotics and their mixtures towards photosynthetic aquatic organisms: implications for environmental risk assessment. *Water Res.*, 47: 2050-2064.
- González-Pleiter, M., Cirés, S., Hurtado-Gallego, J., Leganés, F., Fernández-Piñas, F. and Velázquez, D. 2013. Ecotoxicological assessment of antibiotics in freshwater using cyanobacteria. *Cyanobacteria*, 6(3): 399-417.
- Gothwal, R. and Shashidhar, T. 2015. Antibiotic pollution in the environment: A review. *Clean Soil Air Water*, 43: 479-489.
- Hagel, S. and Scheuerlein, H.J.V.M. 2014. Perioperative antibiotic prophylaxis and antimicrobial therapy of intra-abdominal infections. *Viszeralmedizin*, 30: 310-316.
- Han, Q., Zheng, Y., Qi, Q., Peng, J., Song, J. and Guo, J. 2020. Involvement of oxidative stress in the sensitivity of two algal species exposed to roxithromycin. *Ecotoxicology*, 7: 1-9.
- Hua, X., Zhao, Z., Zhang, L., Dong, D. and Guo, Z. 2018. Role of dissolved organic matter from natural biofilms in oxytetracycline photodegradation. *Environ. Sci. & Pollut. Res.*, 25: 30271-30280.
- Huang, D.J., Hou, J.H., Kuo, T.F. and Lai, H.T. 2014. Toxicity of the veterinary sulfonamide antibiotic sulfamonomethoxine to five aquatic organisms. *Pharmacology*, 38: 874-880.
- Isidori, M., Lavorgna, M., Nardelli, A., Pascarella, L. and Parrella, A. 2005. Toxic and genotoxic evaluation of six antibiotics on non-target organisms. *Sci. Total Environ.*, 346: 87-98.
- Johnson, A.C., Keller, V., Dumont, E. and Sumpter, J.P. 2015. Assessing the concentrations and risks of toxicity from the antibiotics ciprofloxacin, sulfamethoxazole, trimethoprim, and erythromycin in European rivers. *Sci. Total Environ.*, 511: 747-755.
- Kiki, C., Rashid, A., Wang, Y., Li, Y., Zeng, Q. and Yu, C.P. 2020. Dissipation of antibiotics by microalgae: Kinetics, identification of transformation products and pathways. *J. Hazard. Mater.*, 387: 121985.
- Kolar, B., Arnuš, L., Jeretin, B., Gutmaier, A., Drobne, D. and Durjava, M.K. 2014. The toxic effect of oxytetracycline and trimethoprim in the aquatic environment. *Chemosphere*, 115: 75-80.
- Larsson, D.J. 2014. Antibiotics in the environment. *Ups. J. Med. Sci.*, 119: 108-112.
- Laxminarayan, R., Duse, A., Wattal, C., Zaidi, A.K., Wertheim, H.F. and Sumpradit, N. 2013. Antibiotic resistance—the need for global solutions. *Lancet Infect. Dis.*, 13: 1057-1098.

- Laxminarayan, R., Matsoso, P., Pant, S., Brower, C., Røttingen, J.A. and Klugman, K. 2016. Access to effective antimicrobials: a worldwide challenge. *The Lancet*, 387: 168-175.
- Li, J., Min, Z., Li, W., Xu, L., Han, J. and Li, P. 2020. Interactive effects of roxithromycin and freshwater microalgae, *Chlorella pyrenoidosa*: Toxicity and removal mechanism. *Ecotoxicol. Environ. Saf.*, 191: 110156.
- Li, Y., Zhang, B., He, X., Cheng, W.H., Xu, W. and Luo, Y. 2014. Analysis of individual and combined effects of ochratoxin A and zearalenone on HepG2 and KK-1 cells with mathematical models. *Toxins* 6: 1177-1192.
- Liang, X., Chen, B., Nie, X., Shi, Z., Huang, X. and Li, X. 2013. The distribution and partitioning of common antibiotics in water and sediment of the Pearl River Estuary, South China. *Chemosphere*, 92: 1410-1416.
- Liu, B.Y., Nie, X.P., Liu, W.Q., Snoeijjs, P., Guan, C. and Tsui, M.T. 2011. Toxic effects of erythromycin, ciprofloxacin, and sulfamethoxazole on photosynthetic apparatus in *Selenastrum capricornutum*. *Ecotoxicol. Environ. Saf.*, 74: 1027-1035.
- Liu, L., Wu, W., Zhang, J., Lv, P., Xu, L. and Yan, Y. 2018. Progress of research on the toxicology of antibiotic pollution in aquatic organisms. *Acta Ecol. Sin.*, 38: 36-41.
- Liu, Y., Wang, Y., Zhang, J., Sun, L., Zhang, A. and Torres, O.L. 2017. An integrated assessment of ceftazidime and photo products on the feeding behavior of rotifers: From exposure to post-exposure. *Ecotoxicol. Environ. Saf.*, 144: 245-251.
- Machado, M.M.D. and Soares, E.V. 2018. Toxic effects of erythromycin to freshwater and marine microalgae. *Environ. Pollut.*, 242: 357-366.
- Magdaleno, A., Saenz, M., Juárez, A. and Moretton, J. 2015. Effects of six antibiotics and their binary mixtures on the growth of *Pseudokirchneriella subcapitata*. *Ecotoxicol. Environ. Saf.*, 113: 72-78.
- Manzetti, S. and Ghisi, R. 2014. The environmental release and fate of antibiotics. *Mar. Pollut. Bull.*, 79: 7-15.
- Martins, N., Pereira, R., Abrantes, N., Pereira, J., Gonçalves, F. and Marques, C. 2012. Ecotoxicological effects of ciprofloxacin on freshwater species: data integration and derivation of toxicity thresholds for risk assessment. *Ecotoxicology*, 21: 1167-1176.
- Matsumoto, H., Takechi, K., Sato, H., Takio, S. and Takano, H. 2012. Treatment with antibiotics that interfere with peptidoglycan biosynthesis inhibits chloroplast division in the desmid *Closterium*. *PLoS One*, 7: 23-38.
- Mazel, D. and Davies, J. 1999. Antibiotic resistance in microbes. *Cell. Mol. Life Sci.*, 56: 742-754.
- Minguez, L., Pedelucq, J., Farcy, E., Ballandonne, C., Budzinski, H. and Halm-Lemeille, M.P. 2016. Toxicities of 48 pharmaceuticals and their freshwater and marine environmental assessment in northwestern France. *Environ. Sci. & Pollut. Res.*, 23: 4992-5001.
- Mitchell, S.M., Ullman, J.L., Teel, A.L. and Watts, R.J. 2014. pH and temperature effects on the hydrolysis of three β -lactam antibiotics: Ampicillin, cefalotin, and cefoxitin. *Sci. Total Environ.*, 466: 547-555.
- Moullan, N., Mouchiroud, L., Wang, X., Ryu, D., Williams, E.G. and Mottis, A. 2015. Tetracyclines disturb mitochondrial function across eukaryotic models: a call for caution in biomedical research. *Cell Rep.*, 10: 1681-1691.
- Mutiyar, P.K. and Mittal, A.K. 2014. Occurrences and fate of selected human antibiotics in influents and effluents of the sewage treatment plant and effluent-receiving river Yamuna in Delhi (India). *Environ. Monit. Assess.*, 186: 541-557.
- Ngumba, E., Gachanja, A. and Tuhkanen, T. 2016. Occurrence of selected antibiotics and antiretroviral drugs in Nairobi River Basin, Kenya. *Sci. Total Environ.*, 539: 206-213.
- Niu, Z., Na, J., Lv, Z. and Zhang, Y. 2019. How long-term exposure of environmentally relevant antibiotics may stimulate the growth of *Prorocentrum lima*: A probable positive factor for red tides. *Environ. Pollut.*, 255: 113149.
- Noguera-Oviedo, K. and Aga, D.S. 2016. Lessons learned from more than two decades of research on emerging contaminants in the environment. *J. Hazard. Mater.*, 316: 242-251.
- Nweke, C., Orji, J. and Ahumibe, N. 2015. Prediction of phenolic compound and formulated glyphosate toxicity in binary mixtures using *Rhizobium* species dehydrogenase activity. *Adv. Life Sci.*, 5: 27-38.
- Pal, A., He, Y., Jekel, M., Reinhard, M. and Gin K.Y.H. (2014). Emerging contaminants of public health significance as water quality indicator compounds in the urban water cycle. *Environ. Int.*, 71: 46-62.
- Robinson, A.A., Belden, J.B. and Lydy, M.J. 2005. Toxicity of fluoroquinolone antibiotics to aquatic organisms. *Int. J. Environ. Toxicol. Chem.*, 24: 423-430.
- Roose-Amsaleg, C. and Laverman, A.M. 2016. Do antibiotics have environmental side effects? Impact of synthetic antibiotics on biogeochemical processes. *Environ. Pollut. Sci. Res.*, 23: 4000-4012.
- Sebaugh, J. 2011. Guidelines for accurate EC50/IC50 estimation. *Pharm. Stat.*, 10: 128-134.
- Seoane, M., Rioboo, C., Herrero, C. and Cid, A. 2014. Toxicity induced by three antibiotics commonly used in aquaculture on the marine microalga *Tetraselmis suecica* (Kyllin) Butch. *Mar. Environ. Res.*, 101: 1-7.
- Shade, A., Klimowicz, A.K., Spear, R.N., Linske, M., Donato, J.J. and Hogan, C.S. 2013. Streptomycin application has no detectable effect on bacterial community structure in apple orchard soil. *Appl. Environ. Microbiol.*, 79: 6617-6625.
- Siedlewiec, G., Žak, A., Sharma, L., Kosakowska, A. and Pazdro, K. 2020. Effects of oxytetracycline on growth and chlorophyll a fluorescence in green algae (*C. vulgaris*), diatom (*Phaeodactylum tricornutum*), and cyanobacteria (*Microcystis aeruginosa* and *Nodularia spumigena*). *Oceanologia*, 31: 411-431.
- Singh, S.K., Sengupta, S., Antony, R., Bhattacharya, S., Mukhopadhyay, C. and Ramasubramanian, V. 2019. Variations in antibiotic use across India—Multicentre study through global point prevalence survey. *J. Hosp. Infect.*, 3: 54
- Smith, T.C., Gebreyes, W.A., Abley, M.J., Harper, A.L., Forshey, B.M. and Male, M.J. 2013. Methicillin-resistant *Staphylococcus aureus* in pigs and farm workers on conventional and antibiotic-free swine farms in the USA. *Plos One*, 8: e63704.
- Song, C., Wei, Y., Qiu, Y., Qi, Y., Li, Y. and Kitamura, Y. 2019. Biodegradability and mechanism of florfenicol via *Chlorella* sp. UTEX1602 and L38: Experimental study. *Bioresour. Technol.*, 272: 529-534.
- Tian, Y., Zou, J., Feng, L., Zhang, L. and Liu Y 2019. *C. vulgaris* enhance the photodegradation of chlortetracycline in aqueous solution via extracellular organic matters (EOMs): Role of triplet state EOMs. *Water Res.*, 149: 35-41.
- Välitalo, P., Kruglova, A., Mikola, A. and Vahala, R. 2017. Toxicological impacts of antibiotics on aquatic micro-organisms: a mini-review. *Int. J. Hyg. Environ. Health*, 220: 558-569.
- Van Boeckel, T.P., Gandra, S., Ashok, A., Caudron, Q., Grenfell, B.T. and Levin, S.A. 2014. Global antibiotic consumption 2000 to 2010: An analysis of national pharmaceutical sales data. *Lancet Infect. Dis.*, 14: 742-750.
- Van Boeckel, T.P., Brower, C., Gilbert, M., Grenfell, B.T., Levin, S.A. and Robinson, T.P. 2015. Global trends in antimicrobial use in food animals. *Proc. Natl. Acad. Sci.*, 112: 5649-5654.
- Villain, J., Minguez, L., Halm-Lemeille, M.P., Durrieu, G. and Bureau, R. 2016. Acute toxicities of pharmaceuticals toward green algae. mode of action, biopharmaceutical drug disposition classification system, and quantile regression models. *Ecotoxicol. Environ. Saf.*, 124: 337-343.
- Vilvert, E., Contardo-Jara, V., Esterhuizen-Londt, M. and Pflugmacher, S. 2017. The effect of oxytetracycline on physiological and enzymatic defense responses in aquatic plant species *Egeria densa*, *Azolla caroliniana*, and *Taxiphyllum barbieri*. *Toxicol. Environ. Chem.*, 99: 104-116.

- Wan, J., Guo, P. and Zhang, S. 2014. Response of the cyanobacterium *Microcystis flos-aquae* to levofloxacin. *Environ. Sci. & Pollut. Res.*, 21: 3858-3865.
- Wang, G., Zhang, Q., Li, J., Chen, X., Lang, Q. and Kuang, S. 2019. Combined effects of erythromycin and enrofloxacin on antioxidant enzymes and photosynthesis-related gene transcription in *C. vulgaris*. *Aquat. Toxicol.*, 212: 138-145.
- Wang, X., Ryu, D., Houtkooper, R.H. and Auwerx, J. 2015. Antibiotic use and abuse: a threat to mitochondria and chloroplasts with impact on research, health, and environment. *Bioessays*, 37: 1045-1053.
- Wang, X., Zheng, Y., Zhang, Y., Li, J., Zhang, H. and Wang, H.J.C. 2016. Effects of β -diketone antibiotic mixtures on the behavior of zebrafish (*Danio rerio*). *Europe PMC*, 144: 2195-2205.
- Wei R, Ge F, Huang S, Chen M, Wang R (2011). Occurrence of veterinary antibiotics in animal wastewater and surface water around farms in Jiangsu Province, China. *Chemosphere* 82: 1408-1414.
- Wei R, Ge F, Chen M, Wang R (2012). Occurrence of ciprofloxacin, enrofloxacin, and florfenicol in animal wastewater and water resources. *Journal of environmental quality* 41: 1481-1486.
- Wu, M.H., Que, C.J., Xu, G., Sun, Y.F., Ma, J. and Xu, H. 2016a. Occurrence, fate, and interrelation of selected antibiotics in sewage treatment plants and their receiving surface water. *Ecotoxicol. Environ. Saf.*, 132: 132-139.
- Wu, M.H., Que, C., Tang, L., Xu, H., Xiang, J. and Wang, J. 2016b. Distribution, fate, and risk assessment of antibiotics in five wastewater treatment plants in Shanghai, China. *Environ. Sci. Pollut. Res.*, 23: 18055-18063.
- Xiang, L., Wu, X.L., Jiang, Y.N., Yan, Q.Y., Li, Y.W. and Huang, X.P. 2016. Occurrence and risk assessment of tetracycline antibiotics in soil from organic vegetable farms in a subtropical city, south China. *Environ. Sci. Pollut. Res. Int.*, 23: 13984-13995.
- Yan, C., Yang, Y., Zhou, J., Liu, M., Nie, M. and Shi, H. 2013. Antibiotics in the surface water of the Yangtze Estuary: occurrence, distribution and risk assessment. *Environ. Pollut.*, 175: 22-29.
- Yang, L.H., Ying, G.G., Su, H.C., Stauber, J.L., Adams, M.S. and Binet, M.T. 2008. Growth-inhibiting effects of 12 antibacterial agents and their mixtures on the freshwater microalga *pseudokirchneriella* subcapitata. *Int. J. Environ. Toxicol. Chem.*, 27: 1201-1208.
- Yang, W., Tang, Z., Zhou, F., Zhang, W. and Song, L. 2013. Toxicity studies of tetracycline on *Microcystis aeruginosa* and *Selenastrum capricornutum*. *Environ. Toxicol. Pharmacol.*, 35: 320-324.
- Yang, Y., Li, B., Zou, S., Fang, H.H. and Zhang, T. 2014. The fate of antibiotic resistance genes in sewage treatment plants revealed by a metagenomic approach. *Water Res.*, 62: 97-106.
- Zhang, G., Liu, X., Lu, S., Zhang, J. and Wang, W. 2020. Occurrence of typical antibiotics in Nansi Lake's inflowing rivers and antibiotic source contribution to Nansi Lake based on principal component analysis-multiple linear regression model. *Chemosphere*, 242: 125269.
- Zhou, Z., Zhang, Z., Feng, L., Zhang, J., Li, Y. and Lu, T. 2020. Adverse effects of levofloxacin and oxytetracycline on aquatic microbial communities. *Sci. Total Environ.*, 13(9): 499.
- Zorpas, A.A., Dimitriou, M. and Voukkali, I. 2018. Disposal of household pharmaceuticals in insular communities: Social attitude, behavior evaluation, and prevention activities. *Environ. Sci. & Pollut.*, 25: 26725-26735.



The Importance of Public Awareness in Environmental Protection: A Case Study in Paktika, Afghanistan

Hizbullah Rahmani*†, Wafaurahman Wafa** and Fayaz Gul Mazloum Yar***

*Department of Biology, Higher Education Institute of Paktika, Afghanistan

** Department of Environmental Science, Kabul University, Afghanistan

***Department of Geography, Nangarhar University, Afghanistan

†Corresponding author: Hizbullah Rahmani; hezbollah.rahmani@gmail.com

Nat. Env. & Poll. Tech.

Website: www.neptjournal.com

Received: 03-03-2021

Revised: 21-04-2021

Accepted: 01-05-2021

Key Words:

Environmental problems
Public awareness
Environmental protection
Environmental activities

ABSTRACT

Public awareness and knowledge of environmental protection are crucial to avoid environmental pollutions. Lack of relevant scientific principles and lack of public awareness of environmental or other projects are hindrances to controlling environmental pollution. The objective of the study was to identify the importance of public awareness in environmental pollution management. Environmental education and public awareness are crucial to avoid environmental pollutions. The study aims to analyze public awareness of environmental protection. The study was conducted in Sharana, the center of Paktika province, and was attended by 71 students from the Paktika Higher Education Institute's Education Faculty. Questionnaires and field observations have been selected as methodologies for this research. The results of the study show that 59.2 percent of survey participants consider public awareness and 35.2 percent think that enforcement of environmental laws is important. People in Paktika do not take part in environmental activities due to a lack of public awareness and throw away pollutants everywhere. If this situation continues, it is not far off that it will turn into a disaster.

INTRODUCTION

Science's longevity as a discipline is closely connected to the effectiveness of its practice in society's daily lives. Lack of relevant scientific principles and lack of public awareness of environmental or other projects are hindrances to controlling environmental pollution (Ekmekçi & Günay 1997). Public awareness of environmental protection is the ability to be aware of the changes that take place in the environment, including the world around us, the relationship between human behavior, and the quality of the environment. Human activities can have a significant impact on the terrestrial environment. Lack of adequate environmental knowledge is an obstacle in achieving a sustainable future for humankind at both global and local levels (Sola 2014).

The main requirement for high-school graduates is to assimilate not only special environmental awareness, but to enhance, enrich, systematize, and use it under various conditions (Nazarenko & Kolesnik 2018). Curdt-Christiansen, (2020) stated that environmental education is very important in schools even at the start of school for children. Education is one of the major tools for raising public awareness, particularly in developing countries (Debrah et al. 2021).

A key concern for the future of mankind is public understanding of the climate. For reflecting national culture, it is one of the most important indicators. It represents many aspects of environmental situations, such as the awareness, actions, and attitude of people towards a sustainable society (Apichatibutarapong 2018). According to Apichatibutarapong (2018), environmental protection is any activity that maintains the quality of the environment at the individual, administrative or state level for the benefit of both the natural environment and human beings. Protecting the environment is a priority for future generations. Public awareness also gives us a sense of responsibility to keep natural resources for future generations. Environmental problems such as wastewater and waste management (Mukhtar et al. 2016) are among the world's most serious problems. Therefore, public awareness and participation are essential for effective organization and protection of the environment. The United Nations Convention on Climate Change and the Kyoto Protocol can only be achieved through the active participation of the public and key stakeholders. As governments are directly responsible for the reduction in greenhouse gas emissions, they should encourage businesses, communities, and individuals to change their behavior to comply with gas emissions restrictions. Therefore, public awareness and access to information are critical to supporting government policies and laws (UNEP 2006).

Many environmental problems are caused not only by industrial and agricultural pollutants but also by a lack of public awareness. Furthermore, unplanned urbanization is causing some significant long-term implications on humans and the environment; water contamination caused by urban mess and air pollution due to traffic smoke is an emerging and extensive issue (Wafa et al. 2020). Therefore, raising public awareness about environmental protection is very important and necessary (Xua et al. 2011). Climate change can have short-term and long-term adverse effects on health. The number of deaths caused by climate change will rise by 250,000 each year between 2030 and 2050. The participation of the public, in addition to governments, international agencies, and non-governmental organizations, is essential to preventing such environmental problems. Such environmental problems can be easily controlled through public awareness, cooperation, and commitment (Rapaport & Ashkenazi 2016).

Environmental protection education is one of the most important and fundamental goals of UNESCO-UNEP (1978), which enables a person to be active in solving environmental problems through awareness, methods, skills, and participation (Mohamed et al. 2006). The objective of the is article is to identify the importance of public awareness in environmental pollution management. Public awareness and attitude surveys allow an understanding of broader social knowledge and priorities that can contribute positively to the achievement of conservation goals. (Hawkins et al. 2016).

Additionally, in Malaysia, studies of public awareness, consciousness, and attitudes (including WTP) towards air

pollution are uncommon. Thus, by understanding the public's perception of current air pollution, their environmental awareness, and attitudes towards environmental protection, this study attempts to explore this subject (Chin et al. 2019). According to Li et al. (2017), for further consideration during implementation, some constructive policy recommendations have been proposed. The reason for carrying out this study is that without public knowledge and environmental protection funding, the introduction of any initiative or legislation will not be effective (Chin et al. 2019). Therefore, the awareness surveys are crucial for some regulation and policy implementation.

The study will identify the importance of public awareness in environmental pollution management in the Paktika higher education institute. This research will answer the question: what is the level of public awareness in Paktika towards environmental protection? and what types of environmental activities are required for public awareness?

MATERIALS AND METHODS

Study Area

The latitude and longitude of Paktika province are 31.59- and 33.42-degrees latitude and 67.81- and 69.54-degrees longitude, respectively. The nation has a total area of 36360 km² with a 360 km² boundary with Pakistan, which is 210 km from Kabul (Fig. 1).

Paktika is a third-class province according to the Afghan administrative division's political and social divisions. In

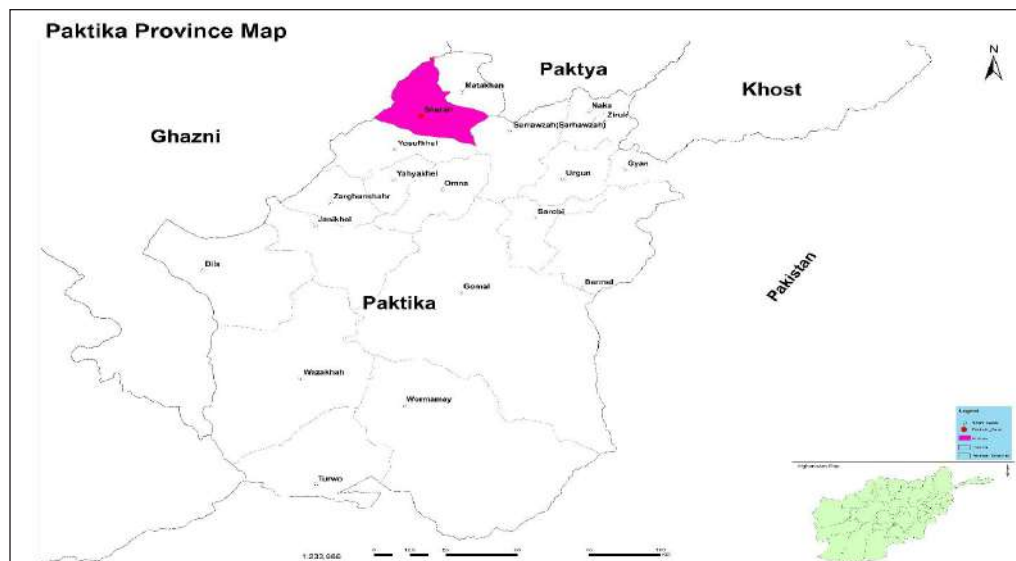


Fig. 1: Paktika Province map.

addition to the capital, it has eight districts. It has a total population of 434742 people, with Pashtuns making up the vast majority of the population, which is divided into different tribes who speak Pashto (Mazloom Yar 2016).

Paktika University

Sampling Size and Population

The total student population of Paktika Higher Education Institute Education Faculty is 1200, and the total sample size based on Cochran's sample size formula for continuous data is:

$$n_o = \frac{(t)^2 * (s)^2}{(d)^2} \text{ (Cochran 1977)}$$

Where t is the value for each tail's chosen alpha stage (the alpha level of .05 indicates the level of risk the researcher is willing to take that true margin of error may exceed the acceptable margin of error.). Where the population's average standard deviation, and d is the acceptable margin of error for the mean estimated (number of points on primary scale * acceptable margin of error). The sample size for this study with a 95% confidence level and 10% confidence interval is 71 students.

Data Collection and Research Instrument

The data is collected from primary and secondary sources. Primary data sources include field observation, and a survey instrument consisting of one set of questionnaires was con-

structed and sent to target respondents to collect information that would later be used for further study to determine public awareness in environmental protection. The data collected through the questionnaires was analyzed descriptively, as well as, the data analyzed was used to support the study's desired results. The questionnaires were constructed in the Pashto National Language of Afghanistan so that the respondents could better grasp the questions and correctly answer them. Secondary data was attained from books, journals, reports, and conference proceedings. The questionnaire had closed-ended questions, and it was distributed to 71 students from the Faculty of Education. The questionnaire was reliable and consistent; therefore, every survey participant answered precisely similar questions. A comprehensive field study was conducted to collect information about the current circumstances of public awareness among the city residents. The results obtained are analyzed descriptively using SPSS 24. The research analysis method was Frequency and Percentage as it is the best and most suitable method for analyzing the question papers.

RESULTS AND DISCUSSION

The questionnaire used in this study has various components such as general information about participants, serious environmental problems of Afghanistan, solutions, public awareness tools, participation in solving environmental problems, and others. Table 1 indicates the findings of the questionnaire.

Questions	Parameters	Survey participants' responses	
		Frequency	Percentage
Respondents education level	First-year student	15	21.1
	Second-year student	23	32.4
	Third-year students	33	46.5
	Total	71	100.0
	S		
Serious environmental problems in Afghanistan	Air pollution	16	22.5
	Noise pollution	6	8.5
	Water pollution	17	24
	Soil pollution	4	5.6
	Mismanagement of waste	5	7
	Demolition of natural resources	13	18.3
	Problems in the municipal system	10	14.1
	Total	71	100
Resolutions	Technological Improvements	3	4.2
	Rising public awareness level	42	59.2
	Enforcement of environmental laws	25	35.2
	Usage of alternative materials in the industry	1	1.4
	Total	71	100

Questions	Parameters	Survey participants' responses	
		Frequency	Percentage
Public awareness tools	Conferences and seminars	25	35.2
	Newspapers, magazines, books	15	21.1
	Radio and Tv	28	39.4
	Activities of Non-governmental organizations	3	4.2
	Total	71	100
Following environment-related publications	Always	9	12.7
	Some times	51	71.8
	Never	7	9.9
	No answer	4	5.6
	Total	71	100
Types of participation in environmental activities	Works as Volunteer	49	69.0
	Financial assistance	14	19.7
	None of them	4	5.6
	No answer	4	5.6
	Total	71	100

The Current Conditions of Public Awareness on Environmental Pollution Management in Paktika

Due to the low level of environmental awareness in Paktika, pollutants are dumped in the water, canals, and other public places (Fig. 2). If the current scenario persists, it is not unlikely that it will devolve into a catastrophe, because the government cannot prevent pollution without the participation of the people. Public awareness is critical to engaging the public in environmental protection activities.

According to the results of the study, the main reason for the government's failure to prevent pollution in Afghanistan is the lack of public awareness about environmental protection. The general public does not cooperate with the government in controlling environmental pollution. This is because they are unaware that these substances are having a detrimental effect on their health and the environment. Environmental pollution prevention cannot be achieved solely by legislation, nor can it be achieved without community participation in environmental protection. If the public is made aware of the effects of environmental problems such as climate change, diversity, ozone depletion, endangered species, illegal trade, environmental pollution, and wastewater, the government will be able to prevent such problems very easily.

People cannot make effective decisions without public knowledge, comprehension of available science and technical evidence, and support for government regulations and acts. Coping skills can be enhanced, health risks can be minimized, and lives can be saved by increasing public knowledge, collaboration, and dedication. It is important in public health practice to keep the public aware of any danger or hazard that can impact their health and well-being (Rapaport & Ashkenazi 2016). Because the majority of pollutants are produced by individuals, the government alone will not be

able to avoid them if they do not help clean up. Therefore, the general public should be involved in environmental protection activities, for which public awareness is very important. Public awareness in the field of environmental protection is very important because only through public awareness and access to information, we can involve the general public in environmental protection activities (Rahmani & Nor Anuar 2019). Rather than asking people to come to you, a good public awareness campaign entails taking the message to them. This necessitates diverse mediums to reach out to various segments of the population, including mass media, magazines (brochures, posters), meetings and hearings, publicity merchandise, social events, role-playing and community theater, and the Internet (Minkova 2002). A broad range of strategies and techniques for improving communication and public awareness are available, and they can be used to engage the public in environmental protection activities. Examples Modern mass media such as newspapers, magazines, radio, television, and film are examples of modern mass media; conventional media such as national broadband radio; printed materials such as posters, leaflets, and illustrated booklets, billboards, wall-writing, messages printed on bags, transport, signs, and other things used or encountered in daily life; use of popular personalities as advocates; school programs; outdoor education programs; and interpretive facilities in protected areas (Solongp 2012).

CONCLUSION

Currently, air pollution, water pollution, destruction of natural resources, and mismanagement of waste are severe environmental problems in Afghanistan. This is because they are oblivious to the fact that the waste products, they generate have a negative impact on their health and the environment. If this situation persists, it is not unlikely that



Fig. 2: a- Sewage at the toilet of the mosque, b- waste materials on the main road, c- waste materials and wastewater next to the Public Health Department and Central Hospital, d- sewage in front of shops, e- emptying wastewater tankers in areas close to homes.

it will devolve into a disaster, as the government cannot prevent pollution on its own. Public awareness plays a very important and fundamental role in environmental pollution management. This is because, through public awareness and access to information, we can encourage the general public to participate in natural resource conservation and environmental protection activities. A wide variety of tools are available such as mass media, traditional media, wall-writing, school programs, and outdoor education pro-

grams for promoting communication and public awareness. Consequently, it is recommended that various environmental activities are required for public awareness to protect the environment.

REFERENCES

- Apichatibutarapong, S. 2018. Factors affecting public awareness concerning the university environment. In: Multidisciplinary Digital Publishing Institute Proceedings, 2(22): 1369.

- Chin, Y.S.J., De Pretto, L., Thuppil, V. and Ashfold, M.J. 2019. Public awareness and support for environmental protection: A focus on air pollution in peninsular Malaysia. *PloS One*, 14(3): e0212206.
- Cochran, W.G. 1977. *Sampling techniques*. 3rd edition. John Wiley & Sons, New York.
- Curdt-Christiansen, X.L. 2020. Environmental literacy: Raising awareness through Chinese primary education textbooks. *Lang. Cult. Curric.*, 1: 1-16.
- Debrah, J.K., Vidal, D.G. and Dinis, M.A. 2021. Raising awareness on solid waste management through formal education for sustainability: A developing countries evidence review. *Recycling*, 6: 106
- Ekmekçi, M. and Günay, G. 1997. Role of public awareness in groundwater protection. *Environ. Geol.*, 30(1-2): 81-87.
- Hawkins, J.P., O'Leary, B.C., Bassett, N., Peters, H., Rakowski, S., Reeve, G. and Roberts, C.M. 2016. Public awareness and attitudes towards marine protection in the United Kingdom. *Marine Pollut. Bull.*, 111(1-2): 231-236.
- Li, Q., Liu, G., Leamon, G., Liu, L.C.C., Cai, B. and Chen, Z.A.A. 2017. A national survey of public awareness of the environmental impact and management of CCUS technology in China. *Energy Proc.*, 114(November 2016): 7237-7244.
- Nazarenko, A.V. and Kolesnik, A.I. 2018. Raising environmental awareness of future teachers. *Int. J. Instr.*, 11(3): 63-76.
- Minkova, Y. 2002. *Developing Skills of NGOs: Public Education to Raise Environmental Awareness*. Ady Endre ut 9-11, 2000, The Regional Environmental Center for Central and Eastern Europe, Szentendre, Hungary,
- Mohamed, E., Kidundo, M. and Tagelseed, M. 2006. *Environmental education and public awareness*. Workshop on Post Conflict National Plan for Environmental Management in Sudan, Khartoum, Sudan, p. 3.
- Mazloom Yar, F.G. 2016. *Political Geography of Afghanistan*, Islah Afkar Publishing Society, Jalalabad.
- Mukhtar, S., Wafa, W., Halimzai, H. and Shams, A.K. 2016. Planning for the solid waste management of the central park in new capital development of Afghanistan. *J. Environ. Protect.*, 7(06): 805.
- Rahmani, H. and Nor Anuar, A. 2019. Challenges and resolutions for sustainable domestic wastewater management in Kabul City, Afghanistan. *Int. J. Eng. Adv. Technol.*, 12: 1398.
- Rapaport, C. and Ashkenazi, I. 2016. Incorporating public awareness into climate change health planning. *SM Trop. Med. J.*, 1: 1-13.
- Sola, A. 2014. Environmental education and public awareness. *J. Educ. Social Res.*, 4(3): 332.
- Solongo, T. 2012. *UNDP-GEF Project: Integrated Natural Resource Management in the Baikal Basin Transboundary Ecosystem*. UNOPS and UNDP.
- UNEP 2006. *Raising awareness of climate change: A handbook for government focal points*. United Nations Environment Programme's Division of Environmental Law and Conventions, CH-1219 Châtelaine (Geneva), Switzerland.
- UNESCO, U. 1978. *Recommendations of the Intergovernmental Conference on Environmental Education* Tbilisi. USSR. France: UNESCO, pp.1-96.
- Wafa, W., Hairan, M.H. and Waizy, H. 2020. The impacts of urbanization on Kabul City's groundwater quality. *Int. J. Adv. Sci. Technol.*, 29(4): 10796-10809.
- Xua, L., Shen, J., Marinova, D. and Guo, X. 2011. *Quantitative Assessment on Public Awareness of Environmental Protection in Response to Environmental Incidents: A Case for Taihu Lake Algae Bloom*. 19th International Congress on Modelling and Simulation, 2011, 12-16 December, Perth Convention and Exhibition Centre in Perth, Western Australia, MODSIM, p. 1718.



Environmental Efficiency of Construction Industry with Considerations to Carbon Emission: A Case Study in Henan, China

Xin Youyang^{*(**)}†, Li Xiuzhong^{*(**)} and Shang li^{**}

*Construction Engineering Quality Testing Research Center, Huanghuai University, Zhumadian 463000 China

**School of Civil Engineering, Huanghuai University, Zhumadian 463000, China

†Corresponding author: Xin Youyang; 20070931@huanghuai.edu.cn

Nat. Env. & Poll. Tech.
Website: www.neptjournal.com

Received: 20-08-2021

Revised: 15-09-2021

Accepted: 22-09-2021

Key Words:

Carbon emissions
Construction industry
Environmental efficiency
Henan province

ABSTRACT

Low energy utilization is observed in China due to the extensive economic growth mode, which further leads to considerable energy wastes and environmental pollution. The construction industry plays an important role in the national economic development of China and consumes tremendous materials; thus, this industry discharges abundant CO₂. The energy consumption growth rate of the construction industry in China is far higher than the national energy consumption growth rate, resulting in the prominent situation of high energy consumption and low yield. A case study based on Henan Province, China, was conducted to further analyze the environmental efficiency of the construction industry. An index system was established by using the Super-slack-based model (Super-SBM). This system chooses the following: labor, energy, capital, and technology of the construction industry as the input variables, economic output as the output variable, and carbon emissions as the unexpected output. This system was also used to investigate the energy efficiency of the construction industry in Henan Province from 2008 to 2019. Results demonstrated that the construction industry in Henan Province has failed to eliminate the extensive development mode thus far. The environmental efficiency of the construction industry presents a fluctuating growth with a mean of 1.048, which generally remains at a relatively low level. The numbers of construction machines and enterprises in the construction industry have redundancy in approximately 50% of the years. Thus, this study can provide some positive references to enrich the evaluation index system and estimation model of energy efficiency of the construction industry, which includes unexpected output. Moreover, the current study can provide a comprehensive understanding of the environmental efficiency of the construction industry in a province in China and realize reasonable allocation of construction industrial resources.

INTRODUCTION

The continuous economic development provides people with pleasant lives, but such a life conceals considerable energy consumption and ecological environmental damages. The most prominent problem is global warming caused by excessive CO₂ emissions. China continuously faces issues in high energy consumption and carbon emissions during economic development. Energy consumption is the primary source of carbon emission, and the construction industry has been one of the industries that consume the most energy in China. Urban scale continuously expands in China, which provides a demanding environment for the construction industry. Consequently, the energy consumption of the construction industry increases, thus generating a substantial amount of CO₂. Except for the direct carbon emission from terminal energy consumption in the construction industry, construction products consume a substantial amount of building materials, such as steel and cement, which can generate abundant CO₂. Assuring stable growth of construction industrial output is an

important premise to reduce emissions of the industry. Such an assurance aims to maximize output and minimize CO₂ emissions in the expected construction production activities. Therefore, increasing carbon emission efficiency shall be used as an important approach to decrease carbon emissions and promote the sustainable development of construction industries. The construction industry in China drives its development at the cost of abundant energy consumption, which prominently leads to high energy consumption and low output. Thus, increasing the energy efficiency of the construction industry in China is of considerable importance to save energy and improve the environment.

Henan Province is an area with an enormous population and large-scaled construction industrial development in central China. Fig. 1 shows that the national construction industry and the construction industry of Henan Province achieved rapid development from 2011 to 2020. The total outputs of the national construction industry and the construction industry of Henan Province increased from 11,646.33 and

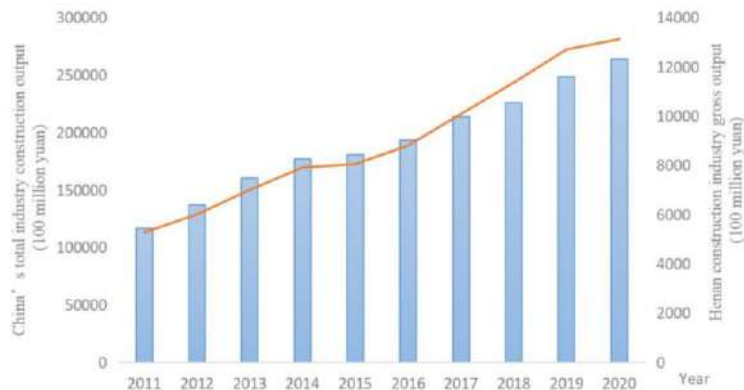


Fig. 1: Total outputs of the national construction industry and the construction industry of Henan Province from 2011 to 2020 (100 million yuan/RMB).

527.936 billion yuan (RMB) in 2011 to 26,394.704 and 1312.255 billion yuan (RMB), showing an annual average growth rate of 14.07% and 16.50%, respectively. Considering the total output of the construction industry, Henan Province is 2.43% higher than the national average level in China, which reflects the strong demands of Henan Province for construction industrial development. Carbon emissions of the construction industry in Henan Province continue to increase and cause serious pressure over ecological environments despite the rapid growth of the construction industry. This phenomenon is due to the generally low utilization of production resources, resource wastes, deficient management mechanisms in construction enterprises, and low construction technological levels. The current carbon emissions of the construction industry in Henan Province were estimated to discuss the carbon emission efficiency and facilitate energy-saving and emission reduction in the construction industry, which are beneficial to realizing the general emission reduction goal of China.

PAST STUDIES

In the background of continuous expansion of the construction industry, addressing the increasingly prominent construction industry-induced environmental pollution has attracted academic research attention worldwide. Numerous empirical studies have been conducted. Some scholars have reported successful studies on the environmental efficiency of construction industries and achieved some progress. Mandal et al. estimated the environmental efficiency of the cement industry in India. Empirical results revealed that the cement industry in India has sufficient potential to improve environmental efficiency, which varies among different states (Mandal et al. 2010). Feng et al. estimated two energy efficiencies and their decomposition indexes of the construction

industry in China from 2004 to 2011. They also tested the influences of different external factors on the energy economic and environmental efficiencies of the construction industry of China. Their results demonstrated an increase in the regional average energy efficiency of the construction industry of China to some extent, and the low pure technological efficiency of construction energy is a major constraint against the energy efficiency of such an industry (Feng et al. 2015). Lin et al. discussed the relationship between CO₂ emission reduction potentials and energy performances of the construction industry in China. They found that CO₂ emission in the construction industry of China quickly increases, and electricity consumption has become a major emission source (Lin et al. 2015). Hu et al. discussed the environmental efficiency of the construction industry in Australia from 1990 to 2013 and found a significant increase during the study period. However, the gap among these industries increased due to seriously poor technological reforms (Hu et al. 2017). Wang et al. analyzed the social responsibility efficiency of the construction enterprises of China from 2012 to 2016. He found that these enterprises have not achieved optimal efficiency in fulfilling social responsibility. Institutional factors have complicated and nonlinear influences on the social responsibility efficiency of enterprises (Wang et al. 2018). Zhang et al. conducted an empirical study on the environmental efficiency of regional construction industries in China during 2006-2015 and found low carbon efficiency of building materials in most regions in the majority of provinces in China due to the low-efficiency material consumption (Zhang et al. 2018). Zhang et al. measured the technological efficiency of the regional construction industry in China by using a three-stage data envelopment analysis (DEA) model. They found that environmental monitoring had significant impacts on construction industrial efficiency in China, and scale efficiency demonstrated the most influence (Zhang et

al. 2018). Xian et al. assessed the internal balance between environments for different types of energy consumption and costs in China's construction industry by using DEA technology. Results showed that the construction industry of China can produce the current level of industrial value-added at low CO₂ emissions and energy input cost by eliminating technologies with low efficiency and adjusting energy consumption structure (Xian et al. 2019). Zhou et al. estimated the total factor carbon emission efficiency of the construction industry in China from 2003 to 2016 by using the super SBM-DEA method. Empirical results revealed that the carbon emission efficiency of China's construction industry is relatively low and presents a decreasing trend. Technological progress and energy restructuring can promote carbon emission efficiency of the construction industry, but the economic scale of the extensive development model may generate some negative impacts (Zhou et al. 2019). Du et al. established a static computable general equilibrium model to discuss the rebounding effect of different energy sources used in the construction industry. Results showed that coal, petroleum, natural gas, and electricity are major energy sources of the construction industry in China, and increasing the energy efficiency of the construction industry had positive effects on relieving GDP and carbon emission (Du et al. 2019). Le et al. studied 600 building material enterprises in Vietnam through a questionnaire and found that environmental efficiency also had strong positive effects on financial efficiency. Therefore, innovative solutions of decreasing environmental pollution can increase the profitability of enterprises (Le et al. 2019). Zhang et al. measured the environmental efficiency of the construction industry in China from 2000 to 2017 and analyzed the degree of influencing factors through Tobit regression. Their results indicated a significant disconnection between the R&D stage and commercial application stage of green technology in the construction industry in China (Zhang et al. 2021). Liang et al. measured energy efficiencies of construction industries in 30 provinces in China from 2008 to 2017 by using a three-stage DEA-Malmquist model. They found that total factor energy efficiency changes (TFEECH) and technological changes (TECH) of China's construction industry had been underestimated. Per capita glass steel, energy consumption structure, industrial development degree, and industrial concentration degree all had positive effects on energy efficiency improvement (Liang et al. 2021). Chen et al. estimated the energy efficiency of China's construction industry from 2005 to 2016 by using an SBM-DEA model. The empirical results revealed that the low management efficiency of the construction industry is an important cause of the low energy efficiency of the construction industry in China (Chen et al. 2021). The literature review on the environmental efficiency of construction industries found that foreign scholars mainly

focused on the micro-enterprise layer, while Chinese scholars conducted measurement and comparative analysis of the local region or national layer. Moreover, most research results show that the construction industry has caused heavy energy consumption and environmental pollution due to its high energy consumption. However, the environmental efficiency of the construction industry has been improving yearly due to the applications of new technologies and high-intensity environmental regulations and policies in different countries. Therefore, a case study based on Henan Province, China, was conducted in accordance with the above studies. Research conclusions are conducive to further comprehend the estimation methods of environmental efficiency of the construction industry and general construction industry development in Henan Province within the corresponding calculation stages.

MODELS AND DATA SPECIFICATION

Models

As an extended model of DEA, SBM has many advantages: setting production function and zero influences of index dimensions in solving efficiency is no longer necessary, considerations to multiple input and output indexes, and objective empowerment. Among these advantages, the unexpected output SBM model offsets the disadvantages of the radial DEA model, including invalid measurement and exclusion of slack variables. Thus, the unexpected output SBM model can analyze specific causes of invalid outputs by reducing (or increasing) the percentage of corresponding slack variables. Therefore, the decision-making units (DMUs) on the data envelope leading edge in the same investigation period (efficiency value is 1) were compared by super-efficiency, thus realizing an accurate measurement of comprehensive DMU efficiency. The model is described as follows. Suppose n DMUs are available. The years of Henan Province were used as DMUs in this study. Each DMU contains m inputs, s expected outputs, and k unexpected outputs. The input elements include labor, capital, and energy of the construction industry when the research object is the energy efficiency of the construction industry. Meanwhile, the expected outputs are the construction industrial output, and the unexpected outputs are chosen as the carbon emission caused by construction industrial development. Consequently, the input matrix of the construction industry is shown in Eq. (1), and the expected output matrix is Eq. (2). The unexpected output matrix is presented in Eq. (3).

$$X = (x_1, x_2, \dots, x_m) \in R_{m \times n}, \quad \dots(1)$$

$$Y = (y_1, y_2, \dots, y_s) \in R_{s \times n}, \quad \dots(2)$$

$$U = (u_1, u_2, \dots, u_k) \in R_{k \times n}. \quad \dots(3)$$

According to Eqs. (1)–(3) and the study of Tone, K., the production possibility set can be obtained as follows (Tone, K., 2001):

$$P = \{(x, y, u) | x \geq \lambda X, y \geq \lambda Y, u \geq \lambda U, \lambda \geq 0\}. \quad \dots(4)$$

The SBM model of the unexpected output is:

$$\rho_0^* = \min \frac{1 - \frac{1}{m} \sum_{i=1}^m \frac{S_{io}^-}{x_{io}}}{1 + \frac{1}{s+k} \left(\sum_{r=1}^s \frac{S_{ro}^g}{y_{ro}} + \sum_{q=1}^k \frac{S_{qo}^b}{u_{qo}} \right)},$$

$$s.t. \begin{cases} x_{io} = \sum_{j=1}^n \lambda_j x_{ij} + S_{io}^-, i = 1, 2, \dots, m; \\ y_{ro} = \sum_{j=1}^n \lambda_j x_{rj} - S_{ro}^g, r = 1, 2, \dots, s; \\ u_{ro} = \sum_{j=1}^n \lambda_j x_{qj} + S_{qo}^b, q = 1, 2, \dots, k; \\ \lambda_j \geq 0, j = 1, 2, \dots, n; S_{io}^-, S_{ro}^g, S_{qo}^b \geq 0 \end{cases} \quad \dots(5)$$

where $x_{io}, y_{ro}, u_{qo}, \lambda$ are the input i of year o , expected output r , unexpected output q , and linear combination coefficient of year j , respectively. $S_{io}^-, S_{ro}^g, S_{qo}^b$ are slack variables of the input i , expected output r , and unexpected output q in the year of o , respectively. ρ_0^* is the efficiency value in the year of o . DMU_k is SBM effective only when $\rho_0^* = 1$ or $S_{io}^- = 0, S_{ro}^g = 0, S_{qo}^b = 0$, and the energy efficiency of the construction industry in the year of k is relatively ideal.

Data Specification

Considering research status, labor, energy, capital, and technology of the construction industry in Henan Province were chosen as input variables according to the research objective

of this study and data availability. Specifically, the following input variables are included: (1) labor input, which is expressed by the number of construction enterprises in Henan Province; (2) capital input, which is expressed by the paid-in capitals of construction enterprises in Henan Province; (3) energy input, which is expressed by the energy input of the construction industry in Henan Province; (4) technological input, which is expressed by the number of construction machines in construction enterprises. The output is expressed by the total construction industrial output. Unexpected output is the carbon emission of the construction industry in Henan Province. The research object used the construction industry in Henan Province considering data availability and consistency, and the study period was determined from 2008 to 2019. All original data came from the Statistical Yearbook of Henan Province, China, Energy Statistical Yearbook, and Statistical Yearbook of China’s Construction Industry from 2009 to 2020. The carbon emissions of the construction industry were calculated in accordance with the previous Regional Energy Sheet of Henan Province. Descriptive statistical results of specific indexes and data are listed in Table 1.

EMPIRICAL STUDY

The calculation of the super-efficiency SBM model considering improved slack variables, including unexpected output, used DEA-SOLVER Pro5.0 in this study. This model evaluated the energy efficiency of the construction industry in Henan Province from 2008 to 2019.

Table 2 shows that most input and output indexes generally have low levels of redundancy and energy efficiency of the construction industry in Henan Province. Thus, the input and output can still be substantially improved.

Fig. 2 shows that the energy efficiency of the construction industry in Henan Province from 2008 to 2019 generally increased slowly in a fluctuating manner. Specifically, the energy efficiency of the construction industry continuously

Table 1: Statistical system index and descriptive statistical results.

Index type	Input indexes			Output indexes		Unexpected output indexes
Specific index	Energy input of construction industry (10,000 tons of standard coals)	Number of construction machines in construction enterprises (pc)	Paid-in capitals of construction enterprises (100 million yuan)	Number of construction enterprise (pc)	Total output of construction industry (100 million yuan)	Carbon emissions of construction industry (100 million tons)
Max	102.00	61,4338.00	453.75	3827.00	2824.05	74.00
Min	569.00	81,8851.00	2143.18	6740.00	12,701.68	297.00
SD	176.06	60,788.09	611.37	891.24	3083.93	90.08
Mean	272.33	691,468.50	1253.27	4898.08	7335.76	155.95
Median	172.34	678,129.00	1168.73	4690.50	7457.55	124.05

increased during 2008-2014, with an annual growth rate of 9%. Subsequently, the energy efficiency generally decreased continuously, achieving an annual fluctuating growth rate of 1.3% from 2017 to 2019. The mean energy efficiency of the construction industry in Henan Province was 1.048 from 2008 to 2019. This value indicated that the construction industry of Henan Province has achieved some success in transition development mode and energy output improvement. Nevertheless, the energy efficiency was generally low, showing an invalid state. This finding revealed that the construction industry of Henan Province is still subordinated to the extensive development mode and has not achieved the coordinated development between output growth and resource

environmental protection. Thus, this industry has a long way to go in development transformation, resource-saving, and environmental protection. For input variables, the number of machines of construction enterprises (pc) and that of construction enterprises (pc) have redundancy in approximately 50% of years. This result proves that technological input to the construction industry of Henan Province has not been maximized, and numerous construction machines have no functions of improving energy efficiency completely. Thus, future work shall provide additional attention to the internal management of construction enterprises and use advanced environmental protection technology to decrease emissions of wastes. Many construction enterprises are available, but

Table 2: Slack Statistical Sheet and Means of Super-Efficiency SBM.

No.	DMU	Score	Excess				Shortage	
			1	2	3	4	1	(OBad)
			S-(1)	S-(2)	S-(3)	S-(4)	S + (1)	S + (2)
1	1	1.145590631	11.99886	65,673.19982	132.1341411	254.95918	0	0
2	2	0.949541904	2.545966266	38,876.84672	0	121.6225195	0	3.849330393
3	3	1.004044659	0	10,521.19357	0	0	0	0
4	4	1.001225432	0	0	3.781438146	0	0	0
5	5	1.027440934	0	2022.017136	0	64.08442227	269.5789778	0
6	6	1.02832062	0	0	17.13265448	0	326.5036423	0
7	7	1.219920843	108.2846129	0	0	60.56679006	508.8824136	0
8	8	1.032799689	0	7625.853782	0	559.3657142	0	0
9	9	1.005185355	0	13,387.75804	0	0	0	0
10	10	1.073532043	0	657.033142	0	0	0	40.13756065
11	11	1.002037367	0	0	0	50.19256551	0	0
12	12	1.087633456	0	18849	0	0	1341.16	12.585348

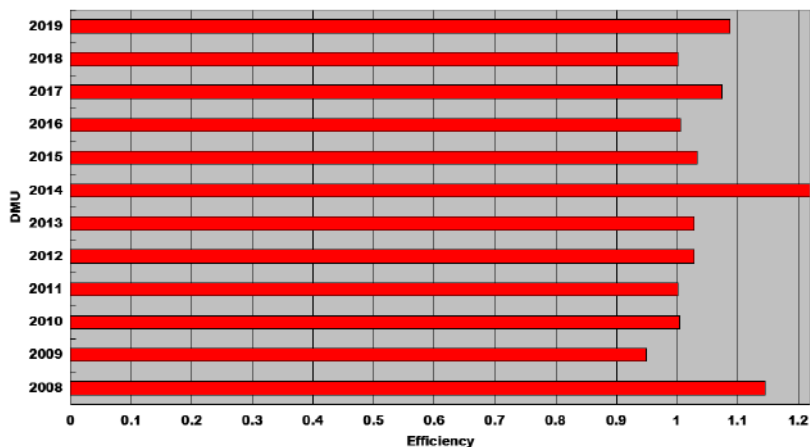


Fig. 2: Mean of annual energy efficiency of the construction industry from 2008-2019.

the general construction industrial level in Henan Province is relatively low. The raw material input increases with the expansion of enterprise production scale, and the resource waste phenomenon emerges, accompanied by rising waste emissions. Therefore, the quantity scale of the construction industry shall be appropriately controlled, and construction industry development shall be strengthened to realize the large-scale economic benefits of construction industries in Henan Province.

POLICY SUGGESTIONS

Strengthen Scientific Input and Control the Scale of Construction Industry Appropriately

The construction industry is a complicated huge system, and many influencing factors affect environmental efficiency. The input scale of the construction industry is recently expanding gradually, and the factor inputs of capital and labor are continuously increasing with the rapid development of the construction industry. Increasing the labor input in a long period may not always promote output growth due to influences by the decreasing laws of marginal benefits. Recent studies indicate that labor input has a small contribution to output growth, and such contributions gradually decrease. Conclusions of most studies disclose to some extent that abundant factor inputs to construction industries have not been properly managed and developed, thus influencing the output growth. This finding implies that simple scale expansion of the construction industry may not always increase environmental efficiency. Hence, the key to improving the environmental efficiency of the construction industry is to change the input-driven extensive economic growth mode rather than expand the industrial scale. Promoting reasonable allocation of resources, comprehending resource demands, comprehensively using construction projects by employing informatization and modernized means, and decreasing resource wastes are suggested. These suggestions facilitate production efficiency improvement of the construction industry.

Adjust Energy Consumption Structure of Construction Industry and Increase its Market Openness

A considerable amount of support shall be given to R&D and the usage of environmental-friendly energy sources. The construction industry heavily relies on traditional energy sources. Carbon emission coefficients of energy sources, such as crude coals and coke, are relatively high and have substantial contributions to direct carbon emissions of the construction industry. Carbon emission coefficients of environmental-friendly energy sources, such as electricity, are relatively low, and these energy sources are renewable.

Hence, these coefficients can adjust prices of environmental-friendly energy sources (e.g., electricity and natural gas) or increase subsidies to the use of environmental-friendly energy sources to encourage the replacement of traditional high-carbon energy sources. Meanwhile, building a platform for communication between universities and enterprises, promoting R&D of environmental-friendly energy sources positively, and decreasing carbon emission caused by traditional energy consumption are also suggested. Such suggestions increase the carbon emission efficiency of the construction industry. Moreover, subsidies to state-owned construction enterprises for innovation shall be increased to promote their enthusiasm for emission reduction. The rich resources and development stability introduced by state-owned systems of construction enterprises decrease the production enthusiasm of workers and reduce technological innovation efficiency. These conditions are disadvantageous to the improvement of the carbon emission efficiency of construction industries. Therefore, the market openness of the construction industry shall be increased and effective market competition shall be formed to promote the technological progress of construction enterprises.

Optimize the Design of Construction Products and Decrease Consumption of Building Materials

The development and use of new environmental-friendly materials shall be encouraged. At present, building materials mainly include steel, cement, glass, and aluminum. Among these materials, only steel and aluminum can be recycled. However, carbon emissions of the five building materials are significantly higher than that of energy consumption. These materials are also major contributors to carbon emissions in the construction industry. Therefore, decreasing the use of traditional building materials is suggested to reduce carbon emissions and thereby promote the improvement of efficiency. On the one hand, the design of construction products shall be optimized to decrease the usage of building materials from the design end while assuring the product performance, finally reducing carbon emissions. On the other hand, R&D of new environmental-friendly materials shall be increased to replace the traditional building materials. Meanwhile, recommendations include reducing the market price of the new materials by combining the market mechanism and providing subsidies to enterprises for using new materials to promote their applications.

Increase Support to Low-Carbon Development of Construction Industry and Strengthen Regional Cooperation

The government shall increase support to the low-carbon

development of the construction industry in economically underdeveloped regions to promote green development of the construction industry, publicize the energy-saving and environmental-protection concept positively, increase subsidies for construction technological innovation, and promote the improvement of production efficiency. Moreover, building a platform for low-carbon construction communication and encouraging provinces with high carbon emissions of the construction industry to learn the construction energy-saving technology from advanced provinces are suggested. Regional cooperation shall be strengthened to promote common development among different provinces in energy saving and emission reduction of the construction industry. Therefore, the government shall strengthen inter-provincial communication and learning, develop the driving role of high-efficiency regions, set up trans-provincial emission reduction plans of the construction industry, break traditional administrative zoning barriers, guide the transfer of low-carbon philosophy and low-carbon technology in high-efficiency regions to low-efficiency regions, and promote coordinated development among regions.

CONCLUSIONS

As a resource-intensive industry, the construction industry absorbs abundant resources, except for human and social resources, during its continuous expansion. This phenomenon causes massive energy consumptions and discharges tremendous CO₂ due to low construction levels, mechanization, and accomplishment of workers in China's construction industry. Consequently, such an absorption causes considerable pressure on the ecological environment. A case study based on Henan Province, China, is conducted in this study. An index system is established by using the Super-SBM model to discuss the energy efficiency of the construction industry in Henan Province from 2008 to 2019. This index system chooses labor, energy, capital, and technology as input variables, economic output as output variable, and carbon emission as the unexpected output. The results demonstrate that the construction industry in Henan Province has failed to eliminate the extensive development mode thus far. The environmental efficiency of the construction industry generally presents a relatively low fluctuating growth with a mean of 1.048. In the construction industry, the numbers of construction machines and enterprises demonstrate redundancy in approximately 50% of the years. Finally, some policy suggestions, including strengthening scientific input to the construction industry, adjusting its energy consumption structure, optimizing the design of building products, and increasing support to the low-carbon development of the industry, are proposed. Future works shall investigate the influencing factors of China's construction industrial development and provincial differences

in carbon emission efficiency of the construction industry by prolonging time frames of data related to the construction industry and choosing appropriate indexes.

ACKNOWLEDGMENT

This work was supported by the Science and Technology Planning Development Project in Henan Province (192102310516); and the Key Scientific Research Project of the Colleges and Universities in Henan Province (21B560007, 22B560009).

REFERENCES

- Chen, Y., Ma, L. and Zhu, Z. 2021. The environmental-adjusted energy efficiency of China's construction industry: a three-stage undesirable SBM-DEA model. *Environmental Science and Pollution Research*, 1-14.
- Du, Q., Li, Z., Li, Y., Bai, L., Li, J. and Han, X. 2019. Rebound effect of energy efficiency in China's construction industry: a general equilibrium analysis. *Environmental Science and Pollution Research*, 26(12): 12217-12226.
- Feng, B. and Wang, X. Q. 2015. Empirical research on energy economic efficiency and energy environmental efficiency of China's construction industry: based on the SBM-tobit two-stage model. *Journal of Beijing Institute of Technology (Social Sciences Edition)*, 17(1): 14-22.
- Hu, X. and Liu, C. 2017. Slacks-based data envelopment analysis for eco-efficiency assessment in the Australian construction industry. *Construction Management and Economics*, 35(11-12): 693-706.
- Lin, B. and Liu, H. 2015. CO₂ mitigation potential in China's building construction industry: A comparison of energy performance. *Building and Environment*, 94: 239-251.
- Liang, X., Lin, S., Bi, X., Lu, E. and Li, Z. 2021. Chinese construction industry energy efficiency analysis with undesirable carbon emissions and construction waste outputs. *Environmental Science and Pollution Research*, 28(13): 15838-15852.
- Le, T. T., Nguyen, T. M. A. and Phan, T. T. H. 2019. Environmental management accounting and performance efficiency in the Vietnamese construction material industry-A managerial implication for sustainable development. *Sustainability*, 11(19): 5152.
- Mandal, S. K. and Madheswaran, S. 2010. Environmental efficiency of the Indian cement industry: an interstate analysis. *Energy Policy*, 38(2): 1108-1118.
- Tone, K. 2001. A slacks-based measure of efficiency in data envelopment analysis. *European Journal of Operational Research*, 130(3): 498-509.
- Wang, X., Lai, W., Song, X. and Lu, C. 2018. Implementation efficiency of corporate social responsibility in the construction industry: A China study. *International Journal of Environmental Research and Public Health*, 15(9): 2008.
- Xian, Y., Yang, K., Wang, K., Wei, Y. M. and Huang, Z. 2019. Cost-environment efficiency analysis of construction industry in China: A materials balance approach. *Journal of Cleaner Production*, 221: 457-468.
- Zhou, Y., Liu, W., Lv, X., Chen, X. and Shen, M. 2019. Investigating interior driving factors and cross-industrial linkages of carbon emission efficiency in China's construction industry: Based on Super-SBM DEA and GVAR model. *Journal of Cleaner Production*, 241: 118322.
- Zhang, J., Li, H., Xia, B. and Skitmore, M. 2018. Impact of environment regulation on the efficiency of regional construction industry: a 3-stage Data Envelopment Analysis (DEA). *Journal of Cleaner Production*, 200: 770-780.

- Zhang, J., Ouyang, Y., Ballesteros-Pérez, P., Li, H., Philbin, S. P., Li, Z. and Skitmore, M. 2021. Understanding the impact of environmental regulations on green technology innovation efficiency in the construction industry. *Sustainable Cities and Society*, 65: 102647.
- Zhang, P., You, J., Jia, G., Chen, J. and Yu, A. 2018. Estimation of carbon efficiency decomposition in materials and potential material savings for China's construction industry. *Resources Policy*, 59: 148-159.



Analysis and Evaluation on Characteristics of Heavy Metal Pollution in the Coastal Farmland Soil along the Wuma River

Xiongfei Cai*, Die Xu*, Shijie Zhao*, Li Lei*, Ji Wang*† and Bin Xuan*

*School of Geographic and Environmental Sciences, Guizhou Normal University, Guiyang, 550025, China

†Corresponding author: Ji Wang; 1907154961@qq.com

Nat. Env. & Poll. Tech.
Website: www.neptjournal.com

Received: 17-11-2020

Revised: 12-01-2021

Accepted: 22-01-2021

Key Words:

Wuma river
Coastal farmland
Soil
Heavy metal

ABSTRACT

The thesis is aimed to provide a reference for the sustainable utilization of farmland soils along the Wuma River, an upstream tributary of the Chishui River in Guizhou Province. Geo accumulation index method, Nemerom comprehensive pollution index method, and potential ecological hazard index method were used based on the experimental data for analyzing and evaluating the heavy metal pollution status of farmland soil along Wuma River. The results showed that: (1) The contents of heavy metals Ni, Cu, Zn, Pb and Hg in farmland soil exceeded the soil background values of 9.82%, 47.80%, 13.72% and 76.06% in Guizhou Province, respectively, but did not exceed the standard limit class II based on the environmental quality. (2) The pollutants of Pb and Zn in the research area mainly come from mineral exploitation, waste residue accumulation, and transportation. The enrichment of Cr and Cu may originate from the domestic garbage dumping and incinerated waste by residents along the coast and irrational agricultural activities. The main contents of Cd, As and Hg come from soil geochemistry. (3) The ranking of accumulations of eight heavy metals was $I_{Pb} > I_{Hg} > I_{Cu} > I_{Ni} > I_{Zn} > I_{Cr} > I_{As} > I_{Cd}$, among which Pb was non-moderately polluted and the remaining heavy metals were at the clean level; Nemerom comprehensive pollution index showed that As, Cr, Zn, and Ni were mildly polluted, while Pb, Hg, and Cu were moderately polluted. The ranking of potential ecological risk levels for the eight heavy metals was Hg, Pb, Cu, Ni, As, Cd, Cr, Zn. The overall ecological risk level is mild.

INTRODUCTION

At present, farmland soils in China are threatened by various kinds of pollution, among which about 50 million mu farmland is moderately and severely polluted with 80% of the soil pollution by excessive contents of heavy metals (Wang et al. 2014, Chen et al. 2016). Heavy metal elements have unique environmental toxicological effects, so they cannot be degraded by microorganisms after entering farmland soil, and gradually accumulate in soil environment and organisms. They not only do harm to the quality and yield of crops but also cause potential harm to human health through the food chain (Massadeh et al. 2006, Zeng et al. 2010). In recent years, domestic and foreign scholars have investigated farmland soil in the basin many times. Marrugo-Negrete et al. (2017) surveyed 83 farmland soil samples from Sinú River in northern Colombia. The results showed that the average contents of Cu, Ni, Hg, and Zn were 1,149, 661, 0.159, and 1,365mg·kg⁻¹, respectively, which exceeded the background values of soil in the same area. Influenced by the coastal industrial zone, Ni, Cu, and Zn were moderate to heavily polluted (Perveen et al. 2017). Based on the comparison and analysis of the contents of heavy metals in farmland soils along the upper and lower reaches of Swan River, an

industrial area adjacent to Islamabad, Pakistan, it was found that the concentrations of Cr, Ni, Cd, Zn, Pb and Cu in the downstream were 149%, 131%, 176%, 139%, 224% and 182% of those in the upstream. Zhou et al. (2008) and Jin et al. (2017) investigated heavy metals in farmland along the Bijiang River in Yunnan Province and found that the concentrations of Pb, Cd, and Zn content could be regarded as serious pollution. Guo et al. (2017) evaluated the distribution characteristics and potential ecological risks of heavy metals in farmland soils along Xinqianghe River in a typical lead-zinc mining area. The results showed that there were many heavy metals in the coastal farmland where Cd dominated, with the existence of As, Cu, Ni, Pb, and Zn. Wu et al. (2011) investigated the contamination status of seven heavy metals in the surface soil of farmland around Puhe River, Hunhe River, Xihe River, and Shenfu Irrigation Canal in Shenyang. According to their investigation, Cd, Hg, and Zn pollution were found to be more common in these river areas.

It is thus clear that the pollution of heavy metals in river basins is becoming more severe. Therefore, researchers pay great attention to the environmental and ecological security of river basins in the current environment. However, there are few reports on the pollution of heavy metals in farmland

in the upper reaches of Chishui River, Guizhou Province. Therefore, it is particularly important to investigate and evaluate the present heavy metals pollution in farmland soil in Chishui River Basin. This thesis conducted a study on the soil along the Wuma River, a tributary of the upper reaches of the Chishui River. The pollution status of 8 heavy metals, such as Ni, Cr, Cu, Zn, Pb, Cd, As, and Hg, was analyzed based on the field investigation and experimental analysis through the methods of the geo-accumulation index and Nemerow comprehensive pollution index. In addition, the potential ecological risk index method was used to assess the ecological risk of farmland soil in the basin. All the above methods were used to provide a reference for the sustainable use of farmland soil and the maintenance of sound farmland ecosystem in the basin.

MATERIALS AND METHODS

Survey on Research Areas

The Wuma River is an important tributary of the Chishui River in Renhuai, is part of the Yangtze River system. The Wuma River Basin is located in the southwest of Renhuai City (106.1-106.6°E, 27.5-27.8°N), and the boundary area between Guizhou and Sichuan provinces. It mainly consists of four townships, including Changgang, Luban, Wuma, and Maoba under the jurisdiction of Renhuai City, Guizhou Province. The total length of it is 39.3 km and an average annual discharge, $4.98 \text{ m}^3 \cdot \text{s}^{-1}$. The climate in the research area is the humid monsoon climate in the middle subtropical zone, with distinct seasons. The rain season and hot season are basically

the same, the annual average temperature is 15.9-18.5 , and the annual average precipitation is 1,081mm. Main soil types can be divided into lime soil, yellow soil, purple soil, paddy soil, and yellow-brown soil. The main produced crops include rice, rape, maize, wheat, sorghum, and tobacco.

Sample Collection

From April to May 2017, a survey was carried out on the Wuma River Basin. According to the distribution of farmland in the basin, one sampling point was set every 1km along the basin, and the location information was recorded by GPS positioning within 1km from the riverbank. In the sampling process, based on the Technical Specification for Monitoring the Environmental Quality of Farmland Soil (NY/T 395-2000), five sub-sampling points were set up in the form of “plum blossom” or “serpentine” within the grid of 10m*10m. The surface soil from 0-20 cm was collected, and then mixed samples were formed. The soil samples were selected repeatedly by the four-point method and only about 1 kg was preserved. A total of 63 soil samples were collected. After air drying, grinding, and sifting (100 meshes), the soil was selected for determination and analysis (Bao 2007). The distribution of sampling points in the research area is shown in Fig. 1.

Sample Processing and Analysis

After using the tetra acid melting sample method (aqua regia, HClO_4 , HF) on an electrothermal plate at 140 for continuous heating and digestion, Copper (Cu), cadmium (Cd), lead (Pb), zinc (Zn), nickel (Ni) and chromium (Cr) were determined

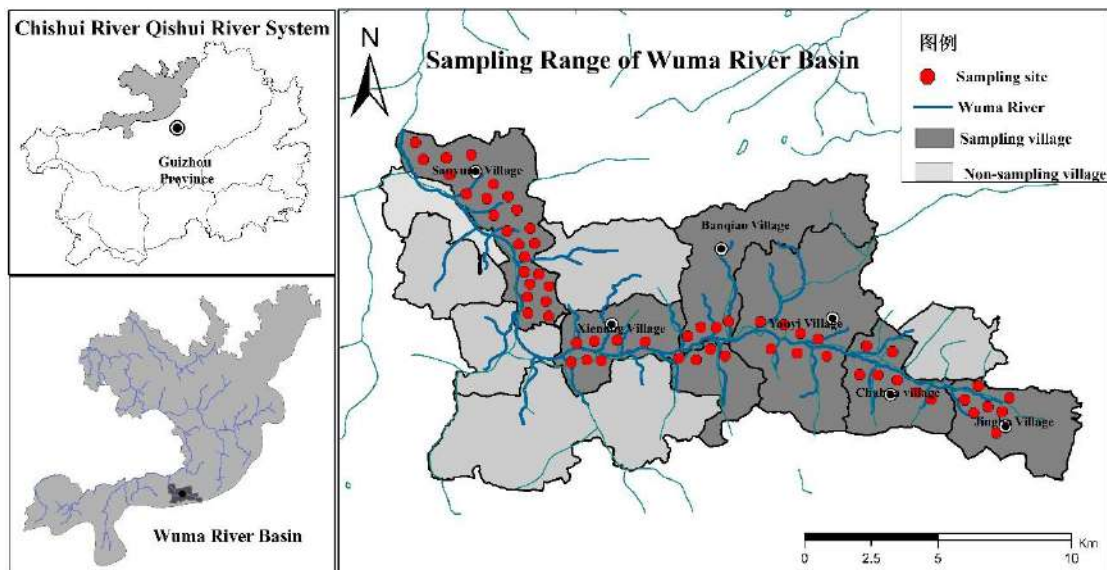


Fig. 1: Location of the research area and sampling sites.

by flame atomic absorption spectrometry (AAS-G800). Mercury (Hg) and arsenic (As) were digested by the aqua regia heating method and determined by atomic fluorescence spectrometry (AFS-E230). For the accuracy of the analysis, the national standard substance (GBW07309) was used for controlling the quality in the experimental process, and the parallel sample analysis was carried out. The test error was controlled within 5%.

Evaluation Methodology

Taking the background value of soil layer A in Guizhou Province as the evaluation criterion. The Muller cumulative index method (I_{geo}) and Nemerow comprehensive pollution index method were used for evaluating the farmland soil pollution in the research area. Based on the Grade II standard (pH > 7.5) of the National Soil Environmental Quality Standard (GB15618-1995), the potential ecological risk index (RI) method proposed by Hakanson (1980) was used to assess the potential ecological risk. The toxicity response parameters of heavy metals T_r^i were adopted based on the reference values proposed by Hakanson (1980) (toxicity response coefficients of T_r^i to heavy metals As=10, Zn = Mn = 1, Cu = Pb = 5, Cr = 2, Cd = 30, Hg = 40) (Li et al. 2015). The specific evaluation methods are shown in Table 1.

The pollution level I_{geo} is graded as follows: $I_{geo} \leq 0$ means pollution-free; $0 < I_{geo} \leq 1$ means pollution-free-to-moderate pollution; $1 < I_{geo} \leq 2$ refers to moderate pollution; $2 < I_{geo} \leq 3$ means medium-to-heavy pollution; $3 < I_{geo} \leq 4$ means heavy pollution; $4 < I_{geo} \leq 5$ means heavy-to-seriously heavy pollution; and $I_{geo} > 5$ means seriously heavy pollution. Nemerow's comprehensive pollution index is graded as follows: $P \leq 0.7$ means clean; $0.7 < P \leq 1.0$ means reaching the warning line; $1.0 < P \leq 2.0$ means slight pollution; $2.0 < P \leq 3.0$ means moderate pollution; $P > 3.0$ means heavy pollution. The degree of single-factor ecological risk pollution E_r^i is divided into the following grades: $E_r^i < 40$ means mild pollution; $40 \leq E_r^i$

< 80 means moderate pollution; $80 \leq E_r^i < 160$ means heavy pollution; $160 \leq E_r^i < 320$ means very heavy pollution; and $E_r^i \geq 320$ means seriously heavy pollution. The total potential ecological risk level R is graded as follows: $R < 150$ is mild; $150 \leq R < 300$ means moderate; $300 \leq R < 600$ means strong; $R \geq 600$ refers to very strong.

RESULTS AND DISCUSSION

Analysis of heavy metals in soil, according to Table 1, show that the upper limits and bottom limits for contents of Ni, Cr, Cu, Zn, Pb, Cd, As, and Hg in farmland soil along the Wuma River Basin varied greatly, ranging from 11.02 to 70.95, 14.57 to 135.20, 9.24 to 80.20, 42.58 to 182.26, 18.34 to 87.13, 0.003 to 0.076, 3.18 to 18.91, 0.074 to 0.307 mg·kg⁻¹, respectively. The average contents of heavy metals Ni, Cr, Cu, Zn, Pb, Cd, As, and Hg were 37.01, 64.55, 37.98, 93.70, 51.58, 0.013, 6.32, and 0.148 mg·kg⁻¹, respectively. The average contents of Ni, Cu, Zn, Pb, and Hg exceeded the Guizhou Province's background values of 9.82%, 47.80%, 13.72%, and 76.06%, respectively. However, the average contents of all heavy metals did not exceed the grade II standard limit according to the national soil environmental quality.

Skewness is statistical data for the shape of data distribution, and kurtosis is statistical data for showing the steepness of all values in the population (Zhan et al. 2011). Based on the heavy metals statistical results of the research area, skewness and kurtosis coefficients of Zn, Cd, As, and Hg were larger, indicating that some soil samples presented high content and were highly accumulated. The coefficient of variation can reflect the average variation degree of heavy metal content in different sites. According to the classification of variation degree by Wilding (1984), Ni, Cd, Zn and Hg (coefficients of variations were 35%, 32%, 32%, and 28%, respectively) were moderate (ranged from 15% to 36%), while Cu, Pb, Cd and As (coefficients of variation were 40%, 38%, 72%, and 41%, respectively) were highly variable (Zang et al.

Table 1: The assessment of geo-accumulation index, Nemerow comprehensive polluted index, and potential ecological risk index for heavy metals.

Index	Expression	Parameter
Geo-accumulation index	$I_{geo} = \text{Log}_2[C_n / (k \times B_n)]$	C_n = Content of heavy metal element n in the soil; B_n = Geochemical background value of heavy metal element n; K = Coefficient of variation of background values caused by different rocks.
Nemerow comprehensive polluted index	$P_{\text{综合}} = \sqrt{\frac{(C_i / S_i)_{\text{max}}^2 + (C_i / S_i)_{\text{ave}}^2}{2}}$	C_i = Concentration of soil pollutant i; S_i = Background concentration of soil pollutant i; $(C_i / S_i)_{\text{max}}$ = The maximum of single factor pollution index for soil pollutant i; $(C_i / S_i)_{\text{ave}}$ = Average value of single factor pollution index for soil pollutant i.
Potential ecological risk index	$RI = \sum E_r^i = \sum (T_r^i \cdot C_n^i) = \sum (T_r^i \cdot \frac{C_n^i}{C_n^i})$	R = Comprehensive potential ecological hazard index of several heavy metals; E_r^i = Potential ecological hazard coefficient of a single heavy metal; T_r^i = Toxicity response coefficient for heavy metals; C_n^i = Pollution coefficient of this element; C_n^i = Evaluation criterion of this element.

2016). If the coefficient of variation exceeds 0.5, the spatial distribution of heavy metal content is not uniform, and the point source pollution may exist (Aguiguri et al. 2017). The coefficient of variation of heavy metal Cd in the soil of the research area was 0.72. It can be seen that the variation of heavy metal Cd was significant, indicating that Cd was more prone to be affected by some local pollution sources. The average value of soil pH value was 7.93 and was of weak alkalinity. The skewness, kurtosis, and coefficient of variation were -1.20, 0.55, and 0.12, respectively. Therefore, the distribution of soil pH value was uniform and no obvious acid-base anomaly was observed.

Relevance and Source Analysis of Heavy Metals in Soil

The heavy metals in soils come from not only the parent soil layer but also agricultural activities (including irrigation

water, agriculture, fertilizer), atmospheric dust, and industrial pollution (Zhang et al. 2012). The correlation coefficients between heavy metals are indicators for the relationship among different pollution sources. Generally, heavy metals with higher correlation coefficients are dependent on each other and may have similar sources. Heavy metals with a low correlation coefficient have weak dependence and different sources (Hu 2014). The results from correlation analysis (Table 3) proved that there was a significant positive correlation between Cd and Hg and between As and Ni ($P < 0.01$), an obvious positive correlation between Zn and Cu, Pb, Cd, and As ($P < 0.05$), and a significant positive correlation between As, Cu, and Hg ($P < 0.05$) in farmland soil along the Wuma River. The above correlations between different elements indicate that the enrichment of these elements might come from similar sources.

Table 2: Statistic of heavy metal concentrations in the research area (n=63).

Elements	Max. (mg·kg ⁻¹)	Min. (mg·kg ⁻¹)	Avg. (mg·kg ⁻¹)	SDANN (mg·kg ⁻¹)	Skewness	Kurtosis	Coefficient of variation	Background value (mg·kg ⁻¹)	National standard (mg·kg ⁻¹)
Ni	70.95	11.02	37.01	12.99	0.18	-0.55	0.35	33.7	40
Cr	135.20	14.57	64.55	20.70	0.85	2.02	0.32	86.6	250
Cu	80.20	9.24	37.98	15.18	0.28	0.01	0.40	25.7	50
Zn	182.26	42.58	93.70	30.19	1.16	1.16	0.32	82.4	200
Pb	87.13	18.34	51.58	19.42	0.04	-1.21	0.38	29.3	250
Cd	0.076	0.003	0.013	0.01	5.06	33.75	0.72	0.133	1
As	18.91	3.18	6.32	2.59	2.70	10.20	0.41	13.3	20
Hg	0.307	0.074	0.148	0.04	1.75	5.14	0.28	0.102	1
pH	8.95	5.23	7.93	0.94	-1.20	0.55	0.12	—	—

Notes: 1) Background value of farmland soil in Guizhou; 2) Grade II Standard according to the National Soil Environmental Quality Standard (GB15618-1995) (pH > 7.5)

Table 3: Correlation coefficients of metals in soil.

	Ni	Cr	Cu	Zn	Pb	Cd	As	Hg
Ni	1							
Cr	0.077	1						
Cu	0.138	0.112	1					
Zn	-0.089	0.018	0.251*	1				
Pb	-0.202	0.017	-0.133	0.262*	1			
Cd	0.332**	0.109	0.17	0.256*	-0.051	1		
As	0.234	0.13	0.278*	0.253*	-0.148	0.559**	1	
Hg	0.198	0.059	0.13	0.233	-0.151	0.504**	0.281*	1

Notes: ** indicates a significant correlation at the 0.01 (bilateral) level, and * indicates a significant correlation at the 0.05 (bilateral) level.

Based on results of principal component analysis on heavy metals in farmland along the Wuma River, the chi-square value of the Bartlett spherical test was 76.518, and the degree of freedom df was 32 (usually $df = 30$, so it had strong reliability). Therefore, the principal component analysis could be made. Table 4 shows that the variance contribution rate of principal component 1 is 29.924%. The positive load coefficients of Cd, As and Hg in principal component 1 are larger, and there is a significant correlation between Cd and As, Cd and Hg ($P < 0.01$), indicating that Cd, As and Hg may have similar sources. The variance contribution rate of principal component 2 is 17.165%. The positive load coefficients of Pb and Zn are larger, and the correlation between Pb and Zn is 0.05 in terms of confidence level. The variance contribution rate of principal component 3 is 12.661%. The

larger positive loads of Cr and Cu show that the enrichment of the same principal component element comes from the same source.

According to the above statistical results (Table 2), the contents of Cd, As and Hg are not significantly different from the background values of soil in Guizhou Province. Therefore, it can be inferred that principal component 1 may be a natural source. The reason is that affected by karst geological origin, the Wuma River Basin has higher geological background contents of Cd, As, and Hg than other elements (Lian 2010). They all originate from the parent material of soil formation and are controlled by soil geochemistry. The average contents of Pb and Zn exceed the background values of soil. The contents of Cr and Cu greatly exceed the standard in some places. Therefore, principal components 2 and

Table 4: Analysis result of principal components of heavy metals in soil.

Items	Principal component 1	Principal component 2	Principal component 3
Ni	0.479	-0.499	-0.01
Cr	0.229	0.012	0.795
Cu	0.472	0.087	0.459
Zn	0.414	0.745	-0.048
Pb	-0.215	0.748	-0.015
Cd	0.816	0.039	-0.218
As	0.754	0.022	0.036
Hg	0.661	-0.001	-0.343
Eigen value	2.394	1.373	1.013
Variance concentration rate (%)	29.924	17.165	12.661
Cumulative variance contribution rate (%)	29.924	47.089	59.750

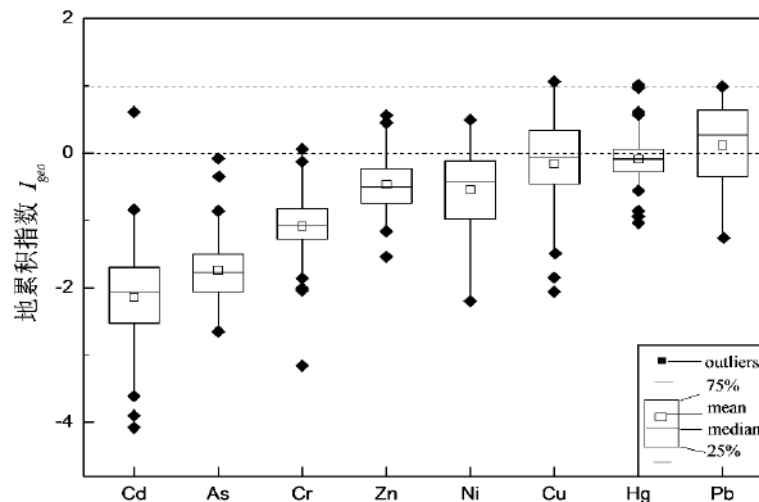


Fig. 2: The map of heavy metals of the index of geo-accumulation in the Wuma river.

3 may be influenced by artificial sources. Coastal farmland mainly depends on the Wuma River for irrigation. However, in the coastal area of the Wuma River, there is Tonglong Coal Mine, Sanyuan Coal Mine, and small-scale Pb-Zn Mine, etc. The waste residue produced in the process of mining and smelting combustion will bring about pollution in the rivers and coastal soil. In addition, due to the narrow landscape, No. 208 Provincial Road and No. 324 Village Road are close to the river coast. The wear and tear of vehicles and exhaust emissions will lead to the pollution of Pb and Zn in the farmland soil. Therefore, it is presumed that principal component 2 mainly comes from mineral mining and smelting, waste residue accumulation, irrigation, and transportation. Previous studies have shown that waste accumulation and incineration, transportation, and unreasonable agricultural activities may lead to the pollution of Cr and Cu (Zhao et al. 2015). Wuma Town in the middle and lower reaches of the Wuma River and the coastal villages in the upper reaches do not have a perfect waste treatment system. As residents along the river dump wasted pesticide bottles directly in the river or set them aside in the river bed for incineration, the river water and the surrounding environment are seriously polluted. At the same time, Cr and Cu have been accumulated in the farmland soil after river irrigation. Therefore, principal component 3 may be presumed to be mainly derived from the dumping and incineration of domestic waste by coastal residents, and unreasonable agricultural operations.

Assessment on Heavy Metal Pollution in Farmland Soil

The results of the geo-accumulation index (I_{geo}) of 8 heavy metals in farmland soils of the Wuma River Basin are shown in Fig. 2. According to the average of I_{geo} , 8 heavy metals are ranked as follows: I Pb>I Hg>I Cu>I Ni>I Zn>I Cr>I As>I Cd. Except for $I_{geo}>0$ of Pb which had no-to-moderate pollution, the I_{geo} of other heavy metals was less than 0 and in a clean level. Several locations of Pb, Hg, and Cu $I_{geo}>1$ had moderate pollution, indicating that there was point source pollution in farmland soil in the basin.

According to statistical results of the Nemeru comprehensive pollution index of eight heavy metals in farmland soil of Wuma River Basin (Table 5), the p -value of Cd was under the warning level, indicating no pollution ($p < 1$). Cr, Zn, and Ni were slightly polluted ($1.0 < p \leq 2.0$), while Hg, Cu, and Pb were moderately polluted ($2.0 < p \leq 3.0$). Nemeru comprehensive pollution index also takes into account the average and maximum values of single factor pollution index, so it can highlight the role of heavy metal pollutants (Wang et al. 2012). However, the evaluation results of the Nemeru comprehensive pollution index basically conform to the cumulative evaluation results.

After calculation on E_r^i for single potential ecological hazard index for heavy metals in farmland soil along the Wuma River (see Fig. 3), the average potential hazard index of eight heavy metals was ranked as Hg > Pb > Cu > Ni > As > Cd

Table 5: Nemeru comprehensive polluted index of heavy metals in soil.

Heavy metals	Cd	As	Cr	Zn	Ni	Hg	Cu	Pb
Comprehensive polluted of P value	0.41	1.06	1.22	1.76	1.68	2.36	2.43	2.44

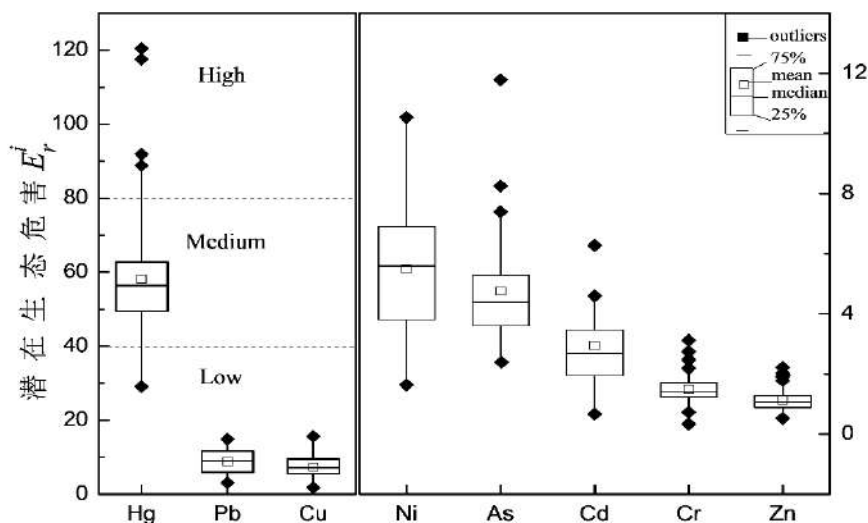


Fig. 3: The map of single potential ecological hazard indexes of heavy metals in soil.

> Cr > Zn from maximum to minimum amount. According to the risk level of ecological hazards, the average potential hazard index of Hg was more than 40 and was at moderate risk. The E_r^i value of some sample points was between 80 and 160, indicating strong ecological hazards. The E_r^i values of the other 7 heavy metals, Pb, Cu, Ni, As, Cd, Cr, and Zn were 8.80, 7.39, 5.49, 4.76, 2.94, 1.49, and 1.14, respectively, so it can be seen that all the E_r^i values were less than 40, and at a slight potential hazard level. The comprehensive index RI of potential ecological hazards of heavy metals in farmland soils in the research area ranged from 56.34 to 183.59, with an average value of 90.21, showing a slight potential ecological hazard as a whole.

After integration of 3 evaluation methods, it was concluded that the accumulative degree of Pb, Cu, and Hg in farmland soil and the comprehensive pollution index of Nemerow were higher in the research area. Although Pb and Cu were highly contaminated, the potential hazards caused by their toxicity were relatively low. Hg had a low pollution degree but relatively high potential toxicity. The pollution degree of Cr and Zn was higher than their potential toxicity.

Potential ecological hazard coefficients are slightly different from the results of the geo-accumulation index method. The reason is that the two evaluation methods have different focuses. The geo-accumulation index method mainly targets the influence of geochemical behavior, emphasizing the influence of exogenous sources on the enrichment of heavy metals through the anthropogenic and natural background values of heavy metals (Yu et al. 2013). In addition to the contents of heavy metals, the ecological hazard index also takes into account the varied environmental toxicity among different heavy metals, but it emphasizes more on the ecological risk of heavy metals and therefore can bring much healthier ecosystems. It is thus clear that the combination of various evaluation methods can provide a more comprehensive and reasonable understanding of heavy metal pollution and hazards in farmland soils in the research area.

CONCLUSION

Through the test, analysis, and evaluation on heavy metal pollution in farmland soil along the Wuma River, the following main conclusions are drawn:

1. In terms of the contents of heavy metals in farmland soil, the average contents of Ni, Cu, Zn, Pb, and Hg exceeded the background values of 9.82%, 47.80%, 13.72%, and 76.06% in Guizhou Province, respectively. Therefore, it can be concluded that all these heavy metals tended to accumulate, but the average contents of all heavy metals did not exceed the limit of the national grade II soil environmental quality standard.

2. The analysis of results of principal components show that Cd, As and Hg mainly come from natural sources and are influenced by geochemistry, with higher background values. Pb and Zn pollution is mainly because of mineral mining and smelting, waste residue accumulation, irrigation, and transportation. The enrichment of Cr and Cu may mainly come from dumped domestic waste, waste incineration from coastal residents, and unreasonable agricultural activities.
3. The geo-cumulation evaluation results showed that $I_{Pb} > I_{Hg} > I_{Cu} > I_{Ni} > I_{Zn} > I_{Cr} > I_{As} > I_{Cd}$. Among them, Pb was in no-to-moderate pollution, and I_{geo} of the rest of heavy metals was in clean level. Pb, Hg, and Cu pollution could be observed in some places. The results of the Nemerow comprehensive pollution index showed that As, Cr, Zn, and Ni were slightly polluted, while Pb, Hg, and Cu were moderately polluted. The calculation of the ecological hazard coefficient showed that the overall ecological risk was mild. The risk of Hg was moderate. At the same time, the potential ecological hazards of 8 heavy metals were ranked as Hg > Pb > Cu > Ni > As > Cd > Cr > Zn from strong to weak level.
4. At present, despite relatively low ecological hazards of the Wuma River Basin, the awareness of relevant departments are expected to be aroused for establishing and perfecting ecological protection measures in the mining areas of the Wuma River Basin, strengthening environmental protection training for coastal residents, properly solving the problems of random stacking of open-pit coal slag and pesticide residue pollution, and improving the centralized treatment system of coastal production and domestic waste. Only in this way, can the ecological environment of the Wuma River Basin develop in a more positive direction.

ACKNOWLEDGEMENT

This work was supported by The Key Project of Science and Technology Foundation, Guizhou Province (Qian Sci. Co. JZ, [2014], NO.2012), Guizhou Provincial Science-Technology Support Program, Guizhou Province (Qian Sci. Co.[2017], No.2580), and Technology Foundation, Guizhou Province (Qian Sci. Co., [2019], NO.1231).

REFERENCES

- Aguiguri, M., Memetilson, E., Eniwal, M., Anival, M., Maituoheti, A. and Ma, G.F. 2017. Heavy metal pollution and potential ecological risk of cultivated land in Oasis downstream of Kaidu river. *J. Acta Entiae Circumstantiae.*, 37(6): 2331-2341.
- Bao, S.D. 2007. Analysis of Soil Agrochemical. China Agricultural Press, Beijing. (in Chinese).

- Chen, Y.Y., Tang, M.Y., Wang, S.T., Wang, Q., Zhan W.X. and Huang G. 2016. Evaluation of heavy metal pollution in farmland soils in China based on Bibliometrics. *J. Chinese Soil Sci.*, 47(1): 219-225. (in Chinese).
- Guo, C.H., Tu, W.J., Wang, P.C., Huang, B., Xiao, X.Y. and Xue, Q. H. 2017. Distribution characteristics and potential ecological risk assessment of heavy metals in farmland soils along rivers in typical lead-zinc mining areas. *J. Agro-Environ. Sci.*, 36(10): 2029-2038. (in Chinese).
- Hkanson, L. 1980. An ecological risk index for aquatic pollution control: A sedimentological approach. *J. Water Res.*, 14(8):975-1001.
- Hu, M. 2014. Distribution characteristics and pollution assessment of heavy metals in farmland soils of Dali county. *J. Resour. Environ. Arid Areas*, 28(1): 79-84.
- Jin, X.Q., Wang, P., Guo, B.L., Guo, J. and Zhou, D.D. 2017. Spatial distribution and pollution assessment of Pb, Zn, and Cd in small-scale farmland soils: A farmland along the Bijiang River in Yunnan province as an example. *J. Chinese Environ. Eng.*, 11: 6190-6195. (in Chinese).
- Li, Y.M., Ma, J.H., Liu, D.X., Sun, Y.L. and Chen, Y. F. 2015. Heavy metal pollution and potential ecological risk assessment of urban soil in Kaifeng. *J. Environ. Sci.*, (3): 1037-1044. (in Chinese).
- Lian, B. 2010. Microbial action in weathering and soil formation of carbonate rocks. *J. Bull. Mineral. Petrol. Geochem.*, 29(1): 52-56.
- Marrugo-Negrete, J., Pinedo-Hernández, J. and Díez, S. 2017. Assessment of heavy metal pollution, spatial distribution, and origin in agricultural soils along the Sinú River Basin, Colombia. *J. Environ. Res.*, 154:380-388.
- Massadeh, A., Alsharif, L., Dalaleh, R. and Hassan, M. 2006. Analysis of lead levels in local Jordanian and imported sheep meat and organs Using atomic absorption spectrometry. *J. Environ. Monit. Assess.*, 115(1/2/3): 87-93.
- Perveen, I., Raza, M.A., Sehar, S., Naz, I., Young, B. and Ahmed, S. 2017. Heavy metal contamination in water, soil, and milk of the industrial area adjacent to Swan River, Islamabad, Pakistan. *J. Human Ecol. Risk Assess.*, (1)-22.
- Wang, J., Zhang, Y.X. and Gao X. 2012. Research progress and prospects of heavy metals in urban surface dust. *J. Geog. Res.*, 31(5): 821-830. (in Chinese).
- Wang, Y.J., Liu, C., Zhou, D.M. and Chen, H.M. 2014. Objectively look at the present situation of soil environmental quality of cultivated land in China: Discussions and suggestions on relevant issues in the national bulletin of soil pollution investigation. *J. Agro-Environ. Sci.*, 33 (8): 1465-1473. (in Chinese).
- Wilding, L.P. 1984. Spatial Variability: Its Documentation, Accommodation, and Implication to Soil Surveys. In Nielson, C. and Bouma, D.R. (eds.), *Soil Spatial Variability. Proceedings of a Workshop of the ISSS and the SSSA.*, Las Vegas PUDOC, Wageningen, pp. 166-193.
- Wu, X. L., Yang, Y. L., Xu, Q., Huang, Y.Y., Lu, G. H., He, J. and Liu, X. D. 2011. Assessment of heavy metal pollution in surface soil of farmland along rivers and irrigation canals in Shenyang. *J. Agro-Environ. Sci.*, 30(2): 282-288.
- Yu, Y., Gao, H.C., Ma, J.H., Li, Y.X. and Kong, Y.H. 2013. Analysis and evaluation of heavy metals in the soil of Chaohu river basin in Miyun county. *J. Environ. Sci.*, 34(9): 3572-3577.
- Zang, X.H., Lu, Y.T., Yao, H., Zhang, S.C. and Jiang, X.X. 2016. Impact of urbanization on the distribution of heavy metals in soils of Shenyang new area and risk assessment. *J. Agro- Environ. Sci.*, 35 (3): 471-477. (in Chinese).
- Zeng, X.B., Su, S.M. and Ma, S.M. 2010. Heavy metal cycling and regulation in farmland ecosystem. *J. Chinese Appl. Ecol.*, 21(9): 2418-2426. (in Chinese).
- Zhan, Y.Z., Jiang, X., Chen, C.X., Gao, H.G., Jin, X.C., Li, C. and Zhao, Z. 2011. Spatial distribution characteristics and pollution assessment of heavy metals in sediments of southwestern Taihu Lake. *J. Res. Environ. Sci.*, 24(4): 363-370. (in Chinese).
- Zhang, Y. X., Wang, J., Qin, F.X. and Zhang, H. 2012. Identification and comparison of sources of heavy metals in road dust and soil in Guiyang. *J. Acta Scientiae Circumstantiae.*, 32(1): 204-212.
- Zhao, X., Huang, Y., Li, J., Chen, G., Song, L.H., Lu, K.D. and Ning, C. 2015. Content level, spatial distribution, source, and potential ecological risk assessment of heavy metals in the soil around large waste incineration plants. *J. Ecol. Environ. Sci.*, 24(6): 1013-1021. (in Chinese).
- Zhou, H.B., Jiao, Y.M., Shi, Z.T., Ming, Q. and He, L. 2008. Magnetometric analysis and heavy metal pollution assessment of farmland soil along the Bijiang river in Yunnan. *J. Agro-Environ. Sci.*, 27(4): 1586-1591.



Study on the Joint Toxicity of Multi-component Mixtures of Quaternary Ammonium Compounds

Y. Jin*, L.Y. Mo*(**)(***)†, L.T. Qin*(**)(***) and J.F. Dai*(**)(***)

*College of Environmental Science and Engineering, Guilin University of Technology, Guilin 541004, China

**Technical Innovation Center of Mine Geological Environmental Restoration Engineering in Southern Karst Area, MNR, Nanning 530023, China

***Guangxi Collaborative Innovation Center for Water Pollution Control and Water Safety in Karst Area, Guilin University of Technology, Guilin 541004, China

† Corresponding author: Ling-Yun Mo; molingyun123@126.com

Nat. Env. & Poll. Tech.
Website: www.neptjournal.com

Received: 20-11-2020

Revised: 02-03-2021

Accepted: 24-04-2021

Key Words:

QACs

Multicomponent mixtures

Joint effects

Non-equitoxic ratio

ABSTRACT

Pollutants generally exist as mixtures in the environment. Their cumulative toxicity and toxicity interactions are potential risks. Therefore, this study aimed to examine the variation of joint toxicity of a multi-component mixture system, which consisted of six common quaternary ammonium salt surfactants in the environment, on *Vibrio qinghaiensis* sp.-Q67 (Q67). *Vibrio qinghaiensis* sp.-Q67 (Vqin-Q67) is a freshwater luminescent bacterium that continuously emits blue-green light (485 nm). The bacterium has been widely used for detecting toxic contaminants. In the mixture system, the luminescent toxicity of each component of the mixture to Q67 was determined by the microplate toxicity analysis method, and the toxicity interaction of the mixture was determined by the toxicity unit method (TU). The combined toxicity of the mixture system was investigated from four aspects, including the number of components, key components, concentration (toxicity) ratio, and exposure time. The results showed that the combined toxic effect of the same mixture system tends to be an additive effect with the increase of the number of components. The combined toxicity of the mixture system was close to that of the key components. Antagonism was presented in the equal toxicity mixture, while synergism was presented in the non-equal toxicity mixture. The combined toxic effect of the multi-component mixture system was not only related to the concentration of the pollutant but also related to the exposure time of the pollutant.

INTRODUCTION

Quaternary ammonium compounds (QACs) are widely used as surfactants and disinfectants (Luo et al. 2020). It has a global output of more than 500000 tons·year⁻¹ and has been listed in the list of high-yield chemicals by the Organization for Economic Cooperation and Development (OECD 2004). They are widely used mainly as disinfectants, detergents, preservatives, and fabric softeners (Ruan et al. 2014, Oh et al. 2014, Zhang et al. 2015). Although surfactants have been widely used, most of the products have not been properly treated and discharged into the water body, resulting in serious water environmental pollution (Brycki et al. 2014, Jardak et al. 2016, Ostman et al. 2017). Surfactants are often detected in surface water at the concentration of $\mu\text{g}\cdot\text{L}^{-1}$ (Ferrer & Furlong 2001, Olkowska et al. 2013). Surfactants may threaten the aquatic ecosystems when they reach a certain concentration in the water body (Rosety et al. 2001, Kobuke 2002).

Contaminants are often present in the form of mixtures (Cipullo et al. 2019, Perez & and Hoang 2017). QACs

generally exist as mixtures in the environment (Kwon et al. 2019, Ruan et al. 2014, Zhang et al. 2015). Warne & Hawker (1995) studied a new hypothesis, the funnel hypothesis, which was derived to explain the variation in toxicity of equitoxic multicomponent mixtures of nonspecific toxicants (narcotics). Results showed that as the number of components in a mixture increases, the range of deviation from toxic additivity decreases. In addition to the number of components and the nature of the compound, the toxicity of the single component also has a large change in the combined toxicity effect (Li et al. 2017). Mixture systems of different components can be considered as one space, and mixtures of different mixture ratios are points dispersed in space (Liu et al. 2016a, Liu et al. 2016b). Therefore, the closer mixtures in this space have similar toxicity because their mixing ratios are similar to the concentration levels (Qu et al. 2019), and most studies have shown that component concentration ratio changes also have an effect on the combined toxicity of the mixture (Feng et al. 2017, Xu et al. 2018, Baek et al. 2019). In addition, considerable attention has been given to

the impact of the exposure period on pollutant toxicities. In the standard toxicity test of algae, bacteria, and large cockroaches, prolonging the exposure time will increase the toxicity of poisons (Vannini et al. 2018, Mo et al. 2020a, Mo et al. 2020b, Hatano & Shoji 2010). Therefore, it can be found that the number of components in a mixture, the component properties (key components), the concentration (toxicity ratio), and the exposure time are the four main factors affecting the combined toxicity effect of the mixture.

However, most of the current research concentrated on the compound system of equal toxicity ratio (Li et al. 2017, Feng et al. 2017, Xu et al. 2018). There is still a lack of a systematic and comprehensive study on the variation law of the combined toxicity effect of the pollutant with complex toxic mechanism and non-toxic ratio mixture system. Therefore, in this study, the quaternary ammonium salt surfactant was used as the research object to determine the combined toxicity effect of a series of mixtures, including binary, ternary, quaternary, five-component mixture, etc.) components. The main factors affecting the toxic effects of the mixture were further revealed. The variation of the toxic effects of the multi-component mixtures was investigated from four aspects: the number of components, the key components, the toxicity (concentration) ratio, and the exposure time.

MATERIALS AND METHODS

Main Reagent

The physicochemical properties of the six quaternary ammonium surfactants are shown in Table 1. The stock solution was prepared using Milli-Q ultrapure water and stored in a refrigerator at 4 °C.

Toxicity test and Mixture Design

The freeze-dried *Vibrio qinghaiensis* sp.-Q67 (Q67) was purchased from Beijing Hamamatsu Corp., Ltd. (Beijing, China). The formulations of liquid medium, concentrated

medium, and solid medium were described in the literature (Yu et al. 2014). Toxicity was determined by microplate toxicity analysis (Yuan et al. 2011).

To investigate the effects of the number of components on the combined toxicity effect, we designed a series of mixture systems with equivalent effect concentration ratios at multiple equal toxicity concentration ratios according to the toxicity data of single QACs compounds. The toxicities of the mixtures were determined by using Q67 as the indicator organism, and the combined toxicities of the mixtures were calculated by using the *TU* method.

As early as 1965, Sprague & Ramsay (1965) proposed the concept of toxicity unit (*TU*) to study the effects of Cu-Zn interaction on the growth and development of Atlantic salmon larvae. In 1975, Anderson and Webbe (1975) revised, improved, and developed this concept.

$$TU_{\text{sum}} = \frac{C_A}{EC_{50-A}} + \frac{C_B}{EC_{50-B}} + \dots + \frac{C_i}{EC_{50-i}} \quad \dots(1)$$

C_A and C_B are the concentrations of the component A and B in the mixture system when the mixture is 50% inhibited, and EC_{50-A} and EC_{50-B} are the concentrations when a single compound is 50% inhibited alone. $TU_{\text{sum}} = 1.00 \pm 0.20$ indicates that the combined toxicity effect is added, $TU_{\text{sum}} < 0.80$ indicates synergism, and $TU_{\text{sum}} > 1.20$ indicates antagonism (Broderius et al. 1995).

RESULTS AND DISCUSSION

Variation of Toxicity Interaction of QACs with the Number of Components

Before determining the toxicity of the mixture, the acute toxicity of a single compound to Q67 was first determined and we obtained the EC_{50} of a single compound, which was shown in Table 1:

The toxicity of the mixture was measured according to the toxicity assay method, the combined toxicity effect was

Table 1: Basic Information and pEC_{50} of Single Compound.

No.	Abbr ^a	Compound	CAS	MW	Purity (%) ^b	Sources ^c	pEC_{50} ^d
1	BLB	C ₂₁ H ₃₈ BrN	7281-04-1	384.44	AR	TRC	5.130
2	TLB	(CH ₃ CH ₂) ₄ NBr	71-91-0	210.16	AR	TRC	0.876
3	BLC	C ₁₃ H ₂₂ ClN	56-37-1	227.77	AR	TRC	2.251
4	CTE	C ₁₇ H ₃₈ BrN	1119-97-7	336.39	AR	TRC	4.885
5	TAC	C ₁₆ H ₃₆ ClN	214-195-7	277.92	AR	TRC	4.795
6	DTC	C ₁₅ H ₃₄ N-Cl	112-00-5	263.89	AR	TRC	2.724

a Abbreviation for a single compound name; b: Analytical purity.

c Truth and Reconciliation Commission of Canada; d: Negative logarithm of 50% effect concentration.

calculated using TU_{sum} . The results are shown in Table 2 and Fig. 1.

The binary equivalent concentration ratio (EC_{50}) of BLB-TLB was used as the initial mixture, and different QACs were added into the binary mixture according to the equivalent concentration ratio (EC_{50}), in turn, to form a series of multi-component equivalent concentration ratio mixtures (Table 2). Since it was difficult to determine the single toxicity of 22 compounds and the combined toxicity of their mixtures simultaneously, the 22 multi-component mixtures used in this study were all 22-component mixtures. As indicated in Table 1 and Fig. 1a, the combined toxic effect of the multivariate isotopic concentration ratio changed from antagonistic to additive effect with the consecutive addition of the QACs chemical for that binary isotopic system of BLB-TLB as the

initial system. Fig. 1b was a histogram of the mixture, the original quaternary mixing system was a multi-hybrid system in which toxic effects were antagonistic. The combined toxic effects of a mixing system tend to have an additive effect as the number of components in the combination increases.

The above results showed that the mixture system had a similar trend when the mixture was mixed with an equal effect concentration ratio for the same system of pollutants. The antagonistic effect increased first and then decreased gradually to concentration addition with the increase of component. For example, as shown in Fig. 1a, the apparent joint toxicity of the six-membered mixture was antagonism ($TU_{sum}=2.53\pm 0.05$) and the joint toxicity of the 22-membered mixture was additive ($TU_{sum}=0.81\pm 0.05$), which indicated that the number of components mixture system had an effect

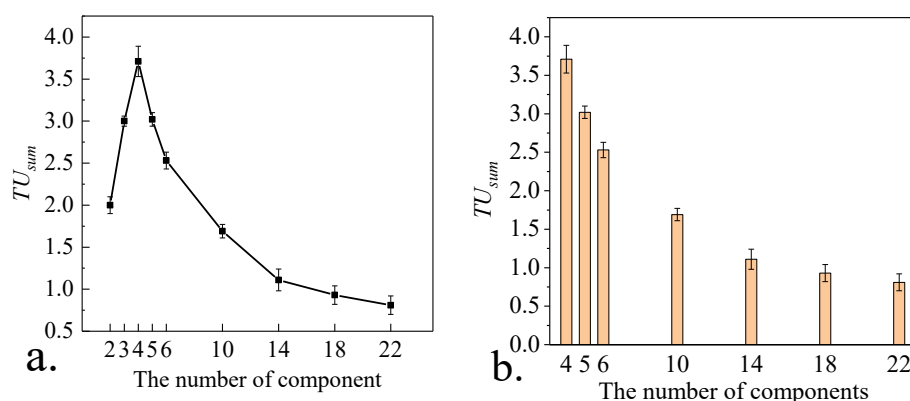


Fig. 1: Effect of Component Number on the Toxicity Effect of Multi-Equivalent Mixture System with Equivalent Effect Concentration Ratio (EC_{50}). (a is CRC of the mixture; b is a histogram of the mixture).

Table 2: Composition of compound pollutants and determination results.

Number of components	1	2	3	4	5	6	TU_{sum}	95%CI ^e
2	BLB	TLB					2	1.95 ~2.05
3	BLB	TLB	BLC				3	2.97 ~3.03
4	BLB	TLB	BLC	CTE			3.71	3.62 ~3.80
5	BLB	TLB	BLC	CTE	DTC		3.02	2.98 ~3.06
6	BLB	TLB	BLC	CTE	DTC	TAC	2.53	2.48 ~2.58
10a	BLB	TLB	BLC	CTE	DTC	TAC	1.69	1.64 ~1.72
14b	BLB	TLB	BLC	CTE	DTC	TAC	1.11	1.08 ~1.21
18c	BLB	TLB	BLC	CTE	DTC	TAC	0.93	0.87 ~0.98
22d	BLB	TLB	BLC	CTE	DTC	TAC	0.81	0.76 ~0.86

a Includes single EC_{50} BLB+TLB and four 2-fold EC_{50} BLC+CTE+DTC+TAC ($2+4\times 2=10$);

b Includes single EC_{50} BLB+TLB and four 3-fold EC_{50} BLC+CTE+DTC+TAC ($2+4\times 3=14$);

c Includes single EC_{50} BLB+TLB and four 4-fold EC_{50} BLC+CTE+DTC+TAC ($2+4\times 4=18$);

d Includes single EC_{50} BLB+TLB and four 5-fold EC_{50} BLC+CTE+DTC+TAC ($2+4\times 5=22$).

e 95% Confidence interval. (the same below)

on the joint toxicity of the mixture system. Therefore, these components can be considered as the key components to determine the joint toxic effects of multi-component mixtures.

Variation of Toxicity Interaction of QACs with Key Components

Fig. 2 showed the effects of key components of the isotope ratio mixture on the TU values. In Fig. 2a, the combined toxic effects of adding 2-fold TAC and 2-fold DTC became stronger. The experimental results of Fig. 2(b-d) further validated the joint toxic effects of binary, ternary, and quaternary mixtures with increasing composition.

The experimental results of Fig. 2(b-d) further validated the joint toxic effects of binary, ternary, and quaternary mixtures with increasing composition. For the binary mixture of BLB and TLB (Fig. 2b), the antagonistic effect was weakened by the addition of BLC, because the combined effect of BLB or TLB in the BLC and the original binary system is stronger than that of BLB and TLB. For the binary mixture of BLB and BLC, the antagonistic effect was weakened by adding TLB, because TLB and BLB could produce a strong antagonistic effect, which was stronger than the concentration addition effect of the original binary mixture of BLB and BLC. As shown in Fig. 2c and Fig. 2d, except for the BLB+BLC+CTE, isovolumetric mixing in Fig. 2c presented a concentration addition effect, and the BLB+BLC+CTE+DTC isovolumet-

ric mixing in Fig. 2d induced a synergistic effect, which was similar to the other mixtures in Fig. 2a.

Fig. 2a showed that the results of this study were not consistent with the funnel hypothesis proposed by Warne and Hawker (2010). The results showed that not only the number of components in the mixture system but also the properties of components (especially the key components) have an effect on the joint toxicity. In these multi-component mixtures, the components that produce the strongest synergistic effects in binary mixtures could be considered as the key components.

It could be seen from Table 3 and Fig. 2 that the combined toxic effects of the mixture system could be enhanced when the newly added components and one of the original components in the system had strong antagonistic effects. The components with strong combined effects could be regarded as the key components to determine the joint toxic effects of multi-component mixtures. The contribution of these key components to the joint toxic effects of multicomponent mixtures was greater than that of other components. The results were showed that the joint toxic effects of multi-component mixtures were close to the joint toxic effects of the key components. In other words, the key components that determine the combined toxic effect of multi-component mixed systems can be determined by comparing the toxic effects of a series of mixtures.

Table 3: Composition of compound pollutants and determination results.

Mixture	Volume ratio	EC ₅₀ (mol.L ⁻¹)	-lgEC ₅₀ (mol.L ⁻¹)	95%CI	TU _{sum}	Toxic interaction
BLB+TLB	1:1	1.22E-01	0.91	0.88~0.95	1.37	ANT
BLB+TLB+BLC	1:1:1	8.61E-02	1.06	1.00 ~1.13	1.27	Slight ANT
	2:1:1	7.53E-02	1.12	1.08 ~1.17	1.39	ANT
BLB+TLB+BLC+CTE	1:1:1:1	1.07E-01	0.97	0.89 ~1.06	1.96	ANT
	4:1:1:1	6.28E-02	1.20	1.11 ~1.30	1.85	ANT
BLB+TLB+BLC+CTE+DTC	1:1:1:1:1	7.27E-02	1.14	1.08 ~1.19	1.61	ANT
BLB+TLB+BLC+CTE+DTC+TAC	1:1:1:1:1:1	2.22E-02	1.65	1.63 ~1.67	0.57	SYN
BLB+TLB+BLC+CTE+DTC+2TAC	1:1:1:1:1:2	5.62E-02	1.25	1.22 ~1.28	0.52	SYN
BLB+TLB+BLC+CTE+2DTC+2TAC	1:1:1:1:2:2	5.67E-02	1.25	1.19 ~1.30	0.48	SYN
BLB+BLC	1:1	2.92E-03	2.53	2.50 ~2.57	1.04	ADD
BLB+BLC+CTE	1:1:1	1.51E-03	2.82	2.79 ~2.85	0.80	Slight ADD
BLB+BLC+CTE+DTC	1:1:1:1	6.10E-04	3.21	3.17 ~3.26	0.43	SYN
BLB+TLB+CTE	1:1:1	9.15E-02	1.04	1.00 ~1.08	1.38	ANT
BLB+TLB+CTE+DTC	1:1:1:1	7.77E-02	1.11	1.05 ~1.16	1.46	ANT
BLB+TLB+BLC+DTC	1:1:1:1	8.65E-02	1.06	1.01 ~1.12	1.59	ANT
TLB+BLC+CTE+DTC	1:1:1:1	9.68E-02	1.01	0.97 ~1.06	1.78	ANT

ANT: Antagonism (the same below); ADD: Addition (the same below); SYN: Synergism (the same below)

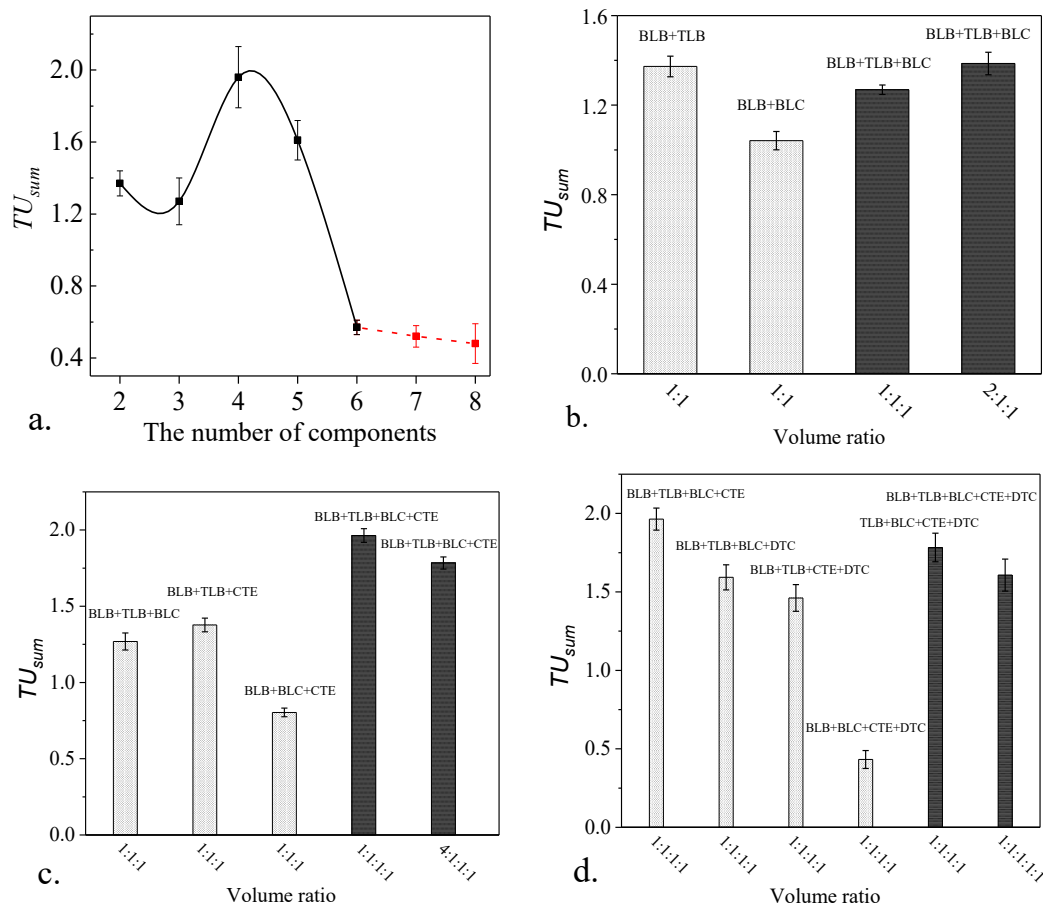


Fig. 2: Effect of key numbers on joint toxicity of mixed systems with multiple equal toxicity ratios.

Variation of Mixed Toxicity Effect of QACs Mixtures with Mixture Concentration

The combined toxicity effects of binary mixture systems with the equal effect concentration ratio are shown in Fig. 3, Fig. 4, and Table 4.

In Fig. 3a, the toxic effects of BLB+TLB mixture except EC₅ mixture were additive effect, and the other equivalent

concentration ratios mixture were antagonistic effects. In Fig. 3b, the toxic effects of BLC-CTE mixed with EC₅ were additive, and the other equivalent concentration ratios were antagonistic. In Fig. 3c, the equivalent concentration of TAC+DTC was antagonistic at the concentration of EC₅, EC₁₀, EC₂₀, EC₃₀, EC₄₀, and EC₅₀, but all the TU_{sum} of the mixtures of EC₅ were 1.62, and the TU_{sum} of the other mixtures was 1.35 ~ 1.42. In Fig. 3b, BLC+CTE mixture

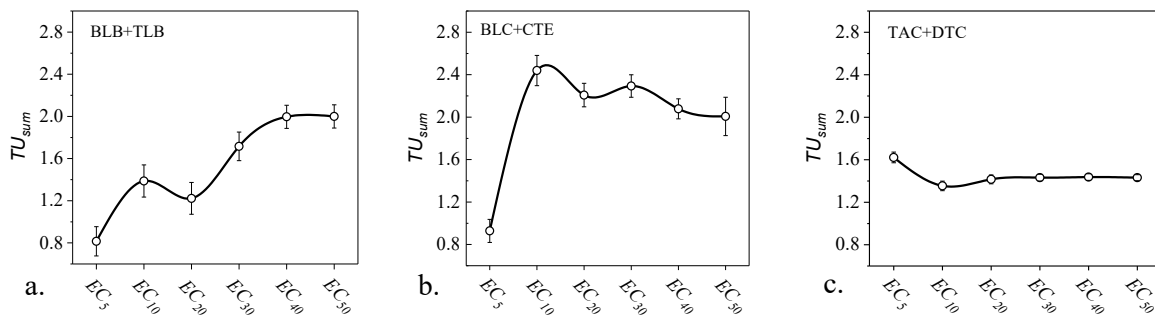


Fig. 3: Effects of mixing with different equivalent concentration ratios on joint toxicity of binary mixtures.

Table 4: Composition and joint toxicity of binary compounds.

Mixture	Equal effect concentration ratio	EC_{50} (mol/L)	$-\lg EC_{50}$ (mol/L)	95% CI	TU_{sum}	Toxic interaction
BLB+TLB	EC_5+EC_5	7.50E-02	1.12	1.10 ~1.15	0.81	Slight ADD
	$EC_{10}+EC_{10}$	1.14E-01	0.94	0.86 ~1.02	1.22	Slight ANT
	$EC_{20}+EC_{20}$	8.98E-02	1.05	1.00 ~1.09	1.39	ANT
	$EC_{30}+EC_{30}$	1.19E-01	0.93	0.85 ~1.00	1.72	ANT
	$EC_{40}+EC_{40}$	1.34E-01	0.87	0.82 ~0.93	1.96	ANT
	$EC_{50}+EC_{50}$	1.33E-01	0.88	0.83 ~0.93	2.00	ANT
BLC+CTE	EC_5+EC_5	2.35E-03	2.63	2.56 ~2.70	0.93	ADD
	$EC_{10}+EC_{10}$	6.36E-03	2.20	2.17 ~2.23	2.44	ANT
	$EC_{20}+EC_{20}$	5.94E-03	2.23	2.18 ~2.27	2.21	ANT
	$EC_{30}+EC_{30}$	6.28E-03	2.20	2.17 ~2.24	2.29	ANT
	$EC_{40}+EC_{40}$	5.77E-03	2.24	2.19 ~2.28	2.08	ANT
	$EC_{50}+EC_{50}$	5.64E-03	2.25	2.16 ~2.34	2.01	ANT
TAC+DTC	EC_5+EC_5	2.16E-03	2.67	2.62 ~2.71	1.62	ANT
	$EC_{10}+EC_{10}$	1.80E-03	2.75	2.72 ~2.77	1.35	ANT
	$EC_{20}+EC_{20}$	1.87E-03	2.73	2.67 ~2.78	1.42	ANT
	$EC_{30}+EC_{30}$	1.89E-03	2.72	2.68 ~2.76	1.43	ANT
	$EC_{40}+EC_{40}$	1.89E-03	2.72	2.68 ~2.77	1.44	ANT
	$EC_{50}+EC_{50}$	1.88E-03	2.73	2.65 ~2.80	1.45	ANT

ANT: Antagonism (the same below); ADD: Addition (the same below); SYN: Synergism (the same below)

systems exhibited additive or antagonistic effects at equal toxicity ratios. It was clear from TAC+DTC in Fig. 3c that the antagonistic effect was present at an equal toxicity ratio. For these two-two mixed systems, their combined toxicity effects did vary with the toxicity ratios.

Fig. 4 showed six component mixtures of five QACs compounds (BLB, TLB, BLC, CTE, and DTC) as the volume ratio of the compounds changed. Fig. 4a showed a ternary mixture system composed of BLB, TLB, BLC, CTE, and DTC in the ratio 1:1:1, 2:1:1, and 4:1:1. It could be seen from the figure that the combined toxicities of the mixture of BLB+BLC+DTC, BLB+CTE+DTC, and BLC+CTE+DTC mixtures were synergistic effects, and toxic effects did not change with the volume change of a single component. The combined toxicity of the BLB+BLC+CTE mixture was additive and basically did not change with the volume change of a single component. The combined toxicity of the BLB+TLB+BLC mixture was concentration additive. The mixture toxicities of the BLB+TLB+CTE and TLB+BLC+CTE mixtures were antagonism at ratio 1:1:1 and became additive at ratio 4:1:1 with the change of volume ratio of a single component.

Fig. 4b showed three ternary mixtures of BLB, TLB, BLC, CTE, and DTC in 1:1:1, 1:1:2, and 1:1:4. The toxicity of the BLB+TLB+CTE mixture was antagonism, and TU_{sum} slightly changed with the increase of volume ratio of CTE, but it did not cause the change of mixture toxicity. The mixture toxicities of BLB+BLC+DTC and BLB+DTC+CTE were synergistic, and the synergistic effect of BLB+BLC+DTC increased slightly with the increase of DTC volume. Fig. 4c showed two ternary mixtures composed of BLB, TLB, BLC, and CTE of ratios 1:1:1, 1:2:1, and 1:4:1. The mixture toxicity of the BLB+TLB+BLC mixture was antagonistic. As the volume of TLB increases, the mixture toxicity tends to increase from antagonistic effect to additive effect. The mixture toxicity of the BLB+BLC+CTE mixture was the synergistic effect, and the synergistic effect was the strongest when the volume ratio was 1:2:1. Fig. 4d showed two ternary mixtures of BLC, CTE, TLB, and DTC in 1:1:1, 1:1:5, and 1:1:10. The toxicity of the TLB+BLC+CTE mixture tended to shift from synergistic to antagonistic as the CTE volume increased. With the increase of DTC volume, the TU_{sum} of the BLC+CTE+DTC mixture had no change. Therefore, the key component may be CTE.

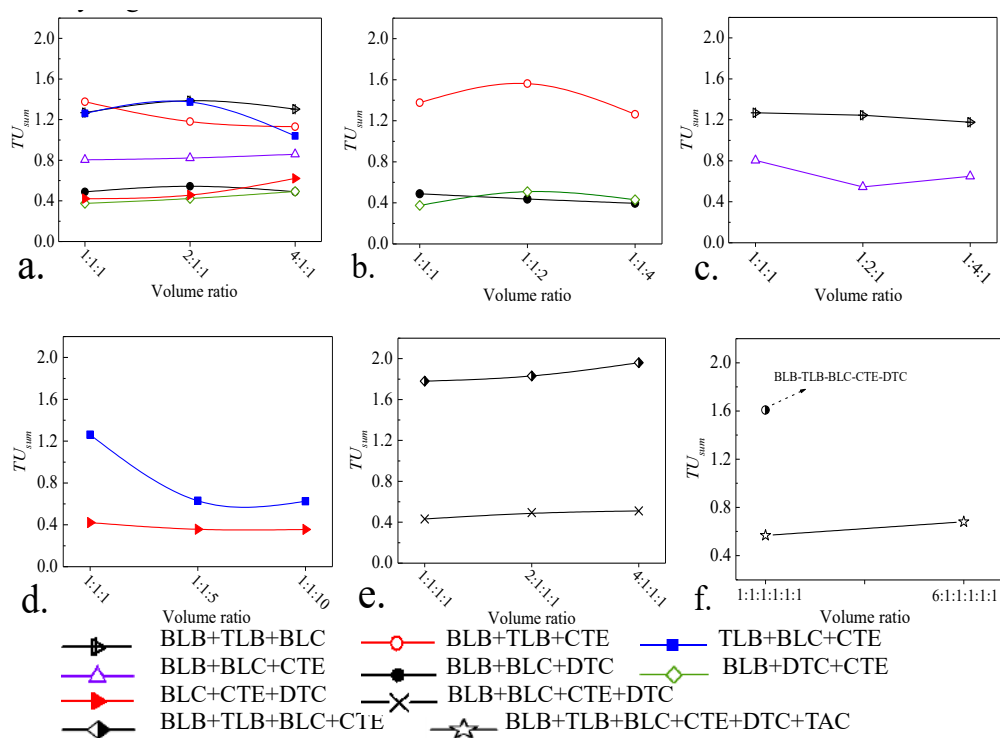


Fig. 4: Ternary and multivariate mixed equal volume ratio.

Fig. 4e shows two quaternary mixtures of BLB, TLB, BLC, CTE, and DTC in 1:1:1:1, 2:1:1:1, and 4:1:1:1. The mixture toxicity of the BLB+TLB+BLC+CTE mixture was antagonistic, and with the increase of BLB volume, the toxicity TU_{sum} had little change. The mixture of BLB+BLC+CTE was added into TLB, which made the mixture toxicity change from additive to antagonistic. The mixture toxicity of BLB+BLC+CTE+DTC was antagonistic. It was the synergistic effect, and TU_{sum} slightly increases with the increase of BLB volume. It could be seen that adding DTC to the BLB+BLC+CTE mixture could increase the toxicity of the mixture, while the toxicity of ternary mixture containing DTC did not change with the change of the volume of other components. It could be seen that DTC was the key component in any ternary mixture and quaternary mixture.

Fig. 4f showed six component mixture of ratios 1:1:1:1:1 and 6:1:1:1:1, and five-component mixture of ratio 1:1:1:1:1. It could be seen from the figure that with the increase of BLB volume, the toxicity interaction of the mixture basically had no change. Compared with Fig. 4e, it could be seen that TLB was added to the BLB+BLC+CTE+DTC mixture, and the toxicity interaction of the mixture changed significantly, that was, from synergism to antagonism. It could be seen that TLB may be the key component in the five component mixture. When DTC was added to the BLB+TL-

B+BLC+CTE mixture, the TU_{sum} of the mixture decreased slightly, but it was still antagonism. When TAC was added to the mixture of BLB+TLB+BLC+CTE+DTC, the TU_{sum} of the mixture interaction decreased significantly, that was, from antagonism to synergism.

It could be seen from Fig. 4 that with the shift of toxicity ratio, i.e. volume ratio, from isotoxicity to non-isotoxicity, its combined toxicity effect changes antagonism-concentration addition-synergy. The results show that the number of fraction items and key components mentioned above, and the toxicity ratio of the components in the mixture system also had an effect on the joint toxicity of the mixed system. Taking the mixture of TLB+BLC+CTE, BLB+BLC+CTE, and BLB+TLB+BLC+CTE in The toxic effect of a binary mixture containing BLC and CTE is $TU_{sum}=0.932.44$, increasing the BLB component was a ternary mixture, and the concentration additive effect of BLB and BLC+CTE ($TU_{sum}=0.80.86$) was greater than the existing combined toxicity effect of the binary mixed system and was increased based on the ternary mixture (see Fig. 4). The synergistic effect of DTC and BLC+CTE+BLB ($TU_{sum}=0.49\sim 0.51$) was greater than the existing combined toxic effect of the ternary mixed system. The toxic effect was enhanced after increasing DTC. However, for the toxic effect of the binary mixtures containing BLB and CTE ($TU_{sum}= 0.8 \sim 2.00$),

except EC_{50} , which is 0.8, it was 1.39 ~ 2.00. The combined toxicity of other mixtures was less than the existing effect of ternary mixtures (BLB+CTE+BLC) ($TU_{sum}=1.27\sim1.38$), so the increase of BLC enhanced the combined toxicity effect of the mixed system.

Variation of Mixture Toxicity of QACs with Different Exposure Time

Fig. 5 showed the change of combined toxic effect of five components (BLB+TLB+BLC+CTE+DTC) mixture system with exposure time. It was shown that the mixture system with equal effect concentration ratio EC_{50} and EC_{10} was antagonistic effects. With the increase of exposure time (0.5h, 2h, 4h, 6h, 8h, 10h, and 12h), the toxic effect of EC_{50} mixture systems was gradually weakened. When the mixture was mixed according to EC_{10} , its toxic effect gradually weakened with the increase of exposure time, and it was the weakest when the exposure time was 4h.

As could be seen from Fig. 5, in the mixture system, it was found that the joint toxic effect of the multiple mixture system was not only related to the dose or concentration of pollutants but also related to the exposure time of pollutants.

Tendency Analysis of Mixed Toxic Effects of QACs

To further analyze the trend of joint toxic effects of multi-component mixtures, we converted the multi-component mixtures into corresponding fraction numbers based on the toxicity ratios of the multicomponent mixtures. For example, a ternary mixture with a toxicity ratio of 4: 1: 1 could be considered as a mixture of six components. Then, the relationship between the combined effect of the mixture and the purpose of the fraction could be obtained. As the purpose of the fraction increases, the possibility of antagonistic or synergistic effects increases gradually. However, it should be noted that it was very difficult to obtain a uniform critical number of components for different reaction-type mixtures. This was because the joint toxicity of the mixture was not

only related to the number of components, but also to the key components, toxicity ratio, and exposure time.

To summarize, those components which can produce strong combined effects were the key components to determine the combined toxic effects of the mixture system. Therefore, we used TU_{min} -binary to describe quantitatively the contribution of the key components in 3, 4- and 5-component mixtures to the mixture system. In the regions with large values of TU_{min} -binary and non-isotoxicity ratios, the joint toxic effects of multi-component mixtures tended to antagonistic effects. The joint toxic effects of multicomponent mixtures tend to have synergistic effects in the region where the values of TU_{min} -binary and non-isotoxic ratios were small because the joint toxic effects of multicomponent mixtures in this region were not determined by a single factor, but by a combination of multiple factors.

CONCLUSION

The results showed that the changes of joint toxic effects were mainly affected by four factors: the number of components, the properties of key components, concentration of components, and the exposure time. In general, the antagonism of the combined effect increased with the increase of the fraction when the newly added components had a strong combined effect with the existing components. On the contrary, if the added components can have a strong combined effect with the existing components, and this effect was much stronger than the toxic effect between the existing components, then the toxic effect of the mixture system would be enhanced with the increase of the new components.

ACKNOWLEDGEMENTS

The authors are especially grateful to the financial support from the National Natural Science Foundation of China (21667013), National Key Research and Development Program of China (2019YFC0507502), Natural Science Founda-

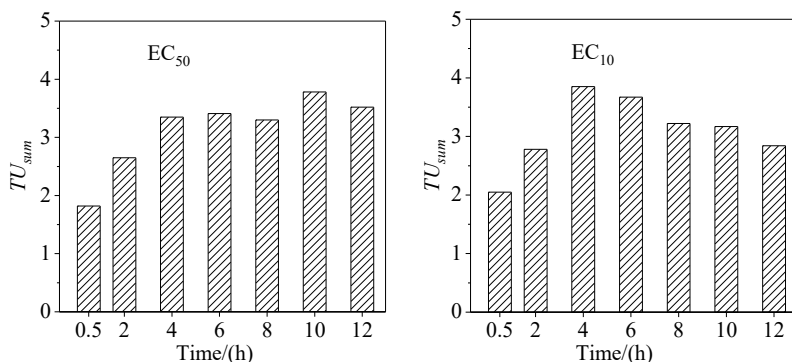


Fig. 5: Effects of a mixture of quintile equivalent concentration ratios on joint toxicity of Q67 in different exposure time.

tion of Guangxi Province (2018GXNSFAA281156), Guilin Scientific Research and Technology Development Program (20180107-5, 20180101-1 and 20190216-2).

REFERENCES

- Anderson, P.D. and Weber L.J. 1975. The toxicity of aquatic populations of mixtures containing certain heavy metals. In: Proceedings of the International Conference on Heavy Metals in the Environment Canada, 27-31 October 1975, The University of Toronto, Toronto Institute of Environmental Studies, pp. 933-953.
- Baek, I.H., Kim, Y., Baik, S. and Kim, J. 2019. Investigation of the synergistic toxicity of binary mixtures of pesticides and pharmaceuticals on *Aliivibrio fischeri* in major river basins in South Korea. *Int. J. Environ. Res. Pub. Health*, 16: 148-162.
- Broderius, S.J., Kahl, M.D. and Hoglund, M.D. 1995. Use of joint toxic response to define the primary mode of toxic action for diverse industrial organic chemicals. *Environ. Toxicol. Chem.*, 14(9): 1591-1605.
- Brycki, B., Walig Orska, M. and Szulc, A. 2014. Nimeric: The biodegradation of monomeric and dimeric alkylammonium surfactants. *J. Hazard. Mater.*, 280: 797-815.
- Cipullo, S., Snapir, B., Prpich, G., Campo, P. and Coulon, F. 2019. Prediction of bioavailability and toxicity of complex chemical mixtures through machine learning models. *Chemosphere*, 215: 388-395.
- Feng, L., Liu, S.S., Li, K., Tang, H.X. and Liu H.J. 2017. The time-dependent synergism of the six-component mixtures of substituted phenols, pesticides, and ionic liquids to *Caenorhabditis elegans*. *J. Hazard. Mater.*, 327: 11-17.
- Ferrer, I. and Furlong, E.T. 2001. Identification of alkyl dimethyl benzyl ammonium surfactants in water samples by solid-phase extraction followed by ion trap LC/MS and LC/MS/MS. *Environ. Sci. Technol.*, 35: 2583-2588.
- Jardak, K., Drogui, P. and Daghrir, R. 2016. Surfactants in the aquatic and terrestrial environment: occurrence, behavior, and treatment processes. *Environ. Sci. Pollut. Res.*, 23: 3195-3216.
- Hatano, A. and Shoji, R. 2010. A new model for predicting the time course toxicity of heavy metals based on the biotic ligand model (BLM). *Comp. Biochem. Physiol. Part - C: Toxicol. Pharmacol.*, 151: 25-32.
- Kobuke, Y. 2002. Environmental risk evaluation for anionic surfactants based on the characteristics of the appearance of high concentration in rivers. *Water Sci. Technol.*, 46(11): 263-268.
- Kwon, D., Lim, Y.M., Kwon, J.T., Shim, I., Kim, E., Lee, D.H. Yoon, B.I., Kim, P. and Kim, H.M. 2019. Evaluation of pulmonary toxicity of benzalkonium chloride and triethylene glycol mixtures using in vitro and in vivo systems. *Environ. Toxicol.*, 34(5): 561-272.
- Li, K., Liu, S.S. and Qu, R. 2017. Application of the combination index in the assessment of combined toxicity of environmental mixture. *Asian J. Ecotoxicol.*, 12: 62-71.
- Liu, S.S., Li, K., Li, T. and Qu, R. 2016a. Comments on the synergistic toxicity of the multi chemical mixtures: Implications for risk assessment in the terrestrial environment. *Environ. Int.*, 94: 396-398.
- Liu, S.S., Xiao, Q.F., Zhang, J. and Yu, M. 2016b. Uniform design ray in the assessment of combined toxicities of multi-component mixtures. *Sci. Bull.*, 61: 52-58.
- Luo, Y.H., Lai Y.J.S., Zheng C.W., Iihan, Z, E., Ontiveros V.A., Long, X.X., Krajmalnik, B.R. and Rittmann B.E. 2020. Increased expression of antibiotic-resistance genes in biofilm communities upon exposure to cetyltrimethylammonium bromide (CTAB) and other stress conditions. *Sci. Total Environ.*, 765: 144-164.
- Mo, L.Y., Ma, W., Kong, S., Qin, L.T., Liang, Y.P. and Dai, J.F. 2020a. Study of the Binding Mode of Quaternary Ammonium Cationic Surfactant to Firefly Luciferase and the Prediction of Binary Mixture Toxicity. *Chinese J. Struct. Chem.*, 39(6): 1167-1177.
- Mo, L.Y., Liu, Y.A., Zhu, J., Qin, L.T., Liang, Y. P. and Zeng, H.H. 2020b. Benefits from hazards benefit from nothing, and benefits from benefits: the combined effects of five quaternary ammonium compounds to *Vibrio qinghaiensis* Q67. *Environ. Sci. Europe*, 32(1): 35.
- OECD. 2004. The 2004 OECD List of High Production Volume Chemicals. http://www.oecd.org/chemical_safety/risk-assessment/33883530.pdf. (Accessed 5 Sept. 2004).
- Oh, S., Kurt, Z., Tsementzi, D., Weigand, M.R., Kim, M., Hatt, J.K., Tandukar, M., Pavlostathis, S.G., Spain, J.C. and Konstantinidis, K.T. 2014. Microbial community degradation of widely used quaternary ammonium disinfectants. *Appl. Environ. Microbiol.*, 80: 5892-5900.
- Olkowska, E., Polkowska, Z. and Namie-Snik, J. 2013. A solid-phase extraction ion chromatography with conductivity detection procedure for determining cationic surfactants in surface water samples. *Talanta*, 116: 210-216.
- Ostman, M., Lindberg, R.H., Fick, J., Bjorn, E. and Tysklind, M. 2017. Screening of biocides, metals, and antibiotics in Swedish sewage sludge and wastewater. *Water Res.*, 115: 318-328.
- Perez, E. and Hoang, T.C. 2017. Chronic toxicity of binary-metal mixtures of cadmium and zinc to *Daphnia magna*. *Environ. Toxicol. Chem.*, 36: 2739-2749.
- Qu, R., Xiao, K., Hu, J., Liang, S., Hou, H. J., Liu, B.C., Chen, F., Xu, Q., Wu, X. and Yang, J. K. 2019. Predicting the hormesis and toxicological interaction of mixtures by an improved inverse distance weighted interpolation. *Environ. Int.*, 130: 104892-104900.
- Rosety, M., Ordonez, F. and Rosety, R.M. 2001. Acute toxicity of anionic surfactants sodium dodecyl sulfate (SDS) and linear alkylbenzene sulphonate (LAS) on the fertilizing capability of gilthead (Sparus aurata L) sperm. *Histol. Histopathol.*, 16(3): 839-843.
- Ruan, T.S., Song, S., Wang, T., Liu, R., Lin, Y. and Jiang, G. 2014. Identification and composition of emerging quaternary ammonium compounds in municipal sewage sludge in China. *Environ. Sci. Technol.*, 48(8): 4289-4297.
- Sprague, J.B. and Ramsay, B.A. 1965. Lethal levels of mixed copper-zinc solution for juvenile salmon. *J. Fish. Res. Board Can.*, 22: 425-432.
- Vannini, A., Paoli, L., Vichi, M., Bačkor, M., Bačkorová, M. and Loppi, S. 2018. Toxicity of diclofenac in the fern *azolla filiculoides* and the lichen *xanthoria parietina*. *Bull. Environ. Contam. Toxicol.*, 100: 430-437.
- Warne, M. and Hawker, D. 1995. The number of components in a mixture determines whether synergistic and antagonistic or additive toxicity predominate: The funnel hypothesis. *Ecotoxicol Environ. Safety*, 31(1), 23-28.
- Xu, Y.Q., Liu, S.S., Fan, Y. and Li K. 2018. Toxicological interaction of multi-component mixtures to *Vibrio qinghaiensis* sp.-Q67 induced by at least three components. *Sci. Total Environ.*, 635: 432-442.
- Yu, M., Liu, S.S., Wang, M.C., Chen, F. and Tang, H. 2014. Mixture toxicities of three pesticides having different time-toxicity profiles. *Chinese J. Chem.*, 32: 545-552.
- Yuan, J., Liu, S.S., Wang, L.J. and Shao, Y.M. 2011. Optimization of microplate toxicity analysis method based on *Chlorella Pyrenoidosa*. *Res. Environ. Sci.*, 24: 553-558.
- Zhang, C., Cui, F., Zeng, G.M., Jiang, M., Yang, Z.Z., Yu, Z.G., Zhu, M.Y. and Shen, L.Q. 2015. Quaternary ammonium compounds (QACs): A review on occurrence, fate, and toxicity in the environment. *Sci. Total Environ.*, 518-519: 352-362.



Erosion Resistance and Fertility of Frost-Resistant Ecological Substrate in Alpine Region

Cailing Xue*, Ailinazaier Ainiwaer*, Jiazhen Gao** and Zhaohui Qin*†

* College of Economics and Management, China Three Gorges University, Hubei Yichang, 443002, China

** College of Civil Engineering & Architecture, China Three Gorges University, Hubei Yichang, 443002, China

†Corresponding author: Zhaohui Qin; mw19630910@163.com

Nat. Env. & Poll. Tech.

Website: www.neptjournal.com

Received: 01-12-2020

Revised: 27-01-2021

Accepted: 03-03-2021

Key Words:

The alpine region

Fertility

Aggregate

Slope ecological restoration

Principal component analysis

ABSTRACT

This research was conducted to quantitatively evaluate the application effect of the frost-resistant ecological substrate in the rock slope of the hydropower station. Field sampling and laboratory tests were conducted to determine the erosion resistance and fertility of frost-resistant ecological substrate, and the test results were compared with those of natural soils with similar site conditions. The research conclusions were as follows. Compared with the natural soil, the content of > 0.25 mm mechanical-stable aggregates, > 0.25 mm water-stable aggregates, average weight diameter, geometric average diameter, organic matter, available nitrogen, available phosphorus, and available potassium of frost-resistant ecological substrate, significantly increased. On the contrary, erodibility factor, percentage aggregate disruption, aggregate degree, and dispersion rate decreased evidently. These results showed that erosion resistance and fertility of the frost-resistant ecological substrate have a better prospect in the engineering application of alpine regions. In addition, the principal component analysis showed that the principal component value of frost-resistant ecological substrate increased by 1.9 times that of natural soil. According to the correlation study, the increase in the amount of > 0.25 mm macro-aggregates and organic matter is the primary reason that ecological substrate has greater stability and fertility than natural soil. In conclusion, the frost-resistant ecological substrate was a suitable soil to create a suitable vegetation growth environment on the surface of rock slope in the alpine region.

INTRODUCTION

Qinghai-Tibet Plateau has abundant hydropower resources, and the rivers in this region have created favorable conditions for the comprehensive development of hydropower (Yuan et al. 2016). A large number of construction measures disturb the original ecosystem function, resulting in the reduction of natural vegetation (Li et al. 2015, Xu et al. 2012). Therefore, the application of slope ecological restoration technology which takes both slope reinforcement and vegetation reconstruction into account is relatively common in Qinghai-Tibet Plateau. At present, the slope ecological restoration techniques (Yang et al. 2015) can be used to build habitats suitable for ecological restoration of vegetation growth in southern areas of China (Cheng et al. 2020, Luo et al. 2016). However, the durability and fertility of ecological substrates will be seriously reduced due to the harsh climatic conditions and frequent freeze-thaw cycles in Alpine Region (Dong et al. 2013, Sharma et al. 2006, Zhang et al. 2017). Therefore, to resist the repeated freeze-thaw damage, a new type of frost-resistant ecological substrate was invented by China Three Gorges University (Zhou et al. 2013), which can create suitable vegetation habitats for the restoration of rock exposed slopes in the

alpine region. The frost-resistant ecological substrate is composed of plant soil, cement, organic materials, green additives, silica fume, and palm fiber. The indoor test results show that the frost-resistant ecological substrate has good frost resistance and high fertilizer efficiency, but the actual improvement effect of its application still lacks specific data support.

In recent years, much research has been carried out on the changes in soil erosion resistance and fertility in the alpine region. Zhao et al. (2019) selected water-stable aggregates, geometric average diameter, and erodibility factor to study the effect of freeze-thaw on the erosion resistance of northern soil. Gu et al. (2020) selected several evaluation indexes such as average weight diameter, aggregate disruption, and the aggregate degree to comprehensively discuss the characteristics of black soil aggregates under freeze-thaw. Du et al. (2020) pointed out that the freeze-thaw process has a significant impact on the soil physical structure, chemistry, and vegetation growth of alpine grassland. So optimal conditions and technical measures to reduce soil nutrient loss during the freeze-thaw period should be explored. Change of fertility is not only a key factor reflecting the quality of the soil (Cai et al. 2008), but also can reflect the restoration

Table 1: Basic properties of planting soil.

Planting soil type	Dry density/ (g/cm ³)	pH	Particle size distribution (%)			
			2-0.5 mm	0.5-0.25 mm	0.25-0.075 mm	< 0.075 mm
Fine-grained sand soil	1.43	6.7	60.82	16.79	9.47	10.91

effect of slope ecological engineering and vegetation growth status (Rivera et al. 2014, Li et al. 2018).

Many studies have contributed to the understanding and evaluation of soil resistance and fertility. However, most of the research subjects are limited to natural soil, and there are few reports of the durability and fertility changes of ecological substrates on slopes in alpine areas. Therefore, this paper takes a rocky slope in the engineering area of Dagu Hydropower Station as the experimental site, spray seeding this frost-resistant ecological substrate according to past research methodologies. Through outdoor sampling and indoor test, the erosion resistance and fertility index were analyzed and compared with natural soils with similar site conditions. The purpose of this study is to deeply understand the application effect of the frost-resistant ecological substrate in the alpine region and to provide a scientific basis for the practical application of ecological substrate in engineering.

MATERIALS AND METHODS

Overview of test area: Dagu hydropower station is located in Zengji Township, Sangri County, Shannan City, Tibet Autonomous Region, on the eastern edge of the Qinghai-Tibet Plateau. The control basin area of the hydropower station is 157400 km² with a length of 49 km main stem and 282 m river fall along the Yarlung Tsangpo River. The minimum elevation at the station is 3400 m above sea level with a gradient of about 5.75‰. The valley width here is around 40–200 m, and the maximum elevation on both banks is more than 6000 m. The characteristic of the landform is a typical high mountain and deep valley. The climate in the region is described as plateau temperate monsoon semi-humid, with less rainfall and drought in winter and more rainfall in summer. According to the statistics date from meteorological stations, the annual average temperature, precipitation, evaporation, and relative humidity are 9.2°C, 540.5 mm, 2084.1 mm, and 51%, respectively, and the maximum frozen soil depth over the years is 19 cm. The soil in the project area is mainly composed of grassland soil, aeolian sandy soil, and skeleton soil. Meanwhile, the lithology of the excavated slope is mainly biotite granodiorite with a medium-fine grained structure.

Engineering construction and sampling: A rocky slope in the engineering disturbance area of the Dagu hydropower station was selected for the ecological restoration with the

frost-resistant ecological substrate. The construction time of ecological restoration was concentrated from June to July in 2019. The mechanical dry spray method is used to spray the surface of the rock slope. Spraying is divided into two layers: the base layer and the surface layer. The base layer and surface layer were sprayed with 10 cm and 2 cm respectively, and the plant seeds were mixed into the surface layer. The plant soil was taken from a natural slope beside the rock slope, and the basic properties of soil are shown in Table 1. The cement is ordinary Portland cement with a strength grade of 32.5, the organic material is made of fir sawdust with a particle size of less than 2 mm, the green additive is a patented product, and silica fume and palm fiber are directly purchased from the local company. The frost-resistant ecological substrate is composed of plant soil, cement, organic material, green additives, silica fume, and palm fiber at a dry weight ratio of 100:10:8:5:3:1 (Zhou et al. 2013). The rocky slope with single spraying of plant soil was selected as the control slope, and the sides of both slopes were facing north, and the slope gradient and height were about 60° and 3.4 m, respectively.

In July 2020, six plots with good vegetation growth were selected as sampling plots in two kinds of slopes, and the size of a single plot was set to 2 m × 2 m. A five-point sampling method was adopted to collect 5–10 cm surface soil from each plot, and the weight of each sample was about 2 kg. The specific method is as follows: Five spots are randomly picked according to the S shape in the depth range of the sample site's soil layer to make a sample, and huge soil blocks are collected when sampling. The soil samples which were packed in plastic boxes were carefully transported to the laboratory, then dried naturally at 25°C. All samples were stripped into 10–12 mm small blocks along the natural structure plane after the sample is air-dried to below the plastic limit while removing plant roots and small stones. The properties of each sample were measured three times in the laboratory, and averaging the experimental results.

Index selection and statistical analysis: In this paper, the evaluation indexes of soil aggregate characteristics and fertility are selected as follows.

1. The content of > 0.25 mm mechanical-stable aggregates (%) = > 0.25 mm mechanical-stable aggregate mass/ the sum of mechanical aggregate mass of each particle size.

2. The content of > 0.25 mm water-stable aggregates (%) = > 0.25 mm water-stable aggregate mass / the sum of water-stable aggregate mass of each particle size.
3. Mean weight diameter (MWD, mm): $MWD = \sum_i^n \bar{X}_i \omega_i$.
4. Geometric mean diameter (GMD, mm):

$$GMD = \exp\left(\sum_{i=1}^n \omega_i \ln X_i\right)$$

$$K = \left\{0.2 + 0.3 \exp\left[-0.0256 S_a \left(1 - \frac{S_i}{100}\right)\right]\right\} \left[\frac{S_i}{C_1 + S_i}\right]^{0.3} \times \left[1 - \frac{0.25C}{C + \exp(3.72 - 2.95C)}\right] \times \left[1 - \frac{0.7S_n}{S_n + \exp(-5.51 + 22.9S_n)}\right]$$

Where, S_a is the content of sand (2 ~ 0.05mm, %); S_i is the content of silt (0.05 ~ 0.002mm%); C_1 is the content of clay (< 0.002mm, %); C is the content of organic carbon (%); S_n is $1 - S_a / 100$. K is the international system unit (t hm² H / (hm² MJ mm).

7. Aggregate degree (%) = > 0.05 mm micro-aggregate analysis value - > 0.05 mm soil mechanical composition analysis value / > 0.05 mm micro-aggregate analysis value × 100%.
8. Dispersion rate (%) = < 0.05 mm micro-aggregate analysis value / < 0.05 mm mechanical composition analysis value × 100%.
9. The indexes of soil fertility: the content of organic matter, available nitrogen, available phosphorus, and available potassium.

Test methods: The particle size distribution of mechanical-stable aggregates was determined by the dry sieving method. The water-stable aggregates particle size distribution is determined by Yoder wet sieving method. According to the mass percentage of the soil particle distribution of each particle size after the dry screening, 50 g of air-dried soil sample was prepared. Then it was placed in the top layer of the set sieve, water was added, and the sieve was artificially vibrated for 10 minutes, after which the sieve residue was dried and weighed. Organic matter was determined by potassium dichromate-external heating method, available nitrogen was determined by alkali hydrolysis diffusion method, available phosphorus was determined by sodium hydroxide alkali solution-molybdenum blue colorimetric method, available potassium was determined by ammonium acetate extraction-atomic absorption method, and soil micro-aggregate and mechanical composition were determined by pipette method.

All date statistical analysis was performed using Excel 2019. SPSS 22.0 was used for one-way ANOVA (P < 0.05), Pearson correlation analysis, and principal component analysis.

5. Percentage aggregate disruption (PAD, %) = 1 - the content of > 0.25 mm aggregates after dry sieving/the content of > 0.25 mm aggregates after wet sieving × 100%.
6. The soil erodibility factor K was calculated by EPIC equation:

RESULTS AND DISCUSSION

Particle size distribution of mechanical-stable aggregates:

The particle size distribution of mechanical-stable aggregates of the frost-resistant ecological substrate and the natural soil is shown in Fig. 1. Overall, the distribution of the two kinds of soils is relatively similar. Both soils have the highest content of > 7 mm aggregates. Then the content of 7 ~ 5 mm and < 0.25 mm aggregates is second. The aggregates content of 5 ~ 3 mm, 3 ~ 2 mm, 2 ~ 1 mm, 1 ~ 0.5 mm, 0.5 ~ 0.25 mm have no significant difference, and the content of 3 ~ 2 mm aggregates is the least. But there is a certain difference between the frost-resistant ecological substrate and the natural soil. Among them, the content of > 7 mm aggregates in natural soil is less than that of the frost-resistant ecological substrate, and the content of < 0.25 mm aggregates in natural soil is about 8.2% higher than that of the frost-resistant ecological substrate. So, the main difference between both soils is that the content of mechanical macro-aggregates of the frost-resistant ecological substrate is significantly increased, while the content of micro-aggregates is significantly reduced.

Particle size distribution of water-stable aggregates:

As shown in Fig. 2, the content of > 5 mm and < 0.25 mm water-stable aggregates in frost-resistant ecological substrate are significantly higher than the content of aggregates of 5 ~ 3 mm, 3 ~ 2 mm, 2 ~ 1 mm, 1 ~ 0.5 mm, and 0.5 ~ 0.25 mm. The content of these five aggregates is all below 6%, and there is no significant difference among them. In comparison, the content of < 0.25 mm water-stable aggregates in natural soil was the highest, which is significantly higher than that of the frost-resistant ecological substrate. The content of > 5 mm aggregates in natural soil is only 16.6%, and it is significantly lower than the frost-resistant ecological substrate (P < 0.05). In terms of the content of 5 ~ 3 mm, 3 ~ 2 mm, 2 ~ 1 mm, 1 ~ 0.5 mm, 0.5 ~ 0.25 mm aggregates, the difference between both soils are not significant. The results show that the content of > 5 mm water-stable aggregates of the frost-resistant ecological substrate is significantly higher than that of natural soil, while the

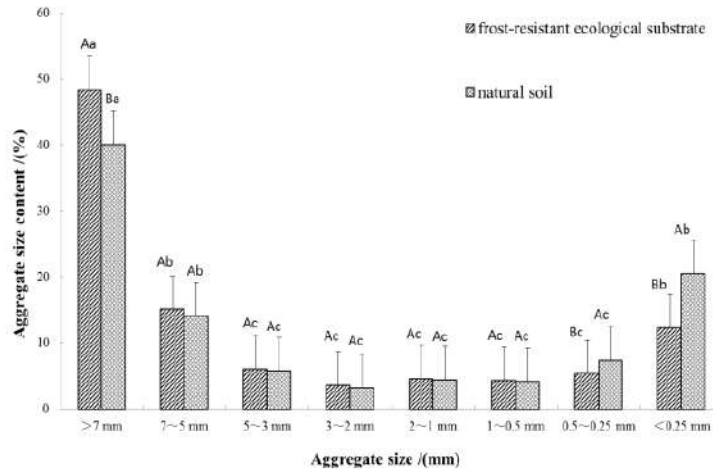


Fig. 1: Particle size distribution of mechanical-stable aggregates.

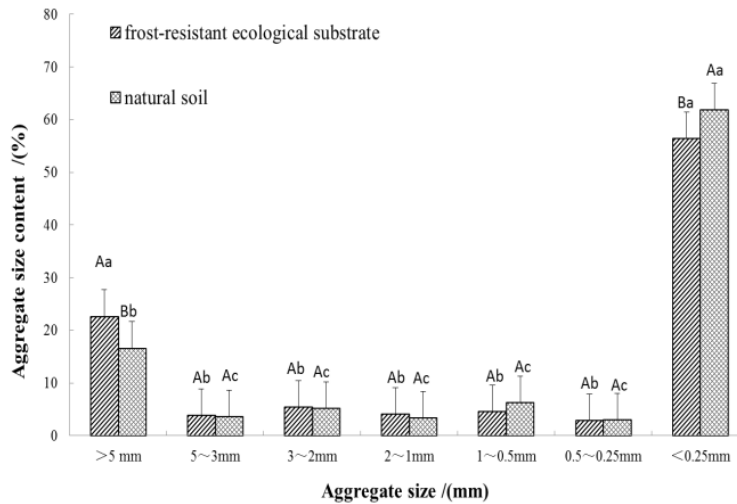


Fig. 2: Particle size distribution of water-stable aggregates.

content of <0.25 mm water-stable aggregates is significantly reduced.

Indexes of erosion resistance and fertility: In terms of

the particle size distribution of aggregates, the content of > 0.25 mm mechanical-stable and water-stable aggregates in the frost-resistant ecological substrate are 10.4% and

Table 2: Erosion resistance and fertility of both soils.

Soil type	Aggregate content (%)		MWD (mm)	GMD (mm)	PAD (%)	K (t hm ² h/ hm ² MJ mm)	Aggregation degree (%)	Dispersion rate (%)	Organic matter (g kg ⁻¹)	Available nitrogen (g kg ⁻¹)	Available phosphorus (g kg ⁻¹)	Available potassium (g kg ⁻¹)
	Mechanical stable	Water stable										
Substrate	87.72 a	43.61 a	2.17 a	0.53 a	50.12 a	0.014 b	29.47 a	57.48 b	22.46 a	0.183 a	0.082 a	0.127 a
Natural soil	79.49 b	38.22 b	1.71 b	0.41 b	52.51 a	0.022 a	21.24 b	71.63 a	14.27 b	0.142 b	0.064 b	0.095 b
Relative change rate	10.4%	14.1%	26.9%	29.3%	-4.0%	-36.4%	38.7%	-19.8%	57.4%	28.9%	28.1%	33.7%

Table 3: Correlation between different indexes.

	X ₁	X ₂	X ₃	X ₄	X ₅	X ₆	X ₇	X ₈	X ₉	X ₁₀	X ₁₁	X ₁₂
X ₁	1.000											
X ₂	0.157	1.000										
X ₃	0.413	0.850*	1.000									
X ₄	0.298	0.959**	0.961**	1.000								
X ₅	0.361	-0.863*	-0.605	-0.761	1.000							
X ₆	-0.307	-0.975**	-0.942**	-0.996**	0.769	1.000						
X ₇	-0.871*	0.080	-0.036	0.007	-0.531	0.009	1.000					
X ₈	-0.818*	-0.032	-0.066	-0.064	-0.407	0.087	0.975**	1.000				
X ₉	-0.454	0.390	0.443	0.441	-0.634	-0.405	0.729	0.779	1.000			
X ₁₀	-0.408	0.366	0.471	0.444	-0.589	-0.401	0.701	0.761	0.995**	1.000		
X ₁₁	-0.443	0.313	0.375	0.360	-0.557	-0.332	0.735	0.807	0.986**	0.918**	1.000	
X ₁₂	-0.474	0.371	0.409	0.406	-0.625	-0.379	0.773	0.824*	0.990**	0.879*	0.885*	1.000

Note: ** is extremely significant correlation at 0.01 level; * is significant correlation at 0.05 level. X₁ is the content of mechanical-stable aggregates (%); X₂ is the content of water-stable aggregates > 0.25 mm; X₃ is the average weight diameter (MWD, mm); X₄ is the geometric average diameter (GWD, mm); X₅ is the percentage aggregate disruption (PAD, %); X₆ is the erodibility factor K (t hm² H / hm² MJ mm); X₇ is the aggregate degree (%); X₈ is the dispersion rate (%); X₉ is the content of organic matter (g kg⁻¹); X₁₀ is the content of available nitrogen (g kg⁻¹), X₁₁ was the content of available phosphorus (g kg⁻¹), and X₁₂ was the content of available potassium (g kg⁻¹). The following is the same.

Table 4: PCA analysis of index.

Principal component	Factor load of each index												Characteristic root	Cumulative contribution rate (%)
	X ₁	X ₂	X ₃	X ₄	X ₅	X ₆	X ₇	X ₈	X ₉	X ₁₀	X ₁₁	X ₁₂		
Y ₁	-0.409	0.638	0.607	0.646	-0.835	-0.624	0.717	0.704	0.944	0.929	0.909	0.942	6.925	57.71
Y ₂	-0.772	-0.709	-0.746	-0.760	0.267	0.775	0.621	0.688	0.208	0.193	0.273	0.249	3.981	33.18

14.1% higher than those of natural soil, respectively. The MWD and GMD of a frost-resistant ecological substrate are 26.9% and 29.3% higher than those of natural soil, respectively. The percentage aggregate disruption PAD and erodibility factor K are 4% and 36.4% lower than those of natural soil, respectively. These results indicate that the aggregate structure and anti-dispersion ability of frost-resistant ecological substrate has improved. In the aspect of fertility, the organic matter content of the frost-resistant ecological substrate is 57.4% higher than that of the natural soil. Meanwhile, the content of available nitrogen, available phosphorus, and available potassium are 28.9%, 28.1%, and 33.7% higher than those of the natural soil, respectively. It also shows that frost-resistant ecological substrate is more conducive to the growth of plants.

Correlation analysis of indexes: Correlation analysis of the twelve evaluation indexes mentioned above in this article is conducted, and the results are shown in Table 3. The results show that the content of > 0.25 mm water-stable aggregates R_{0.25} (X₂) and organic matter content (X₉) of the frost-resistant ecological substrate is closely related to other indexes. For example, the water-stable aggregates content

R_{0.25} (X₂) is significantly and positively correlated with MWD (X₃) and GWD (X₄). The organic matter content (X₉) significantly and positively correlated with available nitrogen (X₁₀), available phosphorus (X₁₁), and available potassium (X₁₂). Therefore, the content of > 0.25 mm water-stable aggregates R_{0.25} (X₂) and organic matter content (X₉) are the most important indexes affecting the erosion resistance and fertility of the frost-resistant ecological substrate, respectively.

The principal component analysis: The SPSS software is used to conduct principal component analysis on the twelve indexes, and the results are shown in Table 4. According to the results, the above-mentioned twelve indexes can extract two principal components, and the two eigenvalues are 6.925 and 3.971 respectively. The contribution rate of principal component Y₁ and principal component Y₂ are 57.71% and 33.18%, respectively. The cumulative contribution rate of both components can reach 90.89%, which meets the requirements of principal component analysis for information coverage.

It can be seen from a load of each index in Table 4 that the nutrient contents of organic matter (X₉), available nitrogen

Table 5: Main component values of both soils.

Soil type	First principal component Y_1	Second principal component Y_2	Comprehensive principal component Y
Frost-resistant ecological substrate	2.557	-0.220	1.543
Natural soil	0.544	-0.850	0.532

(X_{10}), available phosphorus (X_{11}), and available potassium (X_{12}) contribute greatly to the main component Y_1 . For the main component Y_2 , the major contributions are the content of > 0.25 mm mechanical-stable aggregates (X_1), the content of > 0.25 mm water-stable aggregates $R_{0.25}$ (X_2), mean weight diameter MWD (X_3), and geometric mean diameter GWD (X_4).

From the principal component loads and characteristic roots in Table 4, the first and second principal component expressions can be obtained respectively as follows.

$$Y_1 = -0.155X_1 + 0.242X_2 + 0.231X_3 + 0.245X_4 - 0.317X_5 - 0.237X_6 + 0.272X_7 + 0.268X_8 + 0.359X_9 + 0.353X_{10} + 0.345X_{11} + 0.358X_{12}$$

$$Y_2 = -0.387X_1 - 0.355X_2 - 0.374X_3 - 0.381X_4 + 0.134X_5 + 0.388X_6 + 0.311X_7 + 0.345X_8 + 0.104X_9 + 0.097X_{10} + 0.137X_{11} + 0.125X_{12}$$

In conclusion, the principal component values of the frost-resistant ecological substrate and natural soil are calculated as shown in Table 5.

According to the proportion of the corresponding characteristic value of each principal component in the total characteristic value of the extracted principal component as the weight, the comprehensive principal component model $Y = 0.635 Y_1 + 0.365 Y_2$ was obtained, and the comprehensive principal component value of frost-resistant ecological substrate and natural soil was calculated. It can be seen from Table 5 that the comprehensive principal component value of the frost-resistant ecological substrate is 2.9 times that of the natural soil.

DISCUSSION

In this paper, the application of two kinds of soils in the alpine region shows that the erosion resistance and fertility of frost-resistant ecological substrate are significantly higher than that of natural soil. The main reason is that organic material, green additive, cement, silica fume, and palm fiber are added into the frost-resistant ecological substrate. In terms of soil fertility, organic sawdust mixed in the soil would be transformed into organic matter after decay, which will cause the content of organic matter in the frost-resistant ecological substrate to be higher than that in natural soil. The abundant microbial agents contained in the green additives can also promote the growth of various microorganisms

and nutrients in the soil, so soil fertility can be significantly improved in alpine regions. Some studies (Xu et al. 2017, Xie et al. 2019) have shown that the improvement of soil fertility can promote the growth of plants, and the plant roots produced also can increase the soil mechanical properties, which can improve the effect of slope restoration in alpine regions for a long time.

In terms of soil erosion resistance, many scholars (Wang et al. 201, Zhang et al. 2019) have shown that the higher the content of macro-aggregate in soil, the smaller the aggregate dispersion rate, the stronger the soil erosion resistance. One of the reasons is that the hydration reaction of cement generates a large number of gelatin and crystal compounds. These compounds can agglomerate the micro-aggregates to form a crystal network and a solid and dense structure (Zhang et al. 2015), thus increasing the content of macro-aggregates (X_1) and aggregate degree (X_7) in soil, reducing the percentage aggregate disruption (X_5). This result is consistent with Tang's research conclusion (Gao et al. 2020). Second, the addition of silica fume can increase the porosity of the soil, thereby reducing the negative impact of frost heaving and thawing settlement on soil structure and increasing the stability of soil in the alpine region (Liu et al. 2013). The addition of palm fiber can increase the connectivity between soil particles and improve the soil's mechanical properties (Zhang et al. 2018). In addition, studies have shown that the increase of organic matter content is also conducive to the formation of macro-aggregates and the enhancement of soil erosion resistance (Wagner et al. 2007, Yao et al. 2009). Because the organic colloid contained in the organic matter has the function of cementation and agglomeration (Yao et al. 2009), it increases the content of macro-aggregates (X_1 , X_2) and enhances the cohesive force of soil particles. Meanwhile, the organic matter could be decomposed into organic acids under the action of microorganisms, which can prevent the dispersion of aggregates (X_8).

This study also found that the content of water-stable aggregate $R_{0.25}$ (X_2) and organic matter content (X_6) could best reflect the erosion resistance and fertility of frost-resistant ecological substrate respectively because the correlation between the two indexes and other indicators were very high. Zhang et al. (2019) considered that there was a significant correlation between the above two indicators and MWD, GMD, nutrient indicators, which is basically consistent with

the research results in this paper. The principal component analysis also showed that the contribution rate of water-stable aggregate $R_{0.25}$ (X_2) and organic matter content (X_9) to the frost-resistant ecological substrate was higher. Therefore, the above two indicators can be used to evaluate the erosion resistance and fertility of the frost-resistant ecological substrate in future research.

CONCLUSION

In terms of aggregate particle size distribution, the frost-resistant ecological substrate's content of > 0.25 mm mechanical-stable aggregates and water-stable aggregates has increased significantly compared to natural soil, which is reflected in improved erosion resistance compared to natural soil. In terms of fertility, the organic matter content, available nitrogen, available phosphorus, and available potassium of frost-resistant ecological substrate increased significantly compared with the natural soil, which was more suitable for plant growth. The principal component analysis showed that the comprehensive principal component value of frost-resistant ecological substrate is 190% higher than that of the natural soil. Therefore, the erosion resistance and fertility of the frost-resistant ecological substrate are significantly higher than those of the natural soil, so this substrate has a better prospect in the engineering application of alpine regions.

ACKNOWLEDGEMENTS

This study was supported by the Research Fund for Excellent Dissertation of China Three Gorges University (Grant No. 2019BSPY007).

REFERENCES

- Cai, X.B., Zhang, Y.Q. and Shao, W. 2008. Characteristics of soil fertility in alpine steppes at different degradation grades. *Acta Ecol. Sin.*, 3: 1034-1044.
- Cheng, H., Xu, W.N., Luo, T., Xia, L., Xiang, H.Y., Ma, P.F. and Xia, D. 2020. Microbial functional diversity as affected by different engineered eco-restoration methods at Xiangjiaba hydropower station. *J. Environ. Eng.*, 146(3): 56-98.
- Dong, K., Li, S.W., Kang W.L., Long, H.Z. and Liu, G.X. 2013. Study of the changes in microbe amount and its effect factors in the soils along the Qinghai-Tibet highway. *J. Glaciol. Geocryol.*, 35(2): 457-464.
- Du, Z.Y. 2020. Effects of Freeze-thaw Action on Soil Physicochemical and Biological Properties in the Alpine Grasslands. *Ecology and Environmental Sciences*, 29(5): 1054-1061.
- Gao, J.Z., Zhou, M.T., Xu, W.N., Liu, D.X., Shen, J., Peng, S. and Du, Y. 2020. The evolution of structural properties of vegetation concrete under freeze-thaw cycles. *Int. J. Electr. Eng. Educ.*, 5(1): 1-19.
- Gu, W.M., Zhou, J.X., Wang, B. and Guan, Y.H. 2020. Effects of the freeze-thaw cycle on the characteristics of black soil water-stable aggregates. *Sci. Soil Water Conserv.*, 18(4): 45-52.
- Li, R.R., Kan, S.S., Zhu, M.K., Chen, J., Ai, X.Y., Chen, Z.Q., Zhang, J.J. and Ai, Y.W. 2018. Effect of different vegetation restoration types on fundamental parameters, structural characteristics, and the soil quality index of artificial soil. *Soil Till. Res.*, 184: 11-23.
- Li, Z.W., Wang, Z.Y., Yu, G.A., Wang, X.Z. and Zhang, C.D. 2015. Effects on slope stability of the Yarlung Tsangbu grand canyon under future hydropower development. *Mountain Res.*, 3: 331-338.
- Liu, D.X., Xu, W.N., Cheng, Z.L., Zhou, Z.Z., Cai, X.Y. and Zhao, B.Q. 2013. Improvement test on frost resistance of vegetation-concrete and engineering application of test fruitage. *Environ. Earth Sci.*, 69(1):161-170.
- Luo, A.D., Yan, Z.L. and Zhai, W.G. 2016. Initial Analysis on the Improvement of Highway Slope Landscape Based on the Ecological Protection. International Conference on Sustainable Energy and Environmental Engineering, 18-19 December 2016. Xiamen, China, DEStech Publications, Inc., Pennsylvania, pp. 31-37
- Rivera, D., Mejías, V., Jáuregui, B.M., Costa-Tenorio, M., López-Archilla, A.I., Peco, B. and Singer, A.C. 2014. Spreading topsoil encourages ecological restoration on embankments: Soil fertility, microbial activity, and vegetation cover. *PLOS One*, 9(7): e101413.
- Sharma, S., Szele, Z., Schilling, R., Munch, J.C. and Schloter, M.J. 2006. Influence of freeze-thaw stress on the structure and function of microbial communities and denitrifying populations in soil. *Appl. Environ. Microbiol.*, 72(3): 2148-2154.
- Wagner, S., Cattle, S.R. and Scholten, T. 2007. Soil-aggregate formation as influenced by clay content and organic-matter amendment. *J. Plant Nutri. Soil Sci.*, 170(1): 173-180.
- Wang, H., Zhang, G.H., Li, N.N., Zhang, B.J. and Yang, H.Y. 2019. Variation in soil erodibility under five typical land uses in a small watershed on the Loess Plateau, China. *Catena*, 174(3): 24-35.
- Xie, X.J. and Zhang, B. 2019. Comprehensive Evaluation on Recovery of Soil Anti-erodibility by Revegetation Based on Coupling Relationship Analysis. *Soils*, 51(3): 609-616.
- Xu, S.J., Lei, S.T. and Zeng, B. 2017. Stability of root-fixed soil on 4 different slopes in the Three Gorges Reservoir region. *Res. Soil Water Conserv.*, 24(2): 119-123+131.
- Xu, W.N., Xia, Z.Y., Zhou, M.T., Liu, D.X. and Xia, D. 2012. Theory and practice of environmental protection technology of vegetation concrete. China Water Power Press, 45: 55-64.
- Yang, Y., Yang, J.Y., Zhao, P., Shi, C.Q., Xu, Z.N. and Zhou, F. 2015. Two technologies of concrete frame ecological slope protection and application effect: Taking the Anhui Yuewu highway as an example. *Sci. Soil Water Conserv.*, 13(5): 118-124.
- Yao, S.H., Qin, J.T., Peng, X.H. and Zhang, B. 2009. The effects of vegetation on the restoration of the physical stability of severely degraded soil in China. *Ecol. Eng.*, 35(5): 723-734.
- Yuan, J.X., Yi, Z.J. and Wang, S.Y. 2016. Geological challenges in the construction of hydropower projects in Qinghai-Tibet plateau and its surrounding areas. *Journal of Engineering Geology. J.Eng. Geol.*, 24(5): 847-855.
- Zhang, B.H., Liu, D.X. Xu, Y.K. Huang, B. Ding, Yu. and Xu, W.N. 2018. Single polypropylene fiber determines critical fiber reinforcement length and analysis of pullout characteristics for fiber-reinforced soil vegetation-growing concrete. *Bull. Chinese Ceram. Soc.*, 37(9): 2954-2960+2966.
- Zhang, B.J., Zhang, G.H., Yang, H.Y. and Zhu, P.Z. 2019. Temporal variation in soil erosion resistance of steep slopes restored with different vegetation communities on the Chinese Loess Plateau. *Catena*, 182: 104170.
- Zhang, H.Y., Wang, K.Q. and Song, Y.L. 2019. soil erosion resistance under different land-use types in the Jianshan river watershed in middle Yunnan Province. *J. Soil Water Conserv.*, 33(5): 50-57.
- Zhang, L.Y., Liu, D.X., Xu, W.N. and Tong, B. 2017. A study on the change of three functional microorganism quantities in habitat substrate under freezing-thawing cycles. *J. Glaciol. Geocryol.*, 39(05): 1122-1129.

- Zhang, Q.Q., Wang, J.D., Liu, B.R. and Zeng, Y.J. 2015. Quantitative research on microstructure of modified soil with cement. *Hydrogeol. Eng. Geol.*, 42(3): 92-96.
- Zhao, H.C., Wei, X., He, Y. Yu, W.Z. and Wang, T. 2019. Effects of freeze-thaw on soil aggregate characteristics and erodibility factor K. *Res. Soil Water Conserv.*, 26(5):1-6+13.
- Zhou, M.T., Xu, W.N., Hu, H. Hu, X.D., Wu, S.G. and Zhang, S.D. 2013. A Kind of Frost-Resistant Ecological Substrate is Applied in Slope. State Intellectual Property Office of the People's Republic of China.



Briquettes Production as an Alternative Fuel

U.S.P.R. Arachchige

Department of Civil and Environmental Technology, Faculty of Technology, University of Sri Jayewardenepura, Homagama, Sri Lanka

†Corresponding author: U.S.P.R. Arachchige; udara@sjp.ac.lk

Nat. Env. & Poll. Tech.
Website: www.neptjournal.com

Received: 30-12-2020

Revised: 12-03-2021

Accepted: 10-04-2021

Key Words:

Alternative fuel

Briquettes

Energy management

Agricultural crop residue

Waste management

ABSTRACT

Bioenergy, which originated from agricultural crop residue and industrial waste, has been studied for sustainable energy generation. As a raw material for briquettes production, agricultural-crop residue, industrial waste, sewage, sludge, or other plants can be used. Briquettes have numerous advantages as they directly help to reduce waste generation and handling. The possibilities of the briquetting, qualities, and other essential factors for briquette production have been discussed. The alternative methods of Briquetting have been addressed with the comparison. The characteristics of the raw materials for briquettes production have been discussed to identify the best agricultural crop residue for briquettes. The properties of binding agents for the briquetting process have been discussed to identify the most practically available binding agent.

INTRODUCTION

Coal, oil, and natural gas, which are considered fossil fuels, are the primary energy sources that drive the global energy demand process, providing 80 percent of global energy demand until today (Kpalo et al. 2020). Depletion of fossil fuels is at an alarming rate, with environmental pollution concerns as a global issue.

Atmospheric greenhouse gas concentration has been rapidly increasing with industrialization. The greenhouse gas concentration and fossil fuel combustion have a significant relationship with each other (Udehl & Kidak 2019). It has been noted that petroleum, coal, and oil directly contribute to greenhouse gas emissions and global warming.

Renewable energy shows better sustainability while comparing with non-renewable energy sources. Because of global warming and the effects of climate change, the majority of developed countries are shifting to renewable energy sources (Rabbani et al. 2017). Developing countries, on the other hand, continue to lag, despite having high renewable energy sources such as hydropower, biomass, biogas, and other bioenergy sources.

Biomass is one of the primary fuels used for day-to-day life as it is the most precious and versatile resource on earth (Government of Canada 2017). From the day man discovered fire, biomass has been used as a fuel source. One of the main applications of biomass is biomass boilers for industrial

applications. Most industries are currently using biomass boilers to produce steam for industrial processes. Biomass is the most widely used fuel source for heating, cooking, and industrial steam generation (Arachchige & Sandupama 2019). There are varieties of biomass available with different physical properties, given in Fig. 1. Industries based on biomass can foster rural development while providing employment opportunities for the public (Zafar 2016). However, at the same time, the biomass's re-growth has to be promoted to continue that as a sustainable energy source. Numerous applications depend on biomass either for power, steam, or heat generation; however, due to financial benefits, deforestation is alarming around the world by destroying all-natural resources (Scarlat & Dallem 2015). The negative aspects of conventional biomass utilization in developing countries can be mitigated by promoting up-to-date technologies, such as waste-to-energy technologies. Most of the waste generation at industrial premises and agricultural processes plays a vital role in sustainable biomass generation.

One of the main issue with industries are solid waste generated in the industrial process. The majority of industries either incinerate solid waste at a high temperature or dump it in the open ground. At the same time, solid waste and sludge are used for fertilizer production due to biodegradable components. Simultaneously, the solid waste composition is essential if it is to be recycled or used in the manufacturing of biodegradable fertilizer (Abdel-Shafy & Mansour 2018).

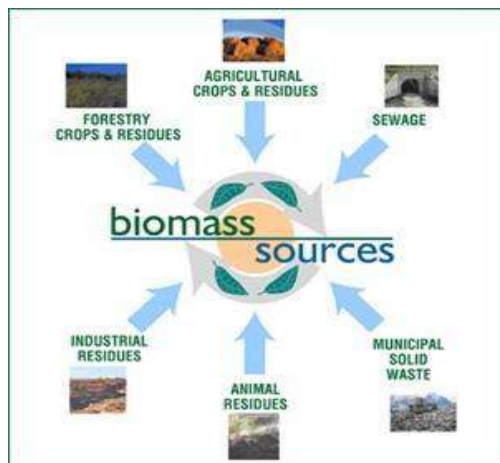


Fig. 1: Biomass sources.

Time is the most crucial factor for the bio-degradation of solid waste as it needs enormous storage capacity until it reaches the final stage (Abdel-Shafy & Mansour 2018).

One of the proven ways of generating energy from waste and converting waste into a sustainable way is biomass briquettes' production (Onukak 2017). Different types of waste have been considered for the production of the briquettes to manage solid waste sustainably. Municipal solid waste has been used to simulate biomass briquettes to produce onsite energy (Romallosa & Kraft 2017). Sawdust, date palm trunk, and various plastic wastes have been used to create biomass briquette without a binding agent (Garrido et al. 2017). They have used locally available solid waste to minimize waste handling.

At the same time, in Uganda, Lubuwama & Yiga (2017) used groundnut shells and bagasse to produce briquettes while Mereteet al. (2014) from Ethiopia made briquettes from coffee husks and pulp.

Biological sludge, cotton flock, and sawdust can produce briquette with binding agents such as shredded paper, organic waste, and citrus peel. Water is commonly used as the principal raw material in the production of all types of briquettes to evenly combine all of the raw materials. The dust created during the briquette production process with charcoal is detailed in the literature (Britta Peters 2014). If briquettes are perfectly produced, they should pass the durability test as follows in Fig. 2 (Britta Peters 2014). The raw material selection for briquetting has to be performed based on the one that has better fuel properties (Mu'az1 2016).

To improve the density of bulky material, briquetting can be done using manual hand pressing and mechanical compaction. The form is defined by converting the fine particles.

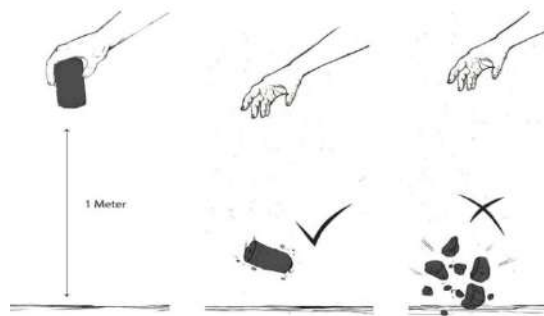


Fig. 2: Testing durability of the briquettes.

Briquette's higher density will prevent the separation of combined material into separate parts during transportation, storage, and combustion. Briquette's moisture content should be maintained between 6-16%, as mentioned in the literature (ASTM Standard E711 – 87 2004).

Biomass briquettes have been demonstrated to be one of the most efficient energy sources. Many different types of waste have been used to make briquettes. Other raw materials have been used in the biomass briquette manufacturing process in a number of studies. The quality and the dimensions of the biomass briquette depend on the raw material type and the production process. The quality of the briquette depends on the characteristics of the raw materials used to produce the briquettes. The key elements of the production of the successful briquettes include the moisture content of the raw material and the calorific value of the raw material.

MATERIALS AND METHODS

Biomass handling at home or industries is not attractive as it occupies larger ground space than fossil fuels. The way agro waste, industrial waste, sewage, or sludge is handled is not environmentally friendly because it is produced at a higher rate. One of the most attractive ways of applying biomass for industrial energy generation is to convert the biomass energy source to briquette, which takes less space. Garrido et al. (2017) used sawdust, date palm trunk, and various plastic waste without a binding agent. One of the main advantages of converting low-density biomass into high-density briquette is that it consumes less storage space while providing higher calorific value. Briquettes are easy to transport, easy to store, and easy to use or generate energy for heating or power generation.

A high-quality fuel source should have a higher density for a longer time of the burning process (Onukak et al. 2017). Furthermore, durability is an important feature because it is linked to the handling, transportation, and storage of the product until the final burning process. One of the

most important aspects to consider when evaluating the best briquette is the time it takes for water to boil. Water boiling is the time taken to boil a specific amount of water when a particular briquette amount is used. If the water boiling time is less, less fuel is required for the combustion process (Onukak et al. 2017). The burning rate is also an important factor in briquette classification since a high burning rate necessitates a large amount of fuel to complete the combustion process. Moreover, thermal efficiency is the most significant physical property because it is directly related to calorific value (Onukak et al. 2017).

There are multiple raw materials available for briquettes production, such as municipal solid waste, industrial waste, sludge, agricultural crop residue, etc. Production of fuel briquettes using municipal solid waste has proven to be an economical product (Diener et al. 2014, Shafie et al. 2012). The quantity of solid waste reduces production costs while also helping to reduce pollution. The properties of the final product are directly linked to the raw material used to make the briquette. Industrial waste plays a significant role in raw material supply in briquettes production. From sawmills as sawdust, rice mills as rice husk, garments produce as flocks and cotton dust, and the water treatment sludge at the industries are the primary sources of raw materials for the briquettes production process. Even septic tank sewage is also a possible source of raw material for briquette production with higher calorific value.

The sludge's higher moisture content is the main issue with the sludge as a raw material as that decreases the calorific value of the product. However, higher moisture content sludge can be used as a binding agent with the municipal solid waste to produce briquettes with higher calorific value. Table 1 summarizes the possible raw materials for fire briquettes production (Diener et al. 2014, Shafie et al. 2012).

Mainly, two analyses have to be done to verify the raw materials for briquettes - proximate analysis and ultimate analysis. The proximate analysis provides the potential efficiency and the durability of the briquettes produced.

Table 1: Raw materials for briquettes.

Origin	Raw materials for briquettes
Agricultural waste	Coconut fronds, coconut fiber (coir), Cassava stalk or leaves, corn stalk, rice straw, palm oil frond, sugar cane leaves
Industrial residue from agriculture	Sugar cane bagasse, coconut shells, Oil palm husk, paddy husk, corn cobs, coffee husk, peanut shells
Other Industrial waste	Water treatment Sludge, cotton flocks, Sewage, Sawdust, paper waste
Other materials	Coal ash or fly ash, charcoal powder

Several physical properties have to be estimated and evaluated for the solid waste, such as total carbon content, volatile matter, fixed carbon, ash content, moisture content, bulk density, particle size, and the calorific value to analyze the proximate analysis (Emerhi 2011).

Total carbon content: The total carbon content represents the amount of carbon available in the waste material, which could be burned for releasing heat.

Volatile matter: High volatile matters are immediately released when the biomass is heated up. Therefore, low volatile matter is essential to complete the combustion process.

Fixed carbon: This factor defines the total amount of solids remaining once the carbonization process has been completed. It should be a higher value of carbon content in the feedstock to produce long-lasting and stable briquettes.

Ash content: A higher quantity of the feedstock's ash content maintains the burning device's operating temperature by ash slugging. The operating temperature maintained at the required level is essential to avoid the unit's overheating to keep the combustion process without interruptions.

Moisture content: Higher moisture content in the feedstock will eventually increase the production cost, hence, moisture must be removed from a feedstock for quality briquette manufacturing. However, a lower amount of moisture is also not suitable as that will decrease the density by forming flakes.

Bulk density: A higher bulk density is required to keep the resistance for shear stress, which causes the product's durability.

Particle size: The raw materials bonding ability increases with the smaller particle size of the raw material. Simultaneously, bonding ability can increase by using different raw material particle sizes for briquette production.

Calorific value: The amount of energy in the briquette represents the raw materials' calorific value. According to the above information, lower moisture content, lower volatile matter and less ash content, higher fixed carbon content, and bulk density are essential to produce efficient fire briquettes (Enweremadu et al. 2004).

Moreover, the ultimate analysis is vital to identify the raw material (waste material) of the briquette production process. Ultimately those factors will contribute to the emissions releasing into the atmosphere when briquettes undergo the combustion process.

Carbon monoxide: The low combustion temperature and poor mixing of the fuel and air will result in Carbon Monoxide (CO) generation.

Fine particulate matter: Emissions of the fine particle is a result of low combustion temperatures.

Nitrogen Oxides: There is a direct relationship between the Nitrogen content of the feedstock and the nitrogen oxide emissions.

Sulfur oxides: Like the nitrogen content of the fuel, the raw materials' sulfur content is directly related to the feedstock's sulfur dioxide emissions.

Therefore, the feedstock's sulfur and nitrogen content must produce a fire briquette with less environmental pollution.

The proximate analysis has to be performed before the production process to select better feedstock (Chin & Siddiqui 2004). Like the nitrogen content of the fuel, the raw materials' sulfur content is directly related to the feedstock's sulfur dioxide emissions (Lela et al. 2016). Therefore, the feedstock's sulfur and nitrogen content must produce a fire briquette with less environmental pollution (Lela et al. 2016). Some fundamental parameter values of the feedstock for briquetting have been reported in the literature, as shown in Table 2 (Ortiz et al. 2013).

RESULTS AND DISCUSSION

To keep the moisture content of the feedstock, the raw materials for briquettes must be dried. Even natural storage conditions over a longer length of time can do this. It's critical to take advantage of the storage time to use natural drying to reduce moisture content. The necessary steps of the briquette production are milling or shredding the raw materials, drying, and pressing to create a final product (Lela et al. 2016).

Table 2: Properties of the raw materials.

	Properties	Unit	Requirement
Proximate Analysis	Moisture Content	%	6-14
	Ash Content	%	<4
	Particle size	mm	1-10 size with 10-20% powdery
	Fixed carbon	%	9-25
	Calorific value	MJ/kg	10-35
	Bulk density	Kg/m ³	>50
	Heating value	MJ/kg	12-20
Ultimate Analysis	Volatile matter	%	50-90
	Carbon (C)	%	40-55
	Hydrogen (H)	%	5-8
	Oxygen (O)	%	35-48
	Nitrogen (N)	%	0-1
	Sulfur (S)	%	0-2
	Chloride(Cl)	%	0-1

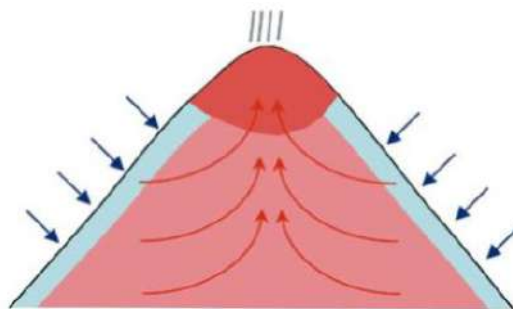


Fig. 3: The chimney effect – natural drying of a biomass heap.

Simultaneously, to achieve better drying conditions, raw materials storage should be done with cement or concrete platforms to avoid missing sand and other unwanted particles. Simultaneously, the storage area must be covered with fabric to prevent moisture from contacting and trapping the heat to vaporize the moisture (Lela et al. 2016). It can be used to maintain the moisture content of the feedstock by pre-drying it before pressing. Natural drying can be applied to minimize the moisture content of the raw material. The raw material can be directly exposed to solar heating or by supplying hot air through the raw material storing pile. The most traditional way of doing the natural heap drying is to use the chimney effect by creating a channel at the heap center for air passing (Fig. 3) (Lela et al. 2016).

Raw material preheating to maintain moisture content is an essential factor while considering the briquette. According to the literature, the moisture content of raw materials should be between 6% and 23% to ensure proper briquette production, as low moisture produces roughness. High moisture, on the other hand, increases the energy cost of moisture removal (Stolarski et al. 2013, Zhang et al. 2013).

The particle size of the raw material is important for the long-term durability of the briquettes produced. Filling the empty spaces between each particle with a mixture of particle sizes is a well-known approach. Previous research has found that particle sizes of less than 6mm are best for mixing raw materials. (Andrejko & Grochowicz 2007).

Preheating the raw material before pressing is essential to maintain the moisture content, increase the grind ability, avoid difficulties during transportation, and increase the final product (Li et al. 2007, Kaliyan & Vance Morey 2009, Kaliyan & Vance Morey 2010).

Compacting or pressing is the heart of the briquette production to increase the density (densification). According to the plant's size, there are numerous ways to achieve the compacting by the manual or automated way. Piston briquetting is one of the most common processes, in which crushed biomass is pushed into a cylinder mold by a piston driven by a flywheel (Fig. 4) (MaxTon Industrial Co 2020).

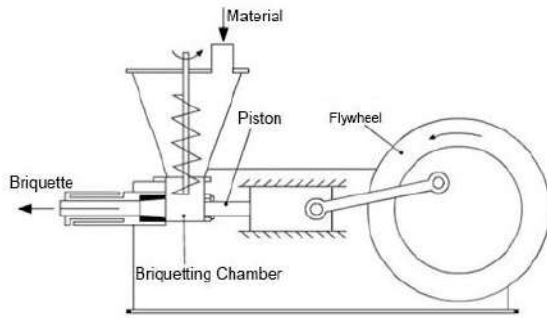


Fig. 4: Piston pressing briquetting machine.

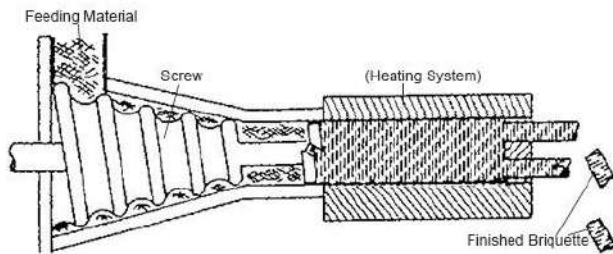


Fig. 5: Screw pressing briquette machine (MaxTon Industrial Co. 2020).

The piston reciprocates the piston using the device’s rotary power, and it pushes the ram to reciprocate in the forming sleeve to provide a force that forms the briquette to the size and shape defined. The briquetting machine’s screw-type can be used similarly to the piston pressing by applying the force to create briquettes (Fig. 5).

One of the most common types of briquetting is a roller-type pressing machine similar to Fig. 6. Closer contact between tow rollers allows them to perform more efficiently. Both rollers have surface holes that coincidentally intersect while rotating in the opposite direction. The rollers move at

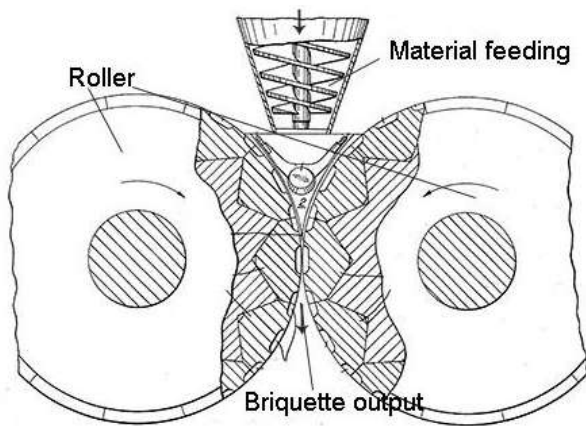


Fig. 6: Roller-type briquetting machine (MaxTon Industrial Co 2020).

the same speed and opposite direction. When they move in the opposite direction, two holes of both rollers meet in the middle of the machine and press the raw material to form the briquette.

According to the waste material and the economic condition, one of the methods mentioned can be applied to produce briquettes. However, the automated process is preferred as that can be used to apply stable high pressure for densification.

The hydraulic type works with a hydraulic pump station which supplies tremendous pressure. With its high pressure, almost all the materials can be briquetted with this system (Fig. 7). One of the advantages of the hydraulic system is briquetting can be produced even with the absence of water due to high pressure applied to raw materials. The briquette working process is in a chamber where materials are fed into; materials are briquetting under very high pressure. It causes their plasticity and causes them to bind together as a block in a stable manner. To keep time on the briquette, the hydraulic type requires a high level of pressure. This avoids short-term material deformation rebound and generates special heating for materials like sawdust to melt its interior lignin, resulting in a stronger briquette.

A. Binders

During the briquetting process, raw material densification will not be entirely stable due to particle distraction. Therefore, binding agents are essential to create internal bonding between the particles during densification. Binders help in obtaining sufficient strength for the finished briquette; with the use of binders, raw material particles are densified, resulting in strong briquettes. The number of binders added to the raw material varies according to the raw materials’ properties and the binding agent. The use of an automated briquette machine with high pressure would reduce the use of a binding agent. There are plenty of binding agents reported

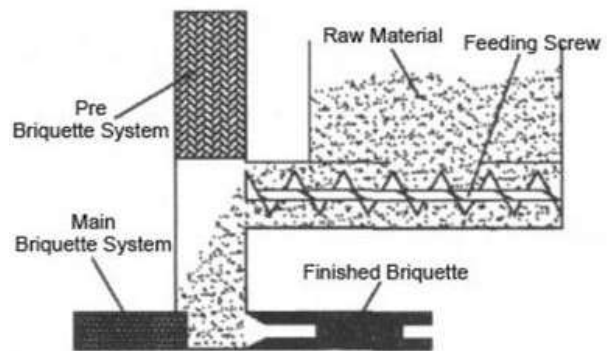


Fig. 7: Hydraulic type briquetting machine (MaxTon Industrial Co 2020).

in the literature that starts from lignin, biodegradable paper soaked in water, char, glycerin, molasses, cassava starch, wheat starch, and waste cooking oil (Bazargan et al. 2004, Massaro et al. 2014, Okegbile et al. 2014, Haykiri-Acma et al. 2013, Njenga et al. 2013, Prasityousil & Muenjina 2013, Fengmin & Mingquan 2011, Chou et al. 2009, Hedman et al. 2005, Rubio et al. 1999). Moreover, material that contains lignin has a better chance for briquetting without a binder agent as that lignin itself acting as a binding agent. Therefore, it is essential to analyze the raw feedstock's lignin content to identify whether external binding agents are necessary or not (Rubio et al. 1999).

B. Quality Parameters

To determine whether a product is suitable for combustion, a few factors must be addressed.

- The average time for briquettes to ignite plays a significant role as that represents the ignition of the briquette.
- Time is taken for the cooking process with a certain briquette or briquette requirement to complete the specific application.
- Soot formation and the ash generated are important as they are directly related to the amount of heat supply to the application.
- Flue gas emission analysis is important to understand environmental pollution compared with conventional biomass.
- Odor during the combustion process will be produced when used for household cooking and industrial heating.

There are significant physical parameters of briquettes to measure to compare and categorized as a quality product. The briquette density is one of the most important parameters as it defines the briquette's energy content (Kpalo et al. 2020).

The feedstock and binding agent density, operating pressure, temperature, and water content will decide the product's eventual density. Based on the density, the total energy content in one unit is varied. Moreover, the burning time of the briquette also i

content is an important parameter that impacts the density of the final product. Moreover, the higher moisture content will lead to a lower calorific value (Miranda et al. 2015). However, a significantly lower moisture limit also leads to lower quality as it will burn out very fast without generating proper energy (Ahmad et al. 2018). Simultaneously, moisture content that is less than 4% or 5% will reduce stability (Tumuluru et al. 2011). The suitable moisture content is around 8% is suggested by many of the previous studies as

it will overcome previously explained drawbacks (Chin & Siddiqui 2004).

The compressive index can also be used to determine the briquette's stability and quality, as well as its transport and storage capabilities (Gendek et al. 2018). Compressive strength is the maximum crushing load a briquette can withstand before cracking or breaking into pieces. However, compressive strength will depend on the material's particle size, water content, operating pressure and temperature, and the type of the material (Gendek et al. 2018). The compressive strength value can be varied between 10 - 22 MPa according to the raw material and the production steps. Among all the factors, the most important one is the final product's calorific value, which will decide the briquette's energy content (Romallosa 2017). The calorific value of the briquette is reported between 13-16 MJ.kg⁻¹ (Gill et al. 2018).

CONCLUSIONS

Briquettes production can be considered as one of the essential waste management practices. Most developing countries have agricultural waste as crop residue or industrial waste as sludge or sewage. The most applicable energy generation in those countries is based on biomass and fossil fuel. However, waste disposal practices are in a deplorable situation in developing countries. As a result, reusing waste to make fire briquettes will improve environmental quality and sustainability while lowering energy generation costs by providing employment opportunities for those living in rural areas. There are multiple raw materials available for briquette production, ranging from industrial sludge, sewage, agro waste, industrial wastes such as sawdust, paddy husk, or cotton flock in the garment industry. The quality of the raw material has to be pre-checked before starting the production process. Multiple physical and chemical properties have to be analyzed to define the production process's operating condition to maintain the moisture content, durability, or stability at the densification stage. The production process of the briquette can be achieved by many different technologies such as piston pressing, screw pressing, roller type pressing as automated, or using manual pressing with the metal mold. During the combustion process and after the combustion process, other qualities such as time taken to ignite, amount of fuel consumption, soot formation, ash remaining, smoke and flue gas analyzing, and odor must be considered to identify the quality of the briquette. Briquetting technology is yet to receive substantial attention in many developing countries with commercial success because of the technical constraints involved and the lack of knowledge to adapt the technology to suit local conditions.

REFERENCES

- Abdel-Shafy, H.I. and Mansour, M.S.M. 2018. Solid waste issue: Sources, composition, disposal, recycling, and valorization. *Egypt. J. Pet.*, 27: 1275-1290.
- Ahmad, K.K.Z., Sazali, K. and Kamarolzaman, A. 2018. Characterization of fuel briquettes from banana tree waste. In *Materials Today: Proceedings*; Elsevier Ltd.: Amsterdam, The Netherlands, 21744-21752.
- Andrejko, D. and Grochowicz, J. 2007. Effect of the moisture content on compression energy and strength characteristic of lupine briquettes. *J. Food Eng.*, 83(1): 116-120.
- Arachchige, U.S.P.R. and Sandupama, P.W.S. 2019. Alternative fuel for biomass boilers in Sri Lanka. *Int. J. Chem. Stud.*, 07: 729-733.
- ASTM Standard E711 – 87. 2004. Standard test method for gross calorific value of refuse-derived fuel by the bomb calorimeter: Annual Book of ASTM Standard [Online]. Available: <http://www.astm.info/standard/E711.Htm2004>. [Accessed on: 27/10/2020].
- Bazargan, A., Rough, S.L. and G. McKay. 2004. Compaction of palm kernel shell biochars for application as solid fuel. *Biomass and Bioenerg.*, 70: 489-497.
- Britta, P. 2014. Charcoal Briquette Production: A Practical Training Manual. UN-Habitat, Nairobi, pp. 1-21
- Chin, O.C. and Siddiqui, K.M. 2004. Characteristics of some biomass briquettes prepared under modest die pressures. *Biomass Bioenerg.*, 18: 223-228.
- Chou, C.S., Lin, S.H., Peng, C.C. and Lu, W.C. 2009. The optimum conditions for preparing solid fuel briquette of rice straw by a piston-mold process using the Taguchi method. *Fuel Process. Technol.*, 90(7-8): 1041-1046.
- Diener, S., Semiyaga, S., Niwagaba, C.B., Muspratt, A.M., Gning, J.B., Mbéguéré, M., Ennin, J.F., Zurbrugg, C. and Strande, L. 2014. A value proposition: Resource recovery from fecal sludge: Can it be the driver for improved sanitation? *Resour. Conserv. Recycl.*, 88: 32-38.
- Emerhi, E.A. 2011. Physical and combustion properties of briquettes produced from sawdust of three hardwood species and different organic binders. *Adv. Appl. Sci. Res.*, 2(6): 236-246.
- Enweremadu, C.C., Ojediran, J.O., Oladeji, J.T. and Afolabi, L.O. 2004. Evaluation of energy potentials in husk from soybean and cowpea. *Sci. Focus*, 8: 18-23.
- Fengmin, L. and Mingquan, Z. 2011. Technological parameters of biomass briquetting of macrophytes in Nansi Lake. *Energy Procedia*, 5:2449-2454.
- Garrido, M.A., Conesa, J.A. and Garcia, M.D. 2017. Characterization and production of fuel briquettes made from biomass and plastic wastes. *Energies*, 10: 850-860.
- Gendek, A., Aniszewska, M., Malat'ák, J. and Velebil, J. 2018. Evaluation of selected physical and mechanical properties of briquettes produced from cones of three coniferous tree species. *Biomass Bioenerg.*, 117, 173-179.
- Gill, N., Dogra, R. and Dogra, B. 2018. Influence of moisture content, particle size, and binder ratio on quality and economics of rice straw briquettes. *Bioenerg. Res.*, 11: 54-68.
- Government of Canada. 2017. Biomass Resources [Online]. Available: <https://www.nrcan.gc.ca/energy/energy-sources-distribution/renewables/bioenergy-systems/biomass-resources/7389>, [Accessed on:16/10/2020].
- Haykiri-Acma, H., Yaman, S. and Kucukbayrak, S. 2013. Production of bio briquettes from carbonized brown seaweed. *Fuel Process. Technol.*, 106: 33-40.
- Hedman, B., Burvall, J., Nilsson, C. and Marklund, S. 2005. Emissions from smallscale energy production using co-combustion of biofuel and the dry fraction of household waste. *Waste Manage.*, 25(3): 311-321.
- Kaliyan, N. and Vance Morey, R. 2009. Factors affecting strength and durability of densified biomass products. *Biomass Bioenerg.*, 33(3): 337-359.
- Kaliyan, N. and Vance Morey, R. 2010. Densification characteristics of corn cobs. *Fuel Processing Technology*, 91(5): 559-565.
- Kpalo, S.Y., Zainuddin, M.F., Abd Manaf, L. and Roslan, A.M. 2020. Production and characterization of hybrid briquettes from corncobs and oil palm trunk bark under a low-pressure densification technique. *Sustainability*, 12: 2468.
- Kpalo, S.Y., Zainuddin, M.F., Abd Manaf, L. and Roslan, A.M. 2020. A review of technical and economic aspects of biomass briquetting. *Sustainability*, 12: 4609.
- Lela, B., Barišić, M. and Nižetić, S. 2016. Cardboard/sawdust briquettes as biomass fuel: Physical-mechanical and thermal characteristics. *Waste Manage.*, 47: 236-245.
- Li, H., Liu, X., Legros, R., Bi, X.T., Jim Lim, C. and Sokhansanj, S. 2007. Pelletization of torrefied sawdust and properties of torrefied pellets. *Appl. Energ.*, 93: 680-685.
- Lubuwama, M. and Yiga, V.A. 2017. Development of groundnut shells and bagasse briquettes as sustainable fuel sources for domestic cooking applications in Uganda. *Renew. Energy*, 111: 532-542.
- Massaro, M.M., Son, S.F. and Groven, L.J. 2014. Mechanical, pyrolysis, and combustion characterization of briquetted coal fines with municipal solid waste plastic (MSW) binders. *Fuel*, 115: 62-69.
- MaxTon Industrial 2020. How does a briquette machine work: Types and making process [Online]. Available: <https://briquettesolution.com/how-does-a-briquette-machine-work-types-and-making-process> [Accessed on: 17/10/2020].
- Merete, W., Haddis, A., Alemayehu, E. and Ambelu, A. 2014. The potential of coffee husk and pulp as an alternative source of environmentally friendly energy. *East Afr. J. Sci.*, 8: 29-36.
- Miranda, T., Montero, I., Sepúlveda, F., Arranz, J., Rojas, C. and Nogales, S. 2015. A review of pellets from different sources. *Materials*, 8: 1413-1427.
- Mu'azil, N.M., Dambatta, M.S., Tukur, S.A., Abdullahi, B. and Abdullahi, U. 2016. Effects of Using Rice Husk and Paper Pulp as Organic Binding Agents on Calorific Value of Biomass (Sawdust) Briquettes. 2nd National Engineering Conference, ACICON, December 2016, Faculty of Engineering, Bayero University, Kano, Nigeria, pp.1-5.
- Njenga, M., Karanja, N., Jamnadass, R., Kithinji, J., Sundberg, C. and Jirjis, R. 2013. Quality of cooking fuel briquettes produced locally from charcoal dust and sawdust in Kenya. *J. Biobased Mater. Bioenergy*, 7(3): 315-322.
- Okegbile, O.J., Hassan, A.B., Mohammed, A. and Irekeola, B.J. 2014. Effect of starch and gum Arabic binders in the combustion characteristics of briquette prepared from sawdust. *Int. J. Sci. Eng. Res.*, 5(3): 1005-1009.
- Onukak, I.E., Ibrahim, A., Mohammed, D., Alewo, O., Ameh Stanley, I.R., Okoduwa, I.D. and Opeoluwa, O.F. 2017. Production and characterization of biomass briquettes from tannery solid waste. *Recycling*, 2(17): 1-19.
- Ortiz, L., Tejada, A., Vázquez, A. and Piñeiro, G. 2013. Use of Forest Biomass Produced by the Monte-Industria Chain. Part III: Production of Densified Elements. *CIS-Madera Magazine*, pp. 17-32.
- Prasityousil, J. and Muenjina, A. 2013. Properties of solid fuel briquettes produced from rejected material of municipal waste composting. *Procedia Environ. Sci.*, 17: 603-610.
- Rabbani, M.G., Sattary, C.T., Mamun, M.R.A., Rahman, M.M. and Khan, M.N.H. 2017. Performance analysis of non-renewable energy in Bangladesh. *Indones. J. Electr. Eng. Comput. Sci.*, 5(2): 290-298.
- Romallosa, A.R.D. 2017. Quality analyses of biomass briquettes produced using a jack-driven briquetting machine. *Int. J. Appl. Sci. Technol.*, 7:8-16.
- Romallosa, A.R.D. and Kraft, E. 2017. Feasibility of biomass briquette production from municipal waste streams by integrating the informal sector in the Philippines. *Resources*, 6: 12-18.
- Rubio, B., Izquierdo, M.T. and Segura, E. 1999. Effect of binder addition on the mechanical and physicochemical properties of low-rank coal char briquettes. *Carbon*, 37: 1833-1841.

- Zafar, S. 2016. Role of Biomass Energy in Rural Development [Online]. Available: <https://www.bioenergyconsult.com/biomass-energy-rural-development/> [Accessed on: 27/10/2020].
- Scarlat, N., Dallem, J.F., Monforti-Ferrario, F. and Nita, V. 2015. The role of biomass and bioenergy in a future bio-economy: Policies and facts. *Environ. Develop.*, 15: 3-34.
- Shafie, S.M., Mahlia, T.M.I., Masjuki, H.M. and Ahmad-yazid, A. 2012. A review on electricity generation based on biomass residue in Malaysia. *Renew. Sust. Energ. Rev.*, 16: 5879-5889.
- Stolarski, M.J., Szczukowski, S., Tworkowski, J., Krzyżaniak, M., Gulczyński, P. and Mleczek, M. 2013. Comparison of quality and production cost of briquettes made from agricultural and forest origin biomass. *Renew. Energ.*, 57: 20-26.
- Tumuluru, S.J., Christopher, W.T., Kenny, K.L. and Hess, J.R. 2010. A Review on Biomass Densification Technologies for Energy Application. Idaho National Laboratory: Falls, Idaho.
- Tumuluru, S.J., Wright, C.T., Hess, J.R. and Kenney, K.L. 2011. A review of biomass densification systems to develop uniform feedstock commodities for bioenergy application. *Biofuels Bioprod. Bioref.*, 5: 683-707.
- Udehl, B.A. and Kidak, R. 2019. The excessive use of fossil fuel and its impact on climate change in Africa. *Curr. J. Appl. Sci. Technol.*, 32(5): 1-4.
- Zhang, Y., Obrist, D., Zielinska, B. and Gertler, A. 2013. Particulate emissions from different types of biomass burning. *Atmos. Environ.*, 72: 27-35.



Influencing Factors of Carbon Emissions in the Construction Industry Based on Logarithmic Mean Divisia Index: A Case Study of China

Wang Lijuan†

Zhengzhou Business University, Gongyi 451200, China

†Corresponding author: Wang Lijuan, 1059514734@qq.com

Nat. Env. & Poll. Tech.
Website: www.neptjournal.com

Received: 20-07-2021
Revised: 12-08-2021
Accepted: 10-09-2021

Key Words:

LMDI
Construction industry
Carbon emission
Influencing factors

ABSTRACT

Carbon emission is further intensified as urbanization and industrialization continue to accelerate. China has maintained its rapid economic development and urbanization in the last 2 decades. The development of the construction industry has not only consumed a large number of energy sources but also resulted in significant carbon emissions, causing some environmental damage. Recognizing the major influencing factors of carbon emissions in the construction industry has become a research hotspot to alleviate environmental pollution caused by the construction industry and meet industrial demands for energy saving and emission reduction. In this study, the factors that influence annual carbon emissions of different building types in China from 2011 to 2018 were decomposed by Logarithmic Mean Divisia Index (LMDI) through a case study in Henan Province. The major influencing factors of carbon emissions have been identified. Results demonstrate that the per capita carbon emission in the construction industry in Henan Province remains high from 2011 to 2018, but it decreases year by year. Carbon emissions from the construction industry in Henan Province increase due to economic development and energy structure. Energy efficiency can inhibit carbon emissions from the construction industry in Henan Province. The obtained conclusions have a positive effect on analyzing annual variations in carbon emissions from the construction industry in a region, identifying influencing factors, and proposing specific countermeasures of energy saving and emission reduction.

INTRODUCTION

Greenhouse gases produced by human activities cause global climatic changes and threaten the survival environment of people in the world. With the acceleration of the urbanization process and improving the living standards of people, building energy consumption in China presents a rigid growth trend. The construction industry is characteristic of high energy consumption, high carbon emissions and low energy efficiency. The huge energy waste and CO₂ emission problems become increasingly prominent with the rapid development of the construction industry. The construction industry accounts for a high proportion in Chinese industries with high energy consumption. Energy saving and emission reduction of the construction industry play an important role in the national economic operation and regional environmental protection. China has assumed the top position around the world in terms of building material consumption and new building areas. CO₂ emissions from the energy consumption for production activities in the construction industry and mass use of building materials have caused serious adverse impacts on the ecological environment. The Green and low-carbon development of the construction industry must be promoted. Construction-induced carbon emissions in China still have

a great growth space. On one hand, industrial technologies continuously develop, and industrial efficiency consistently increases with the continuous progress in industrialization and urbanization in China. The carbon emission caused by industrial production gradually declines, which increases the proportion of consumptive carbon emissions indirectly, such as construction-induced carbon emissions. On the other hand, urban size continues to expand, and the consumption level of residents continuously increases in China, leading to the continuous growth in the energy consumption needs of residents. This situation can directly increase the proportion of construction-induced carbon emissions.

The construction industry is the traditional dominant industry and pillar industry of richening and strengthening of Henan Province. Recently, the total output of the construction industry and gross domestic product (GDP) in Henan Province have been increasing year by year (Fig. 1). The total output of the construction industry in Henan Province was 527.936 billion yuan (RMB) in 2011 and 1312.255 billion yuan (RMB) in 2020, showing an annual average growth rate of 16.51%. However, the construction industry in Henan Province encounters a development bottleneck. Given the highlighted problems of traditional backward

construction structure, the necessity of industrial structural optimization, the inadequate activity of market subjects, and insufficient policy guarantee, comprehensive industrial transformation and updating based on the development philosophy of “innovation, coordination, green, opening, and sharing” must be promoted. It is suggested to change the production mode of the construction industry, renew the project organization, accelerate the transformation from scale expansion to quality benefit improvement, cross from low-middle ends to middle-high ends in the industrial chain, increase the overall competitiveness of the construction industry in Henan Province, decrease carbon emissions from the construction industry comprehensively, and realize the coordinated development of construction industry and regional economy in the province. Nevertheless, energy consumption and greenhouse gas emissions of the construction industry in Henan Province are continuously increasing with the construction economic development, which influences the energy saving and emission reduction to a certain extent. Accordingly, Henan Province must devote itself to the development of green buildings, promote sustainable development of the construction industry, and decrease carbon emissions from the construction industry. The key influencing factors of carbon emissions from the construction industry must be determined, and specific countermeasures of energy saving and emission reduction must be proposed.

EARLIER STUDIES

The threats of global warming to human beings are widely known. Governments across the world have reached a consensus to build a low-carbon economy. The question of how can the construction industry realize low carbonization and recognize influencing factors of carbon emissions from the construction industry has become a research hotspot as carbon emission reduction attracts increasing attention.

Currently, many studies on the influencing factors of carbon emissions from the construction industry are available. These studies mainly decompose influencing factors through econometric model, index decomposition analysis (IDA), structural decomposition analysis (SDA), and logarithmic mean Divisia index. With respect to estimation of carbon emissions from the construction industry and influencing factors, Zhang et al. decomposed the influences on carbon emissions from the construction industry in Beijing by LMDI. The results demonstrated that changes in economic activities, population size, and per capita energy consumption stimulated emissions, while energy intensity, urban–rural population distribution structure, and changes in production and household energy structures decrease emissions (Zhang et al. 2013). Jiang et al. introduced a development ETS monitoring framework in Shenzhen and several challenges and policy choices (Jiang et al. 2014). Kang et al. believed that buildings emit a large amount of CO₂ within the service life, which is an important factor that causes the greenhouse effect (Kang et al. 2015). Sattary et al. demonstrated that construction-induced carbon emissions of the whole building system (floors, walls and roofs) can be decreased by 65% by using the principle of biological climate (Sattary et al. 2016). Jiang found that the energy intensity of residents, per capita housing area, and the total number of households are major driving factors that influence carbon emissions from the construction industry in China (Jiang 2016). Huang et al. developed the calculation method of urban building carbon footprints based on Xiamen City. Results demonstrate that urban building carbon footprints in Xiamen City increased from 8.95 million tons in 2005 to 13.57 million tons in 2009, showing an annual average growth rate of 12.87%. Production of building materials and carbon emission produced by building energy source account for 45% and 40% of building carbon footprints, respectively (Huang et al. 2017). Zhang et

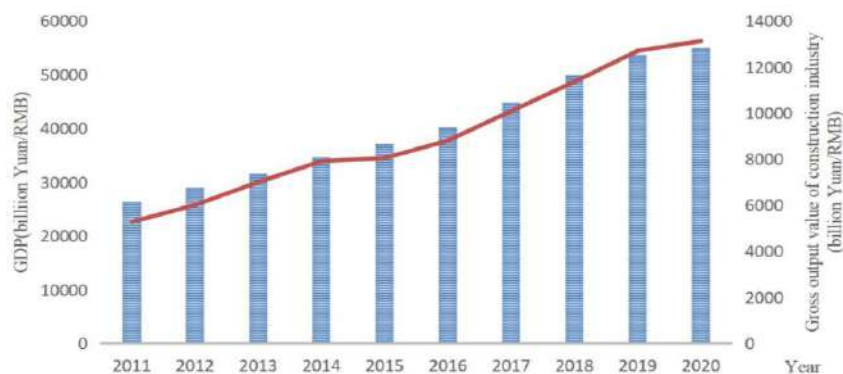


Fig. 1: The total output of the construction industry and gross domestic product (GDP) in Henan Province.

al. analyzed statistical data of China’s construction industry from 2004 to 2013. The results showed that the total emissions of China’s building industry presented an upward trend, and emissions in the building production stage were highest (Zhang et al. 2017). Huang et al. explored and compared the CO₂ emission levels caused by global construction activities by using the world environmental input-output sheet in 2009 and found that CO₂ emission of the global construction industry accounted for 23% of the total CO₂ emissions of global economic activities. China is the biggest contributor to carbon emissions from the construction industry (Huang et al. 2018). Li et al. studied the annual carbon emissions of construction land in Shanghai and its disconnection degrees with economic growth driven by six factors (Li et al. 2019). Lai et al. discussed relations of carbon emission intensity with carbon emissions from the construction industry, energy consumption, and GDP growth rate in China and its trend by using the improved Kaya model. The results showed that carbon emissions from the construction industry were mainly influenced by the GDP growth of the construction scale. Energy consumption was the major driving source to carbon emission growth (Lai et al. 2019). Zhang et al. proposed the China building construction model based on the LCA and discussed energy consumption and carbon emission trends of China’s building construction industry from 2000 to 2016. He found that construction scale, building structural type, and material production efficiency are three important driving factors (Zhang et al. 2019). Han et al. pointed out that the urban employment rate influenced the carbon emission intensity of the construction industry in China the most, and per capita consumption influenced the least (Han et al. 2019). Hao et al. reported that BIM is an effective method to measure carbon emissions of new building construction and prefabrication decreases carbon emission compared with the traditional construction method (Hao et al. 2020). Zhang et al. further decomposed the CO₂ emission connections of the global construction industry by using the multi-region input-output model and hypothesis extraction method. He found that the CO₂ emissions of the global construction industry mainly come from the secondary industry and transportation industry (Zhang et al. 2020). Based on the literature review, we conclude that existing studies on the influencing factors of carbon emissions from the construction industry mainly focus on Kaya identical relation, LMDI, and STIRPAT model. The considered macroscopic influencing factors include population, economic development, urbanization, export and import, and fixed-asset investment. Researches in China and foreign countries use IDA to discuss the influencing factors of carbon emission. IDA is easier to use and obtain data compared with SDA. Moreover, IDA is convenient to implement comparative analysis on time

series and trans-regions. Therefore, a case study based on Henan Province was carried out. The influencing factors of carbon emissions from the construction industry in Henan Province from 2011 to 2018 were decomposed by classical LMDI to provide energy saving and emission reduction measures for the construction industry and decrease carbon emissions from the construction industry in Henan Province.

MODEL INTRODUCTION AND DATA SPECIFICATION

LMDI Model

The influencing factors of carbon emissions from the construction industry are decomposed into Eq. (1) based on the Kaya model:

$$C = \sum_i C_i = \sum_i \frac{E_i}{E} \cdot \frac{C}{E_i} \cdot \frac{E}{Y} \cdot \frac{Y}{P} \cdot P, \quad \dots(1)$$

where C denotes carbon emissions from the construction industry, C_i represents the carbon emissions of the i th energy source in the construction industry, E is the total energy consumption of the construction industry, E_i is the consumption of the i th energy source in the construction industry, Y is GDP, and P denotes the total population at the end of a year. According to existing research results, $S_i = E_i/E$ was defined as the energy structure, which refers to the proportion of the i th energy source in the total energy consumption of the construction industry. $F_i = C/E_i$ is defined as the energy intensity, which refers to the carbon emissions from the construction industry by per unit consumption of the i th energy source. $I = E/Y$ is defined as energy efficiency, which refers to the total energy consumption of the construction industry per unit GDP. $R = Y/P$ is defined as economic development. Hence, Eq. (1) can be rewritten as Eq. (2).

$$A = \frac{C}{P} = \sum_i S_i F_i I R, \quad \dots(2)$$

Eq. (2) shows that the changes of per capita carbon emissions from the construction industry (A) mainly come from S_i , F_i , I , and R .

The changes of A in period t compared with that of the base period can be expressed as follows:

$$\begin{aligned} \Delta A = A^t - A^0 &= \sum_i S_i^t F_i^t I^t R^t - \sum_i S_i^0 F_i^0 I^0 R^0 = \Delta A_S \\ &+ \Delta A_F + \Delta A_I + \Delta A_R + \Delta A_{rsd}, \quad \dots(3) \end{aligned}$$

$$D = \frac{A^t}{A^0} = D_S D_F D_I D_R D_{rsd}, \quad \dots(4)$$

where ΔA_S and D_S are energy structures, ΔA_F and D_F are

energy intensities, ΔA_I and D_I are energy efficiencies, ΔA_R and D_R are economic developments, and ΔA_{rsd} and D_{rsd} refer to decomposition margins. In Eq. (3), ΔA_S , ΔA_F , ΔA_I , and ΔA_R express contributions of different factors to per capita carbon emissions from the construction industry. In Eq. (4), D_S , D_F , D_I , and D_R are contribution rates of different factors to changes of per capita carbon emissions from the construction industry. This study continued to use the LMDI proposed by Ang et al. (1998) for residue-free decomposition in Eqs. (3) and (4). Hence, $\Delta A_{rsd} = 0$, and $D_{rsd} = 1$. According to this method, different factors can be further decomposed as follows:

$$\Delta A = \Delta A_S + \Delta A_F + \Delta A_I + \Delta A_R + \Delta A_{rsd}$$

$$\Delta A_S = \sum_i \frac{A_i^t - A_i^0}{\ln(A_i^t / A_i^0)} \ln\left(\frac{S_i^t}{S_i^0}\right)$$

$$\Delta A_F = \sum_i \frac{A_i^t - A_i^0}{\ln(A_i^t / A_i^0)} \ln\left(\frac{F_i^t}{F_i^0}\right), \quad \dots(5)$$

$$\Delta A_I = \sum_i \frac{A_i^t - A_i^0}{\ln(A_i^t / A_i^0)} \ln\left(\frac{I_i^t}{I_i^0}\right)$$

$$\Delta A_R = \sum_i \frac{A_i^t - A_i^0}{\ln(A_i^t / A_i^0)} \ln\left(\frac{R_i^t}{R_i^0}\right)$$

$$D = D_S D_F D_I D_R D_{rsd}$$

$$D_S = \exp\left(\frac{\ln A^t - \ln A^0}{A^t - A^0}\right) \Delta A_S$$

$$D_F = \exp\left(\frac{\ln A^t - \ln A^0}{A^t - A^0}\right) \Delta A_F \quad \dots(6)$$

$$D_I = \exp\left(\frac{\ln A^t - \ln A^0}{A^t - A^0}\right) \Delta A_I$$

$$D_R = \exp\left(\frac{\ln A^t - \ln A^0}{A^t - A^0}\right) \Delta A_R$$

Data Specification

The estimation method of construction-induced carbon emissions in Henan Province is based on the method of construction-induced carbon emissions. In this study, the mature emission factor method, which is widely used and has a consensus in the industry, was applied to estimate carbon emissions in the building field. Construction-induced carbon emissions are the sum of CO₂ emissions from different fossil energies that are consumed directly (coal, oil, and natural gas) and indirectly (power and thermal power) in the running process of buildings. The calculation formula is as follows:

$$BCE = \sum BE_i EF_i \quad \dots(7)$$

where *BCE* refers to carbon emissions from the construction industry in Henan Province, *BE_i* refers to consumptions of the *i*th energy source in the operation of the construction industry in Henan Province, and *EF_i* refers to the carbon emission factor of the *i*th energy source of the construction industry in Henan Province. Carbon emission factors of fossil energy sources are shown in the General Rules for Comprehensive Energy Consumption Calculation (GB/T2589-2008). Data of consumptions of various energy sources in the construction industry of Henan Province were collected from the Regional Energy Sheet of Henan Province in history, while the rest of the data were collected from China's National Statistical Database (<https://data.stats.gov.cn/>). The investigation period was from 2011 to 2018.

Table 1: Influences on carbon emissions from the construction industry in Henan Province from 2011 to 2018.

	Per capita carbon emission of construction industry Δ	D	Economic development ΔAR	DR	Energy efficiency ΔAI	DI	Energy structure ΔAS	DS
2011	5.769	87.107	0.139	1.113	0.014	1.011	5.617	77.420
2012	4.898	74.106	0.265	1.262	-2.444	0.117	7.077	503.197
2013	3.639	55.306	0.285	1.369	-1.482	0.195	4.836	207.173
2014	3.319	50.544	0.333	1.483	0.729	2.366	2.257	14.405
2015	1.505	23.463	0.225	1.604	0.143	1.348	1.137	10.850
2016	1.898	29.334	0.299	1.704	0.184	1.387	1.415	12.417
2017	1.463	22.841	0.283	1.833	0.071	1.165	1.109	10.702
2018	1.413	22.093	0.323	2.030	-0.027	0.943	1.117	11.538

EMPIRICAL STUDY

The carbon emission factor decompositions of the construction industry in Henan Province from 2011 to 2018 are listed in Table 1, according to Eqs. (1)-(7).

Table 1 illustrates that:

1. The per capita carbon emission of the construction industry in Henan Province maintained at a high level from 2011 to 2018. As a result of the policy adjustment for the construction industry in Henan Province, the financial subsidies facilitate green technological innovation and strengthen the green research and development vitality of construction enterprises. Consequently, many green innovation technologies are developed under environmental regulation stimuli, promoting green construction and applications of environmentally friendly materials. Henan Province advanced construction technologies, expedited the development of environmentally friendly building materials and exploration of new energy sources, and decreased dependence on traditional high-carbon building materials and energy sources. These measures could optimize construction products from the design end and decrease the use of building materials, thus minimizing carbon emissions from the construction industry and increasing carbon emission efficiency. Meanwhile, Henan Province strengthened its promotion of advanced assembly technologies, factorized line production, and safe intelligent equipment. The province strengthened resource integration in the construction industry, reallocation of waste resources, and reproduction in the province, thus decreasing carbon emissions from the construction industry and increasing carbon emission efficiency. Accordingly, per capita carbon emissions in the construction industry decreased year by year, and the residential environment was improved.
2. The regional overall economic development significantly promoted carbon emissions from the construction industry in Henan Province. Economic development is strongly attracted to scientific and technological resources, allowing for the promotion of technological innovations and increased energy utilization. Furthermore, the environmental protection consciousness of government and citizens was strengthened after a certain degree of economic development, which has a favorable influence on carbon emissions from the construction industry. The growth of per capita GDP significantly facilitated carbon emissions from the construction industry, indicating that the relatively high per capita GDP was accompanied by high carbon emissions from the construction industry. Economic development increases the residence demands in urban and rural areas; thus, Henan Province has the ability and motivation to build large infrastructures and promote the construction of public service projects, which will also release high CO₂ contents. Carbon emissions from the construction industry will increase with the promotion of economic development. Hence, economic coordinated development must be achieved while decreasing the growth of carbon emissions from the construction industry. The basic idea lies in the high-quality economic development and driving energy-saving environmental protection needs of the construction industry.
3. Energy efficiency effect refers to the ratio of total energy consumption in the construction industry to total output. The energy consumption intensity of the construction industry has negative effects on carbon emission growth. Table 1 demonstrates that energy efficiency in Henan Province was positive in most years, but it was negative in 2012, 2013, and 2018. This finding indicates that energy efficiency could inhibit the growth of carbon emissions from the construction industry, but it varies in some years. For example, the energy efficiency of Henan Province from 2014 to 2017 could significantly promote carbon emissions from the construction industry in the year. Coals, gasoline, diesel, fuel oil, and power inhibited growth in carbon emissions from the construction industry, while kerosene promoted the growth of carbon emissions. The energy efficiency effect inhibits growth in carbon emissions from the construction industry, and it is a major factor that constrains carbon emissions. In other words, Henan Province achieved certain advances in construction technologies and energy-saving and emission-reduction tasks from 2011 to 2018, which had positive effects on carbon emission reduction.
- (4) Energy structure refers to the ratio of consumption of various energy sources for construction activities to the total energy consumption of the construction industry. The energy structural effect from 2011 to 2018 resulted in an upward trend of carbon emissions from the construction industry in Henan Province. Carbon emissions from the construction industry are positively influenced by kerosene, diesel, and power, while negatively affected coals, gasoline, and fuel oil. Coal and power significantly influence changes in carbon emissions from the construction industry, and they offset variations in carbon emissions. Accordingly, the energy structural effect slightly influences the changes in the carbon emissions from the construction industry. Energy structure gradually transforms to green energy, decreasing the consumption of fossil energy sources

and relieving environmental pollution. Meanwhile, this notion proves that the energy saving and emission reduction have achieved a certain degree of success.

POLICY SUGGESTIONS

Increase Energy Utilization in the Construction Industry

High energy consumption and emission have become the most typical features of the construction industry. Given that the driving contribution of energy intensity effect with the decreased carbon emission intensity of the construction industry in Henan Province still accounts for a low proportion, high-efficiency inhibition of energy intensity effect of construction has become an effective solution to high energy consumption problems. Therefore, energy utilization must be effectively enhanced by using energy sources wisely, and energy wastes during the construction process must be reduced. Henan Province has to strengthen technological innovations of the construction industry. The current energy structure is mainly comprised of coal and petroleum. Coal is critical to the industrialization of the construction industry. Energy utilization and recycling (e.g., coals) must be practically enhanced to strengthen uses and innovations in the deculturation of coals, clean coals, and energy recycling technologies. Substitutive energy sources shall be developed because the combustion of fossil fuels is an important cause of high emissions. Accordingly, low-carbon technologies may be used to improve production equipment and processes. A new substitutive material must be developed while minimizing the usage of fossil fuels.

Optimize the Energy Supply Structure in the Construction Industry

Henan Province increased the proportion of low-carbon energy sources in the building field. Henan Province investigated the potentials of renewable energy sources, such as photovoltaic, wind power, thermal pump, and biomass, by combining them with local features. This initiative supports building photovoltaic integrated building projects in qualified urban areas, such as Zhengzhou. Buildings have become a significant carrier for photovoltaic development, and photovoltaic utilization on the external surfaces of buildings has emerged as an important index to evaluate green buildings. Henan Province supports the construction of zero-carbon buildings and zero-carbon community demonstration projects to promote self-sufficiency of building energies. Some recommendations are as follows: 1) lower carbon emission from local power plants; 2) optimize heating energy structure, support innovations in electric heating technology, construct

renewable energy coupling heating projects, and encourage buildings in qualified regions to replace electrification heating; 3) fully use residual heat resources in industrial data center and improve intelligent heating level; 4) cooperate with renewable power use, optimize the intelligent power supply network, support energy storage technological development, and encourage qualified construction projects to build energy storage projects; and 5) change consumption mode positively, increase the low-carbon environmental protection consciousness, decrease use and purchase rate of high-carbon products, increase uses of energy-saving low-carbon products, such as high-efficiency energy-saving lights, new energy electric cars, and solar energy, and further optimize the market supply structure and energy consumption structure.

Promote Improvement of Energy Efficiency of Buildings

Low-carbon transformation must be encouraged in the construction field, and the green building standards must continuously increase. Moreover, the energy-saving level of building envelopes must be increased, buildings with ultra-low energy consumptions must be constructed, and reduction of carbon emissions through energy saving must be promoted. Existing buildings must continue the implementation of energy-saving reconstruction and effectively decrease carbon emission intensity per unit area. Qualified large public buildings must be investigated for inclusion in the carbon transaction market, and carbon emission reduction must be promoted by market means. The power grid structure of buildings can be optimized by cooperating with relocation and old community reconstruction activities, and a foundation for electric heating and natural gas heating must be established. Heating measurement of buildings must be continually promoted, and units and families must be advised with regard to the reasonable and appropriate use of thermal power. Lastly, waste and lower carbon emissions from ultra-temperature heating must be effectively reduced.

Strengthen Carbon Emission Consciousness of Building Enterprises

The government should strengthen education training of carbon emission reduction to residents to encourage all people to participate in carbon emission reduction in the building field, develop the green life habit of energy-saving and carbon-reduction, and promote the whole society to form a good atmosphere in which everyone is responsible for carbon emission reduction. In addition, the government can encourage building enterprises to use new energy-saving and recycling building materials and support building material

manufacturers to implement green production and relevant application technological reconstruction. Meanwhile, the government shall strengthen the recycling of solid wastes in the building industry. The rapid development of engineering construction continuously increases construction waste production. Processing and recycling of construction wastes are also effective tasks in achieving energy saving and emission reduction. Hence, a construction waste recycling technology must be developed, production technologies and techniques of enterprises for renewable building materials must be strengthened, enterprises must be encouraged to develop green building material technologies, equipment with high energy efficiency in recycling construction solid waste must be created. Finally, and further promote green energy-saving development of the construction industry in Henan Province.

CONCLUSIONS

China's rapid urbanization has resulted in a high concentration of urban population, land usage, and economic activities. This phenomenon increases urban energy demands and energy consumption, especially energy consumption in the construction industry. Carbon emission from the construction industry accounts for a high proportion, with an obvious growth trend and a high growth rate. The construction industry has some emission-reduction potential and claims relatively low emission-reduction costs. Accordingly, reducing carbon emission in the construction industry is a significant step toward China's national energy-saving and emission-reduction goal. In this study, the influencing factors of construction-induced carbon emissions in Henan Province from 2011 to 2018 were decomposed by LMDI, and the major influencing factors were identified. The results demonstrated that the per capita carbon emission of the construction industry in Henan Province remained at a high level from 2011 to 2018, but it decreased year by year. Carbon emissions from the construction industry in Henan Province have been continuously increasing due to economic development and energy structure. Energy efficiency inhibited carbon emissions from the construction industry in Henan Province. Finally, some policy suggestions were proposed, including increasing the energy utilization of the construction industry, optimizing the energy supply structure of the construction industry, promoting energy efficiency improvement of buildings, and strengthening the carbon

emission reduction consciousness of building enterprises. Future studies can measure the influencing degrees of factors related to construction-induced carbon emissions, enrich the full-lifecycle carbon emission estimation models of the construction industry, and deepen scenario prediction and analysis on carbon emissions from the construction industry.

REFERENCES

- Ang, B. W., Zhang, F. Q. and Choi, K. H. 1998. Factorizing changes in energy and environmental indicators through decomposition. *Energy*, 23(6): 489-495.
- Hao, J. L., Cheng, B., Lu, W., Xu, J., Wang, J., Bu, W. and Guo, Z. 2020. Carbon emission reduction in prefabrication construction during materialization stage: a BIM-based life-cycle assessment approach. *Science of the Total Environment*, 723: 137870.
- Han, X., Cao, T. and Sun, T. 2019. Analysis on the variation rule and influencing factors of energy consumption carbon emission intensity in China's urbanization construction. *Journal of Cleaner Production*, 238: 117958.
- Huang, L., Krigsvoll, G., Johansen, F., Liu, Y. and Zhang, X. 2018. Carbon emission of global construction sector. *Renewable and Sustainable Energy Reviews*, 81: 1906-1916.
- Huang, W., Li, F., Cui, S. H., Huang, L. and Lin, J. Y. 2017. Carbon footprint and carbon emission reduction of urban buildings: a case in Xiamen City, China. *Procedia Engineering*, 198: 1007-1017.
- Jiang, J. 2016. China's urban residential carbon emission and energy efficiency policy. *Energy*, 109: 866-875.
- Jiang, J. J., Ye, B. and Ma, X. M. 2014. The construction of Shenzhen's carbon emission trading scheme. *Energy Policy*, 75: 17-21.
- Kang, G., Kim, T., Kim, Y. W., Cho, H. and Kang, K. I. 2015. Statistical analysis of embodied carbon emission for building construction. *Energy and Buildings*, 105: 326-333.
- Li, Y. N., Cai, M., Wu, K. and Wei, J. 2019. Decoupling analysis of carbon emission from construction land in Shanghai. *Journal of Cleaner Production*, 210: 25-34.
- Lai, X., Lu, C. and Liu, J. 2019. A synthesized factor analysis on energy consumption, economy growth, and carbon emission of construction industry in China. *Environmental Science and Pollution Research*, 26(14): 13896-13905.
- Sattary, S. and Thorpe, D. 2016. Potential carbon emission reductions in Australian construction systems through bioclimatic principles. *Sustainable Cities and Society* 23: 105-113.
- Zhang, L., Liu, B., Du, J., Liu, C., Li, H. and Wang, S. 2020. Internationalization trends of carbon emission linkages: A case study on the construction sector. *Journal of Cleaner Production*, 270: 122433.
- Zhang, X. and Wang, F. 2017. Life-cycle carbon emission assessment and permit allocation methods: a multi-region case study of China's construction sector. *Ecological Indicators*, 72: 910-920.
- Zhang, Y., Yan, D., Hu, S. and Guo, S. 2019. Modelling of energy consumption and carbon emission from the building construction sector in China, a process-based LCA approach. *Energy Policy*, 134: 110949.
- Zhang, J., Zhang, Y., Yang, Z., Fath, B. D. and Li, S. 2013. Estimation of energy-related carbon emissions in Beijing and factor decomposition analysis. *Ecological Modelling*, 252: 258-265.



Solid Selective Catalytic Reduction: A Promising Approach towards Reduction of NO_x Emission from Exhaust of CI Engines

M. K. Yadav[†] and A. K. Srivastava

Department of Mechanical Engineering, University of Petroleum and Energy Studies, Bidhauri Campus, Dehradun, Uttarakhand, 248007, India

[†]Corresponding author: M.K. Yadav; mkyadav80@rediffmail.com, ddn@upes.ac.in

Nat. Env. & Poll. Tech.

Website: www.neptjournal.com

Received: 05-11-2020

Revised: 31-12-2020

Accepted: 13-01-2021

Key Words:

Air pollution

Diesel engine exhaust

NO_x reduction

Conversion efficiency

Solid selective catalytic reduction (SSCR)

ABSTRACT

The rising rate of pollution in urban areas has become a worldwide concern in recent years. Diesel engines are considered one of the largest contributors to environmental pollution caused by exhaust emissions, and they are responsible for several health problems as well. Diesel engines contain carbon monoxide, carbon dioxide, unburned hydrocarbons, and oxides of nitrogen. The reduction of Nitric oxides (NO_x) emission from diesel engine exhaust is currently being researched by automotive manufacturers. After much research, selective catalytic reduction (SCR) technology was discovered to be effective in reducing nitrogen oxide emission from diesel engine exhaust. This paper is an attempt to explore the problems associated with the use of selective catalytic reduction (SCR) and compares selective catalytic reduction (SCR) with the latest technology named solid selective catalytic reduction (SSCR) for efficient reduction of NO_x emission from the exhaust of diesel engines. The issue of contamination, malfunctioning, and freezing of diesel exhaust fluid (DEF) at low temperatures are the major problems associated with the application of SCR. It is observed that by controlling the quantity of ammonia slip, SSCR can give better performance in the reduction of NO_x emission from the exhaust of diesel engines.

INTRODUCTION

There is no doubt today that air pollution is a global public health emergency. This is a problem that almost every country is dealing with. Faced with the hazard of deteriorating air composition, many countries over the years adapted to technology and strategies to counter the crisis. The seriousness of the issue has (SSCR) been proven by environmental change as a result of a global temperature increase. Air quality issues related to nitrogen oxides and ozone are of significant concern in the United States, Europe, China, and many other locations (Erickson et al. 2020). Transport is the main sector which causes environmental pollution and climate change. Owing to the rapid increase of motor vehicles and very limited use of emission control technologies, transport emerges as the largest source of urban air pollution, which is an important public health problem in most cities of the developing world. Emissions from transport, and especially motor vehicles, add considerably to the levels of greenhouse gases in the atmosphere, being a significant contributor to global warming. Studies have demonstrated that exposure to diesel exhaust gas causes harm to lungs and respiratory issues, and there is strong evidence that diesel discharges cause malignancy in people (Sydbom et al. 2001, Solomon & Balmes 2003, Lewtas 2007). The fumes

of diesel engines contain unburned hydrocarbons (UHC), particulate contaminants, and nitrogen oxides, all of which are responsible for air pollution. The percentage of fumes outflows from diesel motors is shown in Fig. 1

It is clear from Fig.1 that diesel engine exhaust contains a major portion of nitrogen (67%), whereas CO₂ (12%), H₂O (11%), and oxygen (9%) remain in moderate quantity. Carbon monoxide, hydrocarbons, particulate matter, oxides of nitrogen, and sulfur dioxide (SO₂) remain in very little quantity but represent the most hazardous components of diesel engine exhaust which are highly responsible for disturbing the balance of the environment.

Recent studies have shown that particulate matter emissions and outdoor fine particulates were responsible for 7.6% of the deaths (4.2 million people) globally in 2015 (Kurien et al. 2019). Diverse pretreatment and post-treatment headways have been grasped to decrease exhaust radiations. Exhaust emissions from diesel engines pose a serious threat to the environment and human health. The combined application of pre-treatment and post-treatment techniques is the only solution to reduce these emissions. Pre-treatment techniques include engine modifications like combustion cylinder alteration, injection timing retard, exhaust gas recirculation, fuel injection strategies, and so on (Kurien & Srivastava 2018),

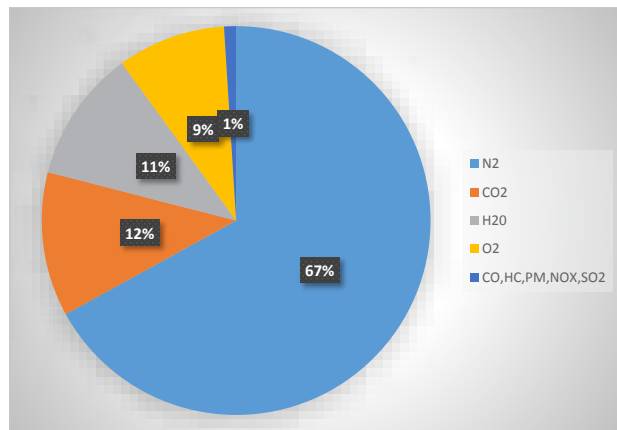


Fig. 1: Composition of diesel engine exhaust (Reşitoğlu et al. 2015).

Regardless, they are still insufficient to minimize nitrogen oxides emission from the exhaust of diesel engines, which is the most difficult task in reducing hazards. Long-term ambient air pollution exposure was reported to increase all-cause mortality. Air pollution is the cause and aggravating factor of many respiratory diseases like chronic obstructive pulmonary disease, asthma, pneumonia, and lung cancer. The presence of a large amount of NO_x in the atmosphere causes a destructive deluge and the formation of smoky clouds. Air pollution in the form of Nitrogen oxides (NO_x) can harm the ozone layer which protects the surface of the Earth from harmful radiation. Aside from the harmful effects on the environment, these oxides have a significant impact on human health (Yan et al. 2014). Due to the above realities, the Euro-VI emission standards specifically noted that a “considerable reduction in oxides of nitrogen emissions from diesel vehicles is necessary to improve air quality and comply with limit values for air pollution. The move from Euro V to Euro VI saw a large reduction in the NO_x emission limit, from 2.0 g.kWh⁻¹ to 0.4 g.kWh⁻¹ in steady-state testing, and from 2.0 g.kWh⁻¹ to 0.46 g.kWh⁻¹ in transient testing, or reductions of 80% and 77% respectively (Williams & Minjares 2016).

A comparison of emission norms in EURO-V & EURO-VI is shown in Table 1 which clearly indicates the necessity of DPF and SCR in diesel engines. The NO_x

Table 1: Requirements of components for EURO -V and EURO-VI norms (Williams & Minjares 2016).

EURO-V	EURO-VI
<ul style="list-style-type: none"> • High fuel injection pressure. • Redesigns to the combustion chamber. • NO_x is controlled mainly by SCR vanadium-based systems. • EGR is offered by some manufacturers and mainly for small trucks. 	<ul style="list-style-type: none"> • DPFs required for EURO-VI compliance with PM and PN standards. • SCR catalyst changes from vanadium to zeolite. • EGR is no longer offered.

reduction efficiency must be greater than 95% as per the EURO-VI discharge standards, and the ammonia slip must be less than 10ppm. In the United States and Europe, SSCR technology is being adopted in big diesel vehicles, which is both practical and cost-effective.

For the reduction of NO_x, various after-treatment technologies such as selective catalytic reduction (SCR), lean NO_x trap (LNT), and SCR channel are used, however, the conversion efficiency of NO_x could surpass 75% (Praveena & Martin 2018). Exhaust gas recirculation (EGR) is an emission control technology allowing significant NO_x emission reductions from most types of diesel engines. However, it cannot achieve a high NO_x reduction efficiency that meets existing discharge standards, particularly, in heavy vehicles. Likewise, because of the decrease of temperature in the chamber, this technology increase hydrocarbon (HC) and carbon dioxide (CO₂) emanations (Bauner et al. 2009). In Diesel engines, the fuel type, engine adjustment, and design affect the content of hydrocarbons. Besides, HC emissions in the exhaust gas depend on irregular operating conditions. High levels of the instantaneous change in engine speed, untidy injection, excessive nozzle cavity volumes, and injector needle bounce can cause significant quantities of unburned fuel to pass into the exhaust (Payri et al. 2009). Despite the fact that SCR has shown promising results in reducing nitrogen oxides, it is not without its disadvantages. Some nitrogen oxides remain unreduced when fluid urea is used as a decreasing agent, which is known as urea slip. This problem arises due to the fact that the catalyst's ability to change state is reduced at low temperatures. Catalyst efficiency is highest when the temperature of the fumes is between 200°C to 400°C (Ma et al. 2019). When functioning at these temperatures, the catalyst chamber should be filled on a regular basis, usually, before the fuel chamber is emptied (Lacin et al. 2011). Urea-based selective catalytic reduction (SCR) of nitric oxides (NO_x) is a key technology for heavy-duty diesel engines to achieve the increasingly stringent NO_x emission standards. The aqueous urea injection control is critical for urea-SCR systems to achieve high NO_x conversion efficiency while restricting the tailpipe ammonia (NH₃) slip. For Euro VI emission regulation, an advanced control strategy is essential for SCR systems since its NO_x emission limits are tighter and test procedures are more stringent compared to Euro IV and Euro V. The complex chemical kinetics of the SCR process has motivated model-based control design approaches. However, the model is too complex to allow real-time implementation. Therefore, it is very important to have a reduced-order model for the SCR control system. (Wang et al. 2018).

Urea SCR

Urea SCR is one of the most effective NO_x reduction tech-

niques, capable of converting around 95% of nitrogen oxides. It can work effectively at a temperature of 200°C. The exhaust after-treatment devices that are applied to vehicles are Diesel Oxidation Catalysts (DOC), Diesel Particulate Filters (DPF), and Selective Catalytic Reduction (SCR) catalysts. The carbon component includes elemental carbon, total carbon, organic carbon, ions, and water-soluble organic carbon. The installation of retrofits such as Diesel oxidation catalyst (DOC), diesel particulate filter (DPF), and Selective catalytic reduction (SCR) is one of the most effective ways for reducing particulate emissions. The installation of retrofits reduced PM mass emissions by over 90% in cruise and 95% of the fumes from the exhaust of diesel engines (Biswas et al. 2009). Penetration of soot on the wall results in a reduction of deNO_x efficiency of the SCR system (Johnson 2016). Most particulate matters (PM) resulted from incomplete combustion of the hydrocarbons in the fuel and lube oil. In an experimental study, it is reported that PM consists of elemental carbon (31%), sulfates and moisture (14%), unburnt fuel (7%), unburnt lubricating oil (40%), and remaining may be metals and other substances (Agarwal 2007). The use of a diesel particulate filter (DPF) reduces elemental carbon by trapping particulates effectively. The amount of organic carbon can be reduced by using catalysts, which oxidize hydrocarbons and reduce the amount of water-soluble organic carbon. The increased amount of sulfate nanoparticles in the DPF manufactured vehicle is caused by a decrease in residue particulate size (Biswas et al. 2009)

Vehicles equipped with catalyzed DPF and urea SCR had 99.9% and 90% efficiency, respectively, in reducing particulate matter. The DPF plasma-assisted burner successfully decreases particulate amount over the whole particle size range (Lee et al. 2015). The Continuously Regenerating Trap (CRT) has been developed to enable diesel engines to meet the proposed future legislation. This passive filter system combines an oxidation catalyst with a Diesel Particulate Filter (DPF); the filter traps the PM and the oxidation catalyst generates NO₂ which combusts the trapped PM at substantially lower temperatures than is possible using oxygen. This combines the CRTTM with SCR (Selective Catalytic Reduction) technology and enables very high simultaneous conversions of CO, HC, PM, and NO_x to be achieved (Allansson et al. 2000).

The DOC+CDPF+SCR retrofit was proved a feasible and effective measurement in terms of reducing particulate emissions and NO_x simultaneously for the in-use engine. The usage of these retrofits has no effect on fuel consumption or engine power (Zhang et al. 2018). These filters can reduce more than 90% of the particulate matter. At the same time, the particulate size is also reduced (Mamakos et al., 2013).

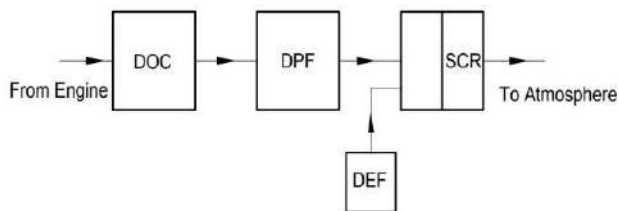


Fig. 2: Schematic diagram of urea SCR (Zhang et al. 2018).

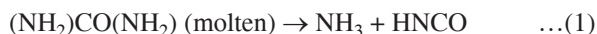
A schematic diagram of urea SCR is shown in Fig. 2 which contains DOC, DPF, DEF and SCR as the main components of the system. Engine exhaust is routed into the DOC, which converts hydrocarbons into carbon particles. The carbon particles are collected and stored by DPF. These soot particles are burned on a regular basis. SCR is used to reduce NO_x emissions in the fume gas by using alkali (NH₃) as a reductant (Biswas et al. 2009).

The exhaust of a diesel engine contains about 17% unused oxygen by volume which is used for the oxidation of hydrocarbons. Hydrocarbons and carbon mono oxides are converted to carbon dioxide and water by DOC. DOC is usually installed before DPF to use nitrate oxidation to regenerate the particles (Kurien & Srivastava 2018). It's been discovered that oxidation releases a lot of heat, which raises the temperature of the exhaust line that supports the DPF. The temperature of the exhaust gas is projected to increase by 90°C for every 1% oxidation of CO (Reşitoğlu et al. 2015).

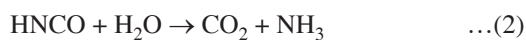
The use of DOC in the upstream affects the CDPF's efficiency. DOCs have been a major invention for diesel motors since their introduction in the 1970s (Wang & Baek 2008). With the use of DOC, the proportion of NO₂ is increased, and a faster rate of particle emission is seen, decreasing the lower side temperature. By oxidizing a portion of the hydrocarbons that are adsorbed onto the carbon particles, DOCs help to reduce the bulk of diesel particulate emissions (Wang et al. 2012). Using the combination of DOC and DPF can reduce 90% of particles, 80% hydrocarbons, and 45% of carbon mono oxide (CO) (Zhang et al. 2018). In the untreated motor that fumes gas, the NO₂ part in the NO_x is just around 10 % at most working focuses. The capacity of the DOC increases the rate of NO₂:NO by inducing thermodynamic concord (Lee et al. 2013, Sampara et al. 2007). Because of the negative effects of NH₃ and to avoid consumption of NH₃ before the response, NH₃ is produced from a fluid arrangement of urea (Hamada & Haneda 2012). DEF is an aqueous solution with 32.5% urea and 67.5% deionized water which is sprayed in the exhaust stream for the reduction of NO_x. The consumption of DEF was found to be 2% of fuel consumption. Spray wall impingement of UWS was investigated in a constant volume chamber by numerical

simulation using STAR CCM+ CFD code. The investigation reveals that wall temperature is the most important parameter that significantly affects spray development after impingement, droplet size distribution, wall film formation, and droplet evaporation. Increasing the wall temperature leads to longer spray front projection length, smaller droplet size, faster droplet evaporation and smaller film thickness, which are preconditions for urea crystallization reduction. The numerical model and parameters were validated by comparing with experimental data (Shahariar et al. 2018)

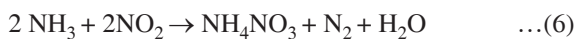
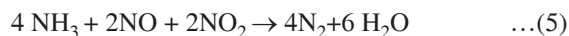
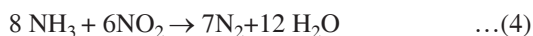
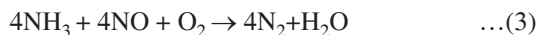
When DEF is injected into the exhaust stream, urea decomposes into ammonia and isocyanic acid due to exhaust temperature.



Due to the hydrolysis of this isocyanic acid, ammonia and carbon dioxide gases are produced.



Now ammonia in the presence of oxygen and a catalyst present in SCR reduces the oxides of nitrogen



Equation (1) shows how urea in molten form is decomposed into ammonia and hydrocyanic acid when it comes in contact with the high temperature of the exhaust. Equation (2) represents the hydrolysis of isocyanic acid in which ammonia and carbon dioxide are the main product. These two reactions occur without the requirement of any catalyst. Equation (3) can be considered as the standard reaction where the same amount of ammonia and NO react with oxygen. Equation (4) represents the slow and fast SCR reactions. Some undesirable reactions also take place as a result of which ammonium nitrate is produced at low temperatures below 200°C. These undesirable reactions reduce the conversion of NOx and result in urea slip (Kurien et al. 2018). The efficiency of conversion of NOx is one of the major parameters in the performance analysis of SCR

$$\text{NOx conversion} = [1 - (\text{NOx out}/\text{NOx in})] \times 100\%$$

(Peng et al. 2015)

Catalysts used in SCR

Copper zeolite and iron zeolite are widely used catalysts in SCR. The reason being their high-temperature stability and good performance when working at low temperatures. Copper zeolite-based SCR was found to be comparatively better than Fe zeolite due to their higher ammonia storage

capacity and oxidation which results in reduced ammonia slip (Guan et al. 2014).

In addition to copper and iron zeolite, Vanadium based SCR catalysts, SiO₂ and TiO₂ are also used as catalysts. Monolith catalysts are also used. Manganese-based catalysts show good performance characteristics while using low-temperature SCR systems as efficiency is not much affected (Gao et al. 2017).

Challenges in SCR

Various urea SCR systems have been used in trucks and passenger cars (Lacin et al. 2011). The solution of Urea is injected into the catalytic tank of SCR with help the of a nozzle but it shows a low ammonia carrying capacity (Qu et al. 2014). The major problem in SCR is the freezing of DEF at temperatures below -11°C which necessitates an integrated electric heater in the tank of DEF. Diesel particulate filter (DPF), consisting of alternately plugged parallel square channels with porous walls that trap the soot particles, must be periodically regenerated. In this work, a new procedure for the preparation of microwave susceptible catalytic DPFS based on a preliminary controlled chemical erosion of the porous structure was optimized, so obtaining catalytic filters with higher catalyst load (30 %wt CuFe₂O₄). The filters showed pressure drop values very similar to those pertaining to the uncatalyzed filters and a higher regeneration activity: consequently, their microwave-assisted regeneration phase, compared to the traditional fuel postinjection, allowed an energy saving of about 60 % (Kurien et al. 2018). With SCR systems the cylinder of DEF needs to be filled frequently usually before the fuel tank gets empty.

Urea-water spray impingement is an important parameter that affects solid deposit formation, should be investigated duly. A study presented an experimental investigation of urea-water spray impingement on the heated wall of automotive SCR systems for diesel engine exhaust gases. The investigation focused on the impingement conditions and distribution of the spray droplets, which are important parameters for system performance. The investigation reveals that high wall temperature produces swirls and bouncing that entrain rebounded droplets of the impinging spray on the wall, which leads to improved mixing. High temperature also causes longer spray front projection length which is an important factor for the mitigation of urea deposits (Hasan et al. 2019)

Solid SCR

The SSCR technology uses a powerful reducing agent with a higher ammonia density. With the help of a nozzle, ammonia is directly injected into the downstream side in this method.

Issues such as urea nozzle blockage, low catalyst productivity, and low NO_x effectiveness are eliminated due to the shorter mixing time and lower decomposition temperature of ammonia salt (Zhang et al. 2014). A solid reductant-based SCR system is observed to be an effective alternative for ammonia generation as compared to urea-based SCR systems. Ammonium salts like ammonium carbamate and ammonium carbonate have the ability to generate ammonia for about 80-90% NO_x conversion for small-, light- and, medium-duty diesel engine applications. Undesired reactions occurring in urea-based SCR systems during cold start and cold transient cycles can be rectified by the introduction of SSCR systems which will also reduce the deposit risks. The performance of the SCR system can be enhanced by using solid reductants for ammonia generation owing to its higher ammonia generation density hence the refill interval can be extended (Kurien & Srivastava 2019). Solid SCR has a lower capacity requirement (up to 28%) than aqueous urea-based SCR, which is an attractive aspect. The usage of Ammonium carbamate also eliminates the freezing problem with aqueous urea. Another advantage of SSCR versus SCR is that ammonia mixes better with exhaust gases. (Krüger et al. 2003). SCR systems that use solid ammonia salts for ammonia generation improve NO_x reduction efficiency while also increasing the energy needed to heat the salt (Kim et al. 2014).

Solid SCR uses a set up involving DOC, Diesel particulate filter (DPF) that maintains the pressure drop. DOC reduces various oxides except for the oxides of nitrogen.

Diesel particulate filter (DPF) uses a ceramic made substrate in form of a honeycomb structure. DPF captures and stores the exhaust carbon particles. Because the exhaust temperature is so high, the carbon particles in this filter are burned and quickly released into the environment. The most typical work is to reduce the oxides of nitrogen. For this purpose, a solid catalyst is used in SSCR systems.

Fig. 3 shows a composite type of SSCR system in which two systems are used for producing heat to decompose the solid salt. When the engine starts, the temperature of water in the water tank remains insufficient to produce heat for the decomposition of solid salt. At this time electronic unit produces the heat, thus providing ammonia gas. When the engine is in running condition and is warmed up, the electronic unit stops working automatically and the heat of the water tank is used for decomposing the solid salt thus providing ammonia gas. Urea in aqueous form is not able to produce a higher amount of ammonia. In SCR systems using DEF produces Cyanuric acid and some other acids which gives rise to blockage of urea nozzle, decreases the catalyst activities thus reducing the NO_x efficiency (Zhang et al. 2014).

Injection of urea at a specific temperature is required in these systems. The above-mentioned problems can be reduced from SCR systems if ammonia is directly injected into the exhaust. This is the basic concept of SSCR where ammonia is generated with the help of a solid reductant. In SSCR systems the mass of reductant is reduced, the reason

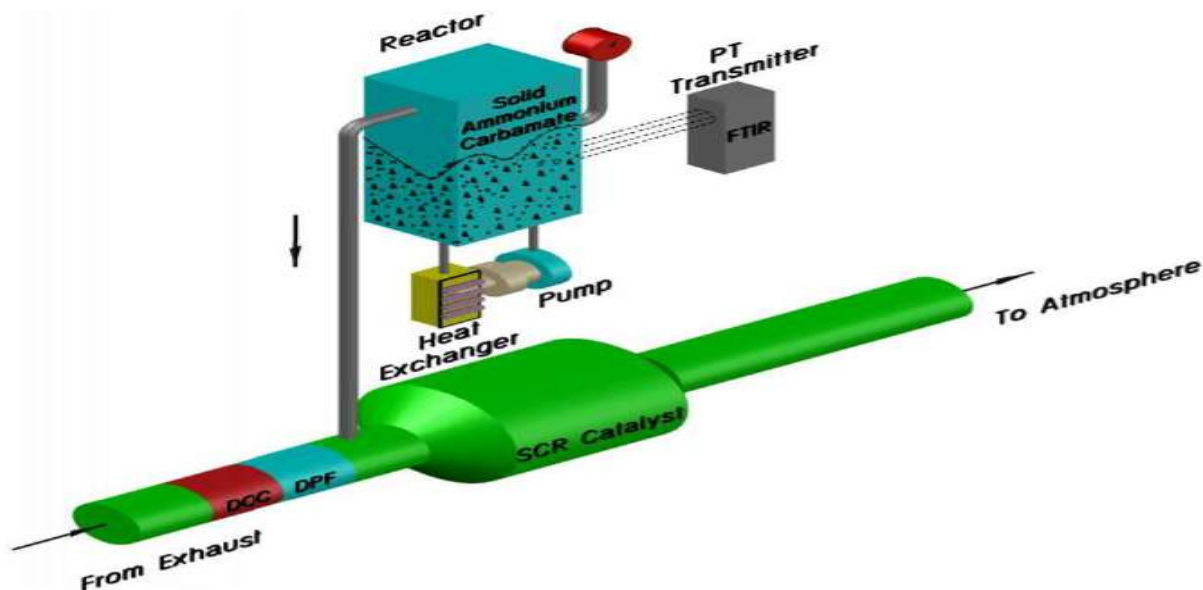


Fig. 3: Solid SSCR system.

being the higher ammonia densities of solid salts. Emission reduction is also increased at lower temperatures which eliminates the problem of deposition risks. Compared to the SCR system, in SSCR decomposition occurs at lower temperatures and also reduces the mixing time. Generally used ammonia salts for the production of ammonia gas are ammonium carbamate, ammonium carbonate, amino strontium chloride, amino calcium chloride, etc. (Zhang et al. 2014). Among various available salts, ammonium carbamate is found to be the best option to use in the SSCR system in India as it has a minimum decomposing temperature. Ammonium carbamate decomposes fully at about 60°C (Zhang et al. 2014). Metal salts of amino having decomposed temperatures of 30°C to 50°C are not opted in India due to their preservation complexities.

Ammonia slip is considerably reduced with the use of CDPF after SCR using slip catalyst. a study concluded that CDPF's reduce ammonia to N₂O and NO_x but the overall conversion efficiency of the NO_x is increased (Girard et al. 2007). The schematic diagram of the diesel after-treatment system using ammonia slip catalyst is shown in Fig. 4

Kim et al. (2014) investigated the possibility of a new ammonia generation system that uses low-cost solid ammonium salt, such as solid urea and ammonium carbonate. The result showed that ammonium carbonate is more suitable than solid urea because of the low decomposition temperature and no change to the other ammonium salt during the decomposition process. This paper also showed the NO_x reduction capability of the new ammonia delivery system that uses ammonium carbonate for the comparison of NO_x reduction using solid urea and ammonium carbonate as salts for producing the reducing agent ammonia.

It was discovered that solid urea requires a high decomposition temperature and that during this process, unwanted chemicals such as cyanuric acid are formed. The ammonium carbonate system was found to be significantly more suitable because of its low breakdown temperature. However, due to the removal of water produced during the process, more attention must be taken when constructing the system. The effect of numerous parameters on the decomposition reaction, such as temperature, pressure, and salt mass, was not taken into account in the experiment (Kim et al. 2014)

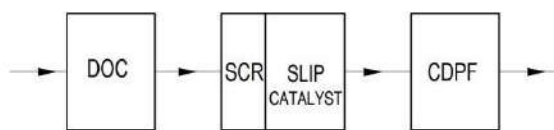


Fig. 4: Diesel after-treatment system using ammonia slip catalyst (Girard et al. 2007).

In 2011 a system containing ammonium carbamate for the production of ammonia was developed by Lacin et al. (2011). This system could not explain the effect of various parameters which affect the thermal decomposition of ammonium carbamate (Lacin et al. 2011).

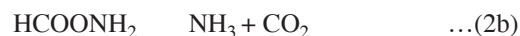
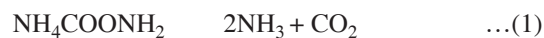
In 2013 an experiment using thermogravimetric analysis and a calorimeter was conducted by Lee et al. (2013) for calculating the energy required for thermal decomposition of ammonium salts. Sufficient data was provided to understand the chemical reaction but they failed to develop any mathematical model for the production of ammonia using ammonia salts (Lee et al. 2013)

Kim et al. (2020) experimentally provided the information regarding optimum production of ammonia for reduction of NO_x using ammonium carbamate as the salt for the production of reducing agents. They also investigated the effect of temperature, pressure, and mass of ammonium carbamate on the decomposition rate of the salt (Kim et al. 2020)

The rate of decomposition of ammonium carbamate varies linearly with temperature. At high temperature, the rate of thermal decomposition is high thus requiring a robust reactor design which can bear high pressure. The size of the reactor must be large enough to reduce the frequency of refilling the reactor with ammonium carbamate. The mass of salt present in the reactor influences the reaction rate of decomposition. The optimized reaction rate of decomposition of salt is obtained only when the mass of salt present in the reactor is high. The reactor should be refilled as soon as the pressure in the reactor is observed less than injection pressure (Kim et al. 2020)

Chemical Kinetics of Decomposition

Ammonium carbamate thermally decomposes into alkali and carbon dioxide. Ramachandran et al. (1998) researched that decomposition of ammonium carbamate happens in two phases hence delivering moderate items.



Equation (1) was given by Kim et al. (2014) and shows that solid ammonium carbamate can remain in equilibrium with the products obtained after decomposition. Equations (2a) and (2b) were predicted by Ramachandran et al. (1998) which explains that the decomposition of ammonium carbamate occurs in two stages.

The thermal decomposition of ammonium carbamate is also influenced by the mass of ammonium carbamate inside the reactor. When the ammonium carbamate mass is low,

an acceptable decomposition rate is impossible to achieve. In this case, it's critical to set a high temperature to ensure a sufficient decomposition even when the ammonium carbamate mass is minimal (Kim et al. 2020).

CONCLUSION

The development of a reliable NO_x reduction method using SCR and SSCR is investigated in this paper. SSCR technology has been found to be a considerably better solution for reducing NO_x emission from diesel engine exhaust. The use of ammonia as a reducing agent improves NO_x emission reduction and so complies with the BS-VI standards. When vaporized ammonia is used as a reducing agent, ammonia slip and lower reduction efficiency are decreased to a greater extent. As a result, due to its large ammonia storing capacity and lower decomposition temperature, ammonium carbamate is shown to be the best option. Because SSCR technology can function effectively at temperatures as high as 200°C, it is useful in diesel engines. The use of ammonia as a reducing agent allows the technology to operate at temperatures below 200°C, resulting in more efficiency in NO_x conversion and hence greater control over decomposing. The findings reveal that a successful SSCR framework can lead to a smaller reductant tank and, as a result, lower filling frequencies. This study concludes that SSCR is a superior method for reducing NO_x emissions from diesel engines' exhaust. The use of ammonia gas instead of urea greatly reduces pollution and malfunctioning issues. The use of SSCR allows for efficient operation even at low temperatures, and the problem of DEF freezing at low temperatures is eliminated. This research lays the groundwork for minimizing ammonia slip in SSCR systems to achieve a highly efficient NO_x emission reduction system.

REFERENCES

- Agarwal, A.K. 2007. Biofuels (alcohols and biodiesel) applications as fuels for internal combustion engines. *Prog. Energy Combust. Sci.*, 33(3): 233-71.
- Allansson, R.P.G., Blakeman, G.R., Chandler, C.A., Maloney, J. E., Thoss, A.P., Walker, and Warren, J.P. 2000. The use of the continuously regenerating trap (CRTTM) and SCRTTM systems to meet future emissions legislation. *Tech. Univ. Vienna*, 12(420): 343-355.
- Bauner, D., Staffan, L. and Norimasa, I. 2009. Evolving technological systems for diesel engine emission control: Balancing GHG and local emissions. *Clean Technol. Environ. Policy*, 11(3): 339-65.
- Biswas, S., Vishal, V., James, J.S. and Constantinos, S. 2009. Chemical speciation of pm emissions from heavy-duty diesel vehicles equipped with diesel particulate filter (DPF) and selective catalytic reduction (SCR) retrofits. *Atmos. Environ.*, 43(11): 1917-25.
- Erickson, L.E., Greg, L.N., Michael, J.H. and Zixian, W. 2020. Nitrogen oxides and ozone in urban air: a review of 50 plus years of progress. *Environ. Prog. Sustain. Energy*, 39(6): 1-9.
- Gao, F., Xiaolong, T., Honghong, Y., Shunzheng, Z., Chenlu, L., Li, J., Yiran, S. and Xiaomi, M. 2017. A review on selective catalytic reduction of NO_x by NH₃ over Mn-based catalysts at low temperatures: Catalysts, mechanisms, kinetics, and DFT calculations. *Catalysts*, 7(7): 199.
- Girard, J.W., Giovanni, C. and Christine, K.L. 2007. The influence of ammonia slip catalysts on ammonia, N₂O, and NO_x emissions for diesel engines. *SAE Trans.*, 116: 182-86.
- Guan, B., Reggie, Z., He, L. and Zhen, H. 2014. Review of the state of the art technologies of selective catalytic reduction of NO_x from diesel engine exhaust. *Appl. Thermal Eng.*, 66(1-2): 395-414.
- Hamada, H., and Haneda, M. 2012. Applied catalysis: General review of selective catalytic reduction of nitrogen oxides with hydrogen and carbon monoxide. *Appl. Catal. A. Gen.*, 421(22): 1-13.
- Hasan, S.G.M., Hyun, J. and Ocktaeck, L. 2019. Analysis of the spray wall impingement of urea-water solution for automotive SCR De-NO_x systems. *Energy Procedia*, 158: 1936-41.
- Johnson, T. 2016. Vehicular emissions in review. *SAE Int. J. Engines*, 9(2): 1258-75.
- Kim, H., Cheon, Y., Junho, L. and Hoyeol, L. 2014. A study on the solid ammonium SCR system for control of diesel NO_x emissions. *SAE Tech. Papers*, 1: 12-18.
- Kim, Y., Hassan, R., Sangho, L. and Hongsuk, K. 2020a. Study on the thermal decomposition rate of ammonium carbamate for a diesel NO_x reducing agent-generating system. *Fuel*, 267: 117-126.
- Krüger, B.M., Patrick, N. and Volker, S. 2003. A compact solid SCR system for NO_x reduction in passenger cars and light duty trucks. *MTZ Worldwide*, 64: 14-17.
- Kurien, C. and Srivastava, A.K. 2018. Geometrical modeling and analysis of automotive oxidation catalysis system for compliance with environmental emission norms. *Nat. Environ. Pollut. Technol.*, 17(4): 1207-12.
- Kurien, C. and Srivastava, A.K. 2019. Solid reductant-based selective catalytic reduction system for exhaust emission control of compression ignition engines. *Nat. Environ. Pollut. Technol.*, 18(3): 969-73.
- Kurien, C., Srivastava, A.K., Gagan, A., Shivam, S., Vivek, S. and Vaibhav, T. 2018. Application of Selective Catalytic Reduction System for Exhaust Emission Control of Compression Ignition Engines. *International Conference on Advanced Materials, Energy and Environmental Sustainability (ICAMEES 2018)*, CCE-University of Petroleum and Energy Studies, 2018 Dec 14-15, ICAMEES, Dehradun, India, pp. 1-2.
- Kurien, C., Srivastava, A.K., Niranjana, G. and Karan, A. 2019. Soot deposition effects and microwave regeneration modeling of diesel particulate filtration system. *J. Energy Inst.*, 93(2): 463-473.
- Lacin, F., Adam, K., Granville, H., Henry, S., Marek, T., Jason, J., Dean, T. and Hoon, C. 2011. SOLID SCR®: Demonstrating an improved approach to NO_x reduction via a solid reductant. *SAE Tech. Papers*, 17: 1-11.
- Lee, H., Cheon, S., Yoon, M. and Hongsuk, K. 2013. A study on the reaction rate of solid SCR for NO_x reduction of exhaust emissions in the diesel engine. *Trans. Korean Soc. Automot. Eng.*, 21(6): 183-94.
- Lee, S.H., Kwak, J.H., Lee, S.Y. and Lee, J.H. 2015. On-road chasing and laboratory measurements of exhaust particle emissions of diesel vehicles equipped with after-treatment technologies (DPF, urea-SCR) *Int. J. Auto. Technol.*, 16: 551-559
- Lewtas, J. 2007. Air pollution combustion emissions: Characterization of causative agents and mechanisms associated with cancer, reproductive, and cardiovascular effects. *Mutat. Res.- Rev. Mutat. Res.*, 636(1-3): 95-133.
- Ma, Q., Dongjian, Z. and Xuehui, G. 2019. Simulation of the flow field and the chemical reaction coupling of selective catalytic reduction (SCR) system using an orthogonal experiment. *Plos One*, 14(7): e0216138.

- Mamakos, A., Giorgio, M. and Urbano, M. 2013. Assessment of the legislated particle number measurement procedure for a Euro 5 and a Euro 6 compliant diesel passenger cars under-regulated and unregulated conditions. *J. Aerosol Sci.*, 55: 31-47.
- Payri, F., Bermudez, V.R. and Tormos, B., Waldemar, G.L. 2009. Hydrocarbon emissions speciation in diesel and biodiesel exhausts. *Atmos. Environ.*, 43(6): 1273-79.
- Peng, Y., Junhua, L., Wenzhe, S., Jinming, L., Yu, W., Jie, F., Xiang, Li., John, C. and Jiming, H. 2015. Deactivation and regeneration of a commercial SCR catalyst: Comparison with alkali metals and arsenic. *Appl. Catal. B. Environ.*, 168(9): 195-202.
- Praveena, V. and Martin, M.J. 2018. A review on various after-treatment techniques to reduce NOx emissions in a CI engine." *J. Energy Inst.*, 91(5): 704-720
- Qu, D., Wei, S., Hua, L., Lu, Y.F. and Jun, Y.M. 2014. Nozzle opening time's impact on flow characteristics of SSCR." *Appl. Mech. Mater.*, 644-650: 718-21.
- Ramachandran, B.R., Arthur, M.H. and Eric, D.G. 1998. Kinetics and mechanism of the reversible dissociation of ammonium carbamate: Involvement of carbamic acid. *J. Phys. Chem.*, 102(22): 3934-3941.
- Reşitoğlu, I.A., Kemal, A. and Ali, K. 2015. The pollutant emissions from diesel-engine vehicles and exhaust after-treatment systems. *Clean Technol. Environ. Policy*, 17(1): 15-27.
- Sampara, C.S., Edward, J.B., Matthew, C. and Dennis, A. 2007. Global kinetics for platinum diesel oxidation catalysts. *Ind. Eng. Chem. Res.*, 46(24): 7993-8003.
- Shahariar, G.M.H., Muhammad, K.A.W. and Ock, T.L. 2018. Investigation of urea-water solution spray impingement on the hot surface of the automotive SCR system. *J. Mech. Sci. Technol.*, 32(6): 2935-2946.
- Solomon, G.M. and John, R.B. 2003. Health effects of diesel exhaust. *Clin. Occup. Environ. Med.*, 3(1):61-80.
- Wang, G., Hafiz, L.A., Jun, Z., Jinzhu, Q., Yang, L., Shiyu, L., Kaiyuan, C., Shi, J.S. and Zhiming, W. 2018. Development of model predictive control strategy of SCR system for heavy-duty diesel engines with a one-state control-oriented SCR model. *SAE Tech. Papers*, 2018: 1-11.
- Wang, T.J. and Baek, S.W. 2008. Kinetic parameter estimation of a diesel oxidation catalyst under actual vehicle operating conditions. *Ind. Eng. Chem. Res.*, (2): 2528-37.
- Wang, X., Dane, W., Jingnan, H., Ye, W., Hang, Y., Xiaochuan, P. and Max, Z. 2012. On-road diesel vehicle emission factors for nitrogen oxides and black carbon in two Chinese Cities. *Atmos. Environ.*, 46: 45-55
- Williams, M. and Ray, M. 2016. Report: A Technical Summary of Euro 6/ VI Vehicle Emission Standards. The International Council on Clean Transportation. The International Council on Clean Transportation (ICCT), Washington DC, USA, pp. 1-12.
- Yan, W., Hoekman, S.K., Broch, A. and Coronell, C.J. 2014. Effect of hydrothermal carbonization reaction parameters on the properties of hydrochar and pellets. *Environ. Prog. Sust. Energy* 33(3): 676-80.
- Zhang, K.L., Lu, Y. F. and Da, W.Q. 2014. Research on SSCR technology to reduce NOx emissions for diesel engines. *Appl. Mech. Mater.*, 14(13): 3989
- Zhang, Y., Diming, L., Piqiang, T. and Zhiyuan, H. 2018. Experimental Study on the Particulate Matter and Nitrogenous Compounds from Diesel Engine Retrofitted with DOC+CDPF+SCR. *Atmos. Environ.*, 177: 45-53.



Upflow Anaerobic Filter for the Treatment of Wastewater from a Natural Rubber Latex Concentration Unit

Nithya Gopinath*, Madhu G.*† and Joseph Francis**

*Division of Chemical Engineering and Division of Safety and Fire Engineering, School of Engineering, Cochin University of Science and Technology, Cochin-682 022, India

**Oman Medical College, National University of Science and Technology, Muscat, Sultanate of Oman

†Corresponding author: Madhu G.; profmadhugopal@gmail.com

Nat. Env. & Poll. Tech.
Website: www.neptjournal.com

Received: 14-10-2020

Revised: 15-02-2021

Accepted: 22-02-2021

Key Words:

Upflow anaerobic filter
Rubber latex wastewater
Volatile acids
Methane

ABSTRACT

In this study, wastewater from a centrifuge rubber latex concentration unit was experimentally treated by an up-flow anaerobic filter (UAF) at variable hydraulic detention time to investigate the COD removal efficiency and the gas production rate. The UAF reactors were made of PVC pipe with an inside diameter of 9.5 cm, 180 cm in height, with a bed volume of 12.8 L, and filled with polyethylene media. The initial COD concentration of wastewater was in the range 4620 - 10400 mg.L⁻¹. HRTs were controlled at 20 days, with the organic loading rate varying from 2.9 to 10.5 kg.day.m⁻³. The findings show that the COD removal efficiency of the system was in the range of 85% to 92% for the varying organic loading rates. In addition, the specific methane production rate varied from 8.2 to 14 L of CH₄ produced/g of COD destroyed/day for the different organic loading rates.

INTRODUCTION

Anaerobic biological treatment of high-strength organic wastes has a number of advantages which makes it preferable to either aerobic biological or physical-chemical treatment methods. The major advantage is that a high degree of waste stabilization can be accomplished with relatively low production of biological solids thus reducing the costs associated with sludge disposal. Methane gas is produced as a result of the anaerobic process and valuable energy can be recovered from the gas by subsequent combustion.

A disadvantage of the anaerobic process is the low bacterial growth rate which may result in a washout of the biomass if the solids in the effluent are not returned to the unit. Young & Mc Carty (1969) therefore developed an up-flow anaerobic filter in which the anaerobic bacteria are present in a film attached to a rock medium to remove organics in the waste flowing upward through the column. The bacteria in the anaerobic filter are firmly attached to the medium resulting in a sludge age of more than 150 days (Behera et al. 2007). The unit can therefore be operated at temperatures substantially below 35°C which decreases the bacterial growth rate while still maintaining sufficient biomass.

The studies carried out by Young & Mc Carty (1969) using synthetic organic waste indicated that at the same organic loading the percentage of COD removal increased

when the concentration of the influent COD increased. The unit consisted of a group of six filters operating in series. Their study based on synthetic wastewater indicated that the percentage removal of organic material is constant regardless of the concentration of the organic load applied to anaerobic filters in a continuous flow system.

Acharya et al. (2008) studied the suitability of an anaerobic filter for the treatment of distillery spent wash. The results of the study showed that up to a certain organic loading, the increase in BOD and COD of the effluent is accompanied by an increase in the percentage removal of COD and BOD, where after the decline in percentage removal with increased organic loading is exponential. A study carried out by Omil et al. (2003) investigated the performance of an anaerobic filter for the treatment of complex dairy wastewater on an industrial scale. During the last three decades, several studies (Tritt 1992, Manariotis & Grigoropoulos 2006, Iscen et al. 2007, Delgado et al. 2000, Rajakumar et al. 2011, Burcu et al. 2016) have been carried out to evaluate the performance of anaerobic filters for the treatment of wastewaters from various types of industries. The anaerobic filter has also been applied successfully as a reactor for the biological denitrification of effluents (Tilche et al. 1994, Hanne & Birgitte 1996, Bodik et al. 2003).

Among the various methods of natural rubber latex processing, the wastewaters from centrifuge latex concentration

units have been found to have the highest pollution potential (Madhu et al. 1994). The purpose of the present study is to evaluate the performance of an upflow anaerobic filter for the treatment of wastewaters from a centrifuge rubber latex concentration unit.

MATERIALS AND METHODS

A bench-scale anaerobic contact filter was fabricated using a PVC pipe of 9.5 cm diameter and 180 cm height having a total volume of 0.012 m³ (12 L). A length of 7 cm was leftover for sedimentation and distribution of wastewater at the bottom of the column. Sampling ports were provided at every 30 cm height of the filter from the perforated plate up to 150 cm. The reactor was filled with polyethylene media with a surface area of 240 m².m⁻³, void 90%, specific gravity 0.95, and standard size 40 mm. A clear liquid column of 30 cm was provided above the media for the separation of the effluent, suspended solids, and gas. A space of 13 cm has been provided for the accumulation of gas produced. The gas was collected by the displacement method. The filter was fed with wastewater at the point just below the perforated support plate from a storage vessel by means of a peristaltic pump. A schematic diagram of the experimental setup is shown in Fig. 1.

Active biomass was grown on the surface of the filter media by daily feeding a mixture of sewage and cow dung slurry (1 %) into the filter. Significant growth of bacteria was observed as evident from the methane gas production after 20 days of continuous operation. Four composite wastewater samples were collected from a centrifuge rubber latex concentration unit and brought to the laboratory with proper preservation. For proper acclimatization, the proportion of sewage was reduced to 90%, 80%, 70%, etc., by adding increasing quantities of the rubber latex centrifuging effluent. After 15 days of this continuous acclimatization, a steady state was achieved for a COD concentration of 9500 mg.L⁻¹. The pH of the feed solution was adjusted to 6.4 by adding sodium carbonate and the solution was fed into the filter at different hydraulic loadings (7.20, 8.64, 10.08, and 11.52 L.day⁻¹).

The following parameters were monitored during the course of the experiments which lasted for 15 days.

- Measurement of pH and alkalinity of the influent and effluent every day.
- Estimation of COD, BOD, and volatile acids content of the effluent daily using standard methods (APHA, AWWA & WPCF 1995).

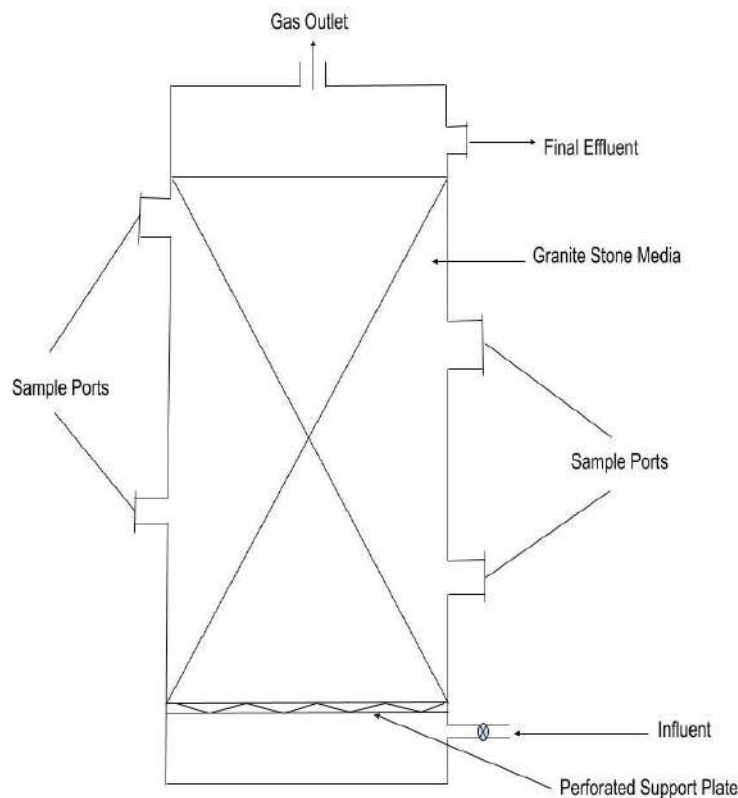


Fig. 1: Experimental set-up for upflow anaerobic filter.

- c. Analysis of the biogas produced for its methane content at the end of 15 days of steady-state operation of the filter using a gas chromatograph.

The above procedure was repeated for other influent COD concentrations of 10400 mg.L^{-1} , 5800 mg.L^{-1} , and 4620 mg.L^{-1} . Adequate time was provided for acclimatization between changes of organic as well as hydraulic loadings.

RESULTS AND DISCUSSION

The characteristics of the wastewater samples used in the study are given in Table 1. The waste analysis indicated that the waste was nutrient-limited by phosphorous. For an unhindered anaerobic treatment of waste at full strength, at least 800 mg.L^{-1} of nitrogen and 160 mg.L^{-1} of phosphorous would be needed (Bodik et al. 2002). To maintain unhindered

anaerobic growth, phosphorous in the form of dibasic potassium phosphate was added to the feed wastewater in sufficient quantities to maintain a phosphorous: nitrogen: carbon ratio of 1: 5.9: 100. The addition of potassium phosphate served two purposes. It not only provided the required phosphorous, but it increased the buffer capacity of the system to a limited extent. During periods of decreased alkalinity, the amount of potassium phosphate added to the feed was increased to provide additional buffer capacity.

pH Value

pH range of 6.4 to 7.3 was observed for various organic loading rates of latex concentration effluent. The pH variation observed for the organic loading rates, 6 kg.day.m^{-3} and $7.2 \text{ kg.day.m}^{-3}$ are plotted in Fig. 2. In all the loading conditions, reduction in pH was observed in one-day detention samples

Table 1: Characteristics of the wastewater samples used for the study.

Parameter	Sample 1	Sample 2	Sample 3	Sample 4
pH	4.2	4.0	4.0	3.9
Total Solids [mg.L^{-1}]	8200	17280	12875	8800
Dissolved Solids [mg.L^{-1}]	6300	11140	10800	8010
Suspended Solids [mg.L^{-1}]	1900	6140	2075	790
COD [mg.L^{-1}]	9500	10400	5800	4620
BOD [mg.L^{-1}]	5700	6100	3100	2800
Total Kjeldahl Nitrogen [mg.L^{-1}]	1500	1880	1580	1560
Ammoniacal Nitrogen [mg.L^{-1}]	630	750	590	710

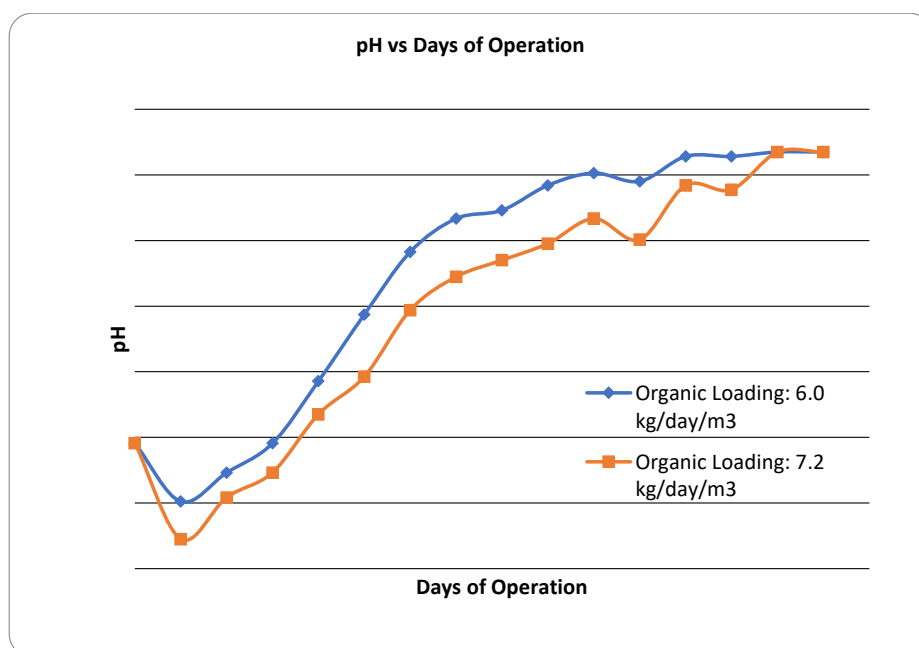


Fig. 2: Variation of pH during the operation of UAF for different organic loading rates.

because of the production of volatile acids but subsequently, it remained neutral because of the conversion of volatile acids to biogas (Kobayashi et al. 1983).

Variation in Alkalinity

The variation in alkalinity experienced in the filter during the experimental run of 15 days is shown in Fig. 3. The alkalinity values were measured for the two organic loadings, viz., 6 kg.day.m⁻³ and 7.2 kg.day.m⁻³, show that the fluctuations

occurring have been taken care of by the bacterial mass in the filter. There is practically no difference between the initial and final alkalinity values which indicates a steady-state operation of the filter.

COD Removal

Steady-state COD removal efficiency was obtained after a period of operation at a given loading. The results of a series of organic loading changes are illustrated in Fig. 4.

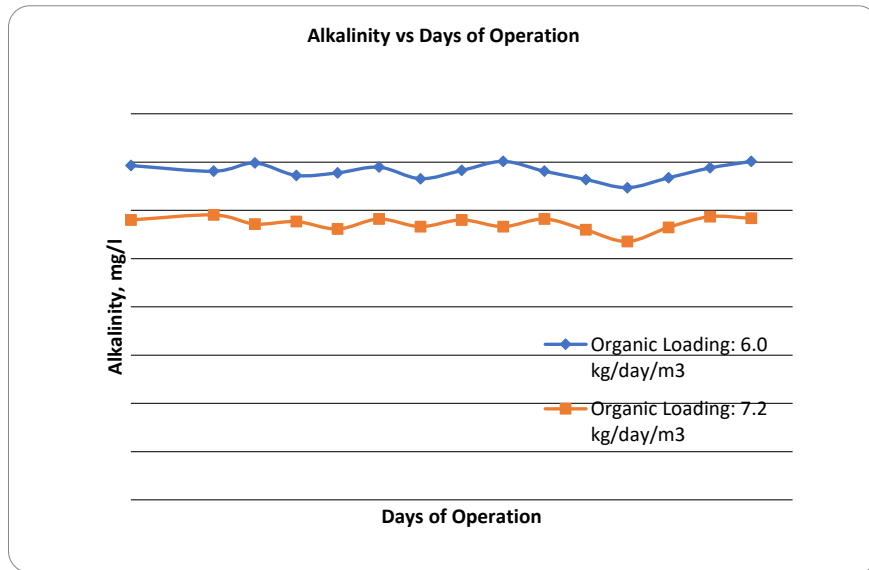


Fig. 3: Variation in alkalinity during the experimental run.

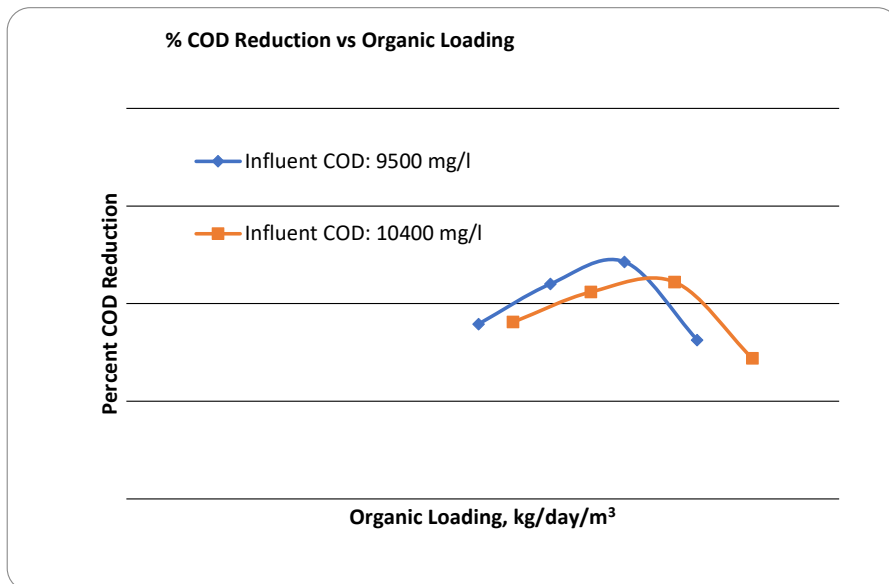


Fig. 4: COD removal efficiency for various organic loadings.

Initially, latex effluent with a COD of 9500 mg.L^{-1} was fed to the filter at a loading rate of $6 \text{ kg.COD.day.m}^{-3}$. This was followed by loading rates of 7.2, 8.4, and $9.6 \text{ kg.day.m}^{-3}$. On increasing the loading rate from 6 to 8.4, the COD removal efficiency increased from 89 percent to 92 percent. But when the loading rate was further increased to $9.6 \text{ kg.day.m}^{-3}$, the COD removal dropped to 88 percent. The same trend was observed at an influent COD concentration of 10400 mg.L^{-1} . Although the COD removal efficiency increased from 89 percent to 91 percent, on increasing the organic loading rate from $6.57 \text{ kg.day.m}^{-3}$ to $9.19 \text{ kg.day.m}^{-3}$, it dropped to 87 percent on further increasing the loading rate to $10.5 \text{ kg.day.m}^{-3}$.

It is seen that the COD removal efficiencies decrease with an increase in organic loadings beyond a particular limit. This may be due to substrate inhibition, or inadequate acclimatization of bacteria, or formation of propionic acids (Ioannis et al. 2006).

The percentage COD reduction obtained on each day of operation of the filter is shown in Fig. 5. The curves plotted for different organic loading rates show that rapid COD removals are obtained in the first-day detention samples. This should be due to the active biomass present on the filter medium which decomposes the organic matter in the feed wastewater very efficiently (Sharma et al. 2014). For all the loading rates, most of the COD removal was found to take

place during the first 10 days of operation. This summarizes the fact that most of the stabilization of the waste should be occurring during the first ten days of operation. The COD removal efficiencies achieved for different influent concentrations are summarized in Table 2.

BOD Removal

As in the case of COD removal, the BOD removal efficiency also increased with organic loading up to a certain limit. The variation of BOD removal with organic loading is illustrated in Fig. 6. When the organic loading rate was increased from 6 kg.day.m^{-3} to $8.4 \text{ kg.day.m}^{-3}$ for an influent COD of 9500 mg.L^{-1} , the BOD removal efficiency increased from 92.5 percent to 96.0 percent. But on increasing the organic loading rate to $9.6 \text{ kg.day.m}^{-3}$, the BOD removal efficiency was found to drop to 91.0 percent. The same pattern was repeated for other influent COD concentrations also. The reason for this behavior should be substrate inhibition or improper acclimatization of bacterial mass.

The variation of BOD with detention time is shown in Fig 7. Rapid BOD removals were observed in the first-day detention samples in all the loading conditions which confirm the presence of active biomass in the filter. The BOD removal efficiencies achieved during the course of the experiments are given in Table 2.

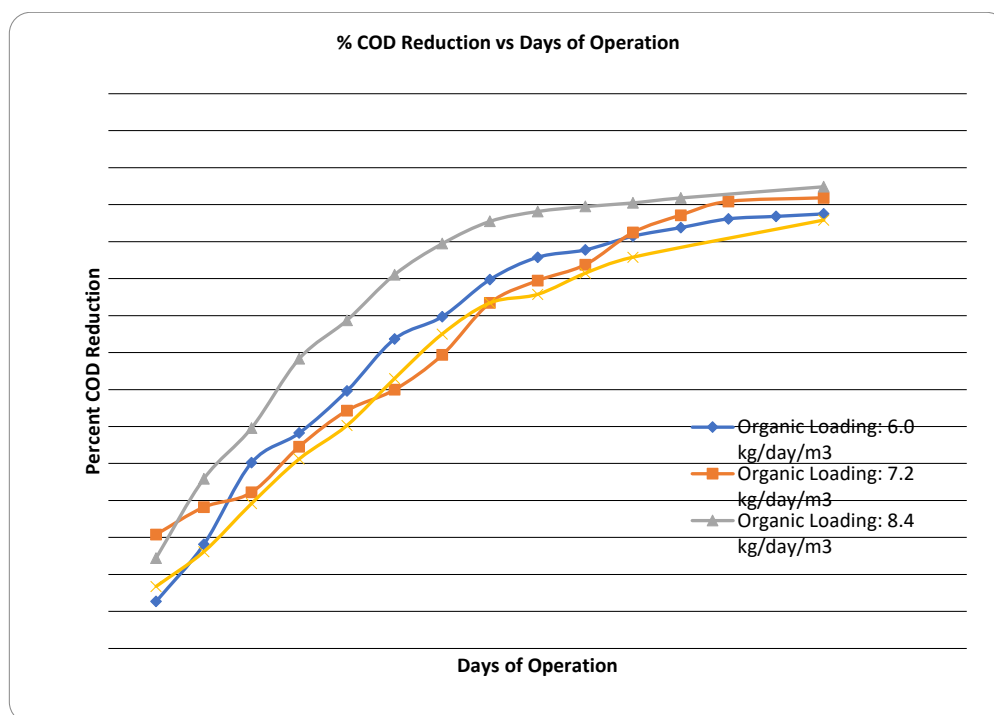


Fig. 5: COD reduction on a daily basis during the operation of the UAF.

Table 2: BOD and COD removal efficiency for different influent concentrations.

Influent COD Concentration [mg.L ⁻¹]	Organic Loading Rate [kg.day.m ⁻³]	Percent COD Removal	Percent BOD Removal
9500	6.0	89.0	92.5
	7.2	91.0	94.0
	8.4	92.0	95.0
	9.6	88.0	91.0
10400	6.57	89.0	91.0
	7.88	90.5	93.0
	9.19	91.0	94.0
	10.50	87.0	90.0
5800	3.66	87.0	90.5
	4.39	88.0	91.5
	5.13	89.0	93.0
	5.86	86.0	88.5
4620	2.92	87.0	90.0
	3.50	89.0	91.0
	4.08	90.5	94.0
	4.67	85.0	90.0

Volatile Acids

The volatile acid concentration of the effluent during the period of operation of the filter is shown in Fig. 8. For all the organic loading rates, there was a steep increase in the production of volatile acids during the initial period. This should be due to the increased activity of non-methanogenic bacteria which produce volatile acids (Zabihollah et al. 2018). But as the detention time increased, the volatile acid

concentration came down. The conversion of volatile acids to methane by bio-methanation should have caused the drop in volatile acids concentration.

Biogas Production

Biogas production is the final step of the anaerobic process and is due to the conversion of volatile acids to gaseous form by methanogenic bacteria. The volume of gas generated

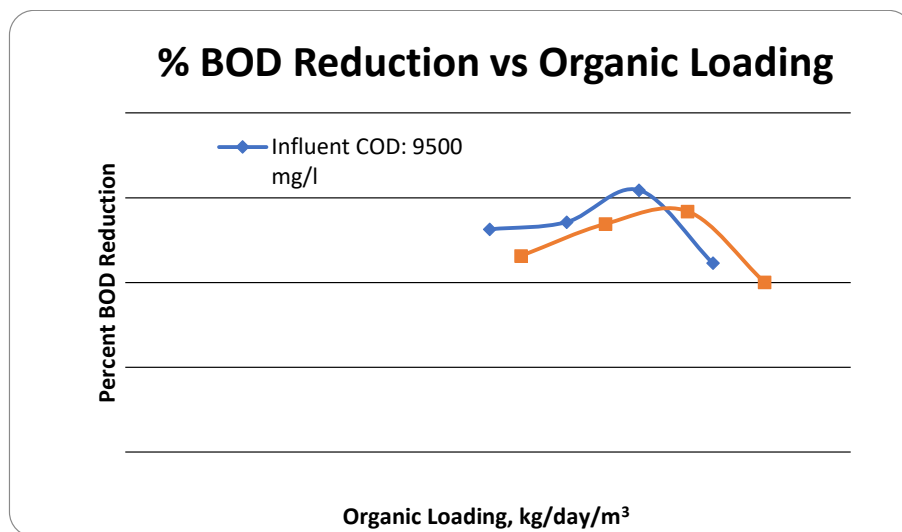


Fig. 6: The variation of BOD removal efficiency with organic loading.

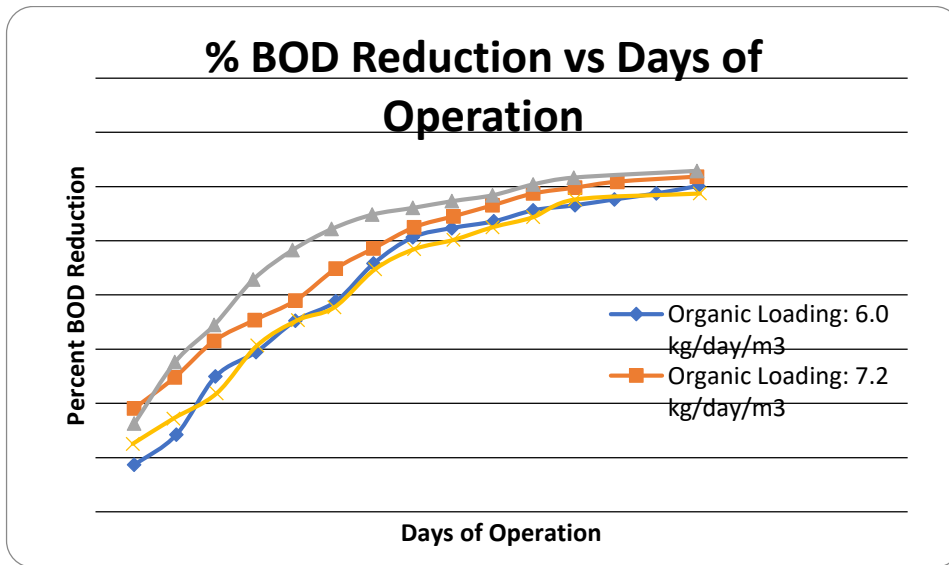


Fig. 7: Variation of BOD with detention time.

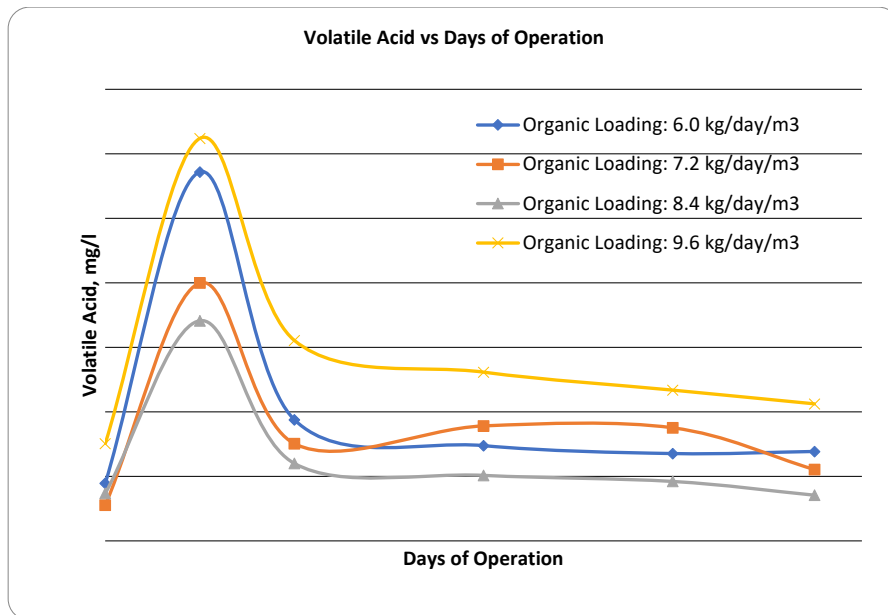


Fig. 8: The volatile acid concentration of the effluent during the period of operation of the filter.

and its methane content for different organic loadings are plotted in Fig. 9.

For an influent COD concentration of 9500 mg.L^{-1} , the volume of gas collected during 15 days of operation of the filter was 1350 L, i.e., 90 L of gas production per day on an average at an organic loading rate of $6.0 \text{ kg.day.m}^{-3}$. The volume of gas collected rose to 1600 L (107 L.day^{-1}) on increasing the organic loading rate to $8.4 \text{ kg.day.m}^{-3}$. But on increasing the organic loading rate further to $9.6 \text{ kg.day.m}^{-3}$,

the volume of biogas produced was found to decrease to 1475 L. The same trend was observed for an influent COD concentration of 10400 mg.L^{-1} . On increasing the organic loading rate from $6.57 \text{ kg.day.m}^{-3}$ to $9.19 \text{ kg.day.m}^{-3}$, the gas production increased from 1425 L to 1750 L. While increasing the organic loading rate to $10.5 \text{ kg.day.m}^{-3}$, the volume of gas dropped to 1520 L.

The methane content of the biogas produced also varied with organic loading. As in the case of gas pro-

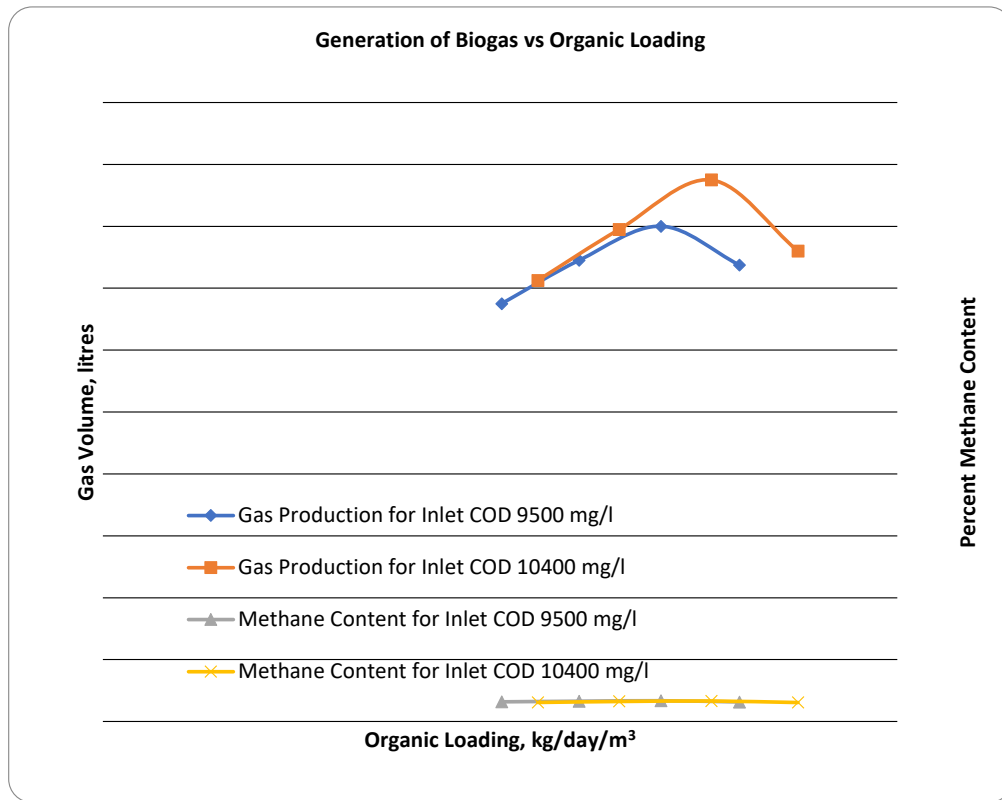


Fig. 9: The volume of biogas generated and its methane content for different organic loadings.

duction, the methane content of the gas increased from 63 percent to 67 percent on changing the organic loading rate from $6.0 \text{ kg.day.m}^{-3}$ to $8.4 \text{ kg.day.m}^{-3}$ for an influent COD concentration of 9500 mg.L^{-1} . The methane content of the biogas was found to decrease to 62 percent on increasing the organic loading rate to $9.6 \text{ kg.day.m}^{-3}$. The same trend was observed for the influent concentration of 10400 mg.L^{-1} .

The drop in gas production and methane content beyond a particular organic loading rate could be attributed to the lesser organic removal at higher organic loadings and lesser activation of methanogenic bacteria (Mata-Alvarez et al. 2000). The specific biogas yield expressed as $\text{lit CH}_4.\text{gm}^{-1} \text{ COD destroyed/day}$ for the various organic loadings studied is given in Table 3.

CONCLUSIONS

1. The upflow anaerobic filter successfully treated the wastewater from a centrifuge rubber latex concentration unit at influent COD concentrations as high as 10400 mg.L^{-1} . The maximum COD removal and BOD
2. The COD and BOD removal efficiency of the filter was found to increase on increasing organic loading up to a certain limit. On increasing the organic loading further, the removal efficiency was found to drop.
3. The maximum volume of biogas production recorded during the period of investigation was 117 L.day^{-1} . The percentage methane content of the gas ranged from 61 to 67 percent.
4. A pH range of 6.4 to 7.3 was observed during the study. Even though a reduction in pH was observed initially, it remained almost neutral subsequently.
5. For all the organic loading rates, there was a steep increase in the volatile acids concentration during the initial period, but subsequently, it came down.

Table 3: The specific biogas yield for various organic loadings.

Influent COD Concentration [mg.L ⁻¹]	Organic Loading Rate [kg.day.m ⁻³]	Specific Methane Production L CH ₄ .g ⁻¹ COD destroyed/day
9500	6.0	13.97
	7.2	13.07
	8.4	12.16
	9.6	9.49
10400	6.57	13.25
	7.88	12.71
	9.19	12.21
	10.50	8.98
5800	3.66	13.53
	4.39	12.79
	5.13	11.97
	5.86	8.31
4620	2.92	13.48
	3.50	12.57
	4.08	10.89
	4.67	8.22

REFERENCES

- Acharya, B.K, Mohana, S. and Madamwar, D. 2008. Anaerobic treatment of distillery spent wash- A study on upflow anaerobic fixed-film bioreactor, *Bioresour. Technol.*, 99: 4621-4626.
- APHA, AWWA and WPCF. 1995. Standard Methods for the Examination of Water and Wastewater. American Public Health Association, Inc, Washington D.C.
- Behera, S.K., Rene, E.R. and Murthy, D.V.S. 2007. Performance of up-flow anoxic bioreactor for wastewater treatment. *Int. J. Environ. Sci. Tech.*, 4(2): 247-252.
- Bodik, I., Herdova, B. and Drtil, M. 2002. The use of upflow anaerobic filter and AnSBR for wastewater treatment at ambient temperature. *Water Res.*, 36(4): 1084-1088.
- Bodik, I., Kratochvil, K., Gasparikova, E. and Hutnan, M. 2003. Nitrogen removal in an anaerobic baffled filter reactor with aerobic post-treatment. *Bioresour. Technol.*, 86: 79-84.
- Burcu, A.C., Cansu, F.I. and Semra, I. 2016. The anaerobic treatment of pharmaceutical industry wastewater in an anaerobic batch and upflow packed-bed reactor. *Desal. Water Treat.*, 57(14): 54-69.
- Delpozo, R., Diez, V. and Beltran, S. 2000. Anaerobic pretreatment of slaughterhouse wastewater using fixed-film reactors. *Bioresour. Technol.*, 71(2): 143-149.
- Hanne, V.H. and Birgitte, K.A. 1996. Integrated removal of nitrate and carbon in an upflow anaerobic sludge blanket (UASB) reactor: Operating performance. *Water Res.*, 30(6): 1451-1458.
- Iscen, C.F., Ilhan, S. and Yildirim, M.E. 2007. Treatment of cake production wastewater in upflow anaerobic packed bed reactor. *Int. J. Nat. Eng. Sci.*, 1: 75-80.
- Kobayashi, H.A., Stenstrom, M.K. and Mah R.A. 1983. Treatment of low strength domestic wastewater using the anaerobic filter, *Water Res.*, 17(8): 903-909.
- Ioannis, D., Manariotis, I. and Sotirios, G.G. 2006. Municipal-wastewater treatment using upflow-anaerobic filters. *Water Environ. Res.*, 78(3): 233-242.
- Madhu, G., George, K.E. and Joseph Francis, D. 1994. Treatment of natural rubber latex concentration wastewaters by stabilization pond. *Int. J. Environ. Studies*, 46: 69-74.
- Manariotis, I.D. and Grigoropoulos S.G. 2006. Anaerobic filter treatment of municipal wastewater: biosolids behavior *J. Environ. Eng.*, 132: 23-31.
- Mata-Alvarez, J., Mace, S. and Llabres, P. 2000. Anaerobic digestion of organic solid wastes. An overview of research achievements and perspectives. *Bioresour Technol.*, 74(1): 3-16.
- Omil, F., Garrido, J.M., Arrojo, B. and Mendez, R. 2003. Anaerobic filter reactor performance for the treatment of complex dairy wastewater at an industrial scale. *Water Res.*, 37(17): 4099-108.
- Rajakumar, R., Meenambal, T., Rajesh Banu, J. and Yeom I.T. 2011. Treatment of poultry slaughterhouse wastewater in upflow anaerobic filter under low upflow velocity. *Int. J. Environ. Sci. Tech.*, 8(1): 149-158.
- Sharma, M.K., Khursheed A. and Kazmi, A.A. 2014. Modified septic tank-anaerobic filter unit as a two-stage onsite domestic wastewater treatment system. *Environ. Technol.*, 35: 2183-2193.
- Tilche, A., Bortone, G., Forner, G. and Indulti M. 1994. Combination of anaerobic digestion and denitrification in a hybrid upflow anaerobic filter integrated into a nutrient removal treatment plant. *Art. Water Sci. Technol.*, 30(12): 405-414.
- Tritt WP. 1992. The anaerobic treatment of slaughterhouse wastewater in fixed-bed reactors. *Bioresour. Technol.*, 41(3): 201-7.
- Young, J.C. and Mc Carty, P.L. 1969. The anaerobic filter for waste treatment. *J. Wat. Pollut. Control Fed.*, 41(5): 160-173.
- Zabihollah, Y., Mohammad, B. and Reza, A.M. 2018. Slaughterhouse wastewater treatment by combined anaerobic baffled reactor and anaerobic filter: Study of OLR and HRT optimization in ABR/AF reactors. *Environ. Health Eng. Manag. J.*, 5(3): 137-142.



Temporal and Spatial Distribution of Zooplankton Inhabiting Sandy and Muddy Shore Habitats at Jazan Coastal Area

A.T. AbdAllah ^(**)†, A.M. Alhababy*, M.G. Shamsy*, M.S. AbdelDayem* and Sahar H. Haroun^(***)

*Biology Department, Faculty of Science, Jazan University, Saudi Arabia

**Zoology Department, Faculty of Science, Al-Azhar University, Assiut, Egypt

***Department of Biological and Geological Sciences, Faculty of Education, Ain Shams University, Egypt

†Corresponding author: A.T. AbdAllah: abdallaht.63@gmail.com

Nat. Env. & Poll. Tech.

Website: www.neptjournal.com

Received: 10-12-2020

Revised: 19-02-2021

Accepted: 24-02-2021

Key Words:

Zooplankton

Seasonal abundance

Sandy shore

Turfa peninsula

Almarjan

ABSTRACT

Few studies were made about zooplankton distribution in Jazan coastal area. The present study dealt with the identification of zooplankton at the sandy shore (AlSalwa coast) and mangrove muddy shore (Turfa peninsula) at the Almarjan coast. Species richness and population density at different seasons were determined for both study areas between May 2016-April 2017. Conductivity, pH, water temperature, and salinity were measured. The relationship between water characters and the seasonal abundance of zooplankton seasons was examined through regression analysis. Ciliates, Rotifers, *Nauplius* larva, *Gammarus* sp., Veliger larva, Nematodes, *Planaria*, Copepods, and Kinorhyncha were recorded for both study areas. The highest species richness and population density were recorded during the summer season for Almarjan sandy shore and Turfa peninsula mangrove. Ciliates were the most abundant zooplankton on the sandy shore, while Kinorhyncha was the least abundant. The zooplankton Nematode was the most abundant at the Turfa Peninsula mangrove, whereas Gnathostomulida was the least abundant. Conductivity, salinity, and water temperature showed a significant regression relationship ($P < 0.05$) with zooplankton abundance. Data was discussed to highlight the role of zooplankton abundance in the mangrove and sandy shore ecosystem.

INTRODUCTION

Zooplankton has well known important ecological role in the marine ecosystem. They are the primary consumers in the marine food web. Zooplankton lives at depths up to 350 meters below the water surface (Castro & Huber 2012, Lee & Stokes 2006). Zooplankton performs dual vertical migration; upward at daylight to follow their prey; upward during the day to follow their prey, the phytoplankton, and downward at night to avoid predators (Castro & Huber 2012).

Zooplankton is the main food source for fishes and other intertidal and epipelagic animals (Lee & Stokes 2006). They live in littoral and sublittoral zones. Marine plankton is classified as “oceanic plankton” (plankters inhabiting water beyond continental shelves), “neritic plankton” (plankters inhabiting water overlying continental shelves), and “brackish-water plankton” (plankters inhabiting brackish-water areas such as estuaries and mangrove). According to the duration of planktonic life, zooplankton is classified into two groups holoplankton and meroplankton. The permanent members of animal plankton are called holoplankton. Meroplanktons are temporary members of the zooplankton, spending only part of their lifetimes as plankton such as larvae of fish, and

arthropods. These larvae differ completely from adult stages at their mode of living as adults either live on the bottom or swim as nektons (Nybakken 1997).

Several authors have defined zooplankton based on morphological criteria (Bradford-Grieve et al. 1983, Heron & Bradford-Grieve 1995, Lee & Stokes, 2006 and Hickman et al. 2011). Kim et al. (2020) used DNA metabarcoding technique to identify zooplankton using the primer (1391F (50-GTACACACCGCCCGTC-30) and EukBr (50-TGATCCTTCTGCAGGTTAC CTAC-30).

Seasonal changes affect the biodiversity of zooplankton and the factors that control their distribution was previously studied by Manickam et al. (2018) and Sharma & Kumari (2018).

Little work was made about the identification of zooplankton in Jazan. Previous studies on the Farasan Islands reported that copepods are the major constituents of the zooplankton community at the water surface (Farasan Report 2000, Abu-Zinada 2001). Calanoid and Euphausiid were recorded as the most important zooplankton as a food source for bream fish in Jazan in the red sea (Bakhsh 1994, Abdul Aziz et al. 2003 and ObuidAllah et al. 2005).

The present work concerns investigating seasonal distribution and abundance of zooplankton inhabiting surface water of intertidal areas on Almarjan sandy shore and mangrove area (Turfa peninsula). Species richness and diversity index were determined. Data were discussed to evaluate the effect of seasonal changes on the distribution of zooplankton in the sandy and muddy mangrove coastal marine ecosystem.

MATERIALS AND METHODS

Study Area

Almarjan sandy shore coast and Almarjan mangrove were the studied sites (E42°33'N16°90')

Sampling

Zooplankton samples were collected seasonally from the littoral zone at the sandy shore of Almarjan coast, and at the mangrove of Almarjan coast about 10:00 am during the period; May 2016- April 2017. Plankton net 353 μ (Forestry Supplies) was used for this purpose. Identification of Zooplanktons was according to Bradford-Grieve et al. (1983), Heron and Bradford-Grieve (1995), Lee & Stokes (2006), and Hickman et al. (2011).

Water Characteristics

Physical and chemical water criteria were measured at littoral areas of Almarjan sandy shore and mangrove habitats using Hanna pH meter instruments for pH and temperature measurement, Hanna salinity meter for salinity measurement, and Genway conductivity meter for conductivity determination.

Population Density and Relative Abundance

Plankton was identified by examining collected water samples by Zeiss Research Microscope. For each plankton group, a number of individuals at a 1 mL water sample determines the population density. The ratio of population density of each planktonic group to total densities of all examined groups was the calculated relative abundance.

Species Richness

Species richness (R) quantifies how many different types the dataset of interest contains (Jost 2006, Tuomisto 2010).

Table 1: Sampling Stations of zooplankton.

Location	Station	Transect
Jazan	Almarjan sandy shore (Salwa coast) S1	16.838854, 42.572049
Jazan	Almarjan mangrove (Turfa peninsula) S2	17.157910, 42.365550

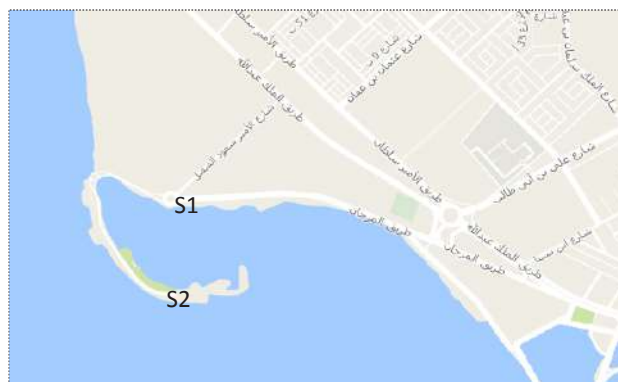


Fig. 1: Map showing the study area.

It calculates the number of different invertebrate species in each of the studied areas.

Statistical Analysis

ANOVA (analysis of variance) was applied using SPSS 22 statistical software program to determine the significance of the spatial distribution of planktonic organisms at the investigated area. $P < 0.05$ was selected as the minimum significance level for statistical analysis. Regression analysis was used to examine the effect of water criteria on zooplankton abundance at both studied sites.

RESULTS AND DISCUSSION

Water Criteria at Different Seasons

The mean seasonal values of pH, salinity, water temperature, and conductivity were detected at Almarjan sandy shore (Table 1) and mangrove (Table 2) studied sites.

Species Richness

The variable richness of zooplankton species was demonstrated during different seasons at Almarjan sandy shore and mangrove studied sites.

At the intertidal zone of sandy shore, species richness was 8 in summer, 5 in autumn, 4 in winter, and 7 in spring seasons. Species richness at mangroves was 7 in summer, 4 in autumn, 6 in winter, and 7 in spring seasons.

Identified Zooplankton

At the intertidal zone of Almarjan sandy shore. Ciliates were the defined protozoan zooplankton. Metazoan zooplankton were nematodes, copepods, rotifers, planaria, kinorhyncha, nauplius larva, and veliger larva.

At Almarjan mangrove, collected metazoan zooplankton were nematodes, copepod, planaria, gnathostomulida,

Table 2: Mean± SD of water criteria determined seasonally at Almarjan sandy shore site.

	pH	water temperature	salinity	conductivity
Winter	7.773 ± 0.304	30.7 ± 0.755	32.267 ± 0.702	56.667 ± 1.778
Spring	7.55 ± 0.266	31.833 ± 0.651	34.833 ± 3.041	61.24 ± 4.097
Summer	7.947 ± 0.142	37.733 ± 0.404	38.367 ± 0.603	62.933 ± 1.756
Autumn	7.383 ± 0.065	31.5 ± 0.866	33.23 ± 0.513	59.967 ± 1.137

Table 3: Mean± SD of water criteria determined seasonally at mangrove site.

	pH	water temperature	Salinity	Conductivity
Summer	8.02 ± 0.094	38.33 ± 1.885	39.97 ± 1.026	63.93 ± 2.783
Autumn	7.38 ± 0.105	30.2 ± 0.36	33.71 ± 0.813	61.4 ± 0.552
Winter	7.44 ± 0.05	27.5 ± 2.082	32 ± 0.816	58.625 ± 0.873
Spring	7.48 ± 0.07	30.7 ± 0.557	34.33 ± 1.527	61.08 ± 2.973

Table 4: Mean seasonal abundance of zooplankton at the intertidal zone of sandy shore habitat at Almarjan coastal zone.

Species	Summer mean±SD	Autumn mean±SD	Winter mean±SD	Spring mean±SD
Ciliates	140 ± 18.257	122.33 ± 4.041	94.6 ± 7.335	131 ± 10.155
Nematoda	132.5 ± 9.574	77.33 ± 6.028	59 ± 6.977	106.67 ± 11.547
Copepods	102 ± 14.142	31.67 ± 4.041	43.67 ± 4.041	75 ± 8.66
Nauplius larva	78.667 ± 7.64	-	-	48.33 ± 5.239
Veliger larva	-	-	-	51.65 ± 6.074
Water flea Cladocera	100 ± 3.605	23.67 ± 4.041	21.67 ± 3.512	90.55 ± 8.351
Rotifers	89.667 ± 4.51	-	-	83.33 ± 10.82
Planaria	46.667 ± 4.041	25.33 ± 3.055	-	-
Kinorhyncha	32.5 ± 2.082	-	-	-
Total	721.001	260.33	218.94	595.53

nauplius larva, trochophore larva, and fish larva. Ciliates were the identified protozoan zooplankton.

Zooplankton Seasonal Abundance

Population density of zooplankton collected at summer, autumn, winter, and spring seasons from Almarjan sandy shore and mangrove coastal zone was tabulated in Table 3 and Table 4 respectively.

Ciliates were the most abundant zooplankton on the sandy shore, while Kinorhyncha was the least abundant. At the Almarjan mangrove, Nematode was the most abundant zooplankton, whereas Gnathostomulida was the least abundant.

Two factors ANOVA showed a significant effect of species ($P < 0.001$), season ($P < 0.001$), and interactions of season and species ($P > 0.001$) on zooplankton abundance at intertidal zone of Almarjan sandy shore.

Two factor ANOVA showed a significant effect of species ($P < 0.001$), season ($P < 0.001$), and interactions of season and species ($P < 0.001$) on zooplankton abundance at the intertidal zone of Almarjan mangrove.

As given from Table 6 zooplankton diversity index was mostly higher in sandy shore than mangrove habitat. Diversity was peaked in summer for sandy shore habitat and spring for mangrove habitat. The Autumn season showed the lowest diversity index for zooplankton in both studied areas.

Zooplankton density and species richness were peaked at the summer season for the intertidal zone of Almarjan sandy shore and mangrove sites.

Based on relative abundance (Fig. 2) the protozoan ciliates were the highest abundant zooplankton at Almarjan sandy shore. Nematodes were the most abundant metazoan zooplankton, while Kinorhyncha was the least abundant. At Almarjan mangrove (Fig. 3) nematodes were the highest abundant zooplankton and gnathostomulida was the least abundant.

Based on abundance data (Table 4 and Fig. 2) zooplankton at summer season can be arranged at the intertidal zone of the sandy shore region as follows:

Ciliates> Nematods> Copepodes> Planaria> water flea (cladocera)> Nauplius larva> Kinorhyncha.

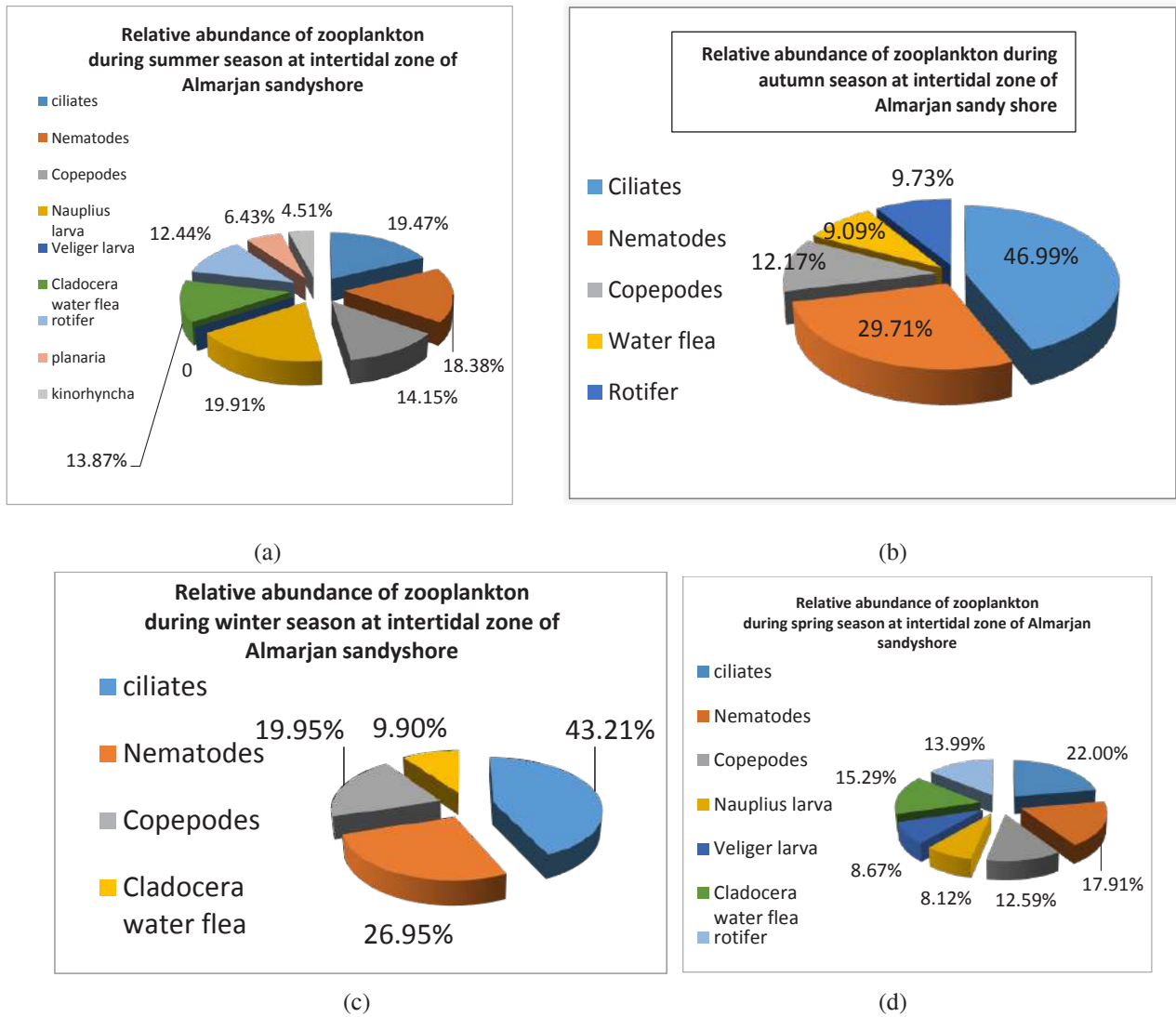


Fig. 2: Seasonal variation of percentage composition of zooplankton at the intertidal zone of Almarjan sandy shore a- summer season, b-autumn season, c-winter season, d-spring season.

Table 5: Mean seasonal abundance of zooplankton at the intertidal zone of Almarjan mangrove coastal zone.

species	Summer mean±SD	Autumn mean±SD	Winter mean±SD	Spring mean±SD
Ciliates	113.75 ± 24.96	103.67 ± 4.04	78.33 ± 7.64	85.75 ± 7.073
Nematoda	132.67 ± 11.15	117.67 ± 3.05	87.75 ± 5.31	82.2 ± 4.651
Copepods	65.33 ± 4.163	49 ± 3.61	81.2 ± 6.76	72.75 ± 5.188
Nauplius larva	78.33 ± 7.63	-	31 ± 1.826	42.67 ± 11.01
Planaria	43.365 ± 6.43	24.714 ± 4.89	-	-
Gammarus	95 ± 5.568	-	-	-
Trochophore larva	-	-	8 ± 2.16	13.25 ± 2.75
Fish larva	-	-	-	36.25 ± 4.79
Gnathostomulida	29.33 ± 1.527	-	16.8 ± 1.702	40 ± 5.305
Total	557.775	295.05	303.08	372.87

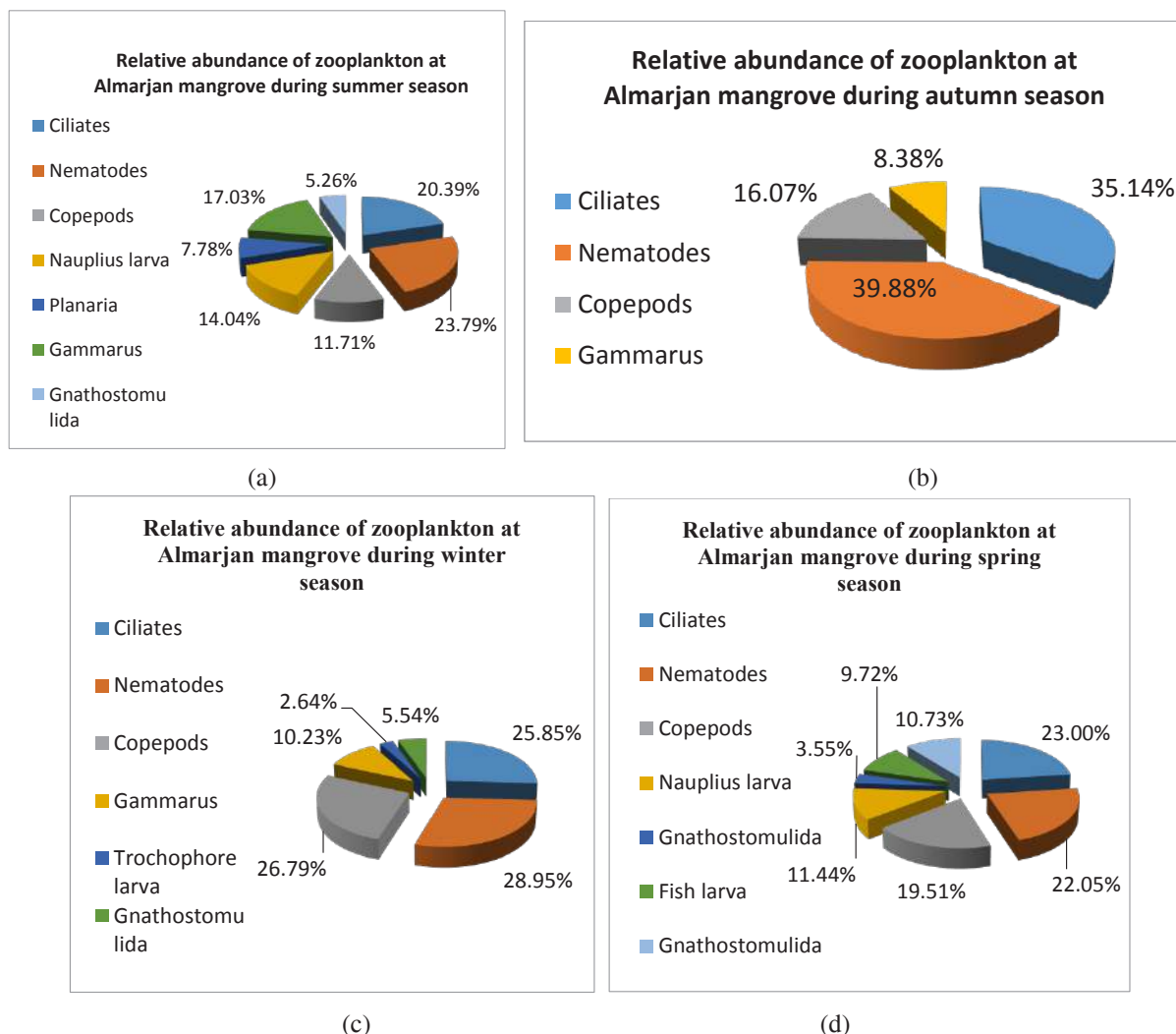


Fig. 3: Seasonal variation of percentage composition of zooplankton at Almarjan mangrove, a-Summer season b-autumn season c-winter season d-spring season.

At mangrove (Table 5 and Fig. 3). zooplankton was ranked as follows:

Nematods>ciliates>*Gammarus*>nauplius larva>copepods> *Planaria*> Gnathostomulida

Total zooplankton abundance data (Fig 4) showed higher population density for sandy shore in summer and spring

Table 6: Shannon-Weiner diversity index (H') of zooplanktons at Almarjan sandy shore and mangrove.

Season	Sandy shore	Mangrove
Summer	0.9	0.709
Autumn	0.688	0.536
Winter	0.548	0.672
Spring	0.835	0.789

seasons. One-way ANOVA showed a significant difference ($P < 0.05$) between total zooplankton density at the intertidal zone of sandy shore and mangrove investigated sites. Duncan's comparison of means test demonstrated that total zooplankton density at the sandy shore was significantly ($P < 0.05$) higher than at the mangrove site.

Effect of Water Criteria on Seasonal Abundance of Zooplankton

Regression analysis between measured water criteria and seasonal zooplankton abundance was calculated.

regression analysis of water criteria with zooplankton abundance inhabiting intertidal zone at Almarjan sandy shore showed nonsignificant relationship with pH ($r = 0.48$, $p > 0.05$), Salinity showed significant relationship ($r = 0.931$,

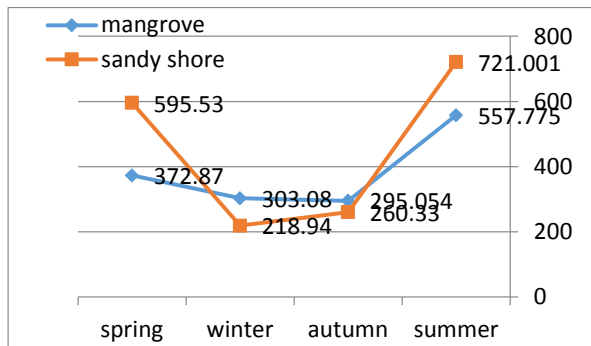


Fig. 4: Seasonal abundance of zooplankton at the intertidal zone of Almarjan sandy shore and mangrove coastal zones.

$p = 0.03$). Surface seawater temperature (SST) demonstrated significant effect on zooplankton abundance ($r = 0.948$, $p < 0.05$). Conductivity showed no significant difference ($r = 0.958$, $p > 0.05$). At Almarjan mangrove; regression relationship was significant ($r = 0.922$, $P < 0.05$) between seasonal variation in SST and zooplankton abundance. Salinity demonstrated significant regression relationship ($r = 0.970$, $P < 0.05$) with zooplankton abundance. Significant relationship ($r = 0.983$, $p < 0.05$) was shown between pH and zooplankton abundance. No significant regression was shown between conductivity and zooplankton abundance ($r = 0.838$, $p > 0.05$).

DISCUSSION

Few works referred to zooplankton in Jazan. However, no previous study concerned the identification of zooplankton species in the Jazan coastal area. It was stated that zooplankton acquires the necessary energy amount required to perform vital activities (Lee & Stokes 2006).

Zooplankton community structure was studied by several authors as bioindicators for global climatic changes due to their sensitivity to environmental stressors. Qualitative and quantitative analysis of the zooplankton community, bioindicator species were selected for analysis of water quality (Ferdous & Muktadir 2009, AbdAllah 2017, Kim et al. 2020). Paul et al. (2016) used zooplankton abundance for the evaluation of abiotic stressors in the temperate estuarine ecosystem. Change in zooplankton abundance at studied habitats might be attributed to the occurrence of inorganic and organic contaminants (Mahdy 2005, ObuidAllah et al. 2005).

Al-Asghah and Bedawi (1988) studied Zooplankton at Jazan Reservoir and recorded copepod, water flea, and rotifers. The present study reported the same groups of zooplanktons. Zooplankton reached their maximum abundance in the summer season. This agrees with previous studies (AlAsghah & Bedawi 1988, Gaughan & Potter 1995).

Bakhsh (1994) stated that the food content of the thread bream *Nemipterus japonicus* at Farsan Islands and Jazan seawater included copepods and amphipods. This result agrees with those of the current study where both zooplankton groups were found.

Calanoid and Euphausiid zooplankton are important zooplankton in the red sea (ObuidAllah et al. 2005). Farasan report stated the presence of copepod as zooplankton in the surface seawater (Abou-Zinada 2001). The current study is in accordance with this study and demonstrated the presence of a high population density of copepod as a holoplankton at the littoral area of sandy and muddy shore.

Surface water temperature, pH, and conductivity had a significant effect on zooplankton abundance. This finding agrees with the previous study by Sharma & Kumari (2018) and Manickam et al. (2018) who found a significant effect of temperature, pH, and salinity on zooplankton diversity in Ukkadam lake.

In the present work, Copepods and ciliates were the most abundant zooplankton in both mangrove and sandy shore intertidal zone. A high number of nematodes was observed among the zooplankton composition at the intertidal zone of sandy or muddy shore studied habitats. This might be due to that the sampling site was the surface water overlying sediments where seawater passed in and out of the underlying sediments. The results agree with Jensen (1981) and Vanreusel et al. (1992) who stated that nematodes exist in different aquatic freshwater or marine habitats. They reported about 4000 diverse marine nematode planktonic species. The presence of vast zooplankton assemblage recorded in the present study indicates good water criteria as zooplankton are sensitive to seasonal changes (Rombouts et al. 2013, Manickam et al. 2018, Xiong et al. 2020).

Future research will focus on the factors and threats that influence zooplankton population density in Jazan coastal habitats.

CONCLUSION

The present work was made due to the shortage of information about the identification of zooplankton in the Jazan coastal zone. The maximum species richness and abundance of collected zooplankton were found in the summer season, whereas the least species richness and abundance of collected zooplankton were found in the winter season. Variable abundance and species richness were shown at different seasons for sandy shore and mangrove studied sites. Water temperature, salinity, and conductivity showed a significant effect ($P < 0.05$) on zooplankton density and species richness.

ACKNOWLEDGEMENT

The authors are thankful to the scientific Dean of Jazan University for financially supporting that work as a part of the six scientific programs, grant number 4357.

REFERENCES

- AbdAllah, A.T. 2017. The efficiency of invertebrate animals for risk assessment and biomonitoring of hazardous contaminants in the aquatic ecosystem, A review, and status report. *J. Environ. Risk Assess. Remed.*, 1(1): 13-18.
- Abdul Aziz, P. K. , Al- Tisan, I. A. , Daili, M.A., Green, T.N. , Dalvi, A. G. I. and Javeed, M. A. 2003. Chlorophyll and plankton of the gulf coastal waters of Saudi Arabiabordering a desalination plant. *Desalination*, 154 ; 291-302.
- Abu-Zinada, A.H. 2001. First Saudi Arabian National Report on the Convention on Biological Diversity. The National Commission for Wildlife Conservation and Development.
- Al-Asgah, N. A. and Bedawi, R. M. 1988. Some observations on water quality and aquatic fauna of the Gizan reservoir in Saudi Arabia. *J. Coll. Agric. King Saud. Univ.*, 10(2): 357-362.
- Baksh, A.A. 1994. The biology of thread bream *Nemipterus japonicus* (Bloch) from the Jizan region of the Red Sea. *J. Kua. Mar. Sci.*, 7: 179-189.
- Bradford-Grieve, J.M. Haakonsen, L. and Jillett, J.B. 1983. The marine fauna of New Zealand: pelagic calanoid copepods: Families Euchaetidae, phaemidae, scolecithricidae, diaixidae, and tharybidae. *Oceanogr.Inst.*, 90: 1-150.
- Castro, P. and Huber, M. 2012. *Marine Biology*. 9th Edition. McGraw Hill Publishers, New York.
- Farasan Report. 2000. Islands protected area master management plan 2000. National Commission for Wildlife Conservation and Development, Riyadh, 11575.
- Ferdous, Z. and Mukhtadir, A.K.M. 2009. A review: Potentiality of zooplankton as bioindicator. *American J. Appl. Sci.*, 6(10): 1815-1819.
- Gaughan, D. and Potter, C. 1995. Composition, distribution, and seasonal abundance of zooplankton in a shallow, seasonally closed estuary in temperate Australia. *Estuar. Coast. Shelf Sci.*, 41(2): 117-135.
- Jensen, P. 1981. Description of the freeliving marine nematode *Dracognomus tinae* n. sp. (Draconematoidea: Prochaetosomatidae). *Cah. Biol. mar.* XXII: 285-289.
- Jost, L. 2006. Entropy and diversity. *Oikos*, 113, 363–375.
- Heron, G. A. and Bradford-Grieve, J. M. 1995. The marine fauna of New Zealand. *Oceanogr. Inst.*, 104: 1-57.
- Hickman, C.P., Roberts, L.S., Keen, S.L., Larson, A., l'Anson, H. and Eisenhour, D.J. 2011. *Integrated Principles of Zoology*. 15th edition. Mc-Graw Hills Higher Education Publishers. Boston, Madrid.
- Kim, H., Lee, C., Lee, S., Oh, S. and Kim, W. 2020. Biodiversity and community structure of mesozooplankton in the marine and coastal national park areas of Korea. *Diversity*, 12: 233
- Lee, G. and Stokes, J. 2006. *Marine Science. An illustrated guide to Science*. Chelsea House Publishers, New York.
- Mahdy, A.A. 2005. Taxonomical and Ecological Studies on Marine Zooplankton of the Red Sea, Egypt. MSc. Thesis, Al-Azhar University, Assiut, Egypt.
- Manickam, N., Bhavan, P.S., Santhanam, P., Bhunasweri, R., Muralisankar, T., Srinivasan, V., Assiakkutti, A., Rajkumar, G., Udayasuriyan, R. and Karthik, M. 2018. Impact of seasonal changes in zooplankton biodiversity in Ukkadam Lake, Coimbatore, Tamil Nadu, India, and potential future implications of climate change. *JoBAZ*, 15: 79.
- Nybakken, J. W. 1997. *Marine Biology an Ecological Approach*. 4th Edition Addison-Wesley Educational Publishers Inc., Boston, p. 481.
- ObuidAllah, A.H., AbdAllah, A.T., Abu-Eldahab, H.M., Abd-Rahman, N.S. and Mahdy, A.A. 2005. Impact of heavy metal contamination on seasonal abundance of planktonic copepods inhabiting mangrove areas in Safaga, Red Sea, Egypt. *Egypt. J Exper. Biol.*, 1: 57-66.
- Paul, S., Wooldridge, T. and Perissinotto, R. 2016. Evaluation of abiotic stresses of temperate estuaries by using resident zooplankton: A community vs. population approach. *Estuar. Coast. Shelf Sci.*, 170: 102-111.
- Rombouts, I., Beaugrand, G., Artigas, L.F., Dauvin, J. C., Gevaert, F, Goberville, E., Kopp, D., Lefebvre, S., Luczak, C., Spilmont, N., Travers-Trolet, M., Villanueva, M.C. and Kirby, R.R. 2013. Evaluating marine ecosystem health: Case studies of indicators using direct observations and modeling methods. *Ecol. Indicators*, 15: 353-365.
- Sharma, R.C. and Kumari, R. 2018. Seasonal variation in zooplankton community and environmental variables of sacred Lake Prashar Himachal Pradesh, India. *Int. J. Fish. Aquat. Stud.*, 6(2): 207-213.
- Tuomisto, H. 2010. A diversity of beta diversities: straightening up a concept gone awry: Part 1. Defining beta diversity as a function of alpha and gamma diversity. *Ecography*, 33: 2-22.
- Vanreusel, A., Vincx, M., Van Gansbeke, D. and Gijssels, W. 1992. Structural analysis of the meiobenthic communities of the shelf break area in two stations of the Gulf of Biscay (N.E. Atlantic). *Belg. J. Zool.*, 122: 184-202.
- Xiong, W., Xuena, H., Chen, Y., Fu, R., Duu, X. Chen, X. and Zhan, A. 2020. Zooplankton biodiversity monitoring in polluted freshwater ecosystems: A technical review. *Environ. Sci. Technol.*, 5(1): 1-11.



Application of Cationic Surfactant Modified Mengkuang Leaves (*Pandanus atropurpureus*) for the Removal of Reactive Orange 16 from Batik Wastewater: A Column Study

Megat Ahmad Kamal Megat Hanafiah* Shariff Ibrahim**†, Nur Izah Fasihah Mohamad Subberi**, Nesamalar Kantasamy** and Is Fatimah***

*Faculty of Applied Sciences, Universiti Teknologi MARA, 26400, Jengka, Pahang, Malaysia

** Department of Chemistry, Faculty of Applied Sciences, Universiti Teknologi MARA, 40450, Shah Alam, Malaysia

***Department of Chemistry, Universitas Islam Indonesia, Kampus Terpadu UII, Jl. Kaliurang Km 14, Yogyakarta, Indonesia

†Corresponding author: Shariff Ibrahim; sha88@uitm.edu.my

Nat. Env. & Poll. Tech.
Website: www.neptjournal.com

Received: 01-12-2020

Revised: 13-02-2021

Accepted: 26-02-2021

Key Words:

Mengkuang Leaves
Reactive orange 16 dye
Cationic surfactant
Fixed bed column
Yoon-Nelson model

ABSTRACT

The feasibility of Mengkuang leaves (*Pandanus atropurpureus*) as a non-conventional low-cost adsorbent for the removal of an anionic dye, Reactive Orange 16 (RO16), was investigated. Among the dyes that have been commonly used in the Batik industry was reactive dye. In this study, Mengkuang leaves were chemically modified with cetyltrimethylammonium bromide (CTAB), a cationic surfactant, to improve their adsorption performance toward anionic dyes. The adsorbent's morphological characteristics were analyzed using a scanning electron microscope (SEM). The surface of modified Mengkuang leaves seems to be irregular and uneven, with more porous structures than raw Mengkuang leaves. Adsorption of RO16 dye in fixed bed column using modified Mengkuang leaves adsorbent indicated that the breakthrough time increased at higher bed height and lower flow rate. The breakthrough times for bed height of 0.5, 2, and 4 cm were at 16, 68, and 165 min, respectively. Meanwhile, breakthrough time for the flow rate of 2.5 and 7 mL.min⁻¹ were at 327, 104, and 43 min, respectively. However, the study utilizing raw Mengkuang leaves showed no significant removal of RO16. Thus, it can be concluded that the cationic surfactant modification of Mengkuang leaves is advantageous for anionic dye removal. This anionic dye removal is significantly influenced by column parameters such as bed height and flow rate as the plotted breakthrough curves obtained from experimental data were similar to the typical breakthrough curve. When applied to the Yoon-Nelson model, the adsorption data provided the best fit with the R² value above 0.95. The time taken for the breakthrough is very similar to model prediction values. Experiments with real batik dye wastewater showed the immense potential of modified Mengkuang leaves where total removal of real Batik wastewater was instantaneous.

INTRODUCTION

Batik industry is one of the oldest cottage textiles industries in Malaysia. More than 1500 batik factories are distributed mostly in Kelantan and Terengganu, Malaysia (Rashidi et al. 2013). The resulting waste is mostly discharged into water bodies with minimal or in most cases it was directly discharged without any prior treatment (Mahmudi et al. 2020). This is because most of these industries are typically practiced on a small scale with no appropriate waste disposal system (Sridewi et al. 2011). Only 5% of these dyes are fixed during the coloring process, where the rest are discarded as liquid waste (Wibowo et al. 2017). Among the many dyes, azo reactive dyes represent the large group as the production volume and number are concerned (Mitrović et al. 2012), where the reactive dyes are the most used in batik textiles industries (Rashidi et al. 2013). The azo reactive dye, which

compounds contain one or more azo groups (–N=N–), could produce potentially carcinogenic in aromatic amines via metabolic cleavage of the azo linkage (Mitrović et al. 2012). Due to this, remediation of dye wastewater is often crucial. Moreover, the wastewater generated from this industry contains a non-biodegradable organic compound, which can cause ecological contamination, especially for the aquatic environment (Wibowo et al. 2017).

Many techniques are employed for dye-containing batik wastewater removals such as the application of hybrid wetland (Rahmadyanti et al. 2020) and membranes (Febriasari et al. 2021). However, due to their simple yet efficient effectiveness, adsorption methods are often preferred (Yagub et al. 2014). The use of plant-based sorbents has been shown to work well for the removal of dye where different biomass has been successfully investigated for the

removal of dye (Yagub et al. 2014). Different functional groups such as carboxyl, hydroxyl, sulfate, phosphate, ether, and amino groups are available on the plant-based sorbent, which has been identified to function as adsorption sites (Nghah & Hanafiah 2008). In this study, Mengkuang leaves, a Pandanus family, have been selected for potential adsorbent of RO16, an azo reactive dye. Mengkuang is the Malaysian name for the *Pandanus atrocarpus*, a plant belonging to the Pandanaceae family (Sheltami et al. 2012). It can be found in wet, damp places such as mangroves and tropical jungles. Mengkuang leaves specifically have not been researched for any adsorbent purpose. But, the Pandanus family was found successful in removing aqueous-based pollutants, such as methylene blue dye (Ismail et al. 2013), copper (Ngadi et al. 2015), and lead (Abdullah & Loo 2006).

Despite the advantages of plant-based sorbent, many works found the less satisfactory raw biomass adsorbent to remove anionic dye due to negative surface charge on the biomass surface (Ibrahim et al. 2010a). This observation has been reported by many works (Oei et al. 2009). Due to this, surfactant modification was employed to render the surface to a positive potential, which is conducive to removing anionic contaminants. This kind of modification has been reported by many works (Akl et al. 2013, Bingol et al. 2004, Ibrahim et al. 2010b). Ibrahim et al. (2010b) found a vast improvement in anionic dye removal, Reactive Blue 4, upon using a modification of barley straw with cationic surfactant for anionic reactive dye adsorption. Hence in this work, the Mengkuang leaves were modified with a cationic surfactant, cetyltrimethylammonium bromide (CTAB). CTAB consists of a 19-carbon chain tail group, is a quaternary ammonium surfactant. CTAB has been used to chemically modify adsorbent surfaces, particularly for removing anionic contaminants in some works (Akl et al. 2013, Bingol et al. 2004). The surfactant was also applicable for attapulgite modification in the enhancement of anionic dye adsorption (Xu et al. 2015).

In this paper, a study on the physicochemical change of CTAB-modified Mengkuang leaves and its applicability for removing model anionic dye, RO16 as well as real wastewater from batik industries, was presented.

Based on the literature search, limited studies on the utilization of modified surfactant adsorbent for removal of dye contaminants, especially real dye from batik wastewater were reported, thus making this study even more interesting.

A continuous column experiment was applied to explore the effects of parameters such as the bed height of the adsorbent and inlet dye flow rate on the column breakthrough volume. The data was fitted to the Yoon-Nelson model to determine the fitness of the column experimental data.

MATERIALS AND METHODS

The Mengkuang leaves were collected, cut into smaller pieces, washed, and dried under sunlight, and further dried in the oven overnight at 80°C. It was then ground to the powder form and labeled as Raw Mengkuang Leaves (RML). The cationic surfactant modification method was adopted from (Zhou et al. 2015) with some modifications. A mixture of RML powder and 200 mL, 1% (w/v) cetyltrimethylammonium bromide (CTAB, Aldrich, USA) solution, were shaken by an orbital shaker at 180 rpm at room temperature for 24 h. RML powder was separated from the mixture and washed with distilled water to remove superficially retained CTAB. Finally, the modified RML powder was dried in an oven at 60°C overnight and labeled as Modified Mengkuang Leaves (MML). The anionic dye solution, Reactive Orange 16 (RO16, MW = 617.54 g.mol⁻¹) obtained from Aldrich, USA, was prepared by dissolving the dye in distilled water. The dye concentrations were measured using the HACH DR2800 Portable spectrophotometer at a maximum absorbance wavelength of 492 nm. The chemical structure of RO16 is shown in Fig. 1.

The RML and MML were then characterized physically and chemically by Fourier Transform Infrared Spectroscopy (Thermo Scientific Nicolet 6700 FT-IR spectrophotometer, USA) at a scanning range of 650-4000 cm⁻¹. Meanwhile, the surface morphologies were observed directly using a Tabletop Scanning Electron Microscope (SEM, Hitachi TM3030 Plus, Japan) with an acceleration voltage of 5kV and magnification of 1000x.

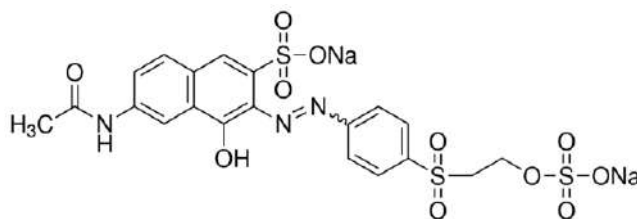


Fig. 1: Chemical structure of RO16.

General Adsorption Column Studies

Column studies were conducted in a transparent cylindrical polypropylene column (2.7 cm and 10 cm height), packed with a known quantity of MML. A layer of the plastic sieve was attached at the bottom of the column. A known amount of the MML was packed in the column to produce the desired bed heights of the adsorbent (0.5, 2, and 4 cm). A 100 mg.L⁻¹ of RO16 dye solution was pumped upward through the column at the desired flow rates (2, 5, and 7 mL.min⁻¹) controlled by a peristaltic pump. The dye solutions at the outlet of the column were collected at regular time intervals. The concentration of the dye effluent was then determined using a spectrophotometer. Breakthrough time was set at 30% of the effluent RO16 to feed concentration, as suggested by Goel et al. (2005). Column operation was stopped when the effluent concentration exceeded 99.0% of its initial concentration. All experiments were carried out at room temperature. The effects of experimental column parameters such as bed height, feed flow rate on the dye removal were investigated by varying the one parameter above while at the same time keeping the other parameters constant. To study the effect of flow rate and bed height, the flow rate was run at 2-7 mL.min⁻¹, whereas the bed height was varied at 0.5 to 4 cm, respectively.

Column Experiment for Real Batik Dye Wastewater

To prove the applicability of MML in remediating batik dye wastewater, the MML was further tested with real batik dye wastewater. The wastewater was collected from Master Wan Batik Industry, located in Dengkil, Selangor, Malaysia at the discharged point. The collected wastewater was preserved with few drops of 1% concentrated nitric acid (HNO₃) and stored in the refrigerator for further use. The column was

packed with MML (2 cm height), and real batik dye wastewater was pumped through the column at a flow rate of 5 mL.min⁻¹. The effluent was collected at the outlet of the column every 1 min. The color variations of the batik dyes were then measured using a stored program in a HACH 16 DR2800 Portable spectrophotometer at 465 nm wavelength, utilizing the color, true and apparent (Platinum-Cobalt (Pt-Co)) method. The results are expressed in mg/L Pt-Co.

RESULTS AND DISCUSSION

Fourier transform infrared spectroscopy (FT-IR) was used to examine the surface groups of the adsorbents and to identify some characteristic functional groups. The FT-IR spectra of RML, MML, and dye-loaded MML were studied in the range of 650-4000 cm⁻¹. The indication of CTAB impregnated on Mengkuang leaves surface was observed at peaks of 2921.66 and 2852.25 cm⁻¹, where's these two peaks were not visible in RML spectra. The same conclusion has been made by Akl et al. (2013), where they assigned these peaks to the asymmetric and symmetric stretching vibrations of the CH₃ and CH₂ of the aliphatic chain of the CTAB. Meanwhile, Spectra for dye loaded- MML does not differ much, except that the peaks at 2921.66 and 2852.25 cm⁻¹ in MML are shifted to 2922.32 and 2851.96 cm⁻¹ in loaded MML with a significant increase in intensity This indicate the dye component combining with hydrophobic groups of surfactant (Ibrahim et al. 2010a). A preliminary study done by soaking the modified MML in DI water resulted in a negligible amount of CTAB being desorbed, indicating the existence of intermolecular attraction between CTAB and MML surface. A similar conclusion has been suggested by Ibrahim et al. (2010) in their study on the modification of barley straw using a cationic surfactant, hexadecylpyridinium chloride monohydrate (CPC).

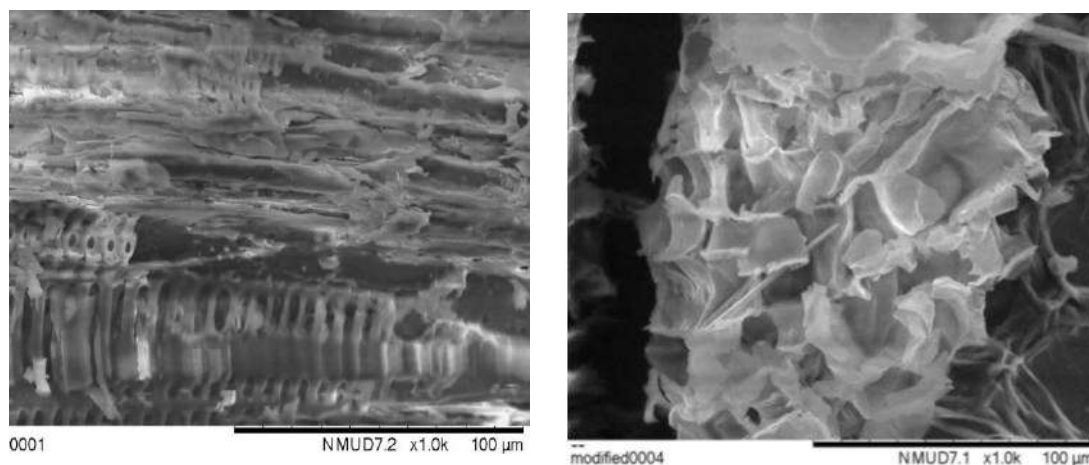


Fig. 2: SEM micrograph of (a) RML and (b) MML at 1000x.

Surface Morphological of Mengkuang Leaves

The adsorbent's surface features and morphological characteristics were studied using a scanning electron microscope (SEM, Hitachi TM3030 Plus, Japan). Fig. 2 shows the images of Mengkuang leaves before and post-modification with CTAB. The surface of MML seemed to be irregular and uneven, with more porousness compared to RML. According to Wang et al. (2020), this feature can be considered as an excellent character with a high possibility for dyes to be adsorbed on its surface. Meanwhile, Hameed and El-Khaiary (2008) suggested uneven and rough surface of an adsorbent offered more opportunity for dyes to be trapped or adsorbed.

Adsorption Column Studies

The effect of bed height on the adsorption performance of MML has been investigated by varying the bed height from 0.5 to 4 cm. The flow rate was fixed at 5 mL.min⁻¹, and the initial concentration of RO16 is at 100 mg.L⁻¹. From breakthrough curves, it was found that by increasing the bed height, the breakthrough time (t_b) increased accordingly. The dye solution had more contact time with the adsorbent, resulting in high dye removal. (Rouf & Nagapadma 2015). The t_b values increased from 16 to 165 min, as the bed height was increased from 0.5 to 4 cm. An increase in the adsorbent's surface area may provide more binding sites for adsorption (Zulfadhly et al. 2001), thus enhancing the breakthrough time. A similar trend was found for the column breakthrough volume (V_b) (Table 1). The effects of the flow rate on the adsorption of RO16 dyes have been studied over a range from 2 to 7 mL.min⁻¹. The bed height was 2 cm, and the initial concentration of RO16 was at 100 mg.L⁻¹. It can be seen that the breakthrough generally occurred faster at a higher flow rate, and it would take less time for the bed to get saturated. Moreover, the higher turbulence at a higher flow rate may cause a weaker interaction and interparticle mass transfer

between the dye molecules and the biosorbent. However, at a lower flow rate, the dye solution has adequate time to get adsorbed on the adsorbent surface (Rouf & Nagapadma, 2015). Table 2 shows the breakthrough time decreased from 327.5 to 42.85 min, increasing the flow rate from 2 to 7 mL.min⁻¹. At a higher flow rate, the contact time of RO16 in the column was shorter, thus decreasing breakthrough time. A consistent trend was as well found for V_b . A similar observation has been made by Jain & Gogate (2017).

Modeling of Column Data: Yoon-Nelson Model

The Yoon-Nelson model basically predicts the possibility of adsorbate breakthrough being proportional to the rate of reduction and the adsorption of adsorbate (Bharathi & Ramesh 2013), but it does not describe the sorption mechanism. The column data were fitted to the Yoon-Nelson model (Yoon & Nelson 1984) to plot the Yoon-Nelson breakthrough curves (Fig. 3). From the plots, the k_{YN} (rate constant), and τ (the time required for 50% RO16 breakthrough) could be determined. As seen in Table 3, in general, the model breakthrough time (τ) showed good agreement with the experimental breakthrough data ($t_{50\%,exp}$). As for Yoon-Nelson's constant (k_{YN}), the value decreased from 0.0667 to 0.0313 min with increasing τ values from 23.7 to 192.5 min as the column bed height increased. This situation was also observed in the inlet flow rate as the k_{YN} values increased from 0.0087 to 0.0606 mL.mg⁻¹.min⁻¹, whereas the τ values decreased from 461.0 to 56.3 min with increasing feed flow rate. The coefficient correlations, R^2 was > 0.96 for all the fitted values in the model, indicating that this model is appropriate to explain the overall kinetics in the column for the RO16 adsorption.

For the actual batik wastewater experiment, color was removed almost instantly. The initial color was 134 mg/L Pt-Co. As batik dye wastewater consists mainly of reactive

Table 1: Effect of bed height on column breakthrough curve.

Bed height (cm)	HRT (min)	t_b (min)	V_b (ml)
0.5	0.27	16	80
2	1.08	68	340
4	2.16	165	825

Table 2: Effect of flow rate on column breakthrough curve.

Flow rate (mL.min ⁻¹)	HRT (min)	t_b (min)	V_b (ml)
2	2.7	327	660
5	1.08	104	490
7	0.77	43	370

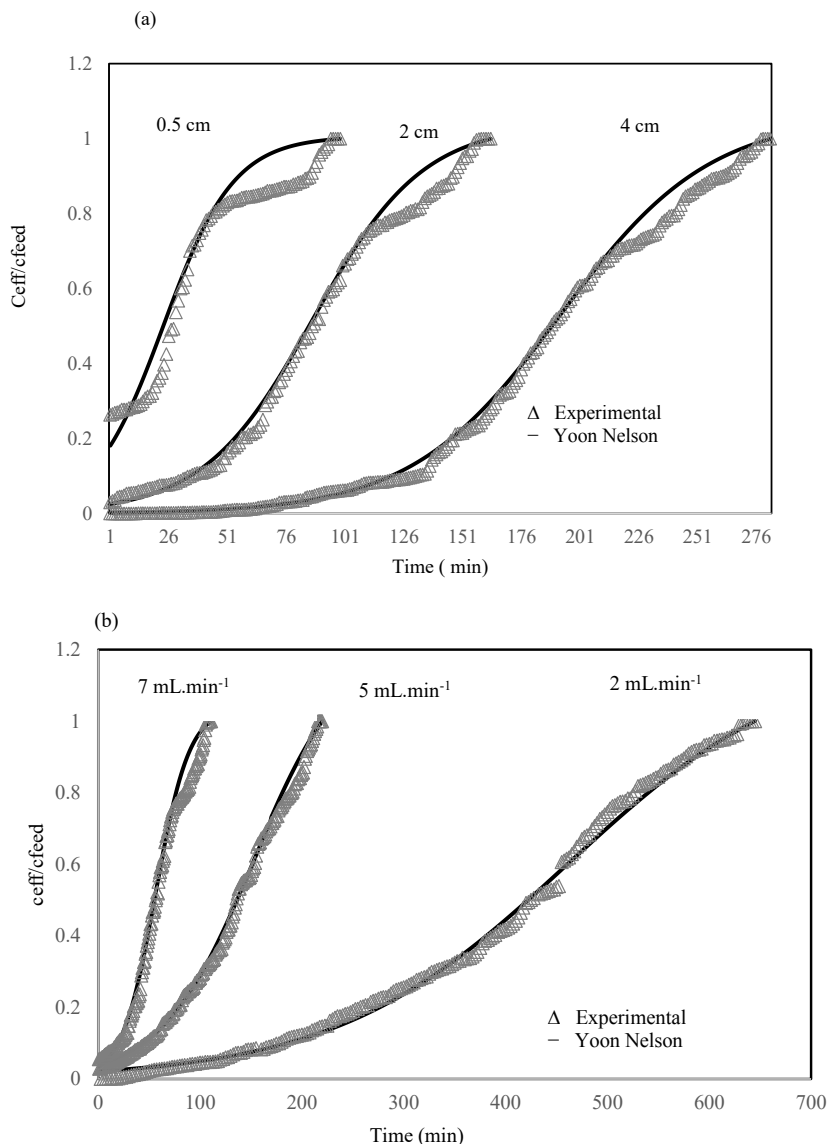


Fig. 3: Experimental and calculated Yoon-Nelson model breakthrough curves for different parameters (a) bed height and (b) flow rate.

dye, this demonstrates our previous finding of the superiority of MML in the removal of reactive dye wastewater.

CONCLUSION

In this study, modified Mengkuang leaves (MML) were prepared, characterized by several physicochemical methods, and tested as an effective adsorbent for RO16 dye removal from aqueous solutions. Some significant conclusions are summarized as follows:

The SEM images showed that the surface of MML seems to be irregular and uneven with more porous compared to RML, which is favorable for the adsorption process.

The column study revealed that adsorption was a function of bed height and flow rate. A higher bed height and a low flow rate were observed to increase the column breakthrough volume.

Yoon-Nelson model revealed that the model agreed well with experimental data as the regression (R^2) values for all the column parameters were > 0.96 . The 50% breakthrough time from the experiment was closed to the Yoon-Nelson breakthrough prediction. The highest k_{YN} breakthrough times were at 192.2 and 461 mL.mg⁻¹ min⁻¹ for bed height of 4.0 cm and flow rate of 2 mL.min⁻¹, respectively.

The column experiment with real batik dye wastewater showed that total removal of color occurred instantly by MML.

Table 3: Yoon-Nelson model at different parameters using A non-linear regression analysis.

Parameter		k_{YN}	Breakthrough Time		R^2
		$\text{mL}\cdot\text{mg}^{-1}\cdot\text{min}^{-1}$	$(t_{50\% YN})$ min	$(t_{50\%,exp})$ min	
Bed Height (cm)	4.00	0.0313	192.5	188	0.99
	2.00	0.0427	87.3	88	0.99
	0.50	0.0667	23.7	28	0.96
Flow Rate ($\text{mL}\cdot\text{min}^{-1}$)	7.0	0.0606	56.3	57	0.99
	5.0	0.0313	192.5	136	0.99
	2.0	0.0087	461.0	421	0.99

ACKNOWLEDGMENT

The authors would like to acknowledge the support from the Faculty of Applied Sciences, Universiti Teknologi MARA (UiTM) Shah Alam, Selangor.

REFERENCES

- Abdullah, M.Z. and Loo, K. 2006. Separation of divalent metal ions using *Pandanus amaryllifolius Roxb* (Pandanus) leaves: Desorption study. WIT Trans. Ecol. Environ., 92: 313-321.
- Akl, M., Youssef, A. and Al-Awadhi, M. 2013. Adsorption of acid dyes onto bentonite and surfactant-modified bentonite. J. Anal. Bioanal. Tech., 4(4): 3-7.
- Bharathi, K.S. and Ramesh, S.P.T. 2013. Fixed-bed column studies on bi-adsorption of crystal violet from aqueous solution by *Citrullus lanatus* rind and *Cyperus rotundus*. Appl. Water Sci., 3(4): 673-687.
- Bingol, A., Ucun, H., Bayhan, Y.K., Karagunduz, A., Cakici, A. and Keskinler, B. 2004. Removal of chromate anions from an aqueous stream by a cationic surfactant-modified yeast. Bioresour. Technol., 94(3): 245-249.
- Febriasari, A., Ananto, A.H., Suhartini, M. and Kartohardjono, S. 2021. Polysulfone-polyvinyl pyrrolidone blend polymer composite membranes for batik industrial wastewater treatment. Membranes, 11(1): 66.
- Goel, J., Kadirvelu, K., Rajagopal, C. and Garg, V.K. 2005. Removal of lead (II) by adsorption using treated granular activated carbon: batch and column studies. J. Hazard. Mater., 125(1-3): 211-220.
- Hameed, B. and El-Khaiary, M. 2008. Removal of basic dye from aqueous medium using a novel agricultural waste material: Pumpkin seed hull. J. Hazard. Mater., 155(3): 601-609.
- Ibrahim, S., Fatimah, I., Ang, H.M. and Wang, S. 2010a. Adsorption of anionic dyes in aqueous solution using chemically modified barley straw. Water Sci. Technol., 62(5): 1177-1182.
- Ibrahim, S., Shuy, W.Z., Ang, H.M. and Wang, S. 2010b. Preparation of bioadsorbents for effective adsorption of a reactive dye in an aqueous solution. Asia-Pac. J. Chem. Eng., 5(4): 563-569.
- Ismail, M.N., Aziz, H.A., Ahmad, M.A. and Kamaruddin, M.A. 2013. Removal of methylene blue dye from aqueous solution using activated carbon prepared from *Pandanus Tectorius* leaves. Int. J. Sci. Res. Knowl., 1(10): 388-403.
- Jain, S.N. and Gogate, P.R. 2017. Adsorptive removal of acid violet 17 dye from wastewater using biosorbent obtained from NaOH and H₂SO₄ activation of fallen leaves of *Ficus racemosa*. J. Mol. Liq., 243: 132-143.
- Mahmudi, M., Arsad, S., Amalia, M.C., Rohmaningsih, H.A., Prasetya, F.S., Ruengruehan, K. and Maraslıoğlu, F. 2020. An alternative activated carbon from agricultural waste on chromium removal. J. Ecol. Eng., 21(8): 1-9.
- Mitrović, J., Radović, M., Bojić, D., Anđelković, T., Purenović, M. and Bojić, A. 2012. Decolorization of textile azo dye reactive orange 16 with UV/H₂O₂ process. J. Serbian Chem. Soc., 77(4): 465-481.
- Ngadi, N., Yahya, N.Y. and Abd Rahman, R. 2015. Sustainable removal of heavy metal using extracted *Pandanus amaryllifolius Roxb*. Appl. Mech. Mater., 56: 28-31.
- Ngah, W.W. and Hanafiah, M. 2008. Biosorption of copper ions from dilute aqueous solutions on base treated rubber (*Hevea brasiliensis*) leaves powder: kinetics, isotherm, and biosorption mechanisms. J. Environ. Sci., 20(10): 1168-1176.
- Oei, B.C., Ibrahim, S., Wang, S. and Ang, H.M. 2009. Surfactant modified barley straw for removal of acid and reactive dyes from aqueous solution. Bioresour. Technol., 100(18): 4292-4295.
- Rahmadyanti, E. and Audina, O. 2020. The performance of hybrid constructed wetland system for treating the batik wastewater. J. Ecol. Eng., 21(3): 94-103.
- Rashidi, H. R., Sulaiman, N. M., Hashim, N. A. and Che Hassan, C. R. 2013. Synthetic batik wastewater pretreatment progress by using physical treatment. Adv. Mater. Res., 6: 394-398.
- Rouf, S. and Nagapadma, M. 2015. Modeling of fixed-bed column studies for adsorption of azo dye on chitosan impregnated with a cationic surfactant. Int. J. Eng. Res., 6(2): 124-132.
- Sheltami, R.M., Abdullah, I., Ahmad, I., Dufresne, A. and Kargazadeh, H. 2012. Extraction of cellulose nanocrystals from mengkuang leaves (*Pandanus tectorius*). Carbohydr. Polym., 88(2): 772-779.
- Sridewi, N., Tan, L. T. and Sudesh, K. 2011. Solar photocatalytic decolorization and detoxification of industrial batik dye wastewater using P (3HB) TiO₂ nanocomposite films. Clean Soil Air Water, 39(3): 265-273.
- Wang, Q., Xi, F., Liang, L., Zhang, Y., Xue, Y., Wu, Q. and Meng, X. 2020. Adsorption of dye reactive brilliant red X-3B by rice wine lees from aqueous solutions. Nature Environ. Pollut. Technol., 19(3): 1085-1093.
- Wibowo, E., Rokhmat, M., Rahman, D.Y., Murniati, R. and Abdullah, M. 2017. Batik wastewater treatment using TiO₂ nanoparticles coated on the surface of a plastic sheet. Procedia Eng., 170: 78-83.
- Xu, M., Li, J., Wang, J. and Wu, Y. 2015. Removal of dyes from aqueous solution by adsorption onto CTAB modified attapulgite. Int. Conf. Chem. Mater. Food Eng., 61: 271-220.
- Yagub, M.T., Sen, T.K., Afroze, S. and Ang, H.M. 2014. Dye and its removal from aqueous solution by adsorption: a review. Adv. Colloid Interface Sci., 209: 172-184.
- Yoon, Y. and Nelson, J. 1984. A theoretical model for respirator cartridge service life. Am. Ind. Hyg. Assoc. J., 66(8): 509-516.
- Zhou, T., Lu, W., Liu, L., Zhu, H., Jiao, Y., Zhang, S. and Han, R. 2015. Effective adsorption of light green anionic dye from solution by CPB modified peanut in column mode. J. Mol. Liq., 211: 909-914.
- Zulfadhly, Z., Mashitah, M. and Bhatia, S. 2001. Heavy metals removal in the fixed-bed column by the macro fungus *Pycnoporus sanguineus*. Environ. Pollut., 112(3): 463-470.



Study on the Prevention and Control of Fe and Mn Pollution by Resistant Mixed Bacteria in Simulated Mining Area

Tianxin Li^(**), Fang Zhang^(**)† and Minjie Zhang^{*}

^{*}School of Energy and Environmental Engineering, University of Science and Technology Beijing, Beijing, 100083 PR China

^{**}Beijing Key Laboratory of Resource-oriented Treatment of Industrial Pollutants, Beijing, 100083, PR China

†Corresponding author: Fang Zhang; b20180082@xs.ustb.edu.cn

Nat. Env. & Poll. Tech.
Website: www.neptjournal.com

Received: 21-12-2020

Revised: 12-03-2021

Accepted: 10-04-2021

Key Words:

Iron pollution
Manganese pollution
Coal mine area
Fe and Mn resistant
microorganisms
Pollution control

ABSTRACT

By simulating the mining environment, the potential of the selected mixed bacteria (*Pseudomonas putida*, *Lysinibacillus xylanilyticus*, *Lysinibacillus macroides*, *Bacillus simplex*, *Brevibacillus agri*) to control Fe and Mn pollutants in mining environment were explored. The results showed that the selected bacteria could inhibit the release of Fe and Mn from ore into the aquifer, and the inhibition effect on Mn was significantly stronger than that on Fe. At the same time, these processes also have a certain degree of impact on the external environment, including the gradual increase of pH, the gradual decrease of oxidation-reduction potential, and the decrease of dissolved oxygen concentration. The changes of these external environmental factors will once again directly affect the degradation and immobilization of Fe and Mn. The selected mixed bacteria can also enhance the adsorption of free Fe and Mn, improve the adsorption efficiency and capacity of Fe and Mn, and slow down the desorption of Fe and Mn to water.

INTRODUCTION

Coal plays an important role in energy generation, and approximately 27% of the world's energy consumption originates from the incineration of coal (Bhuiyan et al. 2010). Industrial production and exploitation of mineral resources are important sources of heavy metal pollution in soil (Bermudez et al. 2012). Heavy metals in coal or coal wastes are released and accumulated in the soil through various processes (leaching, weathering, combustion, and biological reaction) (Shafer et al. 2012, Zhou et al. 2014). Coal mining has resulted in Fe and Mn contamination in mining areas, which has become a key issue in terms of soil ecological environment protection (Guo et al. 2012). By examining heavy metals in mine drainage soil and surrounding farmland in northern Bangladesh, Bhuiyan et al. (2010) discovered that Mn came from human sources, particularly coal mining activities. Zhang & Wang (2009) found that the oxidation of heavy metal sulfide was the main way for coal gangue to release Fe and Mn into the environment. Wang et al. (2005) found that Aha Lake has been polluted by coal mine wastewater for a long time, and Fe and Mn were brought into the lake through this wastewater. Herndon et al. (2019) found that mine spoil continues to produce Mn contamination. Liu et al. (2020) showed that Fe and Mn pollution of the surface

water environment around the centralized mining area of Guizhou Province mainly comes from abandoned coal mines. A high Fe and Mn content will have a significant impact on people's lives and production (Sorensen et al. 2010, Vazquez et al. 2014, Zerling et al. 2008).

Fe and Mn belong to transition metal elements and have similar properties. The common methods to remove Fe and Mn in groundwater include chemical precipitation (Patil et al. 2016), reverse osmosis (Fan et al. 2018), ion exchange (Zhang et al. 2008), and so on. Super enrichment plants are the key technical direction for Fe and Mn soil remediation (Kováčik et al. 2014), chelating agents (Hauck et al. 2006), and microbial remediation (Sasaki 2009). The emerging microbial oxidation method has become a key research direction (Wang et al. 2012). Compared with animals or plants growing in the same soil, microbial activity is more sensitive to heavy metals (Giller et al. 1998). Zhang et al. (2017) tried to use *Fusarium oxysporum* sp. ZHH2-starch-alfalfa to repair the polluted soil in the coal mine area, and achieved good removal effect. Hou et al. (2020) isolated a microbial mixture, which can remove 99.8% and 98.6% of Fe and Mn in an acid mine drainage system, respectively. Krishnan et al. (2007) found that autotrophs and heterotrophs work in tandem, and can mitigate the concentration of Mn and related metals in mangrove sediments. Ling et al. (2011)

screened out three strains of microorganism with strong manganese resistance, and the removal rate was more than 90% when the concentration of Mn^{2+} was $200\text{ mg}\cdot\text{L}^{-1}$.

At present, the Fe and Mn resistant microbial resources are very limited, and the microbial resources have been found to be less applied in the actual remediation process (Chen et al. 2017). The identified potential organism for bioconcentration/biotransformation/biosorption is of great significance for the remediation of metals in a polluted environment (Sharma & Fulekar 2009). The development of the Yimin opencut coal mine in Inner Mongolia of China has caused serious damage to the local ecology (Guo et al. 2014). The soil microorganism used in this paper was derived from directional domestication of Fe and Mn tolerance in the Yimin opencut coal mine, and the potential of the selected mixed bacteria for the prevention and control of Fe and Mn pollution was discussed by simulating the internal environment of the mining area. It can provide some help for the study of microorganisms to assist in the restoration of coal mine ecological environment, and the prevention and control of Fe and Mn pollution (Cui et al. 2010).

MATERIALS AND METHODS

Study Area

Yimin open-pit coalfield ($119^{\circ}39'20''$ - $119^{\circ}46'35''\text{E}$, $48^{\circ}33'00''$ - $48^{\circ}36'24''\text{N}$) is located in the alluvial plain of the middle reaches of Yimin River in the north of Inner Mongolia, under the jurisdiction of Hulun Buir city. The most important basic feature of its hydrogeological conditions is that the coal seam is the main aquifer and strong conductive aquifer.

Experimental Design

Two immersion conditions, bacteria mixed solution, and blank medium were used to carry out the immersion test of Fe and Mn ores in the coal seam aquifer of the mining area to explore the response mechanism of the Fe and Mn immersion process of minerals to the selected bacteria. At the same time, pH, oxidation-reduction potential (ORP), and dissolved oxygen (DO) of leaching solution were determined to explore the influence on external environmental factors.

To study the interaction between the adsorption and desorption behavior of Fe and Mn in the soil medium of the mining area and the selected bacteria, the soil samples of the mining area were used to make the soil column, and the selected mixed bacteria were fixed in it. Different concentrations of Fe and Mn solutions were prepared to carry out the leaching test on the soil column, dynamically simulating the migration process of Fe and Mn in the high background soil medium. The leaching test of Fe solution was divided

into three rounds, which were irrigated with the leaching solution with Fe concentration of $5\text{ mg}\cdot\text{L}^{-1}$, $10\text{ mg}\cdot\text{L}^{-1}$, and $20\text{ mg}\cdot\text{L}^{-1}$ respectively. Each round of leaching test included the adsorption stage (6 days) and the desorption stage (4 days). The leaching experiments were carried out with Mn concentrations of $5\text{ mg}\cdot\text{L}^{-1}$, $10\text{ mg}\cdot\text{L}^{-1}$, and $20\text{ mg}\cdot\text{L}^{-1}$ respectively. Each round of leaching test included the adsorption stage (6 days) and the desorption stage (3 days).

At the end of each adsorption experiment cycle, the desorption test was completed by rinsing with deionized water with $\text{pH} = 5.0$ until the concentration of Fe/Mn in the penetration liquid drops to $0\text{ mg}\cdot\text{L}^{-1}$.

Research Method

The concentration of Fe in the solution was determined by the MR method. Fe was reduced to ferrous ion by Fe MR reagent and then reacted with 1,10-Phenanthroline to form an orange compound. The color produced by the reaction reflects the concentration of Fe in the water sample, which can be directly measured by the photometer (Palintest 8000).

The concentration of Mn in the test solution was determined by potassium permanganate spectrophotometry (National Standard of the People's Republic of China 1990), and it was calculated according to the regression equation obtained from the standard curve of the absorbance ratio of the measured sample.

Source and Treatment of Experimental Materials

Soil samples from Yimin open-pit mine will be used for isolation and screening of Fe and Mn resistant bacteria. After two months of irrigation and domestication of Fe and Mn solution, it was determined that the selected mixed bacteria in this study were: *Pseudomonas putida*, *Lysinibacillus xylanilyticus*, *Lysinibacillus macroides*, *Bacillus simplex*, and *Brevibacillus agri*. Five strains were purified and cultured in a 4°C refrigerator for cold storage. 2 mL of each pure microorganism solution was inoculated into beef extract peptone culture medium, which was cultured at constant temperature for 18hr at 30°C , and then used for the experiment after activation.

The Fe and Mn ore used in the leaching test was provided by the State Key Laboratory of Biochemistry, Institute of Process Engineering, Chinese Academy of Sciences, with a particle size of 400 mesh.

In the leaching experiment, the soil of 50 cm below the surface near the Yimin open-pit coal mine, which is not affected by Fe and Mn pollution, was selected and preserved naturally after being dried. The sample soil and quartz sand were mixed in a ratio of 2:1 to increase the porosity of the leaching test soil. The grain size of quartz sand is 100-200 mesh.

RESULTS AND DISCUSSION

Immersion Experiment

With the increase of the immersion time, the concentrations of Fe and Mn in the solution under both immersion conditions were increasing. In addition, the precipitation rate of Fe and Mn was gradually slowing down (Fig.1). Compared with the two immersion conditions, the concentrations of Fe and Mn in the blank medium solution increased faster. On the 30th day, the concentrations of Fe and Mn in the microorganism immersion solution decreased by 4% and 48.6% respectively compared with those in the blank medium. The mixed microorganism liquid can slow down the increase of Fe and Mn concentrations in simulated coal mine aquifer.

The action mechanism of Fe and Mn resistant microorganisms on Fe and Mn is basically similar, which is mainly reflected in two aspects: Fe and Mn resistant microorganisms can actively promote the enrichment of various elements in cells and generate active compounds, which have strong control on the ORP of the surrounding environment. In addition, Fe and Mn resistant microorganisms

can also produce enzymes or other specific factors to catalyze related oxidation reactions.

The pH of the two immersion solutions increased slowly with the increase of time (Fig.2a). Compared with the blank medium, the pH of immersion solutions was slightly higher. When the time reaches 23 days, the pH of the two conditions was basically the same, the average value was 9.0. The pH gradually increased from 23 to 31 days, and it remained essentially synchronized. The pH level has a significant impact on the removal of Fe and Mn. The increase or decrease of pH can reflect the influence of microorganisms on Fe and Mn (An et al. 2006). Generally speaking, the higher the pH is, the faster the oxidation speed of Fe^{2+} and Mn^{2+} , and the easier the removal of Fe and Mn. When the pH is more than 5.5 and the pH is increased by 1.0, the oxidation reaction speed of Fe^{2+} will increase by 100 times, and the oxidation reaction speed of Mn^{2+} will also increase significantly when the pH is more than 9.0 (Chen et al. 2015, Yu et al. 2004). From the viewpoint of microbiology, the isoelectric point of the microorganism is at $\text{pH} = 2 - 5$. In general, the surface charge of microorganisms living in a neutral and alkaline environment is always negatively charged, which

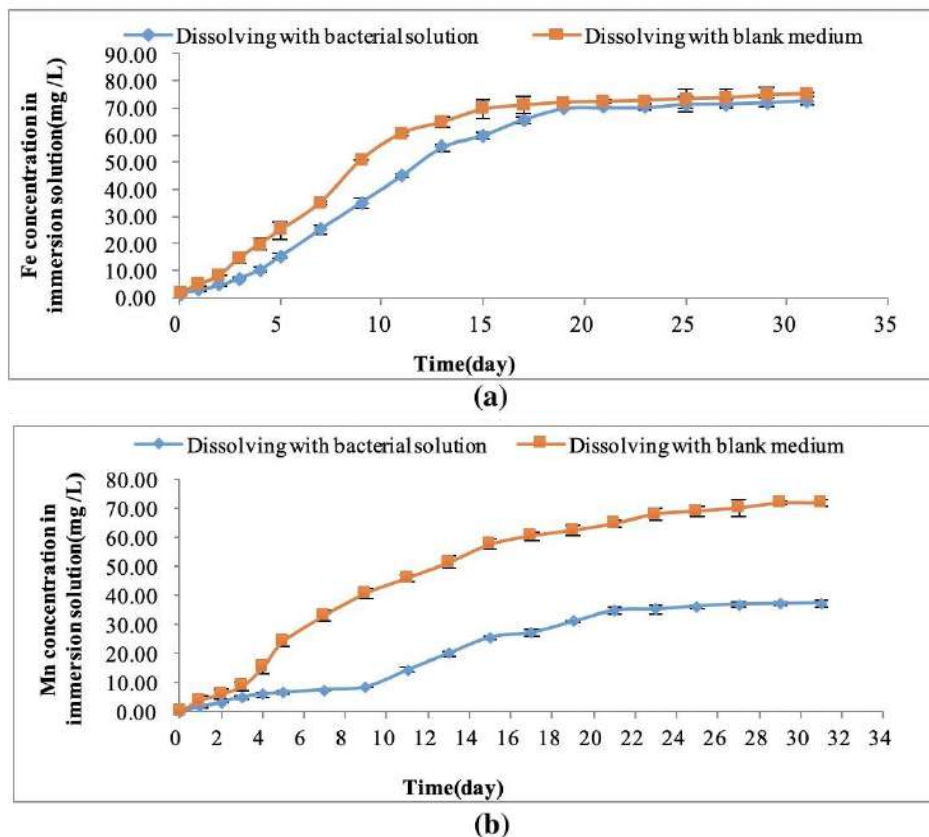


Fig. 1: Changes of Fe and Mn concentrations in immersion solution with time.

is conducive to the adsorption of cations in water, such as Fe^{2+} , Mn^{2+} , and so on. When the pH of the microorganism culture environment varies, the surface charge of the microorganisms changes as well, affecting cation absorption and reducing bacteria' ability to utilize these ions. In addition, if the pH in the environment is too high or too low, it will affect the catalytic ability of the microbial enzyme system (Kulandaivel et al. 2015). The biological enzyme can only play its maximum activity under the optimal pH condition, and the extreme pH condition will reduce the microbial enzyme activity, thus affecting the biochemical process in the biological cells, and even cause the destruction and death of the microbial cells.

ORP of immersion solution decreased slowly with the increase of time (Fig.2b). Compared with the blank medium, the ORP of the microorganism immersion solution was slightly higher. ORP of the microorganism immersion solution and the blank medium decreased to 0 mV for 21 days and 28 days, respectively. On day 31, ORP in the solution both reached the lowest. The form of Mn in nature was closely related to ORP. In the water with neutral pH, the ORP of Mn^{2+} is generally less than 400 ~ 450mv. When

looking at Mn removal from the perspective of oxidation-reduction, the objective is to maximize the ORP of the water environment to the point where Mn^{2+} can no longer exist in a stable state. The groundwater environment in the Yimin Coalfield has strong reducibility, which is very unfavorable to the oxidation reaction of Mn^{2+} , resulting in the high concentration of Mn^{2+} in water.

DO of the immersion solution decreased sharply with the increase of time (Fig.2c). DO of microbial immersion solution and blank medium immersion solution decreased to $0.03\text{mg}\cdot\text{L}^{-1}$ on the 4th and 9th day respectively, and then remained unchanged. A decrease in DO generally leads to a decrease in ORP. Because the selected bacteria were aerobic microorganisms, and the conical bottle mouth was sealed with a cotton cloth during the cultivation process, microorganisms will consume a lot of DO until it reaches the equilibrium state.

Leaching Experiment

The concentration of Fe in penetration liquid increased with the increase of penetration liquid volume (Fig. 3a). In general, compared with the soil column without microbial

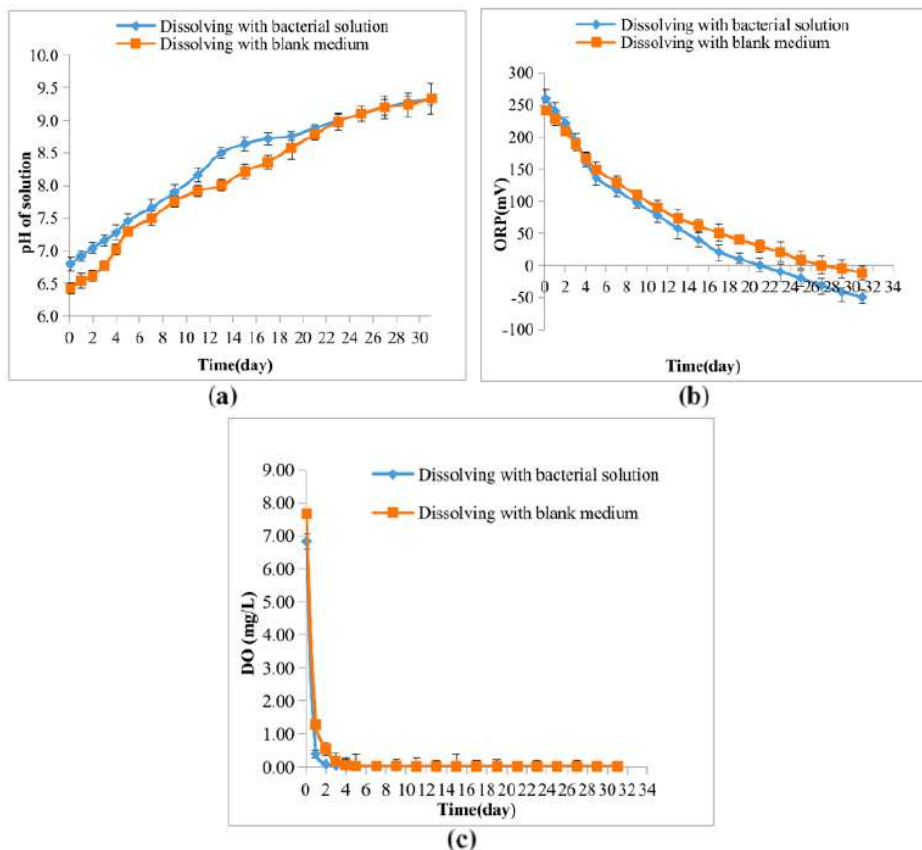


Fig. 2: Changes of pH, ORP and DO in solution with time.

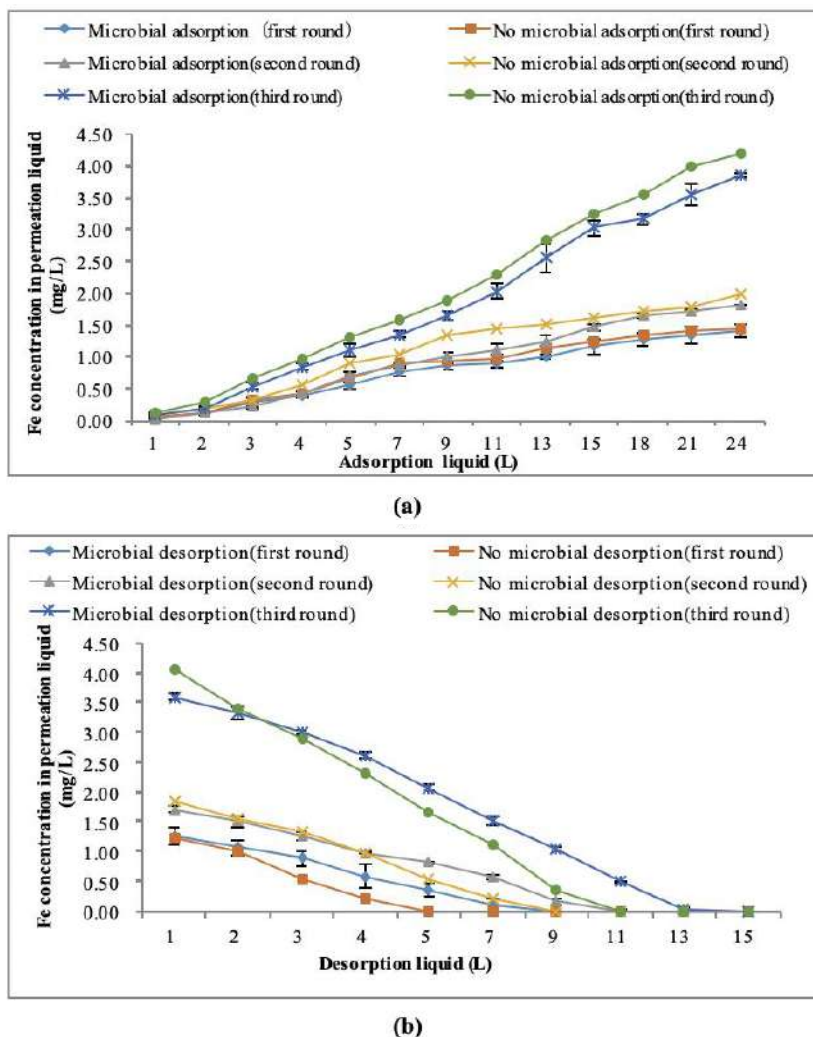


Fig. 3: Variation of Fe concentration in leaching liquid during adsorption and desorption.

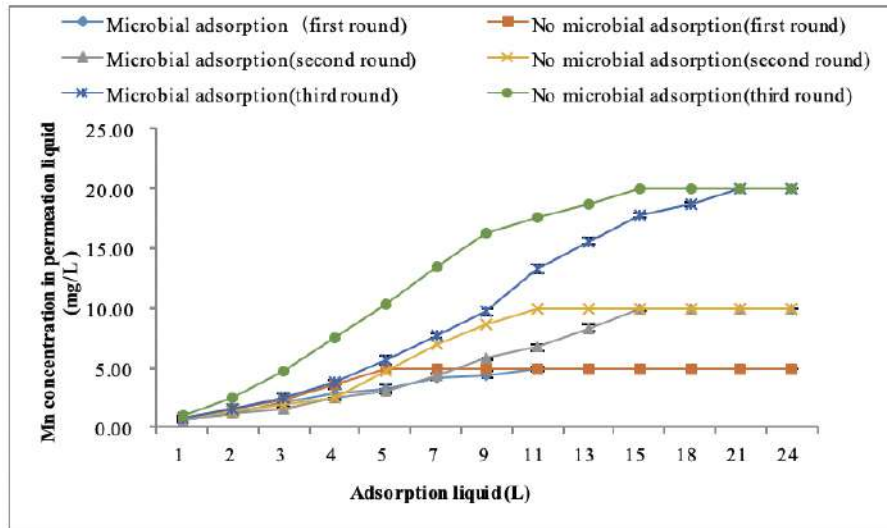
assistance, the soil column with microbial assistance has a stronger adsorption capacity for Fe and a lower concentration of Fe in the penetration liquid. In the first round of the adsorption experiment, with the help of the selected bacteria, the adsorption capacity of the soil column to Fe increased by 2.82%. In the second round of adsorption experiment, with the help of the selected bacteria, the adsorption capacity of soil column to Fe increased by 9.89%, and in the third round of adsorption experiment, with the help of the selected bacteria, the adsorption capacity of soil column to Fe increased 9.07%.

The main reason for this phenomenon was that the adsorption of heavy metal ions depends on the surface energy and local negative charge of soil particles. With the help of the selected bacteria, the adsorption of heavy metal ions in soil includes not only physical adsorption but also biological

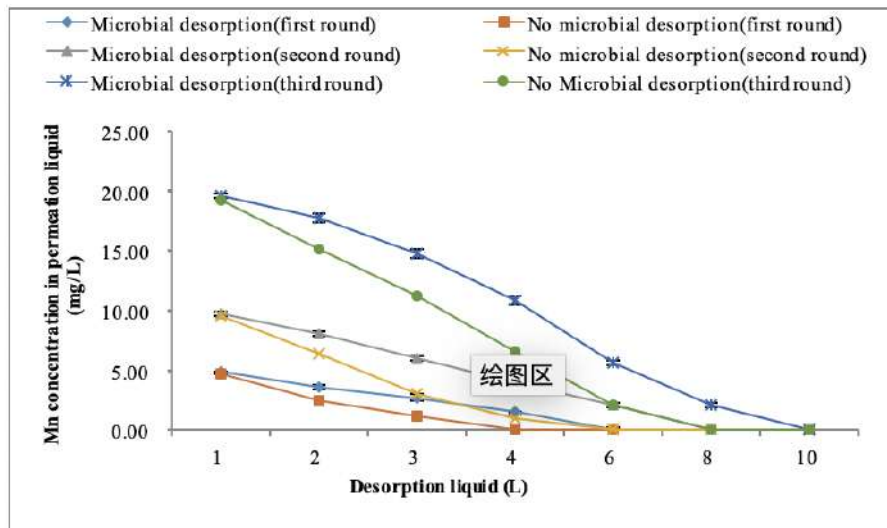
adsorption of microorganisms and adsorption of microbial metabolites.

Furthermore, the experiment revealed that reaching the saturation state of Fe adsorption in the leaching solution was difficult. The reason may be that Fe will form $\text{Fe}(\text{OH})_3$ colloid and $\text{Fe}(\text{OH})_2$ precipitate in the environment when $\text{pH} > 3.5$, and then stay in the soil. To simulate the neutral and alkaline mining system, the pH value of the leaching solution was not adjusted to an acidic environment. Therefore, Fe in the leaching solution was largely retained in the soil column during the leaching process, which also explained the phenomenon of low concentration of Fe in the penetration liquid.

The concentration of Fe in the penetration liquid decreased with the desorption process, and in this experiment, Fe adsorbed in the three-round desorption test soil column



(a)



(b)

Fig. 4: Variation of Mn concentration in leaching liquid during adsorption and desorption.

can be completely eluted into the penetration liquid (Fig. 3b). In addition, compared with the soil column assisted by microorganisms, the Fe in the soil column without the assistance of selected bacteria are more likely to be desorbed and eluted. In the first round of desorption test, in the case of selected bacteria or not, the penetrant of Fe on the soil column is 7 L and 5 L respectively. In the second round of the desorption test, the penetrant of Fe on the soil column is 11 L and 9 L respectively. In the third round of the desorption test, the penetrant of Fe on the soil column is basically eluted. The finished penetration liquid is 15L and 11 L respectively. In sum, the presence of the selected

bacteria can slow down the desorption and elution of Fe in the soil.

With the increase of the penetration liquid volume, the concentration of Mn in the penetration liquid is on the rise and can reach the adsorption saturation state (Fig. 4a). At the same time, with the assistance of the selected bacteria, the adsorption capacity of soil for Fe in penetration liquid was improved. The adsorption of Mn on the soil column without the assistance of microorganisms would reach the saturation state faster. In the first round of the adsorption experiment, under the condition of selected bacteria or not, the breakthrough liquid of saturated adsorption of Mn was 14

L and 7 L respectively. In the second round, the breakthrough liquid was 18 L and 13 L respectively. In the third round, the breakthrough liquid was 21 L and 15 L respectively (Fig. 4b). It can be seen that the selected bacteria also have a certain degree of synergistic effect on the adsorption of Mn in the leaching liquid.

In addition, three rounds of adsorption tests in this experiment have reached the adsorption saturation state, which shows that Mn in the leaching solution is more easily absorbed by the soil than Fe. Mn differs from Fe in that it is easy to form hydroxide colloid or settle in the soil. When the adsorption of Mn by the soil reached the saturation state, the concentration of Mn in the leaching liquid would not be reduced.

With the desorption process, the concentration of Mn in the penetration liquid decreased, and Mn adsorbed in the final soil column would be completely eluted into the desorption liquid. In addition, compared with the soil column assisted by microorganisms, Mn in the soil column without microbial assistance was more likely to be desorbed and eluted. In the first round of desorption test, in the case of selected bacteria or not, 8 L and 6 L of penetration liquid were basically eluted. In the second round, 10 L and 7 L of penetration liquid were basically eluted. In the third round, the finished penetration liquid was 10 L and 8 L respectively. It can be seen that the selected bacteria in the soil column slowed down the desorption rate of Mn in the soil column to a certain extent.

Compared with the desorption experiment of Fe, Mn adsorbed in soil was easier to be eluted. The reason may be that under the condition of $\text{pH} > 3.5$, Fe formed the colloid or precipitate of hydroxide easily, and Fe desorbed at the upper end of the soil column will form the hydroxide again and be detained in the process of migration to the lower end of the soil column. The adsorption of Fe on the soil column has not reached the adsorption saturation state in the adsorption process, so the desorption accompanied by the re-adsorption process was obvious. In contrast, the desorption process of Mn was easier, because Mn was more easily leached by amino acids, organic acids, and other metabolites secreted by microorganisms.

CONCLUSIONS

Through the simulation experiment, it is found that the selected bacteria (*Pseudomonas putida*, *Lysinibacillus xylanilyticus*, *Lysinibacillus macroides*, *Bacillus simplex*, *Brevibacillus agri*) has a certain degree of inhibition on the increase of Fe and Mn concentration in the Fe and Mn ore immersion liquid, and the inhibition on Mn was significantly stronger than that on Fe. The selected bacteria could improve the adsorption efficiency and capacity of free Fe and Mn in

soil, and the desorption of soil iron and manganese by water was alleviated. Therefore, free Fe and Mn in coal aquifer and soil medium could also be immobilized by mixed bacteria. The external environment was influenced by the interaction between the selected bacteria, Fe and Mn, including an increase in pH, a drop in ORP, and a decrease in DO. These external environmental factors would directly affect the dissolution and redox reaction of Fe and Mn.

To sum up, Fe, Mn, the selected mixed bacteria, and the external environment have a complex mutual response mechanism in the coal mine system. It is clear that the selected bacteria have a positive effect on the fixation of free Fe and Mn. The mineral field may be a rich source of microorganisms, which have evolved various mechanisms to resist heavy metal stress and have other metabolic potentials, which can be used for repair and other processes of biotechnological significance. Consequently, suitable growth conditions can be provided for the mixed bacteria to improve the degradation and fixation of free Fe and Mn in the mining environment. It has a lot of implications for future research on iron and manganese pollution prevention and control.

ACKNOWLEDGEMENTS

This work was supported by the National Nature Science Foundation of China under Grant 41303059 for financial support.

REFERENCES

- An, N., Fu, J. and Zhang, D., 2006. Isolation of iron and manganese removal bacteria and their oxidation performance. *Shenyang Jianzhu Univ. J. Nat. Sci.*, 22: 989-994.
- Bermudez, G.M.A., Jasan, R., Plá, R. and Pignata, M.L. 2012. Heavy metals and trace elements in atmospheric fall-out: Their relationship with topsoil and wheat element composition. *J. Hazard. Mater.*, 213-214: 447-456.
- Bhuiyan, M.A.H., Parvez, L., Islam, M.A., Dampare, S.B. and Suzuki, S. 2010. Heavy metal pollution of coal mine-affected agricultural soils in the northern part of Bangladesh. *J. Hazard. Mater.*, 173: 384-392.
- Chen, T., Chen, Z., Jin, S., Li, H., Li, G. and Liang, H. 2015. Effect of pH value on the treatment of groundwater with a high concentration of iron, manganese, and ammonia nitrogen by the filter. *Water Supply Drain. China*, 31: 5-9.
- Chen, Y., Chen, Z., Li, Z., Chen, G., Xiang, Y. and Feng, T. 2017. Research status and Prospect of remediation of manganese contaminated soil. *J. Ecol. Environ.*, 26: 1451-1456.
- Cui, S.J., Gu, L.K., Lian, Y.Y. and Li, G. 2010. Microbial remediation technology of coal mine wasteland. *Metal Mine*, 4: 182-185+188.
- Fan, C., Gao, Y., Zhang, Y., Dong, W. and Lai, M. 2018. Remediation of lead and cadmium from simulated groundwater in loess region in northwestern China using permeable reactive barrier filled with environmentally friendly mixed adsorbents. *Environ. Sci. Pollut. Res.*, 25: 1486-1496.
- Giller, K.E., Witter, E. and Mcgrath, S.P. 1998. Toxicity of heavy metals to microorganisms and microbial processes in agricultural soils: A review. *Soil Biol. Biochem.*, 30: 1389-1414.

- Guo, M.N., Yang, Z.P., Ma, J.J., Gao, J.X. and Jia, Z.B. 2014. Study on landscape ecological risk assessment of Yimin mining area. *Resour. Ind.*, 16: 83-89.
- Guo, X., Gu, J., Chen, Z.X., Gao, H., Qin, Q.J., Wei, S. and Zhang, W.J. 2012. Effects of heavy metal pollution on soil microbial community metabolism and enzyme activity in Tongchuan Coal Mine Area. *J. Appl. Ecol.*, 23: 798-806.
- Hauck, M., Paul, A. and Spribille, T. 2006. Uptake and toxicity of manganese in epiphytic cyanolichens. *Environ. Exp. Bot.*, 56: 216-224.
- Herndon, E., Brianne, Y., Hannah, F. and David, S. 2019. Iron and manganese biogeochemistry in forested coal mine spoil. *Soil Sys.*, 3: 1-19.
- Hou, D., Zhang, P., Wei, D., Zhang, J. and Luo, L. 2020. Simultaneous removal of iron and manganese from acid mine drainage by acclimated bacteria. *J. Hazard. Mater.*, 3: 122-131.
- Kováčik, J., Štěrbová, D., Babula, P., Zvec, P. and Hedbavny, J. 2014. Toxicity of naturally-contaminated manganese soil to selected crops. *J. Agric. Food Chem.*, 62: 7287-7296.
- Krishnan, K.P., Fernandes, S.O., Chandan, G.S. and Bharathi, P.A.L. 2007. Bacterial contribution to mitigation of iron and manganese in mangrove sediments. *Marine Pollut. Bull.*, 54: 1427-1433.
- Kulandaivel, S., Nagarajan, S., Priyanga, A., Saravanapandian, R. and Thangarani, A. 2015. Effect of cement dust pollution on microbial properties and alkaline phosphatase enzyme activity in the soil. *Int. J. Curr. Microbiol. Appl. Sci.*, 4: 641-649.
- Ling, W., Wu, X., Chen, Y., Liu, Q. and Guo, D. 2011. Screening of manganese removal microorganism and its characteristics. *J. Central South Univ. Forest Sci. Technol.*, 31: 152-156.
- Liu, W., Liu, S., Qin, W. and Tang, C. 2020. Pollution characteristics of surface water around the closed pit in the regional coal mining area of Guizhou Province. *J. Subtrop. Resour. Environ.*, 15: 11-19.
- National Standard of the People's Republic of China, 1990. GB 11906-1989 water quality determination of manganese potassium periodate spectrophotometric method State Bureau of technical supervision. http://english.mee.gov.cn/Resources/standards/water_environment/method_standard2/200807/t20080710_125432.shtml
- Patil, D.S., Chavan, S.M. and Oubagaranadin, J.U.K. 2016. A review of technologies for manganese removal from wastewaters. *J. Environ. Chem. Eng.*, 4: 123-129.
- Sasaki, K. 2009. Biomineralization of manganese by microorganisms and its application to environmental remediation. *Shigen-Chishitsu*, 55: 195-202.
- Shafer, M.M., Toner, B.M., Overdier, J.T., Schauer, J.J., Fakra, S.C., Hu, S., Herner, J.D. and Ayala, A. 2012. Chemical speciation of vanadium in particulate matter emitted from diesel vehicles and urban atmospheric aerosols. *Environ. Sci. Technol.*, 46: 189-195.
- Sharma, J. and Fulekar M.H. 2009. identification of potential strain *sutiauxella izardi* dsm 9397 for remediation of cadmium. *Int J Biom. Bioinform.*, 4: 16-24.
- Sorensen, M.A., Chase-Dunn, C.M. and Trumble, J.T. 2010. Chronic exposure to elevated levels of manganese and nickel is not harmful to a cosmopolitan detritivore, *Megaselia scalaris* (Diptera: Phoridae). *Insect Sci.*, 16: 73-79.
- Vazquez, M.C., Rodriguez, H.R. and Villafuerte, B.E.P. 2014. Risk: For whom? Representations of mining activity by different social actors in the Molango Manganese district of Hidalgo, Mexico. *Risk Anal.*, 34: 28-43.
- Wang, F., Liu, C., Liang, X., Wei, Z. and Li, J. 2005. Separation of iron and manganese in sediments of Aha Lake, Guizhou Province. *Environ. Sci.*, 11: 135-140.
- Wang, Z., Wang, H., Li, X., Hou, X. and Liu, L. 2012. Research progress of removing iron and manganese from groundwater. *Environ. Eng.*, 30: 48-51.
- Yu, J., Zeng, G.M., Chen, Y.H., Yao, Z.Q. and Wang, F. 2004. Experimental study on biological removal of manganese from groundwater in Dongting Lake area. *Hunan Univ. J. Nat. Sci.*, 7: 32-35.
- Zerling, L., Hanisch, C. and Sciences, S.A.O. 2008. Iron as a New Water "Pollutant" in Central Germany. *Euro-Mediterranean Information System on Know-How in the Water Sector, United Nations Convention to Combat Desertification*, pp. 1-2.
- Zhang, L., Luan, L., Wang, Y., Guan, S. and Guo, J. 2008. Analysis of ion-exchange test of underground water in Dalong Mine. *Energy Environ.*, 6: 88-89.
- Zhang, L.X., Li, Y., Li, C., Zhao, O.Y., Shi, W., Feng, S.D. and Yang, Z.X. 2017. Study on remediation of HMW-PAHs contaminated soil by *Fusarium sp.*-Starch-Alfalfa in the coal mine area. *J. Soil Water Conserv.*, 1: 350-355.
- Zhang, M.L. and Wang, H.X. 2009. Characteristics of soil heavy metal pollution around coal mine waste piles. *Environ. Sci. Inform. Appl. Technol.*, 2: 90-92.
- Zhou, C.C., Liu, G.J., Wu, S.C. and Lam, P.K.S. 2014. The environmental characteristics of usage of coal gangue in bricking-making: A case study at Huainan, China. *Chemosphere*, 95: 274-280.



Environmental Regulations, Environmental Subsidies and Enterprise Investment for Environmental Protection: Evidence from Pollution Enterprises of China

Chunwei Han

School of Accounting, Henan University of Engineering, Zhengzhou 451191, China

†Corresponding author: Chunwei Han; huehan@126.com

Nat. Env. & Poll. Tech.
Website: www.neptjournal.com

Received: 05-06-2021

Revised: 28-06-2021

Accepted: 09-07-2021

Key Words:

Environmental regulations
Environmental subsidies
Environmental protection
Pollution enterprises
Propensity matching score

ABSTRACT

Environmental protection concerns the global and long-term development of the social economy. The negative effects of production and management activities of pollution enterprises on the environment attract more and more attention from the whole society. The government is not only continuously strengthening production regulation, responsibility monitoring and establishment of rules and regulations of pollution enterprises, but also increasing supports to environmental-friendly development of pollution enterprises. To explore influences of environmental regulations and environmental subsidies on enterprise investment to environmental protection, influences of environmental subsidies under environmental regulations were discussed through the propensity matching using data of listed enterprises in China's pollution industry from 2013 to 2019. Results demonstrate that environmental subsidies promote the growth of enterprise investment to environmental protection significantly and environmental regulations are the primary influencing factor. According to heterogeneity analysis, environmental subsidies have significant positive effects on the investment in environmental protection of state-owned enterprises and private enterprises. The quantity and amplitude of investment in environmental protection of state-owned enterprises are more prominent. Environmental subsidies significantly promote investment in environmental protection of enterprises where senior executives have a technological background, but they have no significant influences on enterprises where senior executives have no technological background. Conclusions have some policy significance: government urges pollution enterprises to increase investment in environmental protection and pursue sustainable development from perspectives of incentives (increasing economic subsidies) and pressure (developing collaborative effect of environmental regulation).

INTRODUCTION

Environmental pollution has become a common problem around the whole world. As an important participant of the market economy and major releaser of pollutants, pollution enterprises shall increase investment in environmental protection and assume environmental protection responsibilities while pursuing economic development. The government of China (GOC) has promoted environmental problems to the strategic level. On one hand, GOC is regulating the pollution industry greatly and eliminating enterprises that fail to meet the industrial access conditions strictly. On the other hand, GOC provides pollution enterprises great supports for investment in environmental protection and practices in sustainable development.

In studies on environmental governance, the government is a power that cannot be ignored. According to classical documents, relevant research conclusions about the influences of government on enterprise investment in environmental protection are inconsistent. Some view government as the “hand of support”, while some view it as the “hand of

pillage”. These involve multiple aspects of reasons. Among them, support and punishment are two intervention factors that shall be considered simultaneously and the government’s preferences to policies of environmental subsidies to enterprises shall not be ignored (Bai et al. 2019, Boeing 2016). For this reason, influences of environmental subsidies on investment of pollution enterprises to environmental protection under environmental regulations were discussed from the above three factors. Moreover, a heterogeneity analysis of the ownership of enterprises and technological background of senior executives was carried out, which provided decision supports to environmental protection policies for enterprises with heavy pollutions.

PAST STUDIES AND HYPOTHESIS DEVELOPMENT

According to the environmental externality theory, the environment is a kind of special economic output that has externality and uncertainty. Due to the existence of externality, environmental pollution cost caused by the production activities of enterprises is assumed by the society rather

than enterprises. Enterprises often prefer tangible current benefits. From the perspective of sustainable development, the environmental output of enterprises involves the balance between future benefits and current benefits, and the future has some uncertainty. Due to objective existences of market failures like externality and uncertainty, enterprises neglect environmental costs to acquire short-term benefits, thus causing environmental deterioration. Hence, the government has to participate in its governance over environmental problem often integrates supports and punishment.

As compulsive environmental governance means, environmental regulations require enterprises to invest in environmental protection; otherwise, they will be punished according to laws. According to the principle of Environmental Protection Law of China that “whoever causes pollution is responsible for treatment”, pollution enterprises which are the main source of environmental pollution must assume responsibility for environmental protection and invest in environmental protection. Nevertheless, the society is difficult to get extra losses of environmental pollution from the responsible enterprises since the environment has a special externality of classical public products. Moreover, pollution governance focuses on social benefits and enterprise investment in environmental protection cannot bring short-term benefits. Therefore, enterprises are unwilling to invest in environmental protection because they pursued profits. Besides, enterprises are generally facing financing constraints of the capital market. Therefore, enterprises are passive and cooperative to environmental protection behaviors even under strict environmental regulations, so they generally have an insufficient investment in environmental protection (Xie, Z. H. et al., 2018). For this reason, GOC has arranged a lot of environmental subsidies and encouraged pollution enterprises to have an investment in environmental protection.

Generally speaking, environmental subsidies provide direct capital supply to pollution enterprises and relieve internal financing pressure. Moreover, environmental subsidies transmit the approval effect of government to the external environment, which are conducive to attracting external institutional investors (e.g. banks) and expanding financial channels for environmental protection activities in enterprises indirectly. On product market, environmental subsidies beautify images and improve the social reputation of enterprises, which are beneficial to expand market demands and improve the supply-marketing relations. In other words, environmental subsidies not only provide capital to enterprises directly or indirectly but also improve the production element environment. Therefore, environmental subsidies can stimulate the investment of enterprises in environmental protection activities and realize benign interaction between enterprise

production and economic sustainable development. Environmental subsidies also bring enterprises stronger pressures of government regulation and supervision (Li et al. 2017). Punishment information for violating environmental regulations may cause negative economic losses and reputation losses. This promotes enterprises to improve the legality of environmental behaviors by increasing investment in environmental protection, especially for those environmental-sensitive pollution enterprises sensitive (Pellegrino et al. 2012).

In a world, the government provides subsidies to enterprises and encourage them to increase investment in environmental protection. In regions with heavy environmental pollution, punitive environmental regulations and supportive environmental subsidies are often applied together (Zhang 2013). This is the called “hand of support”. Nevertheless, the “hand of pillage” cannot be neglected. This is because the government might seek renting by the right of handmade, or is manipulated by some interest groups to pursue private benefits. In this study, some competitive hypotheses were proposed:

H1a: under environmental regulations, environmental subsidies increase investment of pollution enterprises to environmental protection.

H1b: under environmental regulations, environmental subsidies decrease investment of pollution enterprises to environmental protection.

On this basis, we also noticed that many studies have discovered different influences of government on investment of enterprises to environmental protection. In this study, heterogeneous influences of ownership of enterprises and the technological background of senior executives were further analyzed.

State-owned enterprises are under the control of the government and they are the direct influencing objects of government. Compared with private enterprises, state-owned enterprises have natural relations with the government and they are easier to get more policy supports and government resources. State-owned enterprises concern more on investment in environmental protection under influence of the government (Guo et al. 2016). This is because senior executives of state-owned enterprises who are usually selected through political programs prefer to cooperate with the state to complete scientific research plans, realize the goal set by the government and avoid violation of environmental regulations when they are making strategic decisions within the tenure, thus enabling to assure their promotions. However, the high concentration of stock rights in state-owned enterprises and structural redundancy of organizations are extremely easy to cause low initiatives and efficiency in investment. Jin et

al. (2018) pointed out that the positive effects of government intervention on private enterprises become more significant. Based on the above analysis, the effects of government intervention on state-owned enterprises and private enterprises vary due to “political” advantages. Therefore, we propose the following hypotheses:

H2a: under environmental regulations, the promotion effect of environmental subsidies on investment of state-owned enterprises to environmental protection is stronger.

H2b: under environmental regulations, the promotion effect of environmental subsidies on investment of private enterprises to environmental protection is stronger.

When selecting implementing objects of policies, the government makes decisions according to some explicit signals to avoid interferences of information asymmetry. Specifically, the technological background of the senior executive team of enterprises is a key concern of government (Giannetti et al. 2015). According to the upper echelons theory, the different types of characteristics of senior executives may bring different effects. Senior executives with technological backgrounds prefer more to learn and understand the latest dynamics of the industry. During resource allocation, they may give more investments consciously to cope with constraints of environmental regulations in advance. Besides, the senior executive team with professional background and experience has a more scientific control program and estimation of risk premiums when formulating strategies for investment in environmental protection (Han 2021). Therefore, enterprises have to manifest their qualities and attitudes toward environmental protection when acquiring scarce environmental subsidies. Here, we propose the following hypothesis:

H3: under environmental regulations, environmental subsidies have positive promotion effects on enterprise investment to environmental protection where senior executives have technological background.

METHODOLOGY

Modeling

This study aims to evaluate the influences of environmental subsidies on enterprise investment in environmental protection under environmental regulations. The core of policy assessment is to answer the counterfactual problem: if the object of intervention is not intervened, are there any differences in their performances? If objects are selected completely randomly, without any bias error, the difference of investment to environmental protection between the intervened enterprises before intervention and the practically non-intervened enterprises is 0 under the counterfactual conditions. However, this is not random in reality (Bai et al.

2019, Boeing 2016). To solve sample selection bias in policy evaluation, the propensity matching method (PSM) (Rosenbaum et al. 1983) is widely applied to empirical studies.

The matching process is performed according to the following steps:

Step 1: Key influencing factors of environmental subsidies are recognized by the logit model.

$$T_i = \text{Logit}(\beta X_i + \varepsilon_i) \quad \dots(1)$$

T is a binary variable. If the enterprise i is intervened, T is 1; otherwise, T is 0. X is a vector matrix that contains a group of enterprise covariates, β is a coefficient vector, and ε is an error term.

Step 2: Estimate the probability that enterprise i is intervened, which is the tendency score of enterprise i . $P(X_i)$ can be estimated through a probability model:

$$P(X_i) = \text{Pr}(T_i = 1 | X_i) \quad \dots(2)$$

Step 3: match sample enterprises by the nearest neighbor matching method based on tendency score:

$$C(P_i) = \min \|P_i - P_j\| \quad \dots(3)$$

i and j are intervened enterprises and non-intervened enterprises. $C(P)$ represents the neighborhood relationship between i and j . When $C(P)$ is the minimum, enterprises i and j are matching mutually.

Finally, influences of government on investment of pollution enterprises to environmental protection, that is, average treatment effect (ATT), can be calculated as follows:

$$ATT = E(Y_i - Y_j | T_i = 1) = E(Y_i | T_i = 1, P(X_i)) - E(Y_j | T_j = 0, P(X_j)) \quad \dots(4)$$

y is an outcome variable, which is the investment of pollution enterprises in environmental protection in this study. Meanings of other variables and parameters are the same as above. The significantly positive ATT means that government influences investment of pollution enterprises to environmental protection significantly.

Samples and Data

In this study, A-share pollution enterprises in Shanghai Stock Exchange and Shenzhen Stock Exchange, China from 2013 to 2019 were chosen as research samples. Regional environmental regulations and economic level data came from *China Environmental Yearbook*, *China Industrial Statistical Yearbook*, and *China Statistical Yearbook*. Financial data of enterprises were collected from the CSMAR database.

To relieve influences of abnormal values, ST enterprises which are treated specially and samples with data missing of

important variables were eliminated. Finally, 782 enterprises and 5180 valid observation values were gained as the final samples. Among them, state-owned enterprises account for 52.49% and private enterprises account for 47.51%. Enterprises where senior executives have technological background account for 86.04% and enterprises where senior executives have no technological background account for 13.96%. To eliminate influences of extremums, Winsorize treatment was performed on all continuous variables on the 1% and 99% levels. All data processing used the STATA15 software.

Definition of Variables

In this study, there are three major variables, including environmental regulations, environmental subsidies, and enterprise investment in environmental protection. Definitions of these three variables are listed in Table 1.

Environmental regulations: in this study, environmental regulations are measured by the finished investment amount of industrial pollution governance per unit output in different regions (Yuan et al. 2017). Pollution governance investment reflects the degree of government's concern to the local environment and its determination in pollution control problem, and it reflects the intensity of local environmental regulations. This index indicates that given the same total industrial output, the ratio increases, and the regional environmental regulations are stronger with the increase of industrial pollution governance investment.

Environmental subsidies: annotations in the annual reports of listed companies disclose information about environmental subsidies, which are listed in details of government-subsidized projects. In this study, information was organized manually according to keywords related to environmental protection, such as green, emission reduction, environment, sustainability, cleaning, energy conservation, etc. (Bai et al. 2019, Han 2021). All amounts were added to

get the total amount of environmental subsidies. The total assets of enterprises were deflated to control scale differences among enterprises.

Enterprise investment to environmental protection: annotations in the annual report of listed enterprises disclose expenses for environmental protection, which are listed in details of the project under construction and management costs. In details of the project under construction, there are capitalization expenses for wastewater and waste gas governance, expenses for energy, water and electricity conservation, expenses for desulfurization, denitrogenation and denitrification, the expense for refuse disposal, expenses for waste heat recovery and utilization, expenses for monitoring system, etc. Details of management cost include fees for sewage charge and afforestation. These expenses which are directly related to environmental protection are added to get the total enterprise investment to environmental protection. The total assets of enterprises were deflated to control scale differences of enterprises (Xie et al. 2018, Zhang 2013).

To assure the effectiveness of the matching process between intervened enterprises and non-intervened enterprises, it is necessary to accurately estimate the probability that enterprises are intervened and adopt some relevant variables that can reflect characteristics of enterprises to strengthen the matching effect. According to existing studies, 6 variables were chosen in sample matching, including enterprise-scale, financial leverage, ownership and technological background of senior executors, regional environmental regulations as well as regional economic level.

RESULTS ANALYSIS AND DISCUSSION

Influencing Factors of Environmental Subsidies

Influencing factors of environmental subsidies to enterprises were recognized based on the logit model (Table 2). According to regression results, only the constant term fails to reach

Table 1: Definitions of variables.

Name of variables	Codes	Specifications of calculation
Investment in environmental protection	<i>Epi</i>	(investment amount to environmental protection/total assets)×100%
Environmental subsidies	<i>Efund</i>	(Received environmental subsidies of enterprises/ total assets)×100%
Regional environmental regulations	<i>Rule</i>	(Investment amount for per unit industrial pollution governance in a region)×100%
Enterprise-scale	<i>Size</i>	Ln (total assets)
Financial leverage	<i>Lev</i>	(Gross liabilities/total assets) ×100%
Ownership of enterprises	<i>State</i>	1 for state-owned enterprises and 0 for private enterprises
Technological background of senior executives	<i>Tback</i>	It values 1 if the president or general manager has technological background; otherwise, it values 0.
Regional economic level	<i>Gdp</i>	Ln (regional GDP)

the significance level of 10% and all variation coefficients are significantly 5% or higher levels. In particular, the coefficient of environmental regulations is the highest, which is 7.349 and reaches the 1% significance level. This indicates that variable setting is reasonable in this study. Generally speaking, private enterprises which have a relatively smaller asset scale, lower financial leverage, the technological background of senior executives and higher economic development level and locate in places with strict environmental regulations are more likely to get environmental subsidies.

Treatment Effects

Before estimation of propensity matching, it is necessary to have a matching balance test of pairs. It can be seen from Table 3 that after matching processing, the normalized deviations (% reduct) of variables decrease to lower than 10%. According to all t-test results, there's no significant difference between intervened enterprises and non-intervened enterprises, indicating that the selected matching covariates and matching method are appropriate. After matching of

Table 2: Influencing factors of environmental subsidies.

Variable	Whether an enterprise obtains environmental funds (=1 for yes)
Size	-0.0817*** (-5.38)
Lev	-0.7454*** (-3.82)
State	-0.3480*** (-3.77)
Tback	0.3776*** (3.55)
Rule	7.349*** (14.22)
Gdp	0.1180*** (3.73)
_cons	0.3617 (0.55)

Notes: Data in brackets are Z statistics. *, ** and *** indicate the 10%, 5% and 1% significance levels, respectively

Table 3: Balance test.

Variable	Unmatched		Mean	% reduct		t-test	
	Matched	Treated		%bias	bias	t	p> t
Size	U	22.1	22.54	-28.9		-8.46	0.000
	M	22.1	22.15	-3.3	88.7	-1.42	0.157
Lev	U	.4600	.5298	-31.2		-8.45	0.000
	M	.4600	.4479	5.4	82.6	0.67	0.546
State	U	.5055	.7008	-40.7		-10.67	0.000
	M	.5055	.5083	-0.6	98.6	-0.22	0.823
Tback	U	.8799	.8023	21.3		6.07	0.000
	M	.8799	.8666	3.7	82.8	1.61	0.107
Rule	U	.1903	.1290	72.9		19.23	0.000
	M	.1903	.1863	4.8	93.5	1.56	0.120
Gdp	U	.1823	.4703	-20.1		-6.75	0.000
	M	.1823	.2048	-1.6	92.2	-1.07	0.287

tendency scores, there's no significant difference between the intervened enterprise samples and non-intervened enterprise samples. According to equilibrium hypotheses, the estimation results of tendency score matching on this basis are credible.

After matching, ATT of intervention can be estimated by evaluating differences between intervened enterprises and non-intervened enterprises. It can be seen in Table 4 that *t*-value is 2.85 and it is significant on the 1% level. According to the significantly positive differences of investment to environmental protection, environmental subsidies facilitate enterprise investment to environmental protection significantly under fixed environmental regulations. ATT between enterprises with and without environmental subsidies is 0.2253. The investment of enterprises with environmental subsidies to environmental protection is 18.79% higher than that without environmental subsidies. Therefore, H1a is verified.

HETEROGENEITY ANALYSIS

Ownership

According to the results in Table 5, the estimated coefficient of state-owned enterprises is 5.12 and it is significant on the 1% level. The estimated coefficient of private enterprises is 1.88 and it is only significant on the 10% level. The investment of state-owned enterprises with environmental subsidies to environmental protection is 0.3978 (58.5%) higher than that without environmental subsidies and the investment of private enterprises with environmental subsidies to environmental protection is 0.2115 (14.11%) higher than that without environmental subsidies. This demonstrates that given the current environmental regulations, environmental subsidies increase investment of state-owned enterprises

and private enterprises to environmental protection significantly. In contrast, state-owned enterprises show higher significance levels, quantities and amplitudes than private enterprises, thus verifying H2a. As an important pillar of the national economy, the state-owned enterprises become the representatives of the state's willingness to green development due to their political connection with the government. These factors facilitate state-owned enterprises to increase investment in environmental protection. Without political advantages, private enterprises face greater pressures of market competition and financing constraints and they must invest more human resources and capital in market profits. Besides, private enterprises are more passive in investment in environmental protection, and are difficult to increase investments in environmental protection, without touching the bottom line of environmental regulations.

Technological backgrounds of senior executives

It can be seen from Table 6 that when senior executives have the technological background, investment of enterprises with environmental subsidies to environmental protection is 0.4937 (50.13%) higher than that of enterprises without environmental subsidies and the estimated coefficient is 6.85, which is significant on the 1% level. When senior executives have no technological background, investment of enterprises with environmental subsidies to environmental protection is 0.2245 (31.15%) higher than that of enterprises without environmental subsidies and the estimated coefficient is 1.59, which doesn't reach the significance level of 10%. This indicates that enterprises, where senior executives have technological backgrounds, have stronger tendencies to invest in environmental protection and they are more willing to improve environmental governance levels and even exceed requirements of environmental regulations by

Table 4: ATT of environmental subsidies on investment in environmental protection.

Variable	Sample	Treated	Controls	Difference	S.E.	T-stat
Efund	Unmatched	1.424	.9531	.4718	.0664	7.10
	ATT	1.424	1.199	.2253	.0790	2.85***

Notes: *, ** and *** indicate significance levels of 10%, 5% and 1%, respectively.

Table 5: Enterprise grouping based on ownership.

	Sample	Treated	Controls	Difference	S.E.	<i>t</i> -stat
State-owned enterprises	Unmatched	1.077	.9338	.1440	.0896	1.61
	ATT	1.077	.6800	.3978	.0777	5.12***
Private enterprises	Unmatched	1.710	1.458	.2521	.1254	2.01
	ATT	1.710	1.499	.2115	.1128	1.88*

Notes: *, ** and *** indicate significance levels of 10%, 5% and 1%, respectively.

Table 6: Enterprise grouping according to the technological background of senior executives.

	Sample	Treated	Controls	Difference	S.E.	t-stat
Senior executives	Unmatched	1.478	1.403	.0745	.0874	0.85
has technological background	ATT	1.478	.9847	.4937	.0721	6.85***
Senior executives	Unmatched	.9451	.7025	.2426	.1798	1.35
has no technological background	ATT	.9451	.7205	.2245	.1408	1.59

Notes: *, ** and *** indicate significance levels of 10%, 5% and 1%, respectively.

taking advantage of their professional after getting environmental subsidies, thus enabling to avoid reputation loss and economic cost for violating environmental regulations. As a result, it is very necessary to distinguish whether senior executives have technological backgrounds or not to discuss environmental subsidies. Hence, H3 is verified.

CONCLUSIONS

To address the heavy environmental pollution problems, the government not only implements strict environmental regulations but also increases environmental subsidies to enterprises. Based on data of pollution enterprises in the capital market from 2013 to 2019, the influences of the government's environmental subsidies on enterprise investment to environmental protection under environmental regulations were discussed by PSM. Moreover, heterogeneity influences of ownership of enterprises and technological background of senior executives were analyzed. Conclusions could be drawn:

1. Asset scale, liability level, ownership, the technological background of senior executives and environmental regulations and economic levels of local areas of enterprises are key factors that influence pollution enterprises to get environmental subsidies. Among them, environmental regulations show the maximum degree of influence.
2. Environmental subsidies stimulate pollution enterprises to increase investment in environmental protection significantly. The investment of enterprises with environmental subsidies to environmental protection is 0.2253 (18.79%) higher than that without environmental subsidies.
3. Environmental subsidies increase investments of both state-owned enterprises and private enterprises to environmental protection significantly. In particular, the quantity and growth of investment of state-owned enterprises to environmental protection are more prominent.
4. Environmental subsidies significantly facilitate enterprises where senior executives have the technological background to increase investment in environmental protection. However, environmental subsidies show no

significant impacts on enterprises where senior executives have no technological background.

Concerning policy enlightenments, the empirical evidence in this study can provide the following references to relevant government sectors and enterprises:

To stimulate pollution enterprises to increase investment in environmental protection effectively, the government shall continue to implement strict environmental regulations, strengthen deterrence by punishment and approval of industrial access, completely eradicate the fluke mind of enterprises, and adopt emergency environmental governing to cope with environmental supervision of the government. On one hand, the government also shall continue to increase environmental subsidies to pollution enterprises and offset environmental protecting and financing gaps of enterprises. On the other hand, the government shall establish diversified social financing mechanisms and relieve excessive dependence on government resources. During implementation and environmental protection funding policies, government shall generally make full use of collaborative effects of relevant laws and subsidies enterprise investment to environmental protection.

Pollution enterprises shall focus on long-term development and envisage the social-economic effect of improving environmental protection performances. Given high concerns of the government to strict environmental regulations, pollution enterprises shall increase investment to reconstruction of environmental protection technologies and equipment from the production source, adopt clean production modes, decrease pollutant discharges, get supports of government and approval of all involved social stakeholders, and avoid punishment for violating environmental regulations.

It has to point out that increasing investment of pollution enterprises to environmental protection is just one aspect to measure environmental performances and it is only a requirement rather than a sufficient condition to evaluate the validity of environmental subsidy policies. The government also shall concern whether the output index of enterprises is improved to some extent after investment in environmental protection. The external compulsive effect of environmental protection regulations also has limitations. In a word, the

government shall establish a scientific performance evaluation system of environmental protection capital policy, including early investment evaluation, late economic benefit evaluation, social benefit evaluation, and environmental benefit evaluation. Moreover, the government shall not only design a reasonable and comprehensive analysis and evaluation system, but also set up a reasonable and effective policy support model for different types of enterprises, and develop the collaborative effect of policies to the maximum extent.

ACKNOWLEDGMENT

This study was supported by the Soft Science Project of Henan Province in China (No. 182400410659), the Doctoral Foundation Project of Henan University of Engineering (No. D2017027), and the General Project of Humanities and Social Sciences Research for Universities and Colleges in Henan Province (No. 2022-ZDJH-00272).

REFERENCES

- Bai, Y., Song, S., Jiao, J. and Yang, R. 2019. The impacts of government R&D subsidies on green innovation: Evidence from Chinese energy-intensive firms. *Journal of Cleaner Production*, (233): 819-829.
- Boeing, P. 2016. The allocation and effectiveness of China's R&D subsidies: Evidence from listed firms. *Research Policy*, 45(9): 1774-1789.
- Giannetti, M., Liao, G. and Yu, X. 2015. The brain gain of corporate boards: Evidence from China. *Journal of Finance*, 70(4): 1629-1682.
- Guo, D., Guo, Y. and Jiang, K. 2016. Government-subsidized R&D and firm innovation: Evidence from China. *Research Policy*, 45(6): 1129-1144.
- Han, C. W. 2021. Impact of environmental subsidies on environmental technology innovation of polluting enterprises. *Nature Environment and Pollution Technology*, 20(3): 1277-1284.
- Jin, Z. J., Shang, Y. and Xu, J. 2018. The impact of government subsidies on private R&D and firm performance: Does ownership matter in China's manufacturing industry? *Sustainability*, 10(7): 2205.
- Li, D., Zheng, M., Cao, C., Chen, X., Ren, S. and Huang, M. 2017. The impact of legitimacy pressure and corporate profitability on green innovation: Evidence from China top 100. *Journal of Cleaner Production*, (141): 41-49.
- Pellegrino, C. and Lodhia, S. 2012. Climate change accounting and the Australian mining industry: Exploring the links between corporate disclosure and the generation of legitimacy. *Journal of Cleaner Production*, (36): 68-82.
- Rosenbaum, P. R. and Rubin, D. B. 1983. The central role of the propensity score in observational studies for causal effects. *Biometrika*, 70(1): 41-55.
- Xie, Z. H., Sun, Y. X. and Wang, Y. 2018. The influence of environmental regulation on corporate environmental investment of companies: A panel data study based on heavy pollution industry. *Journal of Arid Land Resources and Environment*, (3):12-16.
- Yuan, L. J. and Zheng, X. F. 2017. Coupling induction of environmental regulation and government subsidy on enterprise technological innovation. *Resources Science* (5): 911-923.
- Zhang, G. F. 2013. Government intervention, environmental pollution and corporate environmental protection investment: Evidence from listed companies of heavy pollution industries. *Research on Economics and Management*, (9): 38-44.



Low-Cost IoT Enabled Embedded System for Measurement of Environmental Pollutants

C. Mani Kumar*†, Shahid Ali*, P. Sri Lakshmi*, G. Raja Kullayappa* and K. Tanveer Alam**

*Department of Electronics and Physics, GITAM (Deemed to be University), Visakhapatnam-530045, Andhra Pradesh, India

** Department of Electronics and Communication, Rayalaseema University, Kurnool-518007, Andhra Pradesh, India

†Corresponding author: C. Mani Kumar; mani.k.ele@gmail.com

Nat. Env. & Poll. Tech.

Website: www.neptjournal.com

Received: 12-01-2021

Revised: 12-02-2021

Accepted: 22-02-2021

Key Words:

ARM controller
CO₂ sensor
O₃ sensor
Wireless system
Embedded C

ABSTRACT

In today's world, with ever-changing pollutants and their concentrations, the designing of low-cost meteorological systems is unavoidable for assessing environmental parameters. Wireless instrumentation is an effective way of measuring the physical quantities as it can measure and transmit the data to the targeted location at high speed. In the present work, an IoT-enabled embedded system was developed to measure the concentration of carbon dioxide, ozone, and the presence of smoke. The ARM microcontroller reads the sensor data and processes the information to calculate the pollutant parameters. The measured data is displayed on the LCD, mobile phone, and a computer simultaneously using wireless technology. With Embedded C, the Keil compiler was used to develop the interfacing software for the designed system. Portability, user-friendliness, and reliability are the significant advantages of the device compared with the conventional systems, and it can be widely used as an inexpensive solution for the monitoring of environmental conditions.

INTRODUCTION

Air pollution is a significant threat to human life, which harms the environment, and it is evident in the health of humans as well as the other creatures of this world. Air pollution has become a primary concern for both the developed and developing countries in the world, and it affects the environmental condition every day. One of the leading causes of premature deaths and diseases is the increased levels of different air pollutants in the atmosphere, and as per WHO, almost 8 million premature deaths per annum are recorded worldwide (Xue et al. 2020). Long-term exposure to polluted air can have permanent health effects such as respiratory illness, asthma, heart and lung problems (Flavio et al. 2012). The high concentrations of air pollutants in the air have had negative effects on our daily lives and the global ecology, resulting in changes in climate extremes as well (Wenxia et al. 2020). The increasing use of automobiles and waste emitted by industries are the primary causes of pollution. The continuous burning of fuels in power plants and industries at different places produces hazardous pollutants such as CO₂ and dust particles. The existence of unwanted particles in abnormal quantities causes air pollution and causes health complications (Hanna et al. 2010). There is an inevitable need to control this situation; for this, it is needed

to detect and measure the quantities of these air pollutants continuously (Chun et al. 2016). Conventional techniques, which necessitate a great deal of human effort, are extremely expensive. Designing a cost-effective pollutant monitoring mobile system with different sensors and embedded controllers becomes crucial. The sensors measure the concentration of pollutant gases with high accuracy and the measured values can be shared using IoT-enabled devices. The system can be used to let people know about the increased levels of pollutant gases so that all the necessary steps can be taken to decrease the effects in the future.

Carbon dioxide (CO₂) is an odorless gas produced by burning carbon and different organic compounds. It is one of the most abundant gases in the environment: a colorless, odorless, and non-flammable gas. Carbon dioxide typically enters the body through inhalation. High concentration levels of carbon dioxide (CO₂) may cause different health issues in humans such as incapacitation and unconsciousness. The ozone gas in the troposphere is a very harmful pollutant, and breathing O₃ above 120 ppb can affect lungs, chest pain, and cause coughing, throat infections, and many other severe problems in human beings. The 8 hours' exposure limit of ozone gas is 50 ppb on average as per the guidelines suggested by the WHO (Zhang et al. 2019).

The introduction of the IoT-based pollution measurement system can produce substantial changes in the environmental monitoring systems. The wireless systems can be used in hostile conditions since they are durable enough to survive them (Jayavardhana et al. 2013). Embedded systems are inexpensive to maintain and are proven to be reliable over a long period of time. Apart from the sensors and the control circuitry, the use of sophisticated software development tools creates a user-friendly gadget to achieve the task of environmental monitoring.

The present paper deals with the sensors and their integration for tracking the concentration of carbon dioxide, ozone, and the presence of smoke.

MATERIALS AND METHODS

Instrumentation

The block diagram for the developed gadget can be viewed in Fig. 1. The system was built around the controller LPC 2148 (Barkunan et al. 2019). It is an ARM-based controller with a

32 bit ALU. The microcontroller from NXP semiconductor possesses a vast amount of resources for building an effective embedded system. The availability of different protocols and a couple of 14-channel ADCs makes it perfectly suitable for handling numerous sensors simultaneously. The processor is built to withstand a wide range of temperatures from -40°C to $+85^{\circ}\text{C}$; hence it can be used in domestic as well as industrial applications. The 60 MHz clock, RAM of 40 kilobytes, and the Flash memory of 512 kB assures that the system developed with the processor has enough memory to store and run the program with good speed. It is also enriched with serial communication terminals such as USB, UART, I2C, SPI, and SSP. The watchdog timer takes care in case of erroneous conditions without any human intervention (Seyyed et al. 2018).

Interfacing of Carbon Dioxide Sensor

The MHZ-19B sensor is used to detect carbon dioxide gas concentration using the non-dispersive infrared (NDIR) principle to sense the existence of CO_2 gas in the air. It

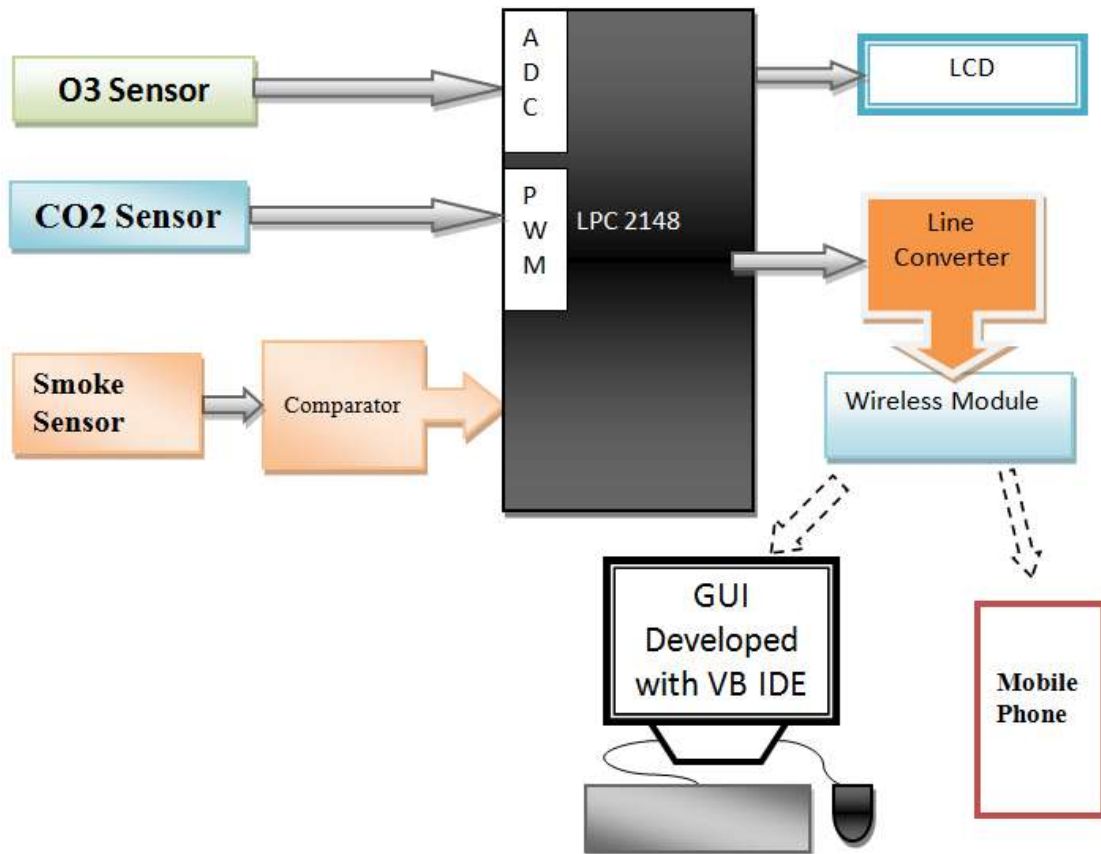


Fig. 1: Block diagram of the designed system.

delivers two digital outputs in the form of UART and PWM output, and it also produces output in analog. The sensor measures the CO₂ ranging from 0 to 5000 parts per million with good stability and non-oxygen dependency (Shahid et al. 2020). The sensor can operate in the temperature range of 0-50°C and the humidity range of 0-90%. The sensor's preheating time is 180 seconds only, which is very less compared to other CO₂ sensors. The NDIR gas sensor is more technically advanced as it has long-term stability, high accuracy, and high selectivity in an open-air environment (Martín-Garín et al. 2018, JongSeon et al. 2010). In the NDIR principle, an infrared beam is passed through the gas to detect the gas concentration. The gas concentration is calculated by measuring the amount of absorbed infrared radiation using the IR receiver at the required frequency. In the present work, the measured analog output is taken from the sensor given to the inbuilt ADC available in the microcontroller to convert the analog output from the sensor into digital form.

Interfacing of Ozone Sensor

The concentration of ozone is tracked by using a MICS-2614 sensor (Nagendra et al. 2019). It is a Metal Oxide Sensor (MOS) with a detection range between 10 ppb (parts per billion) – 1000ppb. MOS-type sensors are often used in the gas sensing field because of their small size, low cost, and high production abilities. In a MOS-type sensor, the sensing material is printed on the sensing element, with the heater created on the reverse side. When the sensing material is in clean air, the free electrons generated by the heating moves freely, and in the presence of ozone gas, the sensor resistance decreases. In this way, the MOS-type gas sensor detects the concentration levels of ozone gas O₃. The voltage from the MICS-2614 sensor connected to the inbuilt ADC of the microcontroller is directly proportional to the ozone concentration in the air.

Interfacing of Smoke Sensor

The MQ-2 sensor is based on the electrochemical variable resistance concept, which is used in smoke detection (Borah et al. 2018). This sensor is highly sensitive to smoke. It is interfaced to the microcontroller through a digital pin using a comparator. The comparator is designed by using an LM358 operational amplifier. When the detected smoke exceeds the threshold point, the comparator sends a signal to the microcontroller's digital pin, triggering an alert in the event of a probable catastrophe. The sensor is also sensitive to consumable gas so that it can be employed to detect gas leakage in a household. The sensing range of the sensor is 300 ppm to 10000ppm.

Wireless System

The detected values can be locally displayed, but most of the time, they need to be accessed in remote locations rather than only showing them on the local device. For remote access, a wired connection can be provided, however, there are some constraints like expensive hardware, installation, and re-configuration. A wireless connection is established to eliminate these constraints by using the microchip ESP8266 (Amir et al. 2018). It follows the IEEE802.11 protocol standard for Wireless Fidelity (Wi-Fi) implementation and is available in many economic modules such as ESP01 and ESP32. The 8-pin ESP01 module works with a power supply of +3.3V, is user-friendly as it can be easily connected and replaced to the system through the socket inserted in the system. The ESP-01 is enriched with antenna diversity, gives a reliable and qualitative link between the transmitter and receiver wirelessly. It also possesses security protocols such as WPA/WPA-II, and data collected from the system is sent to a computer and mobile phone. The detailed schematic diagram of the integrated system is as shown in Fig. 2.

Software Implementation

The software development for the system involves two steps. Primarily, the system needs to collect information from the sensors. Further, the data collected is to be displayed on a Graphical User Interface (GUI) environment. For these, we need the help of a couple of software tools. The sensor interfacing software is developed by Embedded C programming language using Keil Compiler. The sensor readings are continuously collected, and the values are calculated by Embedded C coding and the results are visualized in a liquid crystal display present in the system. Apart from this, the data sent through the wireless network is displayed in a user-friendly environment using the Visual Basic Integrated Development Environment (Ling & Wong 2017). Then, the computer/mobile connected to the Internet, and the measured values can be accessed from wherever the Internet is available. The flowchart of the program is shown in Fig. 3. The parameters displayed on LCD and GUI output on the mobile phone and computer are shown in Fig. 4.

RESULTS AND DISCUSSION

An ARM-based pollutant monitoring mobile system is designed and developed to measure the atmospheric pollutants under different environmental conditions. The system was placed in an industrial area (Port Area) and a heavy traffic area (Dwaraka Nagar) in Visakhapatnam, India, in different seasons during the working hours as depicted in Fig. 5. The port area is an industrial area where a high concentration of

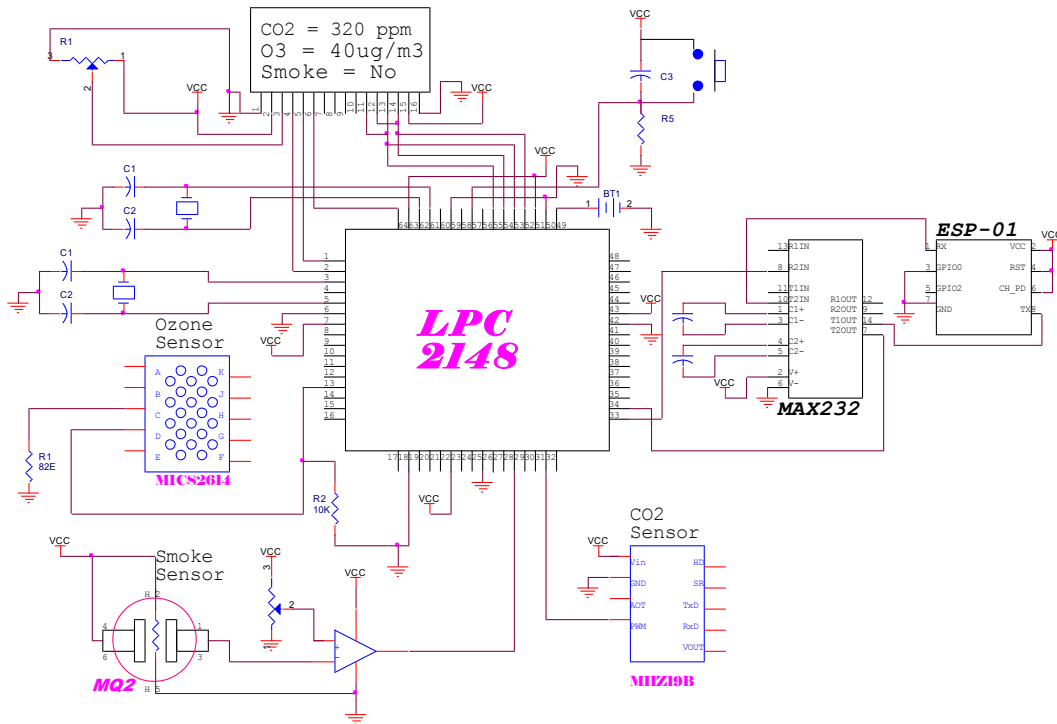


Fig. 2: Hardware schematic diagram.

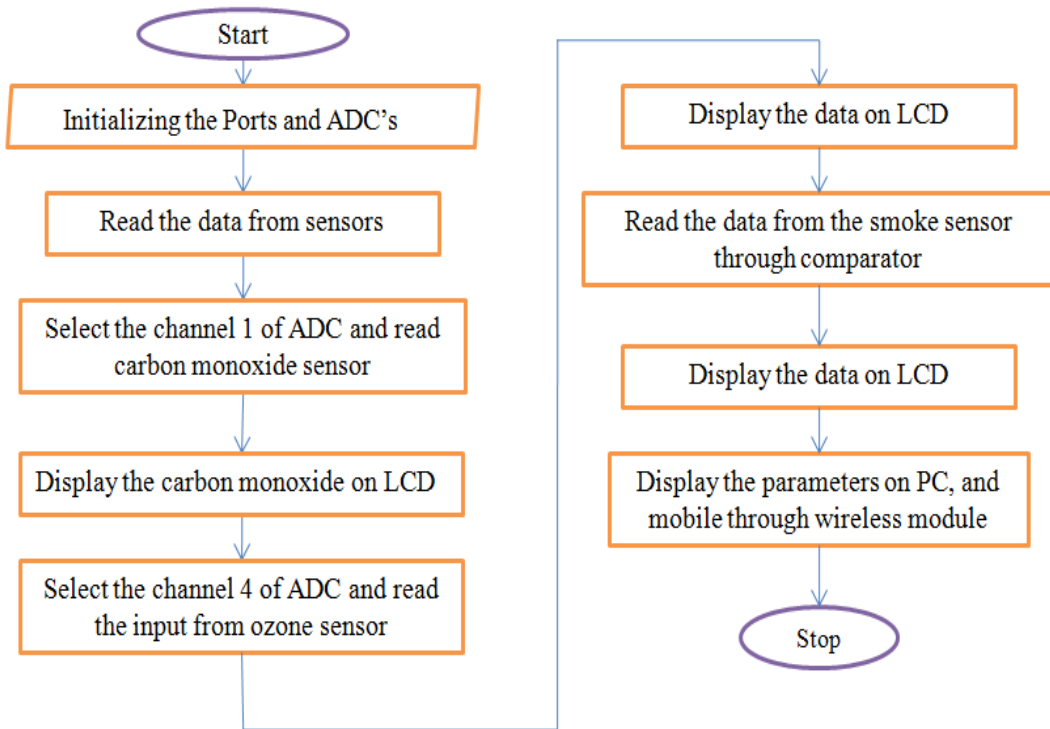


Fig. 3: Flowchart.

pollutants is found due to the different activities performed. Dwaraka Nagar is one of the highest traffic areas in the city where the roads are always full of heavy vehicles such as city buses and lorries.

The values are recorded for these areas on different days during the three seasons. The measured data is in good agreement when compared with the values provided by the Andhra Pradesh Pollution Control Board, Visakhapatnam, India (APPCB). The recorded values plotted with the error bars are as depicted in Fig. 6 and Fig. 7. In summer, the

system was taken to the port area to measure CO₂ and O₃ values during the daytime and the concentration of CO₂ was observed to be high during the afternoon time between noon and 2.00 pm. It was found that different fuels are burned at the port area during this period, and smoke from the industries is emitted, which is the primary cause of higher values being recorded. The concentration of O₃ was tracked high in the summer season compared to the other two seasons as the Sun rays play a major role in the formation of O₃. Ozone being a secondary pollutant is not emitted directly



Fig. 4: Pictorial view of the designed system.



(a)



(b)

Fig. 5: System placed at (a) Port Area and (b) Dwaraka Nagar.

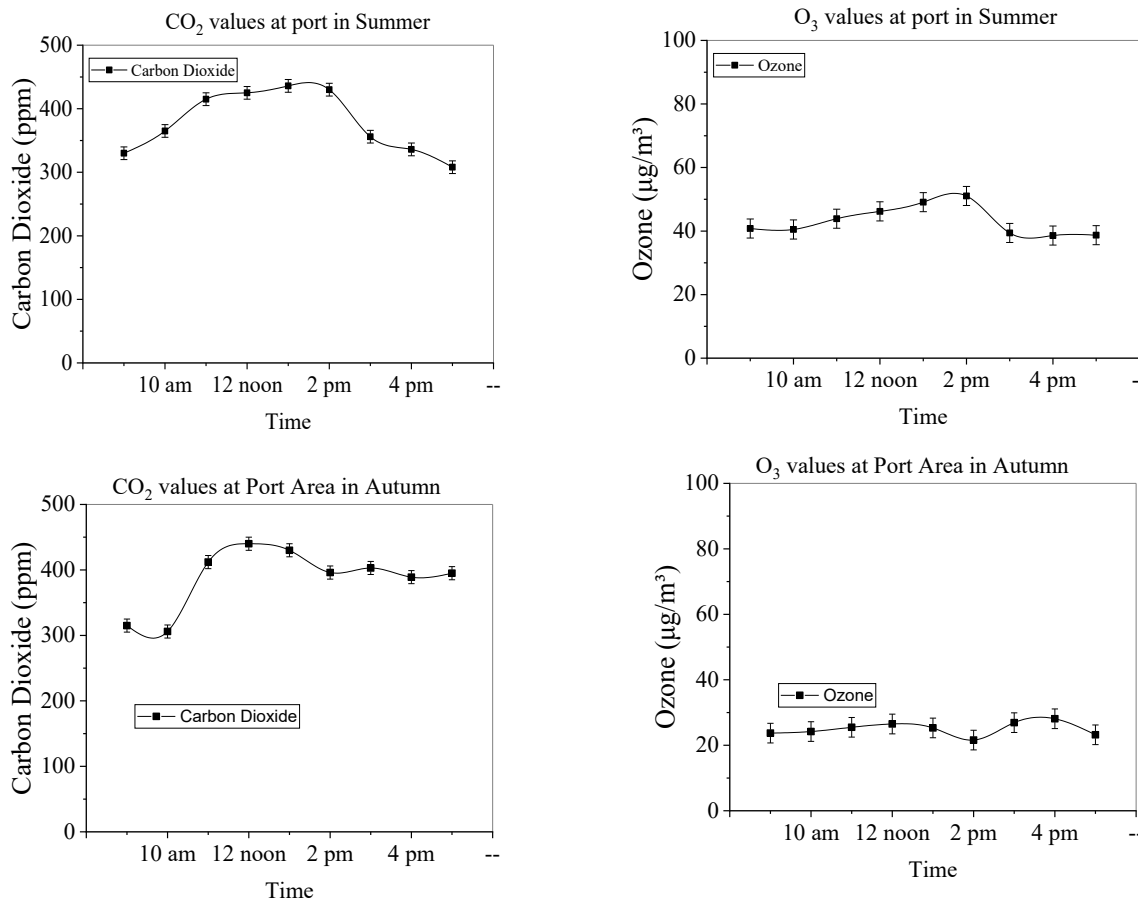


Fig. 6: Values recorded at Port area at different seasons.

by industrial activities or traffic. It is formed by the reaction between ozone precursors such as nitrogen oxides (NO_x) and VOCs under warm sunlight or solar radiation. Hence during the summer, the concentration of ozone measured was high. The developed system was then taken to the Dwaraka Nagar area of the city during the summer season, which is a heavy traffic area of the city. The concentration of CO₂ measured was around 430 ppm, and the concentration of ozone was recorded around 51.05 µg.m⁻³, which is the highest value recorded at 2.00 pm. Owing to the heavy traffic in this area, the concentration of CO₂ and O₃ measured was high during the daytime.

Further, in autumn, CO₂ and O₃ concentrations were measured at both the port and Dwaraka Nagar areas for the same duration. The prototype was first used to measure the pollutants at the port area, where the concentration of CO₂ was found to be high during the afternoon time. The maximum value of CO₂ was at noon as 440 ppm. The concentration of O₃ measured was around 28.2 µg.m⁻³, which was found comparatively less than in the summer season. The

system was then taken to Dwaraka Nagar, where the values were found to be nearly equivalent to those of the summer season in the area, which was plotted in the graph. The maximum concentration of CO₂ was tracked as 428 ppm, and the maximum concentration of O₃ measured was 25.5 µg.m⁻³.

The concentrations of CO₂ and O₃ in the port area measured less during the winter season than during the other two seasons. The maximum concentration of CO₂ measured was 335 ppm, whereas the maximum concentration of O₃ was 22.02 µg.m⁻³. The concentration of ozone is less compared to the summer and autumn seasons, which is also shown in previous studies (Khoder et al. 2009). The designed system was then taken to the Dwaraka Nagar area. In winter, the concentrations of CO₂ and O₃ were observed to be lower in this area. The concentration of CO₂ in this area was found to be high during peak hours of 9.00 a.m. to 11.00 a.m. and 4.00 p.m. to 5.00 p.m., which is primarily attributable to vehicle exhaust gas during high traffic. The maximum value of the CO₂ measure was 340 ppm, and the concentration of O₃ was around 22.59 µg.m⁻³.

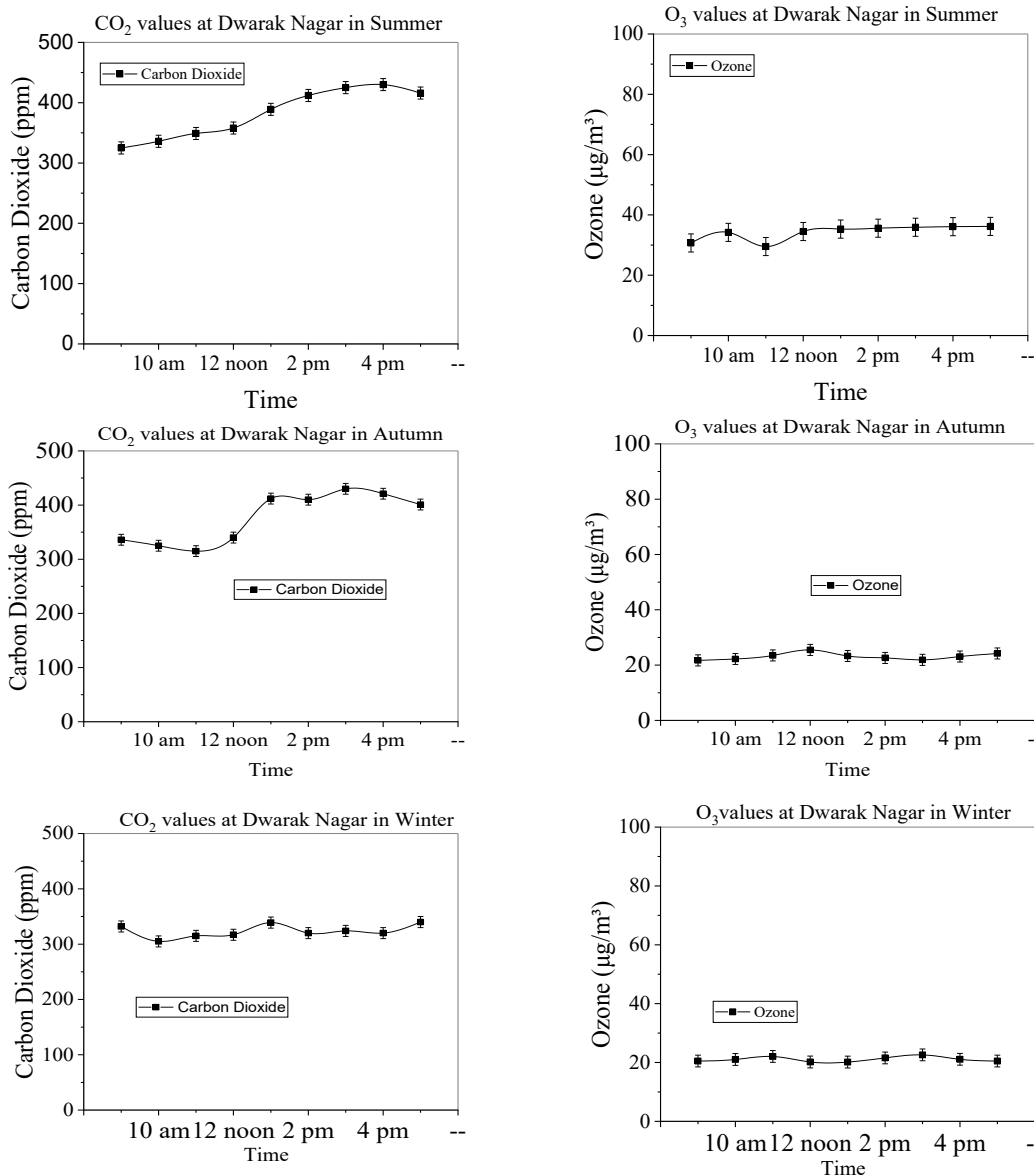


Fig. 7: Values recorded at Dwaraka Nagar in different seasons.

CONCLUSION

An IoT-enabled environmental monitoring device was designed and developed to measure the concentration of pollutant gases under different environmental conditions. The results were in good agreement when compared with the standard values of the pollution control board. The system is equipped with wireless connectivity for incessantly collecting and storing the results. The developed economical device with in-system programmability and low maintenance provides access to a remote location using IoT technology.

REFERENCES

Amir, M.R., Tuan, N.G., Behailu, N., Arman, A., Iman, A., Mingzhe, J. and Pasi, L. 2018. Exploiting smart e-Health gateways at the edge of healthcare Internet-of-Things: A fog computing approach. *Future Gener. Comput. Syst.*, 78: 641-658.

Barkunan, S.R., Bhanumathi, V. and Sethuram, J. 2019. Smart sensor for an automatic drip irrigation system for paddy cultivation. *Comput. Electr. Eng.*, 73: 180-193.

Borah, A., Jangid, S., Kumari, A., Gehlot, A. and Singh, R. 2018. Pollution control by the installation of mq-smoke sensors in car exhausts with IOT-based monitoring. *Intell. Comm. Control Devices*, 624: 1191-1197.

Chun, S.L., Huan, L., Ke, B.H. and Yong, L.M. 2016. Assessment of regional air quality by a concentration-dependent pollution permeation index. *Sci. Reports*, 34891: 1-9.

- Flavio, M.V., Susana, L.D.P. and Marcelo, A.S. 2010. Analysis of the global warming dynamics from temperature time series. *Ecolog. Model.*, 221(16): 1964-1978.
- Hanna, Z., David, Q., Cristian, S., Karin, V., Stefanie, U., Norman, S., Stefanie, M., David, A.G. and Michael, F.S. 2010. Air pollution research: visualization of research activity using density-equalizing mapping and scientometric benchmarking procedures. *J. Occup. Med. Toxicol.*, 5(5): 1-9.
- Jayavardhana, G., Rajkumar, B., Slaven, M. and Marimuthu, P. 2013. Internet of Things (IoT): A vision, architectural elements, and future directions. *Future Gener. Comput. Syst.*, 29(7): 1645-1660.
- JongSeon, P., HeeChan, C. and SeungHwan, Y. 2010. NDIR CO₂ gas sensor with improved temperature compensation. *Procedia Eng.*, 5: 303-306.
- Khoder, M.I. 2009. Diurnal, seasonal, and weekdays-weekends variations of ground-level ozone concentrations in an urban area in greater Cairo. *Environ. Monit. Assess.*, 149: 349-362.
- Ling, T.H.Y. and Wong, L.J. 2017. Elderly Infrared Body Temperature Telemonitoring System with XBee Wireless Protocol. *Intell. Comm. Control Devices*, 22: 103-120.
- Martín-Garín, A., Millán-García, J. A., Bañri, A., Millán-Medel, J. and Sala-Lizarraga, J.M. 2018. Environmental monitoring system based on an open source platform and the Internet of Things for a building energy retrofit. *Automat. Constr.*, 87: 201-214.
- Nagendra, S.M.S., Reddy, Y.P., Narayana, M.V., Khadirnaikar, S. and Rani, P. 2019. Mobile monitoring of air pollution using low-cost sensors to visualize the spatio-temporal variation of pollutants at urban hotspots. *Sust. Citi. Soci.*, 44: 520-535.
- Seyyed, A.A., Mohammadreza, B.M. and Amir, M.R. 2018. Enhancing transient fault tolerance in embedded systems through an OS task-level redundancy approach. *Future Gener Comput Syst.*, 87: 58-65.
- Shahid, A., Kumar, C.M., Kullayappa, G.R. and Saritha, V. 2020. Development of cost-effective measurement system for outdoor and indoor environment parameters using IoT Technology. *Solid State Technol.*, 64(5): 8503-8520.
- Wenxia, Z. and Tianjun, Z. 2020. Increasing impacts from extreme precipitation on population over China with global warming. *Sci. Bull.*, 65(3): 243-252.
- Xue, Y., Chu, J., Li, Y. and Kong, X. 2020. The influence of air pollution on respiratory microbiome: A link to respiratory disease, *Toxicol. Lett.*, 334: 14-20.
- Zhang, D., Zhimin, Y., Peng, L. and Xiaoyan, Z. 2019. Ozone gas sensing properties of metal-organic frameworks-derived In₂O₃ hollow microtubes decorated with ZnO nanoparticles. *Sensors Actuat. B-Chem.*, 7(46): 1-17.



Correspondence Between Technology Options Available for Chemical Industries and the Levels of the Waste Management Hierarchy: A Case Study Approach

S. M. D'Sa*†, D. Patnaik*, V. Acham** and S. Jadhao**

*Department of Economics and Management, Birla Institute of Technology and Science, Pilani, K. K. Birla Goa Campus, Zuarinagar, Sancoale, Goa-403726, India

**Prochem Innovatives, N2 - 408, River Residency Phase 3, Chikhali, Pune-411062, India

†Corresponding Author: Sandra D'Sa; p20130104@goa.bits-pilani.ac.in

Nat. Env. & Poll. Tech.

Website: www.neptjournal.com

Received: 18-12-2020

Revised: 13-02-2021

Accepted: 24-02-2021

Key Words:

Industrial wastewater
Waste management hierarchy
Technology options
Chemical industry

ABSTRACT

The Waste Management Hierarchy is used as a guiding principle for waste management of industrial solid waste. Further, it is extended for the management of industrial liquid effluents as well. The Waste Management Hierarchy consists of the five levels namely; waste prevention, reuse, recycling, recovery, and disposal. This five-tiered Waste Management Hierarchy has been adopted by the European Union under the Waste Framework Directive as a decision-making tool. This paper explores some of the technology options known and available and categorizes them according to the five levels of the Waste Management Hierarchy. This paper presents brief case studies that highlight some benefits to those who embrace this decision-making tool.

INTRODUCTION

The Environment (Protection) Act of 1986 (last amended in 1991) has empowered the Central Government of India to authorize the prevention of environmental pollution and provide environmental solutions through various mandates. This Act encompassed the Water (Prevention and Control of Pollution) Act of 1974 which was specifically concerned with the prevention of water pollution. According to the Hazardous and Other Wastes (Management and Transboundary Movement) Rules, 2016, hazardous waste as defined in the Rules needs to be generated, handled, stored, transported, treated, and disposed of with utmost care (CPCB website). All of the above Acts and Rules have one broad objective, which is to protect the environment along with the people and the ecosystem.

The US Environment Protection Agency (EPA) conducted a study in 2016 to analyze data submitted to the Toxics Release Inventory (TRI) since 1991 in an attempt to quantify the impacts of source reduction activities after implementation. The study revealed that 5 to 15 billion pounds of TRI-listed chemical releases have been prevented since 1991. It was also proposed that the source reduction projects implemented by industries that resulted in the highest reductions may be classified primarily as raw material modifications, product changes, and cleaning and degreasing changes.

Industrial hazardous waste is waste generated from industrial sectors and poses an immediate danger to the environment and the public (LaGrega et al. 2010). Illegal disposal or handling of hazardous waste can affect surface waters. In the Indian context, surface water in the form of rivers and other water bodies is used for drinking, bathing, washing, and irrigation. Therefore, the impact of contaminated water on human health and the environment is very great (Sayal et al, 2016). Surface water bodies can be contaminated or polluted by hazardous waste if run-off from hazardous waste dumps enters them, or if liquid hazardous waste is discharged directly into nearby streams that connect to larger water bodies. (Agrawal et al. 2010).

Industrial hazardous wastes are characterized in terms of toxicity (acute, chronic, and extrinsic), inflammability, reactivity, and corrosiveness (CPCB website). The main important sources of industrial hazardous wastes are mining, chemical, mechanical, pulp and paper industries, cement production facilities, wood remanufacturing facilities, etc. (Mmereki et al. 2016)

Important industrial hazardous wastes include used oil and oil contaminated materials and spent solvent. These include materials such as industrial chemical waste, industrial solvents and sludge, and waste oils (Chandruppa & Das 2012).

Theoretical Framework

The waste management hierarchy: The book, *Silent Spring*, (Carson 2002) highlighted the global problems with herbicides and pesticides and presented a view of the dangers of synthetic contaminants to the ecosystem. This book set off awareness of environmental contaminants and played a pivotal role in the framing of environmental laws. It was largely held in the 1960s, that economic growth and development and the environment could not co-exist (Welford 1995).

The chemical manufacturing process generates waste and reduction of the amount of waste generated can be achieved by adopting waste management practices that are preferred over disposal or release of waste to the environment (Monte et al. 2009). The US Pollution Prevention Act (PPA) of 1990, provides for encouraging manufacturing facilities to first eliminate the generation or creation of chemical waste through source reduction activities (Bayrakal 2006). The waste management hierarchy is the cornerstone of waste management strategies. It consists of a five-tiered hierarchy comprising of the levels of waste prevention, reuse, recycling, recovery, and disposal. This hierarchy has been adopted by the European Union as a decision-making tool.

While prevention in terms of source reduction is the most preferred option, resource recovery, followed by recycling are the next preferred waste management methods for wastes that are generated. For waste that cannot be eliminated by recycling, burning for energy recovery is recommended

followed by treatment. Disposal or release of the chemical waste into the environment is the last resort. By this hierarchy, it is envisaged that over time, manufacturers will shift from disposal or other releases toward the more preferred techniques in the waste management hierarchy that do not result in releases to the environment (Capacity Building Programme on Implementation of Waste Management Rules. 2016).

The principles of the waste management hierarchy can be adopted as the basis for any waste management plan including industrial wastewater management. García et al. (2013) seamlessly connect the Waste Management Hierarchy used in solid waste management to the scenario of industrial wastewaters in viewing organic solvents in wastewaters as resources that can be recovered and reused rather than pollutants that need to be treated and disposed of.

The levels in the waste hierarchy: The waste hierarchy (Fig. 1) establishes an order of priority for the various waste treatment options so that there is the lowest possible impact on the environment and the final waste generated is minimal (Pires & Graça 2019)

The waste hierarchy is a waste management principle that includes the precautionary and prevention principles and provides a framework to enable a decision in waste management. This decision-making tool is useful at all levels; organizational, local as well as national (Van der Vorst et al. 1999).

Waste prevention: This level in solid waste management parlance is also called avoidance and minimization

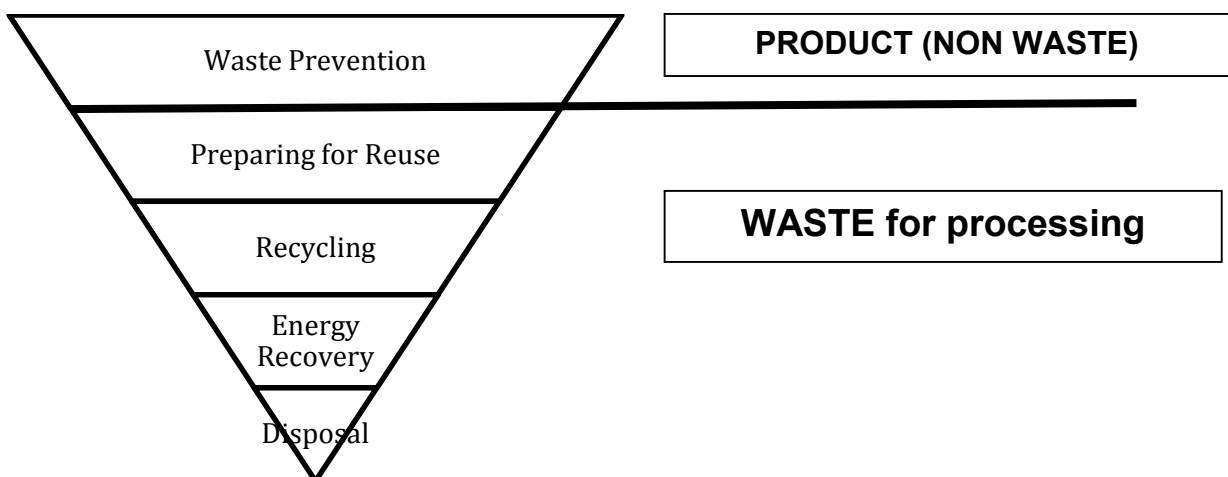


Fig. 1: The five-tiered waste hierarchy of the Waste Framework Directive 2008/98/EC

(Source: EC, 2008. DIRECTIVE 2008/98/EC of the EUROPEAN PARLIAMENT and of the COUNCIL of 19 November 2008 on Waste and Repealing Certain Directives 312, pp. 3-30.)

where waste generation is either minimized or prevented altogether.

Preparation for re-use: This level highlights the fact that industrial wastewater is a combination of water and chemical by-products generated out of an industrial process. With appropriate technologies, these chemicals can be recovered by extraction processes for either captive use or sale and water leftover can be recycled.

Recycle level: In certain situations due to economic or technical constraints, the combinations of chemicals in the wastewater cannot be reused. In this case, the chemicals are recovered as a sludge that is sent to a landfill and the water recovered would be recycled either for industrial processes or for domestic purposes.

Energy recovery: Hazardous wastes that contain toxic chemicals with high calorific value may be incinerated in a co-processing plant replacing fossil fuels. These wastes are used as a waste to energy resource. The organic components are completely converted to carbon dioxide and water while fluorine, chlorine, and sulfur acids are neutralized by the alkaline materials within the kiln. The inorganic constituents react with the raw materials and eventually become part of the clinker matrix. Co-processing is an environmentally friendly and sustainable method of waste disposal as compared to disposal practices of landfilling and incineration because of reduced emissions and the absence of residue after the process.

Disposal: A suitable treatment is resorted to in cases where technologies of recovery or recycle are not applicable based on the characteristics of the wastewater stream generated. The treated and now benign wastewater is scientifically discharged into receiving water bodies.

In a study of the pharmaceutical industry in India, Veleva et al. (2018) extended the Waste Hierarchy to six levels, wherein preparing for reuse has been bifurcated to two relevant levels viz: recovery of chemicals for reuse and recovery of chemicals for sale. Recovered chemicals for reuse can be used for captive consumption and recovery of chemicals for sale can be sold to other manufacturers. The recovery of chemicals for resale is congruent with the concept of a circular economy. The circular economy, also known as circularity, is a regenerative idea based on the principles of reducing waste and pollution, reusing products and materials, and restoring natural systems.

Technology Options

The categorization of technology options commonly used for industrial wastewater management according to the 5 levels of the waste hierarchy is detailed in Table 1.

MATERIALS AND METHODS

The data was collected using an unstructured questionnaire and personal interviews and discussions with senior-level management executives working in the concerned chemical manufacturing firms during the year 2019. The discussions centered on the problem, the level on the Waste Hierarchy the company was at, the technology option adopted, and the impact, both quantitative and qualitative. To the extent possible, costs and benefits of the technological option adopted were sought. However, due to the confidentiality of critical data, the authors collected whatever information was forthcoming. The names of the organizations were also requested to be kept in complete confidence in exchange for the information divulged.

Table 1: Categorization of technology options commonly used for industrial wastewater management according to the 5 levels of the waste hierarchy.

Level	Stages of Waste Hierarchy for Solid Wastes	Stages on Waste Hierarchy for Industrial liquid effluents	Broad Technology options for wastewater management	References
1	Waste Prevention/Avoidance/Minimization	Source reduction	Cleaner technologies, Green chemistry	Lakavat & Rao (2015)
2	Preparing for reuse	Resource recovery - for sale (industrial ecology) - for reuse	Separation and extraction of valuable chemicals	Lema & Suarez (2017)
3	Recycling	Recycling water	Hyphenation of primary, secondary, and tertiary treatment technologies, Reverse Osmosis	Gupta et al. (2012), Dasgupta et al. (2015)
4	Other recovery	Energy recovery	Co-processing of chemical constituents of wastes in cement kilns	Saini et al. (2017), Parlikar et al. (2016)
5	Disposal	Disposal after treatment	Land-filling after treatment, Incineration	Al Yaqout, (2003)

Industrial Wastewater Management Strategies

The Waste Hierarchy can serve to influence the shape of waste management strategies in organizations based on the knowledge of their waste streams, technologies available, and their economic feasibility.

The categorization of the case studies is carried out based on hierarchy levels (L) of waste management and are summarized in Table 2.

RESULTS AND DISCUSSION

Case Study I: Level 1 – Source reduction is also known as Waste prevention - Reduction of waste material generated during reactor emptying operations

Company Name: XYZ Industries Limited, Mumbai, India.

XYZ Industries Limited has a large-scale manufacturing unit located near Mumbai, India. It is a professionally managed manufacturer of organic pigments and chemicals. Organic pigments are used in paint, textiles, plastics, cosmetics, inks, and other relevant products. The company is ISO 9001:2000, ISO 14001:2004, and OHSAS 18001:2007 certified. XYZ Industries Limited has an Effluent Treatment Plant that treats the effluent which is further sent to the Common Effluent Treatment Plant (CETP). However, some part of the waste is incinerated. The solvents are reused in the manufacturing of pigments while the reactor washing water is also recycled in the process. This case study describes the effort of the company in reducing wastewater and other wastes in one of its manufacturing processes.

Process operation: Emptying of water-based viscous mass from the reactor after reaction completion.

Before	After	Benefits
One bar gauge air pressure is taken in a reactor after unloading the reaction charge.	One bar gauge steam pressure is taken instead of air in the reactor after unloading the reaction charge.	The reactor utilization has been extended by 36 hours considering 24 hours of reactor cleaning time every 10 days, three times in a month. Production increased by three batches viz. 30 MT per month. Waste has been reduced by 30 kg per cleaning and cleaning frequency reduced by 1.5 times in a month.
After emptying the mass, the reactor is flushed with water.	After emptying the mass, the reactor is flushed with water.	
There is solid mass scaling on the reactor wall.	There is less solid mass scaling on the reactor wall.	
The reactor has to be cleaned after 10 batch operations and around 50 kg solid waste material is collected from the 10 MT reactor.	The reactor has to be cleaned after 15 batch operations and around 20 kg solid waste material collected from 10 MT reactor.	

Information source: The information was collected during the personal discussion with the senior level management executive working in the concerned chemical manufacturing firm in 2019.

Case Study II: Level 2 – Preparation for Reuse of nitric acid from spent nitration mixture for nitration of chlorobenzene

Company Name: ABC Chemicals Private Limited, Raigad, Maharashtra, India.

ABC Chemicals Private Limited is a medium-scale manufacturing unit located at Raigad, India, manufacturing

Table 2: Categorization of the case studies based on the levels of Waste Management Hierarchy.

Case Study	Title of case study	Hierarchy level
I	Reduction of waste material generated during reactor emptying operations – Mumbai, Maharashtra - India	Level 1- Source reduction
II	Reuse of nitric acid from spent nitration mixture for nitration of chlorobenzene – Raigad, Maharashtra - India	Level 2 -Preparation for reuse
III	Recycle of water/Reuse of proteins from the wash water of Kingfish (Surmai Fish) cleaning process - Goa, India.	Level 3–Recycling of water
IV	Energy recovery during manufacturing of diesel from HDPE waste isolated from Municipal waste in Pimpri- Chinchwad Municipal Corporation, Maharashtra, India	Level 4 -Energy recovery
V	Isolation of heavy metals waste from the metal plating industries – Pimpri-Chinchwad Industrial Estate, Maharashtra, India.	Level 5-Treatment
V	Disposal of solids generated during manufacturing of aromatic aminophenol using sodium hydrogen sulfide - Raigad, India	Level 5 - Disposal

and marketing chemical intermediates used for specialty chemicals and organic dyes. ABC Chemicals Pvt. Limited is a market leader in the manufacture of nitro derivatives of phenols used in dyes, cosmetics, inks, and secondary explosive applications.

The phenol nitration process is conducted safely on an industrial scale using a mixture of nitric and sulfuric acid as a nitrating agent. However, during this nitration process, some spent acid is generated which contains a few traces of un-reacted concentrated nitric acid (~0.5%). The management was concerned about the traces of nitric acid in spent acid which reduced the quality of the waste as at times the consumers of spent acid reject the spent acid as it contains traces of nitric acid which affects the production of their main product.

To remove the traces of spent nitric acid in spent acid, the R&D team of the company devised a solution. The spent acid was washed with halo-aromatic organic solvents, which quantitatively react with nitric acid and forms the nitro-halo aromatic compound as another product. This new product can be captively consumed as one of the starting materials for yet another product.

Process operation: Washing the spent acid containing nitric acid traces with halo aromatic organic solvents.

Before	After	Benefits
The spent acid generated as a waste product of nitration reaction contained traces of nitric acid.	After washing with halo-aromatic solvent the spent acid was converted into nitric acid-free colorless spent acid.	A new compound was manufactured using the colorless spent acid and this compound was used as the starting material for another product. The spent acid is saleable and the demand has increased because it is colorless and free from impurities and consequently contributes to the bottom line of the company.
This waste product, a brownish-colored spent acid, containing nitric acid traces had no resale value.		

Information source: The information was collected during the personal discussion with the senior-level research staff working in the concerned chemical manufacturing firm in 2019.

Case Study III: Level 3 - Recycling of Water-Recycle/ Reuse of proteins from the wash water Kingfish (Surmai Fish) process

Company Name: ABC Fisheries Private Limited, Goa, India.

ABC Fisheries Private Limited, Goa, India is one of the largest producers of seafood in India and a market leader in the manufacture of Kingfish (Surmai Fish) in India. Each kilogram of fish typically required 8 to 10 kilograms of

water thus consuming a huge quantity of freshwater for the washing process. Consequently, it generated a huge quantity of wastewater of approximately 15 to 20 lac liters per day. This wastewater from the washing process also contains proteins. The conventional approach to deal with the waste obtained from the fish washing process did not scientifically recycle or reuse the proteins as well as the water. The company has developed an integrated membrane-based solution for the recovery of valuable proteins from the wastewater from the fish washing process in an economically attractive manner. The company has successfully commissioned two commercial plants based on membrane technology for the recovery of proteins and water from wastewaters generated from the fish washing process operating at a capacity of 600 KLD and 1200 KLD respectively. The recovered proteins after further treatment could be potentially used as fish meal powder. Further, the permeate from this process which has lowered COD (≤ 200 ppm), TDS (≤ 200 ppm) is being reused for washing application of fish thus recycling the water.

Process operation: Washing the spent acid containing nitric acid traces with halo aromatic organic solvents.

Before	After	Benefits
Wastewater is generated during the kingfish washing process as a waste stream containing proteins. Due to high BOD & COD values, it could not be discharged, recycled/reused without treatment. This discharge of such waste streams from the fish washing process without treatment has created many environmental and ecological problems.	After the application of membrane technology for the recovery of proteins from the wastewater of fish processing, the recovered proteins were converted into fish meal powder as well as the permeate was reused for the washing application.	The use of technological solutions has helped the company to make optimum use of water resources. By reusing and recycling proteins and water, the company could ascend the waste hierarchy compared to the other firms in the same industry.
There was an urgent need for a technological solution to this problem because of the huge volume of waste being generated on a daily basis.		

Information source: The information was collected during the personal discussion with the senior-level research staff working in the organization in 2019.

Case Study IV: Level 4 - Energy recovery during the manufacture of diesel from HDPE waste isolated from municipal waste

Company Name: Pimpri- Chinchwad Municipal Corporation, Maharashtra, India

The Municipal Corporation of Pimpri-Chinchwad is locat-

ed in Pune in Maharashtra state, India with a population of 25,00,000 in 2011. Total waste generated in the Corporation area is approximately 1500 MT.day⁻¹. The total quantity of solid waste generation is 500MT Kg.day⁻¹ of which 50% is biodegradable (dry), 25% recyclable, 15.3% green (wet), and 9.7% debris and silt. About 51% of the total solid waste collected from the entire city is biodegradable, processing the energy potential, is harnessed with anaerobic digestion, gasification, or palletization technologies. The waste is disposed of daily and dumped into the landfill site located near the Corporation. Some of the Corporation's waste lies in the form of HDPE, LDPE, PET as non-biodegradable wastes leading to pollution.

Process operation: Pyrolysis of HDPE polymers to manufacture petroleum products and charcoal.

Before	After	Benefits
The waste in the form of HDPE used to be burnt in 'open to air' conditions directly in the dumping ground.	After the installation of the plastic pyrolysis plant, a huge amount of HPDE undergoes pyrolysis which generates petroleum products and charcoal.	Additional revenue by selling petroleum products obtained from plastic pyrolysis plants is generated. Charcoal generated during plastic pyrolysis can be used in water purification plants. This contributed to reducing soil and water pollution in nearby areas.
This process pollutes air, water bodies, and soil in huge quantities along with carcinogens.	Reduction in air, water, and soil pollution was achieved.	
The burning of HDPE has huge carbon and water footprints.		

Information source: The information was collected during the personal discussion with the senior level operation staff working in the plastic pyrolysis plant in the year 2019.

Case Study V: Level 5 (i) – Treatment and disposal

Industry - Isolation of heavy metals waste from the metal plating industries.

The electroplating industry in India is mainly represented by small-scale units having distinct features such as tiny, family-owned jobber units, practices old and obsolete technologies, having unskilled or semiskilled power, located in unplanned and unauthorized areas with lack of industrial infrastructure facilities, and working in small shop areas. Most of the units function in an operating area of 10-25 sqm. Analytical facilities are not easily accessible to the units resulting in a lack of control on process parameters and improper documentation of production details.

Pimpri-Chinchwad Industrial Estate is located in the state of Maharashtra in India and is an industrial hub for automobile manufacturing units and other metal processing industrial units. Many parts of the automobile and die molds need metal plating to improve corrosion resistance and mechanical stress over the surface parts of the components. To improve performances and durability, the machine parts have to be coated with various plating materials like hard-chrome, copper, zinc plating, etc.

Electroplating wastewater contains highly toxic cyanide, cyanide complexes, and metal ions that make treatment a complex problem. As the electroplating industries are located

Table 3: Qualitative and quantitative impact of the Waste Management Hierarchy on manufacturing organizations.

Level on Waste Hierarchy	Environmental	Social	Economic
Waste Prevention	Reduces uptake of raw materials	Green credentials with industry peers	Reduction in waste management costs Waste valorization adds to the bottom line
Preparation for reuse	Impacts material processing by saving natural resources Reduces waste volumes	Preservation of virgin raw materials	Reduction in material costs Control over material input quality
Recycling of Water	Reduction in water withdrawals Less competition with other water users	Sharing of water with local communities for agriculture/domestic uses.	Reduction in water expenses Control over water quality
Energy Recovery	-Destruction of hazardous waste	- Sharing of energy generated with local communities	-Reduction in use of non-renewable fossil fuels - Reduction in energy costs
Treatment and Disposal	- Reduction of sludge to landfill	- Opposition from communities for new or expansion of landfills - Loss of aesthetic appeal of the local environment. - Safe containment of waste	-Costs of transportation, fuel, manpower, regulatory and compliance costs

in small and unorganized sectors in India, the problem becomes more grave. Due to the lack of technology, automation, and process control, the effluent exhibits variable characteristics. It is observed that the effluent has high Biological Oxygen Demand (BOD), Chemical Oxygen Demand (COD), Suspended Solid (SS), Dissolved Solid (DS), Total Solids (TS), Color, and Turbidity and there is depletion of oxygen. The electroplating industry consumes and discharges large volumes of wastewater. The use of various chemicals and metal salts creates pollution-related problems. The major contributor to pollution is rinsed water, spray losses, and solution dumping and leakages. Valuable metals and cyanide along with different chemicals used are lost in wastewater. The loss varies between 2-20% of the chemicals used.

Process operation: Treatment of effluents with sodium sulfide

Before	After	Benefits
The effluent generated as a waste product of metal electroplating reaction contains heavy metal ions such as nickel, chromium, zinc, lead, silver, cadmium, mercury, etc. as well as cyanides, hydrogen sulfides, ammonia, highly toxic chloramines.	After treating the wastewater with sodium sulfide or sodium hydroxide, these heavy metal salts produce corresponding sulfides or hydroxides and precipitates as metal sulfides and metal hydroxides respectively.	The treated stream of the effluents is free from heavy metal waste. The heavy metal sulfides or hydroxides can be easily separated and a few of them (e.g. copper and zinc) are used as micronutrients sources in agro-chemicals.
Electroplating wastewater has high BOD/COD, SS, DS, TS, Turbidity, color, and depletion of oxygen along with metal ions.	This precipitate settles at the bottom of the tank and can be easily removed from the effluent stream.	A heavy reduction in COD, BOD, TS, and turbidity of the effluent stream is achieved.

Information source: The information was collected during the personal discussion with the senior level operation staff working in the plant in the year 2019.

Case Study V: Level 5 (ii) – Treatment and disposal – Disposal of solids generated during manufacturing of aromatic aminophenol using sodium hydrogen sulfide

Company Name - QPR Chemicals Private Limited, Raigad, India

QPR Chemicals has a medium-scale manufacturing unit located at Raigad, India producing dye intermediates. The dye molecules have various organic functional groups such as $-\text{NO}_2$, $-\text{COOH}$, Ar-OH , etc. Sodium hydrogen sulfide is one of the selective chemical reagents for the stoichiometric reduction of the nitro group to an amino group in the presence of the phenolic group.

Selective reduction of nitrophenols to produce aminophenol using sodium hydrogen sulfide produces a colored aqueous stream with a very high content of the mixture of sodium thiosulphate, sodium thiosulphite, and other sodium salts. These salts contain about 9-10 % TDS and TSS content.

Process operation: Application of multiple-effect evaporation (MEE) plant with RVPD (Rotary Vapor Phase Drier)

Before	After	Benefits
The effluent generated in this process contains a high concentration of sodium salts as a toxic waste product.	The application of MEE and RVPD produces low effluent and liquid effluent can be gradually reduced.	The liquid waste with high COD and colored stream has been prevented from occurring which subsequently decreased the amount of effluent generated from the plant.
This effluent has high BOD/COD, SS, DS, TS, Turbidity, Color (red)	The dried solid waste is dispatched for land-filling to Mumbai Solid Waste Management Corporation.	This process decreased the workload on Effluent Treatment Plant.

Information source: The information was collected during the personal discussion with the senior level operation staff working in the plant in the year 2019.

CONCLUSION

The Waste Management Hierarchy has been used in guiding technology options towards higher-order levels on the hierarchy. Initially used in the sphere of Solid Waste, the Waste Management Hierarchy can be translated to be applied to industrial wastewater streams.

The industrial waste management hierarchy was discussed in detail. Five environment management strategies were studied from passive through reactive to proactive approaches and further supported by case studies. Industrialization causes so many problems threatening the planet earth because of wastes, emissions, and pollution. The waste management strategies have progressed from disposal to treatment, recycling, reuse, and reduction at the source itself. In some cases, there is an opportunity to integrate strategy across more than one level of the hierarchy as seen in Case study III where recycling of water and reuse of the waste product are combined. These approaches of waste management although better than disposal are not enough to create a clean environment. To overcome these problems, a cleaner production strategy is one of the options to bring about green growth and ensure sustainable development, where the environment and society are as important as the economy.

Therefore, countries of the world, whether developed or developing, should invest in cleaner production. The various strategies used for various types of effluent-related problems were identified and each one has been solved using different waste management strategies through the decision-making tool as propounded through the Waste Management Hierarchy.

The impact of the Waste Management Hierarchy on the adoption of technology options can be summarized on the three pillars of sustainability as shown in Table 3.

ACKNOWLEDGEMENTS

The authors are thankful to all the organizations that shared the necessary information sought for the sole purpose of this academic work.

REFERENCES

- Agrawal, A., Pandey, R.S. and Sharma, B. 2010. Water pollution with special reference to pesticide contamination in India. *J. Water Resour. Prot.*, 2(5): 432-448.
- Al Yaqout, A.F. 2003. Assessment and analysis of industrial liquid waste and sludge disposal at unlined landfill sites in the arid climate. *Waste Manag.*, 23(9), 817-824.
- Bayrakal, S. 2006. The US pollution prevention act: A policy implementation analysis. *Soc. Sci. J.*, 43(1): 127-145.
- Capacity Building Programme on Implementation of Waste Management Rules. 2016. Your Guide For Hazardous & Other Wastes, <https://www.npcindia.gov.in/NPC/Files/delhiOFC/EM/Hazardous-waste-management-rules-2016.pdf>. (accessed on 5th June 2020)
- Carson, R., 2002. *Silent Spring*. Houghton Mifflin Harcourt, Boston, MA, USA.
- Central Pollution Control Board (CPCB). n.d. Ministry of Environment, Forest and Climate Change, Government of India. <https://cpceb.nic.in/water-pollution/> (accessed on 5th June 2020)
- Chandrappa, R. and Das, D.B. 2012. Wastes from Industrial and Commercial Activities. In Chandrappa, R. and Das, D.B. (eds.), *Solid Waste Management*, Springer, Berlin, Heidelberg, pp. 217-247.
- Dasgupta, J., Sikder, J., Chakraborty, S., Curcio, S. and Drioli, E. 2015. Remediation of textile effluents by membrane-based treatment techniques: a state of the art review. *J. Environ. Manag.*, 147, 55-72.
- García, V., Pongrácz, E., Phillips, P.S., Keiski, R. L. 2013. From waste treatment to resource efficiency in the chemical industry: Recovery of organic solvents from waters containing electrolytes by pervaporation. *J. Cleaner Prod.*, 39: 146-153.
- Gupta, V.K., Ali, I., Saleh, T.A., Nayak, A. and Agarwal, S. 2012. Chemical treatment technologies for waste-water recycling - an overview. *RSC Adv.*, 2: 6380-6388.
- LaGrega, M. D., Buckingham, P. L. and Evans, J. C. 2010. *Hazardous Waste Management*. Waveland Press, Long Grove, US.
- Lakavat, M. and Rao, L.N. Innovative control measures of water: A study on green chemistry. *Amer. J. Mater. Sci.*, 5(3C): 169-174.
- Lema, J.M. and Suarez, S. 2017. Innovative wastewater treatment & resource recovery technologies: Impacts on energy, economy, and environment. *Water Intell. Online*, 16: 81-97. <https://doi.org/10.2166/9781780407876>.
- Mmerekí, D, Adrew, B, Liu H. and Baizhan, L. 2016. The management of hazardous waste in developing countries. *Manag. Hazard. Wastes*, 2016: 39.
- Monte, M., Concepcion, E., Fuente, A., Blanco. and Carlos, N. 2009. Waste management from pulp and paper production in the European Union. *Waste Manag.*, 29(1): 293-308.
- Parlikar, U., Bundela, P.S., Baidya, R., Ghosh. S.K. and Ghosh, S.K. 2016. Effect of variation in the chemical constituents of wastes on the co-processing performance of the cement kilns, *Procedia Environ. Sci.*, 35: 506-512. <https://doi.org/10.1016/j.proenv.2016.07.035>.
- Pires, A. and Graça, M. 2019. Waste hierarchy index for circular economy in waste management. *Waste Manag.*, 95: 298-305.
- Saini, S., Bamniya, B. R., Ramakrishna, G. V. and Kumawat, D. M. 2017. Study of pollution load in the environment during coprocessing of solid waste (carbon black) in cement rotary kiln. *Pollut. Res.*, 36(3):645-650.
- Sayal, A., Amjad, S., Bilal, M., Pervez, A., Mahmood, Q. and Afridi, M.A. 2016. Industrial water contamination and health impacts: An economic perspective. *Pol J Environ Stud.*, 25(2). 60-72
- Van Der Vorst, R., Grafé-Buckens, A. and Sheate, W.R. 1999. A systemic framework for environmental decision making. *J. Environ. Assess. Policy Manag.*, 1(1): 1-26.
- Veleva, V.R., Cue Jr, B.W., Todorova, S., Thakor, H., Mehta, N.H and Padia, K.B. 2018 Benchmarking green chemistry adoption by the Indian pharmaceutical supply chain. *Green Chem. Lett. Rev.*, 11:4, 439-456.
- Welford, R. 1995. *Environmental Strategy and Sustainable Development: The corporate challenge for the twenty-first century*. 6th edition. Routledge, London



Review on BOD/COD Ratio Toxicity to *Daphnia magna*, *Artemia salina* and *Brachydanio rerio*

Latifa Mirzatika Al-Rosyid**†, Harmin Sulistiyaning Titah*, Irwan Bagyo Santoso* and Sarwoko Mangkoedihardjo*

*Department of Environmental Engineering, Faculty of Civil, Environmental, Geo Engineering, Institut Teknologi Sepuluh Nopember (ITS), Sukolilo, 60111 Surabaya, Indonesia

**Department of Civil Engineering, Faculty of Engineering, University of Muhammadiyah Jember, 68121, Jember, Indonesia

†Corresponding author: Latifa Mirzatika Al-Rosyid; latifamirzatika@gmail.com

Nat. Env. & Poll. Tech.

Website: www.neptjournal.com

Received: 09-01-2021

Revised: 26-02-2021

Accepted: 12-04-2021

Key Words:

BOD/COD ratio

Artemia salina

Brachydanio rerio

Daphnia magna

Toxicity

ABSTRACT

This paper review research works on BOD/COD ratio toxicity to three bioindicators, namely: *Daphnia magna*, *Artemia salina*, and *Brachydanio rerio*. Treatment methods are divided into natural, biological, physical, chemical, combined treatment, and phytotechnology for various types of processing operations such as municipal and industrial wastewater treatment plants, various effluent treatment, landfill leachate, and organic matter. *A. salina* shows the lowest toxicity value of the BOD/COD ratio and shows it can withstand processing conditions that are not biodegradable. Then followed by *B. rerio* and *D. magna*. Furthermore, the disposal limits are standardized for the protection of freshwater biota. In addition, it must be considered whether there is any other potential of disposal into the receiving environment, and if so, what form of disposal and how much, to protect the biota.

INTRODUCTION

Toxicology is an understanding of the effects of chemicals that are detrimental to living organisms (Moreno 2018, Li et al. 2018). There are elements in toxicology that interact in specific ways to generate a response in a biological system that can cause damage to the biological system (Xue et al. 2019). Toxicology is divided into pharmacotoxicology and ecotoxicology (Arslan & Karaaslan 2016). This paper discusses ecotoxicology. Ecotoxicology studies the effects of pollutants on life and their effects on ecosystems, which can be used to evaluate the relationship between humans and pollutants that exist around the environment (Cardete et al. 2019). In line with quantity complexity, organic matter has pollutant quality complexity (Paris & Mangkoedihardjo 2020). The BOD/COD ratio itself indicates the biodegradability of wastewater, where the higher the ratio the lower the biodegradability of wastewater (Dincer 2020).

A number of *Daphnidae* family species are commonly used in toxicity tests. Besides being recommended for testing, this organism is available all year round and is easily cultivated in the laboratory (USEPA 2019). *D. magna* is a small invertebrate crustacean and is the main food source for

many fish in freshwater ecosystems (Sa et al. 2018, Bekker et al. 2018, Kruppert et al. 2017). As much as 41.24% of all known fish species are obtained in freshwater (Marzan et al. 2014). In addition, *D. magna* is sensitive to various pollutants and has been widely used as a bio-indicator organism to evaluate various toxic substances (Yan & Chen 2019, Leppanen 2018, Huang et al. 2017, Yasser et al. 2015). This study investigates the acute and chronic toxicity of numerous compounds to aquatic species, with a focus on *D. magna* standard test organisms, with the aim of reducing potential environmental concerns (Borujeni et al. 2018, Xavier et al. 2017, Kocbas & Oral 2015).

Bioindicators based on *A. salina* were used to assess the toxicity of chemicals found in unprocessed and persistent environments (Borba et al. 2019). Rajabi et al. (2015), reported *A. salina* as a bioindicator of toxicity has advantages compared to indirect methods including high sensitivity to toxic substances, fast response, and low cost. *A. salina* is a simple organism from marine biota that is very small and has a high sensitivity to toxins. Research shows that *A. salina* has a positive correlation with bioactive extracts (Arun et al. 2019, Cabrera 2017).

B. rerio is used as a representation of freshwater organisms in toxicity tests, recommended as an organism model according to OECD guidelines (OECD 2019), and has been widely used in toxicology testing (Panzica-Kelly et al. 2015, Boix et al. 2020). *B. rerio* is commonly used in ecotoxicological studies, because of its biological and reproductive properties (short generation and spawning intervals) that are suitable as test fish for toxicological studies (Bambino & Chu 2017). In ecology, *B. rerio* swimming behavior in motility characteristics is an external reaction caused by internal changes, as well as behavioral responses related to environmental pressures, which can provide the latest ecological information in toxicological assessment (Ren et al. 2015). *B. rerio* and *D. magna*, have been used throughout the wastewater toxicity (WET) program to evaluate the removal of acute toxicity of wastewater during anaerobic-anoxic-oxic (A/A/O) (Smol et al. 2018, Deng et al. 2016, USEPA 2016).

Biochemical Oxygen Demand (BOD) and Chemical Oxygen Demand (COD) are the most widely used parameters in the classification of wastewater, each of which has advantages and disadvantages. The choice depends on several factors, namely the time needed to determine each factor itself. Obtaining a correlation between BOD and COD for various wastewater treatment plants is important so that it can help in plant design and operation (Abdalla & Gina 2014). Therefore, the BOD/COD ratio becomes meaningless without knowing the intended use. In line with the quantity complexity, organic matter has a complex quality of pollutants (Paris & Mangkoedihardjo 2020). The BOD/COD ratio indicates the level of wastewater biodegradability; the higher the ratio, the lower the biodegradability of the wastewater (Dincer 2020). However, the researchers used the BOD/COD ratio to describe the level of biodegradability where organic matter containing wastewater decreases the quality of the environment.

This paper review research works on various operating treatment conditions, attempting to figure out BOD/COD ratio toxicity to three bioindicators i.e. *D. magna*, *A. salina*, and *B. rerio*. Treatment methods are divided into natural, biological, physical, chemical, combined treatment, and phytotechnology for various types of processing operations such as municipal and industrial wastewater treatment plants, various effluent treatment, landfill leachate, and organic matter.

In the literature, several review studies have focused on the treatment methods, bioindicator, and the BOD/COD ratio toxicity. However, to the best of our knowledge, studies concerning the various operating treatment conditions of three bioindicators have not been reviewed in detail. This study reviews the state-of-the-art of various operating

treatments and examines BOD/COD ratio toxicity to three bioindicators. In this regard, the BOD/COD ratio toxicity to three bioindicators i.e., *D. magna*, *A. salina*, and *B. rerio* by various operating treatment conditions is presented. Then, the characterization of wastewater, treatment methods, major challenges, and future prospects are discussed in detail.

MATERIALS AND METHODS

The methods applied in this literature review included identification of the relevant studies and preparing a set of questions to be addressed to selected literature relevant to the scope of this review. Identification of relevant literature was performed by searching in Science Direct, Scopus, and Google Scholar using the following keywords: “BOD/COD ratio”, “toxicity”, “*B. rerio*”, “*D. magna*” and “*A. salina*”. After that, the generated literature list was checked manually (reading materials and methods and results) to exclude studies, in which (i) various operating treatment conditions were used; (ii) toxicity assessment of wastewater before and after treatment was not conducted. Moreover, literature reviews were not considered. It should be noticed that only relevant articles published during the period 2010-2020 were included in this review. Moreover, relevant studies found during screening other studies were included in the list during the literature identifying step. The literature search was limited to articles published in peer-reviewed journals in the English language. Reports published in other languages, as well as books, were excluded from the literature search.

RESULTS AND DISCUSSION

Daphnia magna as a Test Species

Complex industrial wastewater

D. magna is used as an assessor and comparison of toxicity between influent wastewater and liquid waste from the activated sludge process, and to compare its relationship with physical-chemical parameters namely BOD and COD. The average ratio of BOD/COD is 0.54 - 0.66, respectively. This shows the amount of high-level material that cannot be decomposed naturally. Very large reductions in BOD are observed between influent and effluent. *D. magna* evaluates high toxicity in waste, indicating that BOD is not the main source of toxicity. The best correlation between bioindicator responses and chemical tests was obtained between nitrogen compounds and COD with *D. magna* in samples from secondary clarifiers. The results of the toxicity test showed that although there was a decrease in the toxicity response to *D. magna*, there were still potential negative effects on the growth of plant roots that could affect plant production (Yan & Chen 2019). No correlation was obtained between the test

results in primary (influent) clarification, but the tendency for correlation was obtained in secondary (effluent) clarification with COD parameters.

Treated Kraft Mill Effluents

Waste from kraft factories treated using activated sludge shows a reduction in acute toxicity. Waste from the kraft pulp mill has been identified as a potential contaminant in the aquatic environment (Chamorro et al. 2016, Peitz & Xavier 2020, Kocbas & Oral 2015). The nature of their compounds comes from the existence of several naturally occurring xenobiotic compounds, which are formed and released during several stages of the process (Koppel et al. 2017). The value of the COD/BOD ratio of each effect is 0.34 - 0.39. This indicates that there are high concentrations of recalcitrant compounds, such as phenolic compounds, tannins, and lignin, among other compounds (Xavier et al. 2017, Peitz & Xavier 2020). The results showed that the effect of kraft mill wastewater treatment indicated acute toxicity of LC_{15-24h} for *D. magna* at 71.72%. While LC_{15-48h} for *D. magna* shows acute toxicity with a value of 20.58%. In this case, it can be seen that there are different sensibilities. The research results obtained that the treatment of activated sludge can eliminate at 100% acute (Kocbas & Oral 2015, Velásquez-Riaño et al. 2019).

Municipal Wastewater Treatment Plant

An acute toxicity test is carried out to evaluate the relationship between the physical-chemical parameters of the waste and its toxicity in the wastewater treatment plant. Toxicity tests are carried out at wastewater treatment plants under various operational conditions (Borujeni et al. 2018). The average BOD₅/COD ratio of each 0.5 - 0.6 was calculated. After 96 hours of exposure, *D. magna* was damaged. The effluent can be safely discharged to surface water with respect to physical-chemical parameters and acute toxicity units (TUa). The relationship between effluent COD and $LC_{50-24hr}$ showed an increase in effluent COD results in increased wastewater toxicity, whereas between BOD₅ and effluent toxicity, no relationship was found.

Municipal Wastewater Treatment Plant Effluents on Freshwater

BOD and COD values in MMWTP wastewater decreased after treatment. This shows that the processing system is working perfectly (Kocbas & Oral 2015). The average value of the BOD/COD ratio was obtained between 0.33 to 0.36. Eco toxicity test results show the mobility of *D. magna* ranges from 0 to 100% in untreated systems and 15 to 100% after being treated (Mendonça et al. 2013). The physical-chemical parameters measured in wastewater show a significant decrease in value. Meanwhile, *D. magna* did not show the

same reduction in toxicity tests. Even for a short amount of time, none of the *Daphnia* individuals are allowed to exist in 100% untreated liquid waste and survive.

However, the toxicity value in immobilized *D. magna* was defined as LC₅₀ and TU with different testing times. Although all MMWTP wastewater is released in accordance with rules for conventional water quality standards, all waste toxicity testing using *D. magna* indicates that it is harmful. In addition, the increase in biological toxic effects is based on the time of exposure to the test. The LC₅₀ value of the test carried out on untreated wastewater is 24.9 after 24 hours. After that, each dropped according to the TU value. The water treated in *D. magna* immobilization is less toxic than untreated water. However, the toxic effects of treated wastewater on *D. magna* increase over a longer period, similar to water not treated before. Although the LC₅₀ value has decreased each.

Of the various types of treatment for *Daphnia*, the range of toxicity ratios of BOD₅/COD that have the most effective effect are 0.3 - 0.6, respectively (Fig. 1).

Artemia salina as a Test Species

Paper Pulp and Mill Wastewater Treatment

The combined treatment of post-bleaching effluents resulted in a BOD/COD ratio of 0.11 to 0.14, respectively. Transparency, colorless and smelly treated water, shows good water quality (Cabrera 2017). *A. salina* bioindicator shows that the expressive decrease in toxic pollutants in the waste occurs after treatment, mainly by a combined process, namely coagulation followed by photocatalysis. Wastewater treatment is carried out together under optimal experimental conditions, giving satisfying results.

Sugar Industry Effluent Treatment

A. salina is used as a bioindicator in the processing of the sugar industry waste. In 60 ppt saline media, *A. salina*, used as a bioindicator for secondary treatment of refining waste, can remove up to 69 percent of total solids and 33.34 percent of BOD. After treatment with *A. salina*, liquid waste showed a significant $p < 0.001$. Obtained COD reduced from a minimum of 14% and then a maximum of 4% (El Fels et al. 2016). The average value of the BOD/COD ratio is obtained for each of 0.14 - 0.19. TDS is measured after each processing stage and shows promising results with *A. salina*, which has the ability to control industrial waste contamination.

Industrial Wastewater

The aerobic process is used for treating wastewater from tannery using *A. salina*. *A. salina* is harvested at the age of 15 days after cysts are inoculated in the hatching tank. 63.09 g (wet weight) *A. salina* was put together in a tank with a

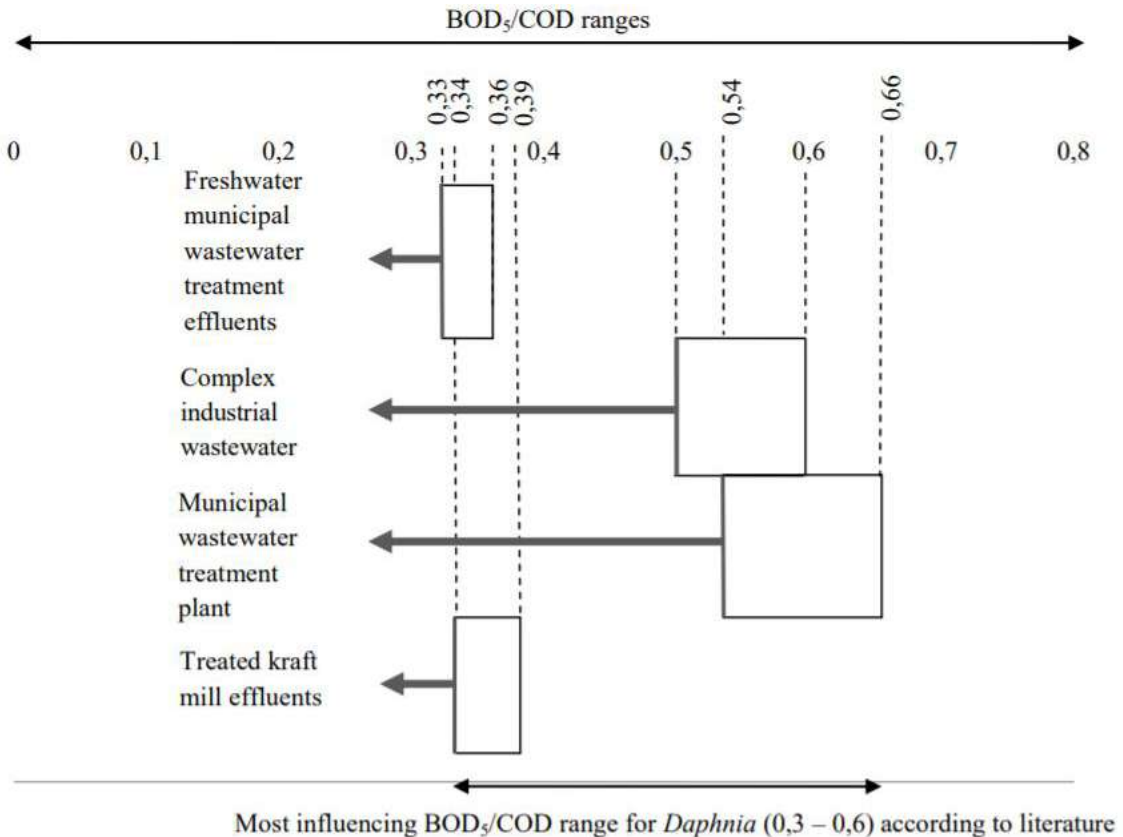


Fig. 1: BOD/COD ratio range yielding maximum removal of *Daphnia magna* as reported in the literature.

weight of 0.0036 g each (Arun et al. 2019). The average value of the BOD₅/COD ratio was obtained for each of 0.12 - 0.17. This is safe within the limits permitted and suitable for disposal into water bodies and recommended for reuse.

From various types of treatments for *A. salina*, the most effective range to the toxicity ratio of BOD/COD is 0.11 - 0.19, respectively (Fig. 2).

Brachydanio rerio as a Test Species

Organic Matter

The BOD/COD ratio shows that glucose, lactose, and sucrose can decompose naturally, while formaldehyde, acetic acid, and oxalic acid, cannot decompose naturally. This result is supported by a toxicity test, which shows that all three are more toxic than substances that can be decomposed naturally (Al-Rosyid & Mangkoedihardjo 2019). The average value of the BOD/COD ratio was obtained for each 0.08 - 0.25. Formaldehyde has the smallest LC_{50-96h}, which is 23.99 so that *B. rerio* response with the highest mortality is obtained. This is consistent with the biodegradability of formaldehyde which is included in the category of non-biodegradable. Lactose

with the largest LC_{50-96h} value is 851.14 and is included in the biodegradable category in laboratory analysis. This also corresponds to lactose biodegradability which is included in the biodegradable category.

Landfill Leachate

Leachate contains a number of distinct properties, including a high level of salinity and low biodegradability. (BOD/COD 0.05). Initially, physical-chemical processing was used, while the second stage consisted of ozone application to improve leachate biodegradability. The final stage consists of biological processing. Stages of the processing carried out bring good results, with an increase in the ratio of BOD/COD from 0.05 to 0.3 after ozonation (Grosser et al. 2019). Toxicity analysis conducted using various bioindicators such as *B. rerio* has confirmed the potential danger of landfill leachate (Ghosh et al. 2017, Sackey & Koci 2020) and the need to process it so that it meets the disposal standards in water bodies. Biological treatment processes, including aerobic and anaerobic processes, are quite effective for leachate produced in the initial stages, with high BOD/COD (Li et al. 2010). However, in general, it has not been successful in treating leachate with BOD/COD which is rather low,

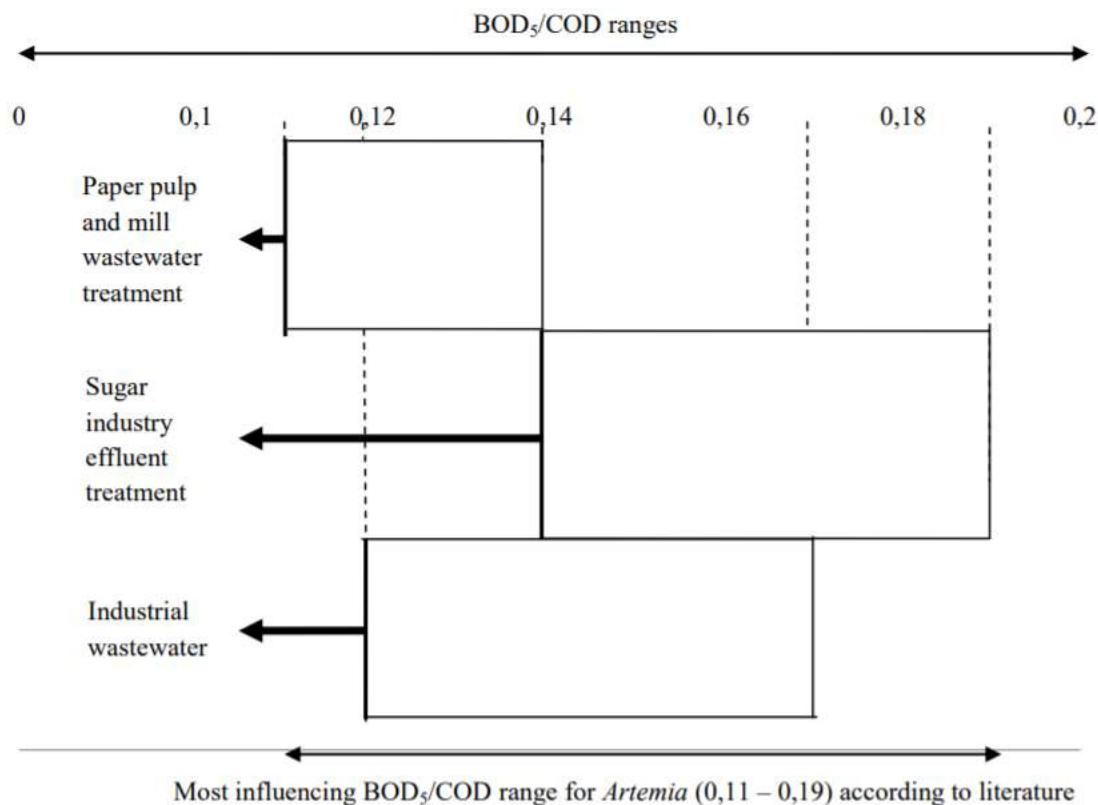


Fig. 2: BOD/COD ratio range yielding maximum removal of *Artemia salina* as reported in the literature.

or high heavy metal concentrations (Banch et al. 2020). Therefore, physical-chemical processes are mostly used for pretreatment or full treatment for leachate types in landfills.

From the various types of processing for *B. rerio*, the most effective range influenced the toxicity ratio of BOD5/COD, ranging from 0.05 to 0.3. (Fig. 3).

Comparison Ranges for *Daphnia magna*, *Artemia salina*, and *Brachydanio rerio*

Each of the three types of bioindicators used, *D. magna*, *A. salina*, and *B. rerio*, has an effective BOD/COD range, with *D. magna*, *A. salina*, and *B. rerio* having the highest influence in their respective processing conditions. *D. magna* has a range of BOD/COD which results in a maximum reduction of 0.3 - 0.6, for complex industrial wastewater, kraft mill effluents treated, municipal wastewater treatment plants, and municipal wastewater treatment plants in freshwater. *A. salina* has a range of BOD/COD which results in a maximum reduction of 0.11 - 0.19, for paper and mill wastewater treatment, sugar industry wastewater treatment, and industrial wastewater. *B. rerio* has a range of BOD/COD ratios resulting in a maximum reduction of 0.05 - 0.3, respectively, for organic matter and landfill leachate. *A.*

salina shows the lowest toxicity value of the BOD/COD ratio. This shows that it can withstand processing conditions that cannot be decomposed naturally. Then followed by *B. rerio* and *D. magna* (Fig. 4).

CONCLUSIONS

This review indicates the future role of *A. salina* bioindicators in aquatic toxicology testing, where *A. salina* can be a reference or quality control in rapid screening tests, as well as predictors of chemical effects on species in the marine environment. Toxicity tests conducted using *B. rerio* show that leachate toxicity is hardly reduced by ozonation. This result is consistent with the fact that although the BOD/COD ratio is higher, biological processes do not show better processing performance. In conclusion, the researchers suggest that toxicity calculation and monitoring of physical-chemical parameters are carried out together in large-scale processing plants. Furthermore, the disposal limits are standardized for the protection of freshwater biota. Furthermore, it must be considered whether additional disposal into the receiving environment is possible, and if so, what form of disposal and how much is possible, so that the biota is preserved.

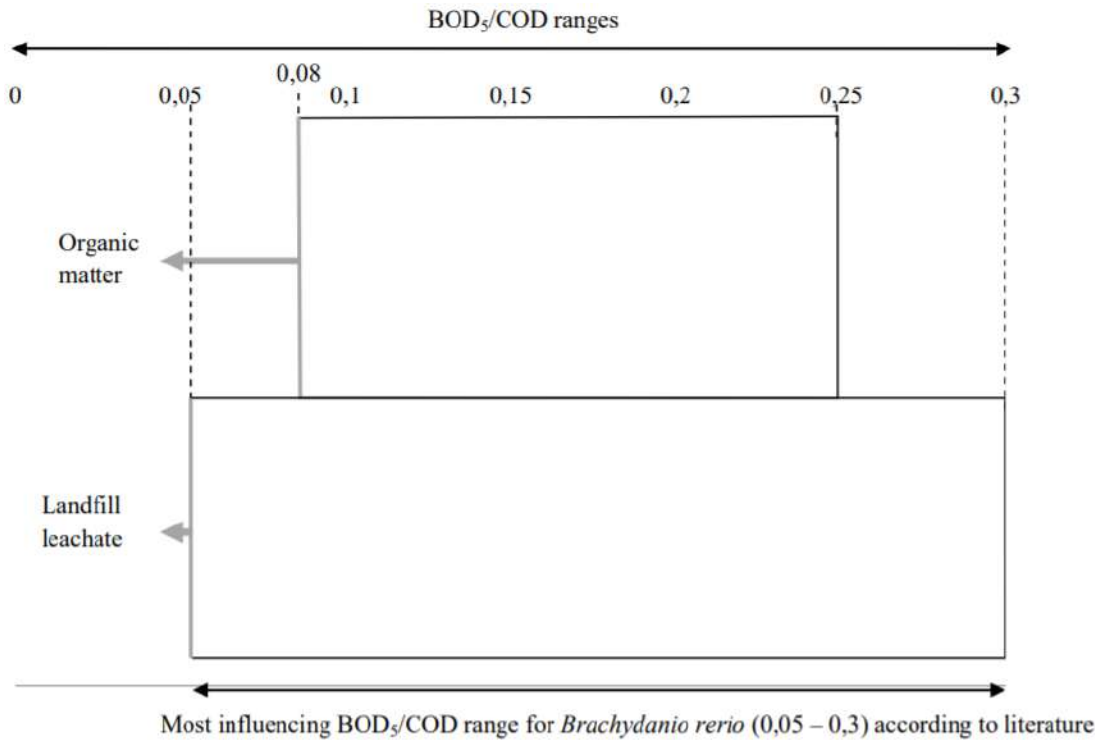


Fig. 3: BOD/COD ratio range yielding maximum removal of *Brachydanio rerio* as reported in the literature.

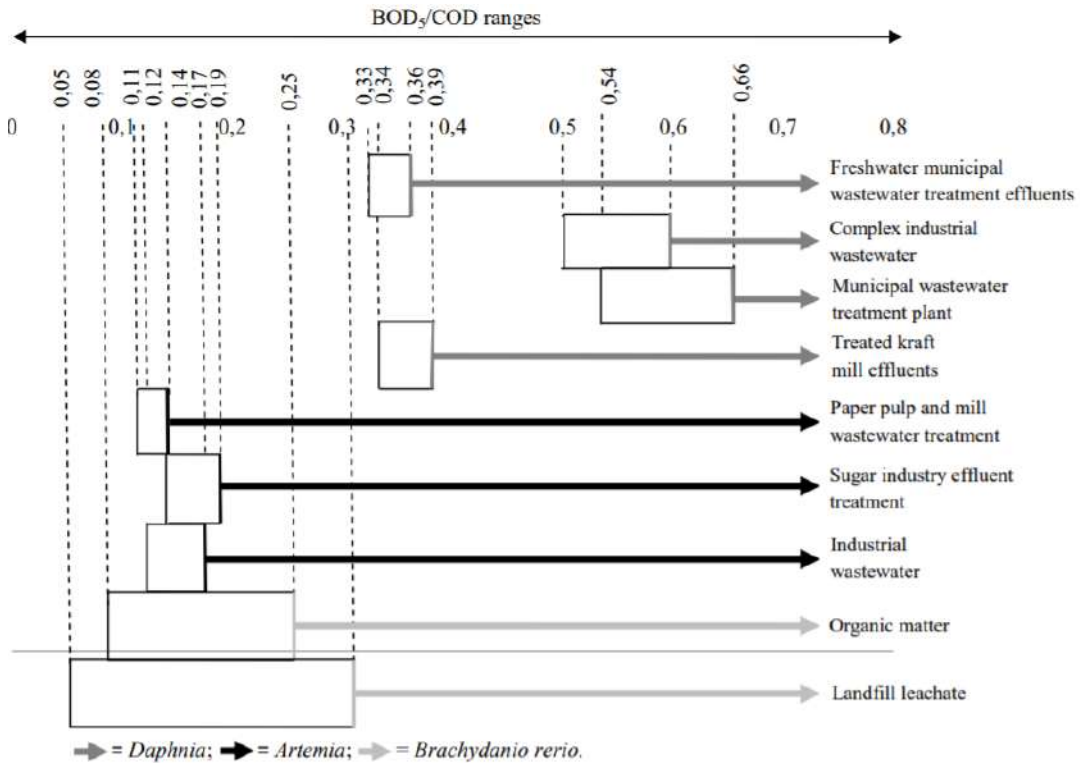


Fig. 4: Comparison of BOD/COD ratio range yielding maximum removal of *Daphnia magna*, *Artemia salina*, and *Brachydanio rerio*

ACKNOWLEDGEMENTS

The authors express gratitude to all lecturers of the Department of Environmental Engineering, Faculty of Civil, Environmental, and Geo-Engineering, Institut Teknologi Sepuluh Nopember for every suggestion and viewpoint.

REFERENCES

- Abdalla, K.Z. and Gina, H. 2014. Correlation between biochemical oxygen demand and the chemical oxygen demand for various wastewater treatment plants in Egypt to obtain the biodegradability indices. *Int. J. Sci. Basic Appl. Res.*, 13(1), 42-48.
- Al-Rosyid, L.M. and Mangkoedihardjo, S. 2019. Relationship between BOD/COD ratio and octanol/water partition coefficient for glucose, lactose, sucrose, formaldehyde, acetic acid, and oxalic acid. *Int. J. Civ. Eng. Technol.*, 10(1): 691-696.
- Arslan, O.C. and Karaaslan, M.A. 2016. Bioavailability of sea urchin to aquatic toxicity tests. *J. Aquat. Pollut. Toxicol.*, 1(1), 1-6.
- Arun, N.C., Satheesh, K. and Dhivakar, K. 2019. Cultivation of *Artemia salina* for reducing BOD in industrial wastewater. *Int. J. Sci. Res. Rev.*, 5(07): 1879-1892.
- Bambino, K. and Chu, J. 2017. Chapter nine: Zebrafish in toxicology and environmental health. *Curr. Top. Dev. Biol.*, 124: 331-367.
- Banch, T.J.H., Hanafiah, M.M., Salem, S., Amr, A., Abbas, F., Alkarkhi, M. and Hasan, M. 2020. Treatment of landfill leachate using palm oil mill effluent. *Processes*, 8(601): 1-17.
- Bekker, E.L., Karabanov, D.P., Galimov, Y.R., Haag, C.R., Neretina, T.V. and Kotov, A.A. 2018. Phylogeography of *Daphnia magna* (Crustacea: Cladocera) in Northern Eurasia: Evidence for a deep longitudinal split between mitochondrial lineages. *PLoS One*, 13(3): e0194045.
- Boix, N., Pique, E., Gomez-Catal, J., Teixido, E. and Llobet, J.M. 2020. Modulation and protection effects of antioxidant compounds against oxidant-induced developmental toxicity in zebrafish. *Antioxidants*, 9(721): 1-13.
- Borba, F.H., Jandira, L., Francine, B., Leandro, P., Jonas, J., Inticher, and Daiana, S. 2019. Pollutant removal and acute toxicity assessment (*Artemia salina*) of landfill leachate treated by a photo-fenton process mediated by oxalic acid. *J. Water Process Eng.*, (28):159-168.
- Borujeni, F.G., Fatemeh, N.B. and Hamed, A. 2018. Data on effluent toxicity and physicochemical parameters of municipal wastewater treatment plant using *Daphnia magna*. Data in Brief, (19): 1837-1843.
- Cabrera, M.N. 2017. Chapter 7: Pulp Mill Wastewater: Characteristics and Treatment. INTECH.
- Cardete, M.A., Mata-A.J., Dosta, J. and Nieto-S.R. 2019. Biological nitrification control by addition of folic acid in a petrochemical wastewater treatment focused on organic matter removal. *J. Environ. Chem. Eng.*, 7(2): 102935.
- Chamorro, S., Lopez, D., Brito, P., Jarpa, M. and Vidal, G. 2016. Sublethal effects of chlorine-free kraft mill effluents on *Daphnia magna*. *Bull. Environ. Contam. Toxicol.*, 97(6): 843-847.
- Deng, M., Zhang, Y., Quan, X., Na, C., Chen, S., Liu, W., Han, S. and Masunaga, S. 2017. Acute toxicity reduction and toxicity identification in pigment contaminated wastewater during anaerobic-anoxic-oxic (A/A/O) treatment process. *Chemosphere*, 168: 1285-1292.
- Dincer, A.R. 2020. Increasing BOD₅/COD ratio of non-biodegradable compound (reactive black 5) with ozone and catalase enzyme combination. *SN Appl. Sci., Sciences*, 2: 736.
- El Fels, L., Hafidi, M. and Ouhouch, Y. 2016. *Artemia salina* as a new index for assessment of acute cytotoxicity during co-composting of sewage sludge and lignocellulose waste. *Waste Manage.*, 50: 194-200.
- Ghosh, P., Thakur, I.S. and Kaushik, A. 2017. Bioassays for toxicological risk assessment of landfill leachate: A review. *Ecotoxicol. Environ. Safety* 141: 259-270.
- Grosser, A., Neczaj, E., Madela, M. and Celary, P. 2019. Ultrasound-assisted treatment of landfill leachate in a sequencing batch reactor. *Water*, 11 (516): 65-78.
- Huang, Y., Campana, O. and Wlodkowic, D. 2017. A millifluidic system for analysis of *Daphnia magna* locomotory responses to water-born toxicants. *Sci. Rep.*, 7(1): 17603.
- Kocbas, F. and Oral, R. 2015. *Daphnia magna* as a test species for toxicity evaluation of municipal wastewater treatment plant effluents on freshwater Cladocera in Turkey. *Turkish J. Fish. Aquat. Sci.*, 15: 619-624.
- Koppel, N., Maini, R.V. and Balskus, E.P. 2017. Chemical transformation of xenobiotics by the human gut microbiota. *Science*, 356 (6344)
- Kruppert, K., Horstmann, M., Weiss, L.C., Witzel, U., Schaber, C.F., Gorb, S.N. and Tollrian, R. 2017. Biomechanical properties of predator-induced body armor in the freshwater crustacean *Daphnia*. *Sci. Rep.*, 7 (9750): 1101-1128
- Leppanen, J.J. 2018. An overview of Cladocera studies conducted in mine water impacted lakes. *Int. Aquat. Res.*, 10: 207-221.
- Li, M., Chen, Z., Wang, Z. and Wen, Q. 2018. Investigation on the degradation behavior of dissolved effluent organic matter, organic micro-pollutants, and bio-toxicity reduction from secondary effluent treated by ozonation. *Chemosphere*, 18 (217): 223-231.
- Marzan, L.W., Barua, P., Akter, Y., Mannan, A., Hossain, A. and Ali, Y. 2014. Molecular investigation on clinicopathological, genetic and biochemical changes in *Channa punctata* infected with internal parasites and subjected to metals pollution in Chittagong, Bangladesh. *J. Biomol. Res. Therap.*, 3: 113.
- Mendonça, E., Picado, A., Paixão, S.M., Silva, L., Barbosa, M. and Cunha, M.A. 2013. Ecotoxicological evaluation of wastewater in a municipal WWTP in Lisbon area (Portugal). *Desal. Water Treat.*, (51): 4162-4170.
- Moreno, M.I. 2018. Resistance of pathogenic and spoilage microorganisms to disinfectants in the presence of organic matter and their residual effect on stainless steel and polypropylene. *J. Glob. Antimicrob. Resist.*, 14: 197-201.
- Organization for Economic Cooperation and Development (OECD). 2019. Section 2 Effects on Biotic Systems: Test Guideline No. 203 Fish, Acute Toxicity Testing. OECD Guidelines for the Testing of Chemicals. https://www.oecd-ilibrary.org/environment/test-no-203-fish-acute-toxicity-test_9789264069961-en
- Paris, D. and Mangkoedihardjo, S. 2020. Detoxification of glucose, ammonium, and formaldehyde using nitrification and plant processes. *Nat. Environ. Pollut. Technol.*, 19 (1) 385-388.
- Panzica-Kelly, J.M., Zhang, C.X. and Augustine-Rauch, K.A. 2015. Optimization and performance assessment of the chorion-off [dechorinated] zebrafish developmental toxicity assay. *Toxicol. Sci.*, 146 (1): 127-134.
- Peitz, C. and Xavier, C.R. 2020. Moving bed biofilm reactor for the treatment of kraft pulp effluent with high organic load rate. *Rev. Amb. Água*, 15(4), e2512.
- Rajabi, S., Ramazani, A., Hamidi, M. and Naji, T. 2015. *Artemia salina* as a model organism in toxicity assessment of nanoparticles. *Daru*, 23(1): 20.
- Ren, Z., Zhang, X., Wang, X., Qi, P., Zhang, B. and Zeng, Y. 2015. AchE inhibition: one dominant factor for swimming behavior changes of *Daphnia magna* under DDVP exposure. *Chemosphere*, (120): 252-257.
- Sa, L.C.D., Oliveira, M., Ribeiro, F., Rocha, T.L. and Futter, M.N. 2018. Studies of the effects of microplastics on aquatic organisms: What do we know and where should we focus our efforts in the future? *Sci. Total Environ.*, 645: 1029-1039.
- Sackey, L.N.A. and Kocif, V. 2020. Assessing the effects of tropical wood leachate on *Desmodesmus subspicatus*, *Lemna minor*, and *Daphnia magna*. *Heliyon*, 6(7): e04268.

- Smol, M., Włóka, D. and Włodarczyk-Makuła, M. 2018. Influence of integrated membrane treatment on the phytotoxicity of wastewater from the coke industry. *Water Air Soil Pollut.*, 229: 154.
- Talalaj, I.A., Biedka, P. and Bartkowska, I. 2019. Treatment of landfill leachates with biological pretreatments and reverse osmosis. *Environ. Chem. Lett.*, 17: 1177-1193.
- United States Environmental Protection Agency (USEPA). 2019. Test Guidelines for Pesticides and Toxic Substances. OCSPH Harmonized Test Guidelines. Washington DC, USA.
- United States Environmental Protection Agency (USEPA). 2016. Whole Effluent Toxicity Methods Errata Sheet: EPA 821-R-02-012-ES. Washington DC, USA.
- Velásquez-Riaño, M., Meneses-Sánchez, J.S. and Arias, C.E.C. 2019. Evaluation of acute toxicity of vinasse by means of *Daphnia magna* and *Aliivibrio fischeri*: a comparative study. *Interdiscip. Toxicol.*, 12(3): 143-148.
- Xavier, C.R., Daniela, L., Gloria, G., Soledad, C. and Anne, S. 2017. Sensitivity study comparing *Daphnia obtusa* (Kurz 1874) and *Daphnia magna* (Straus 1820) exposure to treated kraft mill effluents, diethylstilbestrol, and androstenedione. *BioResources*, 12(3): 6558-6567.
- Xue, F., Tang, B., Bin, L., Ye, J., Huang, S. and Fu, F. 2019. Residual microorganic pollutants and their biotoxicity of the effluent from the typical textile wastewater treatment plants at Pearl River Delta. *Sci. Total Environ.*, (657): 696-703.
- Yan, A. and Chen, Z. 2019. Impacts of silver nanoparticles on plants: A focus on the phytotoxicity and underlying mechanism. *Int. J. Mol. Sci.*, 20(5): 1003.
- Yasser, E.N., Shawkat, E.N. and Samir, A. 2015. Impact of organic contamination on some aquatic organisms. *Toxicol. Int.*, 22(1): 45-53.



Assessment of LULC Changes for Hesaraghatta Watershed Using GIS Tools and Remote Sensed Data

Bharath A.*†, Manjunatha M.*, Ranjitha B. Tangadagi*, Preethi S. and Mukund Dangeti*****

*Department of Civil Engineering, GITAM School of Technology, GITAM University, Bangalore-562163, Karnataka, India

**School of Civil Engineering, REVA University, Bangalore-560024, Karnataka, India

***Department of Civil Engineering, GITAM Institute of Technology, GITAM University, Visakhapatnam-530045, Andhra Pradesh, India

†Corresponding author: Bharath A.; bashu@gitam.edu

Nat. Env. & Poll. Tech.
Website: www.neptjournal.com

Received: 11-01-2021

Revised: 15-02-2021

Accepted: 24-02-2021

Key Words:

Change detection

Landsat

Remote sensing and GIS

Land use/land cover

Image classification

ABSTRACT

Hesaraghatta watershed is one of the most vital and environmentally substantial watersheds in the Arkavathi basin. It has a freshwater lake created in the year 1894 across the Arkavathi River to quench the drinking water requirements of Bengaluru city. The watershed is facing significant stresses due to rapid urbanization and other developmental activities. For this study, an attempt is made to assess the distribution of various land use land cover classes and their temporal changes over 18 years using remote sensed data and GIS tools. The watershed is categorized into four land use land cover classifications: settlement, waterbody, vegetation, and bare soil. The maximum likelihood technique is utilized for the image classification and accuracy assessment is carried out to evaluate the accuracy of image classification. The outcome of the study revealed that there is a substantial change in land use land cover classes in the Hesaraghatta watershed.

INTRODUCTION

From the start of human civilization, humankind has been in a close association with nature and its reliance on the environment is greater than any other living thing (Anees et al. 2017, Wang et al. 2018). Due to the intensification in population and human intervention, there is a substantial modification in Land use (LU) and Land cover (LC) with time. In general, "land cover refers to the physical land kind such as how much of a region is enclosed by forests, impervious surfaces, agricultural lands, wetlands, and open water, whereas land use documents how people are using the land for development, conservation or mixed uses (Chowdhury et al. 2020). LULC changes greatly affect the regional ecological process (Chowdhury et al., 2020), (Belay & Mengistu 2019). Water quality, runoff and groundwater recharge, etc., gets affected due to changes in LULC in a watershed (Butt et al. 2015, Garg et al. 2019). Thus, it becomes necessary to understand the spatial relationship and mechanisms between ecosystem and LULC (Chen et al. 2019, Imran Basha et al. 2018, Salunke & Chavan 2020) and to measure the changes in LULC pattern at the watershed level for planning management strategies (Nayak & Byrne 2019, Preethi et al. 2020, L. Wang et al. 2020). Assessment of LULC change helps to

identify the amount of anthropological impact on the natural environment (Chowdhury et al. 2020). Change detection is a method to identify the condition of a component or phenomenon by perceiving it at a different time (Bharath et al. 2020a, Imran Basha et al. 2018). Change detection helps to identify LULC changes like landscape changes, shifting cultivation, land degradation, desertification, urban sprawl, coastal change, deforestation, quarrying activities, and other cumulative changes (Bharath et al. 2020b, Gebeyehu et al. 2019).

Traditional approaches are not satisfactory for the analysis of multi-complex environmental investigations because of the difficulty of dealing with the multi-disciplinary dataset; hence we need new advances like remote sensing and Geographical Information Systems (GIS) (Mallupattu & Sreenivasula Reddy 2013). GIS and Remote sensing are the most efficient approaches for observing widespread and rapid LULC changes (Ali et al. 2020, Tsai et al. 2019). Remotely sensed data is freely accessible, and developments in spatial, spectral, and temporal resolutions continue to provide tools for detecting changes in LULC at various scales. Landsat satellite systems provide open-access, long-term imageries that are ideal for assessing LULC change (Tsai et al. 2019).

The primary objective of this LULC study is to determine the extent of LULC changes that arisen in the Hesaraghatta Watershed from 2000 to 2018. But the definite objectives are delineating the Hesaraghatta watershed, detecting the changes in LULC classes within the watershed by spatial comparison, and analyzing the capability of integrating GIS with Remote sensing to study the spatial distribution of LULC classes.

Study Area

Hesaraghatta watershed is situated in Bengaluru rural district, and geographically it lies in $77^{\circ} 20'$ and $77^{\circ} 42'$ E longitude and $13^{\circ} 10'$ and $13^{\circ} 24'$ N latitude as shown in Fig. 1. Hesaraghatta watershed is one of the most vital and environmentally substantial watersheds. It has a freshwater lake created in the year 1894 across the Arkavathi River to quench the drinking water requirements of Bengaluru city. The watershed spreads over an area of about 605.2 km^2 with

a width and length of 27.28 km and 33.36 km, respectively (Somashekar et al. 2011).

MATERIALS AND METHODS

Fig. 2 Shows the process flow chart for change detection & LULC mapping.

Data Acquisition

In this study, Cartosat-1: DEM - Version-3R1 collected from the Bhuvan website (<https://bhuvan.nrsc.gov.in/>) is used for watershed delineation. Satellite images of two different years comprising of multi-spectral data procured via Landsat provided by the United States Geological Survey (USGS) Earth Explorer (EarthExplorer n.d.) are used for visual image interpretation and detecting LULC classes. Images collected are of the same months to have minimal seasonal variation (Chowdhury et al. 2020). Table 1 highlights the different data that are used in this study.

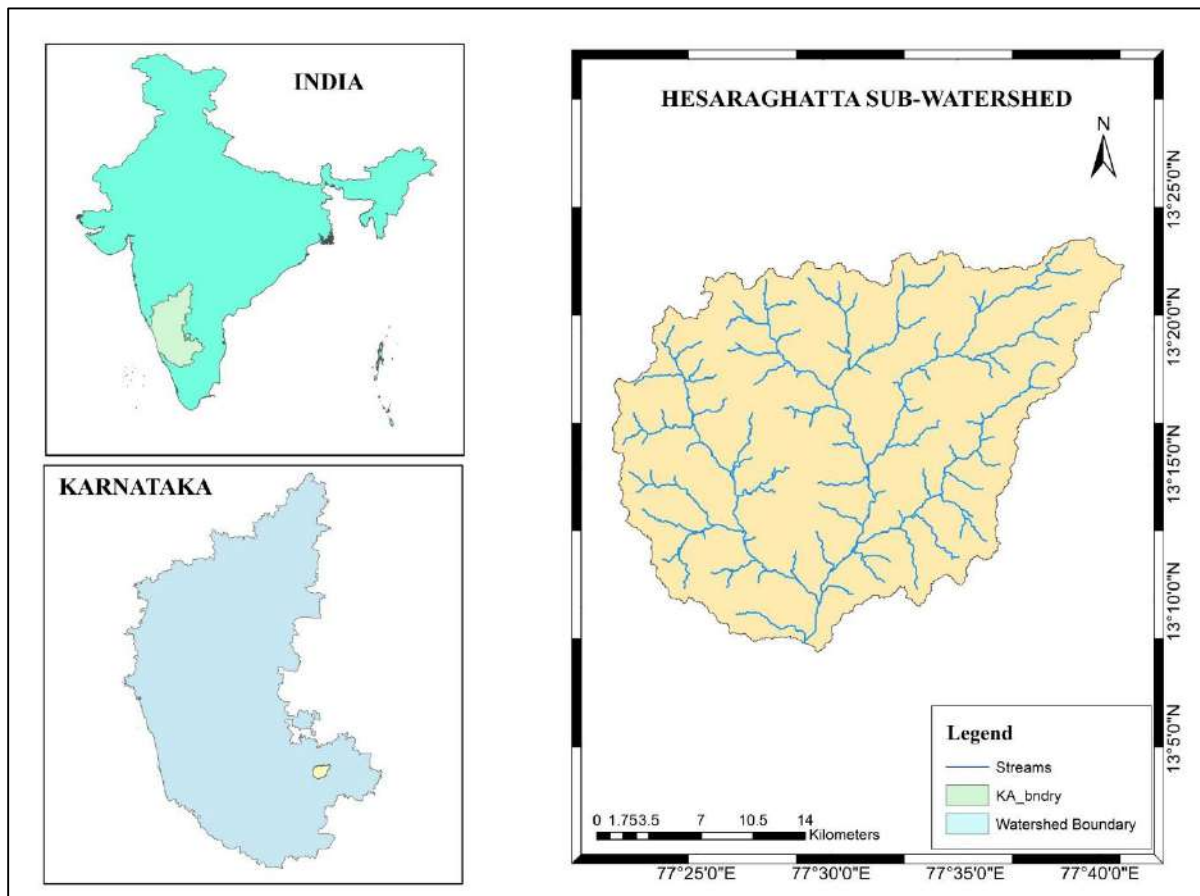


Fig. 1: Location of Hesaraghatta Watershed.

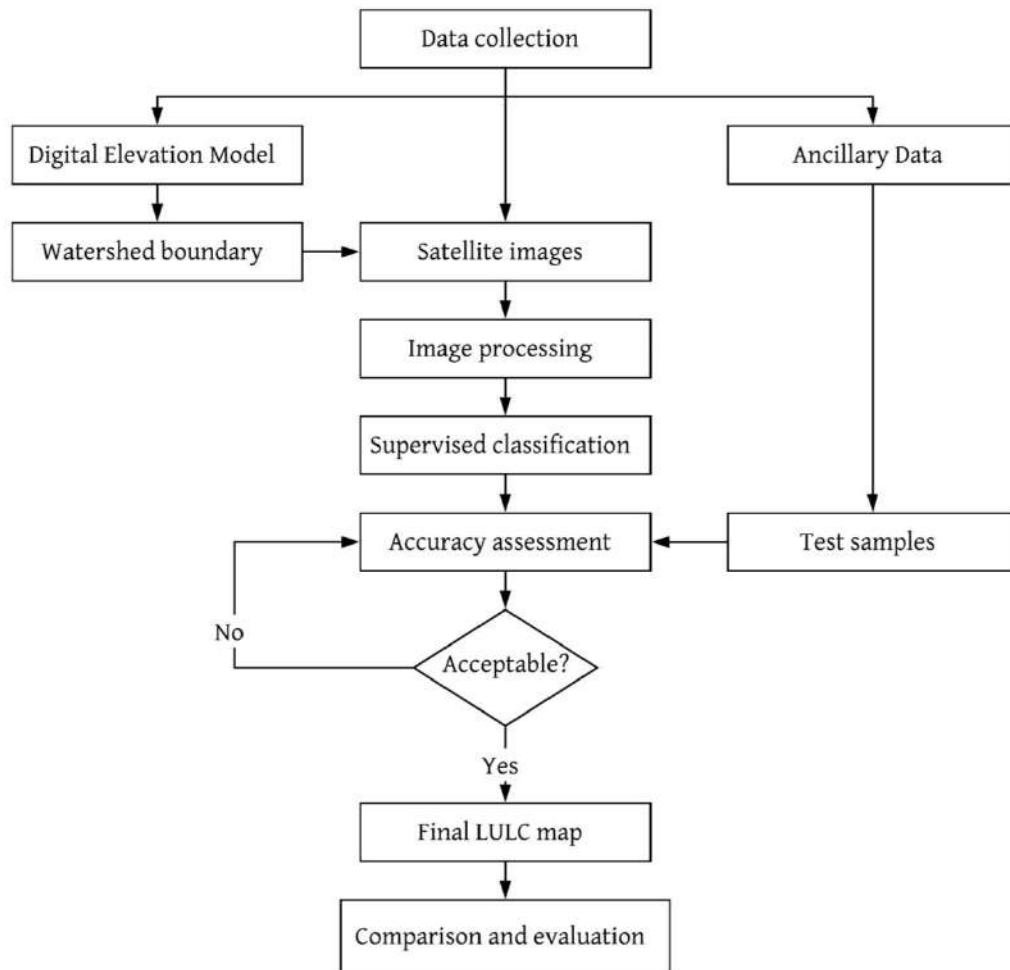


Fig. 2: Methodology for LULC mapping and change detection.

Table 1: Details about the study area.

Data	Source	Satellite	Date of acquisition	Properties
DEM	Bhuvan website bhuvan.nrsc.gov.in	Cartosat-1: DEM Version-3R1	2014	32m resolution
Satellite images	USGS-Earth Explorer earthexplorer.usgs.gov	2000 - Landsat 7 2018 - Landsat 8	16/03/2000 11/04/2018	30m resolution

Watershed Delineation

Watershed delineation is a process of marking a boundary that signifies the area contributing to an outlet (Chowdhury et al. 2020, Rimal et al. 2019). In this research, Cartosat-1 DEM of the study area with a spatial resolution of 30m and QGIS software is used for delineating the watershed. Fig. 3 highlights the process flow diagram for delineating the boundary of the watershed.

Image Pre-Processing & Image Classification

Before image classification, satellite images are enhanced using histogram equalization to increase accuracy (Mallupattu & Sreenivasula Reddy 2013). The resultant satellite images are clipped using the Hesaraghatta watershed boundary. A supervised image classification technique is used for image classification. In supervised classification, training sites are defined by the user based on the pixel signature (Chowdhury

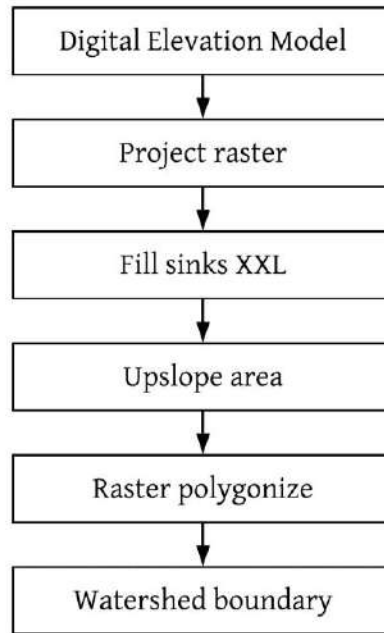


Fig. 3: Process flow diagram for watershed delineation.

et al. 2020, Mallupattu & Sreenivasula Reddy 2013) Both image processing and image classification are done using ERDAS imagine V15. The entire watershed is distinguished into four LULC classes, i.e., vegetation, settlement, bare soil, and water body. For every LULC class, polygons were drawn to training sites. Hence, signatures are located in satellite images by using Google Earth Pro images (Das Kangabam et al. 2019, Tsai et al. 2019) Maximum likelihood algorithm is used for supervised image classification.

Accuracy Assessment

It is a process that compares the classified pixels with the ground-truth points to assess how well the classified image signifies the real world (Chowdhury et al. 2020, Das Kangabam et al. 2019). In the present study, overall accuracy and kappa coefficient are determined to check the accuracy of image classification. This is done by a random sampling method using 200 points based on ground truth data (Abd El-Kawy et al. 2011, Das Kangabam et al. 2019, Tsai et al. 2019)

LULC Change Assessment

After image classification, LULC maps of the years 2000 and 2018 are obtained, which gives information about LULC distribution in the study area. Further, the classified images of two time periods are compared to estimate LULC changes over time (Chowdhury et al. 2020).

RESULTS AND DISCUSSION

Hesaraghatta watershed is delineated using Cartosat-1 DEM of 30m resolution by the QGIS tool. The watershed spreads over an area of 605.2 km². By applying the supervised image classification technique, Landsat data for the years 2000 and 2018 are classified under four LULC classes. The outcomes show that in the year 2000, an area of 98.3 km² was covered with vegetation, 1.1 km² with water, 431.1 km² with bare soil, and 74.6 km² with settlement, whereas in the year 2018, 125.6 km² of the area was covered with vegetation, 2.5 km² with water, 153.3 km² with settlement, and 125.6 km² with bare soil (Table 2). Fig. 4 and Fig. 5 show the LULC maps of the year 2000 and 2018 respectively and Fig. 6 highlights the circulation of different LULC classes in the Hesaraghatta watershed for the years 2000 and 2018. In the results, bare soil includes both barren lands as well as agricultural fallow land because the study area falls under the semi-arid zone. Most of the agricultural activities depend on rainfall only whereas the satellite data which is considered is of the summer season..

Upon comparing the LULC maps of the years 2000 and 2018, it is found that there was a massive change in the distribution of LULC classes. Between the years 2000 and 2018, the settlement increased from 74.6 km² to 153.3 km², vegetation increased from 98.3 km² to 125.6 km²,

Table 2: LULC distribution in Hesaraghatta watershed from 2000 to 2018.

LULC class	LULC in 2000		LULC in 2018	
	Area (km ²)	Percentage (%)	Area (km ²)	Percentage (%)
Water	1.1	0.18	2.5	0.40
Vegetation	98.3	16.24	125.6	20.75
bare soil	431.1	71.23	323.8	53.49
Settlement	74.6	12.32	153.3	25.33

waterbody increased from 1.1 km² to 2.5 km², and bare soil reduced from 431.1 km² to 323.8 km². In between these years, urbanization and industrialization have happened at a very greater rate i.e., 105.54% in the study area due to population growth and developmental activities as it is very nearer to Bengaluru city. There has been a significant decline in the bare soil i.e., 24.89% because most of the land was

converted into plantation and settlement. Table 3 and Fig. 7 highlights the percentage of changes in LULC classes in the study area. Accuracy assessment was done by a random sampling method by selecting 200 sampling points to check the accuracy of the classified images. The outcomes of this analysis indicate that the overall accuracy for the classified images of the years 2000 and 2018 is 92.31% and 87.50%,

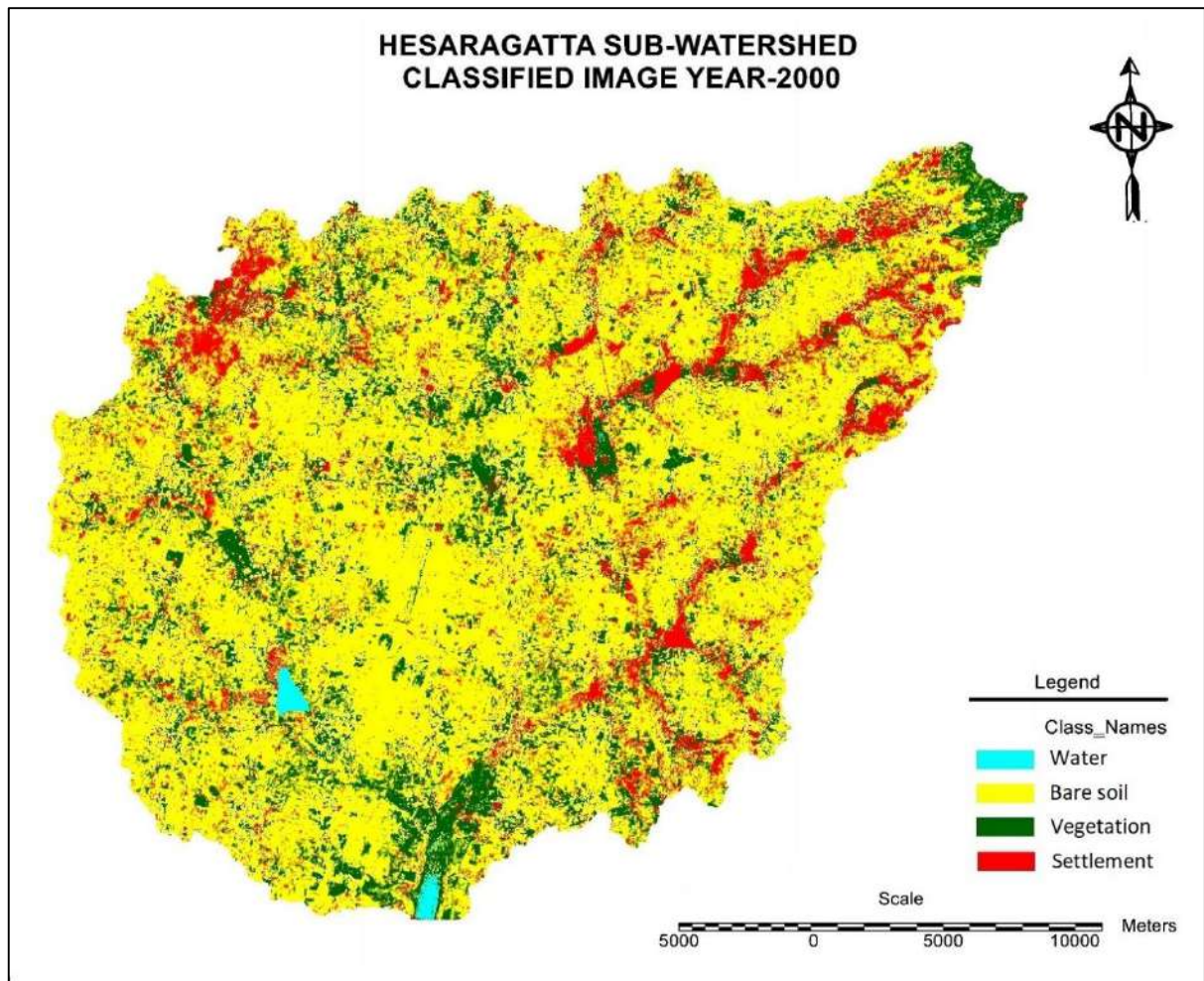


Fig. 4: LULC map of Hesaraghatta watershed, 2000.

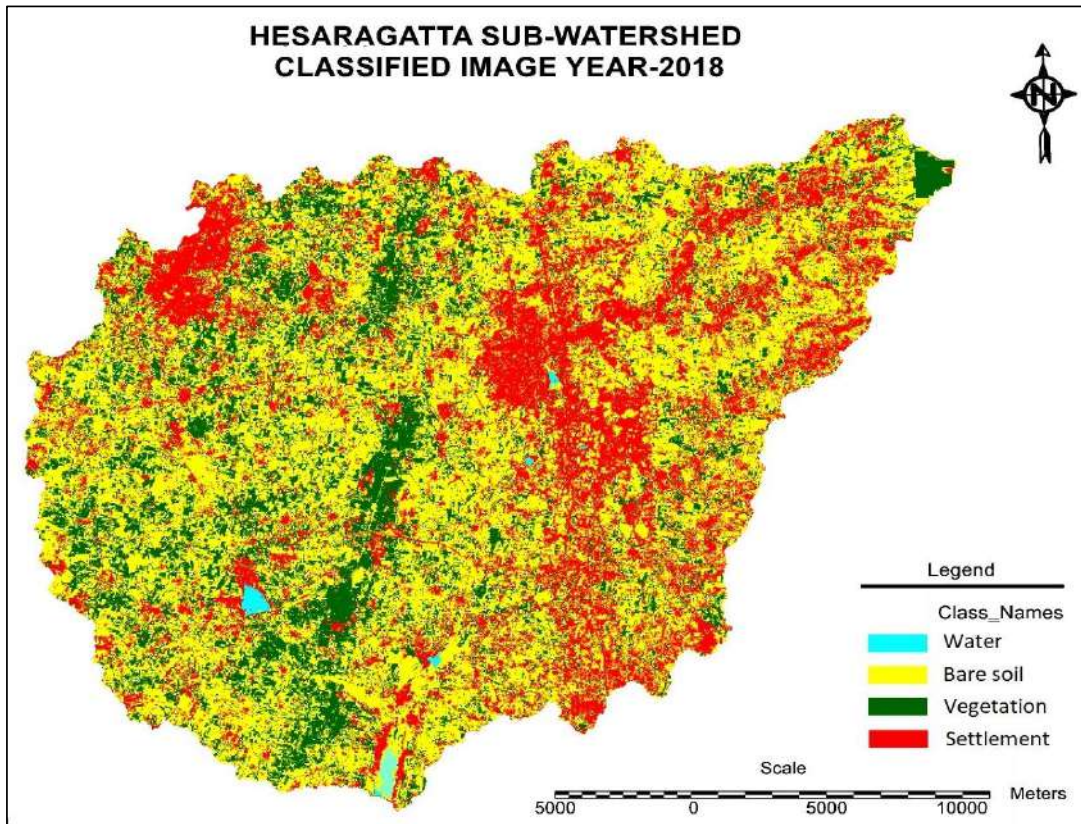


Fig. 5: LULC map of Hesaraghatta watershed, 2018.

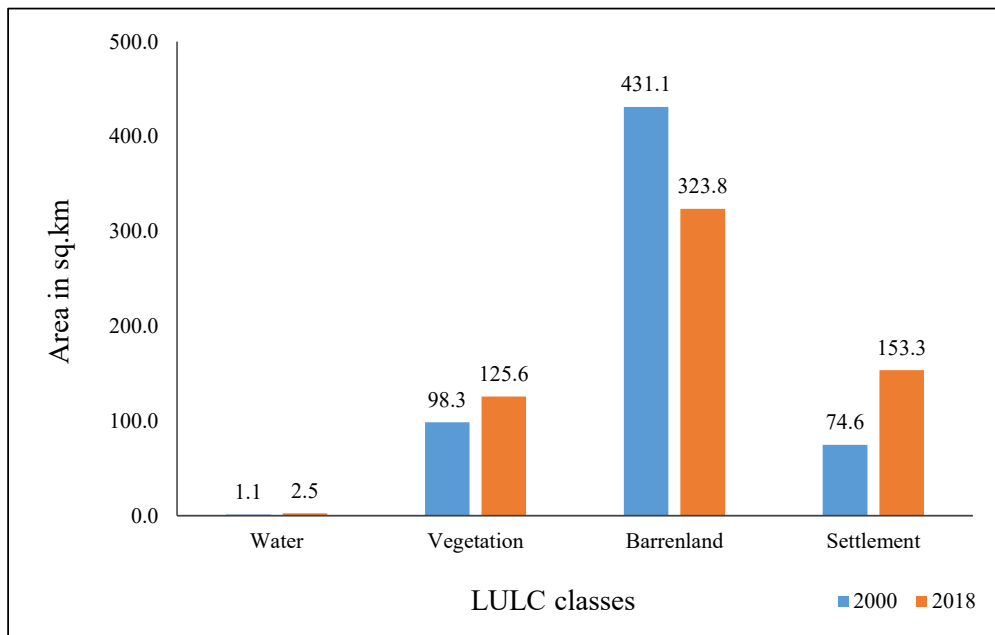


Fig. 6: Distribution of various LULC classes in the Hesaraghatta watershed.

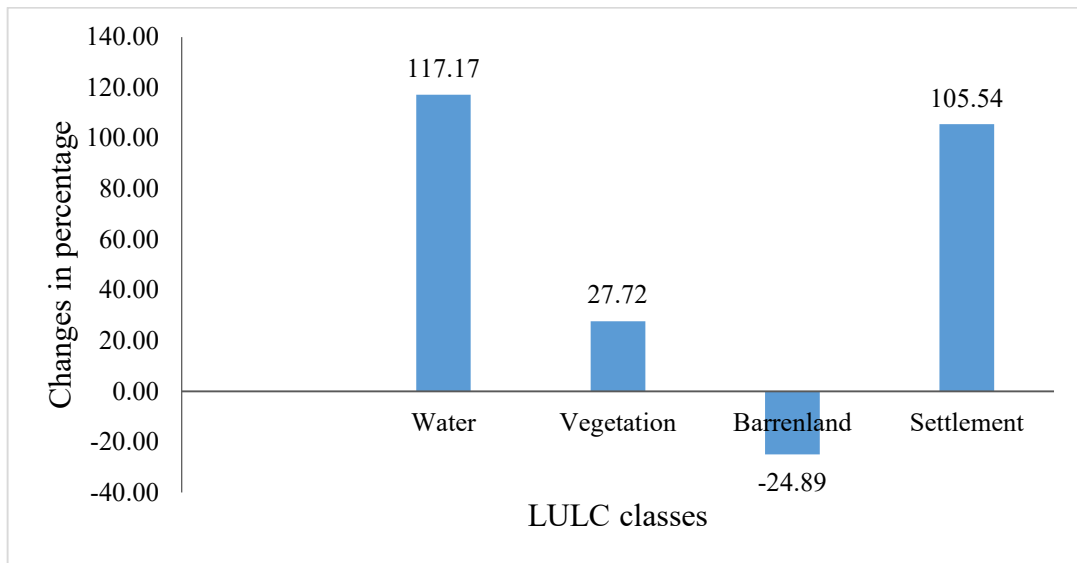


Fig. 7: Change in LULC classes from the year 2000 to 2018 in percentage.

Table 3: LULC assessment of Hesaraghatta watershed area.

LULC class	LULC in 2000	LULC in 2018	Change in the area from 2000 to 2018 (km ²)	Changes in %
	Area (km ²)	Area (km ²)		
Water	1.1	2.5	1.3	117.17
Vegetation	98.3	125.6	27.3	27.72
Bare soil	431.1	323.8	-107.3	-24.89
Settlement	74.6	153.3	78.7	105.54

and Kappa co-efficient for those years are 0.909 and 0.822 respectively. The Kappa coefficient values obtained portray that the accuracy of the image classification is acceptable.

CONCLUSION

The current study aimed at assessing the change in LULC classes in the Hesaraghatta watershed. This study discloses that the LULC pattern in the Hesaraghatta watershed has transformed significantly over 18 years. It is detected that there has been an escalation in the settlement in the study area due to population growth and developmental activities and it is also noticed that there is an increase in vegetation due to an increase in plantation, thereby reducing the amount of bare land. This study has also revealed that integration of GIS and Remote sensing can be a powerful tool for mapping and assessment of LULC changes in an area. Though, the accuracy of results is greatly influenced by interpretation.

REFERENCES

- Abd El-Kawy, O.R., Rød, J.K., Ismail, H.A. and Suliman, A.S. 2011. Land use and land cover change detection in the western Nile delta of Egypt using remote sensing data. *Appl. Geog.*, 31(2): 483-494. <https://doi.org/10.1016/j.apgeog.2010.10.012>
- Ali, D., Batool, S., Techato, K., Gyawali, S. and Suklueng, M. 2020. GIS-MCDM approach to determine forest plantation areas in the U-tapao river basin in Songkhla, Thailand. *Int. J. Integr. Eng.*, 12(2): 294-301. <https://doi.org/10.30880/ijie.2020.12.02.033>
- Anees, M.T., Abdullah, K., Nawawi, M.N.M., Rahman, N.N.N.A., Piah, A.R.M., Syakir, M.I., and Mohd Omar, A.K. 2017. Effect of upstream on downstream due to spatio-temporal land use land cover changes in Kelantan Peninsular, Malaysia. *Nat. Environ. Pollut. Technol.*, 16(1): 29-35.
- Belay, T. and Mengistu, D. A. 2019. Land use and land cover dynamics and drivers in the Muga watershed, Upper Blue Nile basin, Ethiopia. *Remote Sens. Appl.: Soc. Environ.*, 15: 100249.
- Bharath, A., Manjunatha, M., Tangadagi, R.B. and Preethi, S. 2020a. Environmental assessment for rainwater harvesting at GITAM Campus. *J. Green Eng.*, 10(4): 1776-1785.
- Bharath, A., Preethi, S., Manjunatha, M. and Tangadagi, R. B. 2020b. Prediction of temperature data for Ghataprabha. *Sub. Eco. Env. & Cons.*, 26: 140-144.

- Butt, A., Shabbir, R., Ahmad, S.S. and Aziz, N. 2015. Land-use change mapping and analysis using Remote Sensing and GIS: A case study of Simly watershed, Islamabad, Pakistan. *Egypt. J. Remote. Sens. Space Sci.*, 18(2): 251-259. <https://doi.org/10.1016/j.ejrs.2015.07.003>.
- Chen, W., Chi, G. and Li, J. 2019. The spatial association of ecosystem services with land use and land cover change at the county level in China, 1995–2015. *Sci. Total Environ.*, 669: 459-470. <https://doi.org/10.1016/j.scitotenv.2019.03.139>
- Chowdhury, M., Hasan, M.E. and Abdullah-Al-Mamun, M.M. 2020. Land use/land cover change assessment of Halda watershed using remote sensing and GIS. *Egypt. J. Remote. Sens. Space Sci.*, 23(1): 63-75.
- Das Kangabam, R., Selvaraj, M. and Govindaraju, M. 2019. Assessment of land use land cover changes in Loktak Lake in Indo-Burma Biodiversity Hotspot using geospatial techniques. *Egyptian J. Remote Sens. Space Sci.*, 22(2): 137-143. 5
- EarthExplorer. (n.d.). USGS. <https://earthexplorer.usgs.gov/> (accessed January 4, 2021)
- Garg, V., Nikam, B.R., Thakur, P.K., Aggarwal, S.P., Gupta, P. K. and Srivastav, S.K. 2019. Human-induced land uses land cover change and its impact on hydrology. *HydroResearch*, 1: 48-56.
- Gebeyehu, A.E., Chunju, Z. and Yihong, Z. 2019. Assessment and mapping of land-use change by remote sensing and GIS: A case study of Abaya Chamo Sub-basin, Ethiopia. *Nat. Environ. Pollut. Technol.*, 18(2): 549-554.
- Imran Basha, U., Suresh, U., Sudarsana Raju, G., Rajasekhar, M., Veeraswamy, G. and Balaji, E. 2018. Landuse and landcover analysis using remote sensing and GIS: A case study in the Somavathi river, Anantapur district, Andhra Pradesh, India. *Nature Environ. Pollut. Technol.*, 17(3): 1029-1033.
- Mallupattu, P.K. and Sreenivasula Reddy, J.R. 2013. Analysis of land use/land cover changes using remote sensing data and GIS at an Urban Area, Tirupati, India. *Sci. World J.*, 2013: 1-7.
- Nayak, P.M. and Byrne, M.L. 2019. Impact of land use land cover change on a sand dune ecosystem in Northwest Beach, Point Pelee National Park, Canada. *Journal of Great Lakes Research*, 45(6): 1047-1054.
- Preethi, S., Tangadagi B.R., Manjunatha, M. and Bharath, A. 2020. Sustainable effect of chemically treated aggregates on bond strength of bitumen. *J. Green Eng.*, 10(9): 5076-5089.
- Rimal, B., Sharma, R., Kunwar, R., Keshtkar, H., Stork, N. E., Rijal, S., Rahman, S. A. and Baral, H. 2019. Effects of land use and land cover change on ecosystem services in the Koshi River Basin, Eastern Nepal. *Ecosyst. Serv.*, 38: 100963.
- Salunke, S. and Chavan, B. 2020. Imperious approach towards justifiable strategic lake sediment regulation. *Nature Environ. Pollut. Technol.*, 19(1), 339-348.
- Somashekar, R.K., Ravikumar, P., Sowmya, S.V., Dar, M.A., and Ravikumar, A.S. 2011. Runoff estimation and morphometric analysis for Hesaraghatta watershed using IRS-1D LISS III FCC satellite data. *J. Indian Soc. Remote Sens.*, 39(1): 95-106.
- Tsai, Y.H., Stow, D., An, L., Chen, H.L., Lewison, R. and Shi, L. 2019. Monitoring land-cover and land-use dynamics in Fanjingshan national nature reserve. *Appl. Geog.*, 111: 10-20
- Wang, L., Wang, S., Zhou, Y., Zhu, J., Zhang, J., Hou, Y. and Liu, W. 2020. Landscape pattern variation, protection measures, and land use/land cover changes in drinking water source protection areas: A case study in Danjiangkou Reservoir, China. *Global Ecol. Cons.*, 21: e00827.
- Wang, X., Gong, W., Huang, X., Liu, T., Zhou, Y. and Li, H. 2018. Assessment of eco-environmental quality on land use and land cover changes using remote sensing and GIS: A case study of Miyun county. *Nat. Environ. Pollut. Technol.*, 17(3): 739-746.



Biodiesel Extraction from Chicken Fat and Its Effect on the Performance and Emission Characteristics of the Diesel Engine

V. Hariram[†], J. Godwin John, Subramanyeswara Rao, S. K. Baji Babavali, S. Muni Lokesh, D. Tejeswar Reddy and S. Seralathan

Hindustan Institute of Technology and Science, Padur, Chennai-603103, Tamil Nadu, India

[†]Corresponding author: V. Hariram; connect2hariram@gmail.com

Nat. Env. & Poll. Tech.
Website: www.neptjournal.com

Received: 01-05-2021

Revised: 12-06-2021

Accepted: 01-07-2021

Key Words:

Biodiesel
Chicken fat
Emission
Performance
Transesterification

ABSTRACT

This study focuses on the conversion of chicken fat into chicken fat methyl ester (CFME) and its use in the diesel engine. Baseline fuel i.e., diesel and chicken fat biodiesel are the fuels tested to study their effect on the performance and emission characteristics of diesel engines. To enhance the performance and emission characteristics, ethanol up to 20% is added as an additive to the chicken fat biodiesel. The physiochemical properties revealed that the fuel blends properties are closer to the diesel fuel. The experimental investigations revealed that additive blended biodiesel enhanced the performance by reducing the brake-specific fuel consumption and increasing the brake thermal efficiency. Moreover, the emissions are considerably reduced by the additive blended chicken fat biodiesel. Therefore, chicken fat biodiesel can be considered as a substitute fuel to be used in the diesel engine without any modifications.

INTRODUCTION

The rise in the price of fossil fuels, global economy, environmental awareness, and strict enforcement of norms by the pollution control board are the reasons that the development of alternate fuels became important. The search for alternate fuel to the diesel engine has become a recent trend in the research due to the depletion of fossil fuel. Using alternate fuels as biofuel can significantly reduce the implications on the greenhouse gas effects in the environment. In the entire ecosystem, CO₂ is viewed as a serious problem in terms of climate change. In the automobile sector, it is seen as a serious problem as emissions are to be controlled since fuel combustion causes heavy CO₂ emissions.

The search for alternate fuel for diesel engines has intensified in recent years with the imminent depletion of fossil fuel in near future. Among the alternative fuel options, biodiesel is currently favored in the land and sea transportation sectors due to the modern biodiesel production technology, and the compatibility of use of biodiesel with existing compression ignition engines without any major modifications. Waste cooking oil is identified as an alternative resource due to its lower price compared with other fuel sources. Besides this, another widely available resource is animal fat oil. Especially, chicken fat oil can be considered for alternate fuel resource as it has the highest biodiesel potent.

Harsh et al. (2019) detailed the research conducted on reducing emissions through the use of additives in biodiesel. The addition of additives had significantly reduced the emissions in the diesel engine. Mehmet (2019) investigated the emission and performance of the diesel engine when the fuel was added with 15% propanol. The injection pressure was also varied to optimize performance parameters by reducing emission. The reduction in injection pressure improved fuel consumption. Also, there was a considerable reduction in the emission of smoke and oxides of nitrogen due to the addition of alcohol.

Kamel et al. (2019) conducted an experimental study on the emission and performance analysis of ternary waste cooking oil biodiesel-diesel-propanol blends. The results revealed that the addition of propanol to the diesel fuel reduced the emissions of carbon monoxide, oxides of nitrogen, and smoke besides reducing exhaust gas temperature. Deepak et al. (2020) presented the results of an experimental examination into the effects of metal-based additions in biodiesel blends. The chicken fat oil biodiesel was used as the fuel. The experiment was done under varied conditions and the results showed that the addition of the metal-based additives improved the performance of the engine and reduced the engine emissions.

Dhanasekaran et al. (2019) discussed the utilization of waste cooking oil in a light-duty diesel engine to minimize emissions. The research was aimed to replace diesel with waste cooking oil by taking three blend ratios. Finally, the authors concluded that emissions gradually decreased with an increase in n-propanol addition for all the blends. Moreover, instead of treating it as a contaminated waste, the waste oil was put into good usage as fuel to achieve reduced emission. Vivian et al. (2016) investigated the effects of biodiesel made from swine and chicken fat residues on the diesel engine emissions like carbon monoxide, carbon dioxide, and nitrogen oxide. Biodiesel was produced from the chicken and swine fat wastage. It was observed that fuel consumption increased by up to 5%, whereas engine emissions were observed to reduce drastically. This study showed the way that chicken and swine fat wastages can be used to producing biodiesel and its use in the diesel engine.

McCarthy et al. (2011) analyzed and compared the performance and emissions of an internal combustion engine fuelled with petroleum diesel and different biodiesels sourced from canola, palm, and beef tallow. Two different types of biodiesels were tested and analyzed with different blend ratios which showed a lower exhaust emission and better performance for Type 'A' in comparison with Type 'B'. But the performance reported was not so high as compared with the reduction of two emissions namely, CO and NO_x. Mofijur et al. (2016) investigated the role of biofuel and its binary (diesel–biodiesel) and ternary (ethanol–biodiesel–diesel) blend on reduction of emissions in internal combustion engines. Using up to 10% ethanol–25% biodiesel in the petroleum-based diesel provided better results.

Ilker et al. (2017) experimented on the performance, emission, and combustion characteristics of a compression ignition engine using biofuel blends. Biodiesel and bioethanol were used for testing the performance of compression ignition engines. Using Bio-ethanol increased the brake-specific fuel consumption and volumetric efficiency. The combustion analysis was like the diesel fuel. Using bioethanol proved to reduce the emission like HC and smoke opacity. Ali Turkcan (2020) discussed the effects of different types of biodiesels and biodiesel-bioethanol-diesel blends on the cyclic variations and correlation coefficient. It was noted from the result that the fuel properties had much more effective due to the coefficient variation and correlation coefficient while comparing with the engine load.

Zaharin et al. (2017) investigated the influence of physicochemical features of biodiesel-alcohol fuel blends on diesel engine performance and emissions. Alcohol additives had good fuel properties that reduced viscosity and the presence of oxygen. This resulted in better engine combustion and

improved the performance in terms of thermal efficiency which in turn reduced the engine emissions considerably. Hence, adding alcohol-based additives provided better results for biodiesel.

Based on these studies, it can be understood that biodiesel is a good alternative resource for diesel fuel. Also, using biodiesel leads to a significant reduction in CO₂. The disposal of chicken waste is causing ecological problems. Moreover, chicken fat is a waste product that is used as a resource for biofuel production. Hence, the objective of this study is to evaluate the effect of adding an additive to the produced biodiesel from chicken fat which is used as fuel and to optimize the blend ratios in terms of performance and emission characteristics of the diesel engine.

MATERIALS AND METHODS

Oil Extraction

The source for bio-oil production is chicken fat. The chicken fat is collected from the slaughterhouse of the poultry farm. The chicken fat is then washed with water, later it is cleansed with de-ionized water. The fat is made free from the flesh and skin of the chicken. The free fatty acid content present is found to be 4.16% which is high, and hence it should be pretreated. Using the magnetic stirrer, the fat content is dissolved for 30 minutes by maintaining it at a temperature of 60°C upon considering the fat weight and molar to fat ratio of 20% of sulphuric acid as weighed at 40:1 ratio. This acid is added with the alcohol in a beaker (250 mL capacity) and then it is poured into the fat-containing flask. Now, the mixture is taken into a water bath in which temperature is regulated at 60°C and the speed is kept at 150 rpm for 80 minutes. When the process is over, the mixture is left in the

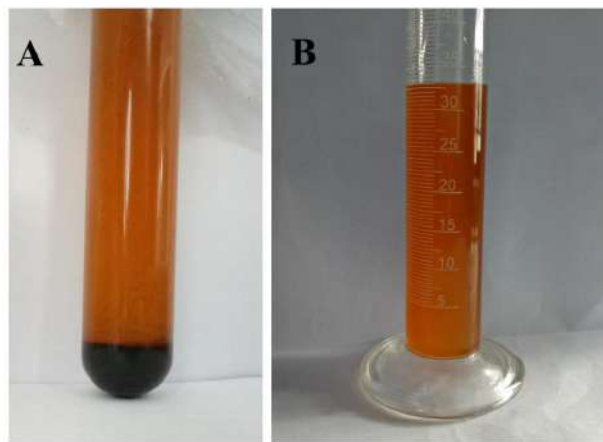


Fig. 1 (A) Chicken fat oil and its (B) biodiesel.

Table 1: Comparison of properties of chicken fat methyl esters and diesel.

Properties	CFME	Diesel	ASTM standards for Biodiesel	Method
Density at 15°C kg.m ⁻³	870	830	860- 900	D4052
Kinematic Viscosity at 40°C mm ² .s ⁻¹	4.386	2.6	1.9 – 6	D445
AV mg of KOH.gm ⁻¹ of oil	0.16	0.35	<0.8	D664
Cloud point, °C	0.8	-8	NA	D2500
Iodine value, G I ₂ /100 gm	80	NA	115	D1959

separating funnel overnight to get settled. Later, three layers are observed in which the underneath layer is chicken fat (Godwin et al. 2017a). This pretreated fat is found to have 0.43% FFA content which can be taken care of with the transesterification process. The bio-oil content is shown in Fig. 1A.

Transesterification

To convert the fat into biodiesel, alkaline-based transesterification is carried out. The fat is mixed with the methanol using an Erlenmeyer flask. The reaction catalyst used is NaOH. This reaction environment is maintained at 65°C, 400 rpm agitating speed, and 120 minutes reaction period. This process yielded 95.2% converted biodiesel. The extracted biodiesel is shown in Fig. 1B.

Fuel Properties

The fuel properties are determined in the Fuels and Lubricant Testing Laboratory, Hindustan Institute of Technology and Science, Chennai. Based on the experimentation, the density of the chicken fat methyl ester (CFME) is found to be 870 kg.m⁻³, and kinematic viscosity is 4.386 mm².s⁻¹. The values of the diesel fuel and Chicken fat biodiesel are shown in Table 1.

Test Fuel Formulation

Ultrasonication is the method used to blend the fuel. The fuels blended are Diesel, Ethanol, and Diethyl ether. Ethanol is added with diesel because it has a high latent heat of vaporization. The globally accepted blend ratio is B20, hence this is used in this research work D80 CFB20 (80% of conventional diesel and 20% of chicken fat biodiesel). In this experimental study 10% of ethanol is added to D80 CFB20 to enhance the performance of the engine (which is D80 CFB20 E10) and further to check its improvisation performance, 20% ethanol is added as the next fuel (which

Table 2: Specifications of the test engine.

Rated power (kW)	5.2
Bore (mm)	87.50
Stroke (mm)	110.00
Compression ratio	17.5:1
Speed (rpm)	1500
Injection pressure (bar)	210
Injection timing	23° BTDC

is D80 CFB20 E20). Based on the mixing capability and stability, the mass balance was achieved in these fuel blends. Considering the miscibility of ethanol additive with diesel – biodiesel blend, the fuel D80 CFB20 E10 was formulated as (Diesel 72.72%, biodiesel 18.18%, and ethanol 9.09%) and similarly D80 CFB20E20 (Diesel 66.67%, biodiesel 16.67%, and ethanol 16.67%) which helps to achieve the mass balance (Godwin et al. 2017b).

Experimental Setup

The experimentation is carried out in the Engine Testing Laboratory, Hindustan Institute of Technology and Science, Chennai. Direct injection water-cooled single-cylinder four-stroke constant speed compression ignition (CI) engine is used to determine the performance and emission characteristics. This engine is attached with an eddy current dynamometer which is water-cooled. The speed of the CI engine is kept constant at 1500 rpm. The engine is tested under stable state conditions and the engine setup is shown in Fig. 2 A and 2B. The technical features of the CI engine are listed in Table 2. The emission characteristics are measured using AVL444 gas analyzer and Bosch Smoke meter.

RESULTS AND DISCUSSION

This section explains the performance and emission characteristics of the test fuel, chicken fat methyl ester (CFME), and its blends used in the direct injection single cylinder compression ignition engine.

Brake Specific Fuel Consumption

Brake specific fuel consumption (BSFC) is the energy spent to produce useful power output, which is a measure of fuel efficiency of the CI engine. Fig. 3 represents the variations in BSFC with respect to brake mean effective pressure of diesel, D80 CFB20, D80 CFB20 E10 and D80 CFB20 E20 blends. For the highest engine load conditions, the data observed for the fuel blends D100, D80 CFB20, D80 CFB20 E10 and D80 CFB20 E20 are 0.24 kg.kWh⁻¹, 0.28 kg.kWh⁻¹, 0.24 kg.kWh⁻¹ and 0.25 kg.kWh⁻¹ respectively.

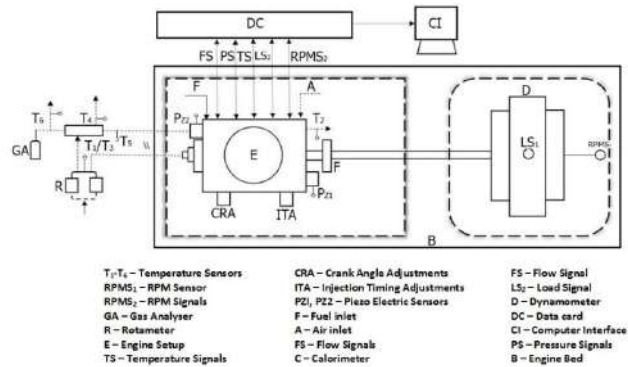


Fig. 2: (A) Engine Testbed, (B) Schematic Setup.

As can be observed, the B20 blend consumed more fuel than other fuel blends. This may be due to higher viscosity and density resulting in improper mixture formation inside the cylinder. Assimilated additive in the blend boosted the combustion thereby lowering the fuel consumption which may be due to higher miscibility (Hariram et al. 2017). Comparing all the blends, D80 CFB20 E10 showed the lowest fuel consumption, and also it is nearly equivalent to diesel fuel.

Brake Thermal Efficiency

The ratio between brake power output and fuel power determines the thermal efficiency of the CI engine. The variations

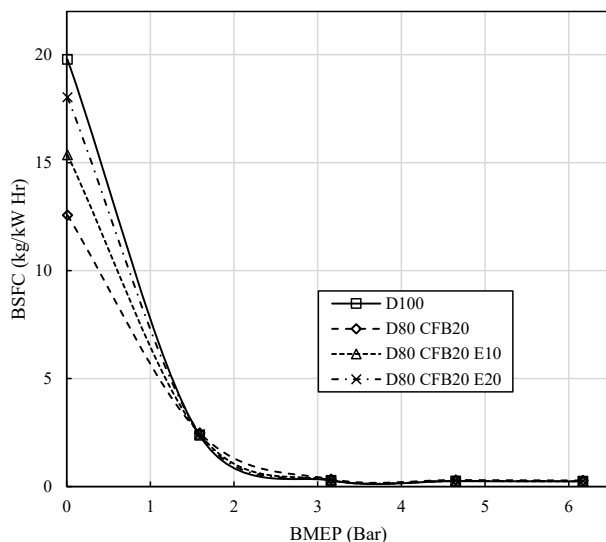


Fig. 3: Brake specific fuel consumption.

of the brake thermal efficiency against brake mean effective pressure is detailed in Fig. 4.

Brake thermal efficiency of diesel fuel and its blends are 35.47% (D100), 33.03% (D80 CFB20), 34.77% (D80 CFB20 E10) and 37.8% (D80 CFB20 E20) at full load conditions. At low load conditions, the diesel fuel showcased a higher brake thermal efficiency. As the load is increased, the additive blend showcased the highest efficiency. This may be due to the availability of the excess amount of oxygen leading to proper combustion (Hariram et al. 2019). Surface tension between the CFME and diesel fuel (D80 CFB20) might be poor because of which the atomization became inferior leading to inferior performance of the CI engine.

Unburned Hydrocarbon Emission

Unburned hydrocarbon (UBHC) emission usually occurs due to improper combustion, deposits of carbon in crevice volume, and low temperatures. The variations of UBHC emission with BMEP are depicted in Fig. 5. The UBHC emissions for D100 and D80 CFB20 are found to be 36 ppm, and 35ppm, respectively at higher loads. The ethanol addition made the evaporation easier at increased cylinder temperature. This leads to better combustion and as can be seen in Fig. 5, at higher loads, the UBHC emission is lower compared to diesel fuel. As observed in Fig. 5, as the load increased, the UBHC emission is reduced due to better combustion.

Carbon monoxide emission

Improper combustion leads to CO emission. The variation in CO emissions with respect to BMEP at various load condi-

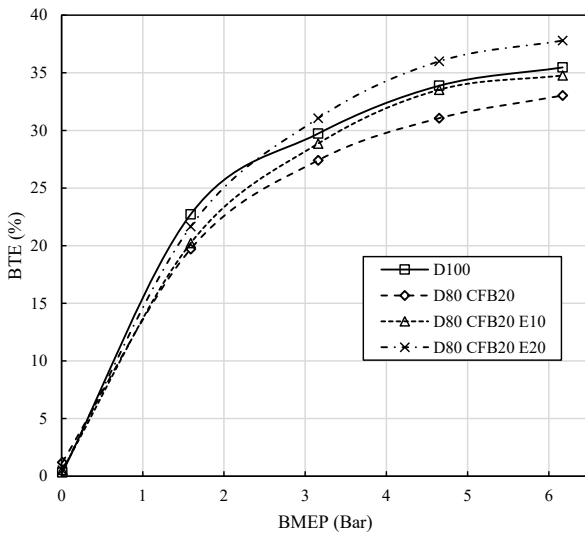


Fig. 4: Brake thermal efficiency.

tions is shown in Fig. 6. The values of the CO emissions as recorded in Fig. 6 are 0.112% (D100), 0.17% (D80 CFB20), 0.083% (D80 CFB20 E10) and 0.073% (D80 CFB20 E20) respectively. D80 CFB20 showcased a higher formation of CO which may be due to the higher density and viscosity of the biodiesel blend leading to incomplete combustion. A decrease in CO emission by supplementation of additive may be due to the complete combustion of the blend inside the chamber because of the reduced viscosity. This may be due to better atomization of the fuel resulting in complete combustion thereby reducing the CO formation.

Oxides of Nitrogen Emission

At elevated temperatures inside the combustion zone, nitrogen mixes with air to forms the oxides of nitrogen. The

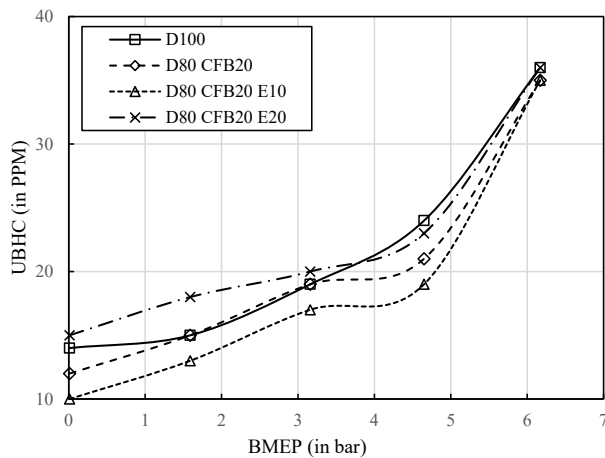


Fig. 5: Unburned hydrocarbon emission.

variations in NO_x emissions are detailed in Fig. 7. At full load conditions, the NO_x emissions released by the fuels D100, D80 CFB20, D80 CFB20 E10, and D80 CFB20 E20 are 1744 ppm, 1685 ppm, 1688 ppm, and 1741 ppm, respectively. All the biodiesel blends showed lower values in comparison with diesel fuel which means that the biodiesel fuel is better with respect to NO_x emissions. The highest value of NO_x emissions among biodiesel blends is reported for the D80 CFB20 E20 fuel blend. This may be due to the additional oxygen content and reduced viscosity which improved the combustion behavior thereby increasing the temperature inside the chamber wherein the Zeldovich Mechanism give rise to the increased level of NO_x emissions.

Smoke Emission

Figure 8 shows the variations of smoke opacity levels with respect to BMEP. It is observed that fuels D100, D80 CFB20, D80 CFB20 E10 and D80 CFB20 E20 showed the

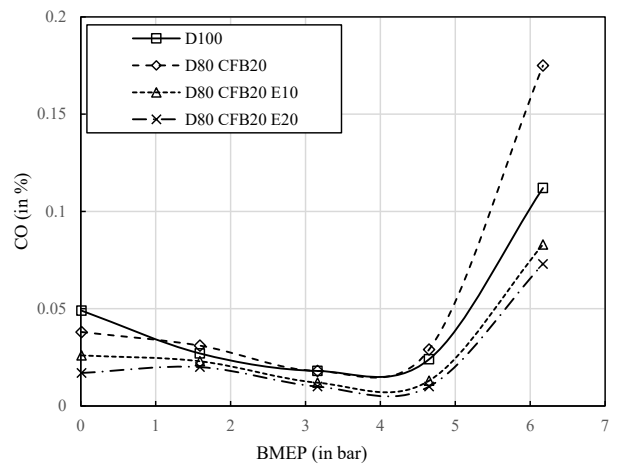


Fig. 6: Carbon Monoxide Emission.

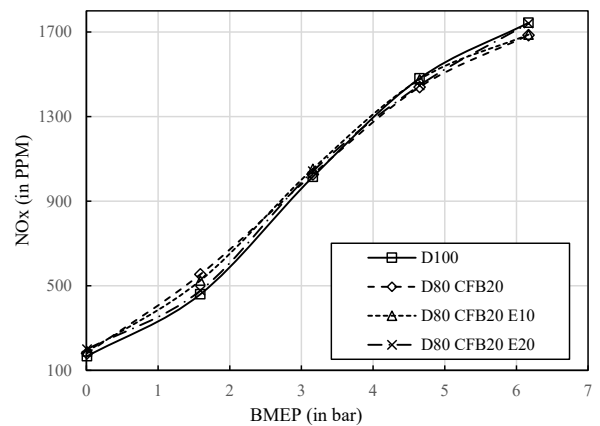


Fig. 7: Oxides of Nitrogen Emission.

smoke opacity values as 61.83%, 64.8%, 57.3% and 57.8% respectively at full load conditions. As can be observed, the diesel and D80 CFB20 blend give higher smoke opacity values than the additive added fuel blends. The reduced smoke formation of the biodiesel blends with additive may be due to the availability of surplus oxygen content at an increased temperature which oxidizes the carbon matter thereby preventing it from getting deposited in the chamber.

Carbon Dioxide Emission

Fig. 9 details the carbon dioxide emission variations with BMEP at all loads for the fuels D100, D80 CFB20, D80 CFB20 E10 and D80 CFB20 E20. As the load is increased, CO₂ emissions also increased. CO₂ emission values are reduced for the biodiesel blends. This is due to the availability of the oxygen content. Also, it can be noted that the results of carbon dioxide emissions at full load condition are 8.85%, 8.8%, 8.49% and 8.45% for fuels D100, D80 CFB20, D80 CFB20 E10 and D80 CFB20 E20 respectively. Due to oxygen content availability, CO is converted into CO₂. Moreover, the conversion of CO to CO₂ is better than the toxic CO emissions coming out as engine emissions. The released carbon dioxide can be considered as an environment-friendly aspect rather than releasing CO emissions to the environment as globally it is known that ground-level CO₂ is manageable.

CONCLUSION

Experimental investigations on the use of chicken fat methyl ester (CFME) and, its blends in the diesel engine are analyzed in terms of performance and emission characteristics. The chicken fat methyl ester is extracted from the waste chicken fat. The performance of the diesel engine is

evaluated in terms of brake-specific fuel consumption and brake thermal efficiency, whereas the emission parameters are evaluated through UBHC, CO, NO_x, Smoke, and CO₂ emission values. Additive-based fuel blend, D80 CFB20 E10 recorded the lowest fuel consumption while D80 CFB20 E20 reported the highest brake thermal efficiency. D80 CFB20 E10 showcased the lowest HC emission throughout different loading conditions whereas the lowest CO emission is given by the D80 CFB20 E20 blend. Among all the tested biodiesel blends, the highest emission values of oxides of nitrogen are released by the D80 CFB20 E20 blend. D80 CFB20 E10 fuel blend showed the lowest smoke emission. Based on the data obtained, it can be concluded that chicken fat biodiesel can be used as a substitute fuel in the CI engine without any modification in the engine. Moreover, adding the additive to this biodiesel further increases the performance and controls the emission levels of the diesel engine.

REFERENCES

- Ali Turkcan, M. 2020. The effects of different types of biodiesels and biodiesel-bioethanol-diesel blends on the cyclic variations and correlation coefficient. *Fuel*, 261: 116453.
- Deepak, K.T., Manjunatha, T.K.S. and Ramesha, D.K. 2020. Experimental investigation on the influence of metal-based additives on diesel engines along with biodiesel blends. *Mater. Today: Proceedings*, 38(1): 407-412.
- Dhanasekaran, R., Ganesan, S., Rajesh Kumar, B. and Saravanan, S. 2019. Utilization of waste cooking oil in a light-duty DI diesel engine for cleaner emissions using bio-derived propanol. *Fuel*, 235: 832-837.
- Godwin, J.J., Hariram, V., Seralathan, S. and Jaganathan, R. 2017a. Effect of oxygenating on emission and performance parameters of a CI engine fuelled with blends of diesel-algal biodiesel. *Int. J. Renew. Energy Res.*, 7(4): 2041-2047.
- Godwin, J.J., Hariram, V. and Seralathan, S. 2017b. Emission reduction using improved fuel properties of algal biodiesel and its blends. *Energy Sour. A: Recov. Util. Environ. Eff.*, 40(1): 45-53.

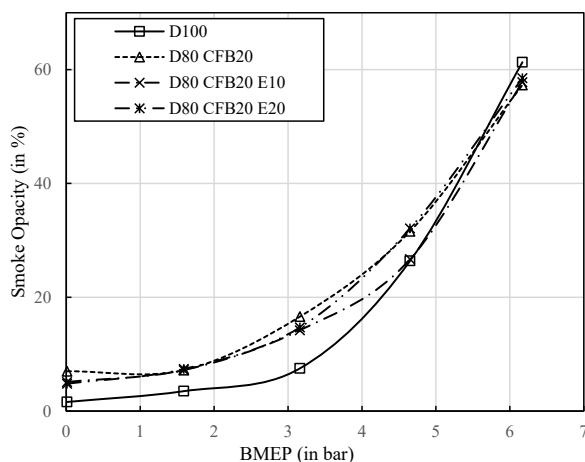


Fig. 8: Smoke Emission.

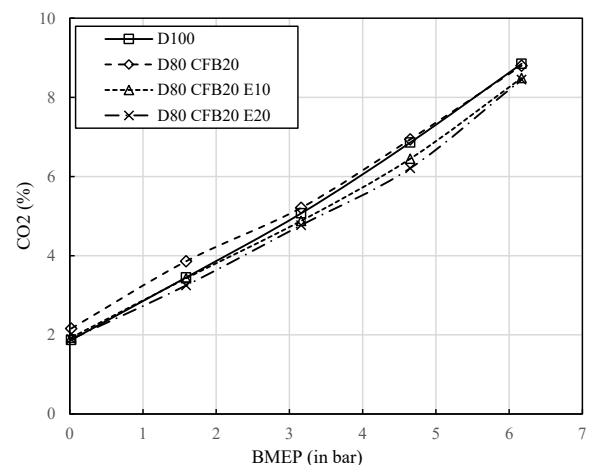


Fig. 9: Carbon dioxide emission.

- Harsh, K., Hardik, B., Yuvrajsinh, D. and Sajan, C. 2019. Investigation of emulsion and effect on emission in CI engine by using diesel and bio-diesel fuel: A review. *Egypt. J. Pet.*, 28: 323-337.
- Hariram, V., Godwin, J.J. and Seralathan, S. 2017. Cottonseed biodiesel as alternative fuel: Production and its characterization analysis using spectroscopic studies. *Int. J. Renew. Energy Res.*, 7(3): 1333-1339.
- Hariram, V., Godwin, J.J. and Seralathan, S. 2019. Impact of oxygenated cotton seed biodiesel on combustion, performance, and emission parameters in a direct injection CI engine. *International Journal of Ambient Energy*, 40 (2): 158-169.
- Ilker, O., Ali, K. and Murat, C. 2017. Performance, emission, and combustion analysis of a compression ignition engine using biofuel blends. *Thermal Sci.*, 21(1B): 511-522.
- Kamel, B., Atabani, A.E., Sutha, S., Mohammed, M.N., Gediz, U., Orhan, A., Gopalakrishnan, K., Abdulkadir, A. and Awais, B. 2019. Fuels properties, characterizations, and engine and emission performance analyses of ternary waste cooking oil biodiesel–diesel–propanol blends. *Sustain. Energy Technol. Assess.*, 35: 321-334.
- McCarthy, P., Rasul, M.G. and Moazzem, S. 2011. Analysis and comparison of performance and emissions of an internal combustion engine fuelled with petroleum diesel and different bio-diesels. *Fuel*, 90: 2147-2157.
- Mehmet, S. 2019. The effect of the injection pressure on a single cylinder diesel engine fueled with propanol–diesel blend. *Fuel*, 254: 115617.
- Mofijur, M., Rasul, M.G., Hyde, J., Azad, A.K., Mamat, R. and Bhuiya, M.M.K. 2016. Role of biofuel and their binary (diesel-biodiesel) and ternary (ethanol-biodiesel-diesel) blends on internal combustion engines emission reduction. *Renewable and Sustain. Energy Rev.*, 53: 265-278.
- Vivian, F., Anildo, C., Marina, C., De, P., Marcio, L., Busi, D.S., Rodrigo, D.S.N., Martha, M.H., Arlei, C. and Paulo, G.D.A. 2017. Effects of biodiesel made from swine and chicken fat residues on carbon monoxide, carbon dioxide, and nitrogen oxide emissions. *J. Air Waste Manag. Assoc.*, 67(7): 754-762.
- Zaharin, M.S.M., Abdullah, N.R., Najafi, G., Sharudin, H. and Yusaf, T. 2017. Effects of physicochemical properties of biodiesel fuel blends with alcohol n diesel engine performance and exhaust emissions: A review. *Renew. Sustain. Energy Rev.*, 79: 475-493.



GIS-Based Digital Terrain Analysis of Assam-Meghalaya Foothills in Kamrup District, Assam

C. Borpujari† and A. K. Bora

Department of Geography, Guwahati University, Guwahati-781014, Assam, India

†Corresponding author: C. Borpujari; chinmoyeeeb@gmail.com

Nat. Env. & Poll. Tech.
Website: www.neptjournal.com

Received: 24-01-2021

Revised: 22-03-2021

Accepted: 14-04-2021

Key Words:

Terrain

Geomorphology

Foothills

GIS

Digital terrain analysis

ABSTRACT

Terrain characteristics and their evaluation usually come under geomorphological study and more particularly the applied geomorphological study (Prasad & Sarkar 2011). Foothills are a geographically defined zone having a gradual increase in elevation at the base of a mountain or hill range. Detailed assessment of the present terrain parameters of the study area using GIS is significant as it shows the influence on the landscape of the area. It is a prerequisite in effective management of the impact of transition upon the landscape and its natural resources for sustainable management. In the study, an attempt has been made to delineate the foothill belt of the Assam-Meghalaya border in Kamrup District, Assam using Geographical Information system (GIS), and remote sensing techniques. Datasets available from USGS Earth Explorer, i.e. Shuttle Radar Topographic Mission (SRTM) and Digital Elevation Model (DEM) are used for analyzing the elevation, contour, slope, and terrain characteristics. The present study aims at getting an information archive of the geomorphological and terrain characteristics of the Assam-Meghalaya foothills in Kamrup District, Assam, and its spatio-temporal variations.

INTRODUCTION

The general configuration of the landscape, its geology, climate, and other natural features define the terrain. Terrain means landscape or the 'Lay of land'. Terrain classification is a process of classifying the earth's surface based on the similarities in terrain properties, geomorphology, geological and morphometric properties, soil types, etc. into different units (Saha et. al. 2019). Evaluation of terrain characteristics and analysis of geo-environmental changes are considered important themes in geographical studies. With the introduction of digital spatial technology, the use of quantitative measurements to evaluate, monitor, and interpret landform changes is becoming more prevalent (Summerfield 1997, Wood 1996). The analysis of the terrain characteristics included delineation of the various terrain features, such as elevation, elevation profile, geology, hydrogeology, geomorphological units, soil, and contours. The landforms observed in the present day are the result of the long-term interactions between the elements of the geosphere, atmosphere, and hydrosphere (Manjare et.al. 2020). Surface subsurface materials, as well as the area's landforms, are depicted in the representation of geomorphological features. Sketches and maps of landscapes and landforms (Dykes 2008) have been used in Digital Terrain Analysis to analyze and visualize earth surface features ever since early geomorphological research. Mapping of terrain and geomorphological characteristics can

act as a preliminary tool for the baseline study of landscape ecology, forestry, soil science, land management, geomorphological and geological assessment (Cooke & Doornkamp 1990, Dramis et al. 2011, Paron & Claessens 2011). Digital Elevation Model is simply called the digital description of the earth's surface or terrain condition of earth as a whole or part of it (Bolstad & Stowe 1994). These are widely used in earth sciences for terrain and topographic study. The application of GIS is an essential tool for digital terrain analysis. The analysis of topographic attributes of a particular area depends on elevation data acquired from satellite imagery, contour lines generated from topographic maps, and ground surveys (Wilson & Gallant 2000). Foothills are the transitional eco-sensitive zone with low relief hills between the plains and topographically high mountains. The study of the terrain characteristics of these foothills is thus important in sustainable resource utilization and planned development with an eco-centric viewpoint in the study area.

Study Area

The study area is confined to the Assam-Meghalaya foothill belt bordering the Kamrup district of Assam. Kamrup district is surrounded by Kamrup Metropolitan district in the east, Goalpara district in the west, Darrang district in the north and Meghalaya state in the south (Fig. 1). The foothill zone occupies a total geographical area of 778.27 km². The northern

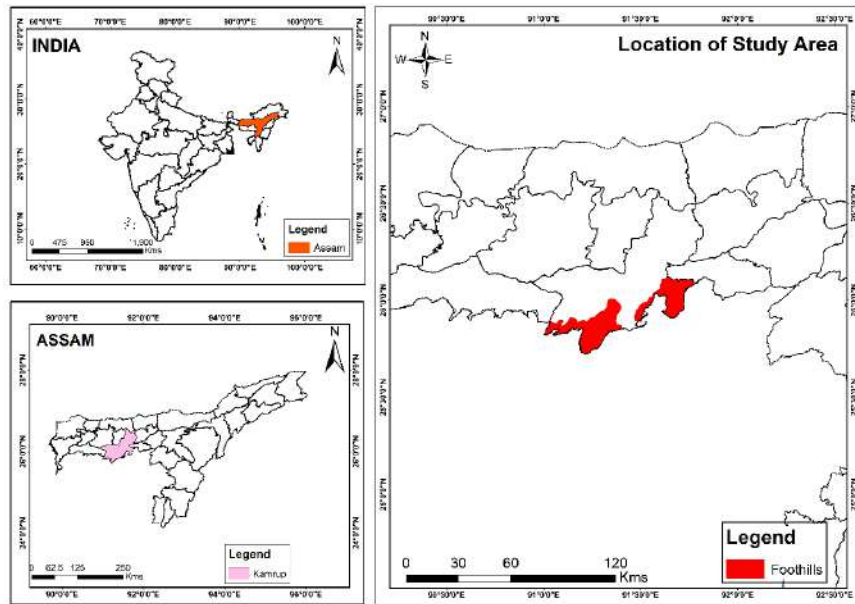


Fig. 1: Location of the study area.

foothills of the Meghalaya plateau along the Assam-Meghalaya border are formed of Achaean rocks, which comprise the metamorphic rock types of gneisses and schist. This foothill belt of the Assam-Meghalaya border is the northward projections of Garo hills and the Khasi-Jaintia hills. These hills gradually lose their elevation northward to merge with the Brahmaputra plains through gentle gradients punctuated occasionally by isolated hills and hillocks. The foothill zone along Kamrup district under study stretches for a distance of about 78.6 km from west to east with an elevation ranging from 42-1124 meters. Geographically, the Assam-Meghalaya foothill belt bordering the Kamrup district lies between geo-coordinates $91^{\circ}0'3.338''$ E and $91^{\circ}46'22.82''$ E longitude and $26^{\circ}0'4.432''$ N and $26^{\circ}13'46.372''$ N latitude.

Objectives of the study

The objectives of the proposed research work are:

1. To analyze the terrain characteristics of the foothill belt of the Assam-Meghalaya region along the Kamrup district of Assam.
2. To analyze the associated geomorphology and relief pattern of the foothill belt.

MATERIALS AND METHODS

The methodology adopted for the study uses both primary and secondary data of the area. The data from various government sources, reports, and publications, is collected and

thoroughly analyzed, and personal observations are made throughout the study area. Using GIS and satellite data, the terrain is classified and mapped. The data prepared is marked and executed on the map. The topographical map numbering, viz. 78 O/1, 78 O/5, 78 O/9, and 78 N/12 on a scale of 1:50,000 prepared by the Survey of India are used for delineation of various features in the foothill zone. Spatial information of terrain and relief characteristics are evaluated using geological data and maps collected from the Geological Survey of India.

RESULTS AND DISCUSSION

Elevation

The altitude of the study area varies between 42 and 1124 meters. This foothill belt is embodied with rugged topography towards the southernmost range, which gradually loses its elevation towards the north and north-western part. The highest elevation is 1124 meters found in the southern part. Altitude is continuously falling from south to north and east. The eastern part of the foothills where river valleys are present is almost flat. The highest elevation is observed in the southernmost part near Rani hills, Lumpi, Ummap, and Lower Lumpi, and, lowest elevated areas have been found in the surrounding valley region of the Kulsi river, Namtarabari area, Hahim, and valley of Rani (Fig. 2).

Relief profiles of the foothill belt in Kamrup show the distribution of the relief and give the elevation profile of the

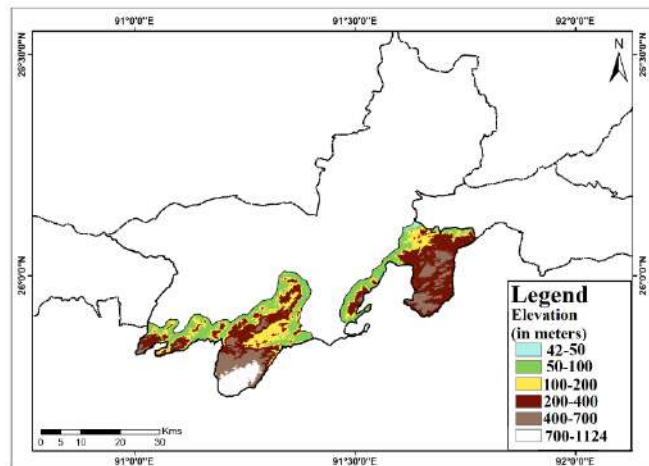


Fig. 2: Elevation of the foothill belt.

hills. The relief profiles along AB and CD cross-sections show the highest elevation in the southernmost part of the Boko revenue circle along the AB cross-section, while the CD cross-section along the Rani-Garbhanga region has relatively moderate relief, i.e. 42 to 650 meters above MSL (Fig. 3).

Geology

Geologically, the study area mainly consists of the Pre-Cambrian gneissic complex (493 km²), and New Alluvium or Recent formation (290 km²). The foothill region of the Assam-Meghalaya border situated in Kamrup district is geologically made up of a Pre-Cambrian gneissic complex composed of granite gneiss, biotic schist, gneiss, and quartz. These hills are the parts of the West Khasi hills, which are

principally composed of gneisses and schists of Gondwana land with intrusive granite, whereas parts of the study area exhibit the characteristics of the Assam valley. Geologically, the foothill zone may be divided into two broad groups, viz (i) Archaean, and (ii) New Alluvium or Recent Formation (Fig. 4).

- (i) **Archaean:** The Archaean group comprises a metamorphic complex of gneisses and schist complex with young acidic/basic intrusive. It covers 493 km² of the area in the southernmost part of the foothill belt.
- (ii) **New Alluvium:** New Alluvium or Recent formation is represented by alluvial deposits of recent age by the Brahmaputra river system and its tributaries. This is the most recent geological classification in the study area.

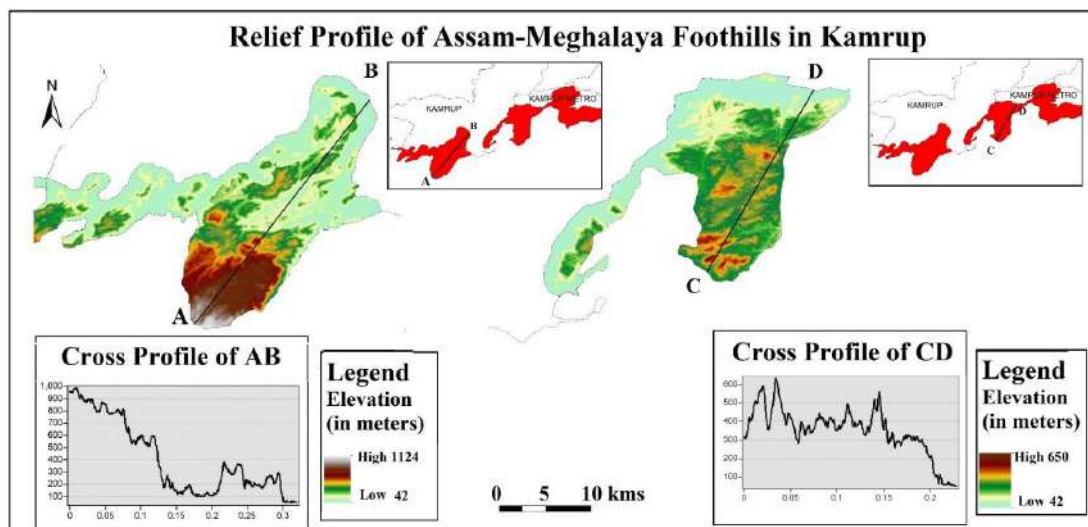


Fig. 3: Cross Profile of AB and CD cross-sections of the foothill belt

Medium to coarse grain sand, gravel, pebbles, cobbles with silt, and clay is the prime characteristics of New Alluvium or Recent formation covering an area of 290 km². The geological formations of the Assam-Meghalaya border situated in the Kamrup district are shown in Fig. 4.

Hydrogeology

Hydrogeologically, the study area is divided into two units, namely consolidated formations and unconsolidated formations (Fig. 5). The newer alluvium zones of the Assam-Meghalaya foothill belt are characterized as unconsolidated formations. This newer alluvium belt of the quaternary and upper Tertiary age group is high in groundwater potential ranging from 150 to 200 m³.hr⁻¹. This belt spreads throughout the northernmost foothills of Kamrup covering a total geographical area of 298.99 km². The consolidated zone of the Archaean age group is the entire structured hill zone of the foothill belt. This belt is found in the southernmost part along the hills of Talimara, Rani, and Garbhanga in Kamrup covering a total area of 484.71 km². Groundwater potential is low at 5 m⁻³.hr⁻¹ (CGWB 2012).

Slope Analysis

The slope is an angular inclination of the region between crests and the base of the valley. Slope analysis of the foothill belt is done by quantifying the maximum rate of change in values of elevation from each cell to its neighbours. It is observed that along the foothill belt, steep slopes are found along the types of ridges and the flat areas aligned with the river valleys. The slope information is useful in understanding the topography, geomorphology, soil types and their erodibility, and surface drainage (Manjare 2013). The slope map was prepared for the study area using SRTM (DEM)

data (Fig. 6). The slope in the study area was calculated in degrees and categorized into five slope classes, namely zero to three degrees, which covered an area of 98.00 km² of the total area of the foothills (12.60 %). These areas were levelled plains. Slope ranging between three to eight degrees which were gentle slope covered an area of 145.36 km² (18.68 %), areas of moderate slope class with slope range of 8 to 18 degrees covered 283.16 km² (36.40 %), areas of steep slope class with slope range of 18 to 29 degrees covered 192.09 km² (24.65%), and high slope values of 29 to 65.6 degrees were distributed over an area of 59.66 km² (7.67%) of the total geographical area of the foothill belt (Table 1).

Geomorphic Units and their Characteristics

The objective of delineating relief zones for terrain classification is taken up to indicate broad and generalized landform types. In the study area, distinct geomorphic units were delineated based on the analysis of SRTM DEM, and SOI toposheets. The geomorphic units identified and delineated in the study area have been categorized under (1) Denudational origin, 2) Fluvial origin, 3) Structural origin and 4) Waterbodies (Fig. 7).

(1) Denudational origin

The denudational structure observed in the foothill zone includes low dissected hill, moderately dissected plateaus, pediment-pediplain complex, residual hill, valley fills, etc. These denudation hills lie between the rugged terrain hills and the valleys distributed unevenly in the foothill belt. The extended low-lying hills of Kamrup covering a total area of 47.8 km² are available at the junction of the plains in the northern part of the foothills.

(2) Fluvial origin

The landforms created due to fluvial agents are of fluvial origin. The fluvial landforms found in the foothill zone are

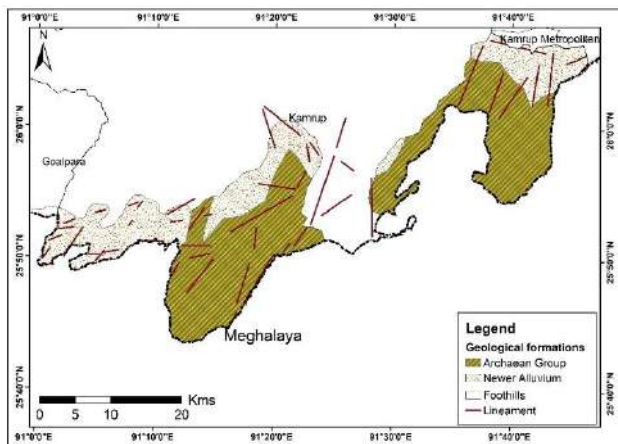


Fig. 4: Geology of the foothill belt.

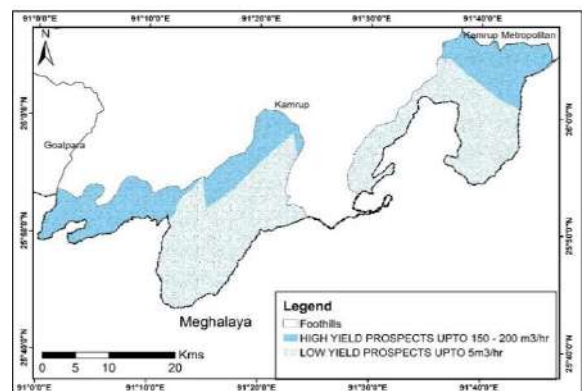


Fig. 5: Hydrogeology of the foothill belt.

flood plains, valleys, alluvial plains, abandoned channels, paleochannels, natural levees, floodplains, etc. These surround the river valleys of Kulsī, Bhatanadi, Kalibog Nadi valley in Kamrup and covers a total area of 55.20 km² accounting for 7.10 % of the foothill belt of the Kamrup district.

(3) Structural origin

The Archaean gneisses complex of the foothill zone is entirely of structural origin. This geomorphic unit has a dramatic effect on the genesis of landforms in the study area and influences the structural setup of the area. These landforms are found in the high elevated extended hills of the Meghalaya plateau, mostly in the dense forested hills of the southernmost part of the foothills. It covers a total area of 674.07 km², i.e. 86.61% of the foothill belt in the Kamrup district.

(4) Waterbodies

In the study area, water bodies include rivers, tributaries, offshoot streams, ponds, wetlands, or more rarely, puddles. Chandubi lake, Deepor Beel are few wetlands in the foothill belt covering a total area of 1.20 km², i.e. 0.15 % of the total area of the foothills under the district.

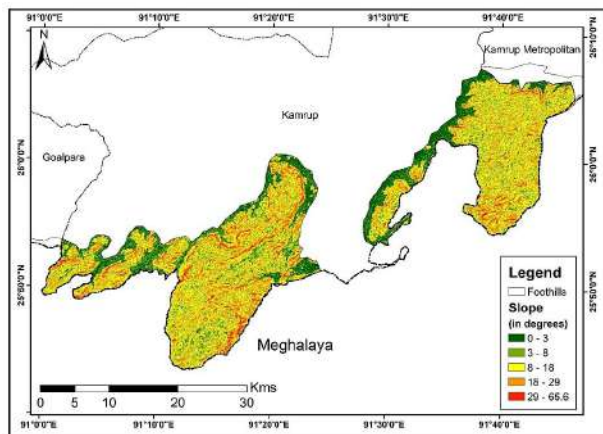


Fig. 6: Slope analysis of the of the foothill belt.

Table 1: Area under different slope classes of the study.

Slope Class (in degrees)	Area under different slope classes (in km ²)	Area (in %)
0 to 3	98.00	12.6
3 to 8	145.36	18.68
8 to 18	283.16	36.4
18 to 29	192.09	24.65
29 to 65.6	59.66	7.67
Total Area	778.27	

Relief units

The objective of delineating relief zones for terrain classification is taken up to indicate broad and generalized landform types. The relief division of the foothills broadly includes three types- valley fill shallows, residual hills, and structural hills (Fig. 8).

a) Valley fill

Valley fills are identified in between the hill ranges and are filled with sand, silt, alluvial deposits, gravel, etc. These valley fills are distributed in large areas over the foothill belt surrounding the tributaries of the Brahmaputra. These are located in the low elevated region of river valleys such as Kulsī, Bhatanadi, Mora Kulsī valley of the foothill zone and covering a total area of 291.37 km², i.e. 37.44 % of the foothill belt of the Kamrup District.

b) Residual hill

Residual hills are complex formations and are in conjunction with both alluvial plains and hills surrounding the foothill zone. These range from 120 to 800 m above mean sea level in the foothill zone. These hills are found surrounding the structural hills of greater elevation. Kahikuchi, surrounding hillocks around Deepor Beel, Pamohi, Rani Hills, and parts of Boko Revenue Circle of Kamrup district are residual hills

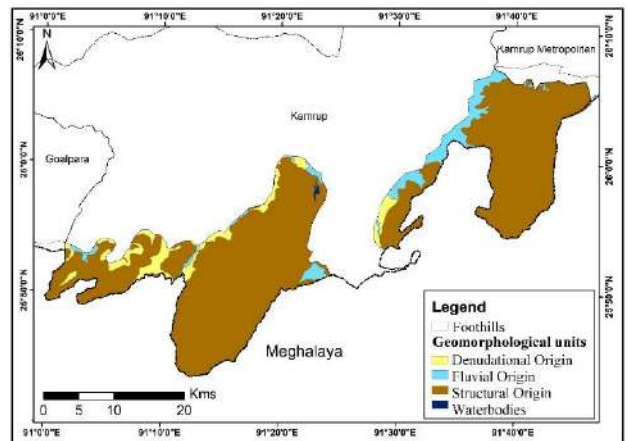


Fig. 7: Geomorphological units of the foothill belt.

Table 2: Area under different geomorphic units of the study area.

Geomorphic Unit	Area (in km ²)	Area (in %)
Structural Origin	674.07	86.61
Fluvial Origin	55.20	7.10
Denudational Origin	47.80	6.14
Waterbodies	1.20	0.15
Total Area	778.27	

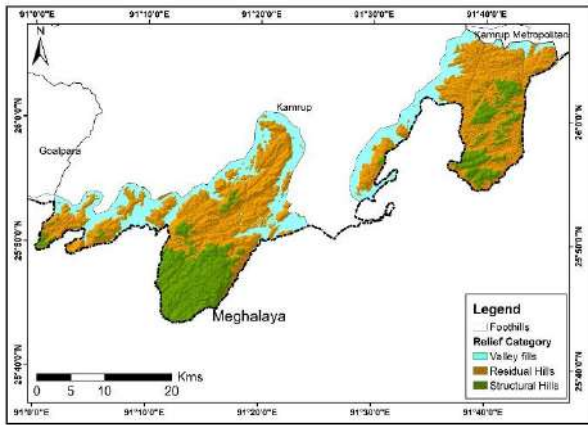


Fig. 8: Relief divisions of the foothill belt.

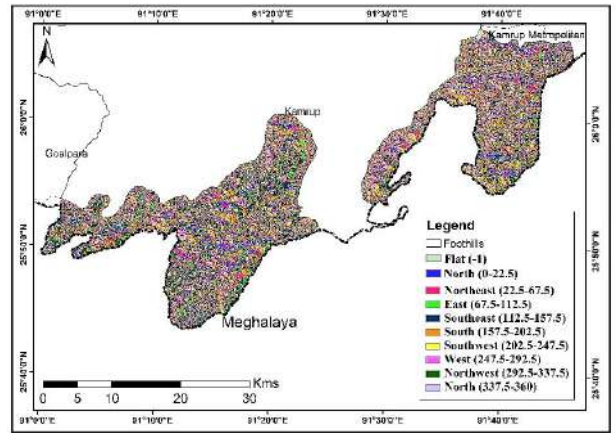


Fig. 9: Aspects of the foothill belt.

and occupy a total area of 377.7 km², i.e. 48.53 % of the foothills of the district.

c) Structural Hills

Structural hills of the Archaean gneissic complex are found in the southern part of the area. These range from 800 to 1124 m above mean sea level in the foothill zone. These are distributed in the southernmost part of Kamrup district in Boko Revenue Circle, Talimara, Garbhanga, and Rani hills. The area covered by the structural hills occupies a total area of 109.2 km² (Table 3).

Aspect

Aspect is the direction of the surface. Aspect is the directional slope measurement. One common way is to divide aspects into eight different directions (N, NE, E, SE, S, SW, W, and NW) and to treat aspects as categorical data. The aspect and slope angle of an area is determined by the difference in incident solar radiation in mountains. It influences the occurrences of soil erosion either directly or indirectly. Aspect is measured clockwise in degrees from 0° to 360°, where 0° is north-facing, 90° is east-facing, 180° is south-facing, and 270° is west-facing showing the orientation of slope. The aspect of the foothill zone is analyzed for the directional measure of the slope. South-East (123.80 km²), South (97.61 km²), South-West (79.56 km²), and North-West (115.17 km²) are the dominant aspect observed in the foothill zone of the study area (Fig. 9).

Hillshade

Hill-shading is a technique used as shaded relief to view the terrain, illuminated by a hypothetical source of light. The illumination value for each raster cell is determined based on slope and aspect, and its orientation to the light

source. Hillshade gives a ground representation of the slope of the terrain. Hillshade of the terrain of the foothill zone is represented in Fig. 10.

Triangular Irregular Network (TIN)

A Triangular Irregular Network is commonly known as TIN. A Triangulated Irregular Network (TIN) is a representation of a continuous surface of triangular facets made to represent the surface. Triangular irregular networks (TIN) have been used to represent surface morphology using GIS. SRTM (DEM) is used to create the TIN of the foothill zone. The TIN model of the foothill belt is a description of the relief using unique color cum shaded relief to depict elevation and surface (Fig. 11).

CONCLUSIONS

In the study area, distinct geomorphological units such as Valley fill, Residual hill, Structural hills have been delineated. The analysis of the geology, hydrogeology, relief profile, TIN, and geomorphic units can be useful in the management the of foothill zone. The information generated at the geomorphic sub-unit level could be effectively used for prioritizing the areas for adoption of appropriate soil and water conservation measures, river basins management, hazards mitigation, geo-environmental planning. Thus, the

Table 3: Area under different Relief Unit of the Study Area.

Relief	Area (in km ²)	Area (in %)
Valley Fill	291.37	37.44
Residual hill	377.70	48.53
Structural Hill	109.20	14.03
Total Area	778.27	

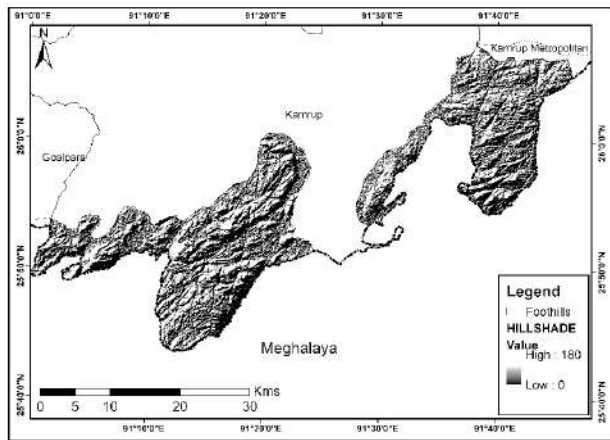


Fig. 10: Hillshade of the foothill belt.

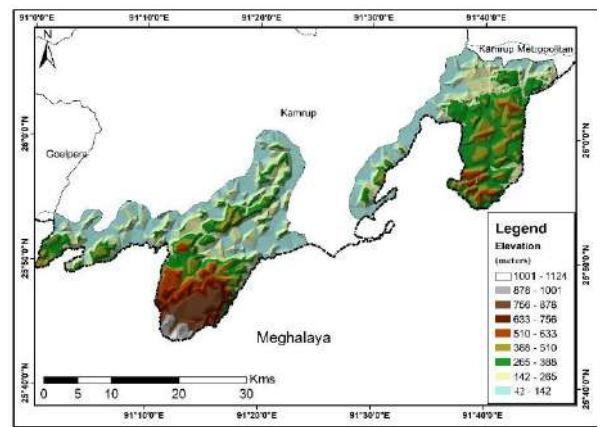


Fig. 11: TIN showing elevation of the foothill belt

Table 4: Area under different aspect classes of the study area.

Aspect Class (in degrees)	Area under different aspect classes (in sq. km)	Area (in %)
Flat	13.39	1.72
North	51.90	6.67
North-East	76.43	9.82
East	73.87	9.49
South-East	123.80	15.91
South	97.61	12.54
South-West	79.56	10.22
West	77.52	9.96
North-West	115.17	14.80
North	69.05	8.87
Total Area	778.27	

foothill belt along the Kamrup district of Assam, with the unique geomorphic characteristics and diverse foothill ecology needs proper management. By detailed terrain analysis, proper management and sustainable development can be implemented.

REFERENCES

- Bolstad, P.V. and Stowe, T. 1994. An evaluation of DEM accuracy: Elevation, slope, and aspect, *Photogramm. Eng. Remote Sens.*, 60(11): 1327-1332.
- CGWB. 2012. Ground Water Information Booklet. Ministry of Water Resources, New Delhi, India.
- Cooke, R.U. and Doornkamp, J.C. (ed.) 1990. *Geomorphology in Environmental Management: A New Introduction*. Clarendon Press, Oxford.
- Dramis, S., Guida, D. and Cestari, A. 2011. Nature and Aims of Geomorphological Mapping. In: Smith, M.J., Paron, P. and Griffiths, J. (eds.), *Geomorphological Mapping: Methods and Applications*. Elsevier, London, pp. 39-74.
- Dykes, A.P. 2008. Geomorphological maps of Irish peat landslides created using hand-held GPS. *J. Maps*, 5: 258-276.
- Manjare, B.S. 2013. Morphometric slope analysis of part of Salbardi and the adjoining region of Amravati District, Maharashtra, and Betul District of Madhya Pradesh, India. *Indian J. Geomorphol.*, 18(2): 59-67.
- Manjare, B.S., Jambhulkar, P., Padhye, M.A. and Girhe, S.S. 2020. Digital terrain analysis and geomorphological mapping using remote sensing and GIS: A case study from Central India. *Sust. Manag. Land Res.-Indian Persp.*, 6(1): 327-345.
- Paron, P. and Claessens, L. 2011. Makers and Users of Geomorphological Maps. In: Smith, M.J., Paron, P. Griffiths, J. (eds.) *Geomorphological Mapping: Methods and Applications*. Elsevier, London, pp. 75-106.
- Prasad, N. and Sarkar, R. 2011. Terrain evaluation: A review. *Int. J. Curr. Res.*, 3(7): 296-301.
- Saha, S., Paul, G.C. and Hembram, T.K. 2020. Classification of terrain based on geo-environmental parameters and their relationship with land use/land cover in Bansloi River basin, Eastern India: RS-GIS approach. *Appl Geomat.*, 12: 55-71.
- Summerfield, M.A. 1997. *Global Geomorphology: An Introduction to the Study of Landforms*. Longman, Essex, England
- Wilson, J.P., & Gallant, J.C. 2000. *Terrain Analysis Principles and Applications*. John Wiley and Sons, New York, 479.
- Wood, J.D. 1996. The geomorphological characterization of digital elevation models. Doctoral Thesis, University of Leicester, United Kingdom.



Spatiotemporal Variation Characteristics of Groundwater Quality in A Semi-Arid Steppe Area in Northwest China

Quansheng Li*, Kai Zhang*, Yingming Yang*, Shan Chong**, Wenfeng Du** and Yunlan He**†

* National energy group, State Key Laboratory of water resources protection and utilization in coal mining, Beijing 100011, China

** State Key Laboratory of Coal Resources and Safe Mining, China University of Mining and Technology (Beijing), Beijing 100083, China

†Corresponding author: Yunlan He; yunlanhe@pku.edu.cn

Nat. Env. & Poll. Tech.
Website: www.neptjournal.com

Received: 01-02-2021

Revised: 26-03-2021

Accepted: 13-04-2021

Key Words:

Semi-arid steppe
Spatiotemporal variation
Groundwater quality
Northwest China

ABSTRACT

In this paper, the open-pit coal mine in semi-arid grassland was taken as the research object. The water samples of the open-pit coal mine and its surrounding areas were collected and the hydrochemical parameters were detected. The temporal and spatial distribution characteristics of the parameters such as pH, electrical conductivity, and dissolved oxygen in the groundwater were studied. The results showed that the groundwater in the study area was alkaline and brackish water. Climate factors might have a certain impact on the pH, conductivity, and dissolved oxygen of groundwater. The pH value of groundwater in the mining area was higher than that in the surrounding pastoral area, while the conductivity value of the mining area was between the pastoral area in the west and the Xilin river area in the east. The parameters of pH, conductivity and total dissolved solids of the four monitoring wells around the mining area showed a slow change or stable phenomenon in the vertical direction with the increase of groundwater depth. This study is of great significance to understand the characteristics of groundwater chemistry in mining areas and the rational development and utilization of groundwater resources.

INTRODUCTION

Groundwater is an important natural resource in human production and life, and also a decisive factor to maintain the balance of the ecological environment, especially in the arid and semi-arid grassland areas. Human activities, such as coal mining, will disturb the groundwater in the grassland area (Liu et al. 2017), and the groundwater level and some water quality parameters may change dynamically with time and space. Therefore, it is of great significance for the protection of groundwater resources and ecological restoration to investigate the dynamic characteristics of groundwater in an arid and semi-arid grassland.

At present, the research on the characteristics of groundwater dynamic change is one of the hot spots of scholars at home and abroad (Jia et al. 2018). By studying the changing law of groundwater dynamic factors, we can not only understand the changing trend of each factor but also take appropriate measures to deal with the possible environmental problems as soon as possible. The temporal and spatial distribution characteristics of groundwater level and hydrochemistry are affected by both natural and human factors, including precipitation, evaporation, terrain structure, and

human exploitation (Jain & Vaid 2018, Barzegar et al. 2018, Thakur et al. 2018). Among them, the research on the spatial distribution characteristics of groundwater quality has direct significance for the identification of groundwater pollution source and degree (Hao et al. 2018, Rasool et al. 2018, Zhang et al. 2017, Oufline et al. 2012). The study on the dynamic change of groundwater can explore the impact of mining activities on groundwater, predict the inflow of mine pit water, and ensure the safety of mining activities (Wu et al. 2019). At the same time, as an important resource, the change of groundwater is of great significance to social development and ecological protection (Sun et al. 2021, Jiang et al. 2020, Zhou et al. 2020). Therefore, it is very important to study the dynamic characteristics of groundwater for the rational development and utilization of groundwater resources.

The current research shows that the original balance state and circulation relationship of groundwater were affected in the process of opencast coal mining due to the discharge of mine water, the drainage of aquifer, the leaching of the waste dump, and the damage of mining, which was manifested by the drop of groundwater level in different degrees and the change of water quality parameters (Oufline et al. 2012). There are many studies on the groundwater quality

in open-pit coal mine areas, such as the evaluation of water quality in coal mining (Lin et al. 2016) and the migration characteristics of groundwater quality along the pollution source (Huang et al. 2016). Although the spatial distribution characteristics of groundwater quality parameters and the analysis of water quality differences are important contents of groundwater research (Kurdi & Eslamkish 2017, Kumari et al. 2014, Arslan & Turan 2014), there are few related studies carrying out in domestic open-pit coal mine areas.

In this paper, we take the open-pit coal mine in a semi-arid grassland area as the research area to study the temporal and spatial variation characteristics of groundwater quality in the mining area and surrounding areas during the development of open-pit coal mines. The spatial differences of groundwater quality parameters distribution were analyzed and the influence of open-pit coal mining on groundwater quality parameters was discussed. This study is of great significance to understand the characteristics of groundwater quality and the rational development and utilization of groundwater resources.

Study Area

The open-pit mining area is located in the middle of Xilingol grassland, which belongs to a part of the hydrogeological unit of the Xilinhot basin. The ground elevation is 980-1093 m, and the terrain is high in the northwest and low in the southeast. This area belongs to a semi-arid grassland climate, cold in winter and hot in summer, with a large annual temperature difference. The extreme maximum temperature is 38.3°C, and the minimum temperature is -42.4°C. The annual average precipitation was 293.45 mm, and the annual average evaporation was 1794.64 mm.

There are faults F1 and F25 in the early mining area of the mine (Jiang et al. 2013), all of which are normal faults

with strike NE and dip angle greater than 50°. The open-pit mine is located in the hanging wall of the fault. The fault forms the water separation boundary, and the east, north, and west are the supply boundary.

MATERIALS AND METHODS

Through sorting out and analyzing various data of the open-pit mine, 16 representative groundwater monitoring points were selected according to the hydrogeological conditions and characteristics of the mine area, as shown in Fig.1. HW1, HW2, HW3, HW4, HW5, HW6, HW7, and HW8 were monitoring points of hydrological wells, CW1, CW2, CW3, CW4, CW5, CW6, CW7, and CW8 were monitoring points of civil wells. The underground water sampling method was as follows: water was pumped to the surface by pumps in civil wells, and water was collected by samplers in hydrology wells at a depth of 1 m. A 1.5 L sampler was used to sample the groundwater from the hydrological well. When the sampler contacted the groundwater-surface in the borehole, the rope was quickly released to the depth of 1 m below the water surface. After waiting for 3-5 min, the sampler was quickly pulled to the ground, and the water sample was quickly poured into the PTFE storage bottle. The indexes of pH, electrical conductivity, and dissolved oxygen were detected by HACH MS5 portable water quality detector on site.

RESULTS AND DISCUSSION

Temporal Variations of Groundwater Parameters

pH is an indicator to measure the acidity and alkalinity of water. According to Fig. 2 (a), the distribution range of groundwater pH in the mining area and surrounding areas was between 7-10, but the pH of most groundwater varied

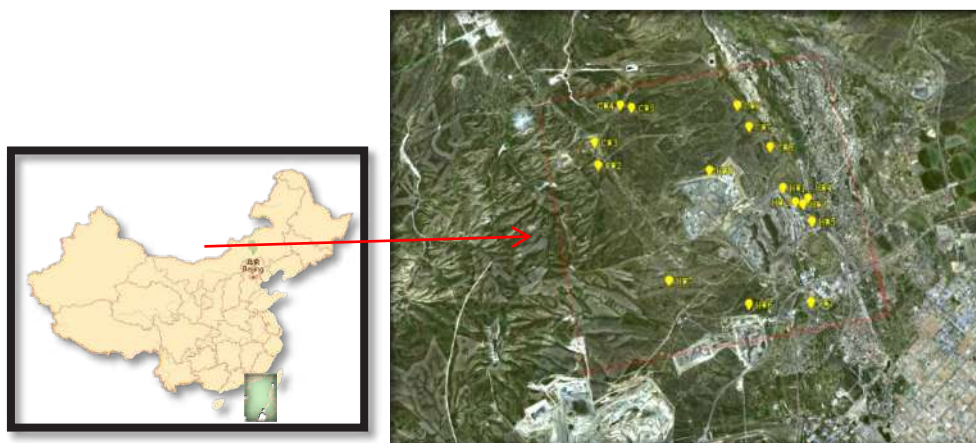


Fig.1: Map of geographic and sampling location.

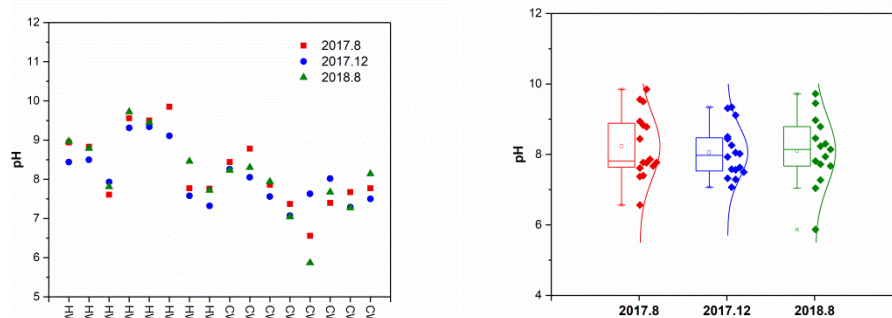


Fig. 2: Temporal variation of pH (a) each well (b) boxplot of all well.

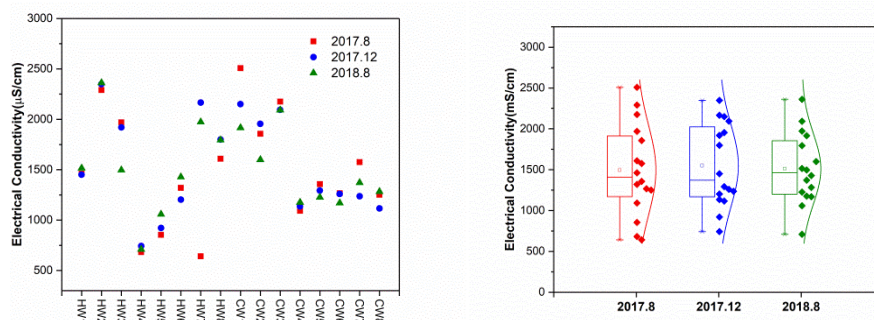


Fig. 3: Temporal variation of electrical conductivity (a) each well (b) Boxplot of all well.

between 7 ~ 9, indicating that the groundwater in this area was neutral to slightly alkaline. In addition, the temporal variation of groundwater pH also showed the following uniform changes: the pH value of groundwater in winter 2017 was lower than that in summer 2017 and 2018; the pH value of groundwater in summer 2018 was higher than that in summer 2017. According to Fig.2 (b), it can be seen intuitively that the pH of most groundwater was between 7-9, among which three wells had a pH value higher than 9, which was reflected in the three sampling periods of August 2017, December 2017 and August 2018.

The electrical conductivity of water was often used indirectly to represent the total concentration of charged matter in water. The distribution of electrical conductivity in groundwater was influenced by comprehensive factors, such as formation lithology, geological structure, and groundwater circulation characteristics. According to Fig. 3 (a) and (b), the distribution range of groundwater electrical conductivity in the mining area and surrounding areas was 500 ~ 2500 $\mu\text{S}\cdot\text{cm}^{-1}$, and the electrical conductivity of most water samples was concentrated in the range of 1000 ~ 2200 $\mu\text{S}\cdot\text{cm}^{-1}$. The electrical conductivity of most groundwater samples in winter 2017 was lower than that in summer 2017, but some samples remained unchanged.

Through the boxplot, it can be seen intuitively that the average electrical conductivity of the groundwater samples first decreased and then increased during the three sampling periods of August 2017, December 2017, and August 2018.

Dissolved oxygen refers to the amount of oxygen dissolved in water, which is an indicator to measure the self-purification capacity of water. As can be seen from Fig. 4 (a) and (b), the distribution range of dissolved oxygen in the mine area and surrounding groundwater was between 0 ~ 9 $\text{mg}\cdot\text{L}^{-1}$, and most of the dissolved oxygen in water samples was within the range of 2 ~ 9 $\text{mg}\cdot\text{L}^{-1}$. The dissolved oxygen value in winter 2017 was higher than that in summer 2017 and 2018, which was caused by the fact that the solubility of gas was related to the temperature of the liquid, and the solubility of oxygen in water decreased with the increase of water temperature. Silva et al. (2013) also found the same phenomenon when the dissolved oxygen in the surface and underground water of Lubango in Angola changed with seasons (Silva et al. 2013). Therefore, the low temperature in Xilingol in winter resulted in the increase of dissolved oxygen concentration in water, while the high temperature in summer resulted in the decrease of dissolved oxygen concentration in water.

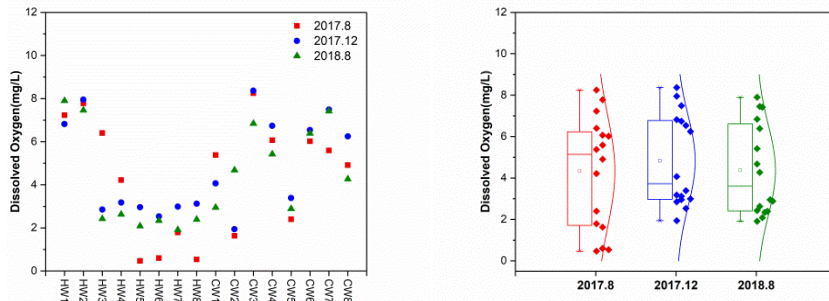


Fig. 4: Temporal variation of dissolved oxygen (a) each well (b) Boxplot of all well.

Horizontal Spatial Distribution of Groundwater Parameters

In this paper, the pH, electric conductivity (EC), and dissolved oxygen (DO) of groundwater in the mining area and its surrounding areas were analyzed. These parameters were drawn by software surfer 8.5 and the Kriging interpolation method, and then the spatial distribution characteristics of physical and chemical parameters of groundwater were described.

As can be seen from Fig. 5, the pH of most water samples was between 7~9, and the pH of groundwater near the mining area was higher than that in the surrounding pastoral areas, among which the pH of groundwater in the western, northern pastoral areas, and the southern vegetable base was lower than 8.5. The pH value of groundwater near the pit and waste dump increased due to the drainage of coal mining. The highest pH value appeared at the HW3 hydrological

monitoring point near the waste dump on the east side of the pit, where the groundwater was alkaline. In comparison to the pH value of groundwater in summer 2017, the pH range in the mining area and surrounding areas had significantly expanded in summer 2018. Therefore, it is inferred that mining activities may have a certain impact on the rise of groundwater pH in the mining area.

It can be seen from Fig. 6 that the electrical conductivity of most water samples was concentrated in the range of 1000~2200 $\mu\text{S}\cdot\text{cm}^{-1}$. The distribution of electrical conductivity was characterized by high in the west and low in the east of the study area. The electrical conductivity value of groundwater in the west pasture was significantly higher than that in the east Xilin River area, while the mining area was in the middle zone. Due to the formation of groundwater funnel, formed by the drainage of open-pit mining, the sand gravel confined water, no.5 coal confined water, no.6 coal confined water and quaternary phreatic water at the top of

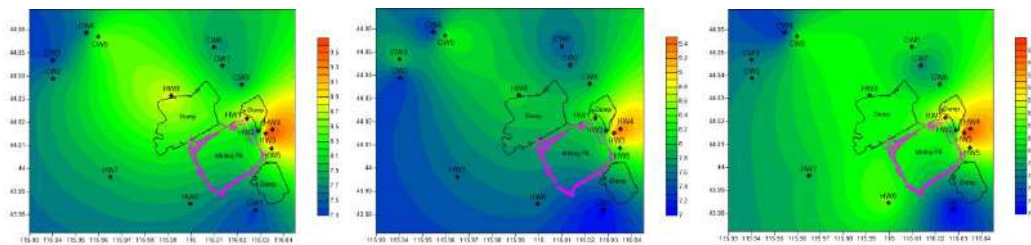


Fig. 5: Horizontal spatial distribution of pH (a) 2017.8 (b) 2017.12 (c) 2018.8.

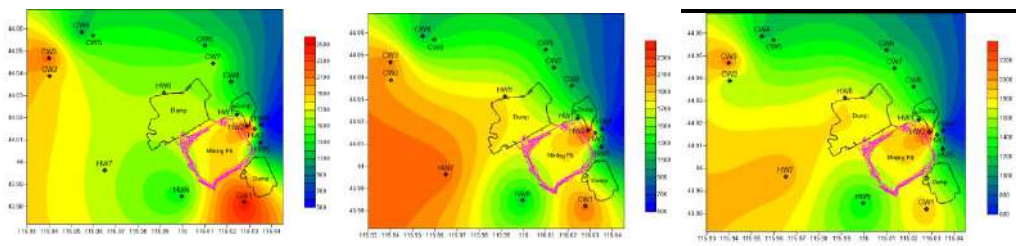


Fig. 6: Horizontal spatial distribution of electrical conductivity (a) 2017.8 (b) 2017.12 (c) 2018.8

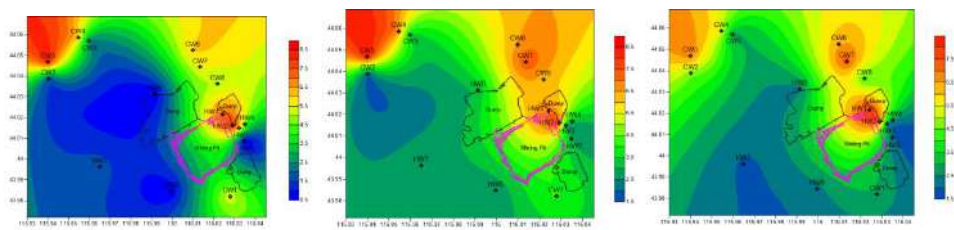


Fig. 7: Horizontal spatial distribution of dissolved oxygen (a) 2017.8 (b) 2017.12 (c) 2018.8

coal measure strata filled the mining pit. The high electrical conductivity groundwater in the west pastoral area and the low conductivity groundwater in the east river were mixed here, resulting in the conductivity value of the mining area between the two. In addition, compared with the summer of 2017 and the summer of 2018, the distribution range of high electrical conductivity in the western pastoral area in winter 2017 was relatively larger, which may be due to the strong evaporation of groundwater in the winter frozen period, while the precipitation recharge was less, resulting in a relatively high conductivity value of groundwater.

As can be seen from Fig. 7, the dissolved oxygen of most water samples was concentrated in the range of 2~9 mg.L⁻¹. The content of dissolved oxygen had a great relationship with the sampling method. In the pastoral area, the main method of groundwater sampling was pumping. The groundwater was mixed with air drastically when it was pumped to the surface, which resulted in the high content of dissolved oxygen in the water samples. However, a sampler was used in the groundwater sampling of hydrologic well, and the sample extraction process had less contact with the air, so the dissolved oxygen content of groundwater samples obtained by this sampling method was relatively low. In addition, since the solubility of oxygen in water increased with the decrease of water temperature (Silva et al. 2013), the dissolved oxygen value of groundwater in winter 2017 was higher than that in summer 2017 and 2018, but the spatial distribution trend of these three periods showed the same characteristics.

Vertical Spatial Distribution of Groundwater Parameters

To further investigate the variation of groundwater chemical parameters with groundwater depth in the study area, we selected four monitoring wells (HW5, CW1, HW7, and HW8) distributed around the mining area, to study the vertical distribution characteristics of pH, electrical conductivity, dissolved oxygen, total dissolved solids, and redox potential parameters. The sampling depth was designed according to the depth of the monitoring wells. Because the depth of the four monitoring wells was different, the sampling depth was

also different. The sampling depth of well HW5 was 1, 5, 10 m below the water surface, well CW1 was 1, 5, 10, 15 m below the water surface, well HW7 was 1, 5, 10, 15, 20, 30, 40, 50 m below the water surface, and well HW8 was 1, 5, 10, 15, 20, 30, 40 m below the water surface. The pH, electrical conductivity, dissolved oxygen, total dissolved solids, and redox potential parameters of the groundwater samples were measured by a portable water quality detection instrument.

As shown in Fig.8, the pH of HW5, CW1, HW7, and HW8 had different trends with depth, and the pH of HW5 and CW1 showed an increasing trend with depth. The pH of HW5 increased from 8.79 to 9.37 with the groundwater depth increasing from 1 m to 5 m, and then the pH remained basically stable within the depth range of 5~10 m. The pH of CW1 increased from 7.04 to 7.42 with the groundwater depth increasing from 1 m to 5 m, and the pH kept stable within the depth range of 5~15 m. With the increase of groundwater depth, the pH value of HW7 decreased first and then increased, and kept stable finally. The pH of HW7 kept stable at about 8.3 with the groundwater depth increasing from 1 m to 40 m. With the increase of groundwater depth from 1 m to 10 m, the pH value of HW8 decreased from 7.94 to 7.41, and then the pH value increased from 7.41 to 7.77 with the depth increasing from 10 m to 20 m, and finally kept stable within the range of 20~50 m. The pH values and trends of the four wells were different, which may be related to the hydrogeological conditions of the location.

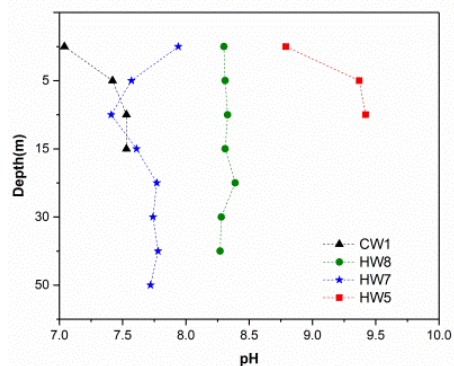


Fig. 8: Vertical spatial distribution of groundwater pH in groundwater.

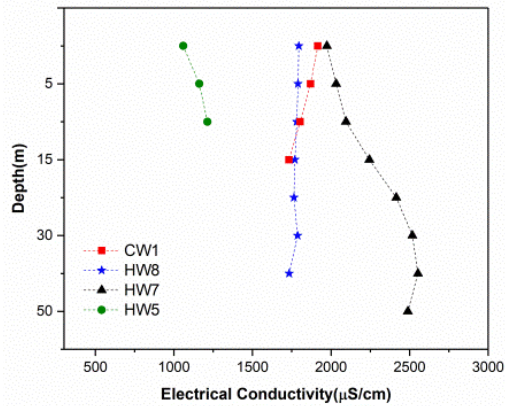


Fig. 9: Vertical spatial distribution of electrical conductivity in groundwater.

As shown in Fig. 9, the electrical conductivity values of four wells HW5, CW1, HW7, and HW8 also showed different variation trends with depth. The electrical conductivity of HW5 showed a slowly increasing trend and it increased from $1059 \mu\text{S}\cdot\text{cm}^{-1}$ to $1213 \mu\text{S}\cdot\text{cm}^{-1}$ with the depth of groundwater increasing from 1 m to 10 m. The electrical conductivity of CW1 decreased from $1619 \mu\text{S}\cdot\text{cm}^{-1}$ to $1732 \mu\text{S}\cdot\text{cm}^{-1}$ with the depth of groundwater increasing from 1 m to 15 m. As the groundwater depth of HW7 increased from 1 m to 50 m, the electrical conductivity increased from $1974 \mu\text{S}\cdot\text{cm}^{-1}$ to $2489 \mu\text{S}\cdot\text{cm}^{-1}$. As the groundwater depth of HW8 increased from 1 m to 40 m, the electrical conductivity was basically stable at about $1790 \mu\text{S}\cdot\text{cm}^{-1}$.

As shown in Fig.10, the changing trend of dissolved oxygen with groundwater depth in HW5, CW1, HW7, and HW8 was basically the same, both of which showed the trend of first increasing and then decreasing. As the groundwater depth of HW5 increased from 1 m to 10 m, the dissolved oxygen increased rapidly from $2.09 \text{ mg}\cdot\text{L}^{-1}$ to $5.03 \text{ mg}\cdot\text{L}^{-1}$. As the groundwater depth of CW1 increased from 1 m to 15 m, dissolved oxygen increased rapidly from $2.95 \text{ mg}\cdot\text{L}^{-1}$ to $4.81 \text{ mg}\cdot\text{L}^{-1}$ and then decreased to $4.18 \text{ mg}\cdot\text{L}^{-1}$, showing a phenomenon of increasing first and then decreasing, and an inflection point appeared at the depth of 10 m. As the groundwater depth of HW7 increased from 1 m to 50 m, the dissolved oxygen increased rapidly from $1.91 \text{ mg}\cdot\text{L}^{-1}$ to $3.88 \text{ mg}\cdot\text{L}^{-1}$, and then decreased slowly to $3.06 \text{ mg}\cdot\text{L}^{-1}$, with inflection points at 10 m and 40 m, respectively. The variation trend of HW8 and HW7 was roughly the same, which increased rapidly from $2.39 \text{ mg}\cdot\text{L}^{-1}$ to $5.12 \text{ mg}\cdot\text{L}^{-1}$ and then decreased to $3.78 \text{ mg}\cdot\text{L}^{-1}$, but the inflection point appeared at 5 m and 20 m, respectively.

As shown in Fig. 11, the changing trend of total dissolved solids with groundwater depth of HW5, CW1, HW7 and

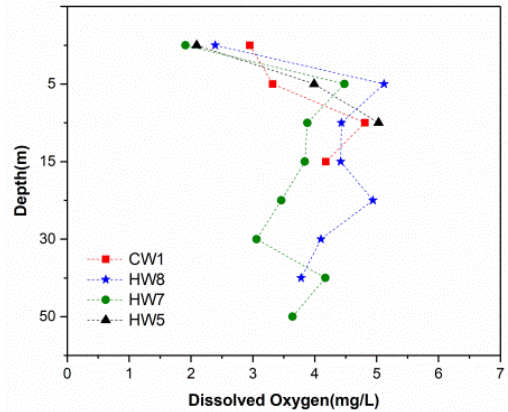


Fig. 10: Vertical spatial distribution of dissolved oxygen in groundwater.

HW8 was roughly the same as that of electrical conductivity. As the groundwater depth of HW5 increased from 1 m to 10 m, the total dissolved solids increased from $528 \text{ mg}\cdot\text{L}^{-1}$ to $573 \text{ mg}\cdot\text{L}^{-1}$, showing a slow increase trend. With the groundwater depth of CW1 increasing from 1 m to 15 m, the total dissolved solids decreased from $897 \text{ mg}\cdot\text{L}^{-1}$ to $832 \text{ mg}\cdot\text{L}^{-1}$, showing a gradual decrease trend. With the groundwater depth of HW7 increasing from 1 m to 50 m, the total dissolved solids increased from $933 \text{ mg}\cdot\text{L}^{-1}$ to $1126 \text{ mg}\cdot\text{L}^{-1}$. The total dissolved solids were basically stable at about $800 \text{ mg}\cdot\text{L}^{-1}$ with groundwater depth of HW8 increasing from 1 m to 40 m.

CONCLUSION

In this paper, groundwater samples were collected from an open pit and its surrounding areas in a semi-arid grassland. The temporal and spatial distribution characteristics of pH, conductivity, dissolved oxygen, and other parameters in

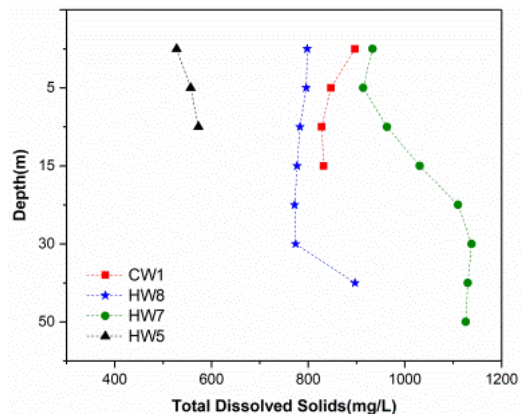


Fig. 11: Vertical spatial distribution of total dissolved solids in groundwater.

groundwater were studied. The main conclusions of this paper are as follows:

1. The groundwater in the study area was alkaline and brackish water. Compared with summer, the pH and electrical conductivity of groundwater samples were relatively low in winter, while the dissolved oxygen was relatively high, indicating that climate factors might have a certain impact on the pH, electrical conductivity, and dissolved oxygen of groundwater.
2. The pH of groundwater in the mining area was higher than that in the surrounding pastoral area, so it is inferred that mining activities may have a certain impact on the rise of groundwater pH in the mining area. The electrical conductivity of groundwater in the west pasture was significantly higher than that in the east Xilin river area. The drainage of coal mining would form an underground funnel near the mining pit, and the incoming water would be mixed near the mining pit, making the electrical conductivity value of the mining area between the two areas.
3. Four monitoring wells HW5, CW1, HW7, and HW8 around the mining area were selected to study the vertical distribution characteristics of pH, conductivity, dissolved oxygen, total dissolved solids, and oxidation-reduction potential parameters. The increase of groundwater depth, pH, conductivity, dissolved total solids, and redox potential showed a slow change or stable phenomenon, while dissolved oxygen changed dramatically. This trend may be related to the hydrogeological conditions of these wells.

ACKNOWLEDGEMENTS

The authors thank the support of the National Energy Group Key Laboratory Open Fund (GJNY 18-73.20), National Key Research and Development Program (2016YFC0501102), the Fundamental Research Funds for the Central Universities (2021YQMT01).

REFERENCES

- Arslan, H. and Turan, N.A. 2014. Estimation of the spatial distribution of heavy metals in groundwater using interpolation methods and multivariate statistical techniques; its suitability for drinking and irrigation purposes in the Middle Black Sea Region of Turkey. *Environ. Monit. Assess.*, 6(12): 187-199.
- Barzegar, R., Moghaddam, A.A., Nazemi, A.H. and Adamowski, J. 2018. Evidence for the occurrence of hydrogeochemical processes in the groundwater of Khoys plain, northwestern Iran, using ionic ratios and geochemical modeling. *Environ. Earth Sci.*, 77: 81-97.
- Hao, A., Zhang, Y., Zhang, E., Li, Z., Yu, J., Wang, H., Yang, J. and Wang, Y. 2018. Review: Groundwater resources and related environmental issues in China. *Hydrogeol. J.*, 26: 1325-1337.
- Huang, X., Deng, H., Zheng, C. and Cao, G. 2016. Hydrogeochemical signatures and evolution of groundwater impacted by the Bayan Obo tailing pond in northwest China. *Sci. Total Environ.*, 543: 357-372.
- Jain, C.K. and Vaid, U. 2018. Assessment of groundwater quality for drinking and irrigation purposes using hydrochemical studies in Nalbari district of Assam. *India. Environ. Earth Sci.*, 77: 111-141
- Jia, Y., Xi, B., Jiang, Y., Guo, H., Yang, Y., Lian, X. and Han, S. 2018. Distribution, formation and human-induced evolution of geogenic contaminated groundwater in China: A review. *Sci. Total Environ.*, 643: 967-993.
- Jiang, D., Li, Z., Luo, Y. and Xia, Y. 2020. River damming and drought affect water cycle dynamics in an ephemeral river based on stable isotopes: The Dagu River of North China. *Sci. Total Environ.*, 758: 143682.
- Jiang, S., Kong, X., Ye, H. and Zhou, N. 2013. Groundwater dewatering optimization in the Shengli no. 1 open-pit coalmine, Inner Mongolia, China. *Environ. Earth Sci.*, 69: 187-196.
- Kumari, S., Singh, A.K., Verma, A.K. and Yaduvanshi, N.P.S. 2014. Assessment and spatial distribution of groundwater quality in industrial areas of Ghaziabad, India. *Environ. Monit. Assess.*, 186: 501-514.
- Kurdi, M. and Eslamkish, T. 2017. Hydro-geochemical classification and spatial distribution of groundwater to examine the suitability for irrigation purposes (Golestan Province, north of Iran). *Paddy Water Environ.*, 15: 731-744.
- Lin, M., Peng, W. and Gui, H. 2016. Hydrochemical characteristics and quality assessment of deep groundwater from the coal-bearing aquifer of the Linhuan coal-mining district, Northern Anhui Province, China. *Environ. Monit. Assess.*, 188: 454-481.
- Liu, P., Hoth, N., Drebenstedt, C., Sun, Y. and Xu, Z. 2017. Hydro-geochemical paths of multi-layer groundwater system in coal mining regions - Using multivariate statistics and geochemical modeling approaches. *Sci. Total Environ.*, 601: 1-14.
- Oufline, R., Hakkou, R., Hanich, L. and Boularbah, A. 2012. Impact of human activities on the physico-chemical quality of surface water and groundwater in the north of Marrakech (Morocco). *Environ. Technol.*, 33: 2077-2088.
- Rasool, A., Farooqi, A., Xiao, T., Ali, W., Noor, S., Abiola, O., Ali, S. and Nasim, W. 2018. A review of global outlook on fluoride contamination in groundwater with prominence on the Pakistan current situation. *Environ. Geochem. Health*, 40: 1265-1281.
- Silva, M.M.V.G., Gomes, E.M.C., Isaias, M., Azevedo, J.M.M. and Zeferino, B. 2013. Spatial and seasonal variations of surface and groundwater quality in a fast-growing city: Lubango, Angola. *Environ. Earth Sci.*, 76: 221-233
- Sun, K., Hu, Li., Guo, J., Yang, Z., Zhai, Y. and Zhang, S. 2021. Enhancing the understanding of hydrological responses induced by ecological water replenishment using improved machine learning models: A case study in Yongding River. *Science of the total environment*, 768: 145489.
- Thakur, D., Bartarya, S.K. and Nainwal, H.C. 2018. Tracing ionic sources and geochemical evolution of groundwater in the Intermountain Una basin in outer NW Himalaya, Himachal Pradesh, India. *Environ. Earth Sci.*, 77: 549-571.
- Wu, C., Wu, X., Zhu, G. and Qian, C. 2019. Predicting mine water inflow and groundwater levels for coal mining operations in the Pangpangta coalfield, China. *Environ. Earth Sci.*, 130: 313-339.
- Zhang, L., Qin, X., Tang, J., Liu, W. and Yang, H. 2017. Review of arsenic geochemical characteristics and their significance on arsenic pollution studies in karst groundwater, Southwest China. *Appl. Geochem.*, 77:80-88.
- Zhou, P., Wang, G. and Duan, R. 2020. Impacts of long-term climate change on the groundwater flow dynamics in a regional groundwater system: Case modeling study in Alashan, China. *J. Hydrol.*, 590: 125557.



Situation and Treatment Methods of Ecological and Environmental Problems during the Process of Urbanization in Rural Areas of China

Xiaoxue Zhang*(**), Faming Sun***†, Jie Yang***, Jian Li***, Jing Liang*, Mei Yang** and Wen Liu****

* School of Finance and Economics, Qinghai University, Xining 810016, China

** Instituto de Ciencias de la Educación, Universidad Pontificia Comillas, Madrid 28049, Spain

*** No. 205 Geological Team, Chongqing Bureau of Geology and Minerals Exploration, Chongqing 402160, China

**** Sichuan Institute of Geological Engineering Investigation Co. Ltd, Chengdu 610072, China

†Corresponding author: Faming Sun; cqdz_yangjie@163.com

Nat. Env. & Poll. Tech.
Website: www.neptjournal.com

Received: 26-02-2021

Revised: 19-04-2021

Accepted: 01-05-2021

Key Words:

Urbanization
Rural pollution
Environmental protection
Environmental economics

ABSTRACT

Rural urbanization is a process of population agglomeration catalyzed by industrialization. At present, China's urbanization process is accelerating against the backdrop of rapid social development. However, in some areas, economic development is emphasized, while the protection of the ecological environment is neglected, leading to the increasingly obvious contradiction between urbanization and rural ecological environment and is not conducive to economic development. In this paper, the development trend of China's rural urbanization, the current situation of environmental pollution, and the progress of important environmental treatment projects are analyzed. Accordingly, the main problems in rural environmental protection and the impact of urbanization are explored. The problems led by industrial and domestic pollutants have been amplified by urbanization, while the improved connection between urban and rural areas will benefit the improvement of environmental infrastructure in rural areas. The government-led projects of rural water improvement, sanitary toilet penetration, methane gas production, and solar water heater have made great progress during the past two decades. Based on these understandings, we put forward feasible countermeasures to implement rural ecological environment protection during the process of urbanization to promote the benign development of rural urbanization. Our results will be helpful in providing some useful references for environmental protection in rural areas and promoting the coordinated development of the economy and environment during the process of urbanization in China.

INTRODUCTION

As one of the ancient civilizations in the world, China is the birthplace of human farming civilization and has always been a big agricultural country. Before China's reform and opening up in 1978, the original agricultural ecological environment was not eroded by modern civilization because agricultural production was always carried out in the traditional way. In the past 40 years, China's market economy has replaced the natural economy, and industrialized agricultural production has replaced primitive agricultural production. With the development of the rural economy, the degree of agricultural modernization has been accelerated unprecedentedly. However, the cost of economic and social development, industrialization, urbanization, and large-scale agricultural development have brought many direct or potential negative impacts on rural ecology and the environment.

Urbanization refers to the natural historical process in which social productive forces are transformed from traditional rural civilization to modern urban civilization in terms

of economic structure, population living, and population quality based on industrialization and informatization (Gibbs & Davis 1958, Gibbs & Martin 1958). From the late 1970s to the early 1990s, urbanization began to develop rapidly in China. In the following ten years, a total of 286 new cities emerged in China, and the population of cities also increased to 312.03 million, with the urbanization rate accounting for nearly 30%. During the process of urbanization and industrialization, the government usually pays more attention to economic growth and neglects environmental problems to a certain extent. However, the coordination between the economy and the environment is very important for sustainable development (Chen et al. 2019, Wu et al. 2021). The deterioration of the rural ecological environment restricts the sustainable development of villages and towns seriously and limits the potential for economic growth in rural areas. Due to the transfer of high-pollution industries from cities to surrounding villages, rural areas are usually faced with an increase in the proportion of industrial land during the process of urbanization, and thus being exposed to higher

environmental health risks (Zhang et al. 2021). In urbanized rural areas, the types of environmental pollution include traditional pollution, industrial pollution, and domestic pollution, and the sources of pollutants are diversified (Ou et al. 2020, Yang et al. 2019, Zhang et al. 2021, Zhu et al. 2019). Traditionally, rural environmental pollution mainly comes from productive sources such as pesticide pollution, chemical fertilizer pollution, and agricultural film pollution produced in agricultural production. The alteration of climate under the influence of the monsoon will limit the intensity of agricultural pollution discharge in the dry season (Xia et al. 2020a, Xia et al. 2019). During the process of urbanization, high-pollution industries move from cities to suburbs, urban-rural fringes, and rural areas, resulting in increased pollution of land, water, and air to varying degrees (Fang et al. 2015, Xia et al. 2020b, Xia et al. 2020c, Zhao et al. 2017). Domestic garbage, human and animal excrement constitute the main source of living pollution. The development of urbanization has promoted the circulation of people and goods in rural areas, and the amount of domestic waste has also increased greatly. In recent years, under the double pressure of increasing population and increasing industrial scale, the situation of China's rural environment is very severe. Although the government tries to solve the environmental pollution by means of technology, legal system, and economy, there are still many gaps in the research on comprehensive management of the rural environment (Yang 2010).

Therefore, it is of great significance to analyze the problems and causes of environmental pollution in rural areas and put forward corresponding solutions. This study summarizes the main environmental problems faced by China's rural areas during the process of urbanization systematically, analyzes the main sources of deteriorating environmental conditions, and sums up the main contents, research ideas, and corresponding technologies and methods of rural environmental pollution prevention and control research. Based on these understandings, this paper proposed some countermeasures to improve the environmental pollution control in rural areas of China and provides suggestions for building a sustainable economic and social development model.

MATERIALS AND METHODS

In this paper, based on results from previous research, combined qualitative and quantitative analyses are adopted. The current situation and main problems of rural environmental problems in China are analyzed based on references; the existing problems are analyzed by quantitative methods using the survey data. The development progress of urbanization in China is obtained through the spatial evolution of remote sensing images. The evolution of urbanization is judged

by land-use data. This data is collected from the "Remote Sensing Monitoring Database of Land Use Status in China" (LUCC) published by the Resource and Environment Data Cloud Platform of the Chinese Academy of Sciences. This data set is based on Landsat 8 remote sensing images and generated by manual visual interpretation. The grid accuracy is 1 km, and the land use is divided into 7 categories in this data set. "Industrial, mining and residential land" is regarded as a substitute index of the urban land use type. By analyzing the trend of some indicators of China's rural environment, corresponding solutions are put forward. Rural environmental data comes from China Environmental Statistics Yearbook published in 2018.

RESULTS AND DISCUSSION

Status of the Urbanization Process in Chinese Rural Areas: The past decades have witnessed the rapid development of China's rural urbanization. Urban expansion has played a remarkable role in promoting the development of surrounding rural urbanization. The distribution changes of working conditions and residential land in China from 1980 to 2015 are shown in Fig. 1. The scale change diagram of this land-use type is shown in Fig.2. In the past 30 years, the proportion of land uses related to cities has gradually increased, indicating the acceleration of urbanization. Generally, China's policy support for rural urbanization includes industry, planning, infrastructure, and community construction. With the improvement of the transportation system, urban-rural integration has been achieved in many areas. However, urbanization not only drives economic development but also increases rural environmental pollution. With the increase of population, the consumption and demand of resources will increase, and the emission of environmental pollution will also increase, thus the pressure of environmental governance will be greater. The rapid development of urbanization has driven a large number of township enterprises to be built in rural areas and become the main economic pillar of the local area. However, most township enterprises lack scientific planning and management, with a small scale of production and extensive management, and then produce a large amount of wastewater, gas, and residue. Enterprises usually pay attention to short-term economic benefits, but lack awareness of environmental protection. They do not bring in environmental protection facilities and supporting pollution treatment equipment, and the phenomenon of irregular sewage discharge is widespread. On the whole, the current situation of rural environmental pollution in the process of urbanization is grim. Although there have been partial improvements, the pollution problems in most areas have not been effectively rectified, and the environmental pollution problems in some areas even tend to worsen.

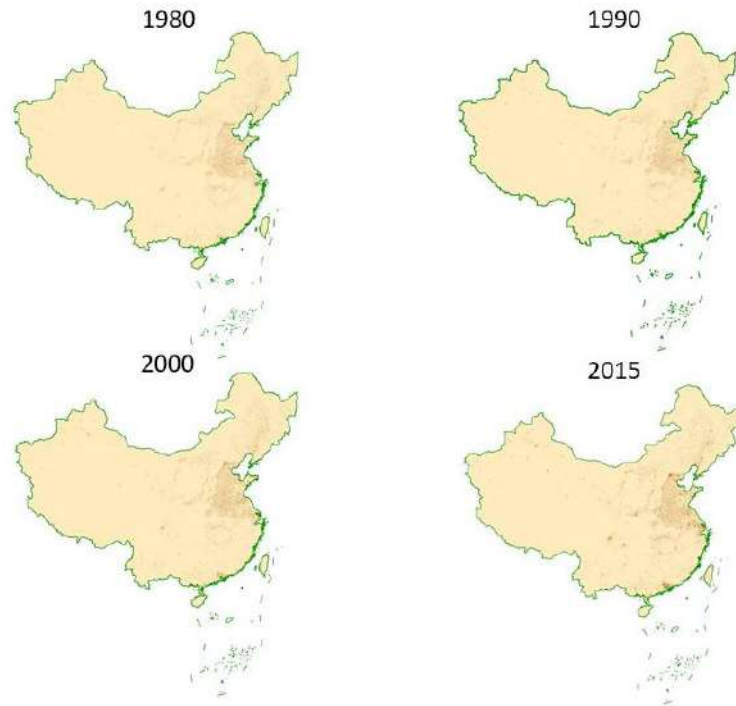


Fig. 1: Variation of the distribution of urban, mining, and residential land from 1980 to 2015. The red scatters represent this land-use type.

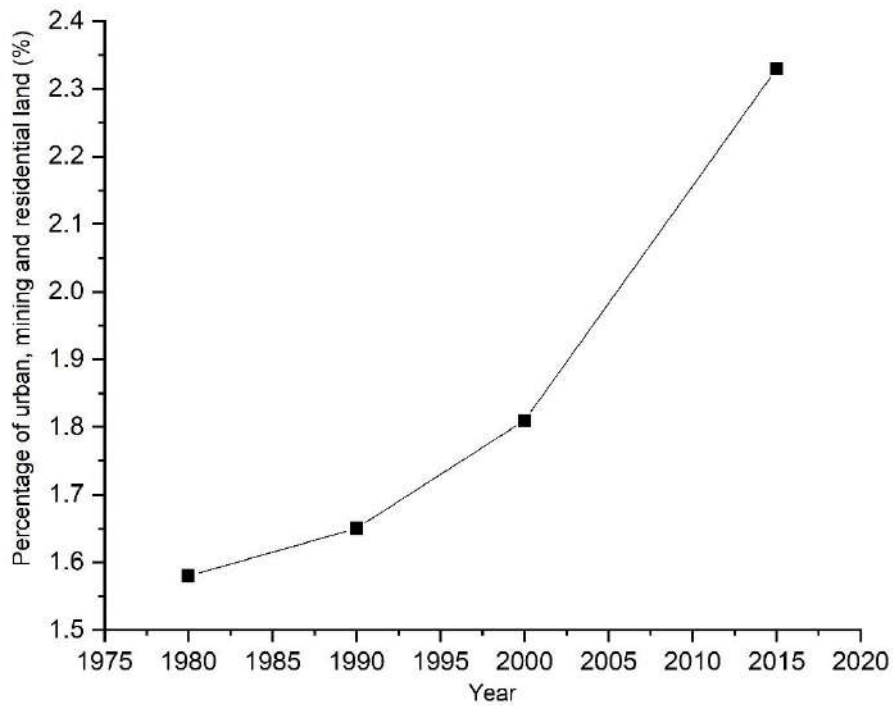


Fig. 2: Temporal variation of the ratio of urban, mining, and residential land in China.

Present Situation and Problems of Chinese Rural Environment: During the process of rural urbanization, the main environmental problems include two aspects: first, the environmental damage caused by ignoring the local natural conditions and disrespecting the objective laws of development. Second, the discharge of pollutants and wastes exceeds the self-purification capacity of the local environment due to the concentration of production and living activities, and the related infrastructure is difficult to keep up, resulting in environmental pollution problems. At present, under the background of increasing agricultural production efficiency and accelerating urbanization, the sources of rural environmental pollution are diverse and can be divided into the following four types:

1. Agricultural pollution. During the process of agricultural production activities such as planting, excessive or improper use of chemical fertilizers, pesticides, and plastic film causes pollution to soil and causes pollution to rivers and other water bodies indirectly. Incineration or random stacking of agricultural by-products will cause air pollution and soil pollution to varying degrees.
2. Farming pollution. Livestock manure, aquaculture wastewater, and aquaculture sludge contain a large amount of nitrate, phosphorus, sulfide, ammonium, carbohydrate, etc. Among them, nitrate and phosphorus will lead to the large-scale growth of phytoplankton, which will gradually cover the water surface reducing the content of dissolved oxygen in water, and further leading to the death of aquatic plants and aquatic animals. These will finally make the water stink and rot and threaten people's health.
3. Domestic-source pollution. Due to the imperfect basic public facilities in rural areas, the sewage produced by residents in their lives, as well as the feces and urine of people and animals, are discharged directly into nearby rivers without any treatment, leading to pollution phenomena such as the odor of water bodies. In addition, urban garbage is usually transported to open areas in rural areas to be buried and piled up. Without any treatment measures, the garbage will gradually pollute the surface water and groundwater, resulting in serious groundwater pollutions.
4. Industrial and mining pollution. During the process of urbanization, a large number of industrial enterprises have transferred high-pollution production lines to rural areas. However, the rural environment has been seriously polluted by industry due to the weak control and supervision of environmental protection in rural towns, and a huge amount of waste gas, residue, and gas have been wantonly discharged, which has become

an important cause of the increasingly serious environmental pollution in rural areas.

Serious pollution is extremely harmful to the rural ecological environment. Traditional agricultural pollution affects the quality of cultivated land and leads to serious desertification. Long-term use of pesticides and fertilizers has seriously damaged the balance of soil nutrients, and the random stacking of domestic and production garbage has brought impacted soil physical and chemical properties. With the advancement of rural urbanization, urban pollution gradually migrates to rural areas, the number of heavy metal pollutants and toxic substances discharged by industry is increasing, leading to the decrease in the number and types of animals and plants. Many rare species have disappeared, which has brought serious damage to the ecological balance and the development of biodiversity.

In China's rural areas, an effective supervision and inspection system has not been established, nor has a perfect garbage removal system been formed. Most of the generated domestic and production wastes are discharged in rivers, seas, and lakes, or stacked directly on the roadside, and they cannot be recovered and treated in time and effectively. Additionally, the education level of Chinese farmers is generally low, and many farmers do not realize the deep harm caused by environmental pollution and the significance of resource protection. Therefore, it is difficult to change their production and living habits. The residents lack the subjective will to participate in pollution control, which limits the development of rural environmental protection.

Measures for Rural Environmental Protection: Currently, the Chinese government attaches great importance to the problem of rural environmental pollution and carries out comprehensive improvements in rural areas. The main measures of environmental governance promoted in rural areas include strengthening the harmless and resource treatment of rural garbage, promoting macro-control and prevention of livestock and poultry breeding pollution, vigorously developing agricultural clean production technology and clean energy, strengthening the management of township enterprises and reducing industrial pollution, and rectifying domestic garbage pollution. For agricultural pollution, the management department promotes clean production technology actively in the process of agricultural planting and processing in the vast rural areas to eliminate the traditional pollutants in rural areas effectively. They also promote the use of low-toxic pesticides and organic fertilizers in the planting process, avoid excessive use of chemical fertilizers and pesticides, and adopt planting varieties with strong insect and disease resistance. Moreover, the financial department increased investment in clean energy and infrastructure and

encouraged rural areas to use solar energy and electricity generated by small hydropower for lighting, heating, and cooking. Construction of biogas digesters is concentrated in breeding and straw production areas, and biogas is produced from collected animal excreta and discarded straw to meet the daily needs of farmers. Rural water improvement projects, sanitary toilet extension projects, biogas production projects, and solar water heater construction projects are representative environmental protection construction projects in rural China in recent years. The development of these four types of projects is shown in Fig. 3. Rural water improvement project focuses on the scientific supply of rural drinking water and aims at ensuring the drinking water safety of rural residents, which is the most important project in rural environmental remediation. Rural water improvement project has been promoted rapidly in recent years and has been basically completed (Fig. 3a). Sanitary toilet extension project aims to achieve the harmless transformation of rural household toilets by the treatment or resource utilization of toilet manure and improvement of rural domestic sewage treatment rate. The popularization rate of sanitary toilets increased from less than 45% in 2000 to about 85% in 2017, and the indiscriminate discharge of rural domestic sewage

was effectively controlled (Fig. 3b). Biogas production increased rapidly from 2000 to 2012 and then began to decline after reaching its peak in 2012 due to the fact that natural gas pipelines began to be laid in rural areas, which was beneficial to further improve energy utilization efficiency (Fig. 3c). The coverage area of solar panels in rural areas increased nearly nine times from 2000 to 2017. Compared with the common coal-fired heating, solar water heaters have the advantages of environmental protection and energy-saving, which can significantly reduce ecological environmental pollution and increase energy utilization rate, and exhibit great potential in rural sustainable energy utilization.

Suggestions for Further Efforts on Rural Environment Protection: Although in recent years, China's rural ecological environment problems have been alleviated in some aspects due to the attention of management and the progress of science and technology. However, there are still many shortcomings. The root causes of these problems mainly include farmers' weak awareness of environmental protection, unreasonable resource structure, insufficient environmental supervision, and insufficient investment in environmental pollution control funds. To further improve the rural environment, the following suggestions are put forward:

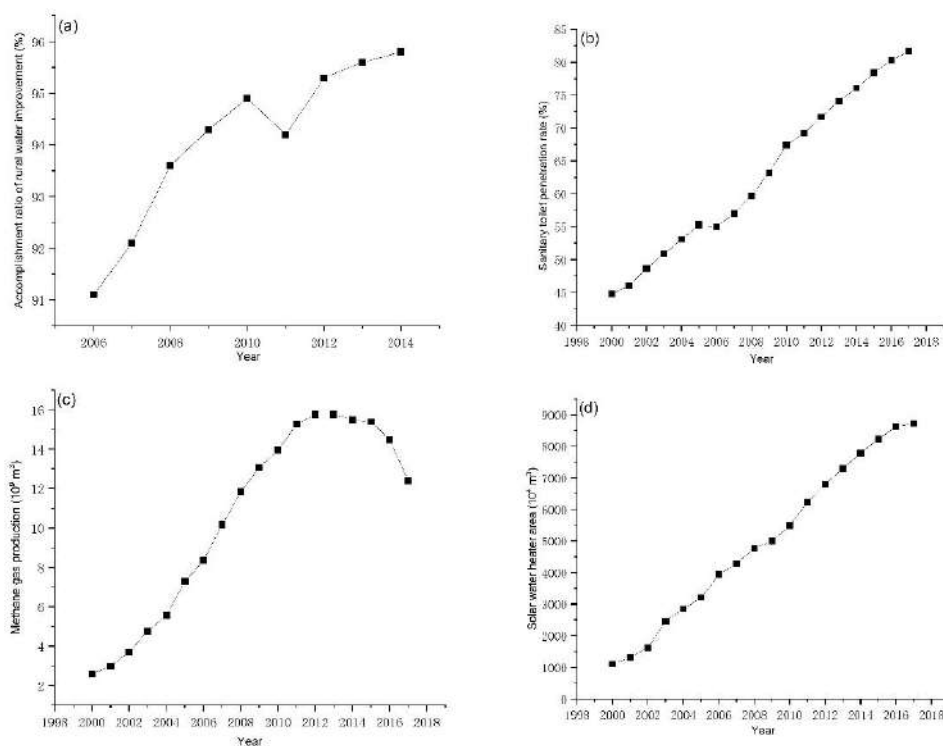


Fig. 3: Variation of environmental protection facilities in China. Panels a, b, c, and d represent the trends of rural water improvement, sanitary toilet penetration, methane gas production, and solar water heater, respectively.

1. Developing ecological agriculture. The promotion of ecological agriculture is the primary measure to improve the rural environment. The vigorous development of ecological agriculture requires the rational development and utilization of existing ecological resources in agriculture, the close combination of ecological benefits and economic benefits, and the optimization of China's agricultural structure. On the one hand, it is necessary to pay equal attention to grooming and governance. The local government needs to guide farmers to develop organic ecological agriculture, reduce the amount of chemical fertilizers and pesticides, reduce man-made pollution, and prohibit the destruction of plants and deforestation. On the other hand, the relevant departments should take inclined measures, invest funds to help farmers to change toilets and circles, build biogas digesters and other pollution reduction engineering measures, and reduce the discharge of domestic and aquaculture sewage fundamentally.
2. Strengthening the propaganda of environmental protection. Improving rural residents' awareness of environmental protection is a fundamental measure to solve the problem of rural environmental pollution in China. Under the background of the Internet age, local governments can use the combination of new media and traditional media as an instrument to carry out environmental protection propaganda, popularize rural environmental protection knowledge, and strengthen environmental protection legal education. The government and the community should pay attention to cultivating residents' awareness of garbage recovery and treatment, and promote ecological education for residents.
3. Promoting the construction of environmental protection facilities. The government should increase investment in rural environmental protection and strengthen infrastructure construction vigorously. On the one hand, it is necessary to promote the centralized collection of rural garbage and the construction of harmless physical facilities. The garbage transfer stations can be established in towns or villages, and all kinds of garbage should be transported to the transfer stations regularly, and then transported to the garbage treatment plants in a unified way. On the other hand, rural sewage treatment is needed to be actively carried out. It is important to adopt a combined measure of decentralized and centralized treatment to comprehensively treat domestic sewage, and actively promote the scientific treatment mode of domestic sewage.
4. Developing the legal system of rural environmental protection. On the whole, the current rural environmental

protection laws and regulations system is still far from perfect and lacks operability. In addition, there are still legal gaps in many areas of the rural environment and resource protection in China. Therefore, it is necessary to gradually establish and improve laws and regulations on the rural environment, strengthen environmental law enforcement and supervision, and protect the rural environment from the level of the legal system. Based on national laws and regulations, it is suggested that localities further formulate local supporting laws and regulations for rural areas according to their own environmental pollution characteristics to fill the legal gaps. In rural areas with rapid urbanization, on the one hand, it is important to deal with the environmental problems from traditional agricultural production, such as livestock and poultry pollution, rural pesticide, fertilizer, agricultural film pollution, domestic garbage, domestic sewage, and other issues. On the other hand, the rectification and standardization of the sewage discharge of key township enterprises is also a challenge for local government.

CONCLUSIONS

In this paper, China's current rural urbanization process is summarized, and various environmental problems in the related rural urbanization development process are analyzed in detail. Countermeasures are put forward for various environmental problems in the current development process. On the one hand, urbanization has increased the types and sources of pollutants in China's rural areas and aggravated the deterioration of the ecological environment. Traditional agricultural pollution and industrial and domestic pollution introduced by urbanization have made rural environmental governance more complicated. On the other hand, urbanization is conducive to urban-rural connectivity and is helpful in promoting rural infrastructure construction and accelerating the development of the environmental protection industry. In the past decades, China's rural environmental improvement has been promoted rapidly, and some achievements have been made in energy conservation and environmental protection. The rural water improvement project, sanitary toilet extension project, biogas production project, and solar water heater construction project have made remarkable progress in rural areas. However, there are still many blanks. It is of great significance for the government and community to strengthen the protection of rural ecology and environment by means of technology popularization, publicity and education, and legal means to accomplish the harmonious development of urbanization construction and ecological environment protection, which will lead to the sustainable development of the rural economy.

REFERENCES

- Chen, M., Sun, Z.H., Wang, Y.J. and Guo, S.F. 2019. Evaluation of coupling coordination among the urban physical environment, economy, and population: A case study of 36 main cities in China. *Adv. Civil Eng.*, 2019: 12.
- Fang, C., Liu, H., Li, G., Sun, D. and Miao, Z. 2015. Estimating the impact of urbanization on air quality in China using spatial regression models. *Sustainability*, 7(11): 15570-15592.
- Gibbs, J.P. and Davis, K. 1958. Conventional versus metropolitan data in the international study of urbanization. *Am. Sociol. Rev.*, 23(5): 504-514.
- Gibbs, J.P. and Martin, W.T. 1958. Urbanization and natural resources - a study in organizational ecology. *Am. Sociol. Rev.*, 23(3): 266-277.
- Ou, C., Zhu, X., Hu, L., Wu, X., Yu, W. and Wu, Y. 2020. Source apportionment of soil contamination based on multivariate receptor and robust geostatistics in a typical rural-urban area, Wuhan city, middle China. *Open Chem.*, 18(1): 244-258.
- Wu, W., Zhou, J., Niu, J. and Lv, H. 2021. Study on coupling between mineral resources exploitation and the mining ecological environment in Shanxi Province. *Environ. Develop Sust.*, 6: 41-58.
- Xia, C., Liu, G., Chen, K., Hue, Y., Zhou, J., Liu, Y. and Mei, J. 2020a. Stable isotope characteristics for precipitation events and their responses to moisture and environmental changes during the summer monsoon period in Southwestern China. *Pol. J. Environ. Stud.*, 29(3): 2429-2445.
- Xia, C., Liu, G., Mei, J., Meng, Y., Liu, W. and Hu, Y. 2019. Characteristics of hydrogen and oxygen stable isotopes in precipitation and the environmental controls in tropical monsoon climatic zone. *Int. J. Hydro. Energ.*, 44(11): 5417-5427.
- Xia, C., Liu, G., Meng, Y., Wang, Z. and Zhang, X. 2020b. Impact of human activities on the urban river system and its implication for water-environment risks: An isotope-based investigation in Chengdu, China. *Human Ecol. Risk Assess.*, 11: 39-53
- Xia, C., Liu, G., Zhou, J., Meng, Y., Chen, K., Gu, P., Yang, M., Huang, X. and Mei, J. 2020c. Revealing the impact of water conservancy projects and urbanization on the hydrological cycle based on the distribution of hydrogen and oxygen isotopes in water. *Environ. Sci. Pollut. Res.*, 16: 111-129
- Yang, W., Xie, S., Zhang, Z., Hu, J., Zhang, L., Lei, X., Zhong, L., Hao, Y. and Shi, F. 2019. Characteristics and sources of carbonaceous aerosol across urban and rural sites in a rapidly urbanized but low-level industrialized city in the Sichuan Basin, China. *Environ. Sci. Pollut. Res.*, 26(26): 26646-26663.
- Yang, Y. 2010. *Management of Agricultural Pollution in China: Current Status and International Experience.*
- Zhang, C., Kuang, W., Wu, J., Liu, J. and Tian, H. 2021. Industrial land expansion in rural China threatens environmental security. *Frontiers Environ. Sci. Eng.*, 15(2): 61-73.
- Zhao, J.J., Shi, X.C., Wang, K.L., Yu, W.H. and Yin, H.C. 2017. The Influence of Land Intensive Use and Urbanization to Air Pollution: Evidence from China. *IOP Conf. Ser.: Earth Environ. Sci.* 94 012139
- Zhu, Y., Wang, D., Li, W., Yang, Y. and Shi, P. 2019. Spatial distribution of soil trace element concentrations along an urban-rural transition zone in the black soil region of northeastern China. *J. Soils Sed.*, 19(7): 2946-2956.



A GIS-Based Methodology to Determine Effect of Vehicular Pollution at Ward Level: Case Study of Jaipur City

A. D. Vyas*†, K. Mahale* and R. Goyal**

*Department of Civil Engineering, Manipal University Jaipur, India

**Department of Civil Engineering, Malaviya National Institute of Technology, Jaipur, India

Nat. Env. & Poll. Tech.
Website: www.neptjournal.com

Received: 09-11-2020

Revised: 26-01-2021

Accepted: 20-02-2021

Key Words:

Air pollution

Linear regression

NO₂

Road density

ABSTRACT

To determine appropriate measures to reduce air pollution in any urban city, the first essential requirement is to estimate the spatial distribution of air pollution parameters in that area. In absence of air monitoring stations, alternative methods are required for the same. In the present work, a GIS-based methodology is presented to estimate the level of NO₂ based on the road density of the road network of different categories of roads. Road network GIS layer and measured levels of the average value of NO₂ for the year 2019 at 12 air pollution monitoring stations of Jaipur city are used to develop a large number of possible linear regression models for estimation of NO₂ values based on road density values. Akaike Information Criterion (AIC) and adjusted r^2 values are used to evaluate and arrive at the best-fitted model. Values from the cities of Jodhpur and Kota are used to validate the model. Using this model, NO₂ levels are determined at 91 wards of Jaipur city and the output is compared with the similar map derived based on interpolation of NO₂ values at the 12 monitoring stations. It is concluded that the methodology developed in this study generates better estimates of NO₂ at the ward levels.

INTRODUCTION

Climate change due to global warming is the major crisis, presently the world is facing. Climate change is closely related to the rise in air pollution. As per Institute for Advanced Sustainability Studies (IASS 2020), these air pollutants are responsible for climate change by affecting the incoming solar radiation. Few pollutants find their way and are absorbed by the atmosphere whereas others are reflected by the atmosphere thereby affecting the earth's atmosphere by cooling or warming it. Ground-level ozone, methane, and black carbons are classified under short-lived climate-forcing pollutants (SLCPs). A report by World Health Organization (2019) predicts that air pollutants are the biggest reason for the major health threat and severely affecting climatic conditions. As per the latest report by Health Effects Institute (2020 a), air pollution is the major cause of 1 in 9 deaths globally. It has been estimated that globally 6.67 million mortalities in the year 2019 were because of air pollution. This is majorly attributed to smog in the outer atmosphere and smoke inside the homes. Heart diseases, strokes, chronic obstructive pulmonary diseases resulting from acute respiratory infections, cancer of the lungs are major contributors to high mortality rates. It is estimated that nine out of ten people are inhaling polluted air with higher levels. UNICEF (2016) press report projected that 300 million children are breathing toxic air. As per the United States Environmental Protection

Agency (2020), particulate matter affects the lungs and heart which is also confirmed through numerous scientific studies across the globe. The United States Environmental Protection Agency (2016) has identified six "criteria" air pollutants as these pollutants are regulated under environmental and human health-based criteria by the Center for Disease Control and Prevention (CDC 2019). These pollutants are CO, NO₂, SO₂, particulate matter, ground-level ozone, and lead. It is mentioned that not enough data may be available on the effects of air pollutants on the health of human beings, still, it is considered a major risk multiplier for the health of human being specially in developing countries. The latest findings on air pollutant impacts on human health as published in the Lancet, "Global Burden of Disease" is very alarming for a country like India. Indeed, Indian population has the maximum exposure to PM 2.5 and the third highest exposure to O₃. It is estimated that almost 1.67 million deaths annually are caused in India due to air pollutants which include 116,000 infants as reported in State of Global Air 2020, Health Effects Institute (2020b).

A study done for natural aerosols in South Gobi Desert by Filonchik & Hurynovich (2020) was found to be of great importance. Data from 2016 to 2019 was analyzed to find the spatial-temporal patterns of atmospheric pollutants in eight cities. It was reported that occurrence rates of pollutants exceeding in concentrations with respect to the

Chinese National Ambient Air Quality Standard (CNAAQs) grade 1 and grade 2 were 40.1% and 5.4% for $PM_{2.5}$ and 82.9% and 11.64% for PM_{10} in the region. Khaniabadi et al. (2020) studied the impact on health due to an increase in the concentration of different pollutants by $10 \mu\text{g}\cdot\text{m}^{-3}$. They studied the effect of PM_{10} , NO_2 , and O_3 in Kermanshah City, Iran. The results indicated that a $\mu\text{g}\cdot\text{m}^{-3}$ change in PM_{10} , NO_2 , and O_3 increases the relative risk by 1.066, 1.012, and 1.020, respectively.

Remote sensing has proved to be useful for depicting spatial variability of air pollutants in an urban area (Bechle et al. 2013). In their study, estimates of surface NO_2 levels recorded by Ozone Monitoring Instrument (OMI) onboard NASA's Aura satellite were compared with values recorded by US EPA ambient monitoring stations. OMI measures the daily level of NO_2 tropospheric column abundance. Scaling factors (surface-to-column ratios) were used to relate satellite data to ground-level measurements. Costabile et al. (2010) studied the distribution of pollutants NO_x , SO_2 , NO_2 , Xylenes, Benzene, and Toluene within the urban area of Lanzhou, China to understand the spatial distribution of these pollutants. The investigation found that it was mainly governed by the factors responsible for the diffusion of emission sources through space.

Nieto et al. (2015) collected levels of CO , PM_{10} , NO_x , O_3 , and SO_2 , for 3 years to build a regression model of air quality for the urban area of Oviedo, Spain. The model was built at a local scale using a multivariate adaptive regression splines (MARS) technique. Mohammad and Juahir (2015) identified the spatial pattern of air pollutants in the northern part of Peninsular Malaysia. The study was carried out from 2008 to 2011, covering seven air pollution monitoring stations. The main pollutants that were part of the study were NO_2 , O_3 , CO , and PM_{10} obtained from the Department of Environment, Malaysia (DoEM). ANOVA, Artificial Neural Network (ANN) and environ metric techniques (HACA and Descriptive Analysis approaches) were used in analyzing the data. They reported that based on ANOVA single test, the p -value of PM_{10} is significantly a smaller alpha level ($p=0.05$) and is therefore suitable for further analysis as compared to O_3 , NO_2 , and CO .

Ryu et al. (2019) used the GIS-based kriging interpolation method to develop a nationwide map of NO_2 concentration over South Korea. Remote sensing data was integrated with the ground observations and a good value of root-mean-square standardized (RMSS) error was obtained. In their study, they compared data for different data sources which include detailed national data besides remote sensing data and other sources. In the study, it was reported that the average concentration was highest when data was taken through

remote sensing. LUR models that are land-use regression models were formulated to analyze the concentration of NO_2 in both urban and non-urban areas. In their paper, Zhu & Lok (2018) described the temporal and spatial variability of nitrogen dioxide concentrations at the level of major streets for densely populated parts of Hong Kong with very high traffic volumes. Using a combination of remote sensing data and direct measurement in the field, temporal variations were differentiated with spatial distributions. This was carried out by ignoring the flow pattern of traffic and concentrating on changes in the spatial distribution of NO_2 .

Walkability one of the measure for air pollutants pertaining to traffic was defined by Cowie et al. (2016). They compared walkability with weighted road density for Sydney neighborhoods, representing 3.6 million population. High walkability and low weighted road density were defined as "sweet spots" and reverse of that as "sour spots" in the neighborhoods. Even short exposure to a higher concentration of NO_2 can aggravate asthma, respiratory diseases and even visiting hospital emergency rooms (EPA, 2016). In a report by the United States Environmental Protection Agency, (2016), it was reported that a long duration exposure of NO_2 severely affected children and elderly citizens. In the atmosphere, NO_2 and NO_x react with other chemicals to form ozone and particulate matter which when inhaled are disastrous to human health, mainly affecting the respiratory systems. Carlsaw et al. (2019) in their report raised concern over the exceeding concentrations of NO_2 of more than $40 \mu\text{g m}^{-3}$ as prescribed by the European Directive limit value. Munoth et al. (2015) reported higher levels of NO_2 and Fluoride in groundwater in Rajasthan state.

Nitrogen dioxide (NO_2) which is mainly emitted from vehicular emissions is yellow-brownish in color is also emitted from industrial activity and power plants. As per the Hindu (2015), the emission of gas has reached significantly high in India and South Asia region during the decade 2005-14 as projected in a study through NASA satellite map. NASA satellite maps predict that exposures of Nitrogen dioxide even for short periods can aggravate respiratory diseases, asthma and can also lead to hospitalizations.

Balakrishnan et al. (2019) discussed that though cardiovascular diseases are the largest cause of death in India but are closely followed by air pollution, which is the second largest reason for premature deaths in India. Till the 1990s, air pollution was relatively lower in the list of causes that caused most deaths in India. In another study, it has been reported that Rajasthan is amongst the leading states in the country with the widespread cause of chronic obstructive pulmonary disease (COPD) (TNN 2017) and asthma induced deaths which in turn is linked to air pollution in more than

half the cases followed by smoking for a quarter of the cases. According to ORGCC (2020), approximately one-third percent of the children in Jaipur suffer from acute respiratory infection (ARI). It was further emphasized that the figure has been increasing recently. Overall, in Jaipur, there has been an increase in Rhinitis, asthma, bronchitis, pneumonia, COPD, chronic cough, sneezing, itching, eye problems ARI, and other respiratory issues. Rajasthan tops the list when it comes to deaths due to air pollution, according to Singh (2019). Using geostatistical and geospatial techniques Dadhich et al. (2018b) estimated the temporal and seasonal variations (2004–2015) of particulate and gaseous pollutants in the city of Jaipur. They performed an ordinary least square (OLS) regression technique to reveal a good correlation between Air Quality Index and weathering features like wind speed, humidity, and temperature for both winter and summer seasons. Similarly, Dadhich et al. (2018a) also used GIS-based approaches for assessing the ambient air quality standards of Kota city.

To reduce the impact of air quality parameters in any area, the first essential requirement is to estimate the spatial distribution of these parameters in that area. This would provide an indication of areas where the air quality is bad or lower than the standard. If this information is available, it becomes easier for urban planners and experts to apply remedial measures and subsequent actions can be taken in the areas which are highly polluted. Adequate measurements thus can be planned and taken in those areas. Estimate of air quality parameters in any area is typically determined with the help of observed values of these parameters at air quality monitoring stations. Different interpolation tools are used to predict the values at other places. However, the density of such air quality monitoring stations is presently extremely too low in many urban areas. Determining air quality in such areas, other than the vicinity of such sensors, is a challenging task. Interpolation typically leads to extrapolation as monitoring stations are usually located in the central part of the city. This leads to the overestimation of air pollution parameters in the urban periphery of big cities. Therefore, a methodology is desired which could estimate the air quality parameter even in the absence of monitoring stations.

In the present study, a new methodology is presented which determines the value of NO_2 due to vehicular pollution, based on the density of the road network of any area. The road network layer, consisting of roads of different categories, such as highways, major roads, and inner roads, of any urban area, can easily be mapped using various remote sensing systems or google earth. Such road network layers could be generated and updated on regular basis. Therefore, a methodology that is dependent on such easily available

information is likely to be of great importance in the absence of a good density of air quality monitoring stations.

Jaipur city with almost 3.5 million urban population as of 2020 (3.1 million as per 2011 census) has three continuous monitoring stations named Continuous Ambient Air Quality Monitoring Stations (CAAQMS) and nine manual stations. Pollutants emitted from vehicular emissions like Nitrogen Dioxide (NO_2) and particulate matter PM_{10} are key pollutants that are continuously monitored at these stations besides other pollutants. The data available is of very limited capacity for a large area of 470 sq km of Jaipur city. Even if it is required to find out the concentration at ward level from these 12 points through GIS spatial interpolation methods, the density is not appropriate, and therefore data is rather extrapolated or interpolated between drastically different points locations. In that case, the values are likely to be not accurate except for those wards where these stations are located. In this paper, there has been an attempt to relate Jaipur road network layer data with available vehicular pollutant data (NO_2) measured at 12 air pollution monitoring stations. A large number of possible models are generated, and their prediction accuracy is compared between different models. Multi-model selection criteria such as the Akaike information criterion and Bayesian information criterion are used to select better-performing models amongst the several hundred models generated. Model output for two additional air quality monitoring stations of Jodhpur and Kota cities are used to validate the model. Estimated values of NO_2 are determined for all the wards of Jaipur city to understand the spatial distribution of vehicular pollution in Jaipur city.

STUDY AREA

Jaipur the capital city of Rajasthan state is a big tourist hub; part of the golden triangle is also called as pink city of India. As per the 2011 census, Jaipur has a population of around 3.1 million which is characterized by high summer temperatures, low rainfalls, and mild winter as shown in Fig. 1. The average yearly rain for the city is just below 600 mm in comparison to India's national average of almost 1100 mm. The city recorded a yearly growth rate of five percent in 2011 in comparison to 2001 and was ranked 10th among India's megacities (Sogani & Vyas 2019). The city is part of the government of India's Smart City Program and there are massive plans for urban infrastructure development. The maps of zones and wards of the city are as per JDA (2020) and were further digitized. Fig. 1 shows the different zones and wards of Jaipur city. Table 1 gives major information about the city.

All the 91 wards of Jaipur city based on 2019 classifications were taken into consideration for this study (Vyas

Table 1: Key statistics of Jaipur City

Study area: Name of city	Jaipur City	
Total Area	467 Square Kilometres	
City Wards and Zones	91 wards and 8 zones	
Total House Holds	737179	
Total Population covered	3046185 (As per the year 2011 census data)	
	Male	1603136
	Female	1443048
	Sex Ratio	900 Females per 1000 Males

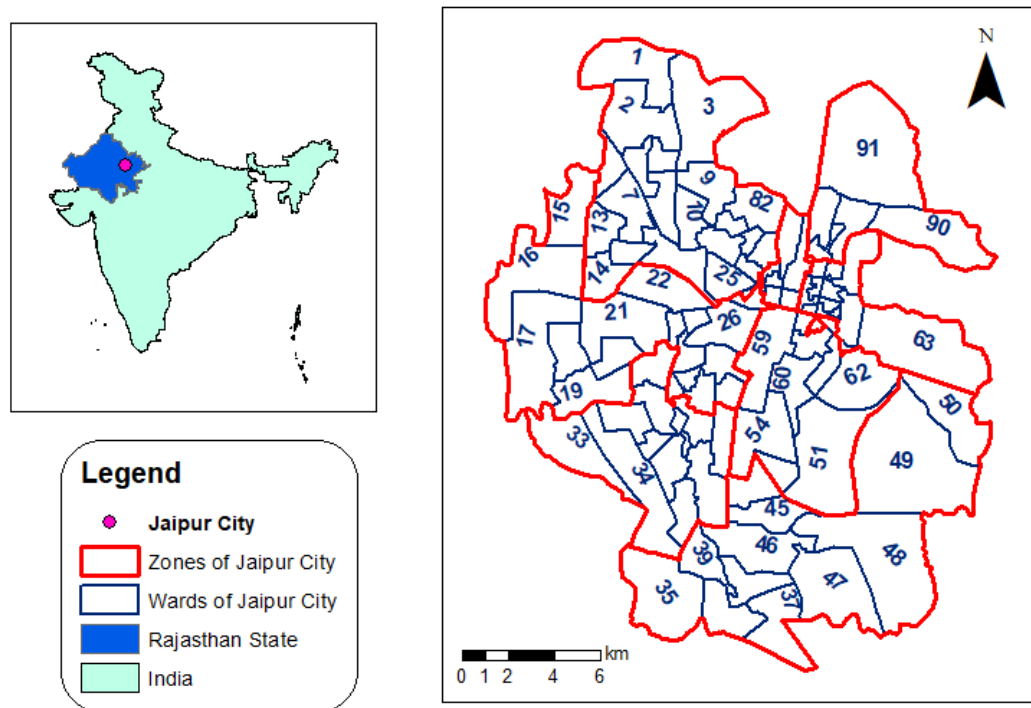


Fig. 1: Zones and wards of Jaipur city.

et al, 2020a). A new bifurcation of city wards was done in December 2019 where the city wards were reclassified into a total of 250 wards. The Greater Jaipur has 150 wards and Heritage Jaipur has 100 wards. This study was confined to 8 Zones and 91 wards as shown in Table 2.

Ambient air quality is continuously monitored in the city as State Pollution Control Board has installed three Continuous Ambient Air Quality Monitoring Station (CAAQMS) and nine manual air quality monitoring stations under National Air Quality Monitoring Programme (NAMP), as shown in Fig 2. At CAAQMS Particulate Matter ($PM_{2.5}$ and PM_{10}), Gaseous pollutants, NO_x , SO_2 , CO , O_3 VOC, and NH_3 , and

Meteorological parameters like Wind Speed, Wind Direction, Temperature, Relative Humidity, Solar Radiation, Pressure, etc. are measured continuously (Vyas et al. 2020). At NAMP stations PM_{10} , NO_2 , and SO_2 are measured twice a week. Due to the dry conditions prevailing over a major part of the year, levels of PM_{10} are found to be in excess. Suspended particulate matter coming from road dust, construction and demolition activities, vehicular emissions, burning of fossil fuels, and solid waste in open, industrial emissions are key air pollutants of the city.

Table 3 shows the annual average PM_{10} and NO_2 values at different stations for the year 2019. Fig. 3 and Fig. 4 show

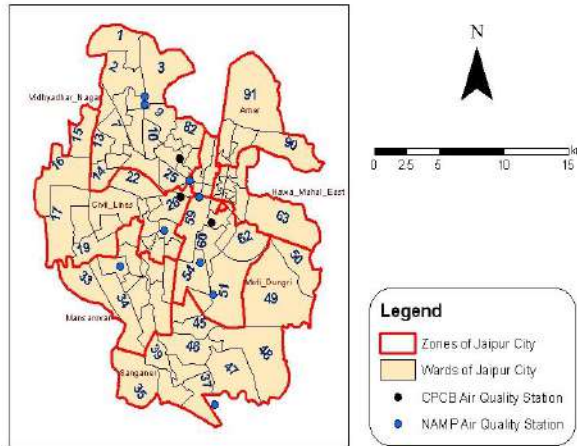


Fig. 2: Location of air quality monitoring stations.

Table 2: Classification of Jaipur city Wards and Zones

S. No.	Name of Zone	Total Wards	Classification of Wards
1	Vidhya Dhar Nagar	21	1 to 14, 23 to 25 and 79-82
2	Civil Lines	16	15 to 22, 26 to 28, 30, 56 to 58 and 76
3	Man Sarovar	11	29, 31 to 34, 40 to 44 and 55
4	Sanganer	12	35 to 39, 45 to 50 and 52
5	Moti Doongri	9	51, 53 and 54, 59 to 62, 64 and 65
6	Hawa Mahal East	11	63 to 73, 85 and 86
7	Hawa Mahal West	6	74 and 75, 77 and 78, 83 and 84
8	Amer	5	87 to 91

the spatial distribution of PM₁₀ and NO₂ concentrations for the year 2019 for Jaipur city based on the annual average observed values of these parameters at the monitoring sta-

tions. As can be seen, most of the variation is visible only in the closed proximity of the air quality monitoring stations. Since monitoring stations only exist inside the city area,

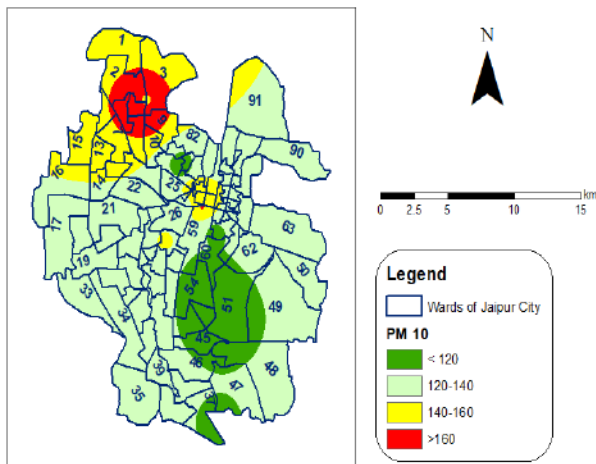


Fig. 3: Spatial distribution of average annual PM₁₀.

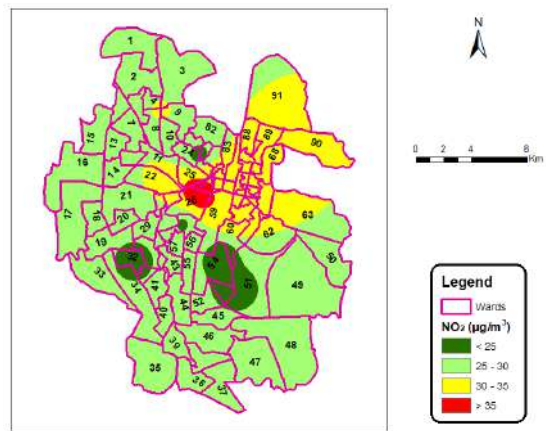


Fig. 4: Spatial distribution of average annual NO₂.

Table 3: Air Quality Parameters of Year 2019

Station Code	Latitude	Longitude	NO ₂ (µg/m ³)	PM ₁₀ (µg/m ³)
101	26.974	75.774	31.41	193.21
102	26.927	75.809	34.21	150.80
103	26.876	75.817	21.41	102.95
104	26.855	75.827	23.36	108.99
105	26.873	75.754	23.64	127.62
106	26.896	75.788	24.30	141.94
107	26.787	75.827	27.46	119.56
108	26.979	75.774	27.00	160.00
109	26.916	75.816	33.80	163.34
110	26.901	75.825	35.08	100.87
111	26.916	75.801	43.15	127.26
112	26.940	75.801	22.57	116.09

where traffic density and hence air pollution parameter levels are generally high, when interpolation is used, most of the outskirts of Jaipur city also show high levels of NO₂ values. NO₂ levels are likely to be lesser in these areas as the traffic density, a major contributor of NO₂ is much less as compared to inner city areas.

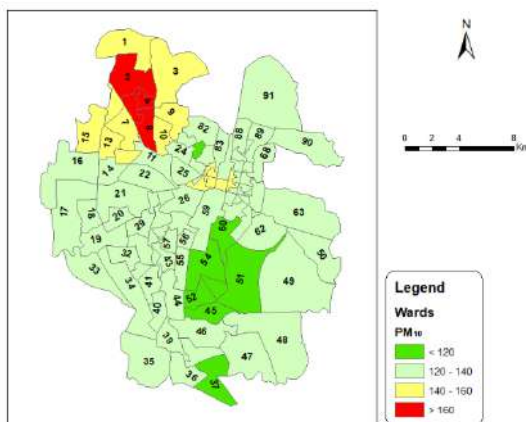
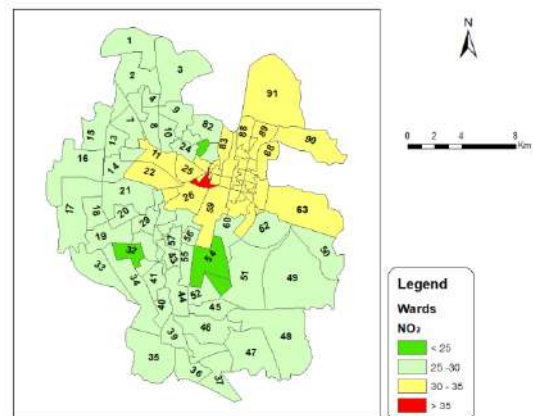
From the interpolated maps and using the zonal statistics tool, the average concentration of PM₁₀ and NO₂ could also be derived at the ward level. Color-coded maps are then plotted showing levels of PM₁₀ and NO₂ for different wards (Fig. 5 and 6). Most of the outer area of Jaipur city is classified under the category of 25-30 for NO₂, which seems to be on the higher side as traffic in these areas is typically lower than in the city area.

All roads of Jaipur cities were classified into three different groups based on estimated traffic on these roads. Level 01 roads are those roads that carry most of the daily vehicular

traffic of the city. Level 02 roads are those interconnecting level 01 roads. Though traffic on these roads is less than the level 01 roads however it is still good enough to generate some level of vehicular pollution. Level 03 roads are inner roads, typically carrying only the vehicular traffic of residents of that area. Though the level of pollution may be less on these roads, however, their density is more than that of other levels of roads. It is also observed that typically inner roads have a better level of plantations around the roads as compared to level 01 and 02 roads. Due to this, these roads may be serving as a sink for NO₂ pollution rather than the generation of pollution. Fig. 7 shows all the three levels of roads in sub maps A, B, and C respectively.

MATERIALS AND METHODS

Road maps of any area could be used to generate road density maps at different search radius levels. The line density tool

Fig. 5: Ward-wise levels of average PM₁₀.Fig. 6: Ward-wise levels of average NO₂.

calculates the density of linear features in the neighborhood of each output raster cell. Road density is determined in m length per m² area within the search radius. Conceptually, a circle of the size of the search radius is drawn around each raster cell center. The length of the portion of each road that falls within the circle is calculated. These figures are summed for all the roads falling within the search radius and the total is divided by the circle's area. Road density maps of different levels were generated for different search radius of 125, 250, 500, 750, 1000, 1250, and 1500 m. Fig. 8 shows the road density map of level 01 roads for the search radius of 750 m. Further buffer tool of GIS was used to generate planar buffers of the same sizes, as the search radius used for road density calculation, around each of the monitoring station. So, planar buffers of sizes 125, 250, 500, 750, 1000, 1250, and 1500 m were generated around each monitoring station. A dissolved type of none was used to ensure that each monitoring station has its own buffer even in case of partial overlap of buffers of different stations. Fig. 9 shows the buffers of 500m for all monitoring stations.

Using the buffer maps (Arc Map 2020a, 2020b) of a particular radius, say 1000 m, and road density maps of the same search radius of 1000 m, the zonal statistics tool was used to calculate the mean value of road density around each individual station for different road levels with different search radius.

Table 4 shows the value of road densities for all three levels of the road network around each monitoring station for a search radius of 750 and 1000 m.

RESULTS AND DISCUSSION

A large number of linear regression models could be developed to find the relationship between air pollution parameters PM₁₀ or NO₂ or a combination of them with the road density values of different levels of roads for different search radius and buffer areas. For examples if RD_{Li}^{SRm} is Road density of road level i and search radius m then some models that could be tried are shown as eqns. 1, 2, 3, and 4 below.

$$NO_2 = f(RD_{L1}^{SR750}, RD_{L2}^{SR750}, RD_{L3}^{SR750}) \quad (1)$$

$$NO_2 = f(RD_{L1}^{SR1000}, RD_{L2}^{SR1000}) \quad (2)$$

$$PM_{10} = f(RD_{L1}^{SR1000}) \quad (3)$$

$$\log(NO_2) = f(\log(RD_{L1}^{SR750}, RD_{L2}^{SR750}, RD_{L3}^{SR750})) \quad (4)$$

A large number of combinations of different road levels and search radius could be taken as independent variables to find the relationship of them with dependent variables of air pollution parameters. Further variations such as linear and log-log combinations could be tried.

A total number of 192 different models were tried using a script developed in R language, out of which 96 models were using normal values of road density and air pollution parameters and 96 of them using log₁₀ values of all parameters. Models with log_e (ln) were also tried, but they were giving poor results as compared to models with log₁₀ and hence are not discussed further. To compare various models and to select which model is performing better, the coefficient of determination (r²) is calculated for each model and com-

Table 4: Road Density Values Around Monitoring Stations

Station Code	Search Radius: 750 m			Search Radius: 1000 m		
	Level 01	Level 02	Level 03	Level 01	Level 02	Level 03
101	2.23	2.59	16.88	1.99	2.76	17.14
102	1.90	4.40	15.18	2.01	4.06	14.17
103	1.46	1.71	10.97	1.50	1.68	10.77
104	1.09	2.14	10.92	0.93	1.93	10.75
105	2.23	2.83	20.49	1.91	2.80	20.45
106	1.52	3.76	18.82	1.54	3.67	18.47
107	2.12	1.29	11.47	1.76	1.40	11.53
108	1.77	3.22	17.11	1.63	3.19	16.72
109	2.77	3.32	9.33	2.63	3.21	10.22
110	2.18	5.00	12.69	2.14	4.56	12.32
111	3.28	3.53	10.43	2.98	3.48	10.68
112	1.61	3.77	18.79	1.49	3.44	17.15

pared. r^2 is a scale-invariant statistic that gives the proportion of variation in the target variable explained by the linear regression model (Analytics Vidya 2020). The R-squared statistic suffers from a major flaw. Its value never decreases no matter the number of variables we add to our regression model, even if redundant variables are added. Therefore “Adjusted r^2 ” (referred to as $\text{adj } r^2$) values are determined. The $\text{adj } r^2$ takes into account the number of independent variables used for predicting the target variable.

It is well known that when fitting linear regression models between two sets of known and unknown variables, more

than one model could be developed with almost comparing values of r^2 or $\text{adj } r^2$. Choosing a specific model between them would require evaluations of uncertainties associated with these models. A number of statistical criteria could be used to evaluate alternative models (Poeter & Anderson 2005). Akaike Information Criterion (AIC) and Bayesian Information Criterion (BIC) are used in the present work (Zhou & Herath 2017, Rajput et al. 2020).

AIC for a model could be calculated using eqns. 5, 6 and 7

$$AIC = n \ln(\sigma^2) + 2k \quad (5)$$

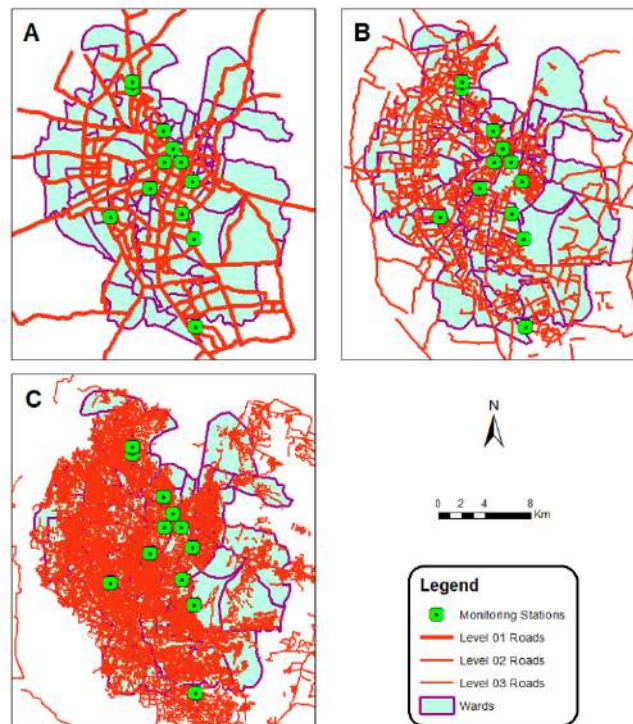


Fig. 7: Road maps of Jaipur city (A – Level 01, B – Level 02 and C – Level 03).

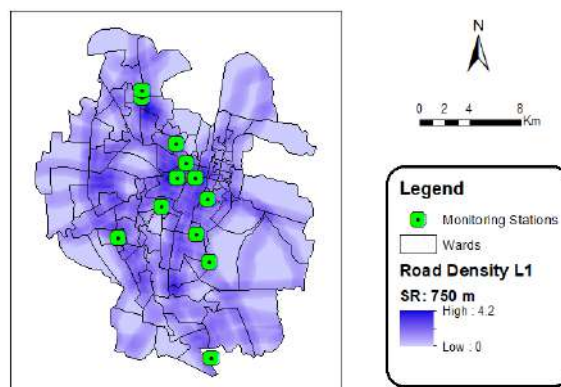


Fig. 8: Road density map of level 01 roads with search radius: 750 m.

$$\sigma^2 = \frac{SWSR}{n} \tag{6}$$

$$SWSR = \sum_{i=1}^n \omega_i [y_i - y'_i(b)]^2 \tag{7}$$

here:

n: number of observations, equal to 12 for all the models;

k: number of model parameters, varies from 1 to 3;

σ^2 : residual variance;

SWSR: sum of weighted squared residuals;

ω_i : weight for the i^{th} observation, taken as 1 for all observations;

y_i, y'_i : measured and model calculated dependent variable, respectively.

BIC is calculated as given in eqn. 8.

$$BIC = n \ln(\sigma^2) + k \ln(n) \tag{8}$$

AIC and BIC values of all models were also evaluated using a script in R language. The model with minimum values of AIC was selected as the best model.

Models were divided into two different streams, one with normal values and another with \log_{10} values of parameters. Table 5 shows the 5 best models of both the streams with the values of r^2 , adj r^2 , AIC, and BIC.

As can be seen, the best values of r^2 and adj r^2 are achieved for model 1, belonging to stream 1 of the models, which is between normal values of NO_2 and road density values of levels 1, 2, and 3 roads with a search radius of 750m. This model also gives the lowest AIC and BIC values in stream 1 of the models. In stream 2, the best model is model 6, which is for the same NO_2 and road density values of levels 1, 2, and 3 roads with a search radius of 750m, however with \log_{10} values of all these parameters. This model gives lower r^2

Table 5: Performance parameters of different parameters

Model number	Stream 1: Normal values of parameters					
	Model description	r^2	adj r^2	AIC	BIC	P_m
1	$NO_2 = f(RD_{L1}^{SR750}, RD_{L2}^{SR750}, RD_{L3}^{SR750})$	0.86	0.81	64.47	66.90	42.6
2	$NO_2 = f(RD_{L1}^{SR1000}, RD_{L2}^{SR1000}, RD_{L3}^{SR1000})$	0.85	0.80	65.20	67.62	28.1
3	$NO_2 = f(RD_{L1}^{SR500}, RD_{L2}^{SR500}, RD_{L3}^{SR500})$	0.83	0.77	66.84	69.27	10.4
4	$NO_2 = f(RD_{L1}^{SR1000})$	0.76	0.74	67.17	68.62	10.0
5	$NO_2 = f(RD_{L1}^{SR1250}, RD_{L3}^{SR1250})$	0.80	0.75	67.18	69.12	8.9
Stream 2: \log_{10} values of parameters						
6	$\log(NO_2) = f(\log \text{ values of } RD_{L1}^{SR750}, RD_{L2}^{SR750}, RD_{L3}^{SR750})$	0.81	0.74	-33.58	-31.16	39.7
7	$\log(NO_2) = f(\log \text{ values of } RD_{L1}^{SR1000}, RD_{L2}^{SR1000}, RD_{L3}^{SR1000})$	0.80	0.72	-32.75	-30.32	27.6
8	$\log(NO_2) = f(\log \text{ values of } RD_{L1}^{SR1000}, RD_{L3}^{SR1000})$	0.72	0.66	-30.76	-28.82	12.1
9	$\log(NO_2) = f(\log \text{ values of } RD_{L1}^{SR500}, RD_{L2}^{SR500}, RD_{L3}^{SR500})$	0.76	0.67	-30.68	-28.25	10.3
10	$\log(NO_2) = f(\log \text{ values of } RD_{L1}^{SR1000})$	0.66	0.63	-30.45	-29.00	10.2

and adj r^2 values, however, AIC and BIC values are negative values and much lower as compared to model 1. Based on adj r^2 values, it can be said that model 1 explains 81% of the variations in NO_2 values whereas model 6 explains 74% of such variation. Thus, it can be concluded that the contribution of road traffic in average NO_2 value is around 75-80% in Jaipur city. To further compare these models, a posterior model probability (p_m) is defined, as given in eqn. 9.

$$p_m = \frac{e^{-0.5\Delta_m}}{\sum_{j=1}^m e^{-0.5\Delta_j}} \quad (9)$$

here

$$\Delta_m = AIC_m - AIC_{min}$$

AIC_m : AIC value for model m ;

AIC_{min} : the minimum AIC values of all models.

Table 5 also shows the values of posterior model probability of all the models considering the two streams separately and considering only the 5 best models per stream. As can be seen, model 1 has about 42.6% probability of being the best amongst the first five models of stream 1 whereas model 6 has a 39.7% probability of being the best amongst the first five models of stream 2.

As a next step, models 1 and 6 are further analyzed to compare them against each other. Fig. 9 shows the scatter plot between NO_2 and RD_{L1}^{SR750} and \log_{10} variant of the same parameters. As can be seen from the graphs there is a trend in both the curves, however, the range of values is considerably lower in model 6 as compared to model 1.

In model 1, coefficients for RD_{L1}^{SR750} , RD_{L2}^{SR750} and RD_{L3}^{SR750} are calculated as 7.10, 2.52, and -0.58 respectively, and the intercept is 15.07. Similarly, the coefficient

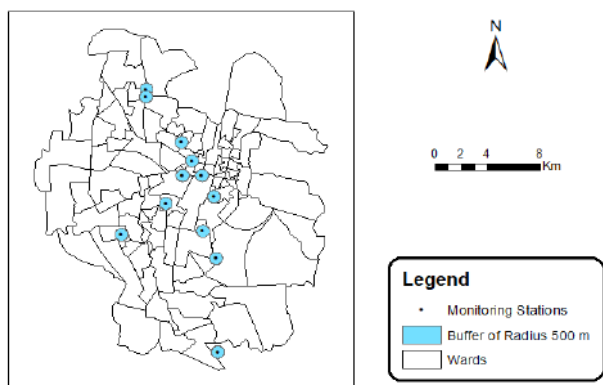


Fig. 9: Buffers around monitoring stations of radius 500 m.

for model 6 are 0.45, 0.23, and -0.31 respectively for \log_{10} values of RD_{L1}^{SR750} , RD_{L2}^{SR750} and RD_{L3}^{SR750} and the intercept is 1.57.

Fig. 10 (a) and (b) shows the graphs between the observed and computed values of NO_2 for model 1 and 6, respectively.

To compare these models for observed values at other cities, two CAAQMS stations of Kota and Jodhpur cities are used. Road maps were prepared in the vicinities of these stations and road density values for levels 1, 2, and 3 roads with a search radius of 750 m were determined. Table 6 below gives details of observed NO_2 values for the year 2019 as well as road density values of different levels for a search radius of 750 m.

Both the cities are also shown in Fig. 10 (a) and (b). It can be seen that model no. 6 poorly estimates the value for Kota city. For Jodhpur city, both models 1 and 6 give similar estimates. Therefore, it is concluded that model 1 is better suited to estimate the value of NO_2 as compared to other models. Therefore, the estimated value of NO_2 values of any area such as wards, roads, plots, or points could be computed by first obtaining road density values of different levels 1, 2, and 3 of the roads at a search radius of 750 m and then using the eqn. 10 below

$$\text{NO}_2 = 15.07 + 7.10 RD_{L1}^{SR750} + 2.52 RD_{L2}^{SR750} - 0.58 RD_{L3}^{SR750} \quad (10)$$

Estimated values of NO_2 have been calculated for all the wards of Jaipur city and the map is shown in Fig. 11. This map is very different from that of Fig. 6, which was developed based on interpolated values of NO_2 and then calculating average value over different wards. Also, it can be seen that wards with NO_2 values of more than 35 are more in Fig. 11 as compared to in Fig. 6. Overall it can be concluded that NO_2 values derived from model 1 give a better estimate for the area which is farther away from the air monitoring station as compared to interpolated maps.

CONCLUSION

A new methodology is developed to estimate the level of air pollution parameter NO_2 , which is mostly caused by vehicular pollution, by using road density levels of different levels of road network in Jaipur city. The road network of Jaipur city is developed for 3 different levels of roads and

Table 6: Parameters for other cities.

City	NO_2	Road Density for Search Radius of 750 m		
		Level 1	Level 2	Level 3
Kota	29.29	2.068	0.404	16.642
Jodhpur	29.25	1.774	1.513	17.16

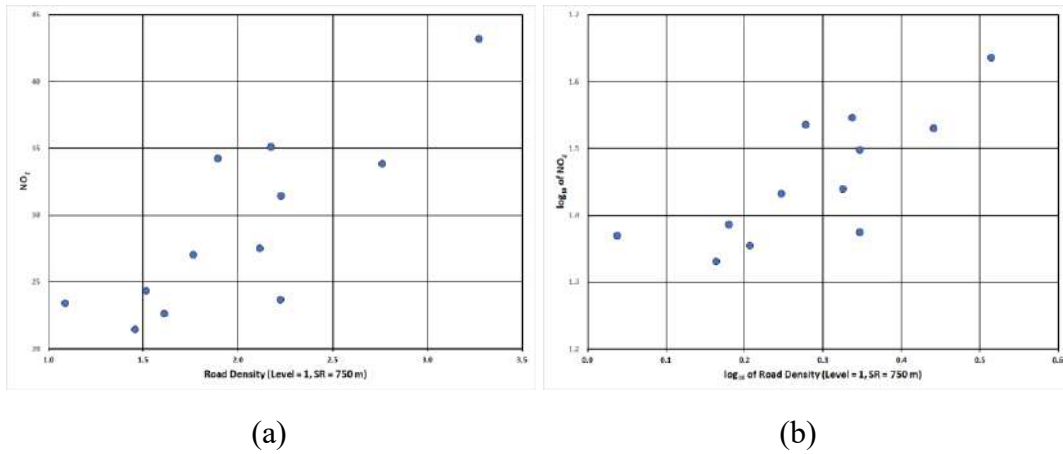


Fig. 10: (a) Scatter plot between NO₂ and RD_{L1}^{SR750} (b) between log10 values.

road density values are determined in the proximity of air pollution monitoring stations of Jaipur city. Proximity is defined in terms of search radius for measuring road density and buffer distance for air pollution monitoring stations.

It is found that for Jaipur city, linear regression model between measured average NO₂ values of 2019 and road density for search radius and buffer of 750 m is found to best-fitted model. Models are compared based on adj r² and AIC values and posterior model probability of the best five models in different streams are determined.

It is found that road networks could explain about 75-80% of the variations in NO₂ values. Also, the finally selected model has a 42.6% probability of being the best model amongst the first five selected from the normal stream of models.

Finally, the selected model is used to calculate estimated values of NO₂ at 91 wards of Jaipur city based on the road network of these wards and this map is compared with another map generated based on interpolated values of NO₂. It is concluded that the map generated from the selected model better explains the spatial distribution of NO₂. This model could also be used in other urban areas where either very few numbers or none at all air pollution monitoring stations are available.

REFERENCES

Analytics Vidya 2020. Key Difference between R-squared and Adjusted R-squared for Regression Analysis. <https://www.analyticsvidhya.com/blog/2020/07/difference-between-r-squared-and-adjusted-r-squared/>
 Arc Map 2020a. Buffer. <https://desktop.arcgis.com/en/arcmap/10.3/tools/analysis-toolbox/buffer.htm>

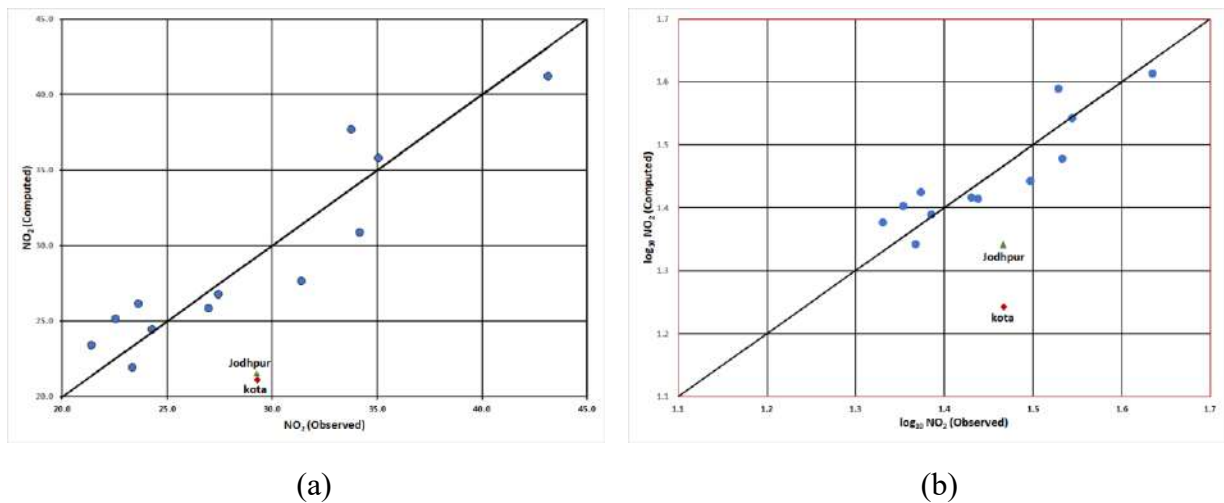


Fig. 11: Estimated values of NO₂ for different wards.

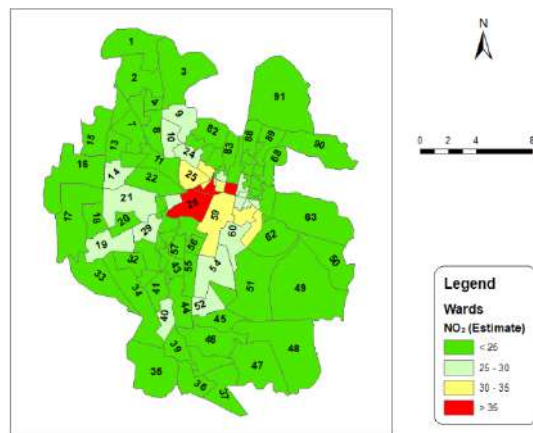


Fig. 12: Observed Vs Computed, (a) Model 1 (b) Model 6.

- Arc Map 2020b. Line Density, Arc GIS for Desktop, ESRI, <https://desktop.arcgis.com/en/arcmap/10.3/tools/spatial-analyst-toolbox/line-density.htm>
- Balakrishnan, K., Dey, S. and Gupta, T. 2019. The impact of air pollution on deaths, disease burden, and life expectancy across the states of India: The global burden of disease study 2017. *The Lancet: Planet. Health*, 3(1): E26-E39
- Bechle, J.M., Millet, D.B. and Marshall, J.D. 2013. Remote sensing of exposure to NO₂: Satellite versus ground-based measurement in a large urban area. *Atmos. Environ.*, 69: 345-353.
- Carslaw, D.C., Farren, N.J., Vaughan, R.V., Drysdale, S.W., Young, S. and James D.L. 2019. The diminishing importance of nitrogen dioxide emissions from road vehicle exhaust. *Atmos. Environ.*, 21: 100002.
- CDC. 2019. Air Quality. Centre for Disease Control and Prevention, U.S. Department of Health & Human Services. <https://www.cdc.gov/air/pollutants.htm>
- Costabile, F., Giuliano, B., Santis, D., Bellagotti, F., Ciuchini, R., Vichi, C. and Allegrini, F. I. 2010. Spatial distribution of urban air pollution in Lanzhou, China. *Open Environ. Pollut. Toxicol. J.*, 2: 8-15.
- Cowie, C.T., Ding, D. and Rolfe, M.I. 2016. Neighborhood walkability, road density, and socioeconomic status in Sydney, Australia. *Environ. Health*, 15: 58.
- Dadhich, A.P., Goyal, R. and Dadhich, P.N. 2018b. Assessment of spatio-temporal variations in the air quality of Jaipur city, Rajasthan, India. *Egypt. J. Remote. Sens. Space Sci.*, 21(2): 173-181
- Dadhich, A.P., Dadhich, P.N. and Goyal, R. (2018a). A GIS-based approach for assessment of ambient air quality in Kota City. *J. Basic Appl. Eng. Res.*, 5(2): 89-93.
- EPA. 2016. Nitrogen Dioxide (NO₂) Pollution. United States Environmental Protection Agency. <https://www.epa.gov/no2-pollution/basic-information-about-no2>
- Filonchik, M. and Hurynovich, V. 2020. Spatial distribution and temporal variation of atmospheric pollution in the South Gobi Desert, China, during 2016–2019. *Environ. Sci. Pollut. Res.*, 27: 26579–26593.
- Health Effects Institute. 2020a. State of Global Air 2020. Global Burden of Disease Study 2019, IHME
- Health Effects Institute. 2020b. State of Global Air 2020. Global Burden of Disease Study 2019, IHME.
- IASS. 2020. Air Pollution and Climate Change. Institute for Advanced Sustainability Studies. Federal Ministry of Education and Research. <https://www.iass-potsdam.de/en/output/dossiers/air-pollution-and-climate-change>. Accessed July 2020.
- JDA. 2020. Master Development Plan 2025, Jaipur. Urban Development and Housing, Government of Rajasthan.
- Khaniabadi, O.Y., Goudarzi, G., Daryanoosh, S.M., Borgini, A., Tittarelli, A. and De Marco, A. 2020. Exposure to PM₁₀, NO₂, and O₃ and impacts on human health *Environ. Sci. Pollut. Res. Int.*, 24(3): 2781-2789.
- Mohammad, A. A. and Juahir, A. (2015). Spatial analysis of certain air pollutants using environmetric techniques. *J. Tech.*, 75: 241-249.
- Munoth, M., Tiwari, M. and Goyal, R. (2015). Fluoride and Nitrate Groundwater Contamination in Rajasthan, India: A Review. Hydro 2015 International IIT Roorkee, India, 17-19 December 2015, 20th International Conference on Hydraulics, Water Resources and River Engineering.
- Nieto, P.J.G., Antón, J.C.Á. and Vilán, J.A.V. (2015). Air quality modeling in the Oviedo urban area (NW Spain) by using multivariate adaptive regression splines. *Environ. Sci. Pollut. Res.*, 22: 6642–6659.
- ORGCC. 2020. India Annual Health Survey 2012 - 13 Fact Sheet. https://www.censusindia.gov.in/vital_statistics/AHSBulletins/AHS_Factsheets_2012-13/FACTSHEET-Rajasthan.pdf.
- Poeter, E.P. and Anderson, D. 2005. Multimodel ranking and inference in groundwater modeling. *Ground Water*, 43(4): 597-605.
- Rajput, H., Goyal, R. and Brighu, U. 2020. Modification and optimization of DRASTIC model for groundwater vulnerability and contamination risk assessment for Bhiwadi region of Rajasthan, India. *Environ. Earth Sci.*, 79: 136.
- Ryu, J., Park, C. and Jeon, S.W. 2019. Mapping and statistical analysis of no₂ concentration for local government air quality regulation. *Sustainability*, 11: 38-49
- Singh, V. 2019. Deaths due to air pollution highest in Rajasthan: Experts “Outlook, The News Scroll. <https://www.outlookindia.com/newscroll/deaths-due-to-air-pollution-highest-in-rajasthan-experts/1592817>.
- Sogani, M. and Vyas, A.D. 2019. Socioeconomic Spillovers Resulting from the Functioning of Sewage Treatment Plants in Jaipur, India: A Case Study of the Delawas Plant. In Yoshino, N., Araral, E. and Seetharam, K.E. (eds.), *Water insecurity and sanitation in Asia*, Asian Development Bank Institute, Tokyo, Japan, pp. 83-106.
- The Hindu. 2015. NO₂ Emission Rising in India, New NASA Air Quality Maps Show. <https://www.thehindu.com/sci-tech/energy-and-environment/no2-emission-rising-in-india-new-nasa-air-quality-maps-show/article7992190.ece>
- TNN. 2017. Rajasthan Has the Highest Deaths Due to Chronic Pulmonary Diseases in the Country. *The Times of India*. <https://timesofindia.indiatimes.com/city/jaipur/raj-has-highest-deaths-due-to-chronic-pulmonary-diseases-in-country/articleshow/61652510.cms>

- UNICEF. 2016 Pollution: 300 million children breathing toxic air - UNICEF report. UNICEF Press release 31 st October 2016.
- United States Environmental Protection Agency. 2016. Nitrogen Dioxide (NO₂), EPA. The United States Environmental Protection Agency, September 08, 2016
- United States Environmental Protection Agency. 2020. Particulate Matter (PM) Pollution, EPA. The United States Environmental Protection Agency, April 13, 2020
- Vyas, A.D., Mahale, K., Ajmera, D. and Goyal, R. 2020. Optimum weights of environmental parameters in evaluating urban environmental sustainability index: A case study of Jaipur city. *ISH J. Hydraulic Eng.*, 28: 143-156
- World Health Organization. 2019. WHO, Health Topics, Air Pollution Overview. www.who.int/2019
- Zhou, Y. and Herath, H.M.P.S.D. 2017. Evaluation of alternative conceptual models for groundwater modeling. *Geosci. Frontiers*, 8: 437-443.
- Zhu, Y. and Lok, C.K. 2018. Analysis of spatial and temporal patterns of on-road NO₂ concentrations in Hong Kong. *Atmos. Meas. Tech.*, 11: 6719-6734.



Dynamic Relationship Between China's Environmental Protection Investment and Regional Environmental Pollution

Xiaowen Qiu

College of Business, Zhejiang Fashion Institute of Technology, Zhejiang, China, 315020

†Corresponding author: Xiaowen Qiu; 2000704015@zjff.edu.cn

Nat. Env. & Poll. Tech.
Website: www.neptjournal.com

Received: 05-06-2021

Revised: 28-06-2021

Accepted: 09-07-2021

Key Words:

Environmental protection investment
Regional environmental pollution
Dynamic relationship

ABSTRACT

The carrying capacity of China's resources and environment has reached a limit. The economic development of different regions has been forced to abandon the original economic development mode manifesting high pollution, high energy consumption, and high emission and to step forward to the new economic development model promoting low energy consumption, low emission, and low pollution. Environmental issues are typical manifestations of market mechanism failure. Government investment in environmental protection, which effectively improves environmental quality, is necessary to achieve sustainable economic development. An index system of the influencing factors that affect regional environmental pollutant emissions was established first in this study to measure accurately the relationship between environmental protection investment in different provinces in China and regional environmental pollution. System GMM (Generalized Method of Moment) method was used to analyze the impact of environmental protection investment on pollutant emissions in 30 provinces in China from 2007 to 2016. Results show that the system GMM method can effectively solve variable endogeneity. Environmental protection investment of explanatory variables has a significant negative effect on pollutant emissions. Among the control variables, per capita GDP (Gross Domestic Product), industrial structure, resident consumption level, and technology market turnover have a significant inhibitory effect on pollutant emissions. Among the control variables, investment in fixed assets and import and export trade is vital in promoting pollutant emission growth. Conclusions provide a reference for improving the governance level of environmental protection investment in China's provinces, controlling environmental pollution and ecological damage, and realizing a green economic development method.

INTRODUCTION

China is a developing country in the process of industrialization. Hence, environmental problems and pressures exist, but the occurrence of these setbacks is a common phenomenon. Moreover, these problems and pressures are determined by the specific development stage and socioeconomic structure. It hasn't been compensated the value of natural resources despite the constant request from nature's resources, thereby bringing a series of environmental problems to mankind, such as air pollution, soil erosion, water pollution, and solid waste pollution. The environmental problems in China mainly include environmental pollution and ecological damage. The following is a rough intuitive judgment on China's environmental problems. Environmental pollution and ecological damage are relatively severe and have been maintained at this relatively serious level for a long time. Neither a sharp deterioration nor a significant improvement exists. The general trend involves partial improvements. Most of these improvements are still deteriorating. As a "poor" output of China's economic growth, environmental issues have now

become the bottleneck of global economic growth while bringing many inconveniences to human society.

Environmental problems are a typical manifestation of market mechanism failure. Government investment in environmental protection is an effective means to improve environmental quality. Fig. 1 shows that China's total investment in environmental pollution control increased annually from 2001 to 2017. In particular, 110.67 billion CNY in 2001 increased to 953.895 billion CNY in 2017, with an average annual increase of 47.62%. Environmental protection investment is the main driving force of environmental protection. Investment size and investment efficiency are directly related to pollution control, environmental construction, ecological protection, and environmental quality improvement. Environmental protection investment is ultimately related to the degree to which the environment bears and supports economic development. However, production investment is an essential source of economic growth. Environmental protection investment is originally part of economic construction. The increase in environmental protection investment

has a crowding-out effect on productive funds. This effect inevitably has a certain negative impact on economic growth. However, environmental protection is also an investment after all, and it has a productive side, with both a supply effect and a demand effect.

PAST STUDIES

The increasing global environmental problems make many people aware of the important role of environmental protection investment in improving and protecting the environment and developing the economy. Many researchers have shown that environmental protection investment has an impact on the sustainable development of enterprises and the reduction of environmental pollutant emissions. Sustainable economic and environmental developments are also important. Porter et al. (1995) showed that the amount of investment in environmental protection by enterprises has increased, and the ability of this investment to control pollution and technical levels has improved. Even if the funds are used for environmental protection, the investment of enterprises in their products and services will still increase. The resources of China are affected, but in the long run, this scenario will be beneficial in environmental protection and the sustainable development of enterprises. Madsen (2009) showed that attracting business investment and protecting local environmental quality are two aspects that must be considered simultaneously. Moreover, environmental protection cannot be ignored because of a large amount of investment and construction. Nakamura (2011) used the data set of 3237 Japanese companies. A regression was conducted to explore the impact of environmental investment on corporate performance. The results showed that environmental investment does not significantly affect corporate performance in the short term, but it significantly improves corporate performance in the long run. Lavrinenko (2013) believed that environmental protection investment

has gradually shifted from corporate interests and public opinion pressure on environmental protection by the state or the public to prevent possible losses caused by environmental pollution, improvement of regional economic development, and improvement of people. Living conditions have also changed, and employment mobility has been reduced. Krajewski (2016) showed that public environmental protection expenditure has no negative impact on economic growth. Its positive impact is the largest among the economies affected by the global financial crisis. The correlation of the country's corporate research and development (R&D) investment and environmental performance of major developed economies have been studied (Alam et al. 2019). Results indicated that the companies actively implementing R&D and innovation activities through their resources are conducive to improving environmental performance and achieving sustainable competitiveness. Yang et al. (2020) determined from Research and Utilization 2009 that in 2018, the data of listed companies in China's A-share heavy pollution industry explored the relationship among internal control quality, corporate environmental protection investment, and financial performance. Moreover, corporate environmental protection investment has a significant positive impact on financial performance. Results provided a basis for the government to issue relevant environmental protection policies, strengthen corporate internal control construction guidelines, and encourage third-party organizations to evaluate the effectiveness of corporate internal control.

The above literature indicated that the early research on environmental issues mainly focused on the environment and economic growth and the impact of environmental protection investment on economic growth. However, the study on the pollution reduction effect and efficiency of environmental protection investment appeared late. Most of the literature research results support that environmental protection

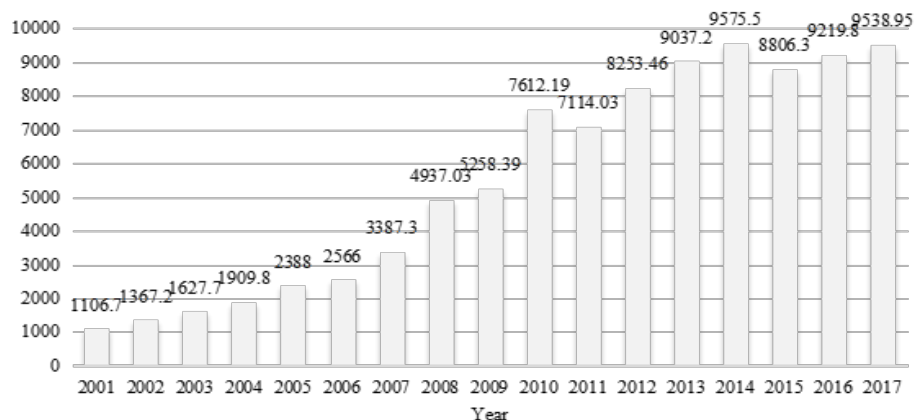


Fig. 1: China's total investment in environmental pollution government in 2001-2017 (100 million CNY).

investment can effectively solve environmental pollution problems. Environmental pollution control investment has a positive effect on environmental pollution control. The role of fiscal environmental protection investment varies greatly in different regions, mainly because the sample objects and the length of time do not necessarily cause some research conclusions to be different. Therefore, this study uses the Generalized Method of Moment (GMM) model method and takes 30 provinces in China (excluding Tibet) as samples to explore environmental pollution control investment by measuring the impact of their environmental protection investment on environmental pollution levels from 2007 to 2016. It provides policy suggestions on the path of pollutant emission reduction and how to use environmental pollution control investment rationally to improve environmental protection investment efficiency and sustainable economic and social development.

MATERIALS AND METHODS

Measurement Model

The influencing factors of environmental pollution in different provinces are relatively complex, and ordinary methods cannot be analyzed systematically. In particular, the selection of factor indicators has always been the focus and difficulty in the research. The author established the index system shown in Table 1 by combining the influencing factors from the existing research literature.

The development of the environmental system itself has a significant time accumulation characteristic. Thus, the level of development in the early stage will have a certain impact in the later stage. Therefore, the lag of the explained variable is added to the model as an explanatory variable, and the

regression result obtained by the dynamic panel model will be more practical. The current period is roughly affected by the lag period of the explained variable. According to the system GMM estimation method, the dynamic panel data regression model used in this study is shown in formula (1) by considering the availability, scientificity, and systematicness of the data. The use of the ordinary least squares method and fixed-effects model causes biased and inconsistent regression results mainly because of the endogeneity in the model. Dynamic panel GMM reduces the impact of endogeneity on the regression by selecting appropriate instrument variables. The regression equation is established as in the following formula (1).

$$y_{ij,t} = \beta_0 + \beta_1 x_{1ij,t} + \beta_2 x_{2ij,t} + \beta_3 x_{3ij,t} + \beta_4 x_{4ij,t} + \beta_5 x_{5ij,t} + \beta_6 x_{6ij,t} + \beta_7 x_{7ij,t} + \beta_8 y_{ij,t-1} + \varepsilon_{ij,t} \quad \dots(1)$$

In formula (1), $y_{ij,t}$ represents the explained variable. $y_{ij,t-1}$ shows the one-period lagging value of the explained variable. $x_{1ij,t}$ is an explanatory variable. The remaining variables $x_{2ij,t}$, $x_{3ij,t}$, $x_{4ij,t}$, $x_{5ij,t}$, $x_{6ij,t}$, $x_{7ij,t}$ represents 6 control variables. b_0 represents the constant term of the regression equation. b_1 to b_8 are the regression equation coefficients. $e_{ij,t}$ represents the error term.

Data

The panel data of 30 provinces (cities, autonomous regions) across the country from 2007 to 2016 are used as the empirical analysis sample based on the availability of actual data. Some indicators of Tibet are not complete; thus, they are excluded. All data can be directly obtained through the Easy Professional Superior data platform. The results of descriptive statistical analysis of all variables are shown in Table 2.

Table 1: Influencing factors of environmental pollution.

Influencing factors	Variable name	Specific index(unit)	Variable type
Exhaust	Y_1	Industrial wastewater discharge (10,000 tons)	Explained variable
Wastewater	Y_2	Industrial sulfur dioxide emissions (10,000 tons)	Explained variable
Dust	Y_3	Industrial smoke (dust) emissions (ten thousand tons)	Explained variable
Environment Protection Investment	X_1	Three Simultaneous Environmental Protection Investment (100 million CNY)	Explanatory variables
Economic Extent	X_2	GDP per capita (CNY)	Control variable
Industry Structure	X_3	The proportion of tertiary industry (%)	Control variable
Consumption Ability	X_4	Resident consumption level (CNY)	Control variable
National Investments	X_5	Total investment in fixed assets of the whole society (100 million CNY)	Control variable
Import and export trade	X_6	Import and export trade volume (ten-thousand dollars)	Control variable
Technology Innovation	X_7	Technical market turnover (ten thousand CNY)	Control variable

RESULT ANALYSIS

This study uses EViews10.0 software to conduct systematic GMM estimation on the model composed of panel data of 30 provinces (municipalities, autonomous regions) across the country from 2007 to 2016. The specific results are shown in Table 3.

Table 3 shows that the corresponding probabilities of the Sargan statistic (J-statistic) of Models 1, 2, and 3 are 0.2196, 0.1727, and 0.2060, respectively, which are all greater than the significance level of 0.05. This finding indicates that the reason for accepting excessive constraints is correct. The

remaining results are as follows:

1. Three simultaneous environmental protection investments have a significant negative effect on industrial wastewater discharge and industrial smoke (dust) emissions, with influence coefficients of -0.0795 and -0.1098, respectively. They are significant at the 1% significance level. The investment in environmental pollution control has a limited effect on the mitigation of environmental pollution discharge in the current period, and most of its effect is on the control of environmental pollution discharge in the previous period. The development of environmental protection industrialization of environ-

Table 2: Descriptive statistical results of each variable.

Variable	Average	Standard deviation	Max	Min
Y_1	72459.21	61640.34	268762.00	5782.00
Y_2	63.91	38.95	182.74	1.70
Y_3	43.27	31.05	179.77	1.31
X_1	68.25	69.56	438.20	0.50
X_2	40654.47	22702.47	118198.00	6915.00
X_3	42.08	9.07	80.23	28.60
X_4	14034.61	8136.11	49617.00	4057.00
X_5	11884.64	9602.38	53322.94	482.84
X_6	5553357.30	11264952.05	59207052.70	414.65
X_7	1897631.40	4592537.70	39409751.79	5556.27

Table 3: Regression results.

Model 1			Model 2			Model 3		
Variable	Coefficient	t-Statistic	Variable	Coefficient	t-Statistic	Variable	Coefficient	t-Statistic
$Y_1(-I)$	0.2882**	2.3420	$Y_2(-I)$	0.7201***	7.1401	$Y_3(-I)$	0.5924***	11.1607
X_1	-0.0795***	-8.3624	X_1	0.0045	0.3978	X_1	-0.1098***	-3.0484
X_2	-0.1757	-0.5421	X_2	-0.6169	-1.1672	X_2	-1.0863*	-1.8725
X_3	-1.5298***	-3.3797	X_3	-0.9928***	-2.5927	X_3	-2.9224***	-7.2434
X_4	-0.4529*	-1.6802	X_4	-1.1341***	-5.9682	X_4	0.3446	0.7726
X_5	0.6155***	4.5205	X_5	1.2714***	5.5752	X_5	1.2350***	5.1087
X_6	0.0265	0.3427	X_6	0.6123***	6.3960	X_6	0.0765	1.5496
X_7	-0.0345*	-1.6624	X_7	-0.2682***	-10.7897	X_7	-0.2064***	-3.4846
Mean dependent var		-0.0484	Mean dependent var		-0.0763	Mean dependent var		-0.0250
S.E. of regression		0.2236	S.E. of regression		0.3177	S.E. of regression		0.3351
J-statistic		26.7831	J-statistic		28.0892	J-statistic		27.1388
Prob(J-statistic)		0.2196	Prob(J-statistic)		0.1727	Prob(J-statistic)		0.2060
S.D. dependent var		0.1931	S.D. dependent var		0.2305	S.D. dependent var		0.2641
Sum squared resid		11.6037	Sum squared resid		23.4117	Sum squared resid		26.0578
Instrument rank		30	Instrument rank		30	Instrument rank		30

Note: ***, **, * indicate significance at the significance level of 1%, 5%, and 10% respectively

mental protection investment should be promoted, and the increase of employment should be promoted. The end treatment of environmental protection investment, such as the construction of sewage treatment plants or the purchase of pollution treatment equipment, should be strengthened to promote the industrialization of environmental protection by developing environmental protection industries and pursuing corresponding employment. The application of environmental protection investment in process control or source prevention, such as improving production technology to reduce the intensity of pollution emissions and using environmental protection investment to improve the level of technology, should be promoted to drive an increase in employment.

2. Per capita GDP has a negative effect on the growth of environmental pollutant emissions. However, this negative effect is not significant. The growth of per capita GDP is not the main factor leading to environmental pollution. Economic development can be effectively achieved with the growth of per capita GDP, and financial resources can be invested in treating environmental pollutants to reduce pollutant emissions effectively.
3. The industrial structure harms the growth of industrial wastewater emissions, industrial sulfur dioxide emissions, and industrial smoke (dust) emissions, and it is significant at the 1% significance level. The optimization and upgrading of the industrial structure have restrained China's environmental pollution to a certain extent by increasing the proportion of tertiary industry in the industrial structure, realizing the industrialization and marketization of science and technology, improving the ability to digest, absorb, and re-innovate imported technologies, and effectively reducing the proportion of primary and secondary industries and industrial emissions.
4. Resident consumption level hurts the growth of industrial wastewater discharge and industrial sulfur dioxide discharge, and it is significant at the 10% significance level. The increase in the consumption level of residents can make residents pay considerable attention to the consumption of environmentally friendly products, such as high and new technology. This scenario has a certain effect on the improvement of environmental pollution.
5. Investment in fixed assets has a positive effect on the growth of industrial wastewater emissions, industrial sulfur dioxide emissions, and industrial smoke (dust) emissions, and it is significant at the 1% significance level. The increasingly large-scale construction investment indicates that the demand for upstream steel,

cement, plastics, electrolytic aluminum, and many chemical products increases. These products belong to high energy-consuming industries. The increase has led to a rapid rise in energy consumption. This pattern is difficult to change because of China's relative lack of oil and natural gas resources and coal-based energy structure. The pollution caused by the burning of coal is the heaviest among all conventional energy sources. The huge scale of energy consumption and the coal-based energy consumption structure are the most important factors affecting the growth of China's environmental pollution emissions.

6. Import and export trade has a positive effect on the growth of industrial wastewater emissions, industrial sulfur dioxide emissions, and industrial smoke (dust) emissions, but it is not significant. This finding fully shows that international trade has a positive role in promoting environmental pollutant emissions. China is a large exporting country. Many products consumed by developed countries can be imported from other countries through international trade. Therefore, the origin of the products and the corresponding pollutant emission regions are also related. The consuming country has moved to the exporting country, thereby changing the spatial distribution of global pollutant emissions.
7. The technical market turnover has a negative effect on the growth of industrial wastewater emissions, industrial sulfur dioxide emissions, and industrial smoke (dust) emissions, and it is significant at the 10% significance level. Technological progress can effectively reduce the discharge of environmental pollutants, and it can weaken the negative impact of the current environmental protection investment of heavily polluting enterprises on the market value through green technological innovation. Strengthening green technology innovation in China's provinces will also help enterprises improve their technological innovation capabilities, assist non-high-tech enterprises to enter the ranks of high-tech enterprises, and help alleviate the increase in environmental pollution emissions caused by environmental protection investment, which is difficult for heavily polluting enterprises. Sustainable development has many benefits.

POLICY RECOMMENDATION

Increase Investment in Environmental Protection and Optimize the Structure of Environmental Protection Investment

Environmental protection investment has not been able to achieve emission reductions through economies of scale. All

provinces in China must increase environmental protection investment to provide financial guarantees for pollution control. With regard to increasing the government's financial investment, the government should include environmental protection funds into the fiscal annual budget and gradually increase investment in this area. According to the principle, "who pollutes, who pays", the environmental protection investment of enterprises should increase. On the one hand, enterprises can play a role in the market economy. On the other hand, the enthusiasm of enterprises to control industrial waste gas will increase. The used structure of environmental protection investment is a way of resource allocation, and different structures will inevitably lead to different pollution control effects. For a long time, China's primary pollution emissions have come from industrial production. However, the investment in urban environmental infrastructure construction is the largest in environmental protection investment, followed by the "three simultaneous" projects in construction projects. The investment in industrial pollution source treatment has the smallest proportion. Therefore, each province should increase the proportion of industrial pollution source treatment investment in environmental protection investment to match the former with the growth of the industrial economy and ultimately achieve the goal of industrial waste gas emission reduction.

Improve Public Financial Investment in Environmental Protection and Implement Pollution Control Funds

Investment is the focus of public fiscal expenditures to ensure that the total environmental protection investment grows. The growth rate of fiscal environmental protection investment can refer to the growth rates of the economy, fixed-asset investment in the whole society, or central and local fiscal revenues. The investment capacity of local governments in environmental protection must be improved, and the budgetary investment of local finances in environmental protection must be strengthened. Market mechanisms must be fully utilized to increase investment guidance and supervision of environmental pollution control. According to the "whoever develops protection, who destroys who restores, who benefits who compensates, who discharges pollution who pays" principle, the use of market mechanisms should be increased to promote pollution control, the law should be strictly enforced to guide enterprises to invest, and government investment should be encouraged to stimulate social investment. Economic policies mobilize market resources and fully implement pollution control funds.

Accelerate the Transformation of Economic Growth Mode and Strengthen Supervision of Key Polluting Industries

At present, most provinces in China are in the middle and late stages of industrialization. The process of industrialization

is accelerating, and the proportion of the industry in the industrial structure remains large. The traditional model of economic growth only considers the speed of economic growth but ignores its quality. The economic growth pattern should be transformed by following the pace of supply-side reforms. The path of sustainable development should be followed. A circular economy should be developed by recycling resources and improving utilization efficiency, thereby reducing the discharge of pollutants and achieving the sustainable development of the use of resources in the entire society. The vigorously developing tertiary industry must realize that the tertiary industry is the future direction of economic development and the green driving mode of economic development to reduce environmental pollution. The control and management of heavy pollution industries must be strengthened because these industries considerably contribute to the total industrial waste gas emissions. Output control in the cement, steel and chemical industries should be strengthened. If these heavily polluting industries are brought under control, the pressure on China's industrial emissions will be eased to a large extent.

Improve the Government's Ability to Monitor the Environment and Increase Corporate Pollution Control Through R&D Investment

Polluters lack environmental awareness and the initiative to invest in environmental protection because of the external characteristics of the environment. Therefore, the government and society should improve enterprise pollution supervision and the role of government regulation. The construction of the monitoring system should be strengthened to support the operation and maintenance of the automatic monitoring system for industrial waste gas pollution sources. Pollution control should persist in accordance with the law, and law enforcement capabilities should be strengthened. R&D investment can promote the emergence of advanced production equipment and production technology, increase the efficiency of resource use, and reduce the pollution output of production. Therefore, policymakers should guide companies to increase investment in R&D and fundamentally reduce the generation and emissions of pollutants. Tax policies should be used to reduce corporate R&D costs. Reasonable and feasible tax incentive policies should be formulated to encourage enterprises to increase investment in R&D. In terms of the establishment of enterprise R&D investment reward funds, certain rewards will be given to enterprises according to the proportion of enterprise R&D investment.

CONCLUSION

China's environmental pollution and ecological damage are relatively severe and have been maintained at this relatively

serious level for a long time. Environmental problems are typical manifestations of market mechanism failure. Government investment in environmental protection can effectively improve environmental quality. In this study, an index system of influencing factors that affect regional environmental pollutant emissions was established and the system GMM method was used to analyze the impact of environmental protection investment in 30 provinces in China on the pollutant emissions from 2007 to 2016. Conclusions could be drawn: the environmental protection investment of the explanatory variables has a significant effect on the reduction of pollutant emissions. The per capita GDP, industrial structure, resident consumption level, and technological market turnover in the control variables have a significant inhibitory effect on pollutant emissions. Fixed-asset investment and import and export trade have a significant role in promoting the growth of pollutant emissions. Environmental pollution can be further achieved by increasing investment in environmental protection, improving public financial investment in environmental protection, accelerating the transformation of economic growth mode, and improving the government's ability to monitor the material emission reduction in the environment. Future research can continue to conduct in-depth research

on enriching the variable index system, extending the time series of research objects, and using spatial measurement to analyze the homogeneity and heterogeneity among different provinces.

REFERENCES

- Alam, M. S., Atif, M., Chien-Chi, C. and Soytaş, U. 2019. Does Corporate R&D Investment Affect Firm Environmental Performance? Evidence from G6 Countries. *Energy Economics*, 78(2): 401-411.
- Krajewski, P. 2016. The Impact of Public Environmental Protection Expenditure on Economic Growth. *Problemy Ekorożwoju*, 11(2): 99-104.
- Lavrinenko, P. A. 2013. Analysis of the Investment Attractiveness of Projects in the Field of Environmental Protection. *Studies on Russian Economic Development*, 24(5): 495-499.
- Madsen, P.M. 2009. Does Corporate Investment Drive a "Race to the Bottom" in Environmental Protection? A Reexamination of the Effect of Environmental Regulation on Investment. *Academy of Management Journal*, 52(6): 1297-1318.
- Nakamura, E. 2011. Does environmental investment really contribute to firm performance? An Empirical Analysis Using Japanese Firms. *Eurasian Business Review*, 1(2): 91-111.
- Porter, M.E. and Linde, C. 1995. Towards a New Conception of the Environment-Competitiveness Relationship. *Journal of Economic Perspectives*, 4(4): 97-118.
- Yang, L., Qin, H., Gan, Q. and Su, J. 2020. Internal Control Quality, Enterprise Environmental Protection Investment and Finance Performance: An Empirical Study of China's A-Share Heavy Pollution Industry. *International Journal of Environmental Research and Public Health*, 17(17): 6082.



Assessment of Soil Environment Pollution Based on Fuzzy Pattern Recognition Model

Xin Huang[†] and Lin Qiu

College of Water Resources, North China University of Water Resources and Electric Power, Zhengzhou, Henan, 450046 China

[†]Corresponding author: Xin Huang; huangxin0013@163.com

Nat. Env. & Poll. Tech.
Website: www.neptjournal.com

Received: 16-11-2020

Revised: 21-12-2020

Accepted: 22-02-2021

Key Words:

Soil environment

Pollution

Fuzzy pattern recognition

General weighted length

Membership degree assessment

ABSTRACT

As one of the basic elements of the ecosystem and natural environment, the soil is closely related to human life. However, the problem of soil environment pollution is becoming more and more serious, which needs to be solved urgently. It will provide a reference for solving the problem of soil environment pollution if a suitable method can be found to evaluate the degree of soil environment pollution. The degree of soil environment pollution belongs to the fuzzy concept. It is a fuzzy pattern recognition problem to evaluate the degree of soil environment pollution according to the soil environment level standard value. The fuzzy pattern recognition method of soil environment pollution assessment makes full use of the fuzzy characteristics existing in soil environment assessment, considers the common influence of the weight of evaluation factors and the index value, and also considers the correlation between indexes and the similarity of index characteristics of different sampling points, therefore, the interference of some man-made certain factors is concealed. The model was applied to the soil sampling point in Wudi County of Shandong Province in the Yellow River basin of China. The results showed that the evaluation of soil environment pollution by this method accorded with the actual situation and can provide a basis for ensuring the stability of soil ecological environment, improving the quality of cultivated land, and improving regional ecological conditions. At the same time, in view of the current problem of soil environment pollution, the paper calls on human beings to pay attention to environmental protection and be responsible for their own safety and also proposes four aspects of treatment schemes and measures.

INTRODUCTION

Soil is one of the basic elements of the ecosystem. It plays an important role in maintaining biodiversity, stabilizing and buffering environmental changes in terrestrial ecosystems. It is a component of the natural environment, connecting the atmosphere, hydrosphere, lithosphere, and biosphere (Newman et al. 2020, Mammo et al. 2019, Ren et al. 2016). It is an important guarantee for promoting sustainable development of the economy and society. Soil is closely related to human life, and the quality of the soil environment has a great impact on human beings. Soil pollution refers to the phenomena in which various toxic and harmful chemicals penetrate the soil and cause changes in soil characteristics, which have a negative impact on plants and animals. Long-term, irreversible, hysteresis, and concealment are all characteristics of soil pollution. Toxic and harmful substances entering the soil environment will have a great negative impact on the structure, composition, and function of the soil, resulting in a significant decline in soil quality, poor soil nutrients, and soil composition necrosis, affecting food

security, ecological security, the physical health of residents (Francisca & Cristina 2019), etc., which will have a great impact on agricultural development and seriously hinder economic development. At present, researches on soil environment pollution mainly focus on the spatial distribution of pollutants, regional pollution characteristics, present situation investigation, soil remediation, and evaluation, etc. There are many methods for soil environment pollution assessment, such as multi-factor comprehensive assessment, Nemerow pollution index assessment, principal component analysis, etc. Among them, the multi-factor comprehensive assessment has wide adaptability and simple application, but the standard boundary is too clear (Su et al. 2016). The mathematical process of the Nemerow pollution index assessment is simple, but it only considers pollution factors with the highest concentrations and excludes pollution factors with low concentrations but high damage. (Kong et al. 2019). Human factors influence the limit value of the load coefficient chosen from each eigenvector by principal component analysis, and the weight changes when the variables are categorized into various principal components, making the

significance test of evaluation factors impossible (Onwosi et al. 2020) Because the evaluation findings of each single soil environment factor are often incompatible, direct use of a relevant standard critical value to divide the level of soil environment pollution cannot produce an exact evaluation in the study of soil environment pollution assessment

The quality of the soil environment is determined by the factors constituting the soil environment. Before the evaluation of soil environment pollution, the advantages and disadvantages of each evaluation factor should be evaluated first. The evaluation factors are gradually changing between the advantages and disadvantages, and show the double-sided property in the intermediate transition. In other words, the level of soil environment pollution is a fuzzy concept, and evaluating the level of soil environment pollution according to the standard level value of soil environment pollution is a fuzzy pattern recognition problem (Poomagal et al. 2020). Therefore, this paper explores the application of the principle and method of fuzzy pattern recognition in the assessment of soil environment pollution and expounds in detail the mathematical and physical significance of the recognition criterion with the minimum sum of squares of weighted distances and the corresponding iterative formula.

MATERIALS AND METHODS

Comprehensive Evaluation Theory and Model of Fuzzy Pattern Recognition

Let a sample set consist of n soil samples, and each sample has m evaluation indexes. Then, the measured index matrix $X_{m \times n} = (x_{ij})$ is obtained, where $i = 1, 2, \dots, m; j = 1, 2, \dots, n$, x_{ij} is the measured value of index i in the sample j . The m indexes are evaluated according to level c soil standard, then the index standard matrix $Y_{m \times c} = (y_{ih})$ is obtained, where $h = 1, 2, \dots, c; y_{ih}$ is the level h standard value of index i .

To describe the fuzziness of soil environment pollution, the matrix $X_{m \times n}$ and $Y_{m \times c}$ were converted into the relative membership degree matrix of measured indexes $R_{m \times n} = (r_{ij})$ and the relative membership degree matrix of index standards $S_{m \times c} = (s_{ih})$ by using the relative membership degree. It is stipulated here that: for the index i that the higher the measured concentration, the heavier the pollution, when $x_{ij} \leq y_{i1}$, its relative membership degree for pollution $r_{ij} = 0$; when $x_{ij} \geq y_{ic}$, $r_{ij} = 1$. For the index i that the higher the measured concentration, the lighter the pollution, when $x_{ij} \geq y_{i1}$, its relative membership degree for pollution $r_{ij} = 0$; when $x_{ij} \leq y_{ic}$, $r_{ij} = 1$; and when x_{ij} between y_{i1} and y_{ic} , r_{ij} is determined according to the linear interpolation formula $r_{ij} = (x_{ij} - y_{i1}) / (y_{ic} - y_{i1})$. It can also be stipulated that the relative membership degree to pollution of the level 1 standard value

of index i is 0; the relative membership degree to pollution of level c standard value of index i is 1. The relative membership degree s_{ih} of level h standard value of index i which is between level 1 and level c was determined by formula $s_{ih} = (y_{ih} - y_{i1}) / (y_{ic} - y_{i1})$.

Sample j is subordinate to soil environmental index standard of level h with relative membership degree u_{hj} , then, the relative membership degree matrix $U_{c \times n} = (u_{hj})$, which satisfies the constraint condition

$$\sum_{h=1}^c u_{hj} - 1 = 0, \forall j; \sum_{j=1}^n u_{hj} > 0, \forall h$$

The relative membership degree matrix of the measurement index $R_{m \times n}$ not only describes the superscalar but also represents the weight. Here, its normalized matrix $W_{m \times n} = (w_{ij})$ is defined as the superscalar weight matrix, which satisfies

$$\sum_{i=1}^m w_{ij} = 1, \forall j.$$

Next, solve for u_{hj} . The difference between sample j and soil environmental index standard of level h can be expressed by general weighted length, which is:

$$D(r_j, s_k) = u_{kj} \sqrt{\sum_{i=1}^m (w_{ij} |r_{ij} - s_{ih}|)^p} \quad \dots(1)$$

The optimal relative membership degree of sample j to soil environmental index standard of level h is obtained by taking the minimum sum of squares of general weighted length as the objective function, which is:

$$\min \left\{ F(u_{hj}) = u_{hj}^2 \left[\sum_{i=1}^m (w_{ij} |r_{ij} - s_{ih}|)^p \right]^{\frac{2}{p}} \right\} \quad \dots(2)$$

Where, distance parameter $p = 1$ is the hamming distance, and $p = 2$ is the Euclidian distance.

The Lagrange equation is constructed according to the objective function (2) and its constraints, which is:

$$L(u_{hj}, \lambda) = u_{hj}^2 \left[\sum_{i=1}^m (w_{ij} |r_{ij} - s_{ih}|)^p \right]^{\frac{2}{p}} - \lambda \left(\sum_{h=1}^c u_{hj} - 1 \right) \quad \dots(3)$$

Then, seeking the partial derivatives of equation (3) respectively for u_{hj} and Lagrange multiplier λ , setting the partial derivatives equal to 0, we get

$$u_{hj} = \frac{1}{\sum_{k=1}^c \left[\frac{\sum_{i=1}^m (w_{ij} |r_{ij} - s_{ih}|)^p}{\sum_{i=1}^m (w_{ij} |r_{ij} - s_{ik}|)^p} \right]^{\frac{2}{p}}} \quad \dots(4)$$

When formula (4) is used for evaluation and calculation, the value range of k is dynamic and should be determined by comparing m indexes of sample j in the matrix $R_{m \times n}$ and the matrix $S_{m \times c}$. Let the value of relative membership degree of m indexes of sample j be $r_j = (r_{1j}, r_{2j}, \dots, r_{mj})^T$. Compare the relative membership degree of r_{ij} of index i ($i = 1, 2, \dots, m$) one by one with the relative membership degree of $s_i = (s_{i1}, s_{i2}, \dots, s_{ic})$ of criteria of index i in $S_{m \times c}$. If the minimum level of index i falling into s_i interval is a_j and the maximum level is b_j , then a_j and b_j are the value range of k , with $1 \leq a_j < b_j \leq c$. In formula (4), the value range of h is the same as that of k ,

obviously when $h < a_j$ or $h < b_j$, $u_{hj} = 0$; $\sum_{h=a_j}^{b_j} u_{hj} = 1$.

In conclusion, the complete form of the theoretical model of fuzzy pattern recognition and evaluation of soil environmental pollution can be expressed as follows:

$$\left\{ \begin{aligned} & u_{hj} = \frac{1}{\sum_{k=a_j}^{b_j} \left[\frac{\sum_{i=1}^m (w_{ij} |r_{ij} - s_{ih}|)^p}{\sum_{i=1}^m (w_{ij} |r_{ij} - s_{ik}|)^p} \right]^{\frac{2}{p}}}, h \in [a_j, b_j] \\ & u_{hj} = 0, h < a_j \text{ or } h > b_j \\ & u_{hj} = 1, r_{ij} = s_{ik} \end{aligned} \right. \dots(5)$$

Where, $j = 1, 2, \dots, n$; $1 \leq a_j < b_j \leq c$; $h = a_j, a_j+1, \dots, b_j$. When $p = 1, 2$, the relative membership degree matrix of the sample set to level h is, ${}_1U_{c \times n} = ({}_1u_{hj})$ and ${}_2U_{c \times n} = ({}_2u_{hj})$ respectively. Here, the average relative membership degree matrix of the sample sets of two kinds of distance parameters for level h : $\bar{U}_{c \times n} = \frac{1}{2}({}_1u_{hj} + {}_2u_{hj}) = \bar{u}_{hj}$ is taken

to eliminate the influence of different values of distance

parameter p on the comprehensive evaluation of soil environmental pollution level identification.

According to the average relative membership degree matrix, the eigenvectors of n soil samples belonging to each level are:

$$H = (1, 2, \dots, c) \cdot (\bar{u}_{hj}) = (H_1, H_2, \dots, H_n) \dots(6)$$

According to the level characteristic values of samples, the classification of soil environmental pollution was comprehensively evaluated (Chen 1998).

RESULTS AND DISCUSSION

Example Application

After the soil environment is polluted, it will have a great negative impact on the structure, composition, and function of soil, leading to the decrease of soil nutrients and soil hardening, resulting in the impoverishment of soil nutrients and the necrosis of soil components. Therefore, the evaluation of nutrient level in soil environment can reflect the degree of soil environment pollution, that is, the higher the nutrient level of soil environment is, the lighter the pollution is; while the lower the nutrient level of soil environmental is, the more serious the pollution is.

In this paper, partial results of soil environmental nutrient determination in the sampling point in reference (Lv 2018) (the sampling point is located in Wudi County, Binzhou City, Shandong Province, China, in the Yellow River Basin) were selected as the basic data for evaluating soil environment nutrient levels, as shown in Table 1.

The second soil survey classification standard in China used the standard concentration values of the soil environment nutrient level evaluation index. Table 2 shows the selected critical values of the evaluation factor level index based on the circumstances of soil sample determination.

According to Table 1 and Table 2:

Table 1: Determination results of physicochemical characters of soil environment nutrient level.

Sampling point number	organic matter (%)	total nitrogen (%)	available nitrogen (mg/kg)	available phosphorus (mg/kg)	rapidly available potassium (mg/kg)
1	0.95	0.085	45	8.5	98
2	1.28	0.071	76	3.9	196
3	2.67	0.274	120	13.6	137
4	1.89	0.937	53	7.7	185
5	6.74	1.136	95	35	230
6	3.86	0.168	104	18	149

Table 2: Critical values of the level indexes of each evaluation factor.

level	I	II	III	IV	V
organic matter (%) (>)	4.0	3.0	2.0	1.0	0.6
total nitrogen (%) (>)	0.20	0.15	0.1	0.075	0.05
available nitrogen (mg/kg) (>)	150	120	90	60	30
available phosphorus(mg/kg) (>)	40	20	10	5	3
rapidly available potassium (mg/kg) (>)	200	150	100	50	30

$$X_{5 \times 6} = \begin{bmatrix} 0.95 & 1.28 & 2.67 & 1.89 & 6.74 & 3.86 \\ 0.085 & 0.071 & 0.274 & 0.937 & 1.136 & 0.168 \\ 45 & 76 & 120 & 53 & 95 & 104 \\ 8.5 & 3.9 & 13.6 & 7.7 & 35 & 18 \\ 98 & 196 & 137 & 185 & 230 & 149 \end{bmatrix} = (x_{ij}),$$

$$Y_{5 \times 5} = \begin{bmatrix} 4.0 & 3.0 & 2.0 & 1.0 & 0.6 \\ 0.20 & 0.15 & 0.1 & 0.075 & 0.05 \\ 150 & 120 & 90 & 60 & 30 \\ 40 & 20 & 10 & 5 & 3 \\ 200 & 150 & 100 & 50 & 30 \end{bmatrix} = (y_{ih})$$

where, $i = 1, 2, \dots, 5; j = 1, 2, \dots, 6; h = 1, 2, \dots, 5$.

The matrix $X_{5 \times 6}$ and $Y_{5 \times 5}$ are transformed into the relative membership matrix of the measured concentration and the relative membership matrix of the standard concentration:

$$R_{5 \times 6} = \begin{bmatrix} 0.897 & 0.800 & 0.391 & 0.621 & 0 & 0.041 \\ 0.767 & 0.860 & 0 & 0 & 0 & 0.213 \\ 0.875 & 0.617 & 0.250 & 0.808 & 0.458 & 0.383 \\ 0.851 & 0.976 & 0.714 & 0.873 & 0.135 & 0.595 \\ 0.600 & 0.024 & 0.371 & 0.088 & 0 & 0.300 \end{bmatrix} = (r_{ij}),$$

$$S_{5 \times 5} = \begin{bmatrix} 0 & 0.294 & 0.588 & 0.882 & 1 \\ 0 & 0.333 & 0.667 & 0.833 & 1 \\ 0 & 0.250 & 0.500 & 0.750 & 1 \\ 0 & 0.541 & 0.811 & 0.946 & 1 \\ 0 & 0.294 & 0.588 & 0.882 & 1 \end{bmatrix} = (s_{ih})$$

The matrix $R_{5 \times 6}$ is normalized by column to obtain the superscalar weight matrix:

$$W_{5 \times 6} = \begin{bmatrix} 0.225 & 0.244 & 0.227 & 0.260 & 0 & 0.027 \\ 0.192 & 0.263 & 0 & 0 & 0 & 0.139 \\ 0.219 & 0.188 & 0.145 & 0.338 & 0.772 & 0.250 \\ 0.213 & 0.298 & 0.414 & 0.365 & 0.228 & 0.388 \\ 0.150 & 0.007 & 0.215 & 0.037 & 0 & 0.196 \end{bmatrix} = (w_{ij})$$

When the distance parameter $p = 2$, the calculation procedure is as follows.

Since the value range of k is dynamic, a_j and b_j are not necessarily the same when using formula (5) to calculate different sample j . Taking the sampling point $j = 1$ as an example, the determination of a_j and b_j is briefly described.

When $j = 1$, from the matrix $R_{5 \times 6}$, $r_{j=1} = (r_{11}, r_{21}, r_{31}, r_{41}, r_{51})^T = (0.897, 0.767, 0.875, 0.851, 0.600)^T$ can be obtained. By comparing $r_{11} = 0.897$ in vector $r_{j=1}$ with the element value in the first row of matrix $S_{5 \times 5}$, it can be seen that it is between 0.882 and 1, that is, it falls between levels 4 and level 5. When $r_{21} = 0.767$ is compared with the element value in the second row of matrix $S_{5 \times 5}$, it is in the interval of 0.667 and 0.833, that is, it falls between level 3 and level 4. Similarly, r_{31} falls between level 4 and level 5, r_{41} falls between level 3 and level 4, and r_{51} falls between level 3 and level 4. In summary, the upper limit value of k is $b_j = 5$, and the lower limit value is $a_j = 3$.

For $j = 1$, the matrix $W_{5 \times 6}$ shows that:

$$w_{j=1} = (w_{11}, w_{21}, w_{31}, w_{41}, w_{51})^T = (0.225, 0.192, 0.219, 0.213, 0.150)^T.$$

Substitute relevant data into formula (5) to obtain: $u_{31} = 0.157$, $u_{41} = 0.604$, $u_{51} = 0.239$.

According to the value conditions of formula (5), $u_{11} = 0$, $u_{21} = 0$.

For $j = 2, 3, \dots, 6$, the lower limit value a_j and the upper limit value b_j of k are 1 and 5, 1 and 3, 1 and 5, 1 and 3, 1 and 3 respectively. Thus, when $p = 2$, the relative membership degree matrix of 6 sampling points for each level is obtained.

$${}_2U_{5 \times 6} = \begin{bmatrix} 0 & 0.005 & 0.030 & 0.016 & 0.102 & 0.024 \\ 0 & 0.016 & 0.531 & 0.055 & 0.375 & 0.869 \\ 0.157 & 0.113 & 0.439 & 0.267 & 0.523 & 0.107 \\ 0.604 & 0.765 & 0 & 0.479 & 0 & 0 \\ 0.239 & 0.101 & 0 & 0.183 & 0 & 0 \end{bmatrix} = ({}_2u_{hj})$$

When the distance parameter p is 1, for $j = 1, 2, \dots, 6$ similar calculations are made separately, the relative membership matrix of 6 sampling points for each level is obtained

$${}_1U_{5 \times 6} = \begin{bmatrix} 0 & 0.005 & 0.033 & 0.014 & 0.132 & 0.032 \\ 0 & 0.016 & 0.677 & 0.048 & 0.304 & 0.878 \\ 0.206 & 0.108 & 0.290 & 0.426 & 0.564 & 0.090 \\ 0.601 & 0.755 & 0 & 0.380 & 0 & 0 \\ 0.193 & 0.116 & 0 & 0.132 & 0 & 0 \end{bmatrix} = ({}_1u_{hj})$$

Thus, the average relative membership degree matrix of $p=1$ and $p=2$ sample sets for each level is obtained

$$\bar{U}_{5 \times 6} = \begin{bmatrix} 0 & 0.005 & 0.031 & 0.015 & 0.117 & 0.028 \\ 0 & 0.016 & 0.604 & 0.052 & 0.340 & 0.873 \\ 0.182 & 0.110 & 0.365 & 0.345 & 0.543 & 0.099 \\ 0.602 & 0.760 & 0 & 0.430 & 0 & 0 \\ 0.216 & 0.109 & 0 & 0.158 & 0 & 0 \end{bmatrix} = (\bar{u}_{hj})$$

The level eigenvector of the six sampling points are obtained from formula (6)

$$H = (1, 2, 3, 4, 5) \cdot (\bar{u}_{hj}) = (4.034, 3.952, 2.334, 3.664, 2.426, 2.071)$$

According to the level eigenvector H , it can be seen that the soil environmental nutrient levels of the six sampling points are: sampling point 1 level 4; sampling point 2 level 3 to 4; sampling point 3 levels 2 to 3; sampling point 4 levels 3 to 4; sampling point 5 level s2 to 3 and sampling point 6 levels 2 to 3. It can be seen that the soil environmental pollution in this batch of sampling sites is medium or lower, and nutrients have reached a relatively deficient level. Local relevant departments should pay attention to it and take positive measures to improve the soil environment and ensure the sustainable development of agriculture and the economy.

CONCLUSION

The problem of soil environment pollution needs to be solved urgently. Soil environment pollution not only affects the basic quality and production quality of crops, but also causes certain harm to air and water resources, and ultimately harms human life and health through food. Soil environment pollution assessment is of great significance to public health, social security, national food security, and ecological balance.

The fuzzy pattern recognition method of soil environment pollution assessment makes full use of the fuzzy characteristics existing in soil environment assessment, considers the common influence of the weight of evaluation factors and the index value, and also considers the correlation between indexes and the similarity of index characteristics of different sampling points, therefore, the interference of some man-made certain factors is concealed. If conditions permit, this method can add other physical, chemical, and

biological indexes, so that the evaluation results can reflect the soil environment conditions more effectively.

The results show that this method is more rigorous in theory, more scientific and accurate in evaluation, and more practical in application, and can provide a basis for ensuring the stability of soil ecological environment, improving the quality of cultivated land, and improving regional ecological conditions. Compared with the membership matrix, the calculation process of this method is more complicated, and still needs to be improved.

In view of the current problems of soil environment pollution, the proposed treatment schemes and measures are as follows: (1) combined with the current situation of agricultural development, it is necessary to further optimize the input structure and production structure of agriculture. (2) Improve relevant laws and regulations, formulate scientific and reasonable prevention and control measures, and strengthen the supervision of soil remediation. (3) Increase the research on soil pollution, actively use advanced soil pollution control technology to improve the soil ecological environment, improve the self-carrying capacity, and self-purification capacity of the ecological environment. (4) Strengthen environmental publicity, and constantly improve the people's awareness of soil environment protection. In the face of environmental protection and economic development, people should pay more attention to the importance of environmental protection. Environmental protection is about safeguarding ourselves and our environment, as well as being responsible for our own safety.

REFERENCES

- Chen, S.Y. 1998. The Fuzzy Sets Theory and Practice for Engineering Hydrology and Water Resources System. Dalian University of Technology Press, Dalian
- Francisca, R. and Cristina, L. 2019. Legal measures to prevent and manage soil contamination and to increase food safety for consumer health: The case of Spain. *Environ. Pollut.*, 250: 883-891.
- Kong, M.Y., Zhong, H.P., Wu, Y.X., Liu, G.D., Xu, Y. and Wang G.X. 2019. Developing and validating intrinsic groundwater vulnerability maps in regions with limited data: A case study from Datong City in China using DRASTIC and Nemerow pollution indices. *Environ. Earth Sci.*, 78(8): 1-14.
- Lv, K.Y. 2018. Spatial and Temporal Variation of Soil Nutrients and Its Influencing Factors: A Case Study on Wudi county. Zhejiang University, Hangzhou.
- Mammo, S., Zhang, K., Chimidi, A. and Ibrahim, H. 2019. Soil quality analysis for the sustainability of forest ecosystem: The case of Chilimo-Gaji Forest, West Shewa Zone, Ethiopia. *J. Environ. Earth Sci.*, 9(3): 1-9.
- Newman, G.S., Coble A.A., Haskins, K.E., Kowler, A.L. and Hart, S.C. 2020. The expanding role of deep roots during long-term terrestrial ecosystem development. *J. Ecol.*, 108(6): 2256-2269.
- Onwosi, C. O., Odimba, J.N., Igbokwe, V.C., Nduka, F.O. and Nwagu, T.N. 2020. Principal component analysis reveals microbial biomass carbon as an effective bioindicator of the health status of petroleum-polluted agricultural soil. *Environ. Technol.*, 41(24): 3178-3190.

- Poomagal, S., Sujatha, R., Kumar P.S. and Nvo, D.V. 2020. A fuzzy cognitive map approach to predict the hazardous effects of malathion on the environment (air, water, and soil). *Chemosphere*, 263: 127926-127926.
- Ren, Y., Deng, L.Y., Zuo S.D., Song, X.D. and Li Z.W. 2016. Quantifying the influences of various ecological factors on the land surface temperature of urban forests. *Environmental pollution*, 216: 519-529.
- Su, H.Z., Yang, M. and Wen, Z.P. 2016. An approach using the multi-factor combination to evaluate high rocky slope safety. *Nat. Hazards Earth Syst. Sci.*, 16(6): 1449-1463.



Evaluation of Cytotoxicity and Genotoxicity of Water from Nag River, Nagpur, India

P. V. Hirapure**†, S. A. Paranjape*, V. S. Sarodaya*, B. A. Mehere* and V. J. Upadhye**

*Department of Biochemistry and Biotechnology, Dr. Ambedkar College, Deekshabhoomi, Nagpur, India

**Department of Microbiology, Parul Institute of Applied Sciences (PIAS), Parul University, Vadodara, Gujarat, India

†Corresponding author: P. V. Hirapure; pradiphirapure@gmail.com, dr.vijaysemilo@gmail.com

Nat. Env. & Poll. Tech.
Website: www.neptjournal.com

Received: 23-01-2021

Revised: 29-03-2021

Accepted: 14-04-2021

Key Words:

Nag river
Cytotoxicity
Genotoxicity
Allium cepa.L.
Water pollution
Mutagenesis

ABSTRACT

The pollution of the river by man-made sewage and waste disposal is not only harmful to animals and plants in it but also for animals higher in the food chain including those close to the food chain. Water is the most vital natural substance, as it plays a role in nearly every aspect of human life. Therefore, there is a great need to ensure that the water used by humans should not contain hazardous substances. Water quality is directly linked to biological life. The Nag River flows from the Lava village of north Ambazari Lake and flows into the center of Nagpur city. As a result of rapid and unstoppable development, significant changes have taken place in the water quality of the Nag River. Because the Nag River's water is frequently used for irrigation, it should be tested for cytotoxicity and genotoxicity. Since the rate of cancer and genetic disorders has recently increased in the Nagpur region, the Nag River's water could be a source of carcinogens in the food chain, affecting the population. This study was conducted to analyze the impact of water collected from various points of the Nag River using *Allium cepa* as a model organism. The results of this study showed that all water samples from the Nag River cause a cytotoxic effect (20-23%) and genotoxic effects (23-28%) in *Allium cepa* cells. Therefore, before the use of Nag River water, it must be treated to diminish its harmful effect.

INTRODUCTION

Nagpur is the third biggest city in Maharashtra after Mumbai and Pune and it is one of India's quickest developing cosmopolitan cities. It is the winter capital of the province of Maharashtra and the second greenest city in India. Nagpur is home to a number of natural and man-made lakes, the largest of which being Ambazari Lake. This lake is where Nagpur's waterway begins. India has a vast and changing topography, which includes a large number of water bodies. Lakes and streams are now widely used for domestic purposes (Patil et al. 2017). Nagpur is fed by the Nag river, which gives the city its name. Originating from the Ambazari lake, the Nag river takes a winding path for approximately 16 km through the city before it joins another stream called Pili Nadi, which originates at another lake. This stream then merges into the Kanhan river on the outskirts of the city. Because Nagpur has experienced fast urbanization and migration to the city in the last five to six decades, there is increased use of water for domestic purposes, as well as, industrial production has increased, causing a sudden surge in sewage quantity (a meager grimy stream of water (Kalyani et al. 2017). Because of the value and importance of freshwater resources, they must be closely monitored biologically to meet water quality stand-

ards (Puri et al. 2010). An enormous amount of wastewater from the Nagpur metropolitan region and numerous enterprises surrounding the urban areas is dumped into streams, such as the Nag river and its tributaries, contaminating both ground and surface water (Manzar et al. 2010). Because this river runs through a city with a population of around 50 lakh people, it is quite dirty. The Nag river was once a lifeline of the city. But today, the river's rich history has got buried in deep silt beneath the millions of litres of sewage flowing in it (Anparthi 2013). The Ambazari Lake which was the prime source of water to Nagpur city is filled with waste and sewage (which gives it an unnatural dark gray color and a foul smell), and despite receiving rainwater during monsoon it is not fit for consumption. Since such contaminated waste affects all metabolic and physiological activities, it is necessary to analyze the physiochemical attributes of water and propose measures to reduce contamination. All said and done, the sewage-water-flooded soils had higher pH, natural carbon, and CaCO₃. Surface skylines of soils (flooded/non-flooded) had higher groupings of DTPA-extractable Fe, Mn, Cu, and Zn, which decreased with depth. When compared to non-flooded soils, sewage-water-flooded soils are associated with moderately higher concentrations of DTPA-Fe, Mn, Cu, Zn, Pb, Cr, and Album (Tayawade et al. 2010).

Exposure to organic and inorganic chemicals over a long period of time can cause ecological health impairment of aquatic ecosystems causing considerable effects on aquatic biota including bioaccumulation of chemicals in organisms and biomagnification in higher trophic levels. Further, these can result in cytotoxic and genotoxic effects in the organisms (Daniels et al. 1989, Kannangara & Pathiratne 2015). Therefore, many ecotoxicological studies focus on the assessment of physical and chemical environmental parameters and biological responses of organisms. However, recent ecotoxicological studies are paying more attention to using bioassays to assess the mutagenic and genotoxic effects of aquatic pollution (Kannangara & Pathiratne 2015). These mutagenic and genotoxic studies have focused on assessing genotoxicity and mutagenic effects of fish species (Alimba et al. 2015, Carrasco et al. 1990) [12, 14], microorganisms (Buschini et al. 2001, Guan et al. 2017), mammals (Chiu et al. 2009, Kim et al. 2010), and higher plants (Iqbal et al. 2019) in relation to variation of chemical parameters in aquatic ecosystems

However, compared to other organisms *Allium cepa* is considered an efficient bioindicator in genotoxicity testing, because of the rapid root growth rate and reduced number of large chromosomes. *A. cepa* assay is commonly utilized as a short-term and cost-effective indicator of toxicity in monitoring water pollution in many parts of the world. This bioassay can provide valuable information on the presence of genotoxic and/or mutagenic compounds in surface waters and sediments of aquatic ecosystems. However, in Nagpur, a few tests have been carried out to analyze the physiochemical parameters of Bother stream water at various locations (Patil 2017, Manzar 2010, Tayawade et al. 2010) yet till today nobody evaluated the cytotoxicity and genotoxicity of the Bother Waterway Water. Therefore, the current study will use an *A. cepa* bioassay to assess the cytogenotoxic effects of water collected from several locations along the Bother Stream of the Nag River in Nagpur. By proving the ability of such substances to cause chromosomal changes in *A. cepa* root cells, the testing would provide important information concerning the presence of cytogenotoxic or potentially mutagenic substances in surface waters of the Bother stream.

MATERIALS AND METHODS

All the experimental work was completed at the Department of Biochemistry and Biotechnology, Dr. Ambedkar School, Deekshabhoomi, Nagpur during the period of October 2019 to Jun 2020. All the chemicals utilized in this investigation were bought from Hi-media Pvt. Ltd and (The basic purple onion, *A. cepa*) bulbs (2.5-2.8 cm in diameter) used in this study were purchased from a local market in Nagpur, Maharashtra (India).

Sample collection: The collection of water samples of Nag River which is spread over Nagpur city. Five different locations were randomly selected to collect the water sample which is given in Table 1. Water samples were collected in clean glass bottles and GPS values of that site were noted down.

Allium cepa Test

A commercial variety of common onions (*Allium cepa*) was used for the determination of different toxicity end points of meristematic cells. Equal sized healthy onion bulbs were chosen and the outer scales of bulbs were removed by gently scraping to make the apices of root primordia exposed. Scarped onion bulbs were germinated in glass test tubes containing distilled water for 24 hours in the dark. The *Allium cepa* bioassay in accordance with Grant (1982) with some modifications was conducted using water samples collected from the study sites. After 24 hours, onion bulbs were exposed to the exposure media (70 mL, Nag River sample taken from each site) in the glass tubes at the time of processing. For each exposure media 10 onion bulbs were tested. Bulbs with exposure media were kept in dark to avoid the direct sunlight.

After 48 hours of exposure, root lengths of randomly selected five onion bulbs from each exposure media were measured in millimeters. Root tips (5-6 from each onion bulb) of 1-2 mm length were processed for microscopic studies of toxicity end points. Root tips were fixed in ethanol: glacial acetic acid (3:1, v/v) solution for overnight at 4°C. Root tips were transferred into 70% alcohol and stored at 4°C until the time of processing.

Table 1: River Water was collected from five different locations of Nag River, Nagpur.

Samples ID	Water collected from different area	GPS Location
Sample 1	Rashimbagh Darsa Road	21°08'19.9"N 79°06'31.3"E
Sample 2	Gangabai Ghat Road	21°08'26.2"N 79°07'13.0"E
Sample 3	Near Airtel express	21°08'30.0"N 79°07'32.5"E
Sample 4	Near RajatSankul apartment	21°08'14.3"N 79°05'43.0"E
Sample 5	Rashimbagh road (Plant growing side)	21°08'18.4"N 79°06'21.0"E

When processing the root tips, they were hydrolyzed in hydrochloric acid (1N) solution for 5 minutes at 60°C and washed with distilled water. Root tips were then placed in watch glasses containing acetocarmine for 30 minutes to allow the stain to penetrate to the primordial cells. After staining, root tips were placed on glass slides and a slight pressure was applied on the cover slip to squash the tip cells over the slide. Prepared slides for each exposure medium were observed under the light microscope at 400x magnification to score mitotic stages, occurrence of micronuclei, and nuclear abnormalities in the interphase cells (Fiskesjo 1985, 1988).

Mitotic index was calculated as the number of dividing meristematic cells into 100 total meristematic cells by counting 1000 meristematic cells in each slide

Mitotic index = Number of dividing meristematic cells / total meristematic cells (500) × 100

RESULTS AND DISCUSSION

Effect of water samples on cell division process, cytological and chromosomal characteristics were assessed by *A. cepa* test and results given in Tables 2, 3 and 4, and Figs. 1 and 2.

Table 2: Effect of water sample collected from different sites of Nag river on cell division.

	No. of dividing cells	Prophase	Pro-metaphase	Metaphase	Anaphase	Telophase	MI in %
Control	163±3.05	78±1.02	24±2.08	21±1.52	29±2.51	11±1.15	32.6
Sample 1	50±2.05	20±1.03	6±0.33	8±2.52	9±1.15	7±0.57	10
Sample 2	48±1.05	18±1.52	8±0.12	7±1.52	10±2.51	5±1.15	9.6
Sample 3	43±1.06	17±0.50	6±0.60	6±0.57	8±1.15	6±0.72	8.6
Sample 4	49±1.52	19±0.8	7±1.01	8±1.15	9±1.15	6±2.51	9.8
Sample 5	40±2.51	17±1.01	5±0.91	7±0.57	6±0.57	5±0.72	8.0

Data are presented as mean ± standard deviation (SD), MI – mitotic index

Table 3: Chromosomal aberrations in *Allium cepa* root tip cells exposed to the Nag river water samples.

	Bridges	Breaks	lagging	Stickiness	Abnormal spiralisation	Multipolarity	Abnormal Ki- netics	Total No. of Aberrant cells (%)
Control	00±00	00±00	01±0.57	01±0.02	00±00	01±0.57	01±0.57	04 (0.8)
Sample 1	09±0.57	17±2.52	00±00	78±2.52	13±0.57	11±2.52	13±1	141 (28.00)
Sample 2	07±1.15	11±1.15	02±0.57	67±1.51	12±2.15	09±0.57	12±2.51	120 (24)
Sample 3	09±2.15	10±1.52	01±0.02	71±0.57	9±1.15	07±1.52	11±2	118 (23.6)
Sample 4	09±0.57	09±1.15	00±00	74±2.52	16±1.52	13±2.51	15±1.52	136 (26.2)
Sample 5	10±0.51	12±2.08	03±0.57	64±3.15	14±2.52	09±1.15	12±2.51	124 (24.8)

Data are presented as mean ± standard deviation (SD)

Table 4: Cytotoxic effects of different collected Nag River water on root tips of *Allium cepa*.

	Cells without nu- cleus	Morphological alter- ations	Plasmolysed cells	BNC	MNC	Total no. of aberrant cells (%)
Control	00±00	01±0.57	01±0.5	01±0.57	00±00	03 (0.6)
Sample 1	07±0.57	20±2.52	34±2.52	07±1.51	50±3.02	118 (23.06)
Sample 2	08±1.15	15±3.08	40±1.52	04±1.52	44±2.52	110(22.00)
Sample 3	07±0.57	24±2.15	30±2.52	06±0.57	40±2.52	107(21.4)
Sample 4	07±1.52	22±1.52	25±2.15	04±1.15	37±0.57	100 (20.00)
Sample 5	08±1.00	19±1.02	29±3.08	07±1.52	49±1.15	112 (22.4)

Data are presented as mean ± standard deviation (SD); BNC-nucleated cells, MNC- micronucleated cells.

The mitotic index of the *A. cepa* root tip cells in the present study ranged from 8% to 10% in Nag River water samples which were low compared to control (32%)

(Fig. 3). A mitotic index of less than 22% is considered fatal to organisms (Antonise-Wiez 1990) As a result, the mitotic indices measured in this study are frequently regarded

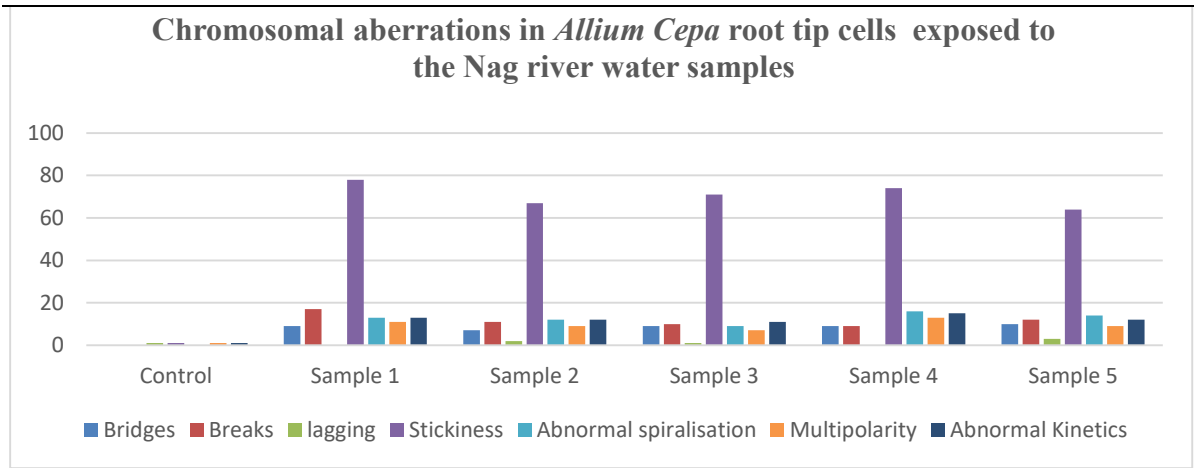


Fig. 1: Chromosomal aberrations in *Allium cepa* root tip cells exposed to the Nag river water samples.

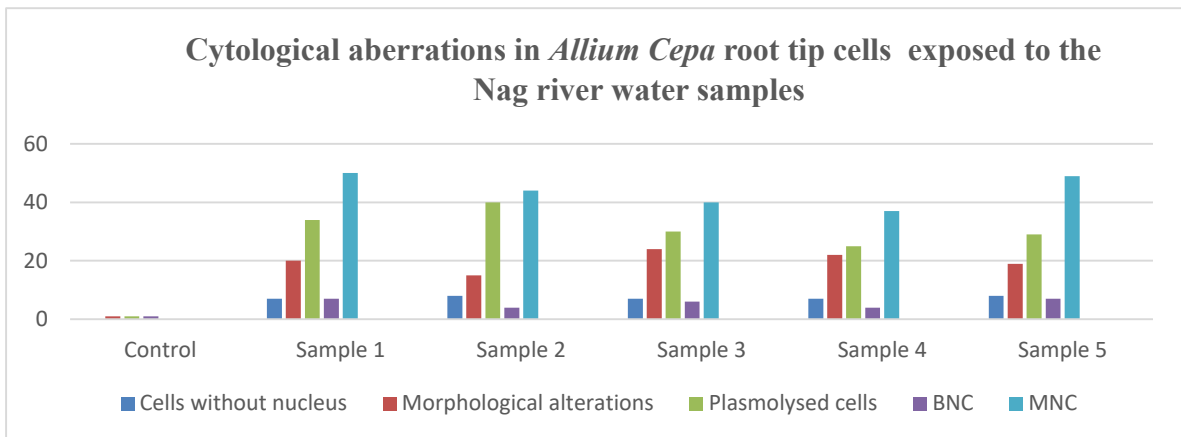


Fig. 2: Cytological aberrations in *Allium cepa* root tip cells exposed to the Nag river water samples.

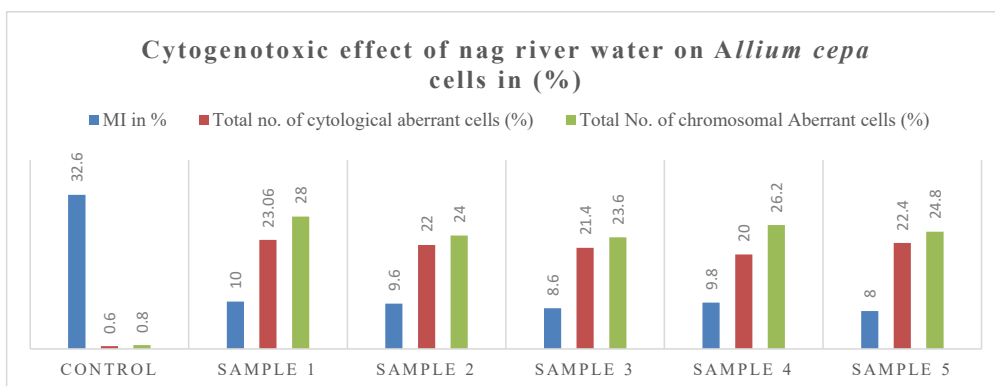


Fig. 3: Cytogenotoxic effect of nag river water on *Allium cepa* cells in (%).

as harmful and indicate high cytotoxic effects within the environment.

The presence of chromosomal abnormalities in *A. cepa* root tip cells indicates that genotoxic compounds may be present in the exposed medium (Kannangara & Pathiratne 2015, Boumaza et al. 2016).

After exposure to the Nag river water sample, chromosomal abnormalities in *A. cepa* root tip cells were observed. Anaphase bridges, breaks, chromosomal lagging and stickiness, aberrant spirulation of chromosomes, multipolarity, and polyploidy were all observed, as shown in Fig. 4.

After treatment with Nag river water, cytological abnormalities were identified during the cell cycle. In all water samples except the control, anomalies such as cells without nucleus, bi-nucleated cells, and morphological alterations were observed. Fig. 5 shows a few examples of cytological changes.

Studies have proven that compounds such as poly aromatic hydrocarbons, copper, arsenic, and other industrial effluents have been shown to have cytotoxic and genotoxic effects in *A. cepa* root tip cells (Kannangara & Pathiratne 2015, Samuel et al. 2010, Da Costa et al. 2012, Olorunfemi 2011)

The *A. cepa* assay is a vital in-vivo assay in which the roots develop in direct contact with the substance of interest, allowing for the prediction of possible DNA damage in humans (Nefic et al. 2013). The test used in this study allows for the evaluation of several genetic endpoints that arise as a result of exposure to various water samples collected from the Nag River in Nagpur, Maharashtra. All 5 samples caused significant inhibition of MI in *Allium cepa* meristem cells and induced chromosomal aberrations, nuclear abnormalities and micro nucleated cells (MNCs).

The mitotic index decreased in all five experimental water samples when compared to the control. The cytotoxic and

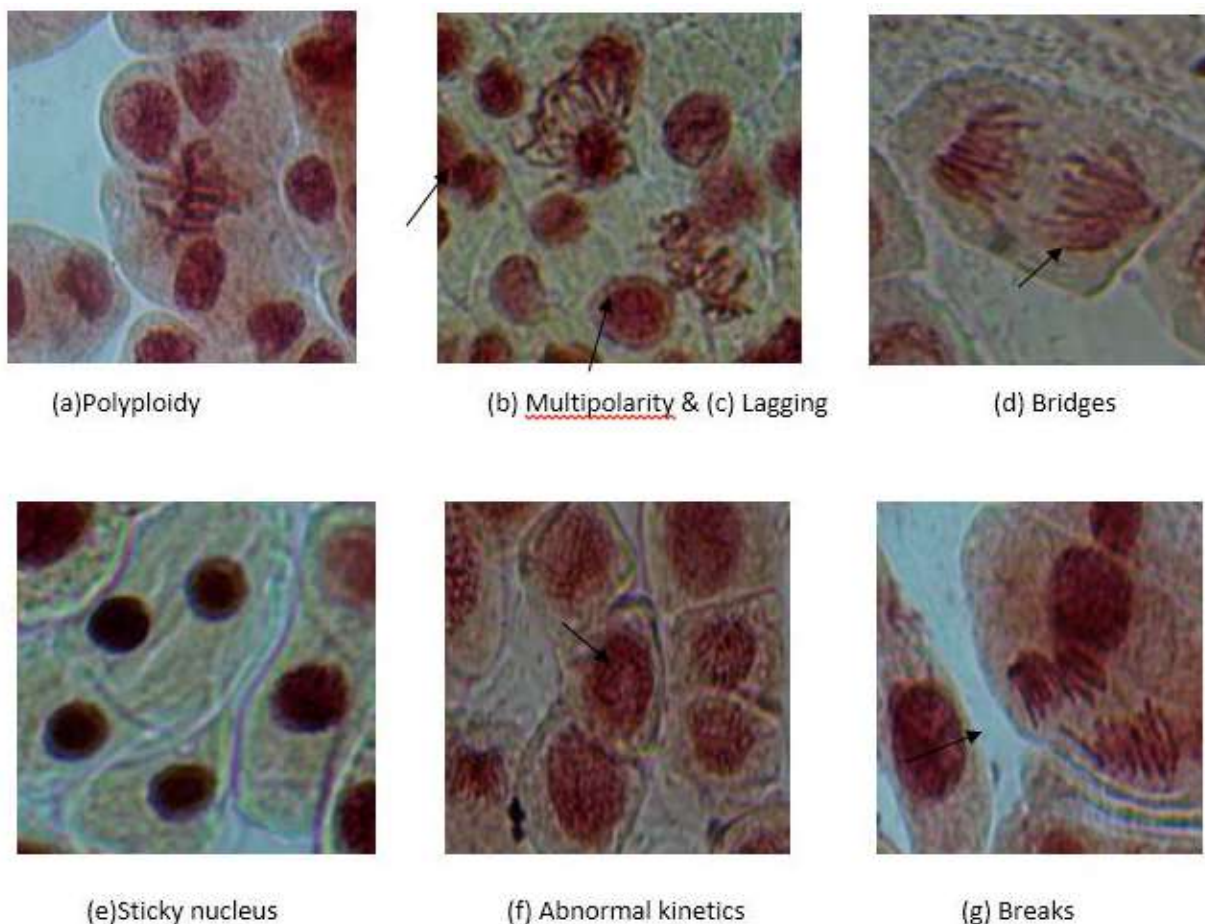


Fig. 4: Photomicrographs of CAs induced by Nag River water in root cells of *Allium cepa*.

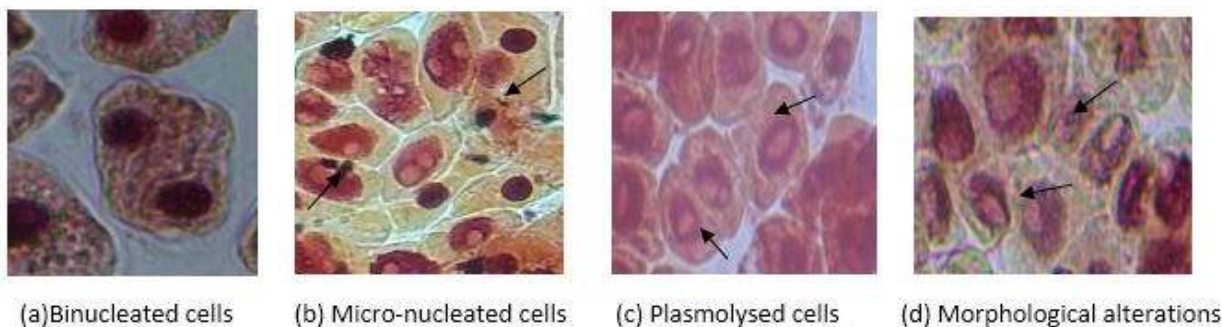


Fig. 5: Cytological aberrations in *Allium cepa* meristem cells exposed to Nag River water

genotoxic potential of Nag river water samples is determined by changes in MI of *Allium cepa* cells. The sample with the most chromosomal abnormalities was no. 1. (28%). The examination of various chromosomal abnormalities types at various stages of the cell cycle allows for a more thorough investigation of the impacts of the Nag river water sample. Breakages may occur and subsequent inhibition of repair mechanisms may lead to base mismatch, mutation and CAs such as fragmented chromosomes and DNA breaks (Nefic et al 2013).

All water samples tested from different points along the Nag River had bridges, breaks, lags, multi-polar anaphase chromosomes, and aberrant spiralization. The findings revealed that all Nag river water samples were capable of inhibiting normal cell division and causing deadly chromosomal abnormalities. Stickiness is due to inter-chromosomal linkages of sub-chromatid strands coupled with excessive formation of nucleoproteins and inappropriate protein-protein interaction (Nefic et al. 2013).

Cytological aberrations are characterized by BNC, plasmolyzed cells, and micronucleus formation as a result of exposure to Nag river Water samples. Also, we observed alterations in the shape and size of cells in all collected Nag river water samples.

CONCLUSION

Domestic as well as industrial activities are important sources of pollution during the flow of these rivers. Domestic sources as compared to industrial sources exceed substantially in terms of organic load addition into the River. The predominant source is untreated sewage discharged by Nagpur Municipal Corporation into Nag and Pili Rivers.

The findings of this study revealed that the water of the Nag River is highly cytotoxic and genotoxic, making it unsafe for drinking and irrigation. No one should grow any vegetables or crops near the Nag River because toxic substances

could enter the food chain and cause diseases due to the phenomenon of biomagnification and bioaccumulation. It's critical to identify the composition and speciation of those cytogenotoxic compounds in the tropical climate, as well as to provide cleanup or treatment options to address this environmental and public health risk. Furthermore, continual water quality monitoring and management are critical for maintaining the ecosystem's ecological health.

ACKNOWLEDGMENTS

The authors wish to acknowledge the Principal of Dr. Ambedkar College, Deekshabhoomi, Nagpur (India), for providing the laboratory facilities to conduct this research and Mr. Avinash Chavhan's laboratory assistant for the kind support.

REFERENCES

- Alimba, C.G., Ajayi, E.O., Hassan, T., Sowunmi, A.A. and Bakare, A.A. 2015. Cytogenotoxicity of abattoir effluent in *Clarias gariepinus* (Burchell, 1822) using the micronucleus test. *Chinese J.Biol.*, 2015: 56-71
- Anparthi, A. 2013. Nag river looks like a sewage drain. *Times of India*, Times News Network, Mumbai, India.
- Antonise-Wiez, D. 1990. Analysis of the cell cycle in the root meristem of *Allium cepa* under the influence of ledakrin. *Folia Histochem. Cytobiol.*, 28(1-2): 79-95.
- Boumaza, A., Lalaoui, K., Khallef, M., Sbayou, H., Talbi, H. and Hilali, A. 2016. Assessment of cytotoxic and genotoxic effects of Clodinafop-propargyl commercial formulation on *Allium cepa* L. *J. Mater. Environ. Sci.*, 7(4): 1245-1251.
- Buschini, A., Cassoni, F., Anceschi, E., Pasini, L., Poli, P. and Rossi, C. 2001. Urban airborne particulate: Genotoxicity evaluation of different size fractions by mutagenesis tests on microorganisms and comet assay. *Chemosphere*, 44(8): 1723-1736.
- Carrasco, K.R., Tilbury, K.L. and Myers, M.S. 1990. Assessment of the piscine micronucleus test as an in situ biological indicators of chemical contaminant effects. *Can. J. Fish. Aquat. Sci.*, 47(11): 2123-2136.
- Chiu, W. A., Okino, M. S. and Evans, M. V. 2009. Characterizing uncertainty and population variability in the toxicokinetics of trichloroethylene and metabolites in mice, rats, and humans using an updated database, physiologically based pharmacokinetic (PBPK) model, and Bayesian approach. *Toxicol. Appl. Pharmacol.*, 241(1): 36-60.

- Daniels, S.A., Munawar, M. and Mayfield, C.I. 1989. An improved elutriation technique for the bioassessment of sediment contaminants. *Hydrobiologia*, 188(1): 619-631.
- Da Costa, T. C., de Brito, K. C. T., Rocha, J. A. V., Leal, K. A., Rodrigues, M. L. K., Minella, J. P. G., ... & Vargas, V. M. F. 2012. Runoff of genotoxic compounds in river basin sediment under the influence of contaminated soils. *Ecotoxicol. Environ Safety*, 75: 63-72.
- Fiskesjo, G. 1985. The *Allium* test is a standard in environmental monitoring. *Hereditas*, 102(1): 99-112.
- Fiskesjo, G. 1988. The *Allium* test: An alternative in environmental studies: The relative toxicity of metal ions. *Mutat. Res/Fund. Mol. Mech. Mutagen.*, 197(2): 243-260.
- Grant, W.F. 1982. Chromosome aberration assays in *Allium*: A report of the US Environmental Protection Agency gene-tox program. *Mutat Res-Rev. Gene. Toxicol.*, 99(3), 273-291.
- Guan, Y., Wang, X., Wong, M., Sun, G., An, T., Guo, J. and Zhang, G. 2017. Evaluation of genotoxic and mutagenic activity of organic extracts from drinking water sources. *PloS One*, 12(1): e0170454.
- Iqbal, M., Abbas, M., Nisar, J., Nazir, A. and Qamar, A. 2019. Bioassays based on higher plants as excellent dosimeters for ecotoxicity monitoring: A review. *Chem Int.*, 5(1), 1-80.
- Kalyani, M. 2017. Nag river's rich history drown in silt. *Articulations*, 2017: 3-9
- Kim, Y. J., Yang, S. I. and Ryu, J. C. 2010. Cytotoxicity and genotoxicity of nano-silver in mammalian cell lines. *Mol. Cell. Toxicol.* 6(2): 119-125.
- Kannangara, D.N.M. and Pathiratne, A. 2015. Toxicity assessment of industrial wastewaters reaching DanduganOya, Sri Lanka using a plant-based bioassay. *J. Natl. Sci. Found Srilanka*, 43(2): 153-163
- Manzar, A. 2010. Report of Government of India Ministry of Water Resources. Central Groundwater Board, India
- Nefic, H., Musanovic, J., Metovic, A. and Kurteshi, K. 2013. Chromosomal and nuclear alterations in root tip cells of *Allium cepa* L. induced by alprazolam. *Med Arch.*, 67(6): 388.
- Olorunfemi D.I. 2011. Cytotoxic and genotoxic effects of Cassava effluents using the *Allium cepa* bioassay. *Res. J. Mutagen*, 1(1), 1-9
- Patil, A.M. 2017. Assessment of Water Quality Parameters of Nag River Flowing through Nagpur, Maharashtra. Monitoring Central Organization, Central Water Commission Nagpur, India
- Puri, P.J., Yenkie, M.K.N., Battalwar, D.G., Gandhare, N.V. and Dhanorkar, D B. 2010. Study and interpretation of physico-chemical characteristics of lake water quality in Nagpur city (India). *Rasayan J. Chem.*, 3(4): 800-810.
- Samuel, O.B., Osuala, F.I. and Odeigah, P. G.2010. Cytogenotoxicity evaluation of two industrial effluents using *Allium cepa* assay. *Afr. J. Environ. Sci. Tech.*, 4(1): 123-140.
- Tayawade, S.S. and Prasad, J. 2008. Characterization of sewage-water-irrigated and non-irrigated soils in nag river ecosystem of Nagpur, Maharashtra. *J. Indian Soc. Soil Sci.*, 56(3): 247-253.



A Study on the Effect of Soil and Sediment Types on the Fugacity Based Multimedia Partitioning of a Contact Fungicide Fluopyram: An Equilibrium Quality Criterion (EQC) Level 1 Approach

A. Thakur*, S. Sharma** and K. Qanungo*†

*Division of Chemistry, University Institute of Science, Chandigarh University, Gharuan, Distt. Mohali-140413, Punjab, India

**N-307, Gilco Heights, Gilco Valley, Kharar, Mohali, Punjab, 140301, India

†Corresponding author: K. Qanungo; kushal.appsci@cumail.in

Nat. Env. & Poll. Tech.
Website: www.neptjournal.com

Received: 16-10-2020

Revised: 24-12-2020

Accepted: 13-01-2021

Key Words:

Fluopyram

Equilibrium quality criterion (EQC)

Environmental fate

Pesticide

ABSTRACT

Equilibrium Quality Criterion (EQC) Level I calculations have been performed with Standard Equilibrium Quality Criterion (EQC) environment to study the environmental partitioning of a fungicide Fluopyram. Equilibrium Quality Criterion (EQC) Level I calculation assumes no degradation of the chemical, steady-state, and equilibrium conditions between the environmental compartments. The results reveal that the concentration of Fluopyram is expected to be maximum in the sediment compartment, followed by soil and water compartments. The effect of soil and sediment types on partitioning has been studied by systematically varying the densities of these two compartments. In the sediment compartment, the Fluopyram concentration is predicted to be highest if the sediment type is 'sandy' and the soil type is 'clay'.

INTRODUCTION

The use of chemical pesticides in farming is one of the principal facets of modern agricultural practices. These pesticides come in a wide variety of types like contact and non-contact pesticides, selective, non-selective, etc., and functions like herbicides, fungicides, bactericides, nematocides, etc. (Duran-Lara et al. 2020). All of these pesticides are toxic not only to humans but also to flora and fauna (Bernardes et al. 2015). After their intended use of these pesticides in agricultural fields, these pesticides are left in the environment to degrade and dissipate. Many of these pesticides end up polluting the sea and surface water, sediments, and air. Their concentrations in these environmental compartments can be determined experimentally using a standard analytical procedure or estimated by the use of environmental fate models (Di Guardo et al. 2018).

Fluopyram is a new pyridylethylamide insecticide with a wide-ranging fungicidal and nematocidal action and has extensive potential use in agriculture worldwide (Persistence Market Research 2020). It is identified to be toxic to aquatic organisms (Malhotra 2018, EFSA 2013) and hence it is not used near places where aquaculture is practiced.

Considering the importance of Fluopyram in agriculture and the need to the study environmental fate of pesticides, this paper describes the effect of soil and sediment type on the environmental fate of Fluopyram using a fugacity-based Equilibrium Quality Criterion Model "EQC Model" (Mackay 2004). The EQC model has been used in several studies to predict the environmental fate of chemicals in the environment (Macleod & Mackay 1999, Cahill et al. 2003, Ellis et al. 2006, Lifongo & Nfon 2009, Ndouba et al. 2020, Kim et al. 2013).

MATERIALS AND METHODS

The Level I of the Equilibrium Criterion (EQC) model has been used in this study (Mackay 2001). There are several assumptions of the Level 1 model (Mackay & Seth 2001) which are as follows: the system containing M moles of the chemical is in thermodynamic equilibrium and the fugacity of the chemical species is the same throughout the system; a multi-compartment "Unit World" is described with the volume of each compartment being v_i ; the chemical does not react and no loss of the chemical is taking place by any means from the unit world, and the system is in steady-state

with no movement of the chemical from one phase to another. For a multicomponent system, the common fugacity is defined as

$$f = \frac{M}{\sum v_i z_i} \quad \dots(1)$$

Where z_i is the fugacity capacity of the particular phase for the chemical and is used to relate concentration and f as follows:

$$c_i = f z_i \quad \dots(2)$$

The concentration c_i in each compartment can then be calculated from Eqn. 2 and the quantities in each of the compartments

$$M_i = v_i f z_i \quad \dots(3)$$

z_i depends upon chemical properties, the nature of the phases, and temperature.

The fugacity capacities of different phases are defined by the following equations:

$$\text{Fugacity capacity of air: } (z_a) \quad z_a = \frac{1}{RT} \quad \dots(4)$$

Fugacity capacity of aerosol: (z_{aerosol})

$$z_{\text{aerosol}} = z_a \times K_{qa} \quad \dots(5)$$

Where K_{qa}

$$K_{qa} = \frac{6 \times 10^6}{P_L} \quad \dots(6)$$

P_L is the subcooled vapor pressure

$$P_L = P \exp \left[6.79 \left(\frac{T_M}{T} - 1 \right) \right] \quad \text{at } T < T_M \quad \dots(7)$$

where T is the measurement temperature, T_M is the melting point, P is the vapor pressure at temperature T .

Fugacity capacity of water: (z_w)

$$z = \frac{S}{P} \quad \dots(8)$$

Where S is the water solubility (mol.m^{-3}) and P is vapor pressure (Pa)

Fugacity capacity of suspended sediments: (z_{sus})

$$z_{\text{sus}} = K_{\text{sus}} \times \rho_{\text{sus}} \times z_w \quad \dots(9)$$

Where K_{sus} is the suspended sediment-water partition coefficient: (K_{sus})

$$K_{\text{sus}} = K_{oc} \times f_{oc} \quad \dots(10)$$

and f_{oc} is the fraction of organic carbon present in the

suspended particles (taken as constant 0.02 in EQC standard environment).

Fugacity capacity of fish: (Z_{fish})

$$Z_{\text{fish}} = K_{\text{fish}} \times \rho_{\text{fish}} \times Z_w \quad \dots(11)$$

Where K_{fish} is the Fish-Water Partition Coefficient or Bio-concentration Factor:

$$K_{\text{fish}} = 10^{\log k_{ow}} \times L \quad \dots(12)$$

Where L is the fraction of lipid content in fish (taken as constant 0.05 in EQC standard environment).

and K_{fish} is the density of fish present (taken as constant 1.0 kg.L^{-1} in EQC standard environment).

Fugacity capacity of soil: (Z_{soil})

$$Z_{\text{soil}} = K_{\text{soil}} \times \rho_{\text{soil}} \times Z_w \quad \dots(13)$$

Where K_{soil} is the Soil-Water Partition Coefficient:

$$K_{\text{soil}} = K_{oc} \times f_{oc} \quad \dots(14)$$

and ρ_{soil} is the density of soil (taken as constant 2.4 kg.L^{-1} in EQC standard environment) and f_{oc} is the fraction of organic compound in soil (taken as constant 0.02 in EQC standard environment) and K_{oc} is the organic carbon-water partition coefficient:

$$K_{oc} = 0.41 \times K_{ow} \quad \dots(15)$$

Fugacity capacity of sediments: (Z_{sed})

$$Z_{\text{sed}} = K_{\text{sed}} \times \rho_{\text{sed}} \times Z_w \quad \dots(16)$$

Where K_{sed} is the sediment-water partition coefficient

$$K_{\text{sed}} = K_{oc} \times f_{oc} \quad \dots(17)$$

Where f_{oc} is the fraction of organic compounds in sediments. (taken as constant 0.04 in EQC standard environment). Additionally, Henry's Law constant can be obtained by the equation given as:

$$H = \frac{P}{S} \times M \quad \dots(18)$$

Where P is the vapor pressure and S is the water solubility and M is the molecular weight.

Model Inputs

An examination of the chemical properties of Fluopyram (see below) indicates that it is a Type 1 chemical (Mackay et al. 1996a, Mackay et al. 1996b, Mackay et al. 1996c) with

vapor pressure $> 10^{-7}$ Pa and solubility in water $> 10^{-6}$ g.m⁻³. The EQC Level 1 model requires the following chemical properties as inputs for Type 1 chemicals, the values of which are given for Fluopyram: a) vapor pressure, 1.20×10^{-6} Pa; b) water solubility, 16.0 g.m⁻³; c) molar mass, 396.72 g.mol⁻¹; d) melting point, 117.5 C; e) data temperature; 20 C (Pesticide Properties Database, 2019). The EQC model assumes a one-time release and instantaneous equilibration of 100,000 kg of the chemical which is 256,067 mols of Fluopyram.

The model has an inbuilt 'EQC Standard Environment' which is mentioned in Table 1. These values are used to calculate the distribution of Fluopyram in the 'Unit World'.

The 'EQC Standard Environment' has been modified to calculate the effect of soil density on the Fluopyram distribution. The following agricultural soil types (Irmak & Djaman 2015) have been used and their density values are mentioned in parentheses (kg.L⁻¹) a) clay soil (1.15) b) silt loam soil (1.13) c) clay loam soil (1.325) d) loam soil (1.38e) sandy loam soil (1.425) and f) sandy soil (1.45). To calculate the distribution of the effect of sediment density on the Fluopyram distribution, the following sediment types (Flemming & Delafontaine 2016) have been used and their density values are mentioned in parentheses (kg.L⁻¹), a) muddy sediment (0.3) b) slightly sandy muddy sediment (0.4) c) sandy muddy sediment (0.6) d) muddy sandy sediment (0.9) e) slightly muddy sandy sediment (1.2) and f) sandy sediment (1.5).

Fugacity-based Environmental Equilibrium Partitioning Model Level I (Mackay 2004) have been used to perform the EQC Level 1 calculations for the 'EQC Standard Environment'. The same calculations were performed using MS Excel for convenience and the results matched with the output of the EQC Level 1 program (Table 2). This served as a check on the calculations performed in MS Excel. The density of the soil and sediment compartments were varied systematically and calculations were performed using MS Excel, and the maximum and minimum Fluopyram concentration in different environmental compartments were

determined, for different combinations of soil and sediments and are tabulated in Table 3.

RESULTS AND DISCUSSION

The amounts of Fluopyram (by weight) and its relative distribution in 'Standard EQC environment' in different environmental compartments have been shown in Table 2. There is a large amount (mols) of Fluopyram present in soil (63%) and water (36%), followed by sediment compartment (1.4%) and negligible quantities in the air. Also, the concentration of Fluopyram is more in sediments > soil > water. The air compartment showed very little concentration of the chemical.

The negligible presence of Fluopyram in the air is understandable because of its low vapor pressure. A chemical with a small vapor pressure does not distribute into the air so there is a possibility for accumulation in water if it is water-soluble or soil. However, if it is not water-soluble, the chemical can accumulate in the soil. The water solubility of Fluopyram is moderately low. The predicted large amount of Fluopyram in the soil compartment was noticed. The Henry's Law constant value for Fluopyram is low $H = 2.98 \times 10^{-5}$ Pa.m³/mol, which indicates that it will distribute to the air compartment. Also, it was noted that in the air compartment Fluopyram concentrations are predicted to be far below the detection limit of 4 µg.m⁻³ (BVL 2017).

The Fluopyram concentrations for all possible combinations of soil and sediment types (details in the Methods section) were calculated and the maximum and minimum values are tabulated for the four main environmental compartments and are depicted in Table 3. The concentrations units used are mol.m⁻³, for easy comparison amongst compartments with varying density of its constituents.

The highest Fluopyram concentration is predicted to occur in the sediment compartment with clay soil-sandy sediment combination (Fig. 1). An increasing Fluopyram concentration is predicted in sediments with different types of soils, and the order of sediment types can be established as

Table 1: Environmental Parameters Under 'EQC Standard Environment'.

	Volume, m ³	Density, kg.m ⁻³	Organic carbon, g.g ⁻¹	Fish-lipid, g.g ⁻¹
Air	1.00E+14	1.21	-	-
Aerosol	2000	2000	-	-
Water	2.00E+11	1000	-	-
Suspended particles	1.00E+06	1500	0.200	-
Fish	2.00E+05	1000	-	0.0500
Soil	9.00E+09	2400	0.0200	-
Sediments	1.00E+08	2400	0.0400	-

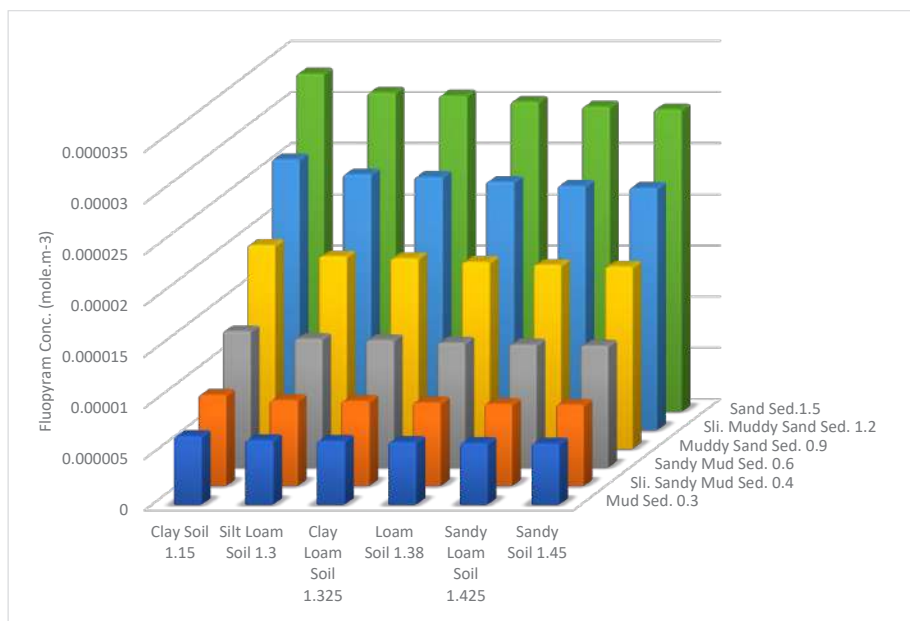


Fig. 1: Graphical representation of variation in concentration of Fluopyram in sediment with different soil and sediment types.

follows: muddy sediment < slightly sandy muddy sediment < sandy muddy sediment < muddy sandy sediment < slightly muddy sandy sediment < sandy sediment. This the same order in which the sediment density increases.

An increasing Fluopyram concentration is predicted in soil with different types of sediment, and the order of soil types can be established as follows: clay soil < silt loam soil < clay loam soil < loam soil < sandy loam soil < sandy soil (Fig. 2). This the same order in which the soil density increases. The Fluopyram concentration is the maximum for

sandy soil-muddy sediment combination (Table 3).

Table 3 would be helpful to identify the soil and sediment combination leading to the highest and lowest concentrations of Fluopyram. This would in turn help to understand and guide the use of Fluopyram in different environments with different types of soil and sediment combinations. At the default value of 100,000 kg application of the Fluopyram, the concentrations of Fluopyram in the soil compartment (Table 2) are above the detection limit ($1.5 \times 10^{-3} \mu\text{g.g}^{-1}$) and lower than the quantification limit ($5.0 \times 10^{-3} \mu\text{g.g}^{-1}$) (FAO

Table 2: Concentration and Amount of Fluopyram in Main Four Different Compartments in EQC Standard Environment at 100,000 kg Emission.

Compartment	Conc. mol.m ⁻¹³	Conc. $\mu\text{g.g}^{-1}$ of solids	Conc. g.m ⁻³	Amount Mol	Amount %
Air	5.48E-15	-	7.17E-12	0.548	2.17E-04
Water	4.49E-07	-	1.78E-04	89778	35.6
Soil	1.76E-05	2.19E-03	6.99E-03	1.59E+05	62.9
Sediments	3.35E-05	5.83E-03	1.40E-02	3525	1.40

Table 3: Maximum and minimum Fluopyram concentration for different combinations of soil and sediments.

Comp.	Soil and Sediment combination producing Max. Fluopyram conc.		Conc. (mol.m ⁻³)	Soil and Sediment combination producing Mini. Fluopyram conc.		Conc. (mol.m ⁻³)
	Soil type	Sed. Type		Soil type	Sed. Type	
Air	Clay soil	Mud sed.	8.30342×10^{-15}	Sandy soil	Sand sed.	7.35×10^{-15}
Water	Clay soil	Mud sed.	6.80161×10^{-7}	Sandy soil	Sand sed.	6.02×10^{-7}
Sed.	Clay soil	Sand sed.	3.30346×10^{-5}	Sandy soil	Mud sed.	5.96581×10^{-5}
Soil	Sandy soil	Mud sed.	1.44174×10^{-5}	Clay soil	Sand sed.	1.26633×10^{-5}

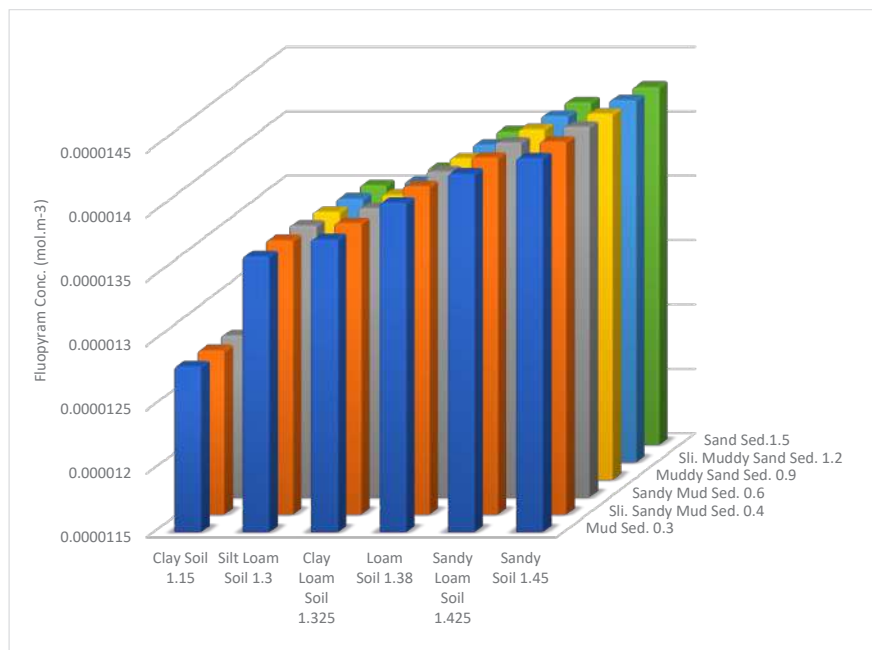


Fig. 2: Graphical depiction of variation in concentration of Fluopyram in soil with different soil and sediment types.

2011). In the case of the sediment compartment, however, the concentration of Fluopyram (Table 2) is above the quantification limit.

CONCLUSION

To conclude, through this evaluative study, it was understood how the densities of soil and sediment in the environment together with the physico-chemical properties of Fluopyram controls the environmental fate of the pesticide. The EQC Model predicts that Fluopyram mainly distributes (in terms of amount) to soil and water. However, its concentration in the sediment compartment would be maximum. It is also predicted that 'sandy sediment' would be able to concentrate most of the Fluopyram while 'muddy sediment' concentrates the least for all possible combinations of soil and sediment types.

REFERENCES

- Bernardes, M.F.F., Pazin, M., Pereira, L.C. and Dorta, D. J. 2015. Impact of pesticides and human health. In: Andrezza, A. C. and Scola, G. (eds.) Toxicology Studies - Cells, Drugs and Environment, IntechOpen, Rijeka, Croatia, pp. 195-211.
- BVL. 2017. Registration Report: National Assessment-Federal Republic of Germany [https://www.bvl.bund.de/SharedDocs/Downloads/04_Pflanzenschutzmittel/01_zulassungsberichte/027208-00-00.pdf?_date=11 October, 2020](https://www.bvl.bund.de/SharedDocs/Downloads/04_Pflanzenschutzmittel/01_zulassungsberichte/027208-00-00.pdf?_date=11%20October%202020).
- Cahill, T.M., Cousins, I. and Mackay, D. 2003. General fugacity-based model to predict the environmental fate of multiple chemical species. *Env. Tox. Chem.*, 22(3): 483-493.
- Di Guardo, A., Gouin, MacLeod, M.T. and Scheringer, M. 2018. Environmental fate and exposure models: Advances and challenges in 21st century chemical risk assessment. *Env. Sci. Process. Imp.*, 20(1): 58-71.
- Duran-Lara, E.F., Valderrama, A. and Marican, A. 2020. A natural organic compound for application in organic farming. *Agriculture*, 10(2): 41-63.
- EFSA. 2013. Conclusion on the peer review of the pesticide risk assessment of the active substance [fluopyram]. *EFSA J.*, 11(4): 3052-3128.
- Ellis, D.A., Cahill, T.M., Mabury, S.A., Cousins, I.T. and Mackay, D. 2006. Partitioning of Organofluorine Compounds in the Environment. In: Neilson A.H. (eds) Organofluorines, The Handbook of Environmental Chemistry (Vol. 3 Series: Anthropogenic Compounds), vol 3N. Springer, Berlin, Heidelberg, pp. 63-83.
- FAO. 2011. Fluopyram. http://www.fao.org/fileadmin/templates/agphome/documents/Pests_Pesticides/JMPR/Evaluation10/Fluopyram.pdf (date accessed 11th October, 2020).
- Flemming, B.W. and Delafontaine, M.T. 2016. Mass physical sediment properties. In: Michael J. (eds.). *Encyclopedia of Estuaries*, Springer, Netherlands.
- Irmak S. and Djaman, K. 2015. Basic Soil and Water Resources and Irrigation Engineering/Agricultural Water Management and Related Terminology. <https://extensionpublications.unl.edu/assets/pdf/ec2009.pdf> (date accessed 6 Nov. 2020)
- Kim, J., Powell, D.E., Hughes, L. and Mackay, D. 2013. Uncertainty analysis using a fugacity-based multimedia mass-balance model: Application of the updated EQC model to decamethylcyclopentasiloxane (D5). *Chemosphere*, 93(5): 819-829.
- Lifongo, L. and Nfon, E. 2009. Evaluating the fate of organic compounds in the Cameroon environment using a level III multimedia fugacity model. *Afri. J. Env. Sci. Tech.*, 3(11): 376-386.
- Mackay, D. 2004. Fugacity-Based Environmental Equilibrium Partitioning Model Level I Model, Version 3.00. Trent University, Peterborough, Canada.
- Mackay, D. 2001. *Multimedia Environmental Models. The Fugacity Approach*. 2nd ed. Lewis Publication, Boca Raton, FL, USA.

- Mackay, D., Paterson, S., Kicsi, G., Di Guardo, A. and Cowan, C.E. 1996a. Assessing the fate of new and existing chemicals: A five-stage process. *Environ. Toxicol. Chem.*, 15(9): 1618-1626.
- Mackay, D., Paterson, S., Di Guardo, A. and Cowan, C.E. 1996b. Evaluating the environmental fate of a variety of types of chemicals using the EQC model. *Environ. Toxicol. Chem.*, 15(9): 1627-1637.
- Mackay, D., Paterson, S., Kicsi, G., Cowan, C.E., Di Guardo, A. and Kane, D.M. 1996c. Assessment of chemical fate in the environment using evaluative, regional, and local-scale models: Illustrative application to chlorobenzene and linear alkylbenzene sulfonates. *Environ. Toxicol. Chem.*, 15(9): 1638-1648.
- Mackay, D. and Seth, R. 2001. Fugacity Modelling to Predict Long-Term Environmental Fate of Chemicals from Hazardous Spills. In: Fingas, E., (eds.) *The Handbook of Hazardous Materials Spills Technology*, McGraw-Hill, New York, N.Y., pp. 483-493
- Macleod, M. and Mackay, D. 1999. An assessment of the environmental fate and exposure of benzene and the chlorobenzenes in Canada. *Chemosphere*, 38(8): 1777-1796.
- Malhotra, S.K. 2018. Minutes of the 384th Meeting of Central Insecticides Board & Registration Committee, Ministry of Agriculture & Farmers Welfare, GoI, <http://164.100.161.213/sites/default/files/384rc2018.pdf> (date accessed 11 October, 2020).
- Ndouba, A.M., Elleingand, E.F. and Wandan, E.N. 2020. Modelling the fate of pesticides applied to banana plantation in the Bia river watershed in Côte d'Ivoire. *J. Chem. Biol. Phys. Sci.*, 10(3): 251-264.
- Persistence Market Research 2020. Fluopyram Market. <https://www.persis-tencemarketresearch.com/market-research/fluopyram-market.asp> (date accessed 11 October, 2020).
- Pesticide Properties Database. 2019. PPDB: Pesticide Properties Database. <http://sitem.herts.ac.uk/aeru/ppdb/en/Reports/1362.htm> (date accessed 11 October, 2020).



Monitoring Methods of Marine Pollution Range Based on Big Data Technology

Q. Zhong*† and X.M. Liu**

*Department of Art Design and Public Management, Yantai Vocational College, Yantai 264670, China

**Department of Information Engineering, Yantai Vocational College, Yantai 264670, China

†Corresponding author: zhongqiang1015@163.com

Nat. Env. & Poll. Tech.
Website: www.neptjournal.com

Received: 20-11-2020

Revised: 23-12-2020

Accepted: 22-01-2021

Key Words:

Big data technology

Marine pollution

Image monitoring

Digital remote sensing

Intelligent monitoring

ABSTRACT

With the development of big data technology, traditional monitoring methods for the scope of marine pollution can no longer meet the current needs of accuracy and timeliness. In light of the outstanding topic, this study proposed to use big data technology to monitor the scope of marine pollution. The intelligent digital remote sensing technology was used for multi-dimensional monitoring of ocean water quality and completed the calculation of data collected by water quality sensors through the improved big data comparative analysis method. Finally, the scope of pollution monitoring was realized. The results verified that the proposed monitoring method could achieve high-precision and time-sensitive monitoring of the range of marine pollutants, and could identify the basic information of pollutants.

INTRODUCTION

The ocean and humans have become increasingly intertwined as science and technology have advanced (Cavallaro et al. 2017). And the protection of the marine environment has become a common concern topic for eco-environmental experts. The current common monitoring method for the scope of marine pollution is low-dimensional detection technology, which is characterized by a narrow monitoring range and applies to the near sea area (Sun et al. 2018). At the same time, the monitoring accuracy of this technology is relatively low, and the monitoring time is comparatively long, which may cause the location of pollutants to change during this period (Rabinskiy et al. 2017). Intelligent digital remote sensing technology has been widely used in many industries and has achieved breakthrough achievements as a major application of big data technology in the field of artificial intelligence, but this technology applied to the monitoring of marine pollution is relatively rare. In view of this, this study proposed the use of intelligent digital remote sensing technology and big data comparison technology as a monitoring method for the scope of marine pollution, aiming to provide technical support for future marine environmental management and help to create a green environment.

MATERIALS AND METHODS

Marine Pollution Scope Monitoring Method Based on Big Data Technology

Intelligent digital remote sensing technology

Research has introduced intelligent digital remote sensing technology for monitoring the scope of marine pollution. The technology, based on remote sensing satellites, detects marine environmental pollution through intelligent data modules (Verfuss et al. 2018), and then, obtains valuable information through multi-layer database comparison. Intelligent remote sensing technology is different from ordinary remote sensing technology. Its characteristics are more intelligent and digital, which can achieve the effective processing of image information more quickly, allowing users to extract valuable information and apply it to real life and work. Remote sensing technology includes information sources, obtaining information, receiving information, processing information, and applying information (Jauzein et al. 2016). The ocean analysis database uses the object features extracted from the ocean object database to realize data analysis and finally displays it on the computer screen through learning mode, machine learning, data mining, etc. The schematic diagram of the structure of the remote sensing database is shown in Fig. 1. The technical structure includes an image layer, a marine information display layer, and a marine analysis display layer. The image layer is to obtain the information of the marine environment through remote sensing recognition of remote sensing satellites and send the obtained images to the marine information processing interface via the wireless network in the form of a packaged file, which involves image processing, retrieval of object attributes and image characteristics (Setala

et al. 2016). The marine information processing layer converts monitoring information into digital information through database processing. Marine object databases and marine environmental physical field analysis databases are used. The ocean analysis display layer accepts the transferred data and then processes the image through data link mode, image data module, and data mining technology (Arslan & Avsar 2020).

Water quality sensor measurement and monitoring technology

Marine pollutants can usually be divided into petroleum and its corresponding products, metal and non-metal pollutants, acidic or alkaline pollutants, pesticides, radioactive substances, organic pollutants, domestic sewage, thermal pollution, solid waste, antibiotics, etc. Marine polluted waters usually have a variety of pollutants, and the main impacts are reflected in the following three aspects (Bonanno & Orlando-Bonaca 2018). First, pollutants will cause a series of physical, chemical, and geological reactions that affect the safety of marine organisms. Second, it threatens human life and health through direct channels and the food chain. Third, marine pollutants have undergone major changes over time and in sea

conditions. Current monitoring of pollutants includes water quality monitoring, bottom quality monitoring, atmospheric monitoring, biological monitoring, etc.

Based on the above analysis and previous research experience, the research selects water quality sensors to collect marine pollution data and then determines the pollution scope (Ternengo et al. 2018). The monitored data information includes seawater PH value, seawater dissolved oxygen content, seawater conductivity, and seawater temperature. The types and related functions of the water quality sensors used in the research are shown in Table 1.

Improved big data comparative analysis method

The research uses a comparative analysis method for the data of marine pollution range. Big data core technologies include four core technologies: big data collection, big data preprocessing, big data storage, and big data analysis. Data preprocessing is directly related to the accuracy of data, and mainly includes four parts: data cleaning, data integration, data conversion, and data specification (Collins & Halliday 2018). Effective information may be derived from the data using intelligent digital remote sensing technology and

Table 1: Types of water quality sensors and their functions.

Sensor	Main functions
PH sensor	Monitoring and measuring the pH value of seawater
Dissolved oxygen sensor	Monitoring and measurement of dissolved oxygen in seawater
TriE Conductivity Sensor	The electrical conductivity of seawater was monitored and measured
Temperature sensor	The temperature of seawater at different depths is monitored and measured

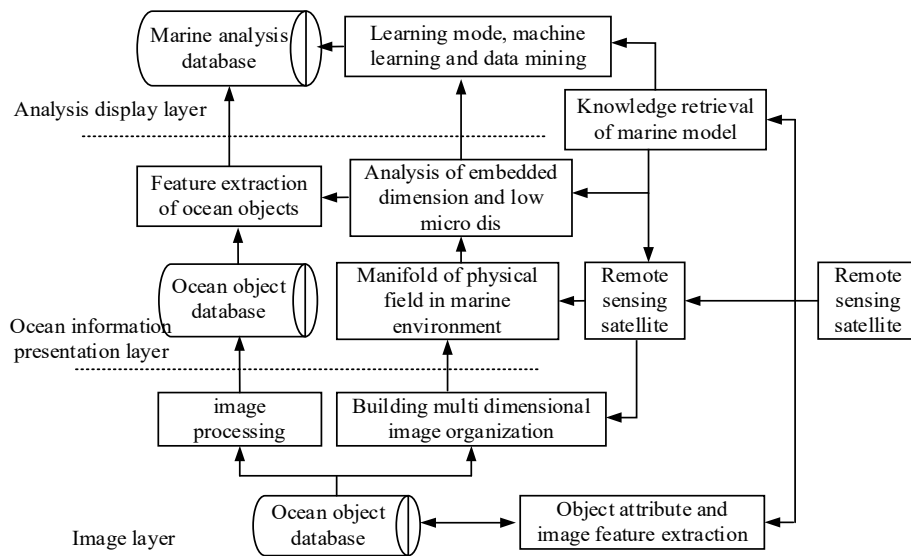


Fig. 1: Structure of intelligent data remote sensing database.

comprehensive data obtained from water quality sensor monitoring technology to realize pollutant range monitoring (González-Fernández et al. 2016). Normally, the scale of data extraction is huge, which increases the difficulty of comparative analysis. This study uses a spatial comparison method, which is to compare spatial index data within the same time range. The specific implementation steps are as follows. First, redefine the type of data source obtained, then extract the picture information and original data, and perform big data analysis with both marine pollution parameters and standard pollution images to obtain the final comprehensive pollution monitoring result (Alothman et al. 2020).

In the ocean reality, there are often upstream, downstream, sea breeze, and low visibility, so the big data obtained has the characteristics of “reasonable quantification”. When the phenomenon of data eddy occurs, the data obtained by the computer will produce analysis and quantitative changes. The law of change is shown in Fig. 2. Fig. 2(a) is a simplified schematic diagram of the vortex degree of the data. The rotation axis of the vortex in the ocean is perpendicular to the earth’s surface. The study only considers the motion of the vortex relative to the earth below, that is, the relative vorticity. Fig. 2(b) refers to the relationship between the precise value of the model and the quantitative analysis.

The data eddy current makes the process of analyzing pollution data more difficult, so the study unified quantification of different data disguise, data vector, and data imbalance. When the data eddy current transformation occurs, the data obtained by the computer will also undergo analysis and quantitative changes. The law of change is shown in Fig. 3. Fig. 3(a) is a simplified schematic diagram of the data eddy current under transformation conditions.

The eddy current transformation is to eliminate data interference through certain processing, which is convenient for the accurate analysis of data information. Fig. 3(b) refers to the relationship between the model’s precise value and the analytical quantification. After the data vortex changes, the data changes have no effect on the degree, and the big data monitoring parameters and quantified values are corrected on average, considerably reducing the difficulty of big data comparison analysis, resulting in well-realized big data comparative analysis.

RESULTS AND DISCUSSION

To test the detection effect of the big data technology proposed by the institute in the scope of marine pollutants, the specific information is shown in Table 2. All the pollution sources used in the simulated pollution source experiment are simulated pollution sources to prevent damage to the marine environment (Emeh & Igwe 2018, Sajil Kumar 2020, Yan et al. 2020). The experiment evaluated the effectiveness of the monitoring method proposed by the institute through the monitoring and identification index. The monitoring identification is the comparison between the number of experiments to find the pollutants and the total number of experiments.

The study selected a fixed 1000 km² monitoring sea area and simulates the monitoring effects of two technologies, the original ocean monitoring technology and the big data monitoring technology, under different pollution source areas. Following the recording of the monitoring results, the pollution monitoring experiment was conducted under the conditions of modifying the sea area and selecting different flow rates and contrasts, and the monitoring data was recorded. The obtained relationship between the degree of

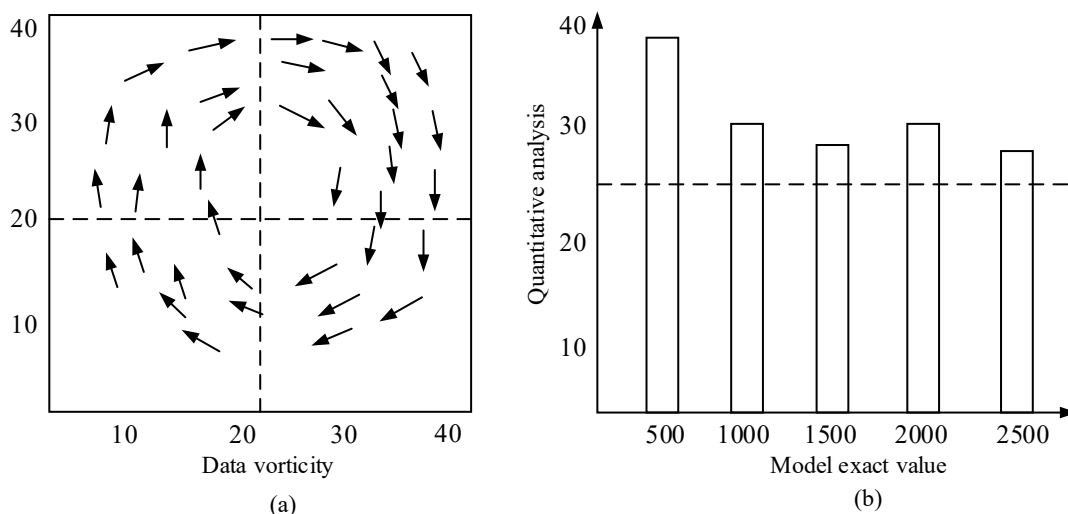


Fig. 2: Analysis and quantification change rule under data eddy current.

identification and the simulated pollution source is shown in Fig. 4. White and black respectively indicate the degree of identification of the original marine pollution monitoring technology and intelligent image monitoring technology. When the area of the monitored pollution source is 200 m² and 300 m², the corresponding monitoring recognition degree is lower than 80% and 85% respectively. When the pollutant area drops again, the data obtained will not be of reference. The intelligent image monitoring method based on big data technology proposed by the research institute can achieve a recognition rate of about 92% even when the pollution area is 72 m², and the monitoring recognition rate stabilizes at about 95% as the pollution area increases.

The experiment further verified the timeliness of the intelligent image monitoring method based on big data technology. Select a certain fixed sea area and compare the monitoring time of 100 km² simulated pollution source through two monitoring methods. Record the monitoring results and draw the curve diagram of the detection time and pollution source as shown in Fig. 5. It can be seen from Fig. 5 that when the pollution source range is small, the monitoring time of the two monitoring methods differs greatly. Traditional monitoring methods have a relatively

long monitoring time when the pollution range is relatively small. In this monitoring method, when the pollution range is within 300 m², the monitoring time is 10 min, and when the monitoring range is within 150 m², the monitoring time is 15 min. The monitoring method based on big data technology has very high monitoring timeliness even under a pollution area of about 50 m². It only takes 5 minutes, and the monitoring time is usually stable at about 5 minutes.

CONCLUSION

Aiming at the current widespread marine pollution problem, this research proposes an intelligent digital image monitoring method for marine pollutants based on big data technology, using a variety of water quality sensors to collect data, and using intelligent digital image sensing technology for image processing and analysis. Finally, the optimized big data comparative analysis method is used for big data analysis, and the final result is obtained. Through the detection of marine pollutant detection range, identification degree detection, and timeliness detection, the results verify that the proposed intelligent digital detection method based on big data technology can achieve good pollutant monitoring. Under the condition of the low pollution area, the recognition degree

Table 2: Experimental data information.

Simulation pollution source / m ²	Monitoring area / km ²	Simulation pollution source / m ²	Monitoring area / km ²
50	500	200	2000
75	750	225	2250
100	1000	250	2500
125	1250	275	2750
150	1500	300	3000
175	1750	325	3250

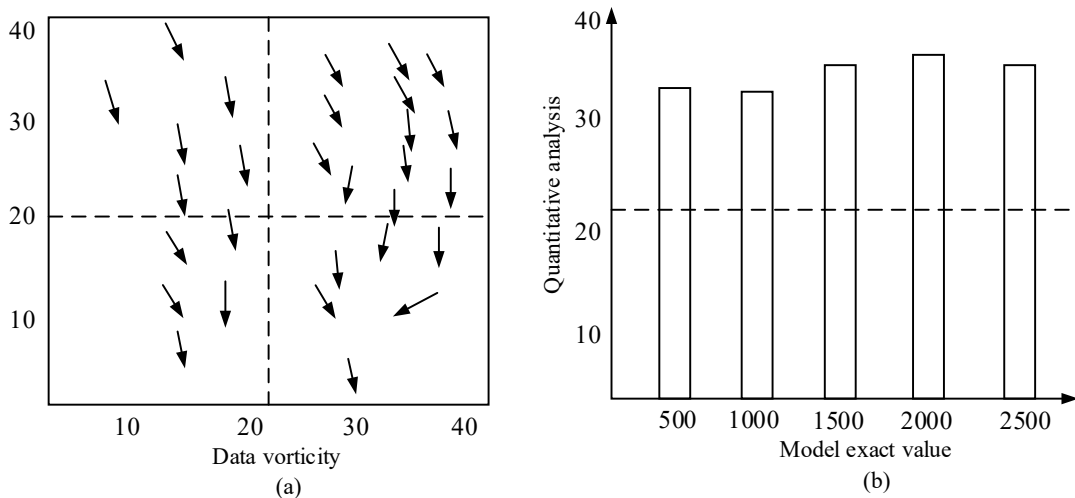


Fig. 3: Analysis and quantification change rule of data eddy current transformation.

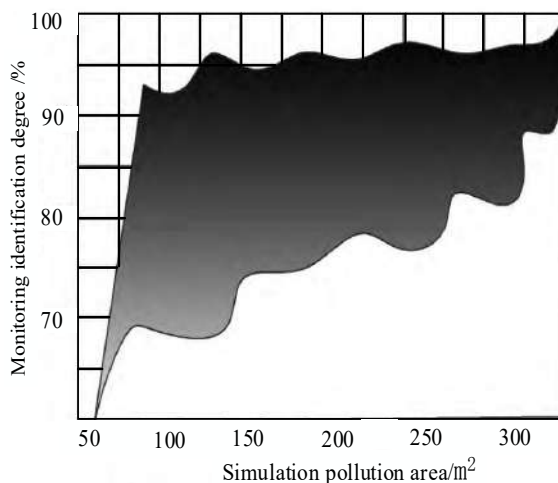


Fig. 4: Simulation pollution source area and monitoring is the rate curve.

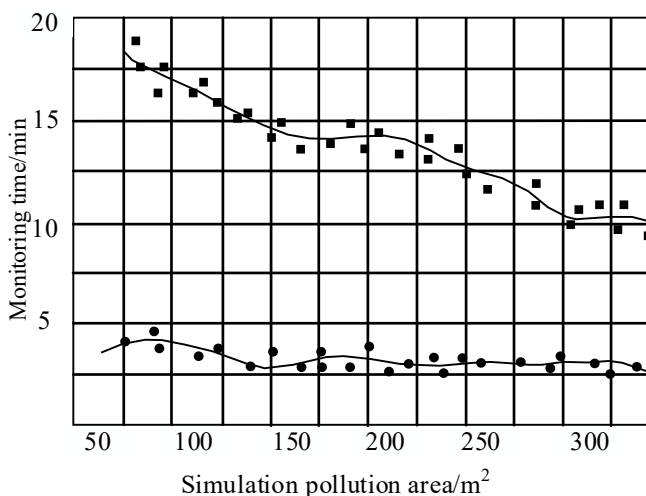


Fig. 5: Simulation pollution source and monitoring time curve.

of the intelligent image monitoring method is about 92%. As the pollution area increases, the recognition degree of monitoring stabilizes to 95%. And the monitoring timeliness of this method is also very high, and the monitoring time is usually stable at 5 minutes. When the original detection method monitors the pollution source area of 200 m² and 300 m², the monitoring recognition rate is as low as 80% and 85%, respectively. At the same time, when the pollution range is within 300 m² and 150 m², the monitoring time is as high as 10 min and 15 min.

REFERENCES

- Alothman, Z.A., Habila, M.A. and Moshab, M.S. 2020. Fabrication of renewable palm-pruning leaves-based nano-composite for remediation of heavy metals pollution. *Arab. J. Chem.*, 13(4): 4936-4944.
- Arslan, S. and Avsar, O. 2020. Assessment of heavy metal pollution in Koycegiz-Dalyan coastal lagoon watershed (Mugla) SW Turkey. *Arab. J. Geosci.*, 13(71915)
- Bonanno, G. and Orlando-Bonaca, M. 2018. Perspectives on Using Marine Species as Bioindicators of Plastic Pollution. *Mar. Pollut. Bull.*, 137C (DEC.): 209-221.
- Cavallaro, G., Riedel, M. and Richerzhagen, M. 2017. On understanding big data impacts in remotely sensed image classification using support vector machine methods. *IEEE J. Sel. Top. Appl. Earth Obs. Remote Sens.*, 8(10): 4634-4646.
- Collins, J.P. and Halliday T. 2005. Forecasting changes in empirical biology: Aiming at a moving target. *Philos. Trans. R. Soc. Lond., B, Biol. Sci.*, 360(1454): 309-14
- Emeh, C. and Igwe, O. 2018. Effect of environmental pollution on the susceptibility of sesquioxide-rich soils to water erosion. *Geol. Ecol. Landscapes*, 2(2): 115-126.
- González-Fernández, C., Albertosa, M. and Campillo, J.A.. 2016. Effect of mussel reproductive status on biomarker responses to PAHs: Implications for large-scale monitoring programs. *Aquat. Toxicol.*, 177: 380-394.

- Jauzein, C., Fricke, A. and Mangialajo, L. 2016. A sampling of *Ostreopsis cf. ovata* using artificial substrates: optimization of methods for the monitoring of benthic harmful algal blooms. *Mar. Pollut. Bull.*, 107(1): 300-304.
- Rabinskiy, L.N., Ripetskiy, A.V. and Zelenov, S.V. 2017. Analysis and monitoring methods of technological preparation of additive production. *J. Ind. Pollut. Control.*, 33(1): 1178-1183.
- Sajil Kumar, P. J. 2020. Hydrogeochemical and multivariate statistical appraisal of pollution sources in the groundwater of the lower Bhavani river basin in Tamil Nadu. *Geol. Ecol. Landscapes*, 4(1): 40-51.
- Setälä, O., Magnusson, K. and Lehtiniemi, M. 2016. Distribution and abundance of surface water microlitter in the Baltic Sea: A comparison of two sampling methods. *Mar. Pollut. Bull.*, 110(1): 177-183.
- Sun, X., Tian, Z. and Malekian, R. 2018. Estimation of vessel emissions inventory in Qingdao Port based on big data analysis. *Symmetry*, 10(10): 452-452.
- Ternengo, S., Marengo, M. and El Idrissi, O. 2018. Spatial variations in trace element concentrations of the sea urchin, *Paracentrotus lividus*: A first reference study in the Mediterranean Sea. *Mar. Pollut. Bull.*, 129 (APR.): 293-298.
- Verfuss, U.K., Gillespie, D. and Gordon, J. 2018. Comparing methods suitable for monitoring marine mammals in low visibility conditions during seismic surveys. *Mar. Pollut. Bull.*, 126(1): 1-18.
- Yan, Y., Sun, L. and Peng, Z. 2020. Effects of pyrolyzed semi-char blend ratio on coal combustion and pollution emission in a 0.35 MW pulverized coal-fired furnace. *Front. Energy*, 5(6): 71-89.



Micro-Fabric Transformations of Ball Clay in Alkaline Environment

V. Sai Kumar†, P. Hari Prasad Reddy and Ch. Rama Vara Prasad

Department of Civil Engineering, GITAM Institute of Technology, GITAM (Deemed to be University),
Visakhapatnam, Andhra Pradesh, India

†Corresponding author: Sai Kumar Vindula; svindula@gitam.edu

Nat. Env. & Poll. Tech.
Website: www.neptjournal.com

Received: 25-10-2020

Revised: 05-01-2021

Accepted: 13-01-2021

Key Words:

Ball clay

NaOH

Transmutation

XRD and SEM

ABSTRACT

Based on the strong evidence of case histories, this study focused on mineralogical and morphological changes of an artificial kaolinitic soil -Ball clay, when exposed to different concentrations of sodium hydroxide (0.1N, 1N, 4N, and 8N) under different curing periods (7, 28 and 100 days). Sediment volume tests are conducted on Ball clay with all combinations and results are analyzed with the help of analytical techniques. XRD and SEM studies are analyzed to understand the micro-level changes of alkali contaminated Ball clay. Mineralogical and morphological transmutations of Ball clay are investigated for 7, 28, and 100 days curing period. Results revealed new mineral formations like Sodalite under 4N and 8N concentrations of NaOH with 100 days interactions are well observed. The morphological transformation from needle shape to pellet shape is clear evidence of the rate of dissolution and precipitation of minerals under 100 days curing periods.

INTRODUCTION

Soil pollution occurs from a broad range of sources which includes over usage of chemicals and accidental spillovers (Ibrahim 2004). All types of soil have direct or indirect, short-term or long-term effects on the soil behavior, which leads to partial or complete transport of contaminants into the ground. The Scientific-Research Institute of Foundations and Underground Structures has investigated the physical and chemical reactions which take place between clayey minerals and acids and alkalis (Sokolovich 1995). In recent years, the detrimental failures of industrial structures are mostly associated with contamination of foundation soils with either acids or alkalis, and alkali contamination has a significant effect on the soil (Sokolovich & Troitskii 1976, Sibley & Vadgama 1986, Rao & Rao 1994, Assa'ad 1998).

Sokolovich & Troitskii (1976) reported the heaving of sand due to leakage of NaOH, NH₄Cl, and soda solutions into the subsoil for five year period of the Krasnopresensk sugar refinery in Moscow. Chunikhin et al. (1988) observed swelling of alkali-saturated soil depends on the gradation, mineral composition, and the amount of clayey fraction contained in the ground. Sivapullaiah et al. (2004) presented the structural distortion of buildings in an alumina extraction plant, Karnataka, India, caused by prolonged contamination with alkali, which led to the heaving of subsoil.

Interaction of clay minerals under highly alkaline conditions results in dissolution and precipitation (Elert et al. 2005,

Taubald et al. 2000, Bauer & Velde 1999, Bauer & Berger 1998, Cuadros & Linares 1996). From the existing literature, it is well-known that transformations of clay minerals depend on the type of the reacting mineral, its chemical composition, and the concentration of the alkaline solutions. Based on the literature on mineral transformations, it was concluded that under high alkaline conditions, dissolution of primary and secondary minerals results in the formation of new minerals which belongs to the family of zeolites. Studies revealed, natural expansive and non-expansive soils under different alkali contaminations significantly affect the engineering properties of soil. Hence in this study, artificially available Ball clay with the same mineral composition with different proportions has been considered. Different concentrations (0.1N, 1N, 4N & 8N) of sodium hydroxide for alternate curing periods (7,28 & 100days).

MATERIAL AND METHODS

Ball Clay

Ball clay known as 'plastic clay' originated from sedimentary rocks becomes highly plastic under moist conditions. Ball clay exhibits highly variable compositions (Table 1) with kaolinite as a predominant mineral along with quartz and mica. A typical Ball clay powder is light grey or cream color in appearance and is extensively used in the field of ceramics. Commercially available Ball clay has been purchased from Godavari Mines and Minerals, Visakhapatnam, Andhra

Table 1: Physical properties of Ball Clay.

Property	Value
Specific Gravity	2.6
Liquid Limit %	49
Plastic Limit %	29
Plasticity Index %	20
Clay	36
Silt	64
Soil Type	CI
Cation Exchange Capacity meq/100g	6.4
Max. Dry Density KN/m ³	16.6
Optimum Moisture Content %	24.5

Pradesh, India. Lumps forms of Ball clay are oven-dried for moisture removal and pulverized in the laboratory. Finally, the soil was allowed to pass through no. 40 (425 μ) sieve before making it useful.

Preparation of Sodium Hydroxide (NaOH) Solutions

Sodium hydroxide, also known as Lye and caustic soda and is commercially available in pellets form, is purchased from Fisher scientific and the required concentration of solutions using distilled water is prepared. Being deliquescent, NaOH readily absorbs moisture from the air, and hence it is stored in an airtight container. The author prepared Sodium hydroxide solutions of 0.1N, 1N, 4N, and 8N by dissolving 4 g, 40 g, 160 g, and 320 g of analytical grade sodium hydroxide pellets with distilled water in glass bottles. As the solution liberates heat, it is placed in a water bath to maintain an average room

temperature. The bottles are closed to avoid evaporation. Later the solution is transferred into a volumetric flask and makes up to 1 L with distilled water (ASTM E 200-08 2008).

Sediment Volume Test

The author followed the procedure established by Rao & Sridharan (1985) for determining the sediment volume test (Fig. 1) by considering the limitations of the test method proposed by Holtz and Gibbs. The soil samples which are more vulnerable to alkali attack with a more specific surface area were sieved through 75 μ m. 10 g of Ball clay with 40 mL of distilled water with the required alkali concentration solution in 100mL graduated cylinders is mixed initially. The suspension is then thoroughly and repeatedly stirred. The sample is allowed to equilibrate for 24 hours to ensure thorough wetting. Suspensions are made up to 100mL with distilled water and closed with caps. The graduated cylinders are left undisturbed for 24 hours duration for significant equilibrium and volume in terms of cc.gm⁻¹ is noted respectively. The supernatant from every cylinder is drained after the completion of sufficient curing periods (7, 28, and 100 days). All wet samples are collected in containers and allowed to dry until the moisture gets vanished. The soil samples were ground into a fine powder, moisture-free to make them fit for X-Ray diffraction (XRD) and Scanning Electron Microscopy (SEM) analysis.

Samples are analyzed from 6°2 θ to 70°2 θ /, at a step size of 0.017, using copper k alpha radiation, X-Ray Diffractometer, PANalytica, and Netherland. X-Ray diffraction patterns are obtained for the chemical mixed soil

Table 2: Chemical composition of soils.

Soil	SiO ₂	Al ₂ O ₃	Fe ₂ O ₃	MgO	CaO	Na ₂ O	K ₂ O	Ti ₂ O	MnO
Ball Clay	44.4	35.3	11.8	2.1	2.7	0.04	0.41	1.97	0.2



Fig. 1: Sediment Volume Test.

Table 3: Quantification of Sediment Volume Test (mL).

Exposure Period (in days)	Distilled water	0.1N	1N	4N	8N
1	11	27	23	26	30
7	12	27	23	25	20
28	12	26	23	25	18
100	13	28	26	37	32

specimens to detect the formation of any new compounds due to the chemical reaction with the soil mineral. SEM is employed for characterizing and examining the morphology of soil samples. SEM-TESCAN was the model used for the present study. A small oven-dried sample is glued to the SEM stub along with the gold-coated sputter before scanning. SEM images under 2 μm , 5 μm , and 10 μm are considered for the identification of morphological changes.

X-Ray Fluorescence Spectrometer (XRF) Test

The chemical composition of clay was evaluated with the help of X-Ray Fluorescence (XRF) spectroscopy technique. Phillips PW 2404 X-Ray fluorescence spectrometer was used for XRF analysis. About 5 g of dried soil sample finer than 20 μ is placed on glass holders and scanned to obtain the chemical composition (Table 2).

RESULTS AND DISCUSSION

Quantification of sediment volume test in Table 3 marked all abnormal changes in terms of swelling behavior occurred in Ball clay exposure to different concentrations of NaOH under various curing periods. Original Ball clay exhibited different mineralogical and morphological changes when exposed to 0.1N, 1N, 4N, and 8N under different curing periods of 7, 28, and 100 days. Results under XRD studies clearly highlighted the primary quartz (peaks at 4.25, 3.34, 1.82, and 1.37 [\AA]) along with kaolinite (major peaks at 7.14, 4.45, 3.57, 2.55, and 2.38 [\AA]) as their major minerals. The micrograph of Ball clay from SEM studies showed fibrous microstructure with layered needle morphology.

Mineralogical Changes of Ball Clay under 7 Days Interactions Period

XRD patterns of Ball clay with different concentrations of 0.1N, 1N, 4N, and 8N NaOH solutions under a constant curing period of 7 days are highlighted in Fig. 2. The commercially available Ball clay primarily consists of quartz (Peaks at 4.25, 3.34, 1.82, and 1.37 [\AA]) and kaolinite (Peaks at 7.14, 4.45, 3.57, 2.49, and 2.38 [\AA]) as their major minerals. No noticeable changes are observed in the XRD patterns of Ball clay under all concentrations of NaOH solutions as it is not inclined towards the dissolution process of kaolinite minerals.

Morphological Changes of Ball Clay (BC) under 7 Days Interaction period

Stratified needle form morphology of Ball clay remained unchanged under 7 days of interaction period though the concentration of NaOH was increased to 8N (Fig. 3).

Mineralogical Changes of Ball Clay under 28 Days Interactions Period

Ball clay with its mineralogical transformations is clearly highlighted in Fig.4. Quartz (Peaks at 4.25, 3.34, 1.82, and 1.37 [\AA]) along with kaolinite (Peaks at 7.14, 4.45, 3.57, 2.49, and 2.38 [\AA]) are identified as their major minerals.

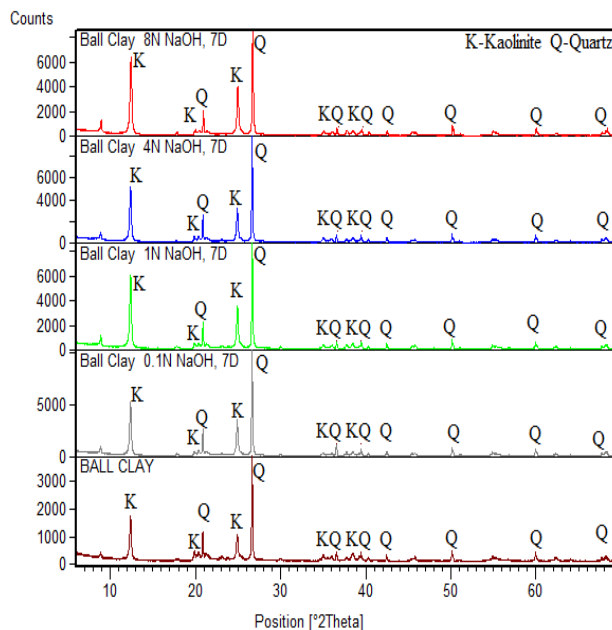


Fig. 2: XRD pattern of Ball clay under 7 days interaction.

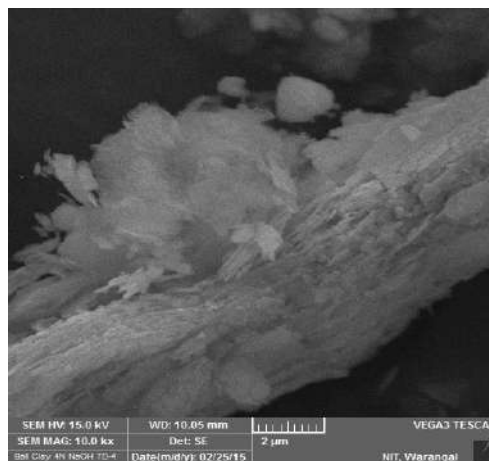


Fig. 3: SEM image of Ball clay under 7 days interaction.

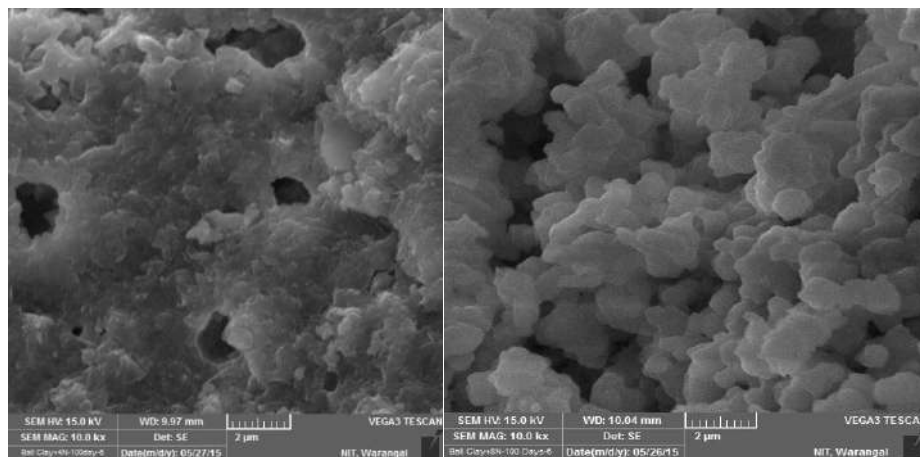


Fig. 7: SEM image of Ball clay under 100 days interaction (Pellet type).

Table 3: Summary of observed transmutations in contaminated ball clay.

Pore fluid	Interaction period	Ball clay	Pore fluid	Interaction period	Ball clay
Water	-	Quartz, Kaolinite	4N	7 days	Quartz, Kaolinite
0.1 N NaOH	7 days	Quartz, Kaolinite	NaOH	28 days	Quartz, Kaolinite, Sodalite, Natrite
	28 days	Quartz, Kaolinite		100 days	Quartz, Sodalite, Natrite
1N NaOH	100 days	Quartz, Kaolinite		7 days	Quartz, Kaolinite
	7 days	Quartz, Kaolinite	8N NaOH	28 days	Quartz, Sodalite, Natrite
	28 days	Quartz, Kaolinite		100 days	Quartz, Sodalite, Cancrinite, Nitratine
	100 days	Quartz, Kaolinite, <i>Sodalite</i>			

peaks pertaining to sodalite (6.34, 3.66, and 2.82 [Å]) - a sodium alumina silicate hydroxide hydrate. However, there is a complete dissolution of kaolinite minerals under 4N NaOH concentrations with strong peaks of sodalite and satrite (3.23, 2.96, 2.71, and 2.62 [Å]). Ball clay when it interacts with 8N NaOH concentration enhanced the formation of sodalite peaks with high intensities along with cancrinite (6.32, 2.42, 1.42[Å]) and nitratine (sodium nitrate). Cancrinite which is identified in 8N NaOH also belongs to the zeolite group. Further, the XRD pattern of 8N NaOH highlights the maximum dissolution of strong peaks pertaining to quartz.

Morphological Changes of Ball Clay under 100s Day Interaction period

From SEM images of Fig. 7, it is clear that there are no specific morphological changes when Ball clay interacts with 0.1N NaOH for 100 days. A subtle change in texture is observed when the same Ball clay interacts with 1N NaOH with initial formations of sodalites. However, Ball clay exhibited drastic changes in its morphology when it interacts with 4N and 8N NaOH solutions. Typical compacted pellet type morphology clearly reflects under 4N concentration

of NaOH indicating the complete dissolution of kaolinite minerals which triggers the formation of sodalite minerals. The micropores with specific sizes on the surface of the texture, confirm the cubic crystalline zeolitic formations. Moreover, cancrinite of zeolite group further made the morphology in 8N NaOH look more compact and denser with pellet type formations. The summary of transmutations of alkali contaminated Ball clay is highlighted in the conclusion under Table 3.

CONCLUSION

Under 0.1N and 1N concentrations of NaOH with 7 days of interactions, Ball clay exhibited low dissolution rates of alumina silicates. At a higher concentration (4N and 8N NaOH) with short-term (7 days) interaction, Ball clay has not shown any significant changes in mineralogy and morphology. However, a higher rate of dissolution and precipitation of Ball clay are observed under 4N and 8N concentrations of NaOH with 100 days of interaction. Transformation of basic needle shape morphology into compacted pellets with open-type textural voids confirms the formations of sodium-based zeolite.

ACKNOWLEDGEMENTS

We acknowledge and extend our regards to University Grands Commission (UGC) for sanctioning and supporting financially the UGC-Major Research Project, New Delhi, India, (File No.43-267/2014; dt:27.10.2017)

REFERENCES

- Assa'ad, A. 1998. The differential upheaval of phosphoric acid storage tanks in Aqaba, Jordan. *J. Perform. Constr. Facil. J.*, 12(2): 71-76.
- ASTM E200-08, 2008. Standard Practice for Preparation, Standardization, and Storage of Standard and Reagent Solutions for Chemical Analysis. ASTM International, West Conshohocken, PA.
- Barnes, M.C., Addai-Mensah, J. and Gerson, A.R. 1999. The mechanism of the sodalite-to-cancrinite phase transformation in synthetic spent Bayer liquor. *Micro. and Meso. Mat.*, 31(3): 287-302.
- Bauer, A. and Berger, G. 1998. Kaolinite and smectite dissolution rate in high molar KOH solutions at 35° and 80°C. *Appl.Geochem.*, 13: 905-916.
- Bauer, A. and Velde, B. 1999. Smectite transformation in high molar KOH solutions. *Clay Min.*, 34: 259-273.
- Chunikhin, V.G., Mavrodi, V.K.H., Kramarenko, O.A. and Dobromil'skaya, N.G. 1988. Effect of leakage of industrial alkali solutions on the construction properties of soils. *Soil Mech. Found. Eng.*, 25(6): 559-561.
- Cuadros, J. and Linares, J. 1996. Experimental kinetic study of the smectite-to-illite transformation. *Geochim. Cosmochim. Acta.*, 60: 439-453.
- Elert, K., Pardo, E.S. and Rodriguez-Navarro, C. 2015. Influence of organic matter on the reactivity of clay minerals in highly alkaline environments. *Appl. Clay Sci.*, 111: 2- 36
- Ibrahim, A.M. 2004. *Soil pollution: Origin, Monitoring & Remediation.* Springer, New York.
- Rao, S.M. and Rao, K.S. S. 1994. Ground heaving from caustic soda solution spillage: A case study, *Soils Found.*, 34(2): 13-18.
- Rao, S.M. and Sridharan, A. 1985. The mechanism controlling the volume change behavior of kaolinite. *Clay. Clay Min.*, 33(4): 323-328.
- Sibley, M.H. and Vadgama, N.J. 1986. Investigation of ground heave at ICI Mond division, Castner-Keller works, Runcorn. *Geol. Society London. Eng. Geol.*, 2: 367-373
- Sokolovich, V.E. 1995. Chemical heaving of soils. *Soil Mech. Found. Eng.*, 32(4): 135-137.
- Sokolovich, V.E. and Troitskii, G.M. 1976. The heaving of a sand base is a consequence of the development of secondary crystal hydrate formations. *Soil Mech. Found. Eng.*, 13(6): 376-378.
- Sivapullaiah, P.V., Allam, M.M. and Sankara, G. 2004. Structural distortion due to heaving of foundation soil induced by alkali contamination. *Int. Conf. Struct. Found. Fail.*, 1: 601-611.
- Taubald, H., Bauer, A., Schaefer, T., Satir, M. and Kim, J.I. 2000. Experimental investigation of the effect of high-pH solutions on the Opalinus shale and the Hammerschmiede smectite. *Clay Min.*, 35: 515-524.



Seasonal Variation of Dissolved Lead Speciation in Tagus Estuary, Portugal

M. Praveen Kumar^{*(**)}†

*Centro de Química Estrutural, Complexo I, Instituto Superior Técnico, 1096 Lisboa Codex, Portugal

**N.B.K.R. Institute Of Science and Technology, Vidyanagar, S.P.S.R Nellore, Andhra Pradesh, India

†Corresponding author: M. Praveen Kumar; praveenm@nbkrist.org

Nat. Env. & Poll. Tech.
Website: www.neptjournal.com

Received: 18-11-2020

Revised: 31-12-2020

Accepted: 13-01-2021

Key Words:

Lead, Speciation
Estuary water
DPASV
Lead species
Seasonality
Tagus estuary

ABSTRACT

The behavior of lead species from Tagus estuarine water collected during winter (January), spring (April), and summer (June) seasons were evaluated. Water samples were titrated with Pb^{2+} followed by differential pulse anodic stripping voltammetry (DPASV). Experimental voltammetric values were interpreted assuming a macromolecular heterogeneous ligand described in a simple way by two types of binding sites, C_{L1} and C_{L2} , where C_{L1} is related to stronger binding groups with lower concentration compared to C_{L2} . Water quality parameters like dissolved organic matter (DOC), pH, salinity, temperature, and total lead concentration were measured during the period under study. The results pointed to a higher concentration of C_{L1} and C_{L2} sites in April probably due to the phytoplankton bloom. The decrease of K_{L1} with the increase of salinity from winter to summer may be caused by the increase of major cations (as Ca^{2+}) in solution. The trend of K_{L2} followed the pH shift in all seasons since an increase of pH favors Pb^{2+} complexation with C_{L2} sites. Finally, the decrease of DOC in summer could be responsible for the decrease in the concentration of the different sites in solution from April to June, with a similar decrease of $35\pm 3\%$ for all of them.

INTRODUCTION

Estuaries are natural water bodies with connections from the river to open sea waters (Pritchard 1967). Mixing of both marine and river waters provides a high level of nutrients, making estuaries the most productive natural habitat (McLusky & Elliott 2004). Estuaries receive a large number of pollutants from effluents if located nearby urban and industrial areas (Reboreda & Caçador 2007, Begona et al. 2020), and play a crucial role in metal transport mechanisms from the river to estuary and estuary to the ocean (Duarte & Caçador 2012, Anderson et al. 2016). The mechanism of metal distribution in salt marsh mainly depends on the physical and chemical conditions of the river and sea waters (Oursel et al. 2013).

Generally, estuaries have rich dissolved organic compounds with different ligand sites which can significantly influence the metal biogeochemical system (Martin et al. 2020). Metal complexation with organic ligands will change significantly metal bioavailability to organisms (Paiva et al. 2015). It is also important to determine the complexing strength because even weak binding sites also may affect significantly metal bioavailability if they are present in large concentrations (Buck & Bruland 2005). Speciation of trace metal in estuaries largely depends on local geochemical factors such as oxides and carbonates, as well as on biogenic particles and organic soluble compounds (Almeida et al. 2004, Anthony et al. 2015).

The studied area of this work, the Tagus estuary, is an important ecosystem in Portugal and one of the largest estuaries on the Atlantic coast of Europe, covering an area of about 320 km^2 . Estuaries are natural sinks for heavy metal pollution. Numerous worldwide studies that focused on the behavior of lead in estuarine waters have shown that it varies from one estuary to another and depends on the time of the year as well as on river-estuarine-sea water mixing zones (Elbaz-Poulichet et al. 1996, Baeyens et al. 1998, Chiffoleau et al. 1994, Matthieu et al. 2007, Martino et al. 2007 & Oursel et al. 2013). A significant number of works have been focused on the distribution of lead and other heavy metals in the Tagus estuary and on the influence of different factors in that process, such as tidal and depth profile (Carlos 1990), flood episodes (Duarte & Caçador 2012), plants (Caçador et al. 1996, Reboreda & Caçador 2007), and sedimentation (Caçador et al. 2000). In the aquatic system, metal toxicity and mobility mainly depend on species distribution rather than on total metal concentration (Mota & Goncalves 1996). Knowledge of trace metal speciation in estuaries is important to understand the biogeochemical cycle. Few papers have reported lead speciation in Tagus estuary (Lindim et al. 2000, Mota et al. 2005), but no data have been published on the influence of the time of the year on lead speciation to the best of our knowledge. The present work is focused on the seasonal variation of lead speciation in the soluble fraction and its correlation with the trend observed for several

parameters such as DOC, pH, and salinity from the winter to summer months.

MATERIALS AND METHODS

Sampling Site and Sample Collection

Tagus river, the longest river of the Iberian Peninsula covering nearly 1038 km long, is the main source of fresh water supply to the Tagus estuary. This is one of the biggest estuaries on the Atlantic coast of Europe where it ends in the Atlantic Ocean near Lisbon. Tagus estuary covers nearly 320 km² comprising a deep, narrow, straight channel, and a wide and shallow inner bay. A large portion of effluents is received from urban and industrial activities. The sedimentation is mainly composed of fine/medium sand, silt, and clay with organic matter. The sampling area receives the flood tide twice a day, with tidal amplitude between 1.5 and 3.2 m (Silva et al. 2013).

Water samples were collected from Tagus estuary, in the saltmarsh of Corroios (38° 39.242' N, 9° 07.700' W) at the end of the low tide during January (winter), April (spring), and June (summer) 2009. In each season three samples were collected and analyzed for complex parameters. The sample location was chosen to represent a non-polluted area, without any industrial activity or habitants. After collection, samples were brought into the laboratory and filtered through a membrane filter paper (0.45 µm). A small fraction was kept in the refrigerator for further metal analysis. Sample pH, salinity, and conductivity were measured in the field as well as in the laboratory.

Chemicals and Glassware

All the glassware used for experiments was pre-soaked with 10% nitric acid (analytical grade) overnight and cleaned with ultrapure water (Millipore Milli-Q system). For pH adjustments, Merck suprapure NaOH and Merck suprapure HNO₃ were used. All other chemicals were of analytical grade and all solutions were prepared using ultrapure water (Millipore Milli-Q system).

Instrumentation

Differential pulse anodic stripping voltammetry (DPASV) experiments were carried out with Metrohm Herisau Autolab, equipped with a 663 VA stand. Hanging mercury drop electrode (HMDE) was used as a working electrode whereas Ag/AgCl and graphite electrodes were used as a reference and auxiliary electrode respectively. All the experiments were done in the deposition step at potential -0.9 V (solution stirred with a rotating bar at 1500 rot min⁻¹), deposition time 60 s, and rest time 30 s. Stripping was performed with 50 mV of

pulse amplitude, by scanning the potential from -0.7 V to -0.25 V at 5mVs⁻¹. Total lead concentrations were measured after acid digestion using DPASV. To check organic adsorption onto the electrode, alternating current (ac) voltammetry was performed with a frequency of 50 Hz, signal amplitude of 10 mV, and phase angle of 90°.

Titration of filtrated samples with Pb²⁺ followed by DPASV were carried out in a room at a controlled temperature (25°C) and dissolved oxygen was removed by bubbling 99.995% purity nitrogen.

Dissolved organic carbon (DOC) was analyzed with a Dohrmann DC-190 equipped with an infrared detector and determined in the form of CO₂ after decomposition of the sample in the furnace at about 6008°C.

Complexing Parameters

Speciation parameters were calculated from the potential-current curves obtained along the Pb²⁺ titrations. Experimental values of peak current (*i_p*) and peak potential (*E_p*) versus total Pb²⁺ concentration added during the water sample titrations were fitted to theoretical curves based on labile complexes, according to the procedure described in our previous papers (Praveen et al. 2016).

RESULTS AND DISCUSSION

Adsorption of organic matter on the Hg electrode will influence significantly speciation parameters determined from voltammetric titrations. To evaluate organic adsorption on the Hg electrode, changes on the double layer capacitance at the electrode surface with the applied potential were measured for the water samples collected and compared with those of the electrolyte solution. For the deposition potential used in DPASV measurements (-0.9 V) no organic adsorption was detected.

Description of Water Quality Parameters

Water quality parameters such as pH, temperature, salinity, DOC, and total lead concentrations in different seasons are shown in Table 1. The value of pH varied from 7.34 to 7.56 and did not show any seasonal pattern. The highest pH value (7.56) was found in January and the lowest (7.34) in April. The temperature was lower in winter and gradually increased up to summer as expected. Salinity also showed a similar trend, increasing from winter (29.6) to summer (35.3), due to higher evaporation with the increase of temperature and decrease of the Tagus river flow in that period. DOC concentration is lower in summer (4.7 ppm) than in winter or spring (6 ppm). Total lead concentration varied from 2.5 nM (winter) to 16.90 nM (summer), both values lower than the

Table 1: Water sample characterization during the studied period.

Sample parameters	January (winter)	April (spring)	June (summer)
pH	7.56	7.34	7.46
Salinity (‰)	29.6	31.9	35.3
DOC (ppm)	6.0 ± 0.6	6.0 ± 0.7	4.7 ± 0.2
Water Temperature (°C)	10.6	15.4	19.1
Total lead (nM)	2.50 ± 0.62	9.94 ± 2.31	16.90 ± 4.35

one reported a decade before (Lindim et al. 2000), probably due to the river trace metal depuration in recent years.

Lead Speciation in Different Seasons

The voltammograms of water samples in all seasons showed a shift to more negative peak potential (E_p) values and a decrease in peak current (i_p) values when compared to the calibration plot (Figs. 1A to 1C). In all experiments, along the titration with Pb^{2+} , E_p tends to a more positive value as expected, since the complexing sites gradually saturate

decreasing the complexing strength. On the other hand, the i_p curve became parallel to the calibration plot because complexing sites are no longer in excess compared to the metal ion concentration. This behavior is commonly observed in estuarine waters (Lindim et al. 2000, Holly et al. 2017).

Table 2 shows the complexing parameters obtained from the best fitting between experimental and theoretical curves of peak current and peak potential along the titration with Pb^{2+} (Fig. 1A to 1C). Voltammetric data was interpreted assuming a macromolecular heterogeneous ligand of humic matter type, simply described by two types of binding sites with concentrations C_{L1} (minor sites with a stronger binding strength) and C_{L2} (major sites with a weaker binding strength). The diffusion coefficient D_{ML} of the macromolecular ligand was obtained from the first points of the titration curve where the mean diffusion coefficient of the labile species presented a near constant value equal to D_{ML} (Lindim et al. 2000, Mota et al. 2005).

From Table 2 it can be seen that both C_{L1} and C_{L2} sites of the macromolecular ligand presented the highest

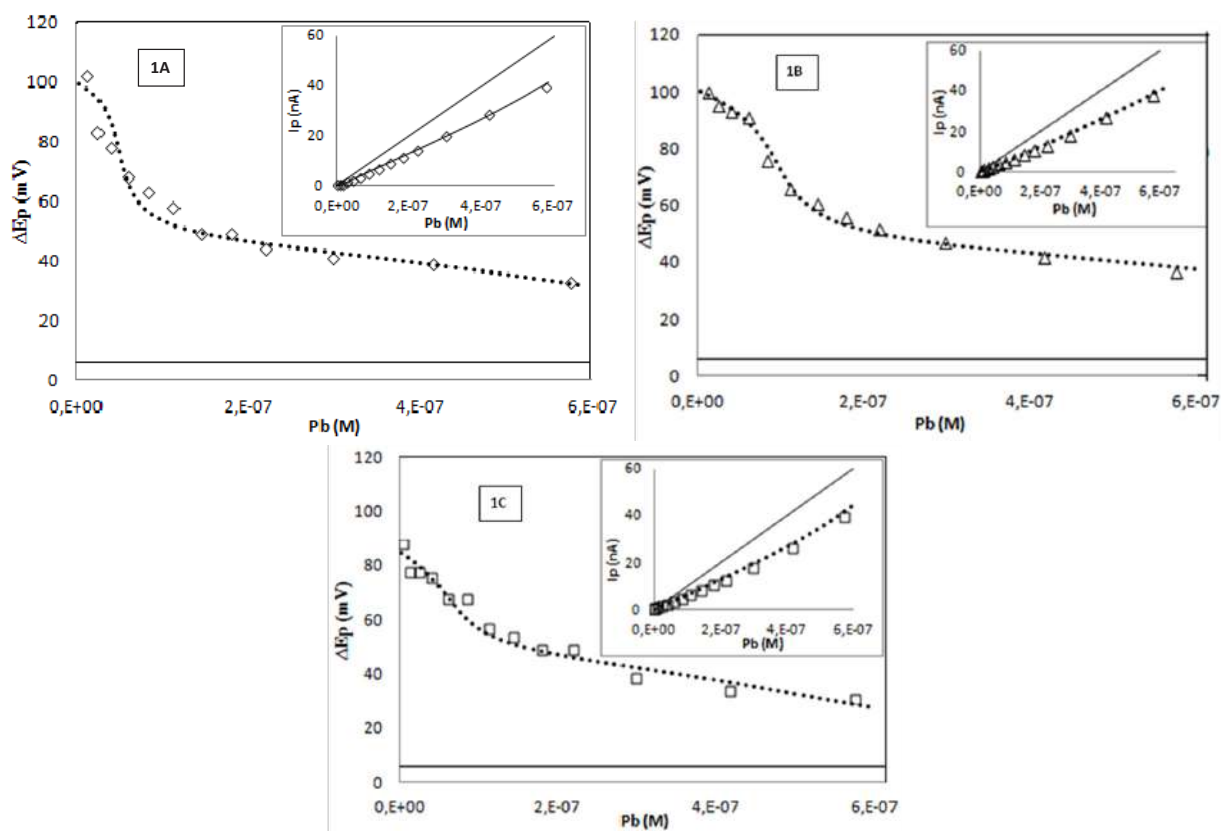


Fig. 1: ΔE_p (shift of the peak potential) and i_p (peak current in inserted figure) versus added lead concentration. (---) - theoretical fitting curve. (\diamond), (Δ), (\square) - experimental values. Figs 1A, 1B, and 1C are samples collected in January, April and June respectively.

Table 2: Ligand complexing parameters during the studied period.

Complexing parameters	January	April	June
D_{ML} ($10^{-6} \text{ cm}^2 \text{ s}^{-1}$)	3.11 ± 0.26	3.11 ± 0.26	3.11 ± 0.26
C_{L1} (10^{-6} M)	1.20 ± 0.1	2.25 ± 0.2	1.52 ± 0.2
K_{L1}	9.49 ± 1.00	9.24 ± 1.33	8.89 ± 2.13
C_{L2} (10^{-6} M)	14.40 ± 1.0	19.40 ± 2.1	12.20 ± 1.1
K_{L2}	6.56 ± 1.1	6.39 ± 0.4	6.63 ± 1.0

concentration in spring, which may be due to the bloom of phytoplankton activity in that season. Between spring and summer, a decrease of $35 \pm 3\%$ in the concentration of all different sites (C_{L1} and C_{L2}) was determined, which may be related to the decrease of DOC in the summer.

The decrease of stability parameter (K_{L1}) from January to June (Table 2) is probably due to the salinity increase, which increases the competition of major cations (such as Ca^{2+}) for the complexing binding sites. This competition depends not only on the affinity of the cation for the binding site but also on the concentrations of the species involved, decreasing with the increase of ligand concentration. The increase of salinity may also contribute to the decrease of stability parameter (K_{L2}) parameter from winter to spring, but to explain the increase of K_{L2} from spring to summer other factors should be looked for. In fact, the pH shift (7.34 in April to 7.46 in June) may lead to an increase of K_{L2} since the de-protonation of C_{L2} with the increase of pH favors Pb^{2+} complexation. It should be noticed that the decrease of pH from winter to spring also favors the K_{L2} decrease observed from January to April. The small seasonal variations in pH and salinity did not significantly affect K_B due to the much larger concentration of B sites in solution.

CONCLUSIONS

From lead speciation results obtained during the study period no systematic seasonal variation was observed for all the sites detected (C_{L1} and C_{L2} sites). However punctual trends observed in the concentration and stability parameters of certain sites could be explained from the variation of water parameters (e.g., salinity, pH, DOC), affected by the time of the year. The increase of salinity from winter to summer may contribute to the decrease of the C_{L1} (minor sites) stability parameter due to the competition of major cations. The seasonal variation of K_{L2} followed the trend of pH, increasing with de-protonation of C_{L2} . The decrease of DOC from spring to summer may explain the decrease in the concentration of all different sites present in solution and the phytoplankton bloom in the spring may be responsible for the higher concentration of C_{L1} and C_{L2} sites in April. To have a more complete picture, factors such as sedimentation, input fluxes and estuarine dynamic have to be included.

ACKNOWLEDGMENTS

Praveen Kumar Mallupattu is highly thankful to Foundation of Science and Technology of Portugal for providing financial support in the form of Postdoctoral Fellowship (SFRH/BPD/37222/2007).

REFERENCES

- Almeida, C.M., Mucha, A.P. and Vasconcelos, M.T. 2004. Influence of the sea rush *Juncus maritimus* on metal concentration and speciation in estuarine sediment colonized by the plant. *Environ. Sci. Tech.*, 38(11): 3112-3118.
- Anderson, A.S.M., Kate, S., Werner, K., Marco, T. and Christiane, Z. 2016. Metal fate and effects in estuaries: A review and conceptual model for better understanding of toxicity. *Sci. Total Environ.*, 541: 268-281.
- Anthony, S., Edward, T. and Stephen L. 2015. Dissolved trace metal speciation in estuarine and coastal waters: Comparison of WHAM/Model VII predictions with analytical results. *Environ. Toxicol. Chem.*, 34(1): 53-63.
- Baeyens, W., Parmentier, K., Goeyens, L., Ducastel, G., De Gieter, M. and Leemans, M. 1998. The biogeochemical behavior of Cd, Cu, Pb and Zn in the Scheldt estuary: results of the 1995 surveys. *Hydrobiologia*, 366(1-3): 45-62.
- Begona P.F., Lucía V. and Victoria B. 2020. Concentrations of organic and inorganic pollutants in four Iberian estuaries, North-Eastern Atlantic. Study of benchmark values estimation. *Mar. Chem.*, 224, 103828.
- Buck, K. and Bruland, K. 2005. Copper speciation in San Francisco Bay: A novel approach using multiple analytical windows. *Mar.Chem.*, 96(1): 185-198.
- Caçador, I., Carlos, V. and Fernando C. 1996. The influence of plants on concentration and fractionation of Zn, Pb, and Cu in salt marsh sediments (Tagus Estuary, Portugal). *J. Aqua. Ecosyst. Health*, 5(3): 193-198.
- Caçador, I. Vale, C., and Catarino, F. 2000. Seasonal variation of Zn, Pb, Cu and Cd concentrations in the root-sediment system of *Spartina maritima* and *Halimione portulacoides* from Tagus estuary salt marshes. *Mar. Environ. Res.*, 49(3): 279-290.
- Carlos, V. 1990. Temporal variations of particulate metals in the Tagus river estuary. *Sci.Total Environ.*, 97/98: 137-154.
- Chiffolleau, J.F., Cossa, D., Auger, D. and Truquet, I. 1994. Trace metal distribution, partition and fluxes in the Seine estuary (France) in low discharge. *Mar. Chem.*, 47(2): 145-158.
- Duarte, B. and Caçador, I. 2012. Particulate metal distribution in Tagus estuary (Portugal) during a flood episode. *Mar. Pollut. Bull.*, 64(10): 2109-2116.
- Elbaz-Poulitchet, F., Garnier, J.M., Guan, D.M., Martin, J.M. and Thomas, A.J. 1996. The conservative behaviour of trace metals (Cd, Cu, Ni and Pb) and As in the surface plume of stratified estuaries: example of the Rhone River (France). *Estuar. Coast. Shelf Sci.*, 42(3): 289-310.
- Holly, B.C.P., Sean D.W.C., Charlotte, B. and Paul J.W. 2017. Predicting copper speciation in estuarine waters: Is dissolved organic carbon a good proxy for the presence of organic ligands? *Environ. Sci. Technol.*, 51(4): 2206-2216.
- Lindim, C., Mota, A.M. and Goncalves, M.L.S. 2000. Influence of UV-B irradiation in lead speciation from an estuarine sample. *Water Res.*, 34(13): 3325-3334.
- Martin, P.P., Véronique, L., Cédric, G., Benjamin, M., Charlotte, R. and Alexandre, J. P. 2020. Dissolved organic matter controls of arsenic bioavailability to bacteria. *Sci. Total Environ.*, 716: 137118.
- Martino, M., Turner, A., Nimmo, A. and Millward, G.E. 2002. Resuspension, reactivity and recycling of trace metals in the Mersey Estuary, UK. *Mar. Chem.*, 77(2-3), 171-186.

- Mathieu, W., Ricardo D.R. and Pierre Le C. 2007. Distribution and seasonal changes of lead in an estuarine system affected by agricultural practices: The Penze´ estuary, NW France. *Estuar. Coast. Shelf Sci.*, 74(3): 570-578.
- McLusky, D.S. and Elliott, M. 2004. *The Estuarine Ecosystem: Ecology, Threats and Management*. Oxford University Press, New York.
- Mota, A.M. and Goncalves, M.L.S. 1996. In: Caroli, S. (Ed.), *Element Speciation in Bioinorganic Chemistry*, Chemical Analysis Series, Vol. 135. Wiley, New York (Chapter 2).
- Mota, A.M., Cruz, P., Vilhena, C. and Goncalves, M.L.S. 2005. Influence of the sediment on lead speciation in the Tagus estuary. *Water Res.*, 39(8): 1451-1460.
- Oursel, B., Garnier, C., Durrieu, G., Mounier, S., Omanovic, D. and Lucas, Y. 2013. Dynamics and fates of trace metals chronically input in a Mediterranean coastal zone impacted by a large urban area. *Mar. Pollut. Bull.*, 69(1-2): 137-149.
- Paiva M.D., Costa Marques, M.R., Baptista, D.F. 2015. Metal bioavailability and toxicity in freshwaters. *Environ. Chem. Lett.*, 13(1): 69-87.
- Praveen Kumar, M., Mota, A.M. and Gonçaves, M.L.S. 2016. Influence of UV-B radiation on lead speciation in the presence of natural particles of estuarine waters. *Environ. Sci. Pollut. Res.*, 23(17): 17503-17510
- Pritchard, D.W. 1967. What is An Estuary: Physical Viewpoint. In Lauf, G. H., *Estuaries*. A.A.A.S. Publishers, Washington, DC., pp. 3-5.
- Reboreda, R. and Caçador, I. 2007. Copper, zinc, and lead speciation in salt marsh sediments colonised by *Halimione portulacoides* and *Spartina maritima*. *Chemosphere*, 69(10): 1655-1661.
- Rosa, R., Cacador, I., Silvia, P. and Pedro, R. A. 2008. Mobility of metals in salt marsh sediments colonised by *Spartina maritima* (Tagus estuary, Portugal). *Hydrobiologia*, 606(1): 129-137.
- Silva, T.A., Freitas, M.C., Andrade, C., Taborda, R., Freire, P., Schmidt, S. and Antunes, C. 2013. Geomorphological response of the salt-marshes in the Tagus estuary to sea-level rise. In: Conley, D.C., Masselink, G., Russell, P.E. and O'Hare, T.J. (eds.), *Proceedings 12th International Coastal Symposium (Plymouth, England)*, *Journal of Coastal Research*, 65: 582-587



Environmental Management: Pragmatic Suitability of Low Cost Activated Carbon in Lead (II) Ion Removal by Continuous Mode of Adsorption

R. Sivarethinamohan*† and S. Sujatha**

*Christ (Deemed to be University), Bangalore, India

**K. Ramakrishnan College of Technology, Tamil Nadu, India

†Corresponding author: R. Sivarethinamohan; mohan.dimat@gmail.com

Nat. Env. & Poll. Tech.

Website: www.neptjournal.com

Received: 05-11-2020

Revised: 08-02-2021

Accepted: 20-02-2021

Key Words:

Activated carbon

Breakthrough curve

Fixed-bed column

Heavy metal

ABSTRACT

Heavy metals such as chromium, lead, and arsenic are usually present in trace amounts in natural waters but many of them are toxic even at very low concentrations. An increasing quantity of heavy metals in our resources is currently an area of greater concern, especially since a large number of industries are discharging their metal containing effluents into freshwater without any adequate treatment. Activated carbons show a significant ability in removing heavy metal ions from an aqueous solution by adsorption, which has been examined by many researchers. Activated carbon derived from Manilkarazapota tree-wood (MZTWAC), which was found to be a suitable adsorbent for the removal of lead ions through continuous adsorption mode, was examined in this paper. A breakthrough curve has been plotted to find the effect of initial concentration and adsorbent bed height in the adsorption of lead (II) ion through MZTWAC. The breakthrough time and the saturation time increased as the initial concentration increased from 40 mg.L⁻¹ to 60 mg.L⁻¹. The saturation time was in the incremental mode when the bed height was increased from 5 cm to 7 cm bed thickness for 40 mg.L⁻¹ concentration. Adams-Bohart's model perfectly fits with this fixed-bed column in the removal of lead(II) from an aqueous solution using MZTWAC. Activated carbon derived from MZTWAC is better suited for the purpose of detoxifying metal-contaminated wastewater.

INTRODUCTION

Heavy metals are defined as metallic elements that have a relatively high density compared to water. With the assumption that heaviness and toxicity are interrelated, heavy metals also include metalloids, such as arsenic, that are able to induce toxicity at a low level of exposure (Duffus 2002). Also, human exposure has risen dramatically as a result of an exponential increase of their use in several industrial, agricultural, domestic and technological applications (Bradl 2002). Heavy metals such as copper are essential in the (Stern 2010) exertion of physiological function in living organisms. They are important constituents of several key enzymes and play important roles in various oxidation-reduction reactions. However, an excess amount of such metals produces cellular and tissue damage leading to a variety of adverse effects and human diseases. For some including chromium and copper, there is a very narrow range of concentrations between beneficial and toxic effects (Tchounwou et al. 2010, Chang et al. 1996). Other metals such as antimony (Sb), cadmium (Cd), aluminum (Al), copper (Cu), arsenic (As), and lead (Pb), have no established biological functions and are considered as non-essential metals (Chang et al. 1996). In recent years, there has been an increasing, global public

health concern associated with environmental contamination by these metals. Reported sources of heavy metals in the environment include industrial, domestic effluents, pharmaceutical, agricultural, and atmospheric sources (He et al. 2005). The pollution of the environment is prominent in source areas such as mining, metal-based production, and fabrication processes (Bradl 2002, He et al. 2005).

Pollution due to lead ion contamination in water has become a serious concern lately. Lead ion pollution can have harmful impacts on human health and can affect the nervous system, digestive system, and cause brain damage leading to fatality (Awual & Hasan 2014, Lim & Aris 2014). Primary sources of lead ion pollution are the discharge of mining wastes, glass and chemical industries, battery manufacturing companies, and ceramic-based industries. Environmental Protection Agency (EPA) has set the maximum contaminant level goal for lead ions in drinking water at 0.05mg.L⁻¹ because lead is a toxic metal that can be harmful to human health even at low exposure levels (Guyo et al. 2015). Thus to lessen the detrimental impact of lead(II) ion contamination in the environment, it is necessary to treat the lead ion polluted water.

Several treatment methods like membrane filtration, ion exchange, chemical precipitation, electrodeposition, coag-

ulation, the solvent extraction process, and adsorption. Of all the methods, adsorption is very effective due to its ease, cost-effectiveness, and superior extraction capacity. Many different adsorbents have been used for the removal of toxic metal ions such as green coconut shells (Sousa et al. 2010), wheat bran (Ozer 2007), waste fruit cortex (Kelly-Vargas et al. 2012), agave bagasse, activated carbon of de-oiled soya (Sujatha et al. 2017), chitosan impregnated with a cationic surfactant (Rouf & Nagapadma 2015).

This study intended to assess the performance of the activated carbon, derived from Manilkara Zapota tree wood (MZWAC), in the removal of lead ions through column adsorption from which its practical applicability can be confirmed. The dynamic behavior of the fixed-bed (continuous adsorption) column was described using a breakthrough curve. The effect of initial lead(II) ion concentration and the effect of bed height on the performance of lead (II) ion adsorption were described in the present study.

MATERIALS AND METHODOLOGY

Manilkara Zapota is a fruit-producing tree that grows extensively in India. The tree branches are collected from a garden in Tamil Nadu.

MZWAC Preparation

The fabrication of MZWAC includes phases mentioned in the authors' previous article (Sujatha & Sivarethinamohan 2019). The carbon that passed through 150 μ sieve and suspended in 90 μ sieve was stored in an airtight container. MZWAC (Sujatha & Sivarethinamohan 2019) is shown in Fig.1.

Continuous Flow Mode or Column Adsorption Mechanism

The practical utility of an adsorbent in removing the pollutants from the wastewater can be assessed by the column



Fig. 1: MZWAC (Sujatha & Sivarethinamohan 2019).

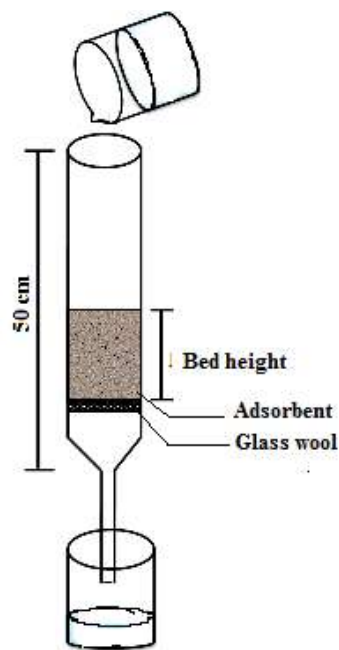


Fig. 2: Graphical representation of investigational setup for column adsorption studies

adsorption process. A fixed-bed column was used in the continuous mode adsorption process. A column made of glass with 1.75 cm diameter and a height of 50 cm was designed and used in the column study. The glass column had an opening at the bottom which could be adjusted by a valve. The column was filled with an adsorbent for a fixed depth over a layer of 1 cm of glass wool which was placed near the opening of the column. Fig. 2 shows the investigational setup for column studies.

To enable uniform filling, a glass rod was used for tapping and tamping. The filled carbon bed was completely dried by exposing it to sunlight for 3 days. The aqueous solution was filled in the column of fixed concentration of lead(II) ion. The input flow rate was preset as 2.5 mL.min⁻¹. At a steady interval of time, the resultant solution was collected and analyzed spectrometrically. The effect of initial lead(II) ion concentration on the performance of lead (II) ion adsorption was experimented by altering the initial concentration of the lead(II) ion in the aqueous solution from 40 mg.L⁻¹ to 60 mg.L⁻¹ and the impact of the bed height was analyzed by altering the bed height from 5 cm to 7 cm. The dynamic response/behavior of the adsorption column was calculated by the breakthrough time and profile of the breakthrough curve. To test the initial part of the breakthrough curve, Adams- Bohart's model was used. The model is particularly useful for estimating characteristic parameters of column experiments.

Adams- Bohart's Model Graph

Adams–Bohart's model was applied to column information which describes the initial portion of the adsorption in continuous adsorption. Based on a theory of surface reaction, the Adams–Bohart' model assumes that equilibrium is not instantaneous and that the adsorption rate is proportional to the adsorption capacity of the adsorbent. This model establishes the basic equation describing the association between $\ln(C_t/C_o)$ and contact time 't' in a continuous adsorption process. The model is particularly useful for estimating characteristic parameters such as maximum adsorption capacity (N_o) and kinetic constant (k_{AB}) used to determine a quasi-chemical kinetic rate expression. The data obtained in the fixed-bed column experiments was applied to Adams-Bohart's equation. Adams – Bohart's equation is as follows (Busto et al. 2016)

$$\ln \frac{C_t}{C_o} = -k_{AB} C_o t + \frac{k_{AB} N_o Z}{U_o} \quad \dots(1)$$

where C_t is the equilibrium metal ion concentration (mg.L^{-1}), k_{AB} is Adams- Bohart's kinetic constant in $\text{L.mg}^{-1}.\text{min}^{-1}$. N_o and Z are the adsorption capacity per unit volume of the adsorbent (saturation concentration in mg.L^{-1}) and the bed depth of the column (cm), respectively. U_o denotes the linear velocity (cm.min^{-1}). The values of k_{AB} and N_o were obtained from the plot of $\ln(C_t/C_o)$ versus time t.

RESULTS AND DISCUSSION

Characterization of MZTWAC

Characterization studies had been undertaken on Fourier Transform Infrared (FTIR) analysis, Scanning Electron Microscope (SEM) analysis, X-Ray fluorescence (XRF), X-Ray diffraction (XRD), and Brunauer- Emmett -Teller (BET) analysis. The characterization study revealed that the MZTWAC has got the potential to remove the lead(II) ion from an aqueous solution.

Continuous Adsorption Study (Fixed-Bed Column Study)

Column adsorption was carried with the designed column at a rate of flow of 2 mL.min^{-1} . At an interval of 1 h, the resultant solution from the column was collected and analyzed spectrometrically. The test was repeated with different initial concentrations of lead(II) ion and with different bed heights of the adsorbents. A breakthrough curve was plotted between contact time in the X-axis and C_t / C_o in Y-axis. Adsorption data was applied to the column model to get the information/data on the influence parameters.

Impact of Initial Concentration on Adsorption

To ascertain the performance and to optimize the adsorption process, the initial concentrations of lead (II)ion were altered between 40 mg.L^{-1} and 60 mg.L^{-1} by keeping the bed height $Z = 5 \text{ cm}$. The breakthrough curve is shown in Fig. 3. The breakthrough curve was linear because, initially, the equilibrium concentration was almost zero. The reason behind this was that at the initial stage the column bed completely adsorbed all the metal ions and as time passed, the bed was completely exhausted because of which it could not adsorb further metal ions from the solution. It was found from Fig. 3 that the unadsorbed metal ion concentration was increased by increasing the initial concentration of the lead(II)ion. The effectiveness of adsorption is the concentration difference between the solute in the adsorbent and the aqueous solution. This showed that the adsorbent bed saturated faster with a greater amount of initial concentration (Lim & Aris 2014)

For 40 mg.L^{-1} initial concentration of lead(II) ion, Fig. 3 shows that the breakthrough time of adsorption was reached at 380 min and the saturation of the bed was reached at 1380 min. Breakthrough time of adsorption was reached at 350 min and saturation of the bed was reached at 1140 min for 60 mg.L^{-1} initial concentration of lead(II) ion.

Impact of Bed Height on Adsorption

The optimum performance of the continuous fixed-bed column adsorption with respect to bed height varied with the bed height from 5 cm and 7 cm. The initial concentration was 40 mg.L^{-1} and a velocity of 2 mL.min^{-1} was kept constant.

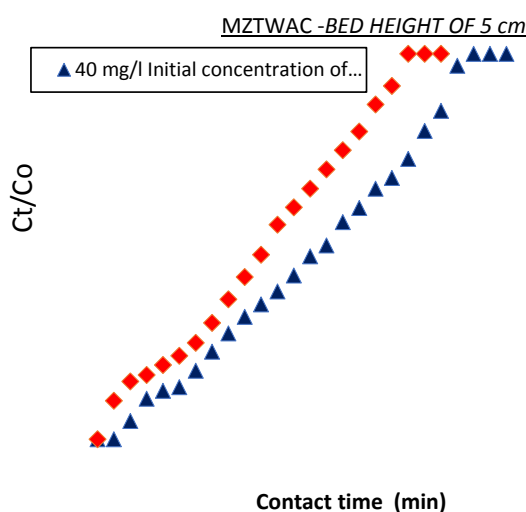


Fig. 3: Breakthrough curve for the impact of initial concentration of lead (II) ion with a bed height $Z = 5 \text{ cm}$.

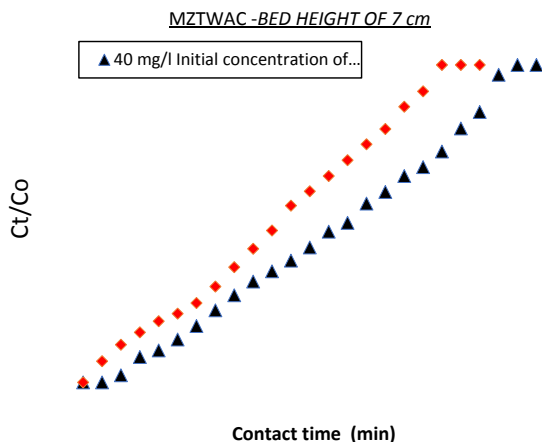


Fig. 4: Breakthrough curve for the impact of initial concentration of lead (II) ion with a bed height $Z = 7$ cm.

By comparing Fig. 3 and 4, it was revealed that as the bed height increased, the saturation time and breakthrough time extended (Biswas & Mishra 2015), since more adsorbent particles were available for the adsorbate. It was found that the breakthrough time was attained at 350 minutes for a bed height of 5 cm bed height and 420 minutes for a bed height of 7 cm.

Adams-Bohart's Model for Fixed Bed Column

The initial part of the adsorption was predicted by Adam-Bohart's model. Equation 1 is Adams-Bohart's column modeling equation. Adams-Bohart constants were derived from the graph (Fig. 5) drawn between the value of $\ln(C_t/C_0)$ versus time, where C_t is the outlet metal ion concentration (mg/L), k_{AB} ($L \cdot mg^{-1} \cdot min^{-1}$) is Adams-Bohart's kinetic constant. N_0 ($mg \cdot L^{-1}$) and Z (cm) are the adsorption capacity per unit volume of the adsorbent column and the bed depth of the column respectively.

Adams-Bohart's column adsorption model with a bed height of 5 cm of lead(II) adsorption is shown in Fig. 5 which shows the Adams-Bohart's model curve of the adsorbate for column adsorption with the bed height of 7 cm.

Analysis and results of Adams-Bohart's constants for the fixed-bed column are summarized in Table 1. From Table 1, it can be explained that the initial concentration of the

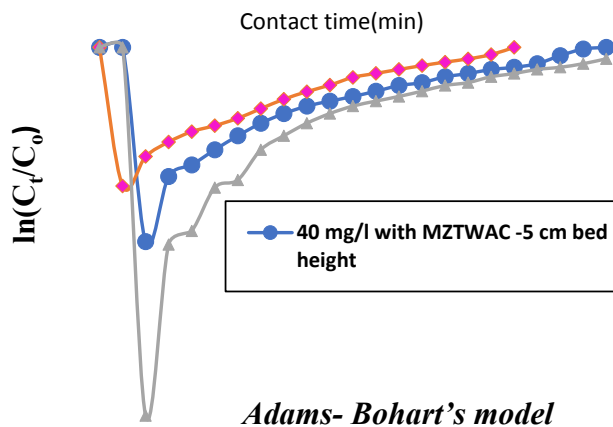


Fig. 5: Adams-Bohart's model on the impact of initial concentration of lead(II) ion.

solute increased N_0 (Sanchez-Machado et al. 2016) whereas K_{AB} decreased. As the bed height increased from 5 cm to 7 cm, N_0 decreased while K_{AB} increased (Sanchez-Machado et al. 2016). The parameters that were applied in this study depicted the influence on the breakthrough for metal ions.

Table 1 shows that any alteration in the bed height of the adsorbent significantly affects the performance of the fixed-bed column by reducing the speed of the exhaustion time. However, the alteration increased the initial concentration of the metal ion in an aqueous solution, which increased the speed of exhaustion of the adsorbent bed.

CONCLUSION

It is concluded that MZTWAC is suitable for removing the lead ion from an aqueous solution. The breakthrough curve depicted that as the initial concentration and impact of bed height increased, the adsorption of lead (II) ions increased. The breakthrough time and the saturation time were 380 minutes and 1380 minutes for $40 \text{ mg} \cdot \text{L}^{-1}$ initial concentration at 5 cm bed height. The breakthrough time and the saturation time were 350 min and 1140 min for $60 \text{ mg} \cdot \text{L}^{-1}$ initial concentration at 5 cm bed height. The breakthrough time and the saturation time were 420 minutes and 1620 minutes for $40 \text{ mg} \cdot \text{L}^{-1}$ for initial concentration at 7 cm bed height. The breakthrough time and the saturation time reduced as

Table 1: Adam-Bohart's parameters at different conditions for the adsorption lead(II) of fixed-bed column.

Concentration of lead ion (mg/L)	Bed height (cm)	K_{AB} (L/mg min)	N_0 (mg/L)	Break through Time (min)	Saturation time(min)
40	5	0.000025	3344.34	380	1380
60	5	0.000017	4859.28	350	1140
40	7	0.000050	1788.64	420	1620

the initial concentration increased. The perfect fit of Adams-Bohart's model with the fixed-bed column showed that activated carbon derived from MZTWAC is better suited for the purpose of detoxifying metal-contaminated wastewater.

REFERENCES

- Awual, M.R. and Hasan, M.M. 2014. A novel fine-tuning mesoporous adsorbent for simultaneous lead(II) detection and removal from wastewater. *Sens. Actuators B Chem.*, 202: 395-403.
- Biswas, S. and Mishra, U. 2015. Continuous fixed-bed column study and adsorption modeling: removal of lead ion from aqueous solution by charcoal originated from chemical carbonization of rubberwood sawdust. *J. Chem.*, 2015: 1-9.
- Bradl, H. (ed.) 2002. *Heavy Metals in the Environment: Origin, Interaction, and Remediation*. Elsevier/Academic Press, London.
- Busto, Y., Palacios, E.W., Aloma, I., Rios, L.M., Cortez, M.F., Calero, M. and Year, M. 2016. Removal continuous studies of chromium (vi) using sugar cane bagasse. *Chem. Eng. Trans.*, 52: 901-906.
- Chang, L.W., Magos, L. and Suzuki, T. (ed.) 1996. *Toxicology of Metals*. Boca Raton. CRC Press, FL, USA.
- Duffus, J. 2002. The heavy metals-a meaningless term? (IUPAC Technical Report). *Pure Appl. Chem.*, 74(5): 793-807.
- Guyo, U., Mhonyera, J. and Moyo, M. 2015. Pb(II) adsorption from aqueous solutions by raw and treated biomass of maize stover-a comparative study. *Process. Saf. Environ.*, 93: 192-200.
- Harvey, L.J. and McArdle, H.J. 2008. Biomarkers of copper status: A brief update. *Br. J. Nutr.*, 99(S3): S10-3.
- He, Z.L., Yang, X.E. and Stoffella, P.J. 2005. Trace elements in agroecosystems and impacts on the environment. *J. Trace. Elem. Med. Biol.*, 19: 125-140.
- Kelly-Vargas, K., Cerro-Lopez, M., Reyna-Tellez, S., Bandala, E.R. and Sanchez-Salas, J.L. 2012. Biosorption of heavy metals unpolluted water, using different waste fruit cortex. *Phys. Chem. Earth*. 37: 26-29.
- Lim, A.P. and Aris, A.Z. 2014. Continuous fixed-bed column study and adsorption modeling: Removal of cadmium(II) and lead(II) ions in the aqueous solution by dead calcareous skeletons. *Biochem. Eng. J.*, 87: 50-61.
- Ozer, A. 2007. Removal of Pb (II) ions from aqueous solutions by sulphuric acid-treated wheat bran. *J. Hazard. Mater.*, 41(3): 753-761.
- Rouf, S. and Nagapadma, M. 2015. Modeling of fixed-bed column studies for adsorption of azo dye on chitosan impregnated with a cationic surfactant. *Int. J. Eng. Res.*, 6(2): 538.
- Sanchez-Machado, D.I., Lopez-Cervantes, J., Correa-Murrieta, M. A. and Sanchez-Duarte, R.G. 2016. Modeling of breakthrough curves for aqueous iron (III) adsorption on chitosan-sodium tripolyphosphate. *Water Sci. Technol.*, 74(10): 2297-2304.
- Sousa, F.W., Oliveira, A.G., Ribeiro, J.P., Rosa, M.F., Keukeleire, D. and Nascimento, R.F. 2010. Green coconut shells applied as adsorbents for removal of toxic metal ions using fixed-bed column technology. *J. Environ. Manage.*, 91(8): 1634-1640.
- Stern, B.R. 2010. Essentiality and toxicity in copper health risk assessment: Overview, update, and regulatory considerations. *J. Toxicol. Environ.*, 73(2): 114-127.
- Sujatha, S. and Sivarethinamohan, R. 2019. Investigation of detoxification nature of activated carbons developed from Manilkara zapota and de-oiled soya. *Mater. Today Proceed.*, 21(1): 663-668.
- Sujatha, S., Venkatesan, G. and Sivarethinamohan, R. 2017. Principal determinants of toxicity reduction by de-oiled soya using multivariate statistics: Principal component analysis and multiple linear regression analysis. *Appl. Ecol. Environ. Res.*, 15(3): 1717-1737.
- Tchounwou, P.B., Newsome, C., Williams, J. and Glass K. 2008. Copper-induced cytotoxicity and transcriptional activation of stress genes in human liver carcinoma cells. *Metal. Ions. Biol. Med.*, 10: 285-290.
- Velazquez-Jimenez, L.H., Pavlick, A. and Rangel-Mendez, J.R. 2013. Chemical characterization of raw and treated agave bagasse and its potential as adsorbent of metal cations from water. *Ind. Crop Prod.*, 43(1): 200-206.



Impact of Government Regulation on Emission Reduction of Environmental Pollutants in China

Kai Wang* and Xin Yang**†

*Admissions and Employment Service Department, Xinyang Normal University, Xinyang, Henan, 464000, China

**Social Science Department, Xinyang Normal University, Xinyang, Henan, 464000, China

†Corresponding author: Xin Yang; xyangxyynu@163.com

Nat. Env. & Poll. Tech.
Website: www.neptjournal.com

Received: 12-05-2021

Revised: 27-07-2021

Accepted: 21-08-2021

Key Words:

Government regulation
Environmental pollutants
Emission reduction
Panel regression

ABSTRACT

In pursuit of rapid economic growth, China ignores the carrying capacity of the natural environment and storage quantity of natural resources, resulting in waste and abuse of a large number of natural resources. With the development of industrialization, environmental and ecological problems are becoming more and more serious. Resources are being wasted seriously, and environmental endurance is faced with a great threat. Government regulation on environmental pollution governance has become a consistent problem to be solved for the further economic and social development of all countries in the world. Most governments adopt the establishment of environmental regulation agencies to regulate enterprise pollution. To explore the impact of government regulation on emission reduction of environmental pollutants, government regulation was taken as an explanatory variable and a multivariate panel regression model was established. The influencing factors of environmental pollutant emission in 30 provinces (cities) in China from 2007 to 2016 were estimated. Results show that the government regulation policy in China cannot significantly promote emission reduction of environmental pollutants. GDP and technological progress can effectively reduce the emission of environmental pollutants. The increasing proportion of the secondary industry and a large amount of foreign investment, both lead to an increase in environmental pollutants emission. Government regulation measures can effectively alleviate ecological environment damage caused by environmental pollutant emission. The policy implication of the findings is that the government of China should formulate appropriate intensity of government regulation. The intensity of environmental regulation cannot be blindly increased. Regulation means of pollution charge, pollution permits, and environmental tax should be flexibly used. According to realistic characteristics of different regions, different degrees of excess production capacity, use of government regulation should be different.

INTRODUCTION

Excessive energy consumption and continuous consumption of deteriorating natural resources have led to an increasingly severe ecological environment in China, which has seriously affected the health of urban residents. The extensive development mode characterized by high energy consumption, high pollution, and high output has caused serious environmental pollution in China. Excessive industrial expansion leads to serious excess production capacity. Industries with excess production capacity are mostly highly polluting. Local governments encourage investment at the expense of the environment, and private costs borne by enterprises are far less than social costs, resulting in excessive investment. This ultimately leads to an unbearable burden on resources and the environment. Some developed countries have realized the seriousness of environmental pollution, and have transferred some high-polluting and high-energy-consuming production and processing enterprises to unwary developing countries by

means of industrial transfer to gain their biggest economic benefits. Although China is rich in natural resources, due to the transfer of foreign high-pollution enterprises and imperfect production of domestic enterprises, the resources are seriously wasted, and the emission of "three wastes" is gradually increasing, posing a great threat to China's environmental tolerance.

With the progress of technology, development and consumption of environmental resources have caused serious environmental pollution and ecological damage, while many countries and regions have achieved rapid economic growth. With the intensification of the industrialization process, China has achieved rapid economic development while bringing about social problems such as environmental pollution. Environmental pollution is becoming increasingly serious, and the importance of ecological environmental protection is realized. As ecological and environmental problems have seriously affected economic development

and social stability, the government of China has issued increasingly strict ecological and environmental regulation measures to strengthen environmental constraints to achieve sustainable development. Through the implementation of government regulation, which can be seen as the replacement of market mechanism, the purpose is to maintain good environmental and economic performance. In particular, China has adopted an environmental management system under which governments at all levels are responsible for local environmental quality. The competent environmental protection administrative departments exercise unified supervision and management, and all relevant departments exercise supervision and management in accordance with the law. It has established an environmental management system supplemented by economic incentives such as pollution charges and emission trading systems, which is the most important policy tool for the government to implement environmental regulation. From 2004 to 2019, the Chinese government increased investment in industrial pollution control, with an average annual growth rate of 6.65%, as shown in Fig. 1. As a result, China's sulfur dioxide emissions decreased year by year, with an average annual decline of 5.31%, effectively reducing the emission intensity of environmental pollutants.

EARLIER STUDIES

As early as the 1970s, economists began to bring regulation into the environment. Environmental pollution governance by government regulation has become an emerging hot field of regulation economics. Local governments are responsible for the implementation and enforcement of government

regulation policies on environmental pollution control in China. Government regulation on environmental pollution governance has become a consistent problem to be solved for the further economic and social development of all countries in the world. Most governments in the world adopt the establishment of environmental regulation agencies to regulate enterprise pollution. In terms of government regulation policies in environmental pollution governance, Rothwell (1992) believed that harmful effects of environmental pollution were becoming increasingly obvious and concerned about ozone layer depletion and global warming were increasing, so it was necessary to formulate stricter environmental laws and regulations. Skinner et al. (2003) investigated changing role of local governments in environmental regulation in Zhejiang Province, and results showed that local governments could selectively implement national and provincial policies according to local priorities, which could effectively improve environmental pollution. Beerepoot et al. (2007) focused on the role of stricter government regulations as innovation incentives for the Dutch residential building industry, and the study showed that stricter government regulations and standards contributed to energy technology innovation in Dutch residential buildings. Smith et al. (2008) believed that government environmental regulation could stimulate the application of "clean" technology. Tang et al. (2010) conducted a questionnaire survey of law enforcement officers of the local Environmental Protection Bureau (EPB) in four counties of Guangdong Province of China and found that both local government support and social support would affect local environmental performance. Aronson et al.

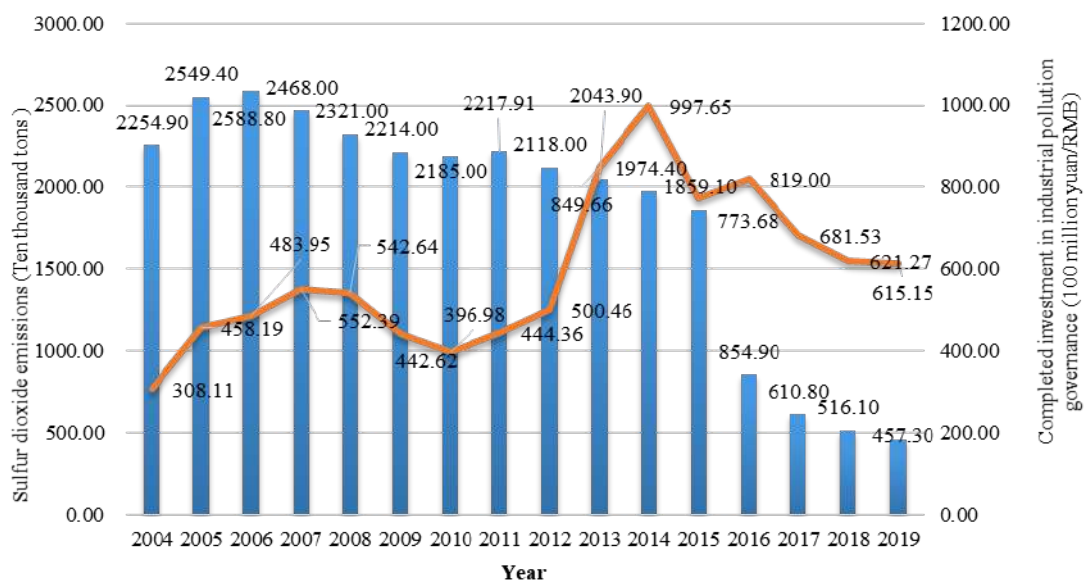


Fig. 1: Sulfur dioxide emissions and completed investment in industrial pollution governance of China from 2004 to 2019.

(2011) believed that the implementation of strict laws and government regulations could effectively promote successful and large-scale tropical forest restoration. Zhao et al. (2016) showed that government environmental regulation had a significant positive effect on enterprise innovation. Hao et al. (2018) investigated the impact of China's environmental regulations on environmental performance, and results showed that current environmental control measures and regulations didn't achieve the expected goal of pollution control and reduction. Zhou et al. (2019) showed that the pollution supervision effect of local governments in China had been strengthened, and green technological innovation and industrial structure optimization caused by environmental regulation could help alleviate haze pollution. Li et al. (2019) analyzed the relationship between government environmental regulation and regional innovation output, and results showed that environmental regulation had a significant negative effect on regional innovation output, and policy suggestions for strengthening environmental protection were put forward from the perspectives of environmental policy diversity, enterprise innovation incentive and sustainable development concept. Pang et al. (2019) studied the reduction effect of government environmental regulations on emission of environmental pollutants by using panel threshold model, and results highlighted timeliness needed to be considered in evaluating environmental regulation efficiency and emphasized the importance of using differential management. It put forward suggestions of local government enhancing the ability of the environmental protection agency system. Deng et al. (2019) investigated the impact of environmental regulation intensity of local governments on regional innovation performance, and the research showed that improvement of environmental regulation intensity improved regional innovation performance through the innovation compensation effect. Zhang et al. (2019) illustrated how the Chinese government's environmental regulations affected smog pollution control through direct and indirect impacts. Results showed that China's current environmental regulation had effectively suppressed haze pollution and achieved the desired effect. Sheng et al. (2020) theoretically analyzed how environmental regulations of the national government and local government affected enterprises' environmental improvement through the three-party evolutionary game model. Results showed that the environmental regulatory policies of the national government were crucial for realizing the goal of environmental protection. Hamman et al. (2021) discussed how Australian laws at the national government level were applied to the impact of agricultural land on the environment. It could be seen from the existing studies that the nature of public goods of environmental resources made the existence of externality possible. Therefore, it was not feasible to rely

on the market mechanism alone, and it would eventually lose control and malfunction. Only the government could add its regulation function. By perfecting government environmental regulation system construction, improving the laws and regulations and policy system, technology innovation, strengthening law enforcement, propaganda and education, and enhancing environmental protection consciousness, China could strengthen ecological environment protection of the government regulation, which could effectively reduce environmental pollutants, and achieve coordinated development of ecological environment and economy.

METHODOLOGY

The multivariate panel regression model constructed in this study is shown in Formula (1).

$$EPO_{ij,t} = \beta_0 + \beta_1 GOV_{ij,t} + \beta_2 GDP_{ij,t} + \beta_3 TEC_{ij,t} + \beta_4 STR_{ij,t} + \beta_5 FAI_{ij,t} + \varepsilon_{ij,t} \quad \dots(1)$$

In Formula (1), $EPO_{ij,t}$ represents environmental pollution as the explained variable. Three indicators, industrial wastewater, industrial waste gas, and industrial solid waste discharge ("three industrial wastes"), are selected to measure the comprehensive environmental pollution index, and the average value of the three indicators represents environmental pollutants. Government regulation ($GOV_{ij,t}$) represents the explanatory variable. According to Lanoie et al. (2008), the proportion of investment in industrial pollution governance in GDP is used to indicate that the larger the index value is, the greater the intensity of government regulation is. Economic growth ($GDP_{ij,t}$) represents the control variable and is represented by the per capita GDP of each region. To eliminate the impact of inflation, the year 2007 is taken as the base period and the value is converted into the actual per capita GDP. Technological innovation level ($TEC_{ij,t}$) represents the control variable, which is expressed by the proportion of internal R&D expenditure in GDP of each region. Industrial structure ($STR_{ij,t}$) represents the control variable and is represented by the proportion of the output value of the secondary industry in GDP. Investment in fixed assets ($FAI_{ij,t}$) represents the control variable and is represented by the total investment in fixed assets of the whole society, which is treated by price adjustment. b_0 represents the constant term of the regression equation, $b_i = (i = 1, 2, \dots, 5)$ is the coefficient of the regression equation and $\varepsilon_{ij,t}$ represents the error term. This study examines 30 provinces (cities) in China (Tibet is not included due to lack of data), with a sample period from 2007 to 2016. The data mainly come from the *China Statistical Yearbook*, *China Environmental Statistics Yearbook*, *China Demographic Statistics Yearbook* and the website of the National Bureau of Statistics.

RESULTS ANALYSIS

Panel data regression model usually involves three models, which are mixed (POOL) model, fixed effect (FE) model and random effect (RE) model. Firstly, the F-test is used to select and compare FE model and POOL model. If *p*-value is less than 0.05, FE model is better. Otherwise, POOL model is used. Secondly, BP test is used to compare the selection of RE model and POOL model. *P*-value is less than 0.05 means that RE model is better. Otherwise, POOL model is used. Thirdly, the Hausman test is used for selecting and comparing FE model and RE model. *P*-value is less than 0.05 means that FE model is better. Otherwise, RE model is used.

As given in Table 1, the panel model involves three models, namely POOL model, FE model and RE model. Firstly,

model testing is carried out to find the optimal model. It can be seen from the above table that F-test showed a significance of 5%. $F(4,40)=14.224$, and $p=0.000<0.05$, indicating that FE model is better than POOL model. Hausman test does not show significance. $\chi^2(5)=2.165$, and $P=0.826>0.05$, indicating that RE model is better than FE model. Based on the above analysis, it is suggested to take RE model as the final result, as shown in Table 2.

1. Impact of government regulation on environmental pollution is significantly positive, and it's significant at the level of 5%, indicating simply increasing the intensity of government regulation cannot reduce environmental pollution. The main potential reason is that the Chinese government's investment in environmental pollution governance is less than the GDP growth rate, which

Table 1: Summary of panel model results.

Variable Model	POOL model	FE model	RE model	Time fixed effect	Two-way fixed-effect
<i>c</i>	12.013** (9.269)	8.507** (3.507)	10.697** (5.581)	17.235** (9.382)	4.995* (2.043)
<i>GOV_{ij,t}</i>	0.140** (2.724)	0.084* (2.269)	0.082* (2.254)	0.019 (0.417)	0.041 (1.994)
<i>GDP_{ij,t}</i>	-0.844** (-8.510)	-0.152 (-0.500)	-0.405 (-1.629)	-0.974** (-11.722)	0.113 (0.545)
<i>TEC_{ij,t}</i>	-0.882** (-2.954)	-1.283** (-3.101)	-1.590** (-4.593)	-0.781** (-2.965)	-0.202 (-0.747)
<i>STR_{ij,t}</i>	0.674** (10.554)	0.246 (1.062)	0.468** (2.703)	0.495** (6.469)	-0.037 (-0.316)
<i>FAI_{ij,t}</i>	-0.106 (-1.961)	0.047 (0.807)	0.027 (0.491)	-0.187** (-4.064)	0.019 (0.674)
<i>R²</i>	0.965	0.368	0.437	0.986	0.159
<i>Adjusted R²</i>	0.961	0.226	0.373	0.98	-0.329
<i>N</i>	50	50	50	50	50
<i>Test</i>	F(5,44)=243.117 p=0.000	F(5,40)=4.660 p=0.002	$\chi^2(5)=34.115$ p=0.000	F(5,35)=485.826 p=0.000	F(5,31)=1.174 p=0.344

Note: In Table 1, * represents $P < 0.05$, ** represents $P < 0.01$, and the corresponding *t* value is in parentheses.

Table 2: Intermediate process value of RE model.

Variable	Value	Coefficient	Standard error	<i>t</i>	<i>p</i>
<i>c</i>		10.697	1.917	5.581	0.000**
<i>GOV_{ij,t}</i>		0.082	0.037	2.254	0.024*
<i>GDP_{ij,t}</i>		-0.405	0.248	-1.629	0.103
<i>TEC_{ij,t}</i>		-1.59	0.346	-4.593	0.000**
<i>STR_{ij,t}</i>		0.468	0.173	2.703	0.007**
<i>FAI_{ij,t}</i>		0.027	0.056	0.491	0.623

$\chi^2(5)=34.115$, $p=0.000$, $R^2=0.437$, $Adjusted R^2=0.373$

Note: In Table 2, * represents $P < 0.05$, ** represents $P < 0.01$

cannot effectively alleviate the massive emission of environmental pollutants caused by other factors. The intensity of formal environmental regulations should not be blindly increased. Such regulatory means as pollution charges, pollution permits, and environmental taxes should be flexibly applied, and differentiated intensity of government regulations should be adopted according to actual characteristics of different regions and different levels of overcapacity.

2. Impact of GDP on environmental pollution is significantly negative, but it's not significant. The main reason is that China's GDP has grown too fast in the past 20 years, and the emission of environmental pollutants is affected by the Chinese government's regulations and other factors. The emission of pollutants does not converge with GDP growth and cannot catch up with GDP growth. In particular, with the profound change of the green GDP concept in China, local governments have implemented a new view of achievements. Therefore, environment-friendly characteristics of GDP growth are becoming more and more obvious. Single comprehensive GDP growth will not easily lead to an increase in the emission of environmental pollutants.
3. Impact of technological progress on environmental pollution is significantly negative, and it's significant at the level of 1%, indicating that strengthening technological innovation can indeed reduce the emission of environmental pollutants. It explains that the increase of R&D of science and technology in the industry promotes the improvement of green technology innovation. The main reason of appearing this kind of situation is that the industrial enterprises of China are in a critical period of traditional economic transformation. Strengthening R&D of technology can increase innovation of pollution governance technology, to further promote the development of technology innovation.
4. Impact of industrial structure on environmental pollution is significantly positive and it's significant at the level of 1%. It shows that an increasing proportion of the secondary industry will lead to an increase in the emission of environmental pollutants. This shows that when the proportion of the secondary industry increases, the level of environmental pollution will worsen. As the secondary industry is an industry with high energy consumption and high pollution, it mainly includes mining, manufacturing, production and supply of electricity, gas, and water, and construction. Mining and manufacturing them need to consume large amounts of natural energy resources, which is the main source of environmental pollution. Coal energy in the process of combustion

will produce large amounts of sulfur dioxide, industrial wastewater and industrial solid waste commonly, and these pollutants in the air, water and ground cause great pollution to the environment.

5. Impact of foreign direct investment on environmental pollution is significantly positive, but it's not significant. It shows that a large amount of foreign investment in China will lead to an increase in environmental pollutant emissions. In the past, to pursue rapid economic development, China had very low environmental requirements for FDI. Developed countries might bring pollution-intensive industries with high pollution and high energy consumption into China, resulting in a large number of pollutant emissions and leading to a large number of pollution-intensive enterprises into China. Due to the requirement of political performance, the incentive of local governments to attract investment and to promote local economy was often greater than that to limit the inflow of foreign investment to protect the environment, which might lead to inflow of polluting foreign direct investment, and the situation that FDI and environmental pollution emissions rose at the same time.

POLICY SUGGESTIONS

Establishing Reward and Punishment Systems to Strengthen Corporate Awareness of Environmental Responsibility

The government should formulate rules and regulations, organize leading groups of enterprises to carry out regular lectures and training on environmental protection, cultivate the environmental awareness of enterprises, and promote green production of enterprises. In the rules and regulations, standards should be set, that is, enterprises do not comply with requirements of environmental protection, and they will be severely punished. Under the guidance of the government's environmental regulations, economic growth mode has changed from the original extensive to intensive growth mode, which has achieved a qualitative leap not only in the production mode, but also in the management mode. When the government strengthens the regulation of environmental pollution, on the one hand, the government can provide technical cooperation to ensure strong technical backing. On the other hand, it can provide financial support, such as low-interest loans, financial subsidies, tax breaks and other preferential policies for enterprises engaged in environmental protection research and development technologies. Green products will be produced after environmental pollution governance by enterprises. The government should strictly regulate polluting enterprises and take restrictive measures

to the non-environmental production of polluting enterprises, to finally reflect the advantages of green products.

Strengthening the Publicity of Green Consumption and Guiding Enterprises to Produce Differentiated Products

Under the condition of environmental pollution regulation adopted by the government, guiding enterprises to produce differentiated products with environmental protection attributes will greatly improve the regulation effect. Green products with environmental protection attributes may not have competitive advantages after being put into the market, because consumers' awareness of environmental protection attributes of products is different. Therefore, the government should cultivate consumers' awareness of environmental protection and guide the concept of green consumption. Demand for environmental protection products in the market depends on the preferences and requirements of consumers. When the public takes environmental protection as their social mission, they will tend to buy such products with environmental protection attributes. Through policy publicity, news media, and organization of environmental protection activities and other means, the government can enhance consumers' awareness of environmental protection, for environmental protection products opening up sales. Enterprises will pay more attention to environmental protection and promote the sustainable and healthy development of China's economy.

Establishing Incentive Mechanisms for Environmental Pollution Regulators

In process of environmental pollution regulation, the government also appears as an agent of the public, representing interests of. As a regulator, but also an actor in the economic society, the goal is also to pursue the maximization of interests, resulting in the choice of behavior against the client. Supervision of regulators should be strengthened. It can improve the overall efficiency of regulation through supervision and can grasp more comprehensive and detailed information about polluting enterprises. In terms of system design and concrete implementation of environmental pollution regulation, the department can independently complete system design and concrete implementation, to prevent the inconsistency of each department to affect implementation effect and specific behavior of enterprises. At the same time, on the basis of the establishment of environmental pollution regulation, the establishment of environmental litigation system in the rear can realize differentiation of environmental regulation rights. Through this method, the implementation of the environmental pollution regulation department is supervised. The establishment of environmental litigation

institution ensures that the environmental pollution regulation department acts in accordance with the rules, and it supervises them to assume corresponding legal responsibilities once they are found to be improper so that the public's demands can be reasonably resolved.

Improving the Public's Ability to Supervise Polluting Enterprises and Giving Them Economic Rewards

If the public can join in the supervision of polluting enterprises, it will not only reduce the occurrence of enterprises' pollution behavior, but also greatly enhance environmental awareness. With the enhancement of environmental awareness of the public, constraints on polluting enterprises will be more and more important. Therefore, the environmental pollution regulation department should regularly disclose pollution information of polluting enterprises to the public, and disseminate harm of pollutants to human beings and impact on the living environment of the public through news, newspapers, magazines and other social media. In process of environmental pollution regulation by the government, many small and medium-sized enterprises violate the rules of emission. The purpose of regulating environmental pollution of small and medium-sized enterprises is not to rule them out of the market, but to regulate their pollution behavior. However, for most small and medium-sized enterprises, high regulatory costs often become an important obstacle to restrict production. In this regard, the government should formulate corresponding policies to provide economic compensation and technical support to them.

CONCLUSION

The extensive development mode characterized by high energy consumption, high pollution and high output has caused serious environmental pollution in China. Government regulation policy is an effective means to realize China's economic transformation and upgrading, to solve environmental pollution problems and to improve environmental performance. To test the impact of government regulation on environmental pollution, government regulation as an explanatory variable was included and a multiple panel regression model was established. The influencing factors of environmental pollutant emission in 30 provinces (cities) in China from 2007 to 2016 were estimated. Conclusions can be drawn that: (1) Government regulation policy in China cannot significantly promote emission reduction of environmental pollutants. (2) GDP and technological progress can effectively reduce emissions of environmental pollutants. (3) Increase in the proportion of the secondary industry and the introduction of large amounts of foreign investment leads to an increase in environmental pollutant emission.

Finally, it puts forward policy suggestions, including constructing rewards and punishment system to strengthen environment responsibility consciousness of enterprises, enhancing the promotion of green consumption to guide the enterprise to produce differentiated products, establishing incentive mechanism for regulators of environmental pollution, improving the ability of the public to supervise polluting enterprises. Those government regulation measures can mitigate ecological environmental damage caused by environmental pollutants. It suggests that further research should be carried out on setting of environmental pollution regulation standards, the impact of environmental information disclosure on pollutant emission, and establishment of green technology innovation mechanism of enterprises.

REFERENCES

- Aronson, J., Brancalion, P. H., Durigan, G., Rodrigues, R. R., Engel, V. L., Tabarelli, M. and Scarano, F. R. 2011. What Role Should Government Regulation Play in Ecological Restoration? Ongoing Debate in São Paulo State, Brazil. *Restoration Ecology*, 19(6): 690-695.
- Beerepoot, M. and Beerepoot, N. 2007. Government Regulation as an Impetus for Innovation: Evidence from Energy Performance Regulation in the Dutch Residential Building Sector. *Energy Policy*, 35(10): 4812-4825.
- Deng, J., Zhang, N., Ahmad, F. and Draz, M. U. 2019. Local Government Competition, Environmental Regulation Intensity and Regional Innovation Performance: An Empirical Investigation of Chinese Provinces. *International Journal of Environmental Research and Public Health*, 16(12): 2130.
- Hamman, E., Deane, F., Kennedy, A., Huggins, A. and Nay, Z. 2021. Environmental Regulation of Agriculture in Federal Systems of Government: The Case of Australia. *Agronomy*, 11(8): 1478.
- Hao, Y., Deng, Y., Lu, Z. N. and Chen, H. 2018. Is Environmental Regulation Effective in China? Evidence from City-level Panel Data. *Journal of Cleaner Production*, 188: 966-976.
- Lanoie, P., Patry, M. and Lajeunesse, R. 2008. Environmental Regulation and Productivity: Testing the Porter Hypothesis. *Journal of Productivity Analysis*, 30(2): 121-128.
- Li, Y., Tang, Y., Wang, K. and Zhao, Q. 2019. Environmental Regulation and China's Regional Innovation Output: Empirical Research Based on Spatial Durbin Model. *Sustainability*, 11(20): 5602.
- Pang, R., Zheng, D., Shi, M. and Zhang, X. 2019. Pollute First, Control Later? Exploring the Economic Threshold of Effective Environmental Regulation in China's Context. *Journal of Environmental Management*, 248: 109275.
- Rothwell, R. 1992. Industrial Innovation and Government Environmental Regulation: Some Lessons from the Past. *Technovation*, 12(7): 447-458.
- Sheng, J., Zhou, W. and Zhu, B. 2020. The Coordination of Stakeholder Interests in Environmental Regulation: Lessons from China's Environmental Regulation Policies from the Perspective of the Evolutionary Game Theory. *Journal of Cleaner Production*, 249: 119385.
- Skinner, M. W., Joseph, A. E. and Kuhn, R. G. 2003. Social and Environmental Regulation in Rural China: Bringing the Changing Role of Local Government into Focus. *Geoforum*, 34(2): 267-281.
- Smith, M. and Crotty, J. 2008. Environmental Regulation and Innovation Driving Ecological Design in the UK Automotive Industry. *Business Strategy and the Environment*, 17(6): 341-349.
- Tang, S. Y., Lo, W. H. and Fryxell, G. E. 2010. Governance Reform, External Support, and Environmental Regulation Enforcement in Rural China: The Case of Guangdong Province. *Journal of Environmental Management*, 91(10): 2008-2018.
- Zhang, M., Liu, X., Ding, Y. and Wang, W. 2019. How Does Environmental Regulation Affect Haze Pollution Governance? An Empirical Test based on Chinese Provincial Panel Data. *Science of the Total Environment*, 695: 133905.
- Zhao, X. and Sun, B. 2015. The Influence of Chinese Environmental Regulation on Corporation Innovation and Competitiveness. *Journal of Cleaner Production*, 112: 1528-1536.
- Zhou, Q., Zhang, X., Shao, Q. and Wang, X. 2019. The Non-linear Effect of Environmental Regulation on Haze Pollution: Empirical Evidence for 277 Chinese Cities during 2002-2010. *Journal of Environmental Management*, 248: 109274.

... Continued from inner front cover

- The text of the manuscript should run into **Abstract, Introduction, Materials & Methods, Results, Discussion, Acknowledgement** (if any) and **References** or other suitable headings in case of reviews and theoretically oriented papers. However, short communication can be submitted in running with **Abstract and References**. The references should be in full with the title of the paper.
- The figures should preferably be made on a computer with high resolution and should be capable of withstanding a reasonable reduction with the legends provided separately outside the figures. Photographs may be black and white or colour.
- Tables should be typed separately bearing a short title, preferably in vertical form. They should be of a size, which could easily be accommodated in the page of the Journal.
- References in the text should be cited by the authors' surname and year. In case of more than one reference of the same author in the same year, add suffix a,b,c,.... to the year. For example: (Thomas 1969, Mass 1973a, 1973b, Madony et al. 1990, Abasi & Soni 1991).

List of References

The references cited in the text should be arranged alphabetically by authors' surname in the following manner: (Note: The titles of the papers should be in running 'sentence case', while the titles of the books, reports, theses, journals, etc. should be in 'title case' with all words starting with CAPITAL letter.)

- Dutta, A. and Chaudhury, M. 1991. Removal of arsenic from groundwater by lime softening with powdered coal additive. *J. Water Supply Res. Techno. Aqua.*, 40(1) : 25-29.
- Hammer, D.A. (ed.) 1989. *Constructed Wetlands for Wastewater Treatment-Municipal, Industrial and Agricultural*. Lewis Publishers Inc., pp. 831.
- Haynes, R. J. 1986. Surface mining and wetland reclamation. In: Harper, J. and Plass, B. (eds.) *New Horizons for Mined Land Reclamation*. Proceedings of a National Meeting of the American Society for Surface Reclamation, Princeton, W.V.

Submission of Papers

- The paper can be submitted by e-mail as an attachment in a single WORD file at **contact@neptjournal.com**
- The paper can also be submitted online in a single WORD file through the **online submission portal** of journal's website: **www.neptjournal.com**

Attention

1. Any change in the authors' affiliation may please be notified at the earliest.
2. Please make all the correspondence by e-mail, and authors should always quote the manuscript number.

Note: In order to speed up the publication, authors are requested to send the publication charges as soon as they get the 'initial acceptance' letter, and also correct the galley proof immediately after receipt. The galley proof must be checked with utmost care, as publishers owe no responsibility for mistakes. The papers will be put on priority for publication only after receiving the processing and publication charges.

Nature Environment and Pollution Technology

(Abbreviation: Nat. Env. Poll. Tech.)

(An International Quarterly Scientific Journal)

Published by



Technoscience Publications

A-504, Bliss Avenue, Opp. SKP Campus
Balewadi, Pune-411 045, Maharashtra, India

In association with

Technoscience Knowledge Communications

Mira Road, Mumbai, India

For further details of the Journal, please visit the website. All the papers published on a particular subject/topic or by any particular author in the journal can be searched and accessed by typing a keyword or name of the author in the 'Search' option on the Home page of the website. All the papers containing that keyword or author will be shown on the home page from where they can be directly downloaded.

www.neptjournal.com

©**Technoscience Publications:** The consent is hereby given that the copies of the articles published in this Journal can be made only for purely personal or internal use. The consent does not include copying for general distribution or sale of reprints.

Published for Proprietor, Printer and Publisher: Mrs. T. P. Goel, A-504, Bliss Avenue, Balewadi, Pune, Maharashtra, India; Editors: Dr. P. K. Goel (Chief Editor) and Prof. K. P. Sharma